MECHANISMS OF SEDIMENT COMPACTION RESPONSIBLE FOR OIL FIELD SUBSIDENCE.

A thesis submitted to the

University of London

(University College London)

for the degree of Doctor of Philosophy

in the Department of Geological Sciences.

by

Michael Anthony Addis

October 1987

to my parents

for all their encouragement

Abstract

During the production of a hydrocarbon reservoir, the compaction of weakly cemented sedimentary materials can result from increases in effective stress, and lead to surface subsidence. Such a phenomenon has recently been observed in the oil and gas bearing chalk fields in the Central North Sea. In order to evaluate the compaction potential of sedimentary materials during exploitation of a reservoir, laboratory experiments were performed on chalks and clays. These experiments were predominantly K_o (zero lateral strain) tests.

The tests were performed in a high pressure triaxial cell, the development of which continued throughout the experimental programme.

Tests performed on chalks from the Central North Sea, and from two onshore sites in southern England showed similar deformational trends. The analyses of these results concentrated on the variables of testing and the possible errors resulting from the use of laboratory data in the modelling of field situations. The analyses of the tests also include a comparison between the experimental methods and the interpretation of the results of this study and those of other workers on the subject of reservoir compaction. A parametric description of the compaction of chalk is presented as a summary to these tests.

Two compaction tests on clay samples from the Central North Sea were also undertaken. The clays were uncemented and show contrasting behaviour to the chalks. These tests were performed to evaluate the amount of compaction likely to occur in the overburden of a hydrocarbon reservoir during production.

The results of the deformational trends obtained from this study

are compared to those obtained by other workers, with particular reference to the changes in physical parameters during compaction. This follows a literature survey into hydrocarbon reservoir compaction.

The K_o tests performed in this study are thought to represent the condition of sediment burial in a tectonically inactive basin. This subject is briefly reviewed, and the relevance of the results presented earlier discussed in terms of the prediction of stresses existing within differing lithologies.

The analysis of the results have been performed using parameters commonly used in soil mechanics, this seemed to be appropriate for the deformations undergone by the materials used in this study.

Acknowledgements

During the period of research the author has been in receipt of a Natural Environment Research Grant, which is duly acknowledged.

During the three years of research the author has been associated with three colleges in the University of London. The first two years of the research were performed while a student at the Geology Department of King's College, now sadly "mergered" in outer London. The final year was spent as a student of University College. During the three years, the experimental work was performed in the soil laboratories in the Department of Civil Engineering, at Imperial College. As such I am indebted to many people from the three institutions to numerous to mention. I would however like to thank the chief technicians from King's and University College, Mr. J Congram and Mr. R Dudman respectively, for ensuring relatively few hickups along the way.

I would especially like to thank the technical staff of the soil laboratories who have provided excellent support to this study, with much input into the equipment design and construction, as well as many other subject areas. I am sure that without their expertise, help and patience this study would not have been possible. Mr. S. Ackerley, Mr. L. Spall, Mr. G. Keefe, Mr. A. Bolsher and Mr. R. Hare are gratefully acknowledged. I would also like to thank Mrs. E. Gibbs for all her help, and for her forgiveness during times of oil leaks. Particular thanks are given to Mr. S. Ackerley whose enthusiasm, general willingness to do the impossible and his patience with an ignorant geologist is gratefully appreciated.

Technical help was also provided by Mr. T. Osbourne and Mr. S. at

University College and Mr. R. Giddons in the Department of geological sciences, Imperial college who are duely thanked. During the initial set up of the apparatus the help of Mr. B. Clarke in the Engineering Geology section in Imperial College was sought and willingfully obtained on many occasions; I would like to express my thanks for his help and advice.

My period of work at the soils laboratory, Imperial College was a true education and I must thank my colleagues in this group for answering my many questions patiently, regardless of the elementary nature of these, and for their encouragement during this study. My many thanks go to Mr A.J. Bond, Dr. G.T. Dounias, Mr. D. French, Mr. J. Hellings, Mrs. G. N. Georgiannou Lesas, Dr. M. Maccarini, Mr. M. Mahmoud, Dr. J. Maswoswe, Mr. D.L. Nyaoro, Dr. E. Ovando-Shelley, Mr. D. Schreiner, Dr. S. Shibuya and Mr. D. Toll, Mrs. T. Tika Vaffilikos. I would also like to thank Dr. M. Maccarini for our many discussions on the behaviour of cemented materials and his ready exchange of ideas. The help of Mr. D. Toll and use of his computer expertise and software for the calculation of results is gratefully appreciated. Use of software developed by Mr. A. J. Bond for the 3-dimensional plots is also gratefully appreciated by the author.

I am very grateful to have been able to work at the soil mechanics laboratories, and as such I must thank the head of the soil mechanics section, Prof. J. B. Burland for this opportunity. I would also like to express my gratitude to the academic staff of the section, Dr. R. J. Chandler, Prof. J. N. Hutchinson, Dr. R. Jardine, Dr. S. Leroueil (visiting academic), Dr. D. M. Potts, Prof. A. W. Skempton, Dr. P. R. Vaughan and particularly Dr. A. E. Skinner, for many stimulating and enlightening discussions.

Many thanks go to the Norwegian Petroleum Directorate for allowing

me the opportunity of working on samples obtained from the North Sea. I would especially like to thank Mr. K. Tonstad, Mr. O. P. Berget and Mr. P. E. Overli, for many fruitful discussions.

Colleagues at King's College and University College are also thanked for all their support and help in very many ways, my thanks go to Dr. H. Chen, Mr. M. J. Leddra, Mr A. Goldsmith, and Miss N. A. Yassir. I am especially grateful to Miss N. A. Yassir for correcting my grammar - a most unenviable task, many thanks. At this point I would like to express my gratitude to my numerous co-tenants/ colleagues for their patience with the author during the period of research, as well as for their welcome distractions and excellent company, these include Mr. H. Davies, Miss K. Jeffrey, Miss K. Lewin, Mr. J. Morris, Mr. A. Pritchard, Mr. M. Shaw, Dr. J. Williams, and Miss M. White.

It only remains for me to thank my supervisor, Dr. M. E. Jones for his help and encouragement, and for directing me towards a very interesting area of study. His support is acknowledged and appreciated especially in times of critisism from the author.

I would finally like to express my appreciation to my family and especially to my parents, who have always encouraged and supported me, not only through this period of research, but through my whole education, the good and not so good times. My thanks are insufficient to express my gratitude.

Contents

List of figures

Plates

List of tables

Glossary of terms

The following list is a glossary of the main terms used in this thesis, other terms used are defined in the discussion.

A Skempton's pore pressure parameter.
B Skempton's pore pressure parameter.
C Compressibility of mineral grains.
C_α Coefficient of secondary consolidation.
C^b Rock bulk compressibility.
C^c Coefficient of volume compressibility.
C^f Pore compressibility
C^m Uniaxial compressibility (= M_v).
C^r Rock matrix compressibility.
C^s Skeleton compressibility.
C^v Coefficient of consolidation.
D^v Depth
e void ratio.
E Young's modulus.
f Fractional porosity.
G Shear modulus.
H Height/Depth.
k Hydraulic conductivity (cm/sec).
K Coefficient of permeability (Darcies).
K_o Coefficient of earth pressure at rest.
$\bar{K}^o$ K_o for incremental stress changes.
$\bar{K}^o$ $\bar{K}^o$ for elastic deformations.
$\bar{K}^{oe}_{onc}$ $\bar{K}^o$ for normal consolidation deformations (Normal consolidation is used to describe materials which exist at stress levels higher than experienced previously, and free of any effects of cementation.
$\bar{K}_{opc}$ $\bar{K}_o$ for pore collapse deformations.
M^{opc} $= {}^oq/p'$
M_v Uniaxial compressibility (= C_m)
n^v Measure of non-linearity of elasticity.
p' Mean effective stress.
p_o Pore pressure of the formation.
p^o_{on} Normal pore pressure gradient (9.79kPa/m).
q, q' Shear stress/deviatoric stress.
t Ellapsed time.
T_v Time constant (= $C_v.t/H^2$)
U^v Pore pressure.
U_h Pore pressure difference across the sample.
V^h Volume.

α Thermal expansivity.
β Ratio of rock matrix to bulk compressibility.
γ Density.
ϵ Strain.
ϕ' Angle of internal friction
σ Total stress.
σ' Effective stress.
$\dot{\sigma}'$ Rate of effective stress change.
ν Poisson's ratio

CHAPTER 1

INTRODUCTION

This thesis presents the results of a experimental study of the volume reduction which occurs in sedimentary rocks when pore fluid is expelled. In nature loss of pore fluid from a sediment may result either because of the increased loading due to burial in sedimentary basins or reduction in pore pressures during production from reservoirs. The reduction in pore volume which occurs as a result of fluid withdrawal during exploitation of oil fields and aquifer systems, is analogous to natural dewatering, and relevant aspects of this subject are therefore discussed both from an engineering and a geological standpoint. The work contained herein is based on an experimental programme of one-dimensional compaction tests (zero lateral strain deformation experiments) performed in a high pressure triaxial cell. A drainage system, a heating facility and special control systems for the tests performed, were developed for the triaxial cell and refined during the testing programme.

The testing programme required samples of a weak sedimentary rock that was porous and cemented. The chalk, which has been shown by previous workers (Blanton, 1981; Jones and Addis, 1985b) to exhibit mechanical characteristics typical of most porous cemented sediments was selected for this purpose. The chalks tested initially were sampled from cores recovered from the Central North Sea and were of varying porosities. These early experiments were then supplemented by a series of deformation tests performed on samples of outcrop

chalk from two onshore sites in southern England. These experiments on samples with the same porosity were performed to evaluate the effects of different test procedures on the mechanical characteristics exhibited by the North Sea samples. The experimental study of the chalks enabled the construction of a model for chalk behaviour during one-dimensional compaction. Two compaction tests on Tertiary clays, cored from the same area of the North Sea as the chalk samples, were also performed. These results provide an interesting comparison with the chalk compaction data, because unlike the chalk the clays were uncemented.

Porosity decrease in sediments has been studied in geology since the earliest days of the subject, and has received the attention of many notable geologists. The methodology behind these early studies has been to correlate porosity with age of strata using outcrop materials. Later studies incorporated samples recovered from drilling operations. From these studies, plots of decreasing porosity with increasing depth have been produced (Rieke and Chilingarian, 1974; Selley, 1978; Baldwin and Butler, 1985).

The experimental study of porosity decrease with increasing applied stress was initiated in the 1930's. The main expansion of this study occured in the 1950's, with the realisation that pore volume decrease significantly affected the prediction of volumes of oil in place, in hydrocarbon reservoir productivity calculations, Hall (1953). Since then, geological work has mainly concentrated on this aspect of volume decrease in sediments and rocks. Also, a number of experimental engineering studies have extended low pressure soil mechanics theory to the high pressures encountered in reservoir engineering - these have proved to be interesting geologically.

The reduction in pore volume of sediments during burial can be

effectively split into two main mechanisms: i) consolidation, the reduction in pore volume by intergranular slip and grain rearrangement, with little alteration of the constituent grains, and ii) cementation, the bonding of the sediment, through filling of the pore volume with mineral material. The former mechanisms have been widely studied at low pressures in the engineering discipline of soil mechanics, but relatively few studies have been performed at high pressures. As a result, there is very little information on the consolidation behaviour of sediments at high pressures, though some notable contributions exist (Rieke and Chilingarian, 1974). The second mechanism, volume reduction through cementation leads to an increase in the competency of a unit of strata, increasing its lithification, and has normally been attributed to a pressure solution mechanism. Pressure solution is the dissolution occurring at compressed points of intergranular contacts, with reprecipitation of the dissolved material in areas of relatively low compressive stress. This differs from cementation of near surface sediments, which is generally due to deposition of salts precipitating from pore fluids, commonly accompanied by mineral breakdown in weathered parent materials. Pressure solution is very dependent upon chemical factors which alter the solubility of the solid material in the transporting medium, whereas consolidation, as a volume change mechanism, has rarely been related to the chemistry of sediments. Another fundamental difference between the two mechanisms is the time dependency associated with them: consolidation has mainly been investigated by engineers over the time scale of decades, whereas cementation of sediments is normally considered as a geological process, occurring over a considerably longer period of time. Cementation due to pressure solution is a very slow process, and it

can only be tested at very slow strain rates. The excessively long times required to undertake laboratory studies of pressure solution, has meant that it has been predominantly studied from a theoretical or descriptive standpoint. (see Addis and Jones (1985) for a brief review of the literature).

The work presented in this thesis applies soil mechanics theory to the problem of compaction of a weak rock under conditions of increasing overburden stress. This increase in the effective overburden stress could result naturally from the progressive burial of a sediment, or from the increase in effective stress due to drawdown of pore pressure during production of a subsurface reservoir. A model of sediment behaviour is used as a framework for the study; this is presented in Chapter 2. The experimental work has mainly concentrated on the study of one-dimensional compaction and consolidation of the chalk. Those factors which have been thought to affect the compaction of the chalk have been investigated as independent variables. This study has also explored in detail the stress path followed by the sample during compaction (Chap. 3), and demonstrates how sample volume change is dependent on the magnitude of all components of the applied stress system. This has been ignored in some of the previous studies which have considered porosity decrease in sediments, during high pressure compaction experiments (Rieke and Chilingarian, 1974). The results of this part of the study indicate that a knowledge of both the magnitude of the stresses acting at depth in sedimentary basins, and the manner in which these stresses vary as the lithology changes, is essential to understanding the compaction of the different sediment units. Such knowledge is also required to understand the generation of overpressures (pore pressures in sediments and rocks, which are in excess of the

hydrostatic gradient). Without such a knowledge a full understanding of the structures in, or associated with sedimentary basins cannot be obtained.

Analyses of the results in terms of the consolidation parameters described in Chapter 3, involves the acceptance of assumptions implicite in Terzaghi's consolidation theory, these assumptions may not be valid for chalk or for other materials at high pressures. This is discussed in detail in the text (Chaps. 2 and 3). The reduction in pore volume due to consolidation will affect the permeability of a sediment. This is obviously an important factor both in terms of consolidation of naturally buried sediments, where low permeabilities will resist further volume change, and in the case of compacting oil reservoirs, where a loss of permeability will have significant economic consequences. Permeability was measured in the samples tested during this study while the samples were deforming; this method of permeability measurement has not been performed at high pressures previously. The results indicate that measurement of the permeability using this test method (Chap. 3) may be a more useful and more time efficient technique than the incremental methods generally employed. The possible errors involved in applying these new testing techniques are discussed in Chapter 3.

Chapter 4 discusses the results of the chalk deformation tests presented in App.5, with emphasis on the variables influencing compaction, and relates the results to similar published work, wherever possible. After discussing the variables affecting the compaction of chalk, the nature and mechanisms of the compaction are discussed. The chapter is terminated by a discussion of deformation of the chalk in terms of the soil model described earlier in, Chapter 2. Chapter 5 is a brief description of the two clay samples tested

from the Central North Sea, to which the chalk experiments can be compared. The tests were each of approximately 6 weeks duration, but because of the low sample permeability, they did not attain the large strains developed during the deformation of the chalk samples. Because of the difficulties encountered in testing the clay samples, the results are not discussed in any great detail, and should be treated semi-quantitatively.

Chapters, 6 and 7, are predominantly literature reviews of hydrocarbon reservoir compaction and the analysis of in-situ stresses in basins, respectively. Initially in Chapter 6, the methods previously used to calculate reservoir compactions and subsidence deformations are reviewed. The results from this study are compared with those reported in the reservoir engineering literature. The chapter is concluded with a review of the reported cases of reservoir subsidence. Chapter 7 is a brief discussion of the state of stress which might exist in tectonically inactive sedimentary basins.

The last section of this thesis (Chap. 8) presents the conclusions of the study, with emphasis on the nature of chalk compaction and on the methodology of K_o testing at high pressures.

Due to the dual application of soil mechanics and reservoir compaction theories in this study, the thesis is deliberately separated into the two parts; the former is a discussion of relevant soil mechanics theory and analyses predominantly used to interpret the results of the experimental programme, whilst the latter considers reservoir compaction theories of sediment volume change as well as the geological applications of the results of the experimental work. The two sections are seperated by the discussion of the results (which are presented individually in the App. 5). This was done because the two subject areas were difficult to combine,

which in turn is due to the different approaches employed in the analysis of deformational volume change.

CHAPTER 2

ASPECTS OF COMPACTION

2.1) INTRODUCTION

This chapter discusses and reviews those aspects of soil mechanics theory which are applicable to the problems of compaction in oil reservoirs, compaction during sediment burial and to the work presented later in this thesis. The chapter is sub-divided, treating separately the various aspects of soil mechanics which are discussed. These are:

a) the principle of effective stress;

b) undrained pore pressure response to loading;

c) one-dimensional consolidation;

d) representation of stress states in sediments;

e) mechanical behaviour of cemented sediments;

f) strain rate effects; and

g) the affect of temperature on consolidation.

The first three subjects consider the effective stress acting on a sedimentary material; the first section reviewing the applicability of Terzaghi's effective stress equation to a material with compressible grains. The undrained pore pressure response to loading, describes the build up of pore pressure during undrained loading of a test specimen. Undrained loading occurred during initial stressing of the sample in the first tests performed in this study (App. 1), and in the oedometer test. The one-dimensional consolidation equation formulated by Terzaghi describes the pore pressure (and hence the

effective stress) distribution in a drained saturated material which has been loaded. The pore pressure under this condition varies with both time and position in the sediment considered. The Terzaghi consolidation equation or equivalent equations have been used as a basis for the constant rate of strain consolidation analyses discussed in Chapter 3. This discussion on the consolidation equation is designed to bring to the attention of the reader, assumptions implicite in the original formulation of Terzaghi (1943), and, as a result, in the constant rate of strain consolidation analyses. Other consolidation equations are discussed briefly for comparative purposes.

The fourth section in this chapter, discusses the different representations of stress states in sediments. The type of axes commonly used to represent the state of stress in sediments and rocks are compared graphically, to assist those readers unfamiliar with the notation which is used to represent the results of this study. The second part of this section then briefly discusses the Critical State model commonly used in soil mechanics. This thesis employs the notation normally associated with this model. The model illustrates how the void ratio or porosity is related to the stress system acting on the sample.

The fifth section briefly describes the mechanical behaviour exhibited by cemented sedimentary materials, e.g. sensitive clays and residual soils, which can be considered to have analogous, but not identical behaviour to weak rocks: like the chalks tested in this study. The introduction of the mechanical behaviour of these low pressure analogs to porous sedimentary rocks, is necessary due to the limited high pressure experimental work that has been published for weakly cemented rocks. In this section information from weak rocks

will also be included where relevant. To complete the fifth section on weakly cemented sedimentary materials, a discussion of the compaction behaviour of chalk is presented from studies reported in the literature.

The chapter is concluded with two aspects of deformation commonly ignored in compaction studies of chalk, they are, however, aspects which should be considered when attempting to investigate burial of a sediment or drawdown of pore fluid pressure in an oil reservoir. These are: 1) strain rate effects - this discusses the increase in compaction strain which occurs when decreasing the loading rate of an experiment; 2) The effect of temperature on compaction - this is relatively unstudied with respect to zero lateral strain compaction tests. These two subjects are reviewed and discussed mainly with respect to the soil mechanics literature, though aspects from rock mechanics and reservoir engineering are presented where relevant information exists.

2.2) THE PRINCIPLE OF EFFECTIVE STRESS

The effective stress acting on a porous material governs its deformation. During the burial of a sediment the effective stress is increased due to an increase in total stress (external stress applied to the boundary of a unit of sediment) ($\bar{\sigma}$). However, during production of a hydrocarbon reservoir the effective stress is increased by reducing the pore fluid pressure (internal pressure) (U) in the pore spaces of the material. This section of the thesis reviews the effective stress equations published in the literature to assess whether the deformation due to an increase in the total stress is equivalent to the deformation due to a reduction of the pore fluid pressure in a porous material, as is often assumed. This

analysis is important to enable the correct modelling of effective stress in laboratory deformation experiments.

Terzaghi (1943) defined the principle of effective stress as relating the external stress or total stress to the internal stress or pore pressure, so that an increase in one of these quantities is equivalent to a decrease in the other, resulting in an identical volume change. This relationship is represented as

$$\sigma' = \sigma - U \qquad .. 2.2.1$$

where σ' is the effective stress, σ is the total external stress and U is the pore pressure or internal stress. This is Terzaghi's equation of effective stress, it is the most commonly used principle of effective stress and is widely applied in engineering and geological studies. It takes no account of porosity or intergranular contact area and assumes the grains are incompressible. Skempton (1960) reviewed the theories of effective stress and concluded that intergranular contact did not influence the relationship. If one takes account of grain compressibility the relationship becomes (Bishop, 1973; Skempton, 1960; Nur and Byerlee, 1971; van der Knaap, 1960)

$$\sigma' = \sigma - (1 - C/C_s)\, U \qquad .. 2.2.2$$

where C = compressibility of mineral grains and C_s = compressibility of the soil skeleton. This was concluded from tests on unjacketed samples, (the increased resistance of the samples to deformation due to increased pressure was considered to be unimportant by Skempton (1960)). The results presented by Skempton

(1960) and Nur and Byerlee (1971) on porous rocks indicate that Eqn. 2.2.2 is a good approximation, and that Terzaghi's equation is valid for most soils where C_s is large in comparison to the grain compressibility (C) (Skempton, 1960; Bishop and Skinner, 1977).

It is normal in compaction experiments performed on reservoir materials to increase the axial stress by increasing the total stress while maintaining a constant pore pressure, however, in a hydrocarbon reservoir the reverse occurs. Van der Knaap (1960) formulated an equation for the effective stress change due to the drawdown of pore fluid pressure under zero lateral strain conditions, i.e. the conditions existing during compaction of a hydrocarbon reservoir, Eqn. 2.2.3.

$$\Delta\sigma' = \left(\frac{1 + \nu}{3(1 - \nu)} + \frac{2(1 - 2\nu).C}{3(1 - \nu)\ C_b} \right) .(U-U_1) \qquad .. \ 2.2.3$$

Where C_b = total compressibility, and ν = Poisson's ratio. In deriving this, an assumption of Eqn. 2.2.1 is made, when a drop in pore pressure is equated to give an equal increase in vertical effective stress.

The determination of C in Eqn. 2.2.2 and Eqn. 2.2.3 has proved troublesome (Mesri et.al., 1976) as this depends on σ' (Nur and Byerlee, 1971; Bishop, 1973; Bishop and Skinner, 1977), this could make the use of these equations impractical. Skempton (1960) pointed out that as the porosity approaches zero C_s approaches C.

Nur and Byerlee (1971) obtained good aggreement for deformations in sandstones and granites with various effective stress increases using Eqn. 2.2.2. This implies that Eqn. 2.2.2 should be used in the analysis of laboratory tests on stiff materials, as opposed to Eqn.

2.2.1. Some C/C_s values quoted in the literature are presented in Skempton (1960); for reservoir type materials, values of 0.46 for a quartzitic sandstone (Skempton, 1960) and 0.36 for Weber sandstone (Nur and Byerlee, 1971; Robin, 1973) are reported, while C/C_s = 0.04 has been given for London Clay at 62.1MPa (Bishop, Kumapley and El Ruwayih, 1975). This suggests a significant error in sandstone experimental data analysed using an incorrect expression for effective stress.

The applicability of the various formulations of the effective stress equation have been reviewed by several workers, Skempton (1960), Nur and Byerlee (1971), Robin (1973), Bishop and Skinner (1977), Carroll (1980). Robin (1973) has discussed the philosophy of the effective stress equation and has concluded that there is no unique relationship (or effective pressure law (EPL)). The relationship between external and internal stress is dependant upon the parameter required, which varies with effective pressure i.e. different effective stress equations apply for volume change, pore compressibility, sonic velocity, etc. (Skempton, 1960; Nur and Byerlee, 1971; Zoback and Byerlee, 1975 ; Bishop and Skinner, 1977). For non-linear elastic materials the EPL does not have any simple analytical expression and hence, as a concept, is meaningless unless it reduces to Terzaghi's basic form. However, during laboratory investigations of reservoir compaction the use of the correct effective stress equation is important. If Bishop's Eqn. 2.2.2 is correct the laboratory investigations of van der Knaap and van der Vlis (1967), Teeuw (1971), van Ditzhuijen and de Waal (1985), van Kooten (1986), de Waal (1986), de Waal and Smits (1986), Smits, de Waal and van Kooten (1986) and this study, overestimate the effective stress, as these studies increase the total stress equivalent to the

pressure decline planned for an oil field - whereas in the reservoir the pore pressure decrease would only give a fraction of the change in effective stress, and thus a proportionately smaller strain. However, an analysis conducted as part of this study has shown that in the case of the chalk, any error is small.

The C/C_s correction has been included in analyses performed on some reservoir materials, Fatt (1957), Marek (1971; 1979). Fatt (1957) uses a pore pressure coefficient of 0.85 for the effective stress calculation required for computation of compressibility in sandstones. This value was obtained from Brandt (see Fatt (Loc.cit.) for reference), for velocity measurements in porous media, and hence may not be valid for Fatt's data.

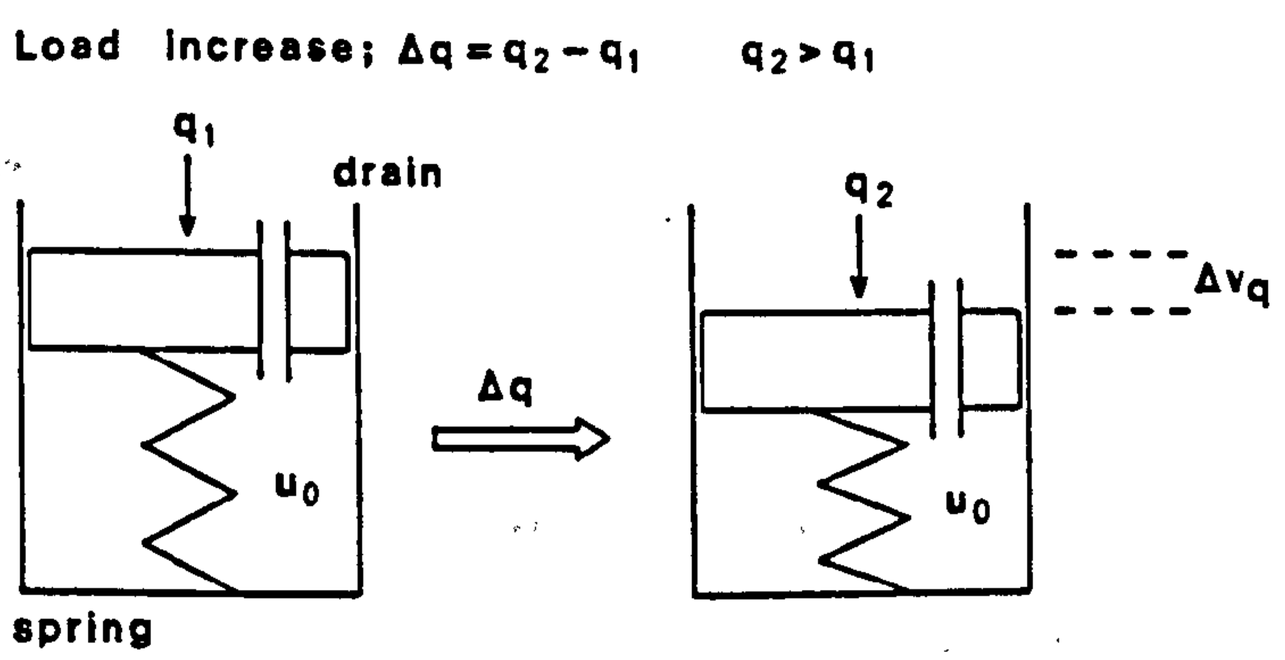

Figure 2.1 The frictionless dashpot analogy of compaction - illustrating two different effective stress increases.

Skinner (pers.comm.) using the analogy of a frictionless dashpot with a spring, Fig. 2.1 (see Lambe and Whitman, 1979), states that the load on the dashpot causing the compression of the spring or the pore pressure under the dashpot so extending the spring, for the application of the same magnitude of stresses, will lead to the same volume change regardless of the stiffness of the spring. The spring represents the mineral skeleton in this analogy. Thus, no correction factor is required, the two stress applications being equivalent. In the view of Skinner, the magnitude of the effective stress in a laboratory triaxial experiment is governed by Eqn. 2.2.1, and is independant of the manner in which the effective stress is applied.

The derivations of the effective stress equations are based on an isotropic homogeneous material which is linearly elastic; the assumption of linear elasticity is not valid for all reservoir materials (Teeuw, 1971) and as mentioned, makes the use of Eqn. 2.2.2 difficult.

During the compaction of high porosity, weakly cemented sedimentary materials, a breakdown of the elastic cemented structure can occur (Chap. 2.6). This leads to deformations in which the recoverable deformation is small, i.e. to a normally consolidated state. In such a case, analysis of volume change in the pre-yield, elastic (low compressibility) response of the structure would neccessitate the use of Eqn. 2.2.2, due to the low C/C_s ratio associated with stiff porous materials, discussed above. However, when the stresses applied to the weakly cemented sedimentary material, approach and exceed the yield strength of the bonding, the compressibility of the mineral skeleton increases significantly. This high post-yield skeleton compressibility allows the Terzaghi effective stress equation, Eqn. 2.2.1, to be employed. Thus, the

progressive compaction of materials such as the chalks investigated in this study should be analysed using, Eqn. 2.2.2 in the pre-yield stress range but this could be simplified using Eqn. 2.2.1 for the post-yield deformations.

To assess the possible analytical errors caused by the initial low compressibility of chalks when using the Terzaghi equation of effective stress (Eqn. 2.2.1), the pore pressure coefficient ($\alpha = 1-C/C_s$) was calculated from published values of chalk pre-yield uniaxial compressibilities (C_m) (van Kooten, 1986), and bulk compressibilities (C_b) (Heiberg, 1974).

Table 2.1

C_m MPa^{-1}	Porosity %	C_b (MPa^{-1})		
		β=0.0	β=0.5	β=0.9
$0.2*10^{-4}$	21	$3.76*10^{-5}$	$7.52*10^{-5}$	$3.76*10^{-4}$
$1*10^{-4}$	32	$1.88*10^{-4}$	$3.76*10^{-4}$	$1.88*10^{-3}$
$2.5*10^{-4}$	40	$4.70*10^{-4}$	$9.40*10^{-4}$	$4.70*10^{-3}$
$9*10^{-4}$	46	$1.69*10^{-3}$	$3.38*10^{-3}$	$1.69*10^{-2}$

Table 2.2

Porosity %	α (1 - C/C_s)		
	C_b β=0	C_b β=0.5	C_b β=0.9
21	0.62	0.81	0.96
32	0.92	0.96	0.99
40	0.97	0.98	1.00
46	0.99	0.99	1.00

The values of uniaxial compressibilities (van Kooten, 1986) presented above have been converted into bulk compressibilities using Eqn.

6.2.19; this involves the assumption of K_o = 0.30, (Teeuw, 1971; Geertsma, 1973; van Ditzhuijzen and de Waal, 1984). The C for calcite is taken as $1.42*10^{-5}$ MPa^{-1} (Skempton 1960). Heiberg (1974) obtained the following bulk compressibilities for Ekofisk chalks.

Table 2.3

Porosity %	bulk compressibility MPa^{-1}	$1-C/C_s$
23.65	$1.160*10^{-4}$	0.89
26.45	$2.538*10^{-4}$	0.94
27.60	$1.638*10^{-4}$	0.91
29.81	$7.106*10^{-4}$*	0.98
32.73	$6.816*10^{-4}$*	0.97
38.14	$2.417*10^{-3}$**	0.99
39.53	$2.709*10^{-3}$**	0.99

Values marked * and ** indicate that the samples underwent pore collapse. Samples marked **, signifies that the compressibilities were averaged over the 13.8 to 20.7 MPa stress range, whilst those marked * were averaged over the stress range 13.8 to 48.3 MPa; all samples had a back pressure of 1.37MPa.

The value "β" is the ratio of the compressibility of the rock matrix to the bulk compressibility, hence, it is the same as the multiplier of U in Eqn. 2.2.2. As such, the calculation of bulk compressibilities from the uniaxial data of van Kooten (1986) assumes values of β. Because of the circular nature of such a calculation, the data is presented to show the effect of this value on the conversion from uniaxial to bulk compressibilities, and to present the possible range of values for $1-C/C_s$ using van Kooten's data. A

comparison of the converted values of van Kooten and Heiberg implies that the value of B approximately equals 0.5 for the C_m to C_b conversion. The conversion is, however, dependent upon the correct K_o value used in the calculation. The values of Heiberg are assumed to be the more reliable of the two data sets considered, due to the inaccuracies and assumptions in the conversion of van Kootens data.

Because of the change in stiffness in the chalk during compaction, and the values obtained for $(1 - C/C_s)$ from compressibilities in the literature, the Terzaghi effective stress, Eqn. 2.2.1, is used in this study.

2.3) UNDRAINED PORE PRESSURE RESPONSE

The response of the pore pressure to undrained loading of a porous material (the undrained pore pressure response) is commonly used in soil mechanics to obtain the degree of saturation of a sediment (Chaney et.al., 1979). The full saturation of a sample is required for the above effective stress equations (Chap. 2.2) to be applicable: for, in partially saturated soils under low stresses (i.e. where grain compressibility can be ignored), other effective stress equations are applicable. Bishop (1973) has shown that the effective stress equation and the pore pressure response are intimately related. The pore pressure response has also been used to interpret the creep deformations occurring in undrained samples, Ohtsuki et.al. (1981). In this study the undrained pore pressure response is used to analyse the results obtained from an oedometer test performed on a chalk from southern England. This section presents a brief review of the published work concerning undrained pore pressure response.

The undrained pore pressure response of a sediment to an increment

of all round stress, or deviatoric stress is given by Skempton's B and A values respectively, Skempton (1954).

$$\Delta U/\Delta \sigma = B(\Delta \sigma_3 + A(\Delta \sigma_1 - \Delta \sigma_3)) \qquad .. 2.3.1$$

The B value is used to obtain a measurement of the degree of saturation; the pore pressure response, $(\Delta U/\Delta \sigma)$ for a fully saturated sediment of high compressibility, is equal to unity. Values less than unity indicates the degree of saturation. This only holds for isotropic soils of high compressibility (Bishop, 1973; 1976; Wissa, 1969; Mesri, Adachi and Ullrich, 1976). A discussion on the effect of anisotropy on the undrained response to loading in the field, is given by Silvestri (1981), and on Skempton's relationship (Eqn. 2.3.1), by Baker and Krizek (1969).

For materials of low compressibility, Bishop (1973) extended Skempton's equation to account for the compressibility of pore fluid (C_w), the sample skeleton (C_s), and of the mineral grains (C).

$$\frac{\Delta U}{\Delta \sigma} = \frac{1}{1 + n(C_w - C)/(C_s - C)} \qquad .. 2.3.2$$

This was generalised further by Bishop (1976) to take into account system compressibility (Wissa, 1969), due to the volume of pore fluid in drainage lines (V_l), the compressibility of the pore lines (C_l), and the compressibility of the pore pressure measuring device (C_m).

$$\frac{\Delta U}{\Delta \sigma} = \frac{1}{1 + \frac{n(C_w - C)}{(C_s - C)} + \frac{V_l}{V} \cdot \frac{C_w}{C_s - C} - \frac{C_l + C_m}{V(C_s - C)}} \qquad .. 2.3.3$$

and B

$$B = \frac{1}{\frac{1}{(\Delta U/\Delta\sigma)_{obs}} - \frac{V_l}{V} \cdot \frac{C_w}{C_s - C} - \frac{C_l + C_m}{V(C_s - C)}} \qquad .. 2.3.4$$

Bishop states that the most important factor affecting the system compressibility is the compressibility of the fluid (Wissa, 1969). Tests on four different rock types, Mesri, Adachi and Ullrich, (1976), show that the latter equation is accurate for the prediction of pore pressure response in porous rocks with an interconnecting pore system. The rock samples used showed that once saturated, (back pressures in the range 0.69 - 1.38MPa), the pore pressure response decreased with increasing external pressure, due to closure of cracks and a decrease in the compressibility of the skeleton. The response ranged from 0.33 to 0.69 at 11.03MPa for the rocks tested (Berea Sandstone, Salem Limestone, Vermont Marble and Barre Granite). Bishop (1973; 1976), calculated $\Delta U/\Delta\sigma$ values (at an effective stress (Eqn. 2.2.1) level of 65 MPa) equal to 0.53 and 0.77 for Berea Sandstones of porosity 15% and 5%, respectively. In practice, pore pressure response values for the Berea Sandstone of 0.48 were obtained for a 18.7% porosity sample.

2.3.1) Sample saturation

Methods of saturation are discussed by Wissa (1969), Mesri, Adachi and Ullrich (1976), Bishop and Henkel (1962), and Chaney, Stevens and Sheth (1979). These methods mainly consist of flushing water through the sample, applying a back pressure, applying a vacuum to the top of

the sample while flushing water, increasing cell pressure and back pressure stepwise, and combinations of these methods. Chaney, Stevens and Sheth (1979), discuss various methods for checking saturation and present data showing the back pressures required to saturate samples of various initial degrees of saturation. They also present the times required for the application of the back pressure to ensure complete sample saturation.

2.4) ONE DIMENSIONAL CONSOLIDATION

The burial or loading of a unit of sediment will lead to a decrease in the volume of pore fluid relative to the volume of solids, if the sediment is allowed to drain freely. Terzaghi (1943), states that "every process involving a decrease of the water content of a saturated soil without replacement of water by air is called a process of consolidation". In highly compressible, low permeability sediments, the flow of water out of a unit of sediment will be slow, and the resulting transfer of the total stress increase to the grains (due to the dissipation of pore water pressure) will be time-dependant. Terzaghi (1943) presents an earlier derived time-dependant equation for the consolidation of sediments. The derivation makes the initial assumptions that: 1) The voids in the sediments are completely saturated; 2) The pore water and the mineral grains are incompressible; 3) Darcy's law is valid; and 4) The coefficient of permeability is a constant. In one dimensional consolidation, the sediment must be laterally confined, the approach also assumes that the sediment is isotropic and homogeneous, and that the coordinate system is an independent variable.

At the instant of subjecting a unit of sediment to a load p, the change in the effective stress is zero (assumimg that the soil has a

B = 1, due to full saturation, Chap. 2.3). The applied load causes an equal increase in stress in the sediment skeleton and in the pore fluid. The complete dissipation of these excess pore pressures (excess pore pressures are those pore fluid pressure due to loading) to the original pre-load hydrostatic pore pressure gradient, increases the effective stress in the sediment by an amount, p. The compressibility or the change in void ratio per stress increment, due to loading is assumed constant. The equation of consolidation arrived at for the time dependent reduction of the pore pressures in sediments is,

$$\frac{d^2u}{dx^2} = \frac{k}{\gamma_w . M_v} \frac{du}{dt} \qquad .. 2.4.1$$

Where, u = the excess pore fluid pressure (Terzaghi's neutral pressure); x = unit thickness of sediment; k = coefficient of permeability (hydraulic conductivity); γ_w = unit weight of pore fluid; M_v = the coefficient of volume decrease (coefficient of volume compressibility); t = time. This equation was derived for small strain increments, and in such a case, k and M_v can be considered constants, therefore $k/\gamma_w . M_v$ is also a constant, called the coefficient of consolidation, and is denoted by, C_v. This equation is for one load application, if the load gradually increases the equation becomes,

$$\frac{d^2u}{dx^2} = \frac{k}{\gamma_w . M_v} \frac{du}{dt} - \frac{d\sigma'}{dt} \qquad .. 2.4.2$$

where σ' = effective stress.

Other refinements of Terzaghi's consolidation theory have been formulated for non-linear compressibility of soils (Davis and Raymond, 1965). The assumption that the coordinate system is an independent variable in the conventional consolidation theory, is valid only for small strains. Gibson, England and Hussey (1967), have developed a large strain consolidation equation, in which variable coefficients of permeability and volume compressibility are incorporated. Again, the pore fluid and the sediment grains are considered incompressible and the self weight of the sediments is ignored. This latter factor has been considered by Gibson, Schiffman and Cargill (1981), Been and Sills (1981), and Koppula and Morgenstern (1982). The results of the consolidation equation derived by Gibson et.al. (1981), show that the excess pore pressures are larger than those anticipated by the conventional theory, which would also over-estimate the time of consolidation. This was also shown by Koppula and Morgenstern (1982) for deltaic sediments. These consolidation theories are generally complex, and their derivations will not be reproduced here; the reader is referred to the above papers for the full analyses.

This brief discussion on one-dimensional consolidation is presented to bring to the attention of the reader the assumptions of the conventional Terzaghi theory, as this equation is used as the basis of the analysis for the constant rate of strain consolidation analysis, (Chap. 3.2).

2.5) REPRESENTATIONS OF STRESS STATES IN SEDIMENTS

The compaction of sedimentary materials in nature and in this study arises from an increase in the magnitude of the applied effective stresses. In the laboratory tests presented in this thesis, the maximum (vertical) effective stress is increased, and the cell pressure is adjusted to maintain a zero lateral strain condition (Chap. 2.2, Chap. 3.2.2, App. 1). The magnitudes of the stress acting on the materials (and the state of the stress) are thus changing during the deformation. The stresses applied in the triaxial cell are $\sigma_1 > \sigma_2 = \sigma_3$, pore pressures are also measured enabling the effective stresses (Chap. 2.2) acting on the materials to be calculated. The deformation of a sediment is dependant upon its previous stress history and the system of effective stresses acting on the material. In this study the effective stresses were continually changing and are presented in terms of stress paths.

2.5.1) Stress paths

The combination of effective stresses ($\sigma_1' > \sigma_2' > \sigma_3'$) acting on a material at any point in the deformation can be plotted as a point on a three dimensional effective stress plot, with continuing deformation numerous points can be plotted, "the line joining all the points of instantaneous states of effective stress is defined as the 'effective stress path'" (Atkinson and Bransby, 1978), Fig. 2.2. In Fig. 2.2 two stress paths are shown in effective stress space, a hydrostatic (isotropic) stress path (A'B') where $\sigma_1' = \sigma_2' = \sigma_3'$, and a drained loading path (B'C') where σ_1' increases while $\sigma_2' = \sigma_3' =$ constant. Since three dimensional plots are cumbersome to use, the effective stress path plot is reduced to a maximum effective stress (σ_1') and minimum effective stress (σ_3') plot, Fig. 2.3; Fig. 2.3

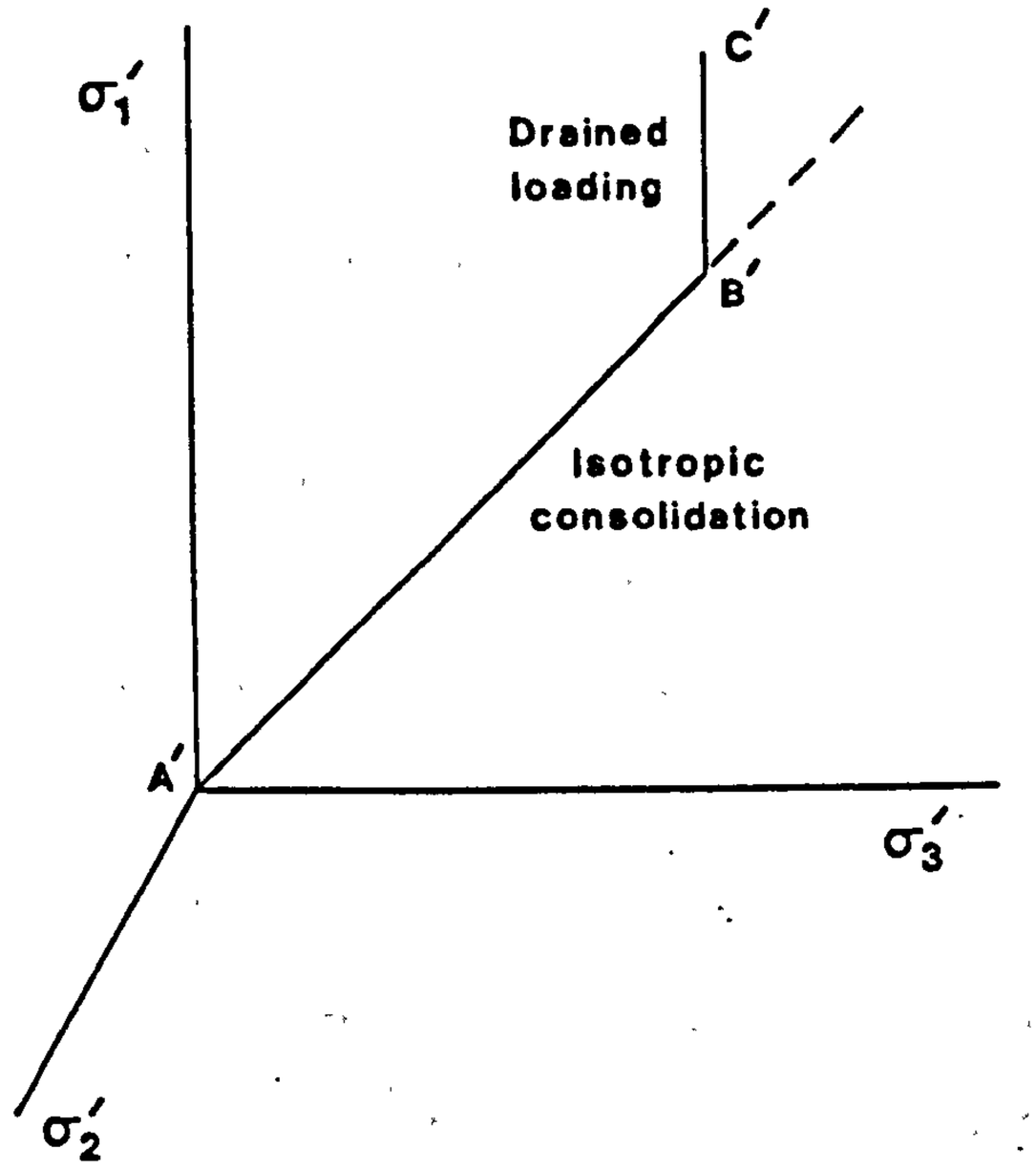

Figure 2.2 Stress paths for hydrostatic and drained loading tests in 3-dimensional principle effective stress space.

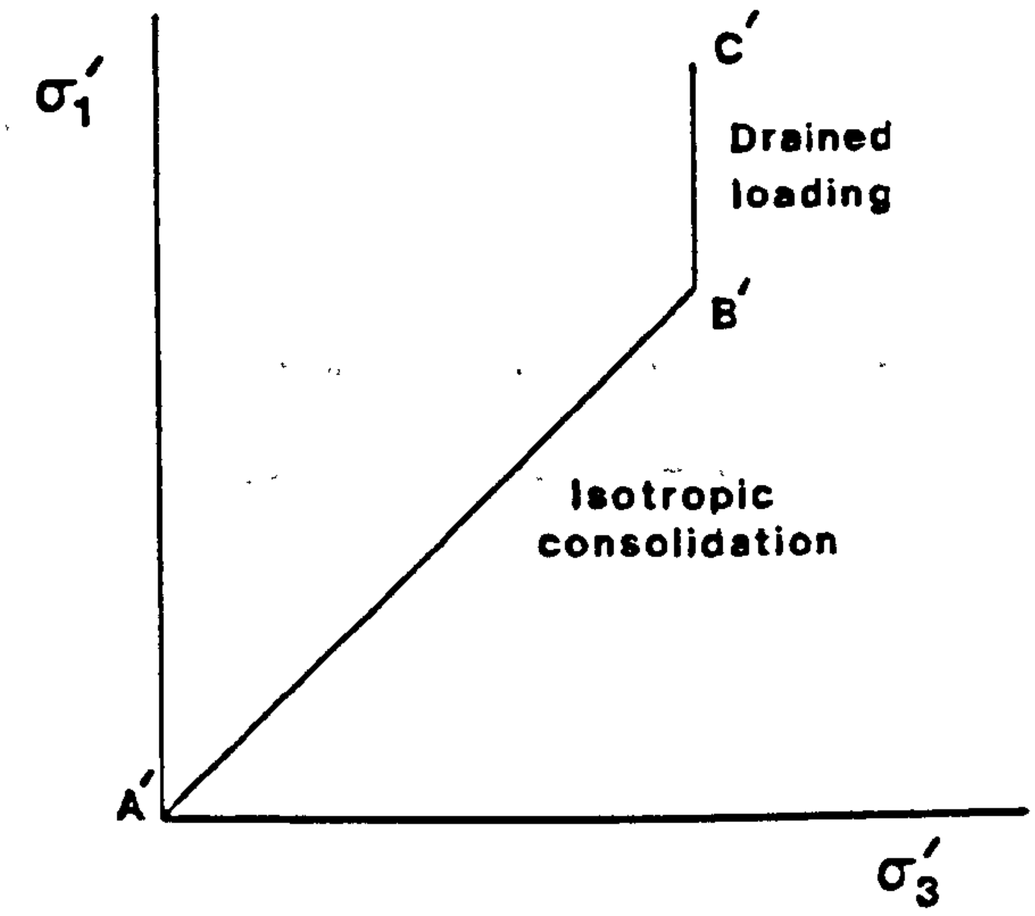

Figure 2.3 Stress paths for hydrostatic and drained loading tests in maximum and minimum effective stress space.

shows the hydrostatic stress path and the drained loading stress path used in Fig. 2.2. With such a plot the intermediate effective stress σ_2' is not considered.

The state of stress acting on a rock or sediment is commonly represented using a Mohr diagram construction, Fig. 2.4. Using this construction, the state of stress acting on any plane in the applied stress field can be determined. The Mohr diagram is generally used to represent the state of stress existing where σ_2' is unknown, or in plane strain conditions, though it can be used to represent a three dimensional stress state. This construction is used to represent the state of stress acting on a unit of material at an instant; and is commonly used to represent the condition at failure or yield. To represent the changing stress state occuring during compaction the use of Mohr circles is impractical, therefore each stress state or Mohr circle is identified by a point, the apex of its circle D with coordinates (s',t'). From Fig. 2.4 it can be seen that

$$s' = 1/2(\sigma_1' + \sigma_3') \qquad .. 2.5.1$$

and

$$t' = 1/2(\sigma_1' - \sigma_3') \qquad .. 2.5.2$$

Different axes are used when the intermediate effective stress is known, in the special case where the $\sigma_2' = \sigma_3'$, the mean effective stress and the deviatoric stress are respectively defined as

$$p' = 1/3(\sigma_1' + 2\sigma_3') \qquad .. 2.5.3$$

and

$$q' = (\sigma_1 - \sigma_3') \qquad .. 2.5.4$$

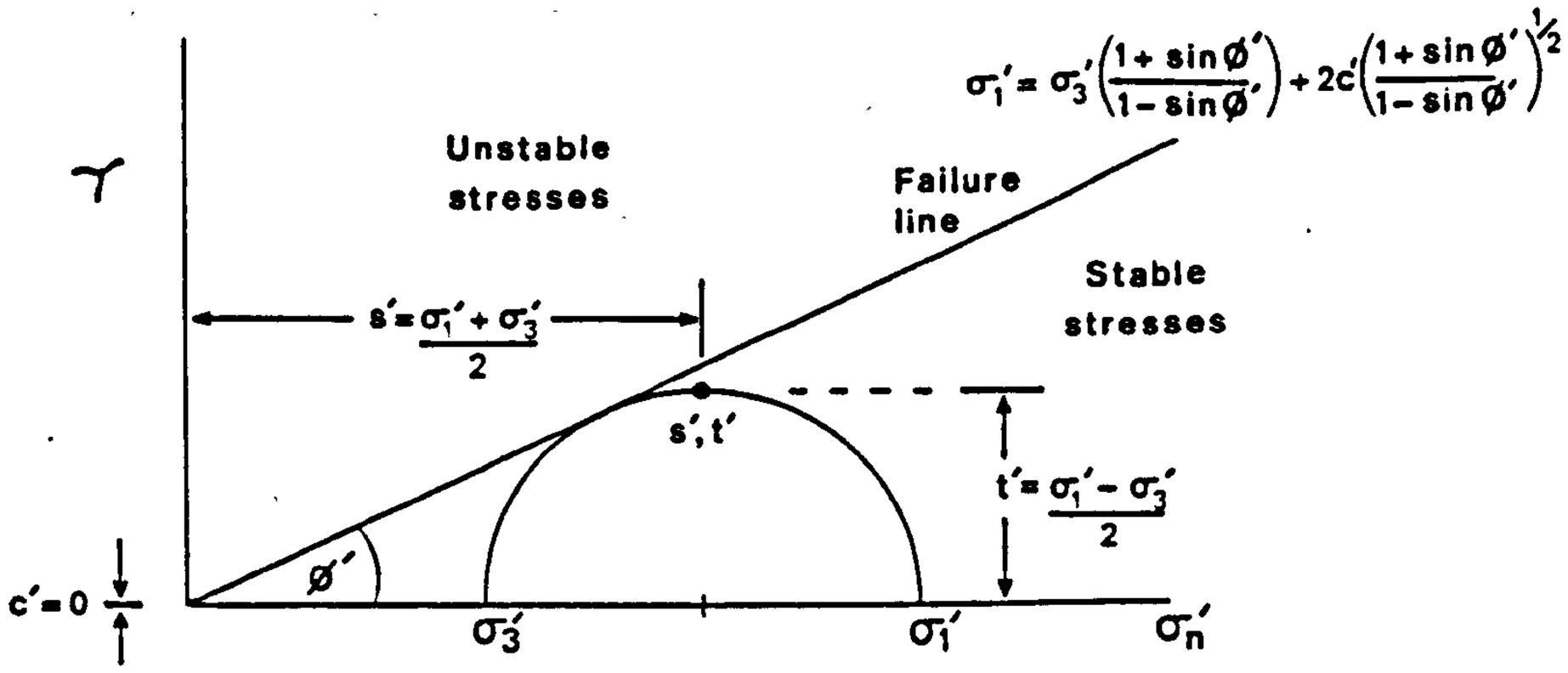

Figure 2.4 Mohr Diagram construction for stress presentation.

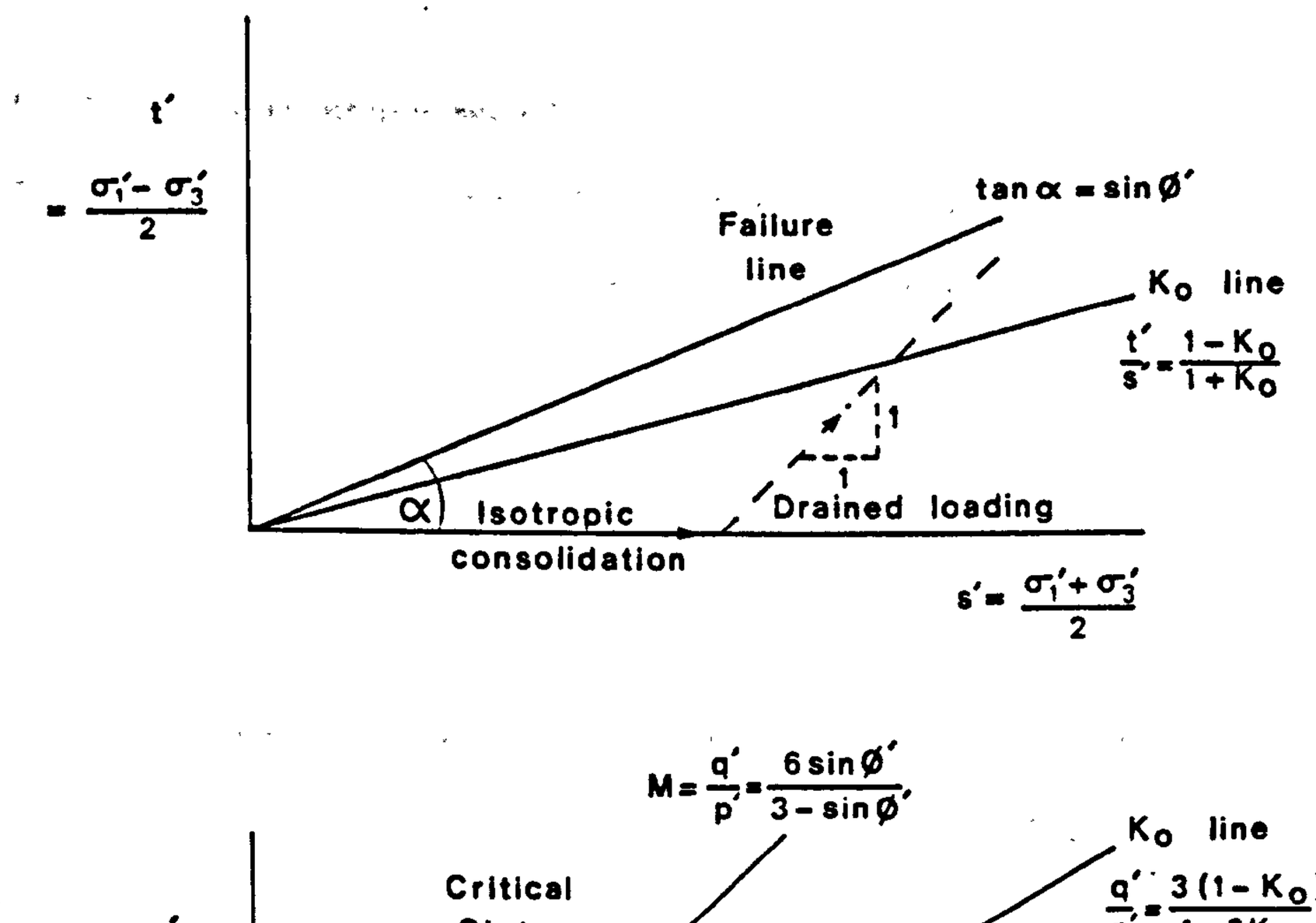

Figure 2.5 Comparison of stress paths and failure lines in t - s' and q - p' stress space.

These representations of stress state are commonly used in both soil and rock mechanics (Atkinson and Bransby, 1978; Elliot and Brown, 1985). For a more comprehensive discussion of these axes and their derivation, the reader is referred to Atkinson and Bransby (1978) and to the references supplied therein.

The stress paths shown in Figs. 2.2. and 2.3 can be represented in both s't' and q'p' stress space, the hydrostatic stress path and the drained loading stress path are shown for these two sets of axes in Fig. 2.5. These are presented for the purpose of comparison, as both sets of axes are commonly encountered in the literature.

2.5.2) Critical state model

The analyses of the results of the chalk and clay compaction (App. 5, Chap. 4 and Chap. 5) have been presented in terms of deviatoric stress (q'), and mean effective stress (p'). These axes are used as the stress axes of a general model of soil behaviour referred to as the Critical State model. During the last decade workers have attempted to extend the principles of this model to the deformation of weak rocks; Gerogiannopoulos and Brown (1978), Brown and Michelis (1978), Price and Farmer (1981), Farmer (1983), Elliot and Brown (1985).

The Critical State model relates the deviatoric stress required to shear a unit of sediment to the mean effective stress and the void ratio of the unit of sediment during shearing. The point of failure therefore is defined by shearing at constant volume, i.e. shearing at constant deviatoric stress and zero volume change. The Critical State line is the failure line defined by constant volume shearing at differing mean effective stresses, void ratios and deviatoric stress, it is a unique failure line for both drained and undrained tests. The

Critical State line plots as a straight line in q'p' space, Fig. 2.6a, while it is a curve of logarithmic form in void ratio-mean effective stress space, Fig. 2.6b.

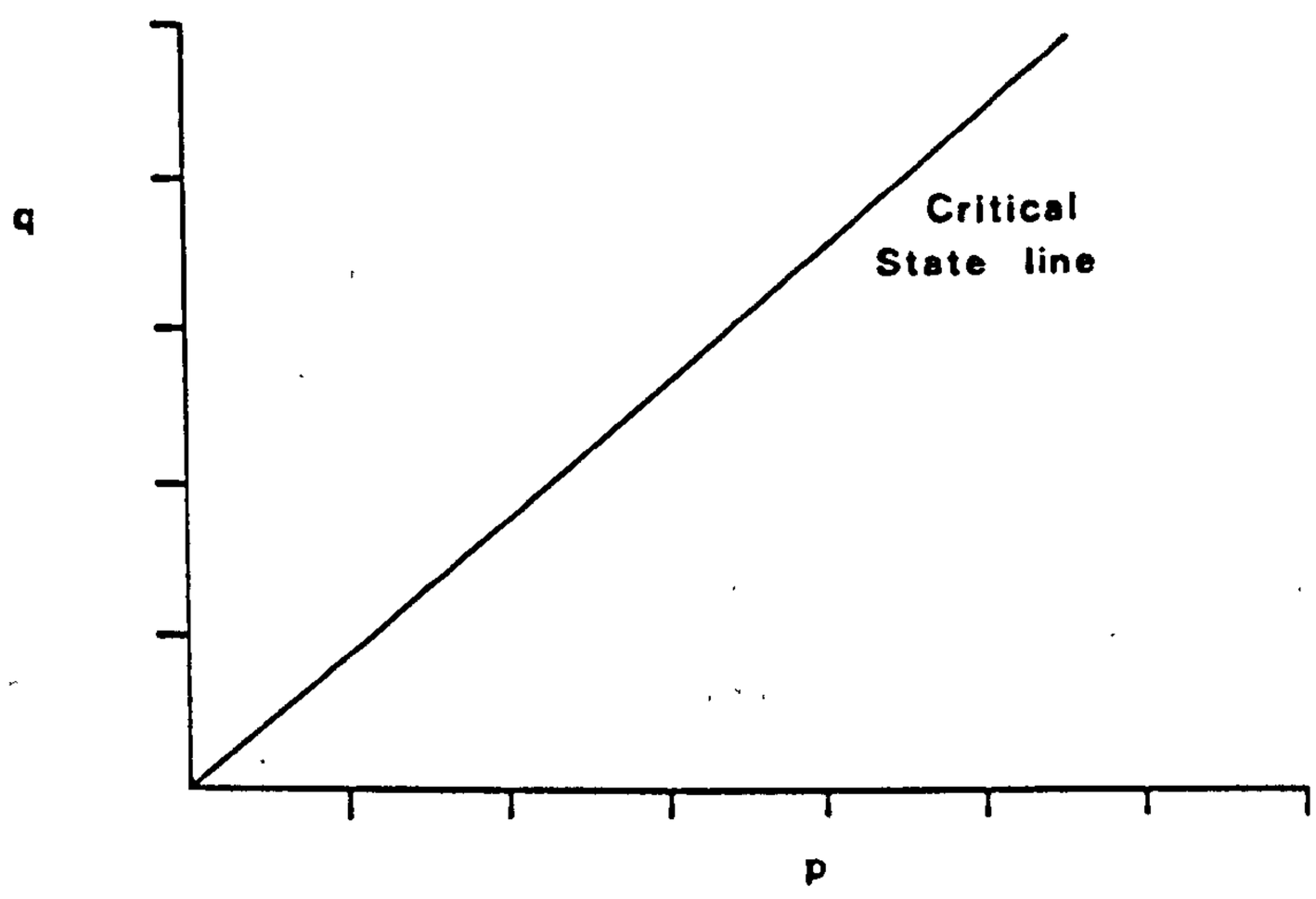

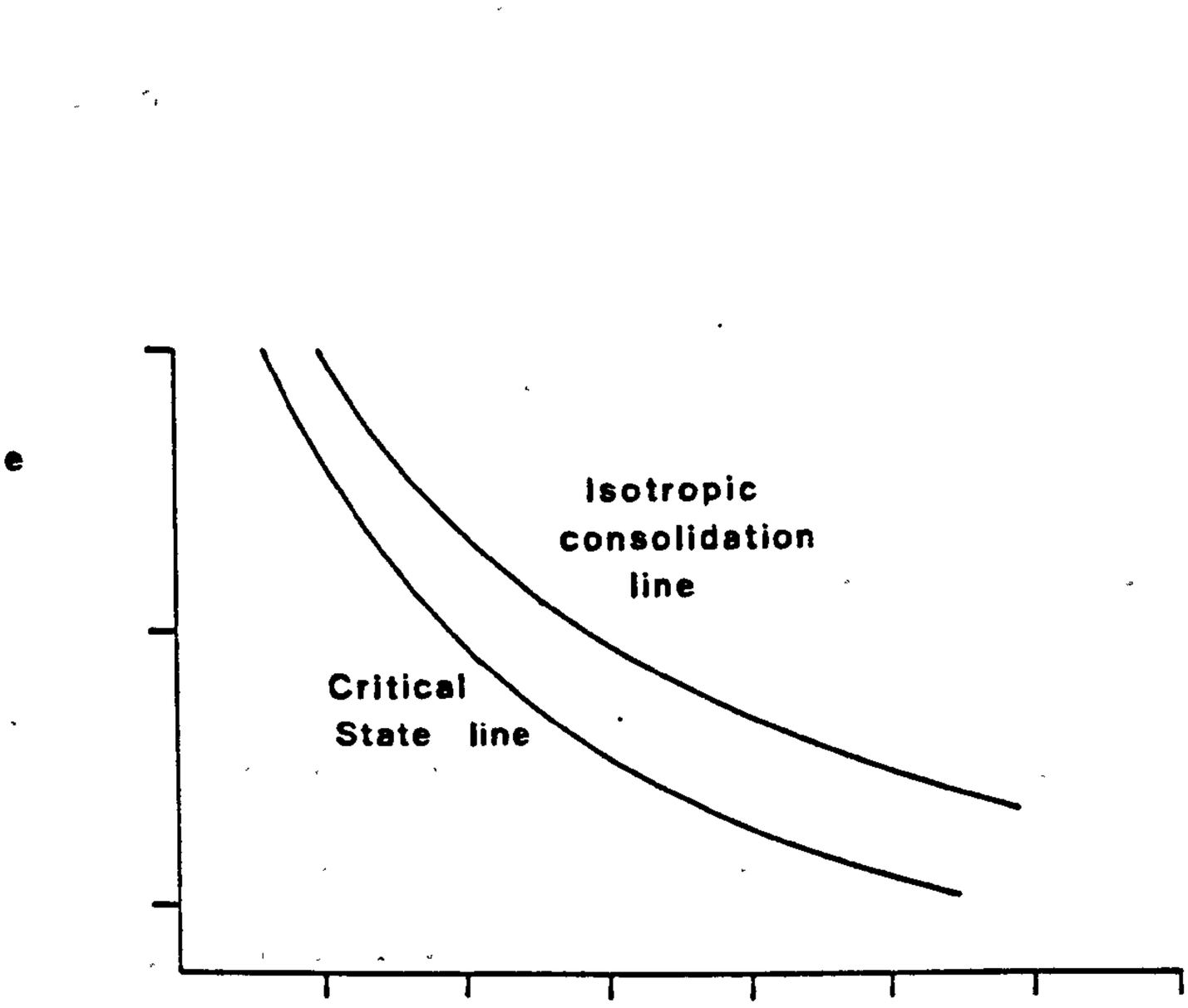

Figure 2.6 Diagrams showing the shape of the Critical State line (After Atkinson and Bransby, 1978).

The Critical State model also defines pre-failure sediment deformation, this can be sub-divided into two regions. The behaviour can be seperately defined for normally and lightly overconsolidated sediments, and another for heavily overconsolidated sediments. The normally consolidated and lightly overconsolidated sediments deform at least partly on the Roscoe surface before reaching the Critical State line. The Roscoe Surface (Fig. 2.7) is a state boundary surface which joins the isotropic consolidation line to the Critical State line. Thus, a sediment which is deformed along the isotropic consolidation line and then subjected to loading will deform following a path on this surface. The stress paths for both drained and undrained loading tests on normally consolidated sediments are constrained to this surface. This can be observed when the stress paths for a drained test initially at isotropic consolidation pressure, p_1', and an undrained test loaded from an initial isotropic consolidation pressure p_2' ($p_2' > p_1'$) cross (Fig. 2.7). At the point of intersection the two samples are at the same q' and p', and have the same void ratio. Families of deformation paths for drained (and undrained) tests of different initial sample void ratio and at different isotropic effective stresses are of the same form but of different sizes in stress space. These families of curves can be normalised to one stress path, showing that the Roscoe surface is of a constant form regardless of initial isotropic effective stress and void ratio. However, the Critical State model has the limitation that it has not been tested to high stresses, to the authors knowledge.

Uniaxial deformation of normally consolidated sediments commonly occurs along stress paths in principle effective stress space (Fig. 2.3) equal to 0.3 to 0.6 ($= K_o = \sigma_h'/\sigma_v'$) (Chap. 3.2). When one dimensional consolidation tests (K_o) are performed on sediments in a

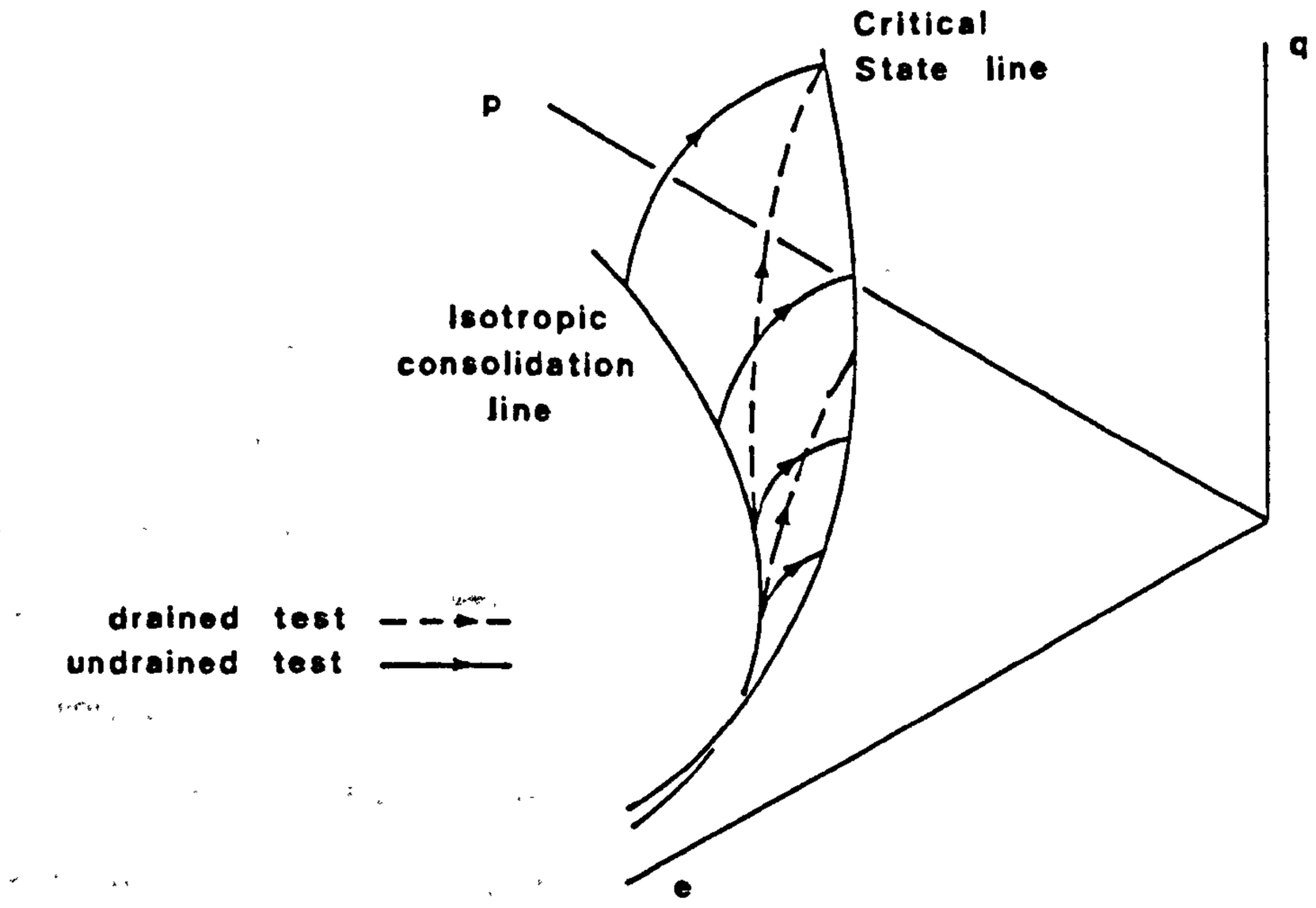

Figure 2.7 The Roscoe surface as defined by drained and undrained loading tests (After Atkinson and Bransby, 1978).

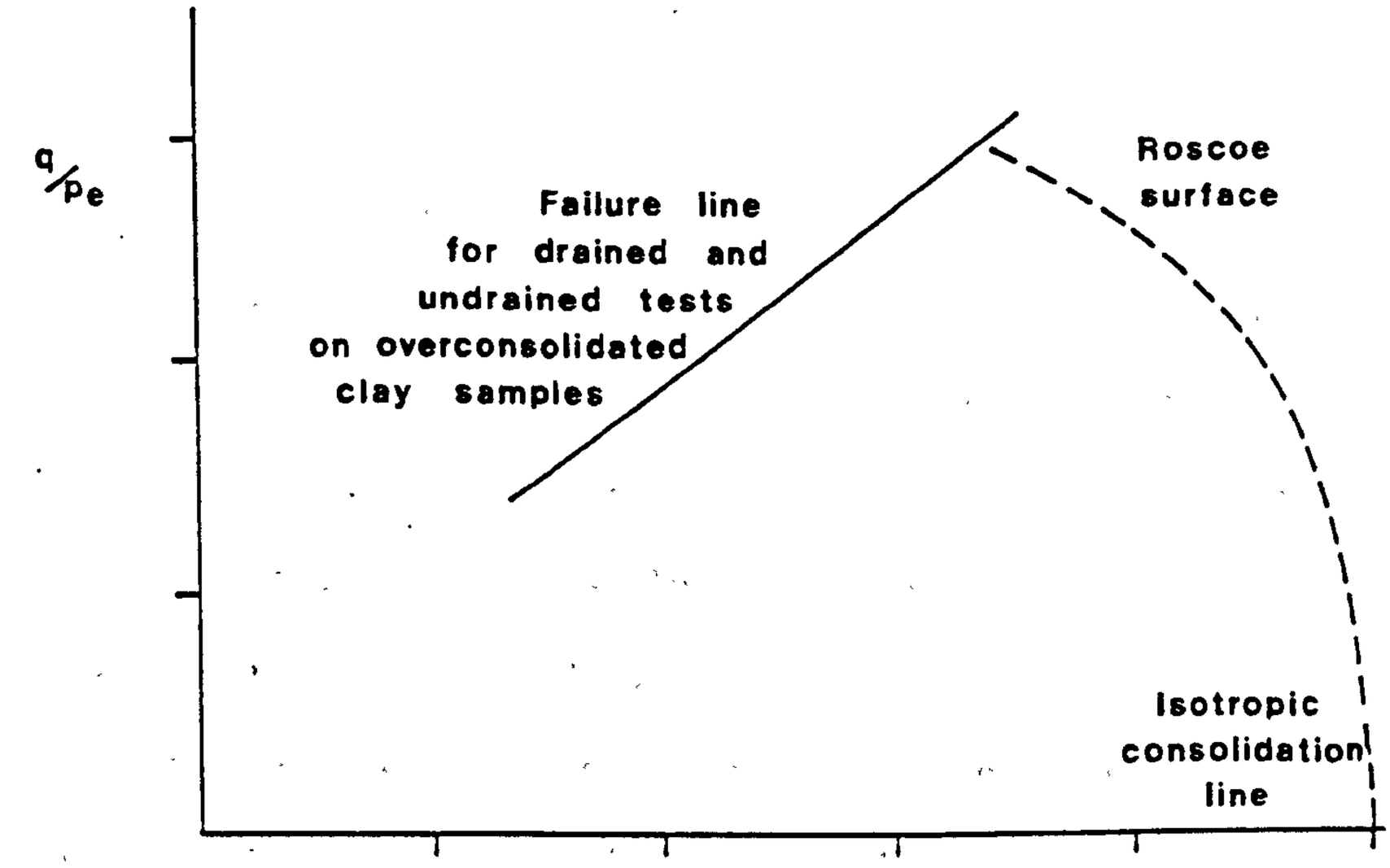

Figure 2.8 The shape of the Hvorslev surface, plotted on normalised axes to eliminate volume variations between different samples (After Atkinson and Bransby, 1978).

triaxial cell, it is very difficult to immediately apply the stress path to maintain zero lateral strain. Therefore the samples are generally consolidated along the isotropic stress path (so decreasing the lateral dimension of the sample), and then loaded under drained conditions until the original radial dimension is recovered, Ovando-Shelley (1986). Thus the one-dimensional consolidation stress path for a normally consolidated sediment exists on the Roscoe surface, the exact position being determined by the K_o of the sediment.

An analogous state boundary to the Roscoe surface is seen to occur for heavily overconsolidated samples; this state boundary is defined by the failure of samples (the peak strength) not by constant volume shearing, as this is not always seen or reliably known (Atkinson and Bransby, 1978). Failure of heavily overconsolidated samples with differing overconsolidation ratios (OCRs) but of the same void ratio define a straight line in q-p' space, Fig. 2.8, with the Critical State line at the lower OCR side of the trend. To account for differences in void ratio at failure, the q-p' plot can be normalised so defining a surface of constant form for overconsolidated samples; this state boundary is called the Hvorslev surface. The Hvorslev surface at the high overconsolidation ratio end is terminated by a tension cut off, and at the low overconsolidation ratio end by the Critical State line, Fig. 2.9.

The complete state boundary surface can be seen as the combination of both the Roscoe and the Hvorslev surface, Fig. 2.9 and Fig. 2.10. The Critical State diagram is used only as a model with which to envisage the volume changes that occur during the compaction and the shearing of the materials used in this study. It is also useful as it shows the effect of stress paths on the volumetric strain of normally

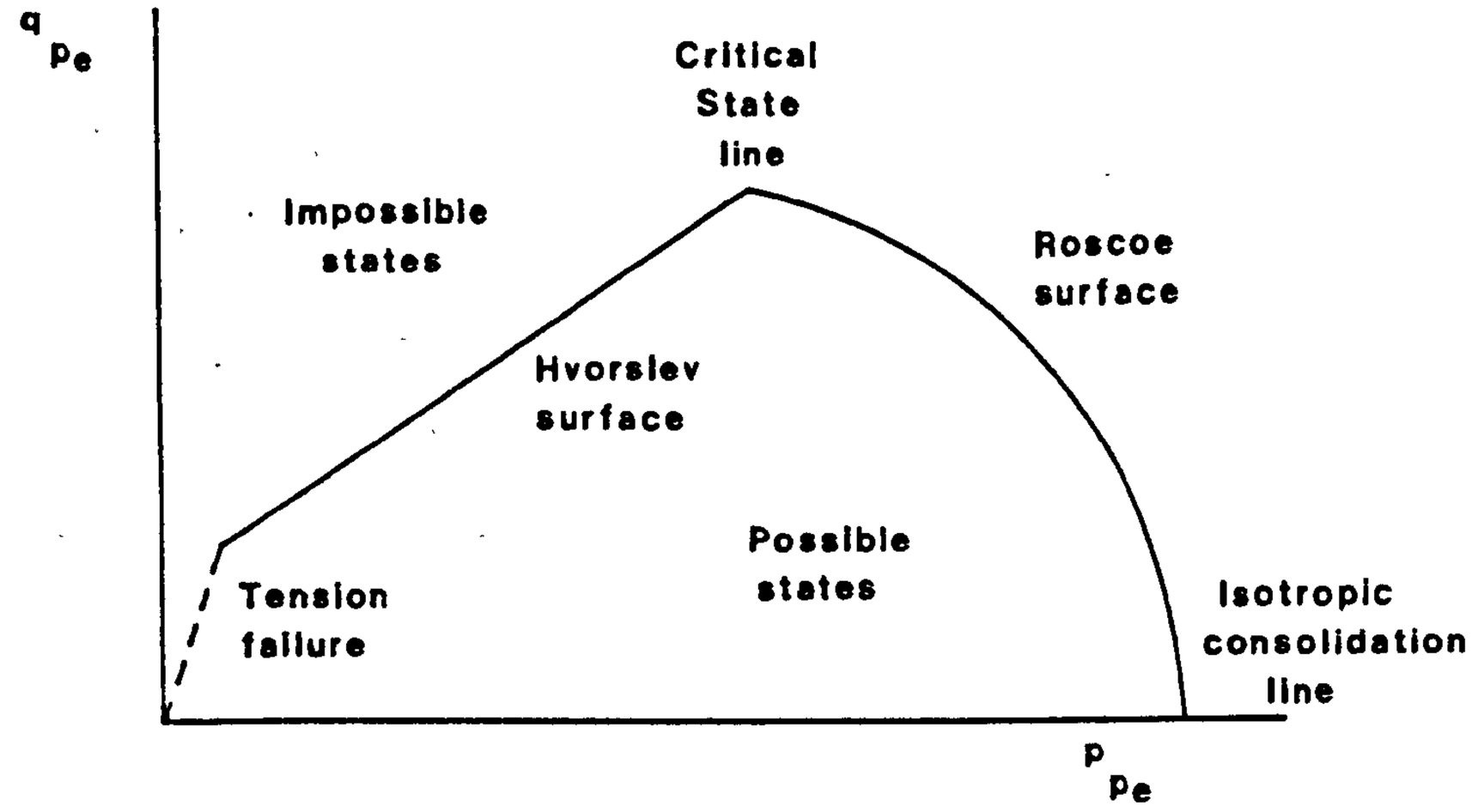

Figure 2.9 An undrained section through the Critical State diagram (After Atkinson and Bransby, 1978).

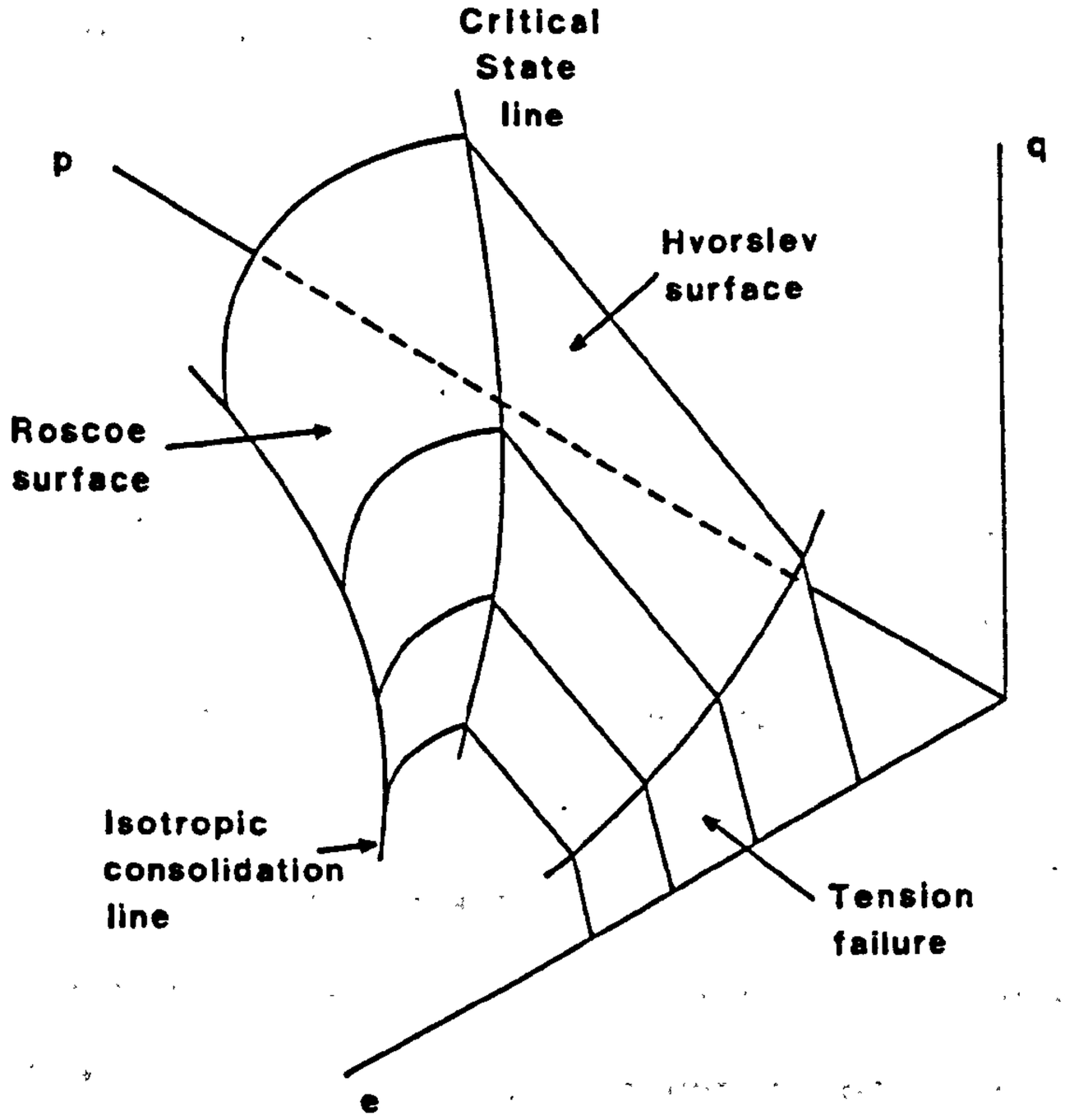

Figure 2.10 The Critical State diagram illustrating the stress dependance of volume reduction for uncemented sediments (After Atkinson and Bransby, 1978).

consolidated samples. The presence of cementation will affect the mechanical properties of sediments, and as such these materials can not be expected to behave as normally consolidated nor overconsolidated sediments, in the conventional sense. The presence of cementation in a sediment, can therefore be expected to alter the behaviour of the sediment with respect to the Critical State diagram. The effect of cementation on the Critical State diagram has been discussed by Jones et.al. (1987) and reviewed in terms of the earlier mentioned rock mechanics studies by Farmer (1983).

For a fuller treatment of the subject of Critical State soil mechanics the reader is referred to Atkinson and Bransby (1978), from which the above discussion was abstracted.

2.6) MECHANICAL BEHAVIOUR OF CHALKS

Chalk is a cemented particulate material (Chap. 3.5.2). This section discusses the mechanical properties of materials which are assumed to have analogous properties to chalk; this is necessary due to the dearth of published data for chalk. Following the discussion of the mechanical properties of cemented particulate materials, a review of the literature pertaining to compaction of chalk and other carbonate materials is presented.

2.6.1) Behaviour of bonded particulate materials

In a compressive regime, sediments can react to applied stresses by deformation of two extreme types, a shearing deformation or a compressional deformation. Bonded sediments exhibit these extremes, but the presence of an elastic bonding material or cement means that, during the shearing of the sample, the cement may induce higher strength or higher resistance to shearing than would the uncemented

grains. In the compactional domain, cementation requires that before large compactional strains are obtained, the sample must react elastically in the pre-yielding stress area. Yielding of the bonds joining grains leads to large compactional strains in the post-yielding region.

Cementation or bonding leads to a low stress area where the sample will behave elastically, with little plastic deformation; outside this area the sample will either behave as a particulate material due to yielding of bonds or will fracture generating a single fracture or a cataclastic shear zone. Between these areas of elastic and non-elastic behaviour there exists a series, or locus of stresses where irrecoverable deformations predominate over the elastic deformation; this is called the yield envelope, and as implied previously, borders the low stress area of elastic response of a rock or soil. A yield envelope is a three- dimensional body in principal stress space (Jaeger, 1969), however, we are only able to study one plane through this body since the triaxial cell and the oedometer have two stress variants and one stress variant respectively with $\sigma_2 = \sigma_3$ in both cases. Investigations of the yield envelopes of carbonate rocks in principal stress space have been performed by Cheatham (1967) and Miller and Cheatham (1972) for Cordova Cream

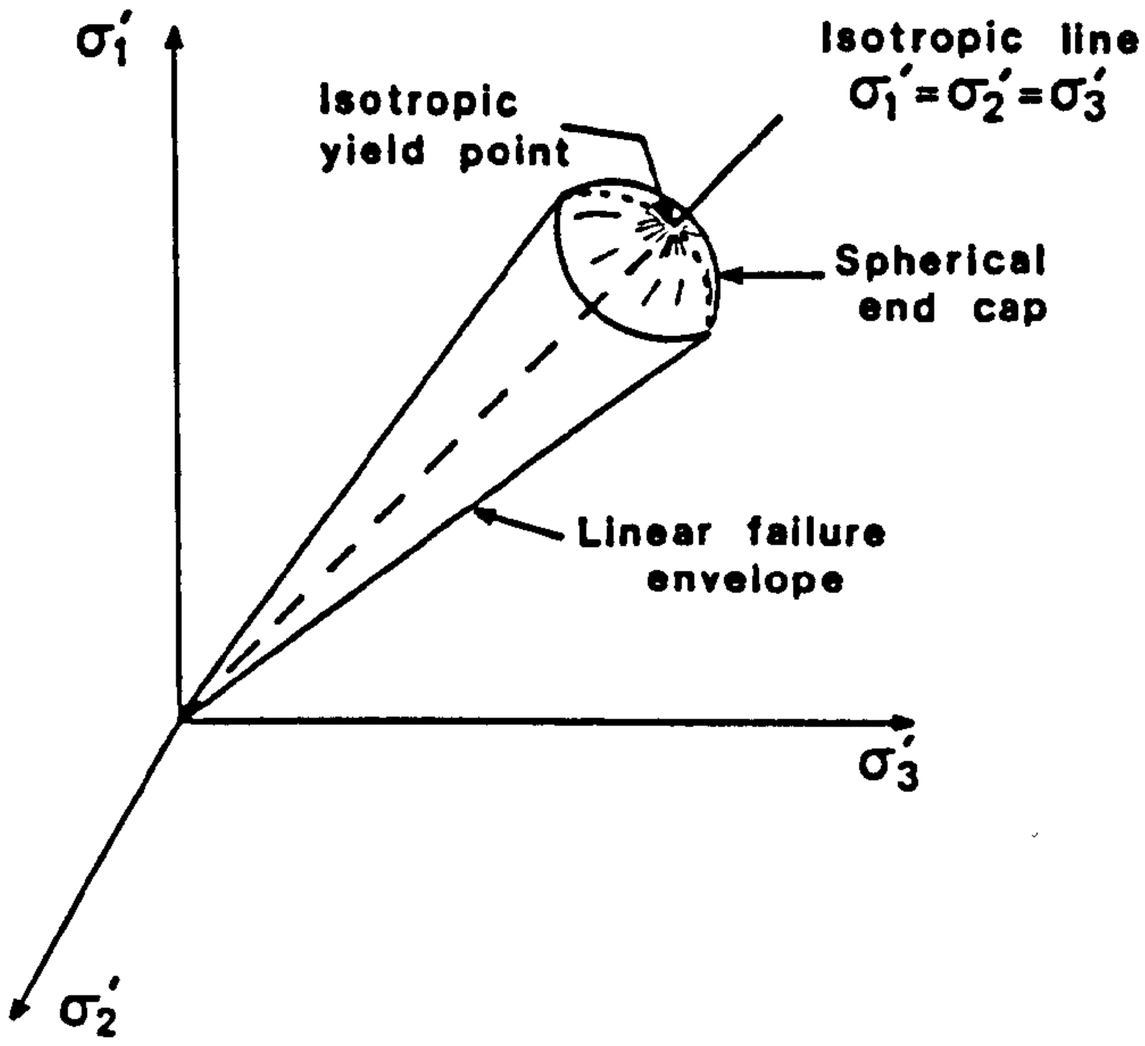

Figure 2.11 Coulombic yield envelope with a terminating end cap.

Limestone, and Batesville limestone. In these studies the yield envelope was assumed to be a Coulombic yield envelope with a terminating end cap, Fig. 2.11.

Yield envelopes have been defined for several weakly bonded sediments (Townsend et. al., 1969; Sangrey, 1972; Uriel and Serrano, 1973) and an excellent review on the subject is given by Vaughan (1985). Sangrey (1972) following earlier work with Townsend et.al. (1969) presents in detail a yield envelope for three sensitive clays (Leda clays) from Canada; he is able to delineate several areas with different properties of the yield envelopes for these clays, Fig. 2.12.

The yield envelope described for the Leda clay, Fig. 2.12, consists of a vertical section on the q-p' diagram at a maximum p' for the yield envelope, i.e. a section independent of p'. This section can be seen by plotting $\Delta V/V_o$ (volumetric strain) against p', which shows a linear trend until the yield point (or quasi preconsolidation pressure of Vaughan (1985)) is reached. The trend is independent of stress ratio up to a $\sigma_1'/\sigma_3' = 1.67$. This value corresponds to the maximum q value on the section of the yield envelope which is independent of p'.

The second section Sangrey describes is a yield surface at lower p', in which the yield surface strength increases as p' increases, until a maximum q value is reached, whereupon it remains constant with increasing p' until a maximum p', defined by the vertical section described above, is attained. The curve of increasing q with p' is gradual, however, Sangrey states that it consists of two yield surfaces, but due to fissures and bond breakage, caused by stress relief, a general increase rather than an abrupt change from increasing q to constant q is seen. The intersection between the

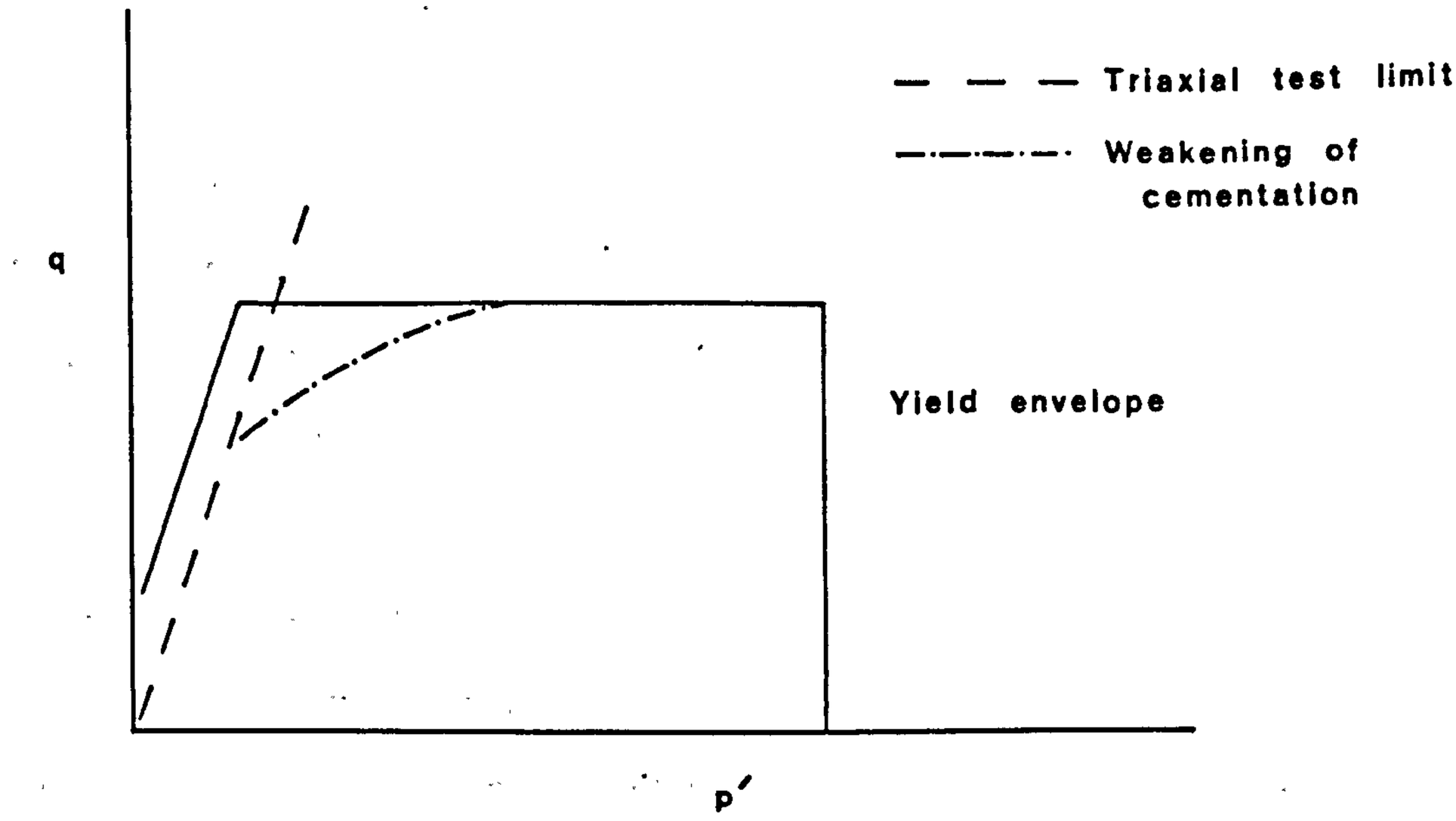

Figure 2.12 Generalised cementation yield envelope (After Sangrey, 1972).

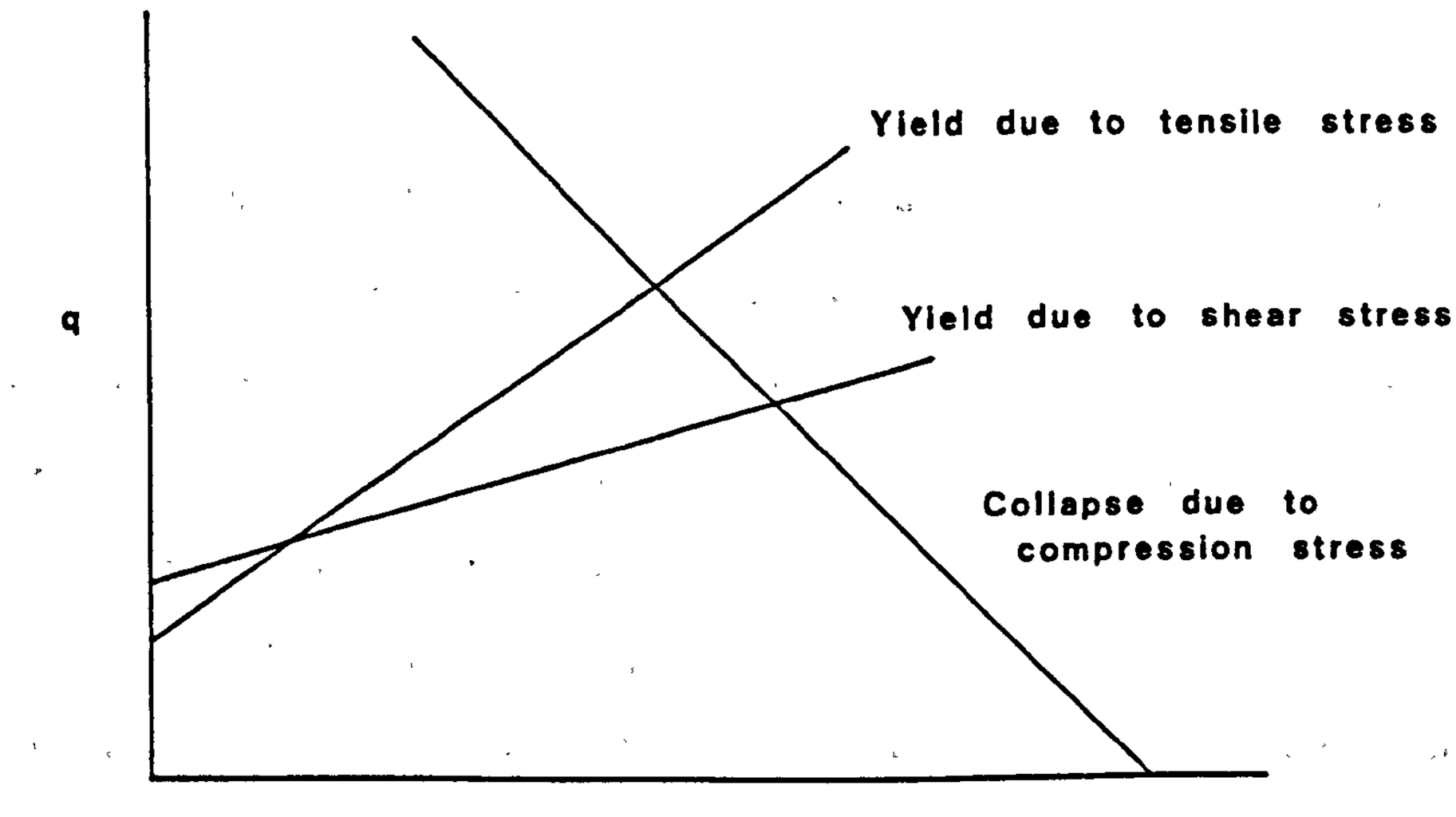

Figure 2.13 Model of yield envelope components present in cemented soils (After Uriel and Serrano, 1973).

p=constant and q=constant is an abrupt change and not gradual, though the yield surfaces from Uriel and Serranos (1973) work on volcanic agglomerate and Ohtsuki et.al's (1981) work on silty mudstones, are represented by curves.

The low stress region is limited by the $\sigma_3'=0$ condition in the triaxial test. Tensile tests are difficult to conduct and interpret due to flaws and fissures in the samples, and will not be discussed further.

The end cap or high pressure area of the yield envelope, forms the main difference between the various examples of yield envelopes determined for different cemented materials. The end caps presented in the literature can be generalised into three types: i) sloped, as in the model of yield envelopes proposed by Uriel and Serrano (1973), Fig. 2.13, Blanton (1978); ii) curved, possibly in the form of a quadratic yield surface, Elliot and Brown (1985), Maccarini (1980), Pattillo and Smith (1982); or iii) a vertical end cap in q-p' space at a constant p', Sangrey (1972), Miller and Cheatham (1972), Uriel and Serrano (1973).

Another feature of cementation yield envelopes reported in the literature, is the slope of the envelope adjacent to the section of decreasing yield strength with increasing p', discussed above. Sangrey suggests that this section in the median pressure range for the yield envelope, is flat and perpendicular or nearly so to the q axis, Fig. 2.12. Other bonded materials have also indicated this tendancy, Meigh and Early (1957), Cheatham (1967), Townsend et.al. (1969), Uriel and Serrano (1973), Blanton (1978). Uriel and Serrano (1973) present a model of modes of failure associated with different sections of cementation yield envelopes. The model yield envelope comprises of three failure lines, one for failure due to a tensile

stress, a second due to shear stress and the third already discussed, the end cap section for collapse due to compressive stress, Fig. 2.13. Uriel and Serrano (Loc.cit.) state that the shearing stress section only occurs in materials which have a short cementation bond length; the failure of long slender bonds occuring in tension or compression, as in porous rocks. The slope of these failure lines (Fig. 2.13) is assumed to be related to the preferential orientation of the cementation in the porous skeleton. This model is supported by work on limestones by Miller and Cheatham (1972), Elliot and Brown (1985), Blanton (1981), where no flat constant q section is observed.

Definition of yield envelopes has generally been obtained from drained and undrained triaxial loading tests, though Sangrey has defined the constant p' end cap using constant stress ratio tests. The application of an isotropic stress to a cemented material prior to loading, will result in a gradual breakdown of the cemented structure, or increased plastic deformation as the isotropic yield point is approached. This would have the effect of reducing the strength of the sample, which could explain the difference between the gradual decrease in q with p' as opposed to the abrupt change seen by Sangrey. However, the author has found no studies in the literature where these different stress applications have been applied to the same material, which would resolve the point.

2.6.2) Stress-strain characteristics of weakly cemented sedimentary materials

The stress-strain characteristics of various weakly cemented sedimentary materials, porous rocks, sensitive clays, residual soils and cemented sands, are very similar. The characteristics of stress-strain curves in cemented materials have been discussed by

Conlon (1966) and Elliot and Brown (1985), from which it is concluded, that the form of these curves is dominated by the shear strength and the frictional resistance of the grains of the mineral skeleton. At low stresses the shear strength due to cementation dominates the behaviour, the granular frictional resistance being small. However, at higher mean - effective stresses, where the isotropic yield point is approached breakdown of bonding and accompaning consolidation increasingly occurs. This consolidation increases the permanent strain in the sample, and gradually mobilises the frictional resistance in the increasingly disrupted structure of the sediment. This breakdown of cementation and consolidation enables the sediment to withstand more shear strength after the yield of the cementation, until failure occurs at large strains. The stress-strain curves shown in Fig. 2.14, shows this gradation of behaviour of weakly cemented sedimentary materials from brittle, through transitional to a ductile response to loading with increasing confining stress (Meigh and Early, 1957; Conlon, 1966; Townsend et.al., 1969; Miller and Cheatham, 1972; Sangrey, 1972; Uriel and Serrano, 1973; Ohtsuki et.al., 1981; Yoshinaka and Yamabe, 1981; Elliott and Brown, 1985; Vaughan, 1985).

The strains developed at yield and failure can be substantially different for a given sediment. For Leda clays (Sangrey, 1972), the axial strain at yield was always less than 2% and usually less than 1% (some plastic deformation was included in this value), while ultimate failure occurred at axial strains of up to 16%. Isotropic and triaxial yielding for cemented materials tested by Uriel and Serrano (1973) occurred below 1% strain, the post-yield failure being about 6%. This change in behaviour with increasing cell pressure has been described as a gradation from strain softening to strain

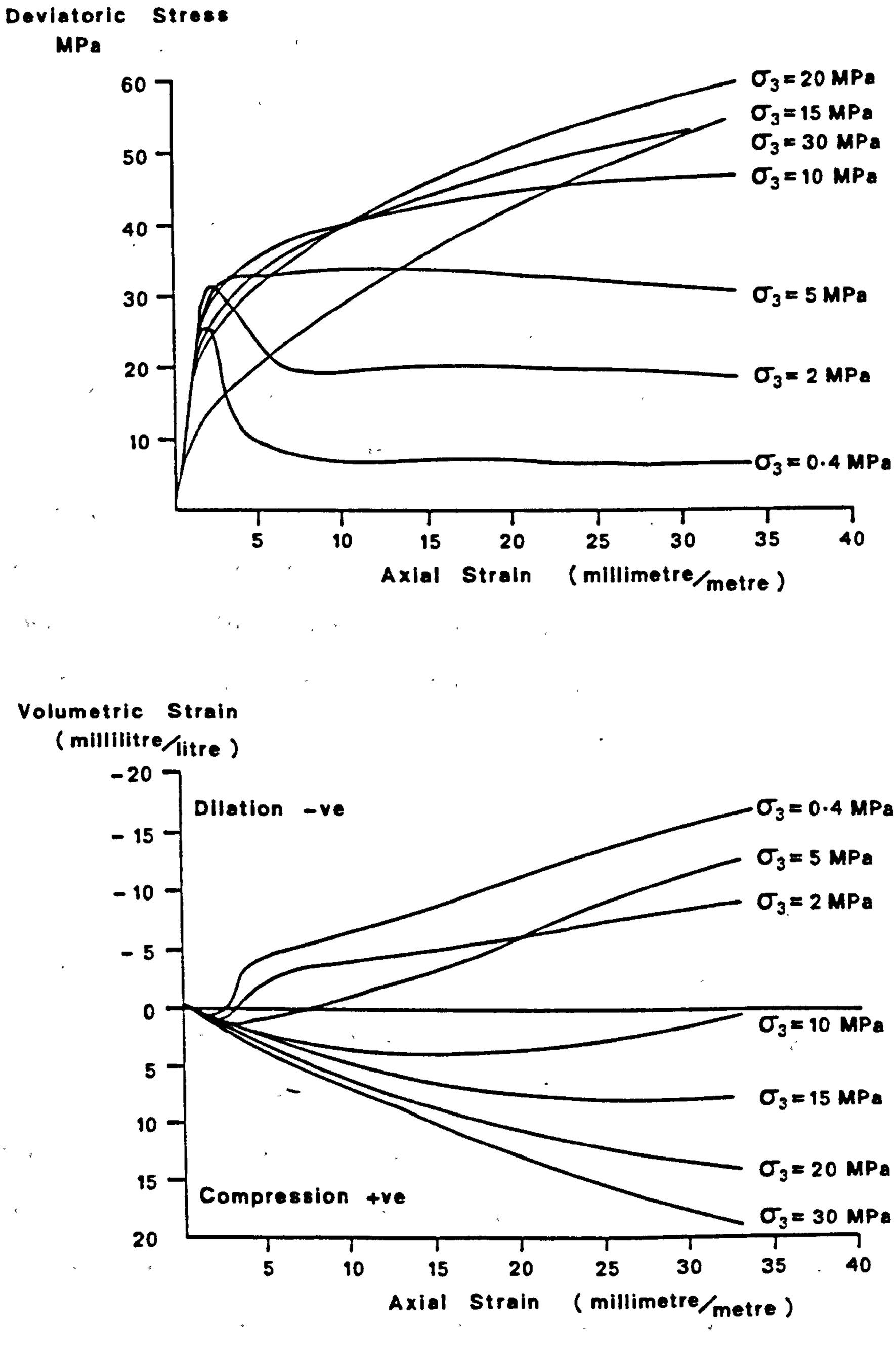

Figure 2.14 Brittle and ductile yield in triaxial tests on dry samples of Bath Stone (After Elliott and Brown, 1985).

hardening (Yoshinaka and Yamabe, 1981; Ohtsuki et.al., 1981; Elliot and Brown, 1985). The intensity of the strain softening decreases exponentially with an increase in confining pressure (expressed by Bishop's brittleness index) (Yoshinaka and Yamabe, 1981), while the Young's modulus tends to increase, Meigh and Early (1957), Yoshinaka and Yamabe (1981), Ohtsuki et.al. (1981), Townsend et.al. (1969), Santerelli, Brown and Maury (1986). Strains at yield for chalks occur at 0.3 to 0.1% for low cell pressures, but at high pressures 5% failure strains occur, Meigh and Early (1957). Hutchinson (1971) observed peak stresses in a shear box occuring at 0.3-1.2% strain when the bedding is parallel to the shear box, and approximately equal to 2% for bedding normal to shearing. In all cases, the cemented structure of the sediment breaks down at relatively small strains.

2.6.3) Compaction of chalk

i) Normal consolidation

Having briefly reviewed the characteristic deformations undergone by weakly cemented materials, the discussion will now focus on the subject investigated during the main part of this experimental study, the compaction of chalk. The studies of chalk consolidation published in the literature will be discussed, as well as the parameters involved in consolidation (Chap. 2.4). Factors thought to affect the magnitude of compaction in chalk will be introduced, these will be discussed with respect to carbonate sediments generally, if no information specifically exists for the chalk.

The compaction of chalk has been discussed by Meigh and Early (1957); Carter and Mallard (1974); Ward, Burland and Gallois (1968); and Burland, Hancock and May (1983); and Smits, de Waal and van

Kooten (1986), the papers by Ward et.al. (1968) and Burland et.al. (1983) describing in-situ behaviour. Carter and Mallard (1974) observed three sections of compressibility during isotropic compression tests, the compression index (Cc) varied from 0.015 psi^{-1}, to 0.5 psi^{-1} and finally to 0.26 psi^{-1}, these values being attributed to an elastic region, an interval of bond breakdown, and a normally consolidated region. This disaggregation of the chalk was also seen in oedometer tests, leading to a structureless silt like material referred to as putty chalk, Higginbottom (1966), Meigh and Early (1957). Putty chalk occurs in the field, due to freeze-thaw or tectonic breakdown of cementation bonds in the chalk, Burland, Hancock and May (1983), Destombes and Shephard-Thorn (1971).

The range of material behaviour exhibited by chalk during compaction, leads to a large range of deformation parameters quoted in the literature. Comparison of published chalk deformation parameters is confusing due to the dependance on both the physical nature of the chalk (intact cemented chalk or disaggregated putty chalk), and on the stress range over which the parameter was determined (for intact chalks, porosity and clay contents are also important). Table 2.4 presents a list of mechanical properties reported in the literature by various workers; a large variation in all of the parameters is observed. The following paragraphs briefly discuss the range of mechanical parameters relevant to compaction and consolidation of chalk; some of the data presented are summarised in Table 2.4.

The breakdown of the cemented structure of chalk, leading to the large variations in mechanical properties will occur at different stresses for different chalk samples. The magnitude of these stresses are dependant upon the strength of the cementation bond and

Table 2.4

REFERENCES	CHALK TYPE	ANGLE OF INTERNAL FRICTION	COHESION (MPa)	M_v (MPa^{-1})	C_v (m^2/yr)	k (cm/sec)	OTHER
Wilson (1948)	Medium and soft	medium 26	0·080	0·465	———	———	
	lumpy chalk	soft 18	0·026	0·186	———	———	
Meigh and Early (1957)	Upper Chalk	d 21	0·896	42·9 < 0·0035 MPa	———	———	E = 0·69 ⟶ 1·39 GPa
	Coulsden, Surrey	u 16,12	2·06 ⟶ 1·51	42·9 > 0·0018	———	———	
	Frost shattered	u 0 ⟶ 16	———	———	———	———	
Wakeling (1966)	Weathered Upper Chalk, Newbury	39	0	0·0186	1136	———	
Lewis and Croney (1966)	Undisturbed	37	0·586	———		soft hard	
	Remolded	38	0·172	———	47·5 ⟶ 66·8	$2·5 \longrightarrow 0·5 \times 10^{-6}$	
Ward et.al. (1968)	Chalk marl	25·8	0·006	0·043	4·92.	———	
Hutchinson (1971)	M. Coranguinum	42	0·131	———	———	———	
	intact/remolded	30	0	———	———	———	
Carter and Mallard (1974)		———	———	0·018	237·5	———	$C_c = 0·15, 0·5, 0·26 psi^{-1}$
Rosenbaum (1978)				20 ⟶ 15	34·9 ⟶ 23·7		$C_c = 0·150 \rightarrow 0·109 kPa^{-1}$
Bell (1977)	Lower Chalk	———	———	0·00014	———	$0·09 \times 10^{-6}$	E_{50} = 14·2 GPa
	Middle Chalk	———	———	0·00015	———	$0·14 \times 10^{-6}$	E_{50} = 13·0 GPa
	Upper Chalk	u 17	2·6	0·00045	———	$2·77 \times 10^{-6}$	E_{50} = 4·4 GPa
Burland et.al (1983)	Soliflucted chalk	40	0	0·04 ⟶ 0·11	———	4×10^{-6}	
	in-situ chalk	———	———	———	———	2×10^{-6}	

the porosity of the material (variations in these, arising due to different burial depths, subjection to tectonic stresses, and possible chemical factors such as clay contents, which are thought to affect cementation mechanisms and the timing of cementation). Carter and Mallard (1974), showed a linear increase in (hydrostatic) preconsolidation pressure (P_c') with depth for the chalk of south east England. The P_c' varies from 3.44MPa at 244m to 10.34MPa at 61m (depths from the base of the lower chalk in south east England), and is in excess of 13.8MPa in Norfolk (the chalk from Norfolk is thought to have undergone greater burial depths than the chalks in S.E.England). Oedometer tests performed by Meigh and Early (1957) support the above data producing uniaxial P_c' values of 10.18, 10.72 and 17.15MPa. In terms of mean stress, assuming a K_o value of 0.3 in the elastic region, these values give P_c' values for hydrostatic loading of 5.43, 5.71 and 9.15MPa respectively. The effects of weathering on the yield strength of chalks was shown by Ward et.al. (1968). The chalks tested by Ward et al (1968) were graded into different recognisable degrees of weathering, grade 5 having the least disrupted or weathered structure. Bearing pressures obtained for these chalks were, for grade 1 chalk <0.2MPa, Grade 2 = 0.2 - 0.4MPa, Grade 3 = 0.4 - 0.6MPa, and Grades 4 and 5 = >1MPa; this chalk classification was devised for upper Turonian chalk near Mundford in Norfolk.

Yield in chalks has been shown to be affected by various factors, such as pore fluid chemistry and temperature. If experiments are to be conducted on chalk in the laboratory, no cleaning operation should be performed as this will affect its measured physical properties. Da Silva et.al. (1985) performed various tests on chalk using different pore fluids and temperatures to assess any weakening effect. They

found that dry samples were stronger than those containing a pore fluid, but did not find any significant difference between samples containing oil or water as a pore fluid. Smits et.al. (1986) obtained contrary results, finding that cleaned dry samples had approximately the same strength as kerosene saturated samples, which were significantly stronger than samples saturated with aqueous solutions. Da Silva et.al. (1985) also observed that water with a high mineral salt content weakened chalks relative to samples with a pure water as a pore fluid. Other workers have also reported the weakening effect of brines on the yield of chalk, (Blanton, 1978; Newman, 1981; Simon et.al., 1982; King, 1986), Smits et.al. (1986) however, observed no significant difference between strengths of chalk containing aqueous solutions of differing salt concentrations.

Coefficients of volume compressibility (M_v) are reported for various occurrences of chalk in southern England, Table 2.4. Meigh and Early (1957) note that the M_v for the chalk tested, at low stress, is equal to $35.4*10^{-4}MPa^{-1}$, decreasing to half this value at stresses above 43MPa. Other workers present compressibility values of $18*10^{-3}MPa^{-1}$ for intact chalk in the 0.2-0.3MPa pressure range, (Carter and Mallard, 1974) and $4*10^{-2}$ to $11*10^{-2}MPa^{-1}$ for soliflucted chalks at low pressures, Burland et.al (1983).

The time dependency of the compaction process in chalk has been considered by Carter and Mallard (1974) who quote a coefficient of consolidation (C_v) (Table 2.4, corresponding to the M_v presented above) of 237.5 m^2/yr. Burland et.al. (1983) considered the time dependancy to be negligable under a test load.

Permeabilities for chalks are generally quoted in two ways, as a relative permeability (or hydraulic conductivity (k)), or as an absolute permeability (K). The latter is measured in Darcies or

millidarcies (mD) and takes account of the viscosity and density of the pore fluid, whereas the former is measured as a velocity and does not. Knowledge of the pore fluid is required for this conversion, and as such, no conversions have been performed by the author on the following data. Chalk permeabilities have been considered by several workers; Burland et.al (1983) give two values of hydraulic conductivity (k), $4*10^{-6}$cm/s for laboratory tests on water saturated soliflucted chalk and in-situ values of $2*10^{-3}$cm/s, Table 2.4. This dichotomy of chalk permeability is not purely due to the soliflucted state of the chalk tested in the laboratory, but also due to the fractured nature of in-situ chalk (Ineson, 1962). Hancock (in; Glennie 1984) and King (1986) state that in high porosity chalks (>30%), low permeabilities (2-13mD) occur due to the small size of pore throats of 0.1-1 microns. Blanton (1978) tested samples of Danian chalk from the North Sea of 43% porosity, these had a permeabilitity of 5.3mD ($5.0*10^{-9}$cm/s), while values generally ranged between 1 and 6mD; Danian outcrop chalks from Denmark have permeabilities of less than 1mD (Simon et.al., 1982; Johnson and Rhett, 1986). Blanton (1978) also tested samples of Austin Chalk, of porosity 26%, these had a permeability of 15.2mD ($1.45*10^{-8}$cm/s) but generally were about 1mD. For chalk-like limestones from the Middle East, permeabilities ranging from 56E-3mD ($5.36*10^{-8}$cm/s) for 9% porosity to 3.44mD ($3.29*10^{-6}$cm/s) for 33% porosity materials have been reported by Marek (1979). Thus, these values obtained from samples from a range of locations show that chalk as a high porosity rock has relatively low matrix permeabilities. Values of permeabilities from on-shore examples are shown in Table 2.4. A trend of permeability with porosity has been presented for samples of pure chalk from many locations by Scholle (1977), Fig. 2.15.

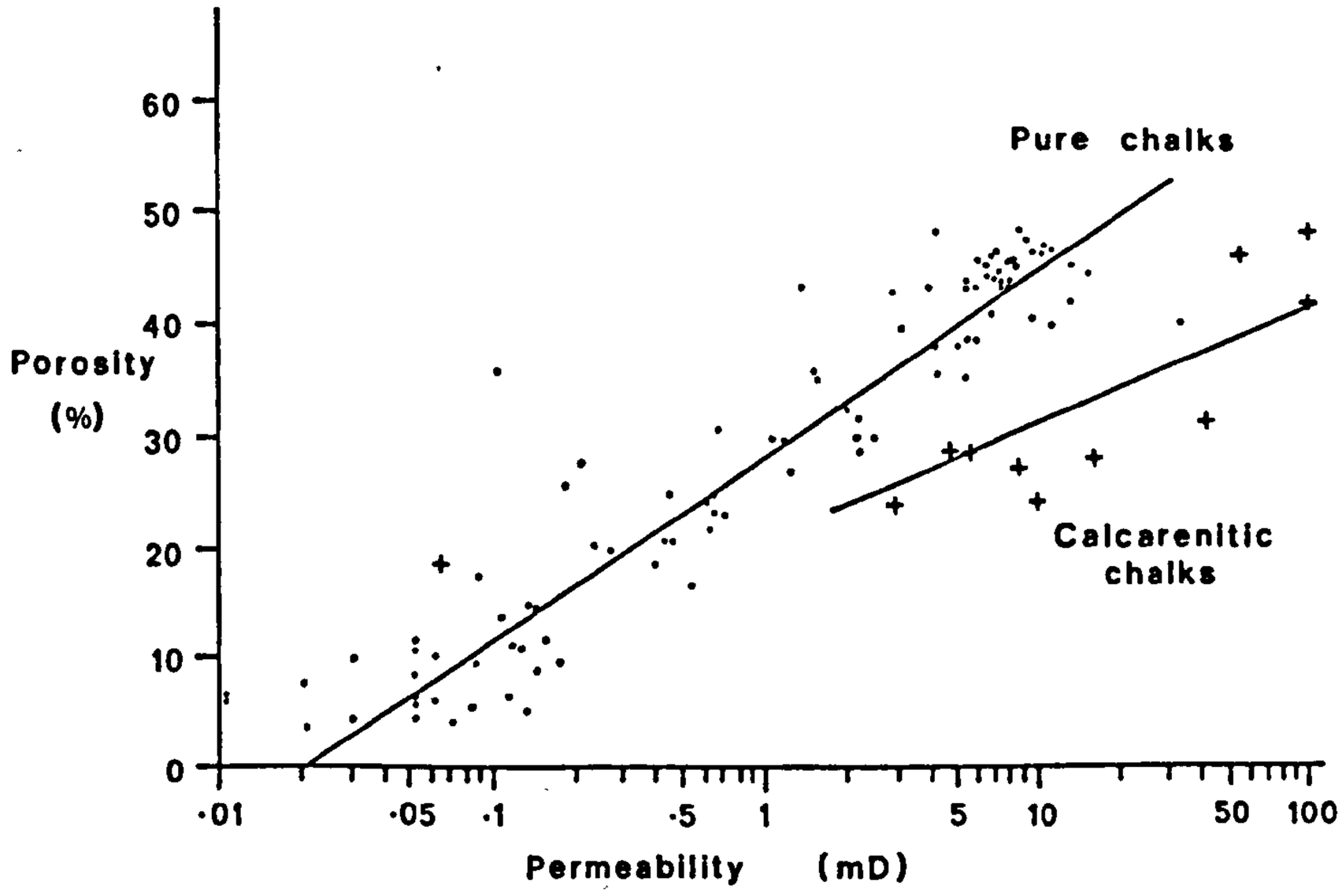

Figure 2.15 A trend of decreasing initial permeability with porosity for pure chalks (After Scholle, 1977).

The post-yield deformation of weakly cemented materials is analogous to the compaction of a normally consolidated sediment; this assumes that the cementation does not affect the nature of the original sediment or its compaction mechanisms. Compaction experiments on carbonate sediments have been performed by Robertson, Sykes and Newell (1962), Fruth, Orme and Donath (1966), Ebhardt (1968), and Rosenbaum (1978). From these studies, factors have been observed which are likely to influence the behaviour of the normally consolidated sediment at most stress levels. The main points which can be derived from these studies are i) Finer sediments show a larger time-dependancy to the deformation than do coarser examples, though the magnitude of the compactions are comparable. ii) When a series of different carbonate sediments with a wide range of porosities are compacted, the compaction curves are of a similar form and sub-parallel at pressures upto 35MPa, this implies that the compaction characteristics are predominantly dependant upon the

mineralogical content of the sediment at the pressure employed in the study. iii) During compaction interpenetration of grains was seen for grapestones with no stylolite production. The deformation was accompanied by minute fractures, suggesting fracture and flow mechanisms predominate and that no pressure solution occurred, Fruth Orme and Donath (1966).

Consolidation experiments performed at high temperatures increase the amount of compaction observed in carbonate sediments (reported in the literature) compared to those tests performed at room temperature. This effect was observed with aragonitic mud (Robertson Sykes and Newell, 1962), artificially precipitated $CaCO_3$ silt, and clayey silt from the Persian Gulf with 65% carbonate content (Ebhardt, 1968). Robertson et.al. (1962), observe a decrease in density of about 20% for a test performed at 500^{o}C which they explain by an increase in the air content in the sample. Ebhardt's experiments on artificially precipitated $CaCO_3$ and clayey carbonate silt both show a 10% decrease in void ratio for tests performed at 90^{o}C, compared to those tests run at 25^{o}C. The tests at both temperatures for the same sediment having the same compression index (C_c). A consolidation experiment where the temperature was increased in a stepwise manner from 25 to 90^{o}C, accompanying the stress increase, showed the same end point void ratio as the experiment run at constantly at 90^{o}C.

ii) Secondary consolidation/creep

Secondary consolidation has been reported from two field studies of chalk foundations, at Mundford (Ward et.al., 1968) and in Salisbury (Burland et.al., 1983). In the earlier study, long term loading tests showed that an additional settlement equivalent to 50%

of the immediate settlement occurred in creep over a 4 month period, all the creep taking place in the top 7 meters of chalk (grades 4 and 3, predominantly in grade 4). For plate loading tests the settlement-log time relationship is linear; the rate of settlement increases linearly with bearing pressure above a certain threshold pressure. Before yield, little secondary creep is seen from the in-situ loading tests. Burland et.al. (1983) observed that total settlements due to construction on chalk amounted 3-10mm, the amount of secondary creep amounting to 3-5mm. At any given pressure the creep rate decreases as the quality of the chalk improves (Ward et.al., 1968).

The effect of creep on the compaction of the chalk in the Ekofisk oil field has been reported in van Kooten (1986), Johnson and Rhett (1986), and Smits, de Waal and van Kooten (1986), (Chap. 6.2).

iii) Summary of salient points

From the above discussion it can be concluded that i) the compaction of the chalk will occur elastically until a yield point is encountered, larger compactions occuring in the post-yield stress range due to the break down of the cementation; ii) factors such as temperature and pore fluid variation may affect the compaction behaviour of the chalks; and iii) creep may possibly be significant.

2.7) STRAIN RATE EFFECTS

Predictions of in-situ sediment behaviour, based on data from laboratory results, are generally erroneous; this has been observed for settlements, calculations of preconsolidation pressures and shear strengths. Work started in the sixties by Crawford (1964) on rates of testing compared to deformation rates in the field, led to the

conclusion that results from laboratories cannot be compared to field behaviour. This is due to the unrealistic rates of compression in the laboratory compared to those existing in the field, and it was stated that "this is a much more influential factor than many of the known errors of testing" (Crawford, 1964). The difference in rates of compaction can be of several orders of magnitude.

In an effort to assess the effect of strain rate on compaction, several authors have produced evidence from various testing methods including incremental loading (IL), constant rate of strain (CRS), constant gradient (CG), single stage loading (SSL), and anisotropically consolidated triaxial testing (ACT), which show that the state of stress at a particular strain is dependant upon the imposed strain rate, Vaid and Campanella (1977). The work has been performed mainly on sensitive clay from Canada (Crawford, 1964; 1965; Vaid et.al., 1979; Leroueil et.al., 1983a; 1983b; 1985) though other work has been performed on non-sensitive clays. These contributions have generally concentrated on the decrease in preconsolidation pressure (P_c') with strain rate. In order to be able to estimate the decrease in the preconsolidation pressure with decreasing strain rate, a parameter $\Delta P_c'/P_c'$ is quoted in the literature. This value denotes the change in the preconsolidation pressure associated with a decrease in strain rate of one log cycle (a tenfold decrease)($\Delta P_c'$), divided by the preconsolidation pressure obtained at a particular strain rate (P_c'). Table 2.5, presents $\Delta P_c'/P_c'$ values for various sediments published in the literature. Data on 11 clays from eastern Canada have been normalised ($\Delta P_c'/P_c'$) to obtain a general value of preconsolidation pressure decrease with strain rate. The 11 clays when normalised, produced a definite trend of decreasing $\Delta P_c'/P_c'$ with decreasing strain rate, with a $\pm$ 9% scatter, Leroueil and

Tavenas (1979), Vaid et.al. (1979), Graham, Crooks and Bell (1983).

Table 2.5

ΔPc'/Pc' per log cycle	Materials	References
12%	sensitive clays Gloucester	Leroueil et.al. (1983a)
10-14%	Champlain sea clays	Leroueil et.al. (1983b)
16%	Belfast clay	Graham et.al. (1983)
20%	Ottawa clay	
10%	Winnipeg clay	
7-23% *	from Ca/Cc values 0.03-0.09	Mesri and Choi (1979)
8-23%	Various clays	Leroueil and Tavenas (1979)
2% *	well-consolidated sandstones	de Waal and Smits (1985)
4% *	consolidated ssts.	
5% *	unconsolidated ssts.	
2-13% *	Danian outcrop chalk various pore fluids.	Smits et.al. (1986)
6-7% *	North Sea chalk.	

Values denoted by * are determined from the displacement of the stress-strain curves caused by a change in the strain rate. These data are for consolidation tests performed at differing strain (or loading) rates. The method and theory relating to the calculation of these values is discussed later.

Leroueil et.al (1983b) related the P_c' from various test results to the strain rate, and showed that standard oedometer tests gave the best results. This was because the CRS experiments were conducted at too fast a rate. This was a consequence of the loading system not being able to operate at slow enough loading rates (Leroueil et.al, 1983a). As such, the standard oedometer tests, being low strain rate

tests, were more comparable with field rates of strain.

The decrease of the preconsolidation pressure or yield point with decreasing strain rate is not independant of strain rate. At low strain rates no further decrease in P_c' is observed. This has been observed by Larsson and Sällfors (1986) and Silvestri, Yong, Soulie and Gabriel (1986).

Following work investigating the preconsolidation pressure variation, the strain rate dependency of the whole stress-strain curve was considered, Leroueil et.al. (1985). The preconsolidation pressure is considered as a well defined point on a stress-strain curve, which occurs over a small range of strains. Stress variations observed for particular strain levels in tests of varying strain rate, demonstrate that the whole stress-strain curve is strain rate-dependent, in the same manner as P_c' (Leroueil et.al., 1985; Graham, Crooks and Bell, 1983; Mesri and Choi, 1979; de Waal and Smits, 1985; Smits et.al., 1986). Leroueil et.al. (1985) have shown that stress-strain curves for one-dimensional compaction tests performed at different strain rates on cemented clays, can be normalised to one curve. The normalisation is obtained by dividing the stress at any strain along the stress-strain curve by the stress at yield, i.e. the preconsolidation pressure. Using this normalisation of stress-strain curves and the decrease in the preconsolidation pressure with strain rate, the stress-strain curve applicable for the in-situ strain rate can be obtained.

The strain rate effect is analogous to variable duration IL tests, with the slower tests giving rise to more compaction of the sediment skeleton per stress increment. This increase in compaction is due to a greater contribution of creep deformation in the slower tests, Fig. 2.16a. Thus, CRS and IL tests move across an e - log σ' - log t

surface in a continual or stepwise manner, respectively, Fig. 2.16.

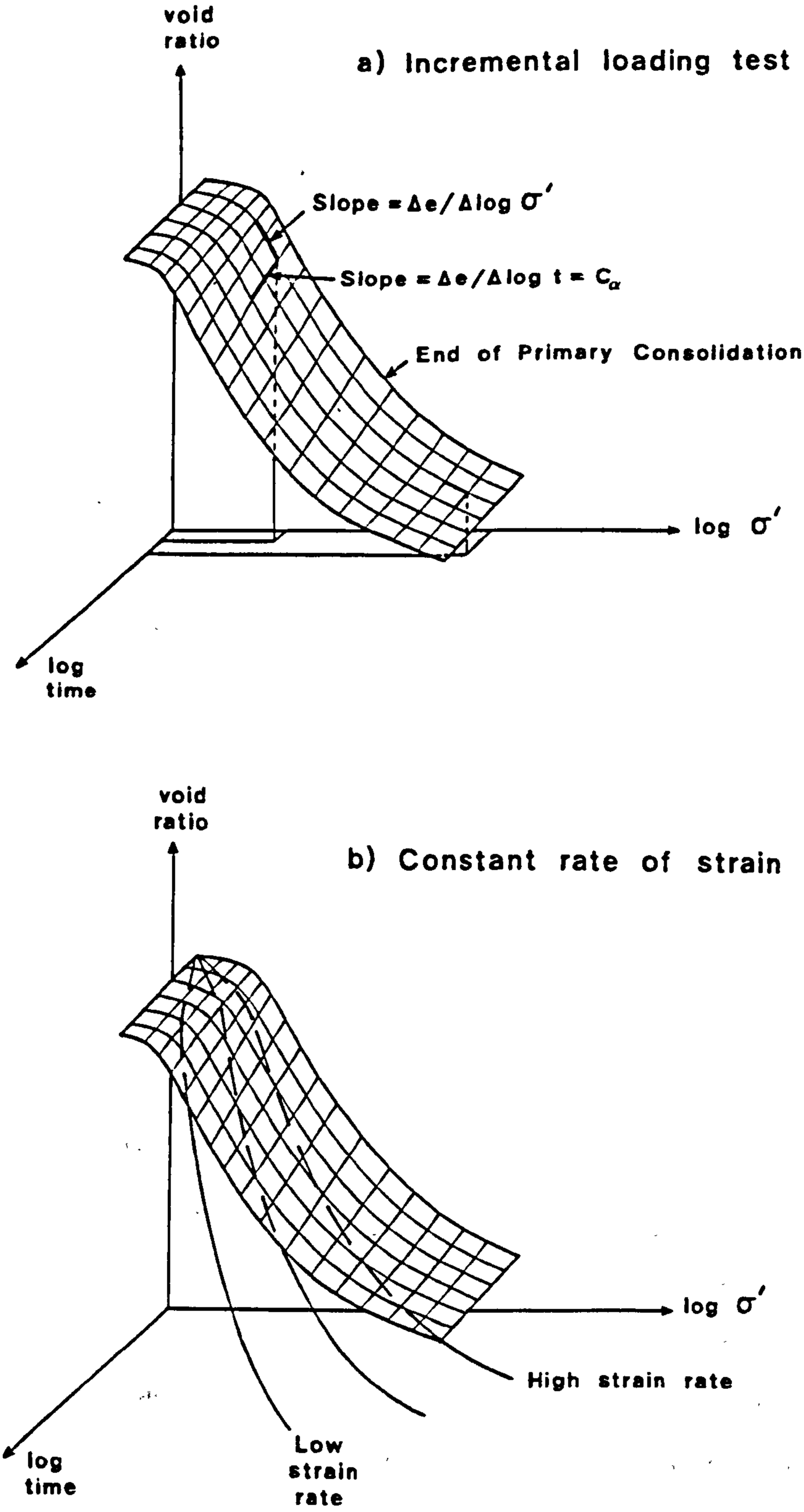

Figure 2.16 Time effects during consolidation (After Mesri and Godlewski, 1977).

Mesri and Godlewski (1977) represent the effect of changing strain rate on sediments in terms of two of the axes in Fig. 2.16a, and have shown that the ratio of these axes C_α (coefficient of secondary consolidation, $\Delta e/\log t$) to C_c (coefficient of compressibility, $\Delta e/\log \sigma'$) is approximately constant, a slight maximum occurring near the pre-consolidation pressure. Inorganic clays typically have C_α/C_c values of 0.03-0.06; the ratio for organic clays ranging upto 0.10. Mesri and Choi (1979) have shown that the preconsolidation pressure (σ_2') due purely to secondary consolidation at a load σ_1', is related to the duration of secondary consolidation (t_2/t_1),

$$\sigma_2'/\sigma_1' = 10^{C_\alpha/C_c} \quad \text{For } t_2 = 10.\ t_1 \qquad .. \ 2.7.1$$

Using the C_α/C_c value, and an initial e - log σ' curve, subsequent curves can be calculated (Eqn. 2.7.1) for increasing consolidation times. Repeating this calculation leads to a family of e - log σ' - t curves.

Similarly strain rates can be used instead of loading durations to obtain P_c' variation or any other strain variation with strain rate.

$$(P_c')_j/(P_c')_k = (E_k/E_j)^{C_\alpha/C_c} \qquad .. \ 2.7.2$$

Hence, it should be possible to predict the e - log σ' curves for any strain rate, if the e - log σ' curve one strain rate, and the C_α/C_c ratio for the sediment are known. It would seem that the C_α/C_c value does not vary considerably with strain rate from the normalised curves of Leroueil et.al. (1985), Mesri and Feng (1986), except at slow strain rates (Larson and Sällfors, 1986; Silvestri et.al. 1986).

An identical result to the above equation Eqn. 2.7.2, relating the stress level (occurring at a particular strain) to the strain rate has been derived for the case of loading rates in response to reservoir depletion in sandstones, Eqn. 2.7.3 (de Waal, 1986; de Waal

and Smits, 1985) (Chap. 6.2). This relationship was derived for use on compaction experiments of reservoir materials, and is applicable to tests where the sample is strained at different loading rates during the compression. As defined by the Eqn. 2.7.3, shifts in the stress-strain curves for differing loading rates occur. Knowing the shifts in the stress-strain curve for different loading rates, the stress-strain curves for the loading rates imposed in the reservoir can be calculated, with the corresponding compressibilities, (c.f. Eqn. 2.7.2 and the discussion in preceeding paragraphs of the work performed by Mesri and Godlewski (1977), Mesri and Choi (1979)). This is the same effect as that described by Bjerrum (1967), with e-log σ' curves occurring at higher stresses for rapid depositional rates.

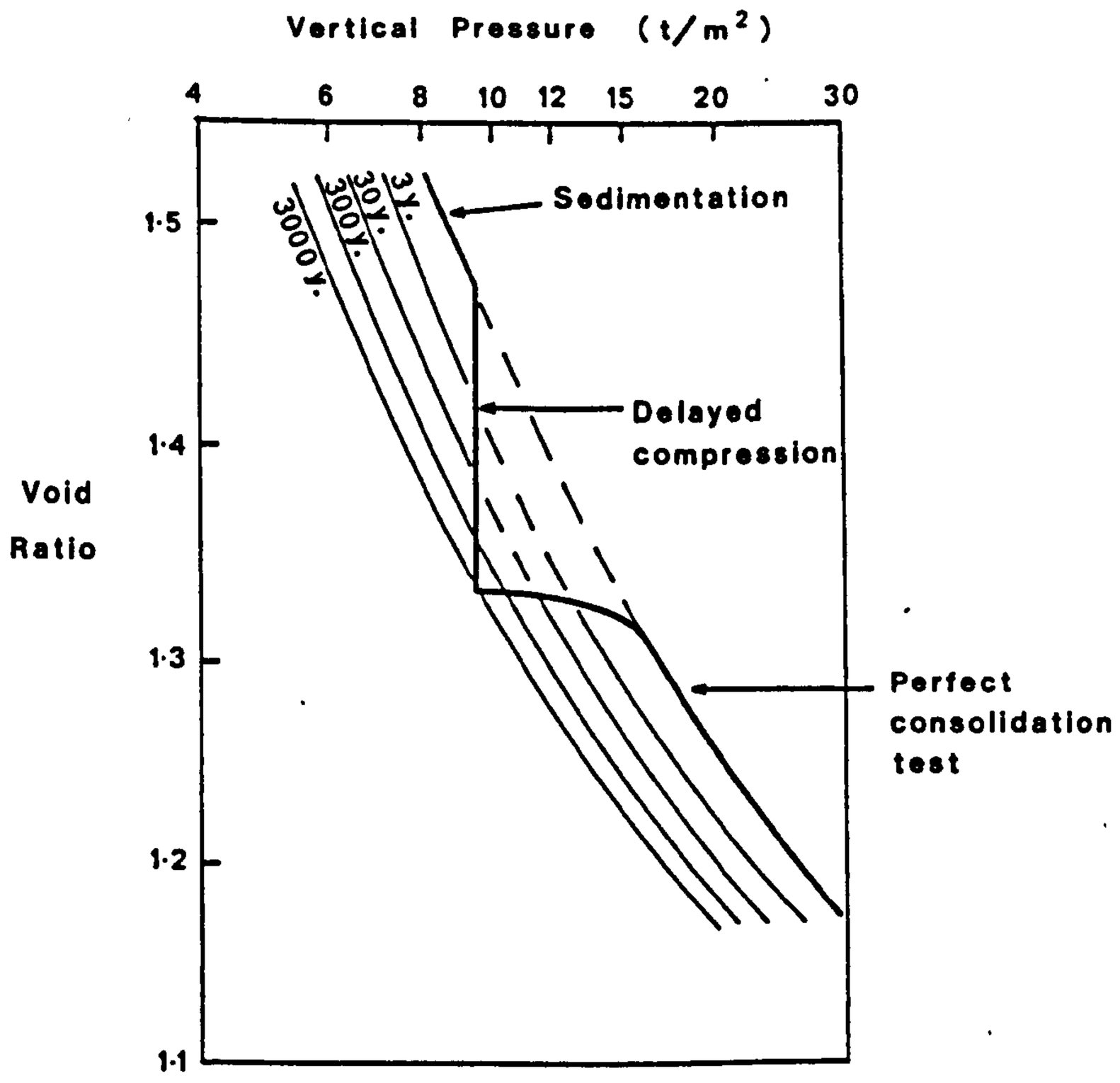

Figure 2.17 Time effects on the compression of a sediment subjected to reloading (After Bjerrum, 1967).

Other characteristics of the tests have also been noted by Bjerrum; e.g. a preconsolidation effect, seen on loading the material at a faster rate, Fig. 2.17. This diagram is a cross section through Fig. 2.16, and shows the different e-log σ' curves obtained for different sedimentation/loading rates. For reservoir problems, the change in loading rate would be that from the geological depositional loading to the enforced stress increase due to drawdown of the pore pressures during production. The relation is presented as

$$\hat{\sigma}'_z = \sigma'_{z,1}\,[(\dot{\sigma}'_{z,2}/\dot{\sigma}'_{z,1})^b - 1] \qquad .. \ 2.7.3$$

and is obtained by curve-fitting procedures of differing loading rates on sandstones. The same equation was obtained (de Waal, 1986; de Waal and Smits, 1985) from theoretical modelling of a rate-type deformation process and was initially expressed as

$$d\sigma'_z = b.\sigma'_z.d(\ln\dot{\epsilon}_z) \qquad .. \ 2.7.4$$

Assuming linear elasticity, this equation becomes

$$\sigma'_{z,2}/\sigma'_{z,1} = (\dot{\sigma}'_{z,2}/\dot{\sigma}'_{z,1})^b \qquad .. \ 2.7.5$$

Even if the assumption of linear elasticity during the conversion from loading rates is questionable, Teeuw (1971), shifts in the stress-strain curve for differing deformation rates could be calculated in terms of strain rate from the Eqn. 2.7.4. Obviously the b value of de Waal and Smits (1985) is the same as the C_α/C_c ratio of Mesri and Godlewski (1977) and Mesri and Choi (1979). The values of b given by de Waal and Smits are given in Table 2.5.

To reproduce the change in strain rates seen in the field, de Waal and Smits (1985), follow a partial unloading technique used by Kenney for shear strength - strain rate determination (Graham, Crooks and Bell, 1983). This can produce a change in loading rate up to a magnitude of 10^7, the amount of unloading required being governed by Eqn. 2.7.3. The curves obtained from these relaxation tests were normalised; the results for a series of sandstones and sands plot on the same normalised curve. The clays of Leroueil et.al. (1985) also showed that the stress-strain curves could be normalised. The regression holds, down to normalised stresses of 0.8 (corresponding to a rate change of 10^7), and is not related to the material properties of the sands. The influence of stress history on the sands is small, but this may affect such methods if applied to a cohesive material (de Waal, 1986).

The decrease in stresses with strain rate for a particular strain (seen by the pre-consolidation pressure variation) is part of a more general dependance of material properties on strain rate. This was seen by Lo and Morin (1972) and Tavenas and Leroueil (1977) who observed a decrease in the size of the yield envelope in stress space of sensitive clays with decreasing strain rate.

From this brief review of the effects of strain (and loading) rates on the degree of compaction observed in sediments and weak rocks, it can be concluded that the displacement of the stress-strain curves is dependant upon a ratio C_α/C_c. This factor is also called a "b" factor in reservoir engineering literature, however, this factor does not have a physical expression, unlike the ratio C_α/C_c. This ratio is the ratio of the relative contributions of primary consolidation and secondary consolidation observed in a compaction experiment. A literature survey of the published C_α/C_c

values show shifts in stress-strain curves of different magnitudes associated with different sediments. As a result, chalk compaction can be expected to be strain rate dependant, as shown by Smits et.al. (1986).

2.8) EFFECTS OF TEMPERATURE ON CONSOLIDATION

Porosity loss during the burial of sediments in a sedimentary basin, occurs through compaction and dewatering under increasing burial with increasing applied stresses (due to continued influx of new sedimentary material). The sediment will also experience an increase in temperature during this burial. This increase in temperature will depend upon the depth of burial of the sediment and the regional geothermal gradient. Hydrocarbon reservoirs occur at various depths, sometimes exceeding 3Km and therefore experience elevated temperatures; bottom hole temperatures in the chalk fields of the Ekofisk group in the Central North Sea are of the order of 130^{o}C. The magnitude of compaction due to drawdown of the pore fluid pressure during the production of an oil field, will depend on how elevated temperatures affect the consolidation mechanism. If compaction is temperature dependant, any evaluation of porosity loss during reservoir compaction or sediment burial should take into account the elevated reservoir temperatures or the geothermal gradient respectively.

This section of the thesis discusses the effect of temperature on compaction and consolidation of sediments, based on published literature, predominantly from the field of soil mechanics. Some effects of temperature on compaction have already been briefly discussed for carbonate sediments (Chap. 2.6.2), the present discussion will consider the effect of temperature on compaction for

a wider range of sediments.

Rearrangement of the structure of a sediment in response to changes in the applied stress, will depend on a number of diverse characteristics, many of which will be sensitive to the applied temperature. These characteristics include; the nature of the mineral skeleton; the nature of the pore fluid; and, the nature and chemistry of the absorbed layer around the grains (often described as the adsorbed water layer). All of these parameters will be temperature sensitive.

When a sediment experiences an increase in temperature, its main response will be a change in the volume of the grains and of the pore fluid. The thickness of the adsorbed water layer surrounding the grains is thought to reduce with increasing temperature, though swelling pressure calculations show that no change in repulsive forces between particles occurs in response to an input of thermal energy (Mitchell, 1969).

Equations for the calculation of changes in volume and pore pressure, with temperature, for both drained and undrained tests, have been presented by Campanella and Mitchell (1968),

$$(\Delta V_{dr})\Delta T = \alpha_w V_w \Delta T + \alpha_s V_s \Delta T - (\Delta V_m)\Delta T \qquad .. 2.8.1$$

and

$$\Delta U = \frac{n\Delta T\ (\alpha_s - \alpha_w) + \alpha_s \Delta T}{M_v + nM_w} \qquad .. 2.8.2.$$

Where V = volume, α = thermal expansion of solids or fluid, ΔT = change in temperature, U = pore fluid pressure, n = porosity and M_v = uniaxial compressibility, and M_w = the compressibility of the pore fluid. Subscripted parameters referred to are; dr = total drained

behaviour, w = water, s = solids, and m = sediment mass. The prediction of pore pressures from these equations agrees well with the those measured in the laboratory.

The increase in pore pressure in an undrained or a low permeability material due to the increase in temperature has been stated as being analogous to an increment of mechanical load, with larger thermal loads leading to larger strains. Thermal loads initiated after sediments have completed their primary consolidation show consolidation curves similar to the type I and type II curves of Leonards and Girault (1961) (Campanella and Mitchell, 1968) for small or large thermal or pressure increments. A sediment consolidated under an increased temperature and then cooled, exhibits similar behaviour, on loading, to an overconsolidated sediment (Plum and Esrig, 1969); with the normally consolidated part of the recompression curve being shifted to a higher stress for a particular void ratio.

The compression curves for sediments at different temperatures have been presented by Finn (1951), Campanella and Mitchell (1968), Laguros (1969), Plum and Esrig (1969), Ebhardt (1968) and Rosenbaum (1978). Plum and Esrig (Loc.Cit.) showed that in consolidation experiments started from low stresses, samples deformed in higher temperature experiments exhibit higher compressibilities at stresses below 0.2MPa. Above this stress level, the compression index remains approximately constant and is equal for the different temperatures. In the high pressure range, this was observed in tests on Fuller's earth by Rosenbaum (Loc.Cit). Other workers have observed this similarity of C_c values with experiments performed at different temperatures. Such tests normally have different initial void ratios, this difference has been attributed to the effect of temperature on

compaction (Plum and Esrig, 1969). One study reports that C_c values converge slightly at higher pressures (50MPa) for different temperature experiments (Ebhardt, 1968). This contradicts the results described above.

Demars and Charles (1982), showed similar trends to those described above in their experiments. Their study consisted of consolidating samples at 25°C until primary consolidation had ceased, heating them to 50°C, during which time the sample further consolidated, then cooling them to 25°C, so obtaining the irreversible deformation due to heating. They found the irreversible volume change to be constant and independent of load; though the magnitude of the irreversible volume change (de), varies from 0 to 0.031 for sands and plastic clays respectively. Thus C_c is constant with temperature, but the change in void ratio as a consequence of changes in temperature will depend on the type of sediment. The magnitude of the decrease in void ratio linearly increases with plasticity index according to Eqn. 2.8.3 (Demars and Charles, 1982).

$$\Delta e = (0.00048 + 0.0000088.I_p)^{\Delta T} \qquad .. 2.8.3.$$

where Δe = the change in void ratio, I_p = the plasticity index and ΔT = the change in temperature (°C).

Tests in which the temperature is varied with pressure show similar trends. Plum and Esrig (1969) load a sample to 0.20-0.27MPa at 25°C then the sample is heated to 50°C and the consolidation is continued at this temperature. Ebhardt compacted samples under increasing loads with a stepwise increase in temperature. In both series of tests the gradually heated sample attained more strain than the equivalent test performed at room temperatures. Plum and Esrig's

tests resulted in a final strain mid-way between the two constant temperature tests (with an additional 1% strain for the sample where the temperature was gradually increased compared to that of the test at 25°C). This was also observed by Rosenbaum (1978). Ebhardt's experiments, however, have effectively the same end point as the sample tested at 90°C, suggesting a standard re-equilibration of the structure to load and temperature, indicated by Eqns. 2.8.1 and 2.8.3. For overconsolidated sediments, the Δe increases with decreasing OCR (Plum and Esrig, 1969; Demars and Charles, 1981).

Campanella and Mitchell (1968) found that the pore pressure pressure response due to a temperature increase rose with confining pressure, and they defined a factor F which is the change in pore pressure per unit change in temperature per unit effective stress (or the change in unit effective stress per change in temperature). The factor, F, was defined for cycled or overconsolidated material, and found to be independent of effective stress. This analysis is therefore not comparable to the tests presented by Demars and Charles which concerned first heating cycle strain.

Time dependency of compaction (or consolidation) has been considered mainly in relation to the variation in the coefficient of consolidation with temperature. Finn (1951) and BS1377 have shown that C_v varies with temperature; the variation being greater than that due purely to a viscosity change in the pore fluid. This change is opposed by a compacting structure which reduces the permeability of the sample (Paaswell, 1967). Laguros (1969) observed only a small decrease in C_v with temperature, and this was probably due to differing initial void ratios for the samples. C_vs for Fullers earth show an increase from 1.1m^2/yr at 15°C to 3.5 m^2/yr at 70°C for low stresses while, for high stresses, C_v varies with increasing pressure

from 1.0m^2/yr to 0.02m^2/yr, the temperature having a marked effect on the C_v. For chalk slurries, C_v decreases from 34.9 to 22.7 m^2/yr for a 20^o to 60^{o}C temperature change. The trend, however, is not distinctive and C_v was difficult to obtain because of the short time span of consolidation, Rosenbaum (1978). In tests where the temperature was increased with pressure, the C_v tended towards the constant elevated temperaure value, Thus showing a similar trend to that observed with the changes in magnitudes of compaction, discussed in the previous paragraphs.

Other factors of sediment deformation are reported in the literature as being temeprature dependant. Secondary consolidation appears to be slightly increased in response to a temperature increase after the equilibration of pore pressures. If the sample is cooled, the C_α decreases in a manner similar to that of an overconsolidated sediment (Plum and Esrig, 1969; Campanella and Mitchell, 1968), though Habebaghai (reported in Gaba, 1980) shows that C_α is unaffected by temperature in the overconsolidated or normally consolidated state for Palisade clays; while all other factors are affected. Other workers have shown that the elasticity modulus decreases with temperature (Murayama, 1969; Zeuch, 1983) as does the strength of granular materials (Zeuch, 1983; Sherif and Burrows, 1969). The decrease in strength is seen to be exponential with temperature increase. Laguros (1969) demonstates this decrease in strength by a decrease in liquid limits and plasticity index with increasing temperature.

From this review, of the effect of elevated temperature on compaction of sediments, it can be concluded that clays are more susceptible to increased compaction at higher temperatures than are sands, while the little information on carbonate materials suggest

that chalks will also be affected to some degree. Various relationships of volume reduction and pore pressure build up have been formulated for increases in temperature, these have however, only been tested at geologically low temperatures and pressures. Extension of these relationships into geologically realistic conditions could be useful for work studies on overpressured clay horizons.

CHAPTER 3

EXPERIMENTAL METHODOLOGY AND MATERIALS

3.1) INTRODUCTION

In the last chapter some of the aspects of soil mechanics relevant to the deformation of weak rocks and sediments during one-dimensional compaction have been discussed. The chapter also included a brief review of the mechanical behaviour of cemented sediments, with emphasis on previous work performed on high porosity chalks and other high porosity carbonate rocks.

The loss of porosity in sediments due to an increase in stress during progressive burial in a sedimentary basin, or as a result of drawdown of pore pressures in a hydrocarbon reservoir has been investigated by previous workers (Teeuw, 1971; Rieke and Chilingarian, 1974; van Ditzhuijen and de Waal, 1984; de Waal and Smits, 1985; Smits, de Waal and van Kooten, 1986) using K_o (zero lateral strain) experiments. This kind of one-dimensional deformation experiment is thought to be representative of large basins and of large hydrocarbon reservoirs (Geertsma, 1973), where only vertical shortening of the sediment layer occurs. The large area is necessary to limit the more complex stress conditions that could be encountered at the margins of the structure (Shepherd and Bryant, 1983). The validity of this test technique obviously depends on the mechanism of basin subsidence and reservoir compaction and the geometries of the structures; but it can be assumed that, for the size of sample tested in the laboratory compared to that of the whole structure, the errors

are negligable.

This chapter reviews the recommended methods for performing one-dimensional consolidation tests in a triaxial cell. These tests allow the ratios of the principle stresses acting on the sediment or weak rock to be evaluated during the deformation. Such tests are referred to in the soils mechanics literature as K_o tests and as zero lateral strain or uniaxial strain tests in the reservoir engineering literature. No recommendations have been suggested in the reservoir engineering literature on test methodology, while in the soils mechanics publications some recommendations have been proposed. This chapter will briefly review the relevant literature pertaining to K_o tests and testing, this information is predominantly obtained from soils mechanics publications; reservoir engineering literature will be introduced wherever applicable.

Historically, one-dimensional consolidation tests have predominantly been performed in oedometer tests, and have been used to evaluate the consolidation parameters. A stepwise increase of the stress is applied to the sample in oedometer tests, and as such is unrepresentative of the stress increase undergone by a reservoir during drawdown. New methods of performing one-dimensional consolidation in soil mechanics have proved very efficient, these include tests where the strain is increased at a constant rate and tests of constant stress increases, however these testing methods have required new analytical expressions to interpret the results. In this study constant rate of strain (CRS) consolidation experiments are performed, and as such, the second part of this chapter reviews the analysis of these tests, in order to obtain consolidation parameters such as the coefficient of consolidation (C_v), and the permeability (K). Determination of these parameters is very

important, as they define the time dependancy of the deformations involved in the pore volume reduction of sediments and weak rocks. This review is obtained purely from the soil mechanics literature.

The Chapter is terminated with a description of the materials used in this study, the description includes the geological setting in which the materials are found, and the age of the formation. A review of any literature concerning relevant studies on the composition of the materials is also included, however the number of these found by the author was very few, therefore, analyses of the compositions of the materials performed by the author are included in this section.

3.2) THE COEFFICIENT OF EARTH PRESSURE AT REST

3.2.1) Introduction

The stresses acting on a unit of sediment or rock in-situ, may not be equal in all directions. The ratio of stresses required to maintain a condition of zero horizontal strain during sediment burial is called the coefficient of earth pressure at rest, and is denoted by K_o. This condition holds for burial in a tectonically inactive area, where a unit of sediment is constrained to deform, by shortening only in the vertical direction; in response to increasing overburden pressure.

$$K_o = \frac{\sigma_h'}{\sigma_v'} \qquad .. 3.2.1$$

Bishop (1958) defines the coefficient of earth pressure at rest as 'the ratio of the horizontal and vertical effective stresses corresponding to the condition of zero lateral strain' and states

that 'shear stress can significantly alter the "at rest" pressure'. The K_o stress path has no unique property, but is part of a spectrum of behaviour for the system $\sigma_v'K = \sigma_h'$ (Andrawes and El Sohby, 1973; Chap. 2.5) the only requirement of K_o being the zero lateral strain condition. A sediment unit may undergo deformation along any stress path, after which a passive (no tectonic stresses) K_o stress path may be followed. Eqn. 3.2.1, would register this past history and misrepresent the stresses in the passive system. To avoid this Andrawes and El Sohby (Loc.Cit.) have suggested that the coefficient of earth pressure at rest should be defined as ' the ratio of the increment in the minor principle effective stress to the corresponding increment in the major principal effective stress when no strain occurs in the direction of the minor principal stress'.

i.e.
$$\bar{K}_o = \frac{\Delta\sigma_h'}{\Delta\sigma_v'} \qquad .. 3.2.2$$

The ratio will be distinguished by $\bar{K}_o$ as opposed to K_o for Eq 3.2.1), (Garga and Costa, 1977).

The values of K_o for normally consolidated sediments generally range between 0.3 and 0.5 for sands (Bishop, 1958; Al Hussaini and Townsend, 1975; Mayne and Kulhawy, 1982) and between 0.5 and 0.7 for clays (Brooker and Ireland, 1965; Abdelhamid and Krizek, 1976; Moore and Cole, 1977; Mayne and Kulhawy, 1982). Many studies have been performed on overconsolidated sediments and for sediments under successive loading (Brooker and Ireland, 1965; Mayne and Kulhawy, 1982) with K_o measured for these conditions. K_o for overconsolidated clays generally increases to values greater than unity, while in recompression the values generally decrease from the overconsolidated

value to the normally consolidated value at the preconsolidation pressure. Relationships between K_o for various stress histories have been formulated by many authors (Mayne and Kulhawy, 1982).

The K_o stress path for a soil with an initial elastic section has been presented for residual soils by Vaughan (1985), for loess by Kane (1973), for sensitive clays by Silvestri (1981) and for overconsolidated clays by Leroueil et.al. (1983b). This is illustrated diagramatically in Fig. 3.1, which shows that the different paths followed in the elastic part of the deformation are dependent upon the initial starting conditions. However, the K_o line in the normally consolidated region of the deformation, is reached, regardless of the initial stress conditions, as long as the initial stress state is within the elastic envelope.

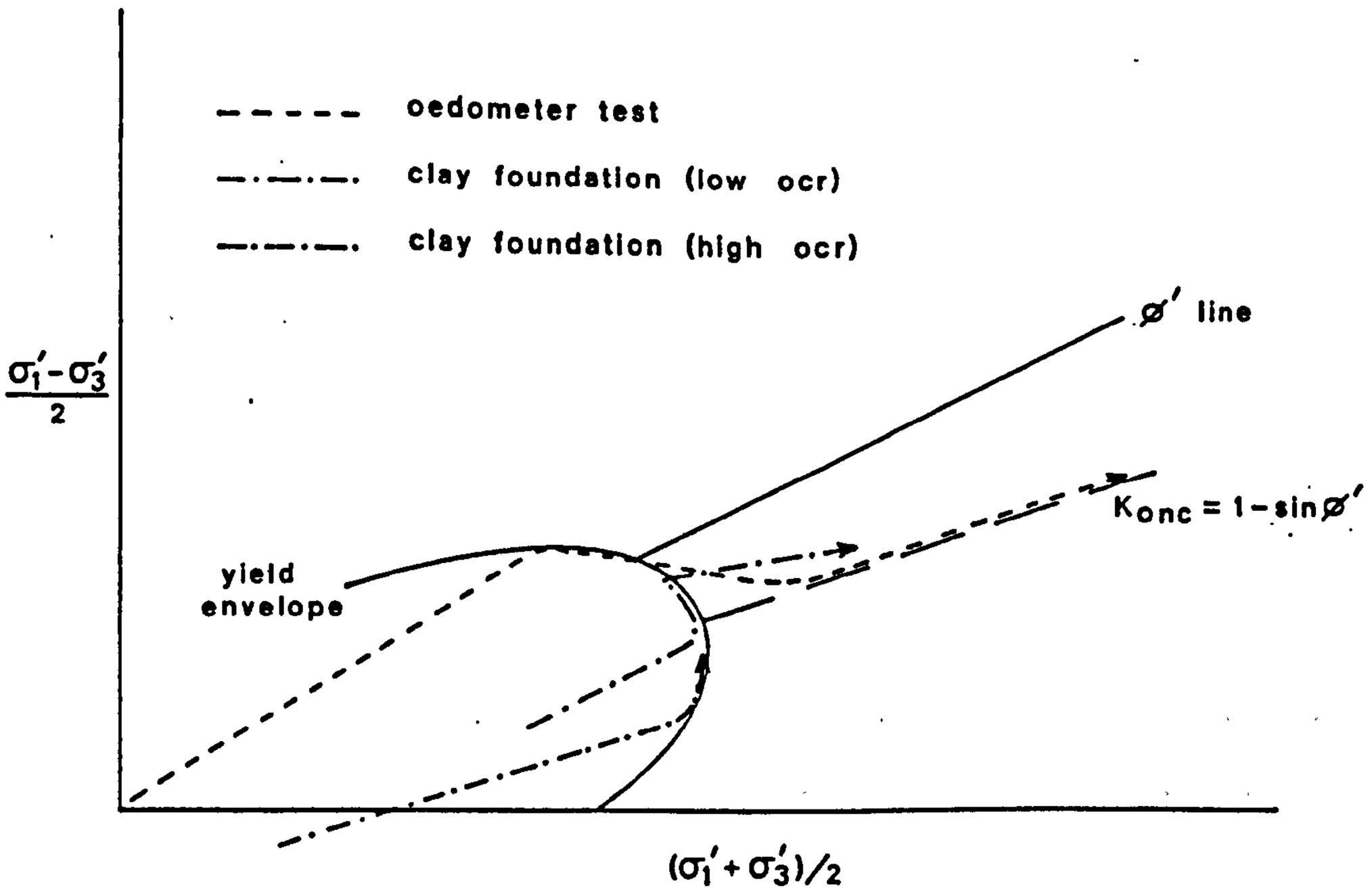

Figure 3.1 K_o stress paths for overconsolidated clays (After Leroueil et.al., 1983).

3.2.2) Relationships of K_o

i) K_o - ϕ' relationship.

Deformation of a sediment under conditions of zero lateral strain involves a deformation in response to the maximum effective stress (which in passive sedimentary basins of large areal extent is assumed to be vertical). The deformation will consist of a structural rearrangement of component mineral grains forming the load carrying skeleton of the sample. The deformation has been divided into distortional and volumetric strains (Hanrahan, 1977; Phillips, 1984). This implies that K_o should be related to other deformational parameters of the sediment. One of the first and most commonly used relationships of K_o is that suggested by Jaky (1948b), in which he related K_o to the angle of internal friction, ϕ'.

$$K_o = 1 - \sin \phi' \qquad .. 3.2.3$$

This equation is a simplification of an equation given by Jaky (1944), Table 3.1. Other workers have suggested relationships between K_o and ϕ, but most are only refinements of the Jaky equation, and generally only hold for specific sediments (Schmidt, 1967). Various relationships are given between K_o and ϕ in Table 3.1.

From Table 3.1, it can be seen that the deviation from Jaky's original equation is always small. Hendron's equation is based on the packing of spheres and is suggested by Schmidt (1967) to represent a lower limit to the K_o - ϕ' relationship. The Hendron equation gives good results for well-rounded sands, though other sands fit Jaky's equation (Schmidt, 1967; Al Hussaini and Townsend, 1975). After testing a series of clays, Brooker and Ireland (1965) deduced the

Table 3.1

K_o =	Reference	Material
$(1 - \sin\phi').\frac{1+2/3\ \sin\phi'}{1+\sin\phi'}$	Jaky (1944)	
$1 - \sin\phi'$	Jaky (1948b)	
$\frac{1}{2}.\frac{1+1/8\sqrt{6}-3/8\sqrt{6}\ \sin\phi'}{1-1/8\sqrt{6}+3/8\sqrt{6}\ \sin\phi'}$	Hendron (1963)	
$1 - 0.987\ \sin\phi'$	Mayne and Kulhawy (1982)	normally consolidated clays
$1 - 0.998\ \sin\phi'$ $1 - 1.003\ \sin\phi'$		cohesionless soils
$0.95 - \sin\phi'$	Brooker and Ireland (1965)	normally consolidated clays
$1 - 1.2\ \sin\phi'$	Schmidt (1966)	normally consolidated clays
$0.9\ (1 - \sin\phi')$	Fraser (1957); in Phillips (1984)	
$0.97\ (1 - 0.97\ \sin\phi')$	Saglamer (1975); in Phillips (1984)	

above equation (Table 3.1); the data of which was re-analysed, and a better fit to the data obtained by Schmidt (1966). Moore and Cole (1977) found a good agreement with Brooker and Ireland's equation for tests on kaolinite, while other workers' tests agree with Jaky's equation (Abdelhamid and Krizek, 1976).

Mayne and Kulhawy's (Loc.Cit.) equations for normally consolidated clays and cohesionless soils (Table 3.1) were obtained from statistical analysis of published values. The equation for cohesive soils accounts for about 75% of the variability observed in the results; the remaining 25% has been attributed to other factors such as initial porosity, plasticity index, liquid limit, and clay fraction, though no relationship could be found for these factors. The structure of the soil has been suggested as a factor affecting K_o though this was not seen to be the case for kaolinite with

flocculated and dispersed structures (Abdelhamid and Krizek, 1976).

The initial void ratio or density of the sample have been seen to affect the measured value of K_o, though this is a result of the variation of the angle of internal friction, (Al Hussaini and Townsend, 1975), however, no effect due to variations in void ratio was found by Moore (1971).

ii) $K_o - \nu$ relationship

The ratio of the horizontal to vertical effective stresses is related to the Poisson's ratio (ν) for a material by the expression

$$K_o = \frac{\nu}{1-\nu} \qquad .. \ 3.2.4$$

This assumes that the properties of the sediment are isotropic, which in most geological cases would not be true. Thus, in an anisotropic material, the relationship between K_o and Poisson's ratio would involve the Young's moduli and Poisson's ratios of the major and minor principle effective stress directions,

$$K_o = \frac{E_h'}{E_v'} \ \frac{\nu_{vh}'}{1 - \nu_{hh}'} \qquad .. \ 3.2.5$$

This was derived for a static case, where ν_{vh} and ν_{hh} are the Poisson's ratios in the horizontal (minor principle effective stress) direction, due to vertical and horizontal loading respectively. (Phillips, 1984).

The above equations are linear elastic solutions; as stated by Teeuw (1971), non linear elasticity is predominant in reservoir

materials and hence Eqn. 3.2.4 for the non linear case becomes,

$$K_o = \frac{\nu}{1-\nu}^{1/n} \qquad .. 3.2.6$$

where n is a measure of the degree of linearity of the elasticity, this being 2/3 for spheres, and unity for the linear case.

3.2.3) Laboratory determination of K_o

The measurement of the coefficient of earth pressure at rest is regularly obtained in experimental studies of soils and commonly reported in the literature, Chap. 3.2.1. The present study was interested in determining K_o in the laboratory, and thus the in-situ measurement of the coefficient of earth pressure at rest will not be discussed.

The laboratory determination of K_o normally involves the axial deformation of a cylindrical sample, whilst maintaining a zero radial (lateral) strain. The various methods of measuring lateral earth stress and maintaining K_o are reported in Abdelhamid and Krizek (1976) and Al Hussaini (1981), and a historical account of the determination of K_o in the laboratory, is discussed by Hellings (1973).

i) Requirements for the K_o test

Due to the definition of the coefficient of earth pressure at rest, the laboratory procedure to determine K_o must be strict. Bishop (1958) details requirements for the experimental determination of K_o; the points raised can be summarised as follows.

1) During the axial shortening of the sample under a condition of zero lateral strain, the boundaries restraining lateral movement

should not set up any shear forces in the sample.

2) The sample used should have a length to diameter ratio of 2:1, thus ensuring no end effects in the sample.

3) The ram used to load the sample should be of low friction. (Hanrahan (1977) used an internal load cell to avoid ram friction problems. Bishop, however, goes on to say that little side friction is induced in the ram during a K_o test).

4) The sample should be homogeneous.

5) Pore pressures should be uniform through-out the sample, i.e. pore pressure gradients are to be avoided.

6) Continuous rather than stepwise testing is to be recommended.

The use of a triaxial cell is therefore recommended for K_o testing since points 1 and 5 are violated in a standard oedometer, though point five can be avoided using a constant rate of strain oedometer (Bishop, 1958; Hanrahan, 1977).

ii) Methods of measuring K_o during zero lateral strain tests

a) Methods of measuring lateral strain in triaxial cells

Measurement of lateral strain in the triaxial cell can be done by various methods, directly or indirectly. The direct methods require actual measurement of the sample diameter, most commonly achieved by monitoring an lvdt which sits in a framework but which is activated by the radial expansion of the sample (Newman and Martin, 1977; Maswoswe, 1985; Maccarini, 1987). Another method of measuring the lateral strain of a triaxial sample is using a strain gauged belt which sits on the sample (Holubec and Finn, 1969; de Waal, 1986; this study App. 1), or a strain gauged cantilever with the strain gauges attached at the fixed end of the lever at the base of the sample. The measurement of lateral strain should be done on the mid

height of the sample; this obviously raises doubts about the fixed nature of the cantilever. The probes of a cantilever system remain at the same height above the base of the sample while during compression the mid-height of the sample decreases. If a framework with a lvdt is used, it must be lightweight otherwise a counter balance is required. The lvdt frames designed for high pressure triaxial cells are normally attached to the base of the sample and also measure axial strains (Newman and Martin, 1977). Recently ultrasonic methods have also been used (Baranski and Wolski, 1986).

Indirect methods of measuring lateral strain include a) equating the axial strain and the drained volume change in the sample (Bishop and Eldin, 1953; Bishop, 1958; Hanrahan, 1977), and b) the use of special cells where the total volume of the sample can be found, using an inner cell in the triaxial confining pressure chamber (Bishop, Webb and Skinner, 1965; Lewin, 1971), Fig. 3.2.

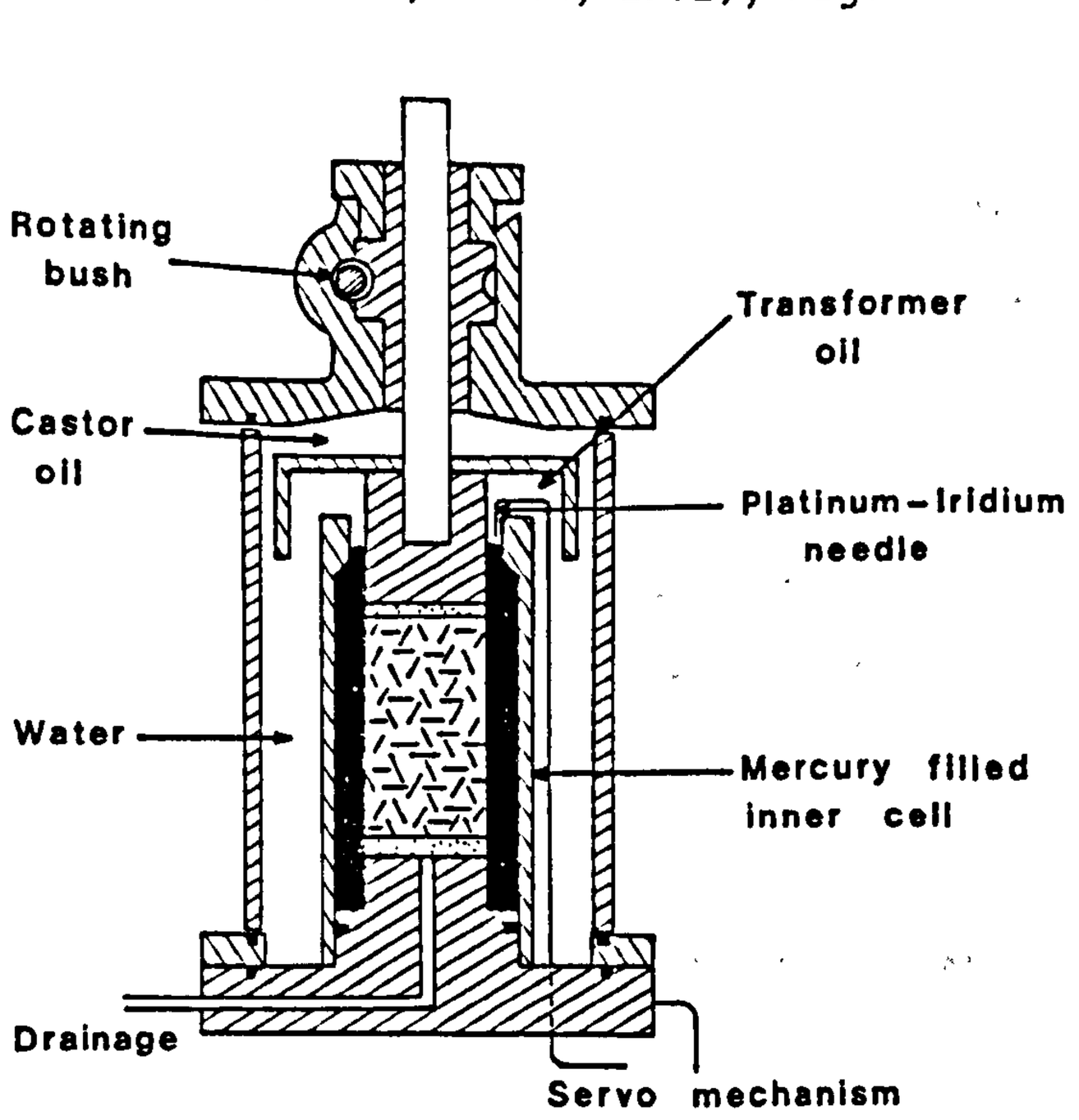

Figure 3.2 Triaxial cell with inner cell for maintaining K_o conditions (After Bishop, Webb and Skinner, 1965).

b) Maintaining zero lateral strain

With the systems described above, the measurement of a radial strain is obtained. This must be reduced to a zero value to maintain K_o conditions; this can be done by adjustment of the stresses. This can be a manual alteration or more desirably can be performed automatically, using either a null indicator (Lewin, 1971), or a servo amplifier or computer responding to a change in voltage from a radial strain belt (Maswoswe, 1985; de Waal, 1986; this study App. 1).

iii) Recommendations for lateral strains during K_o tests

For an accurate determination of K_o, the lateral strain must ideally be maintained at zero. This is impossible in practice, as the systems described above require a strain to be measured, which is then recovered. Therefore, there must be a maximum lateral strain allowable during a K_o test. Schmidt (1967) states that Terzaghi (1934) reports that the transition between earth pressure at rest to a condition of active earth pressure yield for a dense sand required a lateral strain of 10^{-3}, this puts upper bounds for the strain. Bishop (1958) reports that radial strains in a triaxial cell can be measured down to $7.5*10^{-5}$ (for a 4" diameter sample) and, using a mercury filled inner cell, down to $5.08*10^{-7}$m (Bishop, Webb and Skinner 1965). He does not, however, suggest a tolerance for the radial strain.

In oedometer tests Hendron (1963) could maintain lateral strains to $2*10^{-5}$, (Schmitt, 1967). While Brooker and Ireland (1966) maintain K_o in their tests performed on clays, to a circumferential variation of $2.54*10^{-8}$m.

3.2.4) K_o at high stresses

This section will discuss the literature pertaining to high pressure K_o experiments. As discussed in Chap. 3.2.1, K_o can also be derived from values of the angle of internal friction, therefore, values of K_o derived from high pressure determinations of the failure envelope for sediments, will also be briefly reviewed.

i) Previous high pressure K_o experiments

High pressure K_o tests are relatively rare in engineering and geological literature. Experimental studies which measure K_o at high pressures have already been mentioned, these include Brooker and Ireland (1965), Hendron, reported in Schmidt (1967), Bishop, Webb and Skinner (1965), and van Kooten (1986). Other studies reported in the literature included van de Knaap and van de Vlis (1967), Teeuw (1971), van Ditzhuijen and de Waal (1984), de Waal and Smits (1985), de Waal (1986), and Smits, de Waal and van Kooten (1986), however most of these latter cases concentrate on the stress-strain behaviour of the materials tested, as do the studies reported in Rieke and Chilingarian (1974). Studies of normally consolidated clays and sands, show a constant K_o ratio up to stresses of 15.1MPa (2200psi), Brooker and Ireland (1965) and Bishop, Webb and Skinner (1965). The experiments performed by van Kooten (1986) on chalk samples from the Ekofisk region and from onshore sites, do however show variation, Smits et.al. (1986). This is due to the cementation present in the chalks tested by these workers; the variation being similar to that observed in residual soils and sensitive clays, Chap. 3.2.1 (Vaughan, 1985; Kane, 1973; Silvestri, 1981; Leroueil et.al., 1983b; Maccarini, 1987).

ii) K_o derived from angles of internal friction

Few failure envelopes have been investigated at high pressures for sands and clays, notable examples being Bishop, Webb and Skinner (1965) and Bishop, Webb and Lewin (1969), where samples of London clay were remoulded and compacted from a slurry. The angle of internal friction for this material decreases from 19^o at low pressures to 16^o at higher pressures. Using Jaky's equation, this gives K_o of 0.66 to 0.72, increasing with stress. Jaky (1948a) also shows that the failure envelope for sand is curved at high pressures. This has also been shown by Vesic and Barksdale (1963), Hall and Gordon (1963), Hirschfeld and Poulos (1963), Bishop, Webb and Skinner (1965), Lee and Seed (1967), Vesic and Clough (1968), and Hall and Harrisberger (1970). Hall and Harrisberger (1970) showed that at low stresses, sands have different angles of internal friction, however, at higher stresses where grain crushing has occurred, the angle of internal friction is less varied and approximately equal to 29^o; this is equal to a K_o of 0.51.

From the above discussion of the published literature, it can be concluded that the one-dimensional consolidation of materials is most accurately performed in a triaxial cell with a constant loading rate, which is slow enough to allow full dissipation of excess pressures generated by the loading. The accuracy in maintaining the zero radial strain condition however has not been studied, this factor is obviously of great importance. In this study measurement of the radial strain was performed at ambient and elevated temperatures using a strain gauged radial strain belt, App.1.

Factors and relationships such as the effect of elevated temperatures on K_o have not been studied, and the extension of Jaky's

relationship in the high pressures used in this study have not been investigated. The work on cemented materials shows that a change in the values of K_o and $\bar{K}_o$ can be expected during the compaction of chalks.

3.3) CONSTANT RATE OF STRAIN TESTS

3.3.1) Introduction

In order to understand compaction in sediments and weak rocks, the magnitude of strain resulting from increases in the effective stress and its time dependancy must be found. The necessity to obtain fundamental parameters of sediment compaction, and monitor their variation through simulated burial requires that the coefficient of consolidation (C_v), the coefficient of volume compressibility (M_v) and the coefficient of permeability (k) are evaluated from the constant rate of strain experiments, Chap. 3.2 (as opposed to oedometer testing-the standard method of obtaining these parameters (Head, 1982; Vickers, 1983; BS 1377)).

The requirements of the K_o test listed in the last section suggest that the test should be performed in a triaxial cell with a steadily increasing load, the rate of loading being slow enough to enable any excess pore pressures remote from the drainage to dissipate. The latter requirements are accommodated by the controlled gradient test and by the constant rate of strain test. These are two testing procedures introduced to soil mechanics as alternatives to the standard oedometer tests, (Leonards and Girault, 1961; BS 1377) . The controlled gradient (CG) test is performed on an oedometer-type sample but with constant loading rather than the incremental loading of standard tests. The loading is controlled by the pore pressure at

the undrained or impermeable boundary, a servo loop being used to control the rate of loading, to maintain a constant pore pressure gradient across the sample. The constant rate of strain (CRS) consolidation is similar to the CG test in that oedometer samples are generally used. However, in the CRS test, the loading rate is kept constant and the excess pore pressure is allowed to vary. This is more convenient to use as it only requires the use of a loading frame with a range of loading rates (Gorman et.al., 1978) .

In this study the CRS test was used due to the availability of a loading frame with a large range of strain rates. The loading frame used was a 498 KN (50 ton) loading frame with loading rates varying from 0.9999mm/min to $1*10^{-6}$mm/min. The zero radial strain condition for one-dimensional consolidation and K_o was initially maintained by manual adjustment of the cell pressure, in later experiments a servo loop controlling the cell pressure was employed (App. 1).

3.3.2) Interpretation of the CRS test

The constant rate of strain is a misnomer, and should be referred to as a constant rate of deformation test, as the loading piston is brought down at a constant rate (hence the strain rate increases as the test proceeds). However, due to the compression of the loading system, a constant deformation rate is not obtained. Since the variation in the strain rate is very small at the strain involved in normal consolidation, the term "constant rate of strain" (which is well established in the literature), will be retained here.

The boundary conditions for CRS consolidation testing differ from the standard oedometer increment loading and hence the interpretation of the former test results requires a theoretical analysis of the consolidation, with due account of the boundary conditions.

Several approaches have been formulated with the aim of obtaining C_v from the tests. This being one of the most important parameters obtained from standard oedometer tests. Knowing the coefficient of volume compressibility (M_v), and the specific gravity of the pore fluid, the permeability can be calculated, if the C_v is known.

The CRS test is a one-dimensional consolidation test with constant straining rate of the sample. In most tests an oedometer type sample is used in an oedometer ring to restrain any lateral deformation. Drainage generally occurs from one end of the sample, the other being undrained. Pore pressure measurements at both ends of the sample are required. The movement of the piston is monitored by a displacement transducer or a dial gauge. In the theoretical analysis of CRS tests, the variables involved must be restricted to the those which are measurable in the experimental apparatus during the period of the test.

Quantitative evaluation of the CRS test was initiated by Smith and Wahls (1969); subsequently several workers have approached the problem (Wissa et.al., 1971; Lee, 1981; Znidarcic et.al., 1984; Znidarcic et.al., 1986). The approaches have assumed a homogeneous sample, with both the sediment grains and the pore fluid being considered incompressible. These assumptions are derived from the conventional consolidation theory of Terzaghi, Chap. 2.4.

The following section briefly presents the three main relationships used to calculate values of C_v from CRS tests. The brevity of the discussion is due mainly to the limited use of the analysis in this thesis, as well as the complex nature of the formulations of the relationships. The reader is referred to the above mentioned papers for the individual analyses, and to the excellent review in Znidarcic et.al. (1984).

Smith and Wahls (1969) formulate an analysis based on assumptions used in Terzaghi's consolidation equation (Chap. 2.4), to obtain Eq. 3.3.1.

$$C_v = \frac{rH^2(1/2 - b/12r)}{a_v . U_b} \qquad .. \ 3.3.1$$

Where r = the change in average void ratio with time; H = height of sample; b = a constant which depends upon the variation in void ratio with depth in the sample and time (b/r ranging from 2 to 0); U_b = excess pore pressure at the undrained end of the sample; and a_v = the coefficient of compressibility ($de/d\sigma_1'$).

This relationship was seen to agree well with experiments performed in standard oedometer tests, so long as the U_b/σ_1 ratio did not exceed 50%. The main criticisms directed to this derivation are that a linear variation in voids ratio in time and space are invoked, which may not be justified, and secondly the b parameter is not known and its determination is not discussed (Znidarcic et.al., 1984).

Wissa et.al. (1971) describe an analysis of the CRS test based on a strain equation for consolidation. Relationships for two stress-strain theories are then incorporated into the analysis,

1) $M_v = \Delta\varepsilon/\Delta\sigma_1$

2) $-de = C_c . \ d(\log \sigma_1')$

the first being a linear and the second, a non-linear stress-strain theory for sediments. The resultant expressions for C_v are, for the

linear theory,

$$C_v = \frac{rH^2}{2U_b.M_v} \qquad .. 3.3.2$$

and for the non-linear theory,

$$Cv = \frac{-0.434\ rH^2}{2.\sigma_v.M_v\ \log(1 - U_b/\sigma_v)} \qquad .. 3.3.3$$

where U_b/σ_v is averaged over a time interval Δt. Wissa et.al. (Loc.Cit.) show that the variation in C_v calculated from the two stress-strain relationships tend to diverge at large U_b/σ_1 values and therefore suggest that this ratio should not exceed 5%. In comparison with oedometer test results their analysis gives good results. Criticisms of the Wissa analysis are that it assumes a steady state condition during the loading, purely on the assumption that C_v in the sample is constant, whereas this is not the case. This analysis also considers that M_v for the linear and C_c for the non-linear case are constants (Znidarcic et.al., 1984).

The previous analyses have been based on a Terzaghi type consolidation equation, consequently they are valid for small strain consolidation (Gibson et.al., 1967; Gibson et.al., 1981). Some reported tests that have used these analyses have strains of 20%. Lee (1981) formulates a relationship for a finite strain analyses, using a moving boundary theory of consolidation, which considers a dynamic frame of reference following the method of Gibson et.al. (1967; 1981). The resulting equation is

$$C_v \simeq \frac{h^2.\Delta\sigma_1}{2U_b.\Delta t} \qquad .. 3.3.4$$

where h is the current thickness of the sample. This equation defines C_v for the drained end of the sample, C_v for the undrained end of the sample is given by,

$$C_v \simeq \frac{h^2.(\Delta\sigma_1 - \Delta U_b)}{2U_b.\Delta t} \qquad .. 3.3.5$$

The first assumption by Wissa of a constant C_v is also incorporated in the derivation of the finite strain theory of Lee, together with a infinitesimal strain assumption to generate parabolic strain isochrones. This analysis is restricted to small strains and to times greater than T_v>0.5 (Znidarcic et.al., 1984).

Theoretical analyses of constant rate of strain tests have produced similar relationships for C_v, the difficulty being to produce a relationship that is generally applicable using parameters which are measured in the laboratory test. The similarity is also partly a result of the mathematical difficulties and assumptions of material properties that are incorporated in the analyses.

The Wissa analysis was used in this study, as the value of M_v was required from tests with and without excess pore pressure generation. The Lee (1981) analysis calculates the M_v from the C_v, thus, since pore pressure generation is required to compute the C_v this method of M_v determination can not be used on all tests in this study. Both analyses show a variation of results dependant upon the stress interval used in the calculations and the values can therefore only be considered as qualitative.

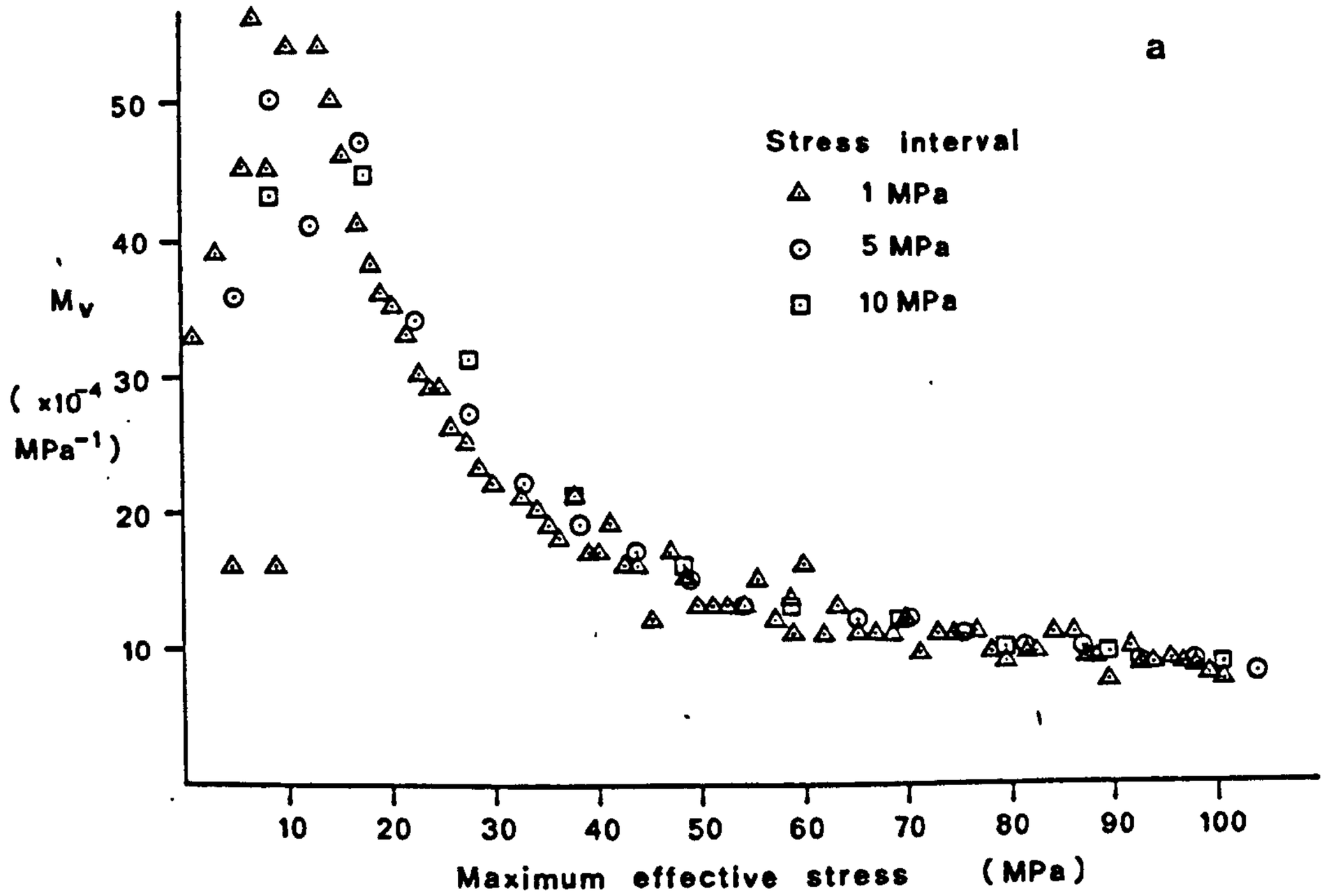

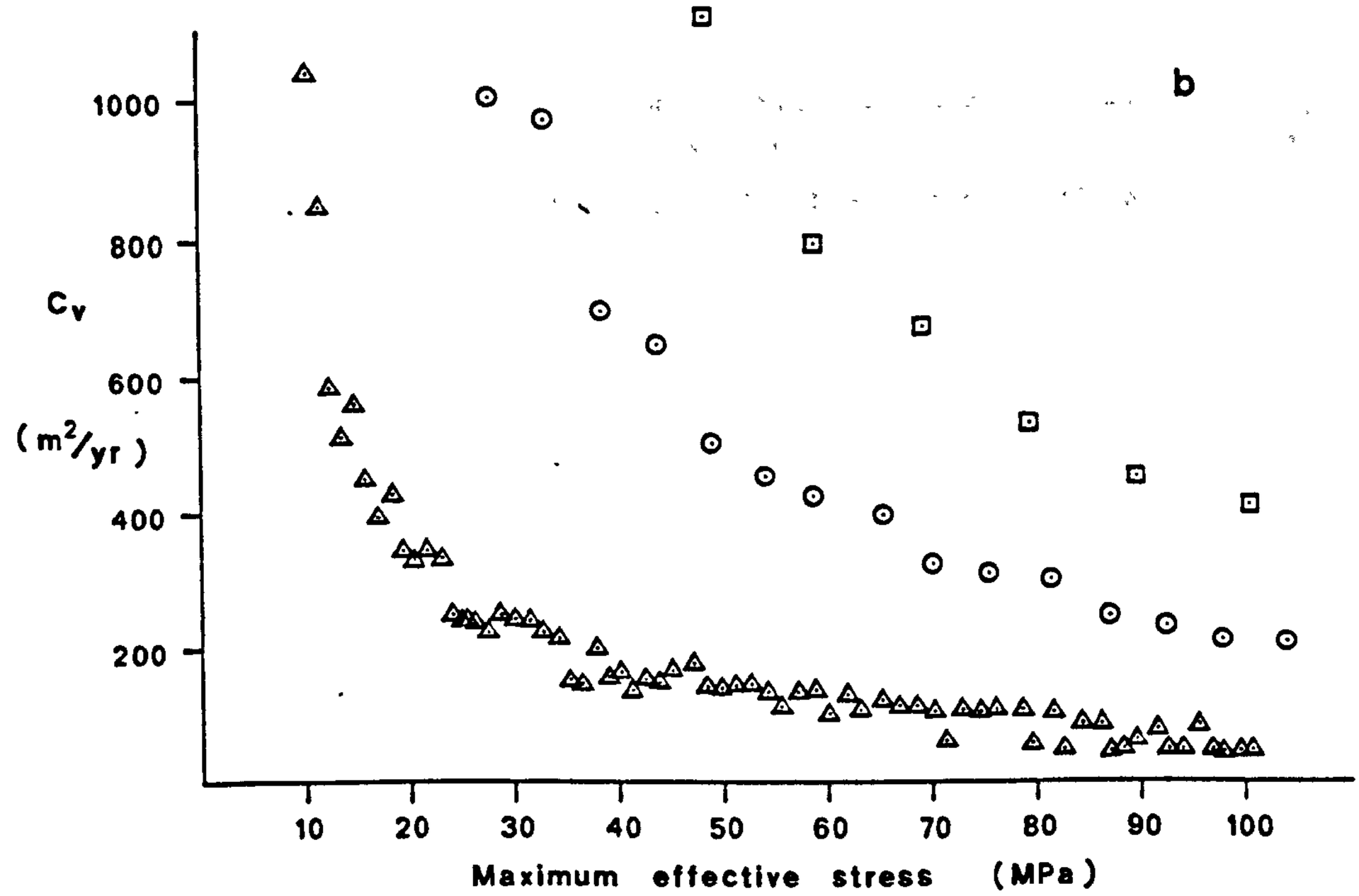

Figure 3.3(a-c) Effect of stress interval on the Wissa analysis.

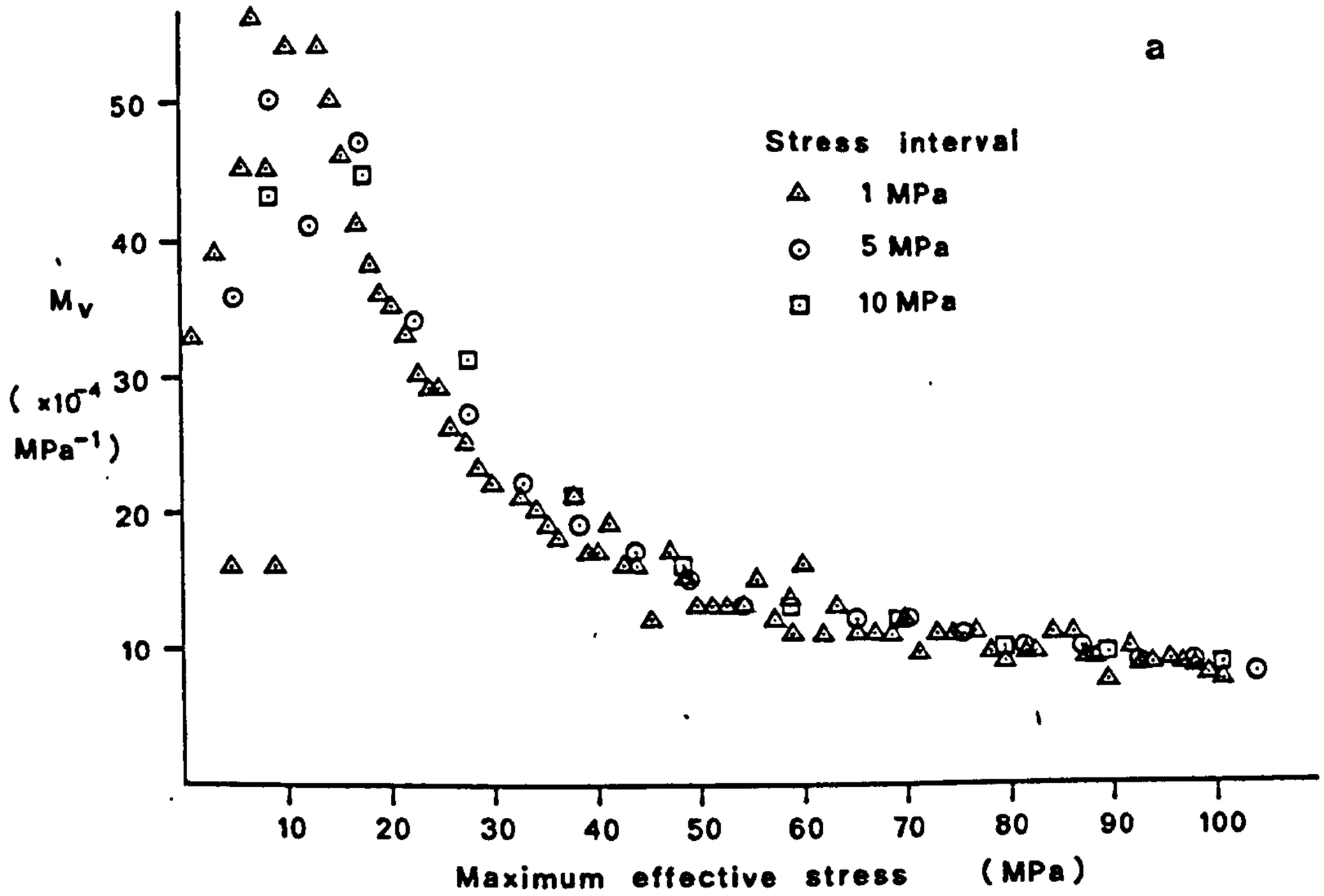

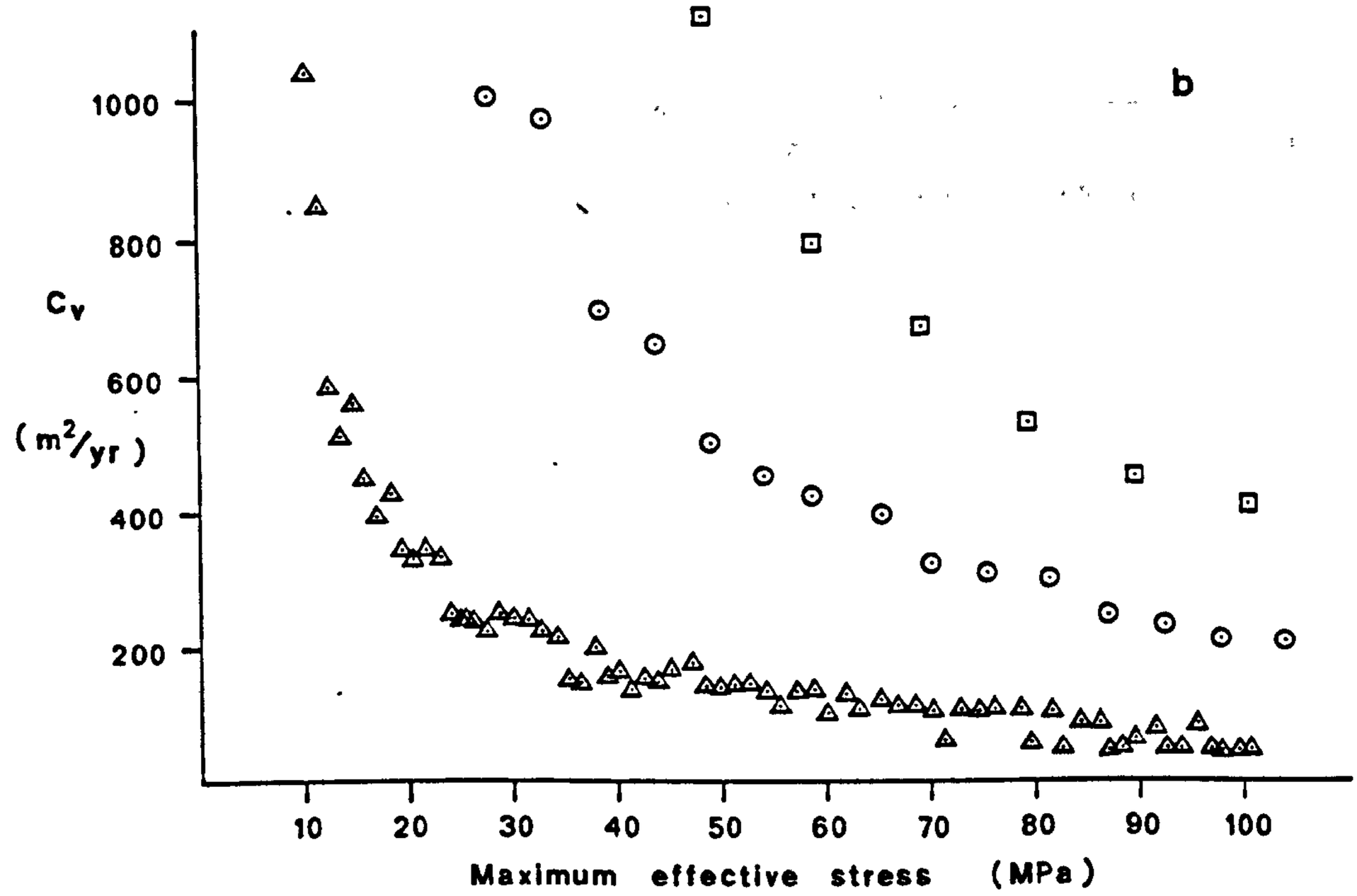

Figure 3.3(a-c) Effect of stress interval on the Wissa analysis.

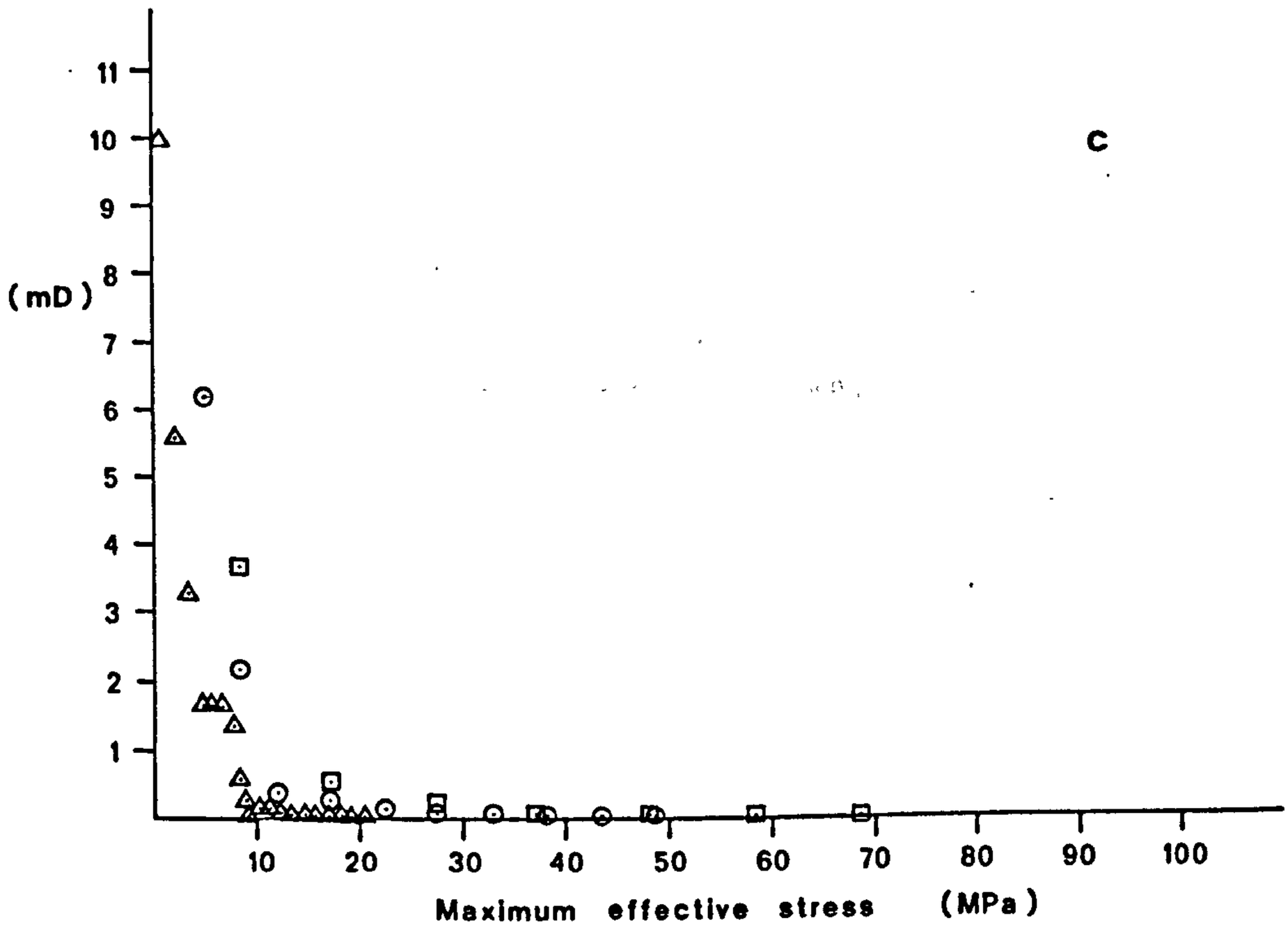
11
10
9
8
7
6
5
4
3
2
1
(mD)
C
10
20
30
40
50
60
70
80
90
100
Maximum effective stress (MPa)

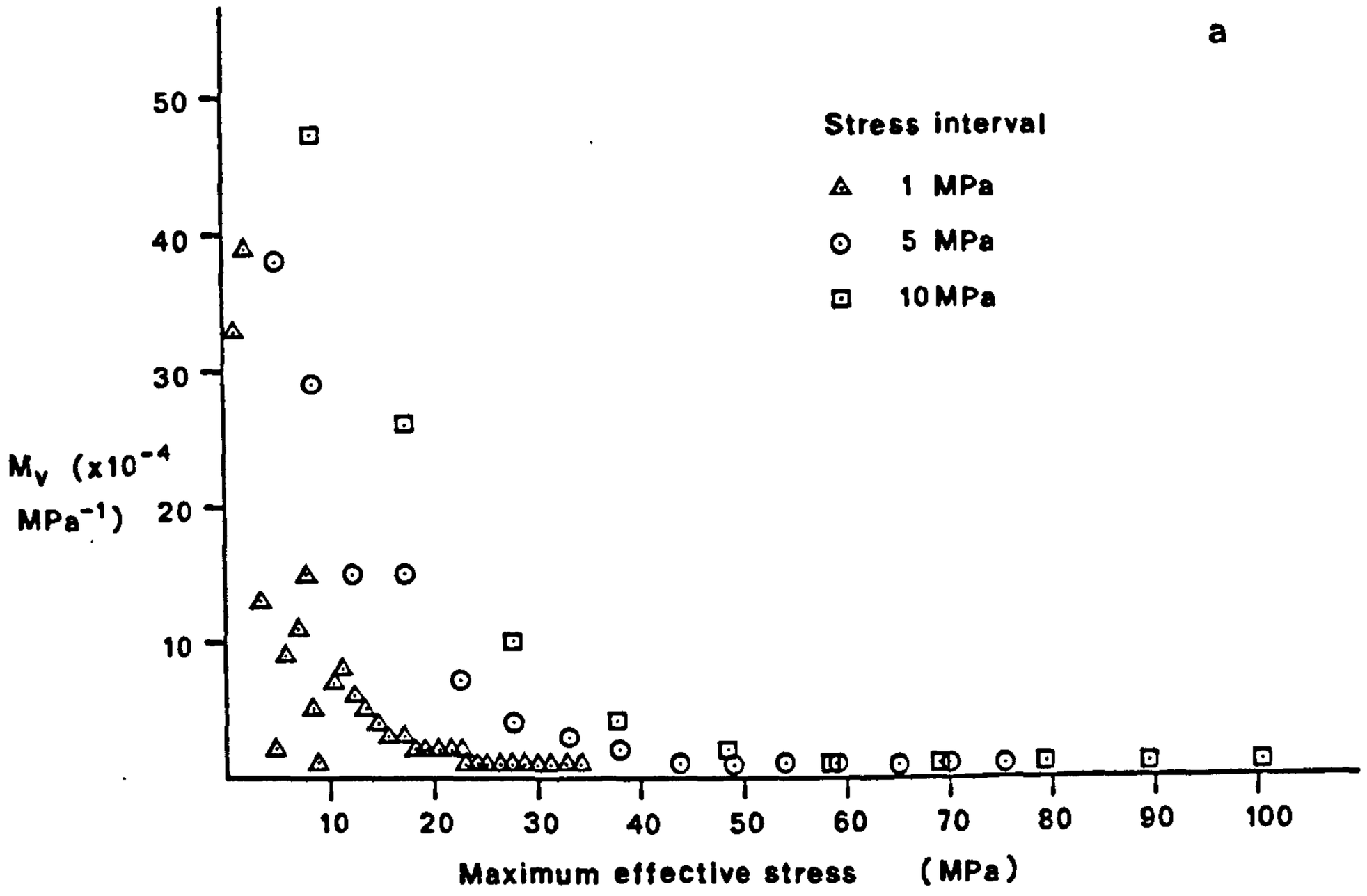

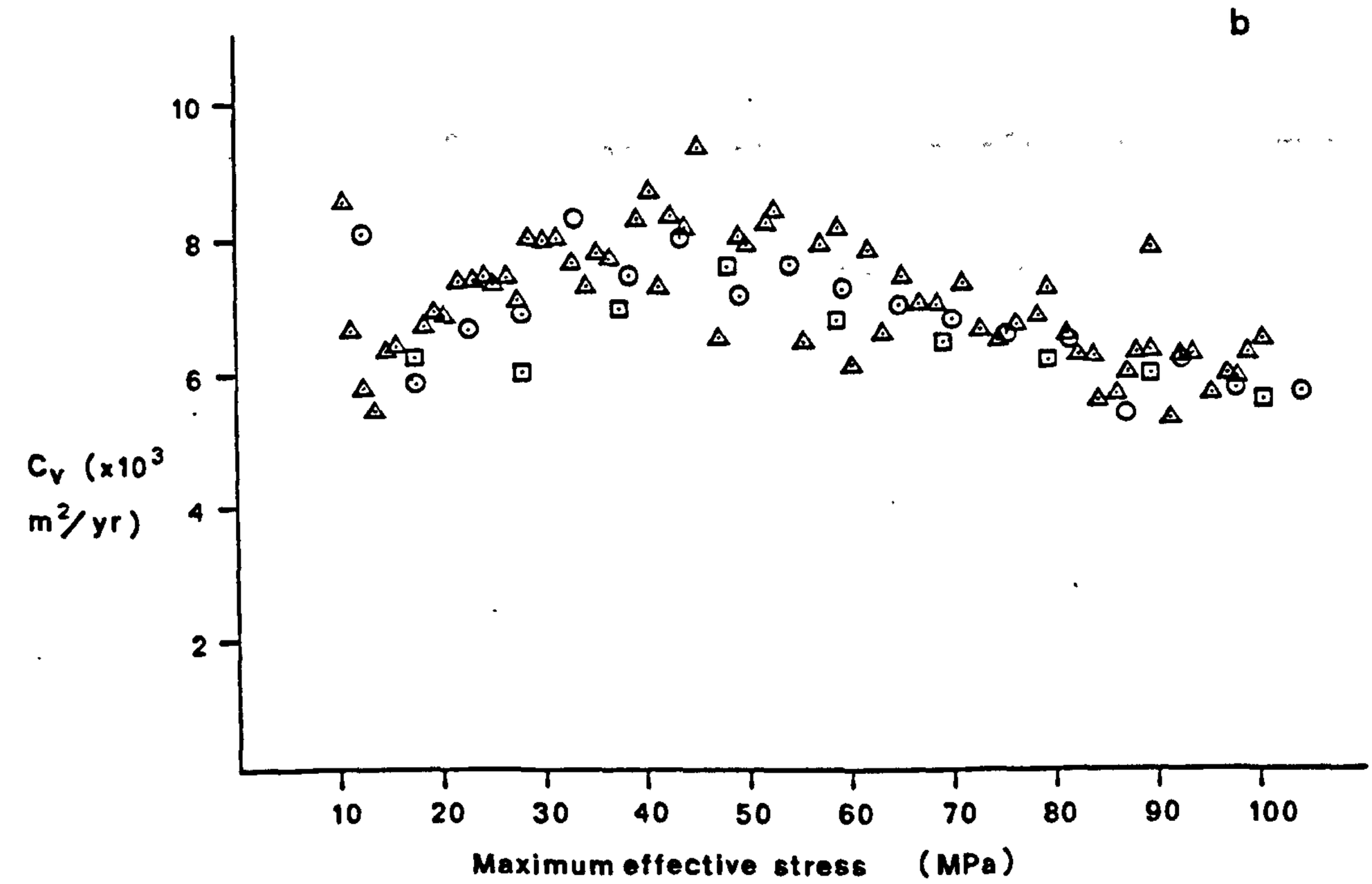

Figure 3.4(a-c) Effect of stress interval on the Lee analysis.

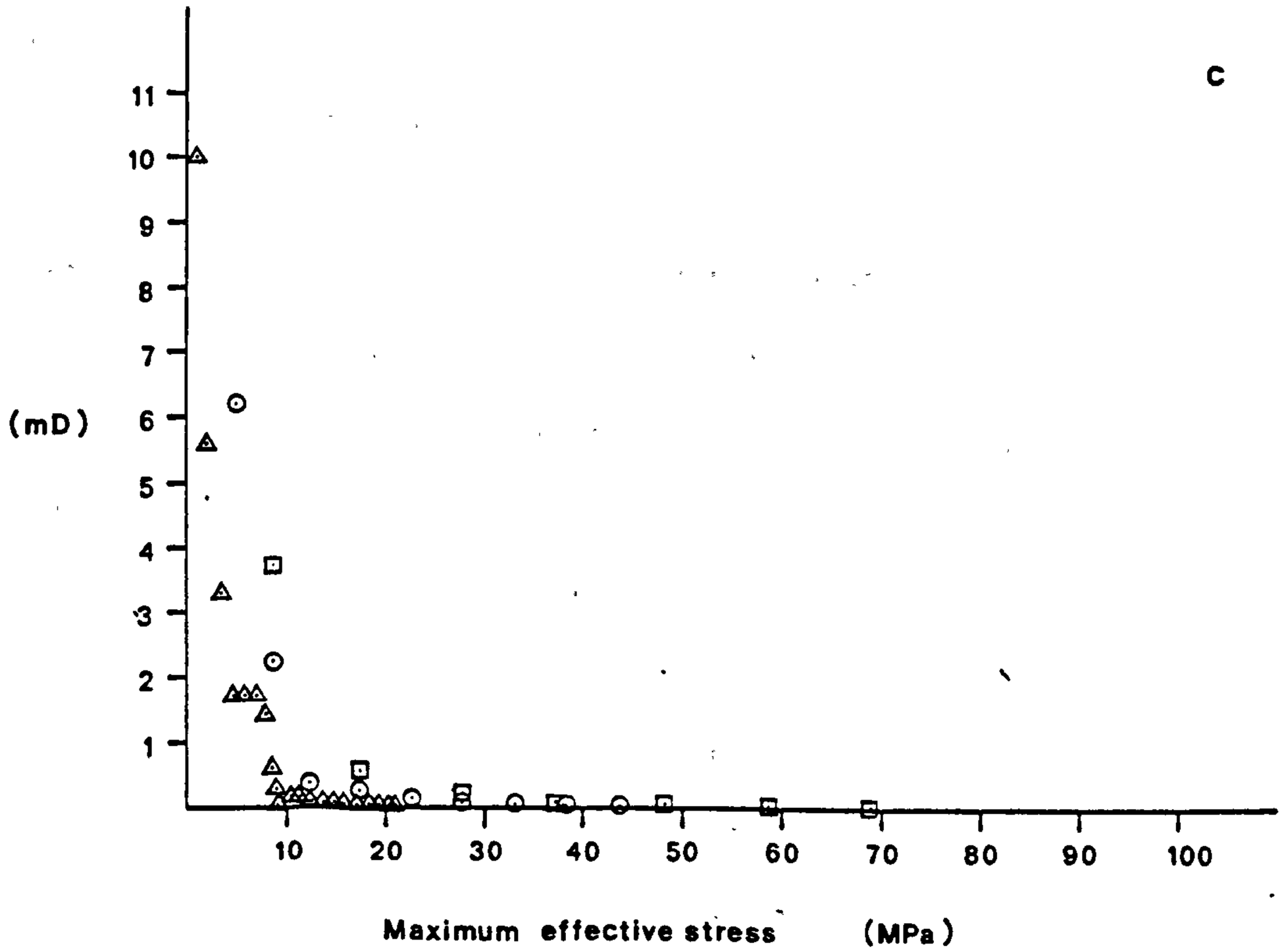
C
11
10
9
8
7
(mD)
6
5
4
3
2
1
10
20
30
40
50
60
70
80
90
100
Maximum effective stress (MPa)

The Wissa analysis and the Lee analysis were applied to one test performed in this study to assess the difference in the analyses. The M_v, C_v, and permeability variations are shown in Figs. 3.3 and 3.4 (plotted against vertical effective stress) for the two analyses for stress intervals 1, 5 and 10MPa. The results of the Lee analysis give higher values than the Wissa analysis, and are more consistent for stress interval variations, Fig. 3.4. Selection of the most representative values can only be obtained by standardizing the results using conventionally measured permeabilities.

3.4) COMPACTION TESTS IN THE HIGH PRESSURE OEDOMETER

Results from the oedometer test can be variable depending upon height to diameter ratio, pore fluid, side friction, temperature, duration of increment and loading increment ratio. The height to diameter ratio has been recommended to be 1/4 (Som, 1968) to reduce side friction which is also reduced by lubricating the side walls; the temperature is usually recorded to enable a correction to be made for C_v. Normally, water is used as a pore fluid. The main areas of contention still remaining are therefore, the loading increment ratio and the duration of the stress increments (Leonards and Girault, 1961; Som, 1968; BS 1377, Vickers, 1983). The standard loading ratio ($\Delta P/P$) is 1 i.e. the load is doubled for each increment, the load normally being applied for 24 hours (BS 1377; Vickers, 1983). This is, however, a purely arbitrary time period and with different soils primary consolidation may occur very quickly or may not be complete in the 24 hour period. This leads to differing degrees of secondary consolidation and stiffening (Graham, Crooks and Bell, 1983; Mesri and Choi, 1979; Mesri and Feng, 1986). For cemented soils Lerouiel et.al. (1983a; 1983b), use a load increment ratio $\Delta P/P = 0.5$, and

show that a higher Pc' is obtained from tests where the increment duration is equal to the time to the end of primary consolidation (E.O.P.), rather than the 24 hour increment duration (Chap. 2.7).

In this study, the oedometer was used to obtain the consolidation characteristics of the chalk by an alternative method to the triaxial cell. The load increment ratio used in the oedometer test was 0.5, as recommended by Leroueil et.al. (1983a; 1983b), this was chosen so that the yield point could be determined more accurately than with a load increment ratio of 1. The duration of the loading increment was approximately 18 hours, the choice of this was purely arbitrary, as the primary consolidation of the approximately 2.5cm thick sample of chalk was normally over in less than ten seconds.

3.5) MATERIALS USED IN THIS STUDY

3.5.1) Introduction

The materials used in this study include two onshore chalks from south east England and offshores chalk from the Greater Ekofisk area in the Central North Sea. These chalks have a range of porosities between 30-45%, and should be representative of high porosity chalks. The clays tested were obtained from wells in the Greater Ekofisk area of the Central North Sea. The materials have been tested in parallel with a study into the compaction and subsidence of the Ekofisk oil field due to the withdrawal of pore fluids (Jones et.al., 1985a; 1985b; 1986).

3.5.2) The geology of chalk

i) General description

Chalk is a fine-grained sedimentary rock which is generally white

or grey in colour; it is a carbonate sediment with low magnesium calcite as its primary mineral phase. Large areas of chalk exist onshore in England and France, a large percentage of this chalk containing <2% of the bulk volume of minerals other than calcite (Hancock, 1975). The chalk in north western Europe accumulated in a variety of depositional modes and contains many structures upon which the relative percentages of impurities depend, the pelagic sediment being the purest form. The common absence of detritus in these chalks points to the deposition of the chalk of north western Europe at a time of eustatic rise in sea-level, accompanied by an arid climate. This severely restricts any possible erosion of the small areas of land mass above sea level at this time. The minerals that do occur as insoluble residue in chalks are a) clays, both depositional and authigenic (Hancock, 1975), b) silica and iron oxides, often in finely dispersed aggregates (this does not include silica predominant in flint bands which is thought to be due to a supersaturation of silica in sea water in areas of high organic content (Hancock, 1975; Clayton, (pers.comm.)) and c) phosphates (Hancock, 1975). The time of deposition of the chalks in north western Europe ranges from the Cenomanian in the Cretaceous (95MY) to the Danian in the Palaeocene (60MY).

The main source of calcite comprising the chalks, occurs as broken laths which form rings or discs called coccoliths; these are disaggregated spheres of the golden brown algae Haptophycaea. The Haptophycaea are digested by copepods, whose faecal pellets contain tens of thousands of coccoliths which are deposited on the sea floor. The coccospheres comprise up to 20 coccoliths and are roughly 13 microns across, the coccolith discs being about 5 microns in diameter. The spheres degraded into the coccoliths during settlement.

Further break up is triggered by initial compaction, causing the coccoliths to split into their composite laths (0.5 - 1 micron long). This is the dominant grain size in chalk, larger particles being derived from skeletal remains of foraminifera and macrofossils (Hancock, 1975; Hancock (in Glennie, 1984)).

Due to the open and granular nature of the chalk sediments, they commonly have a high porosity ranging from 25 - 47%. The initial depositional porosity is about 70% and an early cementation, can maintain an open structure; with evidence of carbonate cementation at less than 200m burial (Datta et.al., 1982). Because of the small grain size, pores and pore throats are resultantly small, which dictates that matrix permeabilities (approx. 2-20mD) are small in relation to the porosity; smaller porosities and permeabilities occurring with increasing overburden pressure, if natural overpressures and hydrocarbon influx do not prevent compaction and cementation (Hancock, 1975; Scholle, 1977).

The chalks in north western Europe were deposited in sea water of normal salinity (35ppt) with depositional rates varying from 3.5 $m/10^6$ years (Cenomanian of Norfolk) to 117$m/10^6$ years (Maastrichtian chalk in the Danish trough). Some doubt is inherent in these figures. Chalk is deposited in 100 - 600m of water i.e. on a continental shelf due to eustatic sea level rise in the upper Cretaceous, though extremes of chalk deposition are estimated to vary from 20 - 4000 metres (Hancock, 1975; 1983; Kennedy, 1983).

Steady pelagic sedimentation of the chalks leads to regularly-bedded strata which has been deposited over large areas, and breaks in sedimentation lead to omission surfaces and hard grounds (Hancock, 1975). Structures, such as banks up to 50m high have been reported in northern France (Skovbro and Kennedy, 1985),

and when the chalk is deposited on slopes, slumping of the deposits can occur possibly activated by tectonism. Also, debris flows, mudflows and turbidites are common, these structures are seen in the Greater Ekofisk area of the Central North Sea where they are associated with fault movement. Chalks often contain many forms of burrowing and boring animals which can severely disrupt the primary fabric of the deposit (Hancock, 1975; 1983; Kennedy, 1983; Skovbro and Kennedy, 1985). The geology of the chalks used in this study will now be discussed.

ii) Ekofisk area chalk.

The chalk in the Central North Sea will be discussed with emphasis on the chalk in the Greater Ekofisk group of oil fields. The major oilfield in this region is the Ekofisk field which is a large elongate dome with an areal closure of $49km^2$, the long axis trends north-westerly and the structure is formed above a salt diapir which became active at the end of the Maastrichtian. The halokinetic movements continued through and after the Palaeocene; this is seen by thinning at the structural crest and by post lithification fracturing (Byrd, 1975).

The chalk occurring at depth beneath the Central North Sea consists of 4 main sedimentary cycles comprising: 1) Rodby and Hidra formations, 2) Plenus Marl formation to the top of the lower Hod, 3) Middle and Upper Hod and the Tor formation, 4) Ekofisk formation. The Ekofisk reservoir consists of two of the four cycles given above. The two cycles can be considered as hydraulically separate since the base of the upper cycle (Ekofisk formation) is a low porosity 'barrier' of silica and carbonate cemented chalks and marls; this is called the Ekofisk 'Tight zone'. Thus the field can be divided into an upper and

lower reservoir. The lower field, part of cycle 3, consists of the late Campanian to late Maastrictian Tor formation which varies in thickness from 762 to 914 meters, but only the top 76m is of interest as an oil reservoir. Interpretation of the cores and seismic logs suggests that this is a series of major debris flows, succeeded by a progression of distally-stacked turbidites to intraclastic debris flows; these are followed by a thick sequence of slumped chalks at the top of Tor Formation. Pelagic deposition occured between mass movements, some of which have been caught up in the slump folding. The source of the material involved in the mass movements is thought to have come from the north east. Burrowing occurs throughout the Tor sequence. The change from the Tor to the Ekofisk formation varies across the greater Ekofisk area; in the area of the Ekofisk field the boundary consists of a debris flow with Maastrictian clasts and a shaly matrix.

The Ekofisk formation is the 4th cycle and depositional regime, the unit being 137m thick. The base of the Ekofisk formation is condensed, and called the 'tight zone'; it is a rhythmically bedded argillaceous limestone marl alternation in which the clay content increases to in excess of 48%. This is interpreted as large debris flows or turbiditic calcarenite, followed by terrigenous clay rich periodites (Skovbro and Kennedy, 1985) with minor turbidites. These sediments are overlain by a debris flow of Maastrichtian material (30-80m thick) which is referred to as the 'reworked zone' (Kennedy, 1983; Skovbro and Kennedy, 1985). The movement of material in this zone is thought to have been triggered off by fault movement in the area. Small disturbed periodites overlie this zone and continue the tight zone, but with increasingly less terrigenous material up the succession.

Table 3.2

Sample	Porosity %	Perm. mD	Insoluble residue %	Description and enviroment
EC1.50	34.8	3.0	-	Homogeneous chalk with shearing and plastic deformation. Steep dips point to slump folding.
EC2.50	43.5	7.2	-	Homogeneous chalks with debris flows.
EC3.20	35.8	5.5	3.1	Homogeneous chalks showing faint burrow mottling. Some laminations and plastic deformations - mudflows.
EC4.50	41.2	5.3	38.1	Spectacular slump complex with dips upto 50^{o} - debris flow with clasts of lower Ekofisk periodite.
EC5.20	~40	-	1.6	Allochtonous chalks, some laminations and plastic deformations, mudflows and slumping rare debris flows with Maastrichtian material
EC6.20	~36	~2.0	13.3	Upper Ekofisk member - debris flows with some plastic deformation.
EC7.130	36.6	2.4	-	Upper Ekofisk member - clast free flows seperated by burrowed ommision surfaces. Indication of internal shear and plastic deformations.
EC8.20	40.9	-	11.9	Upper Ekofisk member - clast free allochtonous chalk units with internal flow and shear structures. 27' below Maureen formation.
EC9.20	37	-	-	

The boundary between the upper and lower Ekofisk formation is gradational and is accompanied by an increase in calcitised sponge spicules and numerous radiolaria. The upper Ekofisk unit is normally featureless but large slumps and slides have been proposed in the general area. In the Ekofisk field a slump complex with evidence of bioturbation and high porosity called the 'porous zone' occurs (Skovbro and Kennedy, 1985).

The top of the Ekofisk formation grades with increasing clay content into a marl and into the overpressured cap rock shale of Maureen formation age (Skovbro, 1983; Byrd, 1975; Kennedy, 1983; Skovbro and Kennedy, 1985).

The description and enviroment of the chalks obtained from the Central North Sea, that were tested in this study, was obtained from Skovbro and Kennedy (1985). A summary of the samples tested from the Central North Sea are presented in Table 3.2.

iii) Pegwell Bay chalk

Pegwell Bay is situated in the south of the Isle of Thanet region of Kent. The Isle of Thanet area is a post-Eocene anticline trending roughly east-west. The steeper side of the fold is in the south, with dips of 8-10^{o} to the south-west, while there are some minor flexures occurring on the northern limb. Faulting is of minor importance in the area, while fractures follow a general north-westerly trend (Bevan and Hancock, 1986), though a more general distribution of fractures was presented by Cawsey (1977).

In this area of Kent the chalks belong to the Middle and Upper Chalk groups, the zones being:

SANTONIAN	Marsupites testudinarius - Marsupites band - Uintacrinus band	UPPER CHALK
CONIACIAN	Micraster coranguinum	
	Micraster cortestudinarium	
TURONIAN	Holaster planus - Hyphatoceras reussianium	
	Terebratulina lata	MIDDLE CHALK

In the Pegwell Bay area the chalk rises from beneath the Thanet Beds at an angle of 8^{o} dipping to the south-west. The succession consists of a brownish-grey laminated flint band, 2.5-7.5cm thick below which is a maximum of 5.5m of lower beds of the Marsupites band of the Marsupites testudinaria zone. 0.6m below this Uintacrinus remains are common. Approximately 270m east of the tunnel by little Cliffsend, the Marsupites zone base is seen, marked by iron-stained chalk of the Barrois sponge bed. 6.4m below the Barrois sponge bed occurs the Whitacker "3 inch" flint band; the north-easterly rise of the beds is seen in the cliffs.

The area the samples were obtained was just west of the Western Undercliff drive (G.R. 36656408), where the Whitacker "3 inch" flint band occurs near the cliff top about 18m above o.d., with Bedwell's columnar flint band occurring 6.7m above o.d.. The wave-cut platform at the base of the cliff is also of the Coranguinum zone (Ordnance Survey sheet TR 36 SE, 6":1 mile) the base of which is found in this area 85m below the Barrois sponge bed.

The Micraster coranguinum chalk is a white chalk containing a larger percentage of flints than any other zone in this region. Above the lower 12m of this zone the chalk is 'harsh to the touch' and the

remainder is soft and homogeneous with occasional thin yellowish and rusty sub-nodular bands containing skeletal remains. The chalk is very pure with insoluble residues reported at 1.206%. The top of the chalk in the Pegwell Bay region consists of the lower 5.4m of the Marsupites band, the remainder being eroded away and now overlain by the Eocene Thanet Beds.

The above description of the Pegwell Bay geology was abstracted from the Geological Survey memoir (Osborne White, 1928), which should be referred to for further details, with the Geological map of the area, sited above.

The Pegwell Bay chalk used is exceptionally pure with dissolution results giving approximately 96% $CaCO_3$, the X-Ray diffraction profiles on the whole rock show this purity, with all the peaks corresponding to calcite, Fig. 3.5.

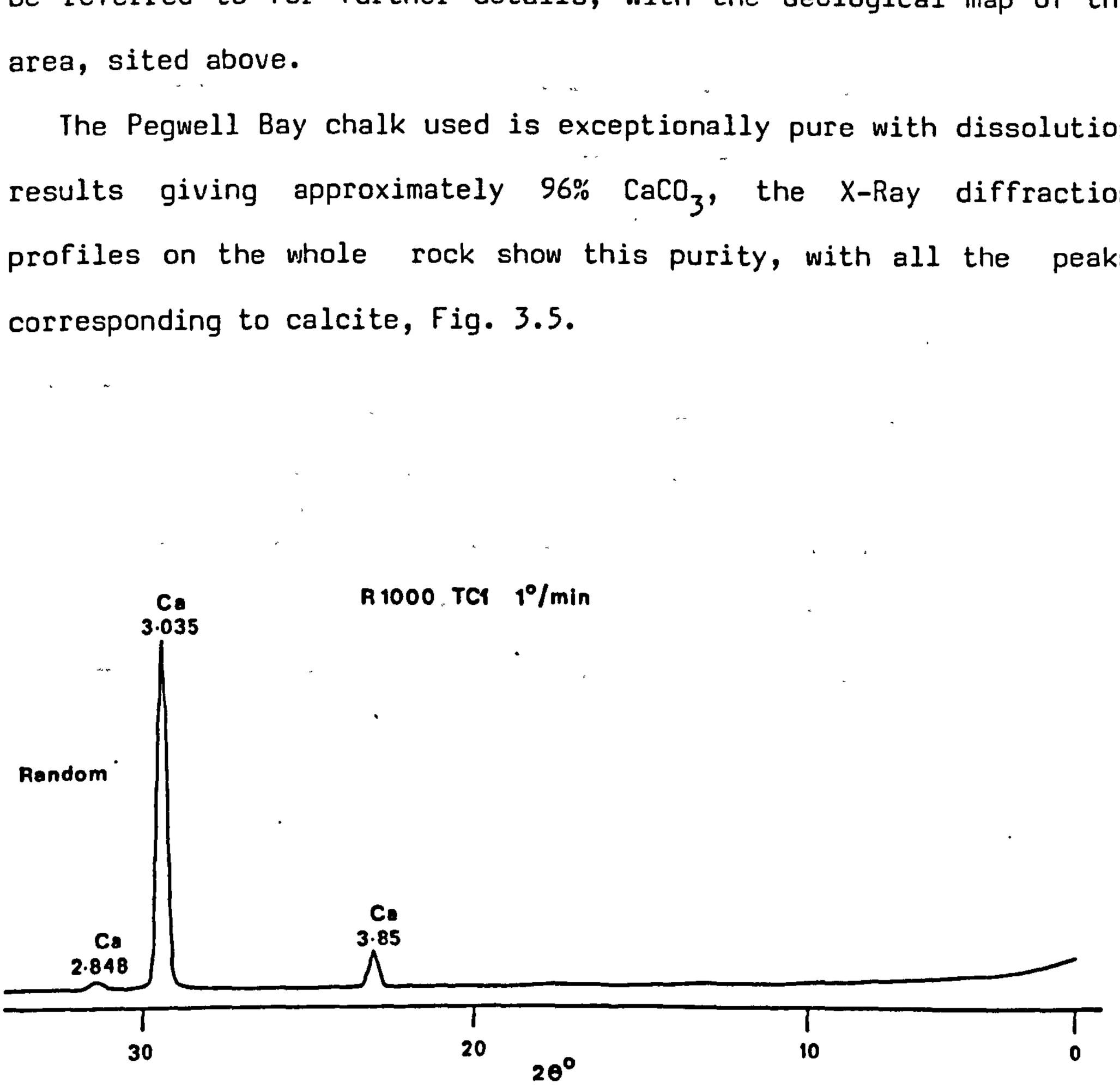

Figure 3.5 X-ray diffraction trace of Pegwell Bay chalk.

iv) Butser Hill chalk

Butser Hill is in Hampshire, south of Petersfield. Its top is 271m above o.d. and lies at the westernmost edge of the South Downs. The area has the regional trend of the Wealden Anticline, with the strata dipping to the south-south-west. However, in the area of sampling, there is a minor fold or flexture running between South Harting and Butser Hill, which is interpreted as a small anticline.

In this area Upper, Middle and Lower chalks occur, the zones found in the area are:

CAMPANIAN	Belemnitella mucronata	UPPER CHALK
	Actinocamax quadrata	
SANTONIAN	Marsupites testudinarius - Marsupites band - Uintacrinus band	
CONIACIAN	Micraster coranguinum	
TURONIAN	Micraster cortestudinarium	
	Holaster planus	
	Terebratulina lata	MIDDLE CHALK
	Rhynchonella cuvieri	
CENOMANIAN	Holaster subglobosus (actinocamax plenus - at summit of the zone)	LOWER CHALK
	Schloenbachia varians	

The samples were obtained from the Butser Hill (Petersfield) Lime Works, 45m north east of some derelict buildings on the northern side of the quarry site. The quarry entrance is on the east side of the Portsmouth to Guildford road (A3), at the northern end of the deep cutting 0.16-0.32 km south of the 15th milestone, to the east of Butser Hill.

The Geological Survey Memoir is confusing concerning the area of sampling, but the sheet, Hamps 60 NE (6":1 mile) (which is a 1910 re-survey of the 1868 original) shows that the area is in the lower chalk. The lower chalk in the region consists of a chlorinitic marl 0.91m thick which passes up through silty marls into bluish marls with some browner marl bands. The bluish marls are of the Schloenbachia varians zone, and pass into yellow - white (grey marly chalk of the Geological Survey sheet) chalks which are massively-bedded and referred to as the Holaster subglobosus zone. The Actinocamax plenus marls top the lower chalks with two 0.3m thick bands of grey laminated marls separated by a 1.22m thick bed of firm white chalk.

The quarry is situated in the chalk marl area in what is thought to be the upper beds of the Schloenbachia zone, with dips of 3^{o} to the north-north-west. The beds are described as bluish - buff, mottled marly chalk with few fossils; the beds sampled were severely fractured or shattered with relatively few massive blocks.

Again this description of the Butser Hill area and geology was taken from the Geological Survey memoir (Osborne White, 1913) and the reader is referred to this publication and the maps of this area, sited above, for more detail.

Two blocks of chalk were sampled from the Butser Hill site, all of the triaxial samples were taken from one block; this block contained 13% insoluble impurities. The second block was used to make oedometer samples and contained 11% insoluble impurities. The X-Ray diffraction profiles of the block used for triaxial samples show a number of non-calcite peaks compared to the Pegwell Bay profile. In the oriented X-Ray profiles these peaks are seen to correspond to clay mineral peaks (Fig. 3.6). The chalk is seen to be heavily

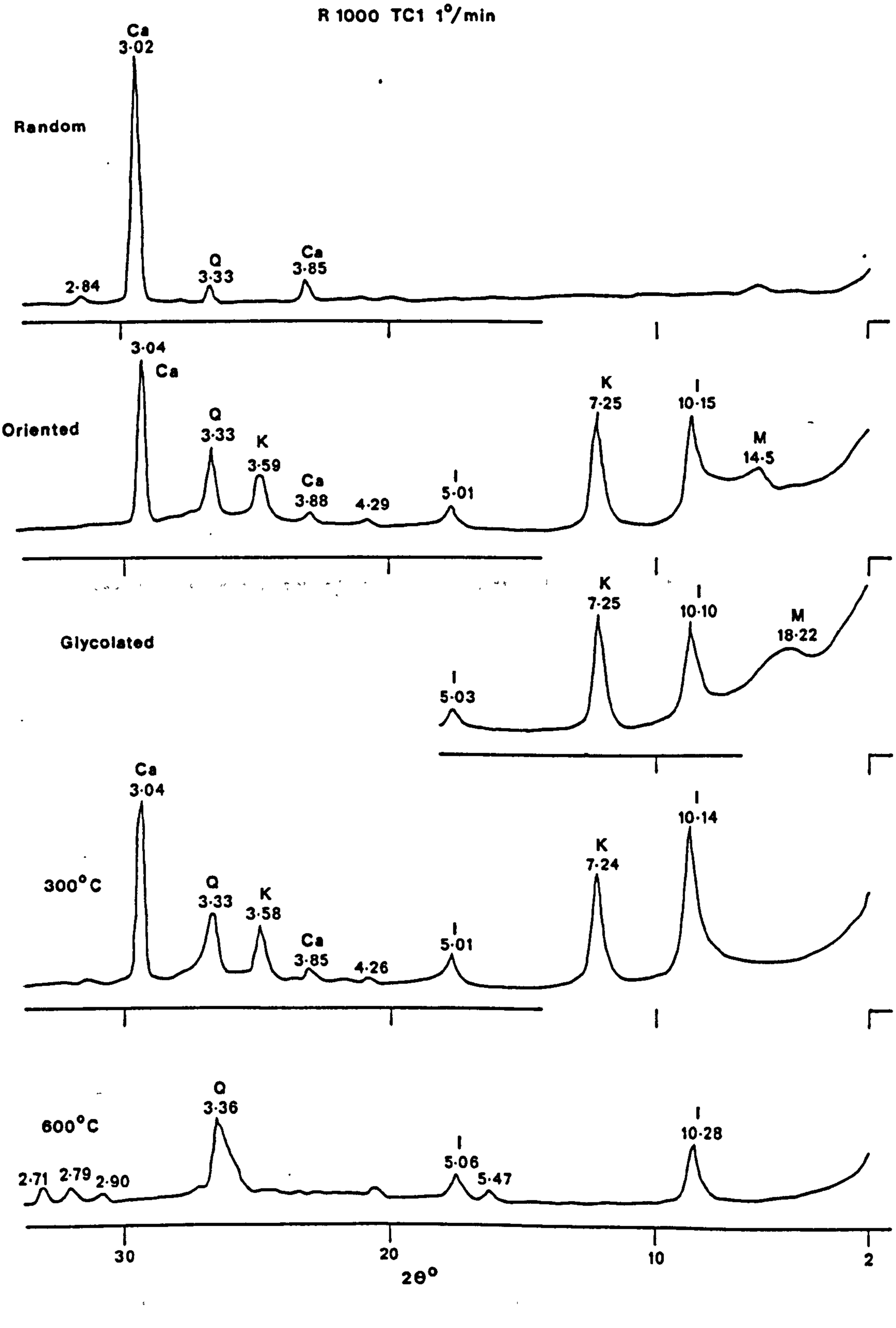

Figure 3.6 X-ray diffraction trace of Butser Hill chalk.

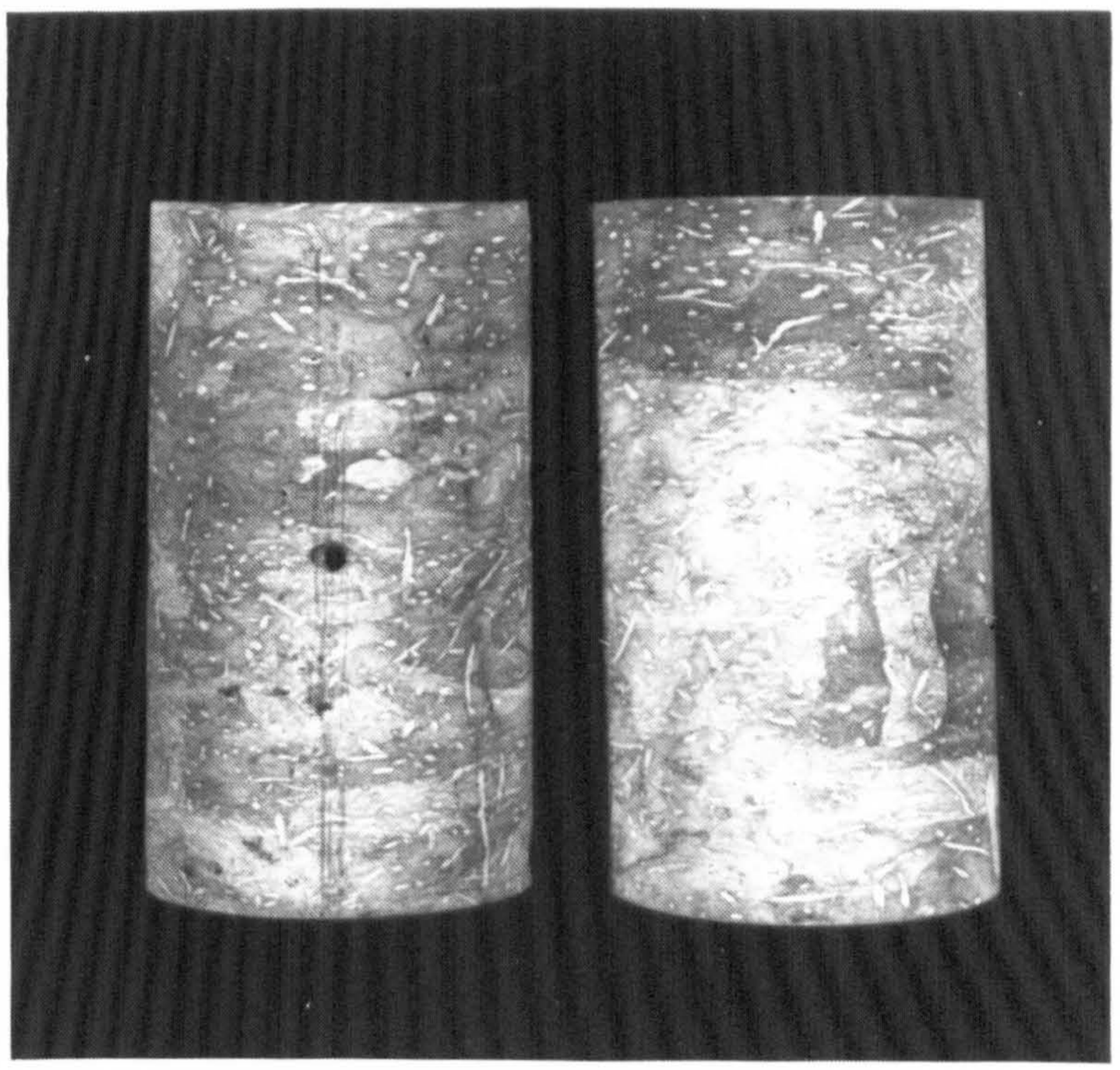

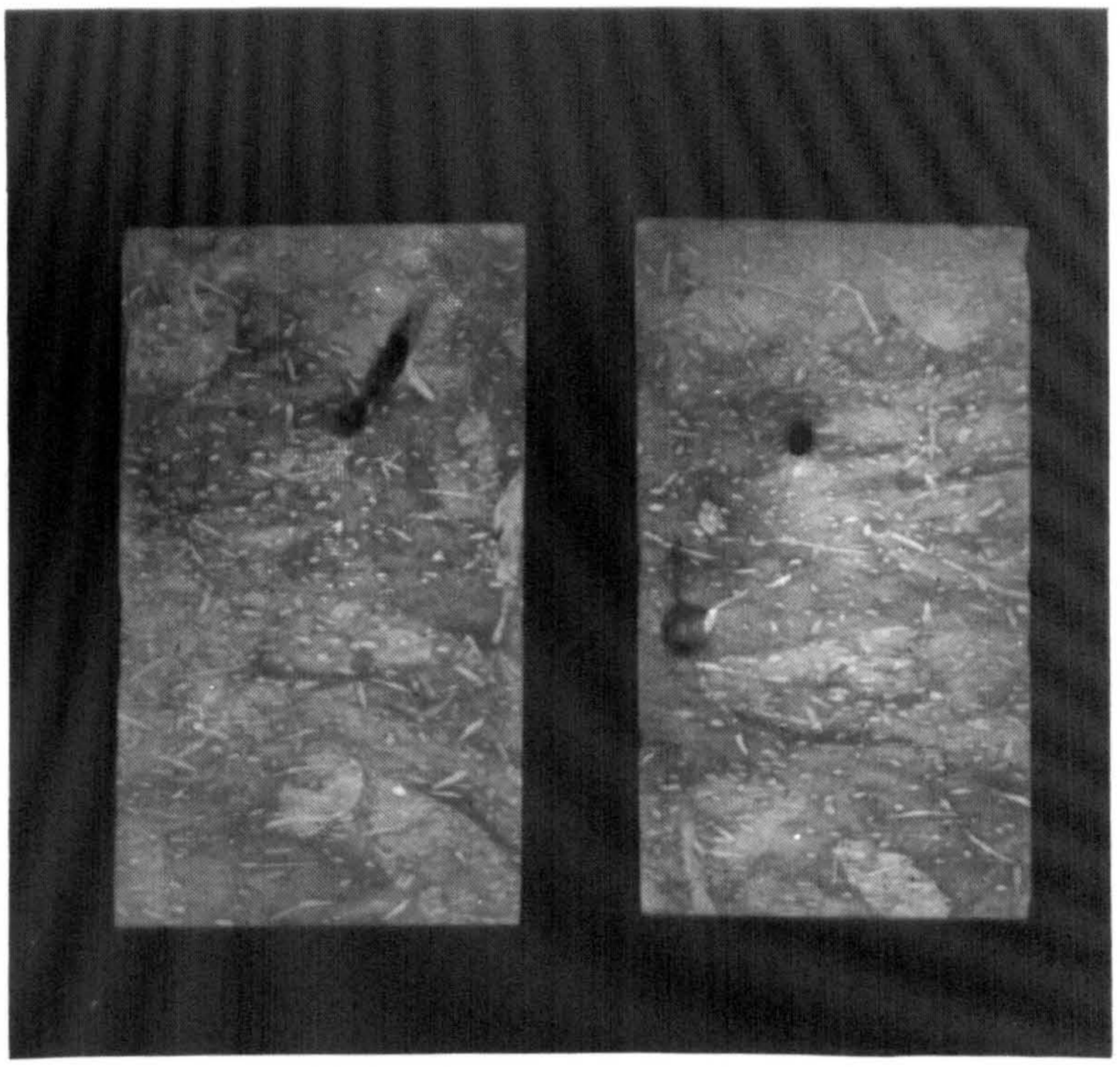

Plate 3.1 Oil saturated Butser Hill chalk showing heterogeneities due to burrows and borings.

burrowed by various organisms at different stages of burial. At least 3 distinct burrowing periods can be recognised: 1) comprising large burrows, with vague outlines, probably the earliest of the visible bioturbation; 2) small well-defined thin cylindrical worm-like burrows; and 3) borings with their channels still remaining open; these are occasionally filled with Fe/PO_4 material. These 3 types of burrows can be seen in the sample which was saturated with oil, heated at 100^oC overnight, and polished, Plate 3.1. This type of technique for investigating structures in chalk have been described in publications by Bromley (Bromley, 1984; also c.f. Hancock, 1975).

3.5.3) North Sea clays

In this experimental programme some clay samples of overburden from the Greater Ekofisk area were tested. The clays are Tertiary deposits, which are overpressured below a depth of 1280m with respect to the normal North Sea gradient of 10.18 kPa/m (0.45 psi/ft) . The Tertiary overburden (in early publications) was considered to be the source rock for the Ekofisk field (Byrd, 1975; van den Bark and Thomas, 1980).

Very little information is available on the overburden of the Greater Ekofisk area, especially concerning its permeability and compressibility, though Young's Modulus and Poisson's ratio have been computed from vertical seismic profile data. The range of Young's moduli for three material layers, used to model the sea-floor subsidence in a finite element program (Jones et.al., 1985a; 1985b) are $41.37*10^5$ to $24.13*10^5$ kN/m^2 (calculated from VSP logs supplied by Philips Petroleum Company Limited), while the respective Poisson's ratios are 0.4 to 0.44. Samples from shallow depths tend to have a lower Young's moduli and higher Poisson's ratio.

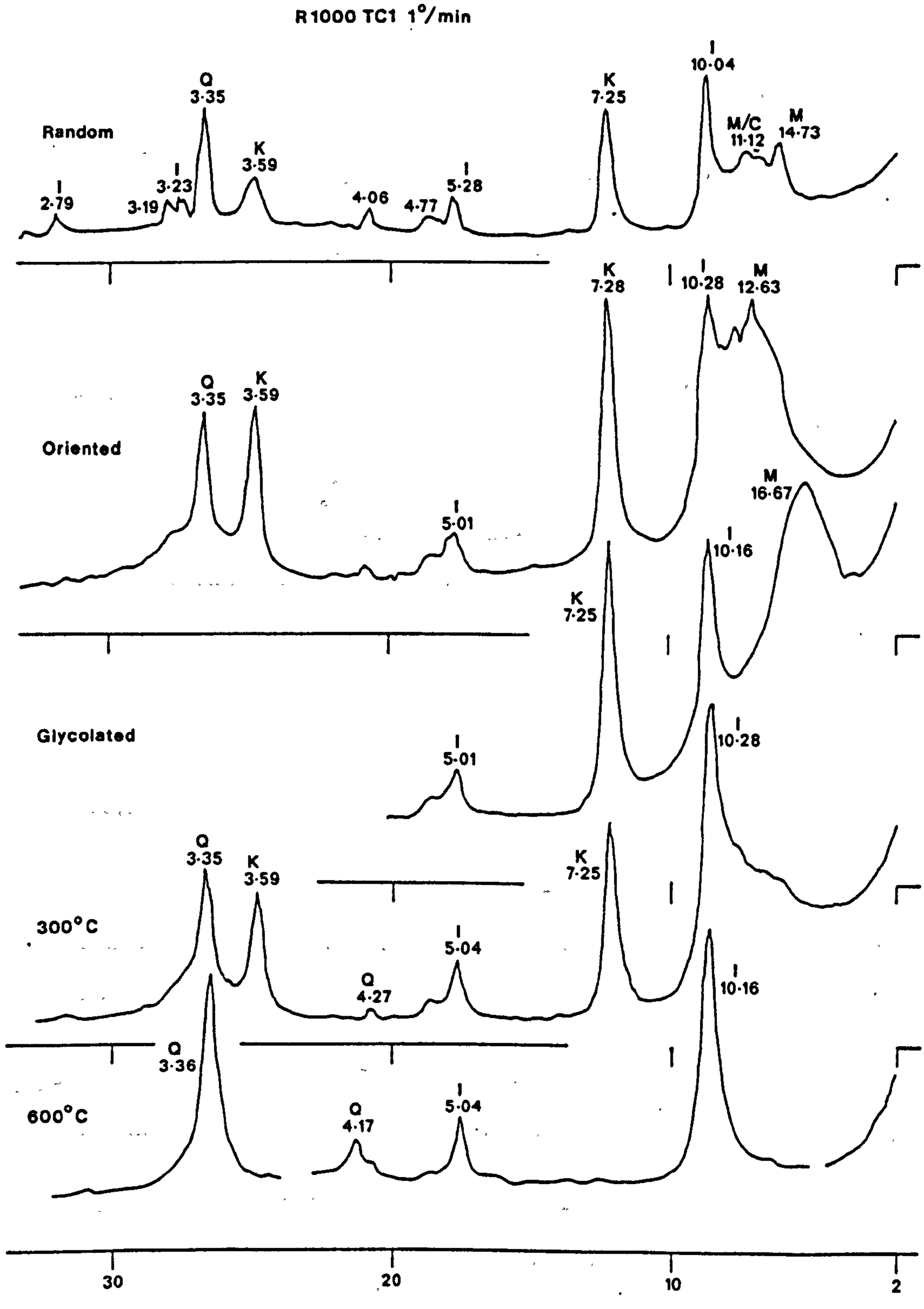

Figure 3.7 XRD for clay test NSC2.20 (Depth 1200m).

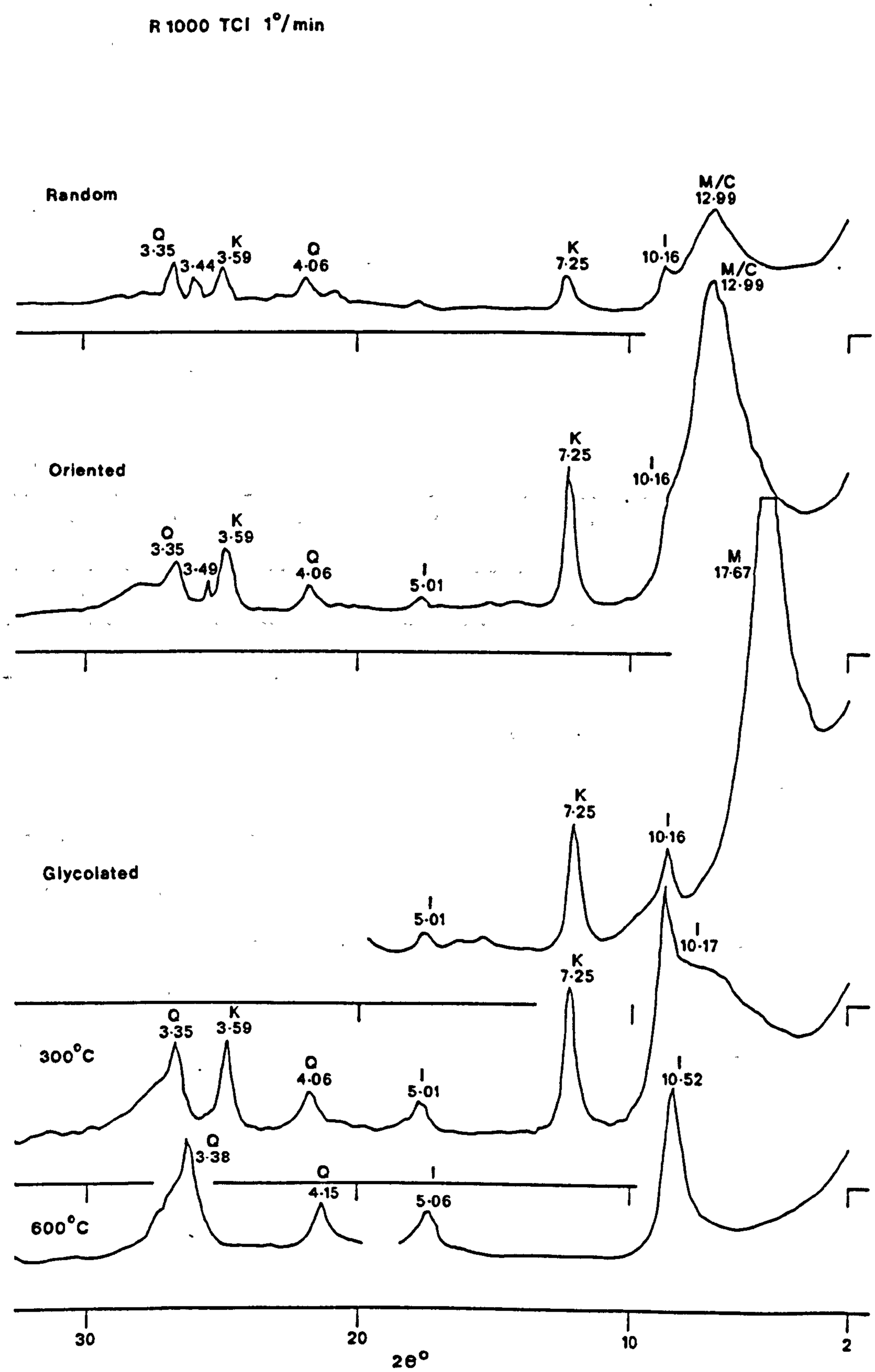

Figure 3.8 XRD for clay test NSC3.20 (Depth 1850m).

The X-Ray diffraction analyses for the two clays tested (from depths of 1200m and 1850m in the same well) Fig. 3.7 and 3.8, show that the materials are very different. The difference cannot be explained by the normal smectite to illite transformation with depth as the two depths show the reverse trend. The percentages of clay minerals in the two clays have been tabulated in Table 3.3, and calculated using method 2 outlined in Pierce and Siegel (1969).

Table 3.3

Sample	Montmorillonite %	Illite %	Kaolinite %	Chlorite %
NSC 2.20	30	47	23	-
NSC 3.20	60	23	17	-

As mentioned earlier only two samples were tested of the clay as each test took approximately six weeks to perform. The work was predominantly performed on the chalk samples as these were thought to be the main cause of reservoir compaction and surface settlement. The range of chalks employed in this study and described above are used to show the deformational similarities between chalks of differing strengths, impurity content and diagenetic history (App. 5).

CHAPTER 4

DISCUSSION OF THE RESULTS

4.1) INTRODUCTION

In this chapter, the results of the experiments performed in the high pressure triaxial cell and high pressure oedometer will be discussed, with emphasis on comparison with other published work. The chalk triaxial test results (presented and described in App. 5) and oedometer results (presented here) will be used to describe the compaction behaviour of chalks.

The discussion will be considered under the following sub-sections:

4.2) The effect of porosity variations on the compaction of chalk,

4.3) Strain rate effects on compaction,

4.4) The influence of sample shape on compaction behaviour,

4.5) The effect of increased temperatures on compaction,

4.6) Hydrostatic to uniaxial strain conversions,

4.7) Time dependency of the compaction,

4.8) The nature of compaction for chalks,

4.9) Yield and failure envelopes for chalk,

4.10) Compaction of chalk: Summary.

The major part of the study concerns uniaxial compaction tests, and results from these are included in all the outlined sections. Triaxial shear tests will also be presented in Chap. 4.9.

4.2) THE EFFECT OF POROSITY VARIATIONS ON THE COMPACTION OF CHALK

The effect of porosity on the uniaxial compaction was studied

using oil-saturated chalks from the Central North Sea (Chap. 3). These samples have porosities between 34.8% and 43.5% and have a range of insoluble residues varying from 1.6% to 38.1%, there is no apparent relationship between these quantities, for the chalks tested. A range of depositional facies and mechanisms are also associated with these chalks (Chap. 3). Once deposited on the sea bed, these chalks should all have followed the same burial history, and hence, any sample variation should be due to initial composition and compaction, degree of cementation (possibly due to initial pre-cementation porosities), and emplacement of oil.

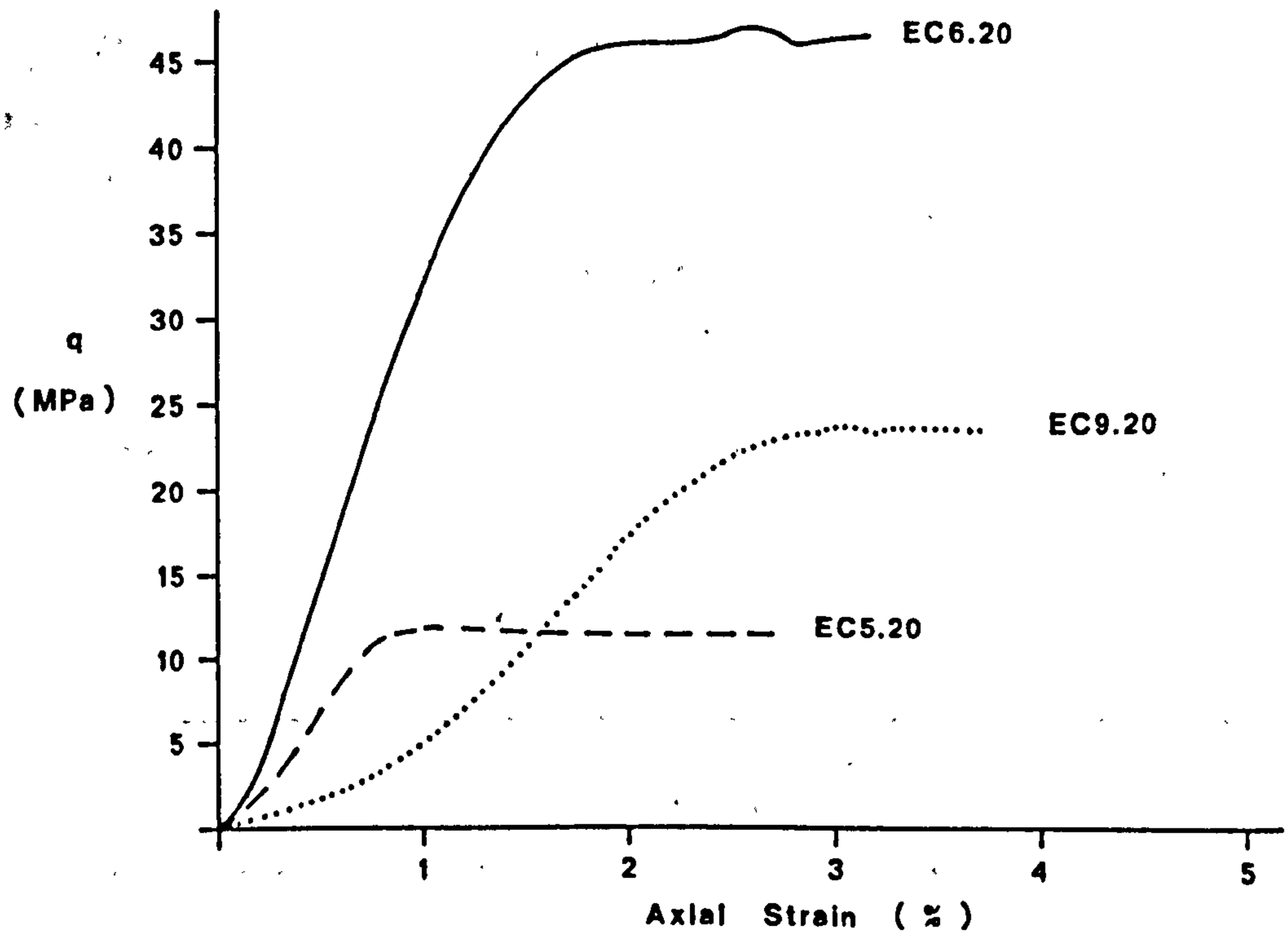

Figure 4.1 Yield strength of EC5.20, EC6.20 and EC9.20.

Uniaxial (K_o) compaction of the North Sea chalk samples show a large variation in the yield point of different samples. In Fig. 4.1 EC9.20, EC6.20 and EC5.20 are shown, these are representative of the

trend of increasing yield point with decreasing porosity. The trend for all of the chalks tested from this area is shown in Fig. 4.2. The trend is not well-defined, but shows an increase from a deviatoric stress at yield of 6MPa at a porosity of 44% to a deviatoric stress of 47MPa at yield of a 36% porosity chalk. The scatter in this diagram, is probably due to errors in the porosity determination as well as variations in sample composition. When compared with other

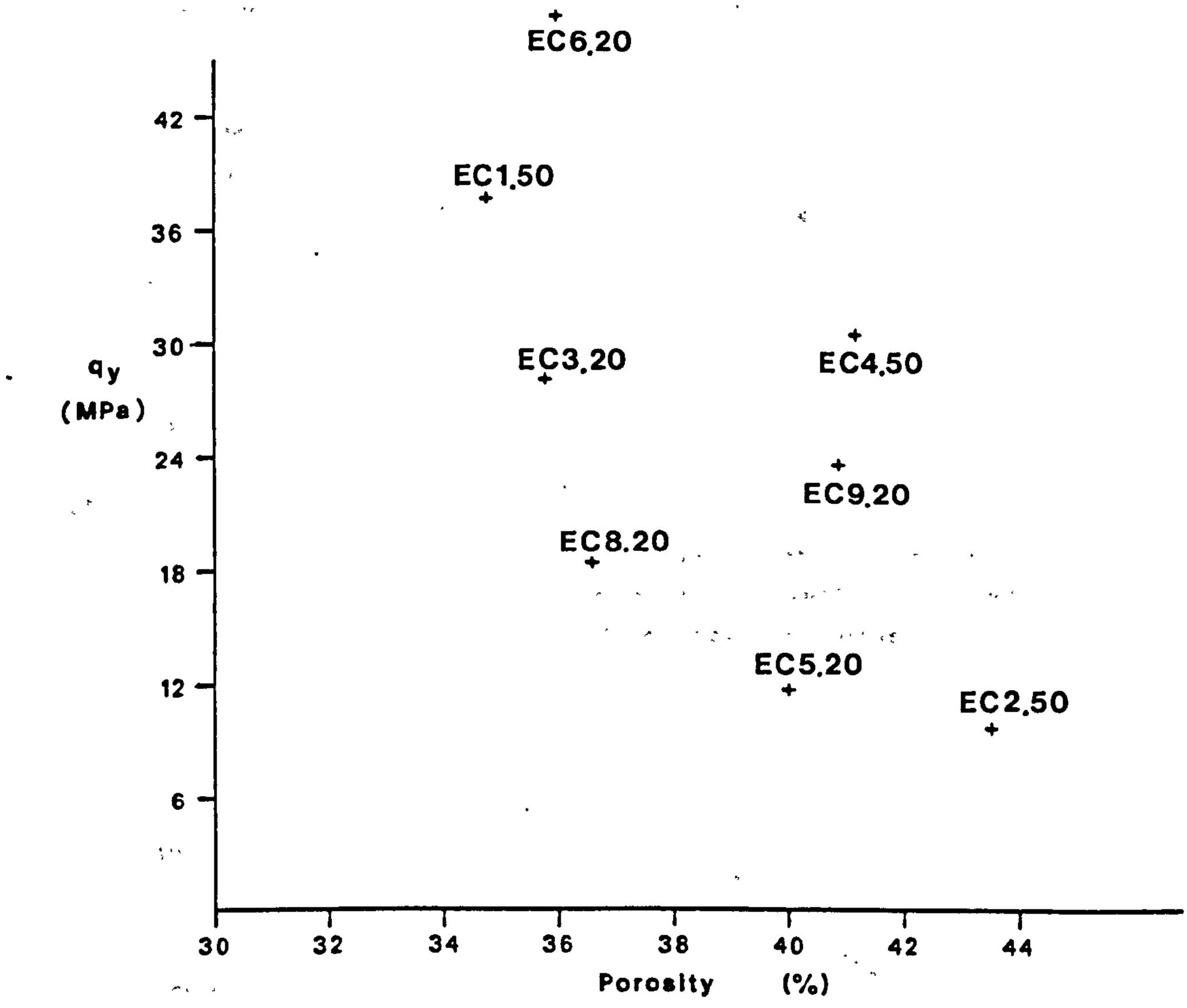

Figure 4.2 Yield point vs porosity for K_o tests on Central North Sea chalks.

published data (over a larger range of chalk porosity and yield strengths), the data obtained from this study can be seen to be in reasonable agreement with the trend observed by Jones (1985) (Fig. 4.3). The data presented by Jones (1985) were obtained from triaxial

compression tests on dry samples at a cell pressure of 60MPa; the trend being defined by brittle failure or by 3.5% axial shortening. In the high porosity range few data points exist for this trend due to the lack of sensitivity of the Hoek cell (used to define this curve). At the cell pressure of 60MPa, the hydrostatic yield would have been exceeded for high porosity chalks, and using 3.5% axial shortening to define yield seems arbitrary in the light of yield envelope determination studies, Chapter 2.

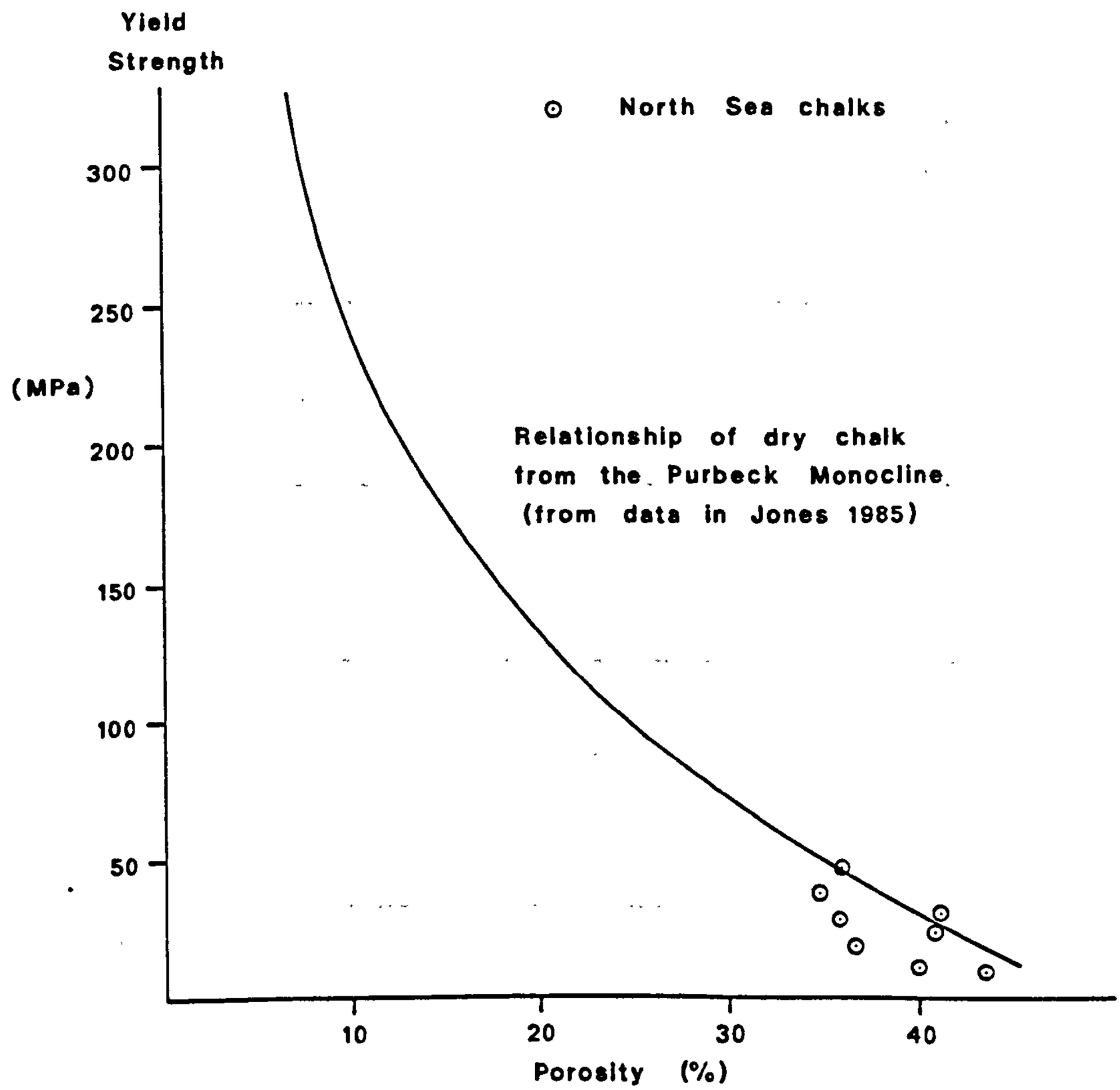

Figure 4.3 Comparison of yield point vs porosity results with data presented by Jones (1985).

Table 4.1

Sample	Porosity %	Insoluble residue %	$\bar{K}_{oe}$	$\bar{K}_{opc}$	$\bar{K}_{onc}$	Young's modulus GPa	Yield point MPa	$\sigma_1'_{nc}$ MPa	p'_{nc} MPa
EC1.50	34.8	---	0.368	0.856	---	- 3.264	37.65	111.1	80.0
EC2.50	43.5	---	---	---	---	- 1.723	9.78	---	---
EC3.20	35.8	3.1	0.492	1.000	0.630	- 2.390	28.11	81.9	61.8
EC4.50	41.2	38.1	0.254	1.115	---	- 2.752	30.42	82.3	60.4
EC5.20	40.0	1.6	0.344	2.055	0.492	1.634	11.85	26.3	21.1
EC6.20	36.0	13.3	0.318	1.077	---	- 3.801	47.25	122.5	90.9
EC8.20	36.6	11.9	0.384	1.432	0.631	- 1.171	18.40	57.6	43.4
EC9.20	40.9	---	0.340	0.973	0.592	- 1.366	23.65	65.7	48.1

The Young's moduli associated with the pre-yield deformation increases with increasing yield stress, both of these quantities exhibiting a porosity dependance, Table 4.1. The variation of Young's modulus with porosity is plotted in Fig. 4.4a, and shows a similar trend to the change in the yield strength with porosity. These results are compared to those obtained by Jones (1985) in Fig. 4.4b. To eliminate the possible errors in porosity determination in Figs. 4.2 and 4.4a, the yield point is plotted against the Young's modulus (Fig. 4.5); however, scatter still exists in the higher porosity chalks which has been attributed to sample variability. The sample stiffness is due to compaction and cementation. Stiffness in high porosity chalks may therefore reflect variability in packing and spot welding of grains.

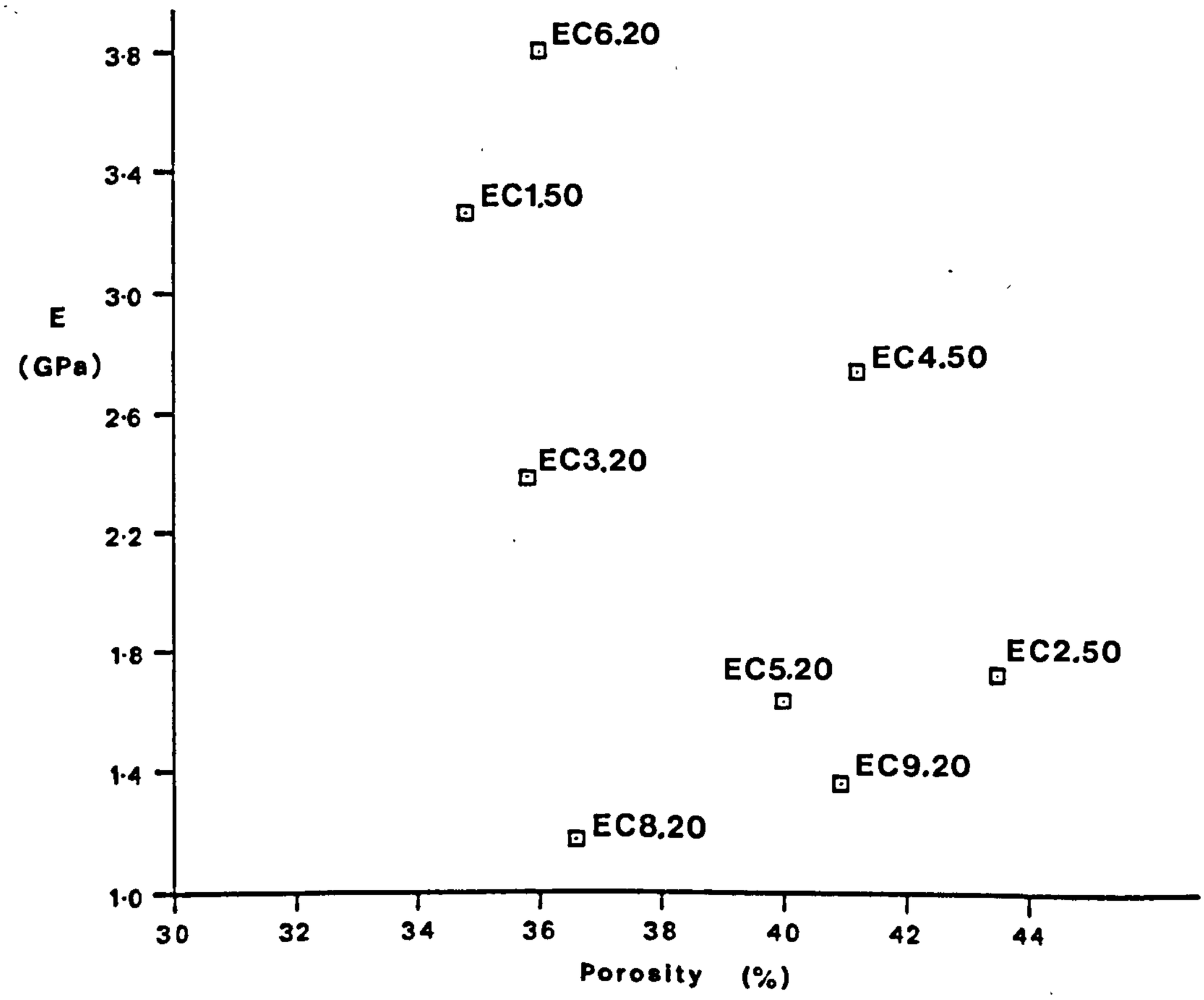

Figure 4.4a Young's modulus vs porosity for K_o tests on Central North Sea chalks.

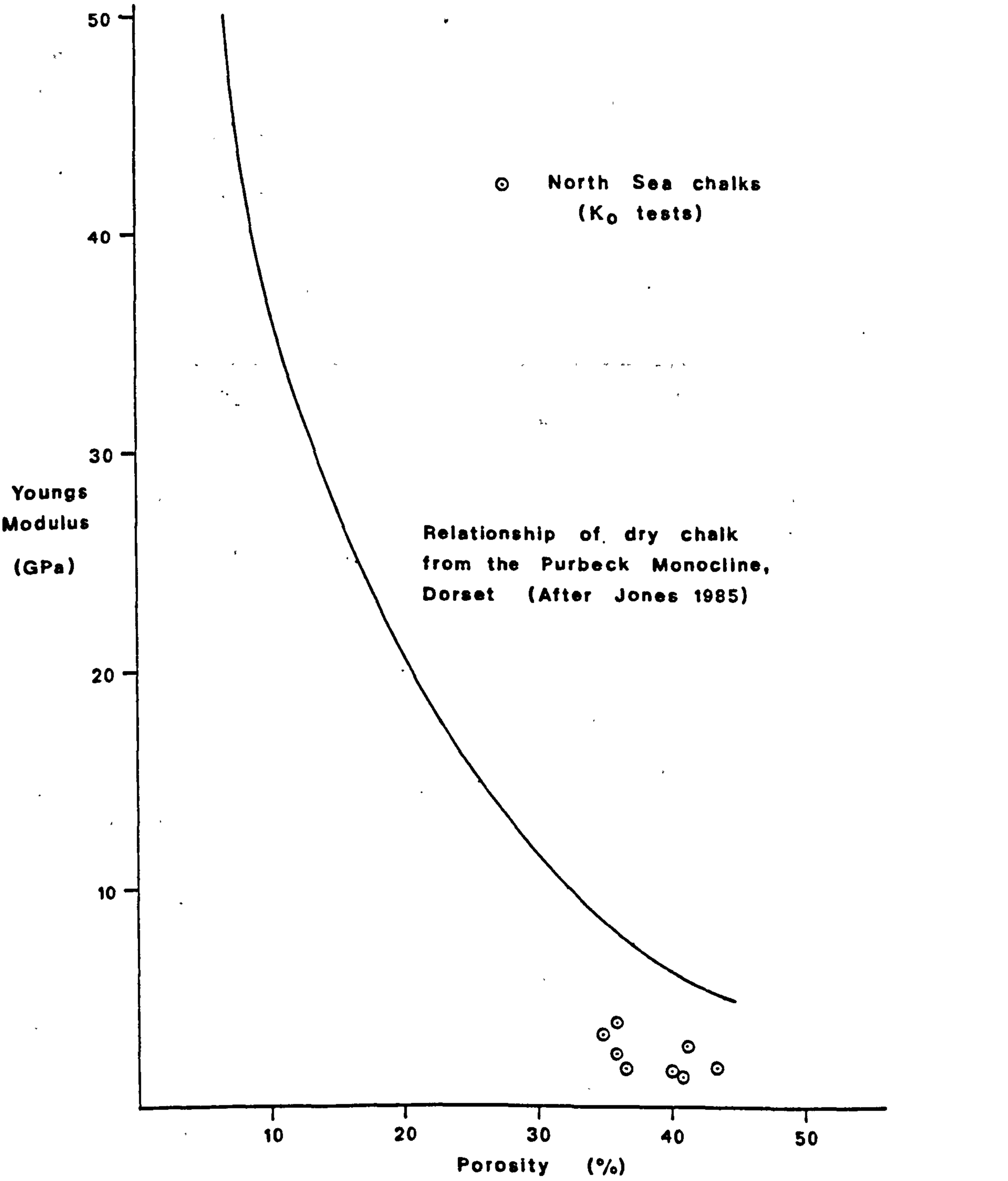

Figure 4.4b Comparison of Young's modulus vs porosity results with data presented by Jones (1985).

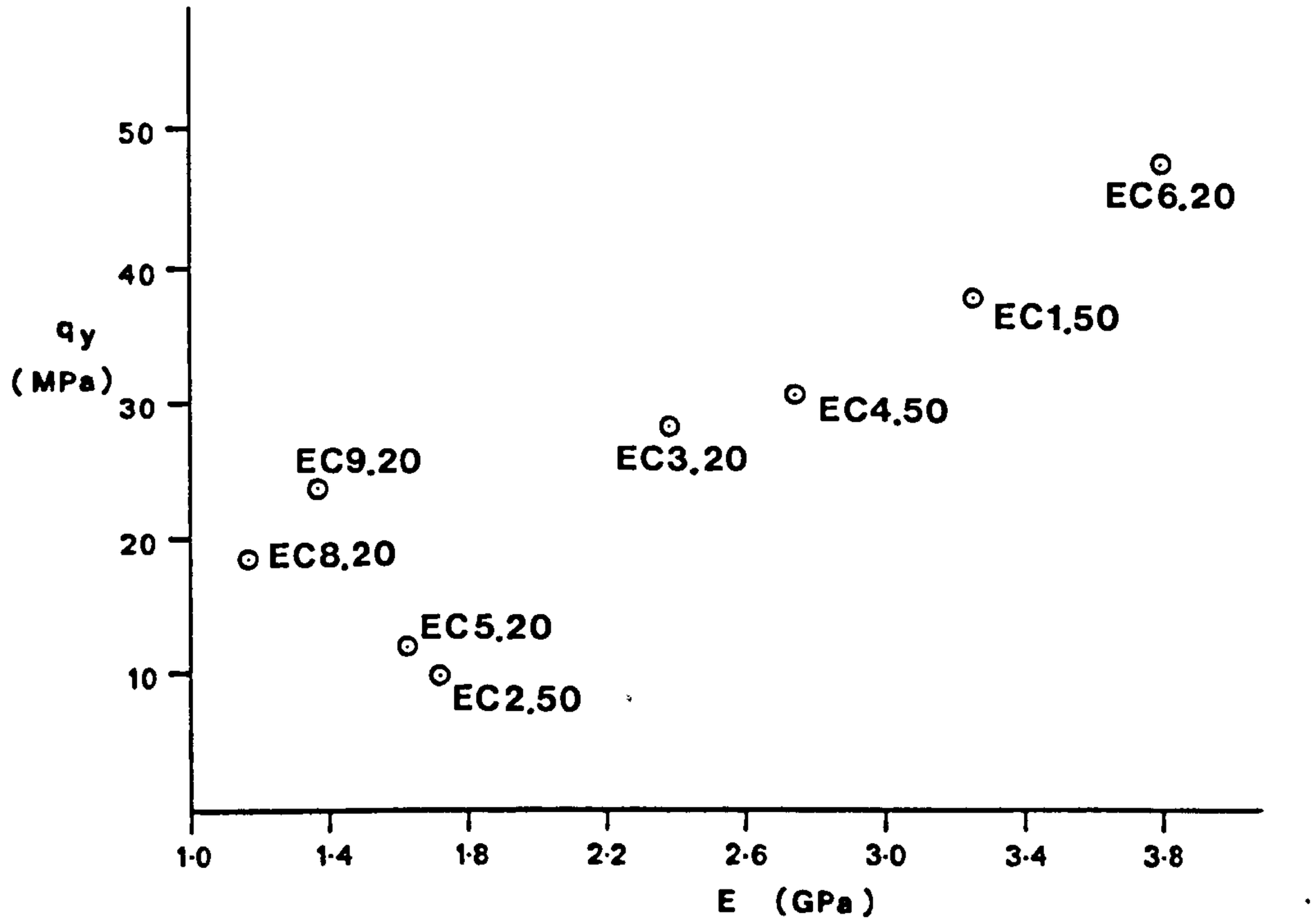

Figure 4.5 Yield point vs Young's modulus for Central North Sea chalks.

The uniaxial compressibility (M_v) (Fig. 4.6a) of the chalks during K_o deformation also shows the effect of cementation on the skeleton rigidity. If it is assumed that all other factors are approximately the same during the diagenesis of these chalks, the density or the degree of compaction controls the degree of cementation and stiffness of the pre-yield response to stress.

The stiff initial response can be seen by analysing the variation of the coefficient of volume compressibility with the porosity, the lower porosities give a smaller M_v for the pre-yield elastic response. The pre-yield response of the North Sea chalks shows a linear trend with porosity on a log normal plot (Fig. 4.6b). The data is seen to fit very well with that of van Kooten (1986) for North Sea chalks. No relationship is seen between M_v and the yield point. The

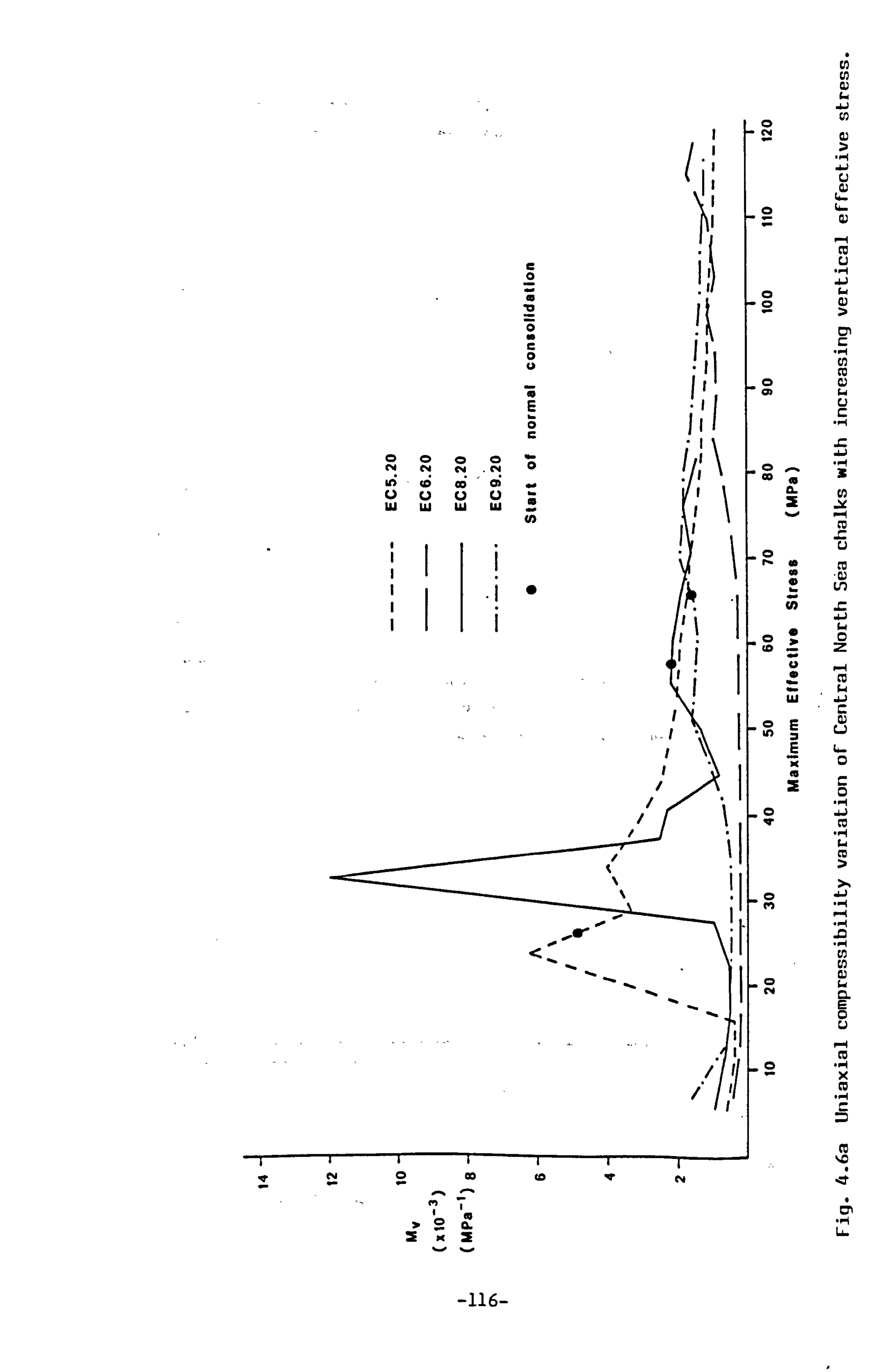

Fig. 4.6a Uniaxial compressibility variation of Central North Sea chalks with increasing vertical effective stress.

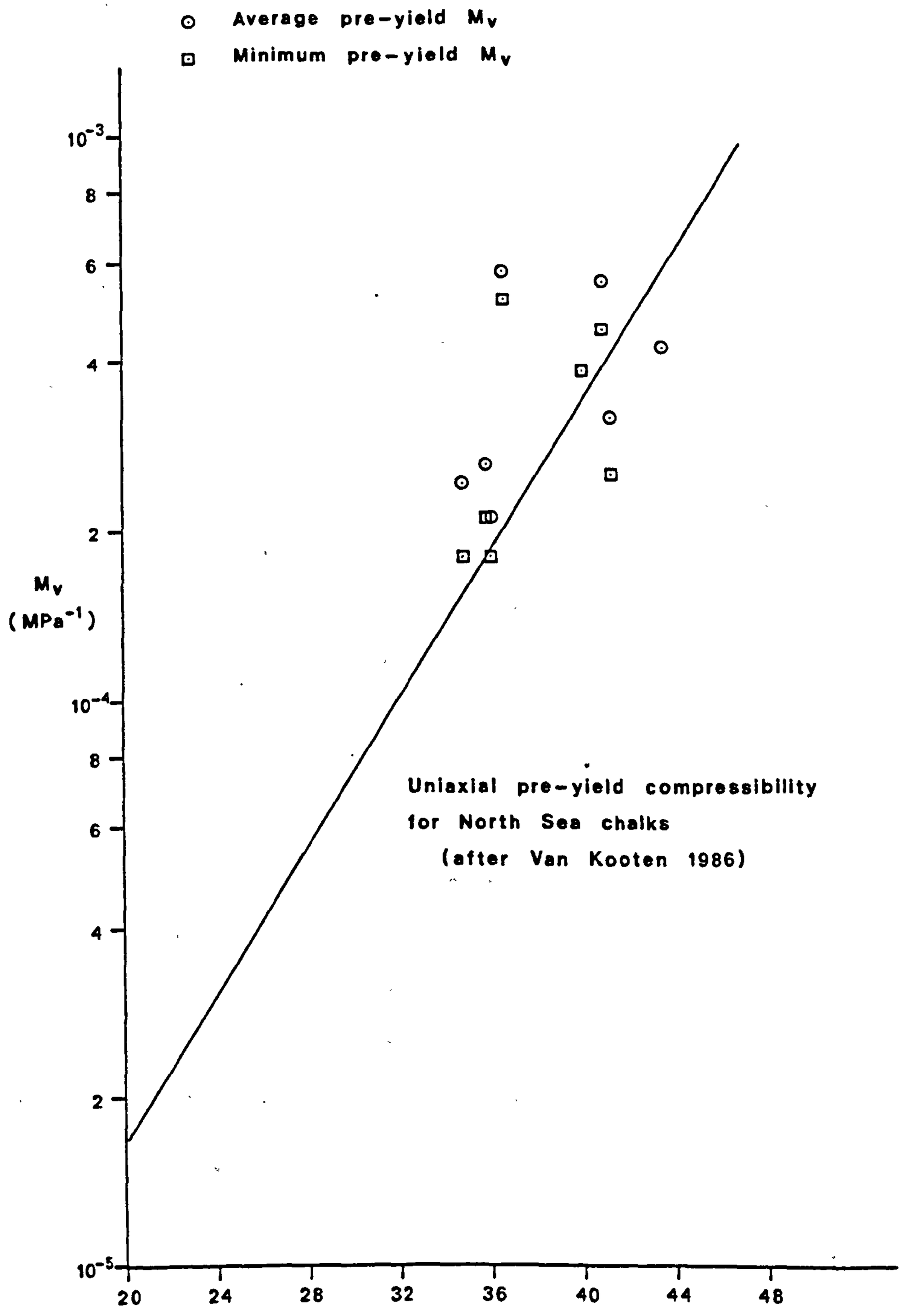

Figure 4.6b Pre-yield M_v variation with porosity for Central North Sea chalks.

post-yield response of the chalks is also seen to be very regular, the M_v values lying along one general trend (Fig. 4.6a), with the maximum coefficient of volume compressibility decreasing with increasing yield stress, and decreasing porosity.

The deformation of the different porosity chalks, and the stresses required to maintain K_o, might be expected to decrease with decreasing porosity, as smaller radial strains would occur with stiffer materials. However, over the range of porosities tested for the North Sea chalks, no variation or trend was noted between $\bar{K}_o$ and porosity (Fig. 4.7). Fig. 4.8 shows that the initial elastic section of the K_o plot extends to higher stresses with decreasing porosity, whilst the slopes in σ_1', σ_3' space remain similar, regardless of the porosity. The post-yield section is also seen to be very regular (EC5.20 has a steeper slope of 2.055 caused by a large decrease in load, which was an experimental error, seen by an increase in the cell pressure, and a sustained reduction in the radial strain, Fig. A5.5e). A trend occurs in the transitional part of the deformation; $\bar{K}_{opc}$ giving a linear trend with de/dp (the change in the void ratio during pore collapse divided by the accompanying increase in mean effective stress), showing that the stress system acting during the cementation breakdown is responsible for the observed volumetric strain (Fig. 4.9). This result contradicts the assumption that the pore collapse deformation is independant of applied stress system, as stated by Johnson and Rhett (1986), Chap. 4.6, Chap. 6.2.1. The value of K_o for the post-yield pore collapse and normally consolidated deformations show no trend with porosity, despite the evidence presented by Al Hussaini and Townsend (1975), which shows a decrease in K_o with increasing relative density for sands. A similar trend is also presented for weakly cemented materials by Maccarini (1987).

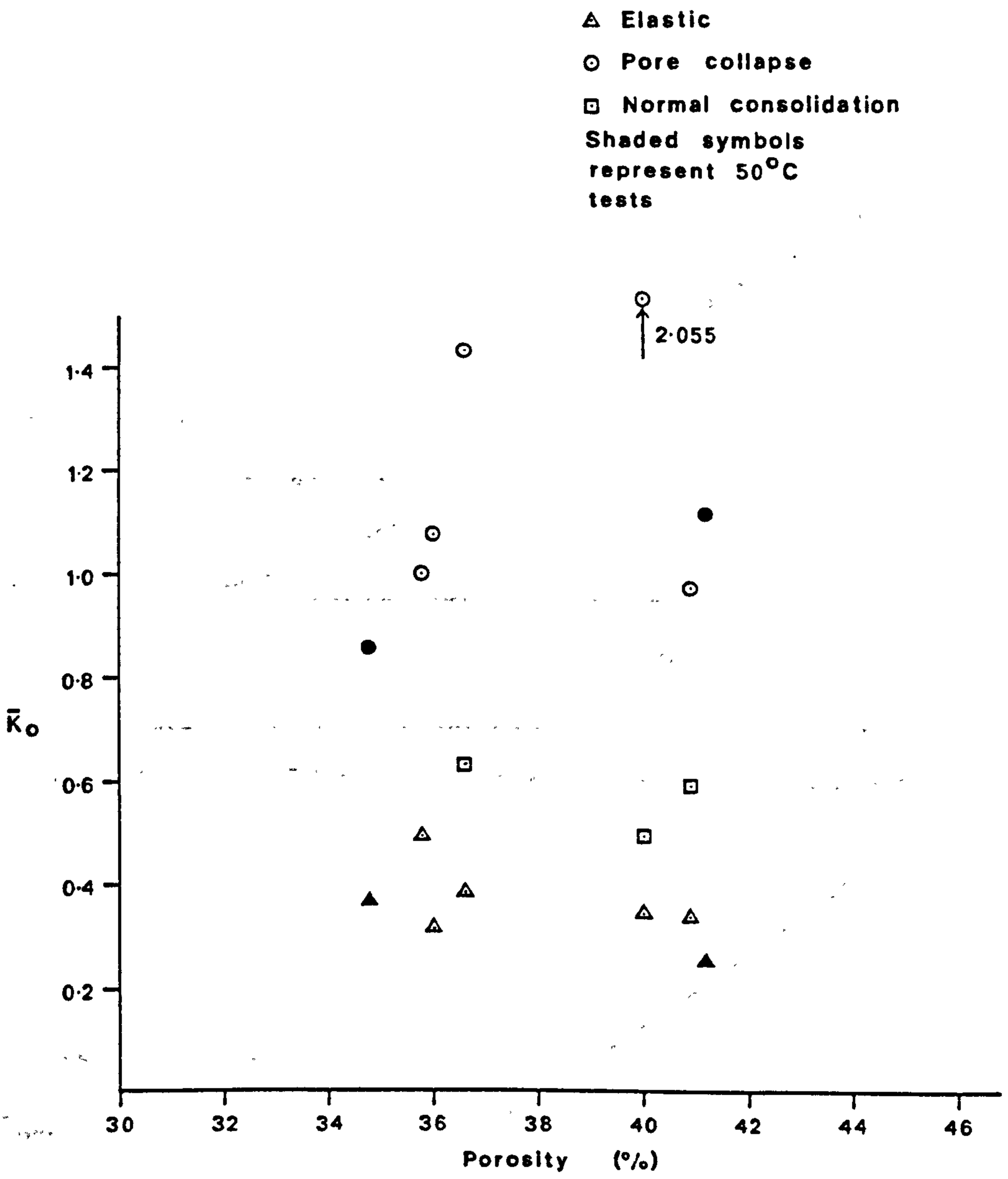

Figure 4.7 K_o vs porosity for Central North Sea chalks.

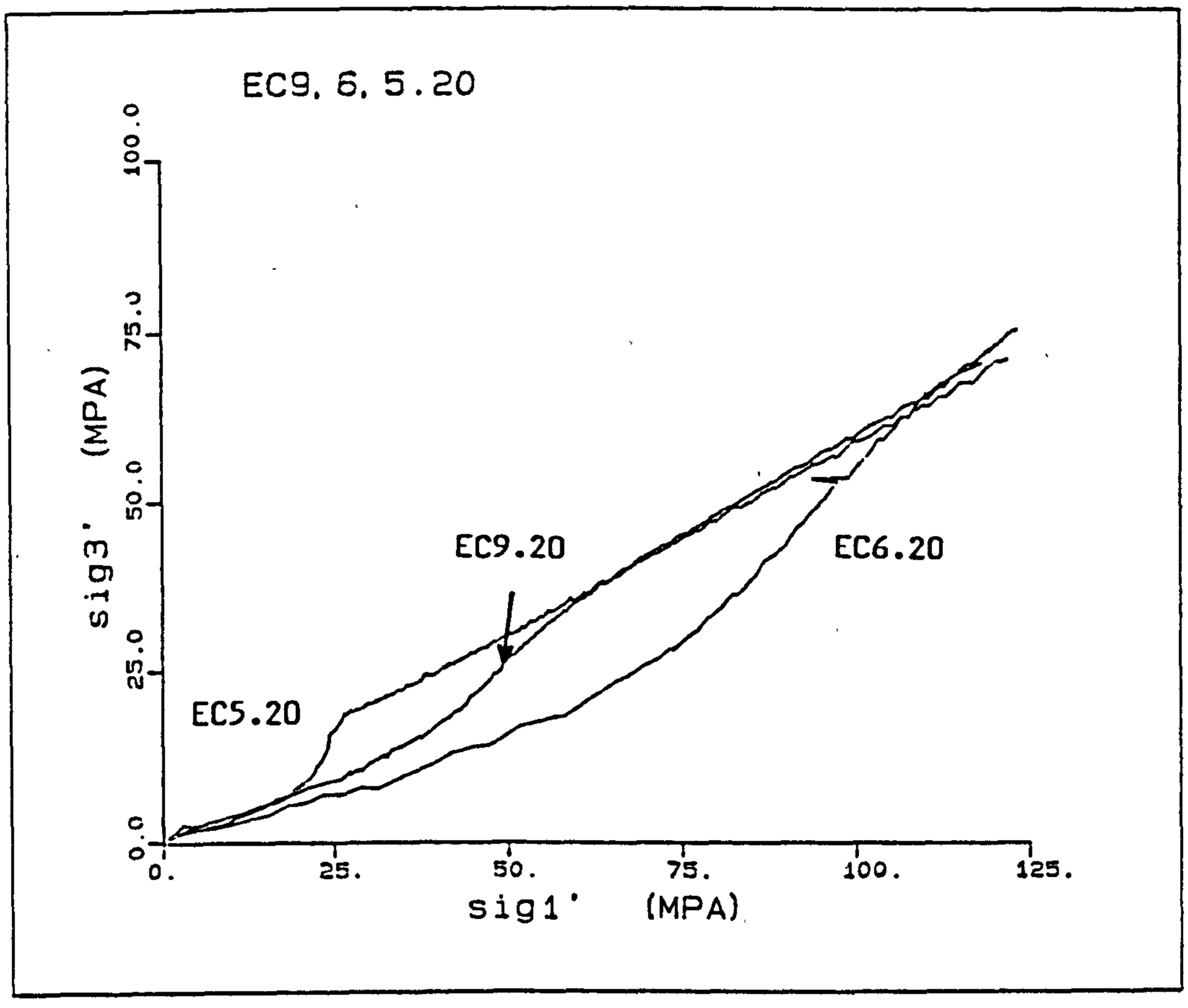

Figure 4.8 σ_3' vs σ_1' plot for three Central North Sea chalks.

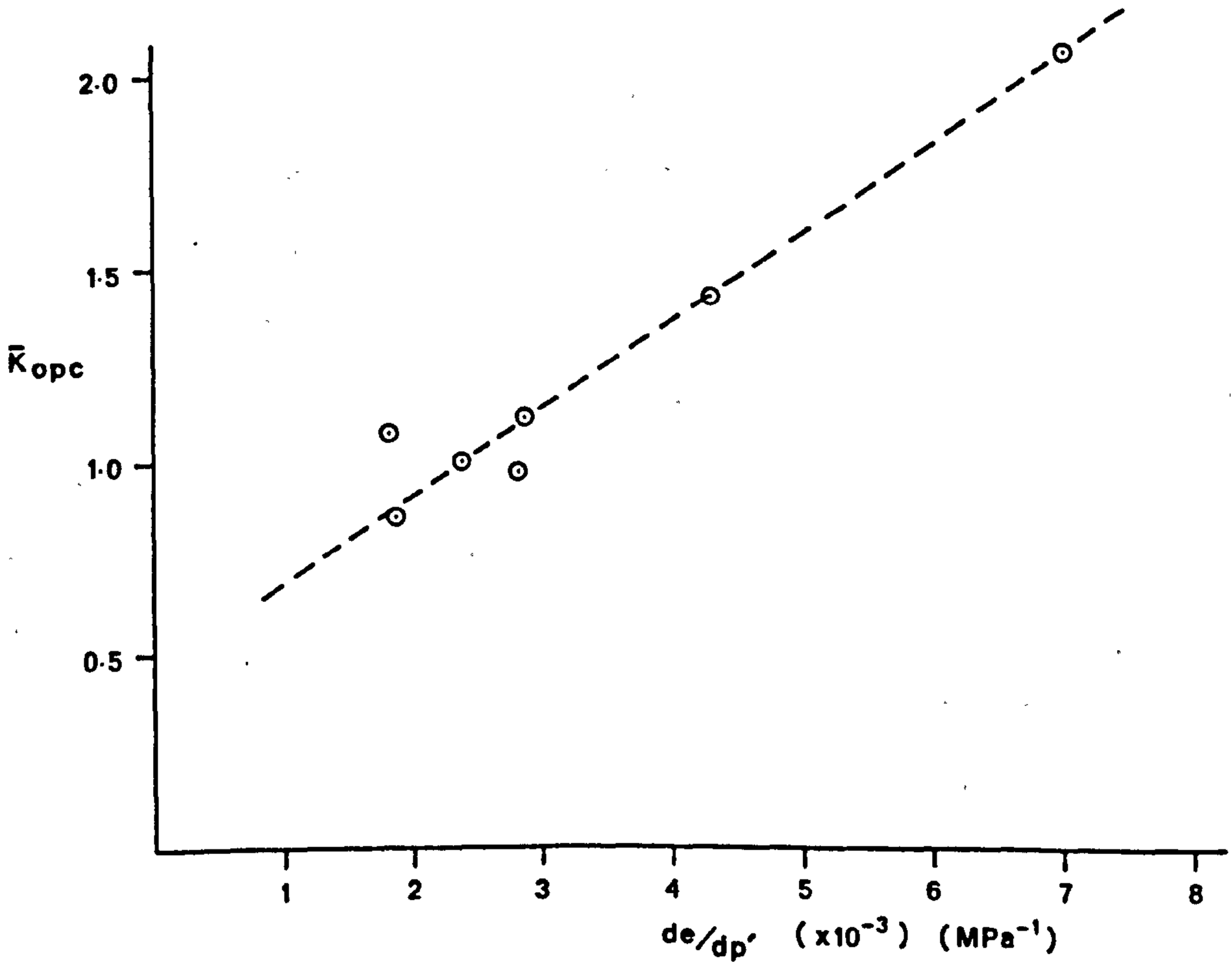

Figure 4.9 Trend of $\bar{K}_{opc}$ with de/dp' for Central North Sea chalks.

It is difficult to fully interpret the volume change characteristics of these chalks, as only part of the picture is seen. This was because the pore volume measuring system did not operate until a pore pressure was obtained, which required some deformation of the sample, App. 1. The void ratio versus maximum effective stress plots are shown in Fig. 4.10; the tests performed at $20^{o}C$ and $50^{o}C$ are plotted separately. These curves have been adjusted from those presented for individual tests in App. 5, to present the correct void ratios at the start of volume measurement (the correction being for the deformation undergone by the sample before volume changes were measured). The figures show no trend for the $50^{o}C$ chalk tests, which is probably due to the limited number of tests performed at this temperature. The data in Fig.4.10a however, show similar void ratio-maximum effective stress relationships (Chap. 2.6.3) which can be adjusted by altering the void ratio axis to give one general volume change-vertical effective stress plot (Fig. 4.11) (Chap. 6.2.1.b). This construction (van Ditzhuijen and de Waal, 1985) assumes that the chalks have undergone similar diagenesis and will undergo compaction along a unique compaction curve, i.e. the clays and cementation have a negligable effect on the magnitude of compaction. The adjustment to the plot is then justified if the variation is assumed to be entirely due to errors in the porosity determination (van Ditzhuijen and de Waal, 1985; van Kooten, 1986; Smits et.al., 1986). The plots were shifted to a median value in the variation of the porosities. The $50^{o}C$ tests do not show any trend, it is interesting to note that EC4.50 shows a markedly different compaction curve which has been attributed to the large clay content present in this sample. The $20^{o}C$ tests show a good trend with only EC5.20 deviating off this trend, the volume strain characteristics of

which are probably affected by the early post-yield deviation from zero lateral strain.

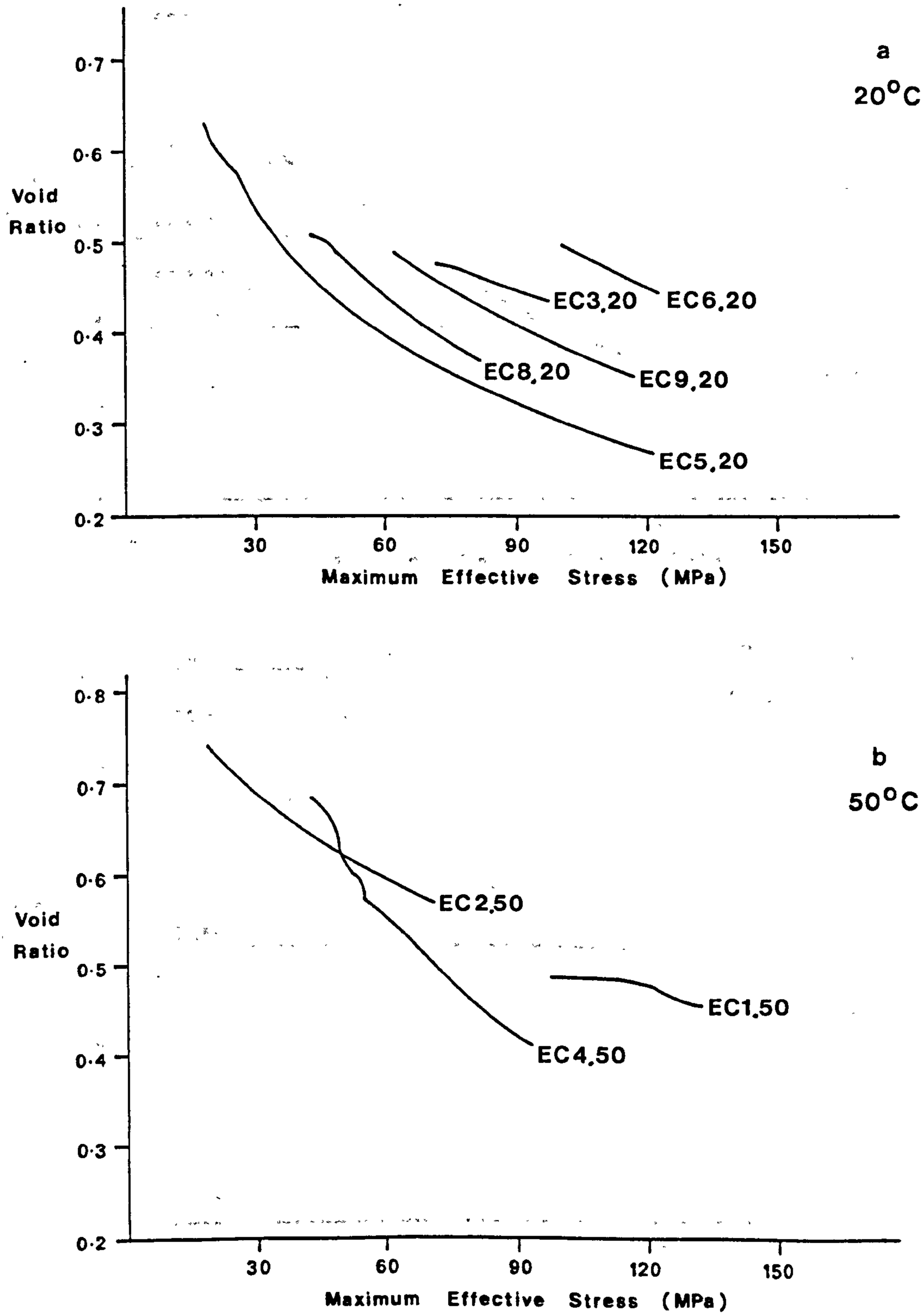

Figure 4.10 Void ratio variation with maximum effective stress for Central North Sea chalks.

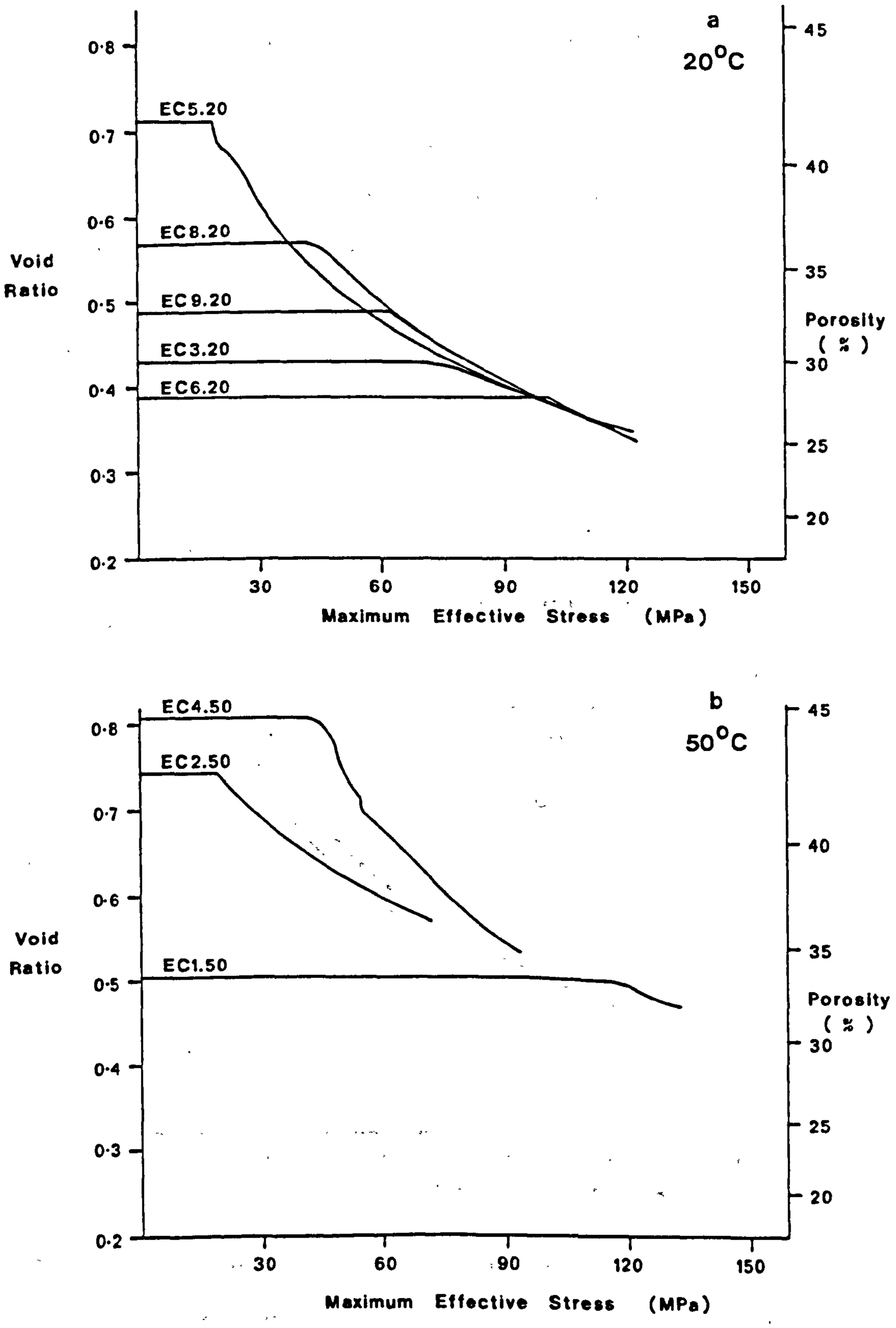

Figure 4.11 Shifted void ratio vs maximum effective stress plots for Central North Sea chalks.

The trend observed in Fig. 4.11 (disregarding EC5.20), is compared with other published compaction trends for chalks (van Kooten, 1986; Smits et.al., 1986) in Fig. 4.12. From this figure it can be seen that it is very similar to the Middle/Lower Danian chalk trend and extends over a larger stress range. The initial part of the trend presented in Fig. 4.12 was not determined in this study due to the lack of high porosity chalks available for testing. The compaction behaviour of chalks from any one diagenetic province seems to be described by a unique porosity trendline.

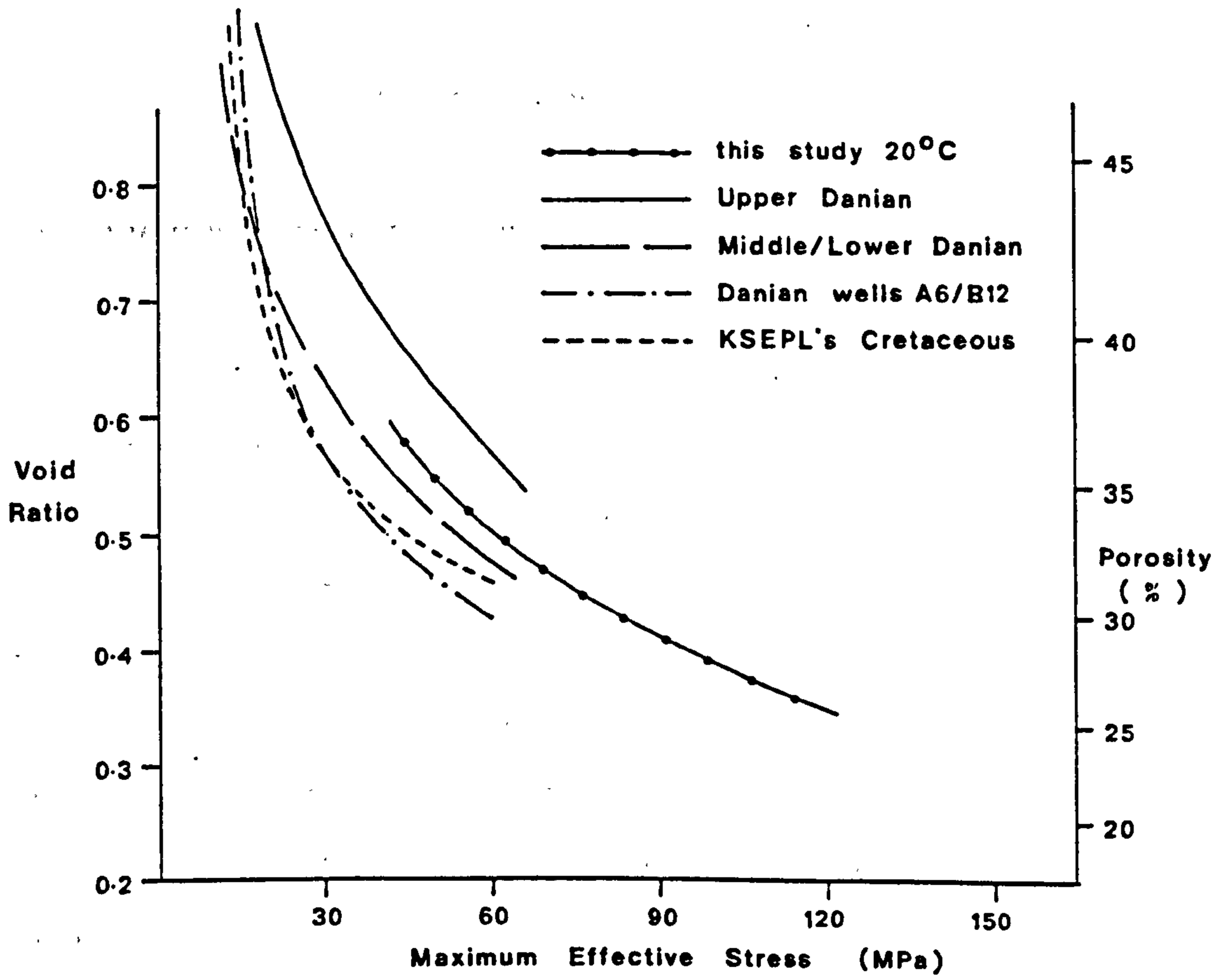

Figure 4.12 Comparison of the compaction trend shown in Fig. 4.11 with published trends.

The unique trendline for the compaction of the materials tested is also seen by observing the variation of the coefficient of volume compressibility (M_v) with vertical effective stress Fig. 4.6a. It can be seen that once yield and pore collapse are terminated, the variation of M_v with vertical effective stress for the normally consolidated region is almost identical irrespective of the initial porosities of the materials. There is some variation in the clay contents of these samples, but this does not seem to adversely affect the trend (at least for the percentages of clay contents of the samples represented in the diagram).

The subject of a unique trendline for the normal consolidation of chalks is discussed further in Chap. 4.10.

4.3) STRAIN RATE EFFECTS ON COMPACTION

The effect of strain rate on the compaction of chalks was investigated using chalks from Pegwell Bay in Kent, these samples had the advantage of having the same porosity and (with the exception of PB7.20) being sampled from the same block, Chap. 3.5.2. All of the tests were performed at room temperature, 20^{o}C. The individual tests are described in App. 5 and the individual plots presented therein.

Due to the similarities in the mineralogy and grain size of most pure high porosity chalks, it is assumed that the strain rate dependancy of different pure chalks of similar porosity will be comparable. This assumption may not hold with the presence of clays in the matrix.

Chalk compaction can be seen to be strain-rate dependent from PB1.20 (Figs. A5.8a; A5.8g; A5.8h; 4.13). Fig. 4.13a is similar in form to the e-log p' plot presented by Bjerrum (1967), (Fig. 2.17). This diagram demonstrates how the amount of compaction increases with

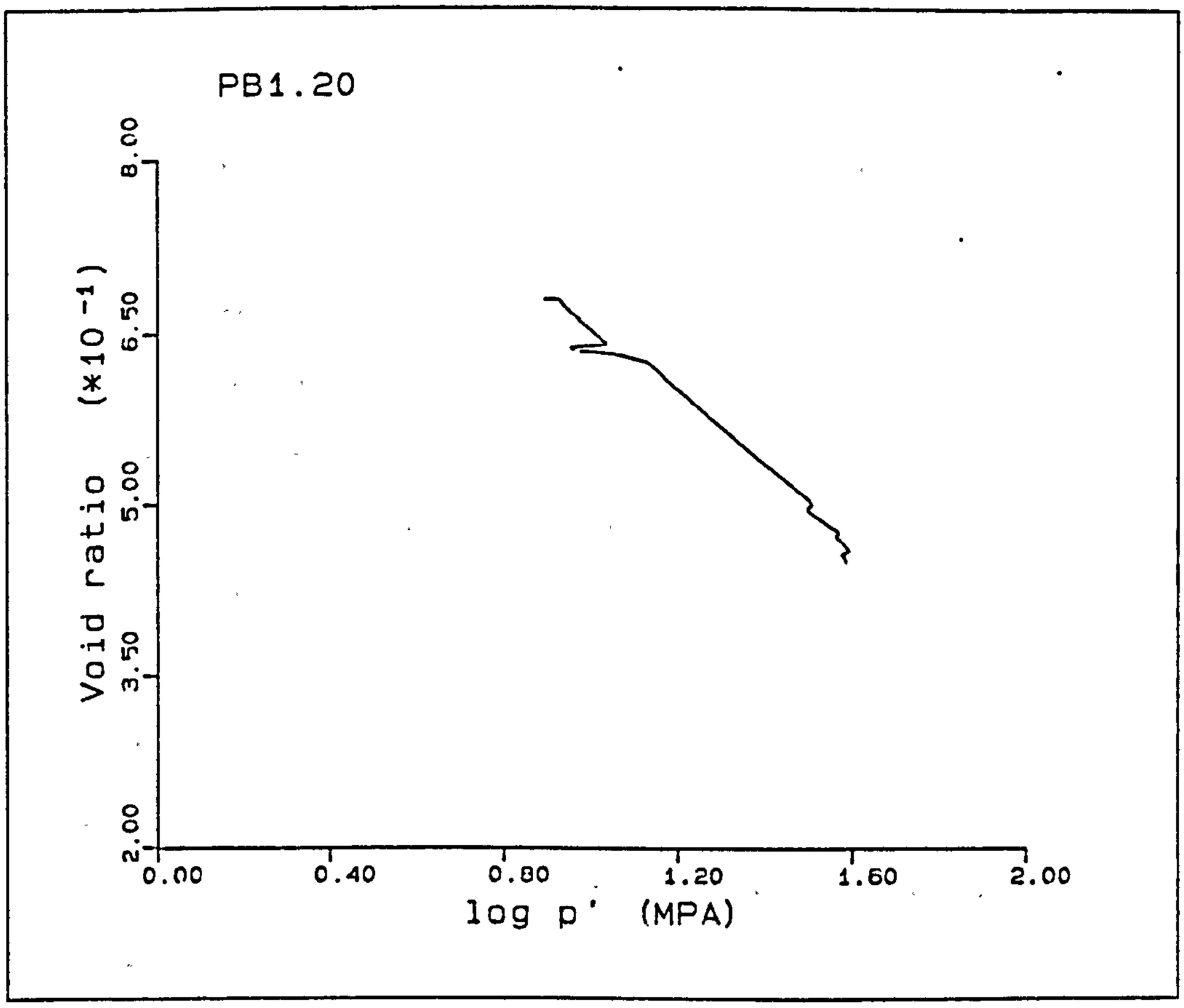

Figure 4.13a Effect of strain rate on e-log p' plot for PB1.20.

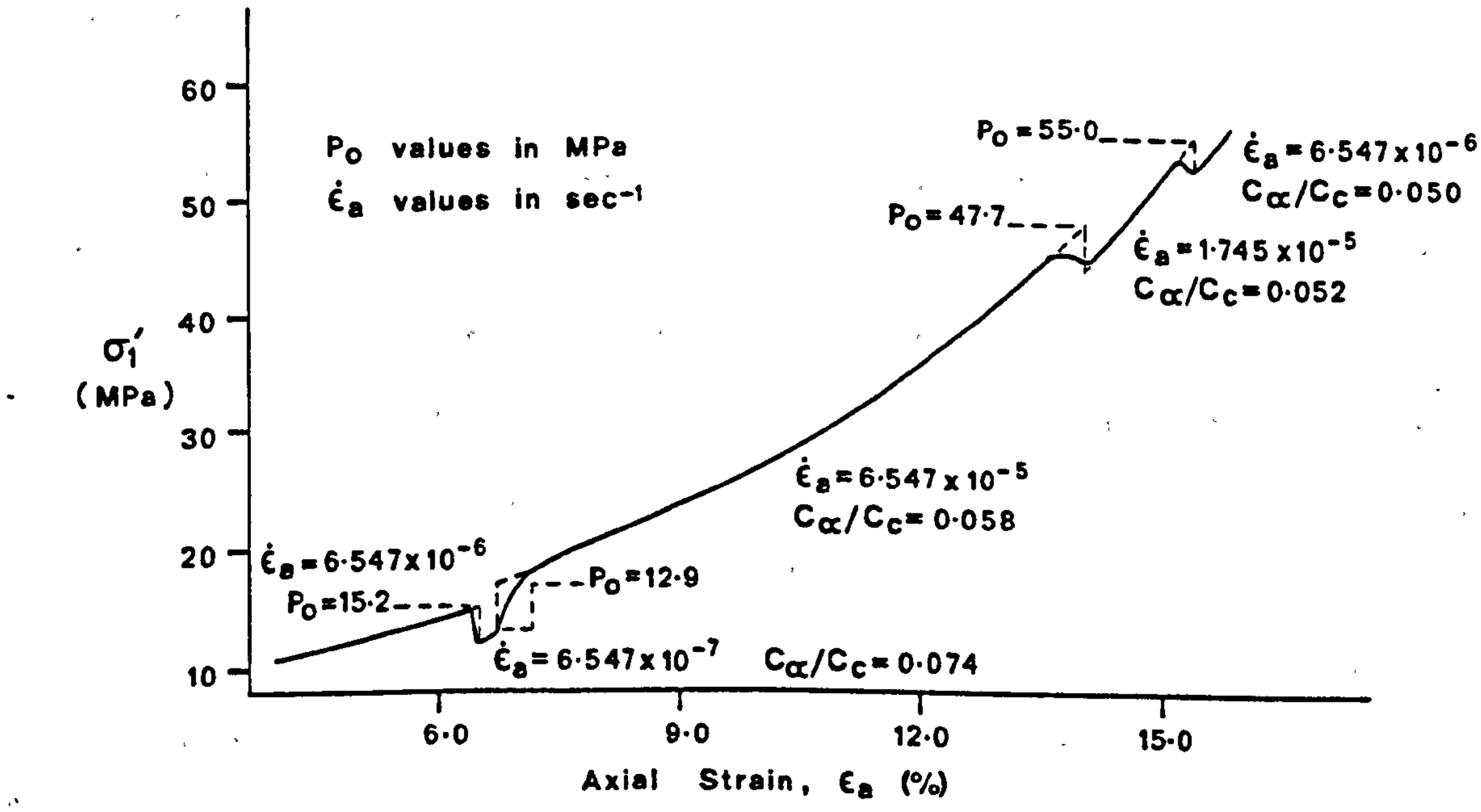

Figure 4.13b Analysis of strain rate variation in PB1.20.

time, due to secondary creep of the sample. At increasingly slower strain rates (in constant rate of strain tests), secondary consolidation becomes an increasingly important factor, contributing to the total deformation of the sample; thus Fig. 2.17 and Fig. 4.13a can be considered to be analogous. This strain rate behaviour, discussed in Chapter 2, can be expressed in terms of the ratio of secondary consolidation (C_α) to the coefficient of primary consolidation (C_c). Following the method of Mesri and Choi (1979) and de Waal and Smits (1985) the C_α/C_c ratio can be calculated. Fig. 4.13b shows that the C_α/C_c ratios decrease, with increasing vertical effective stress, from 0.074 to 0.050; this decrease was observed for Leda clay by Mesri and Godlewski (1977). The decrease can be explained by the larger C_α in the early post-yield deformation, due to slippage and shear of bonds. C_α will decrease with stress due to the smaller proportion of bonds remaining at the higher stress levels, and the presence of a more compact structure.

Testing individual samples at differing strain rates (Fig. 4.14), indicates that identical samples appear to show no trend in compaction, or in the yield point. These data seem to indicate that the chalk deformation does not exhibit any strain rate dependance. This was unexpected in view of the PB1.20 result presented above. The three tests followed very similar stress paths, with the PB3.20 compaction line occurring at slightly higher mean effective stresses in q-p' space, Fig. 4.15 (this will be discussed later, Chap. 4.10). As PB1.20 shows a strain rate effect, the repeatability of the samples and the testing procedure employed must be questioned. PB5.20 was repeated (PB6.20), allowing a slight increase in the radial strain to develop during compaction. As can be seen from Fig. 4.16, 2 microns radial deformation occurred which is shown by the steeper

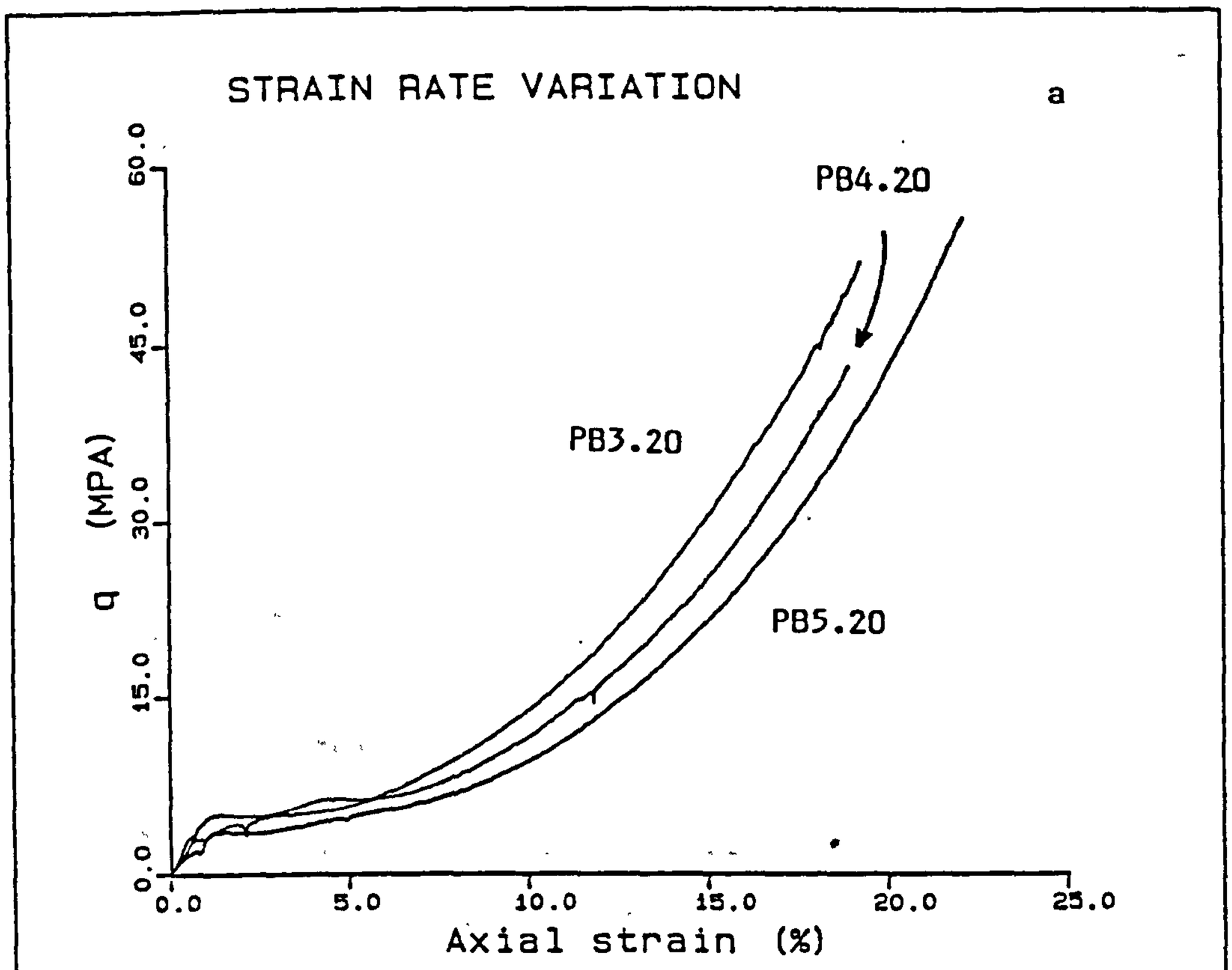

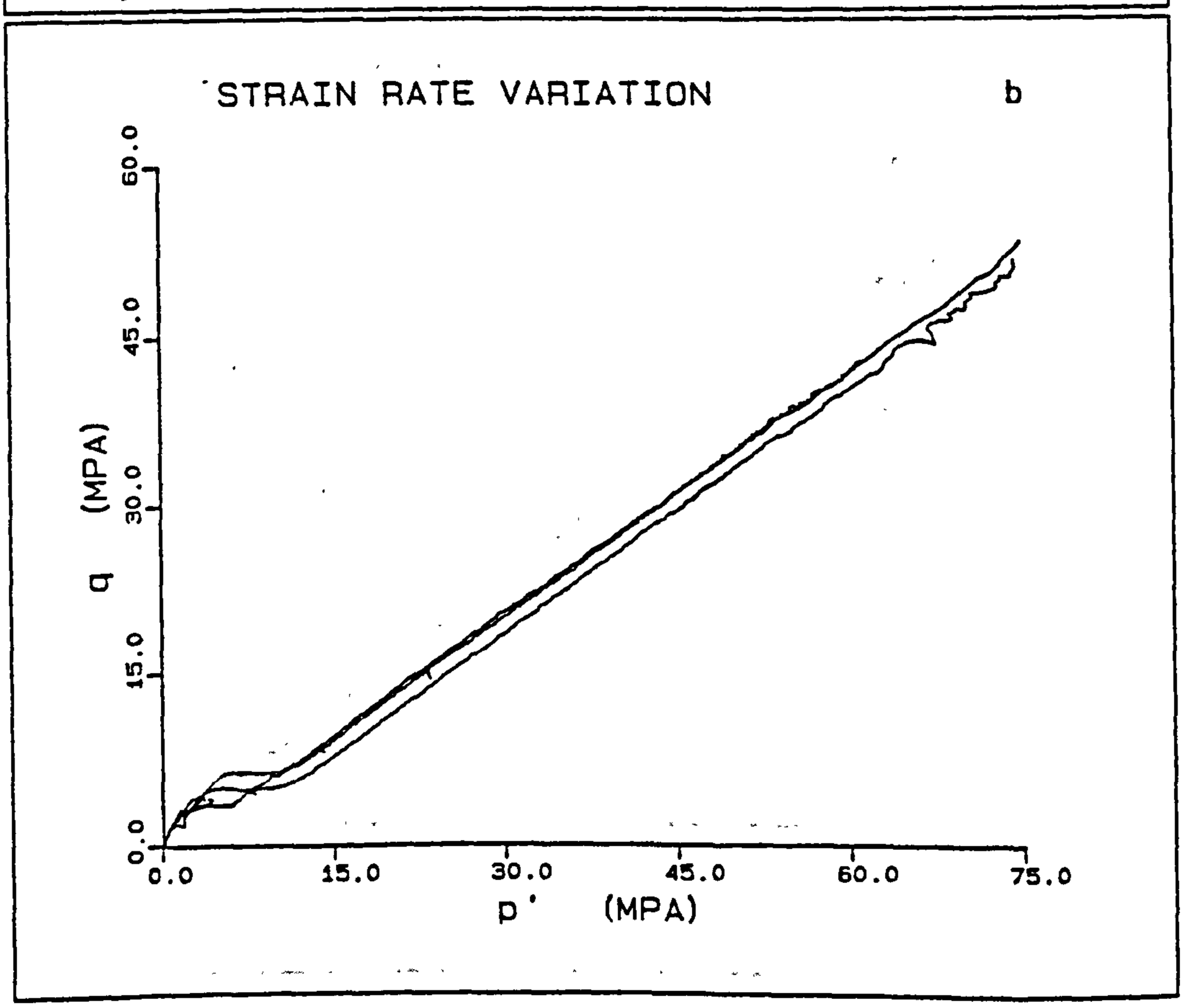

Figure 4.14 and 4.15 Comparison of three strain rate experiments.

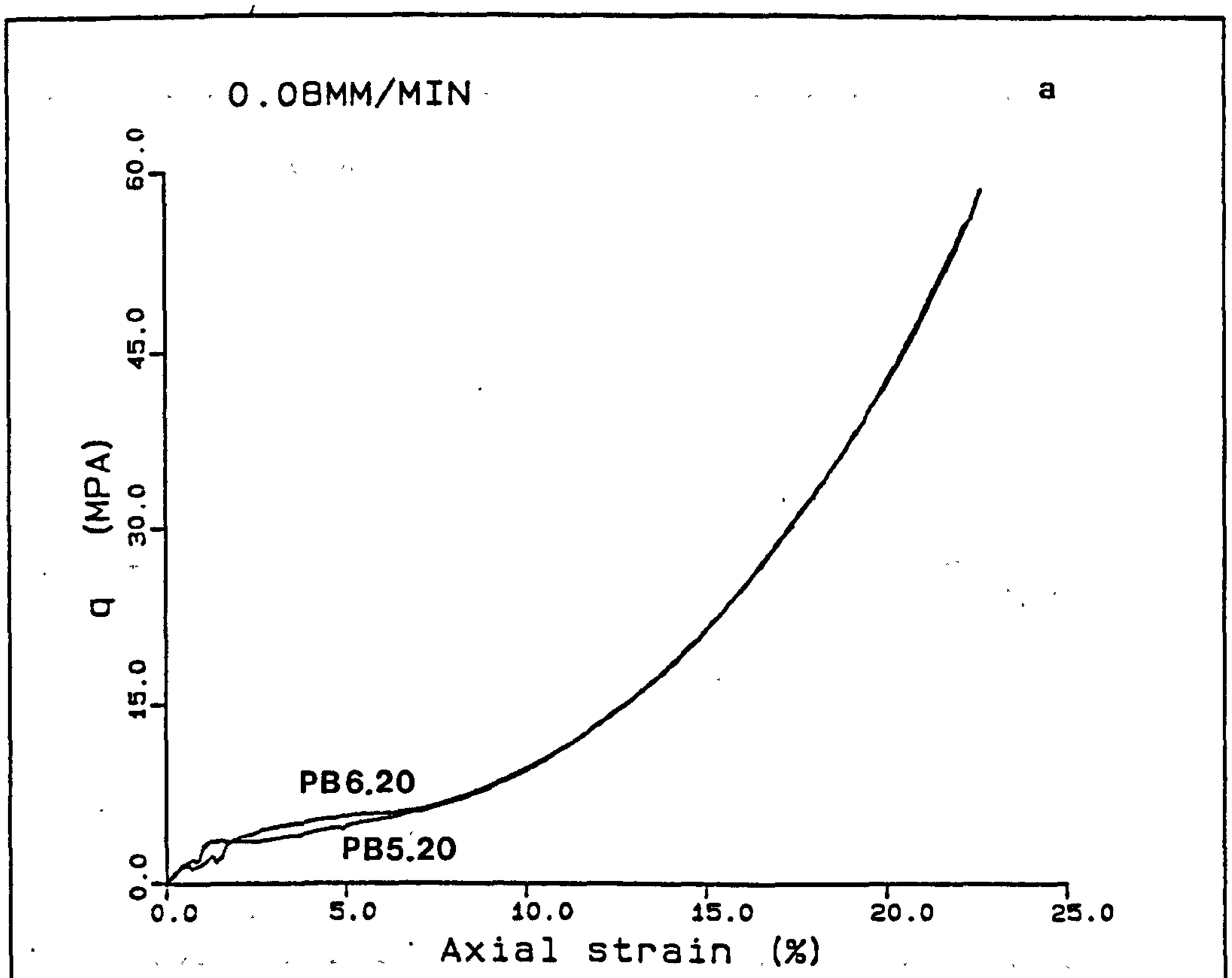

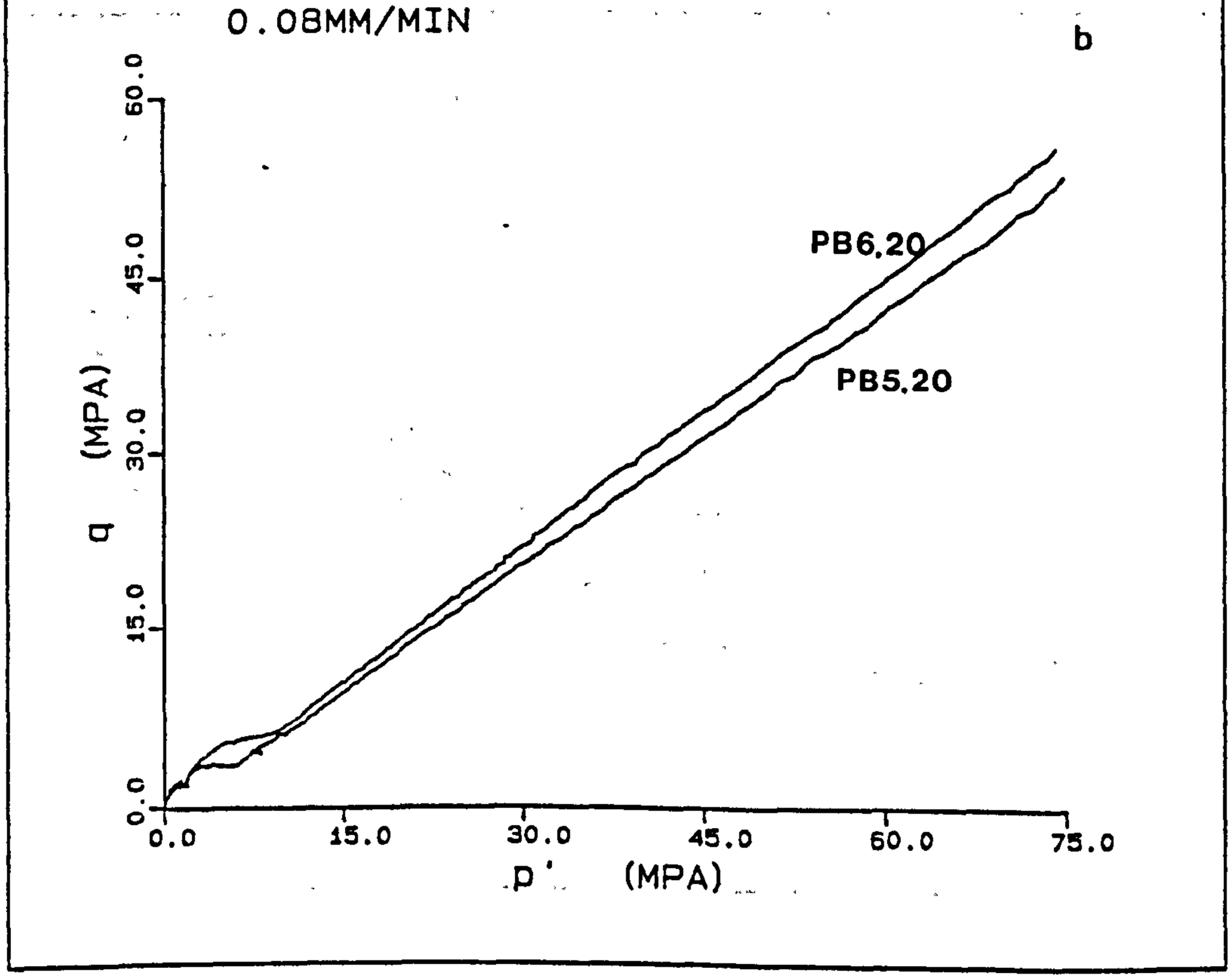

Figure 4.16(a-h) Comparison of tests PB5.20 and PB6.20.

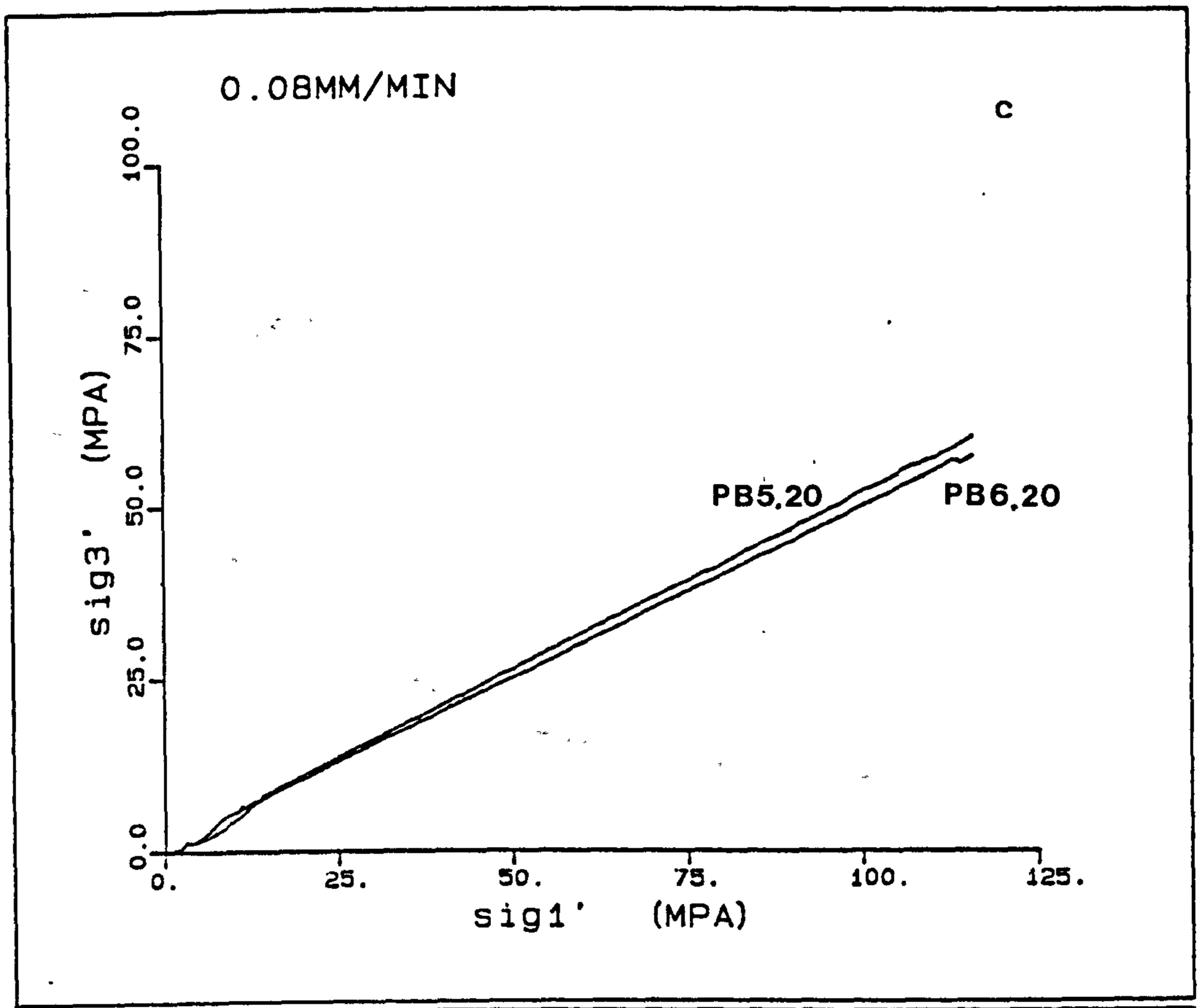
0.08MM/MIN
c
100.0
75.0
50.0
25.0
0.0
sig3' (MPA)
PB5.20
PB6.20
0.
25.
50.
75.
100.
125.
sig1' (MPA)

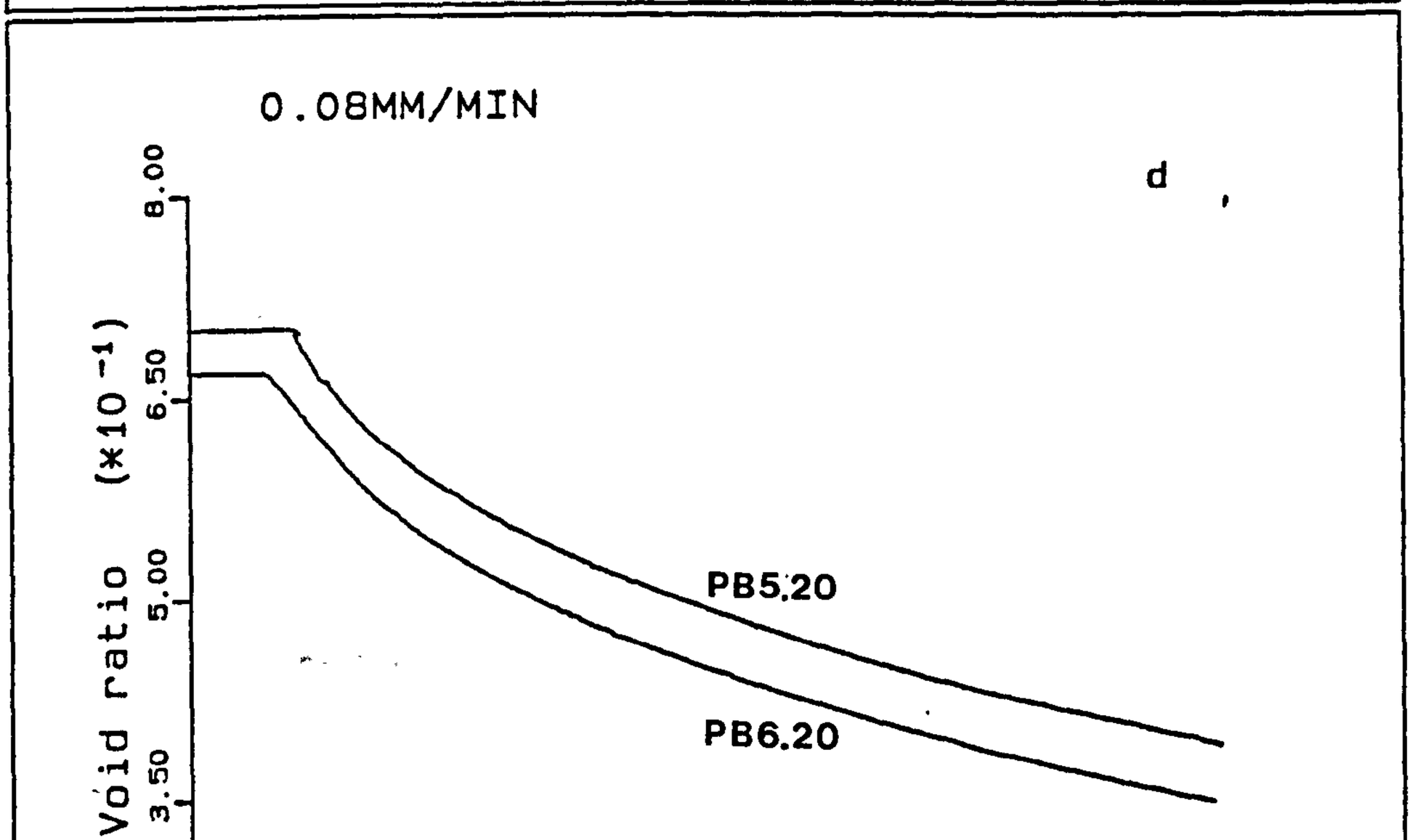
0.08MM/MIN
d
8.00
6.50
5.00
3.50
2.00
Void ratio (*10-1)
PB5.20
PB6.20
0.0
15.0
30.0
45.0
60.0
75.0
p' (MPA)

e

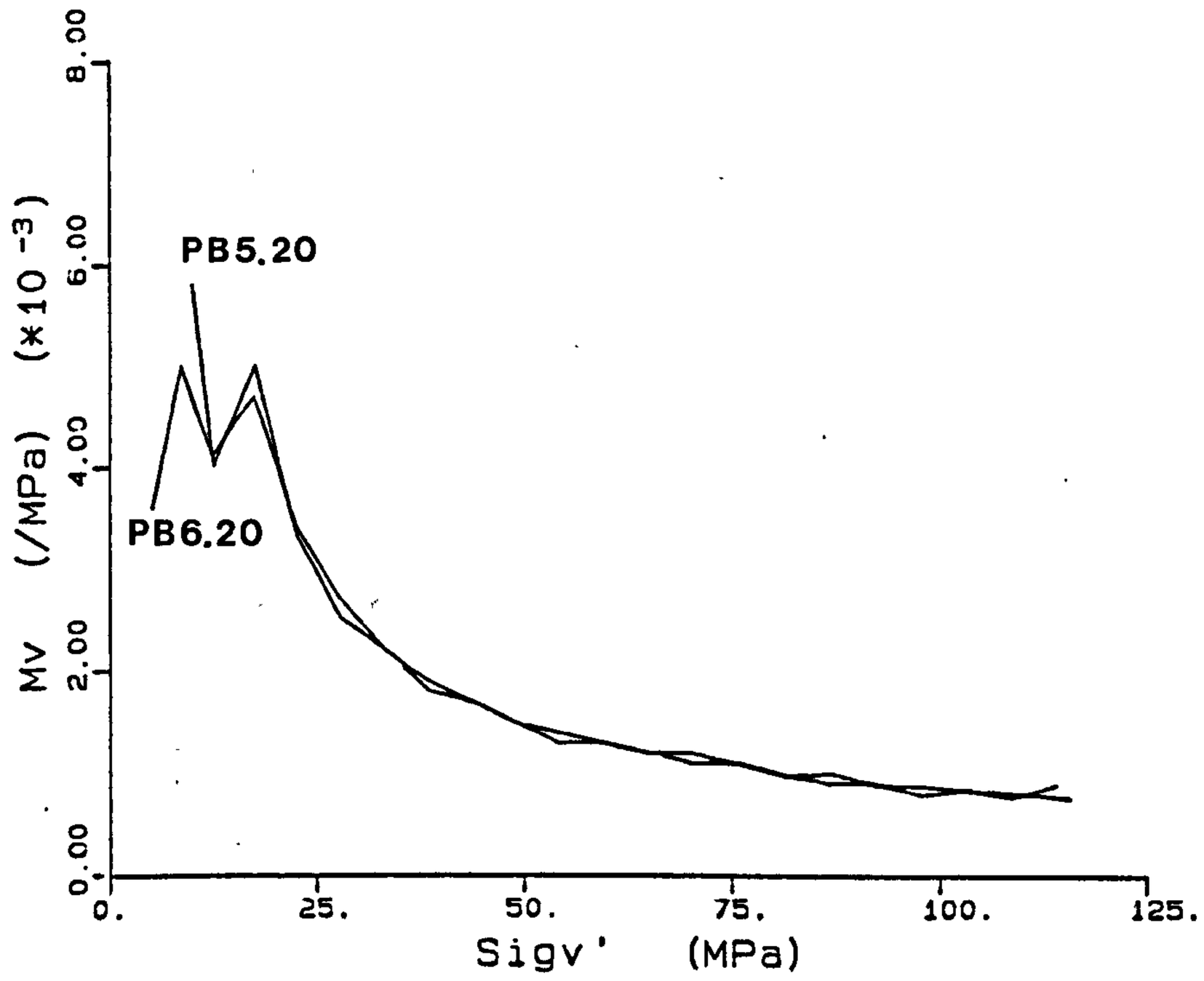
8.00
6.00
4.00
2.00
0.00
Mv (/MPa) (*10 -3)
PB5.20
PB6.20
0.
25.
50.
75.
100.
125.
Sigv' (MPa)

f

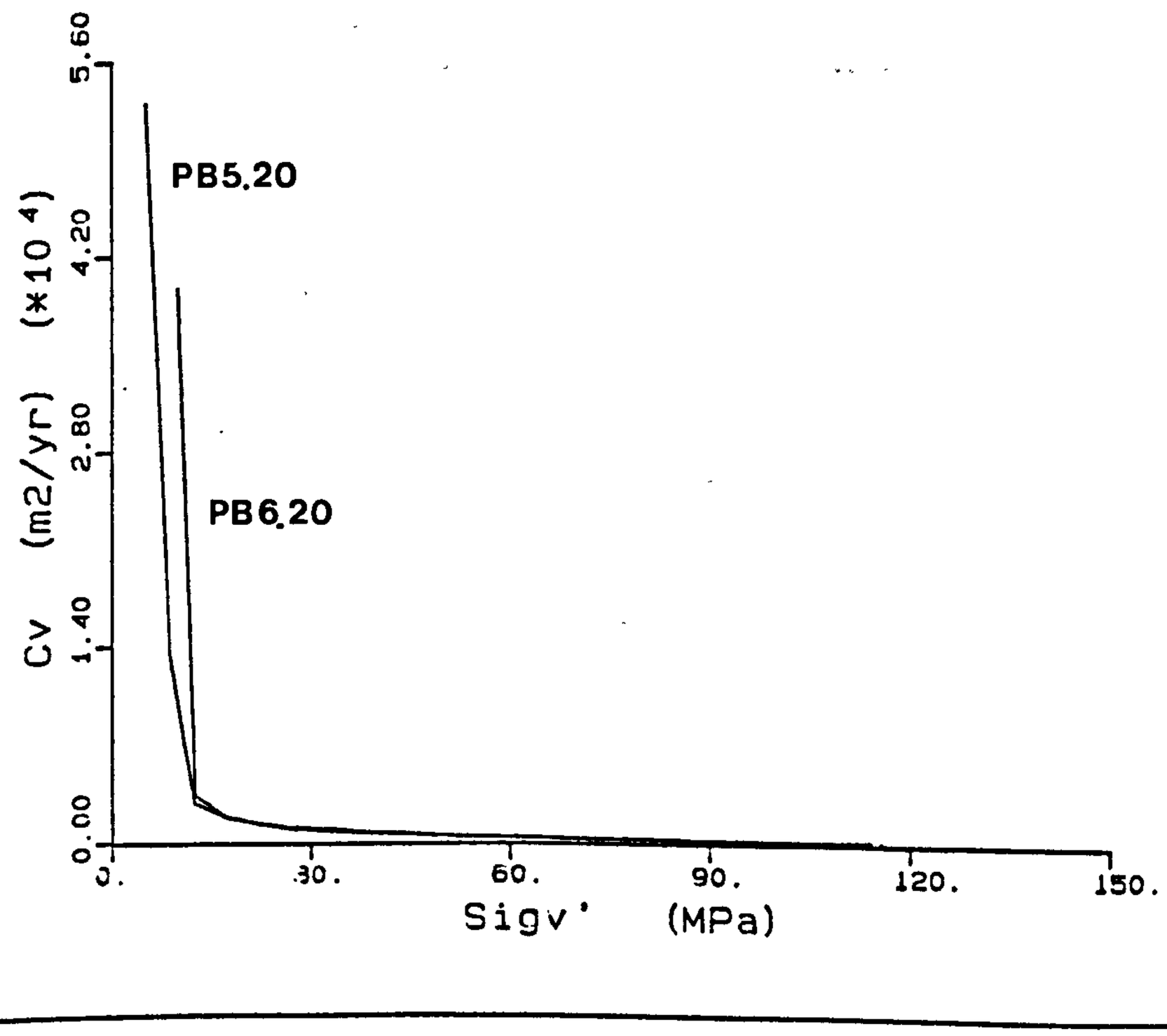
5.60
4.20
2.80
1.40
0.00
Cv (m2/yr) (*10 4)
PB5.20
PB6.20
0.
30.
60.
90.
120.
150.
Sigv' (MPa)

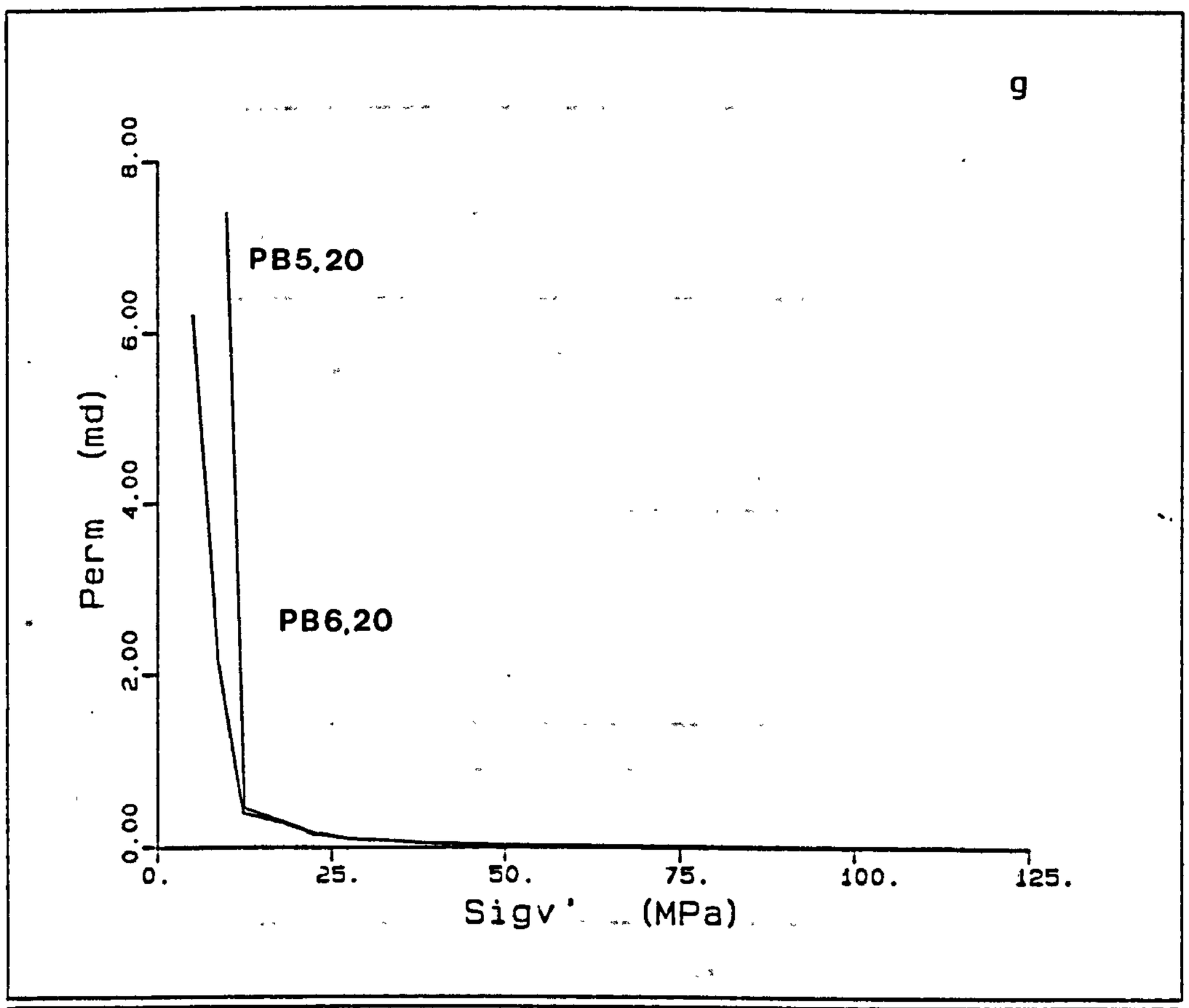
g
8.00
6.00
4.00
2.00
0.00
Perm (md)
PB5,20
PB6,20
0.
25.
50.
75.
100.
125.
Sigv' (MPa)

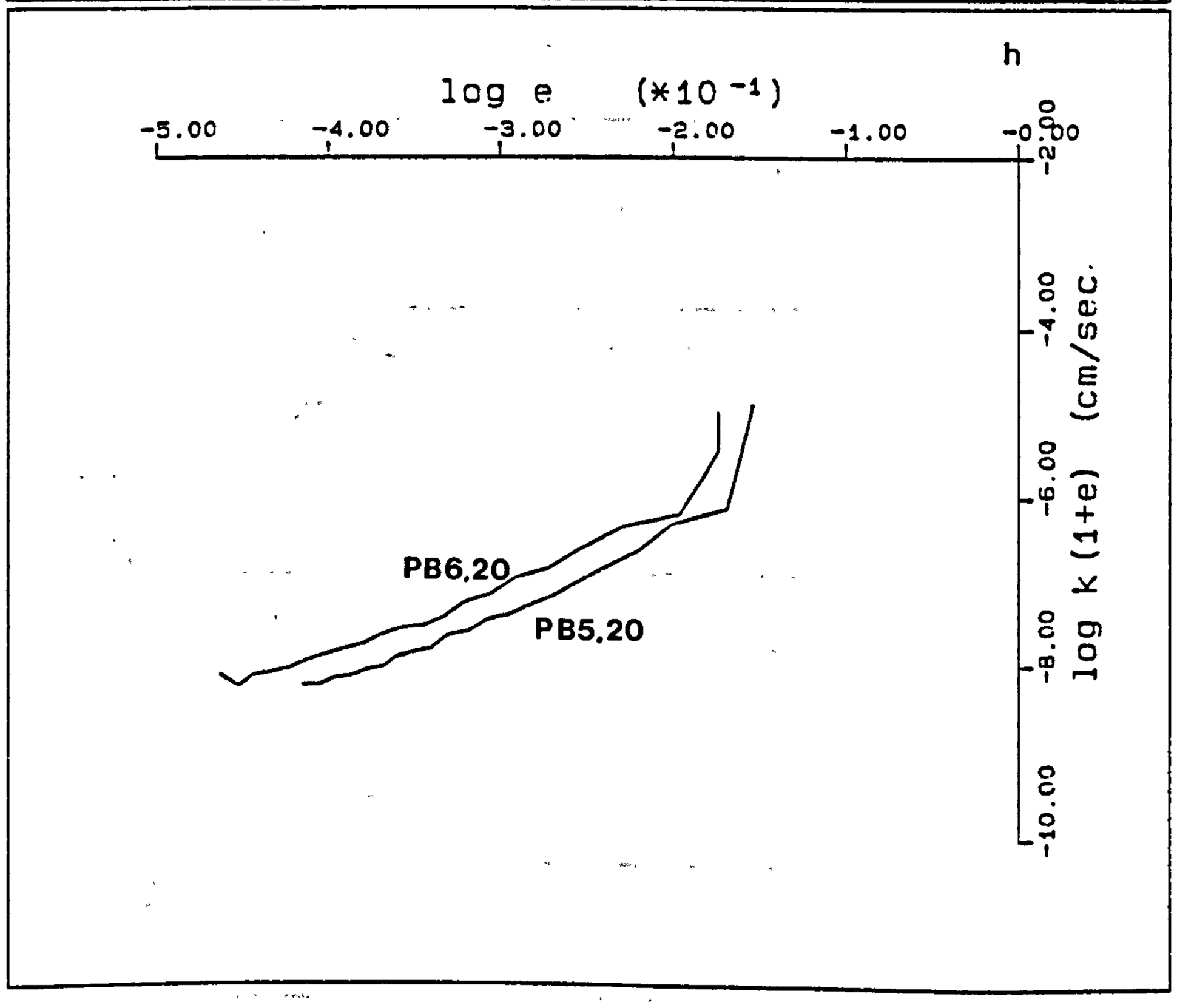
h
log e (*10 -1)
-5.00
-4.00
-3.00
-2.00
-1.00
-0.00
-2.00
-4.00
-6.00
-8.00
-10.00
log k (1+e) (cm/sec.
PB6,20
PB5,20

Table 4.2

Sample	Porosity %	Strain rate $_{-1}$ sec^{-1}	$\bar{K}_{oe}$	$\bar{K}_{opc}$	$\bar{K}_{onc}$	Young's modulus GPa	Yield point MPa	$\sigma_1'_{nc}$ MPa	p'_{nc} MPa
PB3.20	39.0	$6.444*10^{-6}$	---	1.047	0.529	0.629	5.00	15.5	11.7
PB4.20	39.9	$6.512*10^{-7}$	0.383	0.989	0.518	0.350	---	16.8	12.1
PB5.20	41.2	$1.716*10^{-5}$	---	1.000	0.538	0.350	3.68	8.4	6.1
PB6.20	40.1	$1.741*10^{-5}$	0.367	0.854	0.500	---	---	14.3	9.9
PB7.20	40.4	$1.764*10^{-6}$	---	1.294	0.516	1.723	5.03	11.5	8.2
PB8.20	41.3	$6.678*10^{-6}$	0.324	1.470	0.532	1.495	4.50	8.5	6.1

gradient in q-p' space (Fig. 4.16b) and the higher σ_1' at the same σ_3' (Fig. 4.16c). The stress-strain curves of PB5.20 and PB6.20 (Fig. 4.16a), are however, identical at stresses in excess of the deviatoric stress of 6MPa (mean effective stress of 9.8MPa). This is the approximate start of normal consolidation for PB6.20, the normal consolidation for PB5.20 starting at a mean effective stress of 6.1MPa (Table 4.2). Figs. 4.16a-4.16h demonstrate the similarity between experiments PB5.20 and PB6.20.

From the above it was concluded that for an accurate determination of the effects of strain rate, the pore collapse and elastic deformation should be eliminated from the analyses of the effect of strain rate on the compaction of individual samples. (Fig. 4.16a shows that the behaviour during the elastic and pore collapse parts of the stress strain curves is irregular).

The studies of Leroueil et.al. (1985) into the strain rate susceptibility of clay sediments, have been performed by comparing individual samples tested at different strain rates. The results of the studies by these workers have been discussed in Chap. 2.7 and can be summarised as follows:

1) A decrease in the stress at any particular strain, occurs with slower strain rates.

2) The stress-strain curves for compaction tests at different strain rates for clays, are normalisable to one trend, when the stress axis is divided by the stress at a particular strain. Therefore the whole stress-strain curve is normalisable and undergoes the strain rate reduction defined by the trend described in the above point, (1).

The stress-strain curves for the normal consolidation part of the compaction for the tests presented in Fig. 4.14 and of a fourth test PB7.20 (sampled from a different block) was considered, to see if any

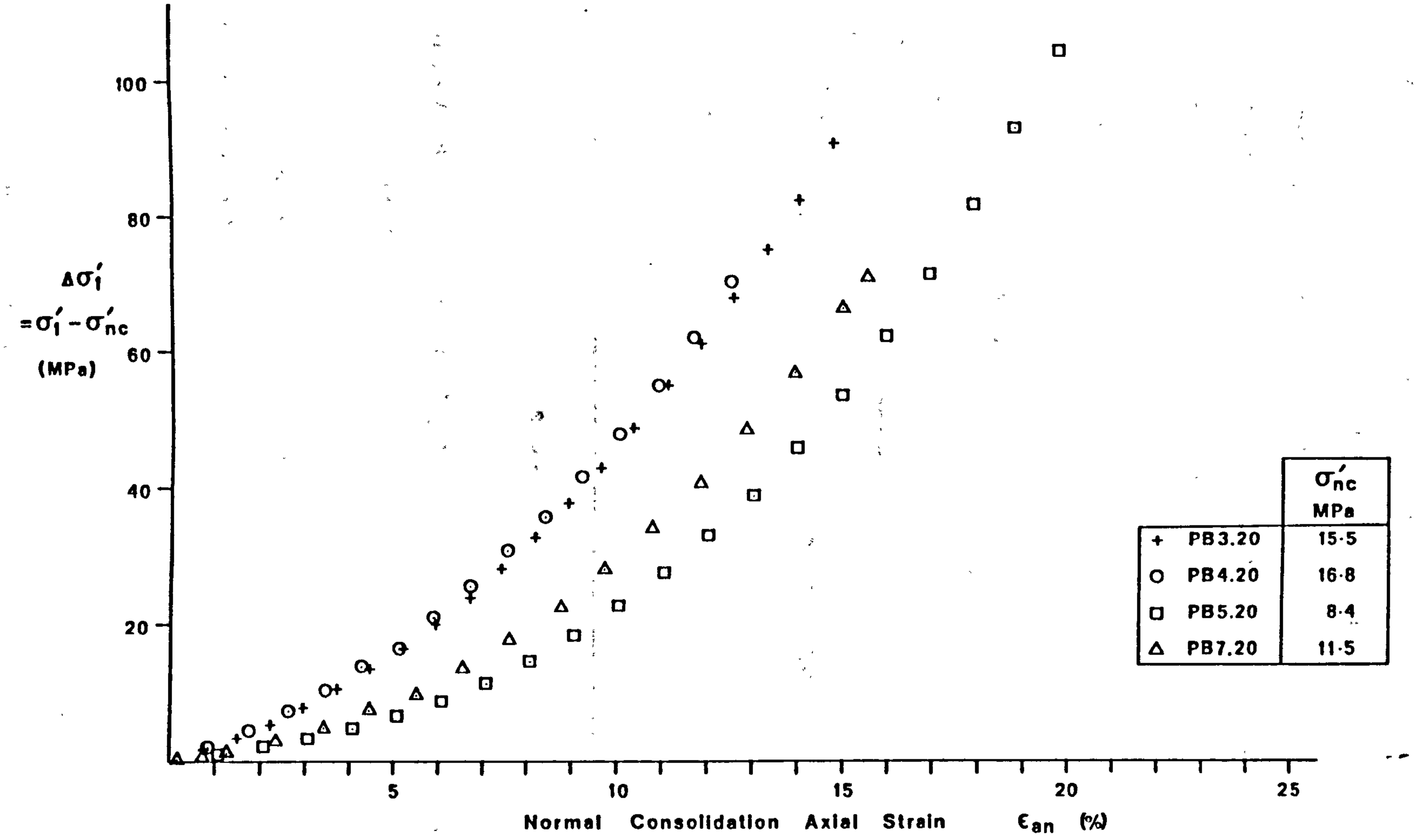

Fig. 4.17 $\Delta\sigma_1'$-Normal consolidation axial strain for samples tested at different strain rates.

trend was observed for this deformation, with strain rate (Fig. 4.17). This figure shows that a variation is seen, though the moduli of the curves seem to vary more regularly with the stress at the start of normal consolidation than with the strain rate. The axes of the stress-strain curves are, the difference in stress since the start of normal consolidation on the ordinate, and the strain since the start of normal consolidation on the abscissa.

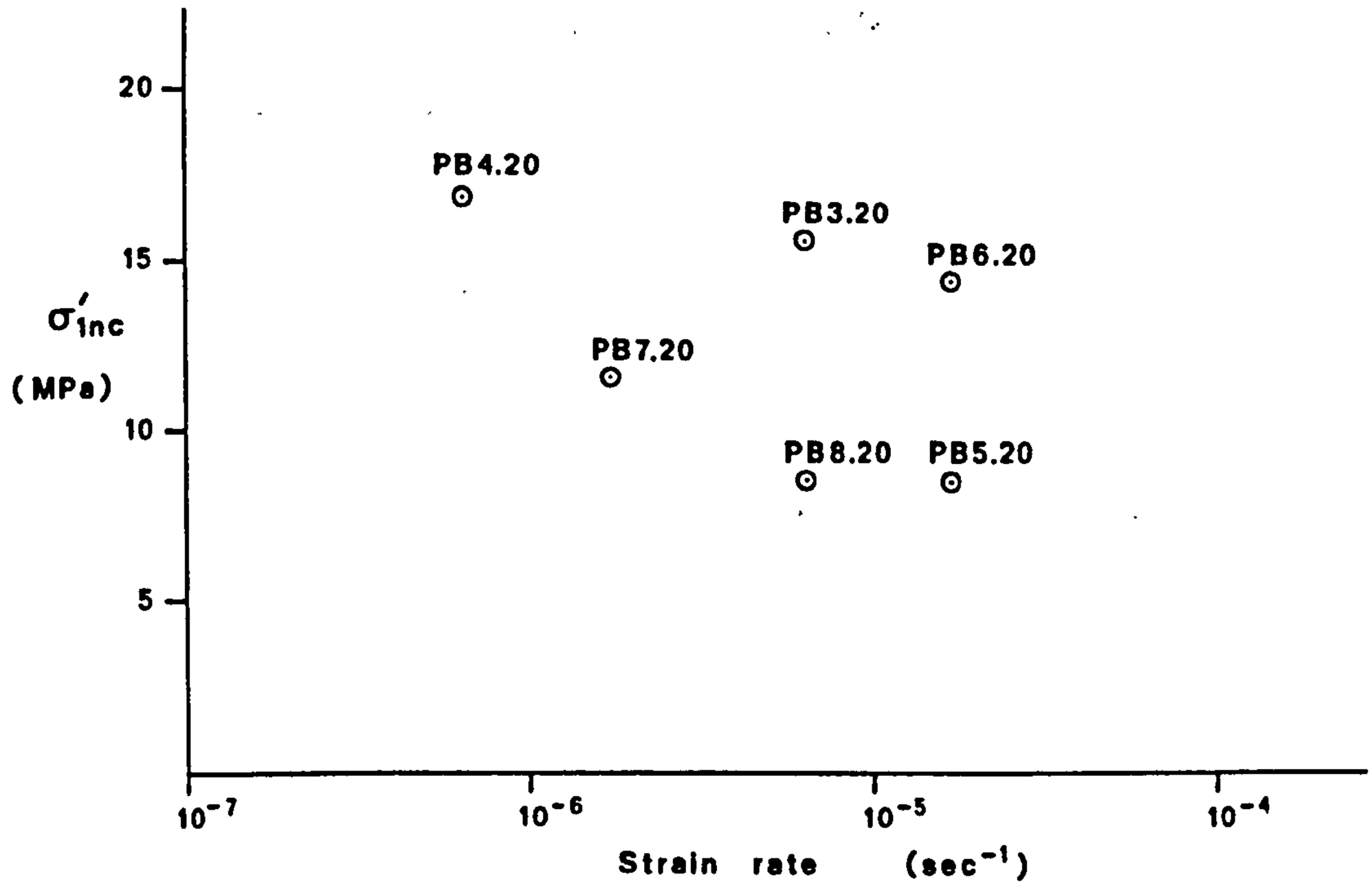

Figure 4.18 Variation of σ'_{inc} with strain rate for Pegwell Bay chalk.

When the stress at the start of normal consolidation for different strain rate tests is analysed (Fig. 4.18), a reverse trend to that observed by Leroueil et.al. (Loc.Cit.) for the preconsolidation pressures is seen. The maximum effective stress at the start of normal consolidation increasing with decreasing strain rate. The trend described by the data is very irregular as suspected from Fig.

4.17. The normalisation of the curves by Leroueil and his co-workers entailed dividing the stress axis of the individual tests by the stress at a particular strain. In the tests presented here the stress-strain curves were divided by the maximum effective stress at the start of normal consolidation (Fig. 4.19). The strain used in this diagram is the actual strain undergone by the sample, the diagram shows that the strain at the start of normal consolidation increases with decreasing strain rate, as does the stress (Fig. 4.18). These observations indicate that the elastic and the pore collapse deformation are strain rate dependant but not in the same manner as the normal consolidation compaction (Chap. 4.5). Unfortunately, the irregular breakdown of these chalks has eliminated the possibility for evaluating the strain rate dependance of the lower stress deformations.

To consider the normal consolidation compaction and to see if it is normalisable in the same manner as clays, the strain axis in Fig. 4.19 was adjusted by removing the strain due to the pore collapse and the elastic deformations. This is shown in Fig. 4.20. As a refinement of this, the actual axial strain since the start of normal consolidation was plotted in Fig. 4.21. Good agreement is obtained in both of these normalised plots. From these diagrams it can be seen that the normalised stress-strain curves for the normal consolidation compaction of the chalk are of the same form and identical. The sample reproducability between blocks, seen by PB7.20, is also excellent, samples from different blocks being normalised to the same normalised stress-strain curve.

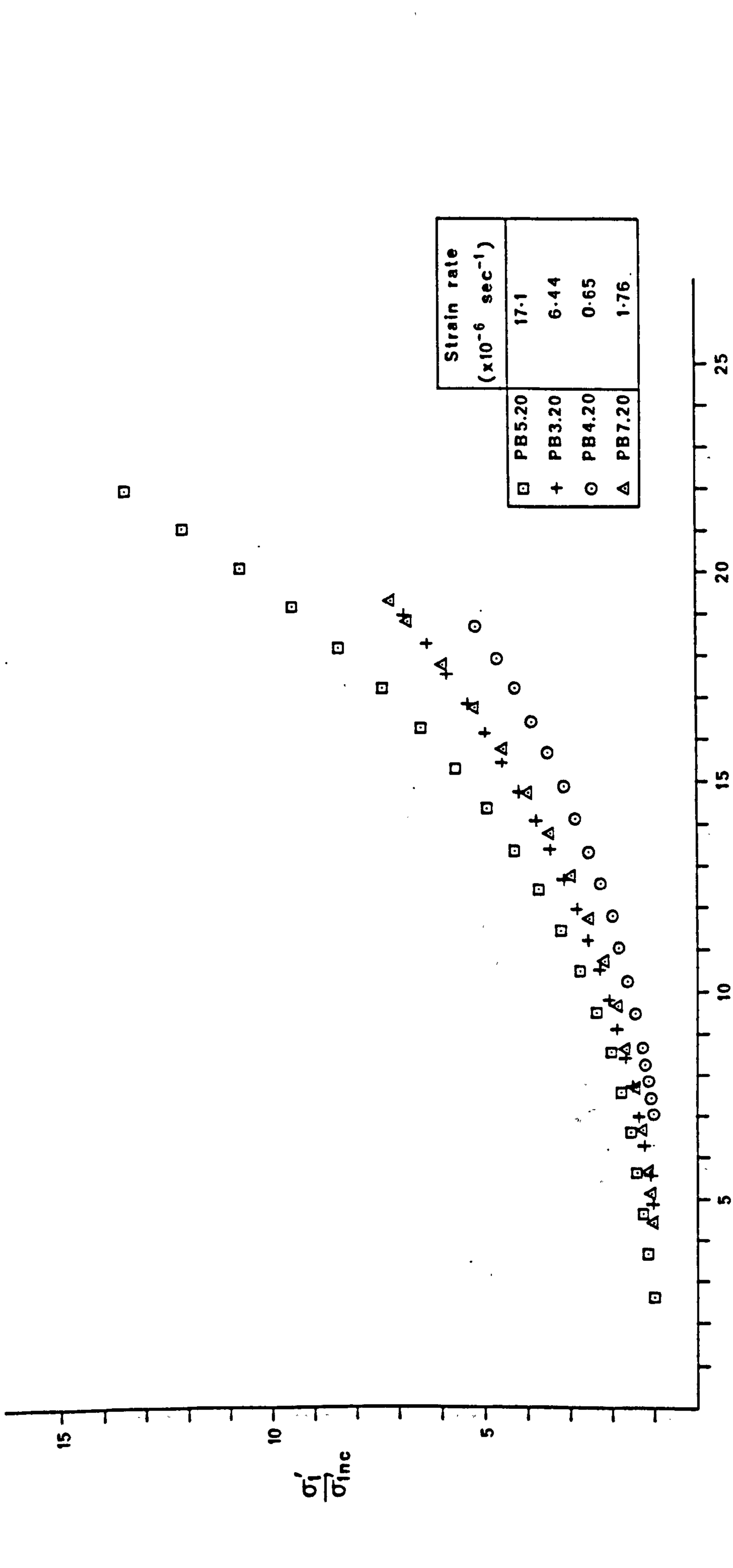

Fig. 4.19 Normalised stress-strain plots for samples of Pegwell Bay samples tested at different strain rates.

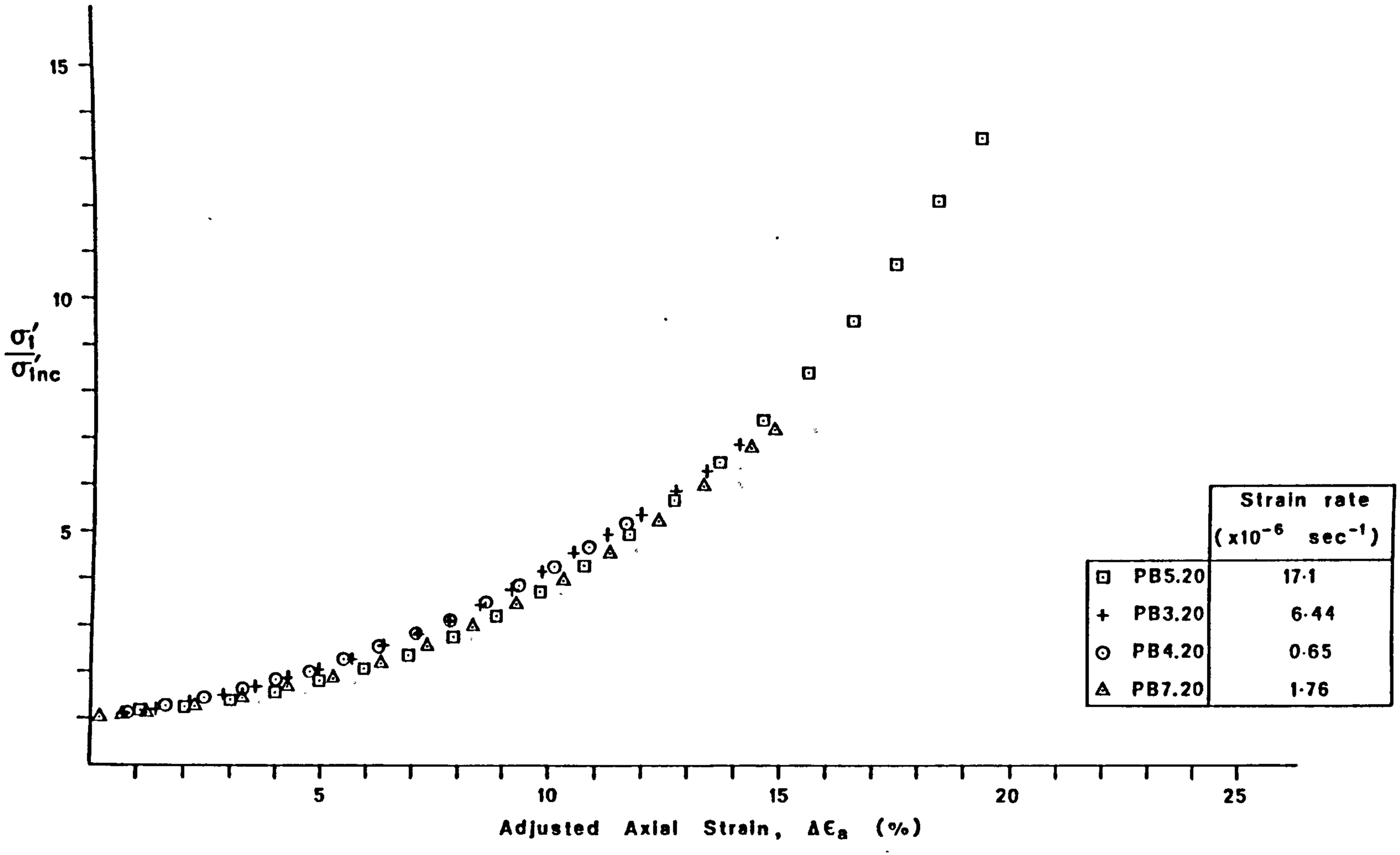

Fig. 4.20 Normalised stress-adjusted strain plots for samples tested at different strain rates.

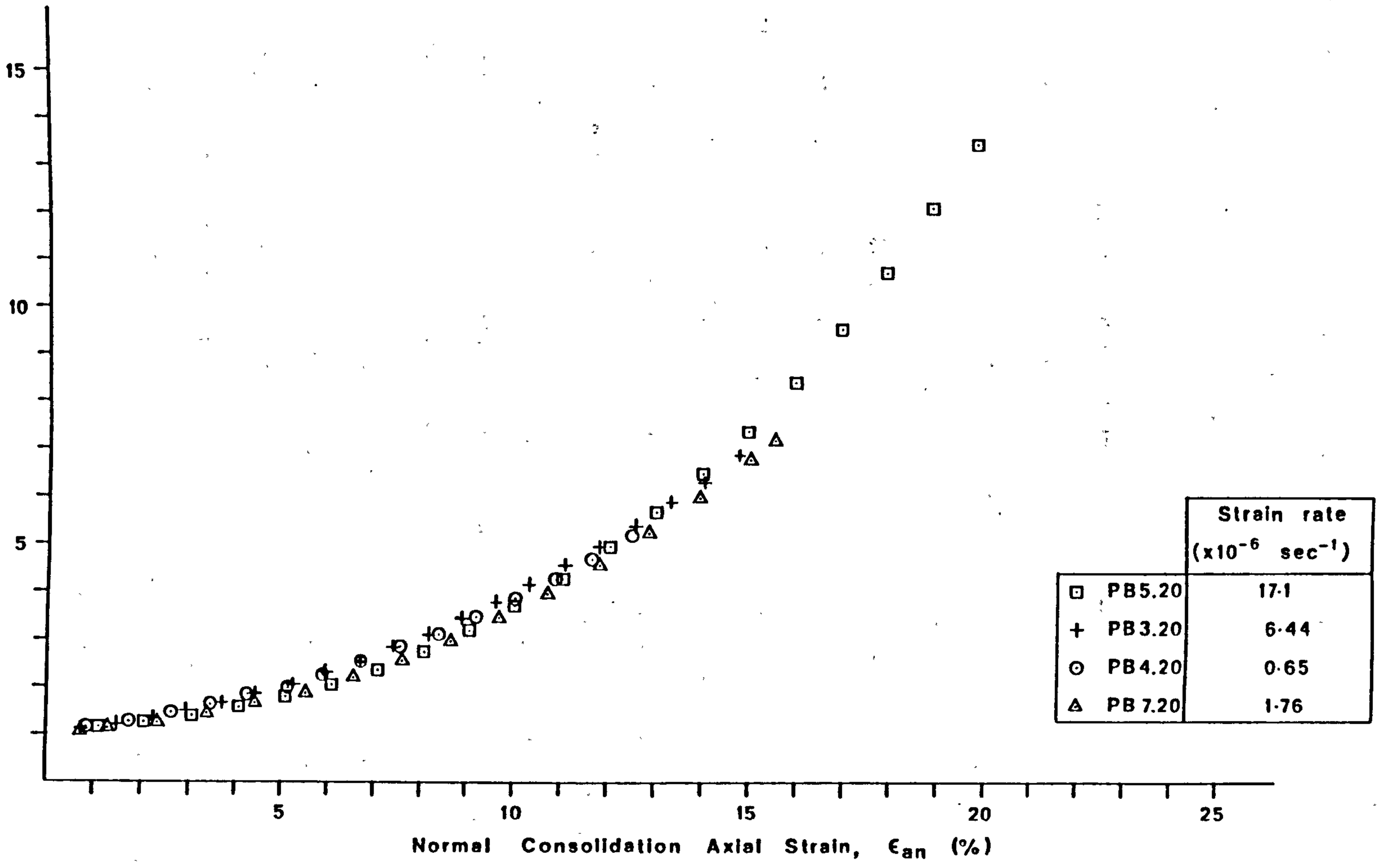

Fig. 4.21 Normalised stress-normal consolidation axial strain plots for samples tested at different strain rates.

The lack of a definite trend between the stress at the start of normal consolidation and strain rate, is probably a product of two factors: 1) the small number of samples tested, 2) the small range of strain rates employed. If such a trend could be observed, extrapolation of test data to field strain rates could be performed by denormalising the curves in Figs. 4.20 and 4.21.

4.4) THE INFLUENCE OF SAMPLE SHAPE ON THE COMPACTION BEHAVIOUR

The work on high pressure compaction reported in the literature, Teeuw (1971; 1973), van Ditzhuijen and de Waal (1984), de Waal and Smits (1985), de Waal (1986), van Kooten (1986), and Smits, de Waal and van Kooten (1986), samples used have a height to diameter (H/D) ratio of 0.600. The samples in this study have a H/D ratio of approximately 2 (Table A5.1, A5.2, A5.3), as recommended by Bishop (1958) (Chap. 3.2.2). Studies in rock and soil mechanics show that the sample size affects deformation parameters measured in the triaxial test (Brown and Gonano, 1974; Bishop and Green, 1965); hence, tests were run to see if the H/D ratio affected the amount of compaction observed in the chalks, and to see if the K_o ratio was affected by the end effects of the loading pistons.

The effect of H/D ratio was tested using three samples of chalk from Pegwell Bay of H/D ratios 1.962, 1.333, and 0.649; these were PB15.20, PB16.20, and PB17.20 respectively. All of the samples were water saturated and taken from one block. These samples were deformed at 0.01mm/min, 0.0068mm/min, and 0.0033mm/min respectively, so keeping the strain rate constant (Table 4.3). The stress-strain plots of these samples are shown in Fig. 4.22a. It can be seen that there is a large increase in the strain undergone at a particular deviatoric stress with decreasing H/D ratio. For these tests it can

Table 4.3

Sample	Porosity %	Strain rate sec^{-1}	$\frac{\text{Height}}{\text{diameter}}$	$\bar{K}_{oe}$	$\bar{K}_{opc}$	$\bar{K}_{onc}$	Young's modulus GPa	Yield point MPa
PB8.20	41.3	$6.678*10^{-6}$	1.988	0.377	1.441	0.529	1.49	4.5
PB9.20	41.3	$2.015*10^{-6}$	0.658	0.324	1.470	0.532	---	6.1
PB15.20	42.5	$2.169*10^{-6}$	1.962	0.311	0.000	0.528	---	3.5
PB16.20	42.5	$2.259*10^{-6}$	1.333	---	---	---	---	3.9
PB17.20	43.0	$2.255*10^{-6}$	0.649	0.250	1.528	0.532	---	3.6

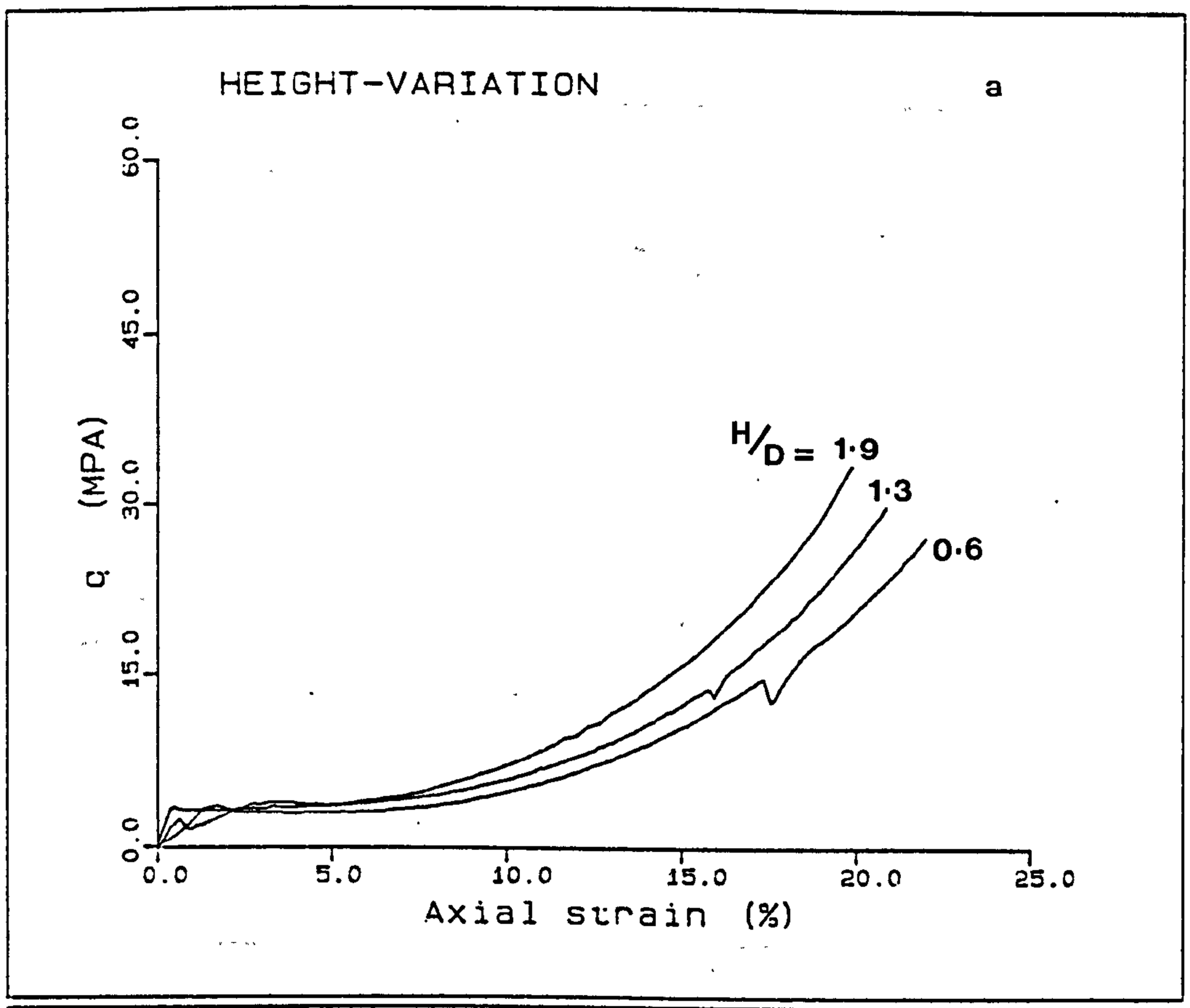

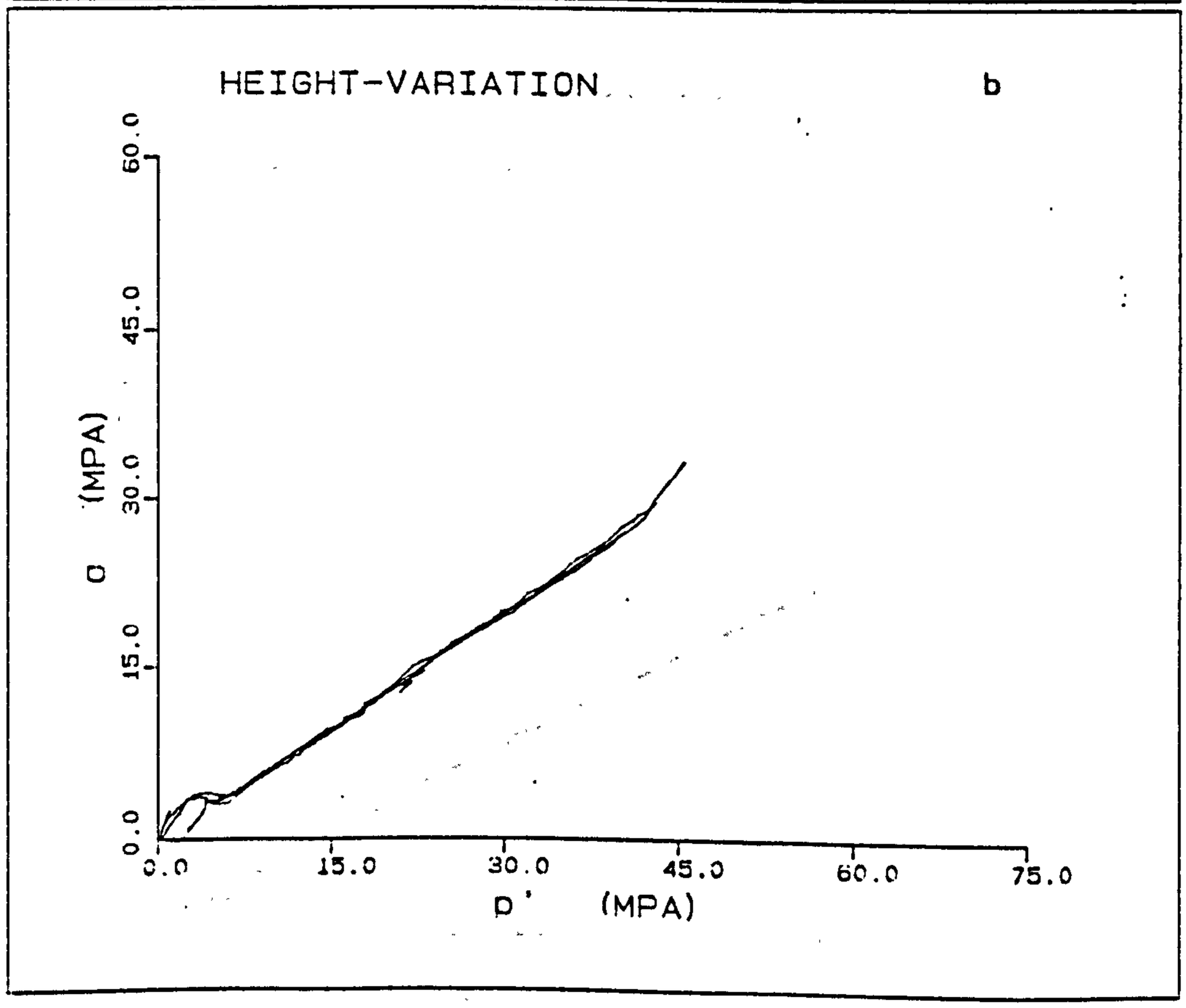

Figure 4.22(a-d) Effect of sample shape on K_o deformation

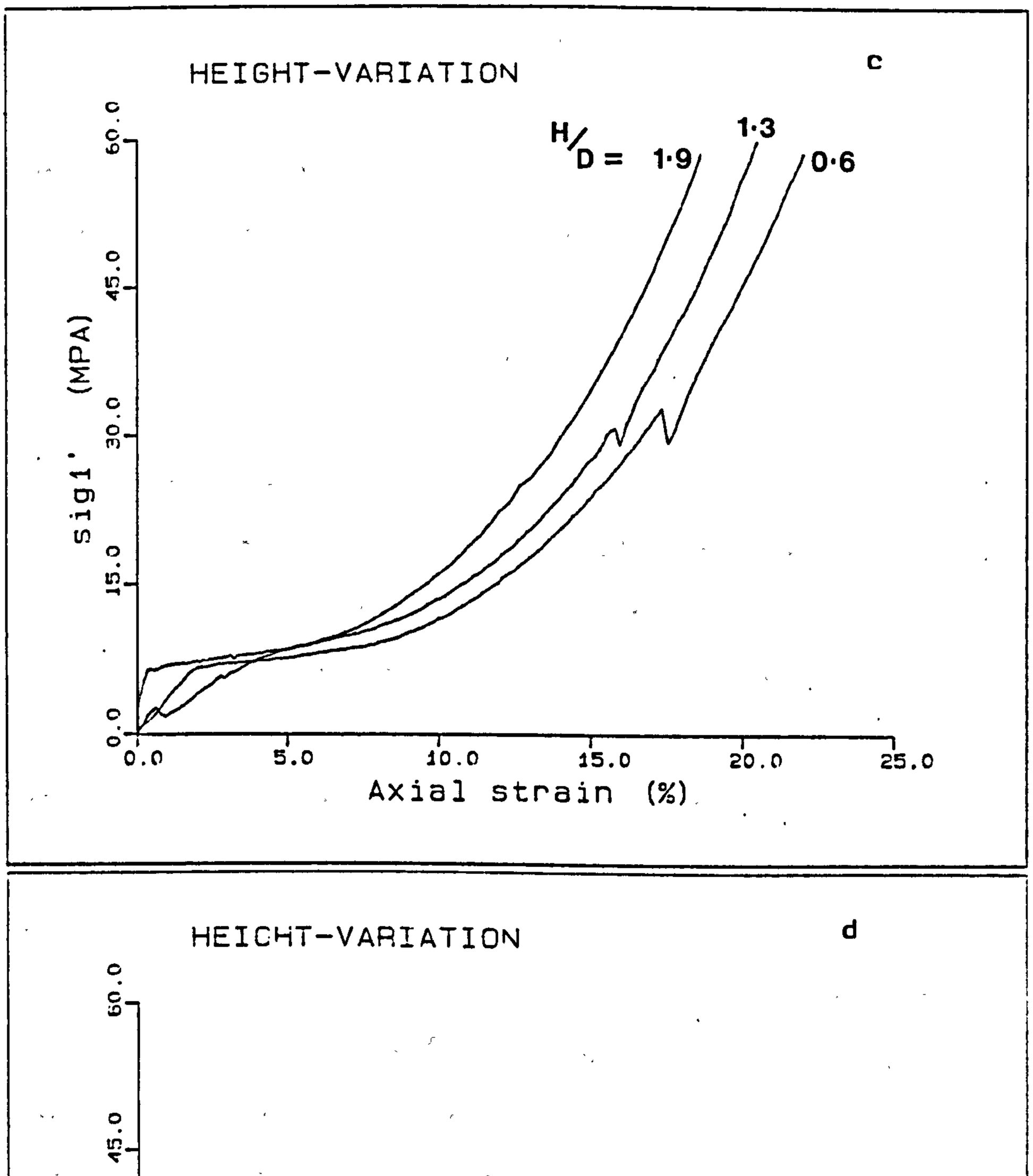
HEIGHT-VARIATION
c
H/D = 1·9
1·3
0·6
sig1' (MPA)
0.0
15.0
30.0
45.0
60.0
0.0
5.0
10.0
15.0
20.0
25.0
Axial strain (%)
HEICHT-VARIATION
d
sig3' (MPA)
0.0
15.0
30.0
45.0
60.0
0.0
15.0
30.0
45.0
60.0
75.0
sig1' (MPA)

be seen that the stress paths are identical, with the exception that the test PB15.20 was started at the higher cell pressure of 2.2MPa, and the elastic deformation was shifted to a higher p'. Analysis of the size effect on the elastic deformation is difficult because sample PB16.20 showed a step in its stress-strain curve where the load decreased. Nonetheless, if the initial tangent modulus is considered, this is seen to decrease with decreasing H/D ratio.

In the context of reservoir subsidence where the maximum effective stress is considered as opposed to the deviatoric stress, Fig. 4.22c shows the same characteristics as Fig. 4.22a: a) the whole curve shifted to higher axial strain at a constant maximum effective stress and b) there was a less stiff elastic pre-yield response with lower H/D ratio. The decrease in stiffness in the elastic region is not due to differing cell pressures as indicated by the similar $\bar{K}_o$ values for the elastic deformation for the three samples (Fig. 4.22d).

PB15.20, PB16.20 and PB17.20 show how the whole compaction curve is affected by the H/D ratios. To isolate the effects of the H/D ratio on the normal consolidation compaction curve, PB15.20 and PB17.20 were compared with PB8.20 and PB9.20. These latter tests have H/D ratios of 1.988 and 0.658 respectively, both were deformed at a constant deformation rate of 0.03mm/min, resulting in different strain rates to those of PB15.20 and PB17.20. The same normalisation procedure used for the strain rate analysis was performed on this data, Figs. 4.23 and 4.24, to eliminate strain rate effects from the comparison. The above diagrams show that in normalised stress-strain space, the effect of sample height on the magnitude of compaction is significant. The data have been extended across a small range of strain rates, and the magnitude of the effect is not altered to an observable extent.

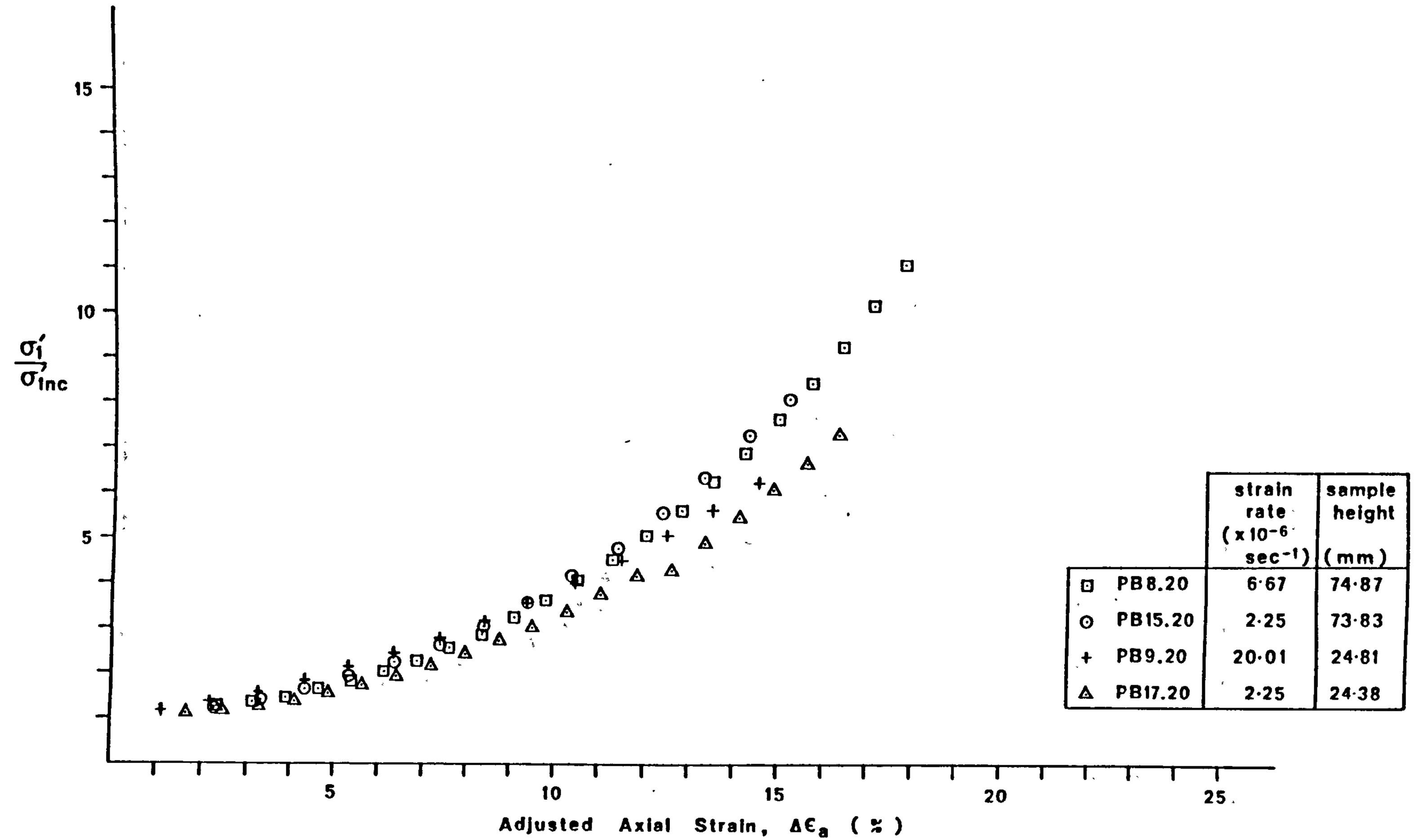

Fig. 4.23 Normalised stress - adjusted strain plots for samples of different H/D ratios and strain rates.

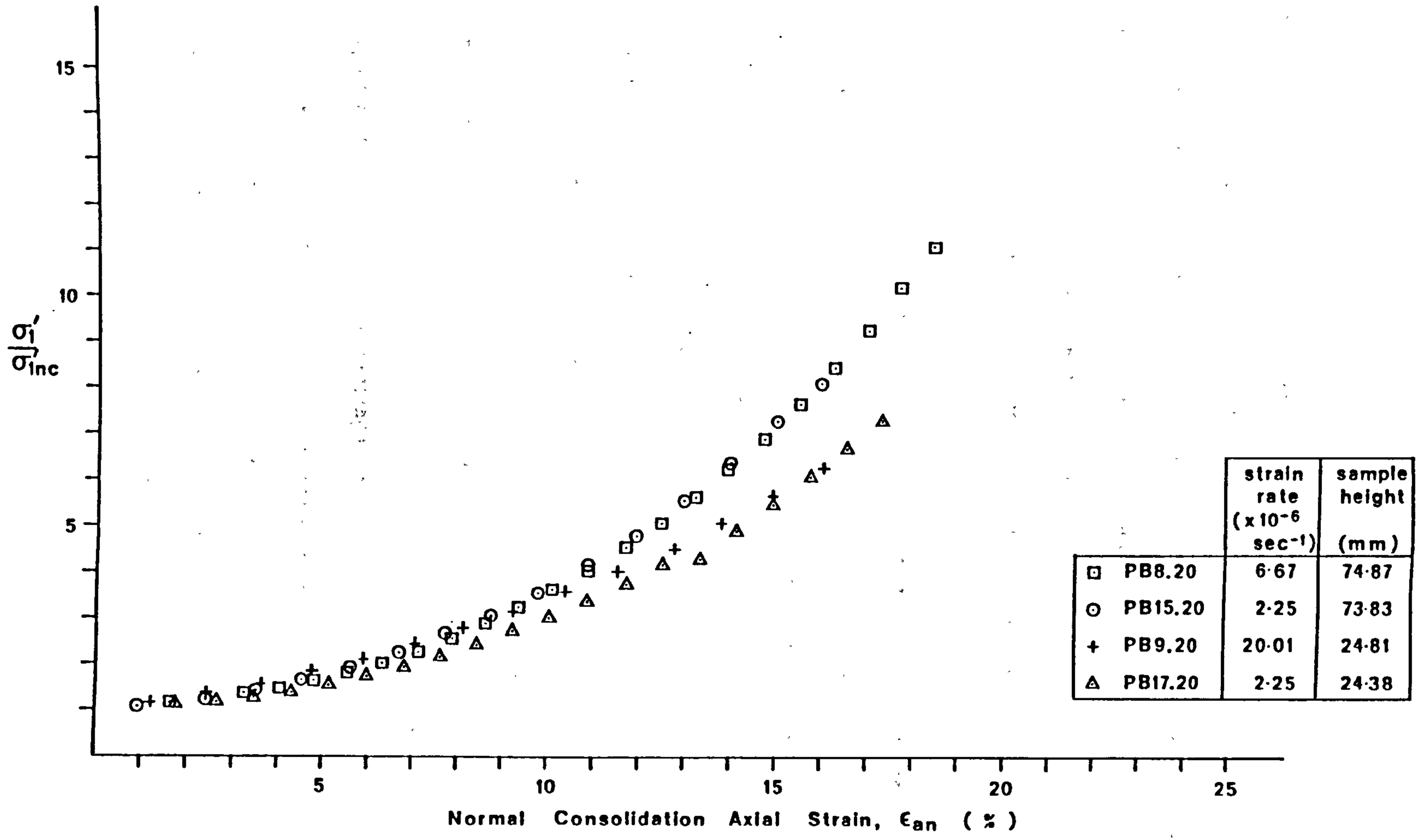

Fig. 4.24 Normalised stress - normal consolidation axial strain plots for samples of different H/D ratios and strain rates.

Based on the limited number of experiments performed on the effect of sample shape on the K_o compaction characteristics of chalk, it can be stated that stress-strain deformation of the chalks are dependant upon the relative dimensions and the shape of the sample. Two sets of tests in which strain rate was varied for samples of similar H/D ratio showed the same pattern of normal consolidation deformation as other samples of the same shape, supporting the results from samples of differing H/D ratio performed at identical rates of strain. A comparison between these samples required normalisation of the normal consolidation part of the stress-strain curve to eliminate strain rate effects.

The results of this part of the experimental programme are of great importance in oil field subsidence prediction, because as stated at the start of this section, most workers use a short sample of H/D ratio 0.6 and since the results presented here suggest varying magnitudes of deformations depending upon sample shape, the question concerning the most applicable sample shape to the problem of oil field subsidence studies must arise. Before this question is seriously approached more studies on different materials are required to verify the results presented above.

4.5) TEMPERATURE EFFECTS ON COMPACTION

The effect of temperature on the compaction of sediments has been reviewed in Chapter 2. In this section the effect of temperature will be discussed with reference to the Butser Hill chalks tested at elevated temperatures of 60^oC and 100^oC which are compared with the tests at 20^oC. The North Sea chalks tested at 50^oC show no deviations from the behaviour of those at 20^oC (Figs. 4.2, 4.4, and 4.5), although subtle changes could be obscured by the gross effects of

porosity differences, especially in such a small number of samples tested.

The Butser Hill samples tested at elevated temperatures were BH14.60 and BH17.60 at 60°C and BH15.100 and BH16.100 at 100°C. Unfortunately during BH15.100 one of the wires connecting the strain belt strain gauges became detached, and so a hydrostatic experiment was attempted. However, during the early stages of the hydrostatic stress increase, the sample membrane failed and the test abandoned. As described in App. 5, BH14.60 underwent a large deviation off the K_o stress path, and the test was repeated in BH17.60, whereupon a collapse of a void or burrow caused an initial large increase in the top pore pressure and in the volume change measurement, Figs. A5.25d,f,g,h. The two experiments are compared in Fig. 4.25. It can be seen that there is only a slight deviation in stress-strain curves, Fig. 4.25a, BH17.60 having approximately 0.55% axial strain less than BH14.60 (at an axial strain of 7% in BH14.60). The q-p' plot, Fig. 4.25b, shows that these two experiments have almost exactly the same stress path, with the exception of the deviation off K_o by BH14.60. Fig. 4.25c shows this in principle effective stress space. The pore pressures do not correspond at all well due to the collapse in BH17.60, which raised the pore pressure initially to 5.8MPa. The void ratio plots, Fig. 4.25e and 4.25f parallel each other despite the collapse offsetting BH17.60 from BH14.60, and despite the deviation off K_o by BH14.60. So for comparative purposes with the other temperature tests BH14.60 was used and the data from the deviation off K_o ignored.

Fig. 4.26 shows the comparison between BH18.20, BH14.60 and BH16.100; the data for these tests are presented in Table 4.4. From Fig. 4.26a, it can be seen that the samples have different yield

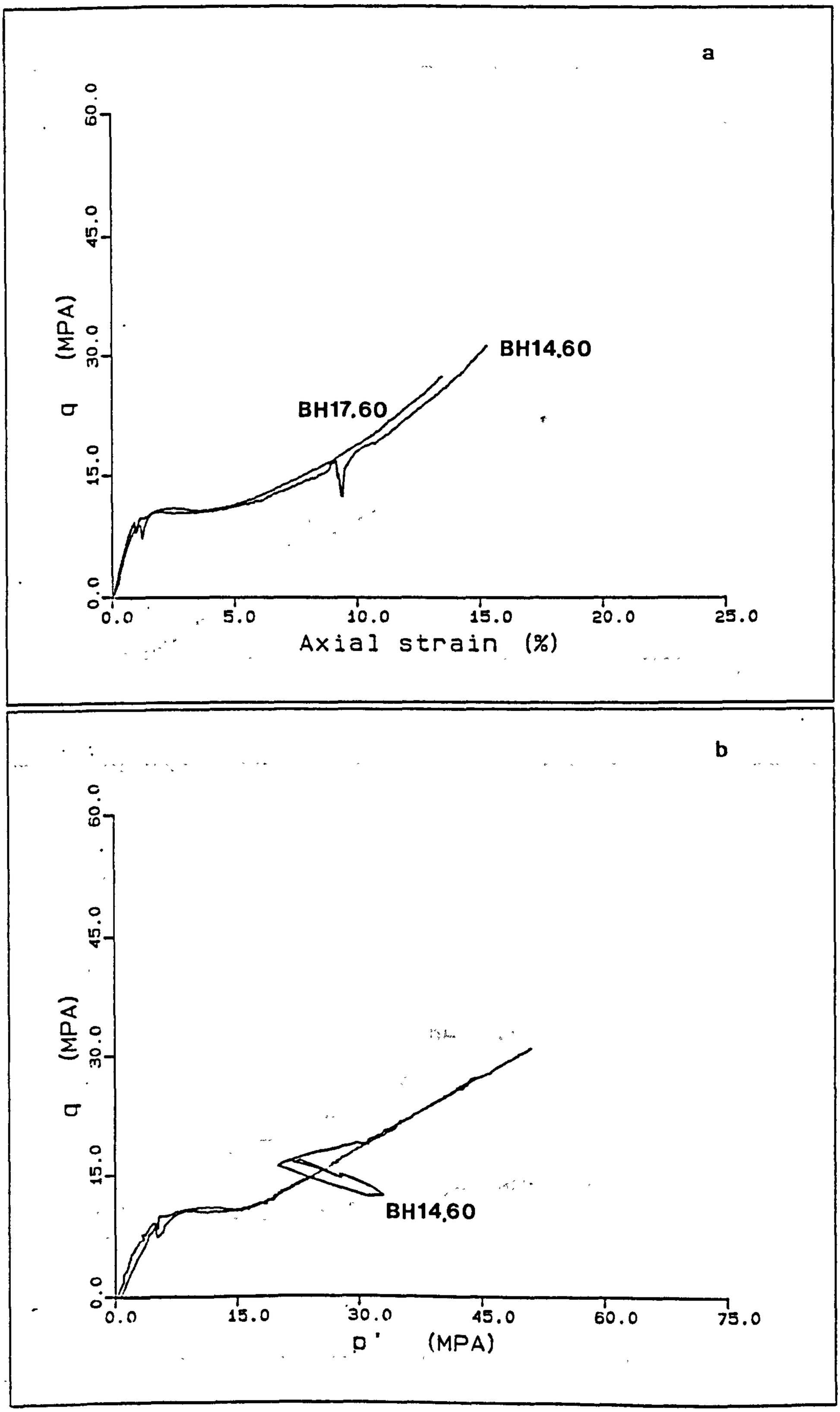

Figure 4.25(a-f) Comparison of BH14.60 and BH17.60

c

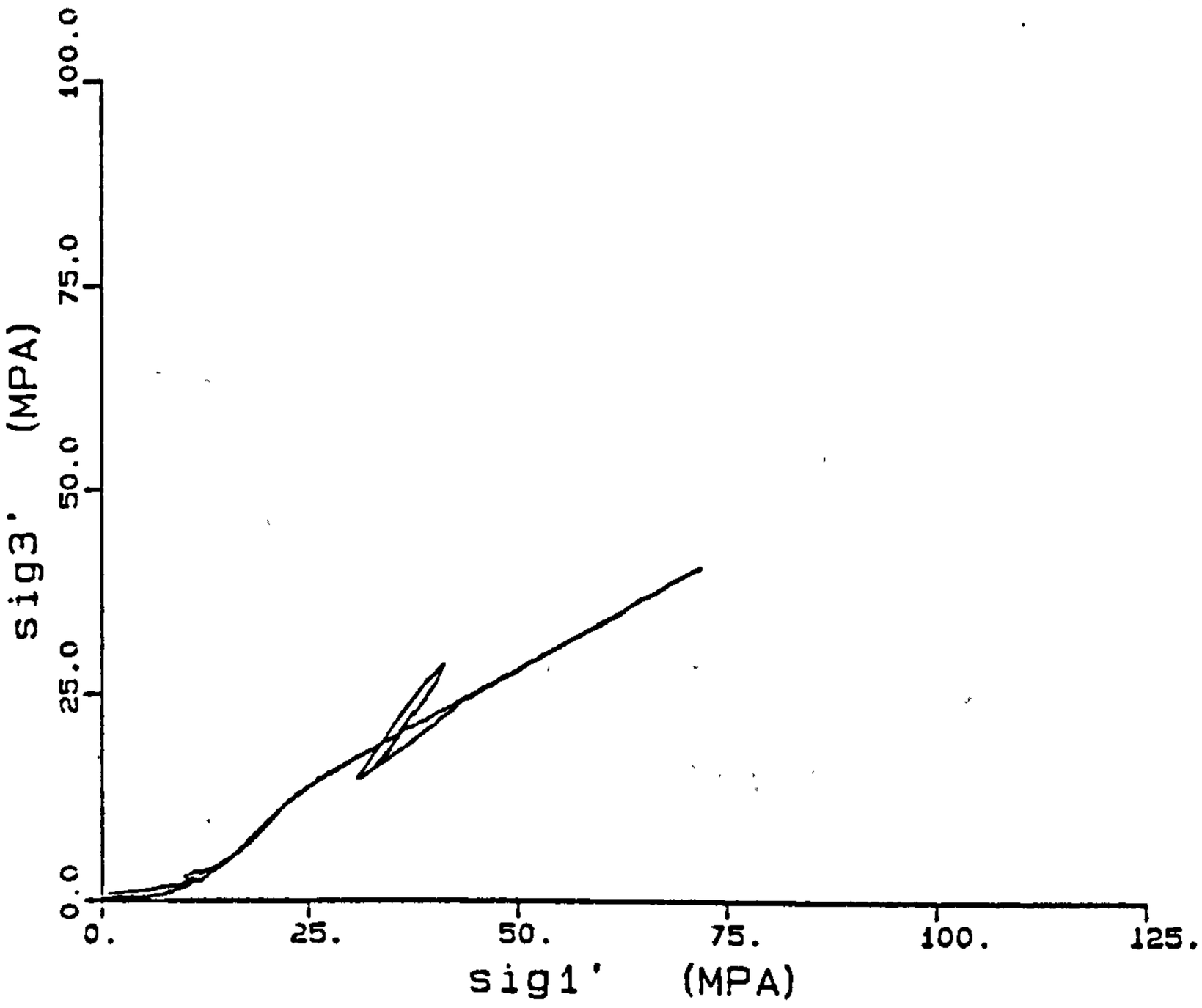
sig3' (MPA)
0.0
25.0
50.0
75.0
100.0
0.
25.
50.
75.
100.
125.
sig1' (MPA)

d

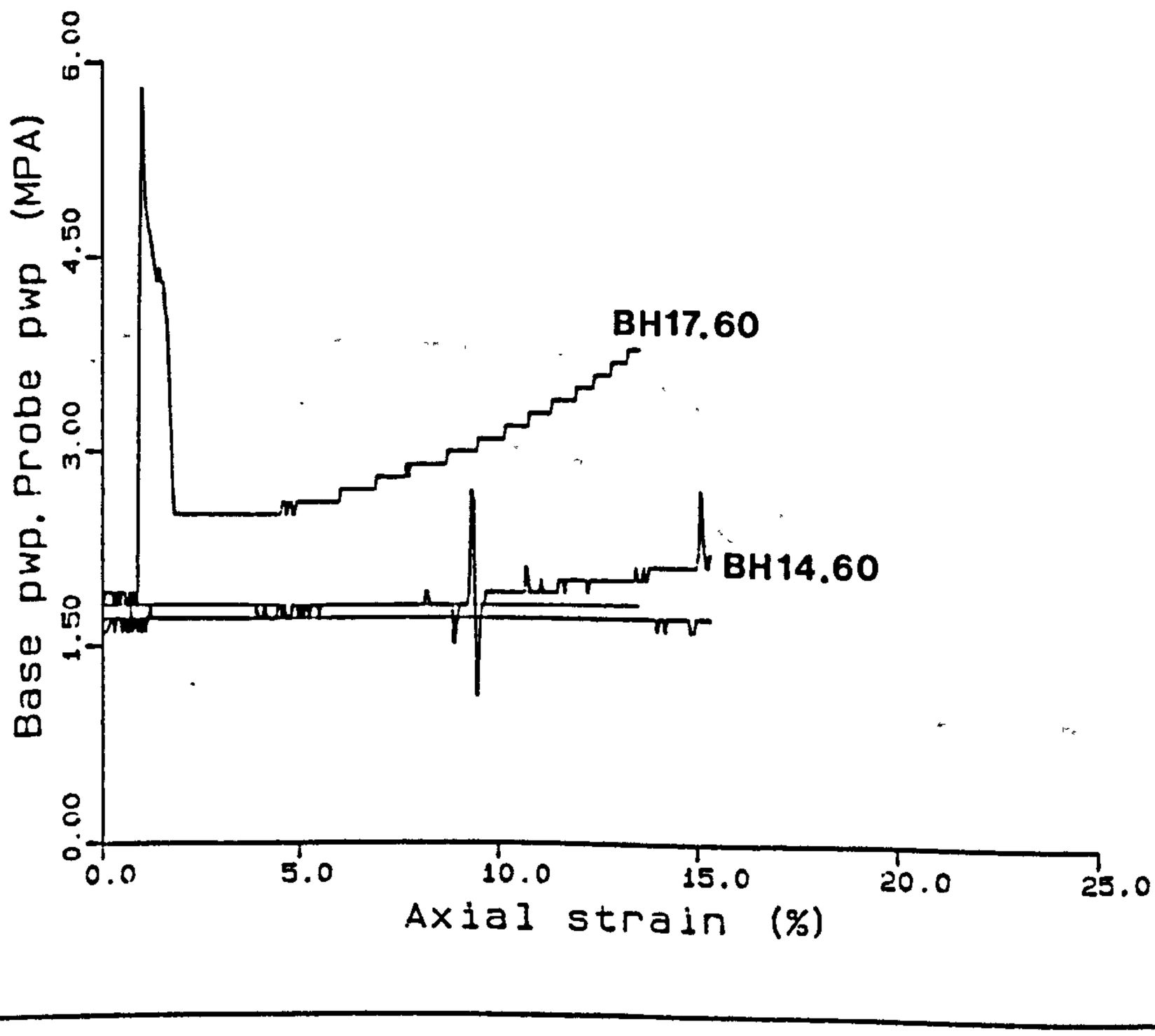
Base pwp. Probe pwp (MPA)
0.00
1.50
3.00
4.50
6.00
BH17.60
BH14.60
0.0
5.0
10.0
15.0
20.0
25.0
Axial strain (%)

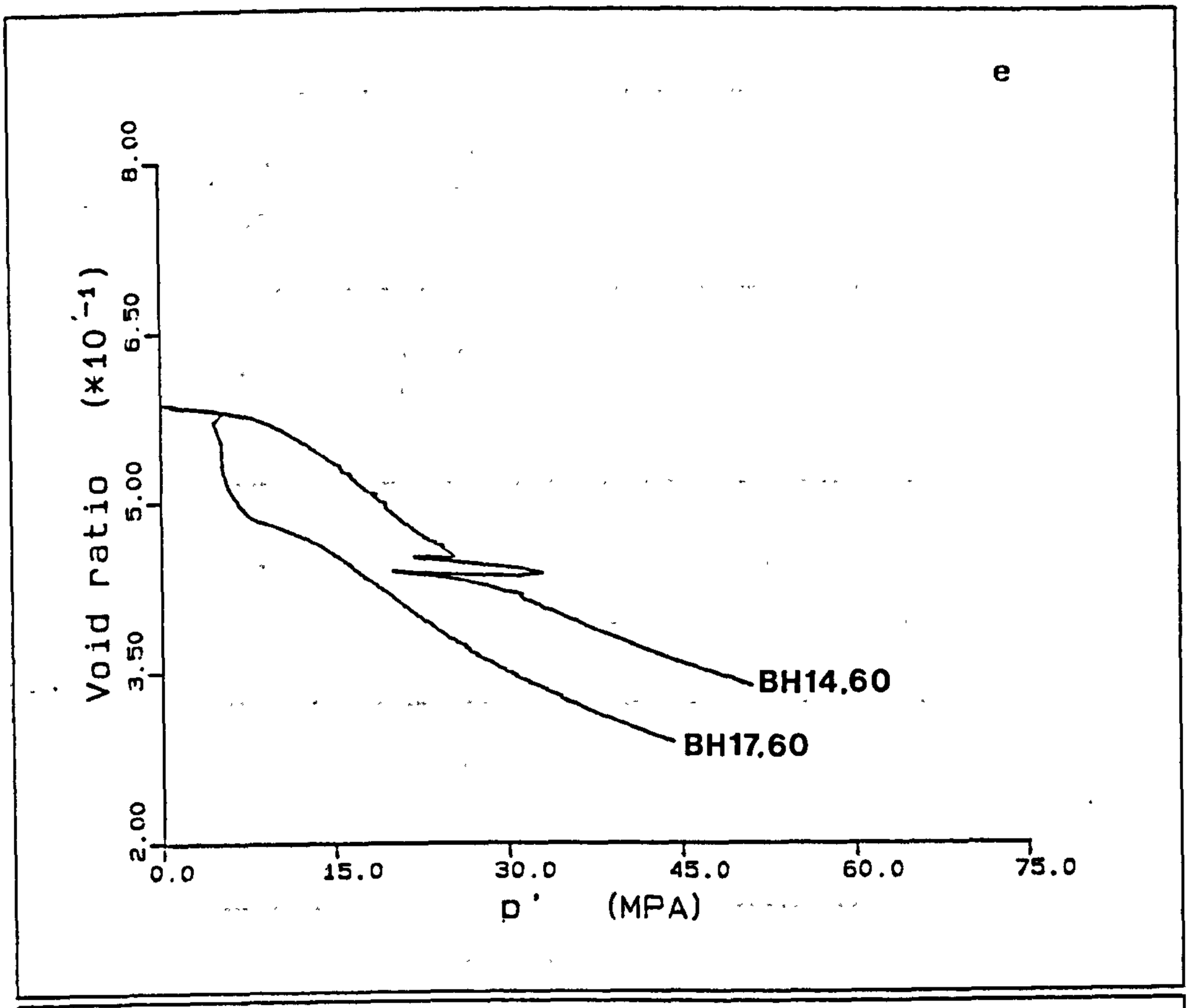
e
Void ratio (*10-1)
8.00
6.50
5.00
3.50
2.00
0.0
15.0
30.0
45.0
60.0
75.0
p' (MPA)
BH14.60
BH17.60

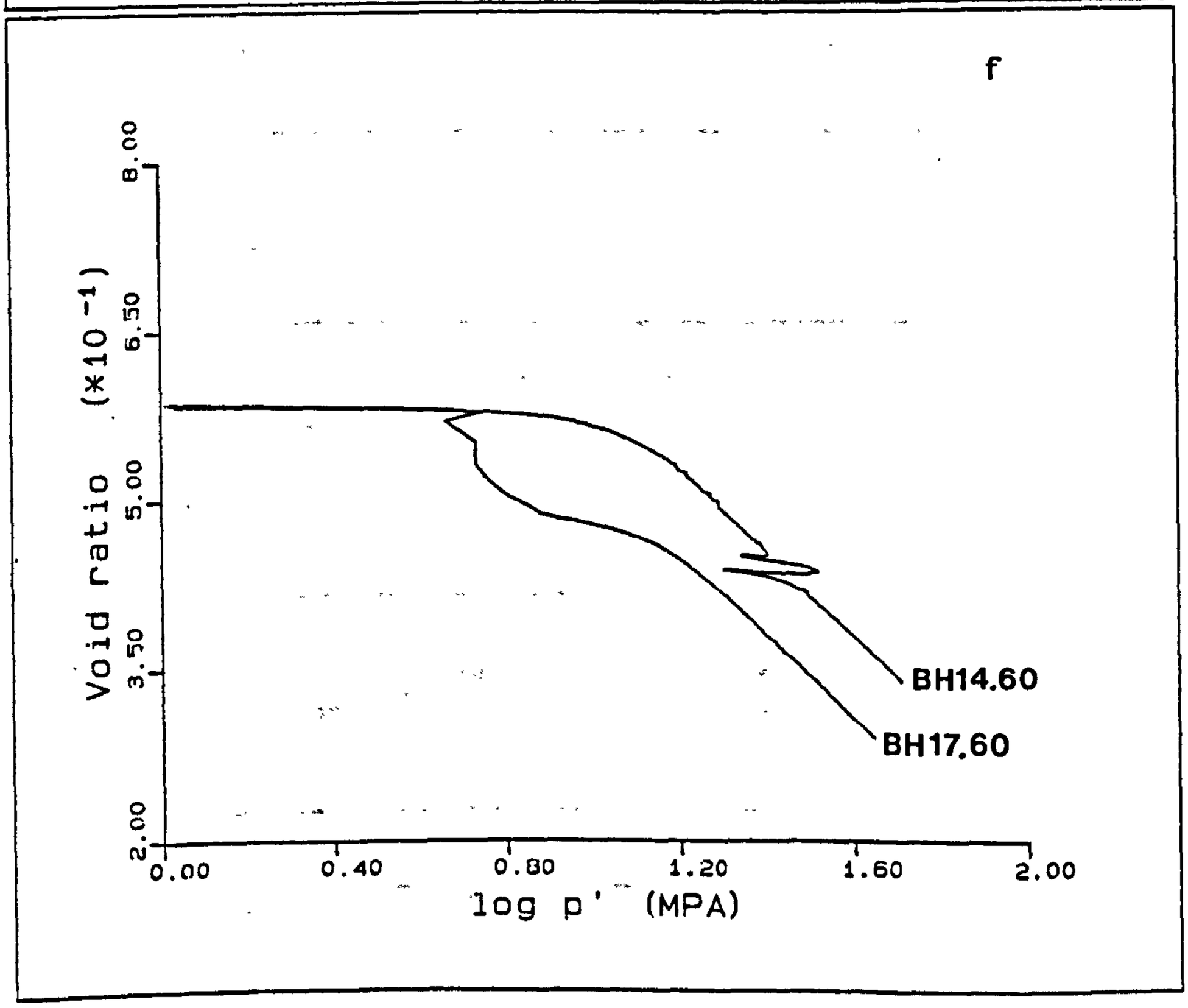
f
Void ratio (*10-1)
8.00
6.50
5.00
3.50
2.00
0.00
0.40
0.80
1.20
1.60
2.00
log p' (MPA)
BH14.60
BH17.60

Table 4.4

Sample	Porosity %	Strain rate sec^{-1}	$\bar{K}_{oe}$	$\bar{K}_{opc}$	$\bar{K}_{onc}$	Young's modulus GPa	Yield point MPa	$\sigma_1'_{nc}$ MPa	p'_{nc} MPa
BH3.20	36.7	$6.554*10^{-6}$	---	1.018	0.572	1.30	11.71	31.2	22.5
BH4.20	37.2	$4.374*10^{-6}$	0.405	1.470	0.558	1.50	11.72	23.4	16.5
BH5.20	36.8	$4.371*10^{-6}$	0.215	0.978	0.613	0.72	10.24	23.0	15.9
BH7.20	36.2	$4.373*10^{-6}$	---	1.052	0.568	1.48	12.21	29.6	12.5
BH14.60	36.9	$8.739*10^{-6}$	---	0.969	0.567	1.26	10.55	26.1	18.4
BH16.100	37.3	$8.746*10^{-6}$	---	0.915	0.547	1.36	11.78	34.7	24.0
BH17.60	36.9	$8.729*10^{-6}$	0.140	0.944	0.560	1.17	11.00	27.8	19.7
BH18.20	36.2	$8.744*10^{-6}$	0.047	1.023	0.574	1.84	12.58	35.2	25.6

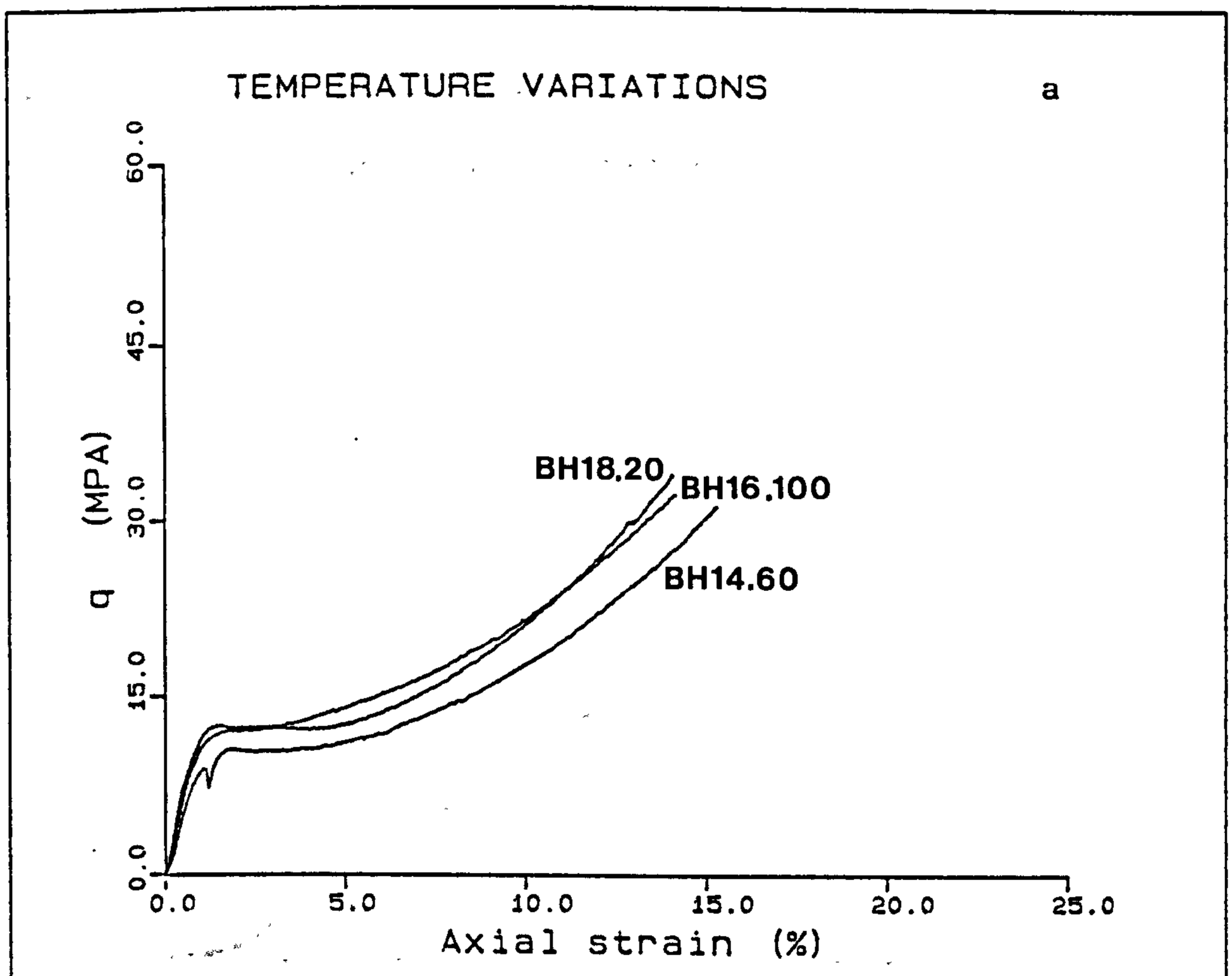

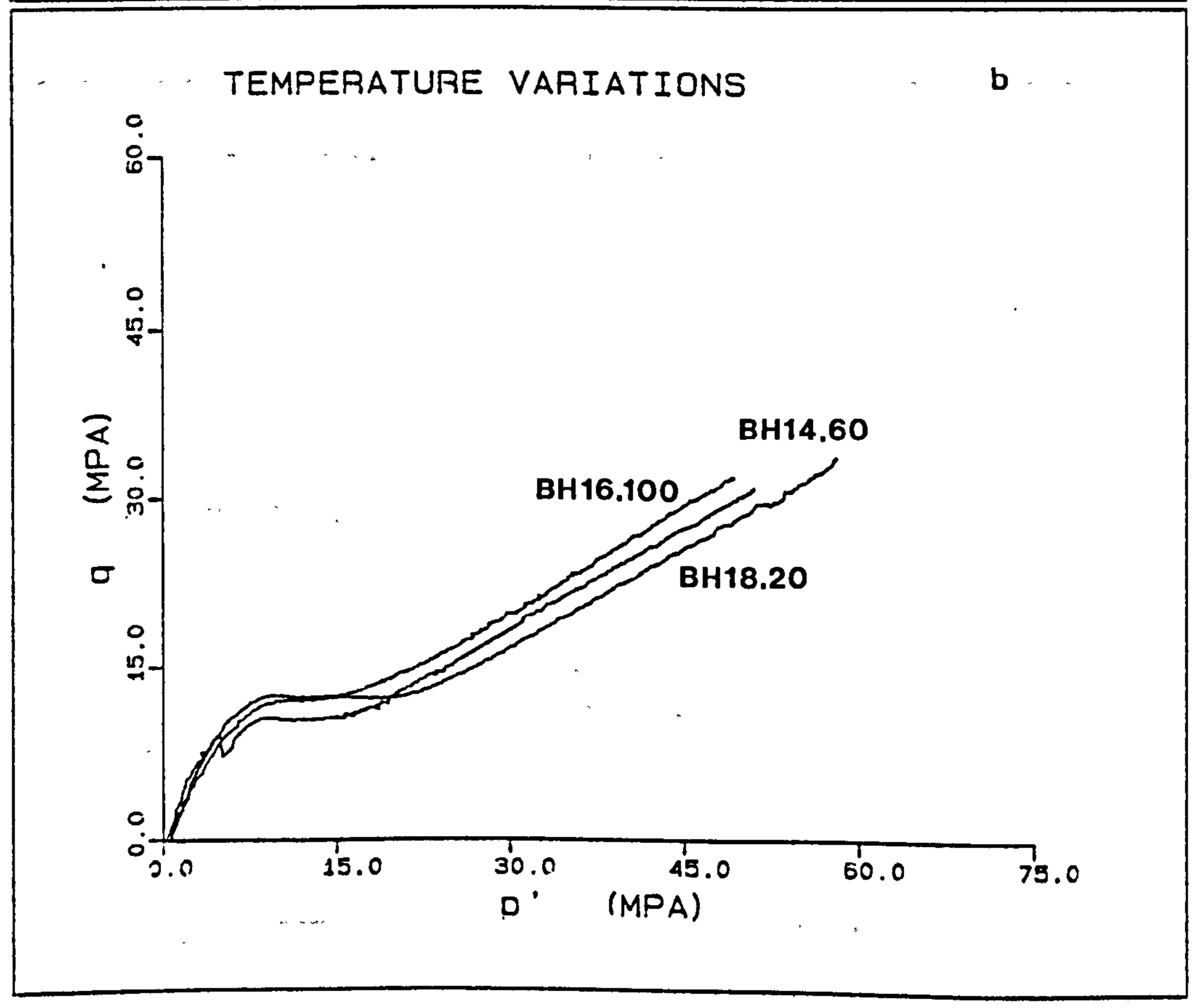

Figure 4.26(a-d) Comparison of BH14.60, BH16.100 and BH18.20.

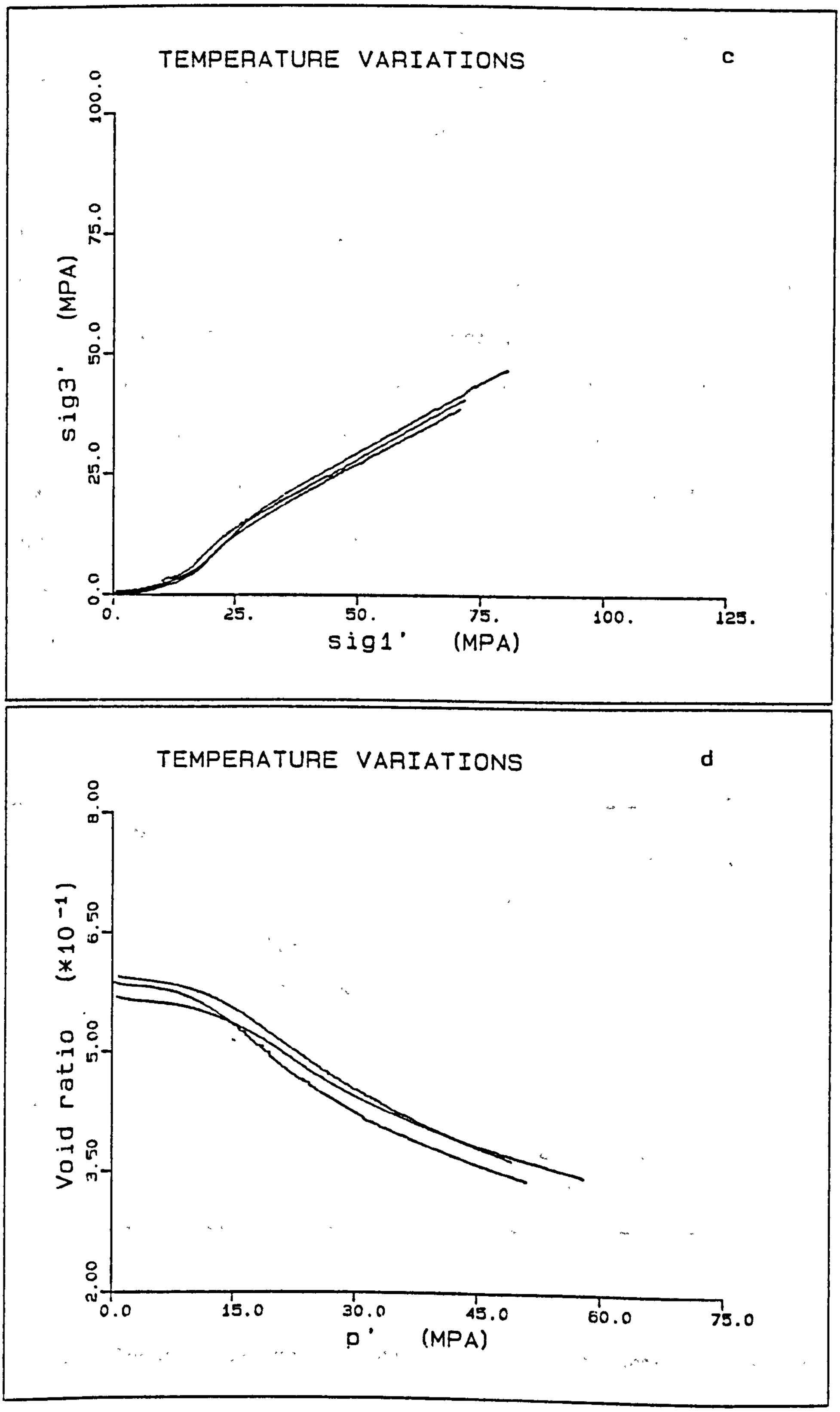
TEMPERATURE VARIATIONS
c
sig3' (MPA)
100.0
75.0
50.0
25.0
0.0
0.
25.
50.
75.
100.
125.
sig1' (MPA)
TEMPERATURE VARIATIONS
d
Void ratio (*10-1)
8.00
6.50
5.00
3.50
2.00
0.0
15.0
30.0
45.0
60.0
75.0
p' (MPA)

points, though no trend is seen with temperature or porosity. All of the tests were run at the same deformation rate of 0.04mm/min to ensure a slight pore pressure build up, even in the 100°C experiment. From Fig. 4.26b, the normal consolidation deformation stress paths can be seen to be slightly different, with $\bar{K}_{onc}$ values of 0.574 for BH18.20 to 0.547 for BH16.100, BH14.60 having an intermediate value of 0.567 and BH17.60 a value of 0.560. This could be due to either the temperature effects or the porosity variation, despite no apparent correlation with porosity for the North Sea chalks. The shift of the normal consolidation part of the deformation in q-p' space also fits a trend with respect to porosity. No trend in the volumetric strain and the temperature is apparent from the e-p' plot shown in Fig. 4.27, with the initial void ratios shifted to the same value (for comparison purposes).

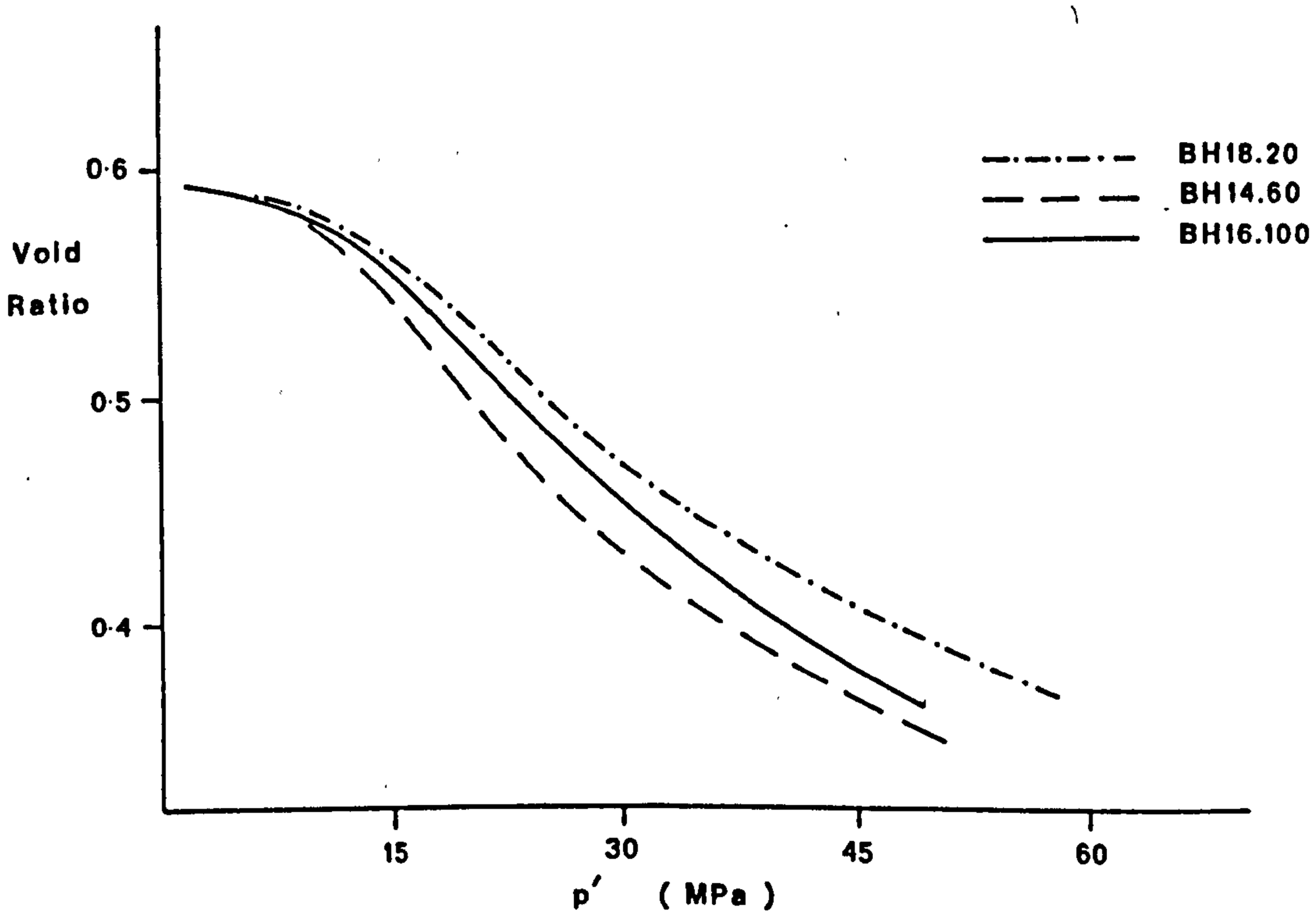

Figure 4.27 Temperature experiments shifted to the same initial void ratio.

Following the analyses performed on the Pegwell Bay samples for strain rate and sample shape effects, the compaction part of the temperature experiments were normalised. Initially these were normalised with respect to the yield point, after Leroueil et.al. (1985); the axial strain was also normalised to the axial strain at the yield point (Chaps. 4.3, 4.4), Fig. 4.28. This process is possible on these chalks, as the yield point is well-defined, and no gradual breakdown of structure as observed in the Pegwell Bay samples, is seen. This procedure also normalises the pore collapse section of deformation. The plot shows no apparent trend. The normalisation of the stress-strain curves was then performed using the start of normal consolidation as the normalising stress, and strain. Fig. 4.29 shows the plot of the three normalised stress-strain curves for the three tests performed at different temperatures, and a trend of increasing strain during normal consolidation with temperature. The gap in the plot of BH14.60 is due to the ommission of the data from the area where the test deviated from K_o. The change in strain (taking the start of normal consolidation as zero strain) between the different temperatures is small-in the order of 1% at a normalised σ_1'/σ_{1nc}' of 2. As seen from Fig. 4.25a, there is a difference in the stress-strain behaviour of different Butser Hill chalk samples. To evaluate the magnitude of errors and sample variability on Fig. 4.29, the two tests at 60^oC were normalised (as with the tests presented in Fig. 4.29) and plotted in Fig. 4.30. The experiments show excellent agreement and repeatability after the normalisation. They also show that the magnitude of the pore pressure, and its build up has a negligible effect on the normalising process, and that use of average pore pressure, calculated from the top and base pore pressure transducers

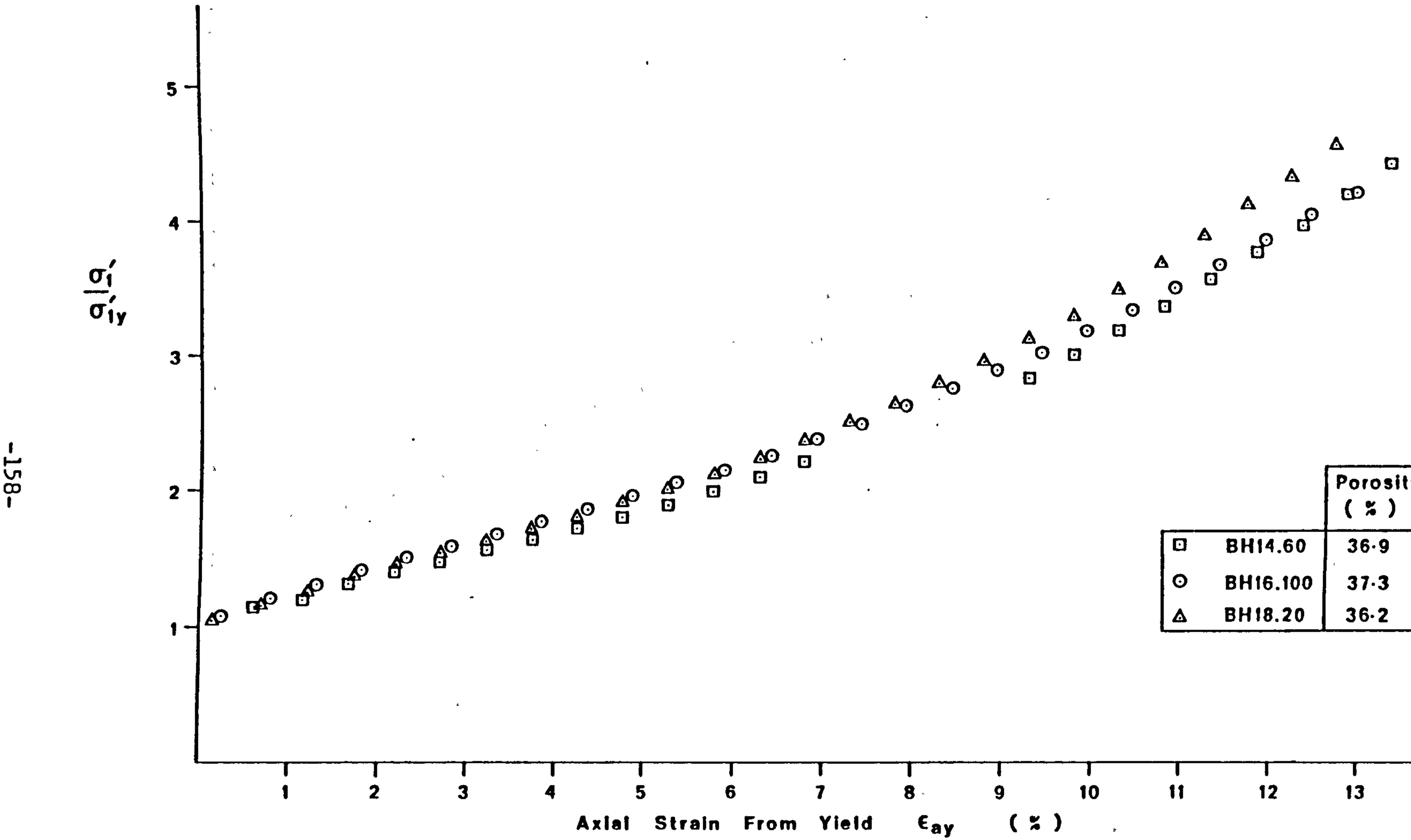

Fig. 4.28 Normalised stress-axial strain from yield, stress normalised to the yield point for the temperature experiments.

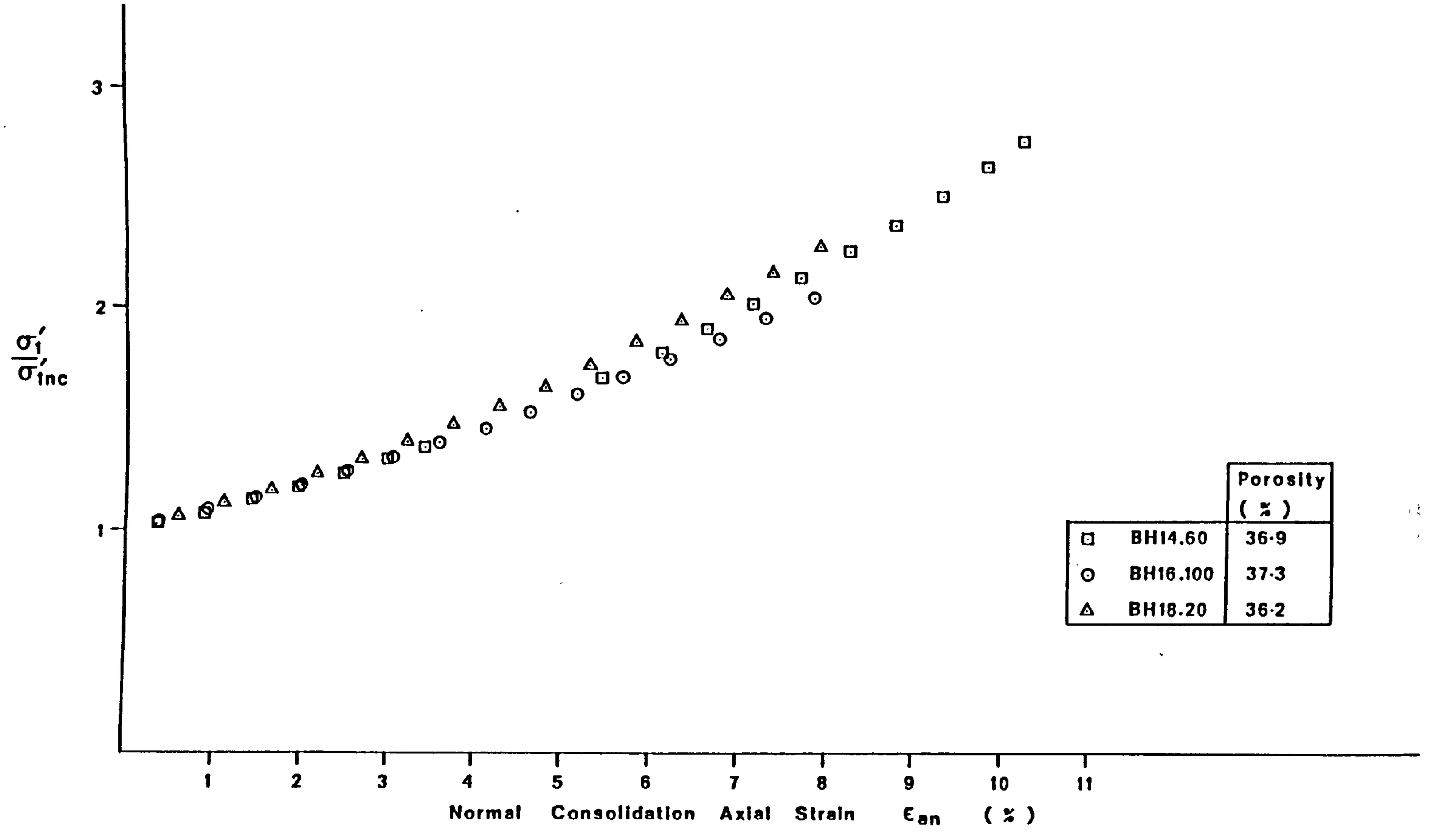

Fig. 4.29 Normalised stress - normal consolidation strain for the temperature experiments.

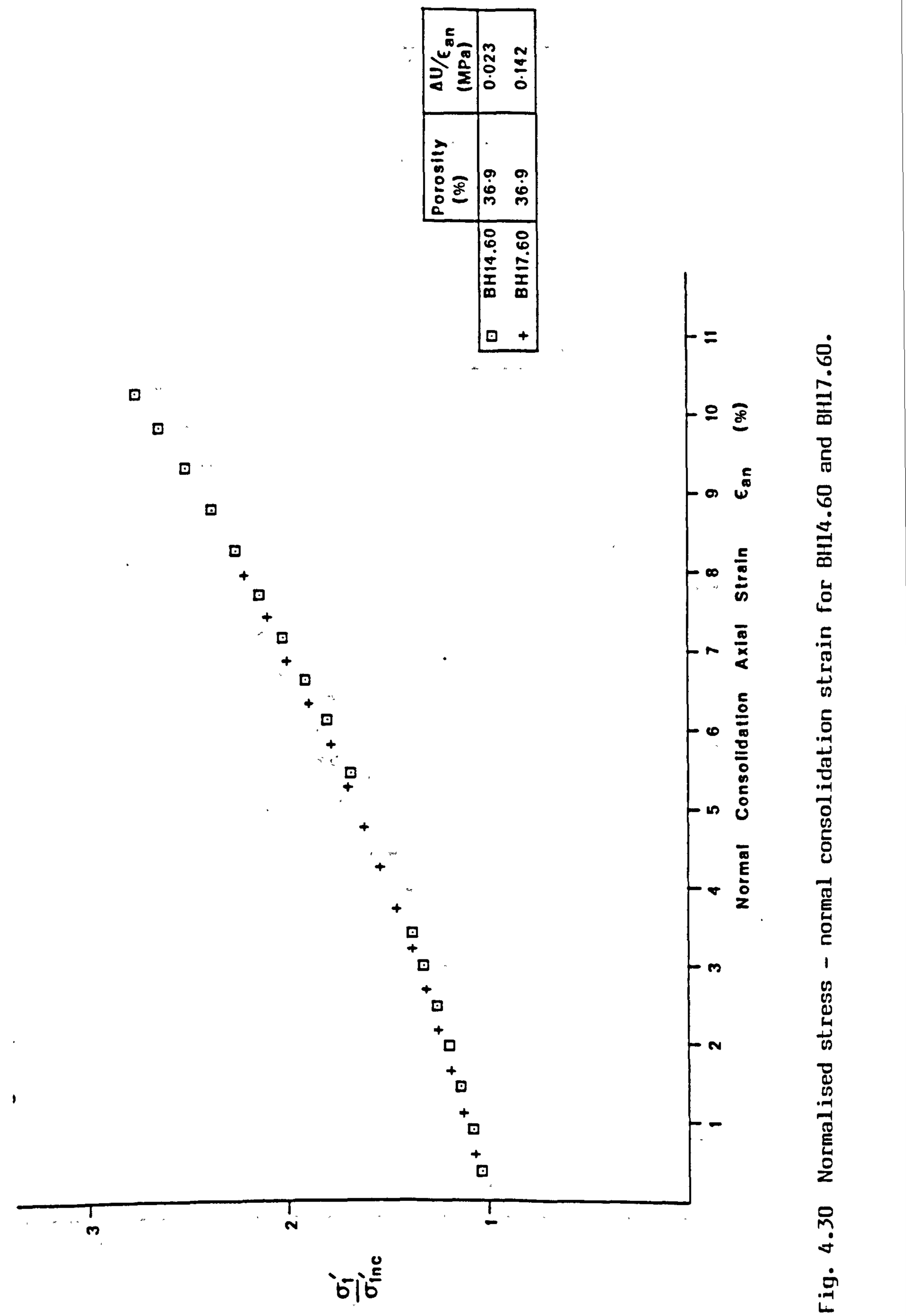

Fig. 4.30 Normalised stress - normal consolidation strain for BH14.60 and BH17.60.

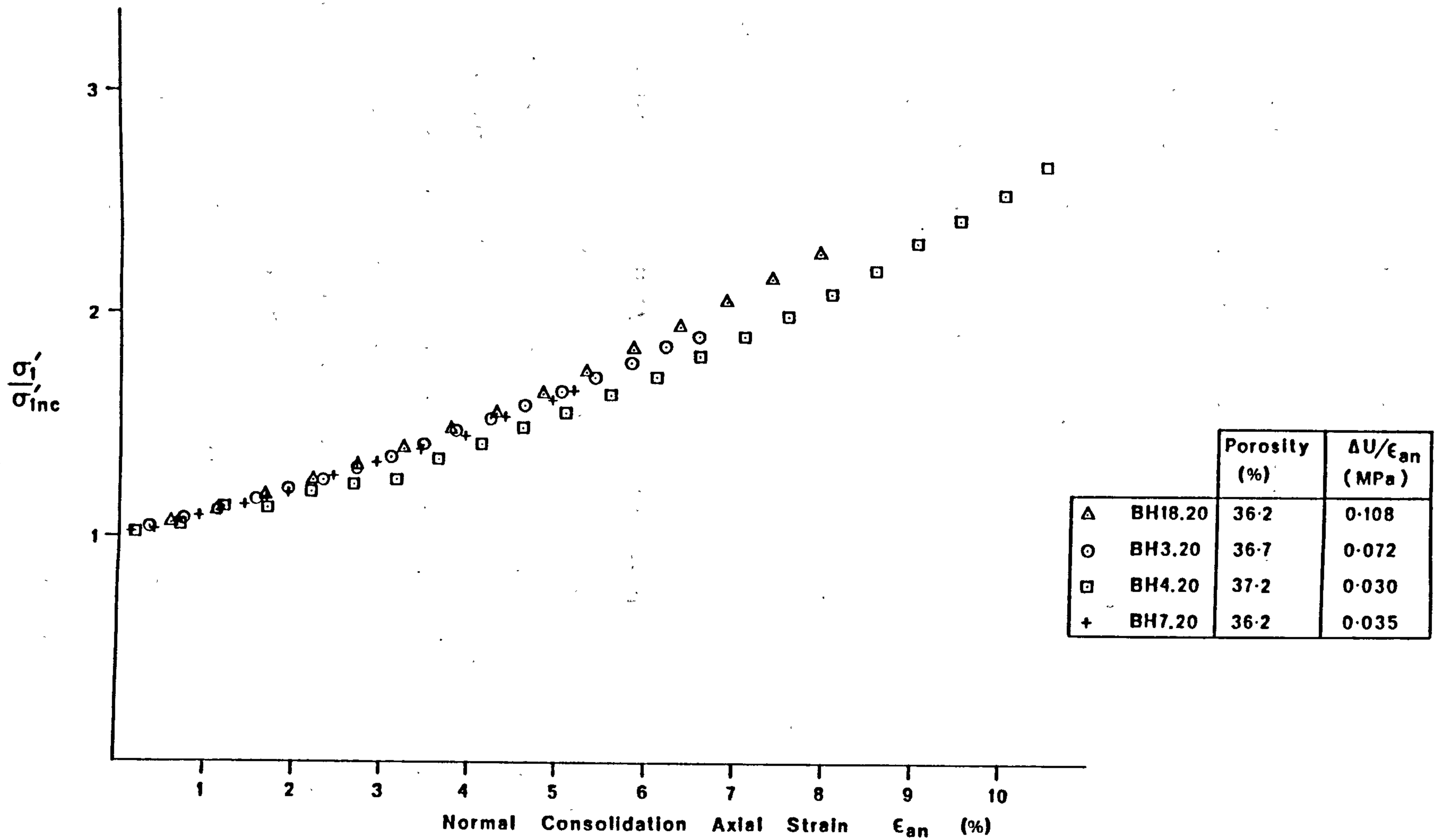

		Porosity (%)	$\Delta U/\epsilon_{an}$ (MPa)
△	BH18.20	36·2	0·108
⊙	BH3.20	36·7	0·072
⊡	BH4.20	37·2	0·030
+	BH7.20	36·2	0·035

Fig. 4.31 Normalised stress - normal consolidation strain for Butser Hill chalks tested at 20°C.

is justified, at the magnitudes of pore pressure generation produced in these tests.

The plots indicate that the temperature has a small effect on the compaction of chalk. However, this effect is within the reproducibility of samples in a normal rock mechanics study and can be ignored as a variable when investigating hydrocarbon reservoir compaction. In the above plots the effect of porosity variation between the samples have been ignored. To analyse this, all of the $20^{o}C$ K_o tests performed on the Butser Hill chalks, Table 4.4, were normalised. These $20^{o}C$ tests (Fig. 4.31), show similar normalised stress-strain curves to those reproduced in Fig. 4.29 for elevated temperatures. As these data sets both cover the same range of porosities, the trend of increasing strain with temperature seen in Fig. 4.29 can be attributed solely to porosity variation in the samples.

4.6) HYDROSTATIC TO UNIAXIAL STRAIN CONVERSION

In Chapter 6 the methods used in calculating the vertical strain due to a drawdown situation are discussed. One popular method is to obtain samples of reservoir rock and test them in hydrostatic compression; the volumetric strain is then converted into uniaxial strain using elastic theory. Teeuw (1971) has described the manipulation of the data and various papers use or refer to it, Lachance and Anderson (1983), Anderson (1985) and Johnson and Rhett (1986). The method was used to compare the hydrostatic test BH6.20 with the uniaxial results performed on Butser Hill chalk. Unfortunately, BH6.20 was performed to obtain the isotropic yield point and, as a result, the amount of post-yield deformation is limited. The BH6.20 results are compared to the K_o test, BH5.20, as

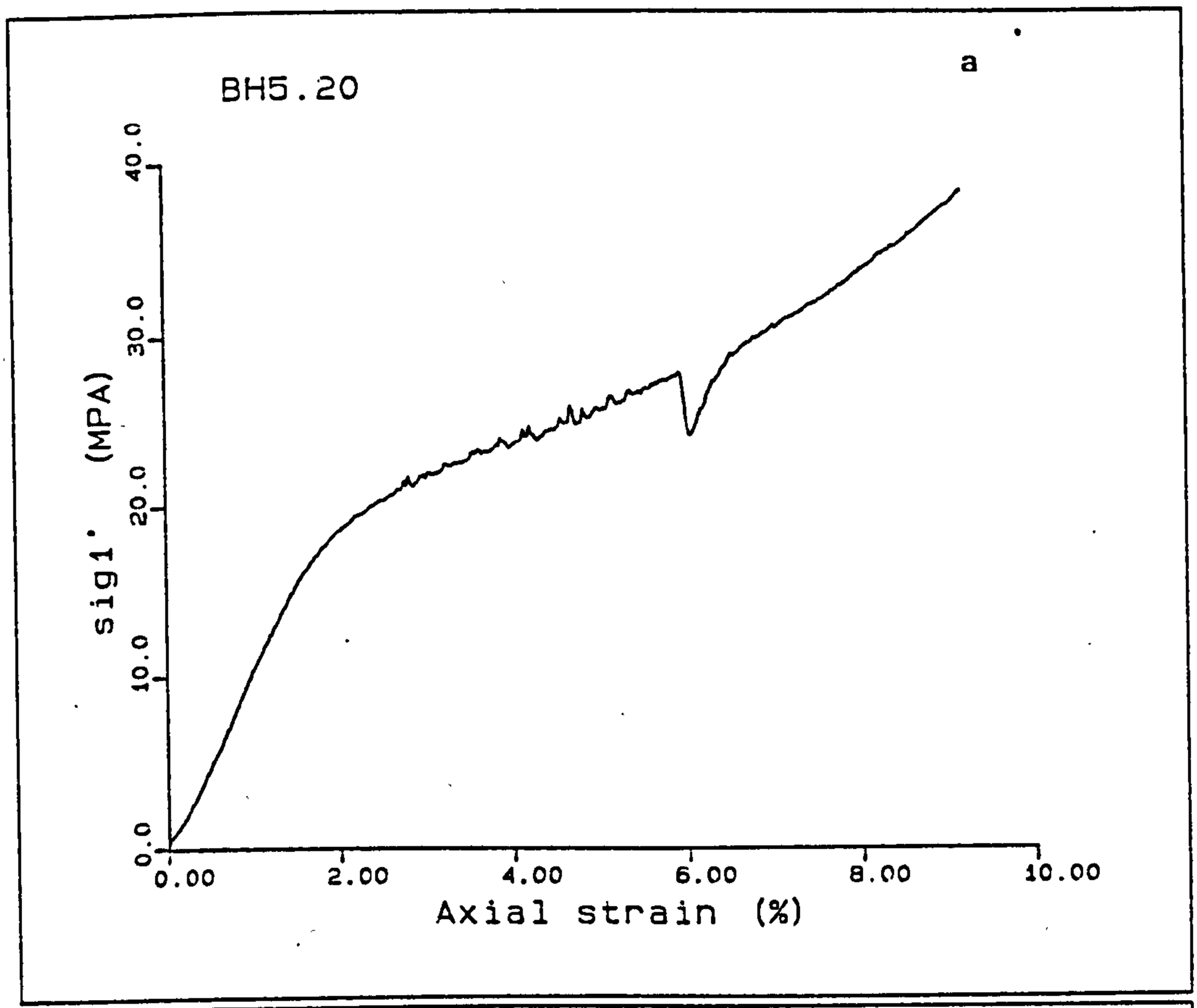

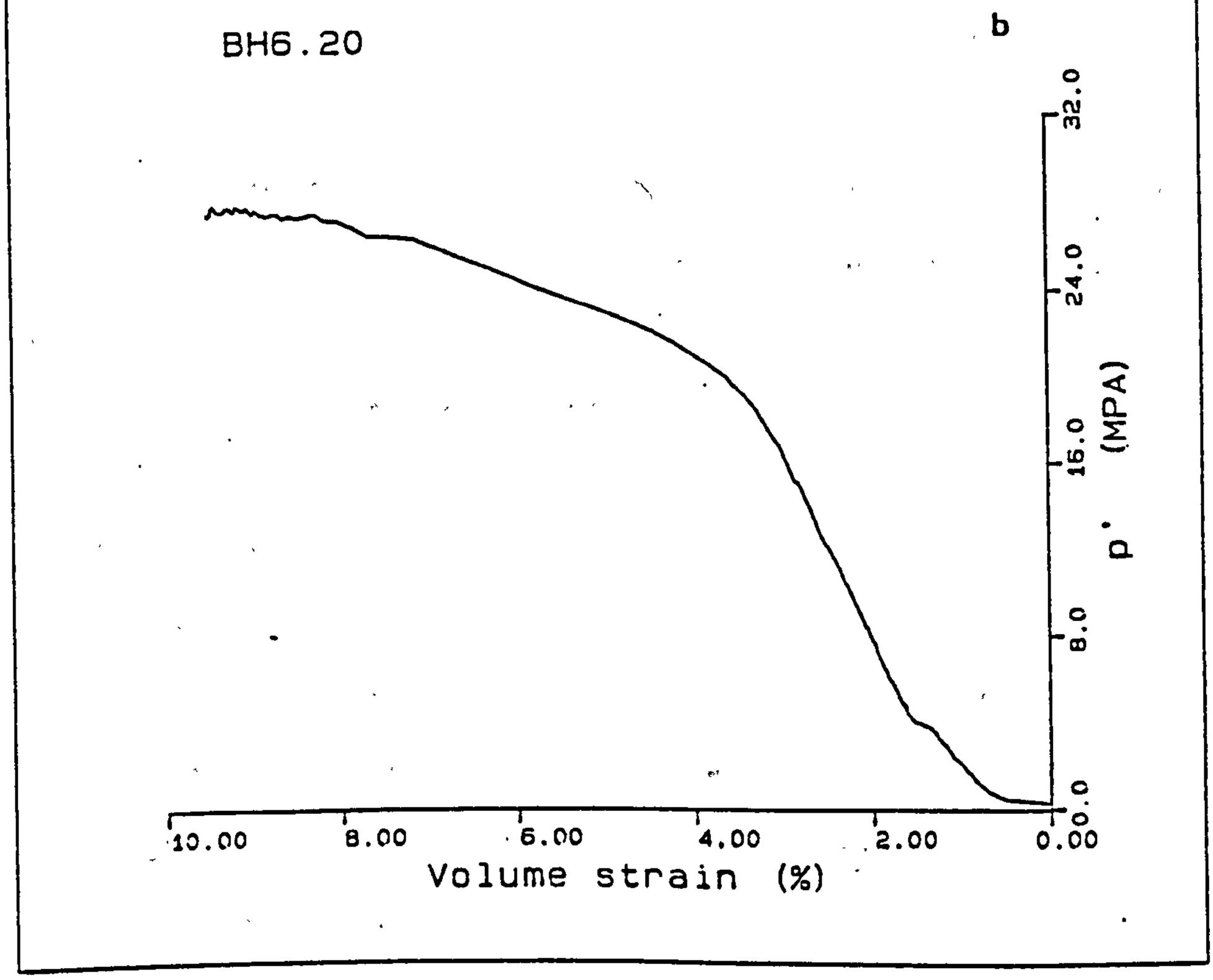

Figure 4.32 Stress-strain curves for uniaxial and hydrostatic tests.

this has the smallest pore pressure increase of the K_o tests performed on Butser Hill chalk samples. The drop in load in BH5.20 is substituted by a smooth curve for the analysis.

In Fig. 4.32 the volume and axial strain are shown with respect to p' and σ_1' respectively. For the conversion of hydrostatic data to uniaxial strain, a Poisson's ratio must be inserted into the equation

$$\epsilon_a = (1+\nu)e/3(1-\nu)$$

where ϵ_a = uniaxial strain, and e = volumetric strain in response to σ_1' and p' respectively; ν is the Poisson's ratio. After Johnson and Rhett (1986) who performed this analysis on Ekofisk chalk from the Central North Sea, a Poisson's ratio of 0.3 was chosen. Fig. 4.33 shows the plot of the uniaxial strain from the K_o test BH5.20 against the converted volumetric strain from BH6.20. The slope of these strains should equal one if the above conversion is accurate, and should plot along the 45^o line shown passing through the origin. Initially the converted data overestimates the strain then, after 2.1% converted volumetric strain, the conversion under-estimates the strain compared to that in BH5.20. At higher volumetric strains, the predicted values from the hydrostatic test and actual values from the K_o test, indicate that these will cross again but the strains are not large enough to see this.

A possible error in the conversion of the hydrostatic volume strain to uniaxial strain, is the value of Poisson's ratio used in the above equation. In order to check this, the value of Poisson's ratio required to obtain an exact fit between the hydrostatic data and the uniaxial data was back calculated. This was found by plotting the axial strain from BH5.20 against the true volumetric strain from BH6.20, Fig. 4.33, the slope of which should be equal to the correction factor $[1+\nu/3(1-\nu)]$; an enlarged section of the low strain

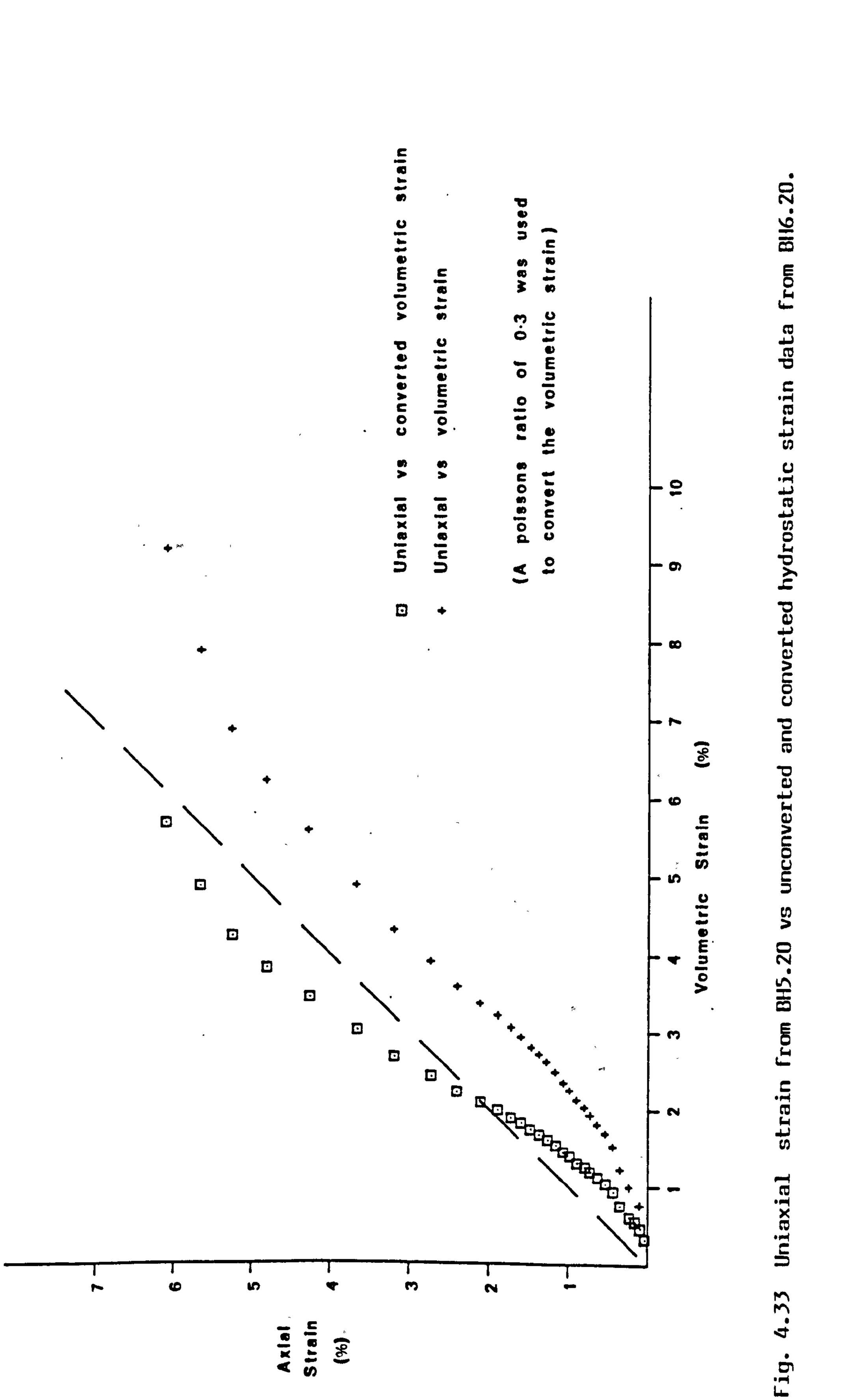

Fig. 4.33 Uniaxial strain from BH5.20 vs unconverted and converted hydrostatic strain data from BH6.20.

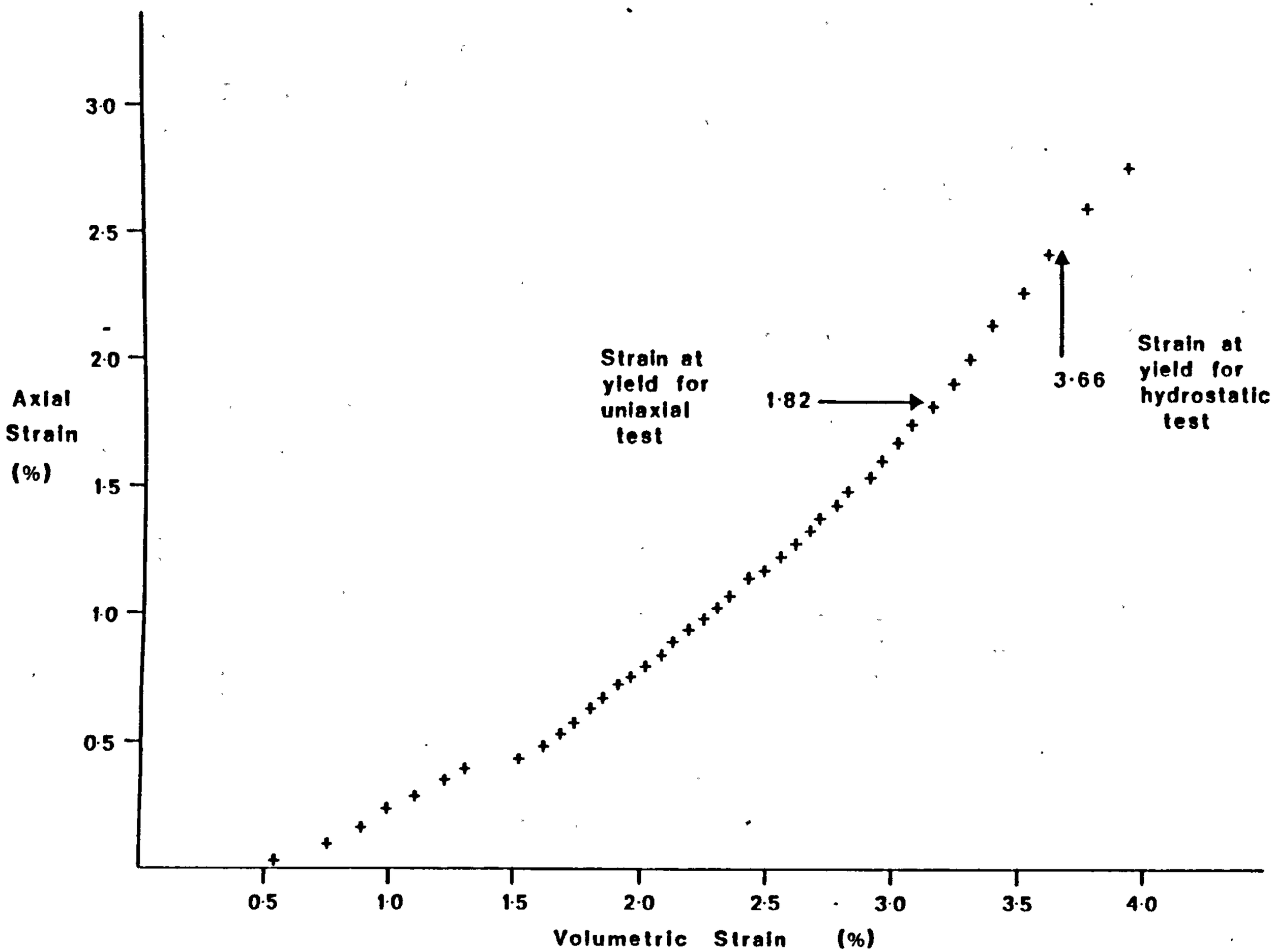

Fig. 4.34 Enlarged low strain area of Fig.4.33.

region of this plot is shown in Fig. 4.34, on which the yield points are marked for the two tests. This plot can be generalised into 6 linear sections with the Poisson's ratio being obtained from the slopes of the plot. The Poisson's ratio varies from 0.221 to 0.596 but decreases down to 0.038 at high volumetric strains. The Poisson's ratio of 0.596 has been attributed to the fact that this occurs when the K_o sample (BH5.20) has yielded whereas the hydrostatic sample (BH6.20) has not. Even the data before this point shows that the Poisson's ratio varies for these samples, therefore an exact fit of the curves using a single Poisson's ratio value is not possible. This can be attributed to variations in the samples compared.

If the data are plotted in terms of stress-strain curves used in subsidence analysis, Fig. 4.35 is produced. The triangles represent volumetric data which has been converted into uniaxial strain; the circles indicating the volumetric strain; the closed triangles denote the uniaxial test and the open points representing the hydrostatic strain data. This plot shows the same characteristics as those observed in Fig. 4.33, with the converted volumetric data overestimating the strain up to a strain of 2.1% thereafter underestimating the strain with a trend to overestimate the deformation at even higher strains.

Johnson and Rhett (1986) found that the conversion using a Poisson's ratio of 0.3 shows a divergence of results of the converted data from uniaxial (K_o) data on chalks. So to construct the uniaxial stress-strain curves they "assume that the uniaxial and the hydrostatic results become equivalent in the pore collapse region", where pore collapse is used by Johnson and Rhett (Loc.Cit.) to include all post yield deformation in the chalk. This is represented in Fig.4.35, with the construction suggested by Johnson and Rhett as

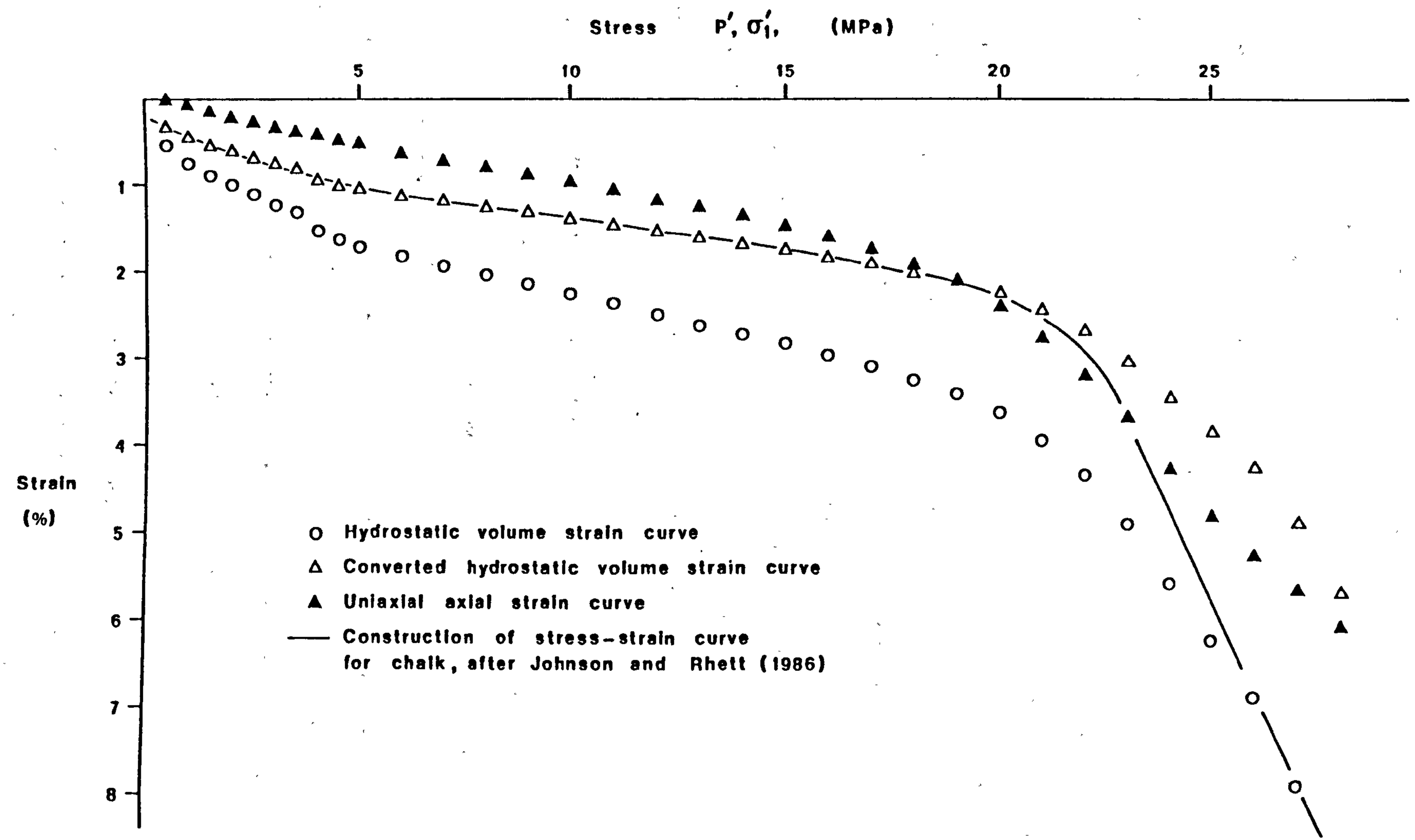

Fig.4.35 Stress-strain curves for K_o, hydrostatic, converted hydrostatic, and curve construction after Johnson and Rhett.

a solid line; the deviation of this from the K_o test (solid triangles) is apparent even for small post-yield strains. This is as expected, since the volume strain in the chalks in the hydrostatic case has a larger mean effective stress. The average mean effective stress on the sample in the uniaxial test will have 0.7 times that of the hydrostatically stressed sample, resulting in less volumetric and axial strain.

This section has shown that in elastic materials conversions from hydrostatic data to uniaxial data are reasonably accurate, however, after the breakdown of the elastic structure no such conversion can be applied. The assumption that hydrostatic strains and uniaxial strains are equivalent in post-yield deformations in chalk, has been shown to be incorrect, with the two strains deviating with increasing stress. This can be observed by considering the Critical State diagram (Chap. 2). Thus, to calculate the compaction behaviour of materials such as chalk, uniaxial (K_o) experiments must be performed.

4.7) TIME DEPENDENCY OF THE COMPACTION

The reduction in porosity due to collapse and compaction of the skeleton will lead to a reduction in both the pore and pore throat size. The reduction will be intensified by any production of fine-grained material due to particle crushing, so reducing the pore sizes further. The lower the permeability, the longer time a sample will require to dissipate any excess pore fluid pressure due to loading, thus, the distribution of effective stress across a sample will change with time, and the resulting deformation will be time-dependent. The time dependency of primary consolidation (reduction of excess pore fluid pressure) is represented by C_v, the coefficient of consolidation and is discussed in Chapter 2. In this

section, the values of C_v and the permeabilities (K) of the chalks will be discussed, the quantities being calculated from the analyses outlined in Chapter 3.

These K and C_v values have been obtained for PB5.20 and PB6.20 for the Pegwell Bay samples, BH14.60, BH16.100 and BH18.20 for the Butser Hill chalks, and from samples EC5.20, EC6.20, EC8.20 and EC9.20 for the North Sea chalks. The North Sea chalks are oil-saturated and have been in storage for several years, as such, the oil in the pores will have increased in viscosity (seen on extended exposure to the atmosphere). Hence, the values of permeability may be lower due to the inaccuracy of the viscosity values used in the analysis for these samples.

The two Pegwell Bay samples PB5.20 and PB6.20 generated pore pressure at a 0.08mm/min deformation rate, the two tests are plotted together to observe the repeatability of the test and the analysis (Fig. 4.16). As observed previously, the radial strain allowed in PB6.20 is seen to have little effect on the results (Fig. 4.16). The M_vs (Fig. 4.16e) are seen to be repeatable, these being a representation of the strain in the sample. The coefficient of consolidation and the permeabilities are seen to decrease at the maximum compressibility of the sample. The permeabilities tail off with increasing maximum effective stress, to values of $0.42*10^{-2}$mD at 115MPa and $0.56*10^{-2}$mD at 114MPa for PB5.20 and PB6.20 respectively. Samarisinghe et.al. (1982), show that the permeability decrease in normally consolidated clays with compaction is linear in log k(1+e) versus log e space, the slope and the intercept of this linear trend are considered to be material constants. Fig. 4.16h was plotted to see if this linear relationship holds for chalk (in which particle crushing occurred), the plots are seen to show a slight upwards

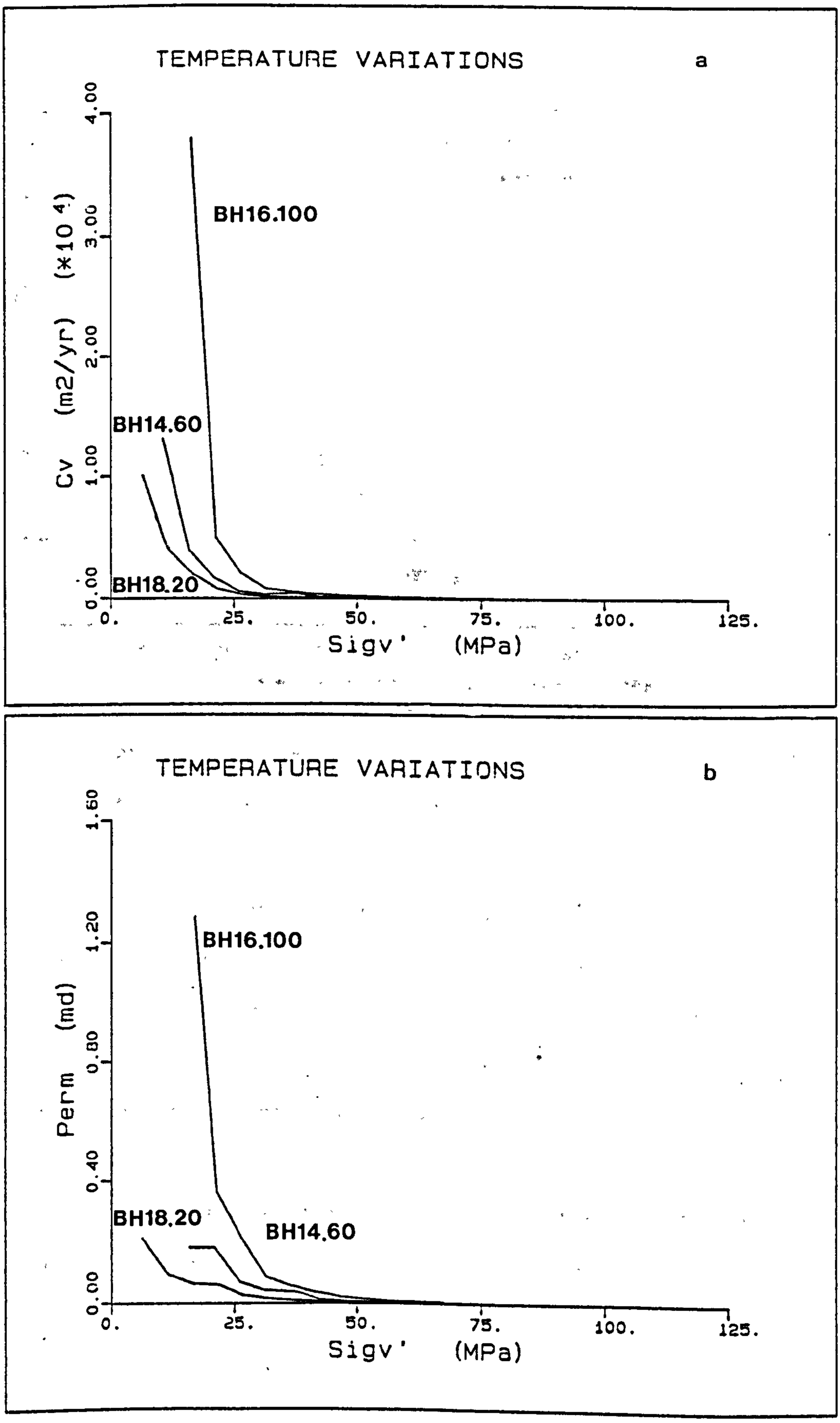

Figure 4.36 The effect of temperature variations on C_v and K.

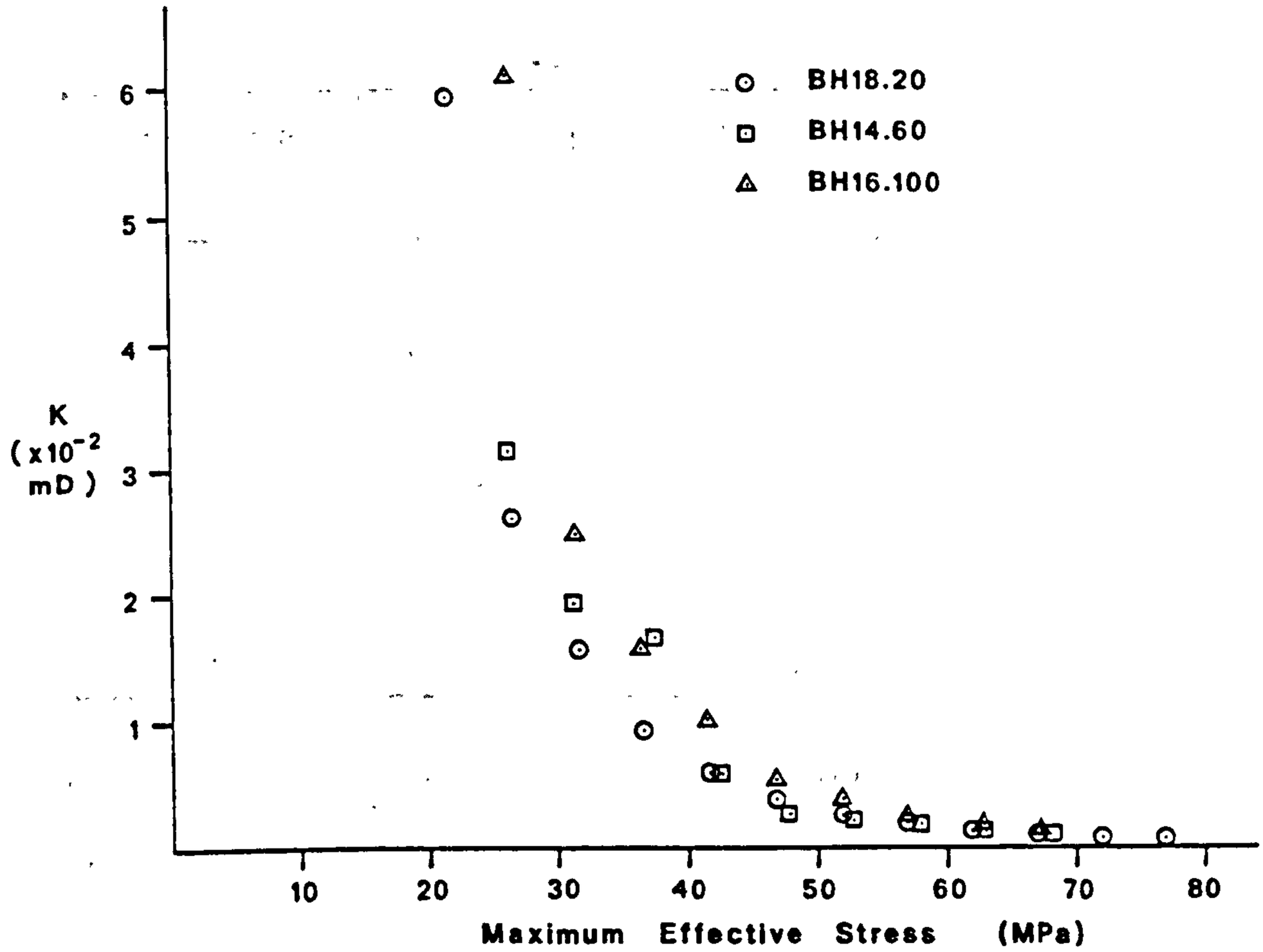

Figure 4.37 Absolute permeability vs maximum effective stress for temperature variation tests.

concavity, which is assumed to be a consequence of grain crushing.

The Butser Hill samples show the effects of temperature on C_v and permeability; these tests are presented in App. 5 and are shown in Fig. 4.36. When the permeabilities are calculated using the correct viscosities and densities (Table 4.5) for the temperature of the experiment (Fig. 4.37), the permeabilities are seen to be very similar, which shows that the C_v is, to a large extent, dependent upon the values chosen for the viscosity and density of the pore fluid.

Table 4.5 (from: CRC handbook of chemistry and physics, 60^{th} Ed., 1981).

Temperature ^{o}C	Viscosity Cp	Density g/cm^3
0	1.781	0.99987
10	1.307	0.99973
20	1.002	0.99823
30	0.7975	0.99567
40	0.6529	0.99224
50	0.5468	0.98807
60	0.4665	0.98324
70	0.4042	0.97781
80	0.3547	0.97183
90	0.3147	0.96534
100	0.2818	0.95838

In Fig. 4.37, there is still a slight trend for increasing permeability with temperature below a stress of 40MPa; and this could be attributed to the use of unrepresentative viscosities and densities, as the values reproduced in Table 4.5 are for pure de-aired water at atmospheric pressure. However, it is more likely that these differences in permeabilities is due to the porosity variation for these samples as shown in Chapter 4.5.

The North Sea chalks (Fig. 4.38) show a decrease in C_v and permeability with increasing stress. The yield is seen in Fig. 4.38a, where the values of M_v increase to a maximum then gradually decrease. Although there are some inaccuracies in these permeability calculations (as outlined earlier), the data indicates a significant decrease with increasing stress. Further inaccuracies possibly arise from the application of Wissa's analysis, and through this, the assumptions present in the formulation of the consolidation equation (the main point of contention being the compressibility of the grains) (Chap. 3). The extents of such errors are difficult to assess and are probably best evaluated by comparing the results of a

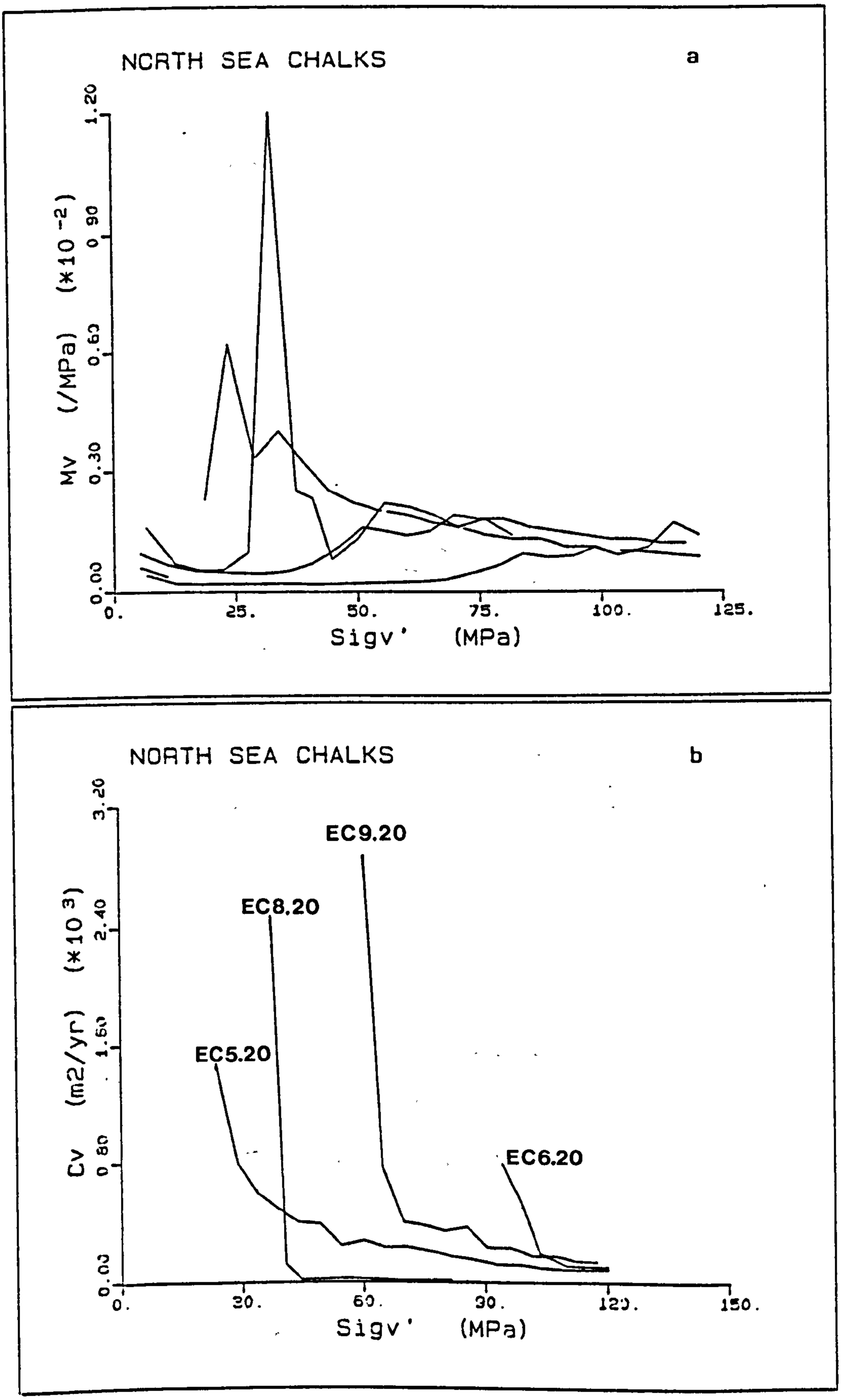

Figure 4.38 C_v and K reduction for Central North Sea chalks.

c

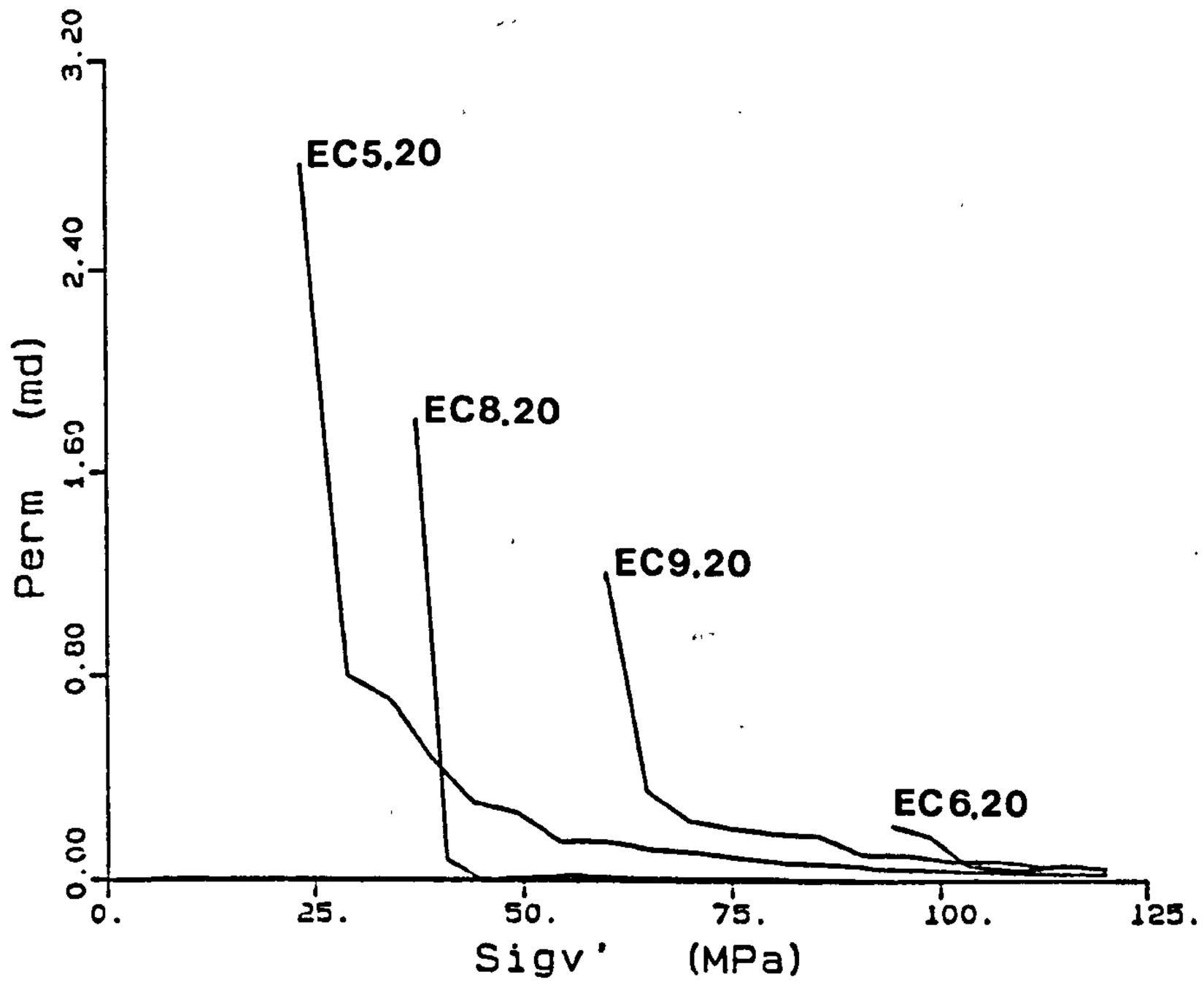

d

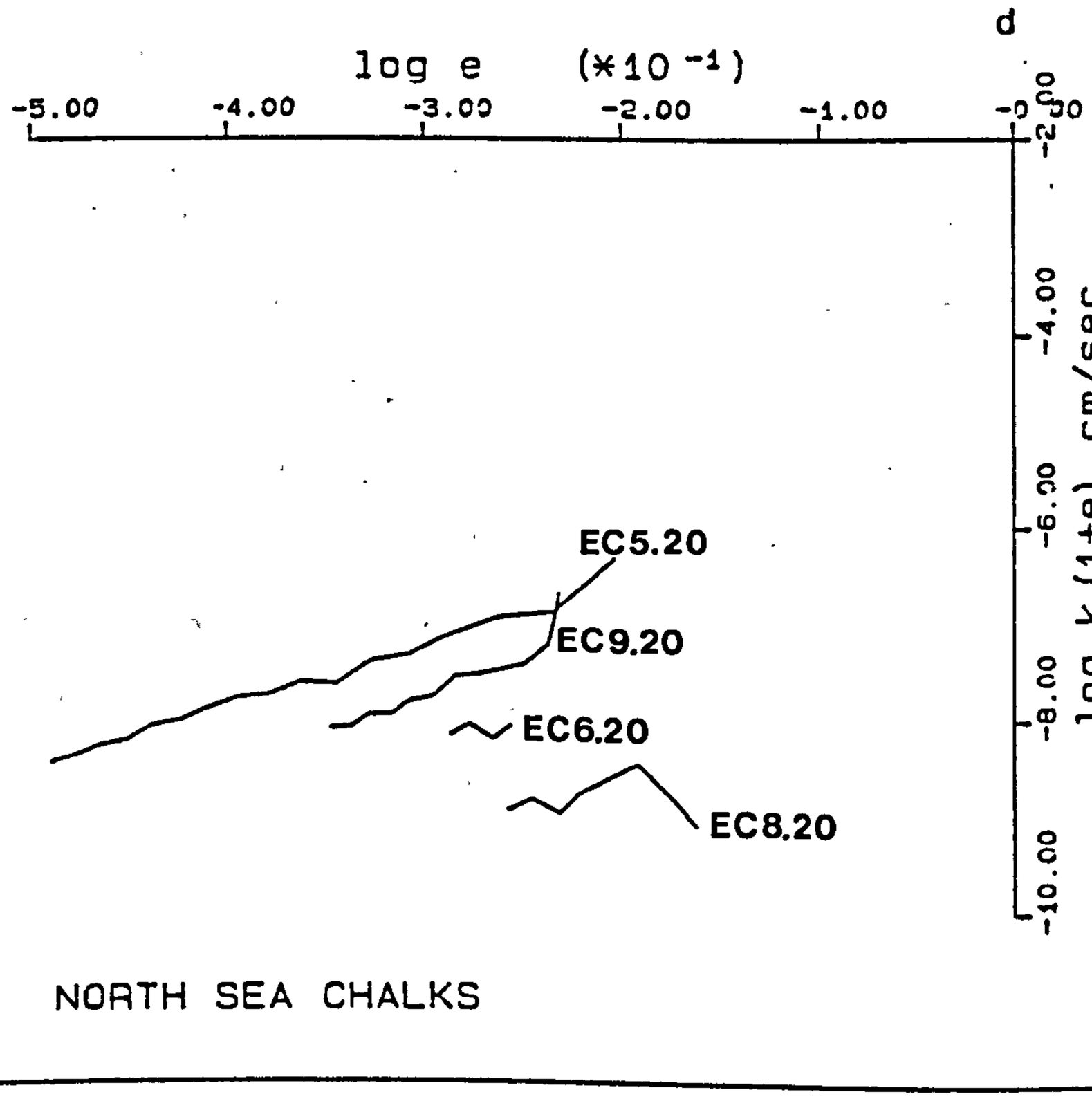

NORTH SEA CHALKS

CRS test using the Wissa analysis with an incremental loading test employing constant head permeability tests. The permeabilities calculated for the North Sea chalks appear to be in good agreement with other published data on permeabilities, and permeability decrease due to increase in vertical effective stress (King, 1986; Simon et.al., 1982; Chap. 6).

The plots of log k(1+e) against log e for the Pegwell Bay samples (Fig. 4.16) and for the samples from the North Sea (Fig. 4.38), show reasonably linear trends. This is probably only the case for the post-yield deformation. The trends of the permeability plots for chalks of different areas differ, but the data for the four North Sea samples show the same slope, suggesting some form of geological influence on this behaviour. The linearity of the slopes for the North Sea chalks would suggest smaller degrees of grain crushing than observed in the Pegwell Bay samples.

The calculation of permeability and the coefficient of consolidation performed in this study, must render the results of this section semi-quantitative. Though reasonable agreement exists between the permeabilities calculated in these tests and those reported in the literature for similar chalks. Initially a large decrease in permeability occurs at the yield point the reduction in permeability decreasing with increasing stress. The trends observed show a linear decrease in plots of log k(1+e) vs log e, with increasing curvature developing with increasing grain crushing.

4.8) THE NATURE OF COMPACTION OF CHALK

From the foregoing discussion and the appendices, we can draw conclusions on the nature of compaction of high porosity chalk. This section will draw upon the general results reported in the appendices, and the result of an oedometer test DBH2.20 performed on Butser Hill chalk.

The chalk deforms under uniaxial conditions by three deformational styles, the predominant style being dictated by the strength of the cementation and the axial strain developed during the deformation. In the small strain region, the cementation dominates the deformational characteristics of the chalk. The strength and elastic properties of the cementation dominate the yield stress required to break the bonding. In chalk the cement and the skeletal grains are both calcite and thus the structural breakdown may not be purely attributed to the breakdown of cementation. With relatively weak bonding the cementation will gradually breakdown with increasing strain; with more competent samples the yield occurs over a small strain range, though stresses of two or three times those at yield are required to break all the bonds in the sample (Maccarini 1987). In the post-yield deformation, a gradual breakdown occurs which is interpreted as a brittle breakdown of the remaining bonding, with accompanying particle crushing and interparticle shear. This occurs at a more-or-less constant deviatoric stress, which indicates that once a stress has been reached to initiate breakage of bonds, the load is transfered from the failed grains to the remaining intact bonds, so increasing the interparticle stress until the stronger bonds fail due to the concentration of load through the ever decreasing number of intact bonds. Thus assuming a normal statistical distribution of bond strength through the sample, a domino-type failure can be

envisaged. The deformation at constant deviatoric stress is therefore considered to involve pore collapse through the progressive failure of the individual bonds, with considerable grain rearrangement and particle crushing at the stresses employed in this study. This process terminates when the grains have reached an equilibrium void ratio for the particle size and grading, for the load predominating in the pore collapse section. Thus, the bonding maintains a higher porosity than would exist in the uncemented sediment, under equivalent effective stresses. During yield the breakdown of the cementation leads to the chalk starting to behave as if uncemented. The gradual collapse is envisaged as the establishment of porosity and stress state equilibrium within the material for the uncemented sediment. Following yield and pore collapse, the chalk behaves as a sediment, and becomes stiffer with further increases in compaction, i.e. work hardens.

The increases in vertical and horizontal effective stresses which are required to maintain zero lateral strain during pore collapse are seen to be equal ($\bar{K}_{opc} = 1$). This is probably due to the intergranular slip subsequent to bond shearing. During continued deformation, the uncemented grains will try to compact in the vertical direction, this will involve a wedging action between grains, which obviously tries to displace the wedged grains laterally. Thus, the horizontal stress (the cell pressure) increases until an equilibrium is established, and the intergranular friction has increased. The large increase in horizontal stress (minimum effective stress), is due to the amount of wedging which occurs as the cementation breaks down. This type of compaction, due to the degradation of the cemented skeleton and rearrangement of the grains to a more dense structure, has been observed for uncemented

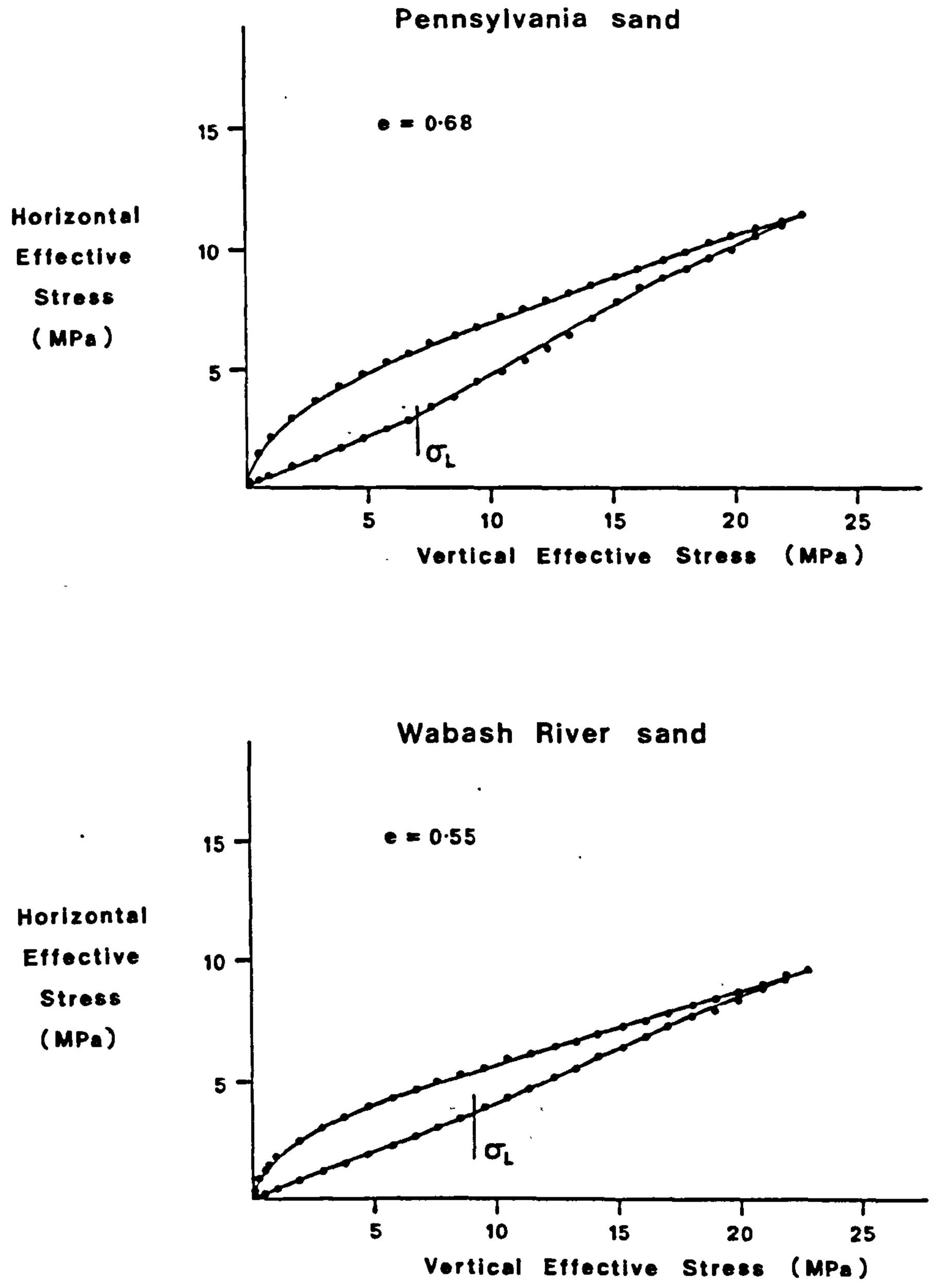

Figure 4.39 The effect of grain crushing during K_o tests on sands (After Schmidt 1967).

materials. Schmidt (1967) shows that, at high stresses, sand grains fracture during one-dimensional consolidation, the structure after yield (σ_L) increasing in density, Fig. 4.39. This diagram does not show the rearrangement of stresses due to the degradation of sand

grains as well as the chalk; this is probably due to the fact that being cemented, the chalk at yield, is further from its equilibrium void ratio for the disaggregated sediment, than is the sand. The evolution of lateral stresses in overconsolidated clays shows the same trends as seen in these experiments and is discussed by Silvestri (1981).

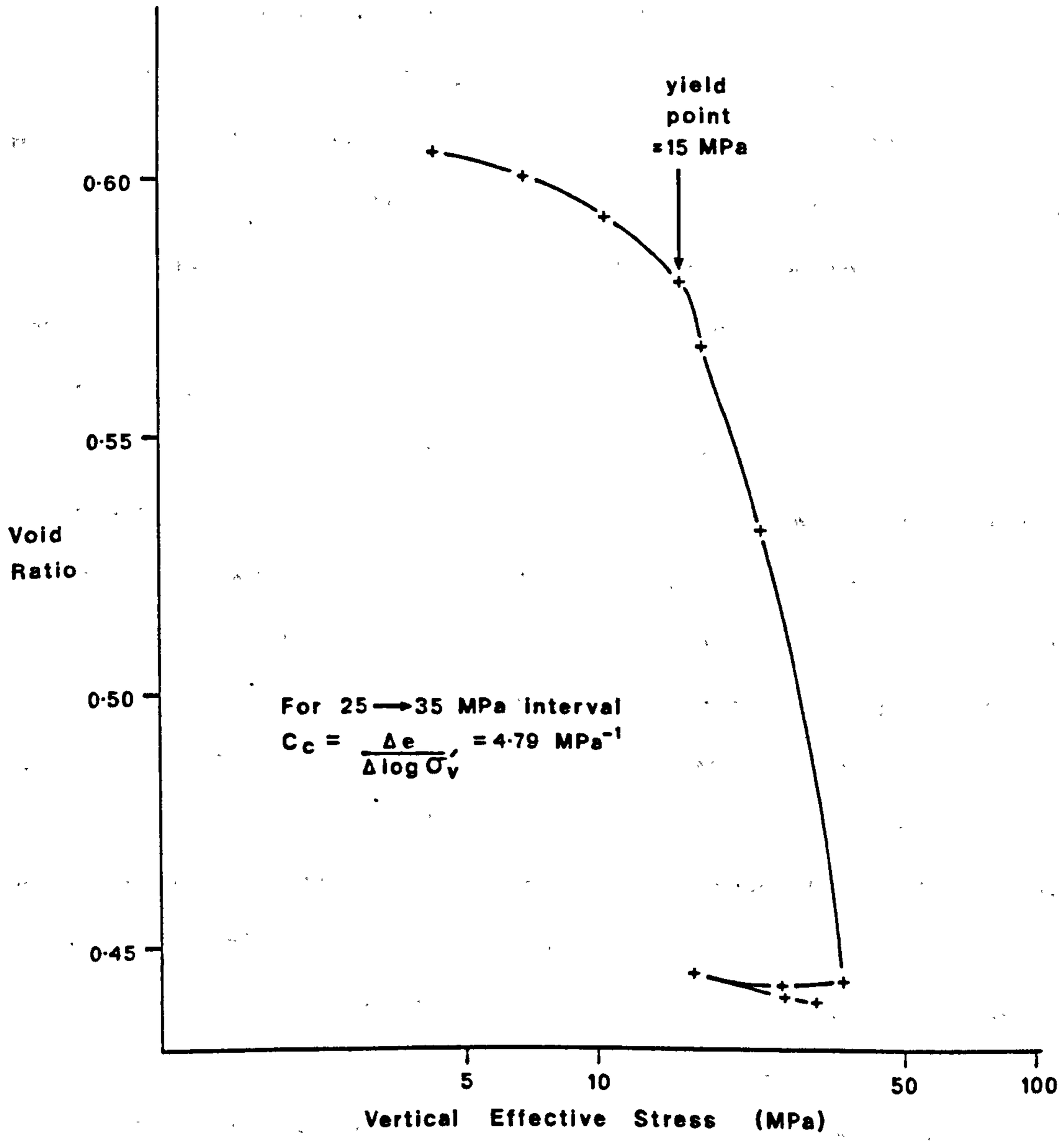

Figure 4.40 e-log p' plot for the oedometer test performed on Butser Hill chalk.

Some of the preceeding observations can be deduced from the oedometer test performed at 20°C on Butser Hill chalk. The stress increments were applied in an increment ratio (IR) of 0.5, which enables the yield to be more accurately defined than by the usual procedure where the IR is equal to 1 (Chap. 3). Trouble with the cell pressure control unit caused some of the stresses to decrease overnight, and the e-log p' curve (Fig. 4.40), is constructed using the value of stress that the reduction leveled off to. The yield can be seen to occur at 15.5MPa, while there is a post-yield kink after which the plot increases in slope with a C_c of $4.79MPa^{-1}$ for the higher stress range of this test. This is similar to a value obtained by Carter and Mallard (1974). The yield in this oedometer test can be seen to be slightly higher than that obtained from the K_o triaxial experiments.

The problem with testing brittle materials in an oedometer is that a perfect fit can never be achieved, and a gap between the sample and the oedometer wall will cause circumferential shearing of the sample in the initial part of the deformation. Associated with this gap and the shearing is a high undrained pore pressure response to the applied stress. Fig. 4.41 shows the undrained response to the stress increments used in the oedometer test. As the stress increases the pore pressure response initially tends to decrease to a value assumed to be the actual pore pressure response of the cemented material. The yield in the sample is seen by the increase in the pore pressure response, which is not immediate, but increases with time (Fig. 4.41). This time-dependent build up of pore pressure can be attributed to a time-dependent crushing deformation of the structure of both the grains and the existing bonding, this has also been observed by Lee and Farhoomand (1967).

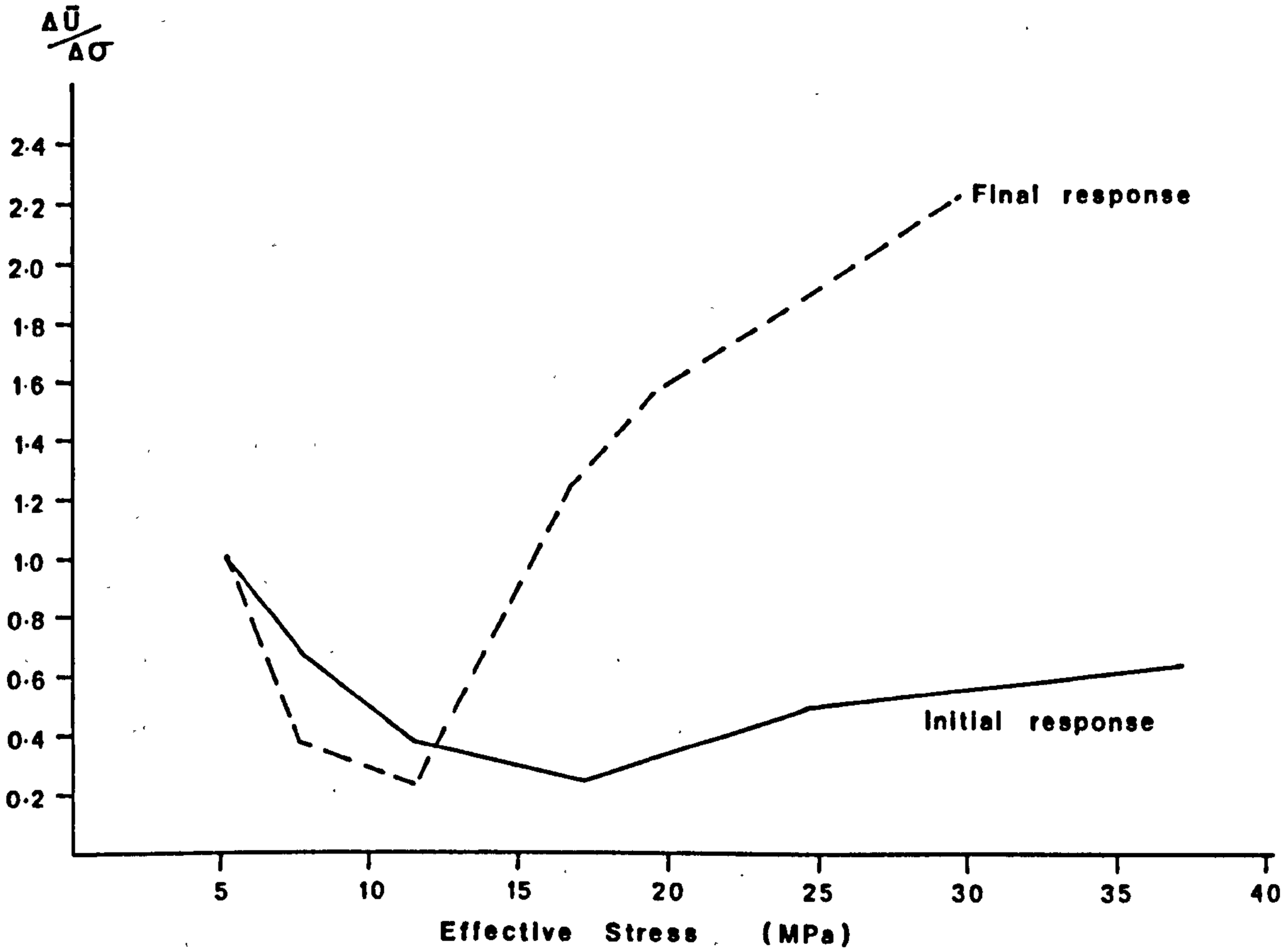

Figure 4.41 Undrained pore pressure response of incremental loads in the oedometer test on Butser Hill chalk.

From the plot of Skempton's pore pressure parameter, B (Chap. 2.3) against the applied effective stress, Fig. 4.41, it can be seen that the initial value of pore pressure response at 1-5MPa corresponds to circumferential shearing, some of the load being transferred to the pore water. At higher stresses, the pore pressure response decreases, which as mentioned, is attributed to both the decrease in the shearing of the sample and the low pore pressure response of cemented materials (Chap. 2.3). At a value approximately equal to the yield point, the pore pressure response increases with stress, the time dependence of which has been discusssed above. The B values reach 2.4, which is unusual, as the pore pressure response of a fully saturated soil is a maximum of 1. Membrane penetration into the

sample can be ignored as the membrane thickness is 0.6mm, and the pore sizes of the chalks are calculated to be between 3.5 and 1.5 microns for soft and hard chalk respectively, Lewis and Croney (1966), Chap. 2. This pore pressure observation is reliable, as the transducers reacted as expected in the drained parts of the test, for each stress increment, hence equipment error was ruled out. The high pore pressure response is attributed to structural breakdown as the effective stresses increase above a certain threshold value for the breaking strength of the particles and skeleton (Schmidt, 1967). The breakdown of the structure under undrained conditions will transfer the load from the skeleton to the pore water, assuming 100% saturation (Chaps. 2.2 and 2.3). Hence, in the extreme case of a very large collapse of structure creating strains larger than the vertical strains due to the compressibility of the water under the applied load, the pore pressure increase will equal the pressure of the load as opposed to the incremental increase in the load. In practice, the pore pressure response will level off when the pore pressure reaches a value that reduces the effective stress on the skeleton to a point where no further breakdown of grains occurs.

If the test had been continued to higher stresses the increase in pore pressure response would be expected to reach a peak at a particular stress and decrease after this - ultimately to a value of $B<1$, due to the structure work hardening.

4.8.1) Particle degradation during compaction

Particle crushing has been observed by many workers, mainly in association with shearing, though some crushing has been observed in compaction experiments, (Roberts and de Souza, 1958; Lee and Farhoomand, 1967; Schmidt, 1967; Roberts, 1969; Valent et.al., 1982;

Demars, 1982; Datta et.al., 1982). Lee and Farhoomand (1967) summarise the factors affecting the degree of particle crushing:

1) Coarse particles,

2) More angular particles,

3) Uniformity of particle grain size,

4) Increasing time of applied load.

Tests performed on sands (Roberts and de Souza, 1958; Roberts, 1969) show all these features at high pressures, and Valent et.al 's experiments on carbonate sediments show that the e - log p' plots for sediments where particle crushing occurs tend to increase in compressibility with increasing stress. A constant slope is not obtained as with sediments where no crushing occurs (Fig. 4.42). From the K_o triaxial tests (App. 5) it can be seen that the e-log p' curve is divided in to three sections, a shallow pre-yield slope, an initial post-yield steep slope followed by a section of lower C_c which gradually increases in C_c with increasing pressure (Figs. A5.10h to A5.12h). This has mainly been seen with the Pegwell Bay samples, though the initial post-yield steep slopes have been observed in the experiments shown in Figs. A5.10h, A5.15h, A5.17h, and A5.18h. This fits the trends presented by Lee and Farhoomand (1967), Roberts (1969) and Valent et.al. (1982).

Butser Hill chalks show less steepening of the e - log p' plot with increasing stress than do the Pegwell Bay chalks, due to the increased clay content in the samples, which distributes the load more evenly around the particles. This has been seen for carbonate sediments by Demars (1982) and Valent et.al. (1982). In addition, the Butser Hill chalk has a lower porosity than the Pegwell Bay sample and this also reduces the degree of particle crushing.

Crushing of particles is normally investigated using grain size

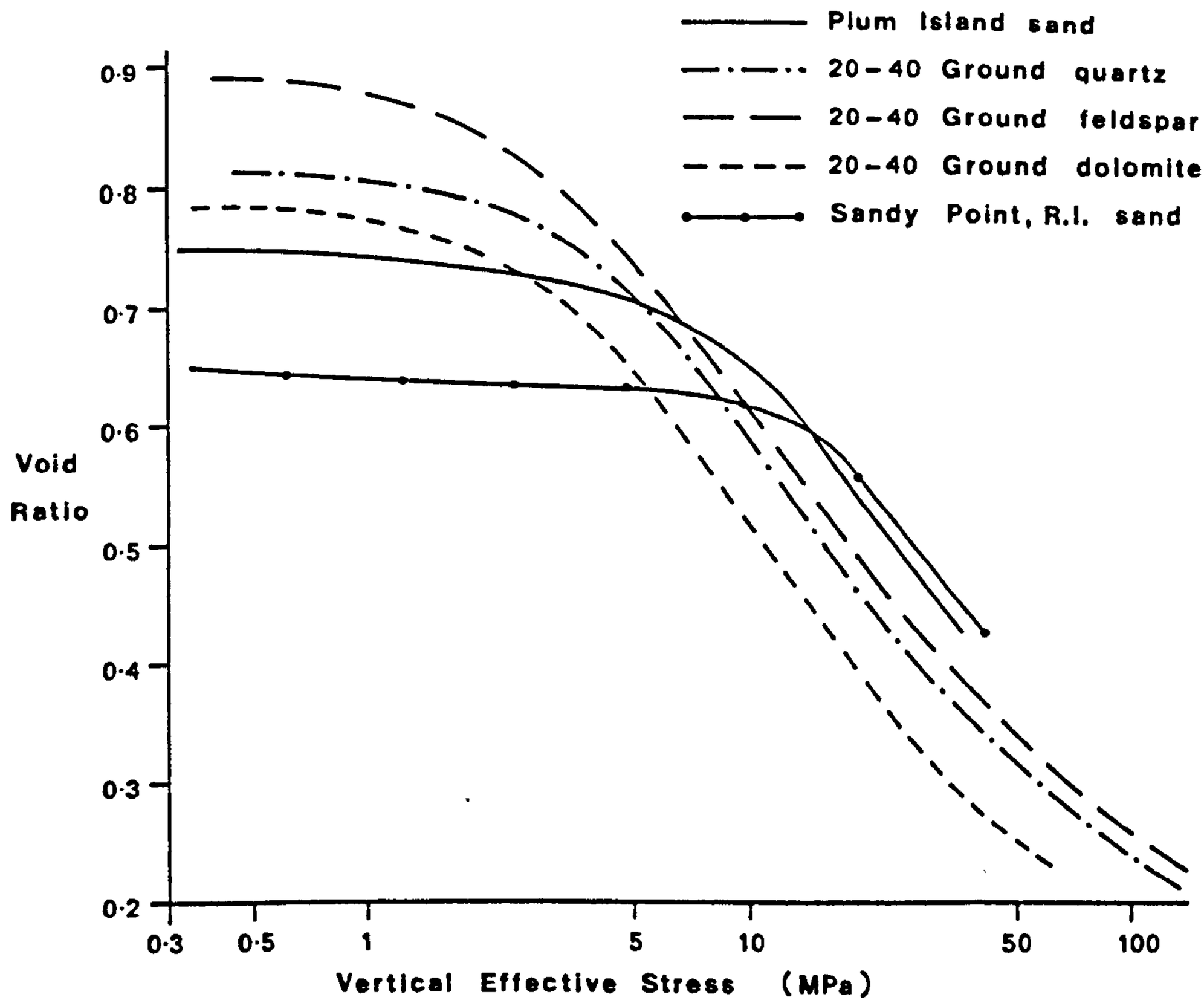

Figure 4.42a Uniaxial compressibility of sands (After Roberts 1969).

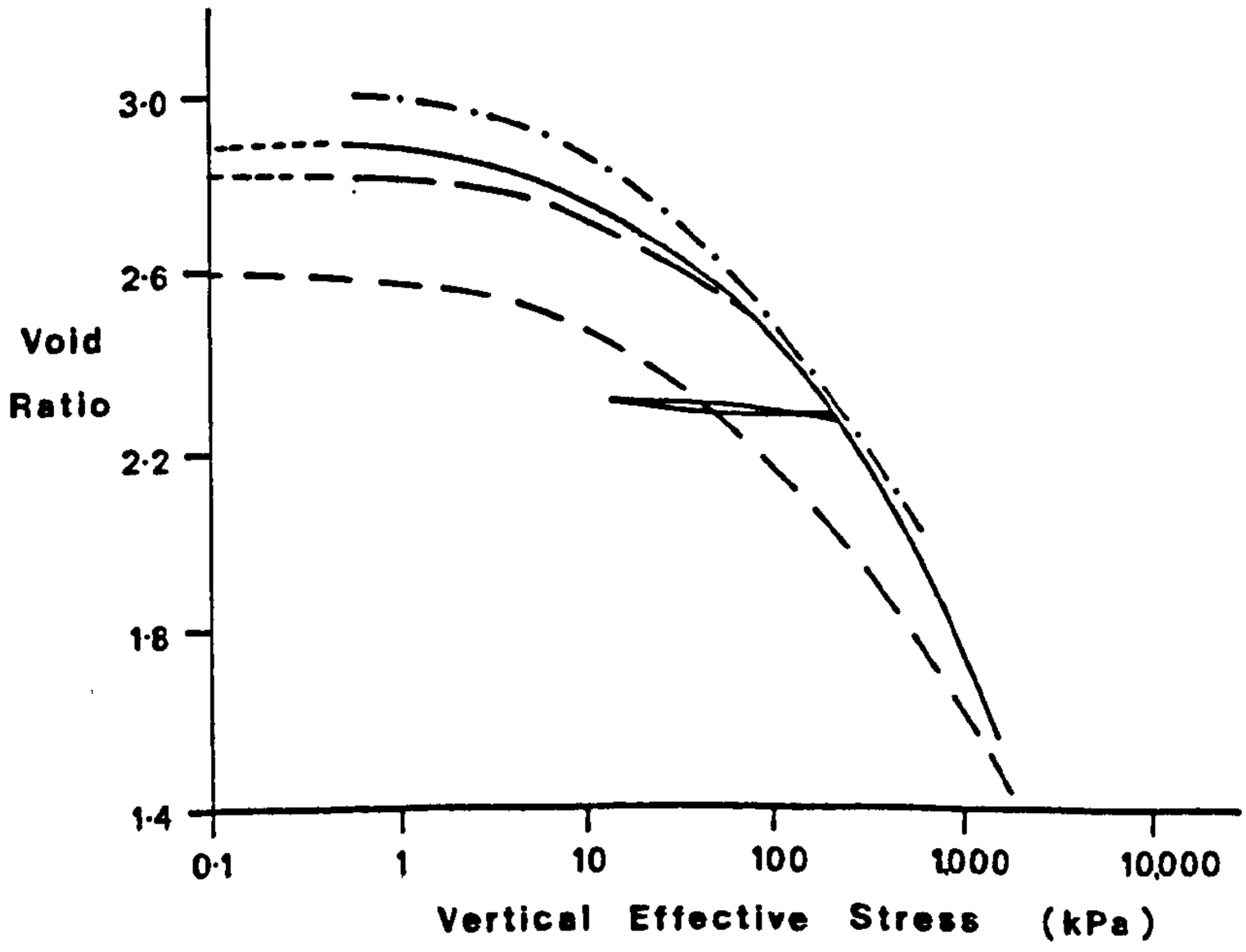

Figure 4.42b Uniaxial compressibility of carbonate sediments (After Valent et.al. 1982).

analysis; this cannot be used on chalks due to the small grain size, and the initial presence of the cement, while crushing the chalk to break the cement bonds will inevitably degrade the particles, as both grains and cement are calcite. Thus, to see if any crushing of particles is apparent in these tests, polished thin sections of the undeformed and deformed chalks were obtained, oriented parallel to the axis of the test samples. The untested samples were offcuts adjacent to the compacted samples, and are assumed to be directly comparable. All of the samples prepared were Pegwell Bay samples these being M1A (PB10.20) and M1, P3A (PB7.20) and P3, M5A (PB17.20) and M5, the A signifying the tested materials. Polished sections of the materials were then examined using the scanning electron microscope. These specimens were cut in the axial direction to observe the maximum strain, and could therefore not be studied using the conventional 3-dimensional SEM image because of the oriented nature of the axial stress in the specimens. Back scatter images as well as secondary electron images were recorded, as the former give a striking contrast between Araldite filled pores and the calcite skeleton. Back scatter can also give evidence of chemical changes in the minerals (Huggett, 1982; White, Shaw and Huggett, 1984).

The main characteristics of the SEM and back scatter SEM microphotographs will now be discussed.

i) Low magnification

In the Scanning Electron Microscope (SEM) photomicrographs at low magnification, 4277 and 4273, a large percentage of the porosity in the chalk is seen to be due to foraminiferal shells or tests (Chap. 3), the matrix of the chalks in these plates is not well-defined. The compaction is evident from these plates as the tested sample (4277)

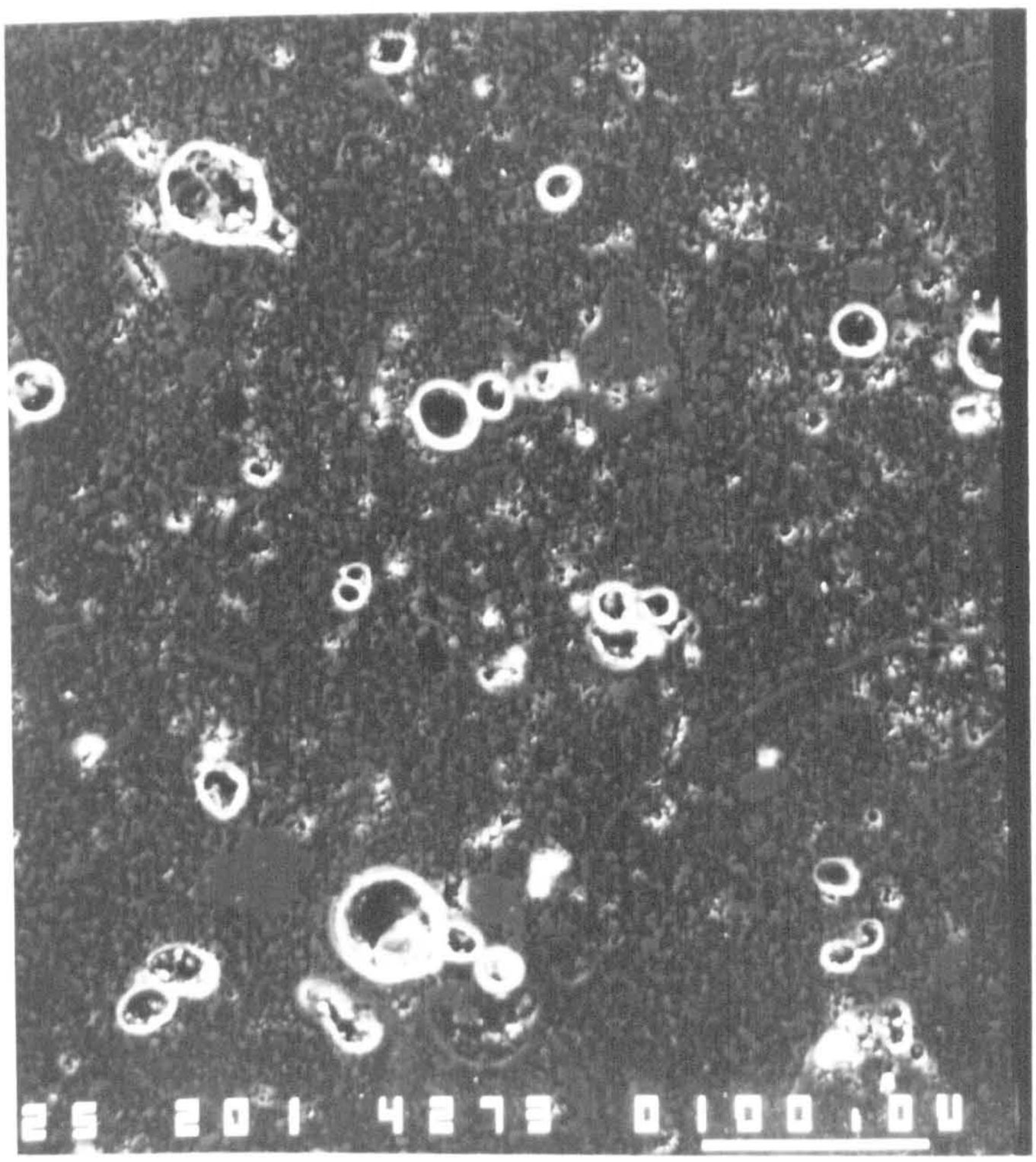

direction of compaction

SEM 4273 M3 - Low magnification (x200).

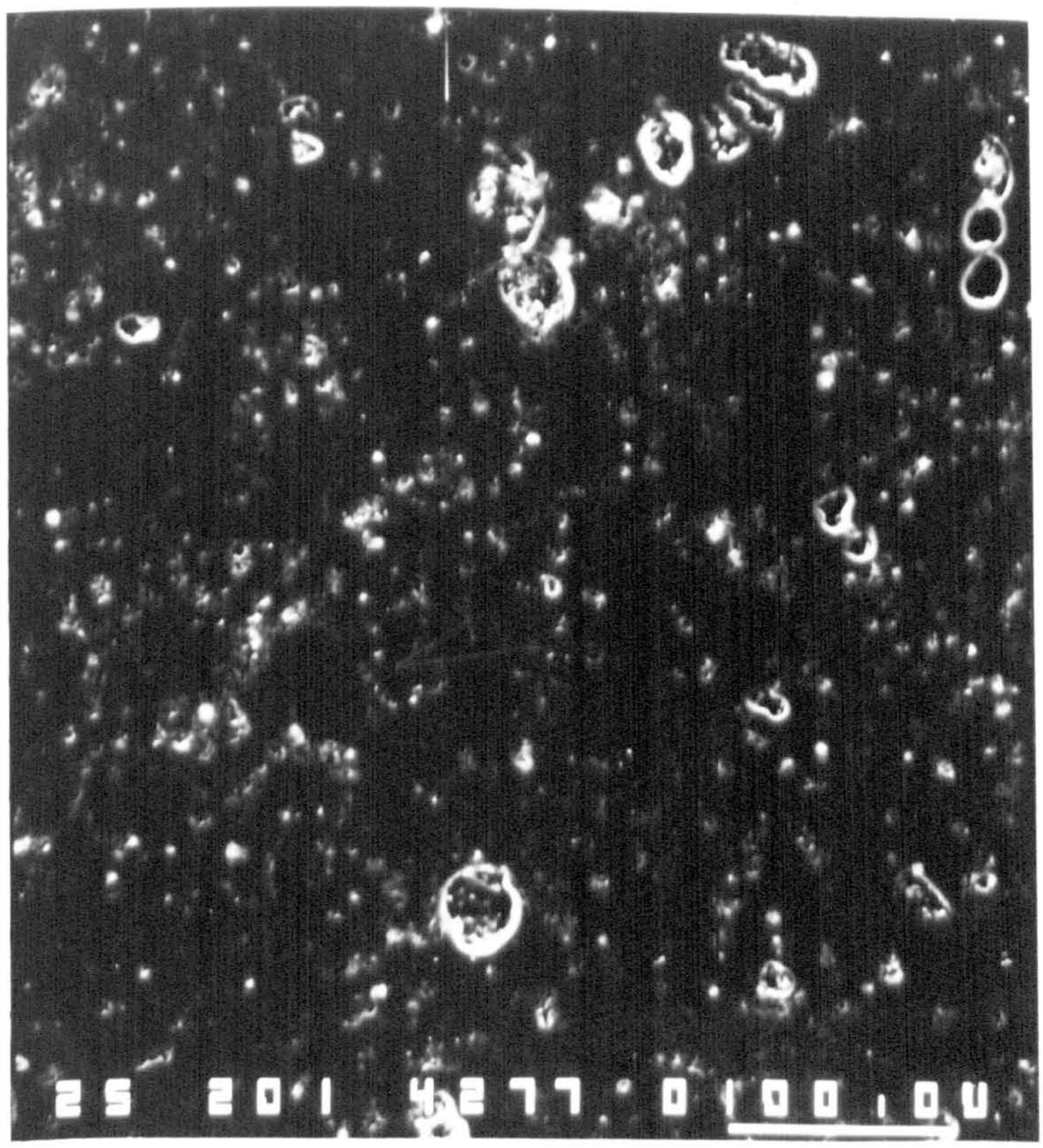

direction of compaction

SEM 4277 M3A - Low magnification (x200).

direction of compaction

SEM 4276 M3A - Medium magnification (x600).

shows less distinct forams with bright nebulous patches in greater abundance than in the untested materials. These are interpreted as collapsed forams in and out of the plane of the section. Not all of the forams collapse, e.g. top right of 4277; the bottom two of three chambers are seen to be intact while the top one has collapsed. An example of these collapsed forams occurs in the top centre of photomicrograph 4277; the collapsed foram is shown at slightly higher magnification in 4276, where the foram test can be seen with granular matrix inside the test. This is also seen in 4272 as a large mass of circular shell with matrix inside the shell. Relic forams exist in the untested samples but these are relatively uncommon in comparison with the tested samples.

ii) High magnification

The matrix of the chalk is shown in photomicrographs 4264 and 4269; these show the matrix in secondary electron image, with 4265 and 4270 being back scatter images of 4264 and 4269 respectively. The scale bar on these photomicrographs is 10 microns. The plates show, for the tested and untested samples, the lower porosity present in the compacted samples, as would be expected. However, the plates also show a marked increase in the percentage of fine grained material. In the electron photomicrographs of the compacted samples, no large areas of black pore space can be observed.

The photomicrographs do show a degradation of coccoliths, although, as with the forams, some coccolith remain intact after testing, c.f. 4269. The back-scatter electron images, although blurred (due to the resolution limit on the back scatter electron detector at this magnification), shows a significant reduction in the amount of black Araldite-filled pore space in 4270 relative to the

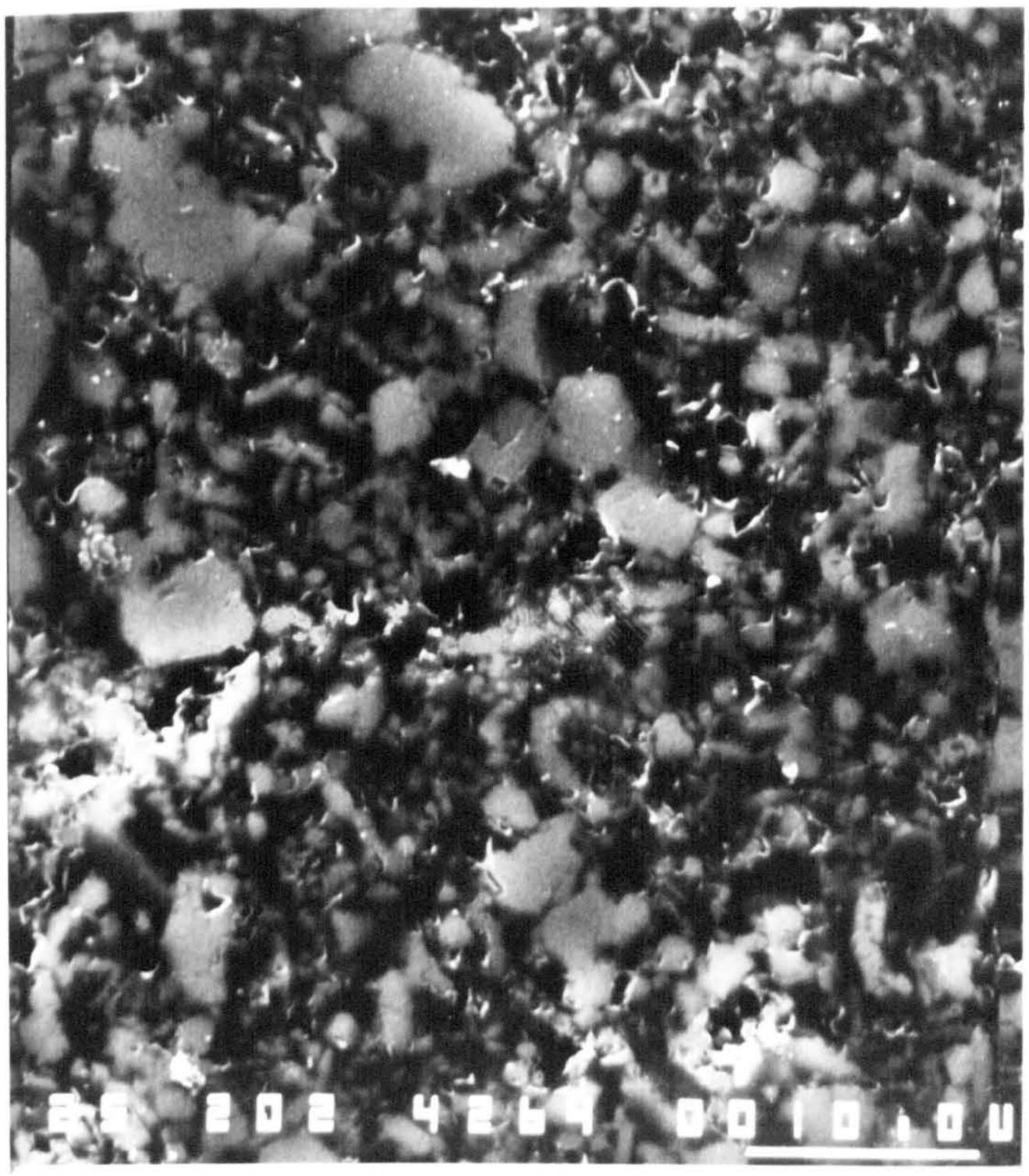

direction of compaction

SEM 4264 P5 - High magnification (x2000).

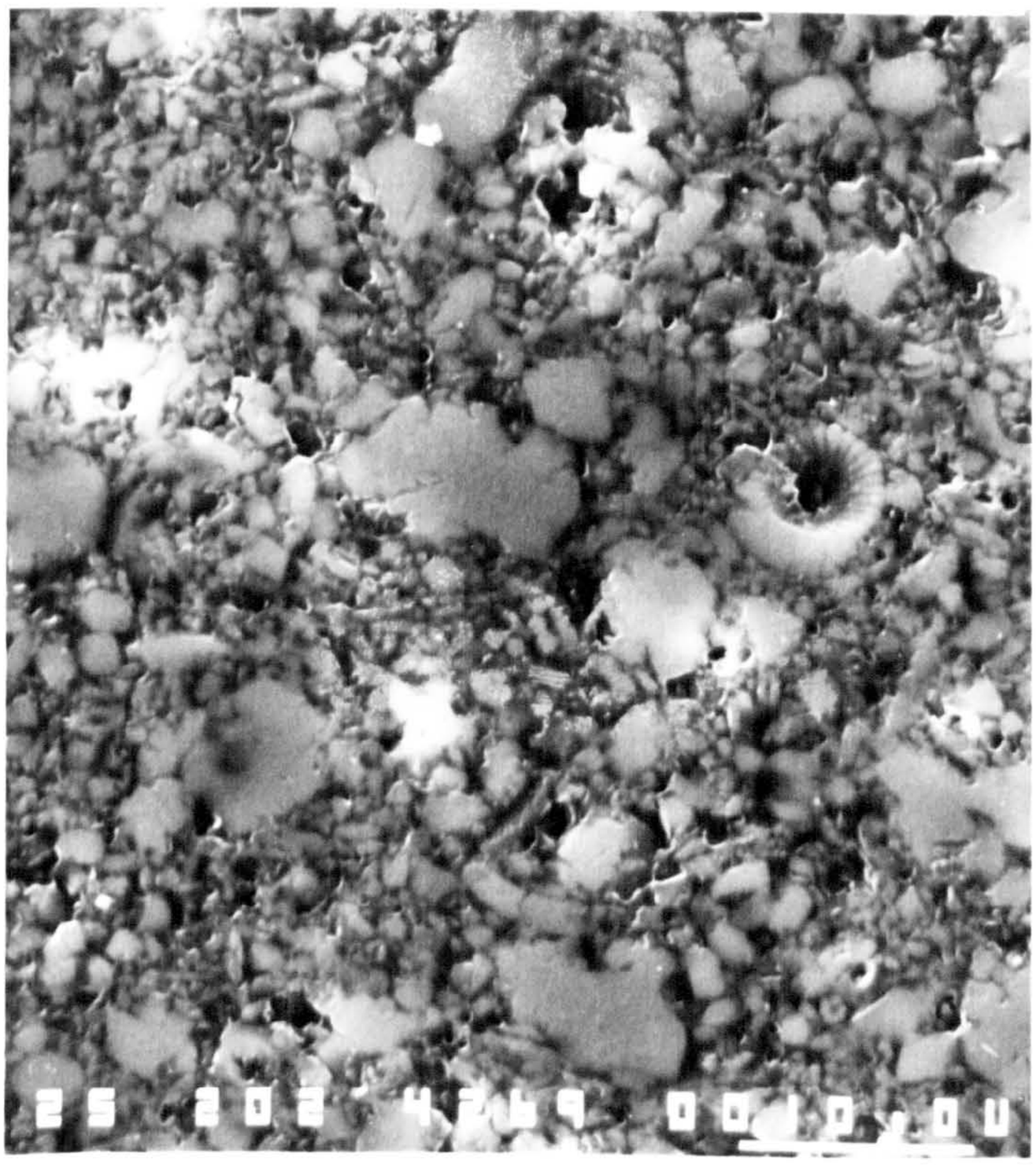

direction of compaction

SEM 4269 P5A - High magnification (x2000).

direction of compaction

SEM 4265 P5 - Back scatter image, high magnification (x2000).

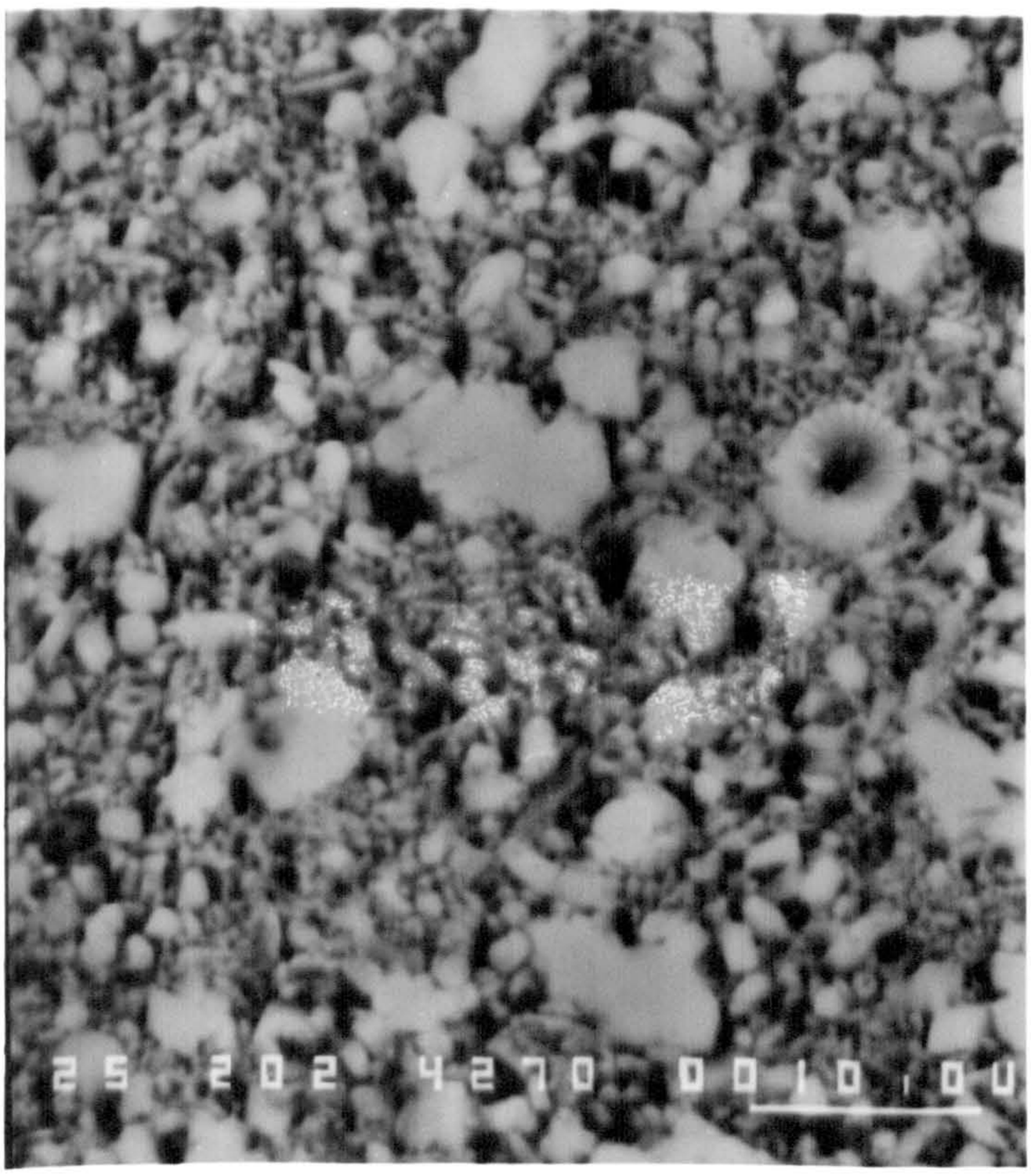

direction of compaction

SEM 4270 P5A - Back scatter image, high magnification (x2000).

untested 4265. Again, the decrease in grain size is apparent. This decrease in the pore volume and the production of fine grained material will decrease the permeability markedly, as discussed in Chap. 4.6.

This section has shown how the compaction of chalk consists of grain crushing as well as grain rearrangement. The breakdown of the chalk due to creep of the structure has been observed under undrained conditions in an oedometer test. This is similar to the results obtained by Othsuki et.al. (1981). The gradual breakdown of the cementation during the pore collapse deformation is seen by the gradual increase in the value of C_c in the e-log p' plot, and the time dependant build up of pore pressures in the oedometer test.

4.9) YIELD AND FAILURE SURFACE OF CHALK

The tests reported in App.5 were performed to investigate the nature of the yield envelope and to see if Jaky's relationship (Eqn. 3.2.3) holds at the high stresses used in this study. The tests performed include drained and undrained shear tests, with one hydrostatic test (Table 4.6).

The yield envelope, Fig. 4.43, was defined using 7 tests to obtain an approximate shape for the compactional yield surface (end cap), though more tests are required to define it in its entirety. The results show that the yield surface has a constant q section analogous to that found by Sangrey (1972) on sensitive clays. The deviatoric stress at yield seems to decrease gradually from 11.3MPa at a mean effective stress of 14.4 to an isotropic yield point of 20.8MPa. The repeatability of the tests seems reasonable, though BH8.20 gives a higher deviatoric stress than expected.

The failure line was not obtained for the three drained shear

Table 4.6

Sample	Porosity %	Strain rate sec^{-1}	Consolidation pressure MPa	Young's/Bulk(*) modulus GPa	Yield point MPa	Poisson's ratio
BH8.20	36.3	$1.78*10^{-6}$	18.2	2.86	6.72	0.021
BH10.20	37.3	$1.70*10^{-6}$	5.7	2.10	11.47	0.394/0.334
BH11.20	37.5	$1.79*10^{-6}$	10.7	2.05	11.37	---
BH12.20	37.0	$1.82*10^{-6}$	15.0	2.16	7.14	0.281
BH20.20	36.9	$1.90*10^{-6}$	15.6	1.48	6.72	0.301
BH6.20	36.9	---	---	0.87 *	20.87	---

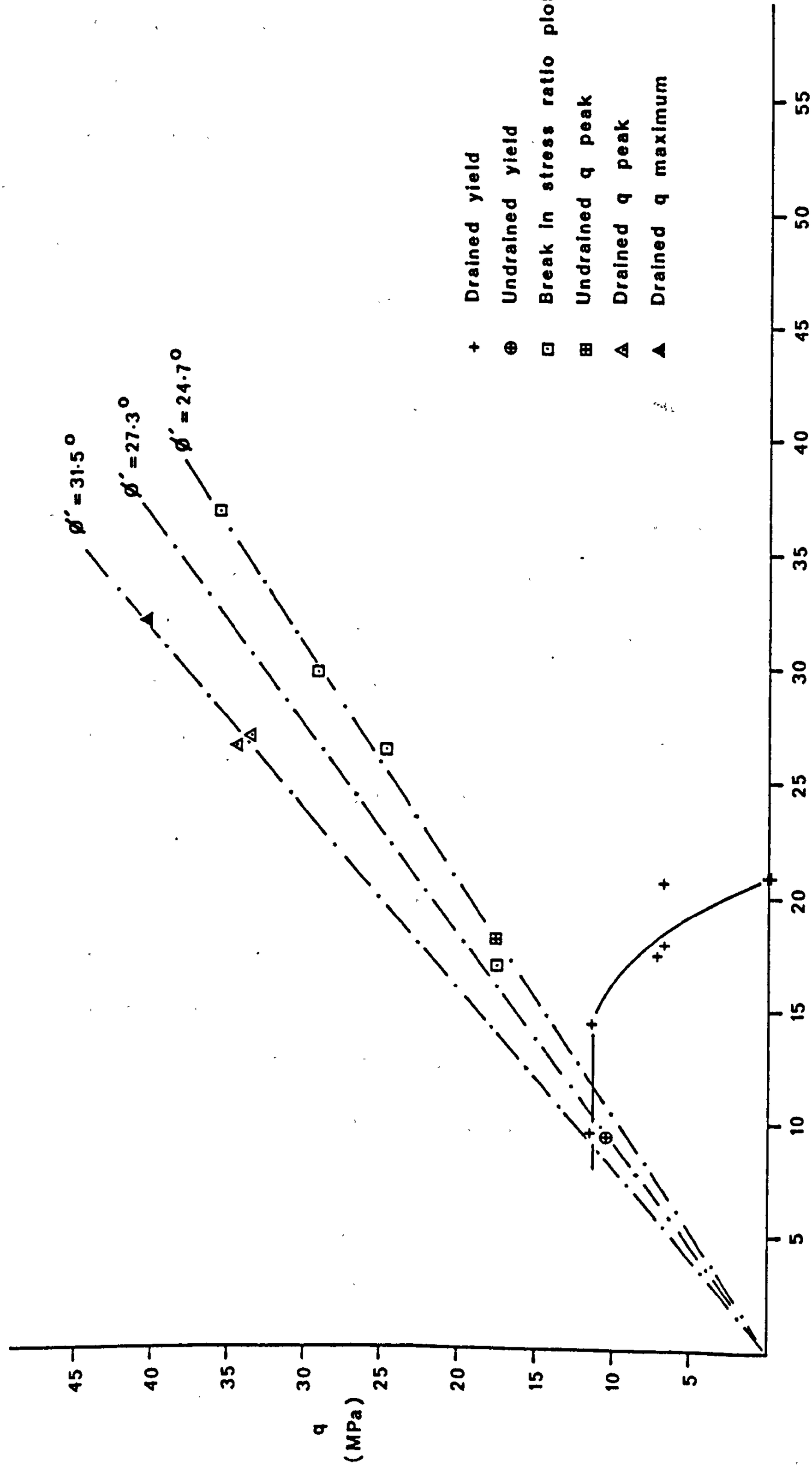

Figure 4.43 Yield envelope and failure line for Butser Hill chalks.

tests performed; only one reached a peak load, during which the volume of the sample was still decreasing. The undrained shear tests performed after K_o consolidation do not reach a maximum load, though USB18.20, USB3.20 and USB5.20 tend towards a value of maximum q/p'. The undrained shear at approximately a minimum p' shows a change in modulus when the principle effective stress ratio is plotted against axial strain, indicating a change in the material behaviour. This is seen with all of the samples; with USB5.20 the change occurs at post-peak load.

In summary the failure defined by the maximum load only occurred in one drained sample, though the other tests showed changes in behaviour during shear. The loads attained for the drained tests are far higher than those in the undrained tests for equal values of p'. The drop in the cell pressure during these tests obviously complicates the interpretation of the failure, App. 5, and so the results should be treated with some caution.

Three possible failure lines were defined by 1) the extension to the origin of the drained tests, 2) the line drawn from the tangent to USB18.20 passing through USB5.20, to which USB4.20 and USB3.20 tend, and 3) a line passing through the break in the stress ratio-axial strain plots. The equivalent angles of internal friction for these slopes are 31.5^o for the drained tests, 27.3^o using the tangent to the undrained shear tests, and 24.7^o using the change in modulus, the equivalent K_o values for these friction angles (using Jaky's equation) being 0.478, 0.548 and 0.583 respectively. These can be compared to the almost constant K_o of 0.55 to 0.61, averaging 0.577, determined from the 20^oC uniaxial experiments. As can be seen the closest agreement occurs with the stress ratio failure line. However, further experimentation is required to make more firm

conclusions about the tests.

This type of analysis is complicated due to the particle crushing during consolidation and shear. As the degree of particle crushing will affect the friction angle for the sediment, the amount of particle crushing during compaction should be matched during shear if relationships between K_o and the angle of internal friction are sought.

4.10) COMPACTION OF CHALK: SUMMARY

This section discusses the overall behaviour of the chalks tested during one dimensional compaction. It combines the characteristics determined from the chalk samples with similar porosities from onshore sites with the variable porosity chalk samples from the Central North Sea. This is done to obtain a general picture of chalk compaction, which is applicable to high porosity chalks from other areas.

The compaction of chalk can be seen to involve an initial elastic deformation, due to the cementation maintaining a rigid structure. The reaction of the chalk to this cementation depends upon the porosity and the strength of the cement. The plot of tangential Young's modulus with porosity for the three types of chalk tested are shown in Fig. 4.44. There is considerable variation in Young's modulus at a specific porosity and vice versa. However, the range of this graph is small compared to range of porosity and Young's moduli for chalks. The results of the North Sea chalks have already been compared to the results of Jones (1985) (Fig. 4.4b). This trend has been obtained using an acoustic velocity method for measuring Young's modulus for various porosity chalks, while the results plotted in Fig. 4.44 are from K_o tests and as such would be lower than those

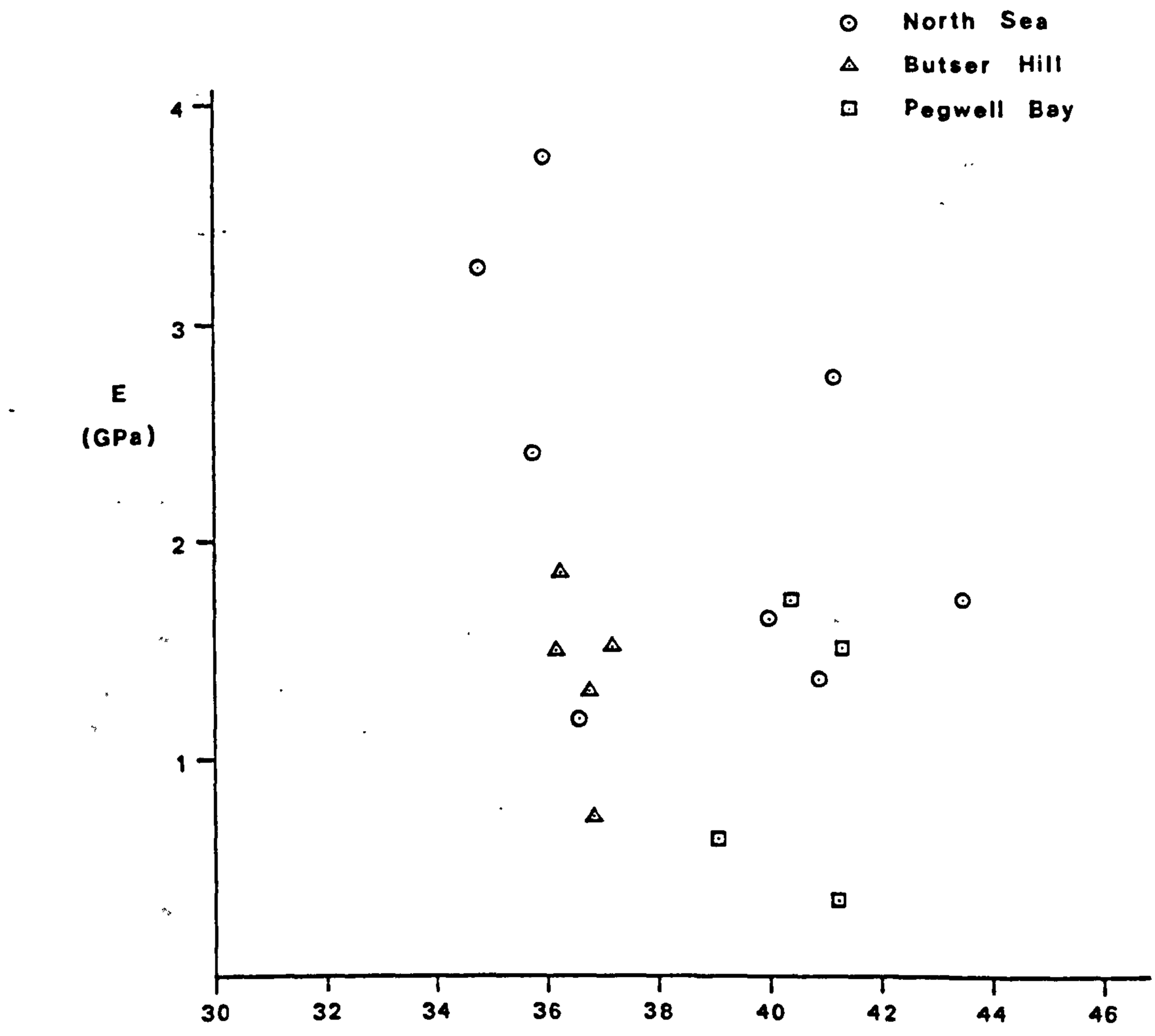

Figure 4.44 Young's modulus vs porosity for K_o tests on three chalks.

obtained from drained triaxial shear tests, as shown in Table 4.4 and 4.6 for the Butser Hill samples. The elastic section has not been deliberately unloaded and reloaded and, as such, has not been proven to be elastic; it is assumed, however, that the reaction to stress has a dominantly elastic component. This section of deformation is terminated by a breakdown in cementation in the K_o tests at the yield point. The yield point is defined as the abrupt change in deviatoric stress with increasing axial strain, and is shown for chalks tested in Fig. 4.45. Again, a large scatter is seen for the deviatoric yield

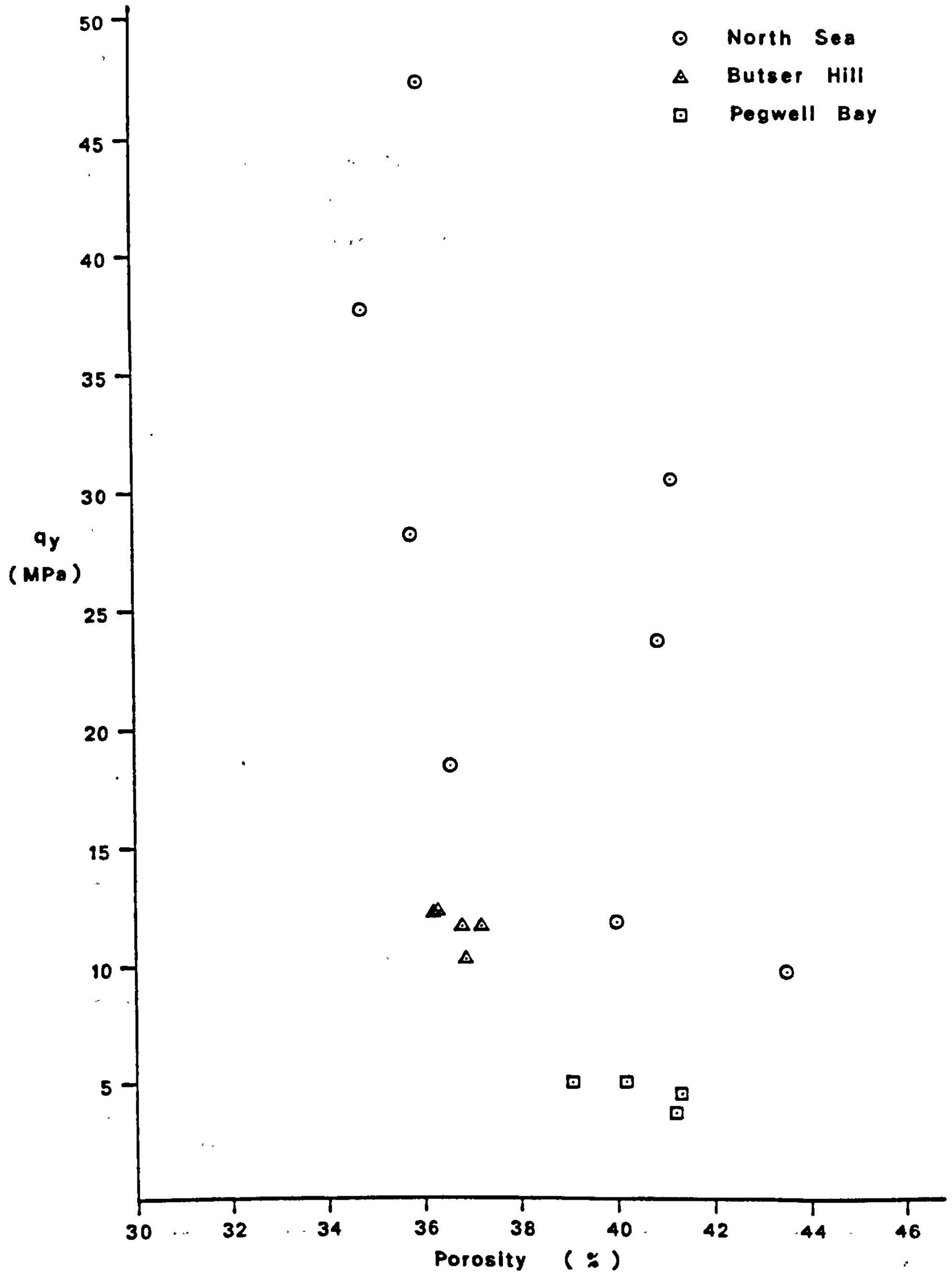

Figure 4.45 Yield point vs porosity for K_o tests on three chalks.

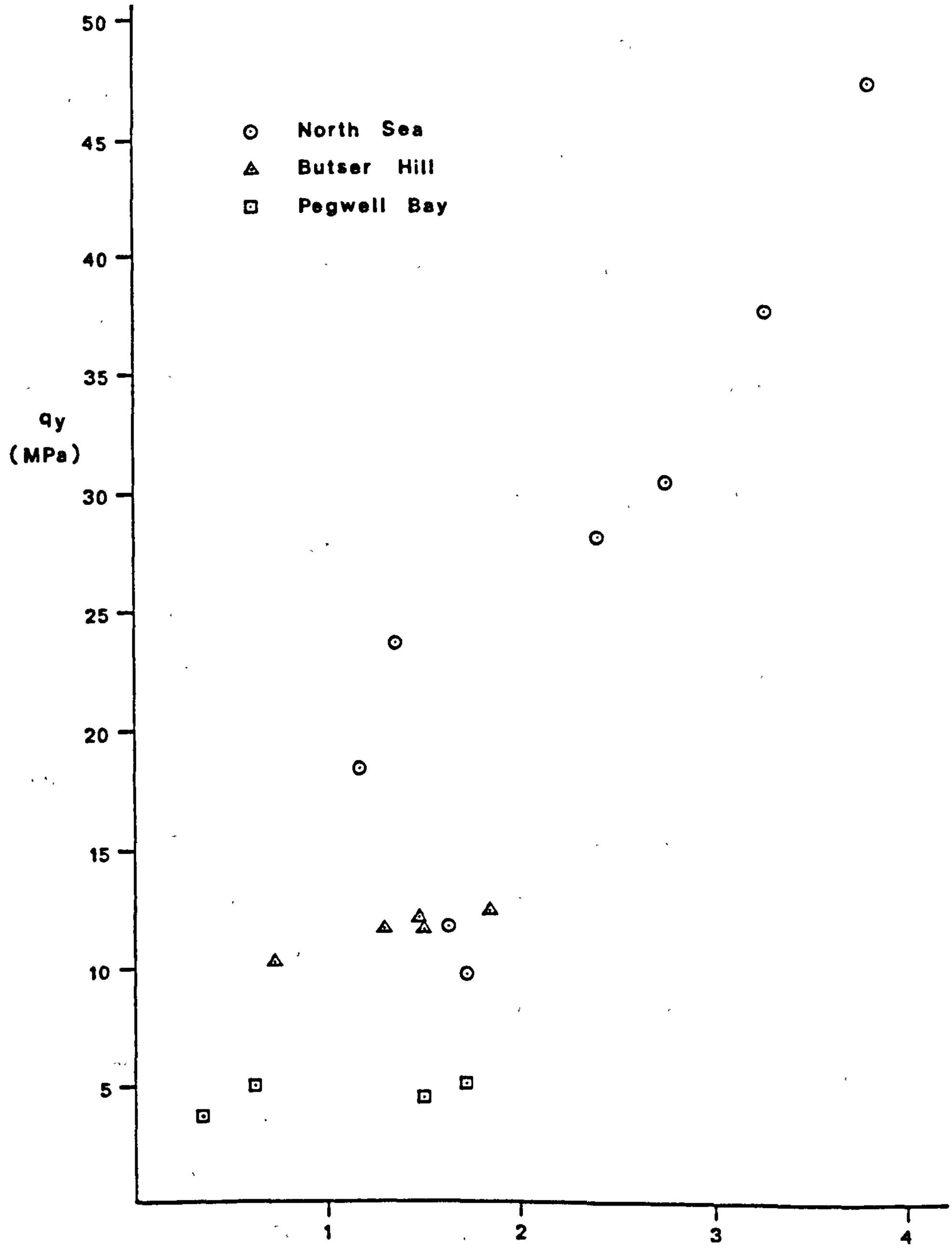

Figure 4.46 Yield point vs Young's modulus for K_o tests on three chalks.

point versus porosity plot. At a deviatoric stress of 10MPa, the range of porosities that yield vary from 36 - 44%, while at a constant porosity of 36.5%, the yield point can vary from 10MPa to 48MPa deviatoric stress. The Pegwell Bay and Butser Hill samples lie beneath the general and broad trend shown by the North Sea chalks. This is attributed to different diagenetic histories, the lower values possibly being a result of lower burial depths and/or weakening by ground water infiltration. In addition, the North Sea chalks, have oil as a pore fluid, which is generally assumed to limit the the amount of pressure solution occurring during burial of a sediment (Hancock, 1983; Sørensen et.al., 1986). Thus, a unique trend in material properties may not be generalised for chalks of different diagenetic histories.

To eliminate the porosity variable, as performed earlier, the deviatoric stress has been plotted against the Young's modulus for representative chalks in Fig. 4.46. Scatter is still seen, and must be attributed to sample variation. The Pegwell Bay samples are seen to occupy the lower stress area, with two samples having a deviatoric stress of approximately 5MPa and Young's moduli of 1.5 and 1.7GPa, whereas the samples from a different block from Pegwell Bay have Young's moduli values below 1GPa. The Butser Hill chalks lie at the lower end of the North Sea chalk trend, at deviatoric stress values of 10 to 13MPa and Young's moduli values ranging from 0.72 to 1.84GPa. The North Sea chalks show an approximately linear trend of increasing Young's modulus with deviatoric stress.

The elastic surface along which the samples deform in the low stress regime, when observed in e-q-p' space, is inclined on the e-p' surface, as seen by the elastic section of the hydrostatic test (see BH6.20 in App. 5). The surface may also be inclined to the e-q

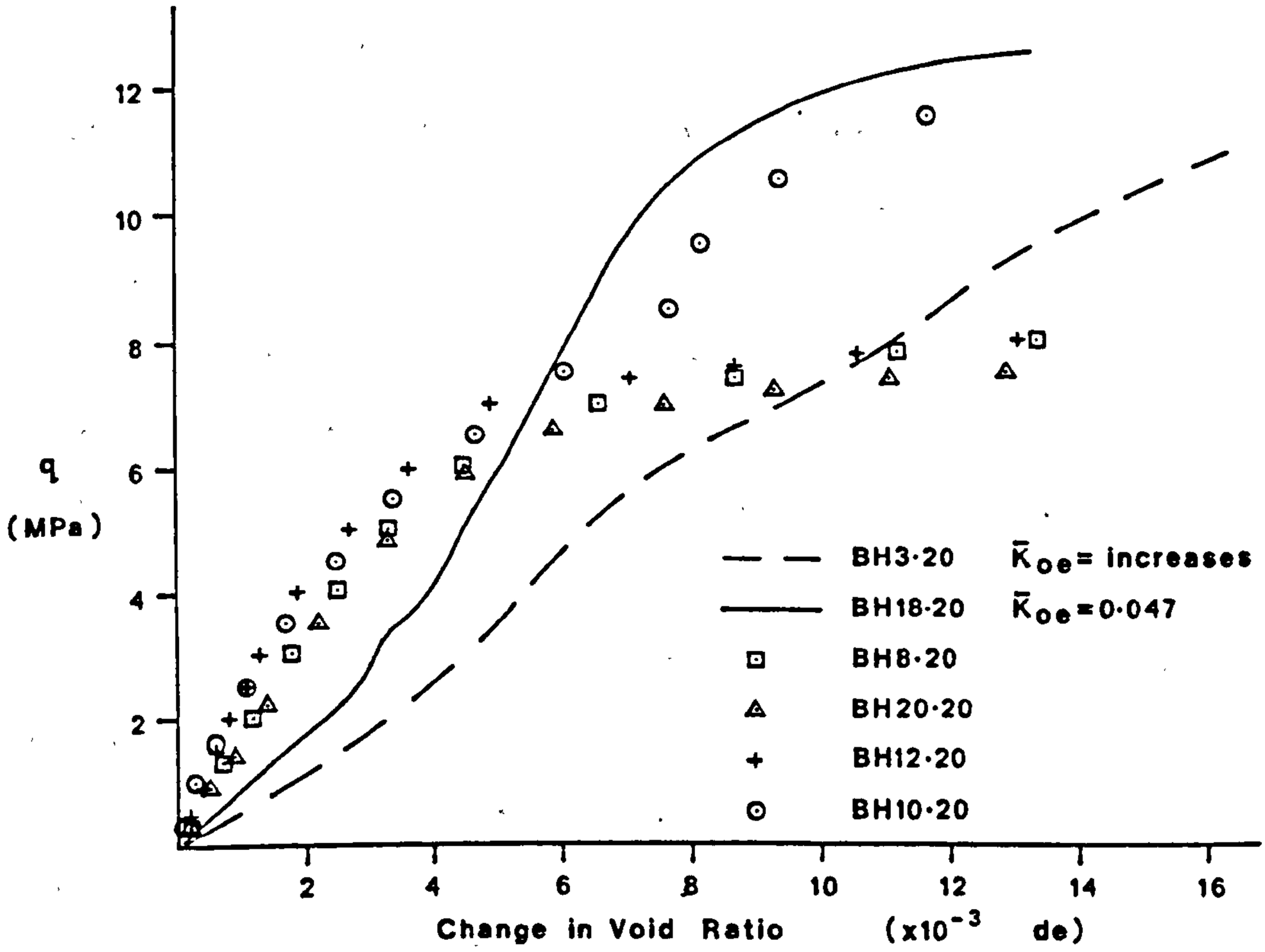

Figure 4.47 Deviatoric stress vs change in void ratio during the elastic deformation of K_o and drained shear tests on Butser Hill chalk.

plane; this inclination, if it exists, remains constant with increasing p'. This can be seen from the plot of the load (q) vs the change in voids ratio due to loading (de) (Fig. 4.47), which shows four drained shear tests and two K_o tests. The drained shear tests have an inclination of 1 in 3 in q-p' space, so in Fig. 4.47 the effect of increasing p' on the void ratio is included. The diagram shows a constant inclination of q-de with increasing p'. To eliminate the effect of p' on de, the de values in Fig. 4.47 were adjusted for the change in p' with q. The relationship used for this reduction or adjustment of de is the generalised gradient of volume reduction for the elastic deformation in the hydrostatic test. When this was done, the inclination in Fig. 4.47 could be seen to be purely attributed to

the volume change due to the increase in p' (Fig. 4.47). The actual values for this correction varied about a zero void ratio change per increase in deviatoric stress, the values occasionally being negative due to the "rounding off" of the computer calculations, with respect to the mean effective stress, and differences in samples. However, the magnitudes of the variations were small generally less than 0.0003. Fig. 4.47, shows how the K_o tests have a larger change in the void ratio than the drained shear tests; this is due to the fact that they have a lower gradient in q-p' space, and hence p' is larger for a particular value of q and a larger volume change is observed. For the two K_o tests presented, BH18.20 has a $\bar{K}_{oe}$ = 0.047 and, is seen in Fig. 4.47 to have a similar initial modulus (ignoring the initial bedding errors) as the drained tests; conversely, BH7.20 has a lower modulus due to the extra void ratio change, which in turn is caused by the larger and gradually increasing p', on its $\bar{K}_{oe}$ stress path. From this it can be assumed that the K_o stress path passes up the vertical elastic surface which can be defined by the drained shear tests.

The results from the pore collapse section of the deformation are generally confusing, one example of this is seen by the different shifts of the normally consolidated part of the deformation in the q-p' plots. To rationalise this pore collapse deformation two parameters are used, de - the change in the void ratio during pore collapse (void ratio for the start of normal consolidation minus the void ratio at yield), and dp' - the change in the mean effective stress between the yield and the start of normal consolidation. Normal consolidation has been defined as the first point of the linear increase in deviatoric stress with increasing mean effective stress; although other definitions could be used e.g. the point of

intersection of the $\bar{K}_{opc}$ and $\bar{K}_{onc}$ lines in principle effective stress space.

The size of the pore collapse section and the stiffness of the elastic section will be controlled by, 1) the porosity at the onset of cementation, and 2) the strength of the cementation and diagenetic alterations. With increasing strength, the size of the pore collapse section will increase as the cemented sediment at yield becomes increasingly further from its equilibrium value (on the normal consolidation surface of the Critical State diagram). From this we can say that for identical $\bar{K}_{oe}$ stress paths (and a constant deviatoric stress, post-yield deformation), the material with the higher bond strength will have a less steep de/dp pore collapse section due to the large increase in p' required to reach the K_o line on the normal consolidation surface. This assumes that the de remains constant, which will generally not be the case due to the slope in e-p' space of the Roscoe surface.

The shift observed in the $\bar{K}_{onc}$ stress paths to higher values of p' (for similar deviatoric stresses), Figs. 4.15, 4.26b, and 4.48, is seen to be related to the size of the volumetric strain undergone in the transitional, pore collapse region (Fig. 4.49a), the relationship being linear for the small variation in the Butser Hill samples. From Fig.4.49b, the shift is seen to be unrelated to the strain rate or the accompanying pore pressure response (u being the average pore pressure, du being the change of pore pressure, and du/dp' being the pore pressure increase with mean effective stress during the pore collapse deformation). The shift in dp', and hence de, is therefore attributed to the porosity or structure of the Butser Hill chalks seen in Figs. 4.48, and 4.49a, and envisaged to be a shift of the normally consolidated surface relative to the elastic cementation

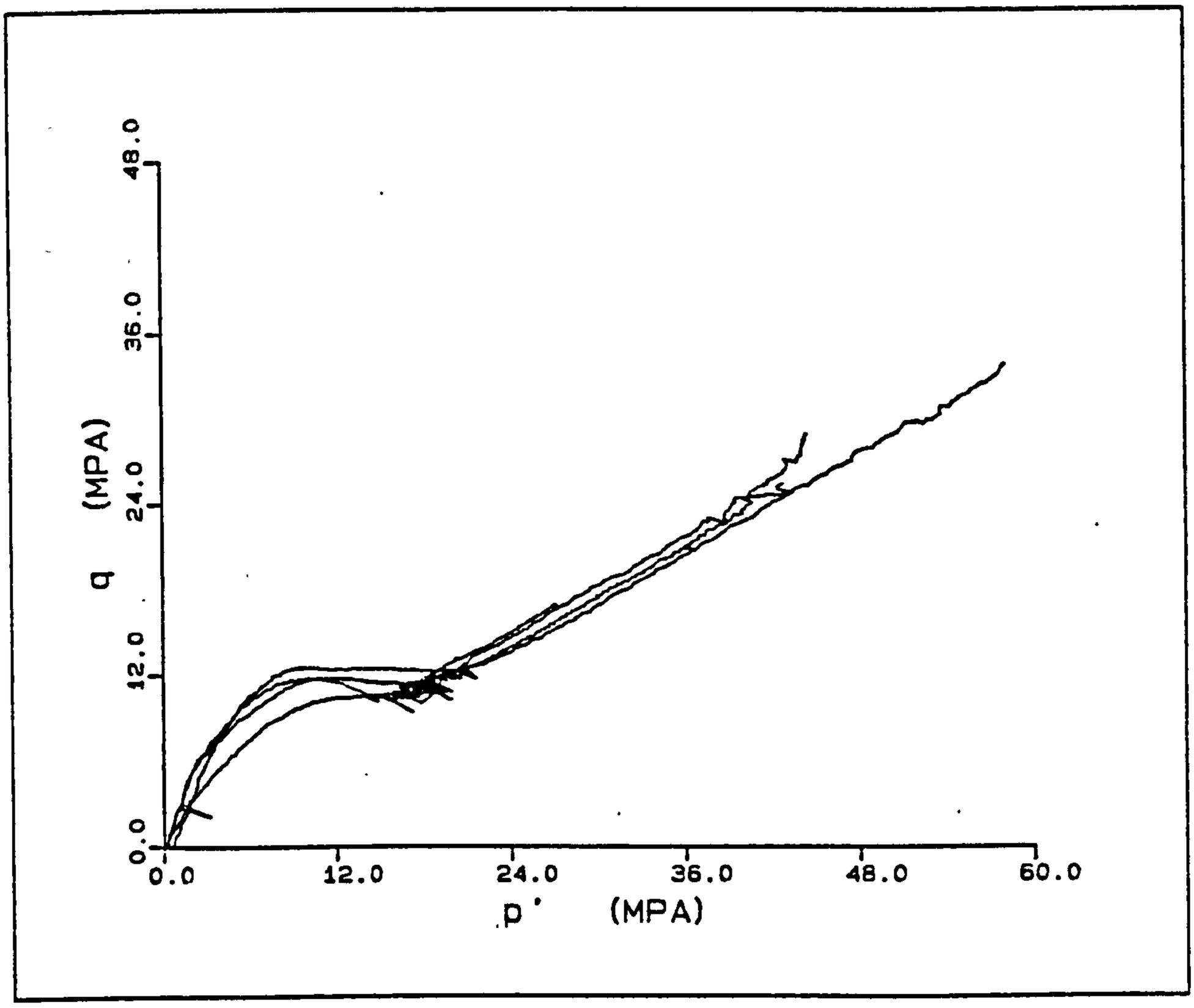

Figure 4.48 Stress paths for four K_o tests on Butser Hill chalks.

surface along one unique de/dp' line for these samples, defined by Fig. 4.49a (Addis, 1987). The variation of de/dp' with porosity will depend upon the geometry of the normal consolidation surface and the porosity at cementation; the yield point versus de/dp' for North Sea chalks is shown in Fig. 4.50. No relationship was observed between de and the yield point for the North Sea chalks. In Fig. 4.50 a trend is seen of decreasing de/dp' with increasing yield stress. The lowest value of yield is given by EC5.20; because of errors in the control of K_o this may have a rather high value of de/dp', Fig. A5.5. This plot does not take into account any variation in q with deformation, i.e. it assumes a constant q stress path. Fig. 4.9 indicates how the stress path affects de/dp', which increases with the $\bar{K}_{opc}$ so that

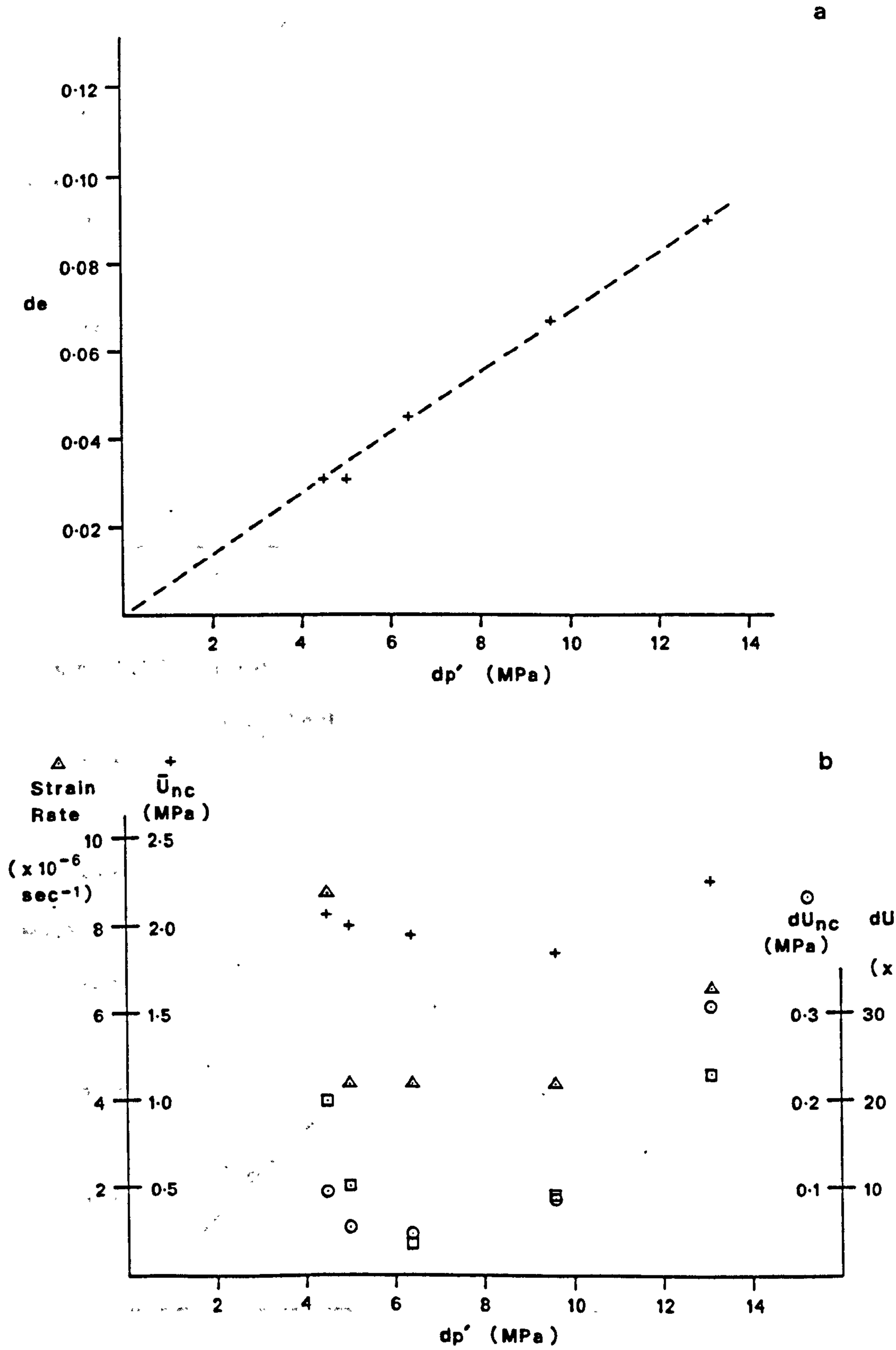

Figure 4.49 Analysis of the pore collapse deformation for K_o' tests on Butser Hill chalks.

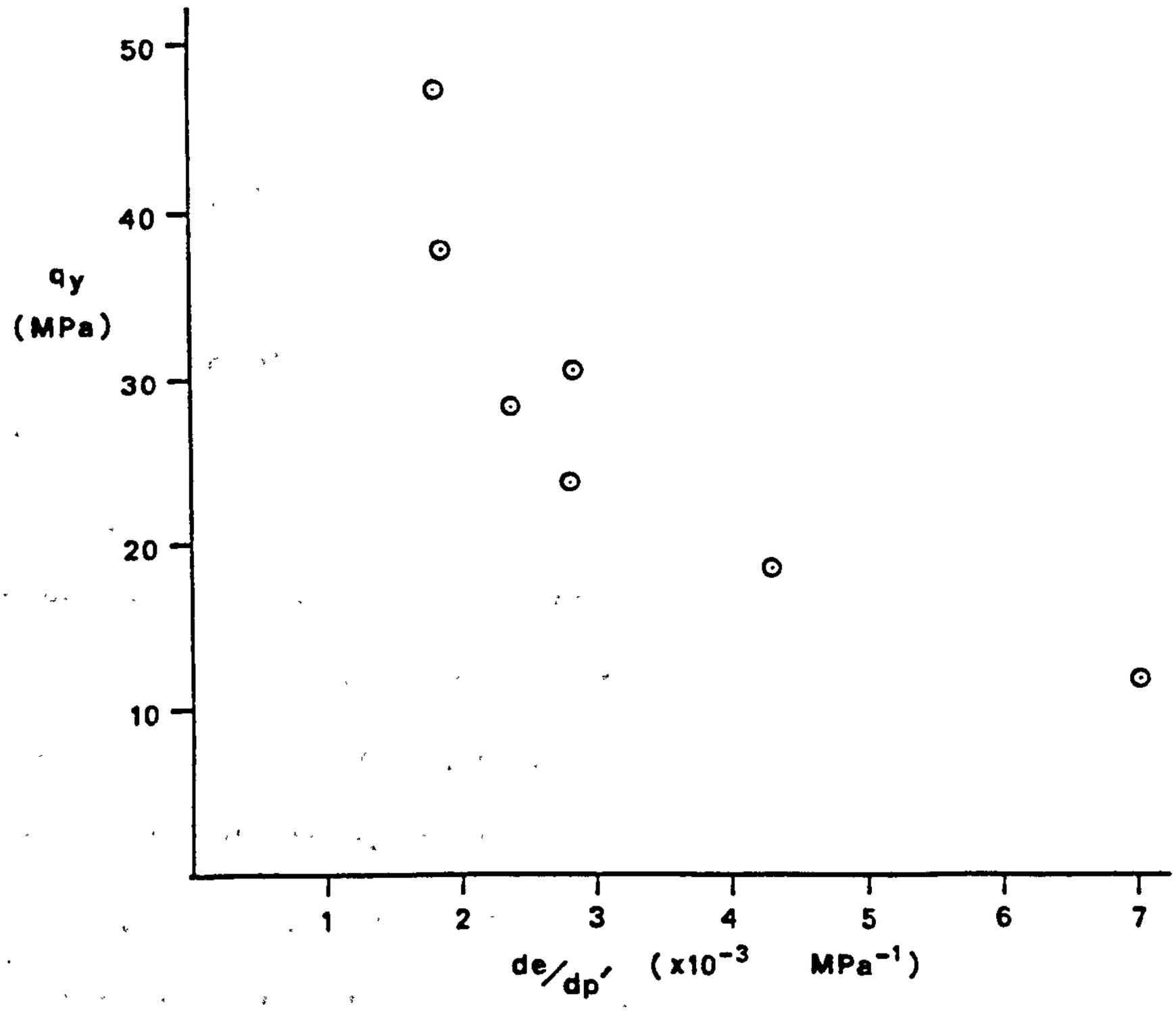

Figure 4.50 Variation of pore collapse deformation with yield point for K_o tests on Central North Sea chalks.

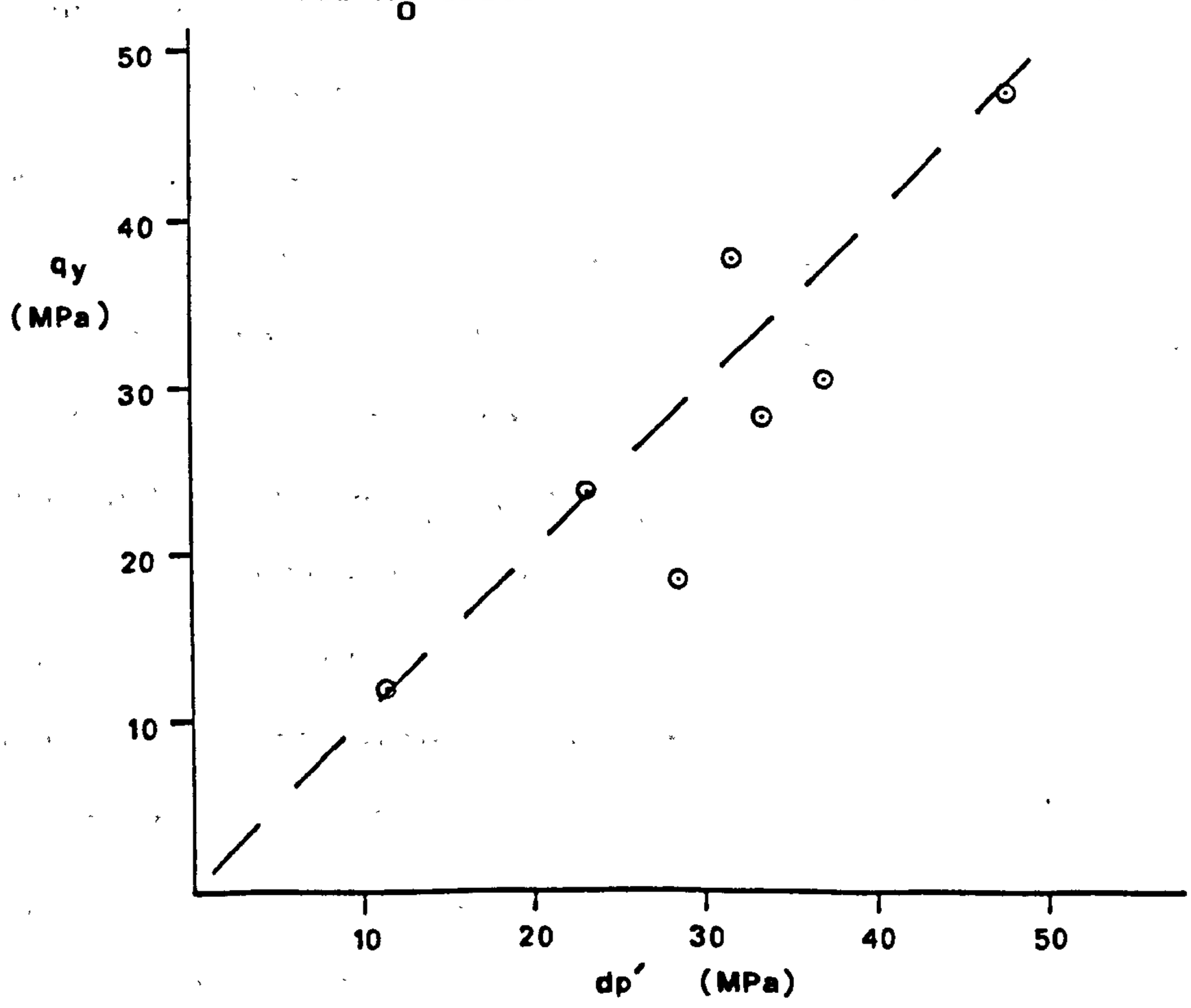

Figure 4.51 Variation of the size of the pore collapse deformation in q-p' space for Central North Sea chalks.

with higher K_o values the dp' is smaller, and the return to the normal consolidation surface is more abrupt. Hence, the trend observed in Fig.4.50 is probably less curved than indicated by the data.

The size of the transitional or pore collapse deformation will be dependent upon the yield point, as seen in Fig. 4.50; the higher the yield, the larger the de for this section. With this increase in de there will be an accompanying increase in dp'. This increase in dp' is a result of the elastic stress path ($\bar{K}_{oe}$) to yield being steeper than the $\bar{K}_{onc}$ stress path, so with increasing deviatoric stresses the paths diverge, increasing dp' with q. Evidence for this was sought, by plotting the size of dp' for the North Sea chalks against mean effective stress and deviatoric stress at yield, Fig. 4.51. An approximately 1:1 relationship is seen between the above mentioned quantities in both plots, with the deviatoric stress plot having slightly less scatter. On this plot the 45^o line plotted is not a best fit line - most of the variation lies beneath it. This could be attributed to the method of defining maximum effective stress at the start of normal consolidation, and hence, dp'. $\bar{\sigma}_{1nc}$' is taken as the first point on the linear $\bar{K}_{onc}$ line, if it were taken as the intersection of the $\bar{K}_{onc}$ and $\bar{K}_{opc}$ lines the dp' would be reduced.

Another difficulty in quantifying this pore collapse or transitional deformation was seen in Fig. 4.22b, where a higher consolidation pressure was used before loading. This resulted in a $\bar{K}_{opc}$ of zero, as deformation occurred at approximately constant q and p'. Thus in such a situation the deformation occurred at approximately constant q and proceeded at 90^o to the q-p' diagram. The consolidation pressures were kept as low as possible for the results presented above, though variation will inevitably lead to

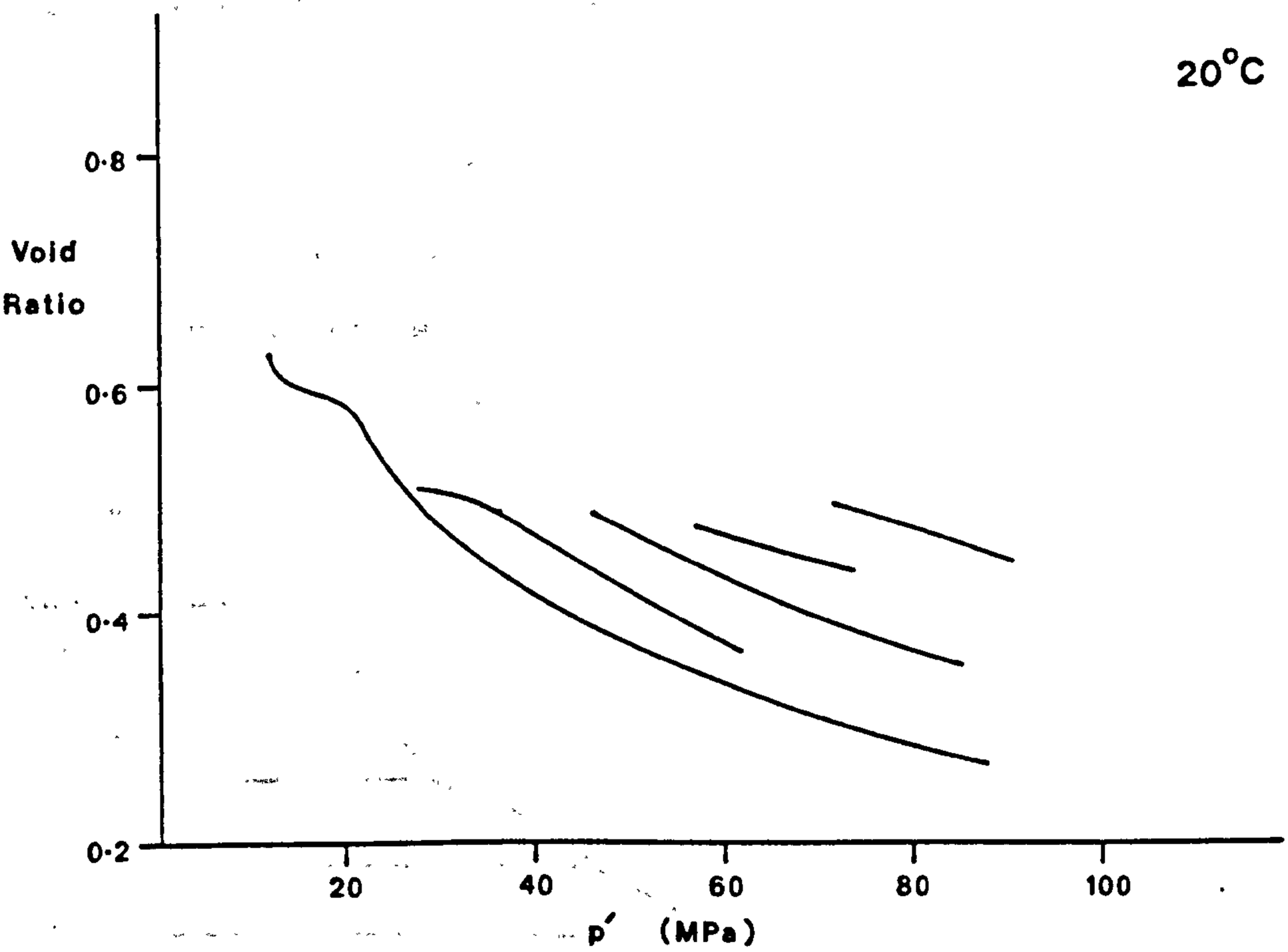

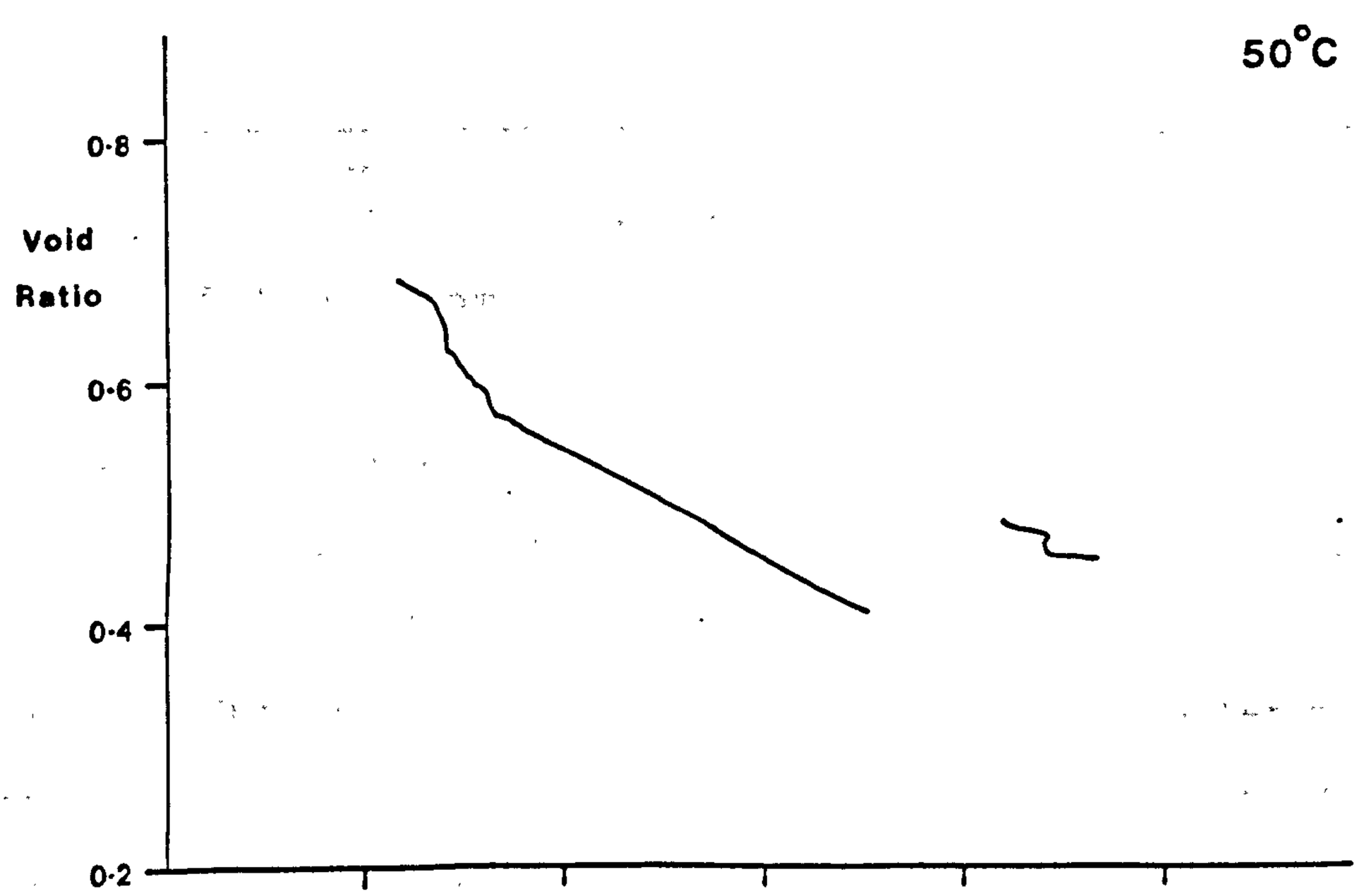

Figure 4.52 Trends of void ratio with mean effective stress for normally consolidated deformation of Central North Sea chalks.

some error in the values of dp' with a relatively smaller error for de. This increase in the consolidation pressure will obviously lead to an increase in the compressibility of the pore collapse deformation up to a point. The condition described above, where the pore collapse occurs with zero change in q or p', will result in the highest compressibilities for this region (Addis, 1987).

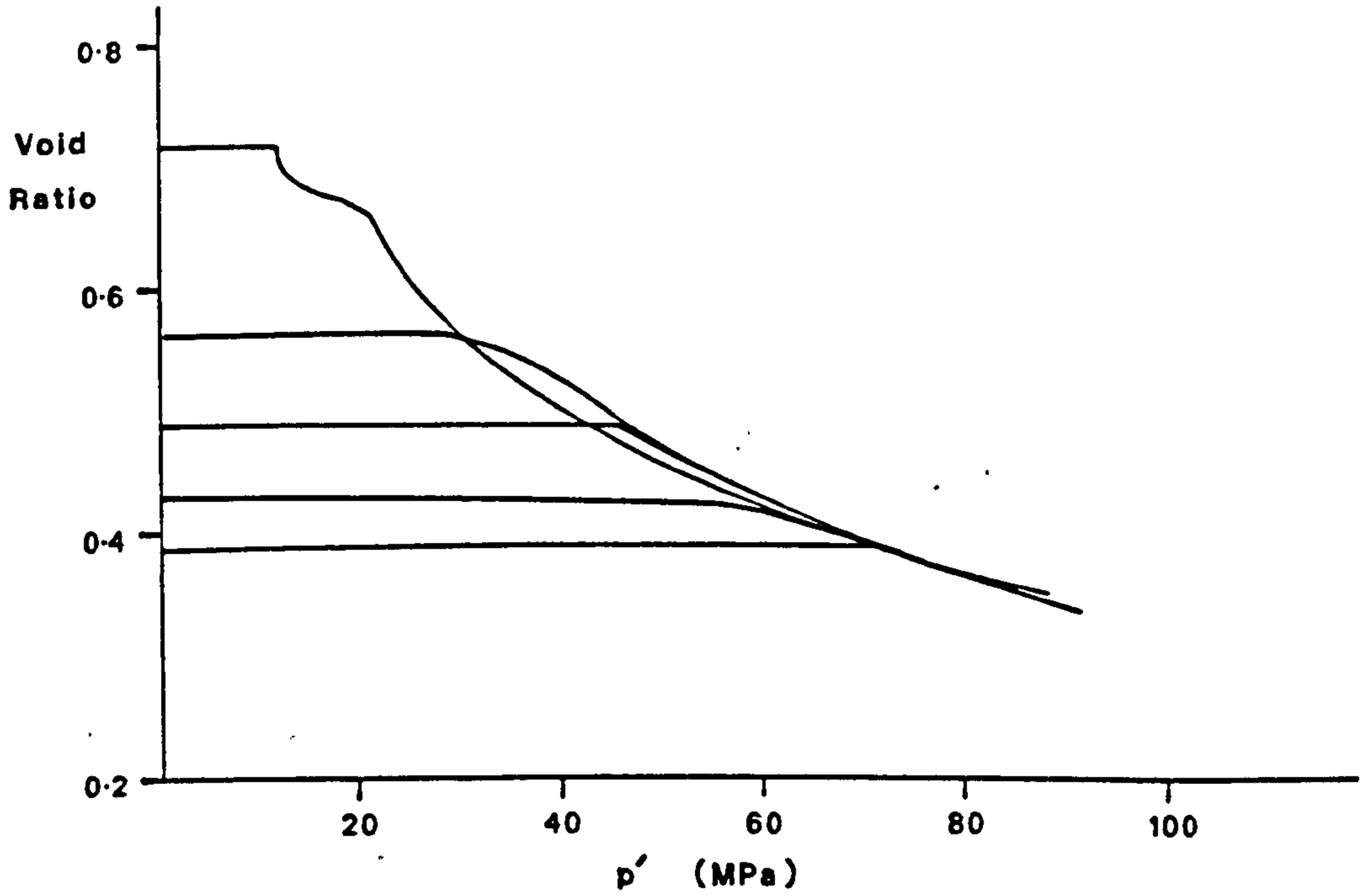

Figure 4.53 Shifted compaction curves for Central North Sea chalks.

The plastic surface of the normally consolidated sediment is shown in Fig. 4.52. As seen, the curves are offset, (presumably due to errors in porosity determination), and are shifted to a median value (van Ditzhuijen and de Waal, 1984) (Fig. 4.53). Whether or not there is one unique surface for the normal consolidation of the chalks of similar diagenesis has been discussed earlier. The compaction of a sediment along the Roscoe surface involves no particle degradation, thus for a single chalk the normal consolidation surface is envisaged to cut across a series of Roscoe surfaces of successively lower void ratio (for a particular q and

p'). With increasing stress the chalk compacts and degrades, so becoming displaced onto a lower void ratio plane due to the production of fine grained material.

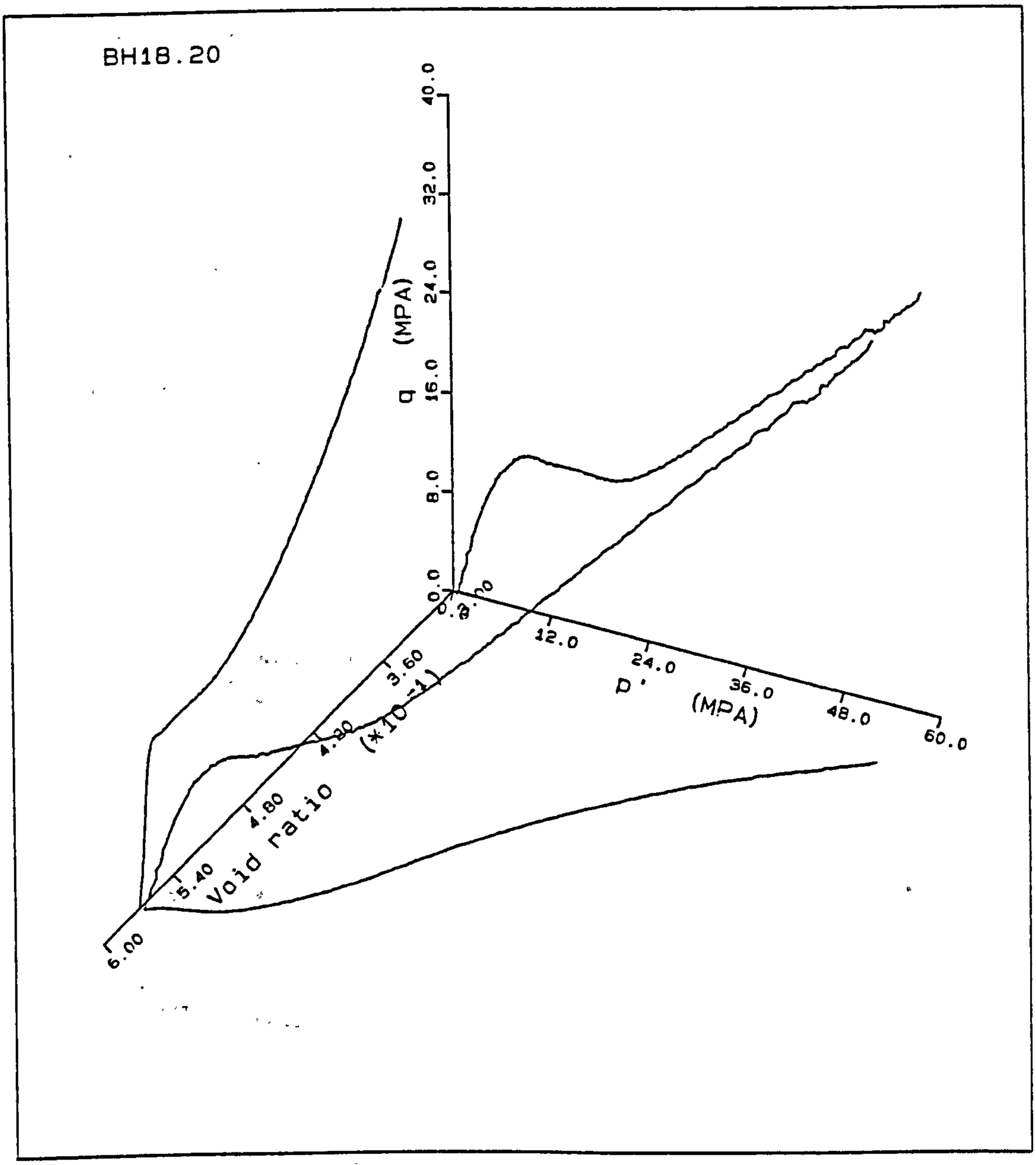

Figure 4.54 K_o stress path in q-p'-e space.

The complete K_o stress path for the chalk can be represented in q-p'-e space. Fig. 4.54 illustrates the results of BH18.20, which also shows the projection of the stress path onto the planes of the axes. This demonstrates the relationship between q-p', e-p' and e-q,

the latter being related to the axial strain by $dh/h_o = de/(1+e_o)$, where h_o and e_o are the initial sample height and void ratio, respectively. The relationship is also seen in the other K_o tests in this series, (with the exception of the earlier tests, where the volume measurement only occured over the post-yield measurement). The deformation shown in Fig. 4.54 is illustrated in Fig. 4.55, which superimposes the stress path onto the Critical State type diagram, including the plane of the elastic surface due to cementation (the yield envelope defining the boundary of this elastic surface). As stated earlier, the normal consolidation may not be restricted to one Roscoe surface, because the material degrades.

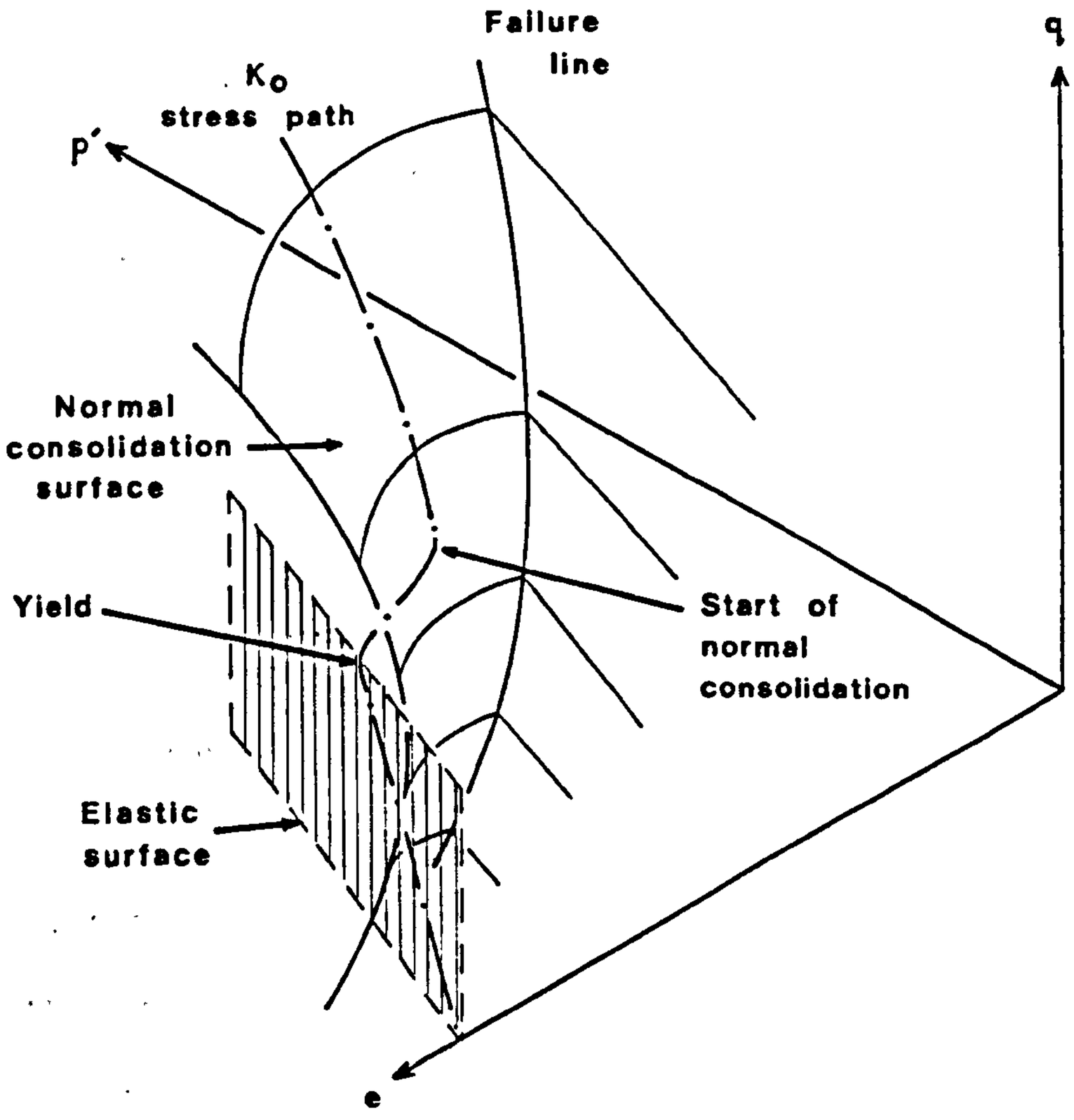

Figure 4.55 Diagrammatic K_o stress path for chalk.

The main conclusions of this chapter and of the experimental work on the chalks can be summarised as followed: -

1) The one-dimensional consolidation of chalk consists of three deformational styles, elastic, pore collapse and normal consolidation.

2) A general variation in the elastic properties of the chalk is seen with variations in initial porosity.

3) The stress-volume change characteristics of the pore collapse deformation are dependant upon the yield stress of the sample and indirectly on the porosity.

4) The normal consolidation deformation is not related to the initial porosity of the cemented sediment.

5) The yield and pore collapse in the chalk corresponds to a change in structure from a rock to a sediment, which exhibits normal consolidation.

6) The breakdown of cementation in chalks and the compaction of the disaggregated sediment is accompanied by grain crushing.

7) The consolidation of the chalks occurs at rates which are to fast to be easily observed in standard oedometer tests.

8) Constant rate of strain tests indicate that the coefficient of consolidation for chalks can initially be higher than $1000m^2/yr$.

9) Relationships between K_o and angles of internal friction were not obtained during these experiments, partly due to the presence of grain crushing.

10) The deformation of the chalks is seen to be strain rate dependant, though an exact strain rate dependance could not be concluded.

11) The shape of triaxial samples used in compaction experiments were observed to affect the resulting stress-strain curve.

12) The compaction of the chalks determined in this study was not temperature dependant to any significant extent.

13) Compaction curves in the normally consolidated range can be normalised to enable rationalisation of data, however, a similar process could not be applied to the pore collapse deformation.

14) The conversion from hydrostatic to uniaxial strain, which is widely used in reservoir engineering cannot be performed on the chalk except for the elastic deformation.

CHAPTER 5

DISCUSSION OF THE CLAY TESTS

5.1) INTRODUCTION

The previous chapter discussed the compaction of chalk, which can be regarded as a granular material with little time dependence involved in the dissipation of excess pore fluid pressure due to loading. This chapter will present and discuss the results of uniaxial (K_o) compaction experiments conducted on two clay samples (described in Chapter 3). The procedure for the preparation of the two clay samples is described in App. 4. These tests were performed to see if the shales overlying a chalk hydrocarbon reservoir could compact through underdrainage and thereby contribute to the overall magnitude of compaction in a draw-down situation.

The potential sources of error in this part of the study are large, due to drill disturbance in the well, and stress relief on recovery from the well (one of the core samples had developed a well-defined cleavage, presumably as a result of stress relief during recovery of the core from depth). Negative pore water pressures associated with the relatively undrained stress decrease (Bishop et.al., 1975), results in the infiltration of drilling muds into the samples. This is seen in the recovered core as a circumferential corona of lighter coloured clay. This will obviously affect the permeability and consolidation characteristics of the affected parts of the core. In addition, the cores had dried out subsequent to recovery and it was not possible to re-saturate them fully before

testing, so that full saturation was not achieved during the initial part of the tests. It is therefore suggested that the results of these clay tests be judged semi-quantitatively as far as the deformation parameters are concerned. The important point under investigation is the axial shortening possible for a certain effective stress increase.

The volume strains will not be considered because of the unsaturated state of the samples and because the samples contain oil-filled pore space, thus making porosity and specific gravity determinations difficult. The presence of large amounts of oil in the samples was seen when hydrogen peroxide (H_2O_2) was added to the samples (BS 1377). The H_2O_2 oxidises hydrocarbons to water and CO_2. Several additions of H_2O_2 were added to the sample, in amounts well above that recommended by BS 1377 for organic rich soil samples. However, with each addition of Hydrogen Peroxide the sample was seen to continue effervescing, showing the presence of organic material.

The two clay samples tested will now be discussed.

5.2) THE COMPACTION TEST ON SAMPLE NSC2.20

This was the first test performed on the clay samples. The sample was obtained from an approximate depth of 1200m. The initial minimum effective stress applied to the sample was high (6.9MPa) with a top pore pressure of 10.4MPa, and a back pressure of 2.9MPa. The loading of the sample caused only an initial rise in the deviatoric stress - axial strain plot, Fig.5.1a, the magnitude of the stress being less than 1.0MPa on average. The deviatoric stress increased from this level after an axial strain of 1.9%. This initial part of the deformation is seen in Fig.5.1d to have a very small radial strain component ($<10^{-2}$%) as compared with the rest of the deformation.

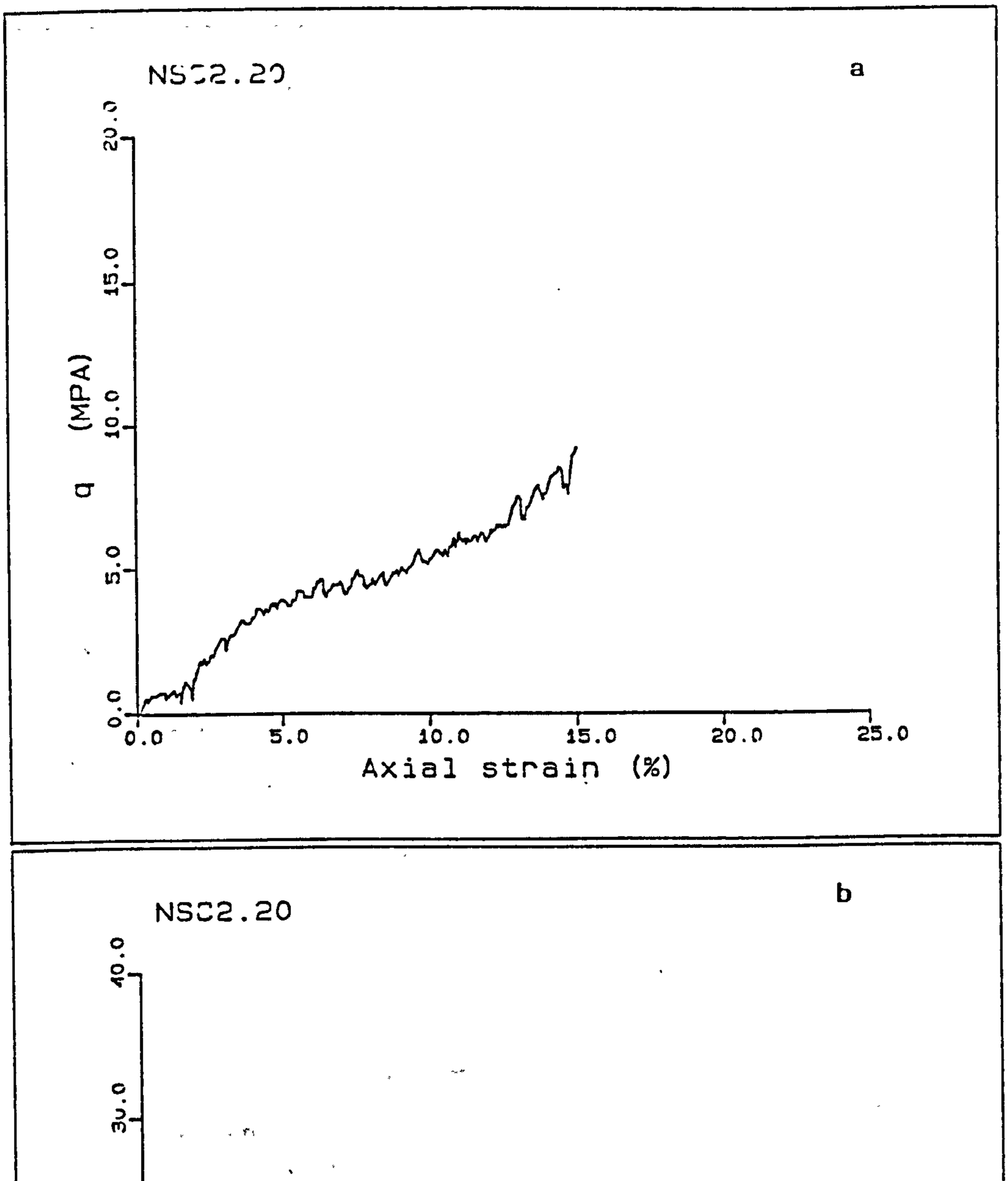

Figure 5.1(a-d) K_o test of North Sea clay NSC2.20.

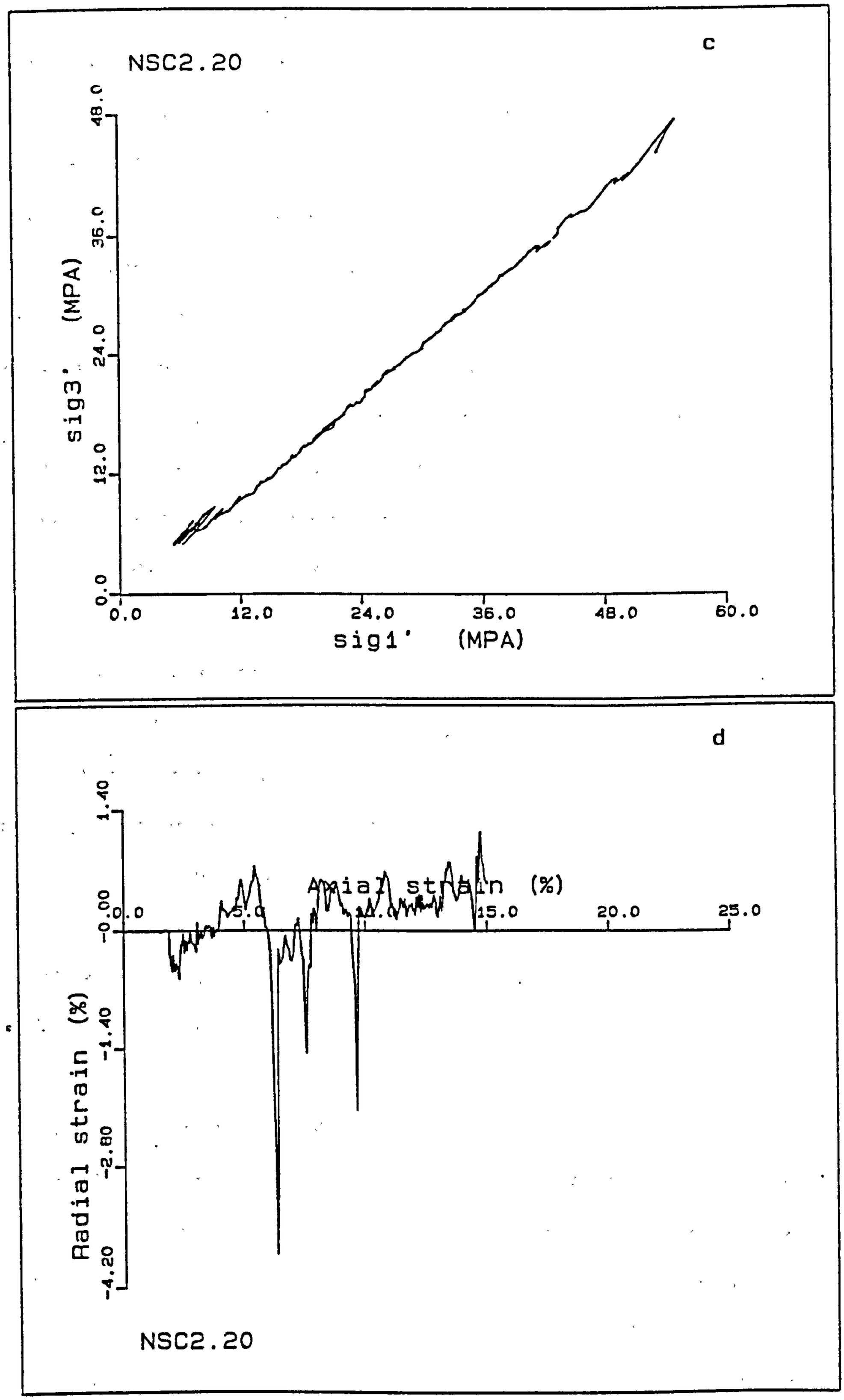
c
NSC2.20
sig3' (MPA)
48.0
36.0
24.0
12.0
0.0
0.0
12.0
24.0
36.0
48.0
60.0
sig1' (MPA)
d
Axial strain (%)
1.40
0.00
-1.40
-2.80
-4.20
0.0
5.0
10.0
15.0
20.0
25.0
Radial strain (%)
NSC2.20

After this initial 1.9% axial strain, the stress-strain characteristics of the sample show a high deformation modulus to approximately 5% axial strain, decreasing after this. The q and p' values for this 5% axial strain are 3.9 and 14.9MPa respectively. In q-p' space, the deformation consists of an initial steeply curved section followed by a reasonably shallow linear increase in deviatoric stress with mean effective stress, Fig.5.1b. The 3.9 and 14.9MPa stresses occur on the linear section of the plot. These stresses are probably an over-estimate of the in-situ stresses, as Fig.5.1a has a curved nature with no abrupt change. However, if the plot of maximum effective stress against minimum effective stress is analysed, a break in the slope of the plot is seen as shown by the intersection of the two $\bar{K}_o$ lines, which gives a value of maximum (vertical) effective stress of 13.7MPa. This corresponds to an axial strain of 3.7%. The initial $\bar{K}_o$ for the deformation is 0.70 up to a maximum (vertical) effective stress of 13.7MPa. The $\bar{K}_o$ then increases to 0.88, thereafter remaining reasonably constant. This value of 13.7MPa is taken as the preconsolidation pressure.

The apparent overconsolidation of the sample can be attributed to two possible factors,

i) stress relief subsequent to coring and sample recovery,

ii) the decrease in temperature existing in the sediment.

Both of the factors contribute to the observed overconsolidation effect, the stress relief probably having the larger affect on the sediment. The two above factors cause a relaxation of the sample, which upon subsequent reloading in the triaxial cell, shows an initial, predominantly elastic reaction to stress. The amount of plastic deformation, in the form of compaction, increases at the preconsolidation pressure. The change in the nature of the

deformation for the pre and post preconsolidation pressure stresses, can be observed in the plots of stress and strain and maximum versus minimum principle effective stress. In the latter plot, the $\bar{K}_o$ (the slope of this plot) is initially relatively shallow, indicating a stiff structure with little radial stress. In this sample part of this deformation is due to closure of cleavage planes. At stresses higher than the preconsolidation pressure, normal consolidation is continued along the virgin consolidation line on the Roscoe surface, Chapter 3, with accompanying larger horizontal stresses. The effects of temperature on sediments and the apparent overconsolidation caused by cooling of sediments, is discussed in Chapter 2.

The radial strains in this test are far larger than in the chalks, as seen in Fig.5.1d, generally staying below $\pm$ 1% radial strain, though occasionally exceeding this limit.

The pore pressure at the top of the sample at the start of the experiment, decreased to 6.0MPa at 2% axial strain, subsequently increasing to 14MPa with increasing axial strain. The coefficient of consolidation was calculated for 5MPa stress increments (for comparison with the chalk results, and assuming that water is the pore fluid). The assumption of water in the pore fluids, was due to the lack of knowledge concerning the viscosity and density of the oil present in the clay. The C_v was seen to decrease from $5m^2/Yr$ at 14.6MPa vertical effective stress, to less than 0.1 by 37.0MPa. Over the interval of 14.6MPa to 67.2MPa the volume compressibility decreases from $7.9*10^{-3}MPa^{-1}$ to $2.6*10^{-4}MPa^{-1}$. The permeability was seen to decrease from $1.1*10^{-3}mD$ to $2.6*10^{-6}mD$ for the same stress interval. The pore pressure difference across the sample divided by the vertical total stress, increases with deformation from 0.1468 to 0.2050, and as pointed out by Wissa et.al. (1971), is subject to

large errors when using constant rate of strain analyses, due to the deviation of linear from non-linear theory above values of 5%, Chapter 3.

5.3) THE COMPACTION TEST ON SAMPLE NSC3.20

This sample was obtained from a depth of approximately 1850m; it was a much better sample than NSC2.20 with less cleavage, but was much more difficult to cut, though the resultant sample was more uniform dimensionally than NSC2.20. The stress-strain plot, Fig.5.2a, shows an initial linear increase in deviatoric stress, with a decrease in modulus with increasing strain; the maximum curvature occurring at around 4% axial strain. The initial tangential modulus of this clay is 0.30GPa, the initial 0.3% axial strain has a low modulus, and is possibly a product of bedding errors in the sample. The preconsolidation effect is seen in the change in modulus in Figs.5.2a-c, as the sample moves from the over-consolidated to the normally consolidated deformations. Fig.5.2c, shows that the $\bar{K}_o$ is 0.24 at stresses below the preconsolidation pressure, increasing to 0.87 in the normal consolidation stress range; the intersection of these deformations occurs at a maximum (vertical) effective stress of 12.96MPa, this is taken as the preconsolidation pressure.

The low initial $\bar{K}_o$ obtained for this sample is seen to be reminiscent of the values obtained from the elastic reaction to loading, obtained for the chalks. The difference between the values obtained in this test and in the previous test (0.24 and 0.70 respectively) are possibly due to this sample having greater stiffness. An alternative explanation is the presence of a more disrupted structure in the previous sample, seen by the presence of cleavage, and possibly due to the higher initial stresses applied

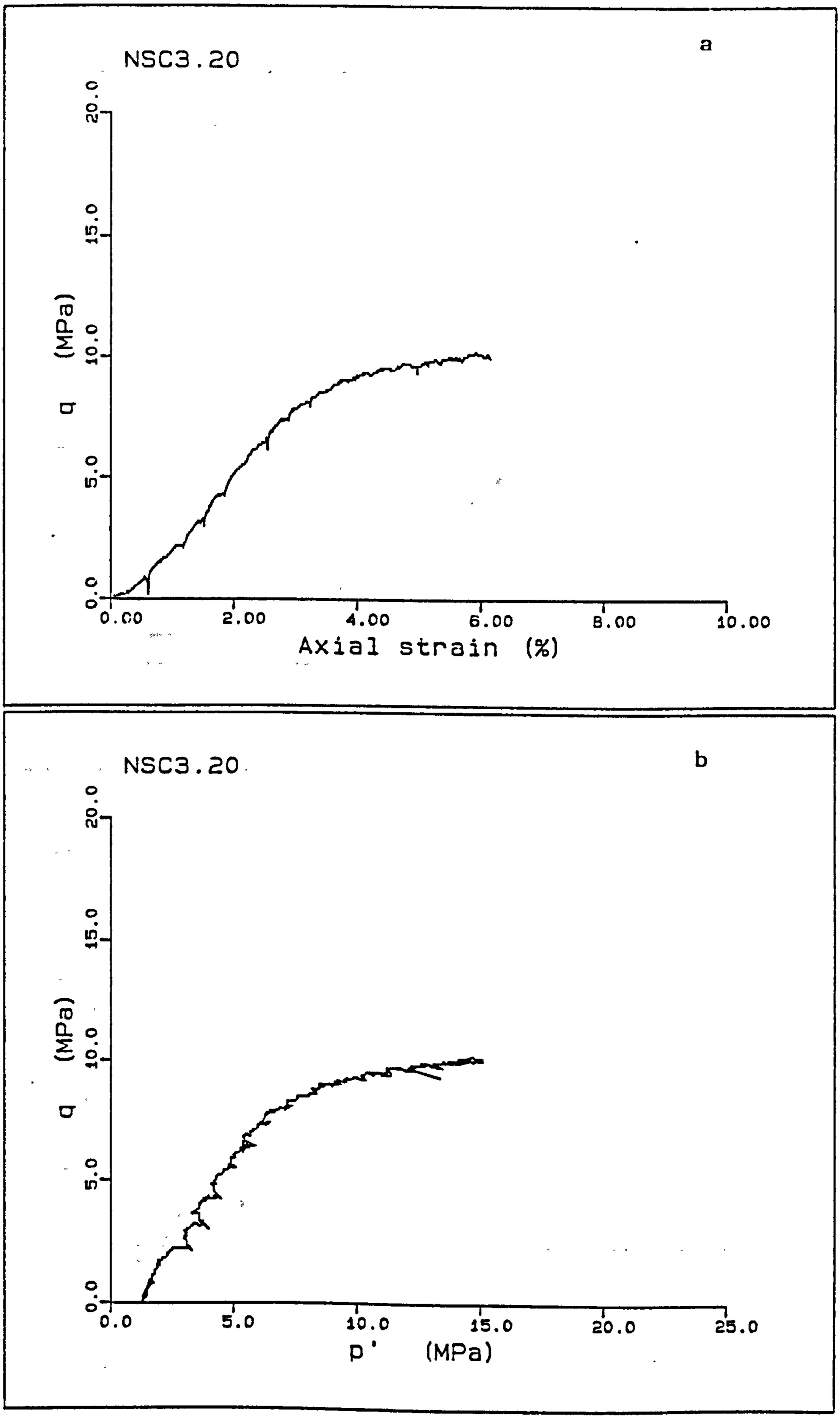

Figure 5.2(a-d) K_o test of North Sea clay NSC3.20.

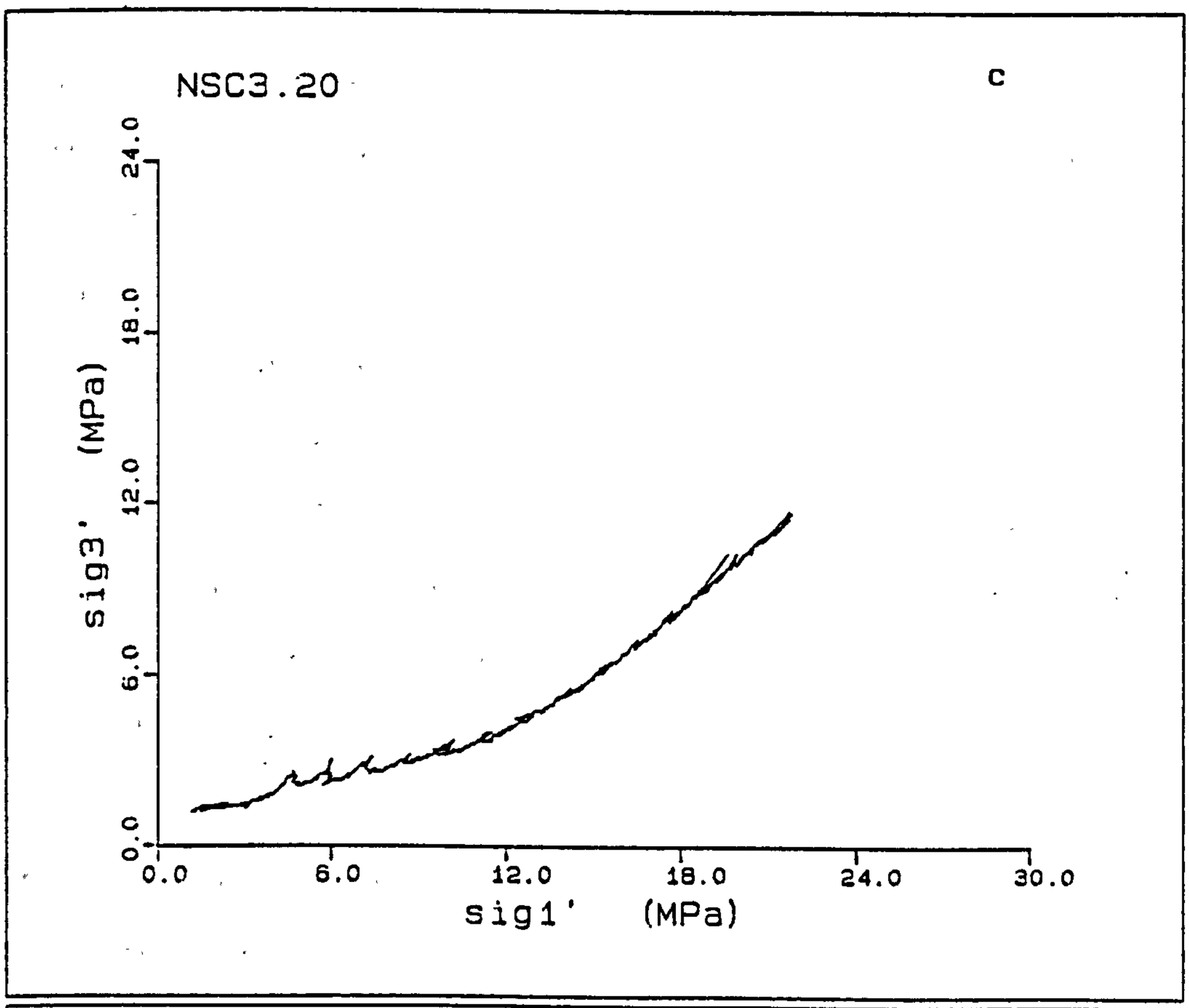
NSC3.20
c
sig3' (MPa)
0.0
6.0
12.0
18.0
24.0
0.0
6.0
12.0
18.0
24.0
30.0
sig1' (MPa)

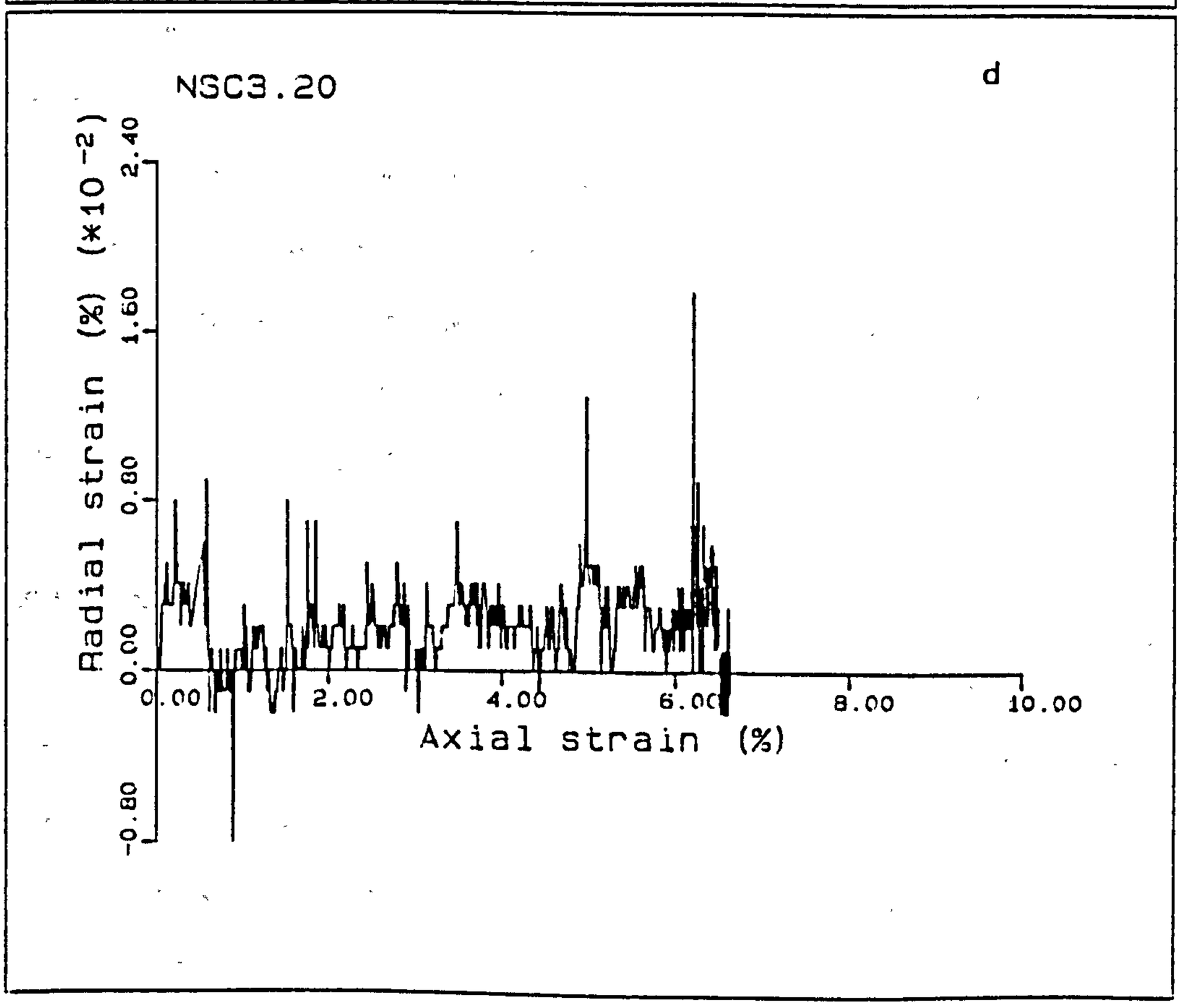
NSC3.20
d
strain (%) (*10-2)
2.40
1.60
0.80
0.00
-0.80
Radial
0.00
2.00
4.00
6.00
8.00
10.00
Axial strain (%)

during the experiment. However, no firm conclusions on this matter have been formulated.

The pore pressures started at zero, reaching 3.2MPa at 5.5% axial strain (this is equivalent to the loading on the back pressure regulator). There was a lag in the top pore pressure response (0.2MPa) at this axial strain. Once the pore pressures had reached this level, the loading rate was decreased but the pore pressures still continued to rise. The pore pressure rise was seen to be affected by the diurnal temperature changes in the laboratory. The test was stopped as the deformation rate was far to slow ($1*10^{-4}$ and subsequently $5*10^{-5}$mm/min), for the test to be of any further use in a reasonable time scale, the experiment already having run for 672 hours, since loading had started.

The radial strain during this experiment was much improved from NSC2.20, the recorded radial strain generally being less than $\pm 10^{-2}$%. The test was run under partially saturated conditions and thus the effective stresses may be erroneous. This lack of saturation could not be avoided at the time of this experiment, App.1. However, saturation of a sample is now possible, due to the addition of a volume gauge to the equipment which can supply high back pressures to ensure dissolution of air in the samples (Bishop and Henkel, 1962; Chaney, Stevens and Sheth, 1979).

5.4) DISCUSSION

Both uniaxial (K_o) experiments presented above show that considerable deformation of clays such as those tested in this study could occur if the clay is subjected to a draw-down situation. The first experiment NSC2.20, shortened vertically by 15% at a vertical effective stress of 53.3MPa, while NSC3.20 showed a similar

shortening of 6.6% axial strain at a vertical effective stress of 21.8MPa. If the strains in the overconsolidated range are subtracted (due to the strain accompanying the stress relief during core recovery), the respective strains are 11.2 and 3.4%, both strains to preconsolidation pressure being between 3-4%. The tests showed reasonable agreement on the preconsolidation pressure, despite NSC3.20 being sampled from approximately 650m deeper than NSC2.20. This can be explained by the over-pressures present in the clays in the Central North Sea, Byrd (1975), Chap. 3. The deformations at stresses in excess of in-situ pressures are seen to be similar, with $\overline{K}_o$ values of 0.88 and 0.87 respectively for NSC2.20 and NSC3.20.

The C_vs obtained from NSC2.20 despite being approximations, show that the pore fluid pressure dissipation is slow and the amount of compaction in a draw-down situation may be relatively small because of the low permeabilities. Thus, the clay could not contribute a great deal to the total reservoir compaction in the normal lifetime of an oil field, unless there are drainage boundaries within the clays, such as sandstone or siltstone lenses, or, a well developed joint pattern, which remains in pressure communication with the reservoir. These discontinuities must enable the clay to be subjected to the pressure draw-down, and thus must be continuous in their nature if they are to act as a drainage boundary for clay consolidation.

Many analogous examples of underdrainage due to fluid withdrawal from ground water aquifers at low stress levels, have been reported in the literature (AIHS, 1969; AIHS, 1976). One of the earliest and probably the most relevant case for this study, is the reduction in the pore water pressure in the chalk aquifer in the London Basin. The compaction of the overlying clays were calculated and showed

reasonable agreement with field determinations of subsidence. The calculation of the clay compaction for this example assumed one drainage boundary, the chalk aquifer, with no drainage effect due to joint systems, Wilson and Grace (1942), Chap. 6.2.3.

CHAPTER 6

HYDROCARBON RESERVOIR COMPACTION AND ASSOCIATED GROUND SUBSIDENCE

6.1) INTRODUCTION

During the production of an oil field, the removal of hydrocarbons can lead to a decrease in the pore fluid pressure. This will result in an increase in the effective stress acting through the rock due to a transference of load from the pore fluid to the mineral skeleton (Chap. 2). The response of the rock to this increase in effective stress can be in two main forms: by compaction of the porous matrix or by shearing of fractures and joints. If the reservoir rock reduces in bulk volume, the process is referred to as reservoir compaction. The reservoir is generally buried beneath a pile of more recent sediments up to several kilometers thick. The volume reduction in an oil field as a result of fluid draw-down can be transfered through the overburden to produce a permanent deformation at the surface (van der Knaap and van der Vlis, 1967). The ratio of land surface subsidence to reservoir compaction (the transfer ratio) is usually less than unity, though in some cases, ratios larger than one have been recorded, generally for short time intervals (Geertsma, 1973; Principia Mechanica, 1986). Shear displacements of joints present in reservoir material may occur in response to a reduction in the pore fluid pressure; its contribution towards reservoir compaction has rarely been assessed, one example is the recent study by the Norwegian Geotechnical Institute (Barton et.al., 1986) of the effect of fractured chalks on the subsidence in the Ekofisk area,

this will not be discussed here.

This chapter will review theoretical and experimental approaches to assess reservoir compaction and the associated subsidence, it will also compare some of the parameters involved with reservoir compaction published in the literature with the results obtained from this study. A brief literature review of the recorded cases of oil field subsidence is also presented.

6.2) HYDROCARBON RESERVOIR COMPACTION

Reservoir compaction resulting from hydrocarbon production has been observed since the beginning of this century. However, serious assessment of the phenomenon with the prediction of the amount of compaction possible only started in the late 1950's. Reservoir compaction is a vertical shortening of a reservoir rock column, due to the increase in effective stress. This is normally considered to be a deformation of the rock matrix. The vertical shortening, or volume reduction of the rock matrix, associated with the increase in effective stress, or pore fluid pressure decrease, have been suggested to be the result of three kinds of deformation:

1) Rock matrix compressibility (C_r).

$$C_r = \frac{1}{V_r}\left(\frac{dV_r}{dU}\right)_{\bar{\sigma}-U,T} \qquad .. 6.2.1$$

2) Rock bulk compressibility (C_b).

$$C_b = \frac{-1}{V_b}\left(\frac{dV_b}{d\bar{\sigma}}\right)_{U,T} \qquad .. 6.2.2$$

3) Pore compressibility (C_f).

$$C_f = \frac{1}{V_p}\left(\frac{dV_p}{dU}\right)_{\sigma,T} \qquad .. 6.2.3$$

In these equations the subscripts r,b and p refer to rock matrix, bulk and pore respectively. σ = average external (total) stress, U = pore fluid pressure, T = temperature and V = volume.

The bulk compressibilities and the pore volume compressibilities are presented as shown (Eqns. 6.2.1 - 6.2.3) by Scorer and Miller (1974), but these quantities can be measured as functions of external stress at constant pore pressure or vice versa.

Two approaches seem to have been dominant in the prediction of oil reservoir compaction, the theoretical and the semi-empirical or empirical approach. The theoretical approach involves the analysis of the deformation of a unit of reservoir material, and relates the analysis to parameters measurable in the laboratory. The second approach is to determine the vertical strain resulting from a particular pore pressure decline. Both methods are simplifications, and as such, include various assumptions, and unknown parameters.

6.2.1) Theoretical approach to reservoir compaction

The theoretical approach was initiated by Geertsma (1957) (though earlier works exist on theoretical sediment compaction, see Geertsma (1957) and de Witte and Warren (1957)) when he analysed the effects of pore pressures and total stresses on the three deformations described above. In the derivation of expressions for pore and bulk volume deformations, Geertsma states that the

hydrostatic stress drives the volume change in the rock as opposed to the deviatoric component (Chap. 4). The analysis is based on elastic theory and assumes that Terzaghi's law of effective stress holds (de Witte and Warren, 1957). The expression obtained for bulk volume change (dV_b) is,

$$\frac{dV_b}{V_b} = -(C_b - C_r)dU + C_b.d\sigma \qquad .. 6.2.4$$

and for pore volume (V_p) change,

$$\frac{dV_p}{V_p} = \frac{-1}{f}(C_b-(1+f)C_r)dU + \frac{1}{f}(C_b-C_r)d\sigma \qquad .. 6.2.5$$

where U = pore pressure; σ = total mean stress and f = the fractional porosity. The strain in one direction "i" as a result of the volume reduction is expressed as

$$\frac{dL_i}{L_i} = \frac{-1}{3}(C_b-C_r)dU + \frac{d\sigma_1 - d\sigma}{2G_b} + \frac{1}{3}C_b.d\sigma \qquad .. 6.2.6$$

G_b = rock bulk shear modulus.

The above equations are for the elastic deformations only, considering plastic deformations, viscous parameters E_b and E_r are substituted for elastic constants in the analysis.

$$\frac{dV_b}{V_b} = -(\frac{1}{E_b} - \frac{1}{E_r})dU + \frac{1}{E_b}d\sigma \qquad .. 6.2.7$$

$$\frac{dV_p}{V_p} = -\frac{1}{f}\left(1 - \frac{1+f}{E_r}\right)dU + \frac{1}{f}\left(\frac{1}{E_b} - \frac{1}{E_r}\right)d\sigma \qquad .. 6.2.8$$

The equivalent equation for strain in one direction due to viscous deformations being

$$\frac{dL_i}{L_i} = -\frac{1}{3}\left(\frac{1}{E_b} - \frac{1}{E_r}\right)dU + \frac{d\sigma_i - d\sigma}{2\mu_b} + \frac{d\sigma}{3E_b} \qquad .. 6.2.9$$

In Eqn. 6.2.9 μ_b = rock bulk shear viscosity.

These are time-derivative equations (Brighenti, 1967), due to the viscous nature of the deformations. Most reservoir rocks undergo deformations which have elastic and viscous components; it is difficult to assign relative amounts of these deformations, hence for applications to real cases approximations must be built into the model. The experimental procedures for obtaining the viscous deformation constants are not described by Geertsma.

The applicability of such the approach used by Geertsma (1957) is obviously restricted to isotropic materials with a low viscous deformation, such as sandstones. As a result of this work, values of pore volume compressibility and bulk compressibility have been obtained for various sandstones (Fatt, 1957; Marek, 1971; Newman, 1973; Scorer and Miller, 1974); most workers follow Geertsma in the assumption that the rock matrix compressibility is negligible.

i) Conversion of hydrostatic strain data to uniaxial strains

Due to the stringent conditions required to perform tests representative of the deformation of reservoir materials during production, i.e. K_o testing, the general consensus has been to test

rock compressilbility in a hydrostatic stress system, and convert the results into a uniaxial strain (zero lateral strain , or K_o) condition (Geertsma, 1957; Teeuw, 1971; 1973; van Ditzhuijen and de Waal, 1984).

Following the earlier analysis of the pore volume reduction in granular materials presented above (Eqns. 6.2.1 to 6.2.9), the effect of pore volume reduction on specific lithologies were examined by Geertsma (1957). Certain assumptions were made concerning the compressibilities of the lithological types, to enable a reduction of the parameters needed to assess the volume reduction of the rock. The most straight-forward case is that of a high porosity sandstone where

$$\frac{dV_p}{V_p} \approx \frac{C_b}{f} (d\sigma - dU) \qquad .. 6.2.10$$

this assumes that $C_b > C_r$. For the case of constant hydrostatic stress, $d\sigma = 0$ which, from the above relationship, gives a volume change

$$\frac{dV_p}{V_p} \approx \frac{-C_b}{f} dU \qquad .. 6.2.11$$

The boundary condition for uniaxial shortening leads to $d\sigma = 2/3\ d\sigma$, where $d\sigma$ is the change in stress in the minor principle direction; this gives a change in average stress

$$d\sigma = \frac{C_b + 1/pE_b - C_r}{(C_b + 1/pE_b) + 3/4(1/G_b + 1/p\mu_b)} .dU \qquad .. 6.2.12$$

which for a sandstone (assuming a Poisson's number of 5) gives a uniaxial volume change

$$\frac{dV_p}{V_p} \approx \frac{-1}{2} \frac{C_b}{f} dU \qquad .. 6.2.13$$

This shows that the ratio between hydrostatic and uniaxial volume changes (Eqn. 6.2.11 and 6.2.13) for a sandstone is equal to approximately 2, Sawabini et.al. (1974). Approximations for limestones and shales are given but are not calculated as C_b, U_b, and pE_b are required.

This work was superceeded by the work of Teeuw (1971) who outlined a procedure for the hydrostatic to uniaxial strain conversion, based on previous experimental evidence. The approach, was to use a non-linear case of elasticity, obtained from volumetric strains of hydrostatic tests (Geertsma, 1957). The elastic constants are assumed to be of the form

$$\frac{d\sigma}{d\varepsilon} = E = b.\sigma_e^{\ q} \qquad .. 6.2.14$$

where σ_e is an isotropic stress, b and q being material constants. Using these constants with a constant Poisson's ratio, the translation from hydrostatic (isotropic) strain to uniaxial strain can be found. The non-linear relationship of Young's modulus to the stress level, for E_y and E_z was introduced into

$$d\varepsilon_x = \frac{d\sigma_x}{E_x} - \frac{\nu d\sigma_y}{E_y} - \frac{\nu d\sigma_z}{E_z} \qquad .. 6.2.15$$

to obtain an expression relating the vertical and horizontal strains. On applying the boundary conditions for the uniaxial case, the vertical strain is given by

$$\varepsilon_z = \frac{(1+\nu)(1-2\nu)}{b(1-\nu)(1-q)} (\sigma_z)^{1-q} \qquad .. 6.2.16$$

Similarly for hydrostatic loading, the strain is given by

$$\varepsilon = \frac{(1-2\nu).(\sigma_e)^{1-q}}{b(1-q)} \qquad .. 6.2.17$$

where ε is the strain in any principle stress direction. The 3-dimensional volumetric strain (e) is assumed to be three times this (Lachance and Anderson, 1983). Hence, by equating the two relationships, the vertical shortening is given by

$$\varepsilon_z = \frac{1}{3} \frac{(1+\nu)}{(1-\nu)} e \qquad .. 6.2.18$$

where the multiplier of e is equal to alpha of Anderson (1985). If a Poisson's ratio of 0.3 is taken as an average value, the ratio between hydrostatic and uniaxial strain is 1.6 which is close to Geertsma's approximation of 2. A correction was made to this equation to account for rock grain compressibility relative to rock matrix compressibility (β) (Geertsma, 1973), the equation being of the form for compressibilities rather than for strains.

$$C_m = \frac{1}{3}\frac{(1+\nu)}{(1-\nu)}.(1-\beta)C_b \qquad .. 6.2.19$$

Brighenti (1967) and Sawabini et.al (1974) have presented evidence for the ratio of C_b/C_m being equal to approximately 2.

One result of this analysis was considered by Teeuw (1971); a volumetric relationship of the same form as Eqn. 6.2.14 is observed (Scorer and Miller, 1974; Anderson, 1985).

$$e = a\sigma_e^{\ n} \qquad .. 6.2.20$$

where n = 1-q for the last analysis. Substituting this into an equation for horizontal stress at zero lateral strain and integrating over stress 0 to σ_z the following relationship is derived,

$$\frac{\sigma_h}{\sigma_v} = \frac{\nu}{1-\nu}^{1/n} \qquad .. 6.2.21$$

where n = 2/3 for perfect spherical packing and 1 for linear elasticity, Teeuw (1971). This equation was presented in Chapter 3.2.2.

The main critisism of this approach is that when substituting Eqn. 6.2.14 into 6.2.15 to develop the analysis, the same values of b and q are used for Young's modulus in the vertical and horizontal directions, hence this approach only holds for an isotropic homogeneous material. Also, for strain in the vertical and horizontal direction, the same Poisson's ratio is used and, more seriously, is assumed constant (Scorer and Miller, 1974). Kumar (1976), presents evidence for the change of Poisson's ratio with stress level. This

would occur with most rocks, to some degree, if the particles are irregular, as the degree of anisotropy increases with vertical effective stress; this increase in anisotropy would not be recognised in hydrostatic tests (Chierici et.al., 1967).

The experiments performed by Teeuw (1971; 1973) show good agreement between uniaxial and converted hydrostatic tests. Lachance and Anderson (1983) measured differences in compressibilities of 0.35 less in uniaxial tests in comparison to hydrostatic tests; however a Teeuw type analysis gave a difference of 0.54 (Nugget sandstone being employed in the tests). The Lachance and Anderson analysis may be erroneous in its application of stresses, as the value of n required for their "Teeuw type" analysis was obtained by a different method than that used by Teeuw (1971). The above experiments were performed on sandstones (Teeuw also worked on limestones and steel beads). Good agreement between predicted and measured strains was obtained by Teeuw from sandstone samples which had been previously loaded, and Teeuw stated that "deformations only appeared to be elastic after the first cycle".

Anderson (1985) related the hydrostatic volume change to uniaxial volume change for consolidated sandstones. The comparison with uniaxial tests was good, though the results deviated at higher stresses. The equation used in the analysis was of the same form as that derived by Teeuw (1971). When considering bulk strains, the values of a and n (Eqn. 6.2.20) obtained were different to those for volume strain, the differences in Poisson's ratio being 0.22 and 0.38 for the bulk volume strain and pore volume strain respectively. The conversion factors (alpha = $(1+\nu)/3(1-\nu)$) between hydrostatic and uniaxial strain were 0.52 and 0.74 for bulk volume and pore volume determinations respectively. The non-applicability of this analysis

to friable unconsolidated sandstones was noted, as was the fact that repeated loading was necessary to obtain consistant results.

The conversion of hydrostatic to uniaxial strain after Teeuw (1971) has been performed on Ekofisk chalks by Johnson and Rhett (1986). They convert the initial elastic section of the deformation using a Poisson's ratio of 0.3 in Eqn. 6.2.15. The post-yield deformation are considered equal for hydrostatic and uniaxial tests. The full stress-strain curve was constructed by joining the converted hydrostatic data in the elastic region to the unconverted hydrostatic data in the post-yield region. This has been shown to be incorrect (Chap. 4.2 and 4.6; Smits et.al., 1986). The converted hydrostatic data and the uniaxial data in the elastic deformation gives the same kind of trend (Fig. 4.35) but the assumption that the strains in the post-yield deformation are coincident goes against the extensive evidence presented in soil mechanics literature. This statement by Johnson and Rhett, although qualified by the authors as only applicable to Ekofisk chalks, implies that the stress system acting on the sample has no effect on the volume strains. Thus they imply that the only control on volume change is the maximum effective stress, i.e. the "Rutledge hypothesis" is valid (Lee and Farhoomand, 1967). This is not the case with sediments and does not occur in the chalks from the Ekofisk area (Chap. 3) tested in this study.

ii) Empirical approaches of reservoir compaction

Another method of predicting reservoir compaction can be described as the empirical approach. This has been used in relation to carbonate reservoirs though only a few studies have been performed (Jones et.al., 1985a; 1985b; 1986; Leddra et.al., 1987; van Kooten 1985; van Ditzhuijen and de Waal, 1984; Smits et.al., 1986). In such

studies uniaxial compaction tests are performed on samples of reservoir material, whereupon, the resulting stress-strain curves are analysed to compute total strain for a particular increase in effective stress predicted for the reservoir. The strain can be calculated from axial strain (Jones et.al., 1985a) or from volumetric strain. The stress-strain curves used by Jones et.al. were determined from the results of uniaxial tests of the reservoir material. The experimental data is generalised into stress-strain curves for differing porosity bands in the reservoir, in which the strains are normalised to the effective stresses at the start of hydrocarbon production. The trendline concept is a another empirical method, using volumetric strains (van Kooten, 1986; van Ditzhuijen and de Waal, 1984; Smits et.al., 1986); it is based on the assumption, mentioned in Chapter 4, that the volumetric deformations are unique in the post-yield stress range. Thus units of sediment from similar strata will have the same compactional trend, the high porosity material yielding and deforming along this trend at lower stresses than the lower porosity material. The construction of a trendline has been performed on the North Sea chalk samples tested in this study in Fig. 4.11. The application of the concept assumes that the chalks will deform with the same $\bar{K}_o$ values for the normal consolidation compactions, otherwise larger mean stresses will be experienced by different porosity samples; it also assumes that the cementation does not affect the post-yield compaction of the sediments. The trendline approach as used in reservoir engineering, is analogous to the use of e - log p' plots in soil mechanics, and more cumbersome to use.

From the results presented in App. 5 and Chap. 4 the post-yield deformation of chalk consists of two deformational trends, and not

one, as stated by Smits et.al. (1986), these deformations having different $\bar{K}_o$ values. Thus, at a particular vertical effective stress in this post-yield deformation, samples of differing initial porosities at the same vertical effective stress, will require differing stress systems to maintain a condition of zero lateral strain. As such, there will be different volume strains developing within the reservoir for materials of different porosities. This observation arises from the fact that post-yield volume changes in sediments result not only from an increase in the mean effective stress but also depends on the relative magnitudes of the principle effective stresses (Chap. 2). In Chap. 4 it was shown that in chalks, particle crushing constitutes an important part of the deformational style in the post-yield deformation; thus, one unique trend or Roscoe surface would not be expected. However, with a problem such as analysis of reservoir compaction, the system is so complex, that the errors associated with laboratory testing are probably purely academic and of little significance, when compared with the errors associated with specifying the reservoir model and its boundary conditions. The errors involved with laboratory testing are due to,

a) the small number of samples tested per volume of reservoir material, and

b) the transfer of the compaction to the surface which is a large variable when considering surface subsidence.

Thus, although not strictly justified, the trendline concept is a simple analytical model, and any errors associated with it are probably well within the limits of accuracy of the rest of such a study.

This empirical approach is best suited to oil fields with lithologies undergoing a large plastic deformation (a post-yield

component of deformation), or containing a strong anisotropy. During pre-yield compaction, volumetric strains are small. Van Ditzhuijen and de Waal (1984) analysed the strain for specific stress levels by performing hydrostatic tests and converting the deformations to a uniaxial strain, using the method described by Teeuw (1971). This type of analysis was also performed in this study (Fig. 4.35), and shown to give reasonable agreement between converted hydrostatic and uniaxial data within the elastic range. For Chalks from the Ekofisk area, van Kooten analysed the compaction in terms of the uniaxial compressibilities for the pre-yield region. This seems more justified in terms of simplicity and in terms of the assumptions required for hydrostatic test conversion. Jones' analyses (1985a; 1985b; 1986) does not separate the pre- and post-yield deformations, and thus does not require these latter methods.

Because of the difficulties in applying the analytical approach of Geertsma (1957), the lack of correspondence between field examples (Mess, 1978) and the linear predictions of subsidence based on some earlier studies of reservoir compaction, an alternative method for analysis of compaction in reservoirs has been formulated. This is an approach which takes account of the effect of loading (strain) rate on compaction (Chap. 2). Due to the increased compressibility at slower loading rates, reservoir materials have been analysed as rate-type materials; this has lead to the formulation of a 'Rate-Type Compaction Model' (RTCM) (de Waal, 1986; Smits and de Waal, 1985).

For experiments incorporating variable loading rates, an expression for strain shifts ($\Delta\sigma_z'$) (the shift in the stress-strain curves for a material with loading or strain rate), as a function of the stress level (σ_z') and change in loading rates ($\dot{\sigma}_z'$), is obtained. This is the same expression derived by Mesri and Choi (1979).

$$\Delta\sigma_z' = \sigma_{z,1}' \left(\frac{\dot{\sigma}_{z,2}'}{\dot{\sigma}_{z,1}'}^{b} - 1 \right) \qquad .. 6.2.22$$

where b is a material constant (the C_α/C_c value of Mesri and Godlewski, 1977; Mesri and Choi, 1979; and Mesri and Feng, 1986) (Chap. 2.7). The model analyses a non-linear compaction curve of the overconsolidated -normally consolidated type; the curve obtained is referred to as a general compaction curve for the materials tested: sandstones. This general compaction curve is the normalised version of the over/normally consolidated curve, the stress being normalised to a starting stress σ_o' (when the loading rate changes). The strain axis is normalised by a denominator $C_{m,o} * \sigma_{z,o}'$. The characteristic of the resultant curve is that several sandstones of various stress histories plot onto this general compaction trend.

An algebraic expression for the curve is obtained for strain (H) as a function of the normalised stress (x),

$$H(x) = -0.010+g(u)*2.969*u^{3.485} +(1-g(u))*(u-0.30) \qquad .. 6.2.23$$

with $u = x - 0.80$

$$g(u) = e^{-(u/0.43)^{7.58}}$$

Using this, the field compaction behaviour is obtained from

$$\frac{\Delta h}{h} = C_{m,o(field)} * \sigma_{z,o}'.(H(x) - H(x_i)) \qquad .. 6.2.24$$

$$\text{with } C_{m,o(field)} = (1-\beta)\left(\frac{\dot{\sigma}_{z,lab}}{\dot{\sigma}_{z,dep}}\right)^{b} * C_{m,o(lab)}$$

β being the ratio of the compressibilities of the grains to the matrix, and "i" indicates parameters at initial reservoir conditions. b is the material constant found graphically from the change in the compaction curves with loading rate.

Two examples of the non-linear trend of subsidence with continued production (for sandstone reservoirs) are seen in the Bachequero area (van der Knaap and van der Vlis, 1967) and in Groningen (de Waal, 1986). These show that during the initial part of the depletion history, the reservoir undergoes little compaction, though once a threshold stress is reached, compaction and subsidence can occur to a marked extent. Such behaviour is predicted by the RTCM, but could be due to other factors including, a dampening of the reservoir compaction due to the overburden, or an initial stiff elastic behaviour of the reservoir rocks. This two-stage strain response to loading, described by the RTCM is described in earlier works on strain rate and from reloading tests after secondary creep deformations, Bjerrum (1967). Morita et.al. (1984) have suggested that for high pressures, a reservoir should have initially high compaction; however, it is suspected that the experiments of Morita et.al (Loc.Cit) are erroneous with respect to the conclusions drawn from the study.

The approach employed by de Waal and Smits (1985) and de Waal (1986) of variable loading rates during compaction experiments, seems to be promising, but there are areas of doubt about the applicability to reservoir materials other than sandstone (de Waal and Smits, 1985). The $\Delta\sigma_z$ shift must be known between the geological loading

rate and the depletion loading rate, the laboratory simulation of which may be less regular in more plastic materials which tend to retain their stress histories more than a sandstone. Added to this, is the fact that any overconsolidation must be known as the effect is additive to the $\Delta\sigma_z$ shift.

This approach was later adopted for chalks (Smits et.al., 1986); the b (C_α/C_c) values for these materials are given in Table 2.1. This type of analysis was discussed in (Chap. 4), and showed that with the Pegwell Bay chalks, the degree of time dependence of the deformation decreased with the increase in strain and/or effective stress. For the sands tested by de Waal (1986) the b values were seen to remain constant; this was also seen by Mesri and Godlewski (1977) for many uncemented clays. The decrease seen in the values in this study would be expected because of structural breakdown (discussed in Chap. 4). The sheared bonds in the post-yield deformation would show more slip, or creep at low strains than at higher strains, where the structure is more compact and less liable to slip. This increased secondary consolidation at the preconsolidation pressure was seen in clays; however, in the case of clays, a constant ratio of coefficient of consolidation to compaction coefficient (C_α/C_c) was maintained by an accompanying increase in C_c.

Some of the assumptions in the formulation of the RTCM (de Waal, 1986) are not applicable to chalks, as no account is made for particle crushing. However, it seems to provide good agreement between predicted and field-measured subsidence, (de Waal, 1986; and de Waal and Smits, 1985), and is compatible with equations based on plastic deformation of sediments (Mesri and Godlewski, 1977; and Mesri and Choi, 1979).

6.2.2) Changes in physical parameters during compaction

During pressure decline in an oil reservoir, compaction of the reservoir material can cause changes in both the type of deformation and petrophysical parameters of the material, Allen (1968), the most important change being the reduction in permeability.

i) The variation in permeability with increasing effective stress

The decrease of permeability with compaction as a function of increasing effective stress has been studied by many workers, (Fatt and Davis, 1952; McLatchie, Hemstock and Young, 1958; Gray, Fatt and Bergamini, 1963; Brighenti, 1967; and Gobran, Brigham and Ramey, 1981). These studies have concentrated on permeabilities in sandstones and occasionally limestones. Fatt and Davis (1952) recognised the fact that the permeability decreased with overburden stress; reductions in permeability of between 89 and 59% for the values at zero confining stress were measured, the greatest reductions occurring with samples that had the largest permeabilities. McLatchie et.al. (1958), showed the reverse of this trend, with the greater reduction in permeability occurring in those samples with the lowest initial permeabilities. This was due to the higher clay contents in the samples with the lowest initial permeabilities.

In their study on the effects of pore pressure and confining pressure on the permeability of Ottawa sands and fired Berea sandstone Gobran et.al. (1981) show that Terzaghi's effective stress (the cell pressure minus the pore pressure (Chap. 2)) controls the reduction in permeability. This phenomenon was also recognised by Brighenti (1967). However, these observations are contradicted by the work on Berea sandstone by Zoback and Byerlee (1975), who suggest and

empirical effective stress equation of the form

$$K(U,\sigma') = K_i + a(bU - \sigma') \qquad .. 6.2.25$$

controls the permeability. Where K_i is the intrinsic permeability at zero stress, and values of a and b for permeability measured perpendicular to the bedding and parallel to the bedding were a = 0.0143mD/bar and 0.0598mD/bar, and b = 4.0 and 2.2 respectively. Gobran et.al (Loc.Cit.) investigate other possible variables involved in the laboratory determination of permeability in sands and sandstones. They show that the rate of flow does not affect the permeability, though as the quantity of fluid passed through the sample increases, the permeability is seen to decrease. There was no effect on the permeability of their samples when the temperature was increased up to 148^{o}C.

Gray et.al. (1963), Brighenti (1967), and Gobran et.al. (1981) have recognised that an anisotropic stress system acts on sediments at depth (Chap. 7), and have analysed the permeability reduction resulting from such a stress system. Gray et.al. (1963) and Brighenti (1967) compare the results of reductions in permeability under non-uniform stress systems with those observed under hydrostatic stress. In both of these studies a stress path with the minimum effective stress equal to 1/3 of the maximum effective stress, rather than K_o stresses was used. The results of these comparisons between isotropic and anisotropic loading are contradictory; Gray et.al. (Loc.Cit.) show a smaller reduction with increasing stress, while Brighenti (Loc.Cit.) shows a greater reduction in permeability with the anisotropic stress system, when compared to tests performed under isotropic stress conditions. This discrepancy is possibly due to the

different methods of anisotropic stress application in these studies. In the study performed by Gray et.al. (1963), the minimum effective stress on the sample was applied axially by a piston, the maximum effective stress being applied by the cell pressure. In comparison, the study by Brighenti (1967) applied the maximum stress through a piston and the minimum stresses via a hydraulic pressure. Thus, for the same maximum effective stress the mean stresses in Grays experiments are 1.4 times the value of those in Brighenti's tests. More importantly, passive and active stress systems are applied to Gray et.al.'s and Brighenti's studies respectively. The stress system employed by Gray et.al. (1963) were chosen so that the horizontal permeability (parallel to the minimum effective stress) could be measured.

The variation of permeability anisotropy with increasing stress was also studied by Gray et.al. (1963). They state that for an increase in hydrostatic stress, the vertical permeability decreases to a greater extent than the horizontal, in the same sample. For Berea sandstone, the vertical permeability decreases to 89% of its unstressed value at 35MPa, while the horizontal permeability remained constant. The same kind of reduction was seen in the Boise sandstone, with the vertical permeability decreasing to 96% of its initial value, while the horizontal permeability decreased by 0.5%. This is possibly due to the fact that the initial vertical permeabilities are larger than the horizontal and thus undergo a larger reduction, Fatt and Davis (1952). This difference in the changing permeabilities, reflects the tendency of sediments to become more isotropic under a hydrostatic stress system. The ratio of horizontal to vertical permeabilities was observed to increase from approximately 0.63 to 0.73 with an increase in stress from 0 to 35MPa, Gray et.al. (1963).

The decrease in the permeability of the chalk, or chalk-type materials, in response to an increase in effective stress has been discussed by Marek (1981), Simon et.al. (1982), and King (1982). The reduction of the permeability shown by these workers has been performed under hydrostatic stress conditions, and no general trend of reduction with stress or porosity, has to date been formulated. The reduction of permeability with stress shown by some Danian on-shore samples is illustrated in Fig. 6.1.

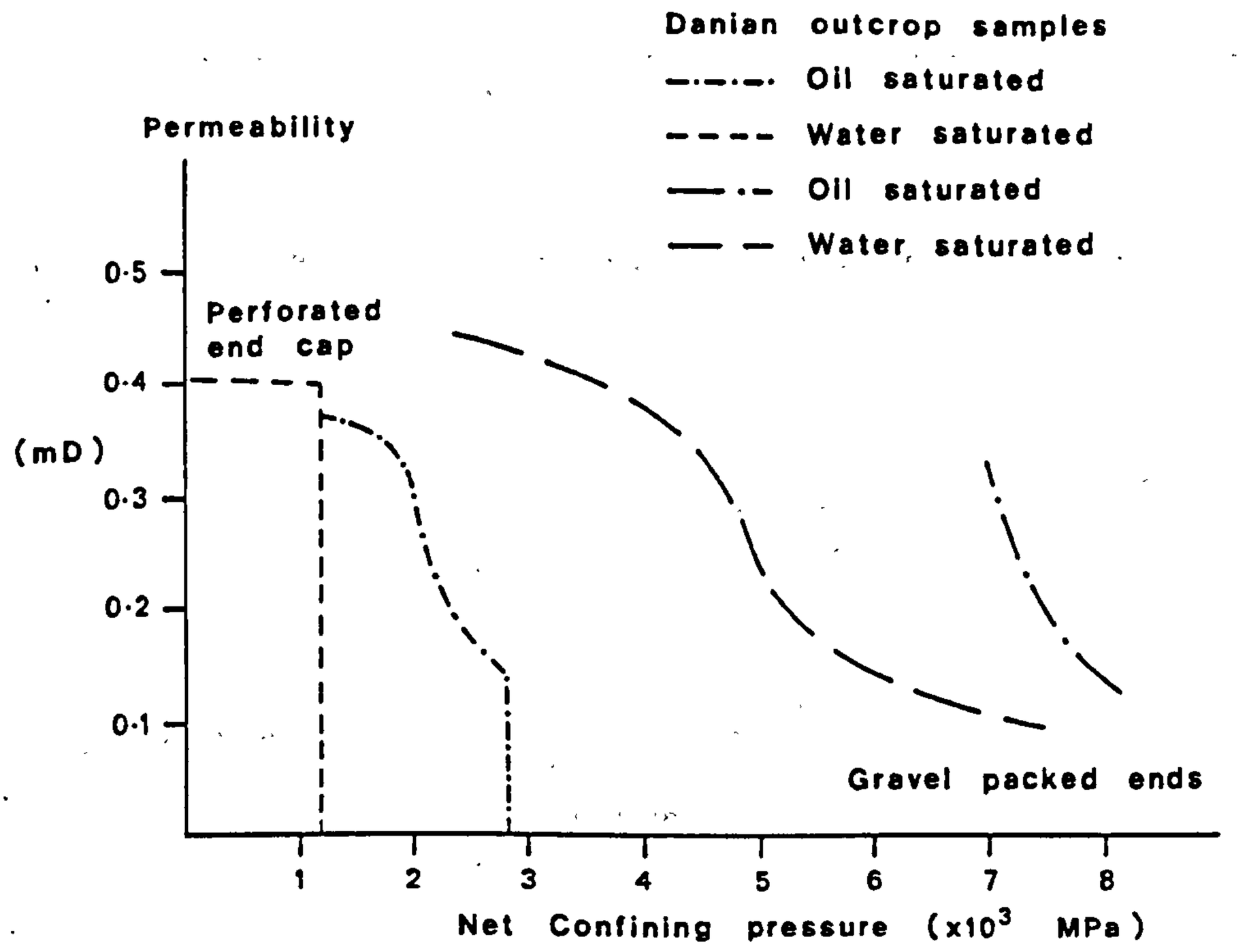

Figure 6.1 Permeability reduction in Danian outcrop chalk due to stress increases (After Simon et.al. 1982).

The results of permeability reduction with increasing effective stress for the chalks tested in this study agree with some of the observations mentioned above (Chap. 4). The permeabilities for all the chalks tested show a significant reduction with increasing stress similar to those shown in Fig. 6.1. The tests performed on Butser Hill chalks show that there is no effect of temperature on the

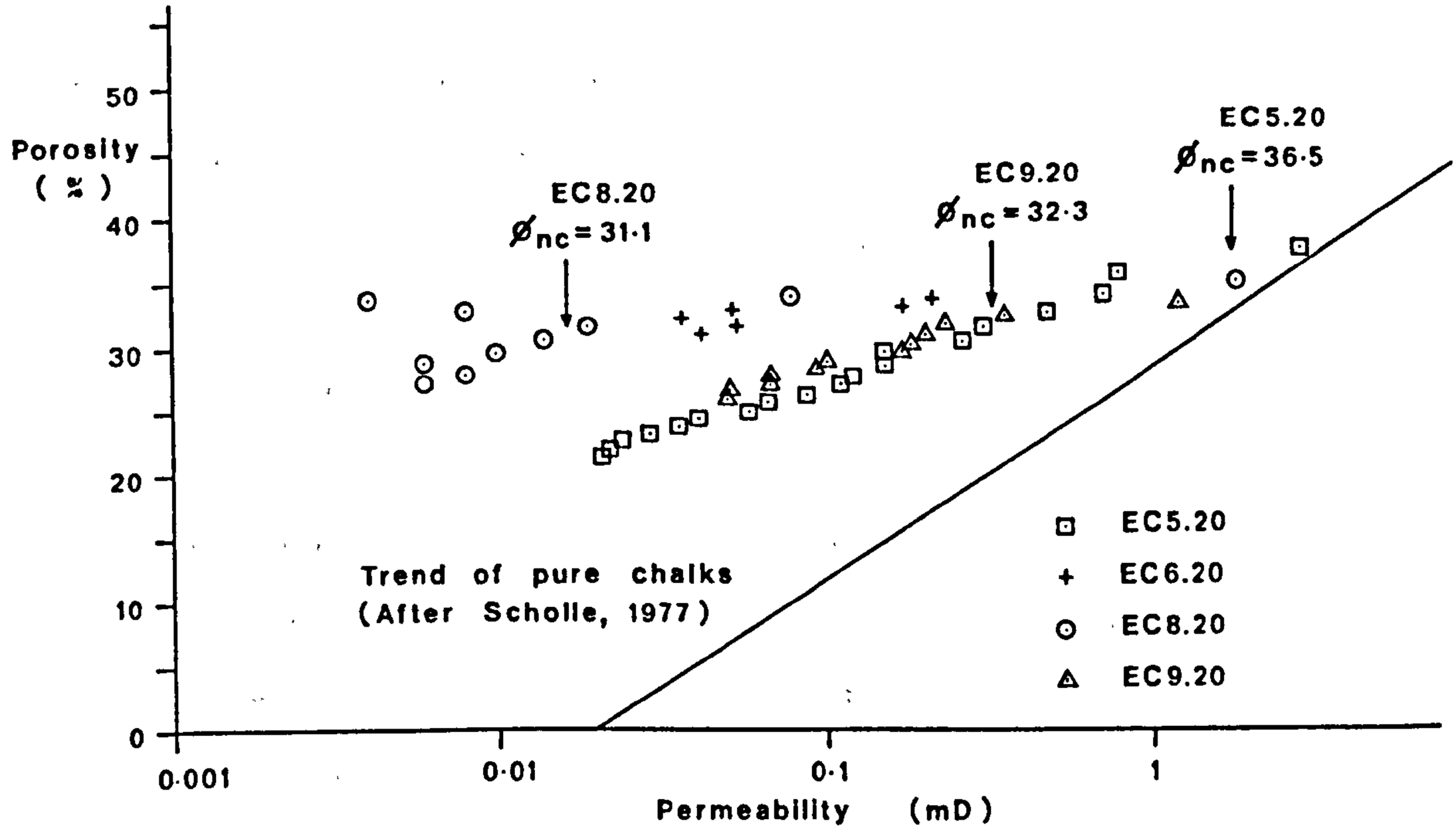

Figure 6.2a Reduction of permeability with porosity in K_o tests on Central North Sea chalks.

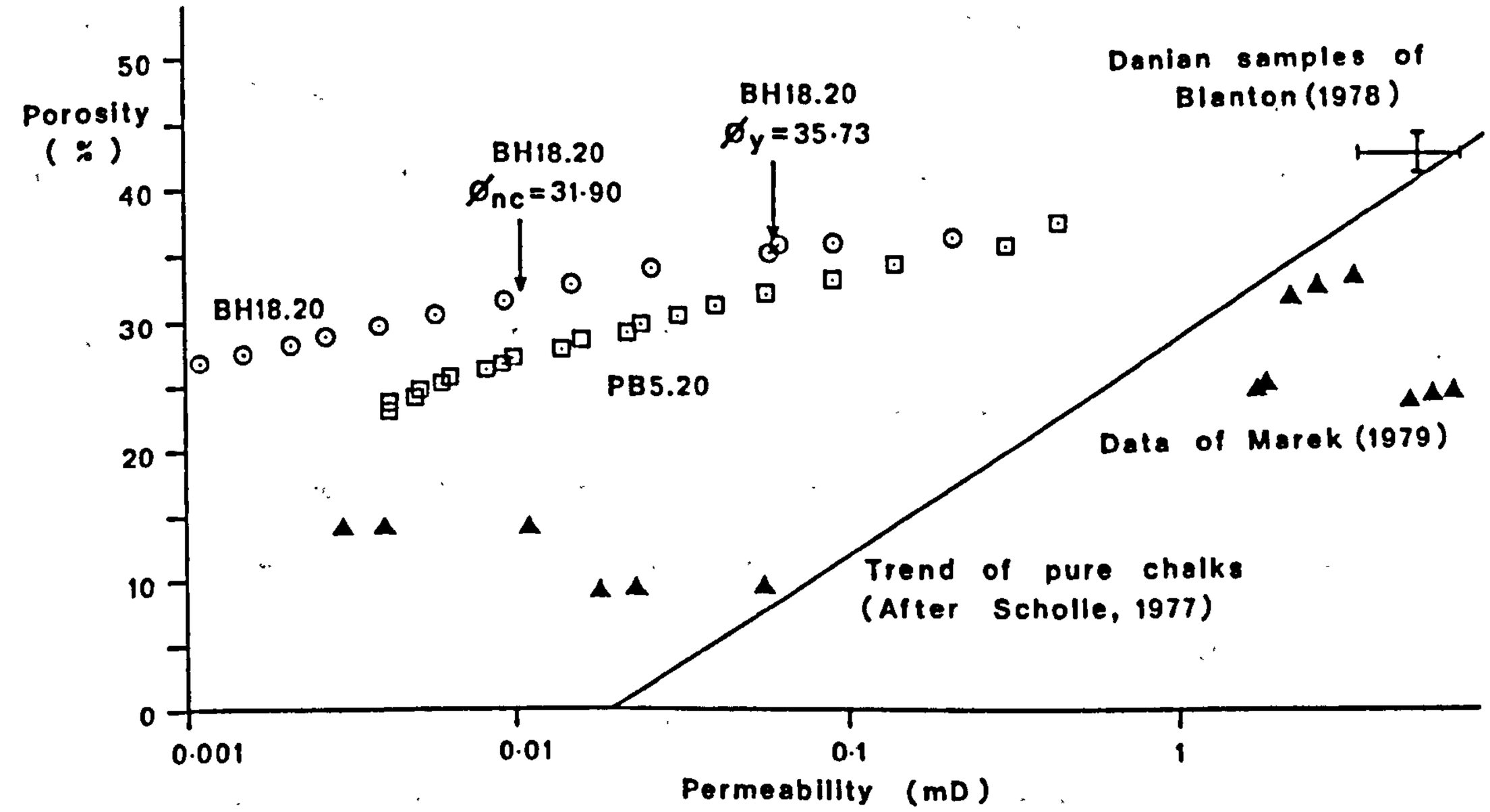

Figure 6.2b Reduction of permeability with porosity in K_o tests on two chalks from southern England.

permeability change up to temperatures of 100°C. The most interesting and significant result of the permeability data obtained in this

study, is the post-yield linear relationship between log k(1+e) and log e (Chap. 4.7), as seen in clays by Samarisinghe et.al. (1982). This relationship shows a deviation from linearity with the Pegwell Bay samples tested which is assumed to be due to the large amount of grain crushing involved in the compaction of chalks. The Samarisinghe et.al. (1982) plots for the chalks from Butser Hill and the Central North Sea show a linear trend in the post-yield deformation. The permeability is thus a function of the void ratio or porosity of the sample as would be expected, Scholle (1977). The results from the permeability measurements obtained from this study are compared to Scholle's (1977) trend, and with other published results of permeability reduction with decreasing porosity (due to stress increases) in Fig. 6.2. Fig. 6.2a compares the North Sea chalk results with those published, while Fig. 6.2b shows the permeability reduction of two onshore chalks with decreasing porosity: one from Pegwell Bay the other from Butser Hill. These figures show that two trends are dominant, a shallow trend with high permeability reduction and little porosity reduction, which occurs before the start of normal consolidation, and a second steeper trend of high permeability reduction associated with a high porosity reduction which is seen to accompany the normal consolidation deformation. Neither of these trends is coincident or parallel to that presented by Scholle (Loc.Cit.), though the normal consolidation trend of the North Sea samples appears to give the closest agreement for the permeability reduction. The data of Marek (1979) is only limited in extent, but two trends could be tentatively proposed for the data.

Although the evidence is so far limited, it appears that the North Sea chalk samples tested in this study all exhibit an identical post-yield permeability reduction in the log k(1+e) vs log e space.

If this trend could be fully quantified more accurate simulations of oil field production could be achieved.

ii) Variation in compressibilities of reservoir materials

The first section of this chapter discussed the methods used to calculate the amount of reservoir compaction from a draw-down situation. In the analyses used by Geertsma (1957), and the conversion from hydrostatic to uniaxial strain (Teeuw, 1971), the input for these equations is mainly some expression of rock compressibility. The compressibility of the rock is important not only for subsidence calculations, but also for calculations of reservoir oil in place. Hall (1953) first showed its importance to material balance calculations in undersaturated reservoirs, using the compressibility of some materials under conditions of constant hydrostatic stress and decreasing pore pressure. The results of this showed that the errors involved in determining the oil in place, calculated ignoring rock compressibility compared to the actual oil in place would vary from 2 to 1.3, for rocks with porosities ranging from 1.5% and 26% respectively. Hall (1953) performed compressibility studies on low porosity, well consolidated materials. Newman (1973) tested a larger range of materials than Hall, and showed that there is a slight trend for a decrease in pore compressibility with increasing porosity for well-consolidated samples, as shown by Hall (1953) and by van der Knaap (1960). For consolidated samples there is a tendency for the compressibility to increase with initial porosity, while friable materials show no trend with porosity.

The compressibility of a reservoir rock can be separated into three components (Geertsma, 1957; Scorer and Miller, 1974), Eqns. 6.2.1 to 6.2.3. However, for calculations of reservoir subsidence,

uniaxial compressibilities are required, as discussed above. Geertsma (1957) related the change in pore volume to approximately half the bulk compressbility for uniaxial strain (Eqn. 6.2.13). Later studies have dealt with the uniaxial compressibility, C_m (Teeuw, 1971; 1973; Geertsma, 1973) which is defined as

$$C_m = \frac{1}{z}\frac{dz}{dU} = M_v \qquad .. 6.2.26$$

where z = height of the unit of material, and U is the pore fluid pressure. Geertsma (1973) presents data obtained from the literature on the magnitudes of uniaxial compressibility which is summarised in Table 6.1.

Table 6.1 Uniaxial compressibilities of sandstones and limestones (After Geertsma 1973).

		UNIAXIAL COMPRESSIBILITY (M_v) (MPa^{-1})	
SANDSTONES	POROSITY %	σ_z' = 9.8-19.6 MPa	σ_z' = 29.4-58.8 MPa
well consolidated	0 - 30	4 - 18	3 - 12
Semi-consolidated	15 - 35	14 - 43	10 - 34
unconsolidated	25 - 40	35 - 460	50 - 200

		UNIAXIAL COMPRESSIBILITY (M_v) (MPa^{-1})	
LIMESTONES	POROSITY %	σ_z' = 9.8-19.6 MPa	σ_z' = 29.4-58.8 MPa
well consolidated	0 - 30	1 - 15	1 - 10
soft	15 - 35	12 - 24	---
vuggy	15 - 35	12 - 50	10 - 37

The compressibility of a material is a function of the applied stress system, this has been demonstrated by Brighenti (1967), where compressibilities for hydrostatic tests varied from those obtained in tests where the radial stress is $1/3^{rd}$ the axial stress. The anisotopically consolidated samples tested by Brighenti (1967) showed higher compressibilities for both sands and sandstones with a calcareous cement than those obtained from hydrostatic tests. This resulted because Brighenti defined the compressibility as a function of the change in mean effective stress, as opposed to the maximum effective stress (c.f. Chap. 2). Therefore, these are not comparable with the lower uniaxial compressibilities predicted from Eqn. 6.2.19. Teeuw (1973), investigating sandstones from Groningen, found that the conversion from hydrostatic to uniaxial strain using Eqn. 6.2.19 predicted the compressibilities obtained from uniaxial tests.

Fatt (1957), van der Knaap and van der Vlis (1967), Brighenti (1967), Geertsma (1973) and Rieke and Chilingarian (1974) have shown that compressibilities are not constant, but change with effective stress. This has also been shown by Mess (1978), who states that "The compaction behaviour of reservoir rock is a function of its stressed state and stress history". Brighenti (1967) and Mess (1978) show that a peak in the compressibility occurs with increasing effective stress; Brighenti (Loc.Cit.) testing sands and sandstones stressed to 10MPa ($100kg/cm^2$) prior to loading, showed compressibility peaks between 15 and 30MPa respectively. Brighenti (Loc.Cit.) also tested sands from the Po Valley gas reservoir, these sands were initially consolidated to different magnitudes of hydrostatic stress before being recompressed with an all round (hydrostatic) stress. The peak compressibility for these sediments occured at higher stress levels for those samples subjected to the higher initial consolidation

stresses (and with a resultingly lower initial porosity). Mess (1978) demonstrated that the peak in the trend for uniaxial compressibility with increasing effective stress, for sands and weak sandstones occurs around the previous stress maximum, though he denies that this increase in compressibility is due to renewed shattering of grains, as suggested by Brighenti (1967). This peak, followed by a gradual decrease in the compressibility of the sample with increasing effective stress, has also been shown for carbonate materials by Heiberg (1974) for hydrostatic loading, van Dizhuijzen and de Waal (1984) and Smits et.al. (1986) for uniaxial compaction. The sand samples compacted under different stress histories tend towards one uniaxial compressibility trend, when subjected to stresses larger than the previous load, Fig. 6.3 (Mess, 1978).

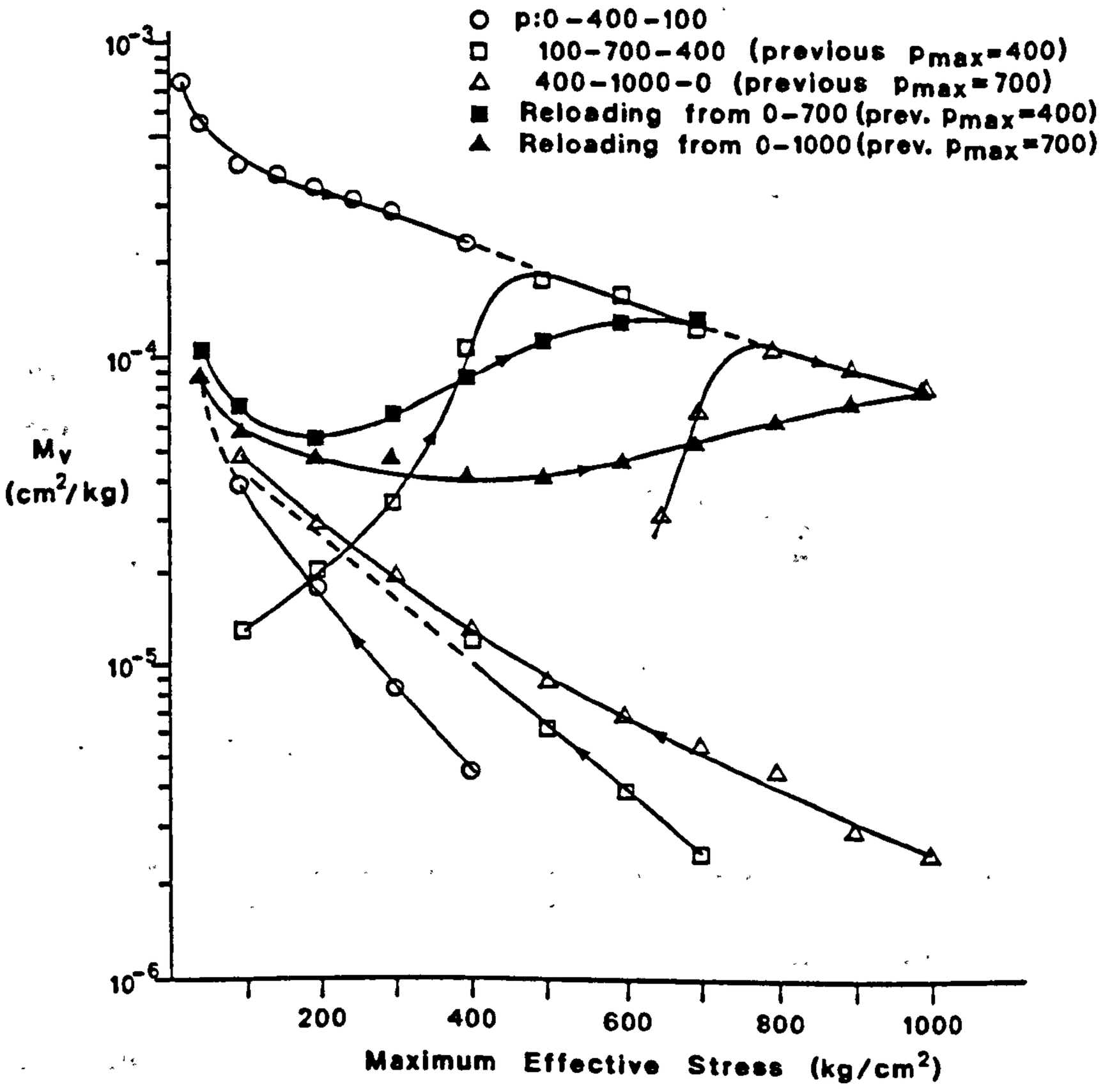

Figure 6.3 Effect of stress history on M_v of sand (After Mess 1978).

This is a similar behaviour to that shown by clays on e-log p' plots, where the consolidation line is rejoined after reloading, Bjerrum (1967), Chap. 2.

The coefficient of volume compressibility (M_v) (equivalent to C_m) has been determined as part of this study and can be seen to change with increasing vertical effective stress, Fig. 6.4. The samples from the Central North Sea show a tendency to deform along a particular compressibility trend in the post-peak compressibility region. This is reminiscent of the compressibility trend seen for the sands studied by Mess (1978).

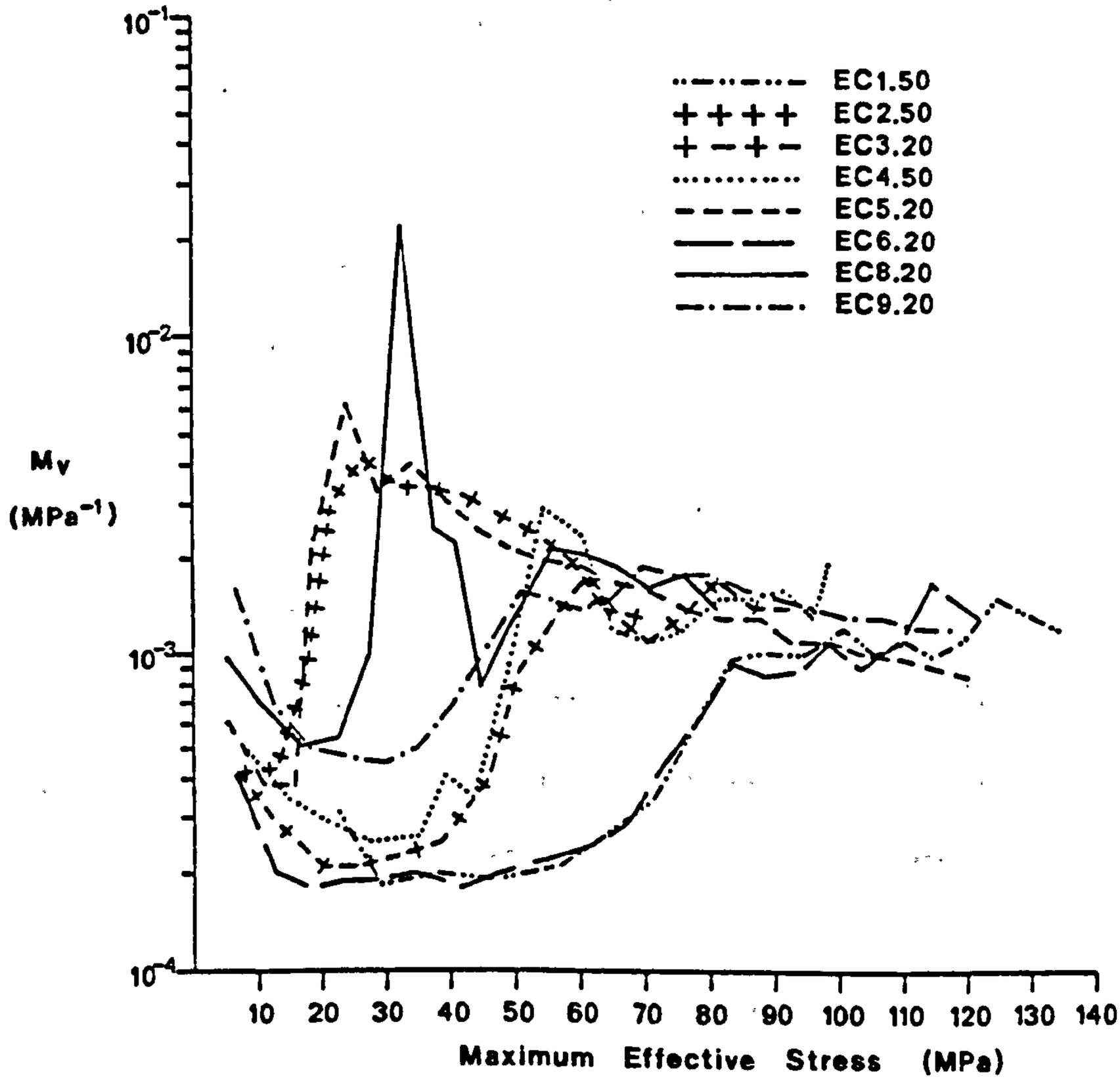

Figure 6.4 Uniaxial compressibility variation with increasing stress for Central North Sea chalk samples.

This apparently unique trend describing the post yield compaction characteristics of these chalks is unexpected due to the variation in the clay contents in these chalks (Table 3.2) (Moshanski and Parabouchev, 1981). Some chalks from onshore sites were plotted on a similar plot to enable a comparison between these and the North sea samples. Such a plot should show if differences in burial history and diagenesis affect such a trend - as would be expected, Fig.6.5.

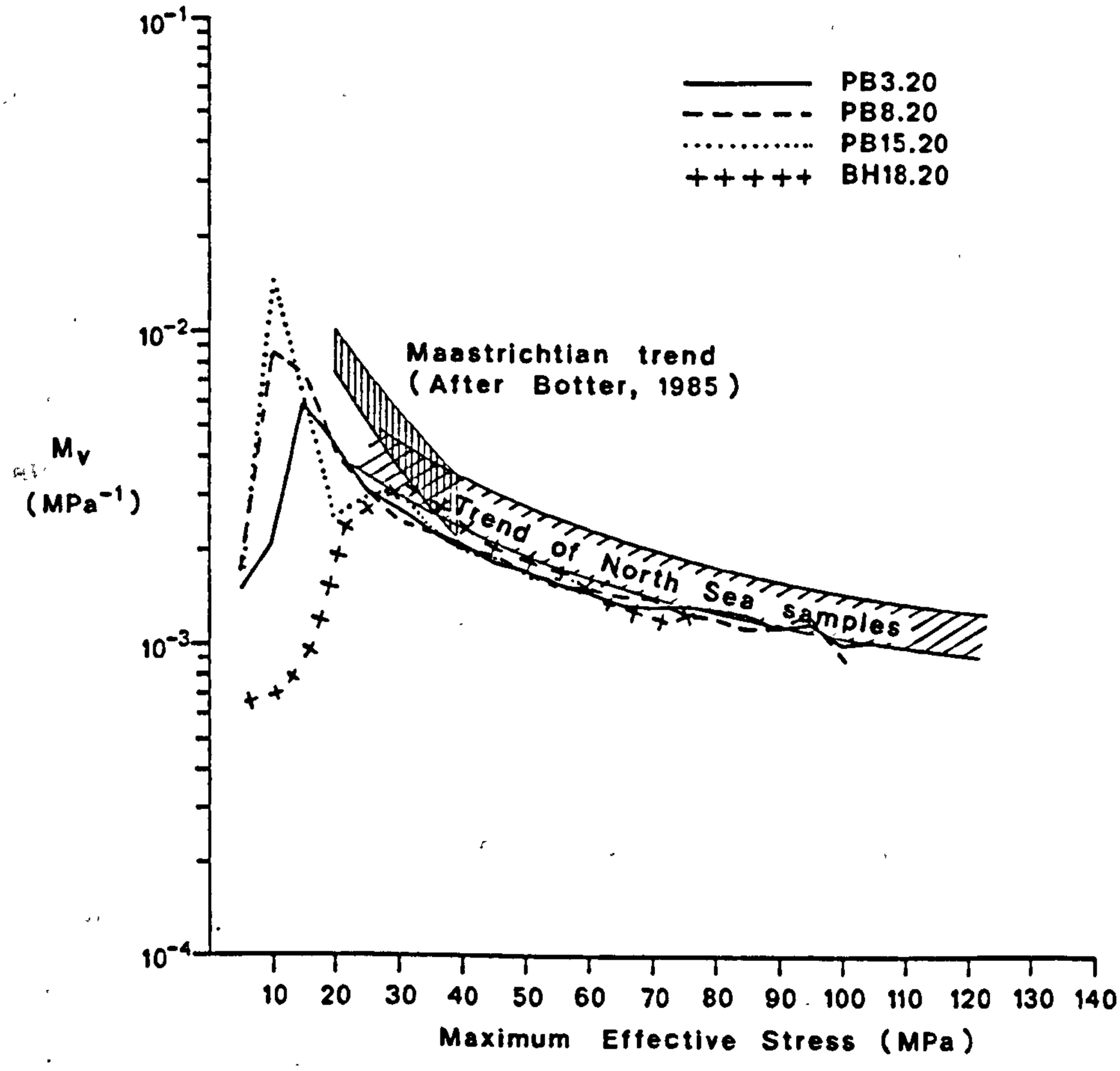

Figure 6.5 Comparison of uniaxial compressibilities obtained from outcrop chalk samples and North Sea samples.

The comparison shows that the uniaxial compressibility of chalk samples obtained from outcrops in southern England lye at the lower end of the trend defined by the North Sea samples. The agreement is very good as the two trends appear to be parallel and coincident.

Fig. 6.4 and Fig. 6.5 suggest that the post-yield compressibility shows little variation between chalks of different burial history and diagenesis, and that the clay contents present in the samples used in this study (generally below 20%) also have little influence. Thus, it must be concluded that once the cementation bonds have been broken, the dominant mineral in the samples, calcite, controls the deformation properties of the sediment. This could be seen by comparing these results with those obtained for the uniaxial compaction of uncemented coccolith ooze.

There is an added complication concerning the laboratory determination of compressibility for use in subsidence and material balance calculations. As discussed by Teeuw (1973) and Mess (1978), the effect of unloading and sample disturbance on the compressibility of weak materials renders the accuracy of compressibilities obtained from first loading questionable. The compressibility values for second and subsequent loadings are generally constant and lower than the first loading. The highest compressibilities being obtained from remolded samples. The compressibility values used by these workers, is the average value obtained from the first and second loadings.

For reservoir compaction and compaction drive calculations in hydrocarbon reservoirs, different values of compressibilities must be used for different magnitudes of pore fluid pressures, during the projected depletion history of the reservoir. As such, the theoretical approaches of volume decrease in reservoir materials, described at the beginning of this chapter, should be integrated over the effective stress increase predicted for the reservoir with the appropriate function of uniaxial compressibility for this stress interval. However, the difficulty still exists of the choice of appropriate values of compressibilities for disturbed samples.

6.2.3) Time-dependent deformation in reservoir compaction

Most theoretical work concerning the prediction of compaction and subsidence in oil reservoirs has focussed on sands and sandstone materials as outlined in the last section. These have a very small plasticity component in their deformation behaviour and therefore respond relatively quickly to increments of effective stress. High pressure uniaxial compression of materials with a more viscous deformation have only really been considered theoretically by Geertsma (1957) (Chap. 6.2.1). Included in this category of materials are limestones, weakly cemented high porosity sandstones and shales or clay-rich materials. High porosity sands and sandstones normally have high permeabilities and as such have a time dependancy of deformation, predominantly due to creep which occurs at a constant stress. Clays and shales have much lower permeabilities than sands and their time dependancy occurs due to both the time dependant equalisation of pore fluid pressure in a unit of sediment, and through creep of the sample under a constant effective stress. Creep or secondary consolidation has been recognised as a time-dependent deformation in reservoir rocks by many workers Newman (1973), de Waal and Smits (1985), van Kooten (1986), and Smits et.al. (1986).

Cases of time dependant compaction in argillaceous materials have been attributed to consolidation of the sediment due to changes in the effective stress. Several examples of subsidence from clay compaction due to aquifer draw-down have been recorded (Wilson and Grace, 1942; Takeuchi et.al., 1969; Nakano et.al., 1969; IAHS-UNESCO 1969; IAHS 1976). Though the aquifers are generally shallow compared to hydrocarbon reservoirs a similar approach can be used to calculate compaction of clay stringers in reservoirs (van der Knaap and van der Vlis, 1967) or for overburden compaction.

An early paper on the subject of clay compaction due to underdrainage was presented for water withdrawal from the chalk aquifer underlying London clay strata in the London Basin area (Wilson and Grace, 1942). The chalk acts as a drainage boundary for the clay, as the pore fluid pressure in the chalk is decreased during draw-down. The settlement of the top of the clay layer was calculated using Terzaghi's consolidation equation (Chap. 2). In their analysis Wilson and Grace (1942) consider a time-dependent withdrawal of pore fluids from the aquifer and a decrease in voids ratio with depth, but do not vary the coefficient of consolidation in response to this decrease, or with time during consolidation. Comparison of their calculated settlements with surface-measured subsidence shows a reasonable agreement, the calculated values being of the same order of magnitude and showing the same general trend. The maximum settlement up to 1931, was 0.21m and occured in the Fulham and Chelsea area of London. The thickness of the strata overlying the chalk in the London area varies considerably and will affect the measured settlement; the uppermost formation - the London clay varying in thickness from zero to 100m over the area. The extent of the drawdown will also affect the magnitude of the settlements - in the London area the largest settlements are seen to follow the areas where greatest drawdown has occured (Wilson and Grace, 1942). The difficulty associated with the study of Wilson and Grace (1942) is the superimposed effect of man-made structures and their settlement at the surface. Deviations of measured settlements from the calculated values of Wilson and Grace (Loc.Cit.) vary widely in the vicinity of heavy construction, the deviation being particularly pronounced in the area around the Bank of England. The London clay strata is fractured to a large extent (Hellings pers.com., 1986);

this would be difficult to model in a study of consolidation due to the irregular nature of fractures; also it is still unclear how fractures would affect the consolidation of a unit of sediment. Since reasonable agreement is obtained by ignoring the fractures, it can be assumed that they have a small effect even at shallow depths.

The consolidation of aquitards due to a pressure draw-down in the strata has been widely studied for low level ground water studies. Delflache (1978) performed oedometer tests on clays from depths of 43 to 371m in the Houston - Galveston area. In these tests the total load was kept constant and the pore pressure was gradually decreased; the analysis of the resultant compaction curves gave values of C_v equal to 0.02 and 0.05m^2/yr. De Simone and Viggiani (1978) formulate a consolidation equation based on the approach of Gibson, England and Hussey (1967), the equation being valid for thick sequences of clays. For the deformation of clays, a non-linear stress-strain equation of the e - log p' type, and a permeability-void ratio relationship is incorporated into the basic derived equation. Using this equation for two aquitard boundary conditions, the consolidation is calculated. Although the examples presented above are for ground water subsidence cases, the application of the consolidation equation can be assumed to be applicable for deeper oil reservoir problems.

Van der Knaap and van der Vlis (1967) have shown that compressibility of sands and clays from a depth of approximately 900m in the Bolivar coast oil fields, Venezuela, are of the same order of magnitudes. Their study considered the consolidation effects of the interbedded clay stringers in the oil- bearing sand strata. They calculated the fractional compaction of various thicknesses of clay strata, and the time dependancy of this compaction, Fig. 6.6. In the calculation, a constant coefficient of consolidation (from Biot's

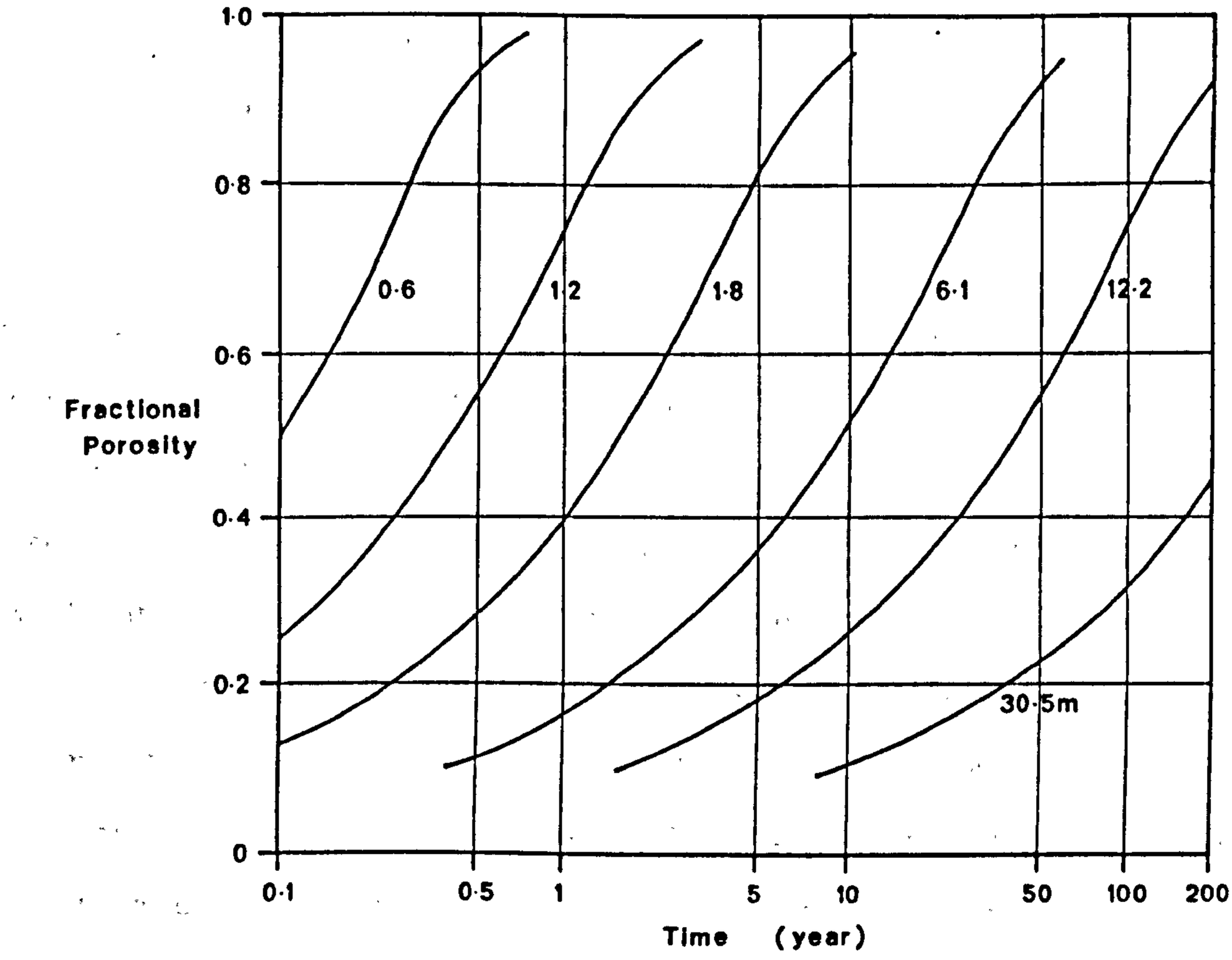

Figure 6.6 Consolidation of clay layers of various thicknesses resulting from an instantaneous stress increase (After van der Knaap and van der Vlis 1967).

theory of consolidation) of $0.2m^2/yr$ was employed.

Creep and secondary consolidation can contribute to the total strain that a material undergoes due to the application of a load; this was briefly discussed in Chap. 2.6. Only a few studies have been performed on high pressure creep of chalk, associated with reservoir compaction (van Kooten, 1986; Johnson and Rhett, 1986). The latter authors show a linear relationship between the reciprocal of volume change and the reciprocal of time at any particular stress with increasing time. At large time intervals the linear trend is seen to level off, with effectively zero volume change with time. This leads to a steady decrease of creep strain rate with time. Johnson and

Rhett project the linear trend to zero reciprocal time, to find an ultimate strain for a specific load. This is an overestimate due to the levelling off of the volume strain at large time intervals.

The Clay samples from the Central North Sea used in this study, Chap. 5, showed similar values of coefficient of consolidation to those given in van der Knaap and van der Vlis (1967). The value of the coefficient of consolidation was also seen to decrease with increasing vertical effective stress, this would increase the consolidation time of a sediment as the effective stress was increased. For a thick sediment where various effective stresses existed in the unit, a spatial distribution of coefficients of consolidation would occur in the sediment, so deviating from the prediction of consolidation formulated by Terzaghi (Chap. 2). The compaction of overburden material as a contributary factor in oil field compaction and subsidence, is generally not considered by most workers. However, the possibility of this should not be ruled out, with the automatic assumption of an elastic overburden (Jones et.al., 1985a; 1985b; 1986). Although the effect of the presence of fractures on consolidation of a shale overburden has not been assessed, it could be significant if the fractures have a small joint spacing and if the joints are pervasive through the overburden. The consolidation of the overburden could also occur through sand lenses, which are in connection with the reservoir or wells. Alternatively, the shales could consolidate radially into the wells due to drainage through the cement surrounding the casing (Skinner pers.com., 1986). However, without such drainage paths the consolidation of clays buried to depths of several kilometres would be very slow, van de Knaap and van de Vlis (1967).

As with friable sandstones, the question of representative samples

of shales being recovered from great depths without significant

i) drilling disturbance,

ii) stress relief,

iii) development of negative pore fluid pressure, with the accompanying infiltration of drilling muds, and

iv) preconsolidation effect caused by cooling the material, is open to some doubt. As such, tests on deeply buried uncemented shales must be treated with caution until these errors are eliminated or evaluated (Chap. 5).

6.3) EXAMPLES OF SUBSIDENCE IN OIL AND GAS FIELDS

Subsidence related to the withdrawal of fluids from porous sediments and rocks occurs due to ground water production, oil and gas removal and, to a lesser extent, steam production for geothermal projects, and brine removal. As stated by Poland and Davis (1969) the separation of field cases into ground water or oil and gas extraction is purely arbitrary as the same principles are involved in the end product: subsidence. The only difference is the magnitude of stresses acting on the reservoirs.

This chapter will a) discuss the factors thought to affect subsidence and b) tabulate the salient features of cases of oil and gas field subsidence reported in the literature. For a full description of the main examples, the reader is referred to Poland and Davis, 1969; Yerkes and Castle, 1969; Principia Mechanica, 1986; Jones et.al., in press; and the AIHS publications on subsidence (1969; 1976).

The number of oil and gas fields that undergo notable subsidence is small relative to the number of producing fields. All oil fields that experience a pore fluid pressure decline will undergo compaction

to some degree, but the amount of associated surface subsidence will normally be negligible. The cases of subsidence commonly reported in the literature are cases where the field is in close proximity to the sea, and the risk of damage due to flooding is high. Cases of minor onshore subsidence are less reported because regular resurveying needs to be performed to detect the movement.

Subsidence above hydrocarbon reservoirs has been attributed to a number of factors (Geertsma, 1973):

1) A large decrease in the pore fluid pressure in the reservoir during production.

2) Production from a large vertical interval of deformable material.

3) High compressibility of reservoir material.

4) Reservoirs at a relatively shallow depth of burial.

To these, Martin and Serdengecti (1984) added a stress transfer factor, this is the transfer of load from the overburden to the compacting reservoir.

Geertsma (1973) obtains the first three factors from the compaction of the reservoir material (ΔH), Eqn. 6.3.1; this assumes a constant mean compaction coefficient (C_m) with decreasing pore pressure (ΔU).

$$\Delta H = C_m(z).\Delta U(z).dz \qquad .. 6.3.1$$

The uniaxial compaction coefficient and the decrease in the pore fluid pressure being functions of the depth in the reservoir. Using the "nucleus of strain" approach to sum the deformations from a large number of nucleii representing the reservoir, Geertsma (1973) presents equations for vertical (u_z) (Eqn. 6.3.2) and horizontal deformations (u_r) (Eqn. 6.3.3) at the surface.

$$u_z(r,0) = -\frac{1}{\pi} C_m (1-\nu) \frac{D}{(r^2 + D^2)^{3/2}} .\Delta UV \quad .. 6.3.2$$

$$u_r(r,0) = +\frac{1}{\pi} C_m (1-\nu) \frac{r}{(r^2 + D^2)^{3/2}} .\Delta UV \quad .. 6.3.3$$

In these equations V is the volume of the nucleus of strain, d = the depth of burial of the nucleus of strain, r = radial distance from the vertical axis through the nucleus of strain.

When these equations are integrated over the whole volume of a simplified disc shaped reservoir, the equation for vertical subsidence in the centre of the field is given by

$$u_z(0,0) = -2 C_m (1-\nu) \Delta U.H \left(1 - \frac{\eta}{\sqrt{1 + \eta^2}}\right) \quad .. 6.3.4$$

where η = depth/radius (D/R) of the disc shaped reservoir. From this Geertsma (1973) derived the following expressions:

Subsidence/reservoir compaction = $- 2 (1-\nu).A \sim - 1.5 A$

"A" is a variable with values ranging from 1 for reservoirs with D/R values of zero, to 0 with both lower D/R values and increasing radial distance from the centre of the field.

From this solution the influence of the fourth factor (burial depth) was derived. This shows that small deeply buried reservoirs will not produce significant subsidence; Geertsma also shows that the

ratio of subsidence to compaction can be larger that unity. This "nucleus of strain" analysis assumes horizontally-bedded strata, and thus does not take into account the structural aspects of the reservoir, e.g. a periclinal structure will have arching effects which will partly suppport it and reduce the aforementioned transfer of stress ratio (S.T.R.). Martin and Serdengecti (1984) bring this into the analysis and state that

$$\text{Subsidence} = (1\text{-d compaction})(\text{S.T.R.})(\text{S.S.F.}) \quad .. \ 6.3.5$$

where S.T.R. is the stress transfer factor, which is the transfer of stresses to the reservoir; and S.S.F. is the subsidence spreading factor, which is the subsidence/compaction ratio.

The stress transfer factor varies with the depth/diameter ratio and with the Young's moduli for the reservoir rocks and the adjacent rock materials. The stress transfer factor decreases markedly for depth/diameter ratios less than 0.5, the decrease being more pronounced with smaller Young's moduli. A finite element analyses performed by Martin and Serdengecti (Loc.Cit.) on reservoirs in Louisiana, shows that the subsidence/compaction ratio (S.S.F.) is only an approximate function of the depth/diameter ratio of the reservoir and not solely dependent on this as stated by Geertsma (1973) (Eqn. 6.3.4). This ratio, even when determined by finite element methods, has a range of values depending on whether the analysis is performed on an axi-symmetic or a plane strain model. Thus the type of deformation expected must be used to assess the validity of these subsidence/compaction values (Jones et.al., 1985a; 1985b; 1986).

The time dependency of reservoir subsidence as discussed in

Chapters 2.7, 4.3, 5 and 6.2.1, with the apparent preconsolidation effect, or non-linear response of subsidence with the reduction in the pore fluid pressure, has been presented in the literature by Bjerrum (1967), Martin and Serdengecti (1984), de Waal and Smits (1985), and de Waal (1986). This effect is attributed to time (strain/loading rate) effects of changes from geological to imposed draw-down loading rates. This non-linear response of subsidence is occasionally attributed to consolidation of clay layers though this is dismissed by Martin and Serdengecti (Loc.Cit.). The consolidation of clay layers can add to compaction of the reservoir, but would not cause this preconsolidation effect unless the deposit was subject to significant creep effects, Bjerrum (1967), Mesri and Godlewski (1977).

Another aspect of subsiding hydrocarbon reservoirs noted in the literature is the relationship between the volume of materials extracted from the reservoir and the volume of the surface subsidence depression (Castle et.al., 1969). This cannot be expected to be equal in all cases, due to the effects of the overburden described by Martin and Serdengecti (1984), and due to the mechanical properties of the materials surrounding the reservoir (Geertsma, 1973).

From the brief description presented above of the factors thought to affect surface subsidence over hydrocarbon reservoirs, a comparison of the various examples of oil field subsidence reported in the literature is unlikely to show any definite trend. Primarily this is due to the relatively few examples of this kind of deformation, and secondly because of the number of variables in the system, which are either not known or not reported in sufficient detail in the literature. The main examples of field subsidence are presented herein (Table 6.2) for comparative purposes of the most

Table 6.2 The main examples of subsidence due to hydrocarbon production

Field	Age and lithology of strata	Structure	Areal extent and depth to strata	overburden lithology pore pressure drop thickness of strata	Max. vertical subsidence, Max. subsidence rate	Start of prod. start of subs. area of subs.
Wilmington, California.	U Miocene-L pliocene Int. sands and clays	Anticline plunges NW, 5 N-S faults	29km^2 650m M = 1000m	sands and siltstones 2MPa (1960) 1500m	9m 71cm/yr (1952)	1936 1937$_2$ >75km^2
Inglewood, California.	Pliocene - Miocene sands	Anticline cut by inverse flower structure	5km^2 244m M = 900m	sands and shales 3.5MPa (1951-2)	1.73 - 3.5m 6cm/yr	1924 <1939$_2$ 31km^2
Buena Vista, California.	Tertiary sands	Active anticline above reverse fault	48km^2 M = 1130m		0.27m 3cm/yr	1910 1932
Kern Front, California.			19km^2 M = 745m		>0.34m	1912
Beverly Hills (East), California.	Miocene 3 sand reservoirs	Overturned anticline + faulting	3.4km^2 975 1630 2057m	163, 138, 129m	0.18m 2cm/yr	1966-7
Huntingdon Beach, California.		Anticline above fault zone	16km^2 M = 930m		1.22m	1920 37km^2
Long Beach, California.			7km^2 M = 1690m		>0.61m	1921 1925$_2$ 31km^2
Goose Creek, Texas.	Oligocene -Pliocene	Domed lenticular deltaic deposits	6km^2 M = 600m	6.9 - 8.2MPa 1160m	>1.0m >0.12m/yr	1917 1918$_2$ 11km^2
Chocolate Bayou, Texas.	Oligocene sands, clays and shales		69km^2 2650m	sands and shales 2500m	0.2m	1940
Saxet, Texas.	Upper Tertiary sands	Rollover fold on listric fault	25km^2 1800m		>0.93m (1942-59) 0.7cm/yr (1950-9)	1920
Bachaquero, Bolivia coast.	Miocene Int. sands + clays thickness 1/1	SW dipping beds, pinching out and onlapping	500-1300m	100m	3.7 (1970)	1936 1954
Lagunillas, Bolivia coast.	Miocene Int. sands + clays thickness 1/1	As Bachaquero	300-1200m		4.1m (1976)	1926 1929
Tia Juana, Bolivia coast.	Miocene Int. sands + clays thickness 1.8/1	As Bachaquero			0.2m (1960)	
Niigata, Japan.	Miocene - recent, sand sandstone + conglomerate	Broad NNE-SSW trough. Small anticlines exist	200m M = 500m	Silts, clays + sands Main prod. 600m	2m (1959-74) 0.5m/yr	1926 1955 600km^2
Po Delta, Italy.	Quarternary calcareous sands, some clay	Gentle undulations breaks in regional dips	Approx. 300m		0.12m (1964) 30cm/yr (1951-6) 20-25cm/yr(1958-9)	1938 1951-6 800km^2
Groningen, Holland.	L Permian Rotliegendes sandstone	Gently dipping strata to N. S,E + W flanks faulted.	900km^2 2900m	Zechstein evaporites Approx. 30MPa S = 70m, N = 240m	0.16m (1986) 0.7m calc. (by 2050)	1968-9
Ekofisk, North sea.	Danian + Maastrichtian chalks (2 reservoirs)	NW trending elongate dome overlying a salt diapir	49km^2 3000m	Tertiary shales Approx 27MPa (1987) 137, 76m	3.6m (1986) 45cm/yr (1986)	1970 1979 Approx. 50km^2

qualitative nature. For more details on the individual fields and examples of ground water extraction, the reader is referred to AIHS-UNESCO (1969), AIHS (1976), Saxena (1978), Reviews in engineering geology (1969; 1984), Verhandelingen van het Koninklijk Nederlands geologisch mijnbouwkundig Genootschap (1973), Proceedings of the Forum on subsidence due to fluid withdrawals (1982), Principia Mechanica (1985) and Jones et.al. (in press) from which most of the data in Table 6.2 is abstracted. The hydrocarbon reservoirs presented in Table 6.2 are the main examples subsidence cases, for which there are details in the literature. Some limited information on smaller fields where subsidence has occured can be found in Yerkes and Castle (1969) and Kreitler (1976); these have not been included in Table 6.2. Fields which are subsiding or suspected to subside in the near future have with the exception of two notable cases, Groningen and Ekofisk, have been ommited from the table also; this is due to the limited information concerning these fields at the time of writing this thesis. The hydrocarbon reservoirs falling in this category include the E11 and F23 fields in Central Luconia (offshore Sarawak), in east Malaysia (van Ditzhiujzen and de Waal, 1984), West Ekofisk (0.5 - 0.6m subsidence) and Eldfisk (0.3 - 1.2m) (Wiborg and Jewhurst, 1986) and Valhall (Jones pers. com.) all in the chalk group in the Central North Sea.

6.4) DISCUSSION

The data for North Sea chalks and clays tested during this study have been used in an analysis to predict the amount of subsidence that is likely to occur in the Ekofisk field in the Central North Sea. The data used in the solution of this problem were the uniaxial stress-strain curves for the chalks and clays presented in this

thesis. results were generalised into stress-strain curves for several porosities thought to be representative of the behaviour of the chalks; the curves were adjusted to zero strain for the vertical effective stress at the start of production. Using these average curves, a model of the field was built up and averaged into the different porosities, i.e. the reservoir was considered to consist of a number of porosity bands. The deformation of the field due to increasing effective stress, was then analysed in a finite element model, the output giving compaction of the field and the amount of surface subsidence. This finite element study has been performed by several workers, is too lengthy to present here to an adequate level and at this time is confidential: This study has been reported by Jones et.al. (1985a; 1985b; 1986) and Leddra (1987). The study does not consider the effects of strain rate, as accurate correction factors for the stress-strain behaviour of chalk have not been formulated to date. However, the analyses presented by these workers, does investigate a number of compaction related variables, and have demonstrated how the transfer factor (S.S.F. of Martin and Serdengecti, 1984) varies with reservoir curvature, and how this alters the total stress distribution acting in the overburden.

From the experiments performed in this study it is shown that the initial reservoir pressures should be reproduced before loading the samples along the K_o stress path is commenced. This initial consolidation eliminates the strain due to the elastic relaxation which occurs during core recovery from depth. As seen in Chapter 4 the initial pre-loading stress affects the compressibility of the pore collapse deformation, the extreme example of this occurring when the pore collapse occurs at constant q and p', Fig. 4.22 and Fig. A5.17.

The prediction of subsidence associated with drawdown in a hydrocarbon reservoir concerns many aspects of sediment deformation and includes numerous variables which should be assessed as important or otherwise to the formation of the surface subsidence depression. Some of the variables required for such a study can be derived from an experimental investigation, the results of such an experimental study on reservoir material generally taking the form of a stress-strain relationship. In reservoirs where only an elastic reaction to stress occurs in the producing formation, such a deformation can be calculated using the conversion from strains obtained in hydrostatic experiments to uniaxial strain, Teeuw (1971), Chap. 4.6 and Chap. 6.2. However, if plastic deformations occur in response to increases in effective stress in the reservoir, K_o (uniaxial) experiments must be performed; as the strain in such materials is due to the applied stress system and not the mean effective stress, Chap. 2.5, Chap. 4.6. The reliability of the stress-strain relationship is paramount to studies of compaction and subsidence, and as such their translation to, field behaviour is required. This translation has been described in Chapters 2 and 6. Other factors which should be taken into account when translating laboratory experiments to field conditions are i) the temperature dependance of the stress-strain relation and ii) the effect of sample size on the results obtained. The first of these is easily studied, though the second is obviously restricted to the size of cores recoverable during drilling operations in hydrocarbon reservoirs. In a study of reservoir compaction, large numbers of samples need to be tested to enable an accurate model of the reservoir behaviour to be determined. The mechanical properties of the overburden and other adjacent formations should also be assessed in parallel with the

studies on the producing formations, and not automatically treated as elastic, especially when for shale overburden, sand lenses and/or a pervasive joint system exists.

Having defined the stress-strain relationship of the reservoir material, the subsequent modelling of the reservoir compaction should be performed by a computer using either a finite element or finite difference method, though the nucleus of strain approach can be used for elastic materials or for a first approximation of subsidence, Geertsma (1973). Finite element and finite difference models allow the arching effects in reservoirs, different reservoir materials, and non-uniform pore pressure decrease in the reservoir to be incorporated into the analyses. The accuracy of any computer modelling is dependant upon the mechanical properties of the materials inserted into the program, and as such, the determination of these parameters as well as the structure (including the spatial variation of porosity, and distributions of faults and joints) in the reservoir is of great importance.

Having presented some points of clarification on certain approaches to subsidence prediction, the conclusion of this chapter will discuss the errors in such a study, which still have to be resolved.

1) The elastic reaction of granular sediments at high stresses (>10 - 20MPa) can only occur if the material is well cemented, and does not yield. Unconsolidated sands generally should not react elastically due to the susceptibility of individual grains to grain crushing - this will be seen during uniaxial loading, with very little effect seen under a hydrostatic stress system, as such, the correct stress system must be used in experiments which investigate subsidence in hydrocarbon reservoirs.

2) The translation of the stress-strain relationships to field loading (strain) rates should, and probably will become established practice during such investigations, and will not be discussed further here.

3) A remaining serious error concerning subsidence prediction concerns the cores tested, and the sample disturbance caused by drilling. The samples recovered from the reservoir are subject to weakening resulting from

a) the increase in stress during the approach of the drillbit,

b) the vibration of the sample by the drillbit,

c) the stress change associated with coring,

d) the stress relief and elastic expansion of the constituents of the rock/sediment skeleton,

e) the thermal contraction of the mineral skeleton,

f) possible generation of negative pore water pressures in low permeability samples (shales) and influx of drill fluid into the sample.

With the exception of points c) and f), these factors could seriously affect the bonds forming the grain to grain contact in cemented samples and lower the strength of recovered samples. These factors have not been assessed to the authors knowledge, partly due to the difficulty in reproducing such effects and assessing the variables parametrically.

The stress-strain relationships obtained for reservoir material will allow the prediction of the porosities of materials present in the reservoir at any time during the pore pressure drawdown. The accuracy of such a calculation can be correlated against porosities determined from down hole measurements, performed at times during the drawdown and production of the field. However, it has been observed

in the Ekofisk field that high porosity chalk still exists for effective stresses under which the chalk should have collapsed to lower porosity levels (Jones pers.com. 1987). The evaluation of maximum porosities which should have existed in the Ekofisk field (for particular effective stress increases), was calculated from laboratory tests. It is suggested that the above factors of sample weakening could be responsible for such an observation. However, such factors as non-uniform pore pressure reduction in the reservoir and arching effects above high porosity lithologies make the weakening effect due to drilling disturbance of lesser importance.

4) This study has not involved computer modelling of subsidence, but one aspect will be briefly introduced to terminate the above discussion on possible errors in subsidence studies. The area of doubt concerns the transfer factor of compaction in the reservoir to the surface subsidence, values of the transfer factor have been predicted for Ekofisk by Barton et.al (1986), and range from 0.5 to 0.7, the range being the error in the prediction of possible subsidence; the values obtained being dependant upon the type of computer modelling employed (Jones et.al., 1985a; 1985b; 1986, in press). The accurate determination of this factor is obviously of great importance, the value being dependant upon the reservoir geometry, structure and mechanical properties of the overburden. One possible method of more accurately evaluating such a transfer factor, is to construct a scale model of the overburden with scaled stresses, dimensions and material properties (Sauer and Gonano, 1979; Bandis et.al., 1987).

The compaction of a hydrocarbon reservoir involves many complex and misunderstood factors, until such factors are assessed and are of a form which can be modelled, many errors will occur in such studies.

The understanding of some of these factors would also allow a greater understanding of reservoir behaviour, with possible improved productivity due to more accurate reservoir production planning.

CHAPTER 7

THE STATE OF STRESS DURING BURIAL OF SEDIMENTS

7.1) INTRODUCTION

This chapter contains a brief discussion of the state of stress existing in sedimentary basins which are unaffected by tectonic forces. This is an idealised case which the K_o test represents in the laboratory. A knowledge of the state of stress in basins is required for evaluating the initial stress conditions for subsidence problems and for hydraulic fracturing studies.

7.2) VERTICAL STRESS

Many studies in the past have analysed the porosity loss that occurs in sediments during burial (see Rieke and Chilingarian (1974) for a review). The porosity of a sediment is a function of the stress system and not simply a function of the depth. If the total stress system is completely passive, then the horizontal stresses acting will be related to the vertical stress, and both will increase with depth. The corresponding effective stresses may not increase however, if excess pore pressures exist in the sediment. Therefore to describe the probable stresses acting on a unit at depth, one must first know the vertical effective stress; this is assumed to be the maximum effective stress for a tectonically passive area.

The increase in vertical stress with depth of burial in a basin, is described as the geostatic gradient and is assumed to be more or less constant for most applications at 23kPa/m (1.0 psi/ft) (Prats, 1981;

Breckels and van Eekelen, 1981). This assumes that the amount of total stress supplied by a unit of sediment to underlying units is constant regardless of depth of burial, and hence does not take into account the effect of compaction on the density of a unit of sediment. Jaky (1948a) separated the volume reduction of a sediment, based on compression of dry sand to 20MPa, into two sections: the first was linear in e-log p' space. This was valid to a maximum of $\sigma_{1,1}'$ = 0.4MPa. The second section for compression obeys a power parabolic law, which is of the form

$$e = e_o - C_1.\sigma_1'^{m} \qquad .. 7.2.1$$

The geostatic stress at stresses less that $\sigma_{1,1}'$ can be represented by the equation

$$y = \frac{A.\sigma_y}{S} - \frac{C_1}{S} \ln \sigma_y - 1 \qquad .. 7.2.2$$

while at stresses greater than $\sigma_{1,1}'$

$$y = \frac{\sigma_y}{\gamma_o} - \frac{C_1}{S(m+1)}.\sigma_y^{m+1} \qquad .. 7.2.3$$

Where y = depth, σ_y = the stress at depth y, γ_o = the specific weight of the sediment in the original state, and equal to $S/(1+e_o)$, and S = density of the mineral grains. The deviation of the two formulae at low stresses is small, and Eqn. 7.2.3. is assumed to hold. Using a constant specific weight in the calculations, gives values 10% lower than the real situation, where the specific weight of a unit of

sediment increases with depth.

The case described above is obviously idealised, where the nature of the sediment is assumed to be constant, real sedimentary basins generally contain a sequence of different sediments, with differing compaction properties. Therefore in a field situation the only accurate method of obtaining the vertical stress is to integrate the information from well logs. In a real basin overpressuring (underconsolidation) and overconsolidation occurs, which will also affect the sediment's specific weight. The total stress supplied by a unit of sediment at depth also includes the contribution of pore fluid. The specific gravity of the pore fluid will vary not only with depth but also with formation, as will the pore fluid pressure. Thus, the vertical effective stress will be, in most cases, an approximation.

7.3) HORIZONTAL STRESS

Several workers have attempted to calculate the horizontal stresses acting in basins, using geometrical indicators of stress (Currie, 1967), theoretical considerations (Prats, 1981), analysing data from hydraulic fracturing and formation integrity tests (Hubbert and Willis, 1957; Breckels and van Eekelen, 1981), and more recently from strain recovery measurements from core material (Voight, 1968, Teufel, 1982; 1983; Blanton, 1983; Blanton and Teufel, 1983; Teufel and Warpinski, 1984; Lacy, 1984).

Currie (1967) describes the methods that could be used to determine the stress in a basin using hydraulic fracturing, and also how the evolution of stresses in a basin can be estimated from structures, such as folding and faulting. Prats (1981) through considering the burial of two adjacent strata, a shale and a sandstone state that the

horizontal stress in the shale will be larger than in the sandstones. This is based on a variation of elastic response in the sediments, and a response to increasing temperature during burial. This qualitative study assumes an exponential variation with depth of the elastic properties, density, and horizontal strain, the quantity of geothermal expansion of the sediments was assumed to be the same for both strata. Various conditions were assumed for different cases, to assess the sensitivity of the study to the aforementioned parameters. The geothermal gradient was assumed to be constant in all eight cases considered. The only significant difference between the eight cases of varied conditions, arose from differences in the thermal expansions of the strata, and from applying a creep law to the sediments. The higher the thermal expansions of the shale relative to the sandstone the larger the difference between the stresses in the contiguous strata. The creep also caused an increase in the stress in the shale relative to that in the sandstone. The approach is qualitative and the variations in parameters are not accurate but assumed, better knowledge of the properties of these sediments at depth would help to quantify this approach. The horizontal stress gradient calculated for the sandstone is 12 to 17kPa/m (0.53 to 0.77psi/ft) while for the shale it is 15 to 20kPa/m (0.67 to 0.87psi/ft) (Prats, 1981).

Breckels and van Eekelen (1981) present horizontal stress gradients obtained from hydraulic fracturing tests and formation integrity test data from the Gulf Coast Texas, Venezuela, Brunei, the North sea, and the Netherlands. They show that the same kind of trend in horizontal stresses with depth occurs in each of the five areas for normally consolidated formations, and they present relationships for the increase in horizontal stress with depth taking into account pore pressure variations. The data are used to evaluate the

difference for horizontal stresses obtained from the two methods mentioned above, which suggest that the leak-off tests (formation integrity) give results 11-15% higher than the instantaneous shut-in pressure (ISIP) obtained from hydraulic fracturing tests. The effect of lithology was also analysed for the Netherlands and North Sea areas. Breckels and van Eekelen (1981) show that shales have horizontal stresses 3-7MPa (30-70bars) higher than sandstones (depending on the sandstone) at a depth of 2500m for the Netherlands while the difference between shales and sandstones in the North Sea is between 0-5%. The difference in the Netherlands is 3-4 times as large as in the North Sea and considered to be significant.

The trends of horizontal stress with depth obtained by Breckels and van Eekelen (1981) are presented in Table 7.1 and 7.2. Table 7.1 summarises the trends for hydraulic fracturing tests. The second set of relationships (Table 7.2) relate to formation integrity tests, and as described above give higher stresses for a given depth, due to a hoop stress effect in the tests.

Table 7.1 Variation of horizontal stress with depth, calculated from hydraulic fracturing data (From Breckels and van Eekelen, 1981).

Area	Hydraulic fracturing tests S_h =	Depth
Gulf Coast	$0.053D^{1.145}+0.46(p_o-p_{on})$	(D<3500m)
Venezuela	$0.0565D^{1.145}+0.56(p_o-p_{on})$	(1800<D<2800m)
Brunei	$0.061D^{1.145}+0.49(p_o-p_{on})$	(D<3000m)

Table 7.2 Variation of horizontal stress with depth, calculated from formation integrity tests (From Breckels and van Eekelen, 1981).

Area	Formation integrity test Leak-off pressure =	Depth
Gulf Coast	$0.059D^{1.145}$	(D<3500m)
North Sea	$0.089D^{1.091}$	
Netherlands	$0.085D^{1.104}$	

The relationships shown above are seen to obey a power law for the increasing horizontal stress with depth. This is what one would expect when the analysis of the vertical stress gradient (Jaky, 1948a) is combined with the observation of an approximately constant K_o for normally consolidated sediments. The tests shown in App.5 indicate that for normally consolidated sediments, the K_o remains reasonably constant up to pressures of 120MPa (1200bars), though this does include some degradation effects of the grains. Thus, if the stress - depth relationship does increase as described by Jaky, the horizontal stresses obtained from the series of tests described in this study would agree with the observations and analysis described by Breckels and van Eekelen (1981). The effects of temperature in tests reported in this thesis did not appear to alter the K_o, though during gradual heating with increasing stress, this may occur as described by Prats (1981). This constant linear trend of K_o for normally consolidated sediments with increasing stress has been shown by other authors (Abou-Sayed, 1982; Chap. 3), and would thus seem a reliable way of predicting horizontal stress in "tectonically relaxed" areas

(Abou-Sayed, 1982). However, under sub-surface conditions, reservoir material may be fractured and jointed and these discontinuities will affect the state of stress acting in-situ (Barton et.al., 1986).

In a passive sedimentary basin the maximum effective stress is assumed to act in the vertical direction due to the weight of the overburden. The intermediate and minimum effective stresses will not be equal if tectonic stresses are present; even though both may act in the horizontal plane. This has been demonstrated by Teufel (1982; 1983) and Teufel and Warpinski (1984) for the Piceance Basin in Colorado. The stresses acting in the basin have been determined by strain relief techniques (Voight, 1968) as well as by hydraulic fracturing tests. The orientations of the principle effective stresses determined from these two techniques being coincident. The magnitudes of the stresses acting in the basins give reasonable agreement, with the results obtained from the anelastic strain recovery measurements being 12% higher than those obtained from the hydraulic fracturing tests. The difference in magnitudes of the two horizontal principle effective stresses for the Piceance Basin range between 2.6 and 2.8 MPa, when calculated from either of the aforementioned techniques (Teufel and Warpinski, 1984).

The in-situ stress determinations using the strain relaxation method, gives in situ effective stress ratios of $\sigma_{Hmax}'/\sigma_v' = 0.87 \pm 0.2$ and $\sigma_{Hmin}'/\sigma_v' = 0.70 \pm 0.2$ for the Rollins sandstone (Teufel and Warpinski, 1984) while for Devonian shales in Ohio, $\sigma_{Hmax}'/\sigma_v' = 1.60 \pm 0.05$ and $\sigma_{Hmin}'/\sigma_v' = 0.73 \pm 0.08$. These values are not in accordance with the values obtained from hydraulic fracturing data presented above nor with the K_o values obtained in this study, where distinct differences in the ratio of effective stresses are obtained between sand or sandstones and clays or shales. This probably reflects

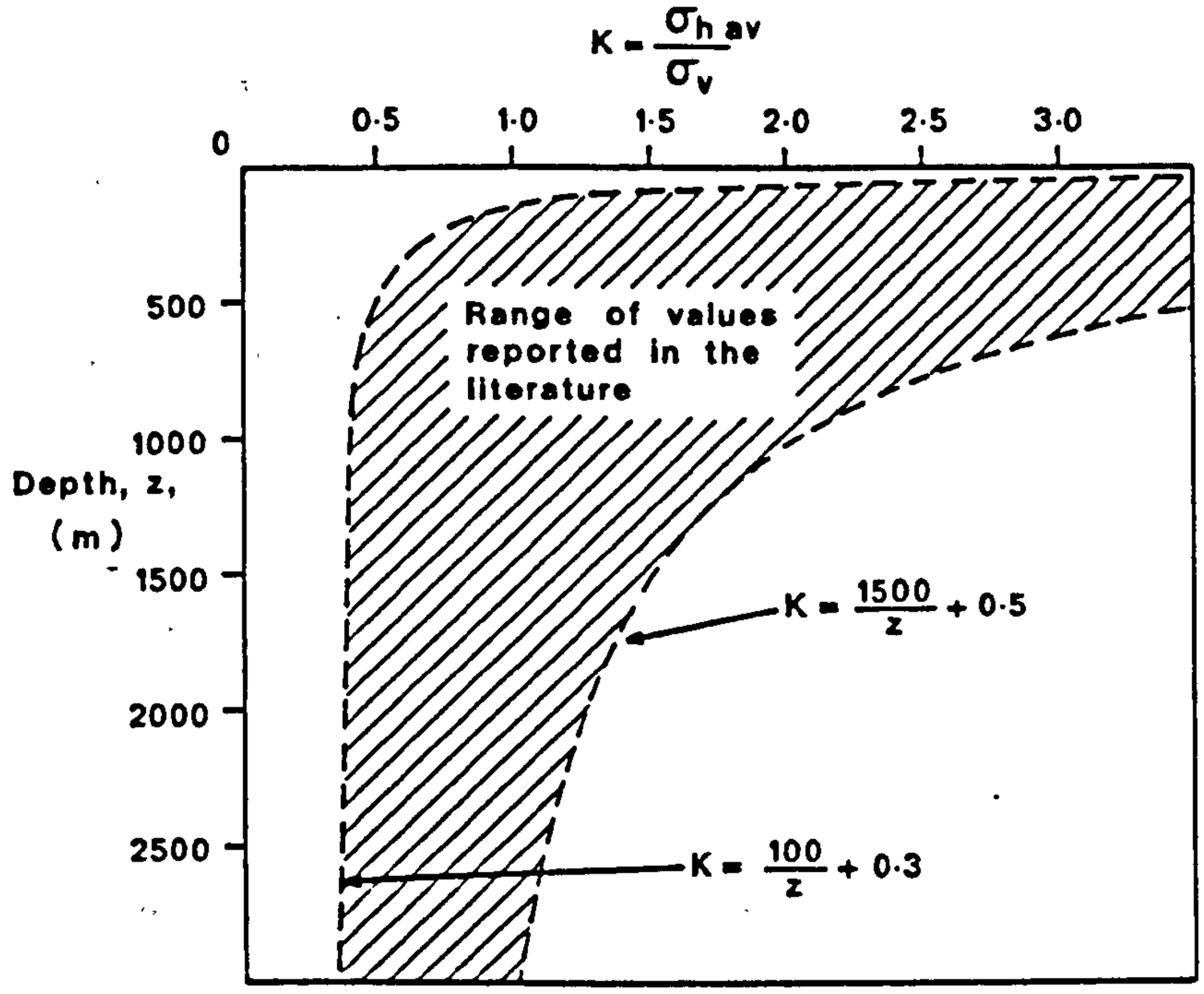

Figure 7.1 Variation of ratios of horizontal to vertical stress with depth reported in the literature (After Brown and Hoek, 1978).

the influence of the tectonic stress field on the in situ stresses.

In areas of large tectonic stresses the tectonic forces tend to dominate the local stress system. This has been discussed extensively by many workers for onshore sites. Brown and Hoek (1978), have reviewed the data on this subject, and show that a tectonic stress can predominate over large areas, with trends for horizontal stresses against depth being applicable on a "sub-continent basis". They present evidence which shows that for tectonically stressed areas the horizontal stresses can be larger than the vertical, with a greater spread of results at shallow depths.

It is apparent from the above discussion that K_o tests can not be used to predict horizontal stresses which exist in basins, other than

in those basins which have not been subjected to tectonic stresses. However, this fact has to be established before K_o results are used; therefore K_o test results can be used only as a first approximation for the prediction of horizontal effective stresses occurring in different lithologies. During the increase of stress through hydrocarbon production or through the application of tectonic stresses, yield of a cemented rock can occur. Any tectonic stresses locked into the rock will be lost upon yield and the K_o stresses could dominate, the re-establishment of tectonic stresses will only occur after substantial strain hardening. This condition requires that a large strain occurs in the rock, which will only occur over a long period of time at geological strain rates . Over short periods of time, yield occurring in soft high porosity layers leads to the dissipation of tectonic stresses, however, stronger low porosity layers will remain intact and retain the original built in stresses. Therefore a situation will exist where the competant rocks will deform towards the yielded rocks, this deformation occurs until the yielded material has compacted enough to resist the displacements. This can be thought of as an analogous process to that existing upon excavation of a cavity or tunnel, with the possibility of large shear deformations existing juxtaposed to the boundary of the yielded and intact material. Subsequent to the yielding of sedimentary materials and during compaction of unconsolidated sediments generally, the possibility of sediment flow from crests of structures to the flanks in dipping strata may occur. Alternatively, lateral flow of sediments might occur in extensional areas resulting in greater magnitudes of compaction (Shepherd and Bryant, 1983). However, such questions as these require numerical simulations to evaluated the importance of these mechanisms, and will not be discussed further.

The influence of sediment deformations and K_o stresses on sedimentary structures has been discussed briefly in the literature (Jones and Addis, 1984; 1985b; 1986; Addis and Jones, 1985a), and for the sake of brevity will not be discussed here. The reader is referred to the aforementioned references for discussions on this subject.

CHAPTER 8

CONCLUSIONS

The experimental programme reported in this thesis, is one of only a few high pressure studies performed under K_o conditions in a triaxial cell, and one of even fewer studies on the high pressure compaction of chalks. The studies of the mechanical behaviour of hydrocarbon bearing chalks that have been undertaken during the last couple of years, have primarily been in response to the subsidence, and other reservoir engineering problems pertaining to the chalk fields in the Norwegian sector of the North Sea. The released data on this subject will hopefully increase in the coming years, as further studies are completed.

The experimental study presented in this thesis considers and discusses many aspects of compaction of both chalks and clays at large consolidation stresses. The chalk can be considered as an ideal bonded material, and is therefore a good model for the behaviour of cemented, porous rocks. The few clay experiments are included primarily for comparison and indicate that bonded and particulate materials exhibit different behaviour at these stress levels. K_o tests form the majority of the tests performed, and a number of questions concerning the testing methodology of high pressure K_o tests have also been addressed. The study has elucidated several aspects of the uniaxial compaction of chalk, and has tried to independently rationalise the influence of different mechanical variables on the deformations. These studies have lead to the

formulation of an outline description of the compaction behaviour, specifically for the chalk, and for bonded sedimentary materials in general. The main points brought out in this thesis will now be briefly summarised.

1) The hydrostatic testing of reservoir materials predominant historically in reservoir subsidence studies cannot be applied to chalks, this has been discussed in Chapter 4 and is in full agreement with the conclusions of Smits et.al. (1986). The testing method required to perform tests representative of sediment burial or drawdown in a reservoir is the uniaxial or K_o test.

2) The K_o test is very sensitive to small changes in the radial strain, a gradual variation of 2 microns having a marked effect on the stress path plotted in q-p' space, Fig. 4.16b. The data concerning short term large lateral strains, is conflicting. The North Sea samples EC5.20, Fig.A5.5, and EC8.20, Fig.A5.7, show the effect of a negative radial strain of 2.7 microns for approximately 0.7% axial strain, this resulted in a offset in the stress-strain curve of 4MPa deviatoric stress. EC8.20, encountered a large positive radial strain of approximately 10 microns which caused a drop in the deviatoric stress of 3MPa. Both of these variations occurred in or close to the pore collapse region of the deformation. However, a large radial strain variation was observed in BH14.60, Fig.A5.25, whereupon the strain was recovered, the stress-strain curve was not radically affected, the plot being continuous after recovery of the strain with no offset, as was seen in the tests EC5.20 and EC8.20. Large strains are also observed in other tests with little effect on the stress strain curve. Therefore it is assumed that relatively

large radial strains (>5 microns) can be experienced by the sample in a K_o test without any great effect, as long as the strain is recovered relatively quickly, in terms of axial strain. The tests PB5.20 and PB6.20 showed that a gradual radial change of 2 microns affected the q-p' plot markedly, while the stress-strain plots remained unaffected. This suggests that the North Sea chalk samples where the condition of zero radial strain were controlled by hand, may have undergone larger strains than recorded by the logging system. The amount of strain allowable for a particular material will probably depend upon the dominant grain size.

3) The variables of chalk compaction have been discussed in Chapter 4. The porosity and cementation strength were seen to be the main factors affecting each sample. The test variables also affected the deformations. The strain rate was seen to affect the stress-strain curves of the chalk, however for the chalk tested, from Pegwell Bay, no regular trend with strain rate could be observed for the whole curve as might be expected. The normal consolidation part of the deformation was however found to give a reasonable trend when normalised from the start of normal consolidation. It was concluded that the lack of any definite trend was probably a function of the weak cementation in this chalk, the few samples tested and the small range of strain rates incorporated in the study. Variations in the height of the sample, at constant diameter was seen to have a marked effect on the deformation of the samples. The $\bar{K}_o$ values were not affected, as expected, by the closer proximity of the end platens, however the stress-strain curves showed far more strain with the shorter samples, for similar deviatoric stresses. This should be investigated independantly on different equipment before conclusions

are drawn. This sample shape effect was seen to be independant of strain rate. The effect of temperature on compaction was investigated, as the oil reservoirs in the Central North Sea are at temperatures of approximately 120-130^{o}C. Three tests on onshore chalk from Butser Hill with 13% insoluble residues in the form of clay minerals, showed that the temperature did not affect the the magnitude of the compaction, the variation in the magnitude of the compaction being attributed to porosity variations in the samples. For the above tests the results were analysed for the normally consolidated part of the deformation by a normalisation procedure modified slightly from that suggested by Leroueil and his co-workers.

4) The samples of chalk were seen to deform with three distinctive sections. The first was an elastic response to stress, the second following the yielding of the cementation was one of bond breakage and grain rearrangement, the third being one of consolidation, or further compaction. These deformations were analysed in terms of a Critical State type soil model. The chalks were seen to degrade slightly during the compaction process. The yield strength of the chalks were seen to increase with decreasing porosity, the Young's modulus increasing also, as observed with other carbonate sediments (Saxena, 1982).

5) The coefficient of consolidation of chalks is difficult to measure in standard laboratory tests, Rosenbaum (1978), so for the tests performed in this study, the constant rate of strain analysis was used. The results from this analysis seem to give very reasonable results for the magnitudes of the C_vs and the permeabilities, and the decrease of these quanities during compaction. The C_v and

permeabilities were not seen to be affected significantly by temperature variations, once the values of viscosity and density of the pore fluid had been corrected for the test temperature. The permeability decreases with increasing stress and decreasing void ratio, were seen to be different for the three sets of chalk samples tested. The decrease for the North Sea samples were seen to be identical despite the different porosities of the samples. This is assumed to be due to the diagenetic history of the sediment. The Pegwell Bay samples showed slight curvature of the plots, showing a tendancy to one value. This curvature was attributed to the greater grain crushing in the Pegwell Bay samples. The North Sea and Butser Hill samples showed linear decreases in the normal consolidation deformations in the plots presented, Chapter 4. These permeability data are the only results for high pressure uniaxial compaction experiments so far reported.

6) The compaction of the high porosity chalks can be seen to involve large deformational strains, and as such the use of pre-existing methods of analysis of reservoir compaction, based on elastic theory, cannot be applied to the compaction of chalk reservoirs. The use of soil mechanics theory to build a model for the compaction of chalk is is necessary because of the degradation of the cementation bonds during compaction, leading to a silt like sediment which is able to flow into wells and has been likened to "putty" and "toothpaste". It is likely that other high porosity cemented sediments will exhibit a similar type of structural breakdown. Probably the closest material analogs to the chalks are the "sensitive clays".

7) The K_o stress path for the deformations in the normally

consolidated range of stresses for the chalks and the clays was seen to be constant up to stresses used in this study. The vertical effective stresses attained in this study were 120MPa, in the light of earlier published work on sand compaction, it would seem reasonable to assume that the chalk particles gradually degraded during compaction in the normal consolidation deformation, the particle breakdown being initiated in the pore collapse region.

8) The breakdown of chalk skeleton and mineral grains during the undrained incremental loading of the chalks in an oedometer lead to B values greater than unity.

9) The relationship between the friction angle and the K_o for a material, Jaky's equation, has not been extended into the high pressure region (where grain crushing occurs) in this study. It was hoped that the results would permit this analysis to be performed, however, due to experimental difficulties during shearing, these results were not sufficiently reliable. In addition, too few samples were tested to obtain the failure envelope of the chalk.

10) The results of the experiments performed on clays show that these will compact, over a pressure increase commonly encountered in overpressured reservoirs. The time dependancy of the deformation is however large, and as such, the contribution of this to the deformation of a reservoir will be dependant upon the number of drainage boundaries within the clay stratum.

This thesis has addressed many questions concerning the compaction of sediments at high stresses, and as such may not be as complete as

might be expected. The individual parameters investigated such as strain rate, temperature, sample shape etc. would probably each take the equivalent of a thesis to study thoroughly, and thus, this work must be considered as an overview of sediment and chalk compaction at high stresses.

None of the principles or laws of soil mechanics can be automatically assumed, at the stresses used in this thesis, as is possible at the stress levels normally used in soil mechanics studies. As such the work presented herein asks many questions fundamental to the deformation of sediments at high stresses. Hopefully future studies will approach and answer these.

REFERENCES

Abou-Sayed A.S. (1982): Laboratory evaluation of in-situ stress contrast in deeply buried sediments.
SPE paper 11069, SPE 57th Annual Conf., New Orleans, Sept. 26-29

Abdelhamid M.S. and Krizek R.J. (1976): At-rest lateral earth pressure of a consolidating clay.
J. Soil Mech. Found. Div., Proc. ASCE, v102, GT7, p721-738

Addis M.A. (1987): Material metastability in weakly cemented sedimentary rocks.
Memoir of the Geological Society of China, No.9, Taiwan (in Press)

Addis M.A. and Jones M.E. (1985): Volume changes during diagenesis.
Marine and Petroleum Geology, 1985, v2, p241-246

AIHS-UNESCO (1969): Land subsidence, Proceedings of the 1st Int. Symp. on Land subsidence, Tokyo 1969, v1 and 2. AIHS Publication Nos. 88 and 89

AIHS (1976): Land subsidence symposium, Proceedings of the 2nd Symp. on Land subsidence, Anaheim 1976, AIHS Publication No. 121

Al-Hussaini M.M. and Townsend F.C. (1975): Stress -deformation of sand under K_o conditions.
Proc. 5th. Panamerican Conf. Soil. Mech. Found. Engng., v1, Buenos Aires, p129-136

Al-Hussaini (1981): Comparison of various methods for determining K_o. Laboratory shear strength of soil, ASTM STP740, R.N.Yong and F.C.Townsend, Eds., American Society for Testing and Materials, 1981, p78-93

Allen D.R. (1968): Physical changes of reservoir properties caused by subsidence and repressuring operations.
J. Petrol. Tech., Jan 1968, p23-29

Alva-Hurtado J.E. and Selig E.T. (1981): Survey of laboratory devices for measuring soil volume change.
Geotech. Test. J., GTJODJ, v4, No.1, p11-18

Anderson M.A. (1985): Predicting reservoir condition pore- volume compressibility from hydrostatic-stress laboratory data.
SPE paper 14213, SPE 60th Annual Conf., Las Vegas, Sept 22-25

Andrawes K.Z. and El-Sohby M.A. (1973): Factors affecting the coefficient of earth pressure K_o.
J. Soil Mech. Found. Div., Proc. ASCE, v99, SM7, p527-539

Atkinson J.H. and Bransby P.L. (1978): The mechanics of soils-An introduction to critical state soil mechanics.
McGraw Hill Book Company (U.K.) Ltd.

Baker W.H. and Krizek R.J. (1969): Pore pressure equation for

anisotropic clays.
J. Soil Mech. Found. Div., Proc. ASCE, v95, SM2, p719-724

Baldwin B. and Butler C.O. (1985): Compaction curves.
Am. Assoc. Petrol. Geol. Bull., v69, No.4, p622-626

Bandis S.C., Lindman J. and Barton N. (1987): Three-dimensional stress state and fracturing around cavities in overstressed weak rock.
6th Int. Cong. Rock. Mech., Montreal, Sept. 1987, v2, p769-775

Baranski T. and Wolski W. (1986): Lateral strain measurement by an ultrasonic method.
Consolidation of soils: Testing and evaluation., ASTM STP 892, R.N. Yong and F.C. Townsend, Eds., American Society for testing and Materials. p516-525

Barton N., Harvik L., Christianson M., Bandis S.C., Makurat A., Chryssanthakis P. and Vik G. (1986): Rock mechanics modelling of the Ekofisk reservoir subsidence.
Proc. 27th U.S. Rock Mech. Symp., Tuscaloosa, p267-274

Been and Sills (1981): Self-weight consolidation of soft soils: an experimental and theoretical study.
Geotechnique, v31, No.4, p519-535

Bell F.G. (1977): A note on the physical properties of the chalk.
Engineering Geology, v11, p217-225

Bevan T.G. and Hancock P.L. (1986): A late Cenozoic regional mesofracture system in southern England and northern France.
J. Geol. Soc. Lond., v143, part 2, p355-362

Bishop A.W. (1958): Test requirements for measuring the coefficient of the earth pressure at rest.
Proc. Brussels Conf. on Earth Pressure Problems, p2-14

Bishop A.W. (1973): The influence of an undrained change in stress on the pore pressure in porous media of low compressibility.
Geotechnique, v23, No.3, p435-442

Bishop A.W. (1976): The influence of system compressibility on the observed pore pressure response to an undrained change in stress in saturated rock.
Geotechnique, v26, No.2, p371-375

Bishop A.W. and Eldin A.K.G (1953): The effect of stress history on the relation between 0 and the porosity in sand.
Proc. 3rd Int.Conf. SMFE, v1, p100-105

Bishop A.W. and Green (1965): The influence of end restraint on the compresssion strength of a cohesionless soil.
Geotechnique, v15, No.3, p243-266

Bishop A.W. and Henkel D.J. (1962): The measurement of soil properties in the triaxial test. 2nd Ed.
Edward Arnold Publishers Ltd.

Bishop A.W., Kumapley N.K. and El-Ruwayih A. (1975): The influence of pore water tension on the strength of clay.
Phil. Trans. R. Soc. Lond., 278A, (1286), p511-554

Bishop A.W. and Skinner A.E. (1977): The influence of high pore water pressure on the strength of cohesionless soils.
Phil. Trans. R. Soc. Lond., 284A, (1318), p91-130

Bishop A.W., Webb D.L., and Skinner A.E. (1965): Triaxial tests on soil at elevated cell pressures.
Proc. 6th Int. Conf. S.M.F.E.,

Bishop A.W., Webb D.L., and Lewin P.I. (1965): Undisturbed samples of London Clay from the Ashford Common shaft: Strength - effective stress relationships.
Geotechnique, v15, No.1, p1-31

Blanton T.L. (1978, 1981): Deformation of chalk under confining pressure and pore pressure.
European Offshore Conf. 24-27th Oct. 1978
also; Soc. Petrol. Eng. J., Feb 1981, p43-50

Blanton T.L. (1983): The relation between recovery deformation and in-situ stress magnitudes.
SPE/DOE paper 11624, SPE/DOE Symp. on Low Permeability, Denver, March 14-16

Blanton T.L. and Teufel L.W. (1983): A field test of the strain recovery method of stress determination in devonian shale.
SPE paper 12304, Eastern Regional Meeting, Champion, Nov. 9-11

Botter B.J. (1985): Pore collapse measurements on chalk cores.
Chalk Research Group Symp., Stavanger, May 1985, v2

Breckels I.M. and van Eekelen H.A.M. (1981): Relationship between horizontal stress and depth in sedimentary basins.
SPE paper 10336, SPE 56th Annual Conf. San Antonio 1981

Brighenti G. (1967): Influence of pore pressure decline on the behaviour of petroleum reservoir rocks.
7th World Petrol. Cong., Mexico City, v3, p97-105

Bromley R.G. (1984): Bioerosion.
Workshop notes on "processes in carbonate enviroments", held at Wye College, University of London. 28th June - 3rd July 1984

Brooker E.W. and Ireland H.O. (1965): Earth pressure at rest related to stress history.
Can. Geotech. J., v2, No.1, Feb 1965, p1-15

Brown E.T. and Gonano (1974): Improved compression test technique for soft rock.
J. Geotech. Eng. Div., Proc. ASCE, v100, GT2, p196-199

Brown E.T. and Hoek E. (1978): Trends in relationships between measured in-situ stresses and depth.

Int. J. Rock. Mech. Min. Sci and Geomech. Abs., v15, p211-215

Brown E.T. and Michelis P.N. (1978): A critical state criterion for strain-softening rock.
Proc. 19th U.S. Rock Mechanics Symposium, p515-519

British Standards 1377 (1975): Methods of test for soils for civil engineering purposes.
British Standards Institution, Gr10, BS1377:1975

Burland J.B., Hancock R.J. and May J. (1983): A case history of a foundation problem on soft chalk.
Geotechnique, v33, No.4, p385-395

Byrd W.D. (1975): Geology of the Ekofisk Field, offshore Norway. in A.W.Woodward, Ed., Petroleum and the continental shelf of north-west Europe:
John Wiley and Sons, v1, p439-445

Campanella R.G. and Mitchell J.K. (1968): Influence of temperature variations on soil behaviour.
J. Soil Mech. Found. Div., Proc. ASCE, v94, SM3, p709-734

Carroll M.M. (1980): Mechanical response of fluid-saturated porous materials.
Int. Union of Theoretical and Applied Mechanics, 1980, p251-262

Carter P.G. and Mallard D.J. (1974): A study of the strength, compressibility and density trends within the chalk of South East England.
Q. J. Eng. Geol., v7, p43-55

Castle R.O., Yerkes R.F. and Riley F.S. (1969): A linear relationship between liquid production and oil-field subsidence.
1st Land Subsidence Symp., Tokyo, AIHS Publications 88 and 89

Cawsey D.C. (1977): The meaurement of fracture patterns in the chalk of southern England.
Engineering Geology, v11, p201-215

Chaney R.C., Stevens E. and Sheth N. (1979): Suggested test method for determination of degree of saturation of soil samples by B value meaurement.
Geotech. Test. J., GTJODJ, v2, No.3, p158-162

Cheatham J.B. (1967): Strain hardening of a porous limestone.
Soc. Petrol. Eng. J., Sept 1967, p229-234

Chierici G.L., Ciucci G.M., Eva F. and Long G. (1967): Effect of the overburden pressure on some petrophysical parameters of reservoir rocks.
7th World Petrol. Cong., Mexico City, v3, p309-338

Conlon R.J. (1966); Landslide on Toulnustouc River, Quebec.
Can. Geotech. J., v3, No.3, p113-144

Crawford C.B. (1964): Interpretation of the consolidation

test.
J. Soil Mech. Found. Engng., Proc. ASCE, v90, p87-102

Crawford C.B. (1965): The resistance of soil structure to consolidation.
Can. Geotech. J., v2, p90-97

Currie J.B. (1967): Evolution of stress in rocks of a sedimentary basin.
7th World Petrol.Cong., Mexico City, v3, p41-51

Da Silva F., Sarda J.P. and Schroder C. (1985): The mechanical behaviour of chalks.
Chalk Research Group Symp., Stavanger, May 1985, v2

Datta M., Gulhati S.K. and Rao G.V. (1982): Engineering behaviour of carbonate soils of india and some observations on classification of such soils.
ASTM, STP 777, K.R.Demars and R.C.Chaney, Eds., American Society for Testing and Materials, 1982, p113-140

Davis E.H. and Raymond G.P. (1965): A non-linear theory of consolidation.
Geotechnique, V15, p161-173

Delflache A.P. (1978): Land subsidence versus head decline in Texas.
In: Evaluation and prediction of subsidence. Ed. S.K. Saxena Published by ASCE

Demars K.R. (1982): Unique engineering properties and compression behaviour of deep-sea calcareous sediments.
ASTM, STP 777, K.R.Demars and R.C.Chaney, Eds., American Society for Testing and Materials, 1982, p97-112

Demars K.R. and Charles R.D. (1982): Soil volume changes induced by temperature cycling.
Can. Geotech. J., v19, p188-194

De Simone P. and Viggiani C. (1978): Consolidation of a thick aquitard due to ground water withdrawal.
In: Evaluation and prediction of subsidence. Ed. S.K. Saxena. Published by ASCE

Destombes J.P. and Shephard-Thorn E.R. (1971): Geological results of the Channel Tunnel site investigation, 1964-65.
Rep. No. 71/11 Inst. Geol. Sci. 12p

De Waal J.A. (1986): On the rate type compaction behaviour of sandstone reservoir rock.
Ph.D. Thesis, Delft Technical University.

De Waal J.A. and Smits R.M.M. (1985); Prediction of reservoir compaction and surface subsidence: Field application of a new model.
SPE paper 14214, SPE 60th Annual Conf. Las Vegas 1985

De Witte A.J. and Warren J.E. (1957): Discussion of "The effect of fluid pressure decline on volumetric changes in porous rocks" and

closure by J.Geertsma.
Trans AIME, (1957), v210, p339-340

Ebhardt G. (1968): Experimental compaction of carbonate sediments. From; Recent Developments In Carbonate Sedimentology Of Central Europe. Ed - Muller G. and Friedman G.M.. Springer-Verlag.

Elliot G.M. and Brown E.T. (1985): Yield of a soft high porosity rock.
Geotechnique, v35, No.4, p413-423

Evaluation and Prediction of Subsidence (1978): Ed. S.K.Saxena. Int. Conf. on Evaluation and Prediction of Subsidence. Pensacola Beach, Florida, 1978. American Society of Civil Engineers

Farmer I. (1983): Engineering behaviour of rocks.
Chapman and Hall Ltd.

Fatt I. (1957): Pore volume compressibilities of sandstone reservoir rocks.
J. Petrol. Tech., March 1958, p64-66

Fatt I. and Davis D.M. (1952): Reduction in permeability with overburden pressure.
J. Petrol. Tech., Dec. 1952, p16

Finn F.N. (1951): The effect of temperature on the consolidation characteristics of remolded clay.
Symp. Consol. Test. of soils, Special Technical Publication 126, ASTM. p65-71

Fruth L.S., Orme G.R. and Donath F.A. (1966): Experimental compaction effects in carbonate sediments.
J. Sed. Pet., v36, No.3, p747-754

Gaba (1980): The secondary consolidation of clays.
Unpublished MSc. thesis, University of London.

Garga V.K. and Aboim Costa C. (1977): Stress- compressibility characteristics of a residual soil from gneiss.
Proc. 9th. Int. Conf. Soil. Mech., Tokyo 1977, v1, p105-108

Geertsma J. (1957): The effect of fluid pressure decline on volumetric changes of porous rocks.
Trans. AIME, (1957), v210, p331-339

Geertsma J. (1973); Land subsidence above compacting oil and gas reservoirs.
J. Petrol. Tech., June 1973, p734-744

Gerogianopoulos N. and Brown E.T. (1978): The critical state concept applied to rock.
Int. J. Rock Mech. Min. Sci. Geomech. Abs., v15, p1-10

Gibson R.E., England G.L. and Hussey M.J.L. (1967): The theory of one-dimensional consolidation of saturated clays, i. Finite nonlinear consolidation of thin homogeneous layers.

Geotechnique, v17, p261-273

Gibson R.E., Schiffman R.L. and Cargill K.W. (1981): The theory of one-dimensional consolidation of saturated clays, ii. Finite nonlinear consolidation of thick homogeneous layers.
Can. Geotech. J., v18, p280-293

Glennie K.W. (Ed.) (1984): Introduction to the petroleum geology of the North Sea. 2nd Ed., 1984.
Blackwell Scientific Publications

Gobran B.D., Brigham W.E. and Ramey H.J. (1981): Absolute permeability as a function of confining pressure, pore pressure and temperature.
SPE paper 10156, SPE 56th Annual Conf. San Antonio

Gorman C.T., Hopkins T.C., Deen R.C. and Drnevich V.P. (1978): Constant rate of strain and controlled gradient consolidation testing.
Geotech. Test. J., GTJODJ, v1, No.1, p3-15

Graham J., Crooks J.H., and Bell A.L. (1983): Time effects on the stress-strain behaviour of natural soft clays.
Geotechnique, v33, No.3, p327-340

Gray D.H., Fatt I. and Bergamini G. (1963): The effect of stress on permeability of sandstone cores.
Soc. Petrol. Eng. J., June 1963, p95-100

Hall C.D. and Harrisberger W.H. (1970): Stability of sand arches: A key to sand control.
J. Pet. Tech., July 1970, p821-829

Hall E.B. and Gordon B.B. (1963): Triaxial testing with large-scale high pressure equipment.
ASTM, STP 361, p315-328

Hall H.N. (1953): Compressibility of reservoir rocks.
J. Petrol. Tech., January 1953, p17-19

Hancock J.M. (1975): The petrology of the chalk.
Proc. Geol. Ass., v86, p499-535

Hancock J.M. (1983): The setting of the chalk and its initial accumulation.
Japec Course Notes, No.20, A1-A42

Hanrahan E.T. (1977): Lateral stress in one-dimensional consolidation.
Proc. 9th. Int. Conf. S.M.F.E., Tokyo, v1, p117-121

Head K.H. (1982): Manual of soil laboratory testing. Volume 2: Permeability, shear strength and compressibility tests.
Pentech Press, London:Plymouth

Heiberg S. (1974): A review of rock compressibility data for the Ekofisk reservoir and the significance of this data on subsidence and

oil in place.
Phillips Petroleum Company, Project Report

Hellings J.E. (1973): The coefficient of earth pressure at rest.
Unpubl. MSc. Thesis, University of Witwatersrand.

Higginbottom I.E. (1966): The engineering geology of chalk.
Proc. Symp. on chalk in earthworks and foundns., ICE, p1-13

Hirschfield R.C. and Poulos S.J. (1963): High-pressure triaxial tests on a compacted sand and an undisturbed silt.
ASTM/NRC Symp.on laboratory shear testing of soils. ASTM STP NO. 361, p329-341

Holubec and Finn (1969): A lateral deformation transducer for triaxial testing.
Can. Geotech. J., v6, p353-356

Hubbert M.K. and Willis D.G. (1957): Mechanics of hydraulic fracturing.
Petrol. Trans. AIME, v210, p153-168

Huggett J.M. (1982): The growth and origin of authigenic clay minerals in sandstones.
Unpubl. Ph.D. Thesis, University of London.

Hutchinson J.N. (1971): Field and laboratory studies of a fall in Upper Chalk cliffs at Joss Bay, Isle of Thanet.
Roscoe Memorial Symposium, Cambridge University, 29th-31st March 1971

Ineson J. (1962): A hydrogeological study of the permeability of the chalk.
J. Inst. Water. Engineers, v16, 1962, p449-463

Jaky J. (1944): A nyugalmi nyomas tenyezoje.
A Magyar Mernok-Es Epitesz-Egylet Koslonye EV1 zz Szamabol
(The coefficient of earth pressure at rest)

Jaky J. (1948a): State of stress in great depth.
Proc. 2nd Int. Conf. S.M.F.E., Rotterdam, v1, p90-93

Jaky J. (1948b): Pressure in silos.
Proc. 2nd Int. Conf. S.M.F.E., Rotterdam, v1, p103-107

Jaeger (1969): Elasticity, fracture and flow, with engineering and geological applications.
Methuen and Co.Ltd.

Jardine R.J. Brooks N.J. and Smith P.R. (1985): The use of electrolevel transducers for strain measurements in triaxial tests on weak rock.
Int. J. Rock Mech. Min. Sci. & Geomech. Abs., v22, No.5, p331-337

Johnson J.P. and Rhett D.W. (1986): Compaction behaviour of Ekofisk chalk as a function of stress.
SPE paper 15872, SPE European Petrol. Conf., London, 20-22nd October

Jones M.E. (1985): Deformation mechanisms in the chalk.
Chalk Research Group, Symp. Stavanger May 1985 v2

Jones M.E. and Addis M.A. (1984): Volume changes during sediment diagenesis and the development of growth faults.
Marine and Petrol. Geol., v1, p118-122

Jones M.E. and Addis M.A. (1985): On changes in porosity and volume during burial of argillaceous sediments.
Marine and Petrol. Geol., v2, p247-253

Jones M.E., Addis M.A., Preston R.M.F., Goldsmith A., Leddra M.J., Yassir N.A., and Rowbothom J.D. (1985a): Compaction analysis of the Ekofisk field.
Confidential Report for the Norwegian Petroleum Directorate.

Jones M.E., Addis M.A., Preston R.M.F., Leddra M.J., Yassir N.A., Goldsmith A., and Rowbothom J.D. (1985b): Compaction analysis of the Ekofisk field.
Confidential report for the Norwegian Petroleum Directorate.

Jones M.E., Leddra M.J., Preston R.M.F., Addis M.A. and Yassir N.A. (1986): Analysis of the Ekofisk oil field subsidence.
Confidential report for the Norwegian Petroleum Directorate.

Jones M.E., Leddra M.J. and Addis M.A. (1987):
Department of Energy, HMSO Publications Ltd. (in press)

Kane M. (1973): Confined compression of loess.
Proc. 8th. Int. Conf. S.M.F.E., v2.2, p115-122

Kennedy W.J. (1983): Depositional mechanisms in North Sea chalks.
JAPEC Course notes No.20, B1-B20

King G.E. (1982): Identification of causes of formation extrusion and permeability reduction in high porosity North Sea chalks.
Confidential report, Amoco Production Co.

Koppula S.D. and Morgenstern N.R. (1982): On consolidation of sedimenting clays.
Can. Geotech. J., v19, p260-268

Krietler C.W. (1976): Faulting and land subsidence from ground-water and hydrocarbon production, Houston-Galveston, Texas.
2nd., Land Subsidence Symp., Anaheim, AIHS Publication No. 121 p435-445

Kumar J. (1976): The effect of Poisson's ratio on rock properties.
SPE paper 6094, SPE 51st Annual Conf., New Orleans, Oct 3-6

Lachance D.P. and Anderson M.A. (1983): Comparison of uniaxial and hydrostatic stress pore-volume compressibilities in the Nugget sandstone.
SPE paper 11971, SPE 58th Annual Conf. San Fransisco

Lacy L.L. (1984): Comparison of hydraulic fracture orientation techniques.

SPE paper 13225, 59th Annual Conf., Houston, Sept. 16-19

Laguros J.G. (1969): Effect of temperature on some engineering properties of clay soils.
Highway Research Board, Special Report 103, p186-193

Lambe T.W. and Whitman R.V. (1979): Soil mechanics, SI version.
John Wiley and Sons.

Larsson R. and Sallfors G. (1986): Automatic continuous consolidation testing in Sweden.
Consolidation of soils: Testing and Evaluation, ASTM STP 892, R.N. Yong and F.C. Townsend, Eds., American Society for Testing and Materials, p299-328

Leddra M.J., Yassir N.A. and Jones M.E. (1987): Compaction in the Greater Ekofisk Group chalk hydrocarbon reservoirs and related surface subsidence.
Confidential report to the Norwegian Petroleum Directorate.

Lee K. (1981): Consolidation with constant rate of deformation.
Geotechnique, v31, No.2, p215-229

Lee K.L. and Farhoomand I. (1967): Compressibility and crushing of granular soil in anisotropic triaxial compression.
Can. Geotech. J., V4, No.1, p68-99

Lee K.L. and Seed H.B. (1967): Drained strength characteristics of sands
J. Soil Mech. Found. Engng., Proc. ASCE, v93, SM6, p117-141

Leonards G.A. and Girault P. (1961): A study of the one-dimensional consolidation test.
Proc. 5th Int. Conf. S.M.F.E., Paris, v1, p213

Leroueil S., Samson L. and Bozozuk M. (1983a): Laboratory and field determination of preconsolidation pressures at Gloucester.
Can. Geotech. J., v20, p477-490

Leroueil S. and Tavenas F. (1979): Strain rate behaviour of Saint-Jean-Vianney clay: Discussion.
Can. Geotech. J., v16, p616-620

Leroueil S., Tavenas F., Samson L. and Morin P. (1983b): Preconsolidation pressure of Champlain Clays. Part 2. Laboratory determination.
Can. Geotech. J., v20, p803-816

Leroueil S., Kabbaj M., Tavenas F. and Bouchard R. (1985): Stress-strain-strain rate relation for the compressibilities of sensitive natural clays.
Geotechnique, v35, No.2, p159-180

Lewin P.I. (1971): Use of servo-mechanisms for volume change measurement and K_o consolidation.
Geotechnique, v21, No.3, p259-262

Lewis W.A. and Croney D. (1966): The properties of chalk in relation to road foundations and pavements.
Proc.Symp. on chalk in Earthworks and Foundns., ICE, p27-41

Lo K.Y. and Morin J.P. (1972): Strength anisotropy and time effects of two sensitive clays.
Can. Geotech. J., v9, p261-277

Maccarini M. (1980): Triaxial and direct shear tests on a young residual soil from gneiss.
Unpubl. MSc. Thesis, PUCRJ, GAVEA, RJ, Brazil

Maccarini M. (1987): Laboratory studies of a weakly bonded artificial soil.
Unpubl. Ph.D. Thesis, University of London.

Marek B.F. (1971): Predicting pore compressibility of reservoir rock.
Soc. Petrol. Eng. J., Dec 1971, p340-341

Marek B.F. (1979): Permeability loss in depletion of reservoirs.
SPE paper 8433, SPE 54th Annual Conf., Las Vegas, 1979

Martin J.C. and Serdengecti S. (1984): Subsidence over oil and gas fields. In, Reviews in Engineering Geology v4, Ed. T.L.Holzer. Geological Society of America

Maswoswe J. (1985): Stress paths for a compacted soil during collapse due to wetting.
Unpubl. Ph.D. Thesis, University of London.

Mayne P.W. and Kulhawy F.H. (1982): K_o-OCR relationships in soil.
J. Soil Mech. Found. Div., Proc. ASCE, v108, GT6, p851-872

McLatchie A.S., Hemstock R.A. and Young J.W. (1958): The effective compressibility of reservoir rock and its effects on permeability.
J. Petrol. Tech., June 1958, p49-51

Meigh A.C. and Early K.R. (1957): Some physical and engineering properties of chalk.
Proc. 4th Int. Conf. S.M.F.E., v1, p68-73

Mesri G., Adachi K. and Ullrich C.R. (1976): Pore pressure response in rock to undrained change in all-round stress.
Geotechnique, v26, No.2, p317-330

Mesri G. and Godlewski P.M. (1977): Time- and stress- compressibility interrelationship.
J. Soil Mech. Found. Div., Proc. ASCE, v103, GT5, p417-430

Mesri G. and Choi Y.K. (1979): Discussion of: Strain rate behaviour of Saint-Jean-Vianney clay.
Can. Geotech. J., v16, p831-834

Mesri G. and Feng T.W. (1986): Discussion and reply on: Stress-strain-strain rate relation for the compressibilities of sensitive natural clays.
Geotechnique, v36, No.2, p283-290

Mess K.W. (1978): On the interpretation of core compaction behaviour. in; Evaluation and prediction of subsidence, Ed. S.K.Saxena. Published by ASCE

Miller T.W. and Cheatham J.B. (1972): A new yield condition and hardening rule for rocks.
Int. J. Rock Mech. Min. Sci. & Geomech. Abs., v9, p413-423

Mitchell J.K. (1969): Temperature effects on the engineering properties and behaviour of soils.
Highway Research Board Special Report 103, p9-28

Moore C.A. (1971): Effect of mica on K_o compressibility of two soils.
J. Soil Mech. Found. Engng., Proc. ASCE, v97, SM9, p1275-1291

Moore P.J. and Cole B.R. (1977): At-rest lateral earth pressure of a consolidating clay.
J. Soil Mech. Found. Engng., Proc. ASCE, v103, GT7, p820-821

Morita N., Gray K.E, Srouji F.A.A. and Jogi P.N. (1984): Rock property change during reservoir compaction.
SPE paper 13099, SPE 59th Annual Conf., Houston, Sept. 16-19

Moshanski V.A. and Parabouchev I.A. (1981): The nature of strength and deformability of weak carbonaceous rocks.
Proc. Int. Symp. Weak Rock, Tokyo, 21-24 Sept. 1981, p339-346

Murayama S. (1969): Effects of temperature on elasticity of clays.
Highway Research Board Special Report 103, p194-203

Nakano T., Kadomura H. and Matsuda T. (1969): Land subsidence in the Tokyo deltaic plain.
1st Land Subsidence Symp., Tokyo, AIHS Publications 88 and 89, p80-87

Newman G.H. (1973): Pore-volume compressibility of consolidated, friable and unconsolidated reservoir rocks under hydrostatic loading.
J. Petrol. Tech., Feb 1973, p129-133

Newman G.H. and Martin J.C. (1977): Equipment and experimental methods for obtaining laboratory compression characteristics of reservoir rocks under various stress and pressure conditions.
SPE paper 6855, SPE 52nd Annual Conf., Denver,

Newman G.H. (1983): The effect of water chemistry on the laboratory compression and permeability characteristics of some North Sea chalks.
J. Petrol. Tech., May 1983, p976-980

Nur A. and Byerlee J.D. (1971): An exact effective stress law for elastic deformation of rocks with fluids.
J. Geophys. Res., v76, No.26, p6414-6419

Ohtsuki H., Nishi K., Okamoto T. and Tanaka S. (1981): Time dependant characteristics of strength and deformation of a mudstone.
Proc. Int. Symp. on Weak Rock, Tokyo., 21-24 Sept. 1981, p119-124

Osborne White H.J. (1913): The geology of the country near Fareham and Havant.
Memoir of the Geological Survey, sheet 316

Osborne White H.J. (1928): The geology of the country near Ramsgate and Dover.
Memoir of the Geological Survey, Sheets 274 and 290

Ovando-Shelley E. (1986): Stress-strain behaviour of granular soils tested in the triaxial cell.
Unpubl. Ph.D. Thesis, University of London.

Paaswell R.E. (1967): Temperature effects on clay soil consolidation.
J. Soil Mech. Found. Div., Proc. ASCE, v93, SM3, p9-22

Pattillo P.D. and M.B. Smith (1982): The effect of formation flow on the integrity of perforated casing.
SPE paper 11123, SPE 57th Annual Conf., New Orleans, Sept. 26-29th

Phillips (1984): In situ stresses in natural soil deposits.
Unpubl. MSc. Dissitation, University of London

Pierce S.W. and Siegel F.R. (1969): Quantification in clay mineral studies of sediments and sedimentary rocks.
J. Sed. Pet., v39, p187-193

Plum R.L. and Esrig M.I. (1969): Some temperature effects on soil compressibility and pore water pressure.
Highway Research Board Special Report 103, p231-242

Poland J.F. and Davis G.H. (1969): Land subsidence due to withdrawal of fluids. In, Reviews in Engineering Geology, v2, Eds. D.J.Varnes and G.Kiersch. Geological Society of America

Prats M. (1981): Effect of burial history on the subsurface horizontal stresses of formations having different material properties.
Soc. Petrol. Eng. J., Dec 1981, p658-662

Price A.M. and Farmer I.W. (1981): The Hvorslev surface in rock deformation.
Int. J. Rock Mech. Min. Sci. and Geomech. Abs., v18, p229-234

Principia Mechanica Ltd. (1986): A global review of subsidence and seismicity associated with deep-level fluid extraction.
PML Report No.365/86, For Phillips Petroleum Co. Ltd.

Proc. Forum on Subsidence Due to Fluid Withdrawals (1982) Fountain-head State resort, Checotah, Oklahoma. Nov. 14-17

Reviews in Engineering Geology V2 (1969): Eds. D.J.Varnes and G.Kiersch.
Geological Society of America

Reviews in Engineering Geology V4 (1984): Man-induced land subsidence, Ed. T.L.Holzer
Geological Society of America

Rieke H.H. and Chilingarian G.V. (1974): Compaction of argillaceous sediments.
Developments in sedimentology 16
Elsevier Scientific Publishing Company

Roberts J.E. (1969): Sand compression as a factor in oil field subsidence.
1st. Land Subsidence Symp., Tokyo, AIHS Publications 88 and 89, p368-375

Roberts J.E. and de Souza J.M. (1958): The compressibility of sands.
61st. Annual Meeting of ASTM, Boston, June 22-27 1958

Robertson E.C., Sykes L.R. and Newell (1962): Experimental consolidation of calcium carbonate sediments. In; Enviroment of calcium carbonate deposition west of Andros Island, Bahamas. Compiled by P.E.Cloud.
U.S.G.S. Prof. Paper 350, p82-83

Robin P.Y.F. (1973): Note on effective pressure.
J. Geophys. Res., v78, No.14, p2434-2437

Rosenbaum M.S. (1978): Variations in geotechnical properties of argillaceous sediments during burial.
Unpubl. Ph.D. Thesis, University of London.

Samarasinghe A.M., Huang Y.H. and Drnevich V.P. (1982): Permeability and consolidation of normally consolidated soils.
J. Soil Mech. Found. Div., Proc. ASCE, v108, GT6, p835-850

Sangrey D.A. (1972): Naturally cemented sensitive soils.
Geotechnique, v22, No.1, p139-152

Santarelli F.J., Brown E.T. and Maury V. (1986): Analysis of borehole stresses using pressure dependant linear elasticity.
Int. J. Rock Mech. Min. Sci. & Geomech. Abs., v23, No.6, p445-449

Saxena S.K. (1982): Geotechnical properties of calcareous rocks of southern Florida.
Geotechnical properties, behaviour, and performance of calcareous soils, ASTM STP 777, K.R. Demars and R.C. Chaney, Eds., American Society for Testing and Materials, p340-358

Selley R.C. (1978): Porosity gradients in North Sea oil-bearing sandstones.
J. Geol. Soc. Lond., v135, p119-131

Schmidt B. (1966): Discussion of; 'Earth pressures at rest related to stress history'.
Can. Geotech. J., v3, No.4., p239-242

Schmidt B. (1967): Lateral stresses in uniaxial strain.
Danish Geotech. Inst. Bull., No.23., p5-12

Scholle P.A. (1977): Chalk diagenesis and its relation to petroleum exploration: Oil from chalks, a modern miracle?

Bull. Am. Assoc. Petrol. Geol., v61, No.7, p982-1009

Scorer J.D.T. and Miller F.G. (1974): A review of reservoir rock compressibility, and its relationship to oil and gas recovery.
Institute of Petroleum, 74-003, p1-25

Sherif M.A. and Burrows C.M. (1969): Temperature effects on the unconfined shear strength of saturated, cohesive soil.
Highway Research Board, Special Report 103, p231-242

Shepherd L.E. and Bryant W.R. (1983): Geotechnical properties of lower trench inner slope sediments.
Tectonophysics, v279, p279-312

Silvestri V. (1981): Behaviour of an overconsolidated sensitive clay in drained K_o-triaxial tests.
Laboratory Shear Strength of Soil, ASTM STP 740, R.N.Yong and F.C.Townsend, Eds., American Society for Testing and Materials, 1981 p619-630

Silvestri V., Yong R.N., Soulie M. and Gabriel F. (1986): Controlled-strain, controlled-gradient, and standard consolidation testing of sensitive clays.
Consolidation of soils: Testing and evaluation, ASTM STP 892, R.N. Yong and F.C. Townsend, Eds., American Society for Testing and Materials, p433-450

Simon D.E., Coulter G.R., King G. and Holman G. (1982): North Sea completions - A laboratory study.
J. Petrol. Tech., Nov. 1982, p2531-2536

Skempton A.W. (1954): The pore pressure coefficients A and B.
Geotechnique, v4, p143-147
Also in: Selected papers in soil mechanics by A.W. Skempton, FRS, Thomas Telford Ltd., 1985, London.

Skempton A.W. (1960): Effective stress in soils concrete and rocks.
In: Selected papers in soil mechanics by A.W. Skempton, FRS, Thomas Telford Ltd., 1985, London.

Skovbro B. (1983): Depositional conditions during chalk sedimentation in the Ekofisk area, Norwegian North Sea.
Geol.Mijnbouw, v62, p169-175

Skovbro B. and Kennedy W.J. (1985): Sedimentology of the late Cretaceous and early Palaeocene chalk group, North Sea Graben.
Chalk Research Group Stavanger Symp. May 1985

Smith R.E. and Wahls H.E. (1969): Consolidation unde constant rates of strain.
J.Soil Mech. Found. Div., Proc. ASCE, v95, SM2, p519-539

Smits R.M.M., de Waal A. and van Kooten J.F.C. (1986): Prediction of abrupt reservoir compaction and surface subsidence due to pore collapse in carbonates.
SPE paper 15642, SPE 61st Annual Conf., New Orleans, Oct 5-8th

Som N.N. (1968): The effect of stress path on the deformation and consolidation of London clay.
UnPubl. PhD. Thesis, University of London

Sorensen S., Jones M.E., Hardman R.F.P., Leutz W.K. and Schwarz P.H. (1986): Reservoir characteristics of high- and low-productivity chalks from the Central North Sea.
In: Habitat of Hydrocarbons on the Continental Shelf, Norwegian Petroleum Society, Graham and Trotman Publishers Ltd., p91-110

Sawabini C.T., Chilingar G.V. and Allen D.R. (1974): Compressibility of unconsolidated arkosic oil sands.
Soc. Petrol. Eng. J., April 1974, p132-138

Takeuchi S., Kimoto S., Wada M., Shiina H. and Mukai K. (1969): Geological and geohydrological properties of the lad subsided areas.
1st Land Subsidence Symp., Tokyo, AIHS publications 88 and 89, p232-241

Tavenas F. and Leroueil S. (1977): Effects of stresses and time on yielding of clays.
Proc. 9th Int. Conf. SMFE, Tokyo, p319-326

Teeuw D. (1971): Prediction of formation compaction from laboratory compressibility data.
Soc. Petrol. Eng. J., Sept. 1971, p263-271

Teeuw D. (1973): Laboratory measurement of compaction properties of Groningen reservoir rock.
Verhandelingen Kon. Ned. Geol. Mijnbouwk. Gen., v28, p19-32

Terzaghi K. (1943): Theoretical soil mechanics.
John Wiley and Sons Inc.

Teufel L.W. (1982): Prediction of hydraulic fracture azimuth from anelastic strain recovery measurements of oriented core.
Proc. 23rd Symp. on Rock Mech., Berkeley, August 25-27, p238-245

Teufel L.W. (1983): Determination of in-situ stress from anelastic strain recovery measurements of oriented core.
SPE/DOE paper 11649, SPE/DOE Symp. on Low Permeability, Denver, March 14-16

Teufel L.W. and Warpinski N.R. (1984): Determination of in-situ stress from anelastic strain recovery measurements of oriented core: comparison to hydraulic fracture stress measurements in the Rollins sandstone, Piceance Basin, Colorado.
Proc. 25th Symp. on Rock Mech., Evanston, June 25-27, p176-185

Townsend D.L., Sangrey D.A. and Walker L.K. (1969): The brittle behaviour of naturally cemented soils.
Proc. 7th. Int. Conf. S.M.F.E., Mexico, 1969, v1, p411-417

Uriel S. and Serrano A.A. (1973): Geotechnical properties of two collapsible volcanic soils of low bulk density at the site of two dams in the Canary Islands (Spain).
Proc. 8th. Int. Conf. S.M.F.E., Moscow, 1973, v2.2, p251-264

Vaid Y.P. and Campanella R.G. (1977): Time-dependant behaviour of undisturbed clay.
J. Geotech. Engng. Div., Proc. ASCE, v103, GT7, p693-709

Vaid Y.P., Robertson P.K. and Campanella R.G. (1979): Strain rate behaviour of Saint-Jean-Vianney clay.
Can. Geotech. J., v16, p34-42

Valent P.J., Altschaeffl A.G. and Lee H.J. (1982): Geotechnical properties of two calcareous oozes.
ASTM, STP 777, K.R.Demars and R.C.Chaney, Eds., American Society for Testing and Materials, 1982, p79-95

Van den Bark E. and Thomas O.D. (1980): Ekofisk: First of the giant oil fields in Western Europe.
Giant oil and gas fields of the decade 1968-1978. Ed - Halbouty M.T., AAPG Memoir 30, p195-224

Van der Knaap V.W. (1960): Der einflub einer anderung des porenvolumens in erdolhaltigen gestein auf die abschatzung des olvorates.
Erdol und Kohle, 1960, p305-312

Van der Knaap W. and van der Vlis A.C. (1967); On the cause of subsidence in oil producing areas.
7th World Petrol. Cong., Mexico City, 1967, v3, p85-96

Van Ditzhuijen P.J.D. and de Waal J.A. (1984): Reservoir compaction and surface subsidence in the Central Luconia gas bearing carbonates offshore Sarawak, East Malaysia.
5th Offshore South East Asia Conf., Singapore, 21-24 Feb 1984

Van Kooten J.F.C. (1986): Model prediction of Ekofisk compaction and subsidence.
Confidential Report for Phillips Petroleum Co. Ltd.

Vaughan P.R. (1985): Mechanical and hydraulic properties of in-situ residual soils.
1st. Int. Conf. in Geomechanics in tropical lateritic and saprolitic soils, Brasilia, Feb. 1985

Verhandelingen van het Koninklijk Nederlands geologisch mijnbouwkundig Genootschap (1973): The analysis of surface subsidence resulting from gas production in the Groningen area, the Nederlands., v28, 1973.

Vesic A. and Barksdale R.D. (1963): On shear strength of sand at very high pressures.
ASTM/NRC Symp. on Laboratory Shear Testing of Soils, STP 361, p301-305. American Society of Testing and Materials.

Vesic A.S. and Clough G.W. (1968): Behaviour of granular materials under high stresses.
J. Soil Mech. Found. Div., Proc. ASCE, v94, SM3, p661-688

Vickers B. (1983): Laboratory work in soil mechanics. 2nd Ed.

Granada Publishing Ltd.

Voight B. (1968): Determination of the virgin state of stress in the vicinity of a borehole from measurements of a partial anelastic strain tensor in drill cores.
Felsmechanik u. Ingenieurgeol., v6, p201-215

Wakeling T.R.M (1966): Foundations on chalk.
Proc.Symp. on chalk in Earthworks and Foundns., ICE, p15-23

Ward W.H., Burland J.B. and Gallois R.W. (1968): Geotechnical assessment of a site at Mundford Norfolk, for a large proton accelerator.
Geotechnique, v18, p399-431

White S.H., Shaw H.F. and Hugget J.M. (1984): The use of Back-scattered electron imaging for the petrographic study of sandstones and shales.
J. Sed. Pet., v54, No.2, p487-494

Wiborg R. and Jewhurst J. (1986): Ekofisk - Reservoir management in a compacting environment.
Proc. Advanced Projects Conf., Stavanger, Nov. 1985

Wilson G. (1948): Some laboratory tests on chalk.
Proc. 2nd Int. Conf. S.M.F.E., Rotterdam, v3, p183-187

Wilson G. and Grace H. (1942): The settlement of London due to underdrainage of the London Clay.
J. Inst. Civil Eng., v19, No.2, paper No.5294, p199-127

Wissa A.E.Z. (1969): Pore pressure measurement in saturated stiff soils.
J. Soil Mech. Found. Div., Proc. ASCE, v95, SM4, p1063-1073

Wissa A.E.Z., Christian J.T., Davis E.H. and Heiberg S. (1971): Consolidation at constant rate of strain.
J. Soil Mech. Found. Div., Proc. ASCE, v97, SM10, p1393-1413

Yerkes R.F. and Castle R.O. (1969): Surface deformation associated with oil and gas field operations in the United States.
1st Land Subsidence Symp., Tokyo, AIHS publications 88 and 89, p55-66

Yoshinaka R. and Yamabe T. (1981): Deformation behaviour of soft rocks.
Proc. Int. Symp. on Weak Rock, Tokyo, 21-24 Sept. 1981, p87-92

Zeuch D.H. (1983): The mechanical behaviour of Anvil Point oil shale at elevated temperatures and confining pressures.
Can. Geotech. J., v20, p344-352

Znidarcic D., Croce P., Pane V., Ko H.Y., Olsen H.W. and Schiffman R.L. (1984): The theory of one-dimensional consolidation of saturated clays: iii. Existing testing procedures and analyses.
Geotech. Test. J., GTJODJ, v7, No.3, p123-133

Znidarcic D., Schiffman R.L., Pane V., Croce P., Ko H.Y. and Olsen

H.W. (1986): The theory of one-dimensional consolidation of saturated clays: part v. Constant rate of deformation testing and analysis.
Geotechnique, v36, No.2, p227-237

Zoback M.D. and Byerlee J.D. (1975): Permeability and effective stress.
Am. Assoc. Petrol. Geol. Bull., v59, No.1, p154-158

APPENDIX 1

DESCRIPTION AND DEVELOPMENT OF THE TRIAXIAL CELL.

A1.1) THE TRIAXIAL CELL

The triaxial cell has been made by the soil mechanics group in the Civil Engineering Dept. of Imperial College, and is based on soil testing type triaxial cells, with independant control of confining pressure, axial stress, pore fluid pressure, and temperature. The cell (Fig. A1.1 and Plate A1.1.) is made of En25 steel and designed for a maximum confining pressure of 70MPa (10,000 psi), the ram can supply a load of >80kN (>8tons) to a 3.83cm diameter, 7.6cm long sample.

The main parts of the cell (Fig. A1.1 and Plate A1.1) are 1) the base, which contains the main drain for pore fluid, and entry ports which allows internal monitoring of the sample, and connection to the sample: 2) the cylinder, this forms the main body of the cell and is a steel cylinder 2.30cm thick, it contains the oil surrounding the sample. The cylinder sits on the base and is sealed by an "o" ring: the top section of the cell consists of 3) the ram, which supplies the load to the sample: 4) the ram guide and 5) the top cap, which lock together with a perspex-rubber seal and forms an upper oil filled chamber, the top cap containing an oil bleed. The ram is held within this assembly and moves with the ram flange sealing against the walls of the upper chamber with another pespex-rubber seal. This ram flange limits the ram movement to 5.09cm (2.0"), and splits the upper chamber into two smaller chambers above and below the flange.

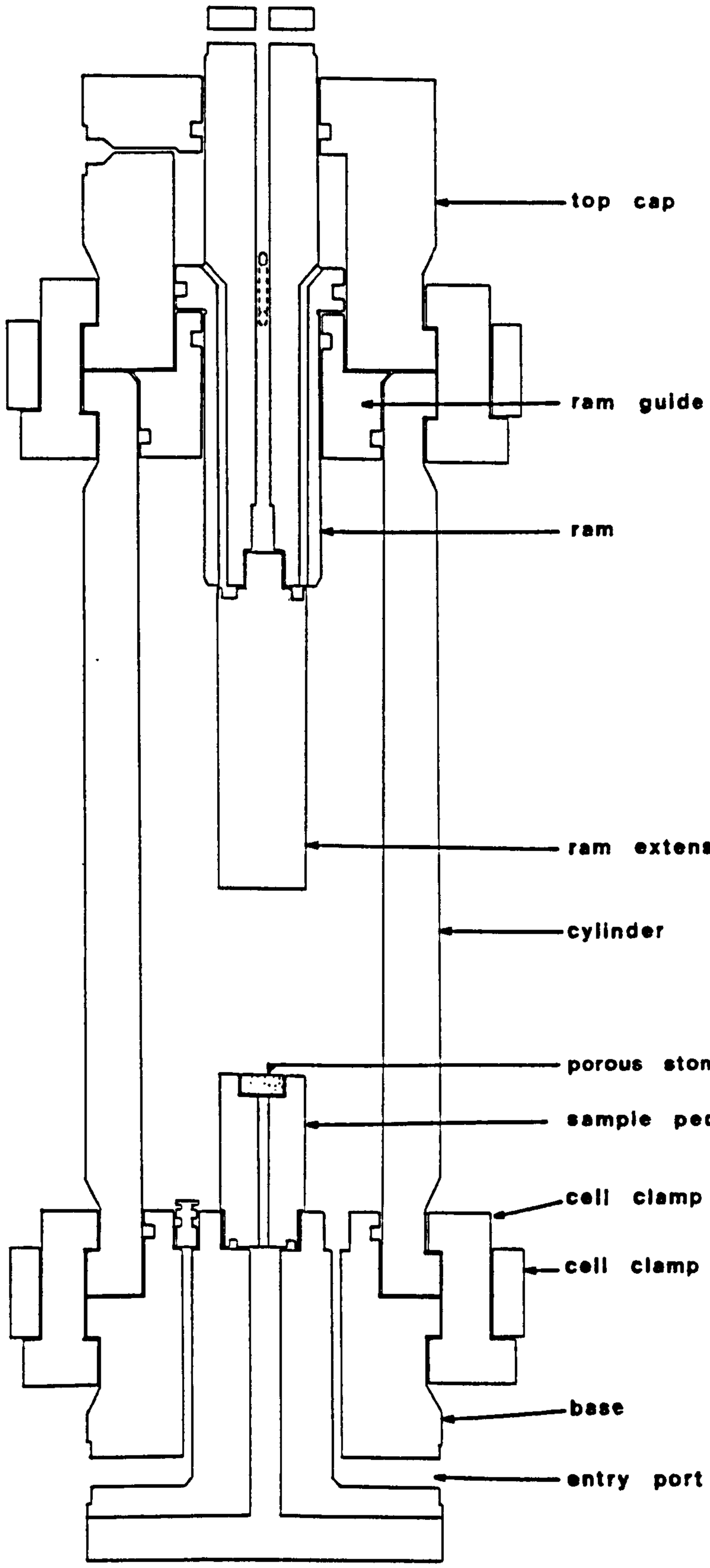

Figure A1.1 The high pressure triaxial cell.

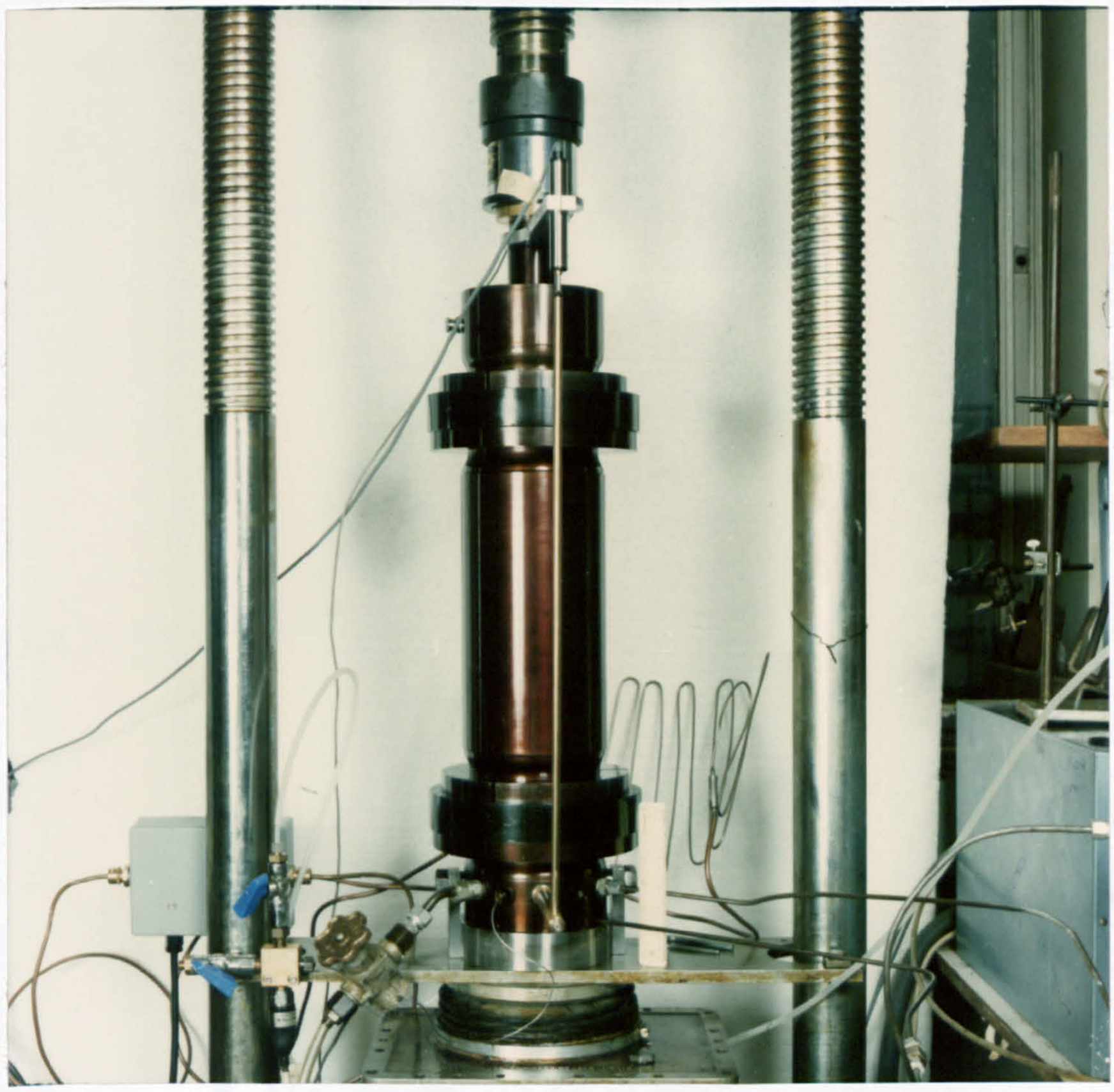

Plate A1.1 The high pressure triaxial cell.

The ram contains drains which run through its length connecting the main oil chamber surrounding the sample to the upper chamber, thus when the ram moves the ram flange has an equal oil pressure on either side of it ensuring no work is done against the confining pressure of the cell (Bishop, Kumapley and El-Ruwayih, 1975). The ram protrudes through an opening in the top cap, sealed by a perspex-rubber seal, to enable a loading frame to move the ram. The ram contains a central hole for connections to an internal load cell (if required) but was blocked off in these experiments by a ram extension, and sealed by an "o" ring (Fig. A1.1). The "o" rings used in the cell in these experiments were viton "o" rings which can sustain temperatures in excess of 200^{o}C. The cylinder is held to the base and the top cap by

three flanges which are locked together to form a segmented ring, the three flanges are held together by an outer ring.

The samples used in this apparatus are generally 7.6cm (3") high and 3.8cm (1.5") in diameter and are held in nitryl or neoprene rubber membranes which seals the sample from the confining pressure oil. The membrane is sealed to the sample top cap and the sample pedestal by "o" rings (Fig. A1.2).

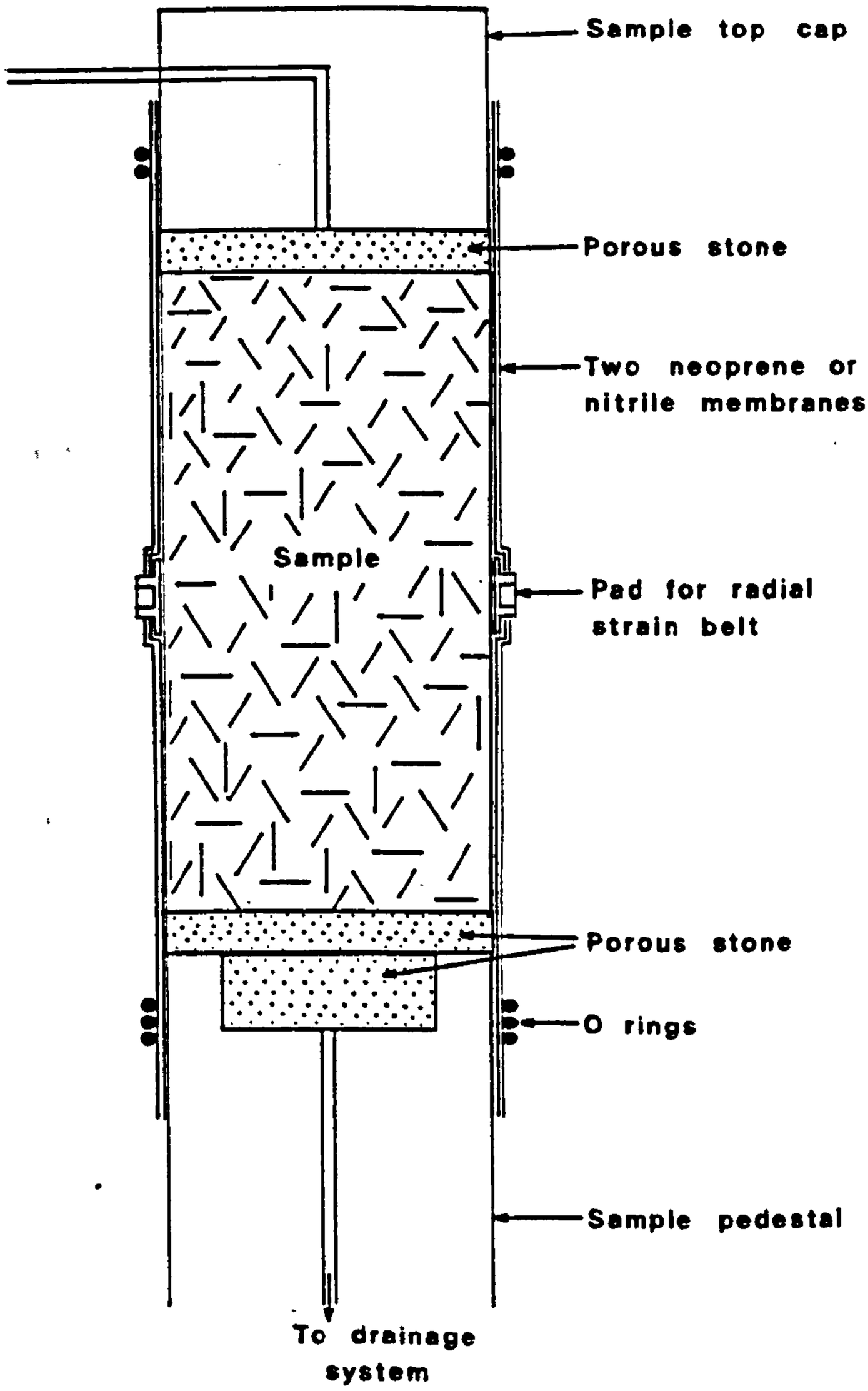

Figure A1.2 Sample set up in the triaxial cell.

The stresses are applied to the sample in two ways: 1) the confining pressure is supplied by a Beacham high pressure oil pump. This is a spring loaded oil pump system, capable of supplying an oil pressure of 70MPa (10,000 psi) to the sample. The oil pressure is monitored by a 70MPa pressure transducer. 2) The axial stress is supplied via a 500KN (50 tons) Clockhouse Engineering Ltd. loading frame, which pushes the ram onto the sample. The loading frame is capable of supplying a constant deformation rate varying from 0.9999mm/min to $1*10^{-6}$mm/min, which for a 7.6cm high sample gives a strain rate varying from $2.2*10^{-4}sec^{-1}$ to $2.19*10^{-10}sec^{-1}$. The axial stresses on the sample are measured externally using a MRE/NCB 25 ton load cell, while the movement of the ram is measured externally by a MRE displacement transducer.

A1.2) THE HEATING SYSTEM

The heating system of the triaxial cell consists of a stainless steel sheathed, ceramically insulated heating cable wound to an elongated sinusoidal shape, which can supply 750 watts to the cell. This enables the cell to be heated to $180^{o}C$. The heater works off 120v and is controlled by a Eurotherm three term controller, proportioning between 2 and 20 seconds and capable of maintaining a temperature to $\pm 2^{o}C$, App. 6. The controllers input is an externally mounted thermocouple, thus allowing any variation in the output of the heater will be dissipated by the diffusion of the heat through the walls of the cell and through the oil. Thermocouples are installed in the cell to monitor oil temperature or sample temperature; All the thermocouples used are Cr/Al mineral insulated thermocouples.

A1.3) THE DRAINAGE SYSTEM

The drainage system was designed to measure volume changes in the sample, while supplying a back-pressure or pore water pressure to the sample. The necessity for back pressures was two fold; firstly to ensure that the sample is fully saturated, a high pore water pressure dissolving any air in the sample (Bishop and Henkel, 1962; Chaney, Stevens and Sheth, 1979; Chap. 2.3). Secondly, a back pressure is needed to suppress boiling of pore water during the heating of the sample (Fig. A1.3)

The drainage system designed was kept as simple as possible, but with emphasis on accuracy and reliability. A Tescom back pressure regulator (App. 6) was chosen as the controlling valve for maintaining the back pressure. This is a spring loaded device which maintains a pore pressure upstream. Once the pore pressure starts to exceed the loading on the regulator, the pore pressure pushes against the spring so lifting the needle valve seal, this allows a leak of pore fluid past the seal lowering the pore pressure and closing the valve. The pore fluid therefore leaks to a lower or atmospheric pressure down stream. Downstream the back pressure regulator is connected to an Imperial College (I.C.) volume gauge which works at a slight back pressure, and is capable of measuring volume changes of $0.01cm^3$. The I.C. volume gauge consists of a piston sealed at both ends by two Bellofram membranes, water enters the volume gauge at one end pushing against the air pressure supplied to the opposite end of the piston. The air pressure has the effect of 'floating' the piston, the maximum pressure the volume gauge can take is 0.41MPa (60psi) (App. 6). The regulator and volume gauge are connected in line from the base of the sample, the system is de-aired using a pressurised de-aired water supply and a hand ram reservoir for use when high

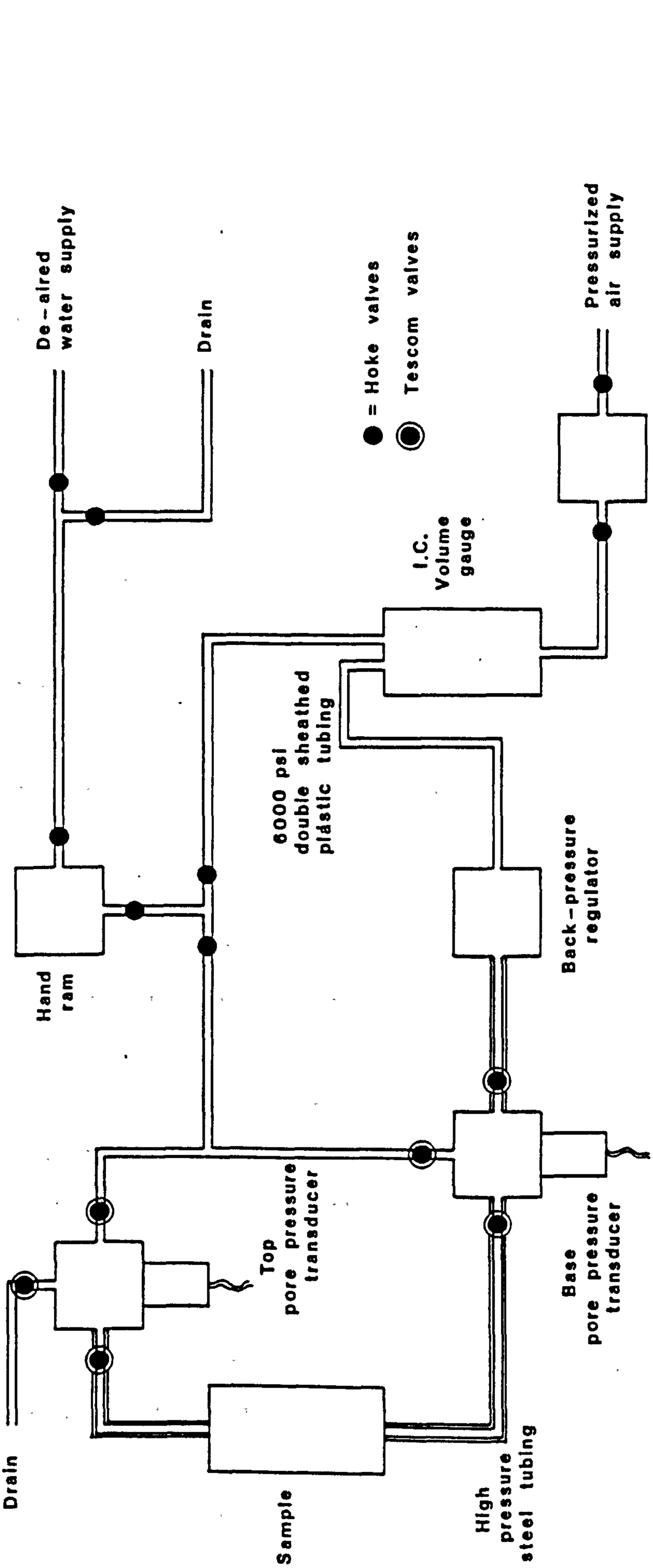

Figure A1.3 Diagrammatic illustration of the drainage system.

water pressures are required. The hand ram can supply water pressures upto 1.8MPa (300psi), and is generally used to flush water through samples or for a controlled movement of water through the system.

This system does not supply a back pressure but maintains a self induced back pressure, when the sample is supplied with an isotropic stress at the begining of the test. Thus at the start of a test an isotropic stress was applied to enable the pore pressure to rise above a value of 0.41MPa (30psi) or to a pressure which suppressed boiling in heated tests. The amount of isotropic stress needed for a sufficient pore pressure response could be calculated from Skemptons B parameter, if the degree of saturation is known. However, in low porosity soils and weak rocks this does not apply (Chap. 2).

There is one main draw back of this system, it relies on a Skempton B type relationship, this is acceptable with plastic soils, but when dealing with cemented materials such as chalk, the pore pressure response to an increment of isotropic stress will generally be small. This obviously has serious consequences when trying to perform high temperature experiments.

The performance of the Tescom back pressure regulator can be seen in the early chalk experiments, where the pore pressures gradually built up. Large strains are needed to breakdown the structure of the chalk and allow build up of pore pressures (App. 5). There appears to be an initial pore pressure build up in the regulator before it starts releasing the pore fluid, this is assumed to be due to frictional forces in the sealing flanges in the valves. After the initial leakage, an almost constant back pressure is maintained.

In tests performed using oil as a pore fluid, an oil-water interface was inserted between the sample and the base pore water pressure transducer block. The interface has a 1cm thick steel

cylnder o.d. of 7cm, with a brass piston sealing against the steel cylinder with a double 'o' ring. The friction in the piston would have the effect of increasing the pore fluid pressure in the sample compared to that measured by the base pore pressure transducer.

A1.3.1) New high pressure volume gauge

Due to the inability of the drainage system in its initial form to supply a pore fluid pressure, and due to the structural damage of the sample whilst trying to saturate the sample using an isotropic stress to induce a high pore pressure, a new volume gauge was designed. The volume gauge was designed to measure small volume changes, and to supply or transmit high back pressures: the first of these required that there be only a small frictional component in the system.

The design of the new volume gauge was based on the I.C. volume gauge wherever possible to make manufacture less troublesome and to reduce costs. The difficulties with the present I.C. volume gauge with regard to high pressure testing, can be summarised as follows: 1) A maximum pressure of 0.4MPa (60psi) can be used, as the Bellofram membranes act as a seal to the piston and are not able to sustain a large pressure differential across them; 2) The transducer is situated outside the main body of the cell, so the Bellofram membranes act as a seal between the pressurised pore fluids and the outside. Other difficulties or reservations have been observed with the volume gauges, though mainly at low pressures: 3) friction present in the system due to the rolling action of the membranes. 4) Tilting of the piston possible, with subsequent apparent volume change registered by the transducer. Despite these last two points, the system has been proven to work exceptionally well in a very wide range of applications.

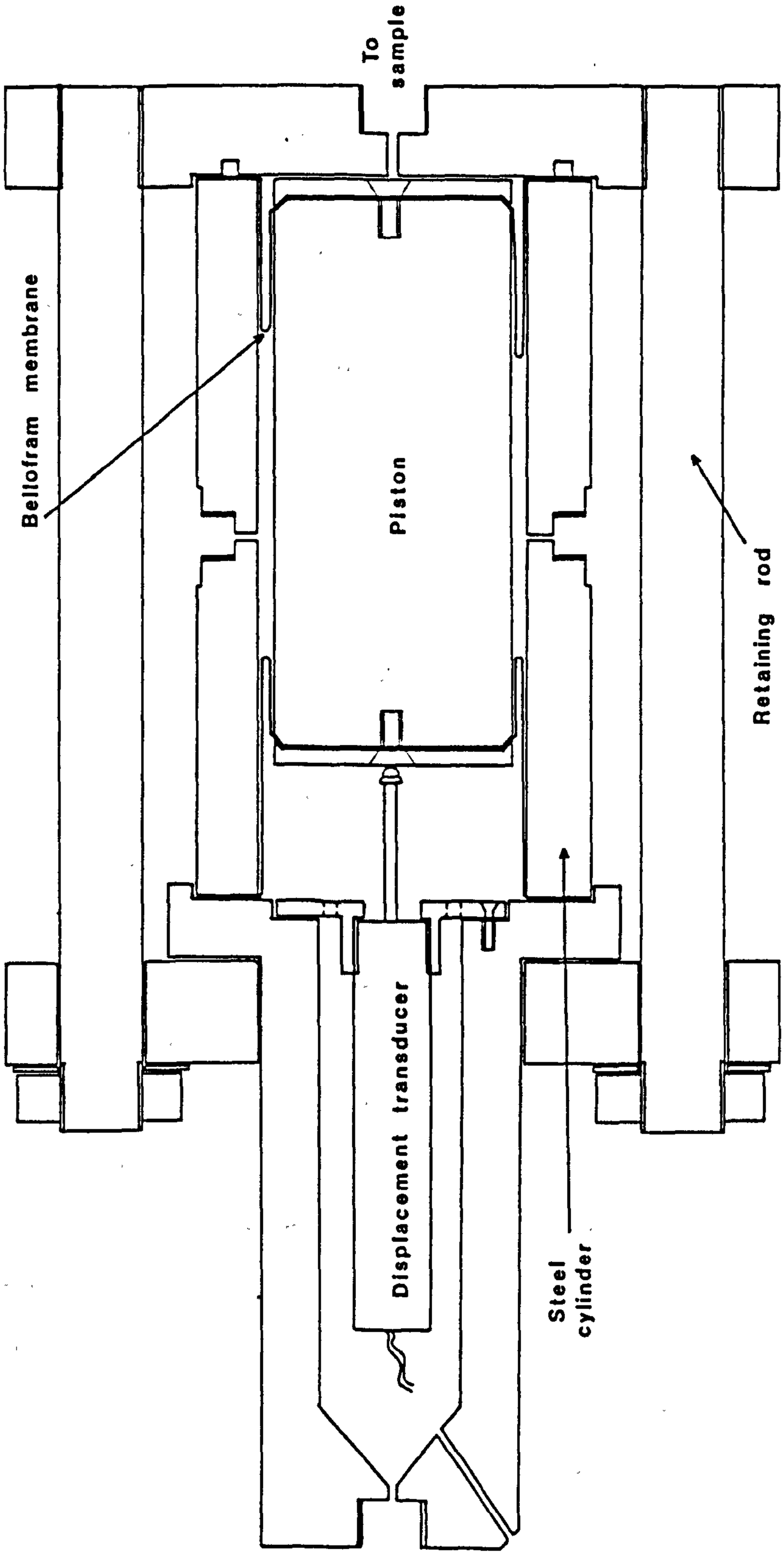

Figure A1.4 High pressure volume gauge.

The new high pressure volume gauge (Fig. A1.4) was designed with the first two points in mind, the latter points may also be reduced to some degree with the new design. The use of high pressures can induce volumetric strain in the components used, especially in the PVC piston. An aluminium piston could be used to reduce the compressibility of the system, enabling the volume gauge to work at higher pressures, up to 70MPa, with variable back pressures throughout the test. When working with a variable back pressure, small errors in volume change due to the compressibility of the system, would need to be "calibrated out". The high pressure volume gauge used in this study had a conventional PVC piston, as only 2MPa back pressure was required during the tests, and kept constant throughout the test.

The new volume gauge, firstly removes any contact between the Bellofram membranes and atmospheric pressure, by placing the transducer inside the pressurised body. The displacement transducer used was a modified MRE displacement transducer (App. 6) which is a dc device used on the I.C. volume gauges. The transducer has a hollow body and under high pressures it was likely to be crushed, so holes were drilled into the side of the body to enable equalization of the pressure across the transducer body. This was very much experimental as the transducers were designed to be sealed. However, because the strain gauges in the transducer should not come into contact with moisture and be surrounded by oil, no problems were envisaged. The modifications also included removal of the end pieces of the transducer body so that the device could be attach to the volume gauge at the core end, and secondly to allow easy access to the electrical connections in the transducer. The electrical connections leave the cell by a ceramic plug glued into a hole drilled into the

lvdt section at an angle of 36^{o} to the long axis of the body.

The sealing of the body and the piston of the volume gauge from atmospheric pressure does not get around the maximum pressure differential sustainable across the Bellofram membrane; the anulus formed between the cylinder and piston would be filled with highly compressible air. This problem was solved by filling the anulus with oil. The oil was pushed into the anulus slowly by a pump, whilst moving the piston backwards and forwards in the chamber so no air was trapped in the anulus. The annulus is sealed by two 1/4" BSP plugs with Dowty seals. The volume of the annulus should remain constant during movement of the piston, due to the opposing effects of the two Belloframs. Hence when pressurised the piston floats in a hydrostatic stress system, the pressure supplied by an oil pump being transmitted to the pore fluid by the piston and by the oil annulus. The oil in the annulus may lubricate the Bellofram membranes so reducing side friction as mentioned in point 3). Errors due to toppling of the piston in the chamber are reduced in this design due to the central positioning of the transducer above the piston.

The high pressure volume gauge was calibrated for four pressures to see if the compressibility of the system, i.e. the PVC piston, would affect the calibration. The pressures used, were controlled by the maximum working pressure of the hand ram and the high pressure double burette used to calibrate the volume gauge. The hand ram displacing a measured volume of fluid from the burette into the volume gauge. The volume gauge back pressure was supplied by an oil pump, the pressure remaining constant during the calibration. The pressures used, the number of cycles of the calibrations and the regressions are presented in Table A1.1.

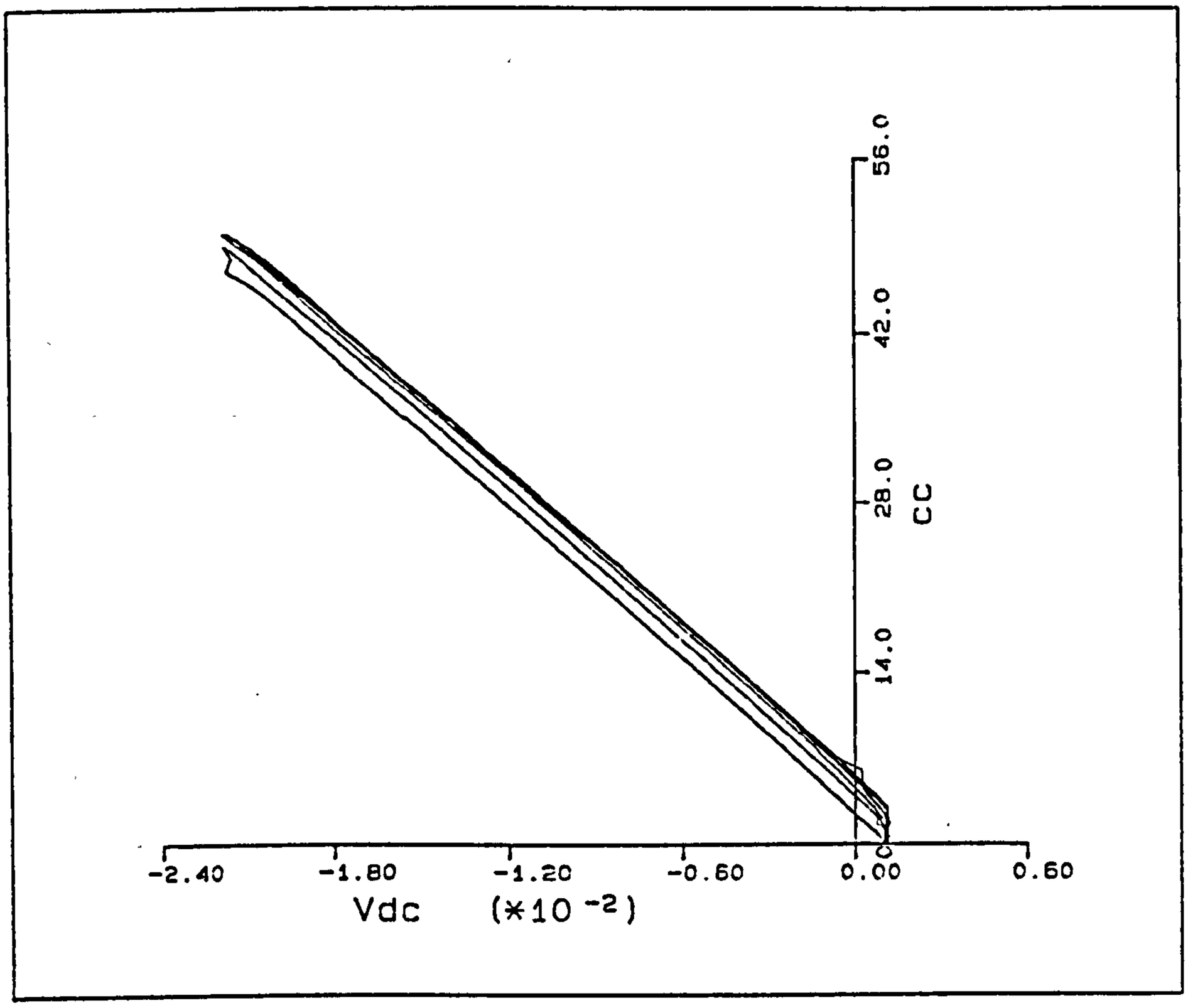

Figure A.1.5 Calibrations of the high pressure volume gauge at various back pressures.

Table A1.1 Calibrations of the new high pressure volume gauge

Pressure MPa	Cycles	Coefficient 0	Coefficient 1 ($*10^3$)	Correlation Coefficient
0.6	1	4.957454	-2.129181	0.99917662
1.43	3	5.360119	-2.112115	0.99924159
2.2	5	2.594971	-2.090903	0.99988186
3.0	7	4.668444	-2.112159	0.99940991

The odd numbered cycles are for filling cycles of the volume gauge, the regressions were calculated for these. The emptying (even

numbered) cycles were ignored for the tests performed. Only linear regressions were calculated for the data, despite higher orders giving better correlation coefficients. Fig. A1.5 shows the plot of the 7 calibration cycles (filling and emptying cycles); the shift in the start of the cycles is purely due to the choice of an arbitrary zero volume at the begining of each odd numbered cycle. The drop between cycles 5 and 6 is due to an adjustment in the volume in the device between cycles. The calibrations show no variation with pressure, at the low oil pressures employed here.

In practice the volume gauge was pressurised from an intensification of the air supply in the laboratory, which is maintained at 120psi. The intensifier approximately doubled this pressure. Preceeding this, the high pressure volume gauge was pressurised via a link off the oil pressure supply to the triaxial cell. The line off the main oil pump - triaxial cell line, contained a restriction and a T junction, to which the volume gauge was attached. The other branch of the T, was attached to a back pressure regulator (App. 6). This system was abandoned as the oil pump could not maintain pressures, since the leak past the back pressure regulator was to great.

A1.3.2) Medium pressure volume gauge

The high pressure volume gauge was considered excessive for the small back pressures used in this series of tests, therefore the intensifier was adapted to work as a volume gauge and intensifier. The unit was constructed by joining the base of a $50cm^3$ I.C. volume gauge to the top of a $100cm^3$ I.C. volume gauge, Plate A1.4. The pistons inside were joined using a packing piece slightly larger than the thickness of the end plate of a normal volume gauge, the

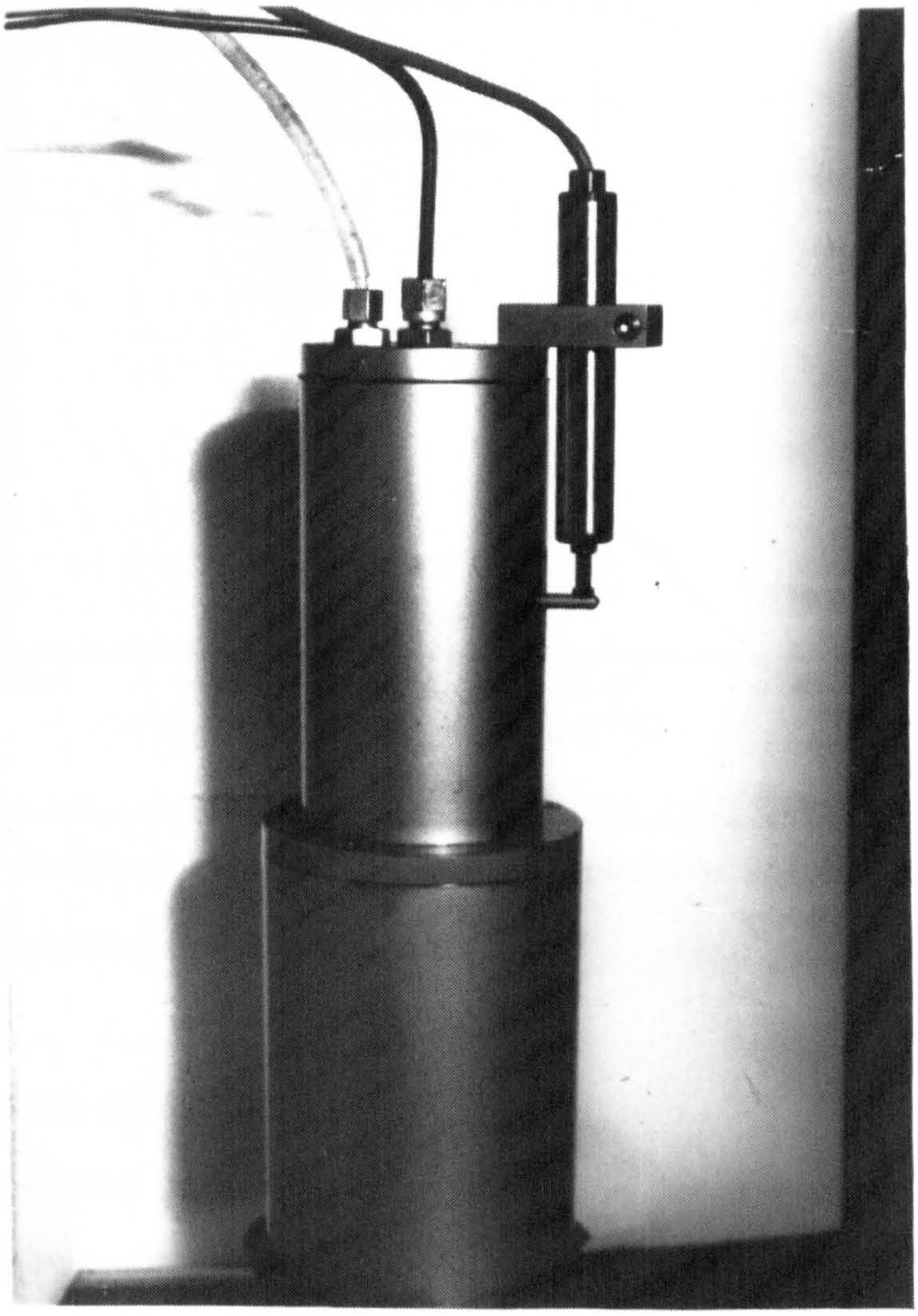

Plate A1.2 The medium pressure volume gauge and intensifier.

Bellofram membranes being removed at the joined ends. The calibration at the required back pressure, is shown in Fig. A1.6, the regression is presented in App. 4.

Some of the points presented above as well as a wider review and discussion of volume measuring devices used in soil mechanics, can be found in Alva-Hurtado and Selig (1981).

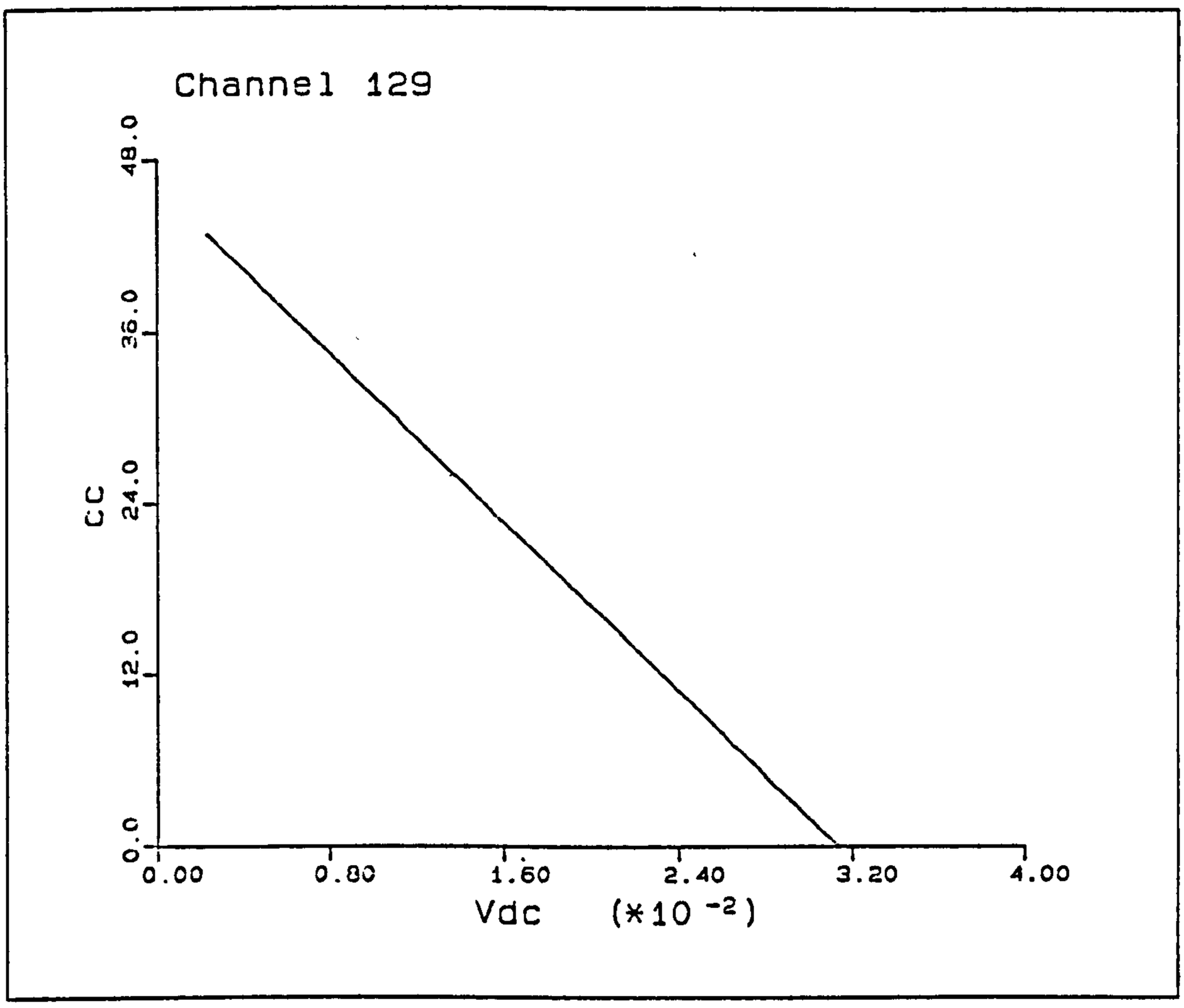

Figure A1.6 Calibration for the medium pressure volume gauge at the working back pressure.

A1.4) THE RADIAL STRAIN BELT

The conventional strain belt used in the laboratory consists of a lvdt in a frame work which is attached to the sample (Maswoswe, 1985; Maccarini, 1987). Because of the limited space around the sample in the high pressure triaxial cell a new radial strain belt had to be devised which would give accurate measurements of radial strain and satisfy the following conditions: a) able to work under high pressures; b) be light enough to attach to the sample so that the belt could always stay in the middle of the sample during compaction; c) be small enough to get in the cell; and d) able to withstand temperatures of up to at least 180^{o}C.

The design that was used, was that of a steel anulus 0.3mm thick,

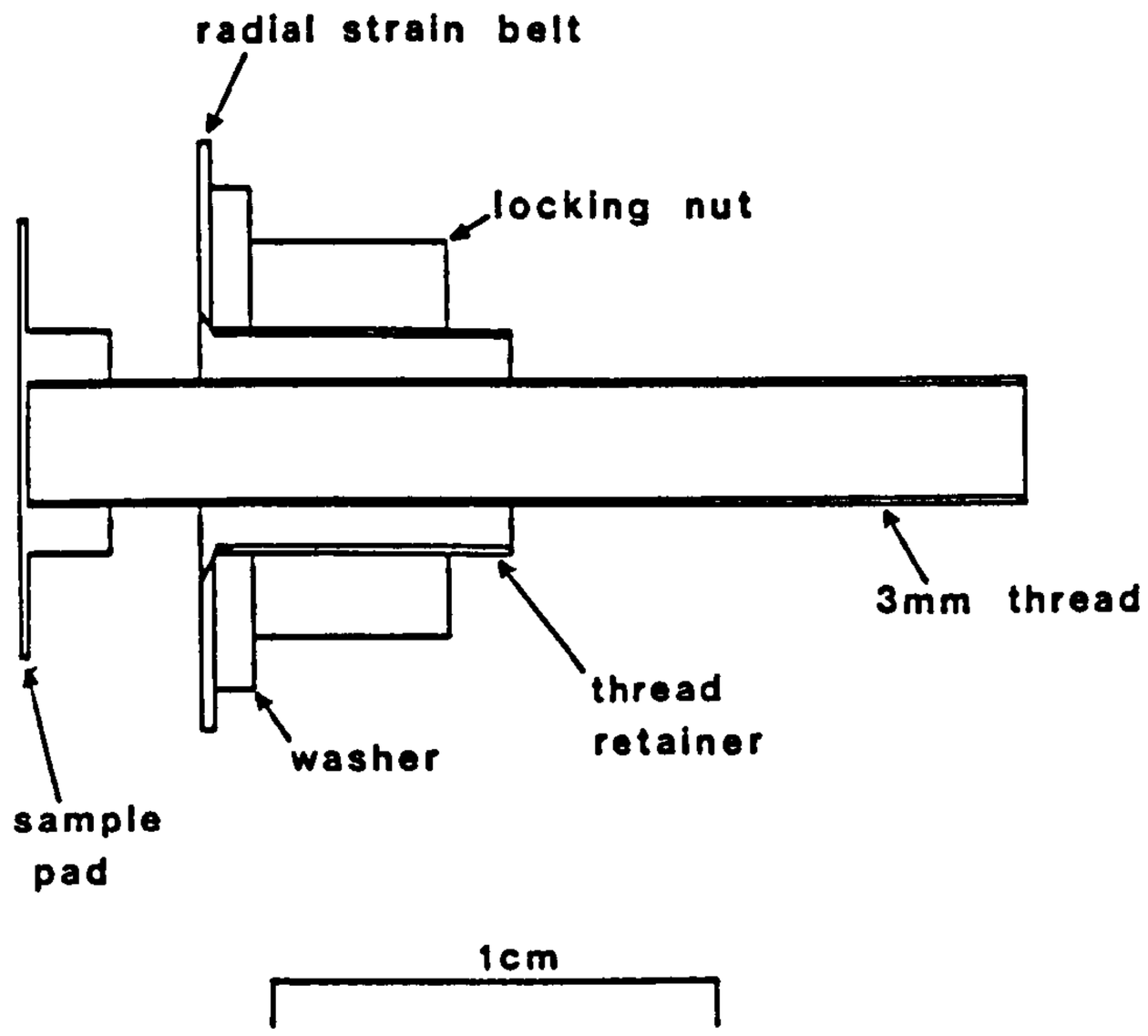

Figure A1.7 Cross section through the pad of the radial strain belt.

with an o.d. of about 46mm and 1cm high. Across the diameter are two pads which screw into position on the sample, and locked on to the belt with two locking nuts (Fig. A1.7). The pads are glued on to the sample membrane. The belt detects strain using four strain gauges attached to the steel anulus at 90^{o} to the pads. Two strain gauges are attached to the inner and outer surfaces and arranged in a full bridge circuit. The wire used is light weight, but has some stiffness which can support the weight of the belt.

The belt worked well, the calibration being linear over a range of over 1mm and repeatable over this range. At slightly elevated temperatures the belt also worked well (see tests EC1.50, EC2.50 and EC4.50 etc), but when subjected to a temperature of $130^{o}C$ the belt became troublesome, the equilibration time for the output to settle down was large (2 weeks), this was followed by a large drop in the output of the belt due to a short circuit of the strain gauges to the belt or to a breaking of the strain gauges. On disassembly of the experiment the insulation on the wires connecting the belt were seen

to have dissolved, and the strain gauges mesh had turned black possibly due to carbonizing of the oil.

Because the strain belt was a closed anulus only small strains could be measured before permanent strain was transfered to the belt, hence no tests using this belt were taken to shear failure.

Considering the above limitations, a second belt was made of similar design, but the ring was cut so allowing larger strains to be measured. The strain gauges were arranged on the complete, uncut half of the anulus again in a full bridge circuit. The anulus was made thinner, about 0.2mm thick so that the belt would be more sensitive despite the gauges being arranged on one half of the belt. The gauges used were WK-06-250BG-350 gauges supplied by Welwyn strain Measurements Co. limited, which can with-stand temperatures of up to 290^{o}C, App. 6.

This belt was built to enable large strains and high temperatures in our experiments. The only drawbacks being that due to the thinness of the belt one still had to procede with caution with the failure part of the tests, and secondly, during straining a rotational component would be felt by the pads, as the cut half of the steel anulus would not be compensated by the uncut half. The rotational aspect will only be important if the axial stresses are calculated by considering the change in the diameter of the sample using the strain belt output. In this case the calculation would need to be adjusted to consider the rotational movement. Alternatively the diameter could be calculated by the changes in volume and axial strain.

An important aspect in the use of this belt is the repeatability of the results. The belt was designed to be used on many samples, therefore the strain undergone by the belt in an experiment should not exceed the belts elasticity, as this would permanently deform the

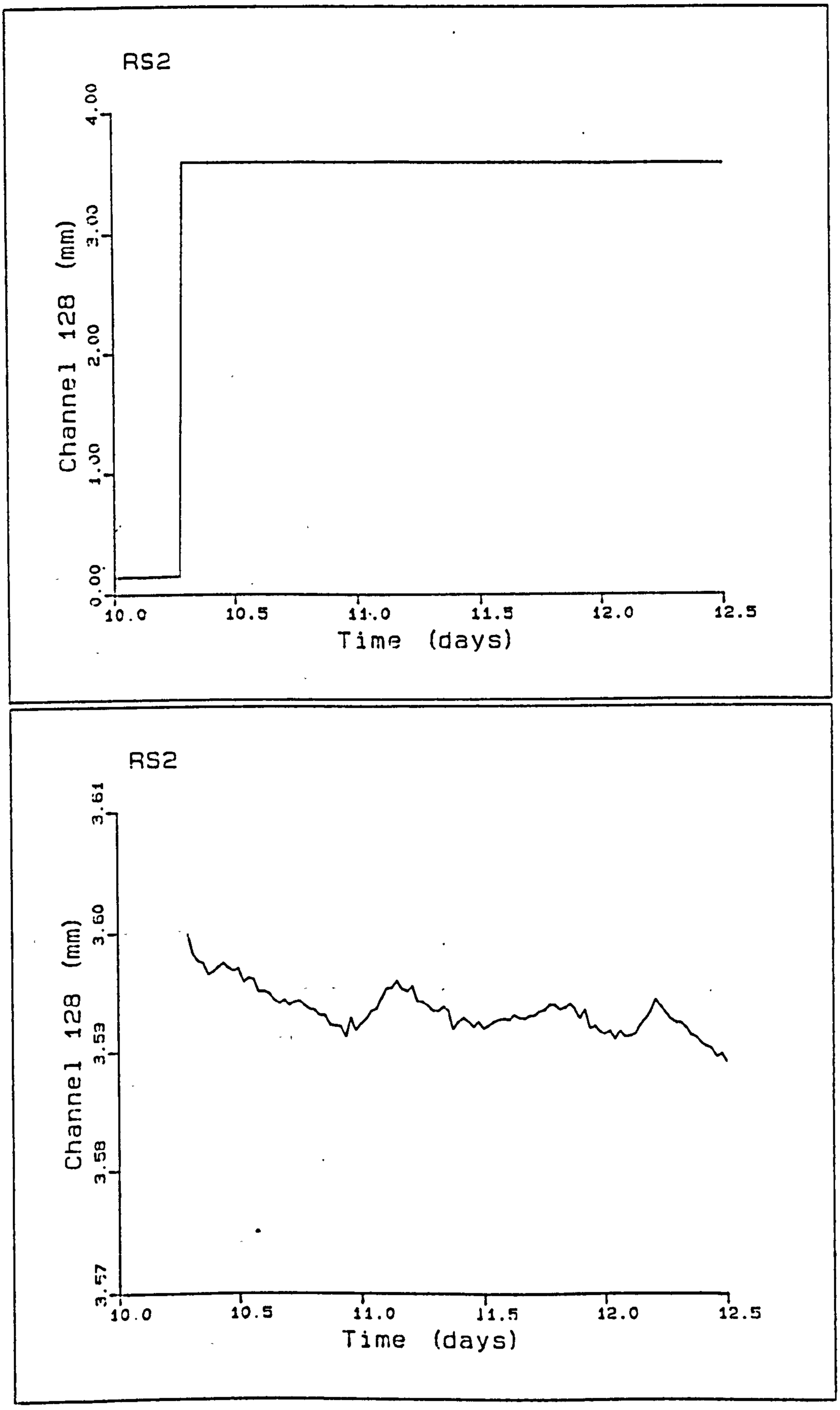

Figure A1.8 Stability of the second radial strain belt.

belt thus altering the calibration for any subsequent tests. If this were the case the strain belt would need recalibrating after each experiment. During calibration, the belt was cycled to strains up to 10% of the sample diameter, which was considered to be the maximum strain required to induce shear in the sample. The calibration consisted of 16 runs of 8 loading and unloading cycles, which were performed on different days, between which the output of the belt was monitored, to analyse output stability. The belt during this period was left for three days at an extension of 3.5mm, this was done to monitor any creep in the belt which could occur at large strains for experiments performed at slow strain rates. The calibrations showed excellent repeatability with only slight base line shift in both the loading and unloading cycles. The output of the belt at approximately 3.5mm radial expansion was very stable showing a variation of less than 5 microns over 2.5 days, Fig. A1.8. The variation is partly due to temperature variations in the laboratory which would be reduced in the triaxial cell.

A1.5) CONTROL OF THE TESTS

The tests in this study were predominantly K_o tests, the tests being performed at a Constant Rate of Strain (Chap. 3), with a constant lateral dimension being maintained by adjusting the confining pressure. The output of the radial strain belt dictated the required variation in confining pressure, which would maintain a condition of zero lateral strain in the sample. In the first experiments, the control of the confining pressure was performed by manually adjusting the loading on the spring of the oil pump. This was superceeded by an automatic adjustment of the confining pressure by a servo control of the loading of the spring of the oil pump. The

output of the radial strain belt was amplified in a Maclellan servo amplifier, the amplified output driving a stepper motor attached to the spring loading pressure valve on the oil pump. The connection between the stepper motor and the spring was through a gear box to reduce the torque of the loading device to make it compatible with the motor rating. The gear box also ensured that the change in the confining pressure was damped so reducing any shock loading of the sample. The first arrangement used a gear reduction of 1/125, this was found to react to slowly, and the motor used with this was seen to be damaged after controlling the first clay experiment (NSC2.20). For any subsequent tests a Maclellan motor was used with a gear reduction of 1/50. This was seen to work well for the short and long term tests.

Monitoring of the sample was performed by 70MPa pressure transducers recording the cell pressure, the pore pressure at the top and the bottom of the sample. Displacement transducers were used to measure the displacement of the ram externally, and to measure the movement of the piston in the volume gauge. The radial strain is measured using the strain belts described above, while the load is measured externally between the piston and the head of the loading frame. The transducers have a continual energisation of 5vdc, the output being logged by the Orion logging system.

A1.6) FUTURE APPARATUS DEVELOPMENT

The apparatus is at the present time being improved and developed in order to make the results obtained more accurate and to simplify results analysis, the development will also make the apparatus far more flexible.

The improvement includes development of an internal load cell

capable of measuring loads up to 80kN, the load cell is based on a design of Dr.A.Skinner, the design being commonly used low pressure research. A 26kN (6,000lb) model has been constructed previously (Bishop, Kumapley and El-Ruwayih, 1975), this load cell will also be strain gauged with high temperature gauges, enabling the load cell to be used with high temperature experiments.

The second improvement required on this apparatus is internal measurement of axial strain. At Imperial College inclinometers are used Jardine et.al. (1985), these cannot be used at high pressures due to their hollow nature. Therefore light weight submersible lvdt's are being considered.

A1.7) DATA ACQUISITION

The logging of the transducer outputs was performed using two systems during the period of experimentation, the first consisted of a Schlumberger Solartron data aquisition unit, which gave output voltages on a paper printout; this was used until October 1985. This system was substituted by the system which recorded and converted results for the laboratory, this was performed by a Schlumberger Orion datalogger linked to a Prime computer.

The Solartron data aquisition system consisted of a digital multimeter, a power supply for the strain gauges a relay switching unit enabling different channels to be logged, a data aquisition unit and a paper printer; the data aquisition unit transfering the readouts for different channels to the printer at set logging intervals.

The power supply energises the transducers with a 5vdc supply, the transducers being energised only momentarily to obtain an output. The relay unit enabled the recording of a maximum of 50 channels. The

data transfer unit contained a built in clock, a data transfer unit, and optional logging intervals, the logging intervals ranging from 1 second to 2 hours, a minimum logging time being dependant upon the number of transducers being recorded. The output voltages were typed into the central computer of the laboratory which converted the voltages to measurements, the measurements then being used to calculate the parameters, presented in App. 5 for the individual tests.

The Orion data logging unit controls the logging for most of the laboratory one user unit normally can have 20 channels recording at any one time. One unit consists of a stabilised power supply supplying a 5vdc supply to energise the transducers continually, the power supply works off 240v mains supply. The Orion logger reads the output of selected transducer channels at periods ranging from 3 seconds to two hours, the data being passed to a Prime computer where it is filed and processed when required.

The logging and data processing programs were written by D.Toll.

APPENDIX 2

HIGH PRESSURE OEDOMETER

The high pressure oedometer is a uniaxial testing device called a Rowe cell, which supplies a hydraulic load to a 10cm (4") diameter, 2.5cm (1") thick sample via a flexible membrane. This differs from the Casagrande type oedometer which supplies a weighted load to the sample via a metal platten. The high pressure oedometer is hydraulically loaded by a spring loaded Beacham high pressure oil pump, which can supply a maximum oil pressure of 70MPa (10,000 psi).

A back pressure/drainage system was fitted to the oedometer so enabling the measurement of volume strains at high back pressures. A heating system was also fitted, to investigate the effects of high temperature on compressibility at high pressure.

A2.1) DESCRIPTION OF THE HIGH PRESSURE OEDOMETER

The high pressure oedometer stands 43cm (17") high and has an outside diameter of 27.9cm (11"), Fig. A2.1. The body is mainly brass and consists of three main sections: The base consists of a stainless steel core 15.2cm (6") in diameter which contains the main drainage lines and the main porous stone 10.1cm * 1.2cm (4" * 0.5"), outside the porous stone sits an "o" ring. The steel core sits in a brass surround the two being locked together with an screw.

On the base sits the oedometer ring assembly: Comprising an oedometer ring of inside diameter 10.1cm (4") outside diameter 15.2cm (6") and an outer ring, the oedometer ring surround, 27.9cm (11")

outside diameter 2.5cm (1") thick. The steel oedometer ring and its surround are locked together by two metal seals. The oedometer ring surround is held to the outer (brass) part of the base by six Allen keys so sealing the oedometer ring to the base core with the "o" ring.

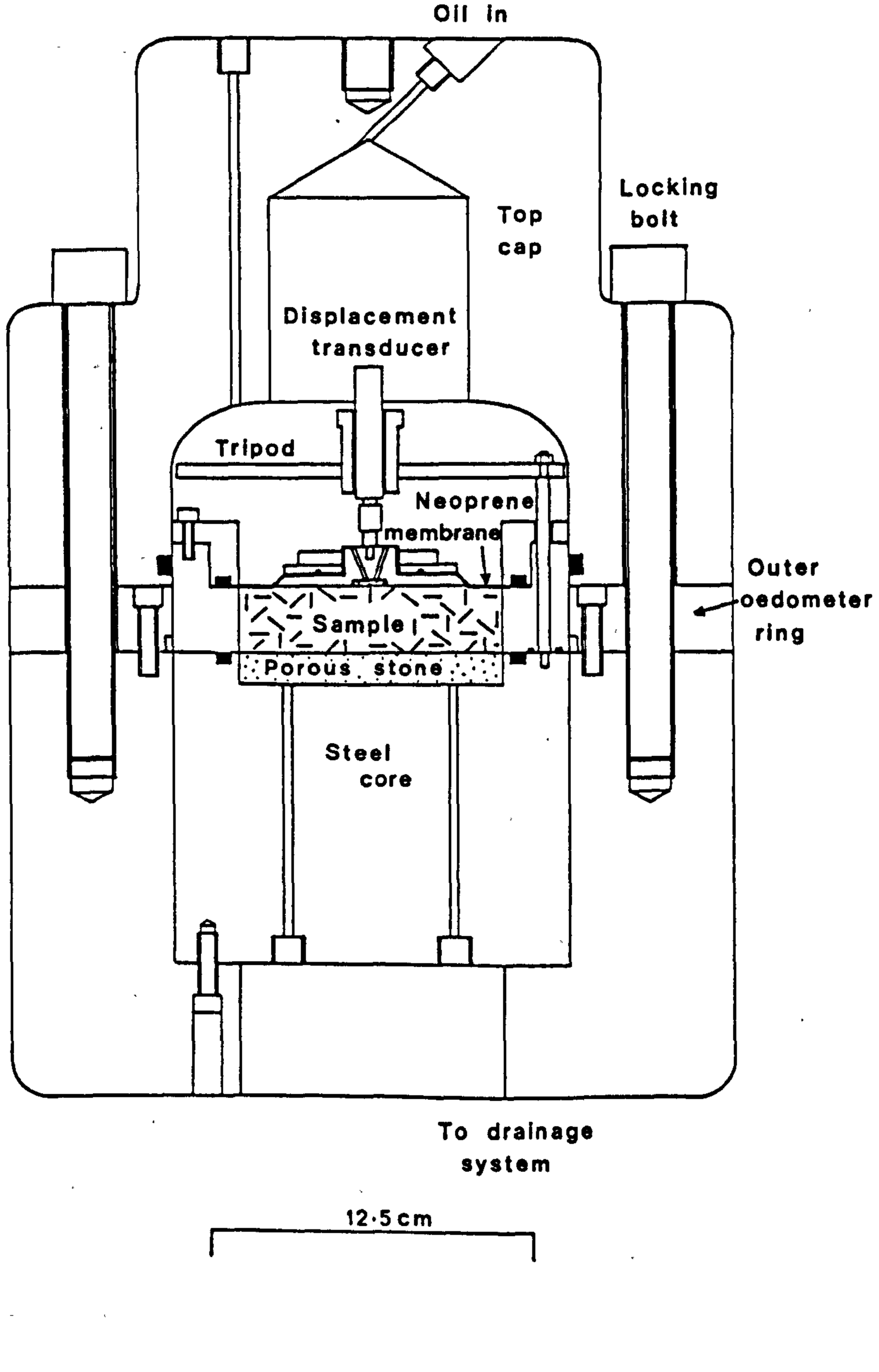

Figure A2.1 The high pressure hydraulic oedometer.

The top of the sample is isolated from the hydraulic loading oil by 0.6mm (0.023") neoprene rubber membrane, with a central island (sample top cap), which contains a porous stone and capillary tube connections to the drainage system. This allows pore pressures at the top of the sample to be measured. The sample top cap also holds the core of the lvdt enabling settlements can be measured. The body of the lvdt is held above the island by a tripod, the three legs of which screw into the steel core of the base. Hence, no movements of the oedometer ring relative to the base, due to compression of the "o" ring, are included in the sample deformation.

The rubber membrane sits on a step in the top of the oedometer ring, and is held in place by an "L" shaped flange. This locks onto the top of the oedometer ring with six allen keys, the flange sealing the membrane via an "o" ring (Fig. A2.1). Connections from the sample top cap and the leads of the lvdt leave the cell via holes through the oedometer ring and grooves in the base of the oedometer surround. The connections pass through plugs which seal the holes in the oedometer ring using "o" rings.

The top cap sandwiches the oedometer ring surround to the base, the whole cell being held together by six 1.9cm (3/4") diameter allen keys. The top cap seals to the outside diameter of the oedometer ring with an "o" ring (Fig. A2.1). The top cap has 4 entry ports and a central eye for lifting the top cap, the oil which supplies the load enters the cell through one of these entry ports. The cell is emptied by a exit port which is situated just above the "o" ring seal between the top cap and the oedometer ring. The oil pressure is monitored by a shape 70MPa (10,000 psi) pressure transducer, which is situated between the cell and the high pressure oil pump.

A2.2) DRAINAGE SYSTEM

The drainage system is effectively the same as that of the triaxial cell (Fig. A1.3). The drainage system measures volume changes at a back pressure which is self induced and regulated by a Tescom back pressure regulator (App. 6). The volume gauge in this system is a 100cc Imperial College volume gauge, which is approximately one half the total volume of the sample, and is capable of measuring a volume change of 0.02cc (App. 6). After the first tests the back pressure regulator was removed, and the back pressure supplied directly by the air pressure, floating the volume gauge.

The sample top cap contains two capillary tubes, enabling water to be flushed from the drainage system through the top porous stone. These tubes are secured into the stainless steel sample top cap by a small Enots connections. The other ends of the capillary tubes are connected to 1) a pressure transducer block in the drainage system to enable pore pressure measurement at the top of the sample, and 2) to an external drain. The main back pressure is measured at the base of the sample as in the triaxial cell. Shape 70MPa pressure transducers are used to measure these pore pressures.

A2.3) THE HEATING SYSTEM

As with the triaxial cell, the high pressure oedometer was supplied with a heating system, to enable the effects of temperature on compressibilities to be evaluated. The heating element used was an Eltron mica insulated band heater (App. 6), this is a 2KW heater working off 240V; it clamps to the outside of the oedometer ensuring a large contact area. A large contact area is important in heating such a large volume of metal, so the maximum transfer of heat to the vessel is obtained. The element used with the triaxial cell has a

very small contact area so large amounts of insulation are required to contain the heat. This heating system was not used during the present series of tests, and will not be discussed further.

APPENDIX 3

SAMPLE PREPARATION AND TEST PROCEDURE

A3.1) SAMPLE PREPARATION

A3.1.1) Chalk

The chalk samples were cored from sections of Ekofisk core or from blocks of chalk obtained from Pegwell Bay or Butser Hill. The blocks from which the samples were cored were cut into slabs approximately 80 mm thick using a large circular saw. The samples were cut using a thin walled 38mm diameter corer, attached to a drill; during coring water was used as a lubricant. The coring was performed at a steady pace to limit distortion in the wall of the corer. Once the cylindrical samples are obtained the top and bottom are squared off using standard soil mechanics equipment (Plate A3.1). The samples are placed in a 38mm diameter, 76mm long cylindrical mold which has perpendicular top and bottom. The sample ends are then made perpendicular to the axis of the sample by trimming them flush to the mold. The variation in bedding is kept to a minimum, differences in the lengths of the samples being kept below 0.2mm. Surface ginding of the ends was ruled out due to the brittle and weak nature of the chalk.

The Pegwell Bay and Butser Hill samples after cutting to size were dried for at least 12 hours in an oven set at 110^{o}C, the samples were then left to cool in a vacuum desiccator for a few hours under a vacuum of 500mm of mercury. Once cool, the samples were weighed to obtain the dry weight, this was done to an accuracy of $\pm$0.0002g and

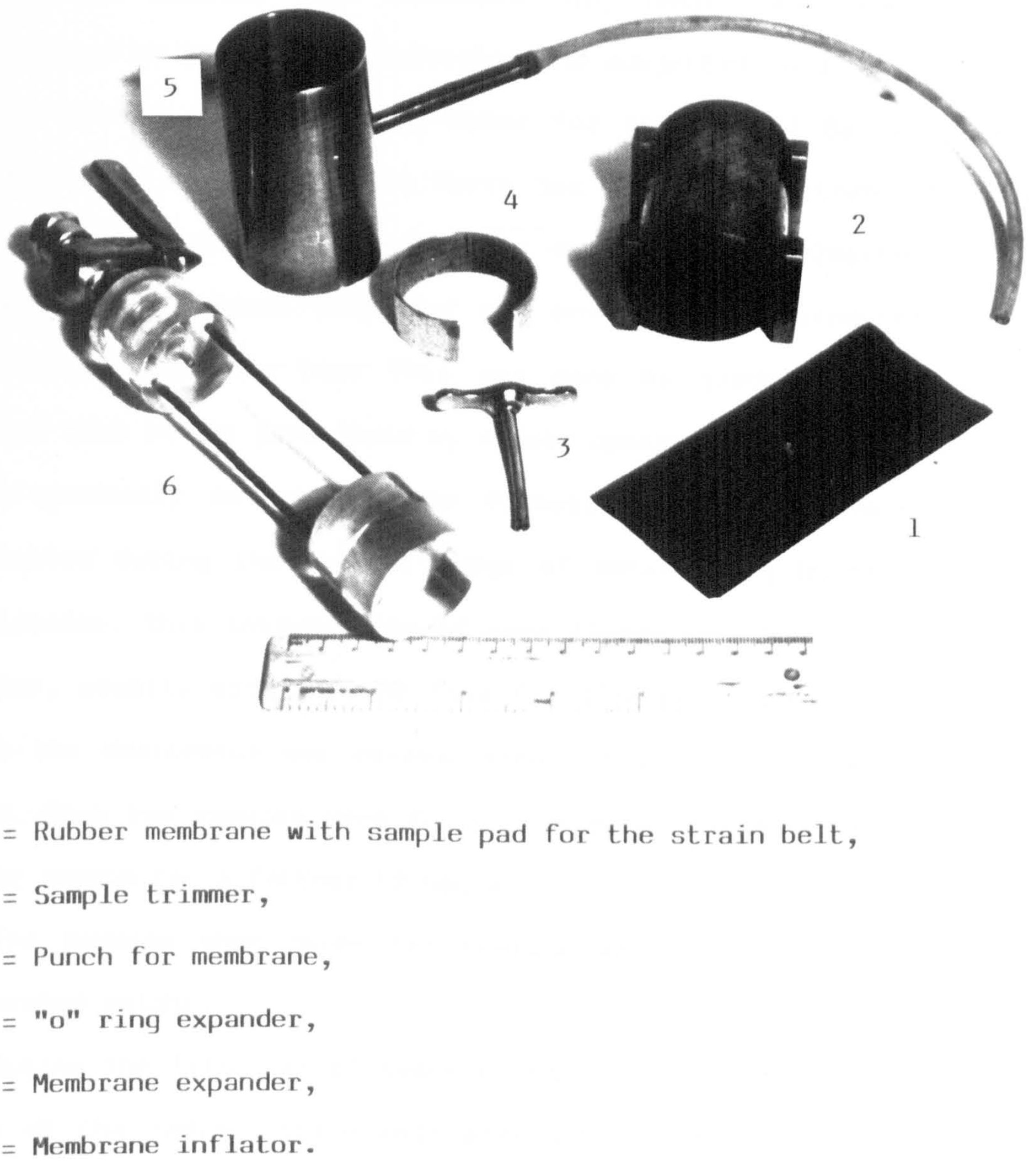

1 = Rubber membrane with sample pad for the strain belt,

2 = Sample trimmer,

3 = Punch for membrane,

4 = "o" ring expander,

5 = Membrane expander,

6 = Membrane inflator.

Plate A3.1 Equipment used during sample preparation.

done as quickly as possible to restrict any rehydration. The oil bearing North Sea samples were not dried as the oil in the sample would be affected.

All the samples were measured for length and diameter and transfered to the vacuum desiccator and subjected to a vacuum for at least 12 hours. Pore fluids, water for the Pegwell Bay and Butser Hill samples and oil for the North Sea samples were then introduced to the desiccator. The vacuum was maintained by closing the tap accessing the vacuum pump and the pore fluids introduced to the desiccator via this tap. This was done by gradually letting the vacuum suck in the pore fluid by slowly opening the tap. This must be done gradually as some of the Pegwell Bay samples fractured and shattered during the initial surge of water being pulled into the desiccator. This introduction of pore fluids was done in a stepwise manner, usually with four or five fluid introductions. Between each step the desiccator was re-evacuated for a period of at least one hour. Once the samples were fully covered by fluid, they were left under vacuum for a further 12 hours.

The samples when ready for testing were weighed to obtain the saturated weight.

During the first set of tests on the Central North Sea chalk, the pads of the radial strain belt were attached to the outside of the membranes; samples were put into the membranes using the method outlined in Bishop and Henkel (1962). The membrane is put on a membrane expander (Plate A3.1), and the expander evacuated so pulling the membrane tight to the expanders walls. Saturated porous stones and filter paper used at both ends of the samples are added to the sample and two rubber strips placed over the circumference of the porous stones which overlap onto the sample. These rubber strips

(38mm diameter, 25mm long) also overlap onto the sample pedestal and the sample top cap for the bottom and top of te sample respectively. The bottom overlapping strip was placed over the sample pedestal and the membrane rolled off the sample expander onto the sample pedestal, the top of the membrane also being rolled off the expander. The sample pedestal before the sample is added contains a meniscus of water so no air is trapped between the pedestal and the stone. A second membrane is put over the sample in the same manner. The membranes are then secured to the base using 3 o-rings. The strain belt and an o-ring expander with 2 o-rings is then placed over the top of the sample. Water is flushed through the top cap on to the porous stone at the top of the sample until a thin layer of water is seen covering the stone, the sample top cap is fitted into the membranes. The membranes and secured to the sample top cap with two o-rings.

Once the membraned sample is attached to the pedestal, the membrane is cleaned of any water or oil using butanone and the strain belt pads glued to the sample mid height (across the diameter), using M-Bond adhesive. With later tests, new pads for the radial strain belt were made and attached to the inside of the membranes before being attached to the sample. The first membrane was punched with two holes at the mid height of the membrane across the diameter. The shaped pads were arranged so that the curvature of the pads, (which are of the same radial curvature as the sample) was perpendicular to the axis of the membrane. The pads were then glued to the membrane using M-Bond or Loctite Superglue. Once dried, the membranes were inverted so that the pads were on the inside. The membrane was then sealed to the outside of the pad using a smear of glue. The sample was fitted into the membrane as before, but ensuring that the pads

lay at the mid height of the sample. The second membrane once fitted, overlapped the screw threads of the pads, so two small circular holes were cut in the outer membrane to expose the threads. The second membrane being glued to the outer partof the pads as with the first membrane. This was to ensure that no oil leaked between the two membranes. The radial strain belt could then be screwed into the pads and secured with the two locking nuts.

During the sample shape variation tests samples shorter than the 76mm standard were made up to this height by adding stainless steel packing pieces 38mm in diameter. This was placed on top of the sample between the top porous stone and the sample top cap.

A3.1.2) Clay

Due to the deviated nature of the wells from which the cores were taken, bedding in the clay and the cleavage was not perpendicular to the core axis. To obtain a sample with bedding at right angles to the long axis of the triaxial sample, a block of the clay was cut along the inclined cleavage/bedding so the block had reasonably square ends. The block was reduced in height to approximately 80mm in length, and secured in a standard soil mechanics 38mm diameter sample trimmer (Bishop and Henkel, 1962). The inclined sides were cut to size and perpendicular to the ends, and plane to the cutting edge of the trimmer. This generally took at least ten hours, so when the core was not being cut, the samples were sealed by wrapping in "Cling Film" and sealed in wax. The ends were cut down to size using the mold used to trim the ends of the chalk samples, Plate A3.1

The samples were weighed and measured before testing and samples or offcuts of samples saved and wrapped in "Cling Film" and sealed in wax for moisture determinations.

The samples were inserted into the membrane in the same manner as the chalk samples. Fractures were seen to appear while cutting with a sub vertical orientation as well as a pronounciation of the cleavage, due to drying of the sample. Saturation of the samples by the vacuum method used on the chalk samples, was not performed on the clay samples as any swelling would damage the sample particularly with regard to the existing fractures.

A3.2) TEST PROCEDURE

A3.2.1) K_o tests

Once the sample is set up in the triaxial cell, and the cell filled with oil, two courses of action were taken.

Initially when no back pressure could be applied by the volume gauge, the sample was subjected to a small confining pressure of approximately 1MPa (100-150 psi), Then loading was started and the cell pressure adjusted either manually while monitoring the radial strain, or the servo system was set up to maintain the initial strain belt output. The loading of the sample was generally set to 0.03mm/min for chalk samples (though for Butser Hill chalk loading was performed at 0.02mm/min), the strain rate tests were run at various strain rates.

i) Applying back pressure

The second procedure involved increasing the cell pressure and the pore pressure up to a back pressure of approximately 1.8 MPa while keeping an effective stress of approximately 0.2MPa constant. After applying the back pressure the sample was left for some time to equilibrate; the loading was then started.

ii) Shearing following K_o loading

Shearing subsequent to K_o loading was performed in the undrained state. The shearing was performed by maintaining a constant cell presssure, by disconnecting the servo system which had controlled the cell pressure during the K_o part of the test. The loading was also changed for the shearing; the loading being decreased to 0.01mm/min.

A3.2.2) Triaxial compression tests

The cell pressure and the pore pressure were increased as in the latter K_o tests to an effective stress of approximately 0.2MPa and a back pressure of 1.8MPa. Then an undrained increment of hydrostatic stress was applied and the sample allowed to equilibrate. The sample was then drained. The end of isotropic consolidation was seen by the equalisation of the pore pressure at the top of the sample to the back pressure. The sample was subsequently loaded either drained or undrained at 0.01mm/min.

In the drained hydrostatic consolidation tests, the cell pressure was increased using the velocity control on the servo amplifier. This increases the loading on the spring controlling the confining pressure unit. The speed of the motor pumping the oil was gradually increased by hand, resulting in a continuous but not constant increase in isotropic stress.

APPENDIX 4

CALIBRATIONS OF THE EQUIPMENT AND TRANDUCERS

A4.1) CALIBRATION OF THE TRIAXIAL CELL

The acquisition of of accurate measurements from the electronic transducers requires their calibration, which enables voltage outputs to be related to actual measurement of parameters and quantities in the tests. For the measurements to be meaningful and to increase the accuracy of the results, certain aspects of the apparatus must be calibrated. The cell being simple in design only required two aspects to be considered.

A4.1.1) Ram friction

Due to the load being measured externally by the MRE/NCB load cell, the load actually experienced by the sample would be the load registered by the external load cell minus the friction of the ram against the upper chamber of the triaxial cell. The determination of the ram friction was evaluated by pushing the ram into the triaxial cell at a constant rate, at various cell pressures. The rate of the ram displacement was not considered to affect the ram friction.

The results of these tests showed that the ram friction increased with the displacement of the ram at constant cell pressure Fig. A4.1; this is possibly due to variation manufacturing of the ram. The cell pressure pump would not affect this measurement as it works against a leak. In addition, the ram is balanced and so the volume change of oil in the cell is negligable.

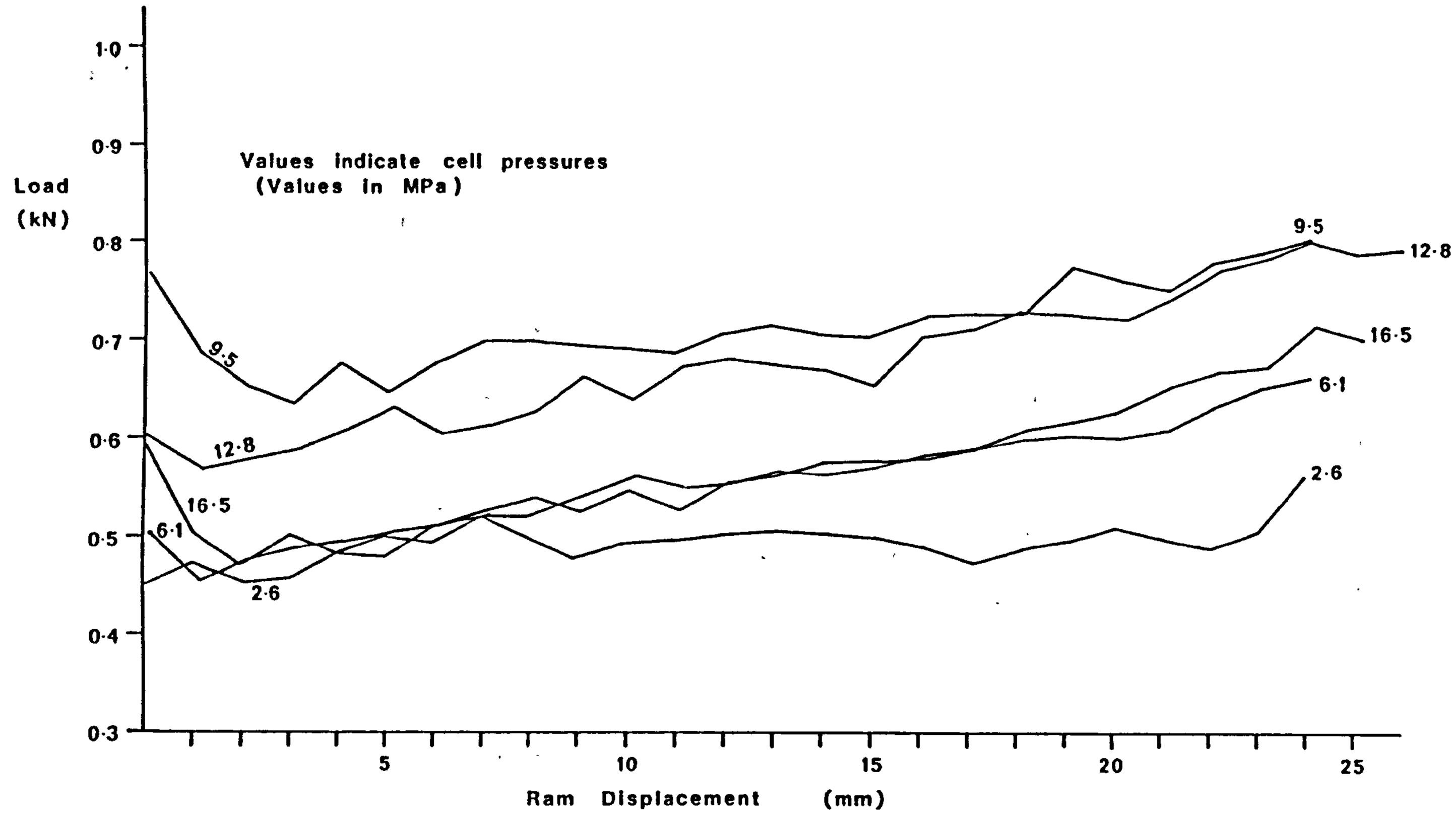

Figure A4.1a Increase of ram friction with ram displacement - Low cell pressures.

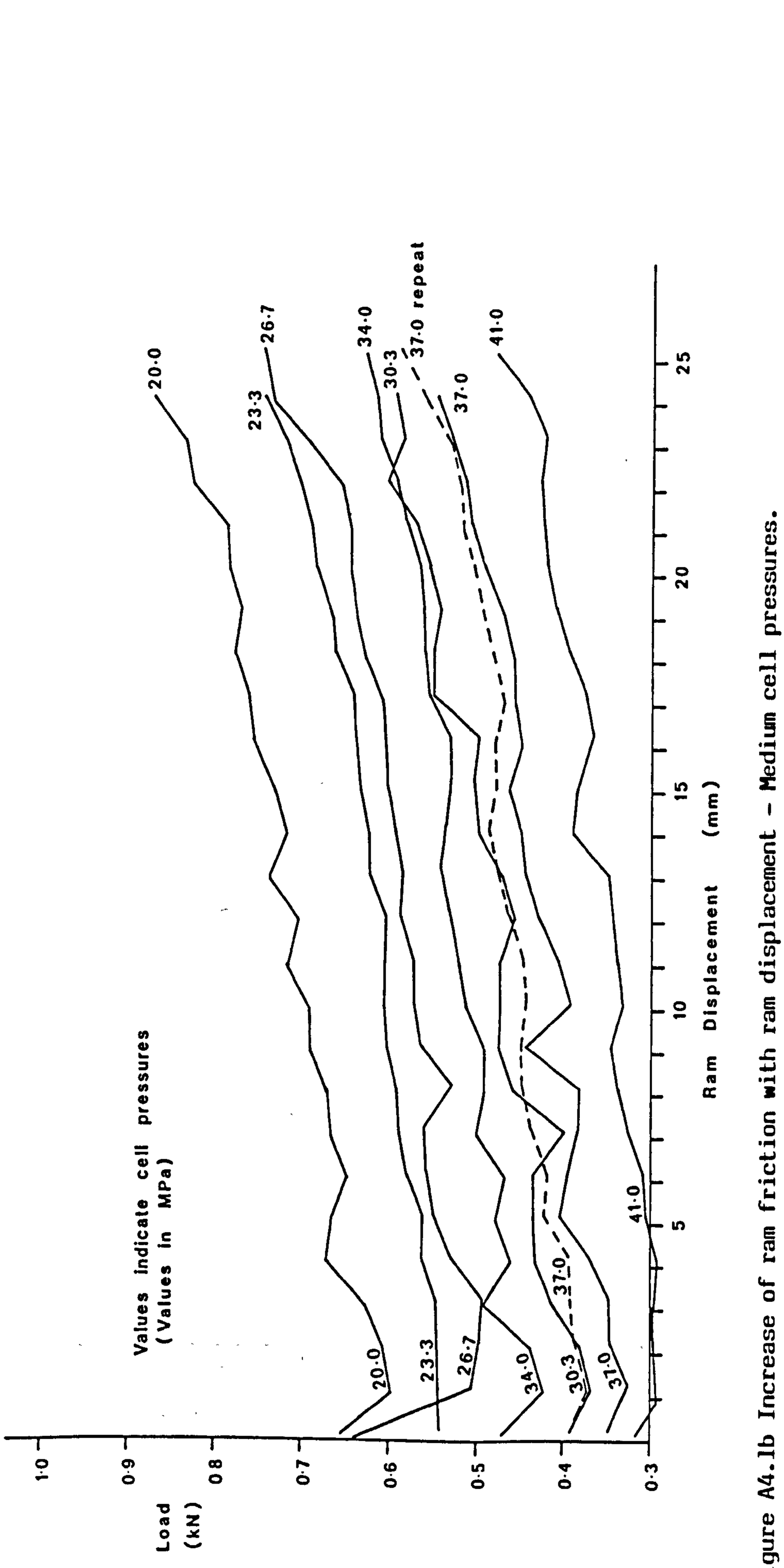

Figure A4.1b Increase of ram friction with ram displacement - Medium cell pressures.

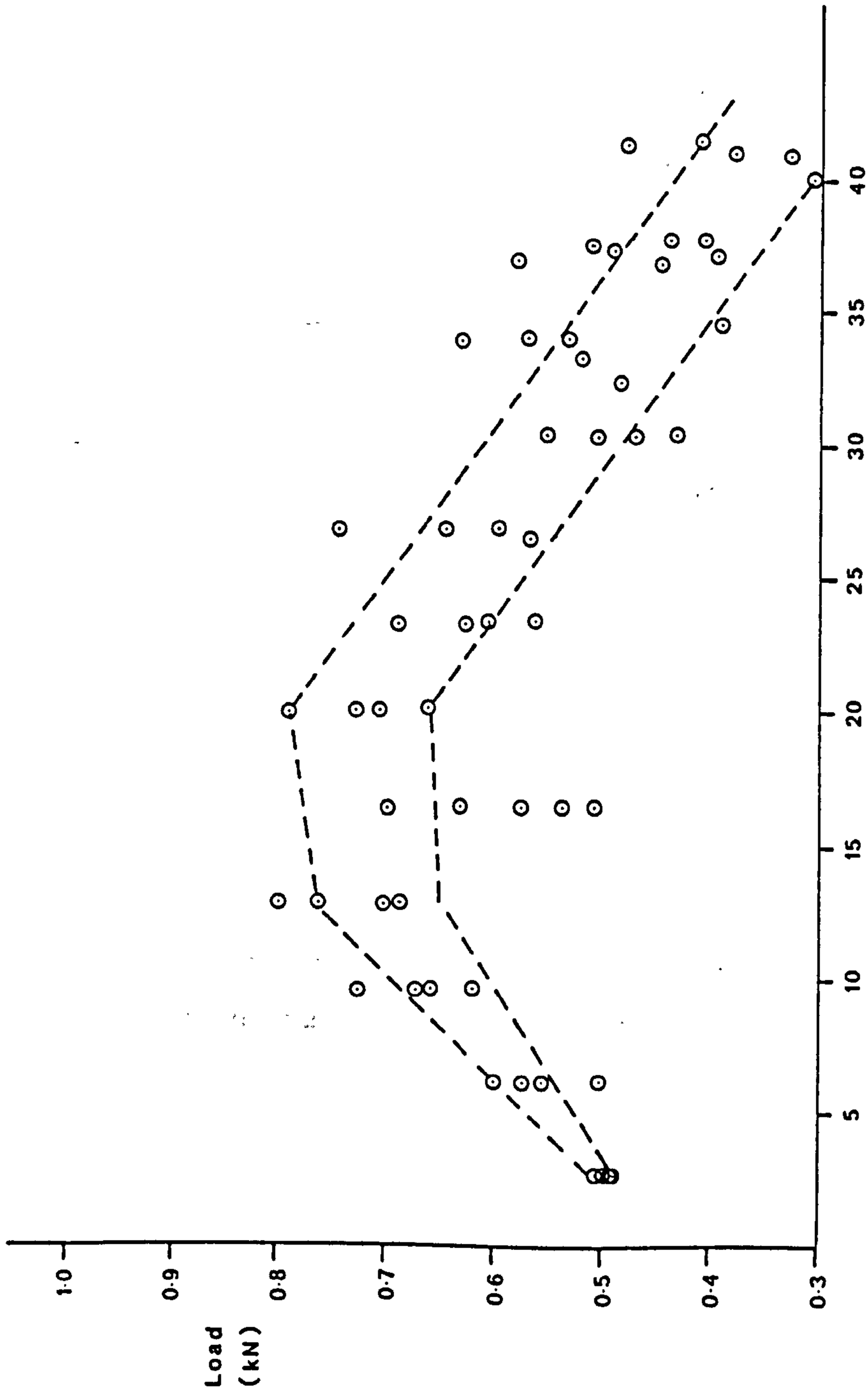

Figure A4.2 Variation of ram friction with cell pressure.

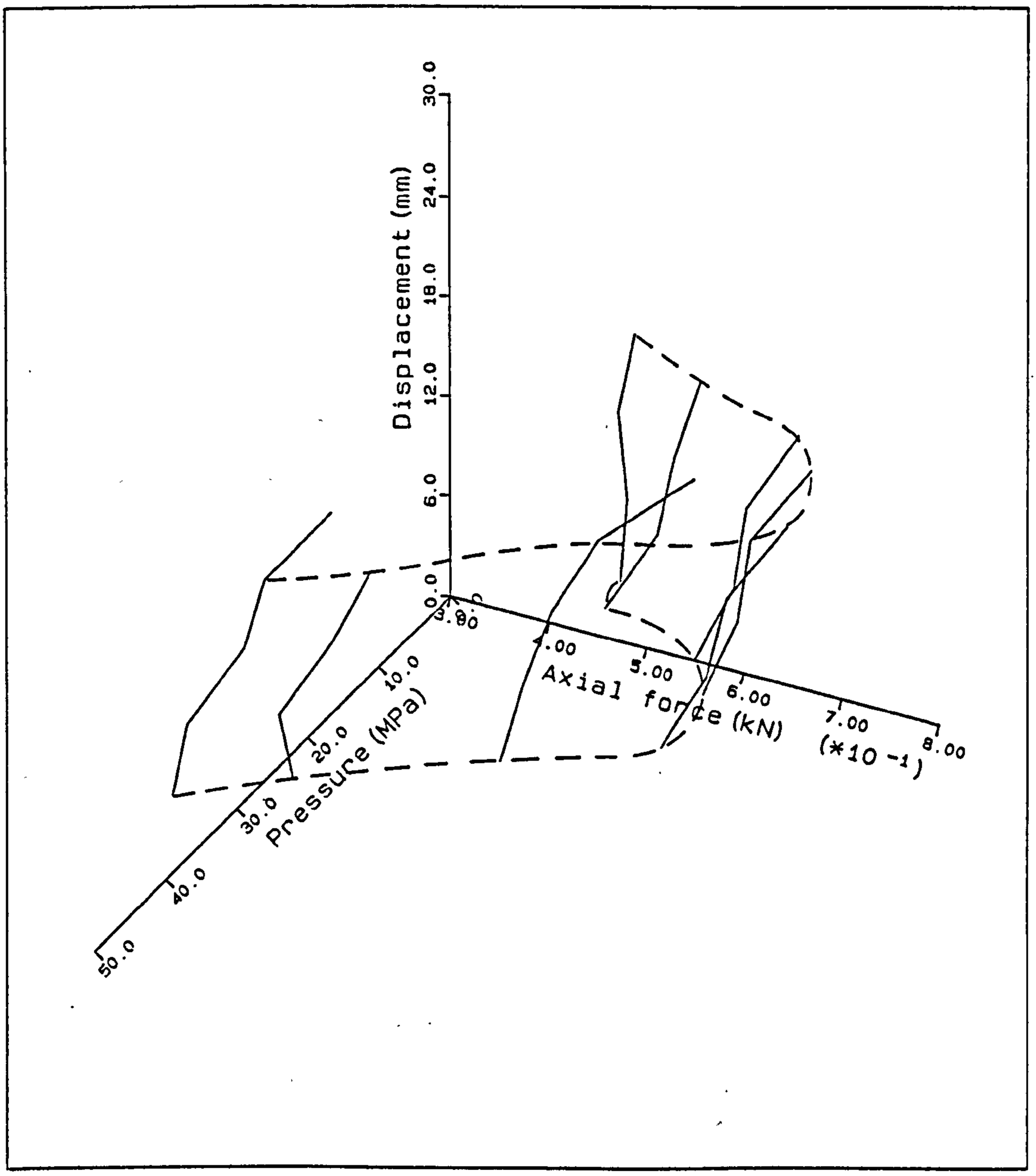

Figure A4.3 3-d plot of ram friction in the triaxial cell.

The increase of the cell pressure can also be seen to affect the ram friction, Fig. A4.2. Initially at pressures below ~20MPa, the ram friction increases with cell pressure, after which it drops with increasing pressure. The design of the ram incorporated an over balancing of the ram to balance the friction of the seals (pers.com. A.E.Skinner). The friction in the seals has reduced with wear and at cell pressures above 40 - 45MPa the ram can drop under its own

weight. The increase and decrease of the ram friction with cell pressure was attributed to an increase in the seal friction with pressure, followed at higher pressures by expansion of the cell (pers. com. A.E.Skinner).

In normal triaxial tests, loading at constant cell pressure the ram friction due to the displacement would only have to be considered for a particular cell pressure. However, in the K_o experiments conducted in this research the ram displacement and the cell pressure varies in the test. Calibrations were generated for the ram friction due to the increase in cell pressure (RF) and for the displacement of the ram into the cell (RD) with the use of software developed by D.G.Toll and A.J.Bond.

$$RF = 3.47959*10^{-1} + 2.66370*10^{-2}.(CP) - 7.23458*10^{-4}.(CP)^2$$

$$RD = 0.0 + 8.09000*10^{-3}.(Disp.)$$

Where CP = the cell pressure, and Disp. = the displacement of the ram into the cell. The overall picture is shown in the 3-d plot, Fig. A4.3.

A4.1.2) Ram shortening

The axial (vertical) displacements of the samples measured during the tests, were measured externally from the top of the ram relative to the base of the cell. During loading of the samples a shortening of the ram and the porous stones on each end of the sample will also occur. The only accurate method of measurement of axial displacement is to measure the shortening of the sample using some displacement measuring system attached to the sample (Jardine et.al., 1985;

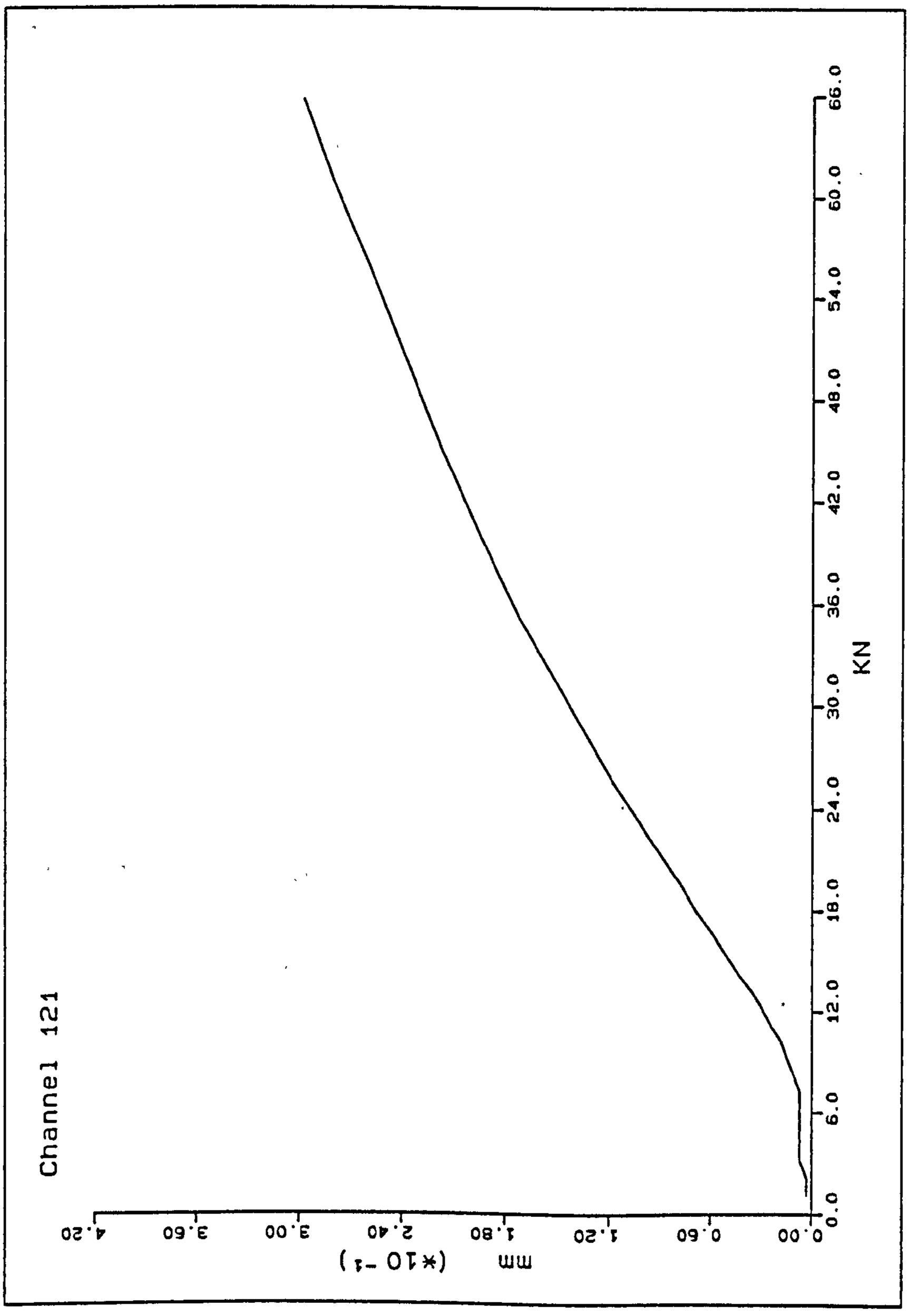

Figure A4.4 Ram and sample pedestal shortening during axial loading.

Newman and Martin, 1977). Such a system has not yet been introduced into this equipment.

To "calibrate out" the effects of both the ram and sample pedestal shortening and the compression of the porous stones, a steel dummy sample was put in the cell and set up with porous stones and filter paper as with test samples; this was then subjected to loading. The steel sample would also shorten in response to the loading; this shortening was calculated using a Young's modulus of 210GPa and deducted from the total displacement. The corrected displacement was plotted against load Fig. A4.4, and a regression obtained for the ram shortening (RS).

$$RS = 5.29218*10^{-3} - 2.04271*10^{-3}.(load) + 4.48226*10^{-4}.(load)^2 - 9.44047*10^{-6}.(load)^3 + 6.28581*10^{-8}.(load)^4$$

The above regressions were stored by the computer and used in the recalculation of the results.

A4.2) TRANSDUCER CALIBRATIONS

The transducers were calibrated and regressions calculated by the computer for each instrument. Calibrations were performed several times to check the reproduceability.

The pressure transducers were calibrated on a Budenberg pressure system over their full range for approximately 30 data points. The displacement transducers and radial strain belts were calibrated on a vernier system which was accurate to 10 microns. The strain belt calibrations for the second belt was seen to be very sensitive to the calibration set up. This was due to the rotational aspect of the pins during loading and subsequent opening of the belt. The load cell was

Table A4.1 CALIBRATION COEFFICIENTS FOR TRANSDUCERS USED WITH THE TRIAXIAL CELL

TRANSDUCER	COEFFICIENT 0	COEFFICIENT 1	COEFFICIENT 2	COEFFICIENT 3	COEFFICIENT 4	CORRELATION COEFFICIENT	NUMBER OF POINTS
LOAD CELL	$2.56016*10^{0}$	$-1.97328*10^{4}$	$9.64966*10^{5}$	$1.96224*10^{8}$	$1.29263*10^{10}$	0.99999952	16
RADIAL STRAIN BELT No.1	$-6.52188*10^{-1}$	$1.96927*10^{2}$	-----	-----	-----	0.99985921	--
RADIAL STRAIN BELT No.2	$1.38904*10^{0}$	$6.18298*10^{2}$	-----	-----	-----	0.99998951	--
CELL PRESSURE	$1.35748*10^{0}$	$-3.66235*10^{3}$	$-3.77351*10^{3}$	-----	-----	1.00000167	29
BACK PRESSURE	$-1.04641*10^{0}$	$1.39376*10^{2}$	$7.18800*10^{0}$	-----	-----	1.00000000	28
PORE PRESSURE	$9.37648*10^{0}$	$-3.46694*10^{3}$	-----	-----	-----	1.00000048	28
DISPLACEMENT	$1.00387*10^{-1}$	$-7.74295*10^{2}$	-----	-----	-----	1.00000525	53
VOLUME GAUGE LOW PRESSURE	$4.10574*10^{1}$	$-1.51902*10^{3}$	-----	-----	-----	0.99996686	30
VOLUME GAUGE MEDIUM PRESS.	$4.63357*10^{1}$	$-1.47835*10^{3}$	-----	-----	-----	0.99998033	52
VOLUME GAUGE HIGH PRESSURE	$4.66844*10^{0}$	$-2.11215*10^{3}$	-----	-----	-----	0.99940991	57

calibrated using an Amstler loading system, the loading being performed up to loads of 200kN (20 tons). The calibrations for two volume gauges used in this series of tests have been presented in Appendix 1.

Regressions for the transducers used in the latter tests are given in Table A4.1 with their coefficients of correlation.

One possible source of error in the K_o tests has been found concerning the radial strain belts. As seen in Table A4.1 the calibrations and regressions give a good correlation coefficient, and the calibrations were seen to be reproducible. The outputs from the belts were also seen to be stable over a period of time, at least for several days (App.1). However, the source of error is seen as the pressure sensitivity of the belts. During K_o tests the cell pressure is increased gradually, and the output from the belts are seen to vary with the increasing cell pressure. The first example of this was when the first radial strain belt was used to investigate the compressibility of rubber membranes, and whether these were being compressed during the K_o tests on the North Sea samples (as in these tests the radial strain belt was glued to the membrane). A dummy Brass sample was used and the output of the radial strain belt (channel 16) monitored while the cell pressure (channel 3) was increased. Fig. A4.5 shows the data obtained from this test. On the basis of this result, for all subsequent tests, the pads of the radial strain belt were attached to the inside of the membranes, and hence, in direct contact with the sample. Later tests with the first and second radial strain belts in direct contact with a steel dummy sample (i.e. the pads of the belt attached to the inside of the rubber membranes) showed similar results. Fig. A4.6 shows the output of the radial strain belts with increasing cell pressure. In this

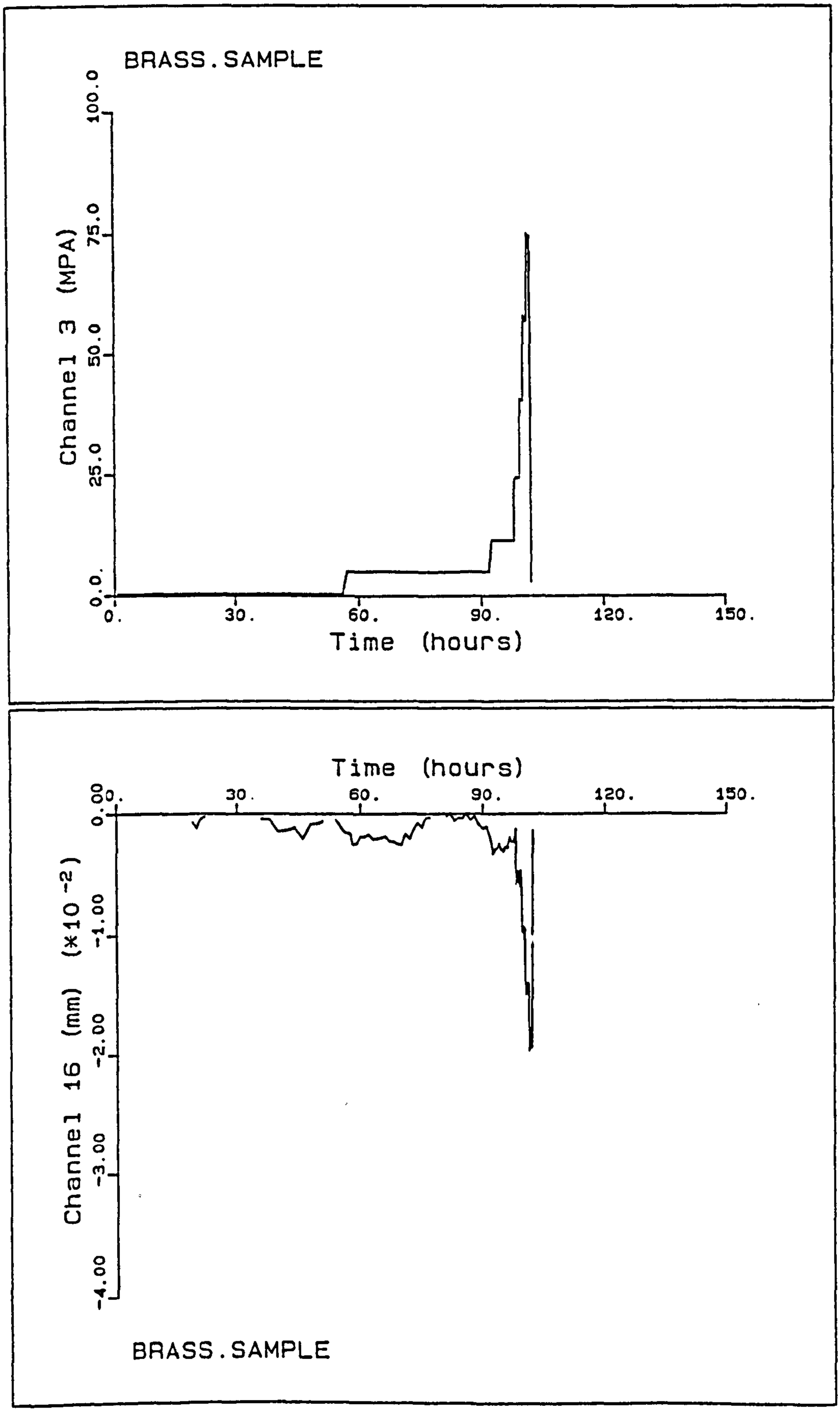

Figure A4.5 Output of first radial strain belt with cell pressure.

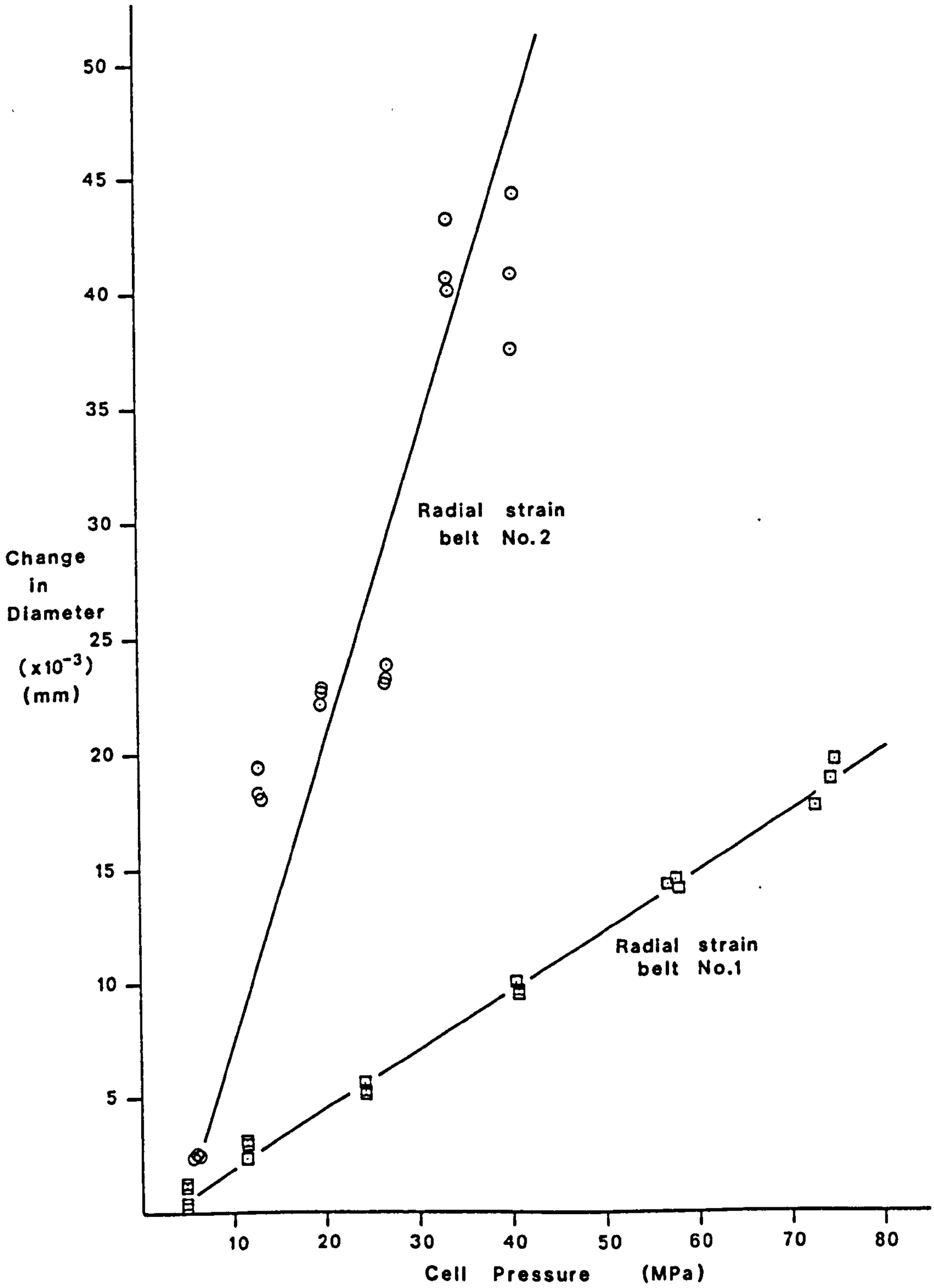

Figure A4.6 Apparent change in diameter of sample due to the pressure sensitivity of radial strain belts.

plot the radial contraction of the steel sample has been taken into account and therefore the presented data does not include this effect.

This observation obviously affects the tests as the servo system tries to maintain a zero change in output fron the radial strain belts. Thus, if there is an apparent reduction in the radial strain, purely due to this pressure sensitivity of the belts, the servo system would maintain the zero change in output from the belts by allowing the sample to undergo an increase in radial strain. This pressure sensitivity of radial strain belts has also been recognised by de Waal (1986). This effect may affect the data obtained from "K_o" tests, as shown in Chapter 4. Work is currently being performed at the Norwegian Geotechnical Institute to produce a radial strain belt whose output is independant of pressure.

APPENDIX 5

CHALK TEST RESULTS

A5.1) NORTH SEA CHALKS

The North Sea chalks samples were obtained from two wells in the Ekofisk area, all of the samples were oil saturated using Ekofisk oil obtained from the centre of the field. The samples were tested under K_o conditions with a constant rate of strain loading, these tests were the first to be performed, with the condition of zero lateral strain maintained by manual adjustment of the cell pressure control system.

Three samples of oil saturated North Sea chalk were tested at an elevated temperature of 50°C, EC1.50, EC2.50, and EC4.50, the others being tested at 20°C. One test EC7.130 was tested at a temperature of 130°C, however, an Araldite seal failed at an entry port in the base of the cell, and the insulation on the wires on the first radial strain belt was stripped or dissolved. This experiment was abandoned.

The experiments were performed to obtain information on the shortening and K_o of different porosity chalks, which have undergone a similar diagenesis. To this end, all the tests were run at a deformational rate of 0.03mm/min with all of the samples having approximately the same proportions, Table A5.1. The first two experiments, EC1.50 and EC2.50, were run with base pore pressure measurement only, the remainder of the tests having base and top pore pressure measurement.

Back pressure in these samples, was supplied by a back pressure

regulator, App. 6. Thus, in the plots of axial strain versus volume strain, no volume change is recorded until the axial strain required to cause an increase in the pore fluid pressure (this included dissolving any air in the sample and as well as increasing the pressure of the fluid) equals the loading of the spring in the regulator. The recording of the output of the transducers was performed by the Solartron logging system.

The initial conditions of each of the samples are given in Table A5.1.

Table A5.1

Sample	Porosity %	Rate of loading mm/min	Average height mm	Average diameter mm	Saturated weight g	Dry weight g	Specific gravity g/cm3
EC1.50	34.8	0.03	76.72	37.72	182.69	149.81	2.68
EC2.50	43.5	0.03	76.37	37.35	165.78	126.71	2.68
EC3.20	35.8	0.03	76.02	37.55	176.76	145.39	2.69
EC4.50	41.2	0.03	76.12	37.64	163.16	132.99	2.67
EC5.20	40.0	0.03	76.23	37.57	168.39	136.89	2.70
EC6.20	36.0	0.03	76.92	37.66	172.68	148.06	2.70
EC8.20	36.6	0.03	76.56	37.60	165.40	135.64	2.70
EC9.20	40.9	0.03	76.63	37.34	169.48	142.74	2.70

EC1.50

This was the first experiment performed, the chalk was of 34.8% porosity, and the initial cell pressure was 16.0MPa. The response of the sample to loading was three fold, an initial linear stiff response is seen with a Young's modulus of 3.26GPa, the yield of this stiff structure occurred at 37.6MPa, this being defined by the point of maximum curvature on the stress-strain curve. The load in the post-yield deformation increases slightly with increasing mean effective stress. The near vertical section of the deformation in q-p' space was due to a deviation off the K_o stress path. The deformation of the chalk is seen in principle effective stress space as three staged, the initial stiff response having a $\bar{K}_o$ designated as $\bar{K}_{oe}$ of 0.368, the second stage of the deformation, the plastic or pore-collapse section has a slope, $\bar{K}_{opc}$ of 0.856. The third deformational response to stress ($\bar{K}_{onc}$), the normal consolidation deformation was not well defined, as the maximum cell pressure was reached soon after the start of normal consolidation, hence no reliable slope could be obtained. The variation in the radial strain was initially large, $3*10^{-2}$% over the first 0.3% axial strain, after which the variation was reduced to $1*10^{-2}$%. At an axial strain of 6%, the sample was loaded at the maximum cell pressure and deviated off K_o. The pore pressure gradually built up in the experiment until an axial strain of 5.8% was attained, whereupon it equalled the loading of the back pressure regulator, and volume changes were recorded.

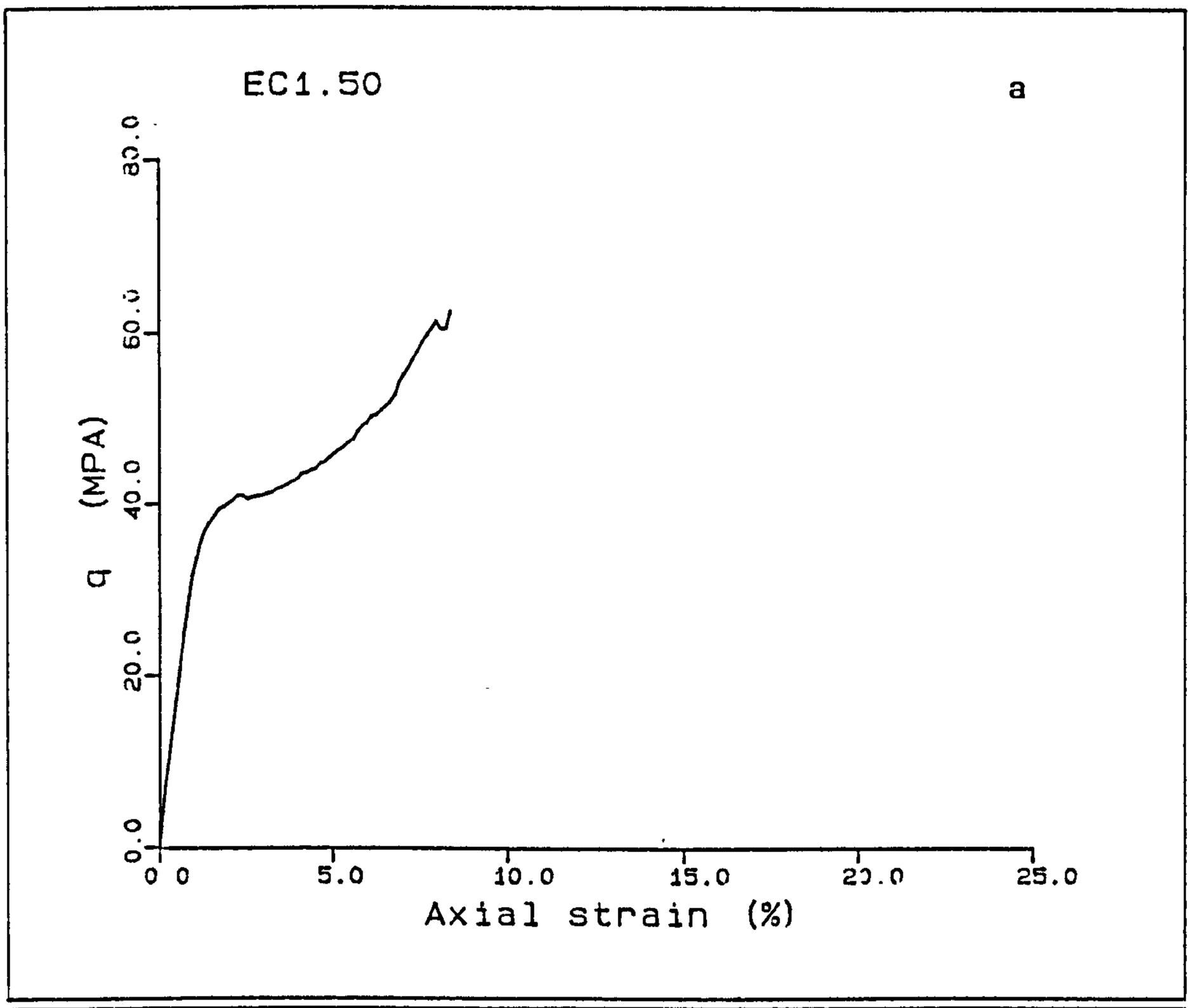

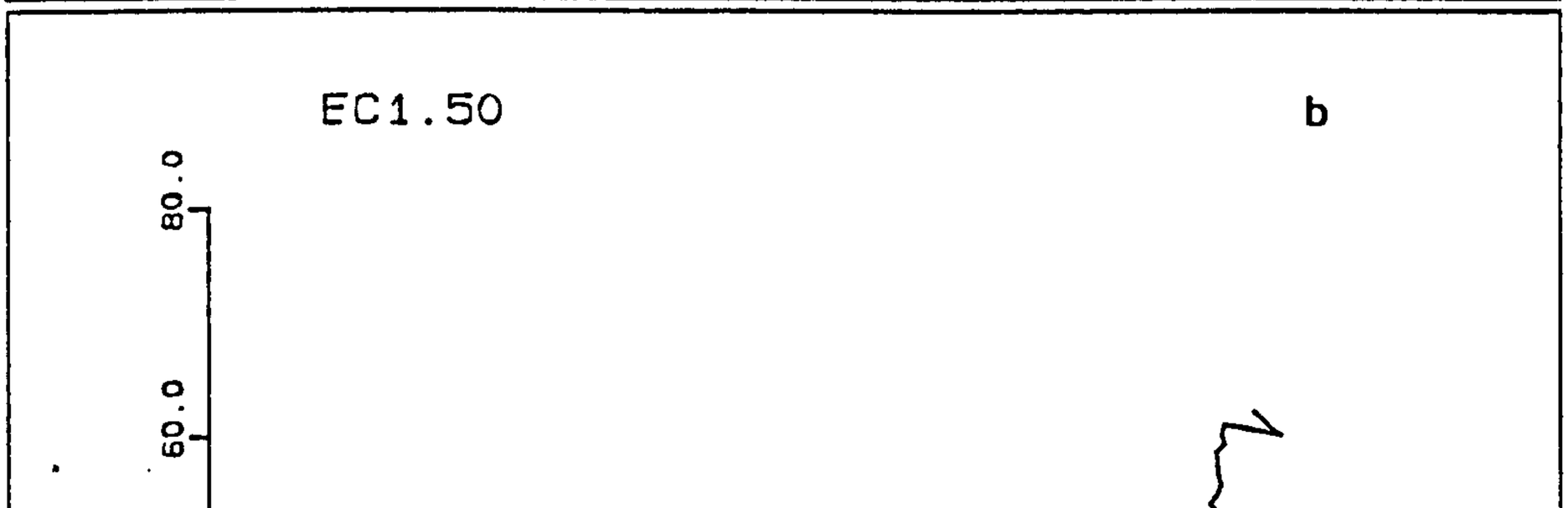

Figure A5.1(a-h) K_o test EC1.50.

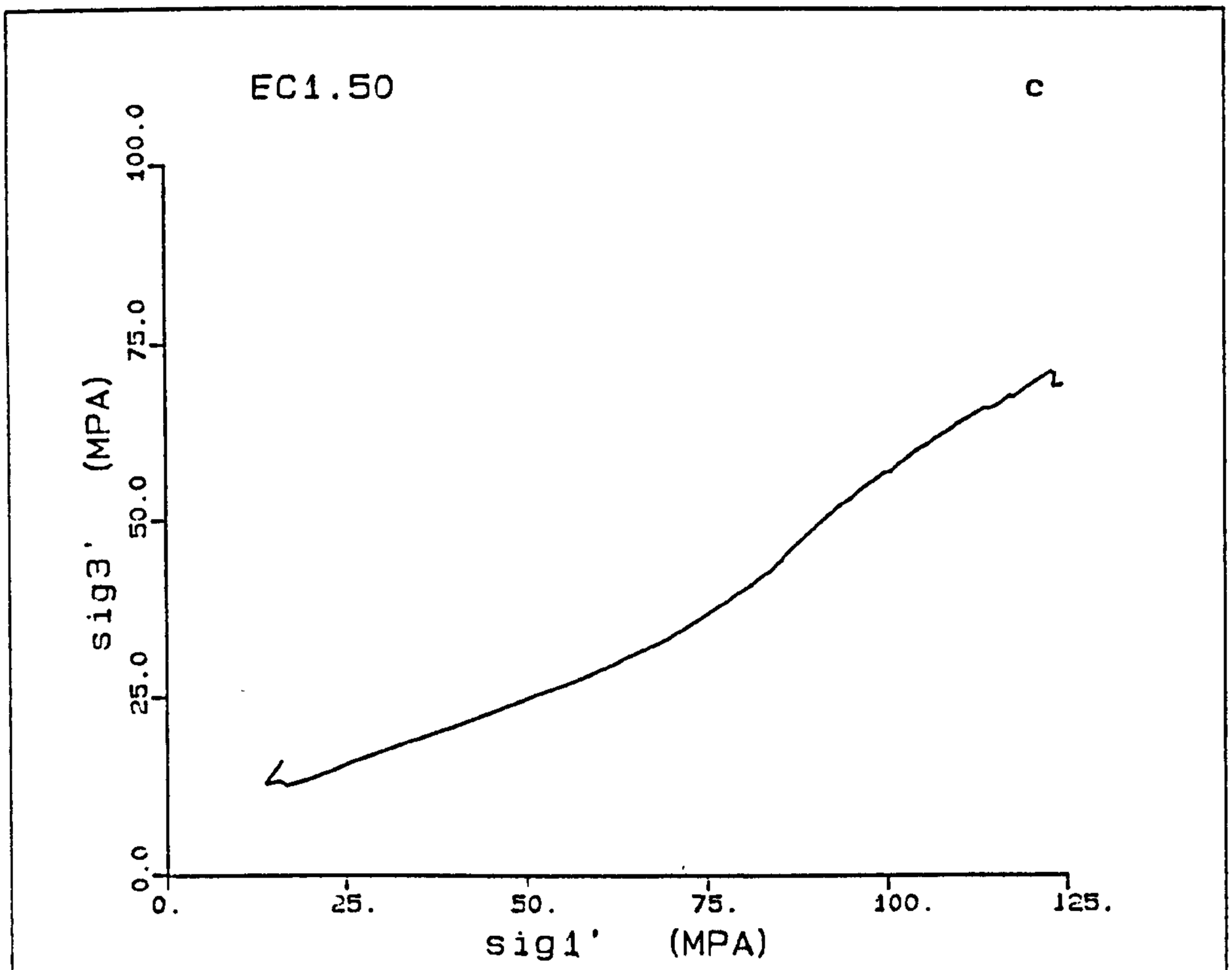
EC1.50
c
100.0
75.0
50.0
25.0
0.0
sig3' (MPA)
0.
25.
50.
75.
100.
125.
sig1' (MPA)

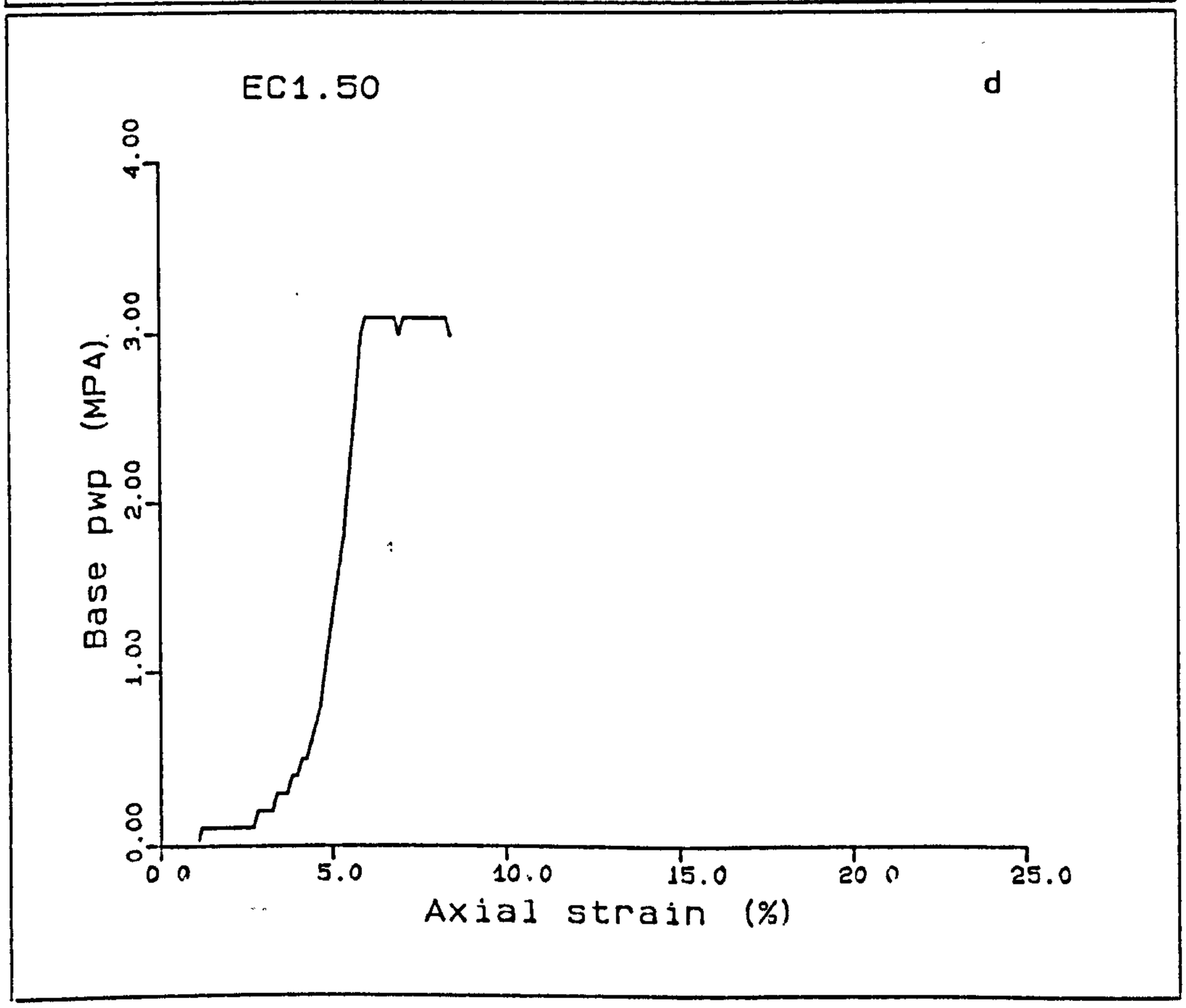
EC1.50
d
4.00
3.00
2.00
1.00
.00
Base pwp (MPA)
0 0
5.0
10.0
15.0
20 0
25.0
Axial strain (%)

EC1.50

e

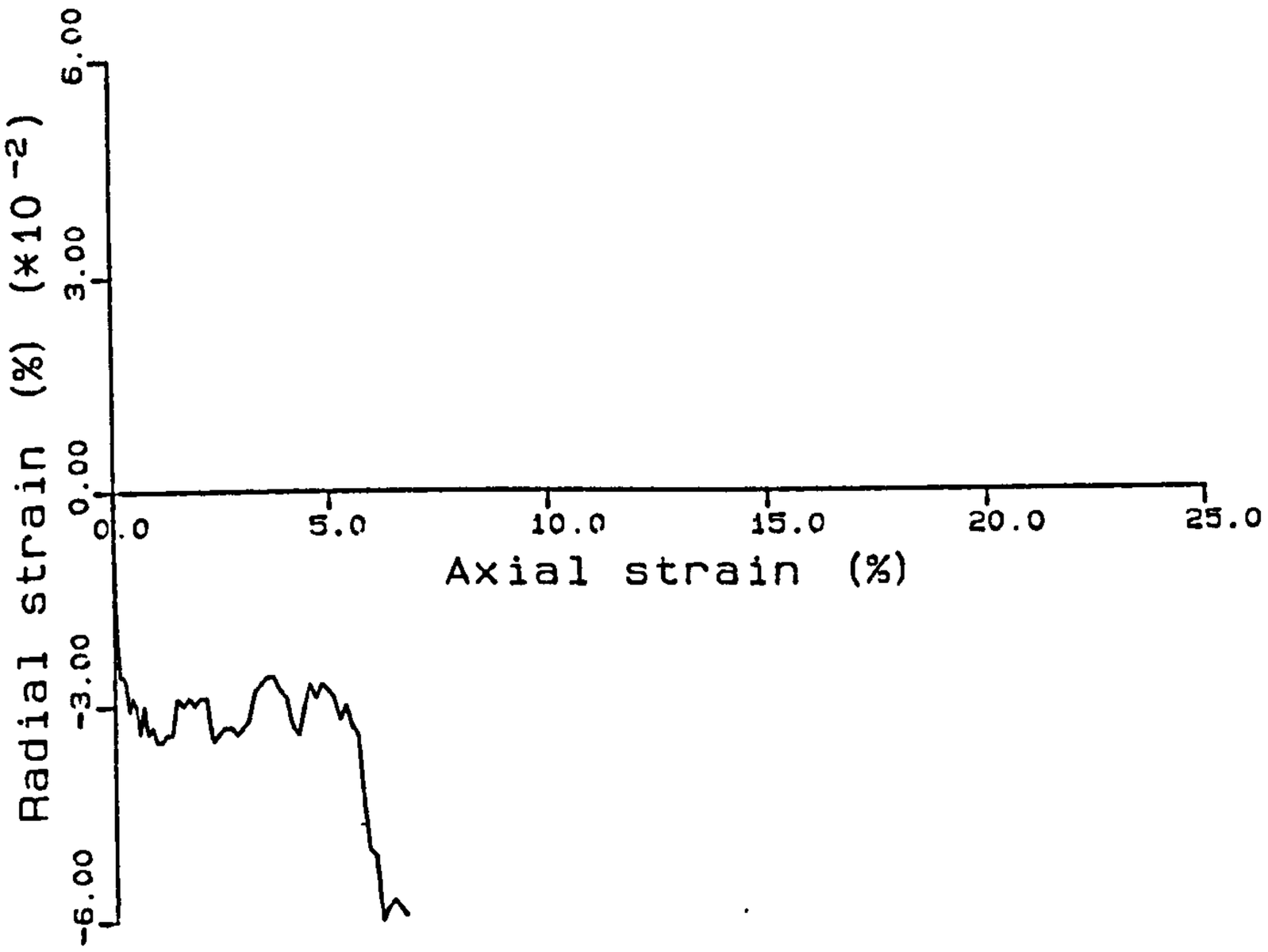

f

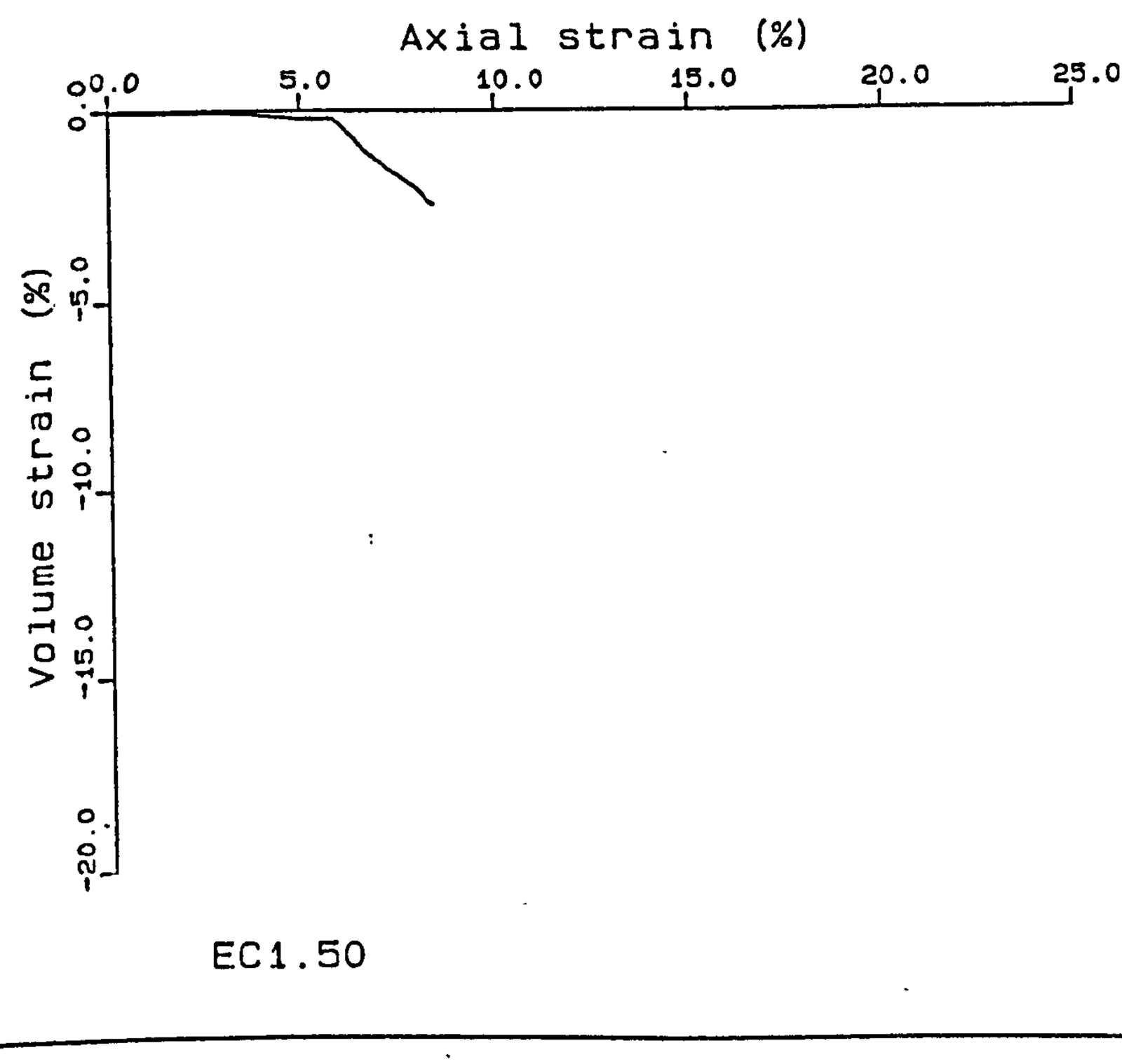

EC1.50

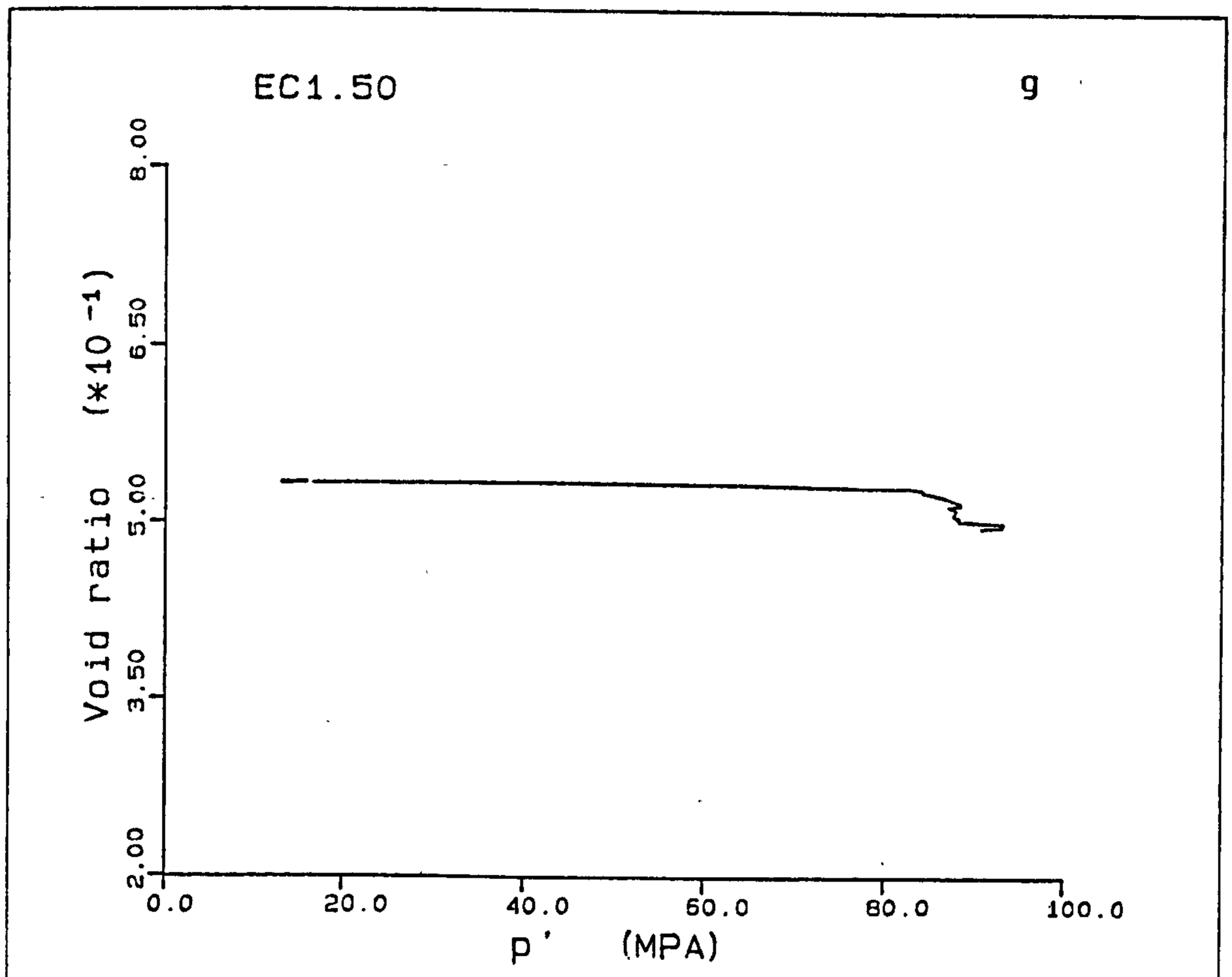
EC1.50
g
Void ratio (*10 -1)
8.00
6.50
5.00
3.50
2.00
0.0
20.0
40.0
60.0
80.0
100.0
p' (MPA)

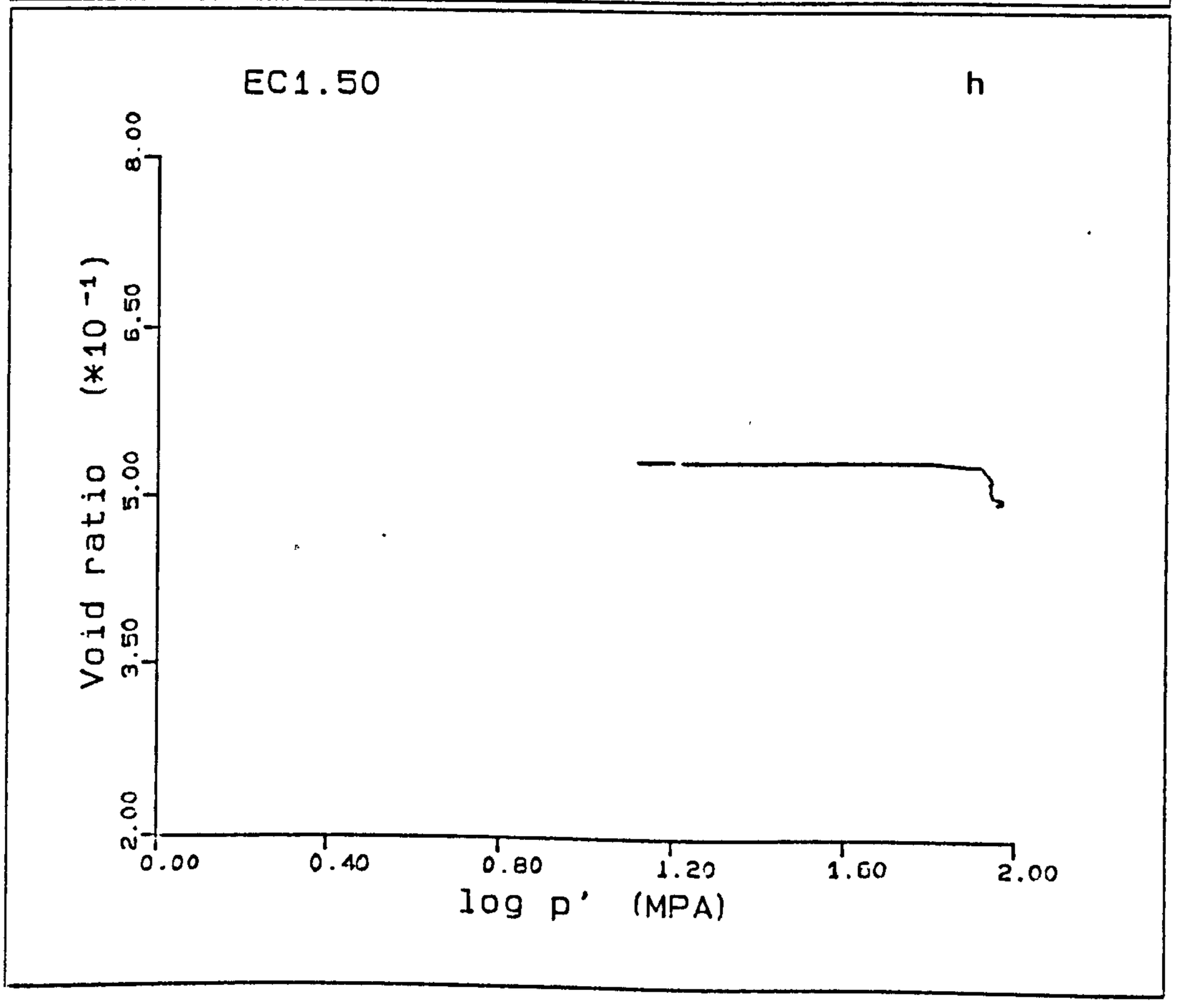
EC1.50
h
Void ratio (*10 -1)
8.00
6.50
5.00
3.50
2.00
0.00
0.40
0.80
1.20
1.60
2.00
log p' (MPA)

EC2.50

This is a 43.5% porosity sample which deforms initially with a Young's modulus of 1.72GPa, the yield (the point of maximum curvature) occurs at a deviatoric stress of 9.7MPa. The stress-strain curve in the post-yield deformation shows a steady increase in stress without any load reduction characteristics of later experiments. This is seen on the q-p' plot as a continuing increase of q with p', until at 24MPa mean effective stress, the increase in q decreases to approach a constant value at 40MPa. This trend is also seen in principle effective stress space. The plot of radial strain with axial strain, and axial strain with volume strain both show that the sample deformed along K_o conditions.

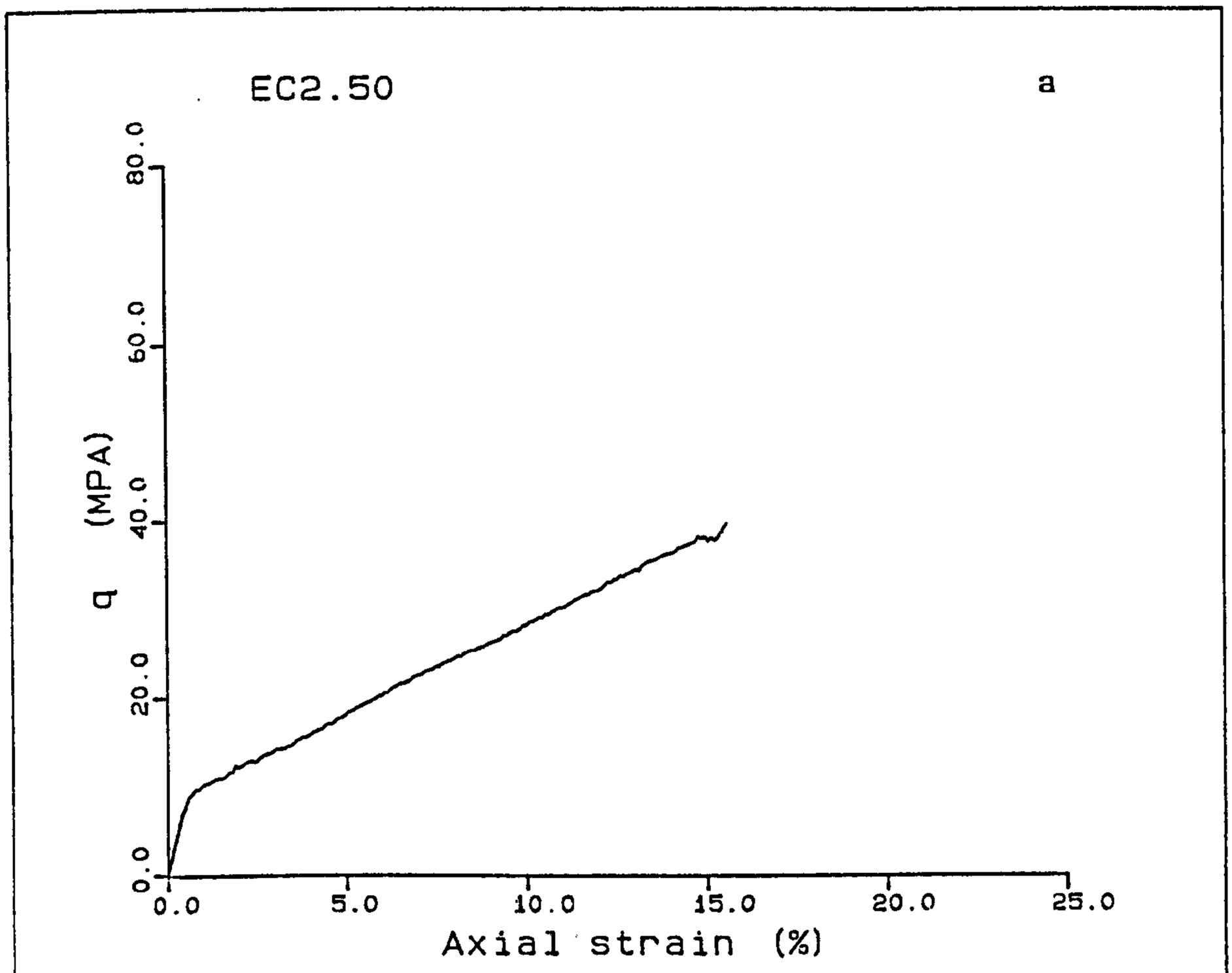

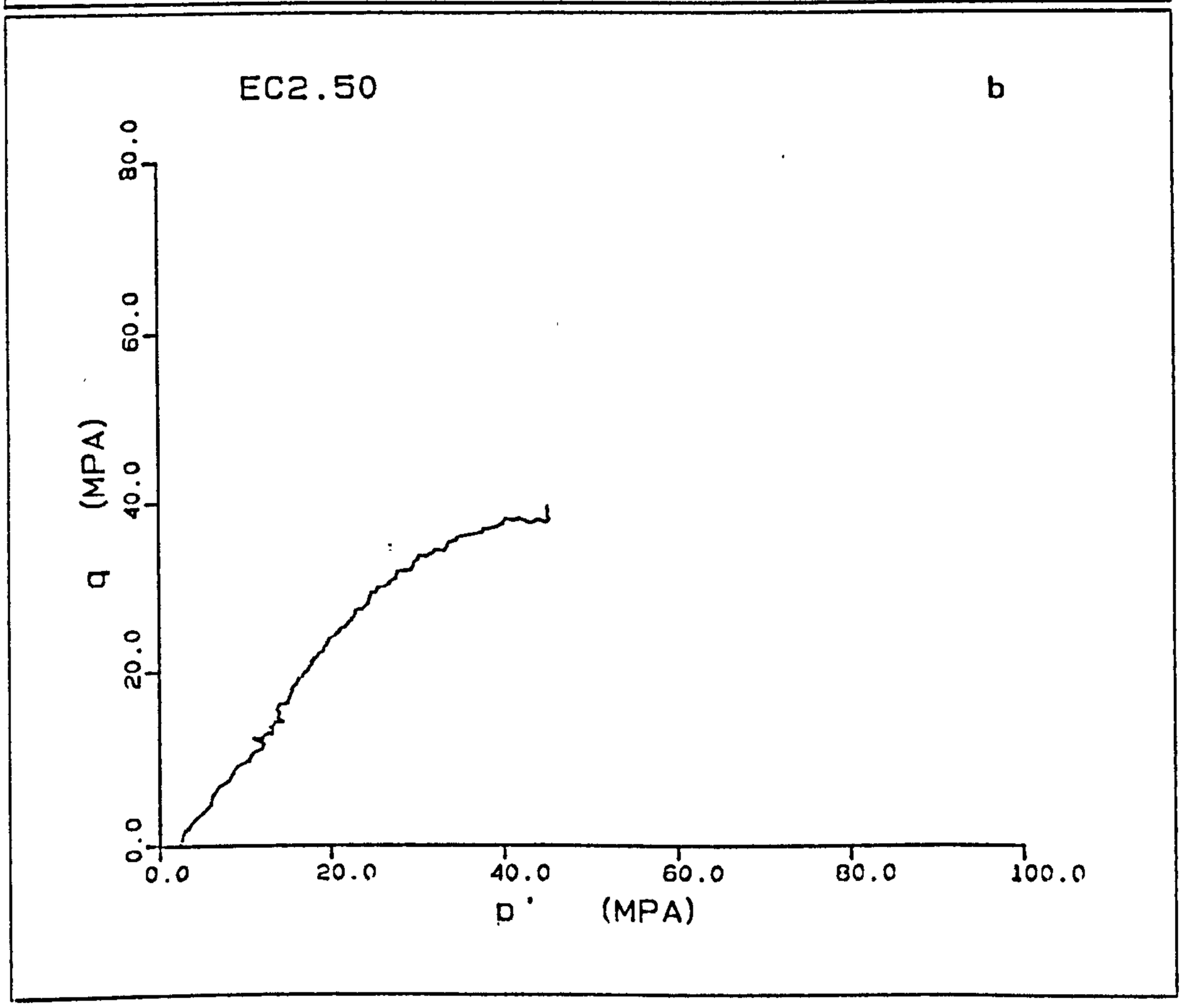

Figure A5.2(a-h) K_o test EC2.50.

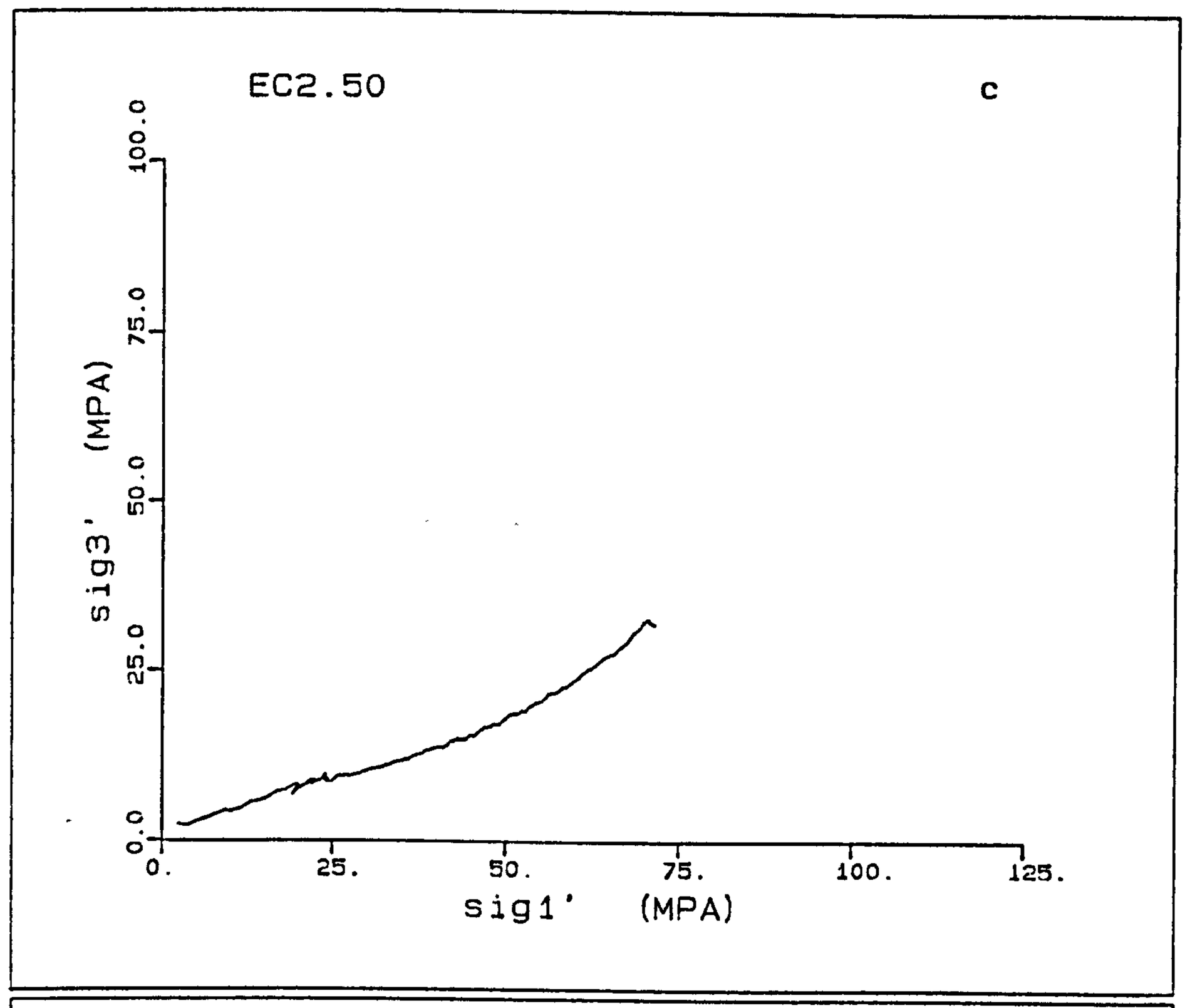
EC2.50
c
100.0
75.0
50.0
25.0
0.0
sig3' (MPA)
0.
25.
50.
75.
100.
125.
sig1' (MPA)

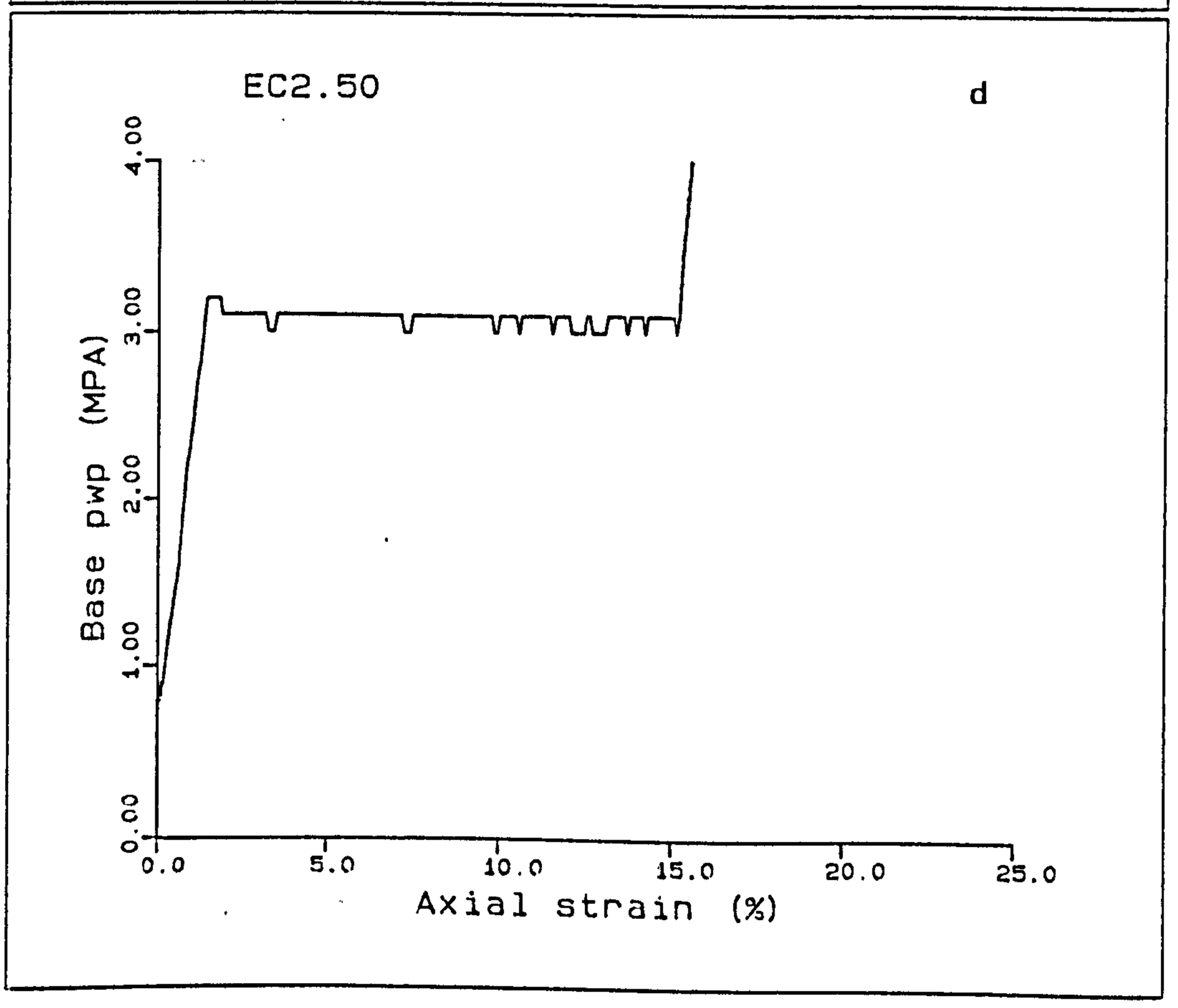
EC2.50
d
4.00
3.00
2.00
1.00
0.00
Base pwp (MPA)
0.0
5.0
10.0
15.0
20.0
25.0
Axial strain (%)

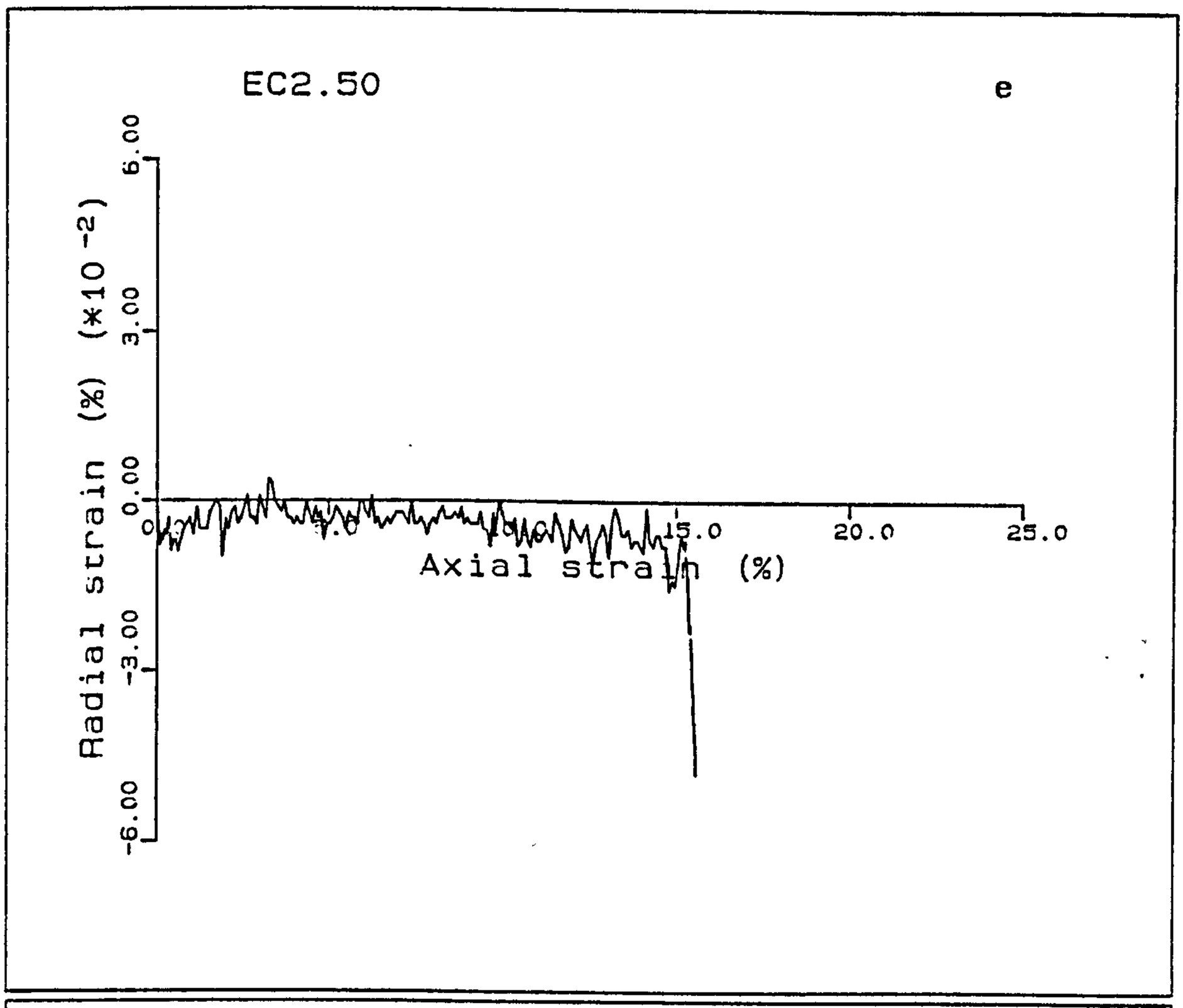
EC2.50
e
Radial strain (%) (*10 -2)
6.00
3.00
0.00
-3.00
-6.00
0
5.0
10.0
15.0
20.0
25.0
Axial strain (%)

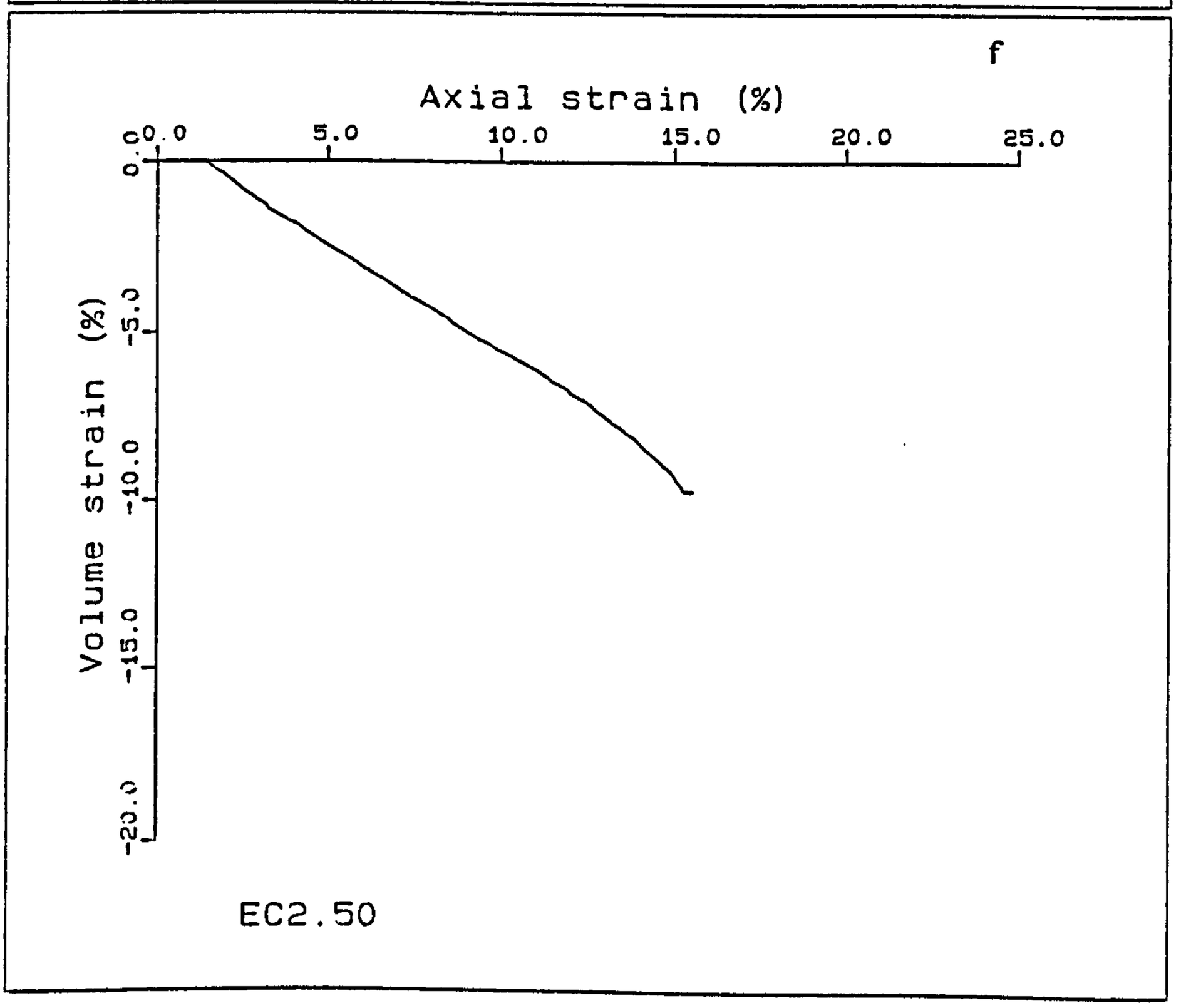
f
Axial strain (%)
0.0
5.0
10.0
15.0
20.0
25.0
0.0
-5.0
-10.0
-15.0
-20.0
Volume strain (%)
EC2.50

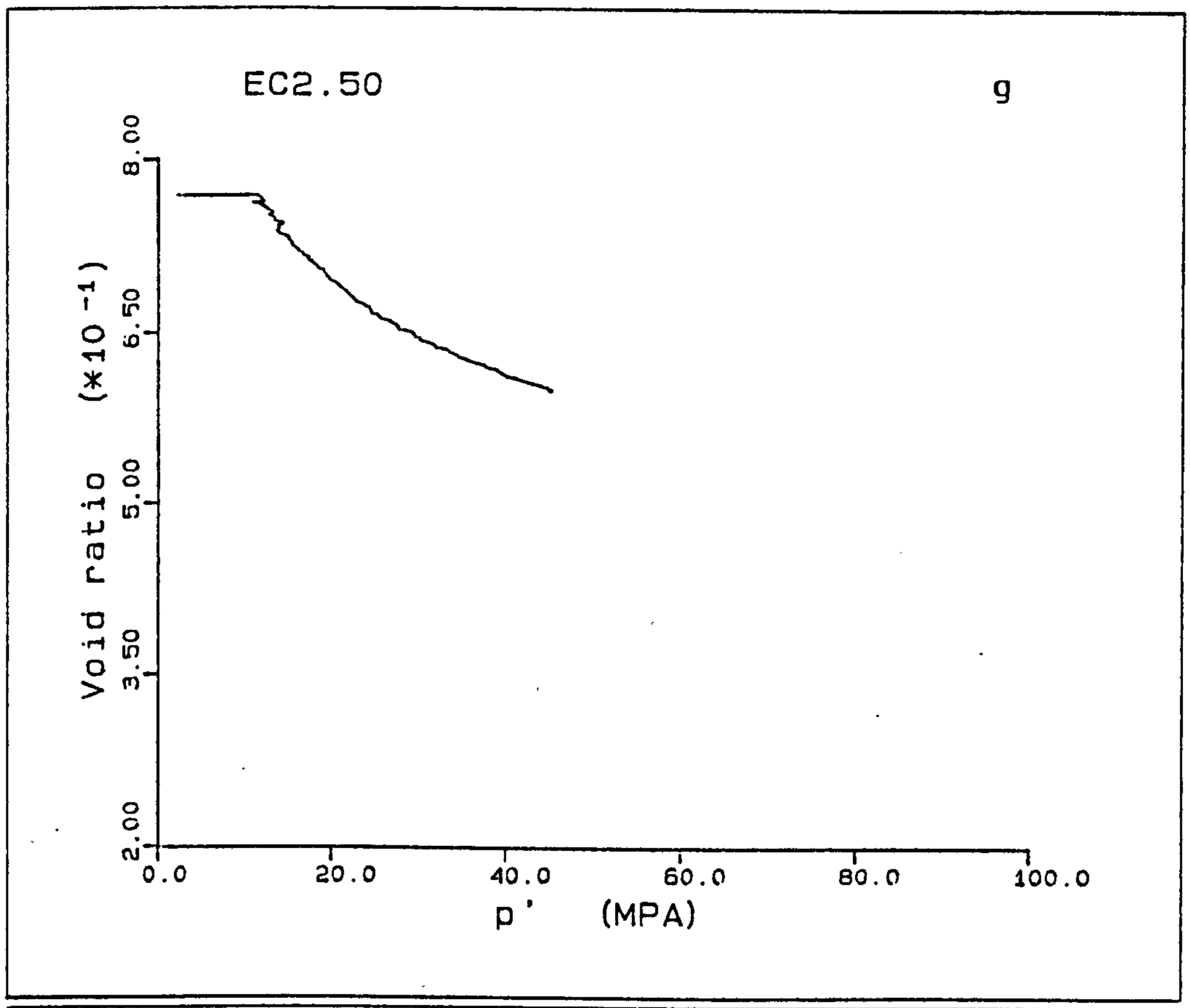
EC2.50
g
Void ratio (*10 -1)
8.00
6.50
5.00
3.50
2.00
0.0
20.0
40.0
60.0
80.0
100.0
p' (MPA)

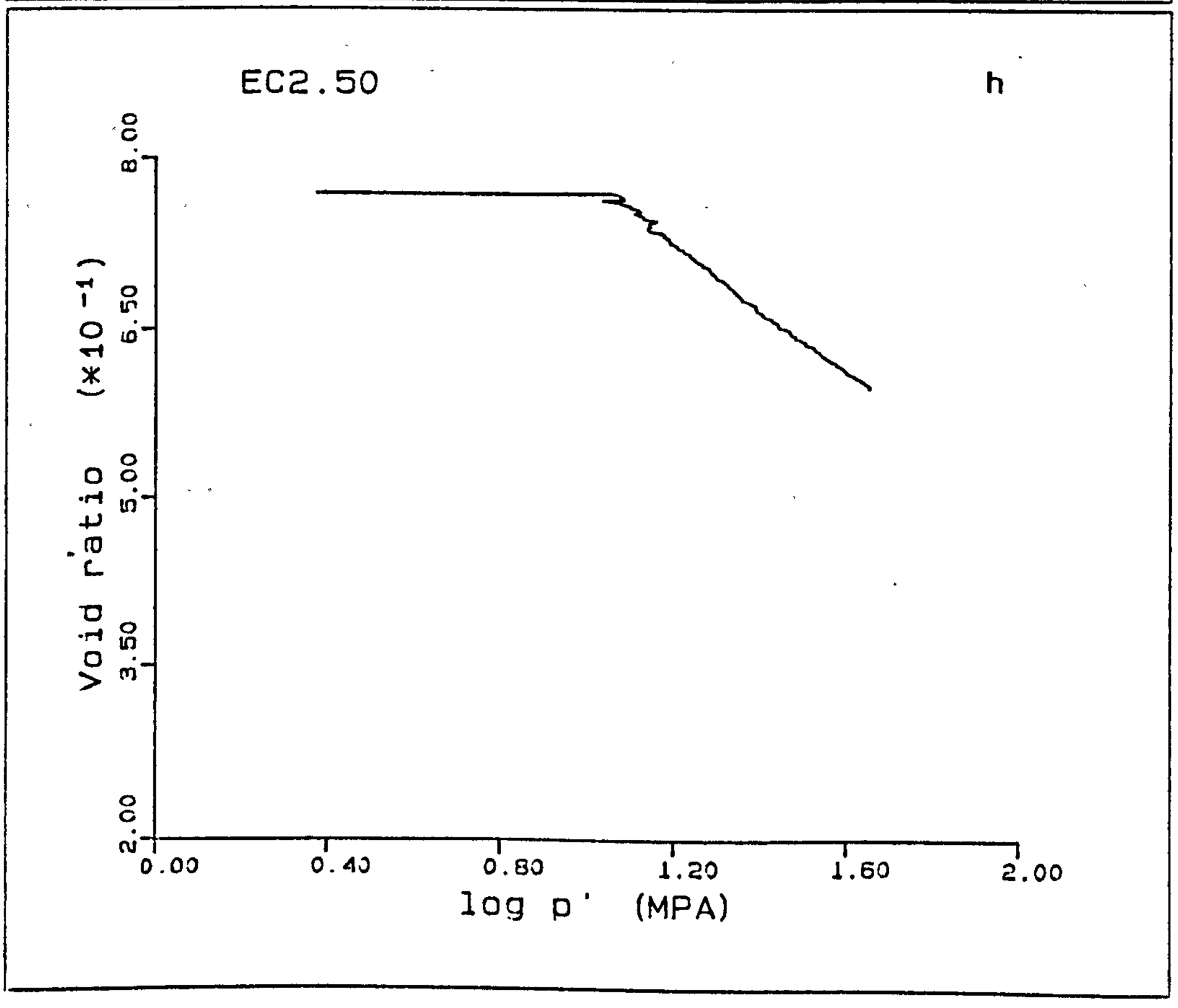
EC2.50
h
Void ratio (*10 -1)
8.00
6.50
5.00
3.50
2.00
0.00
0.40
0.80
1.20
1.60
2.00
log p' (MPA)

EC3.20

EC3.20 is a 35.8% porosity chalk which yielded at a deviatoric stress of 28.1MPa (shown by a peak in the deviatoric stress), the stress-strain curve being linear over the initial pre-yield section Fig. A5.3a, with a Young's modulus of 2.39GPa. In the constant q section, the loading was stopped and unloading occured due to sample relaxation, the deviatoric stress dropped from 27.4MPa to 21.7MPa. Associated with this was an increase in the radial strain of $2.5*10^{-2}$%. The reloading seems to be approximately parallel to the initial elastic section, though the unloading was not large enough to obtain an accurate determination of the reloading modulus. The change in stresses during this unloading are due to a reduction in maximum effective stress, as the minimum effective stress remained constant, Fig. A5.3c. Over the entire test the variation in the radial strain recorded is below $3*10^{-2}$%, with two peaks, one at the unloading part of the deformation, and another during the initial loading of the sample. This initial loading is accompanied by a decrease in the cell pressure, leading to a near vertical section of the stress path in q-p'space.

The principle effective stress plot shows $\bar{K}_o$ values of 0.492, 1.000, and approximately 0.630, for the elastic, pore collapse and the normal consolidation deformations respectively. The pore pressures gradually built up in the test to 3.2MPa at an axial strain of 5.2%.

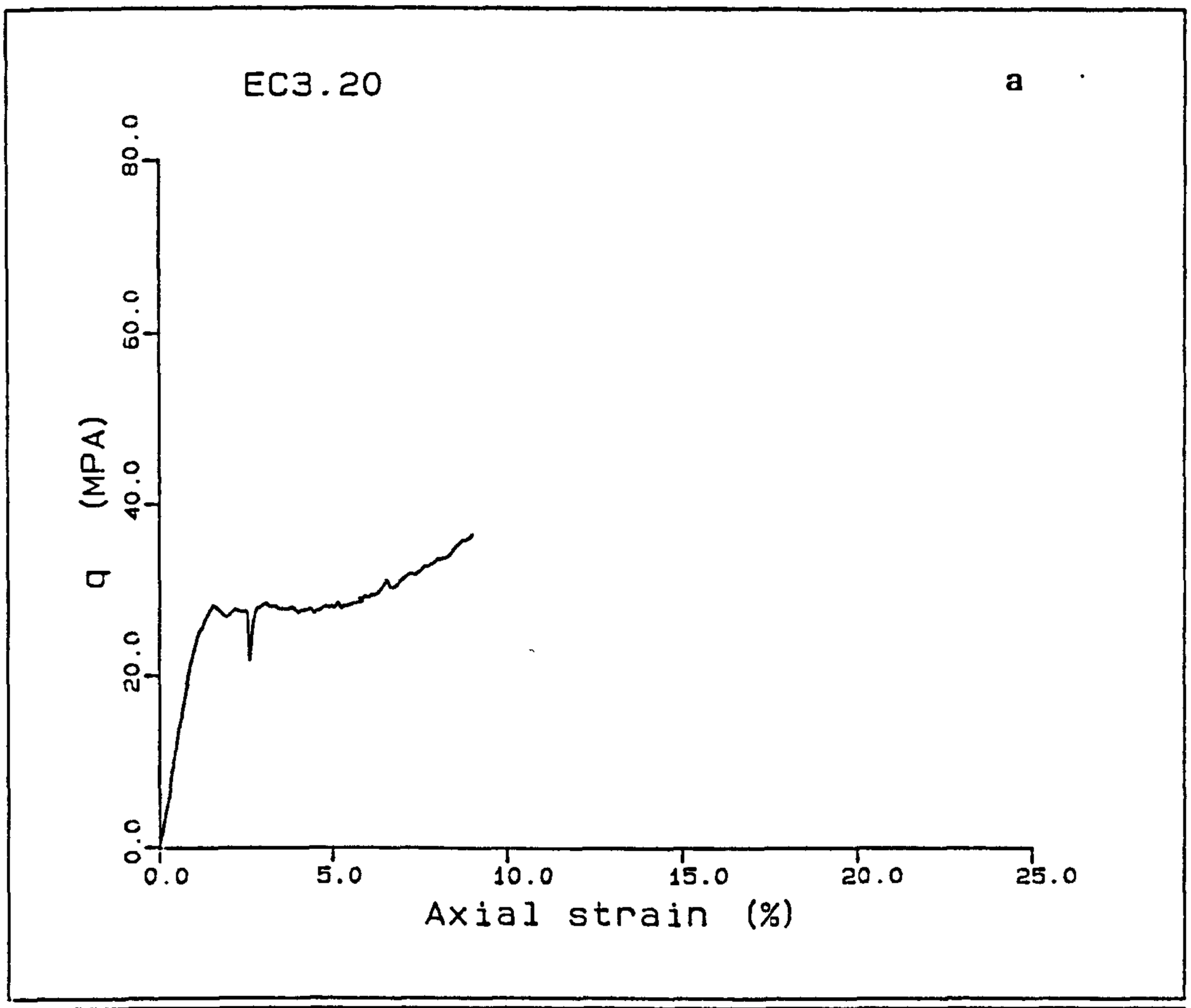

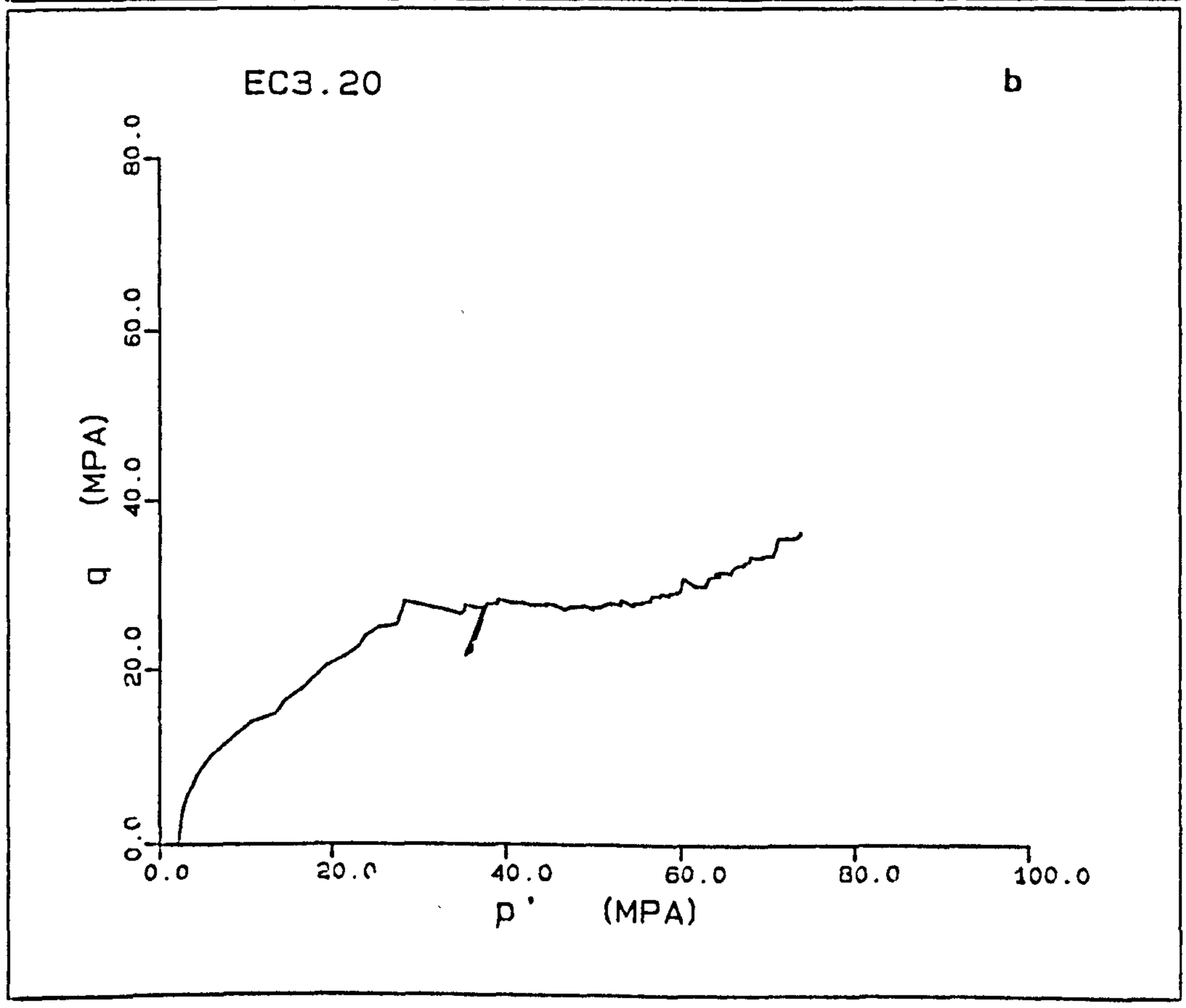

Figure A5.3(a-h) K_o test EC3.20.

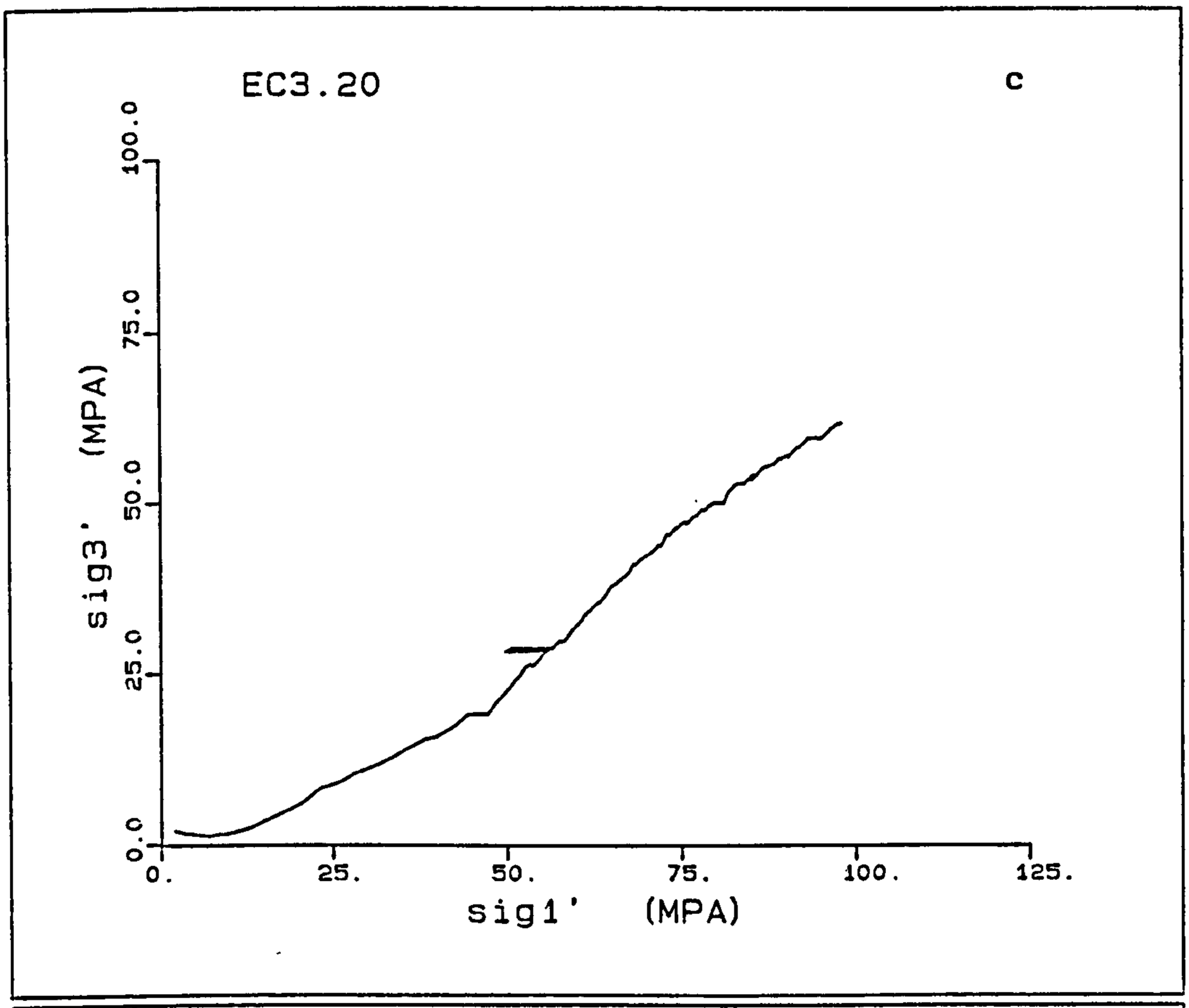
EC3.20
c
sig3' (MPA)
100.0
75.0
50.0
25.0
0.0
0.
25.
50.
75.
100.
125.
sig1' (MPA)

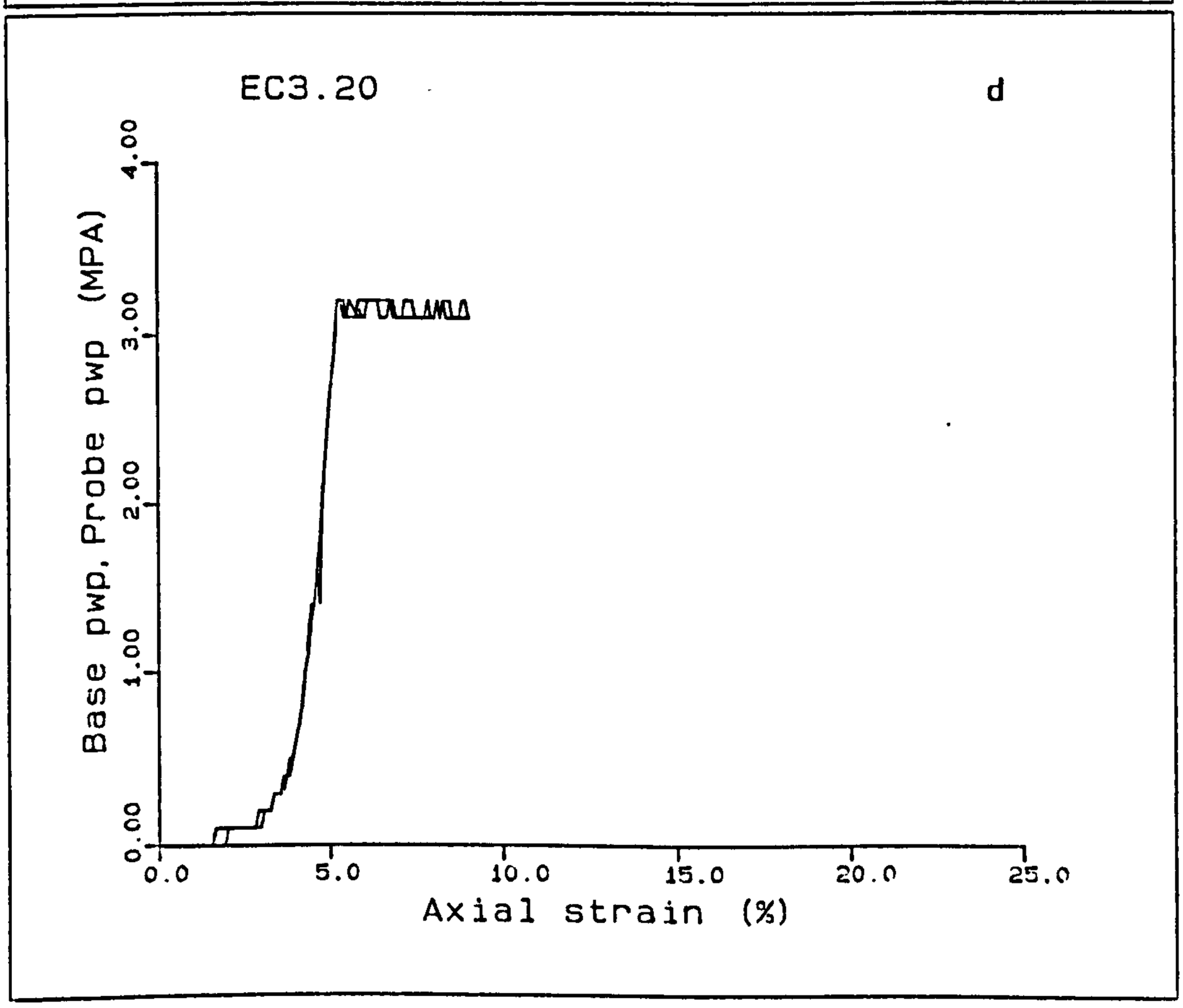
EC3.20
d
Base pwp, Probe pwp (MPA)
4.00
3.00
2.00
1.00
0.00
0.0
5.0
10.0
15.0
20.0
25.0
Axial strain (%)

EC3.20

e

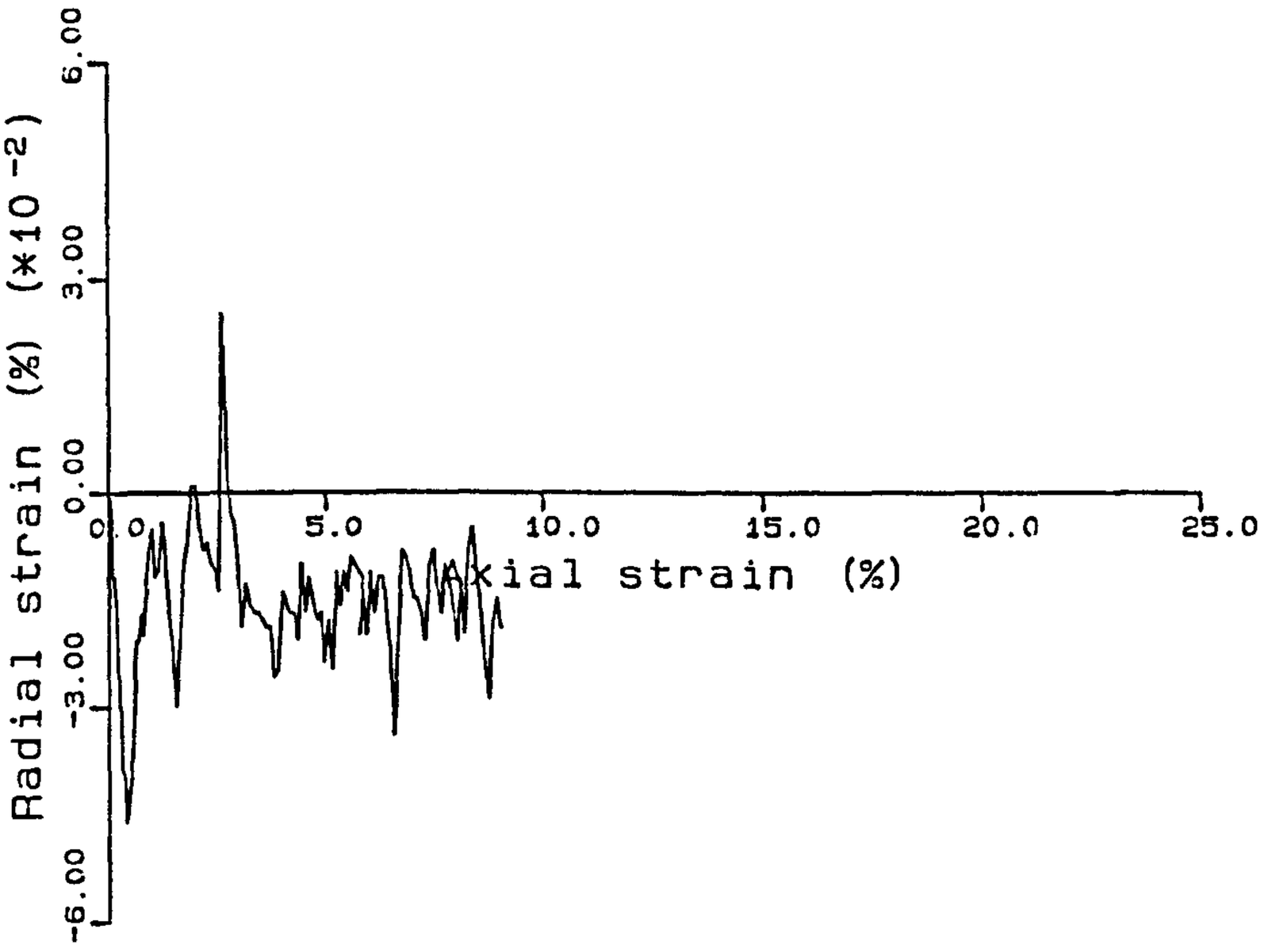

f

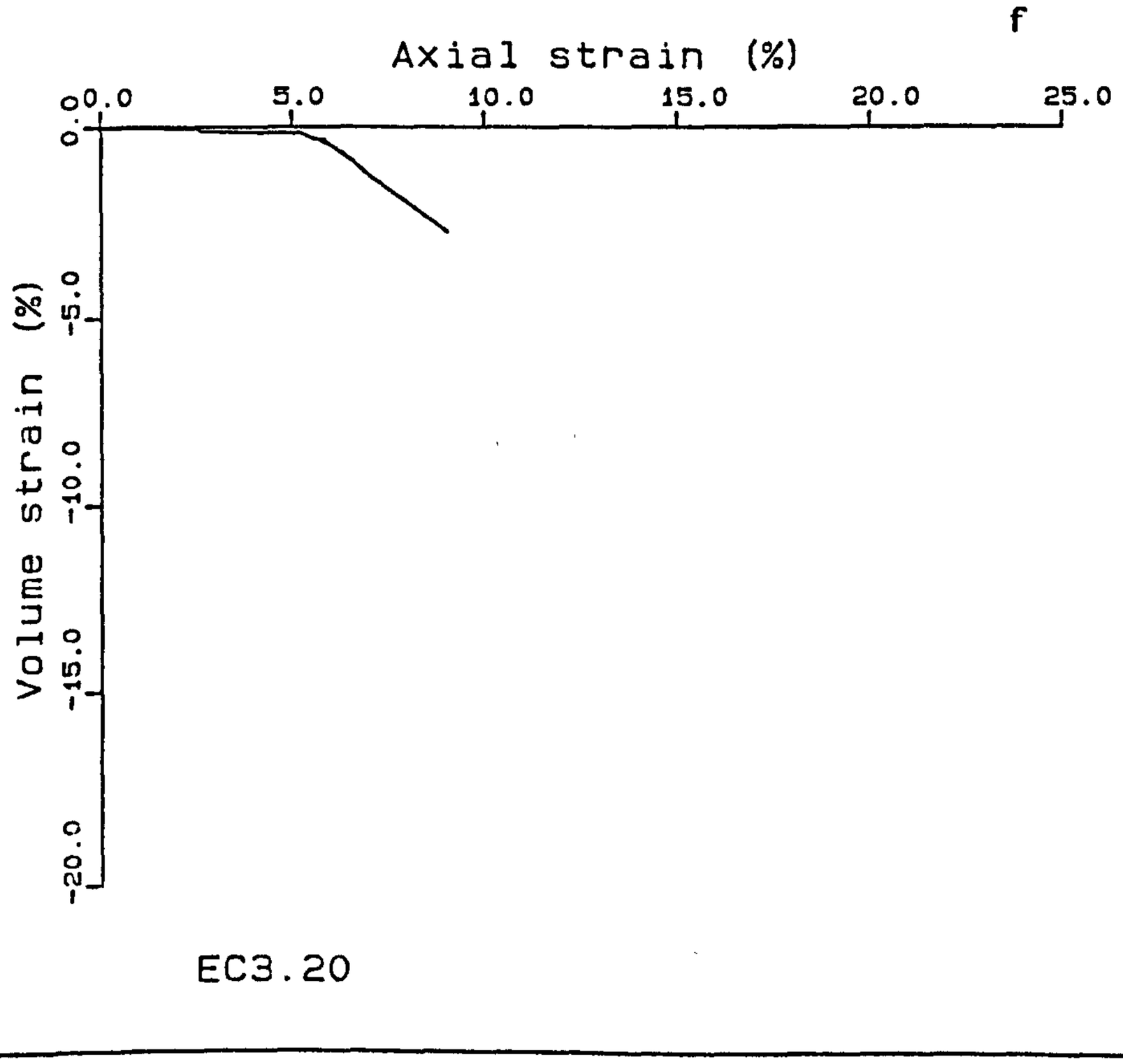

EC3.20

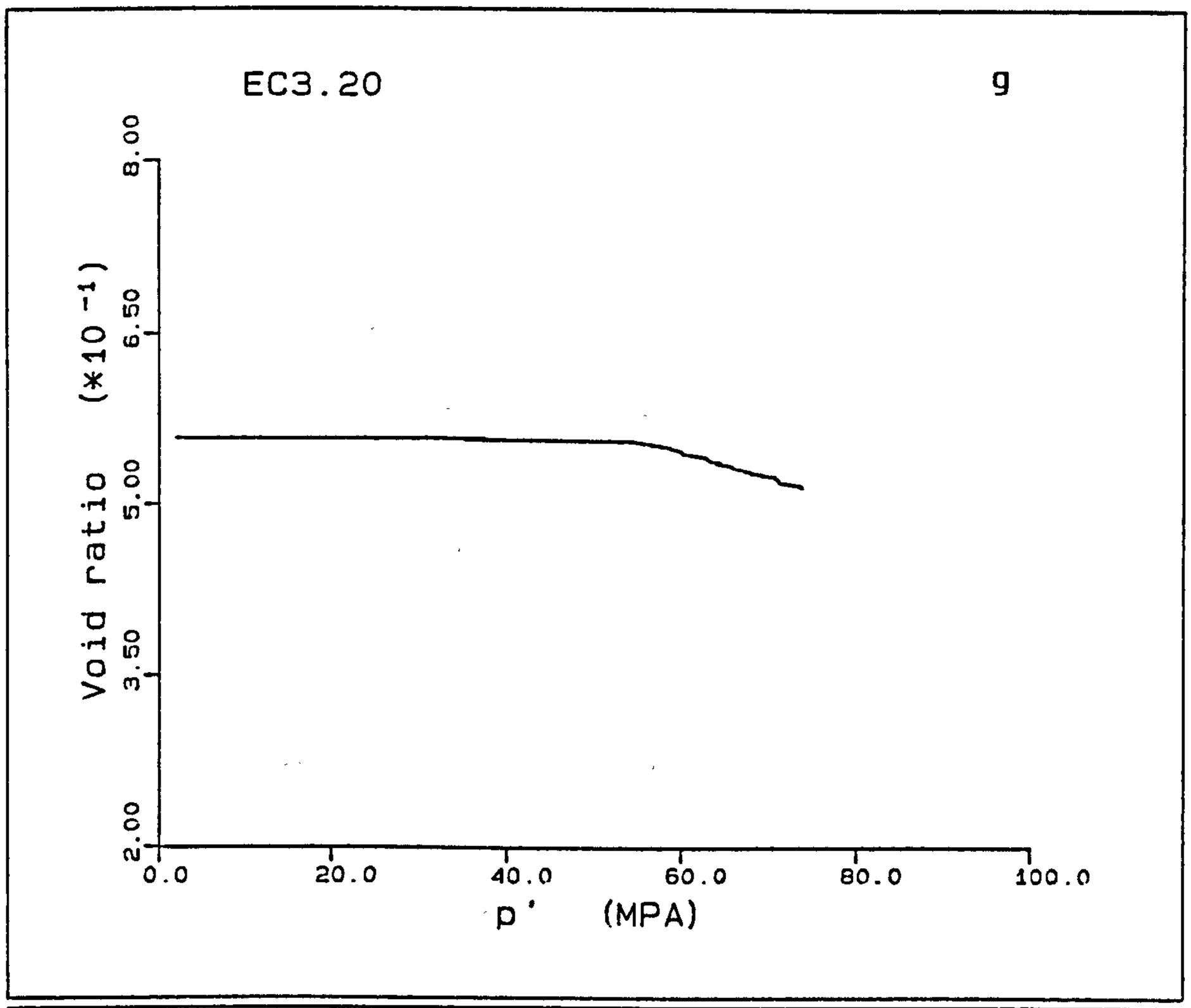
EC3.20
g
Void ratio (*10 -1)
8.00
6.50
5.00
3.50
2.00
0.0
20.0
40.0
60.0
80.0
100.0
p' (MPA)

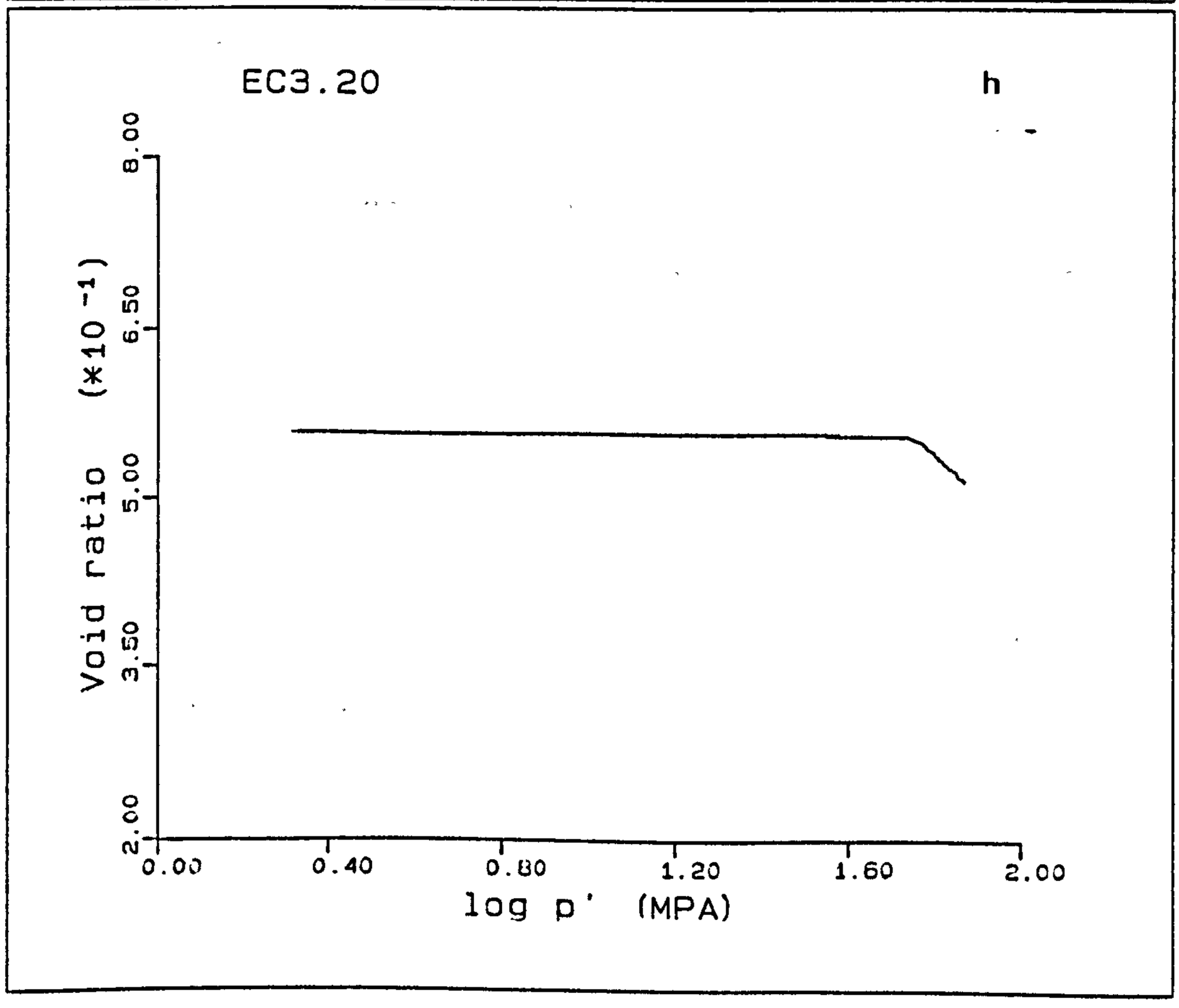
EC3.20
h
Void ratio (*10 -1)
8.00
6.50
5.00
3.50
2.00
0.00
0.40
0.80
1.20
1.60
2.00
log p' (MPA)

EC4.50

EC4.50 is a 41.2% porosity chalk which shows the three sections of deformation typical in the chalk. The elastic section gives a linear stress-strain relationship with a Young's modulus of 2.75GPa; the end of the elastic range is seen as an abrupt change in the slope of the deviatoric stress-axial strain plot with a yield point (q_y) of 30.4MPa. Post-yield, the deviatoric stress shows a slight increase in load followed by a small decrease. This is seen as an almost constant deviatoric stress during a large increase in mean stress, after which the load increases due to work hardening during the normal consolidation deformation. Fig. A5.4c shows the $\bar{K}_o$ values for the elastic and intermediate deformation to be 0.254, 1.115, the normal consolidation section again being indeterminate.

The total radial strain variation throughout the experiment was less than $1.5*10^{-2}$. However, the plot of volume against axial strain does not give a 45^o line, the reason for this discrepancy between the different methods of monitoring K_o is not known. One possible explanation is the presence of collapsible material (c.f. BH17.60). This structural breakdown is also seen in the plots of void ratio against stress, by a large decrease in void ratio at a mean stress of approximately 27MPa, which is early in the post-yield deformation. In the initial part of the pore collapse section, volume changes start recording at an axial strain of 1.4%, the sample deforming with a constant back pressure at strains greater than this.

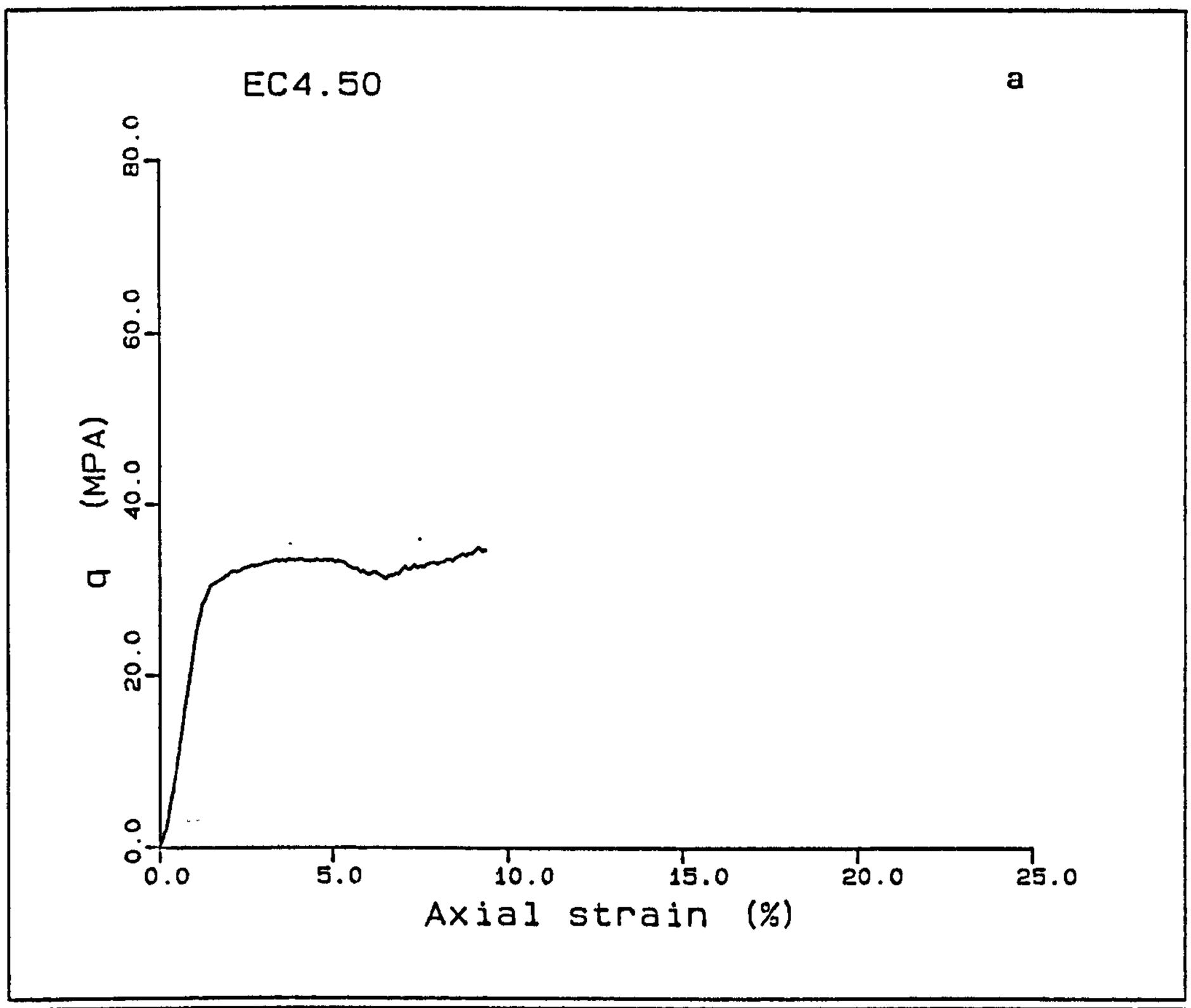

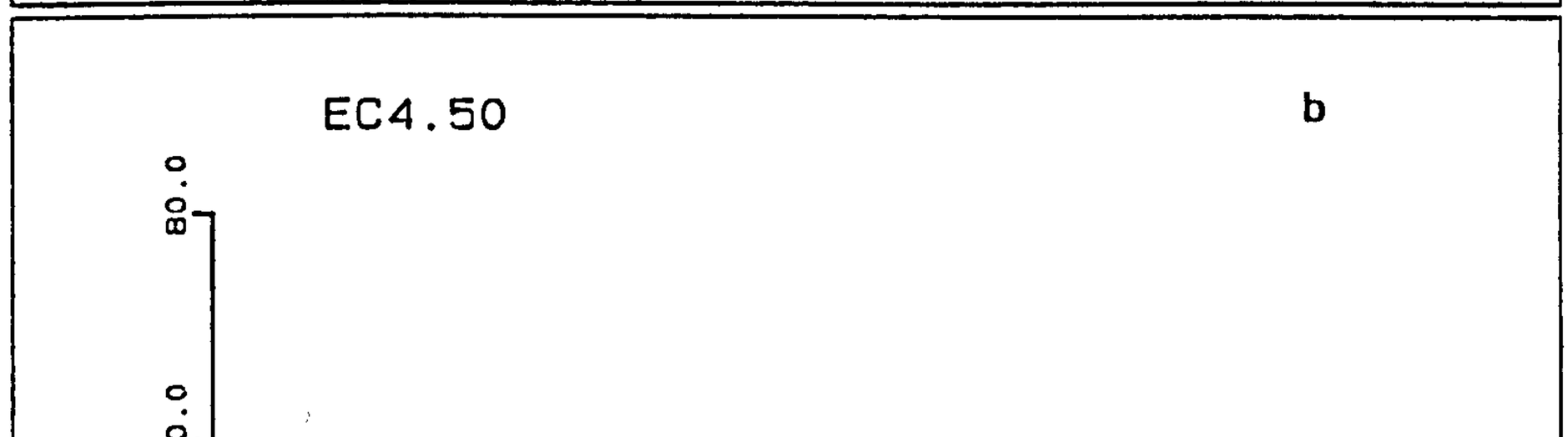

Figure A5.4(a-h) K_o test EC4.50.

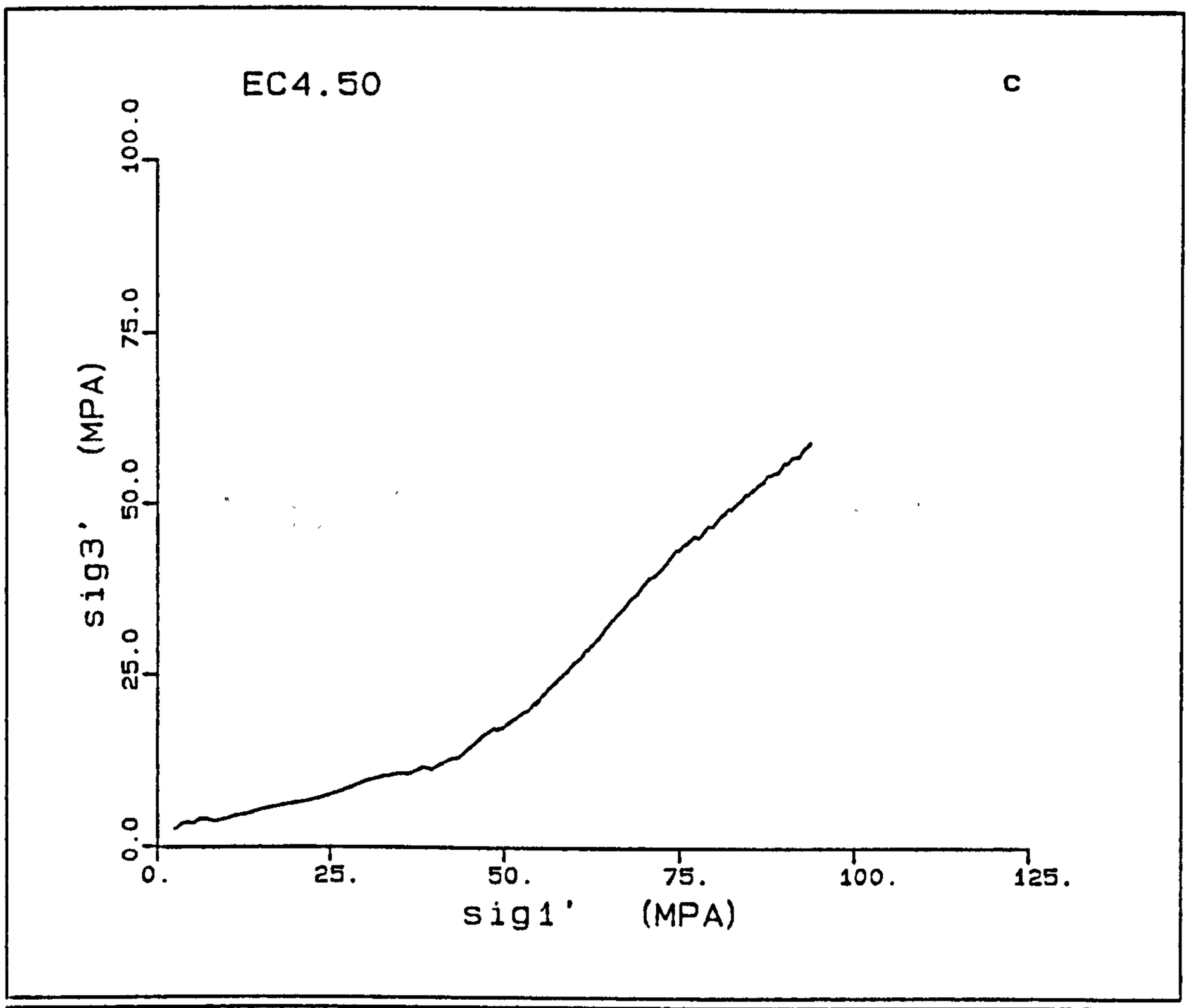
EC4.50
c
sig3' (MPA)
100.0
75.0
50.0
25.0
0.0
0.
25.
50.
75.
100.
125.
sig1' (MPA)

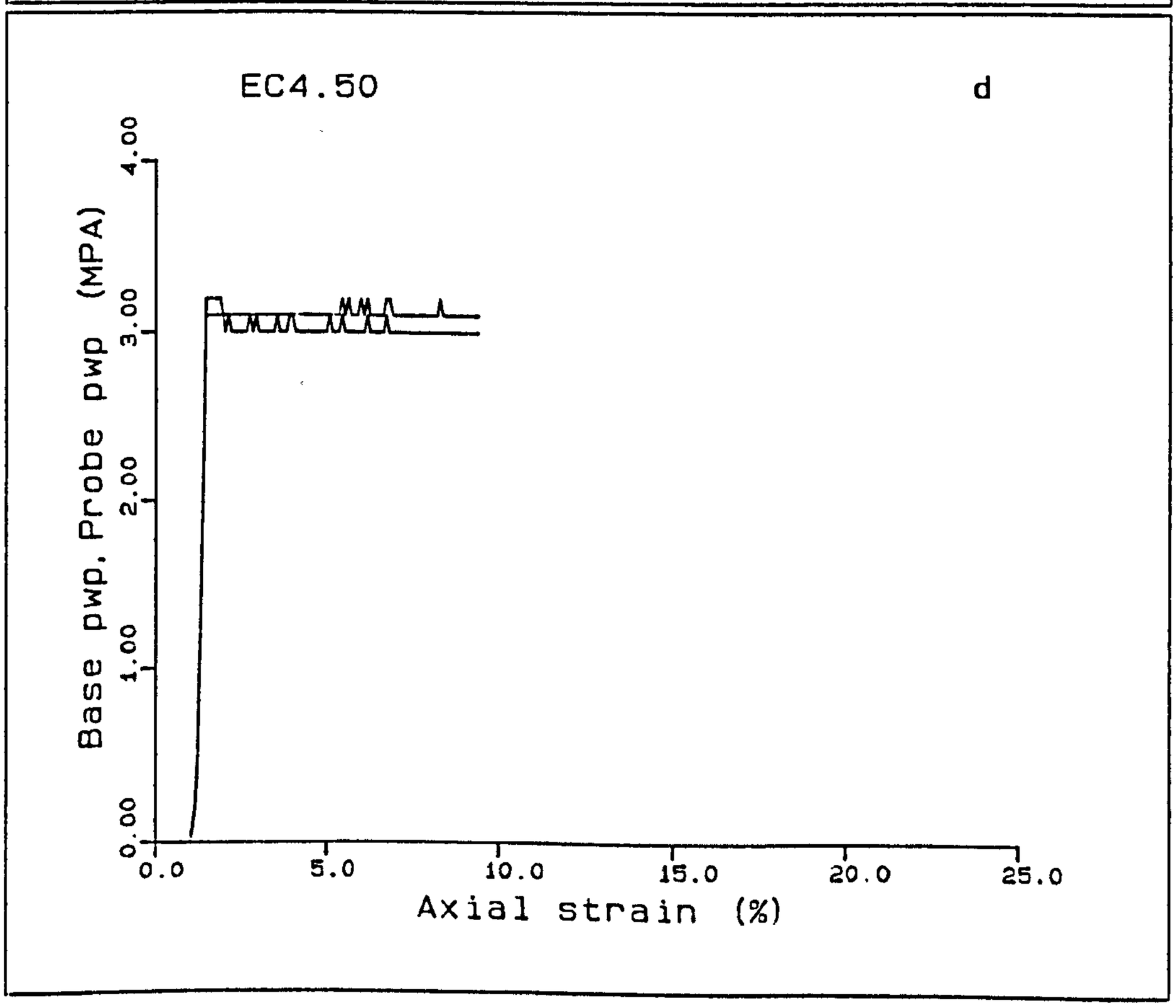
EC4.50
d
Base pwp, Probe pwp (MPA)
4.00
3.00
2.00
1.00
0.00
0.0
5.0
10.0
15.0
20.0
25.0
Axial strain (%)

EC4.50

e

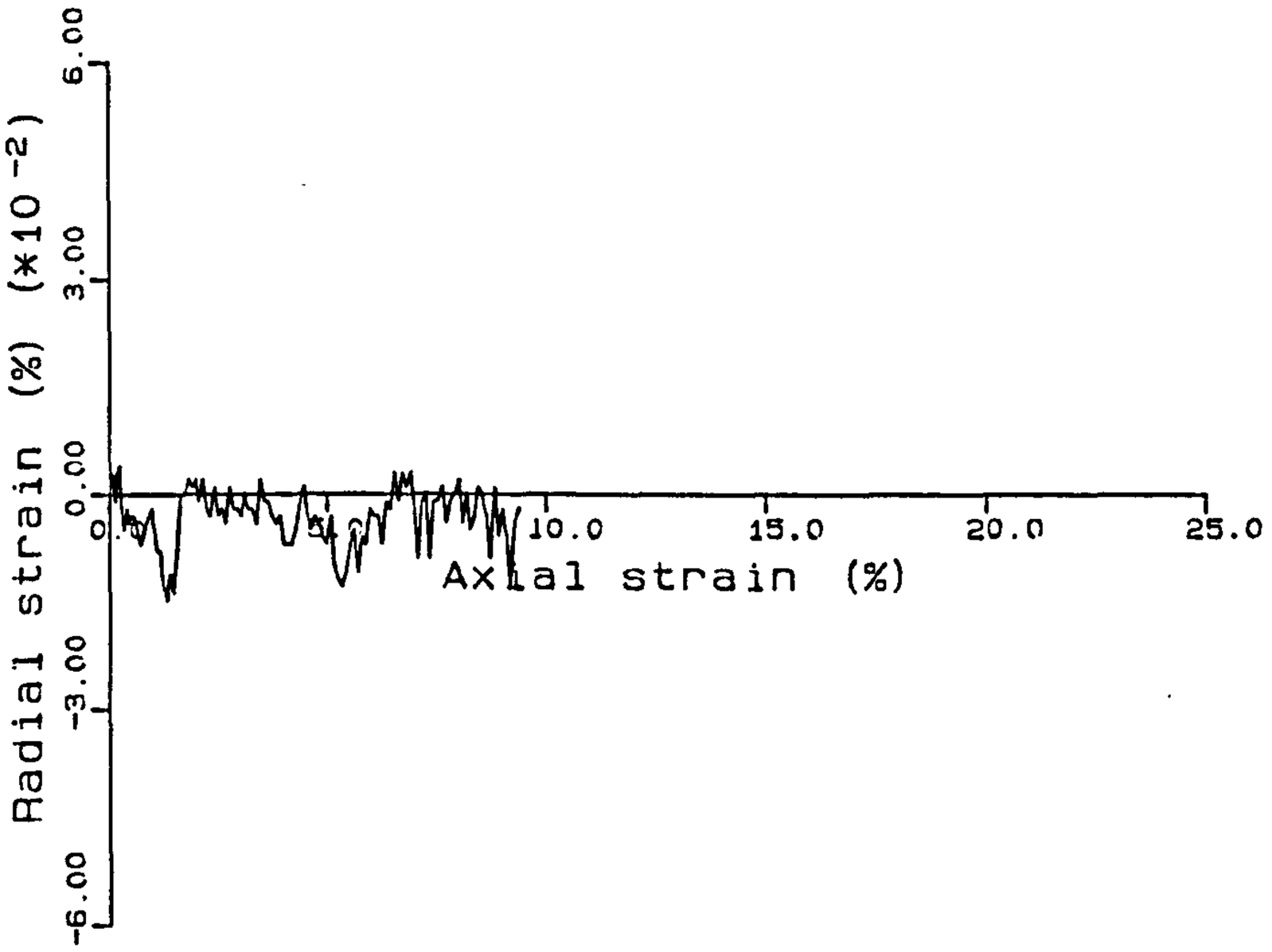

f

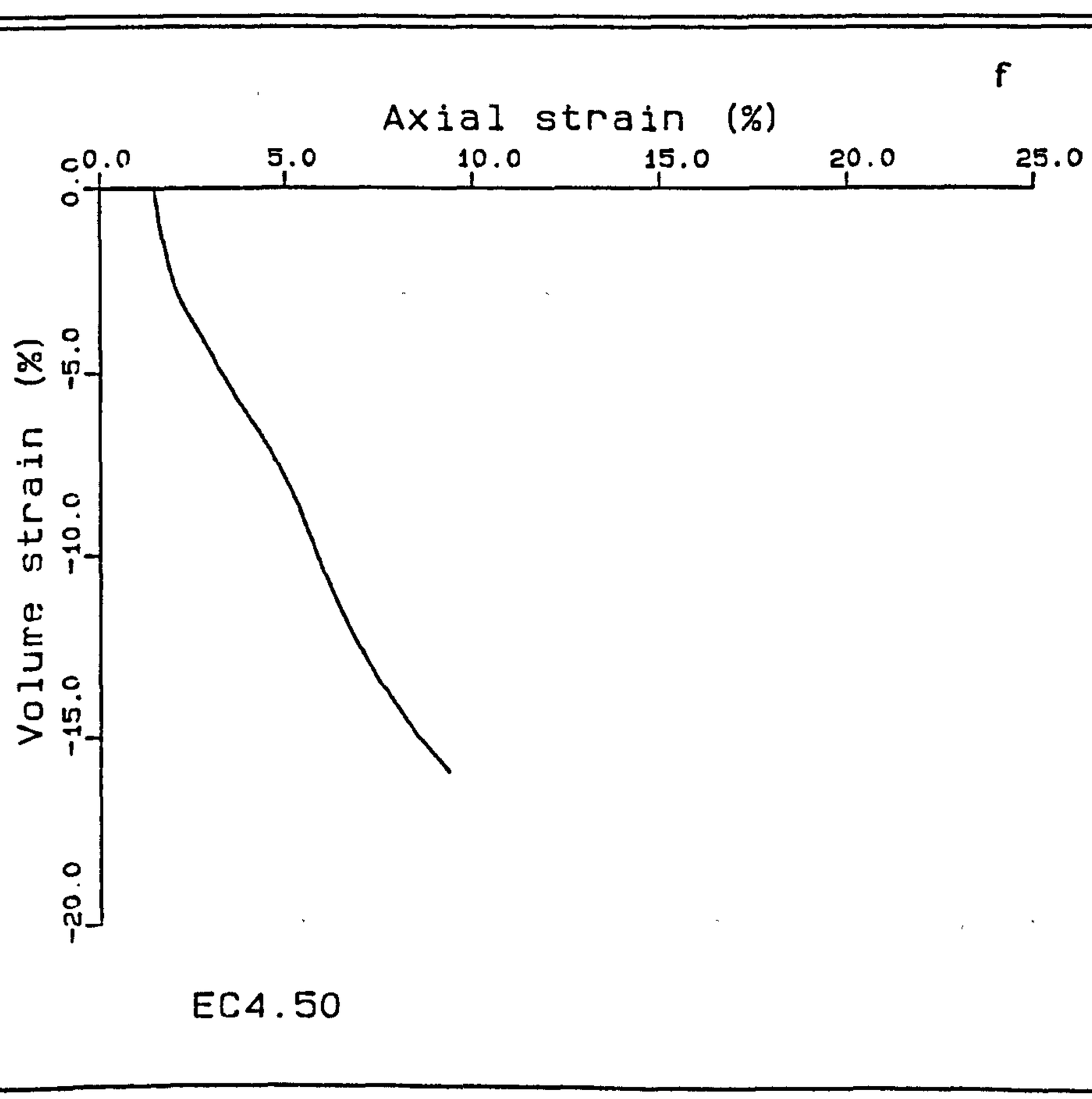

EC4.50

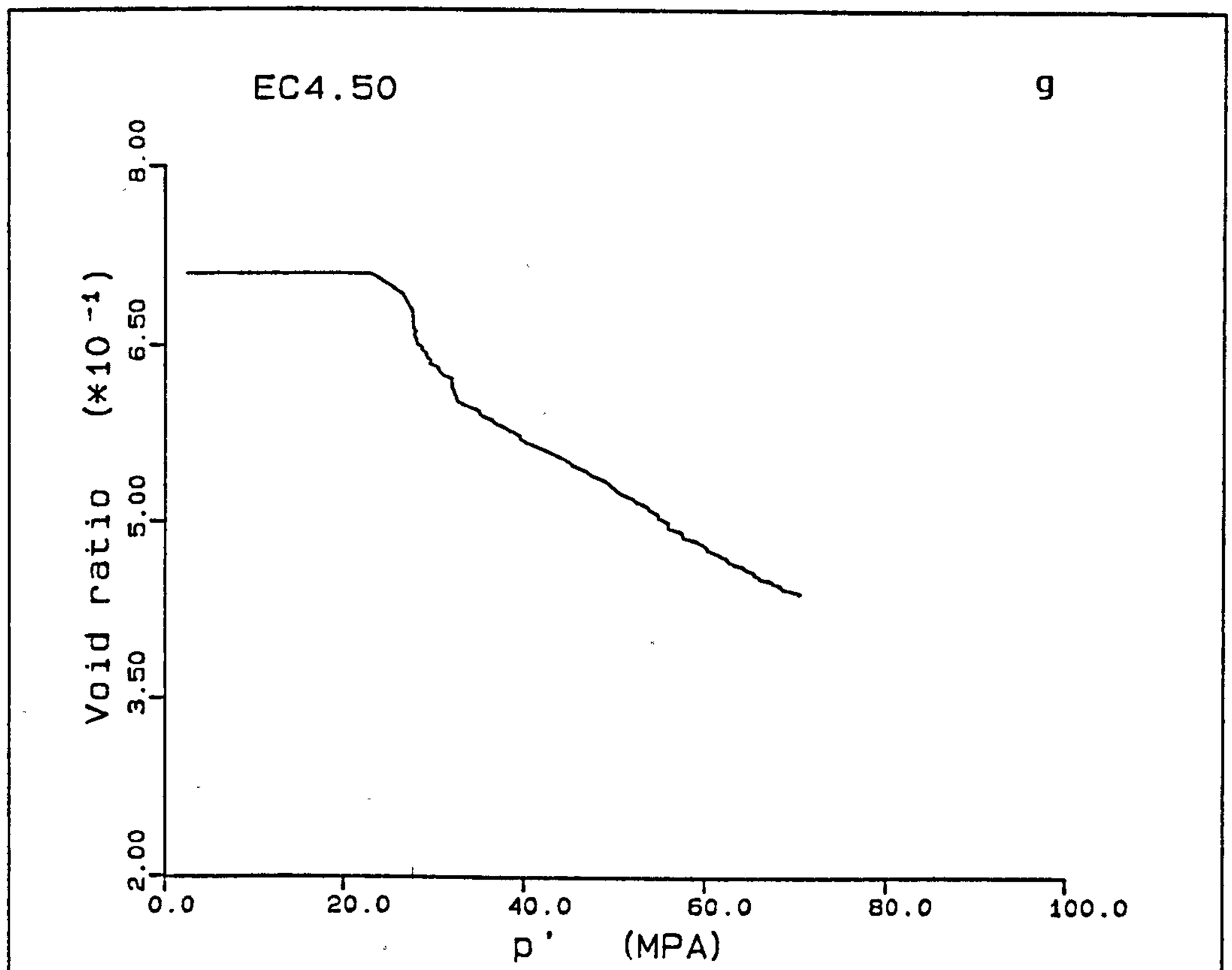
EC4.50
g
Void ratio (*10 -1)
8.00
6.50
5.00
3.50
2.00
0.0
20.0
40.0
60.0
80.0
100.0
p' (MPA)

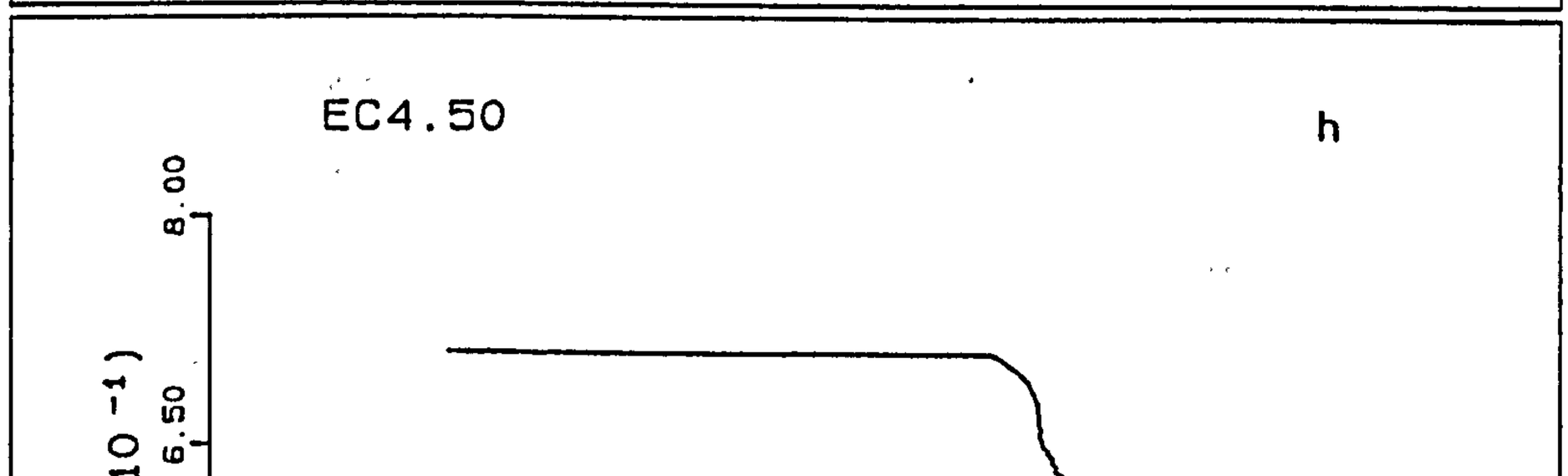
EC4.50
h
Void ratio (*10 -1)
8.00
6.50
5.00
3.50
2.00
0 00
0.40
0.80
1.20
1.60
2.00
log p' (MPA)

EC5.20

This test on a 40% porosity chalk shows that a small radial strain can have a marked effect on the stress strain characteristics. The initial part of the test maintained a radial strain variation of $\pm 3*10^{-3}$% up to an axial strain of 3%. The elastic deformation seen as a linear response to stress with a Young's modulus of 1.63GPa, this is followed by yield at a deviatoric stress of 11.8MPa, where a slight maximum of load is seen, the load reducing slightly and tending to increase in a concave upwards manner during post-yield strains. At 5% axial strain a maximum decrease in radial strain occured of $1.5*10^{-2}$, the radial strain started decreasing at an axial strain of 4.5%. This caused a jump in the stress strain curve with a decrease in load of 4MPa.

This drop in load in q-p' space, due to the radial strain of the sample, was followed by the normal consolidation compaction. The K_o stress path is not linear but curved (concave downwards) initially, and becomes linear after a mean effective stress of 40MPa. The $\bar{K}_o$ for the deformations are 0.344, 2.055, and 0.492, for the elastic, transitional, and normal consolidation sections, respectively.

The decrease in the radial strain is represented in the volumetric strain and void ratio plots, as a step, with reduced volume decrease of the sample during the reduction in load. After the radial strain is restored, a volumetric readjustment is seen with a larger C_c for the e-log p' plot, this becoming linear at approximately log p' = 1.56. The response in the pore water pressure is to increase slightly around an axial stain of 4.5 - 5%.

The compaction of this sample is seen in Figs. A5.5i-1. The average initial pre-yield compressibility of $3.8*10^{-4}MPa^{-1}$ rising to $6.2*10^{-3}MPa^{-1}$ at a vertical effective stress of 23.6MPa, the yield of

the chalk being at 17.1MPa vertical effective stress. After the maximum, the compressibility decreases to a value of $8.5*10^{-4}MPa^{-1}$ at a vertical effective stress of 120MPa. The C_v initially has a value of $1484m^2/yr$ at peak M_v and decreases to $82.4m^2/yr$ at the stress of 120MPa, Fig.A5.5j. An accompanying drop in the permeability of 2.8mD at 23.6MPa to $2.1*10^{-2}$mD at the higher stress is also observed. At a vertical effective stress of 50MPa, the sample permeability was 0.26mD. These value were calculated using viscosity values of 8cp and densities of $0.85g/cm^3$. The log k(1+e) versus log e is seen to be approximately linear over the range of stresses, 23.6 to 120.0MPa. The pore pressure difference across the sample, U_h divided by the vertical effective stress σ_v' ranges between 0.0016 and 0.0019.

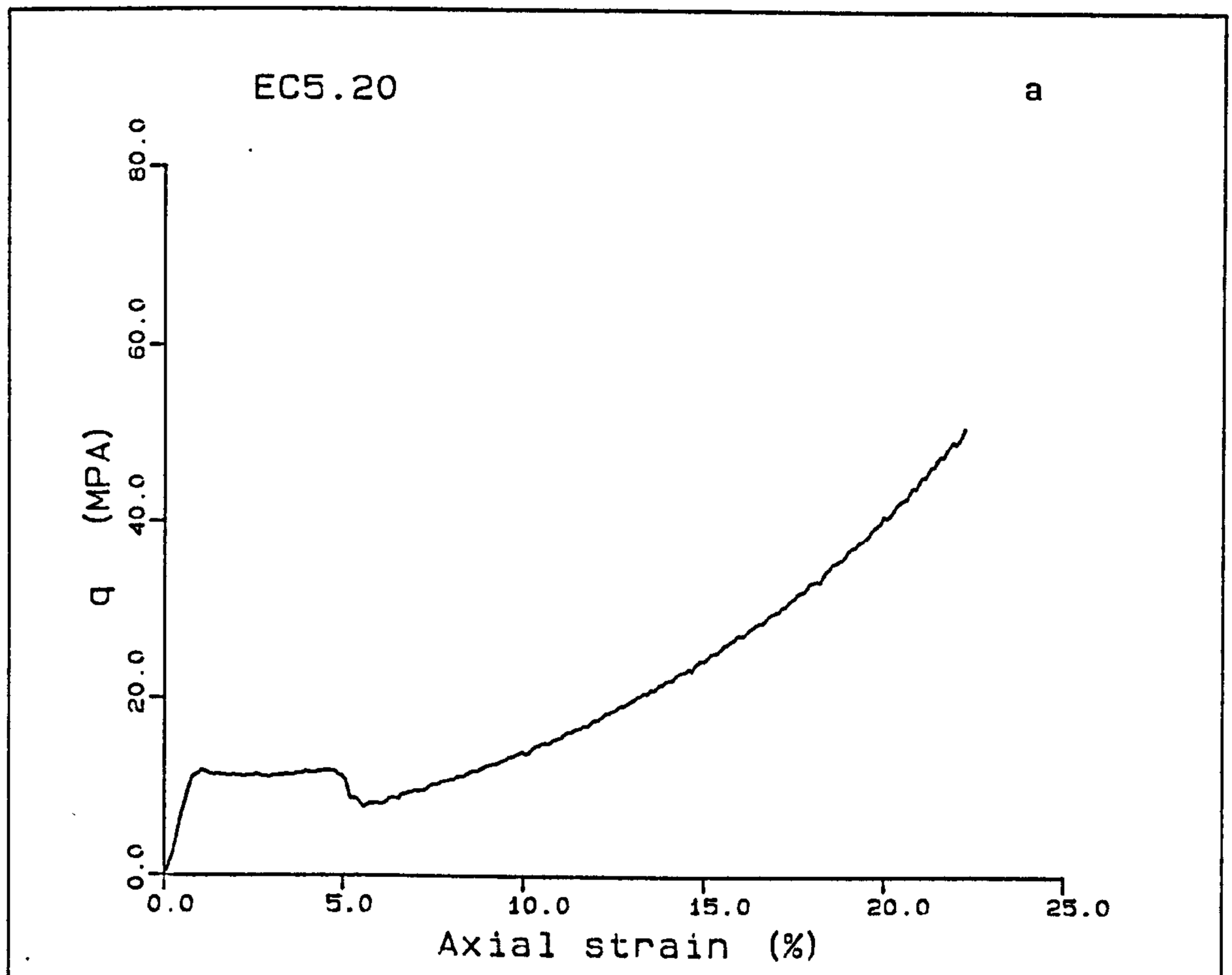

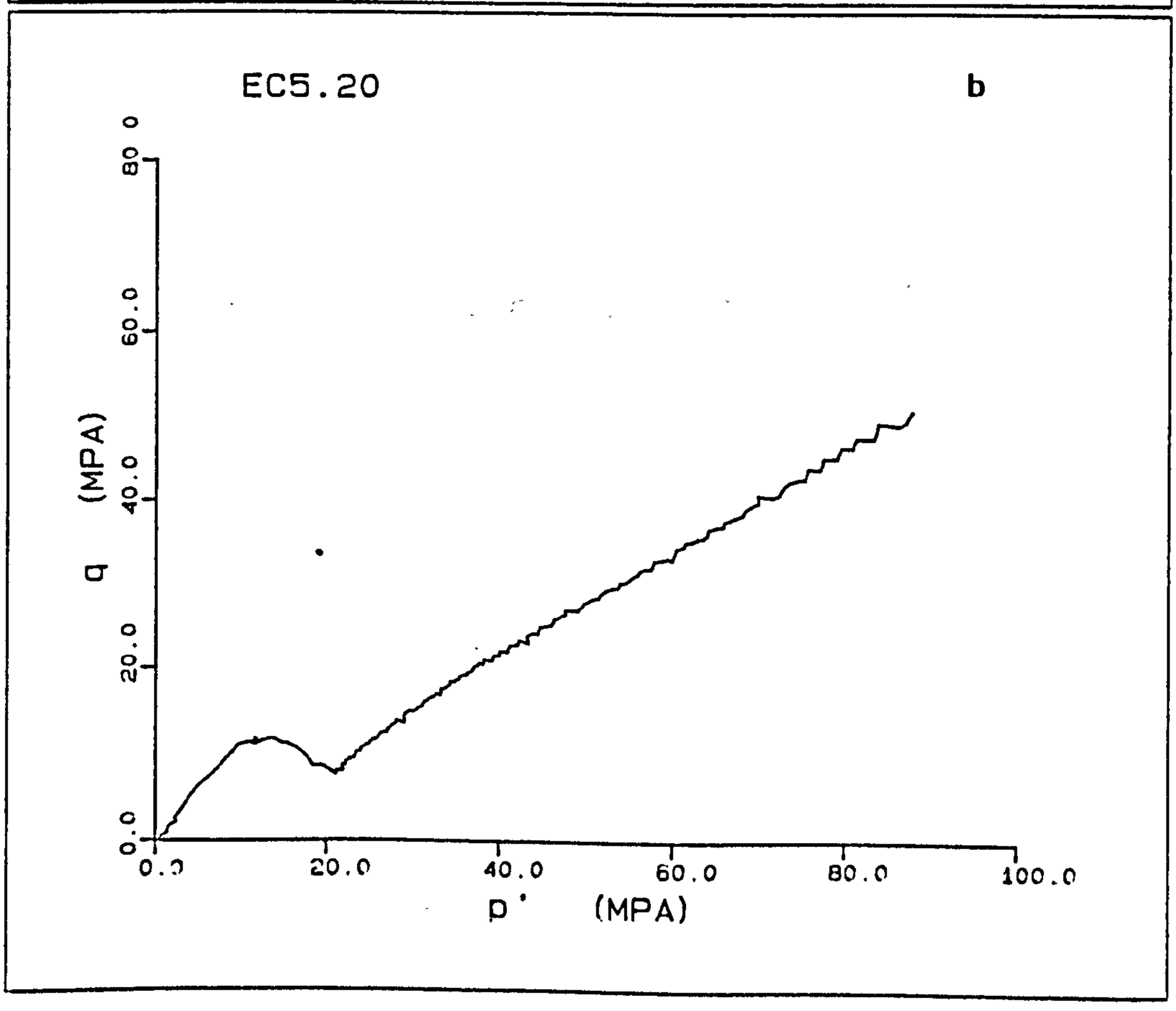

Figure A5.5(a-1) K_o test EC5.20.

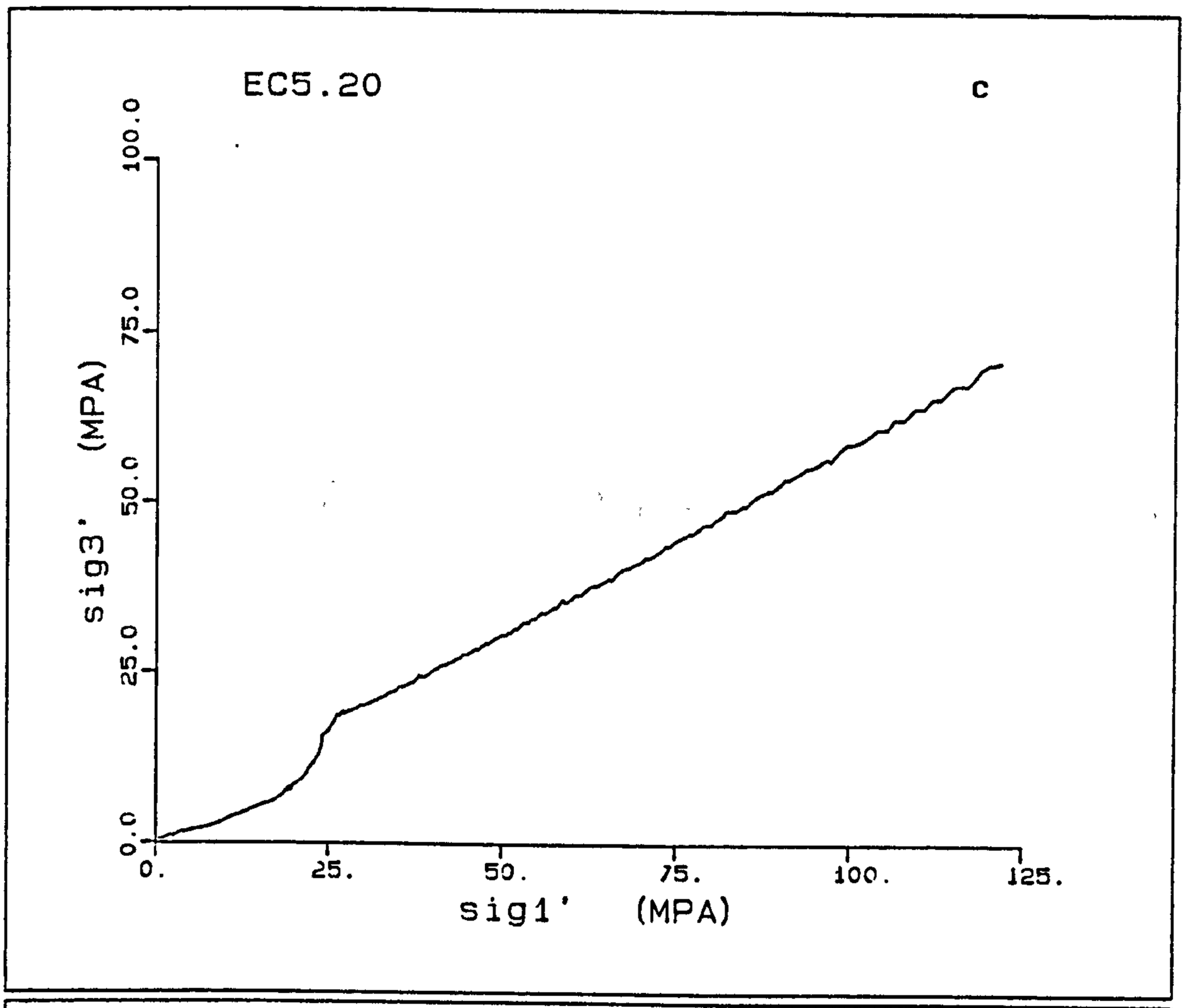
EC5.20
c
sig3' (MPA)
100.0
75.0
50.0
25.0
0.0
0.
25.
50.
75.
100.
125.
sig1' (MPA)

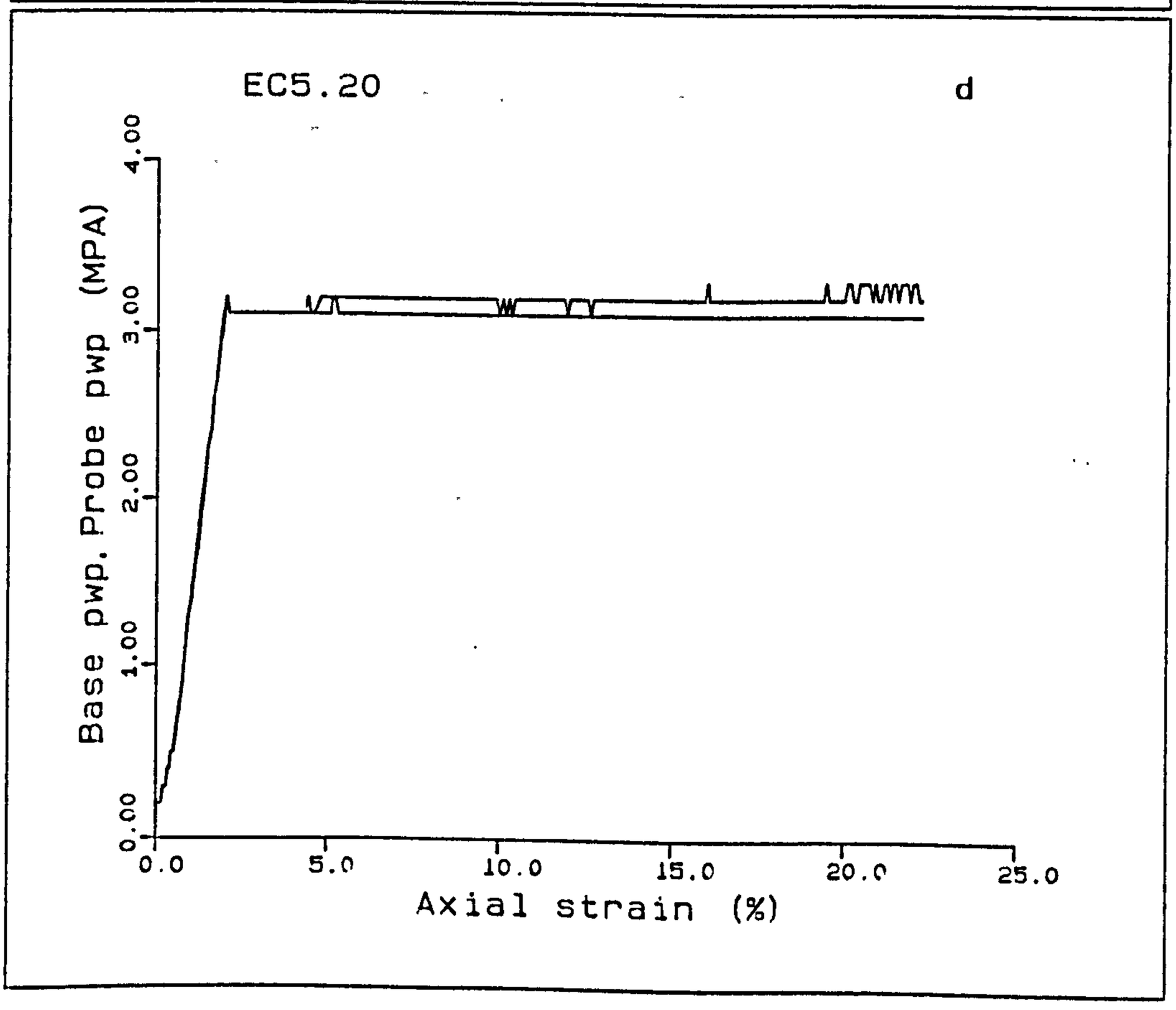
EC5.20
d
Base pwp. Probe pwp (MPA)
4.00
3.00
2.00
1.00
0.00
0.0
5.0
10.0
15.0
20.0
25.0
Axial strain (%)

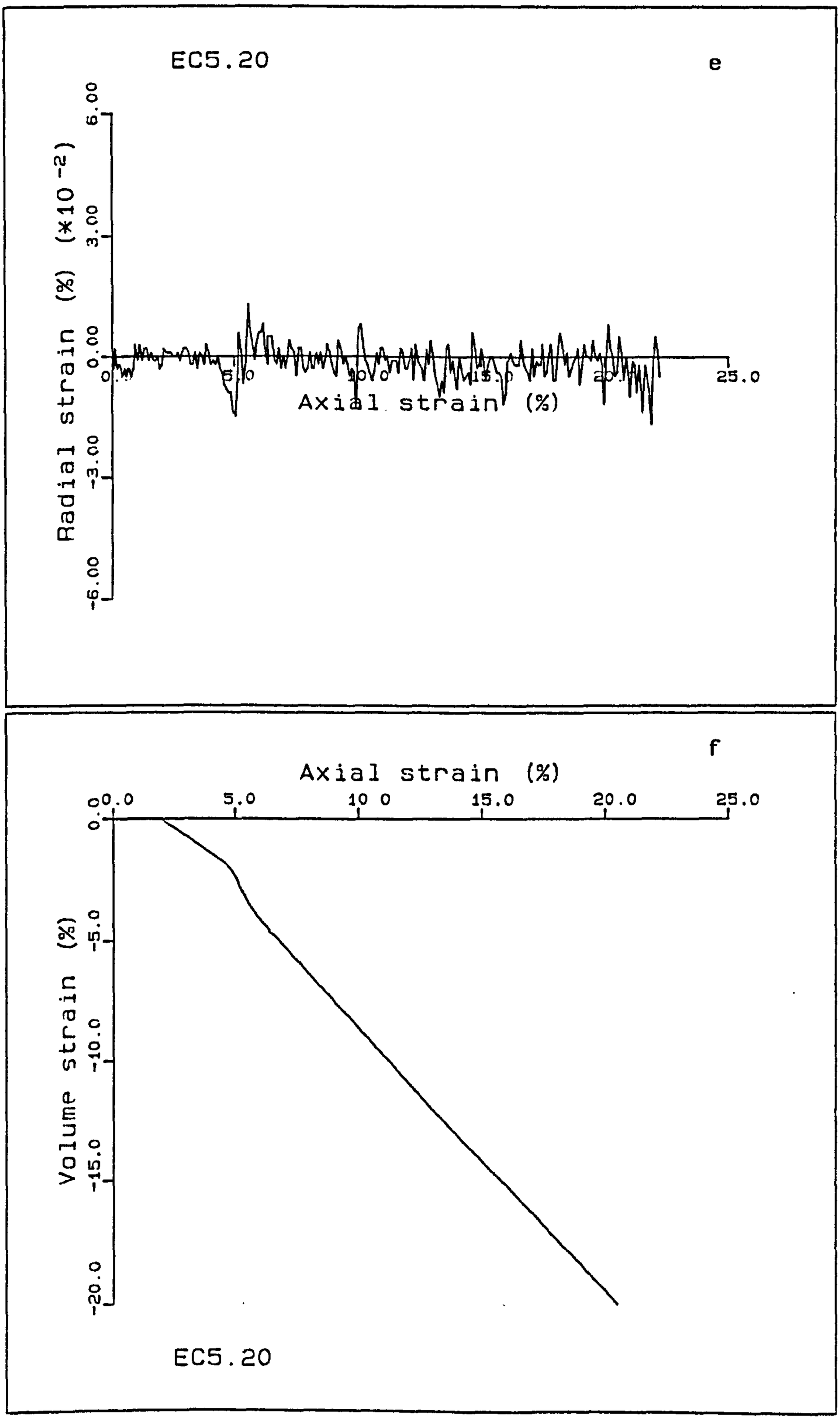
EC5.20
e
Radial strain (%) (*10 -2)
6.00
3.00
0.00
-3.00
-6.00
0
5.0
10.0
15.0
20.0
25.0
Axial strain (%)
f
Axial strain (%)
0.0
5.0
10 0
15.0
20.0
25.0
Volume strain (%)
-5.0
-10.0
-15.0
-20.0
EC5.20

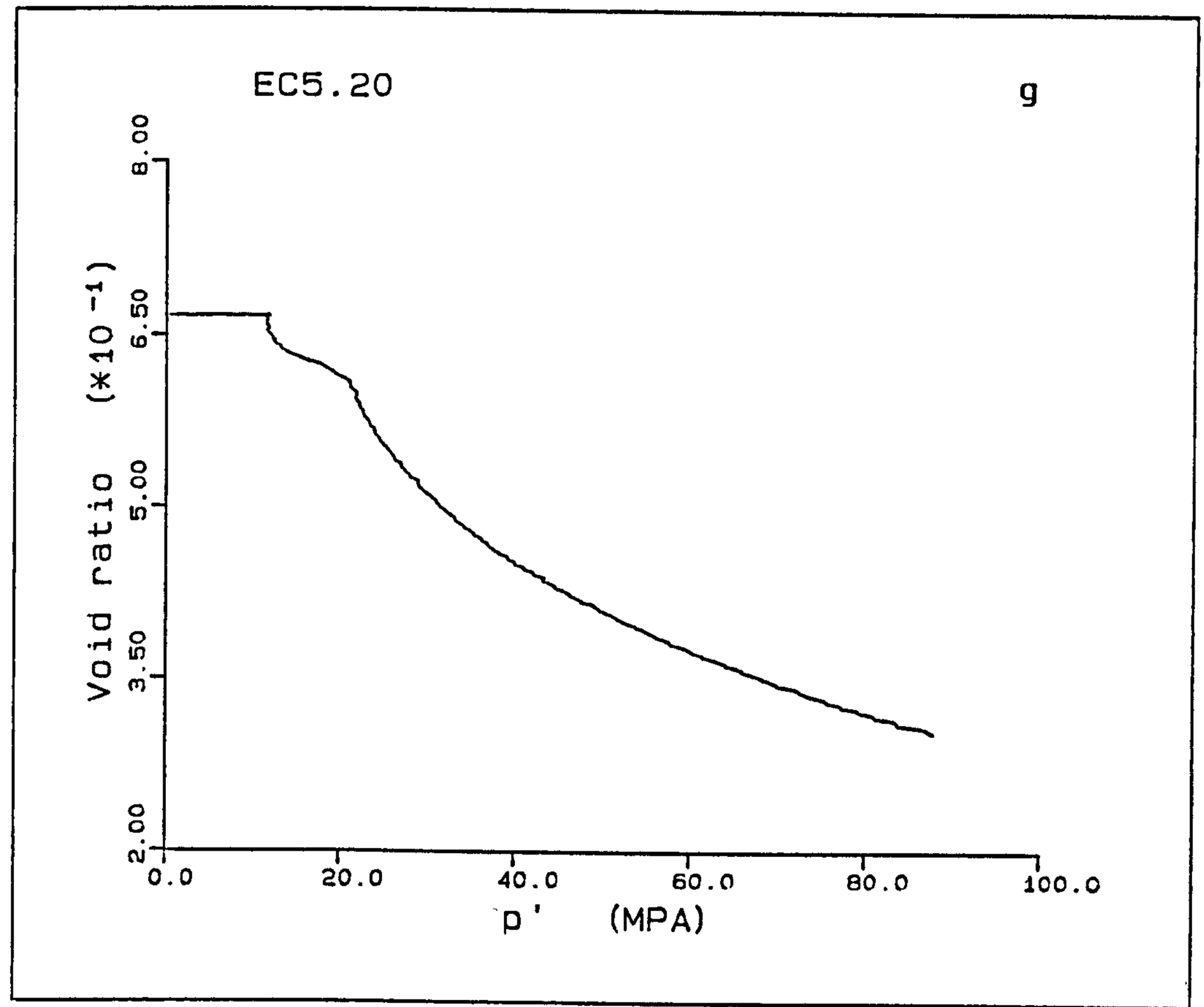
EC5.20
g
Void ratio (*10 -1)
8.00
6.50
5.00
3.50
2.00
0.0
20.0
40.0
60.0
80.0
100.0
p' (MPA)

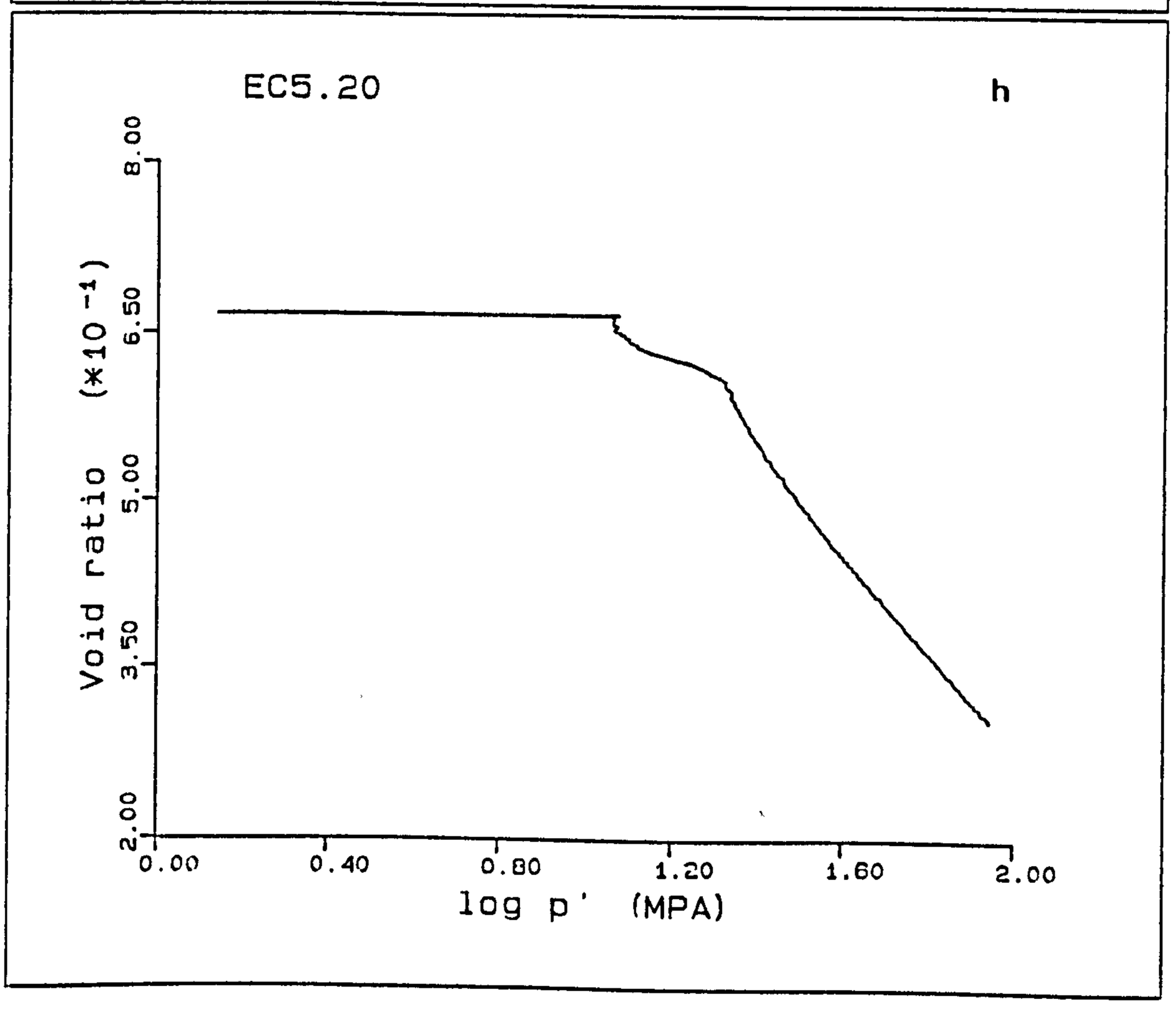
EC5.20
h
Void ratio (*10 -1)
8.00
6.50
5.00
3.50
2.00
0.00
0.40
0.80
1.20
1.60
2.00
log p' (MPA)

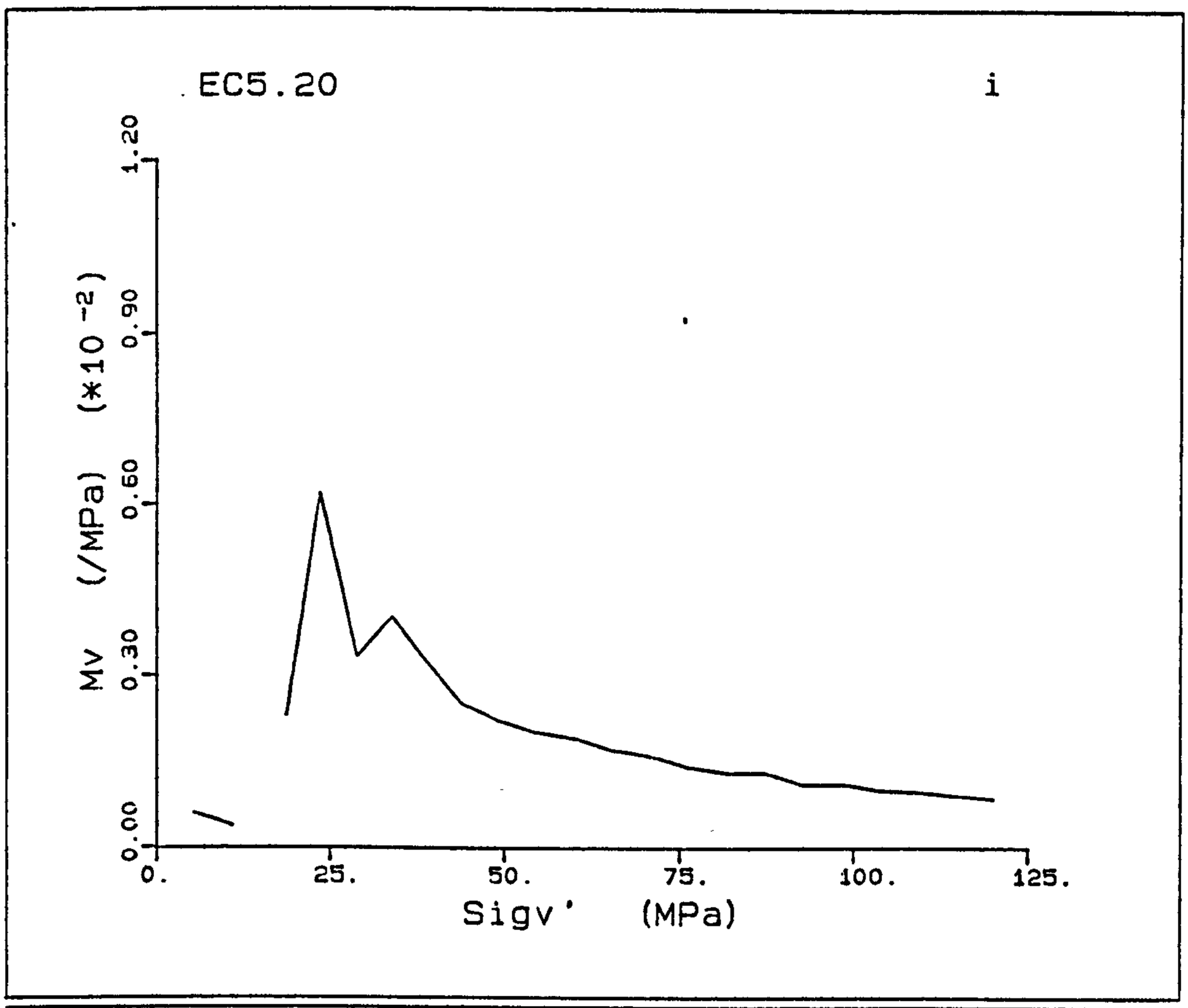
EC5.20
i
Mv (/MPa) (*10 -2)
1.20
0.90
0.60
0.30
0.00
0.
25.
50.
75.
100.
125.
Sigv' (MPa)

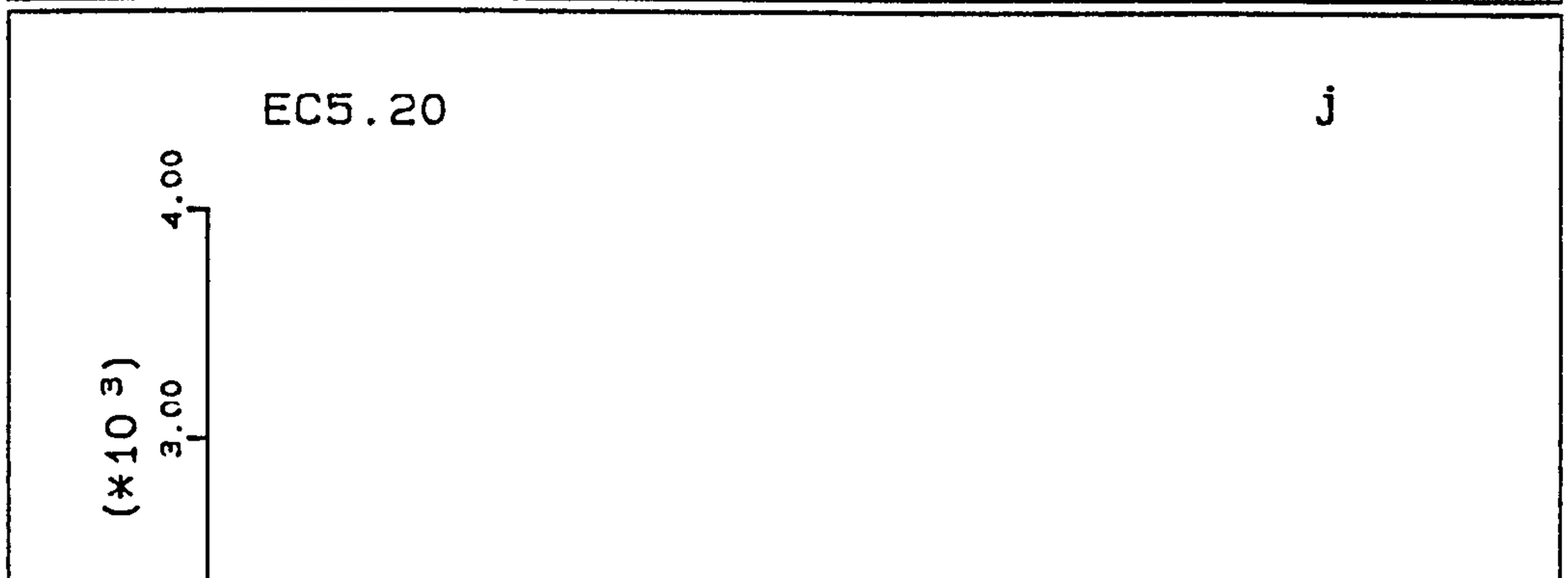
EC5.20
j
Cv (m2/yr) (*10 3)
4.00
3.00
2.00
1.00
0.00
0.
25.
50.
75.
100.
125.
Sigv' (MPa)

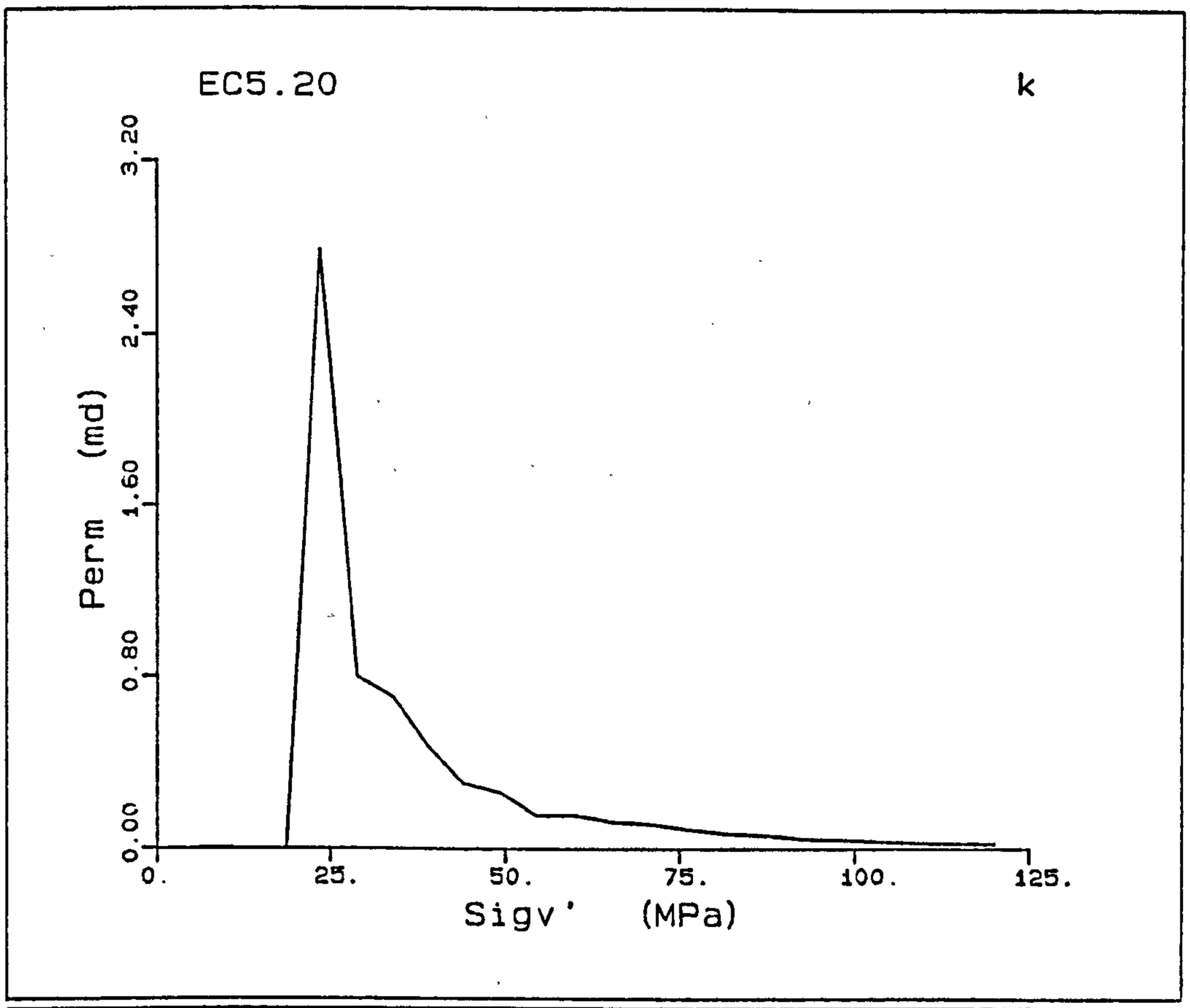
EC5.20
k
3.20
2.40
1.60
0.80
0.00
Perm (md)
0.
25.
50.
75.
100.
125.
Sigv' (MPa)

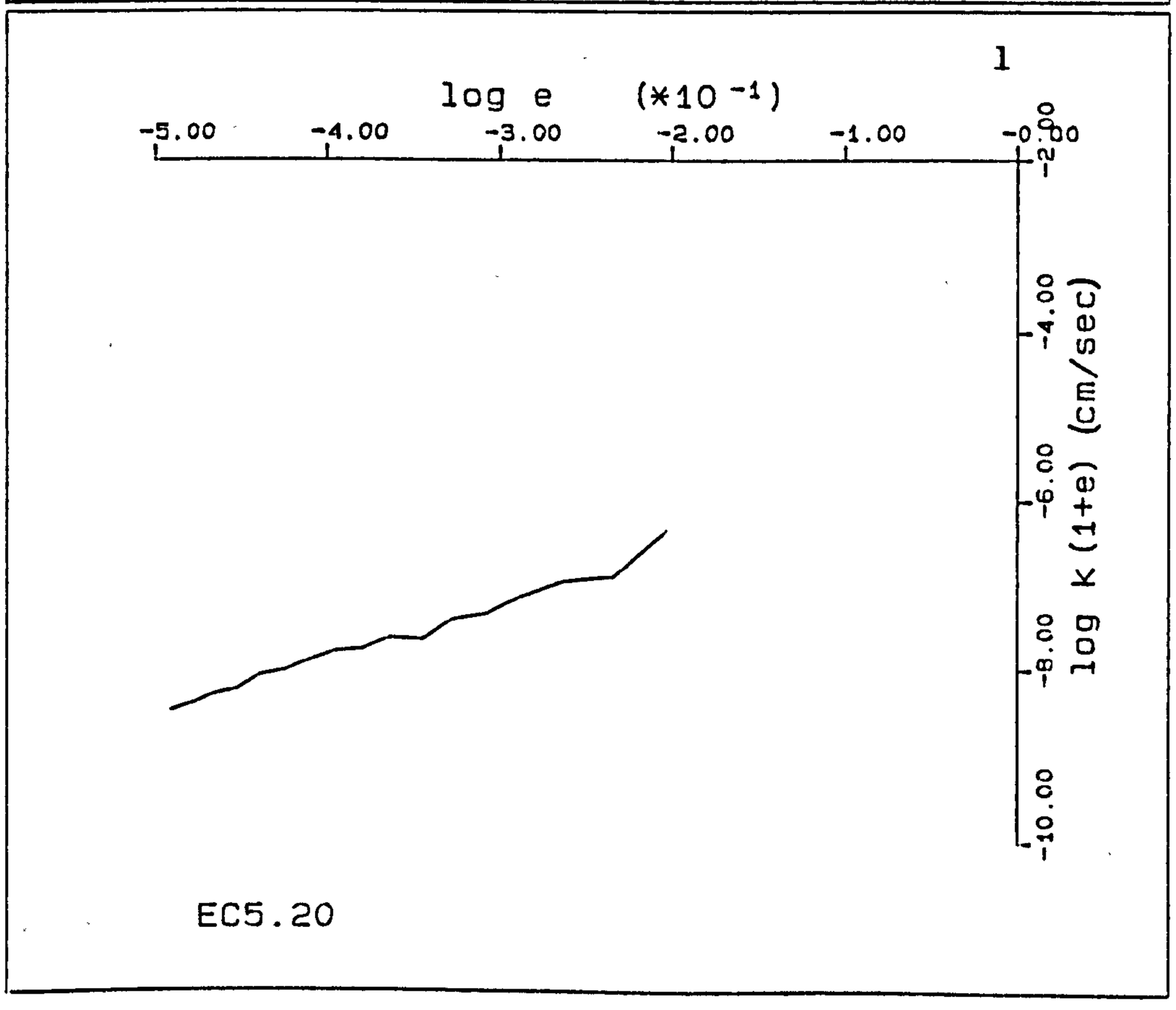
1
log e (*10 -1)
-5.00
-4.00
-3.00
-2.00
-1.00
-0.00
-2.00
-4.00
-6.00
-8.00
-10.00
log K (1+e) (cm/sec)
EC5.20

EC6.20

This is a 36% porosity chalk, which shows a linear elastic section of Young's modulus, 3.8GPa. At a deviatoric stress of 38MPa, the linear elastic section starts curving to a maximum deviatoric stress for this section at a yield point of 47.2MPa. In the pore collapse deformation, the loading was stopped for 15 minutes, when a decrease in the load of 4.5MPa occured. The reloading is over too small a stress range to obtain a modulus, but it appears to be approximately equal to the initial modulus. The normal consolidation deformation seen in this test is small due to the maximum cell pressure being reached. Thus, no reliable $\bar{K}_o$ for this section could be obtained; the $\bar{K}_o$ values for the elastic and transitional stages are 0.318 and 1.077 respectively.

The radial strains were held within $1*10^{-2}$% axial strain throughout the experiment, except at axial strains 4.1 and 5.4%, where the radial strains reached $1.3*10^{-2}$% and $1.9*10^{-2}$% respectively.

The volume change did not start recording until 4.3% axial strain, where upon the pore pressure reached the loading of the back pressure regulator, the pressure remained constant for the rest of the deformation. The top pore pressure increased to 3.4MPa and increased from this value slightly with further shortening.

The compaction of this chalk sample occurs predominantly in the pre-yield, elastic region at the stresses used in this study. The average pre-yield M_v being $2.1*10^{-4}MPa^{-1}$, gradually increasing to a peak value of $1.7*10^{-3}MPa^{-1}$ at an effective stress of 114.8MPa. The yield point occurring at a vertical effective stress of 73.1MPa, which is the point where the M_v starts to increase from its low pre-yield level, Fig. A5.6i. The C_v and permeability are obtained

from a stress of 94.1MPa with initial values of 799m^2/yr and 0.21mD respectively, and decrease at a maximum stress (120MPa) to 100m^2/yr and 0.042mD. U_h/σ_v' from 94.1 to 120MPa increases from 0.0011 to 0.0034.

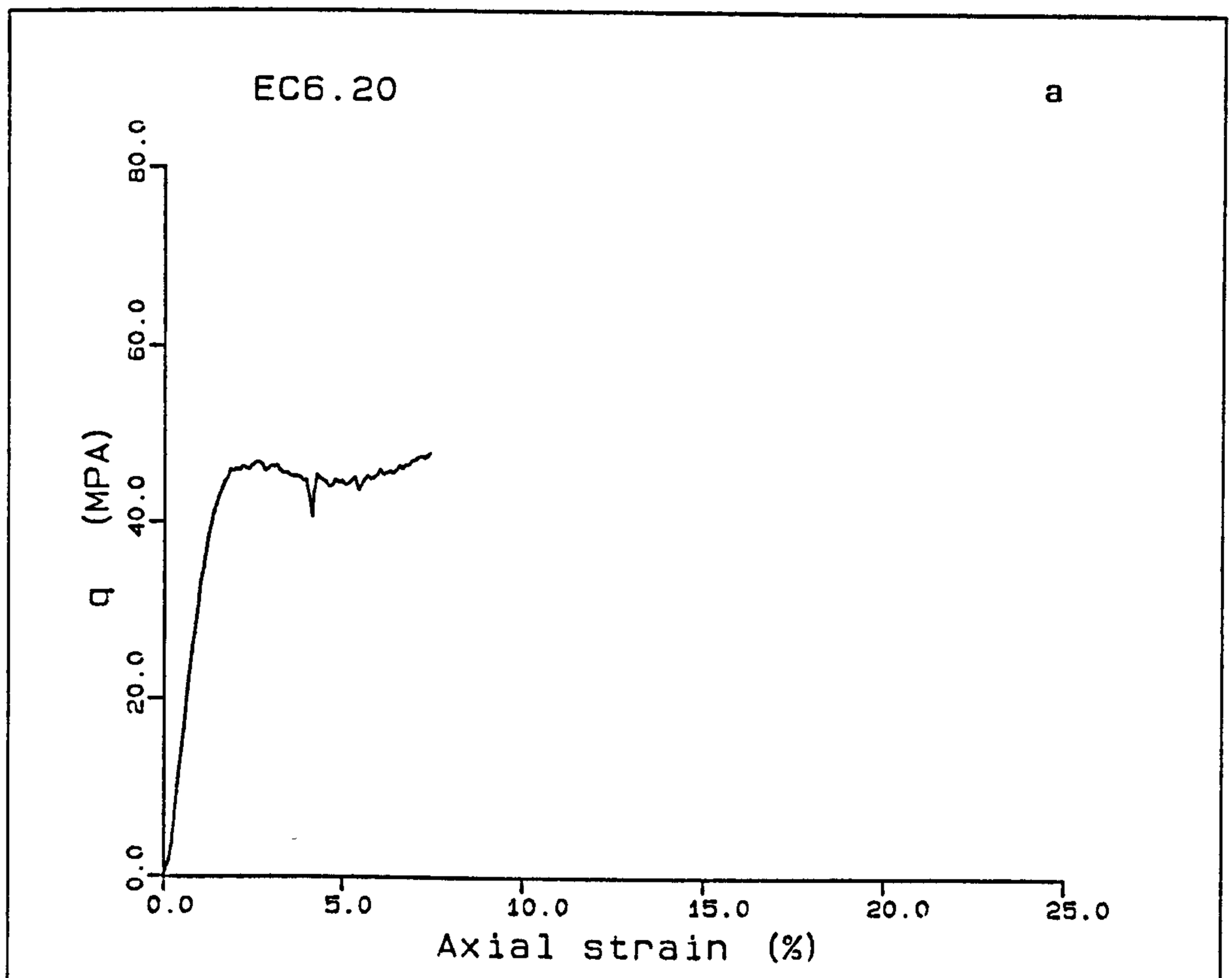

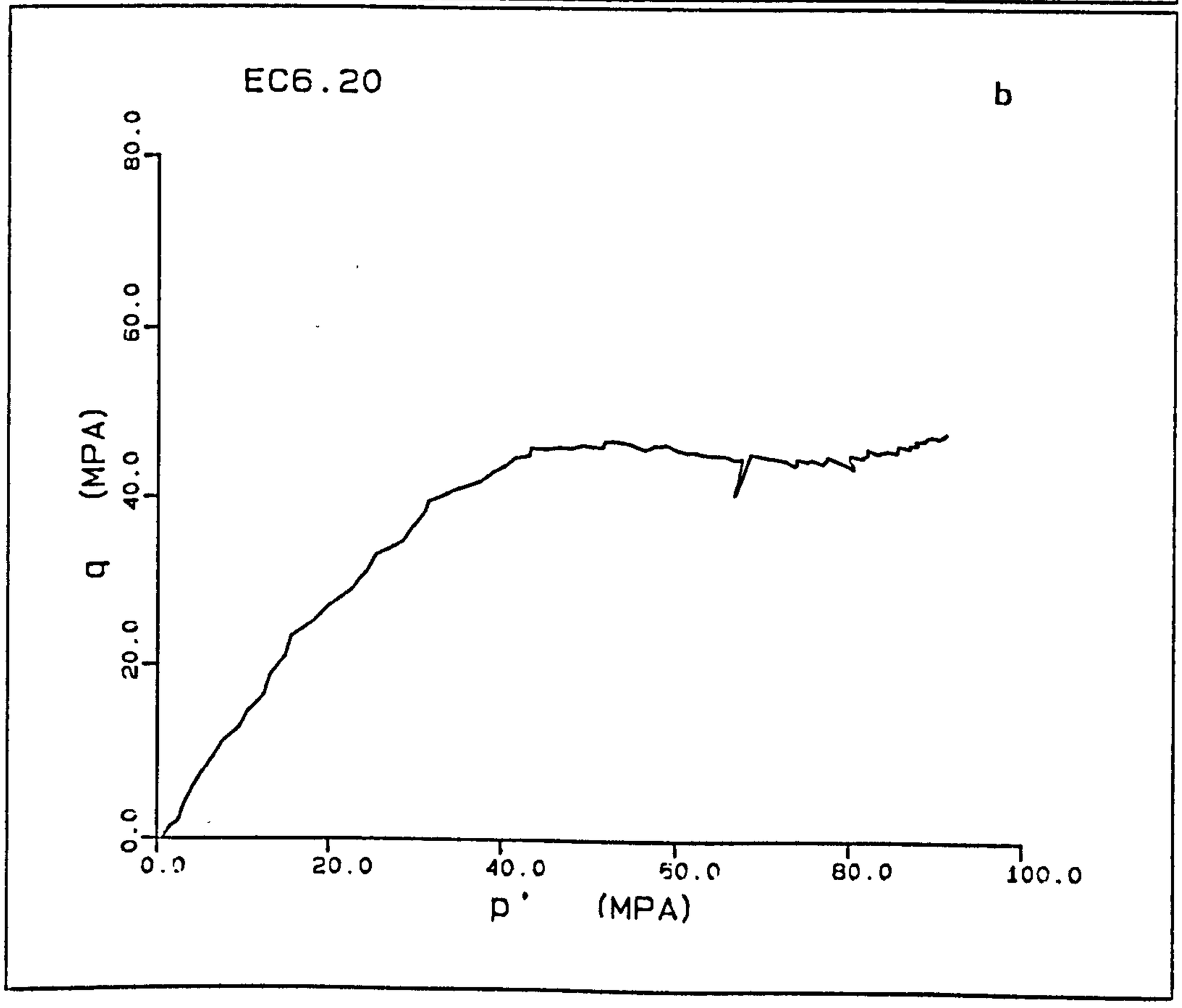

Figure A5.6(a-l) K_o test EC6.20.

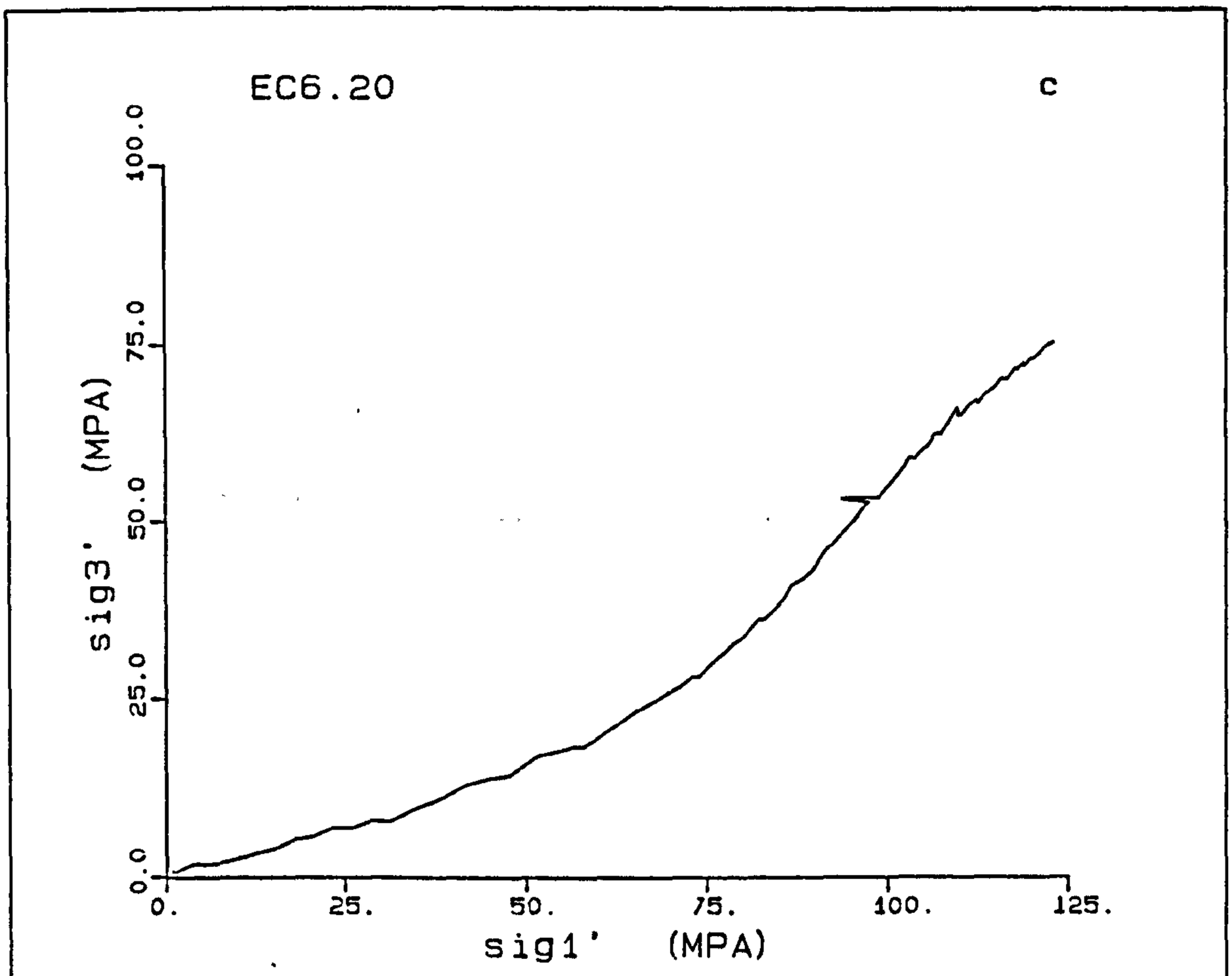
EC6.20
c
sig3' (MPA)
100.0
75.0
50.0
25.0
0.0
0.
25.
50.
75.
100.
125.
sig1' (MPA)

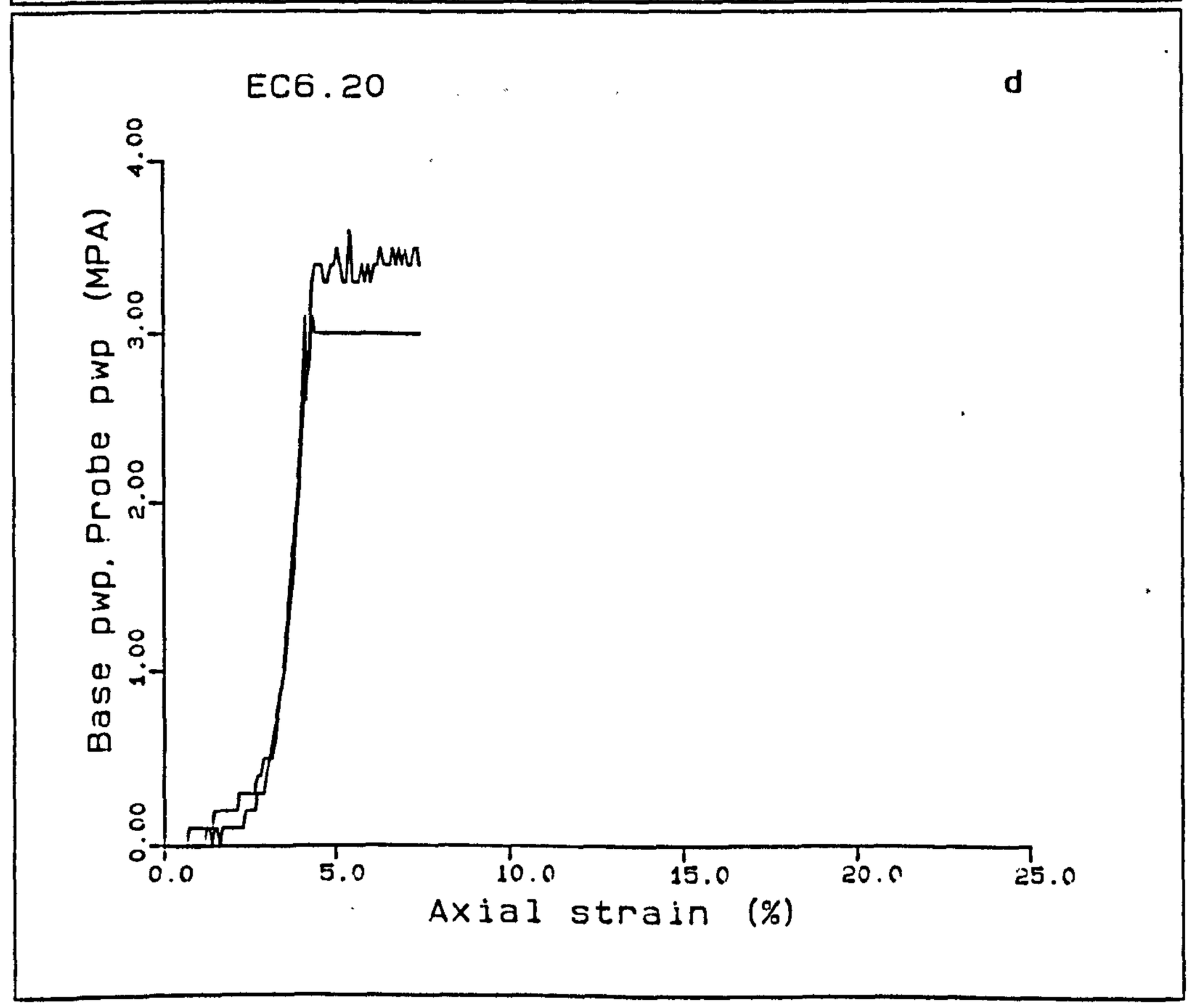
EC6.20
d
Base pwp, Probe pwp (MPA)
4.00
3.00
2.00
1.00
0.00
0.0
5.0
10.0
15.0
20.0
25.0
Axial strain (%)

EC6.20

e

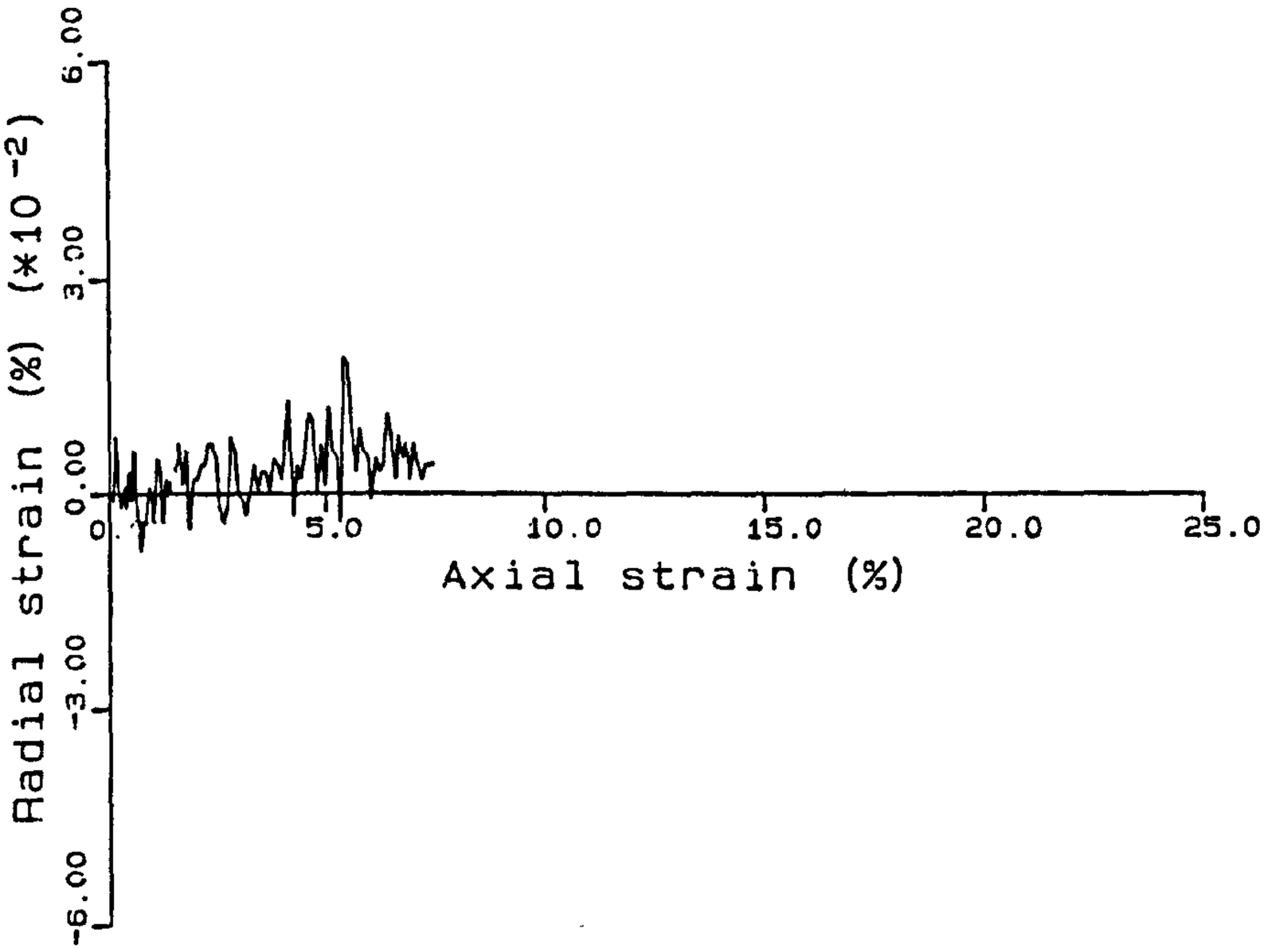

f

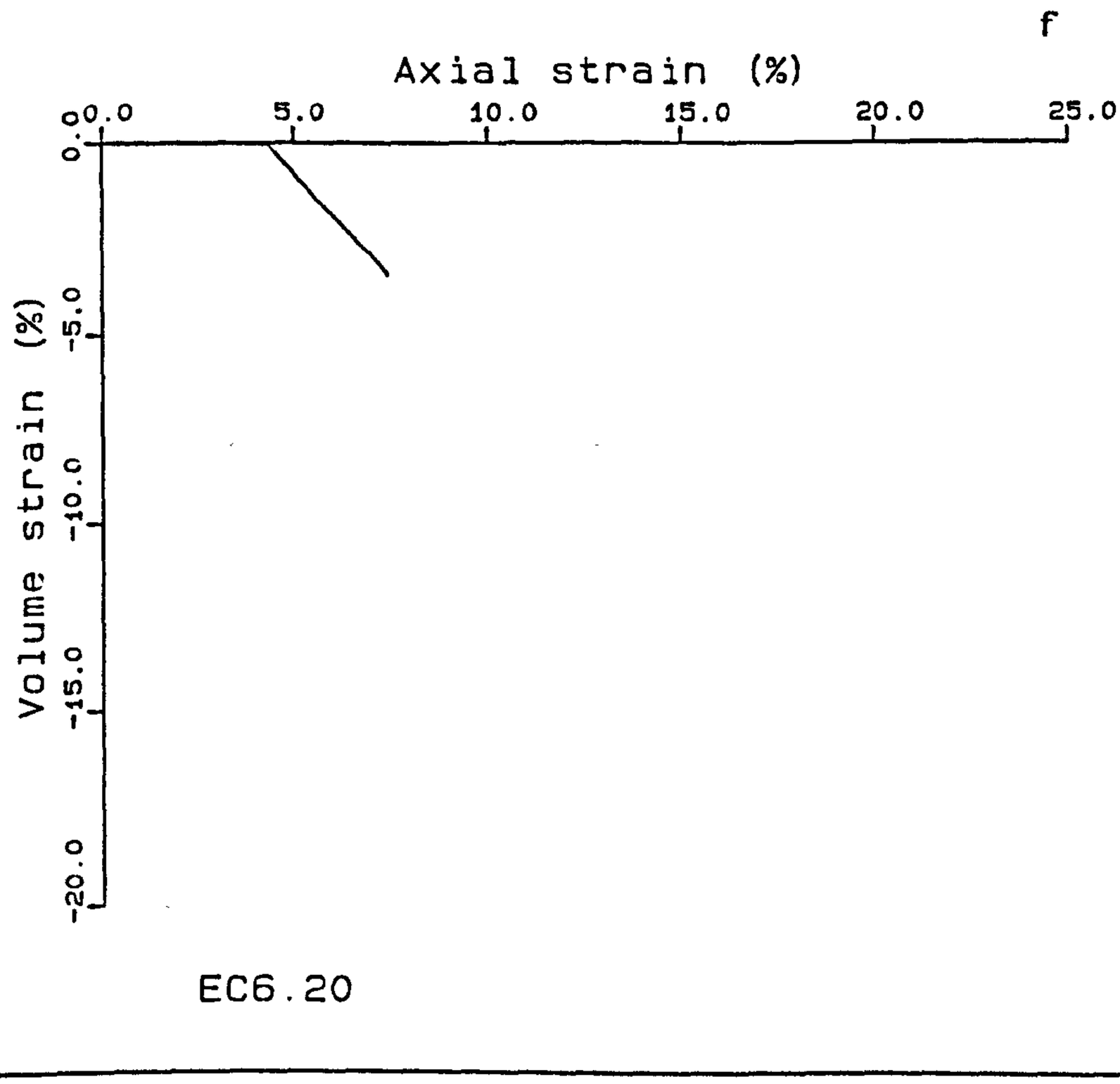

EC6.20

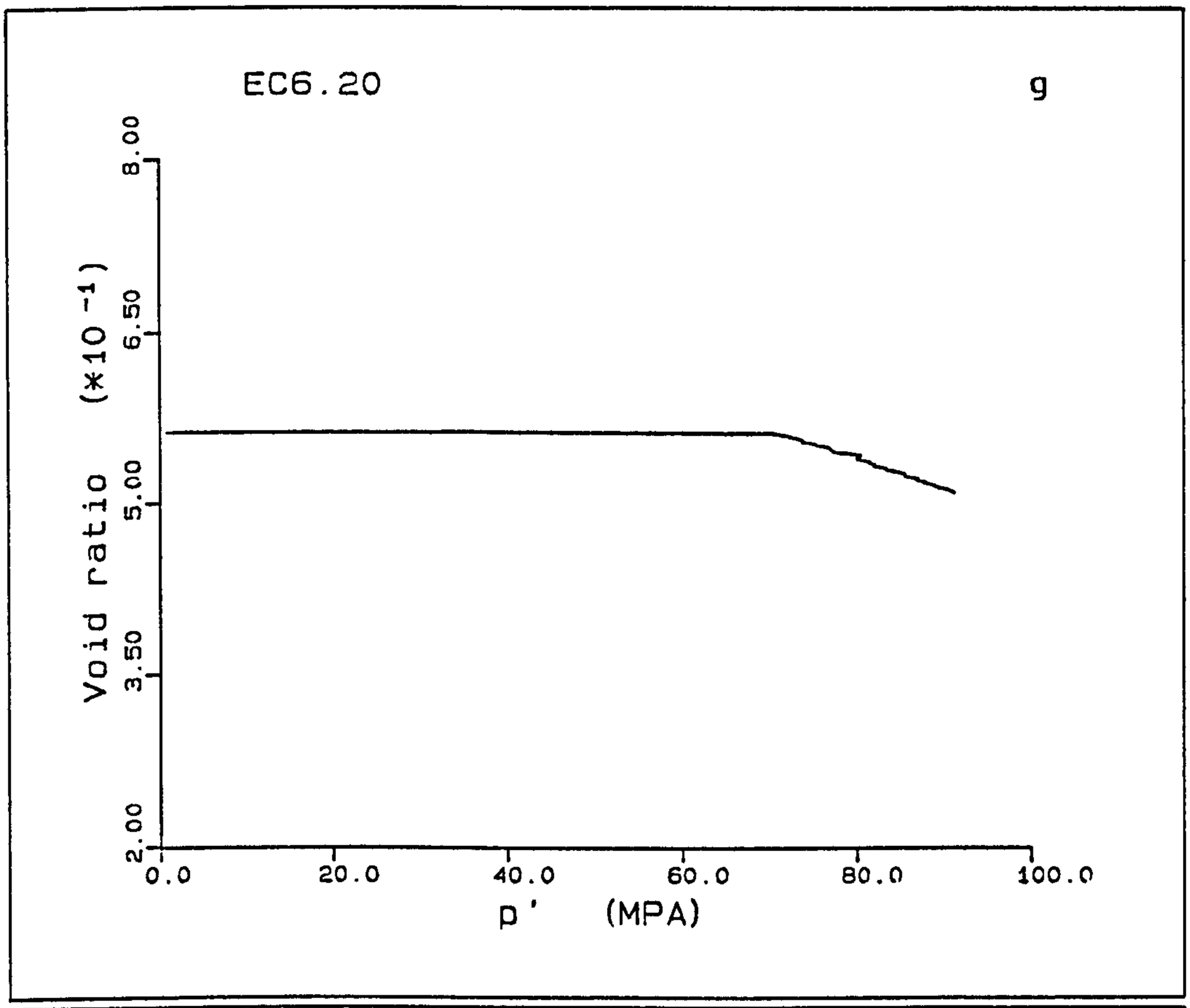
EC6.20
g
8.00
6.50
5.00
3.50
2.00
(*10 -1)
Void ratio
0.0
20.0
40.0
60.0
80.0
100.0
p' (MPA)

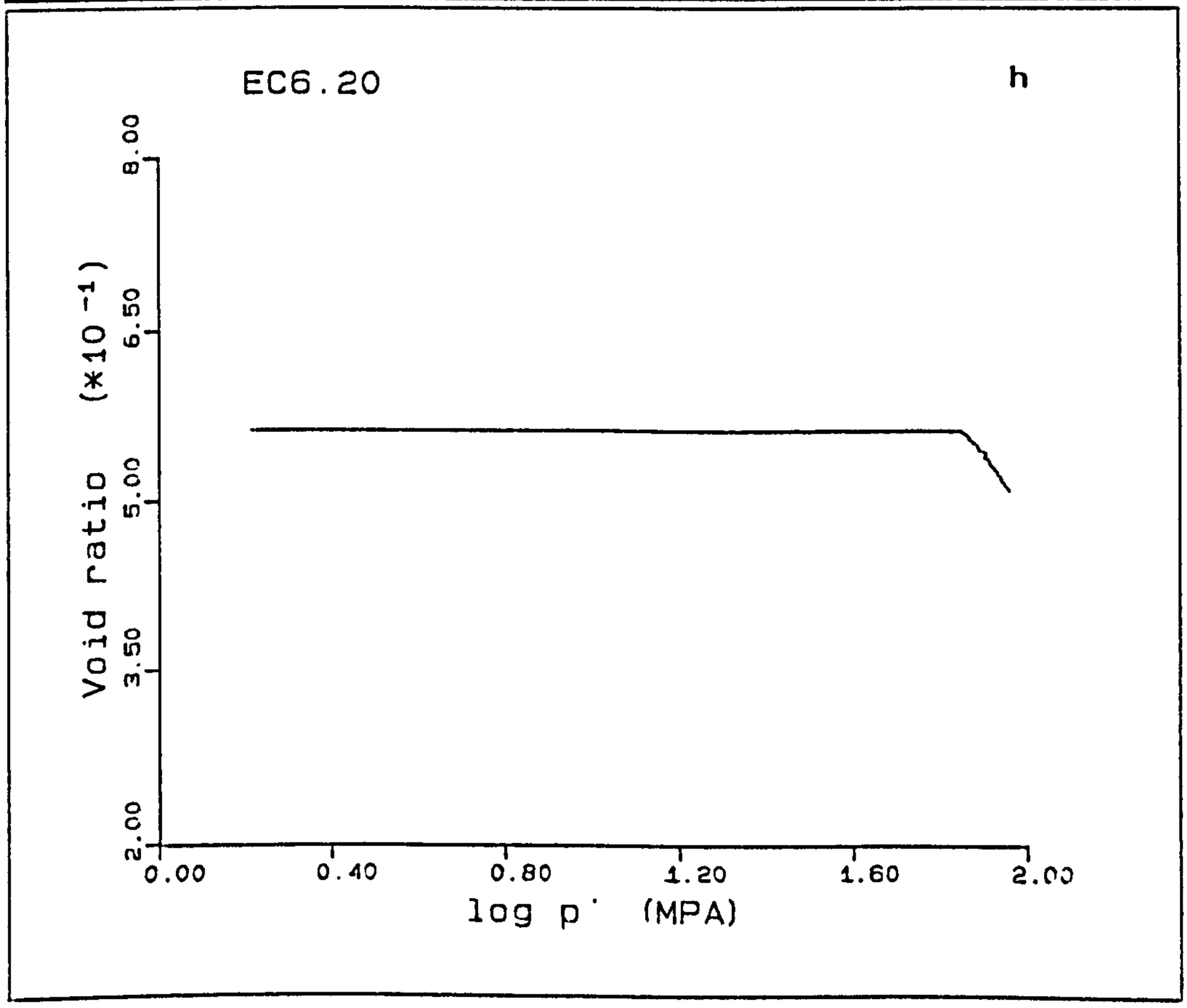
EC6.20
h
8.00
6.50
5.00
3.50
2.00
(*10 -1)
Void ratio
0.00
0.40
0.80
1.20
1.60
2.00
log p' (MPA)

EC6.20 i

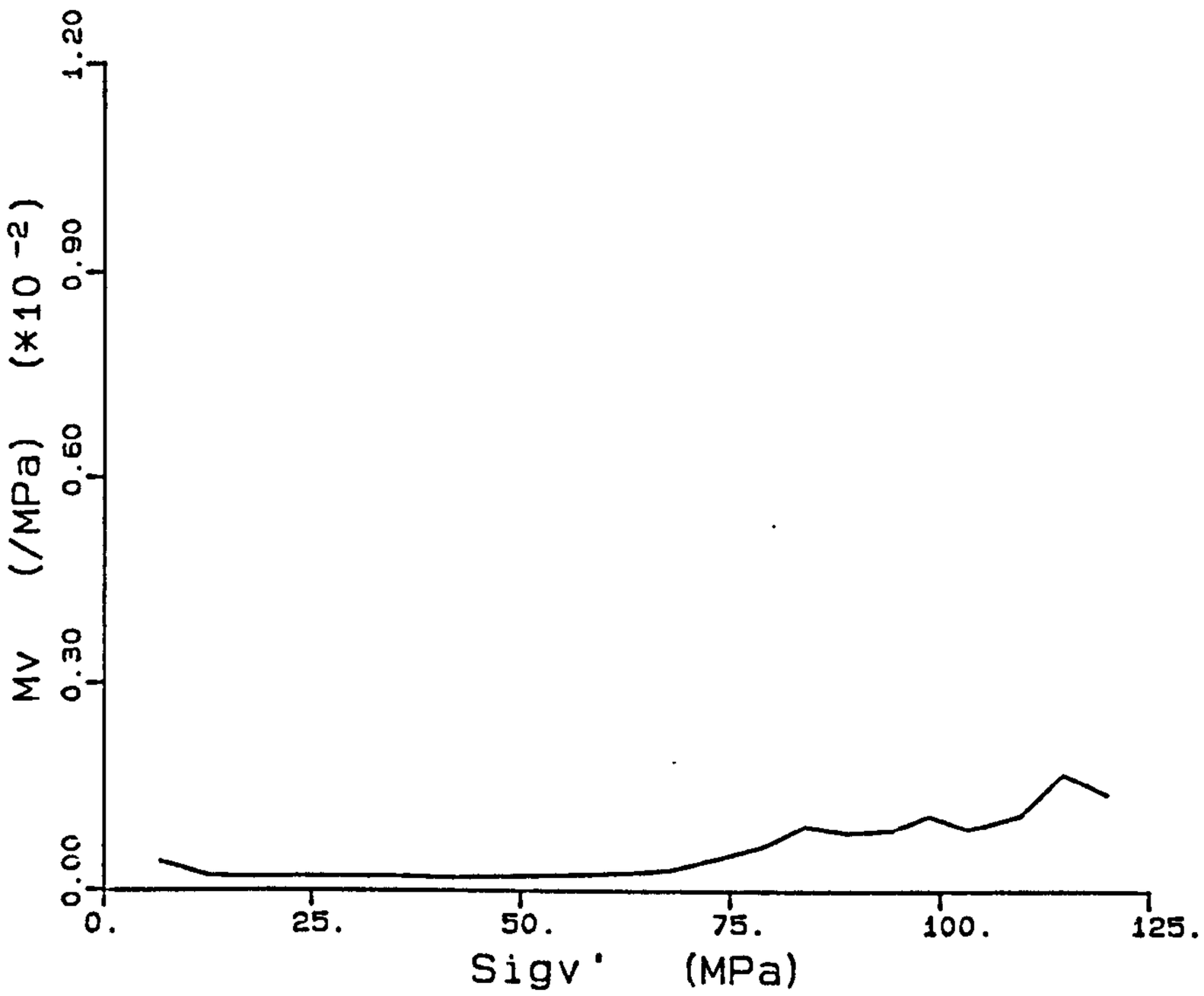

EC6.20 j

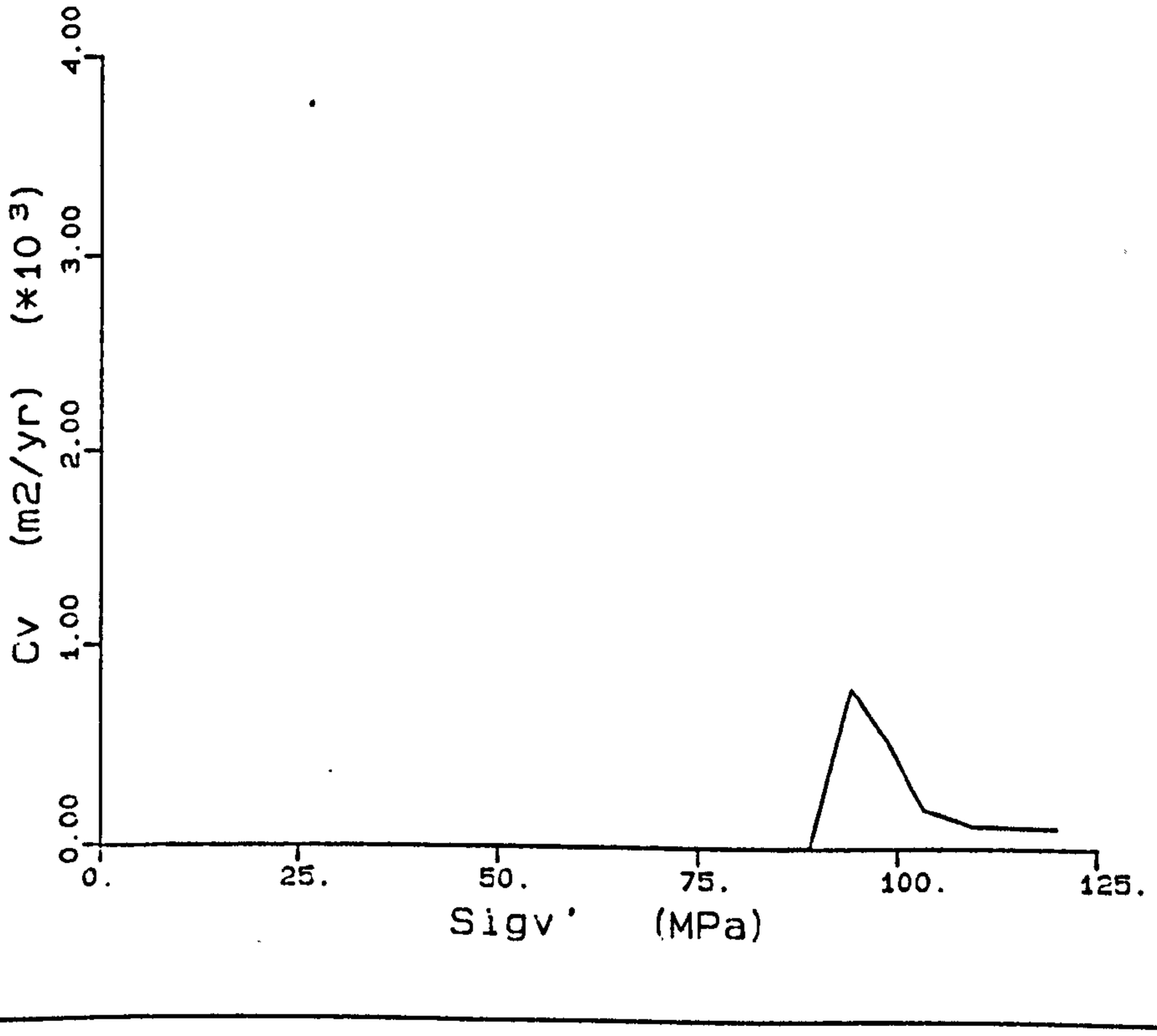

EC6.20 k

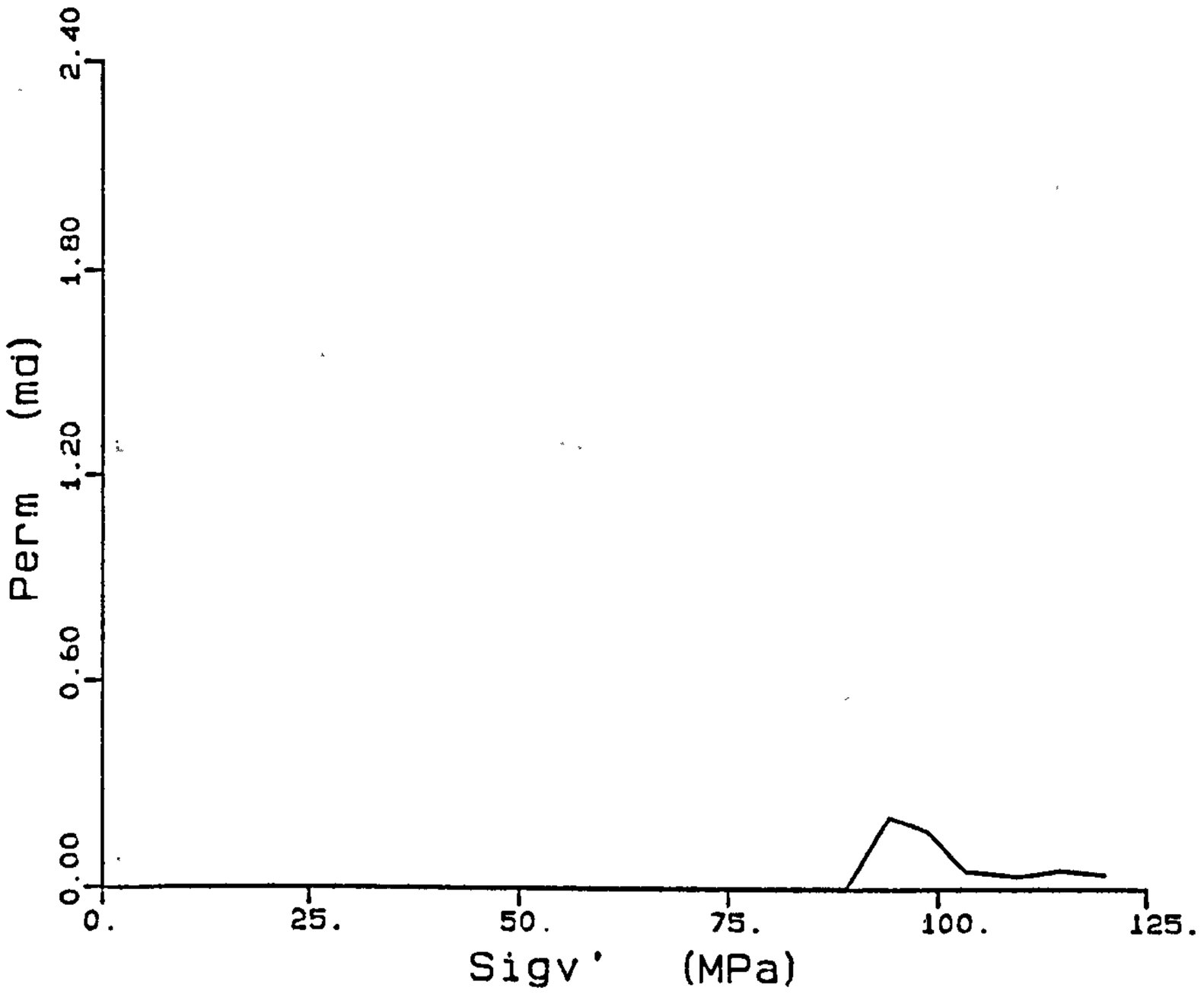

l

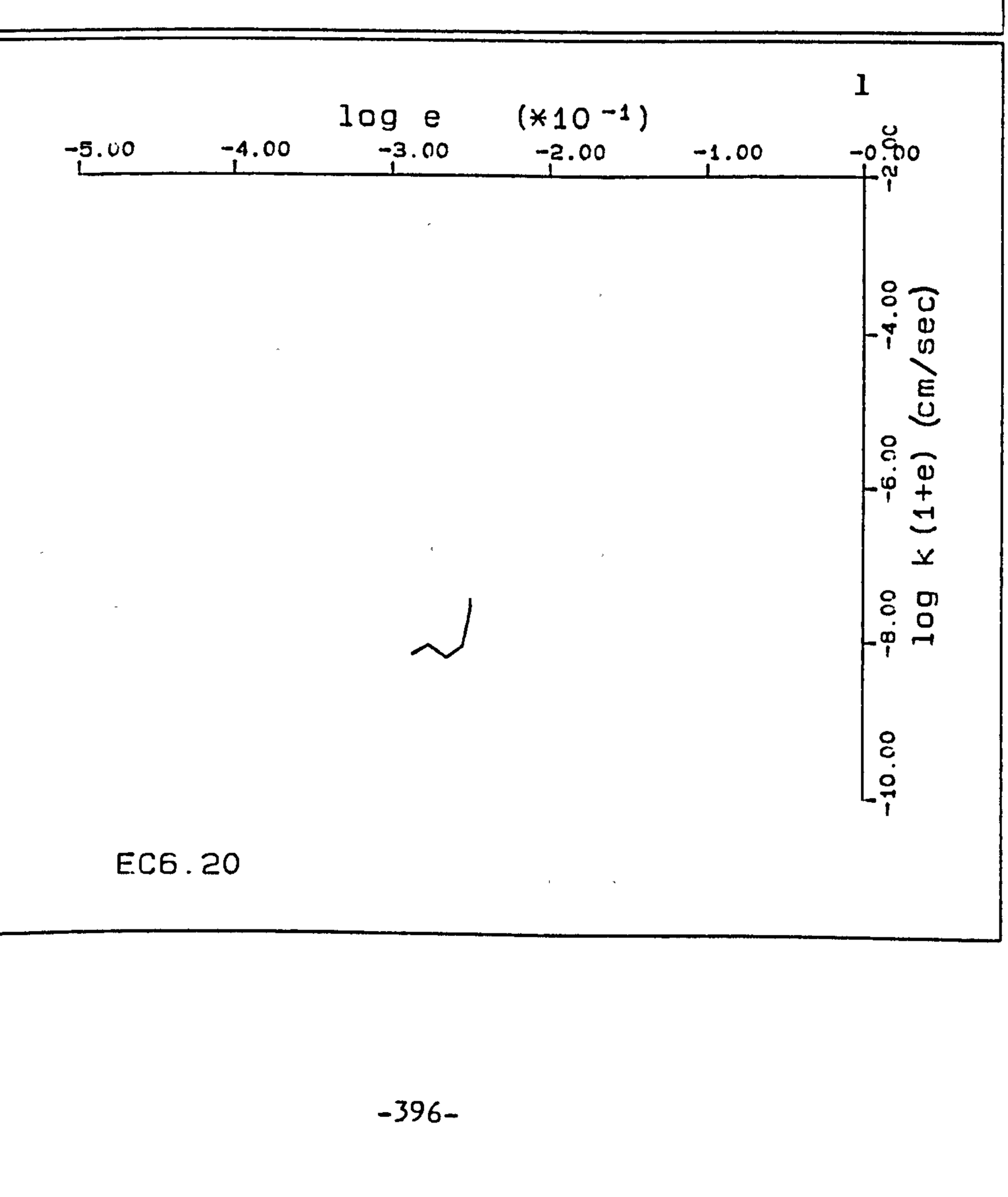

EC6.20

EC8.20

EC8.20 is a 36.6% porosity chalk which has an initial Young's modulus of 1.17GPa, and a yield point (seen by a slight deviatoric stress maximum) at 18.4MPa. In this test the yield point is on the initial slope in the q-p' plot, Fig.A5.7b, after which the plot gradually levels off. In Fig.A5.7a, a slight decrease in the load is noticed after which it seen to increase.

The total radial strain variation up to 9.0% axial strain is less than $1.5*10^{-2}$%, at 9.7% axial strain, an increase in the radial strain occurred reaching a maximum strain of $5.8*10^{-2}$% at 10.9% axial strain. This was accompanied by a reduction in the modulus of deformation on the stress-strain curve. On recovering the radial strain, at 11.5% axial strain a decrease in load of 3.0MPa was observed, shifting the compaction curve by this amount, also seen as a decrease in q in Fig. A5.7b. Subsequently, the radial strain varied by only $1.6*10^{-2}$%, the remaining compaction curve in terms of q-p space, showing only slight perturbations.

The $\bar{K}_o$ values for the elastic, transitional, and normal consolidation deformations are 0.384, 1.432, and 0.631 respectively. The regaining of the strain after the expansion caused a large increase in the pore pressure which started volume change measurement, but the increase was to large to dissipate in the following compaction deformation. The large volume strain caused by the jump and regaining of the zero lateral strain condition is seen by an initially steeper section in Fig. A5.7f.

The average compressibility of the pre-yield response is $5.73*10^{-4}MPa^{-1}$, the peak compressibility being $1.2*10^{-2}MPa^{-1}$ at 32.5MPa, the yield occurring at a vertical effective stress of 27.0MPa. The values of C_v and permeability were first recorded at a

vertical effective stress of 37.3MPa, with values of 2487m^2/yr and 1.8mD. At 49.8MPa the respective values are 21m^2/yr and 0.0083mD, and decreased finally to 15.4m^2/yr and 0.0067mD at a vertical effective stress of 81.6MPa. The decrease in permeability is very abrupt. U_h/σ_v' increases from 0.0004 at 37.3MPa to 0.0361 at 44.6MPa and to 0.0167 at 81.6MPa.

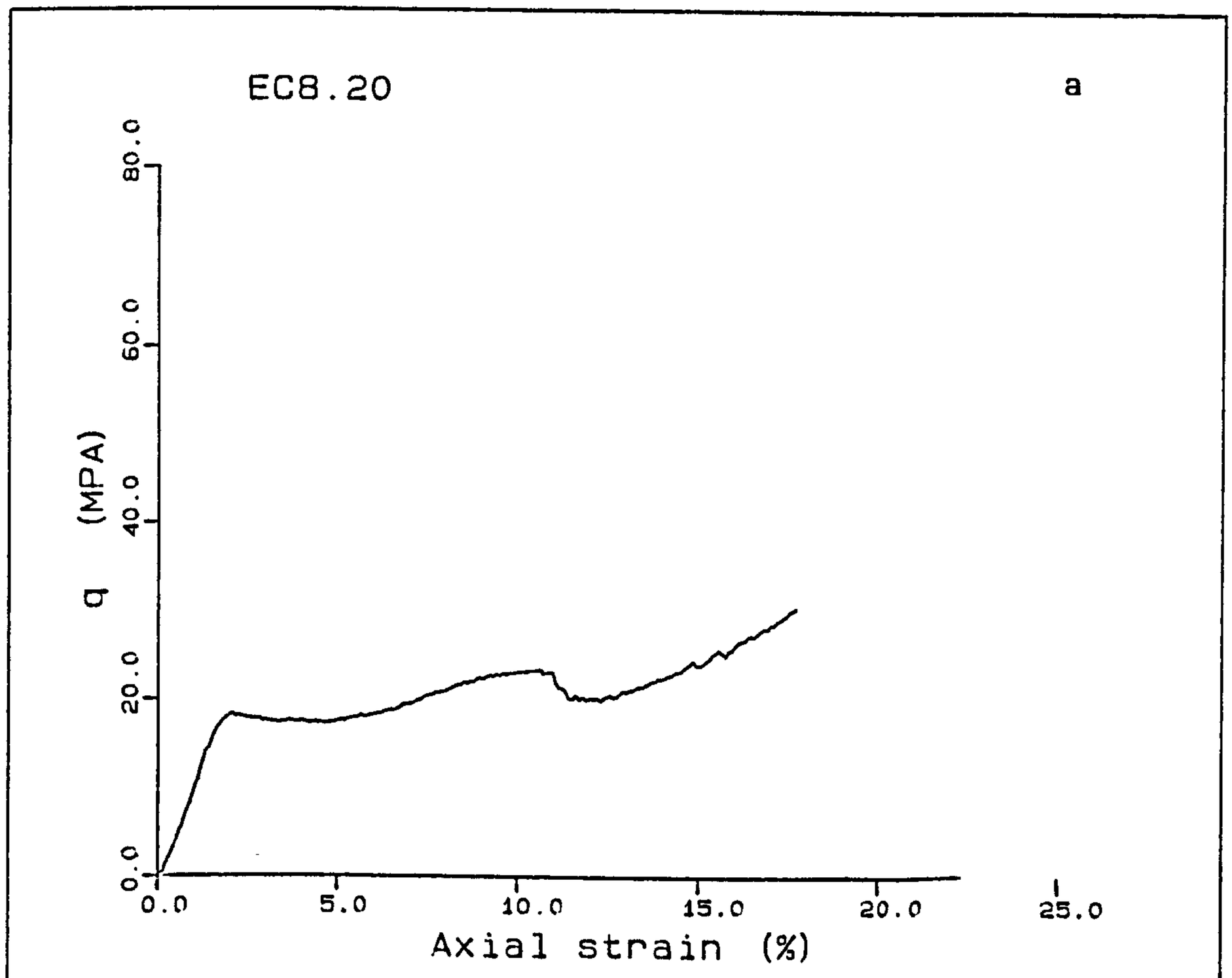

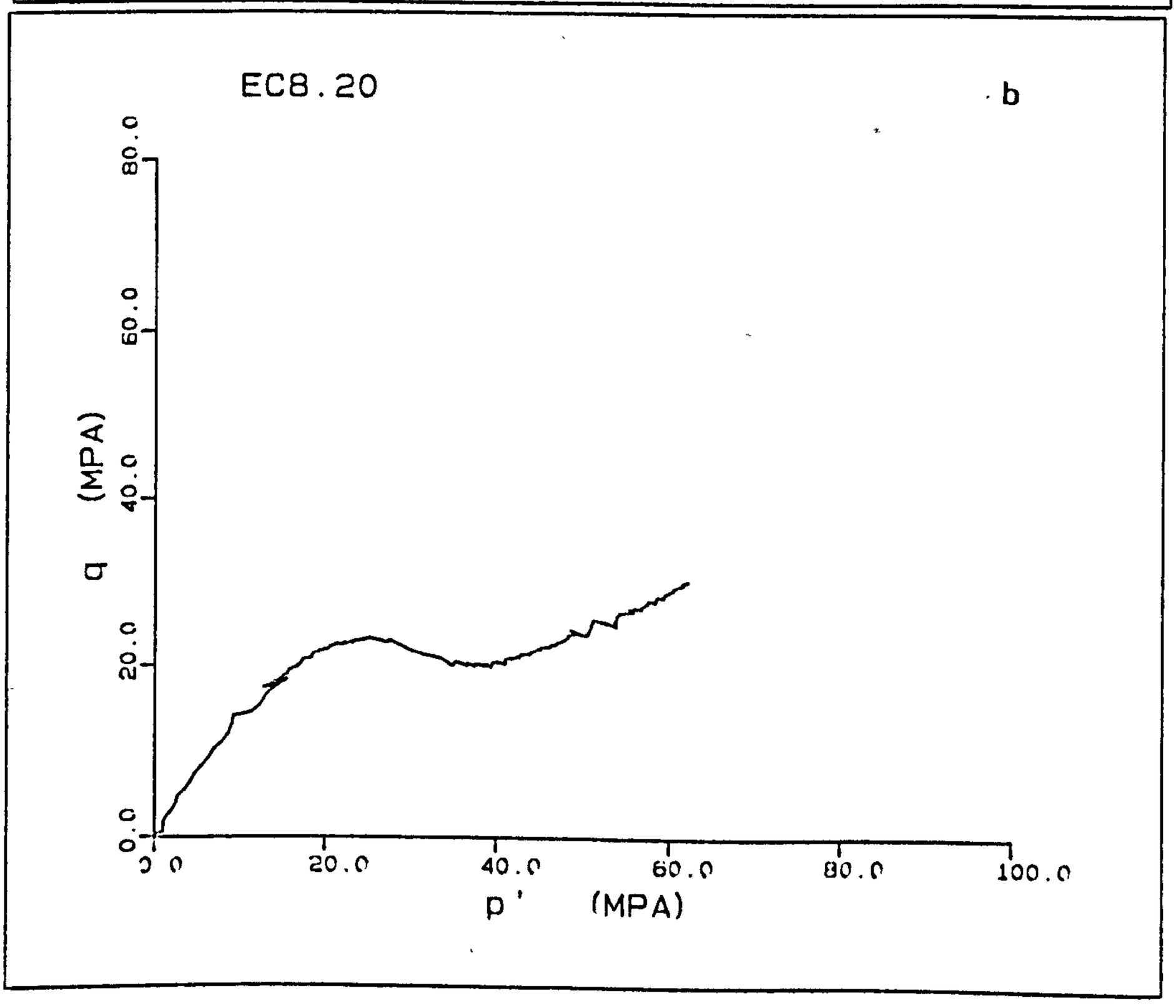

Figure A5.7(a-1) K_o test EC8.20.

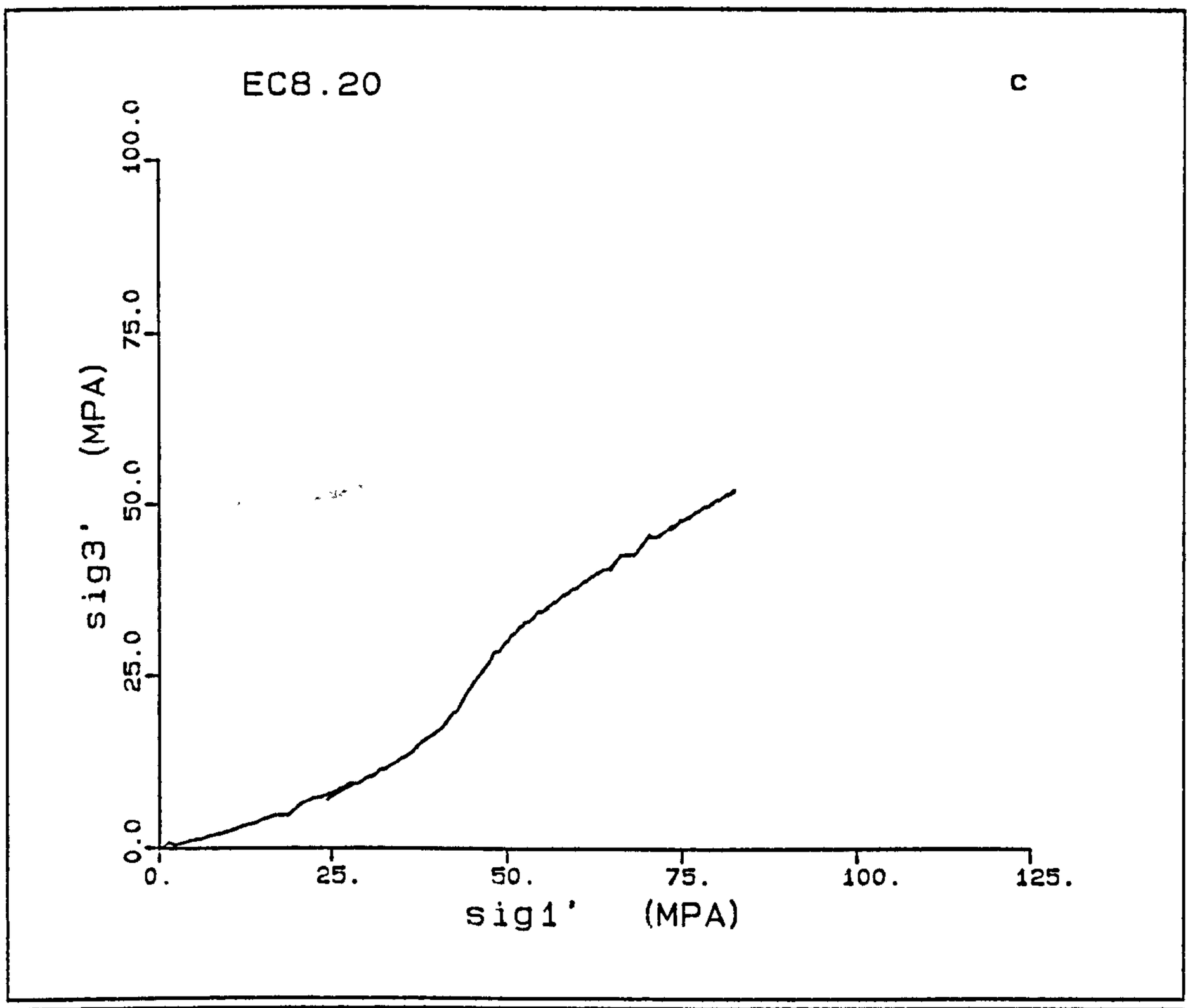
EC8.20
c
100.0
75.0
50.0
25.0
0.0
sig3' (MPA)
0.
25.
50.
75.
100.
125.
sig1' (MPA)

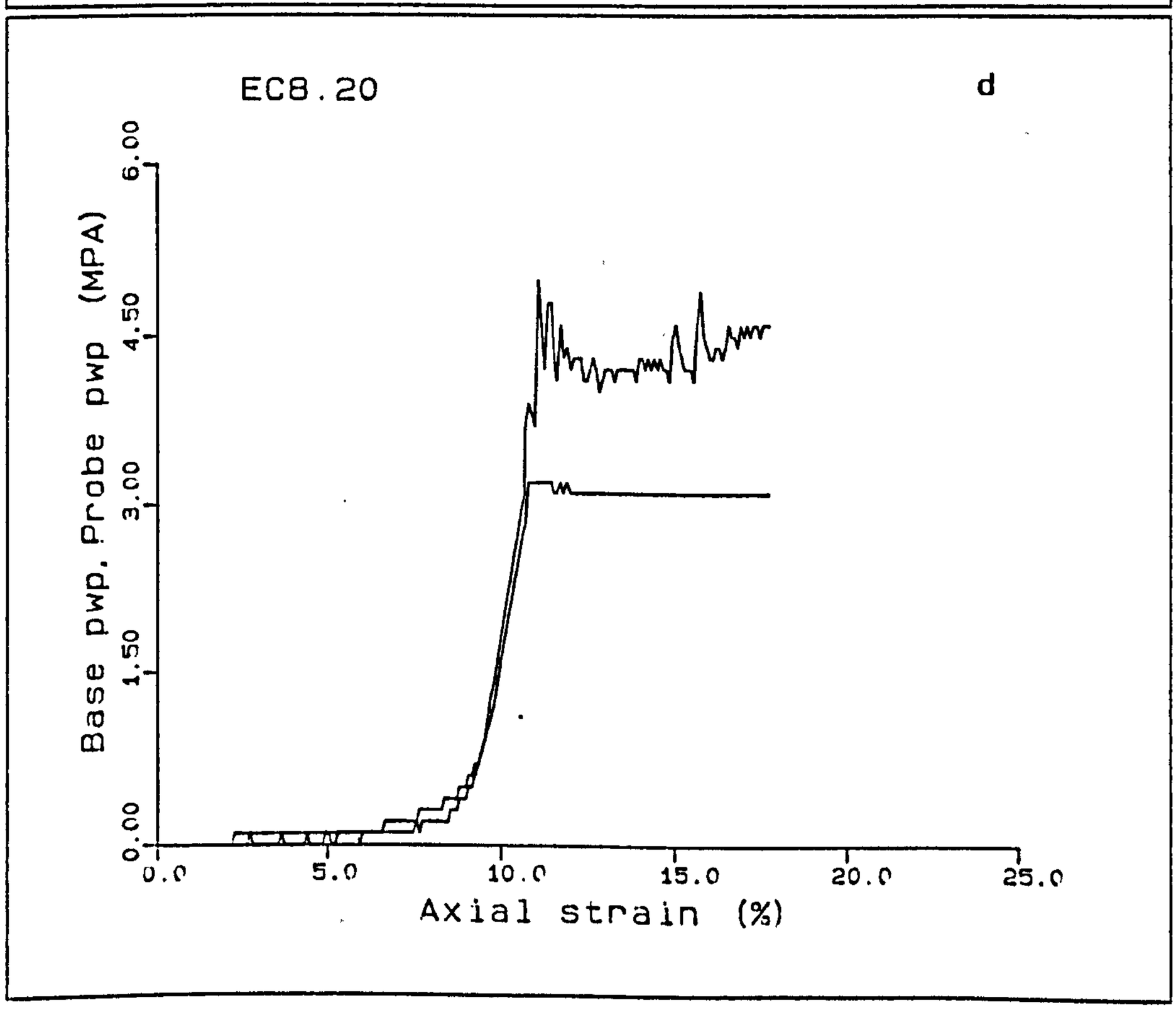
EC8.20
d
6.00
4.50
3.00
1.50
0.00
Base pwp. Probe pwp (MPA)
0.0
5.0
10.0
15.0
20.0
25.0
Axial strain (%)

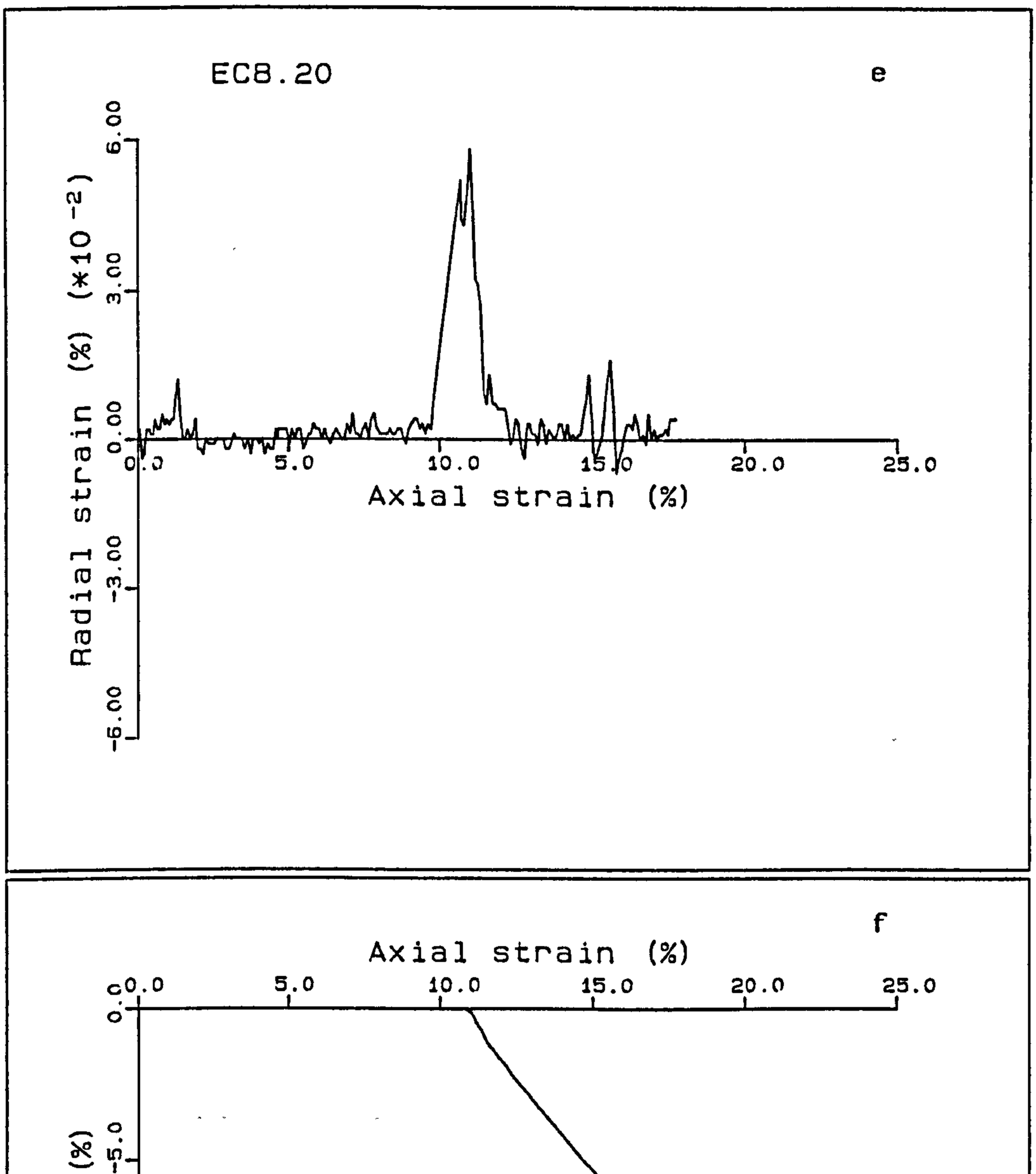
EC8.20
e
Radial strain (%) (*10-2)
6.00
3.00
0.00
-3.00
-6.00
0.0
5.0
10.0
15.0
20.0
25.0
Axial strain (%)
f
Axial strain (%)
0.0
5.0
10.0
15.0
20.0
25.0
Volume strain (%)
0.0
-5.0
-10.0
-15.0
-20.0
EC8.20

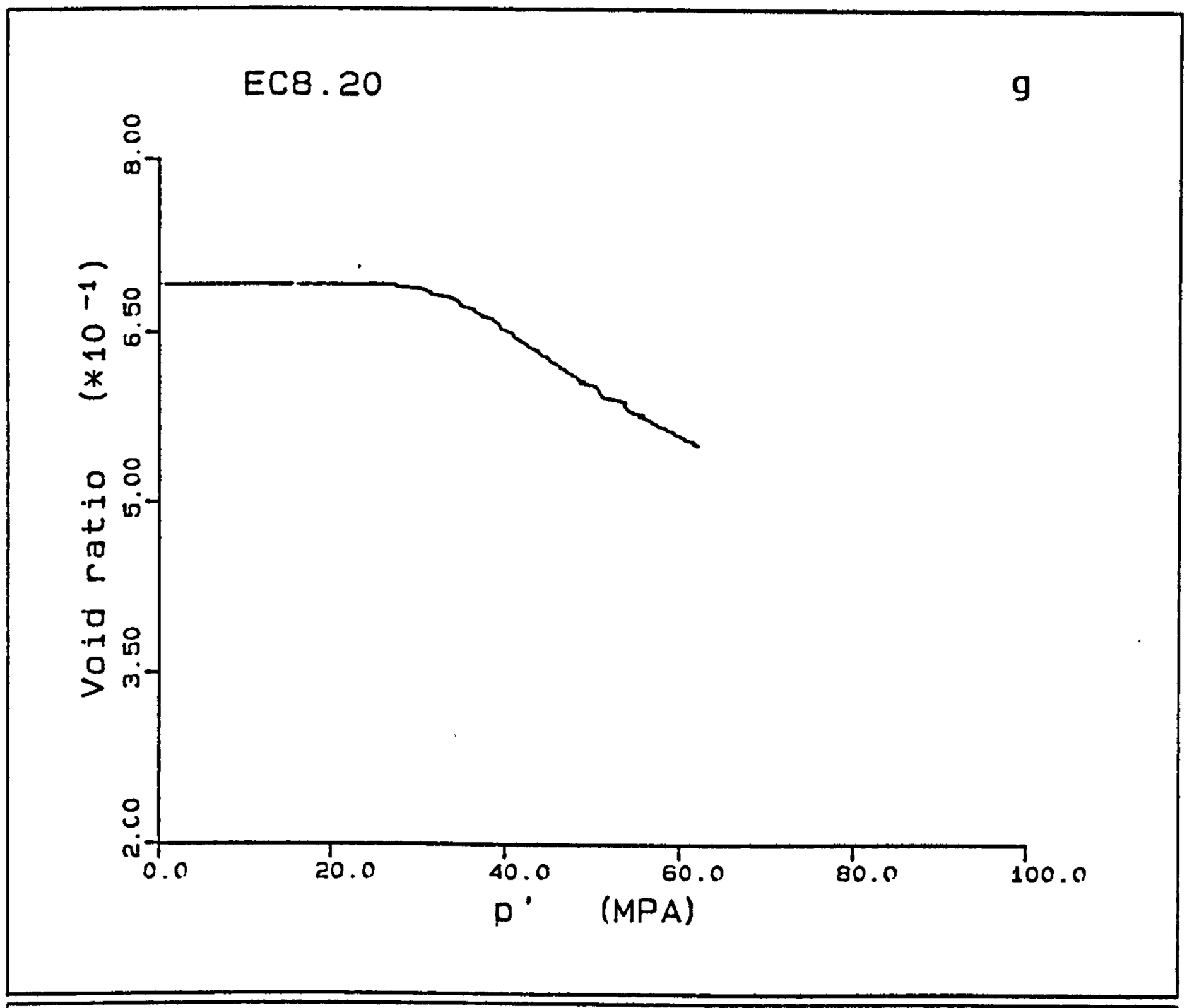
EC8.20
g
Void ratio (*10 -1)
8.00
6.50
5.00
3.50
2.00
0.0
20.0
40.0
60.0
80.0
100.0
p' (MPA)

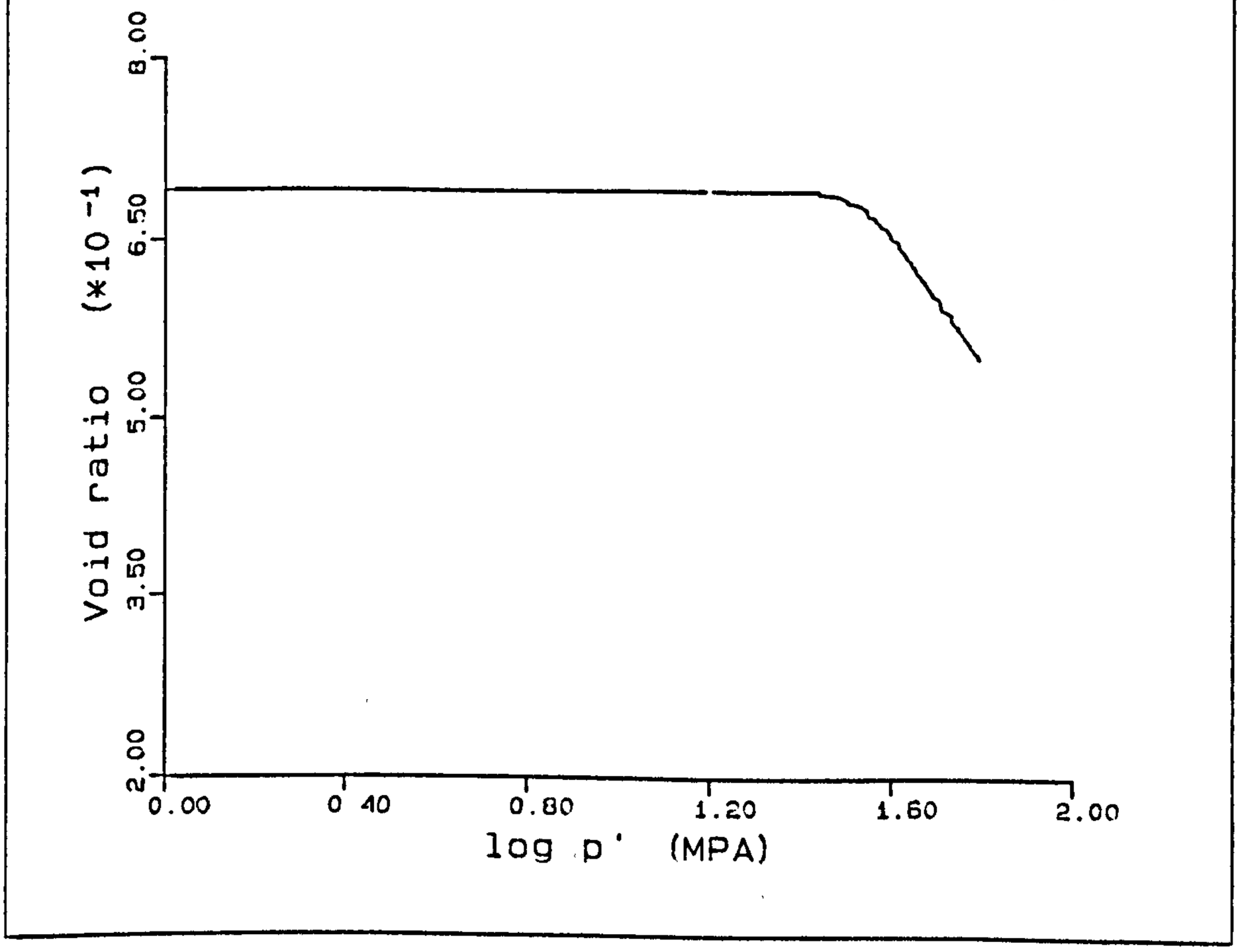
EC8.20
h
Void ratio (*10 -1)
8.00
6.50
5.00
3.50
2.00
0.00
0.40
0.80
1.20
1.60
2.00
log p' (MPA)

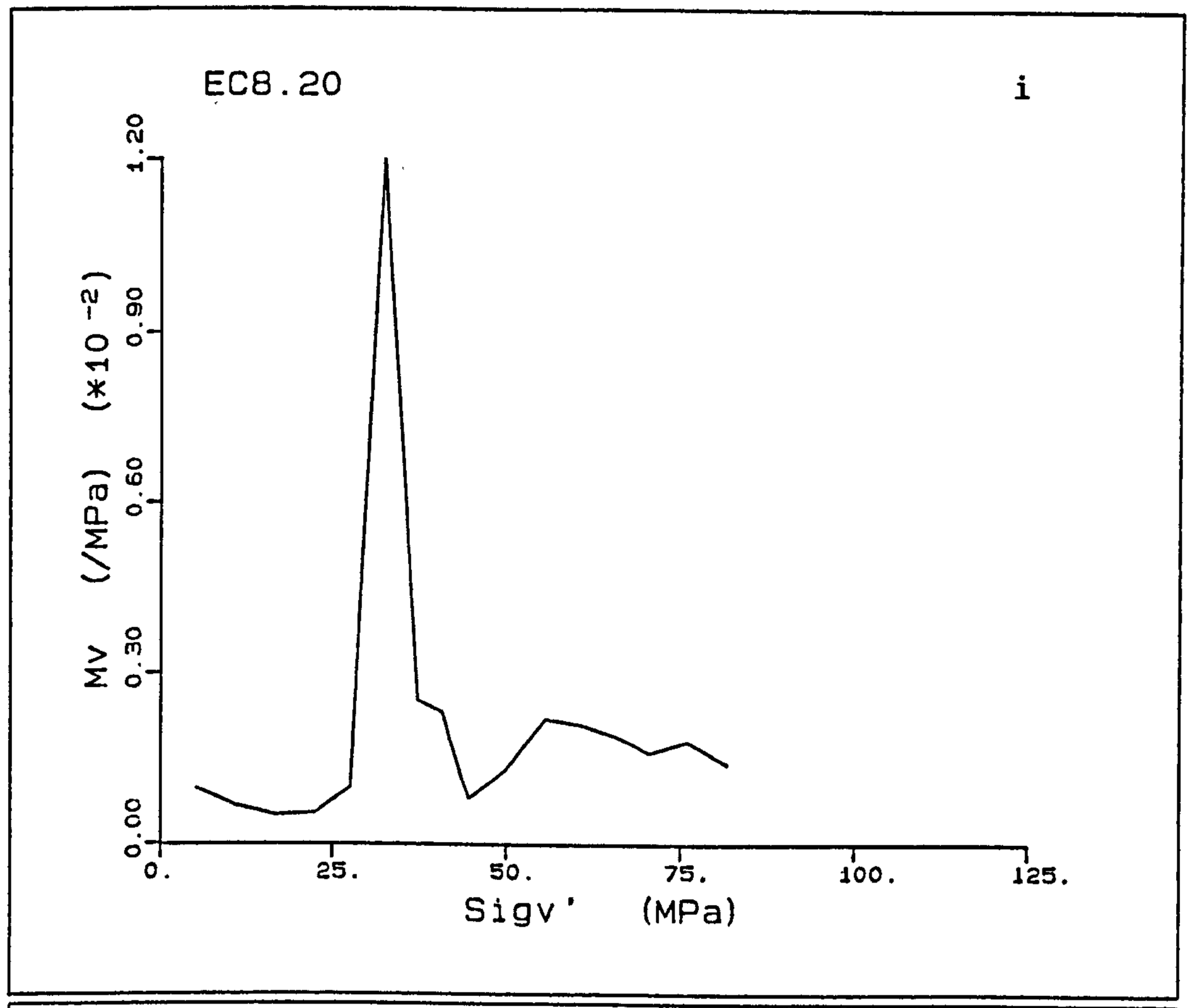
EC8.20
i
Mv (/MPa) (*10 -2)
1.20
0.90
0.60
0.30
0.00
0.
25.
50.
75.
100.
125.
Sigv' (MPa)

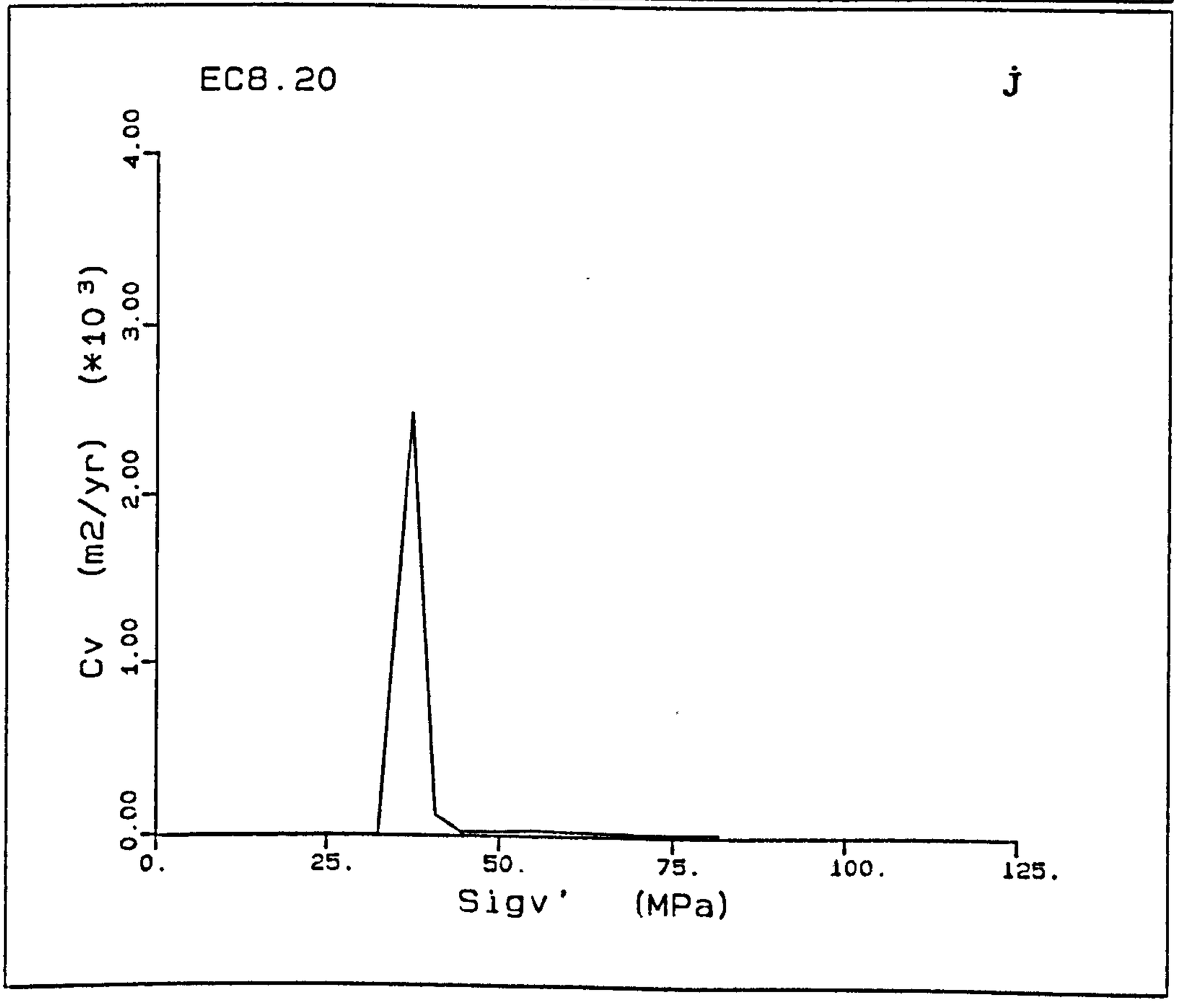
EC8.20
j
Cv (m2/yr) (*10 3)
4.00
3.00
2.00
1.00
0.00
0.
25.
50.
75.
100.
125.
Sigv' (MPa)

EC8.20 k

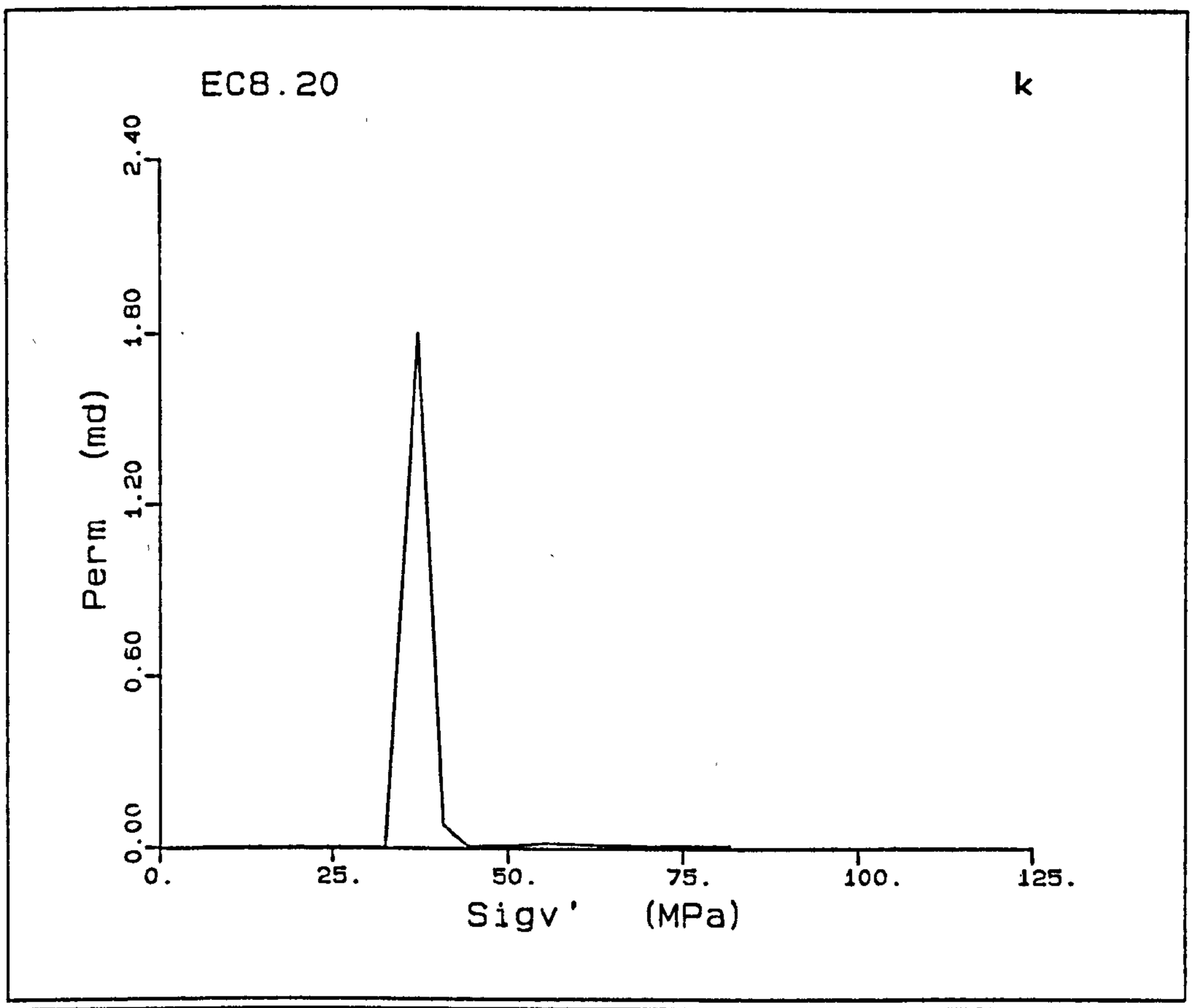

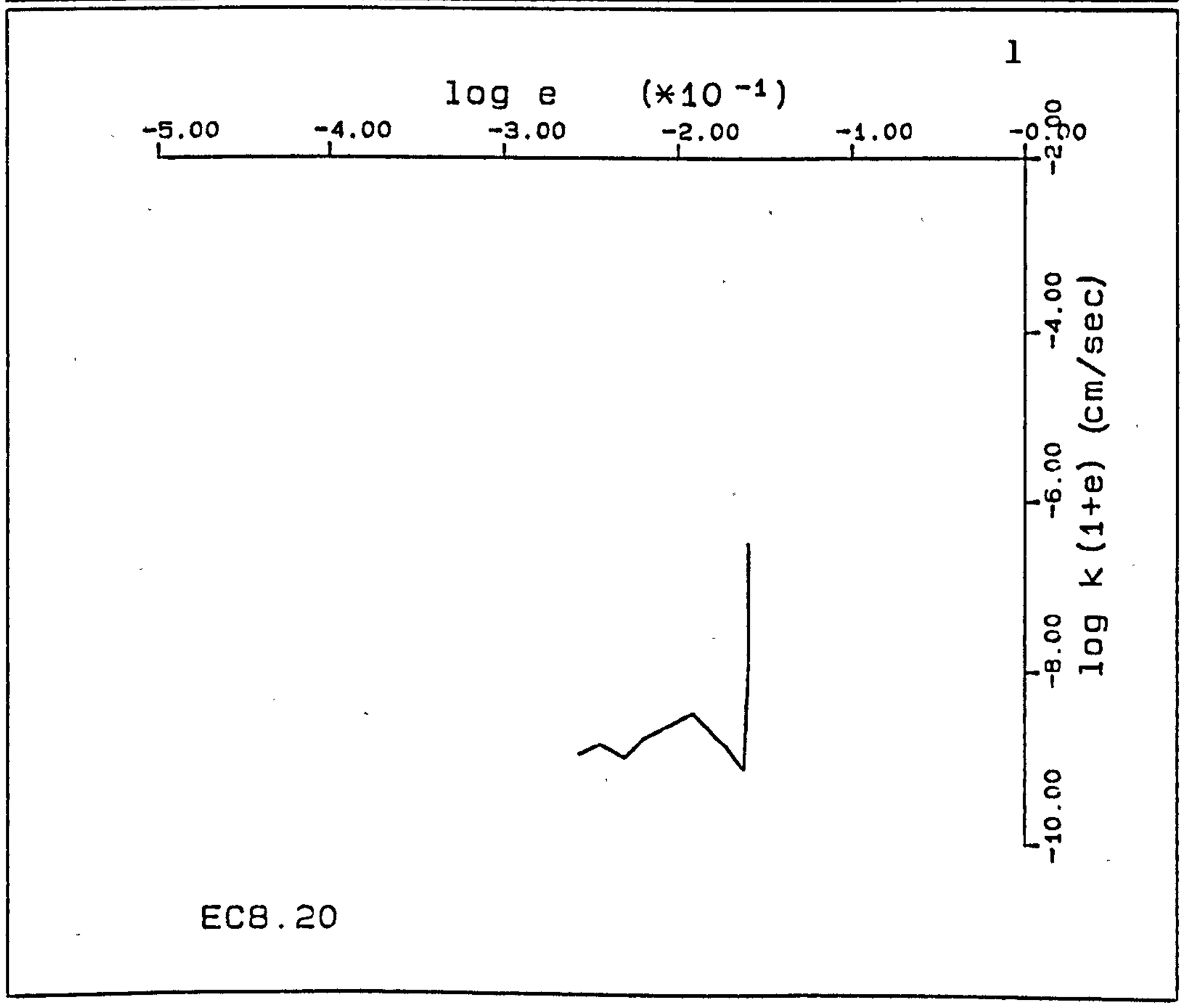

EC8.20

EC9.20

This is a 40.9% porosity chalk, the sample had bedding errors, as seen by the large axial strain required to obtain a linear elastic section of the stress-strain curve. The linear section of the deformation shortened with a Young's modulus of 1.36GPa, eventually reaching a peak deviatoric stress for yield of the cementation, at 23.6MPa. The post-yield deformation consists of a compaction at constant load, with an accompanying large increase in p' . The load starts increasing once more at a mean effective stress of approximately 40MPa, after a mean effective stress of 45MPa a linear increase in deviatoric stress with mean effective is seen. The $\bar{K}_o$ values corresponding to the three deformational styles are equal to 0.340, 0.973, and 0.592 for $\bar{K}_{oe}$, $\bar{K}_{opc}$ and $\bar{K}_{onc}$ respectively. The total variation in radial strain recorded through the test was less than $1.1*10^{-2}$%.

The volume change starts recording at an axial strain of 6.1%, with pore pressures of 3.2MPa at the base of the sample, the top pore pressure increases slightly to 3.4 from 3.3 with increasing compaction.

The initial decrease in compressibility is assumed to be due to the bedding error of the sample, the average M_v in the elastic region (ignoring the first high value) is $5.51*10^{-4}MPa^{-1}$. The increase in M_v is gradual and starts at approximately 40MPa, the yield for this chalk being at 43.1MPa (though considerable curvature of the stress-strain curve occurs at 40.0MPa). The peak M_v value of $1.9*10^{-3}MPa^{-1}$ occurs at a vertical effective stress of 69.8MPa, thereafter decreasing to a value of $1.2*10^{-3}MPa^{-1}$ at 117.3MPa. The values of C_v and permeabilities were initially calculated at 60.0MPa, and equal to $2986m^2/yr$ and 1.2mD and decrease, Fig. A5.8j-k, to

values of $134m^2/yr$ and $5*10^{-2}mD$ at 117.3MPa. The values of U_h/σ_v' increase from 0.0003 to 0.0016 from 60MPa to 117.3MPa respectively.

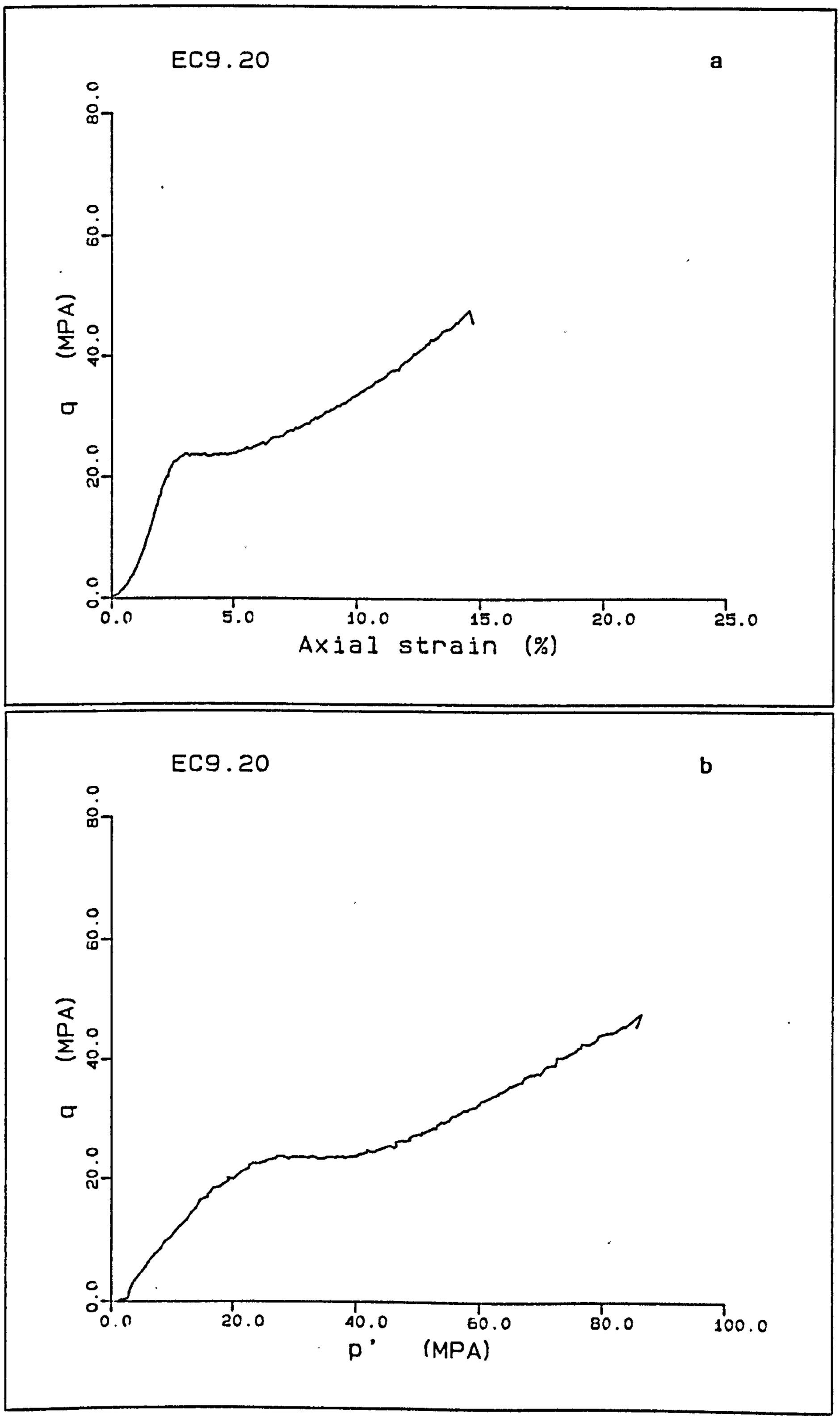

Figure A5.8(a-l) K_o test EC9.20.

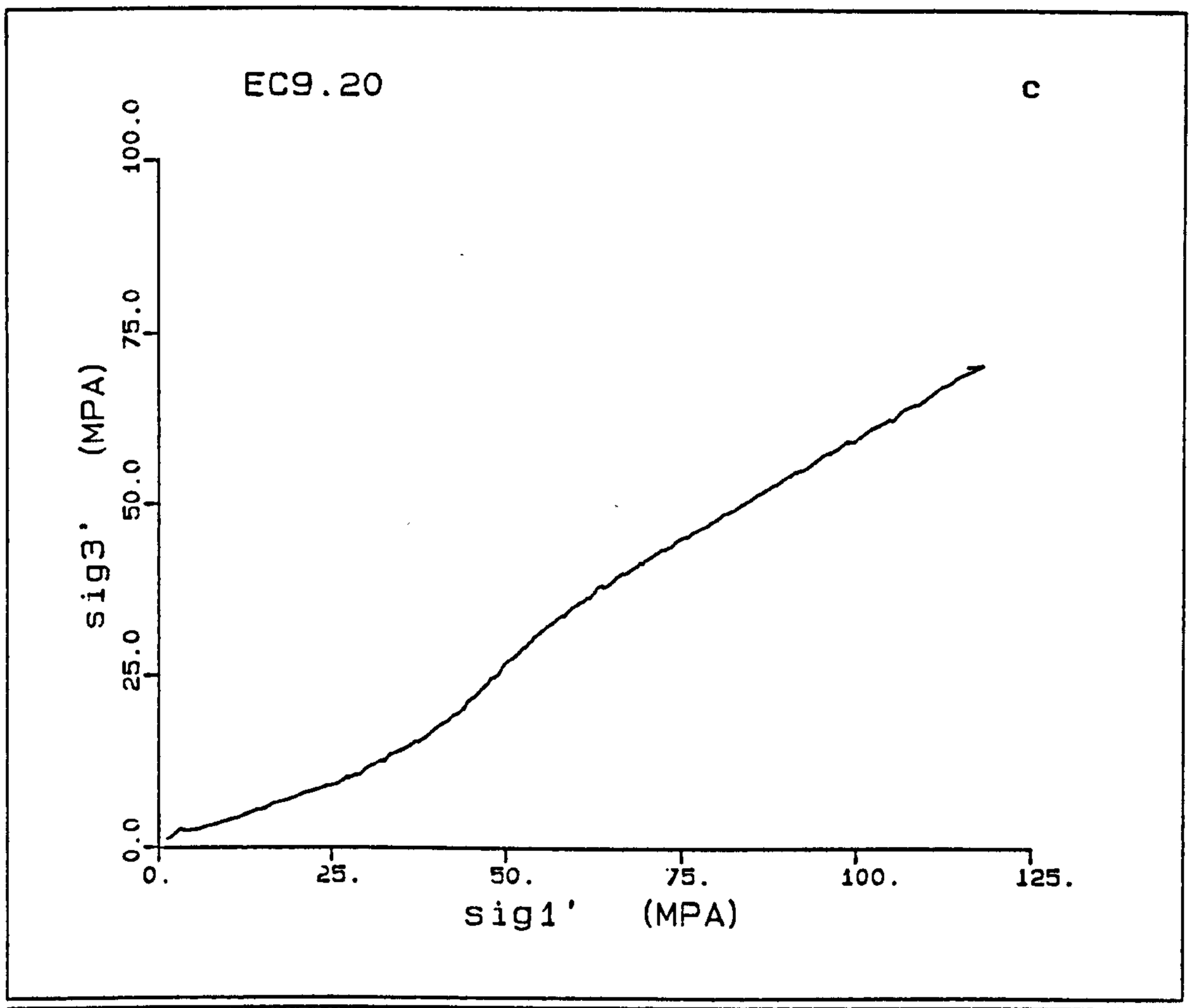
EC9.20
c
100.0
75.0
50.0
25.0
0.0
sig3' (MPA)
0.
25.
50.
75.
100.
125.
sig1' (MPA)

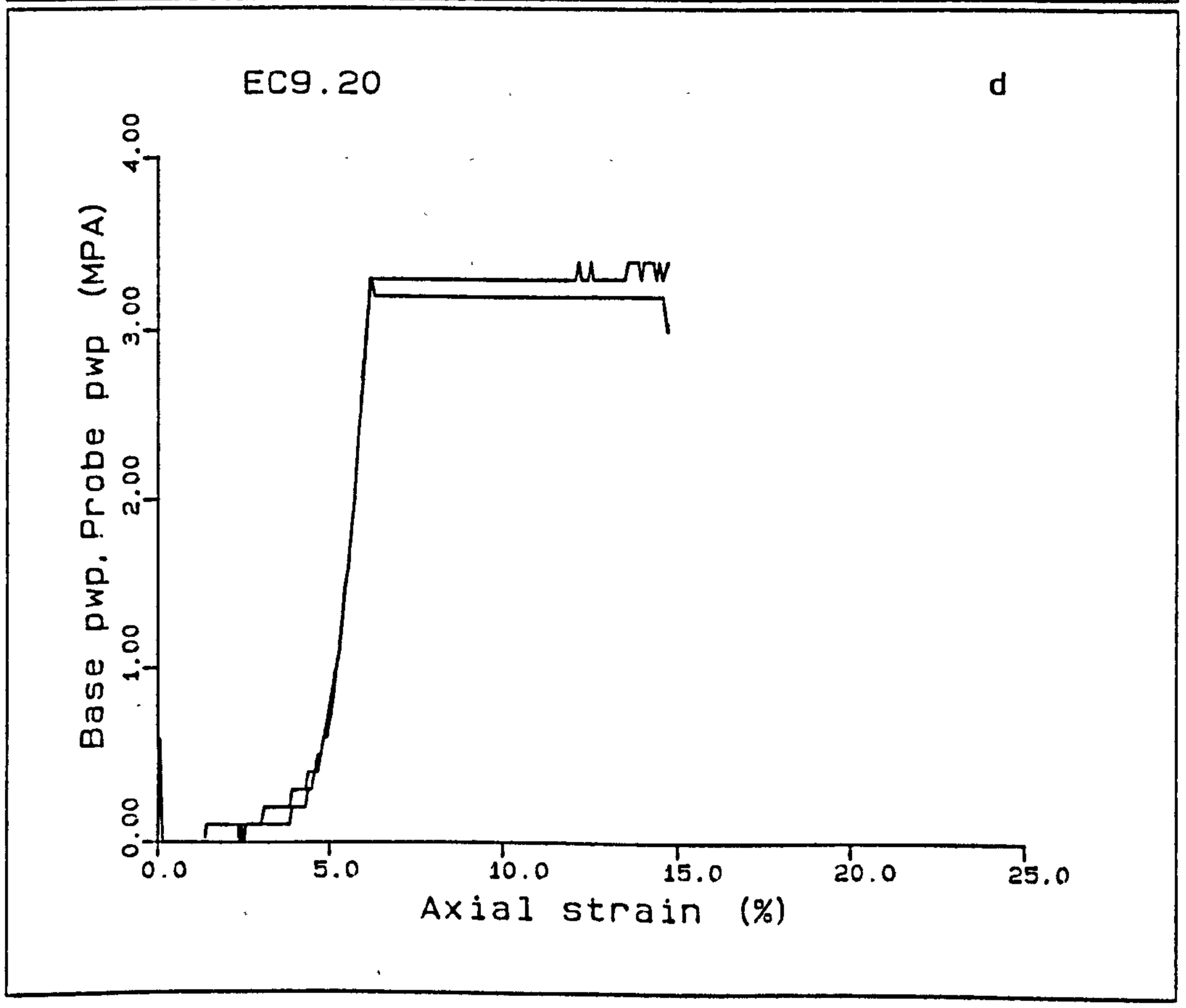
EC9.20
d
4.00
3.00
2.00
1.00
0.00
Base pwp, Probe pwp (MPA)
0.0
5.0
10.0
15.0
20.0
25.0
Axial strain (%)

EC9.20

e

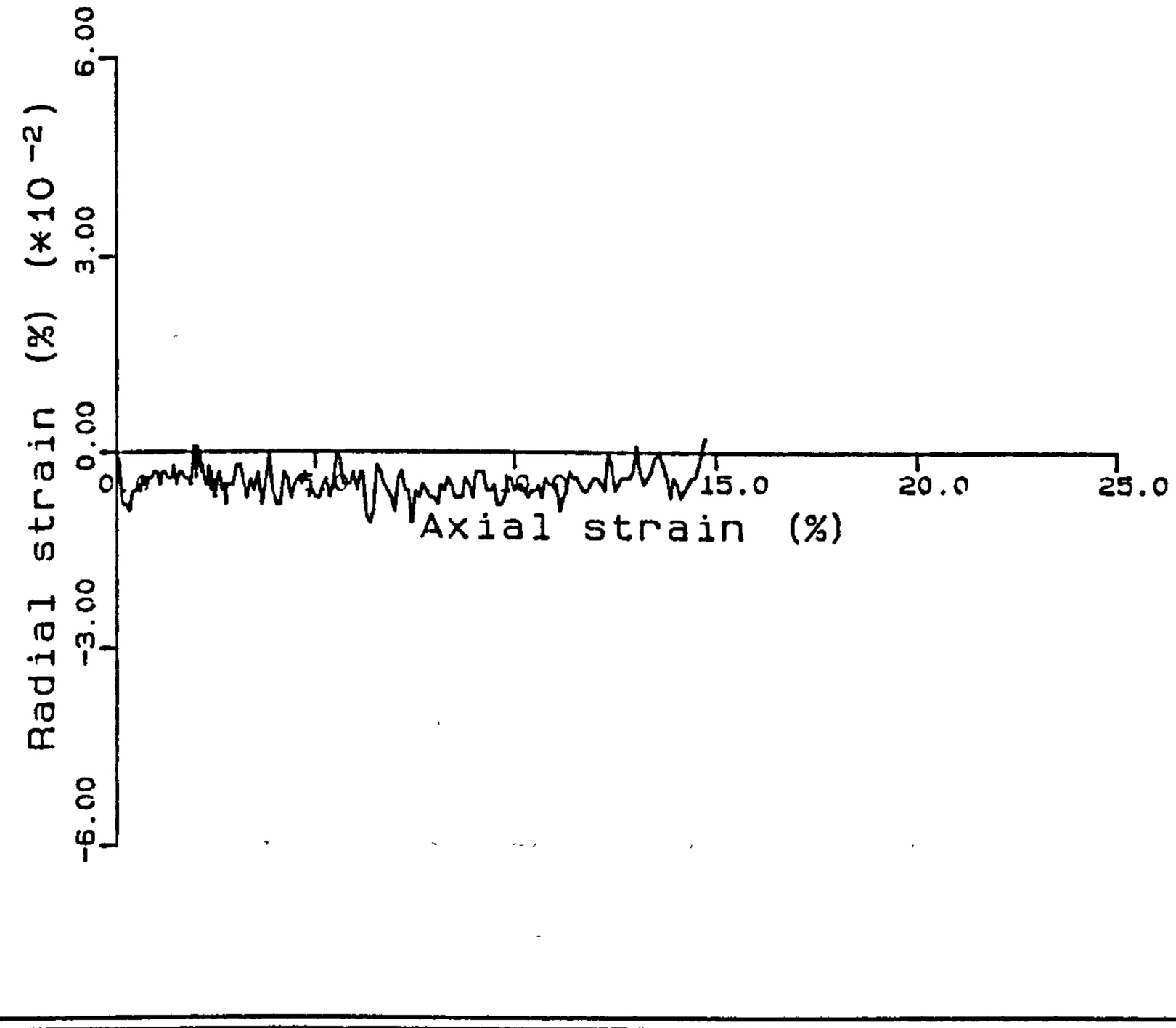

f

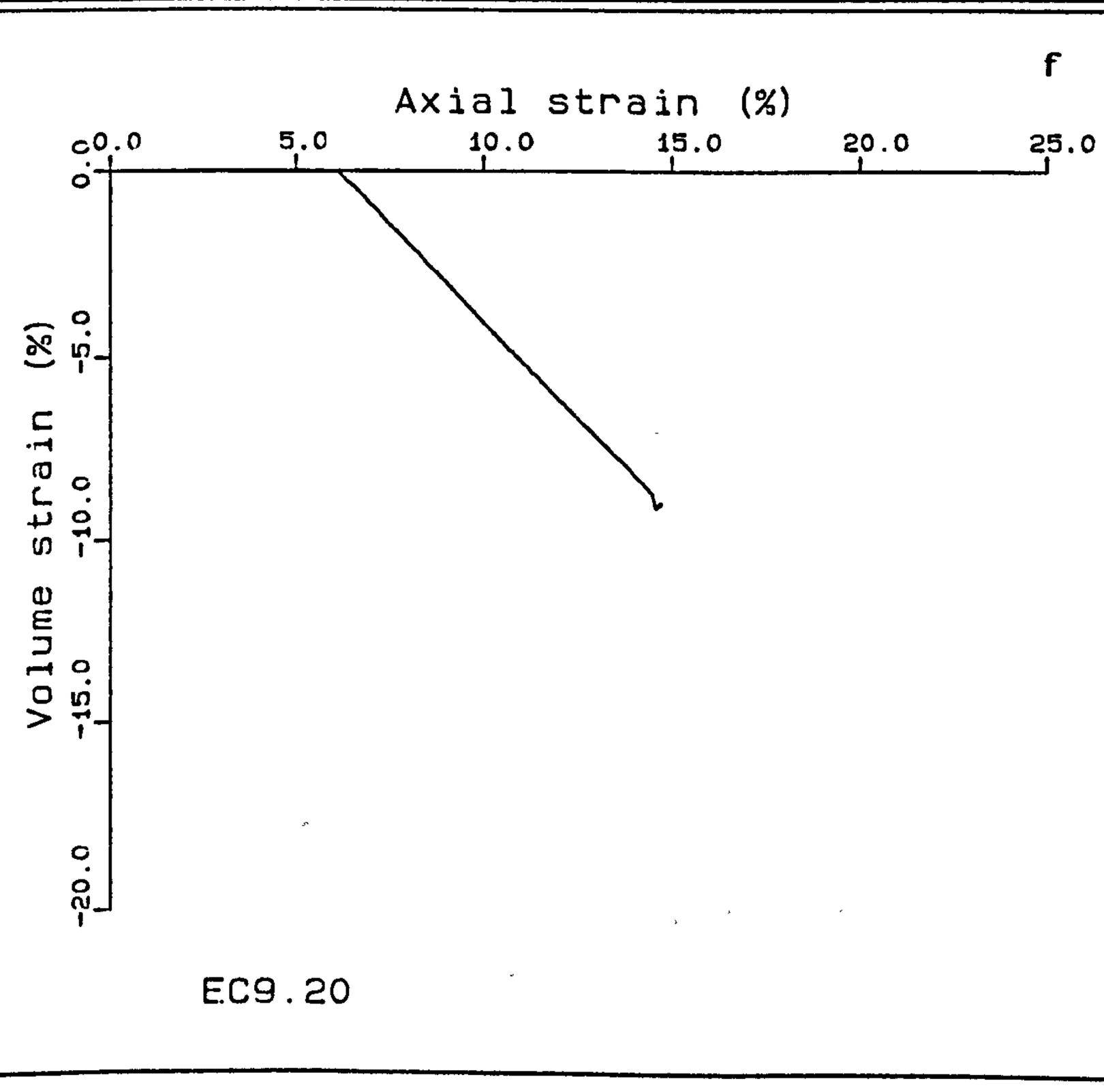

EC9.20

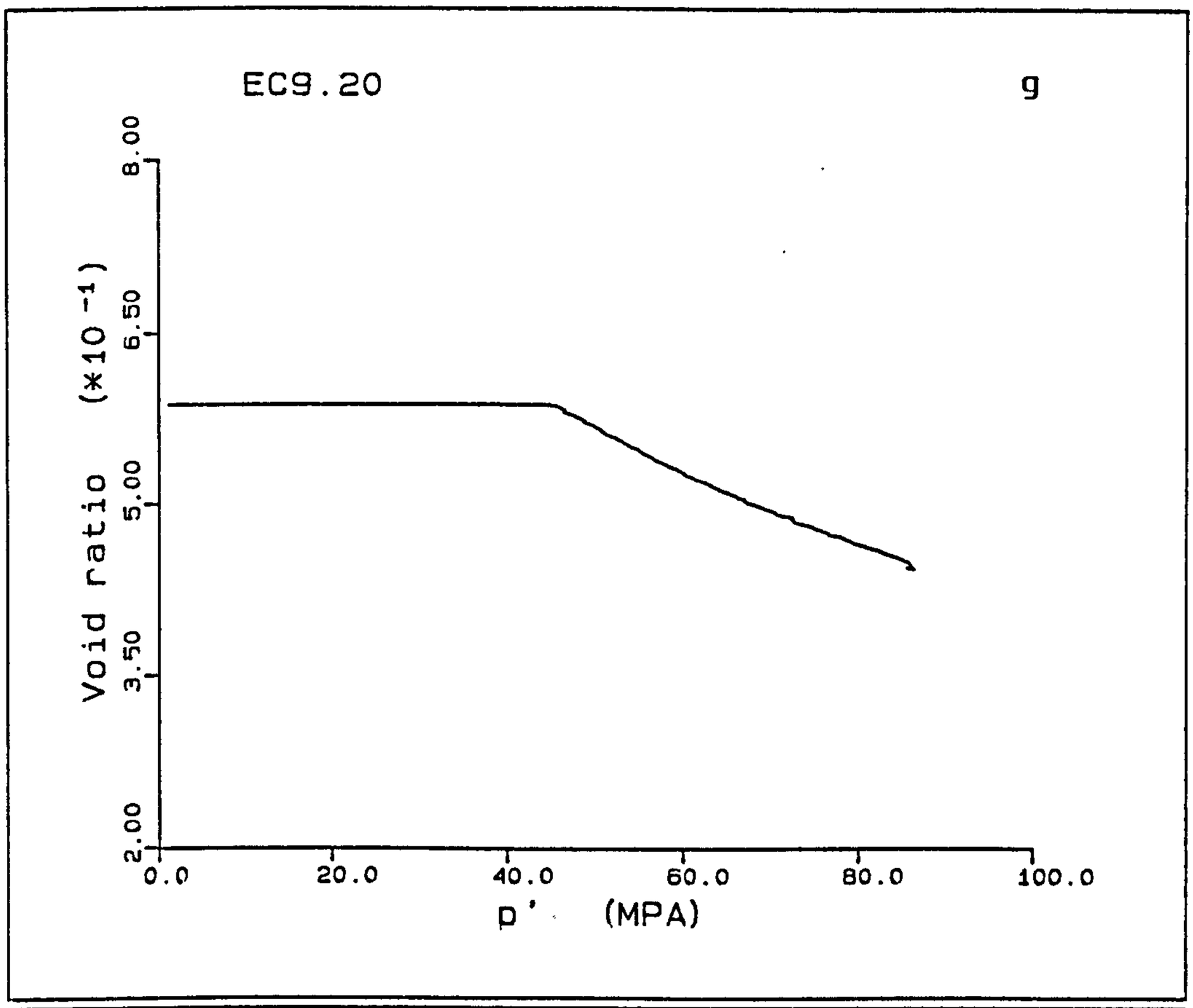
EC9.20
g
8.00
6.50
5.00
3.50
2.00
(*10 -1)
Void ratio
0.0
20.0
40.0
60.0
80.0
100.0
p' (MPA)

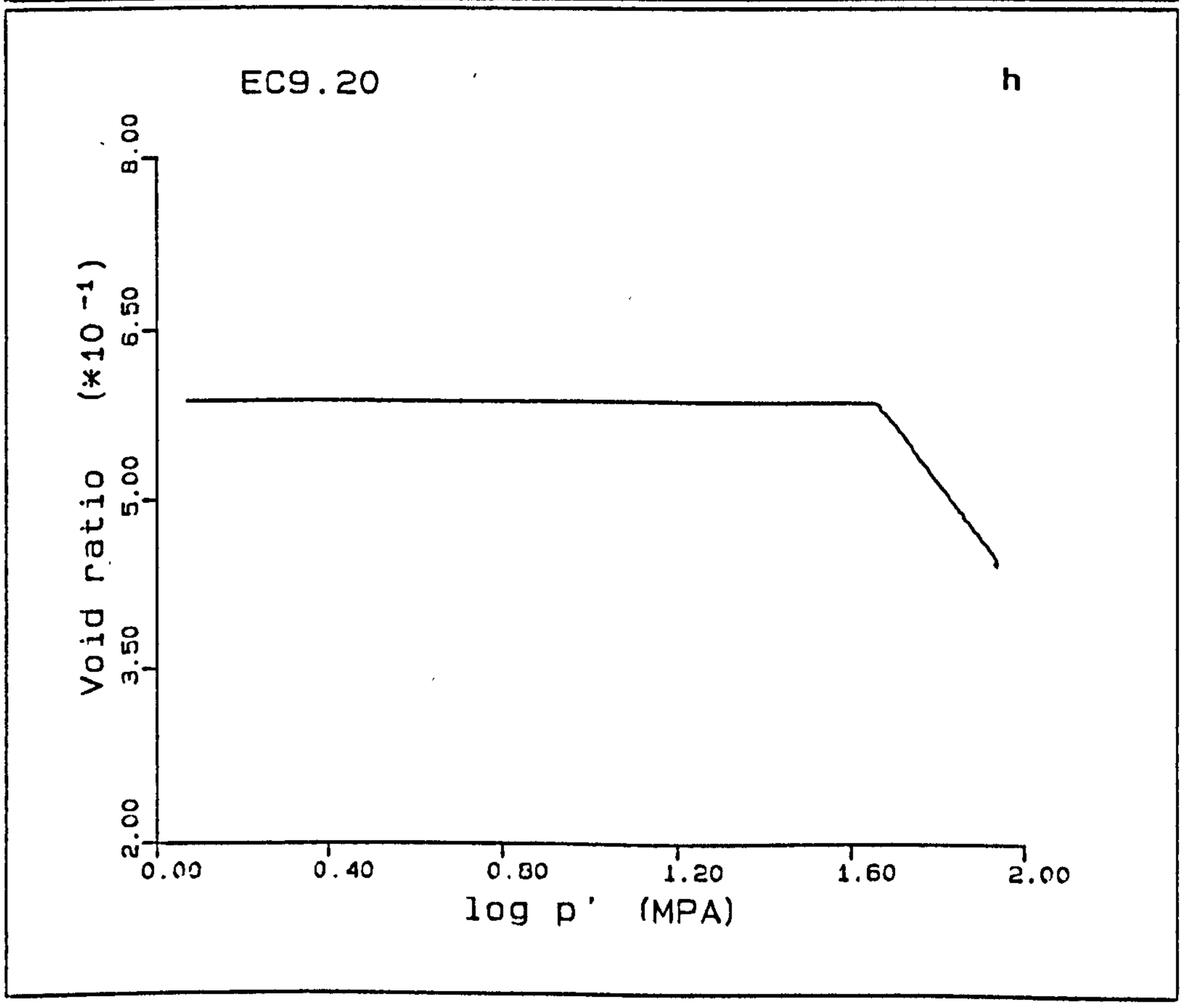
EC9.20
h
8.00
6.50
5.00
3.50
2.00
(*10 -1)
Void ratio
0.00
0.40
0.80
1.20
1.60
2.00
log p' (MPA)

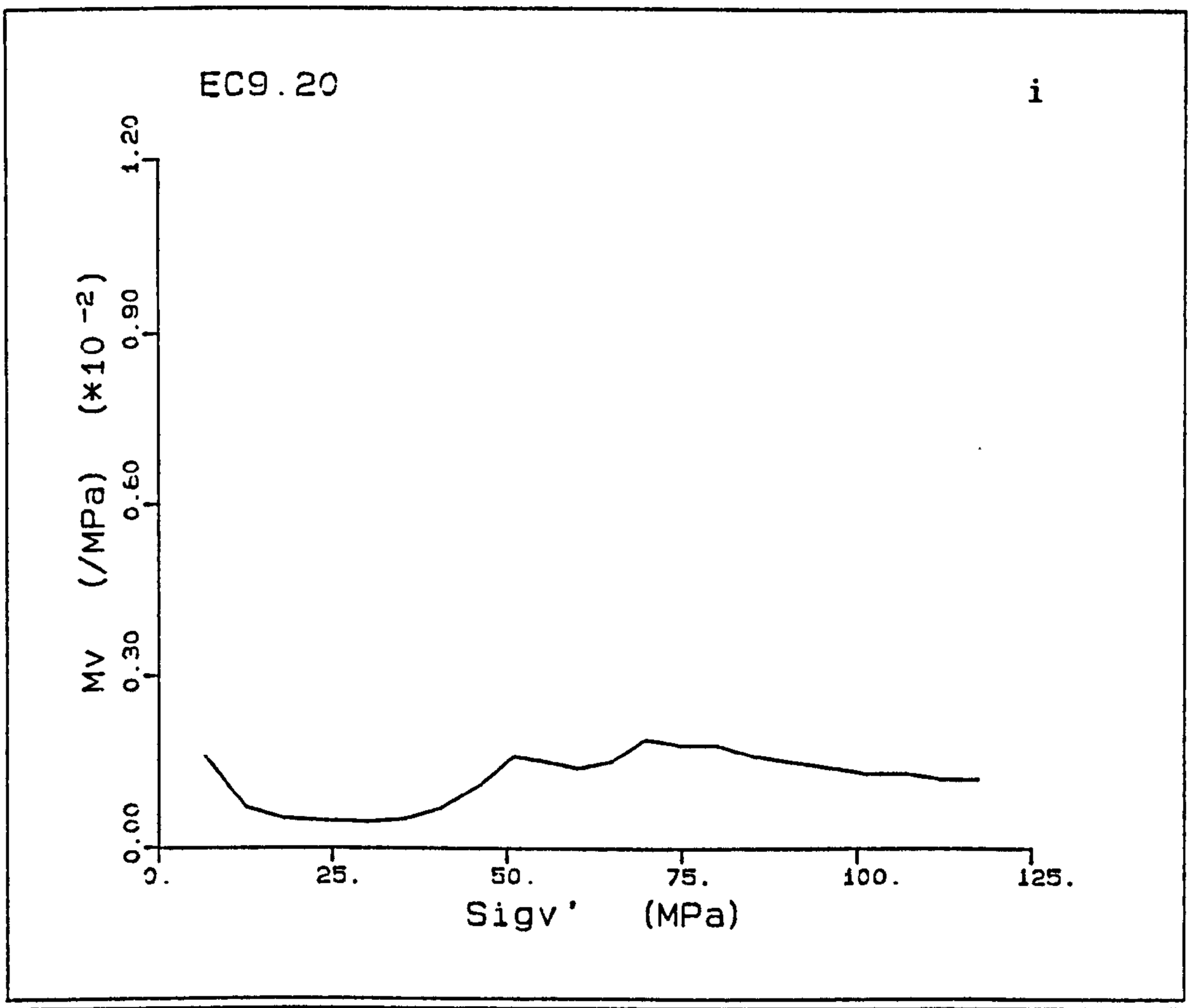
EC9.20
i
1.20
0.90
0.60
0.30
0.00
Mv (/MPa) (*10 -2)
0.
25.
50.
75.
100.
125.
Sigv' (MPa)

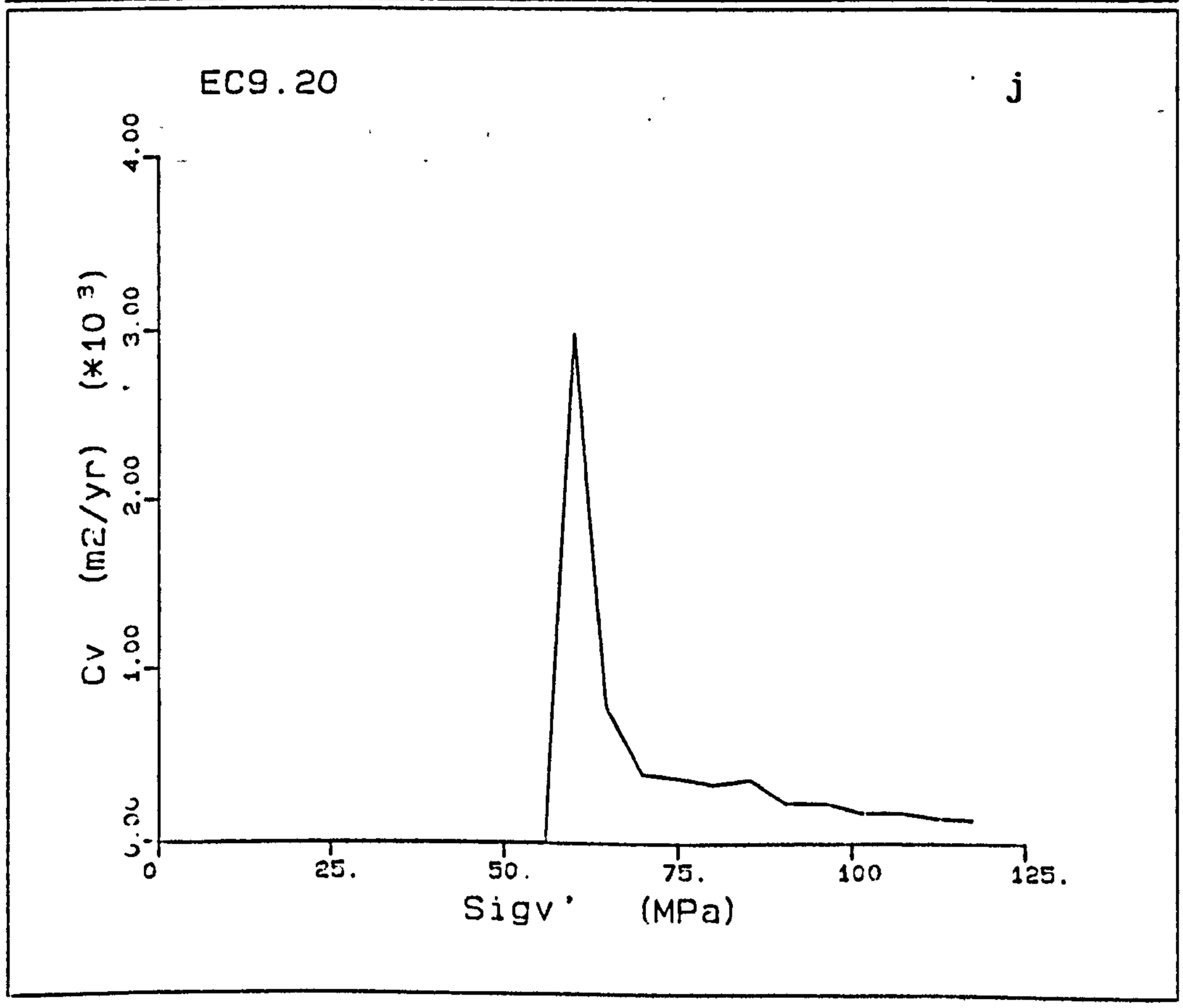
EC9.20
j
4.00
3.00
2.00
1.00
0.00
Cv (m2/yr) (*10 3)
0
25.
50.
75.
100
125.
Sigv' (MPa)

EC9.20

k

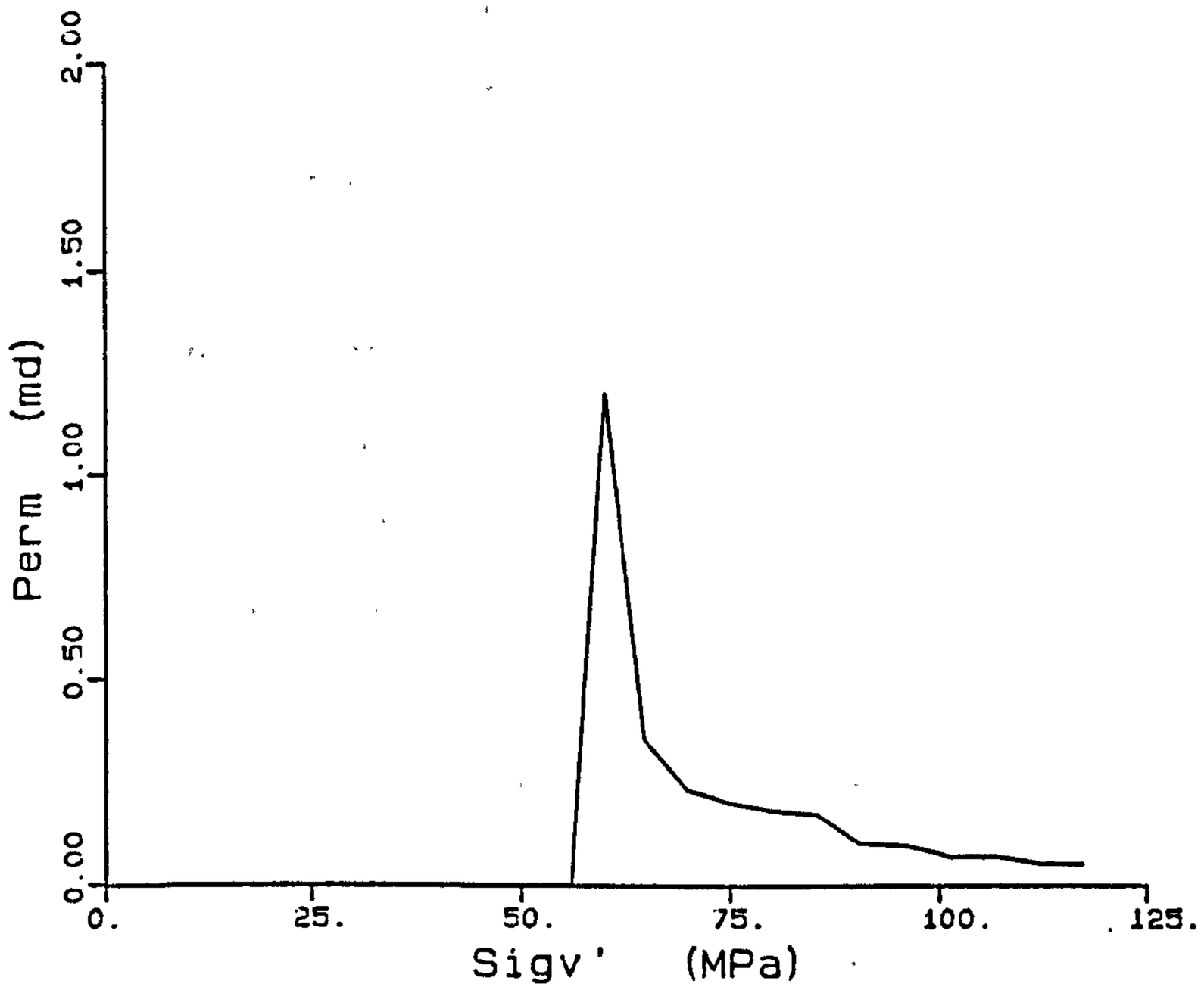

l

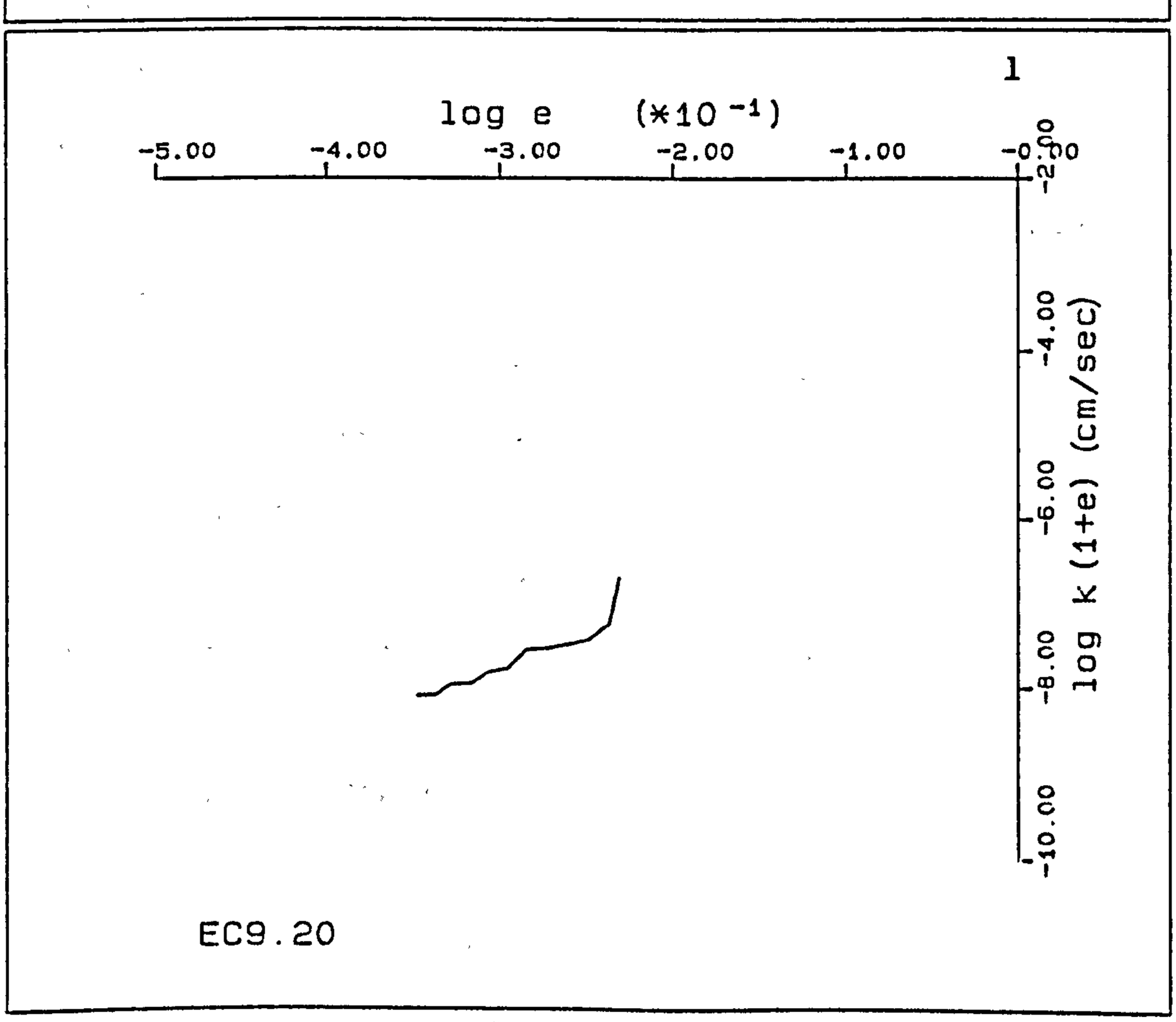

EC9.20

A5.2) STRAIN RATES

Seven experiments were performed to analyse the strain rate effect on the compactional characteristics of chalk. The tests were performed on chalks from an onshore site at Pegwell Bay in Kent, which were water saturated. The onshore chalks were chosen to keep porosity variation between samples to a minimum. The tests PB3.20 to PB8.20 were performed on samples with a 2:1 ratio of height to diameter, and the zero lateral strain condition was controlled by a servo feedback system responding to changes in the output of the radial strain belt, the servo feedback adjusting the cell pressure to maintain a constant voltage output from the strain belt. The first strain belt was used in these tests where the deformation rate was set constant throughout the experiment. PB1.20 was conducted with its deformation rate varied.

PB1.20, PB3.20, PB4.20, PB5.20, and PB6.20 were samples taken from one block, block O, while PB7.20 and PB8.20 were taken from block M. Unfortunately, block M was more competant than the O block, shown by a higher Young's moduli. The chalk has a low yield point with a deviatoric stress of less than or equal to 5MPa, some of the tests, PB4.20 and PB6.20 showed an irregular breakdown of the cementation from which no initial modulus could be obtained. At the higher rate of deformation employed in the testing of PB5.20, the servo controlled system could not 'keep up ' with the axial deformation and the K_o condition was maintained by manually increasing the cell pressure, as required. The test was repeated, PB6.20, and the cell pressure was not adjusted, so the K_o stress path was not maintained. These two tests are useful as a comparison for the effects of stress path on the stress-strain curve, and as a check on reproduceability of the tests. Again, these tests were performed with the back

pressure regulator controlling the back pressure, and hence, the recorded volume change.

With all of the following tests the pads of the radial strain belt were placed on the inside of the the sample membranes, and the transducer output was recorded by the Orion logging system. The initial conditions of the samples with respect to the dimensions of the samples and the rate at which the experiments were performed, are summarised in Table A5.2.

Table A5.2

Sample	Porosity %	Rate of loading mm/min	Average height mm	Average diameter mm	Saturated weight g	Dry weight g	Specific gravity g/cm3
PB1.20	40.4	Varied	76.37	37.66	169.14	136.17	2.69
PB3.20	39.0	0.03	77.59	37.64	175.63	141.43	2.69
PB4.20	39.9	0.003	76.78	37.82	169.26	139.23	2.69
PB5.20	41.2	0.08	77.69	37.82	172.12	137.98	2.69
PB6.20	40.1	0.08	76.58	37.75	171.78	138.07	2.69
PB7.20	40.4	0.008	75.56	37.61	166.54	134.84	2.69
PB8.20	41.3	0.03	74.87	37.65	166.54	131.55	2.69

PB1.20

This sample from block O, was initially deformed at a rate of 0.03mm/min, unfortunately the first part of the experiment was not recorded by the computer, and the starting position of the loading and strain determinations were lost. So the strain rate was varied to see the effect of this in one sample. The deformation rate was varied in the following stages:

1) 0.03 to 0.003mm/min,

2) 0.003 to 0.3mm/min,

3) 0.3 to 0.08mm/min,

4) 0.08 to 0.03mm/min.

From the plots of deviatoric stress vs axial strain, void ratio vs mean effective stress, and void ratio vs log mean effective stress, the change in deformation rate can be seen to cause a step in the deformations. The plots show that the slower deformation rates give lower stresses, both p' and q, at a particular strain, than would a faster deformation (found by extrapolation of deformations at particular strain rates). The control of the zero lateral strain with different deformation rates shows small variation, though at the faster rates, a gradual increase in the radial strain occurs. A peak in the radial strain occurs at an axial strain of 7%, and this is seen as a slight kick in the volume strain vs axial strain plot, Fig. A5.9. Otherwise the volume strain - axial strain plot is unaffected. The pore pressure also builds up gradually during the faster deformation rate. During the last decreases of the deformation rate a loop occurs in the q-p' plot which is a result of the servo mechanism controlling the K_o condition, and probably a relaxation in the sample as the rate is reduced.

The apparently large radial strain is due to the fact that before

loading started the belt slipped and a revised radius could not be obtained since no logging of the initial part of the experiments was performed.

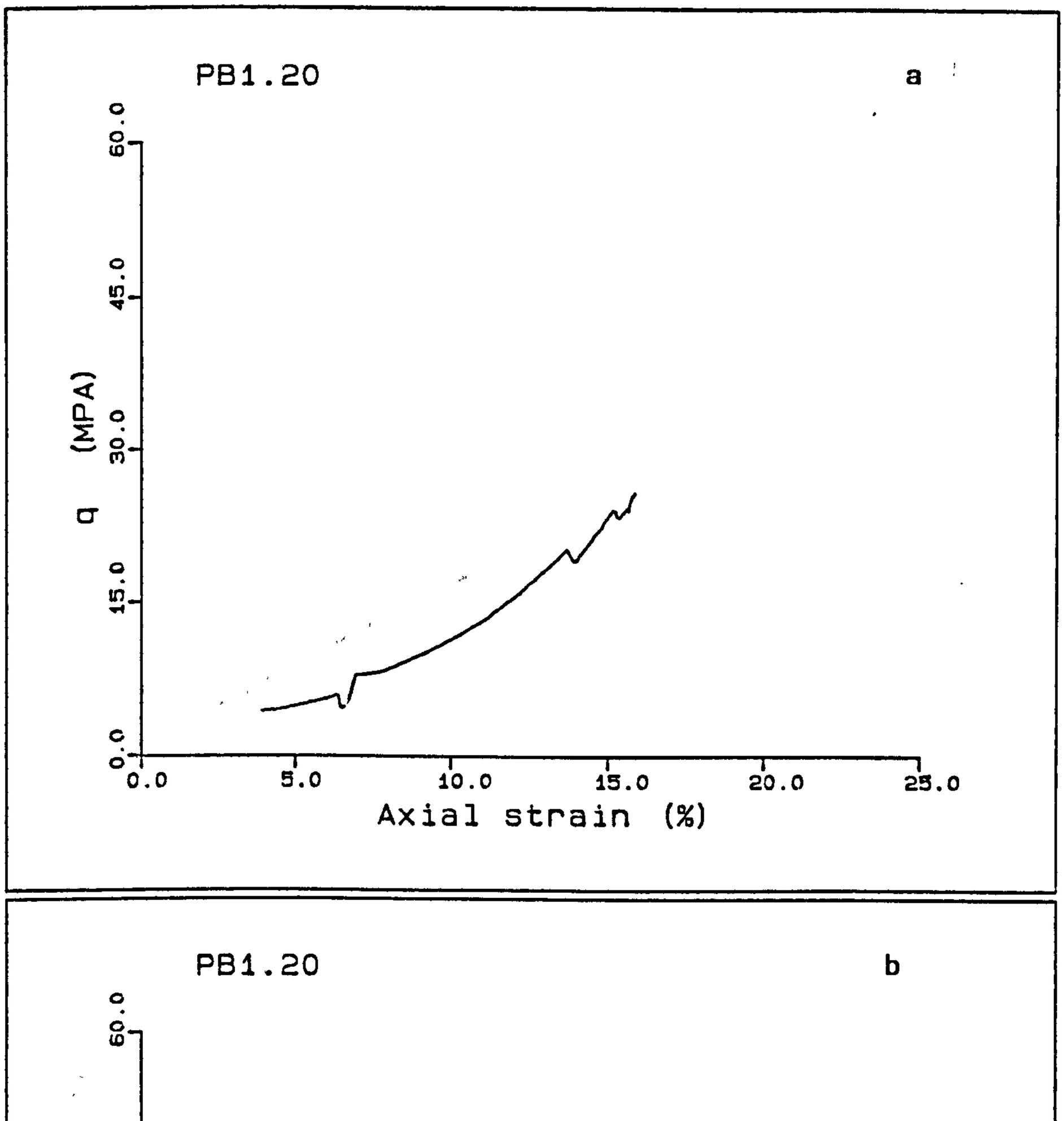

Figure A5.9(a-h) K_o test PB1.20 with varied deformation rate.

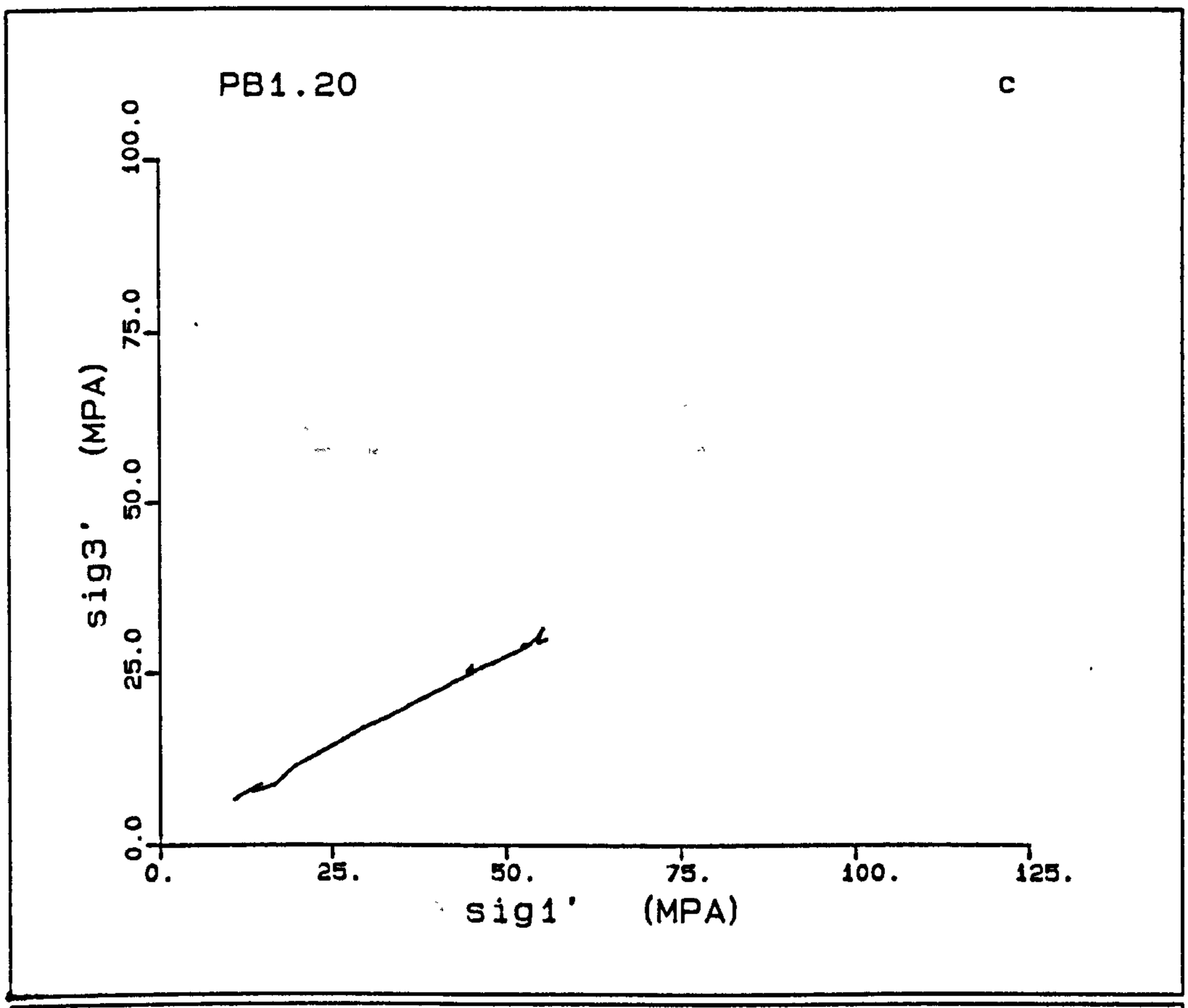
PB1.20
c
100.0
75.0
50.0
25.0
0.0
sig3' (MPA)
0.
25.
50.
75.
100.
125.
sig1' (MPA)

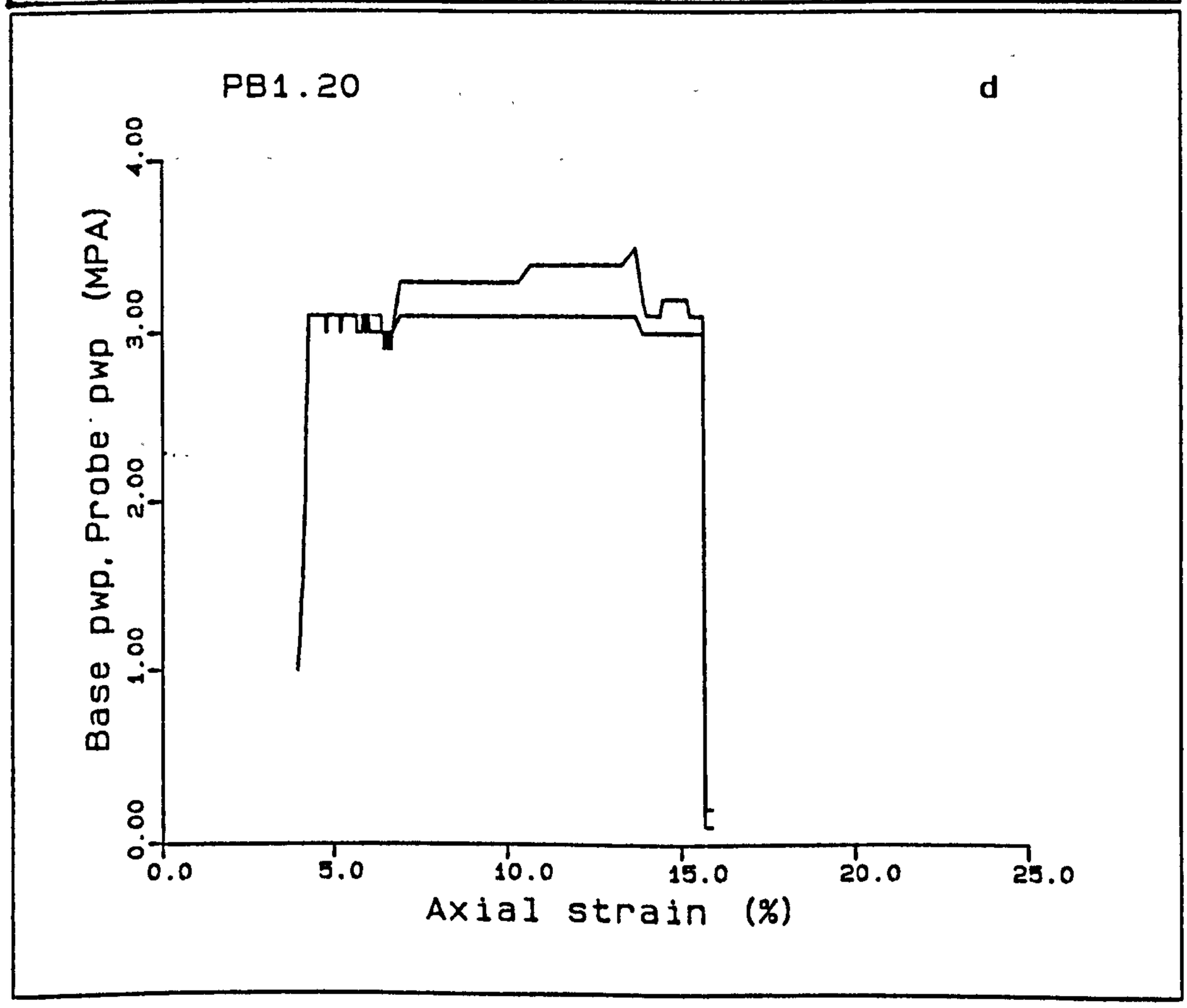
PB1.20
d
4.00
3.00
2.00
1.00
0.00
Base pwp, Probe pwp (MPA)
0.0
5.0
10.0
15.0
20.0
25.0
Axial strain (%)

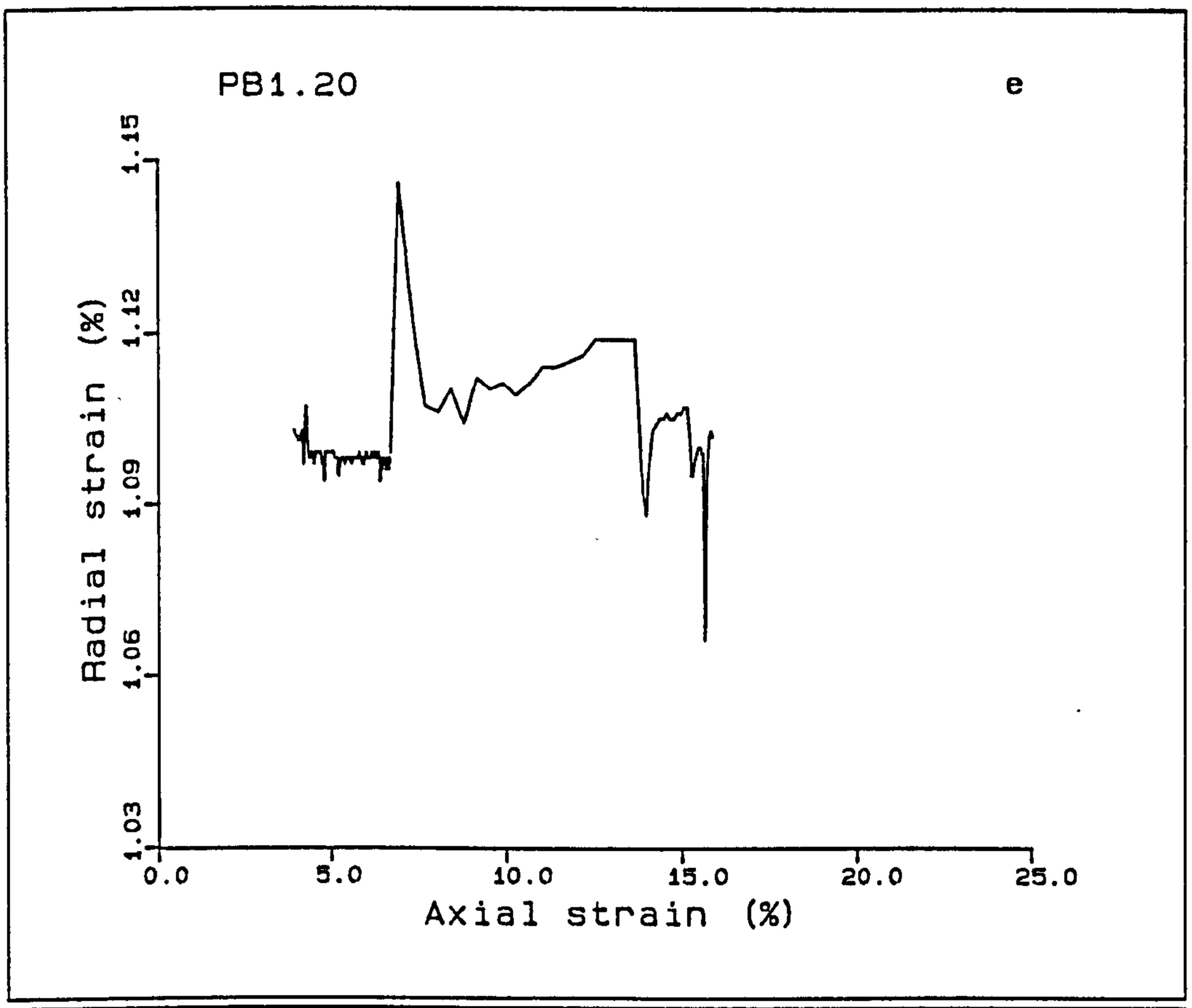
PB1.20
e
Radial strain (%)
1.15
1.12
1.09
1.06
1.03
0.0
5.0
10.0
15.0
20.0
25.0
Axial strain (%)

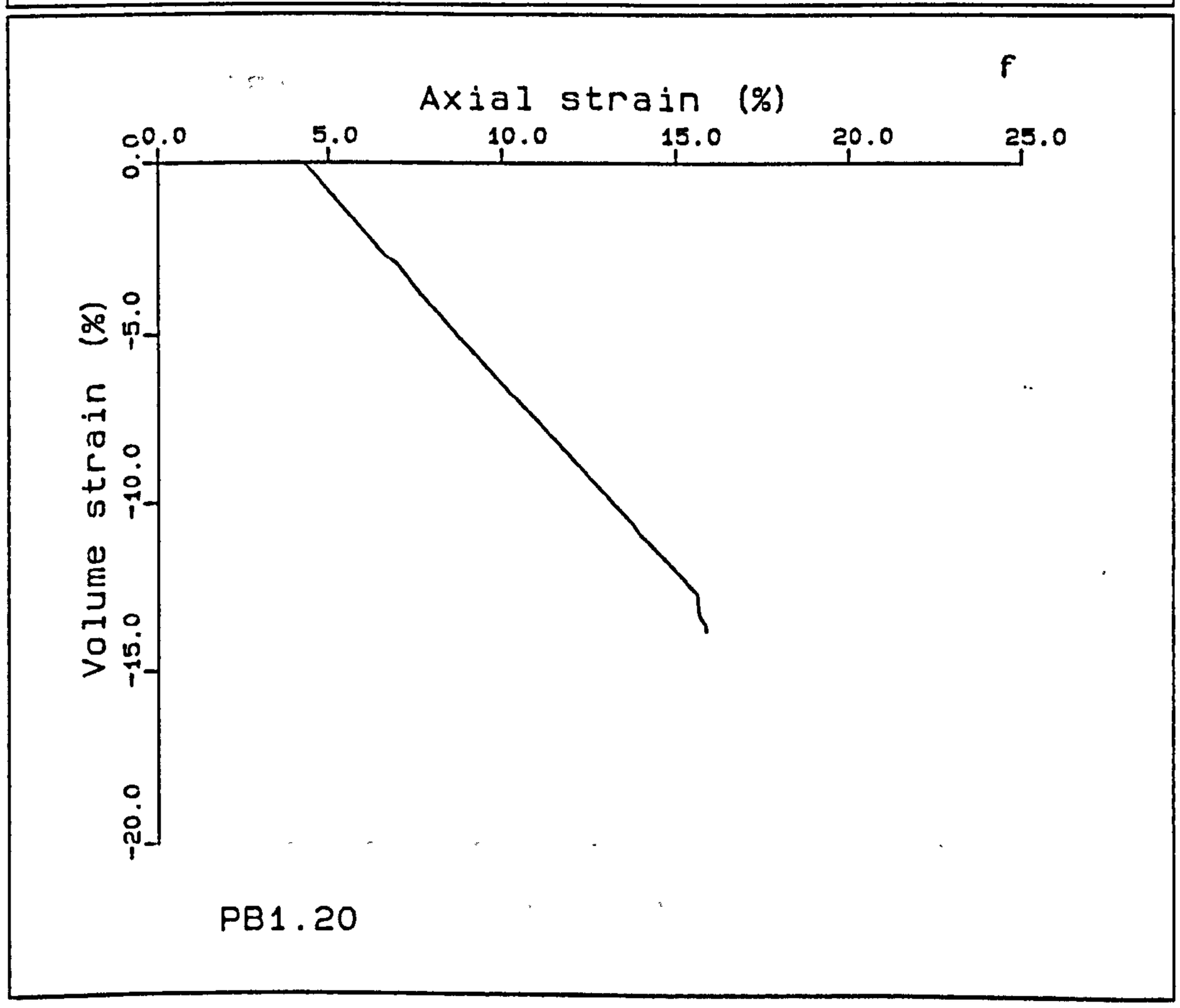
f
Axial strain (%)
0.0
5.0
10.0
15.0
20.0
25.0
Volume strain (%)
0.0
-5.0
-10.0
-15.0
-20.0
PB1.20

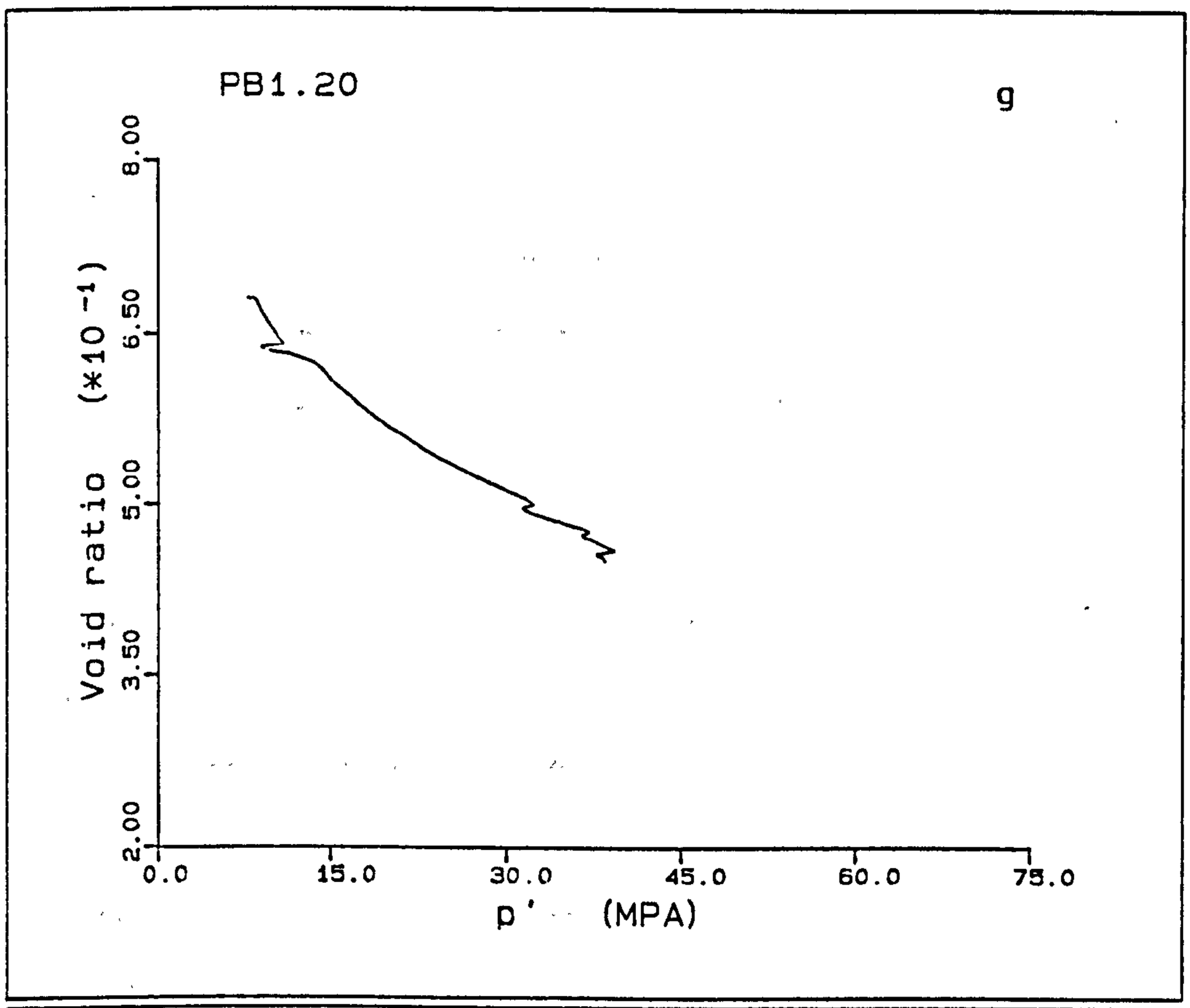
PB1.20
g
Void ratio (*10 -1)
8.00
6.50
5.00
3.50
2.00
0.0
15.0
30.0
45.0
60.0
75.0
p' (MPA)

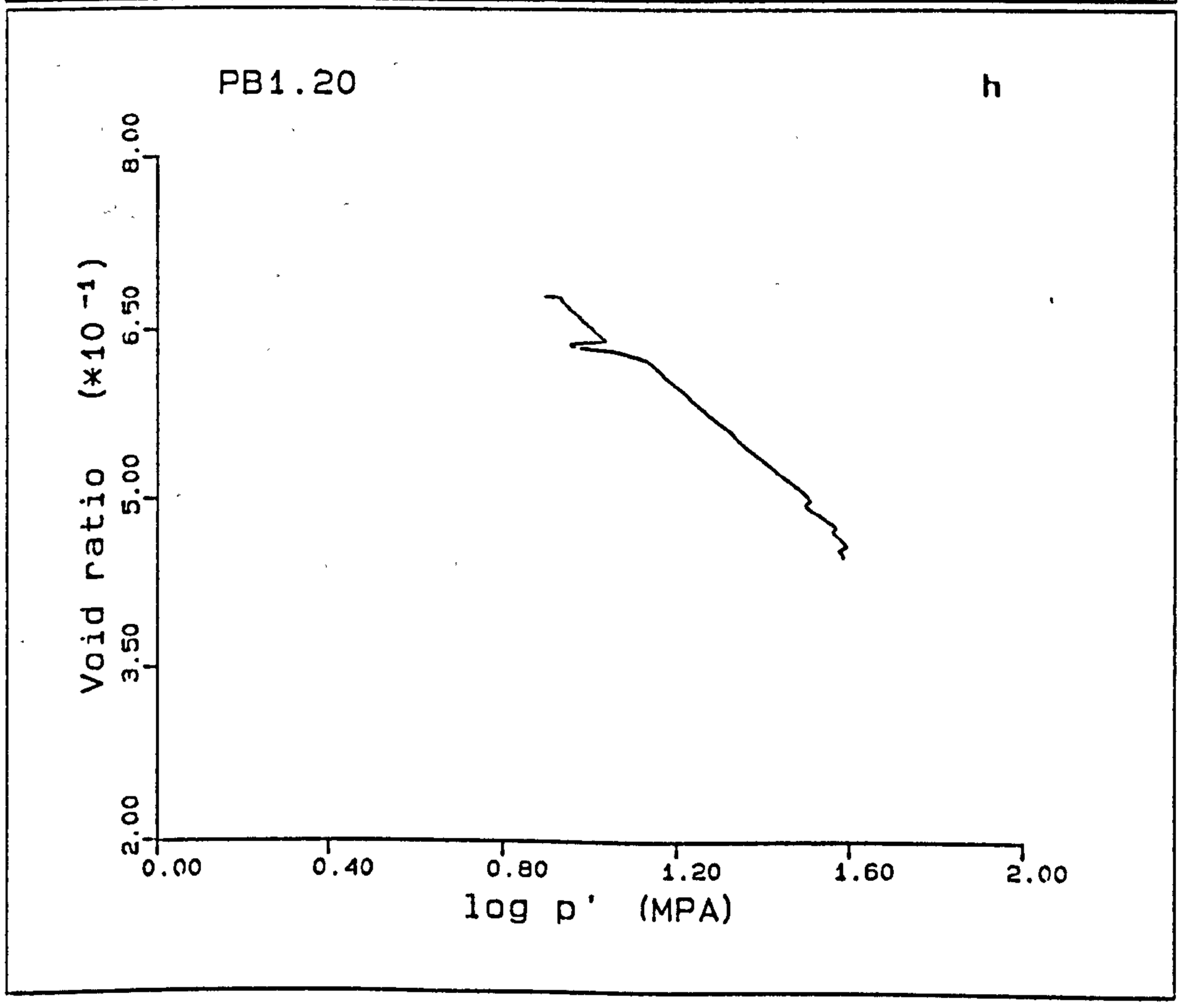
PB1.20
h
Void ratio (*10 -1)
8.00
6.50
5.00
3.50
2.00
0.00
0.40
0.80
1.20
1.60
2.00
log p' (MPA)

PB3.20

This test was performed to repeat PB1.20, and was deformed at a rate of 0.03mm/min. The initial elastic part of the deformation is linear (Fig. A5.10a), with a slight drop in the load near the yield point. The Young's modulus for this deformation is 0.62GPa, the sample yielding at a deviatoric stress of 5MPa, after which the constant q section occurs as in the North Sea samples. The $\bar{K}_{opc}$ for this is equal to 1.047, the normal consolidation deformation is characterised by a $\bar{K}_{onc}$ of 0.529, being essentially linear up to a maximum effective stress of 108MPa. The volume strain is recorded after the pore pressures reach 3.1MPa at 3.3% axial strain, there is a slight over shoot at the begining to 3.2MPa after which the 3.1MPa is maintained until the end of the experiment. The pore pressures changed in response to the cell pressure at high pressures, as it was controlled manually at the high stresses. The radial strains were kept to $2*10^{-3}$% over most of the experiment with two periods of larger strain, the first at an axial strain of 3.2% which gave a lateral strain of $8*10^{-3}$%, and in the last part of the test radial strains varied up to $11*10^{-3}$%.

The e-log p' curve, is not linear over the whole recorded volumetric compaction, the curve being split into 3 sections, an initial relatively steep section a flatter section and at higher stresses, a second steep section.

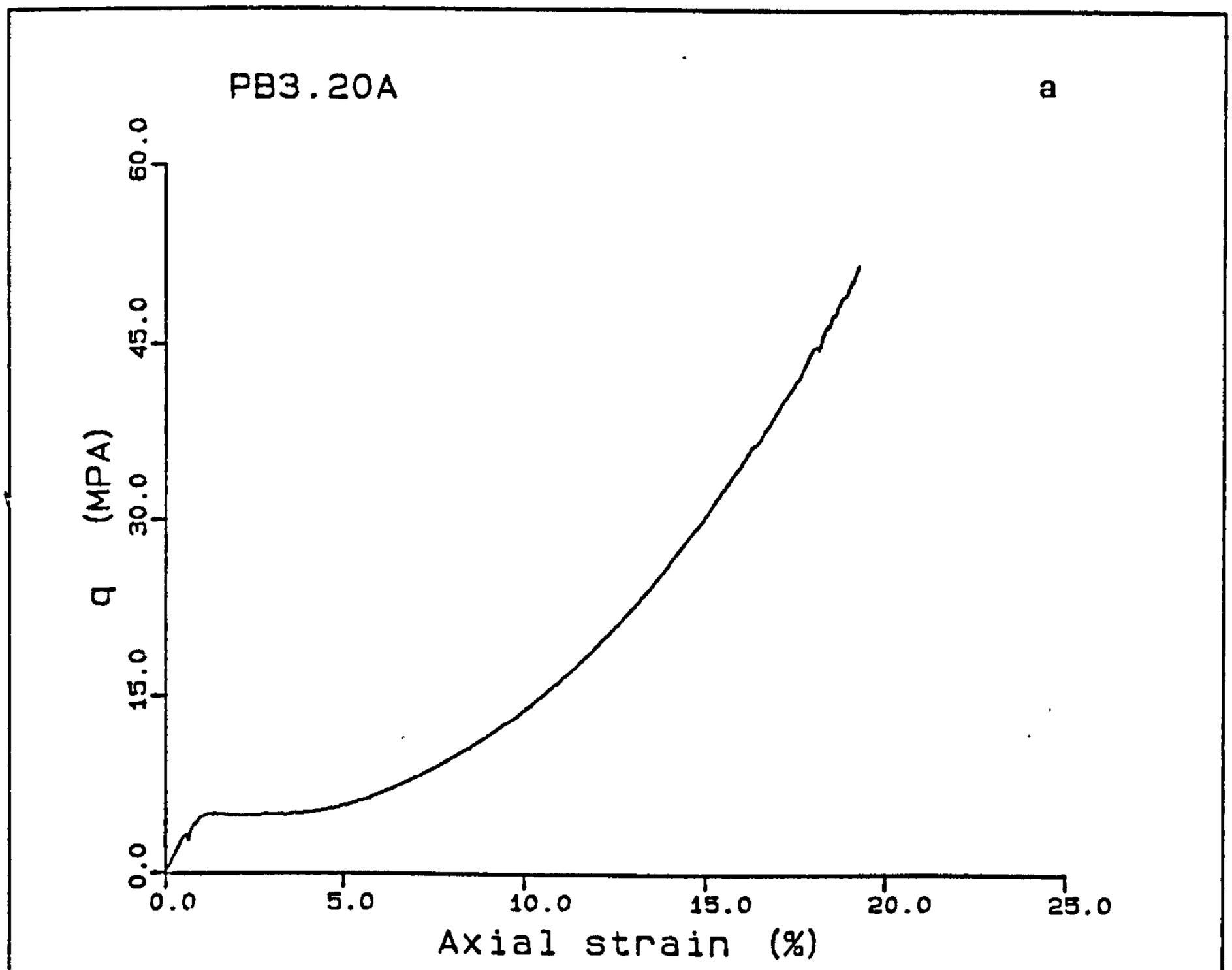

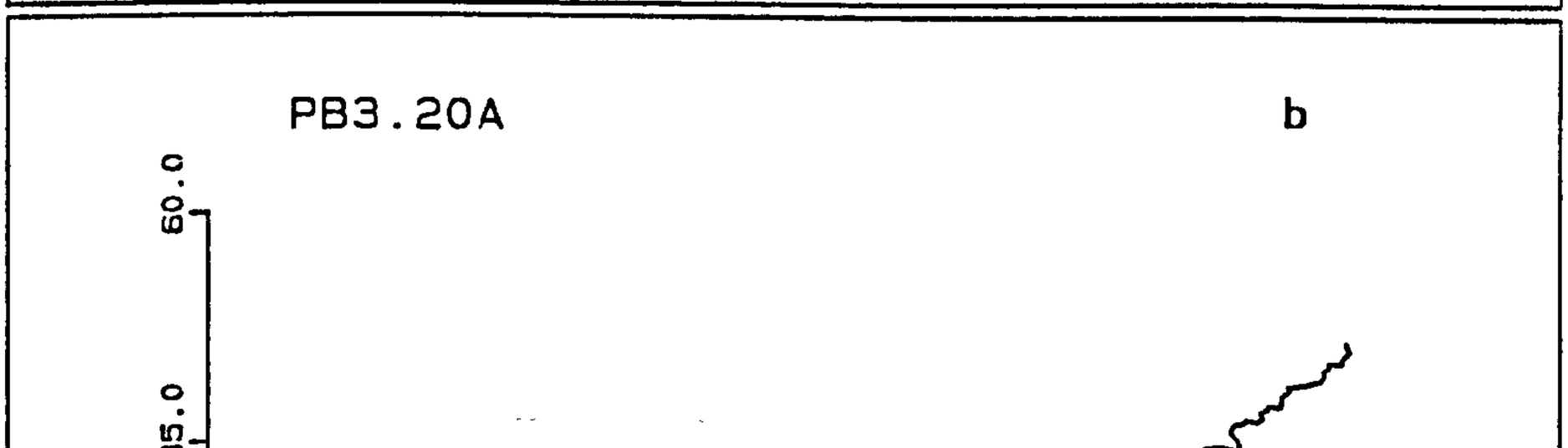

Figure A5.10 K_o test PB3.20.

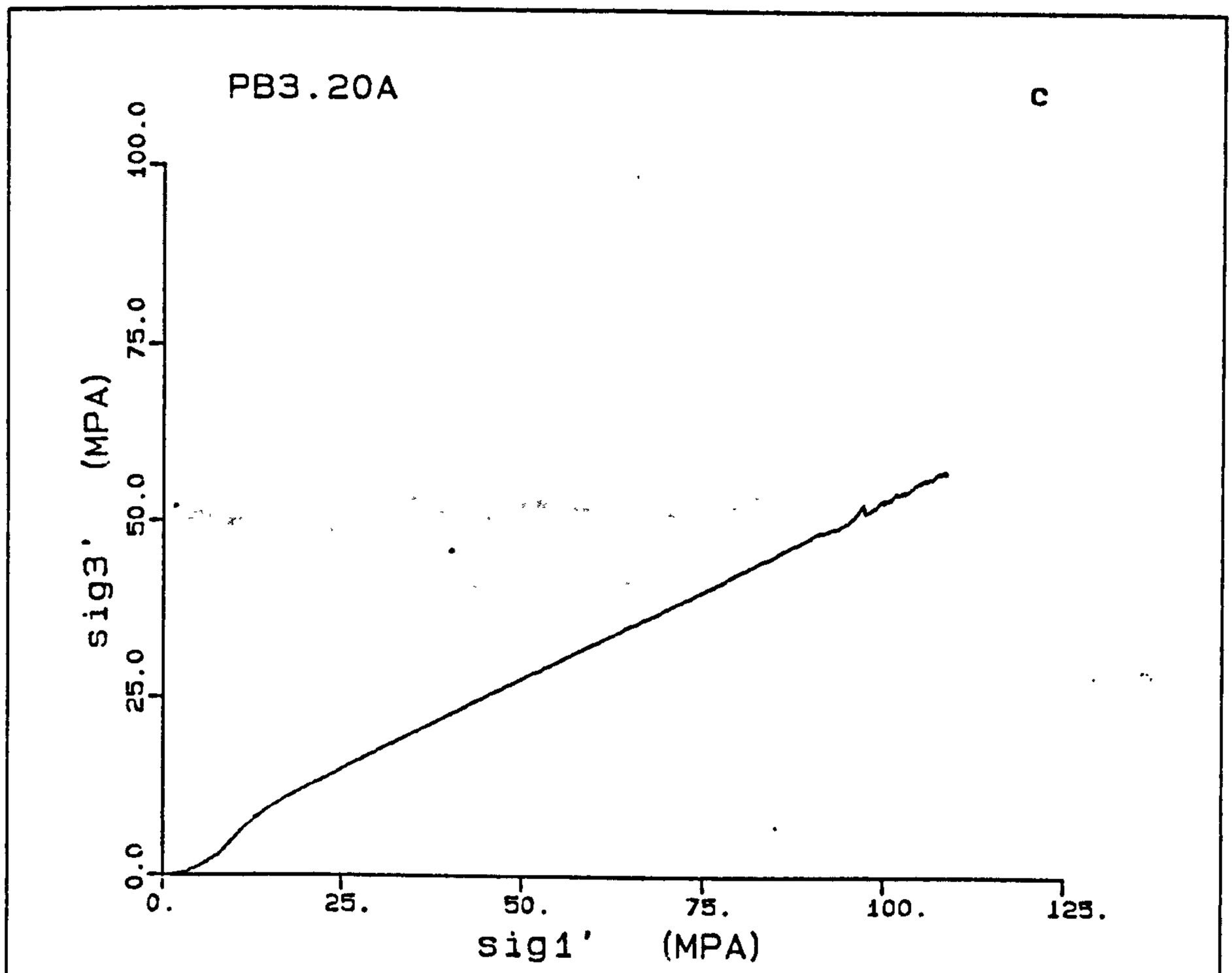
PB3.20A
c
sig3' (MPA)
100.0
75.0
50.0
25.0
0.0
0.
25.
50.
75.
100.
125.
sig1' (MPA)

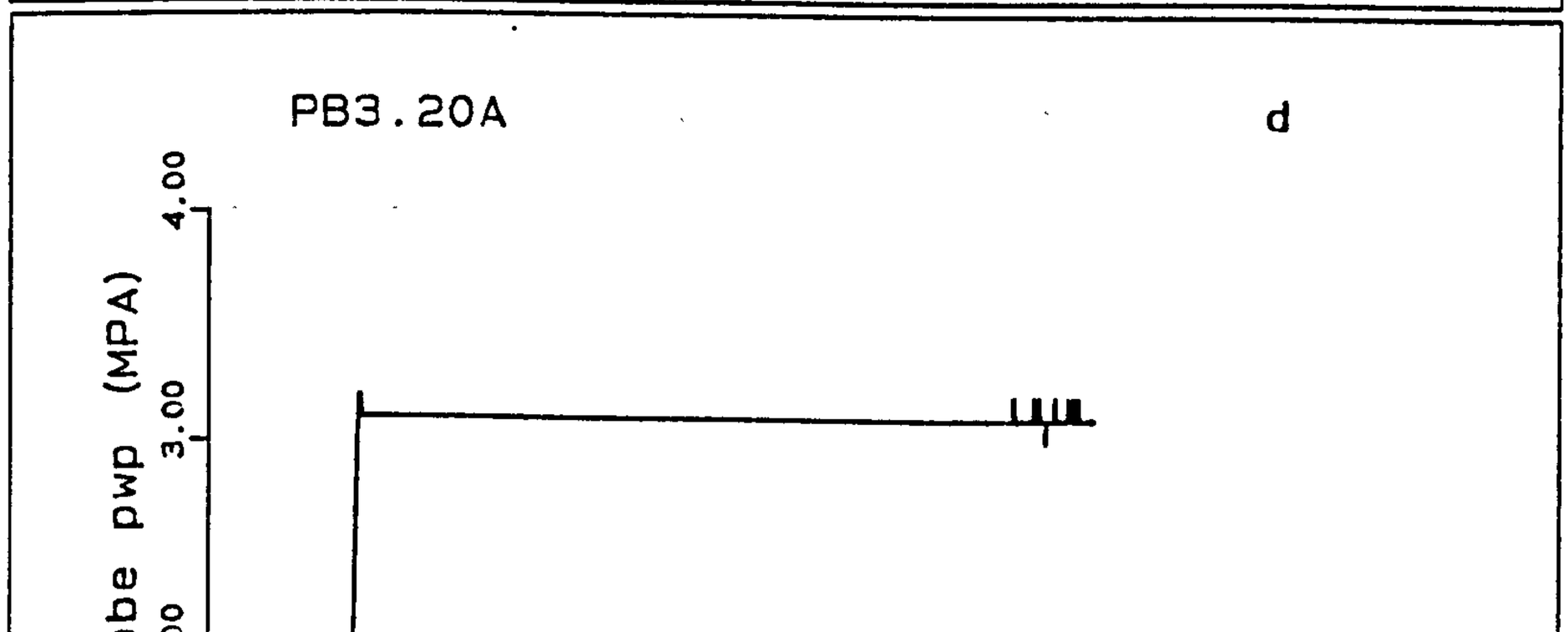
PB3.20A
d
Base pwp, Probe pwp (MPA)
4.00
3.00
2.00
1.00
0.00
0.0
5.0
10.0
15.0
20.0
25.0
Axial strain (%)

PB3.20A

e

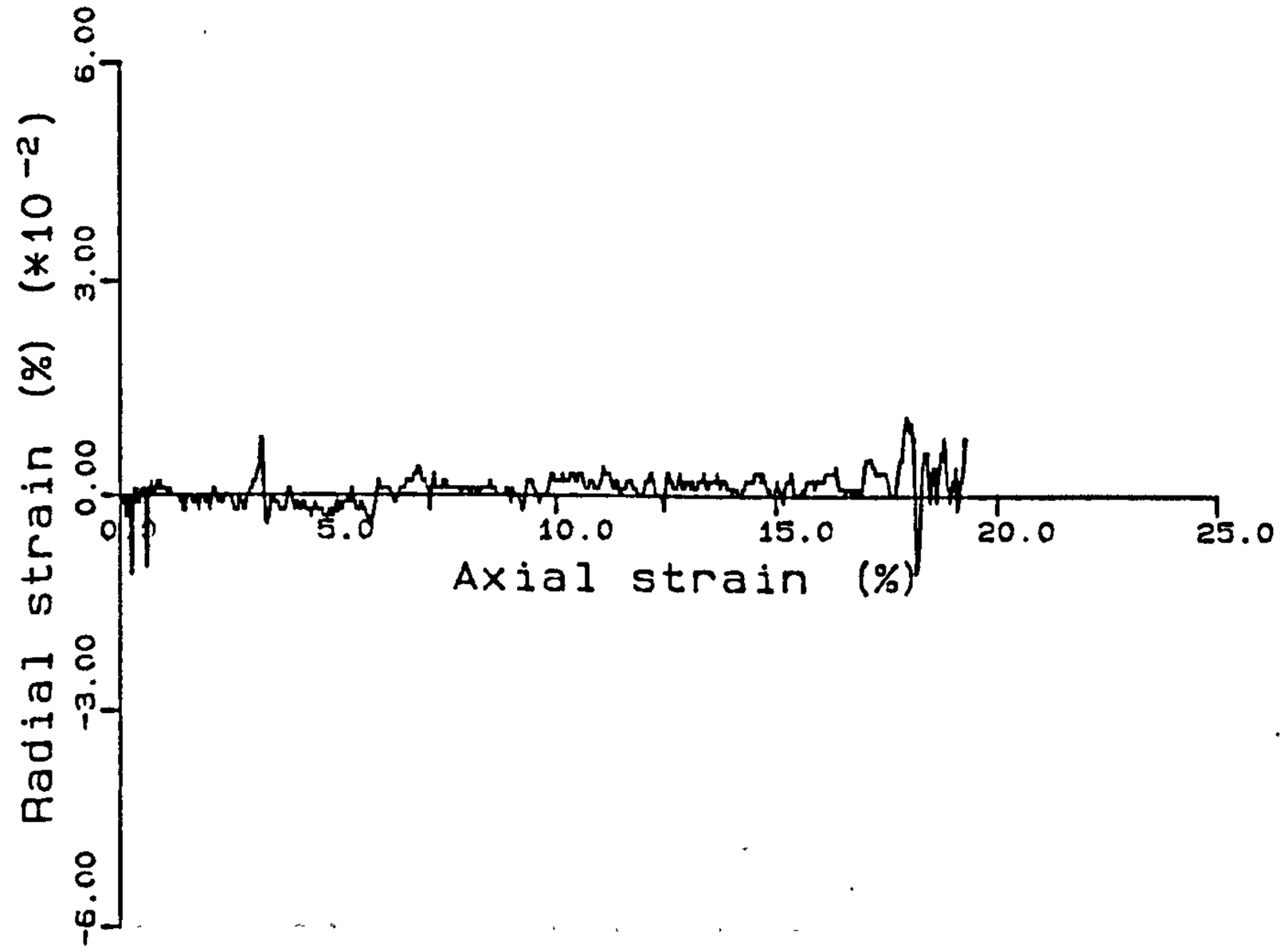

f

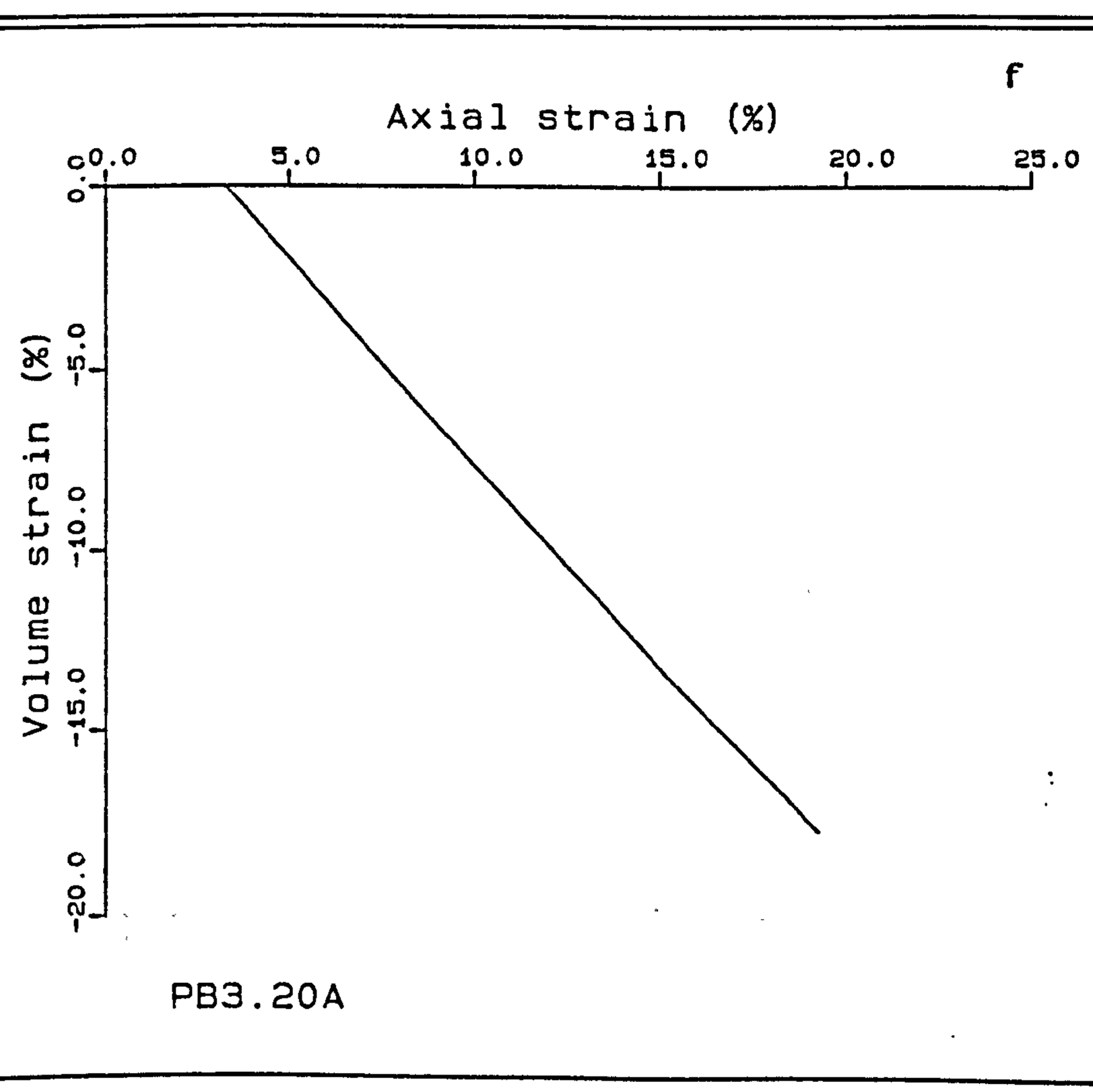

PB3.20A

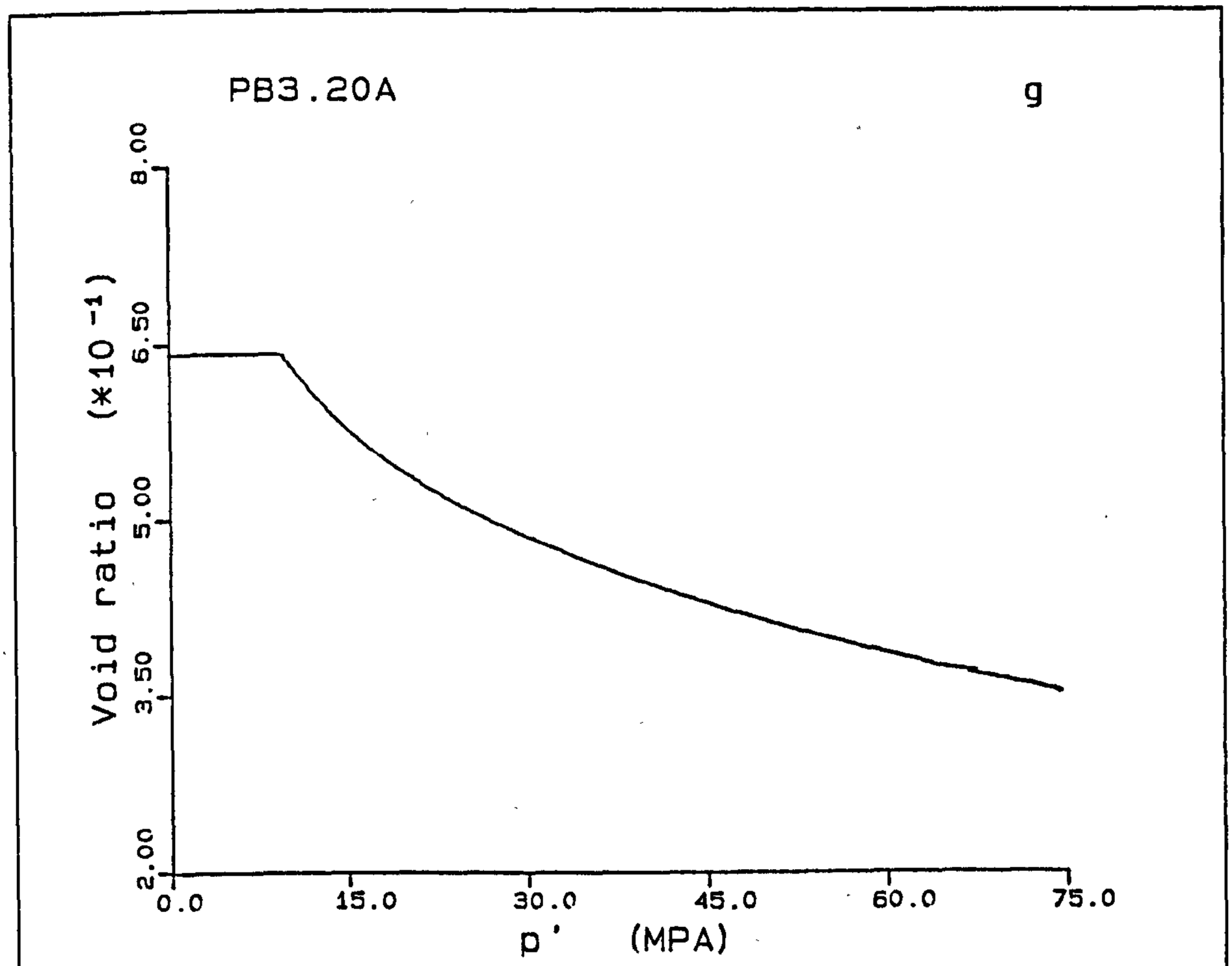
PB3.20A
g
8.00
6.50
5.00
3.50
2.00
Void ratio (*10 -1)
0.0
15.0
30.0
45.0
60.0
75.0
p' (MPA)

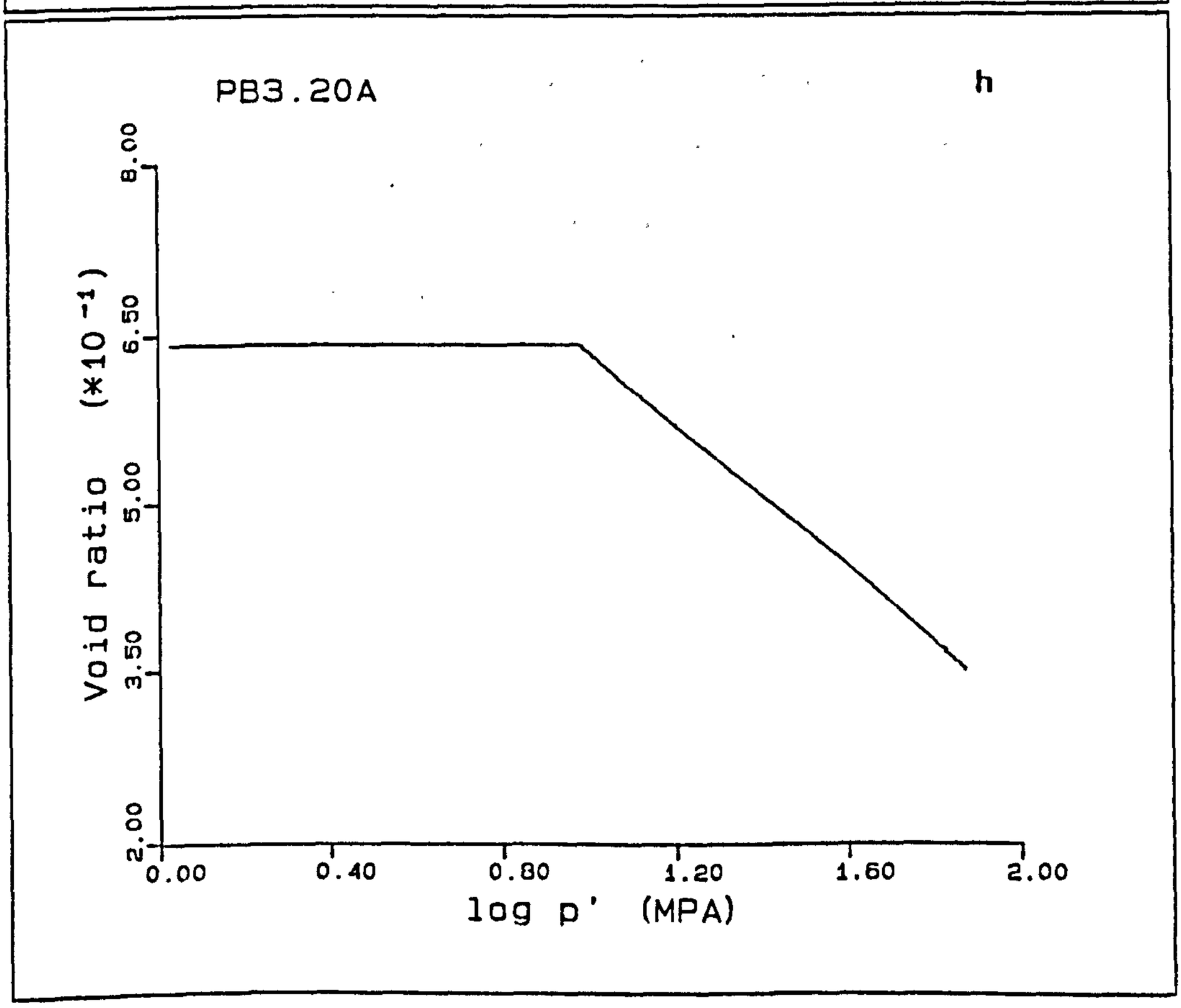
PB3.20A
h
8.00
6.50
5.00
3.50
2.00
Void ratio (*10 -1)
0.00
0.40
0.80
1.20
1.60
2.00
log p' (MPA)

PB4.20

This is a slow deformation test with a deformation rate of 0.003mm/min, the initial part of the test is very irregular, with no well defined linear elastic section as seen in previous chalk samples. The initial irregular build up of load is completed at an axial strain of 4.5% after which a distinct compaction curve is seen. This post-yield section is seen as the constant (or nearly so) q section, there being a slight decrease of 0.2MPa before the load increases again at an axial strain in excess of 5%. The coefficient of earth pressure at rest for the three section of the deformation are $\bar{K}_{oe}$=0.383, $\bar{K}_{opc}$=0.988, $\bar{K}_{onc}$=0.518, the work hardening section is seen to be largely linear over the whole range of stress employed. The radial strains show a total variation of about $1*10^{-2}$%, with two peaks outside this range at 2.1% and at 4.5% axial strain, with radial strains of $3.6*10^{-2}$% and $2.1*10^{-2}$% respectively. The volume strain and void ratio plots show a continually decreasing tangent with increasing stress, an abrupt decrease at an axial strain of 18.1% occurs, whereas no variation is seen in the radial strain - axial strain plot, Fig. A5.12e.

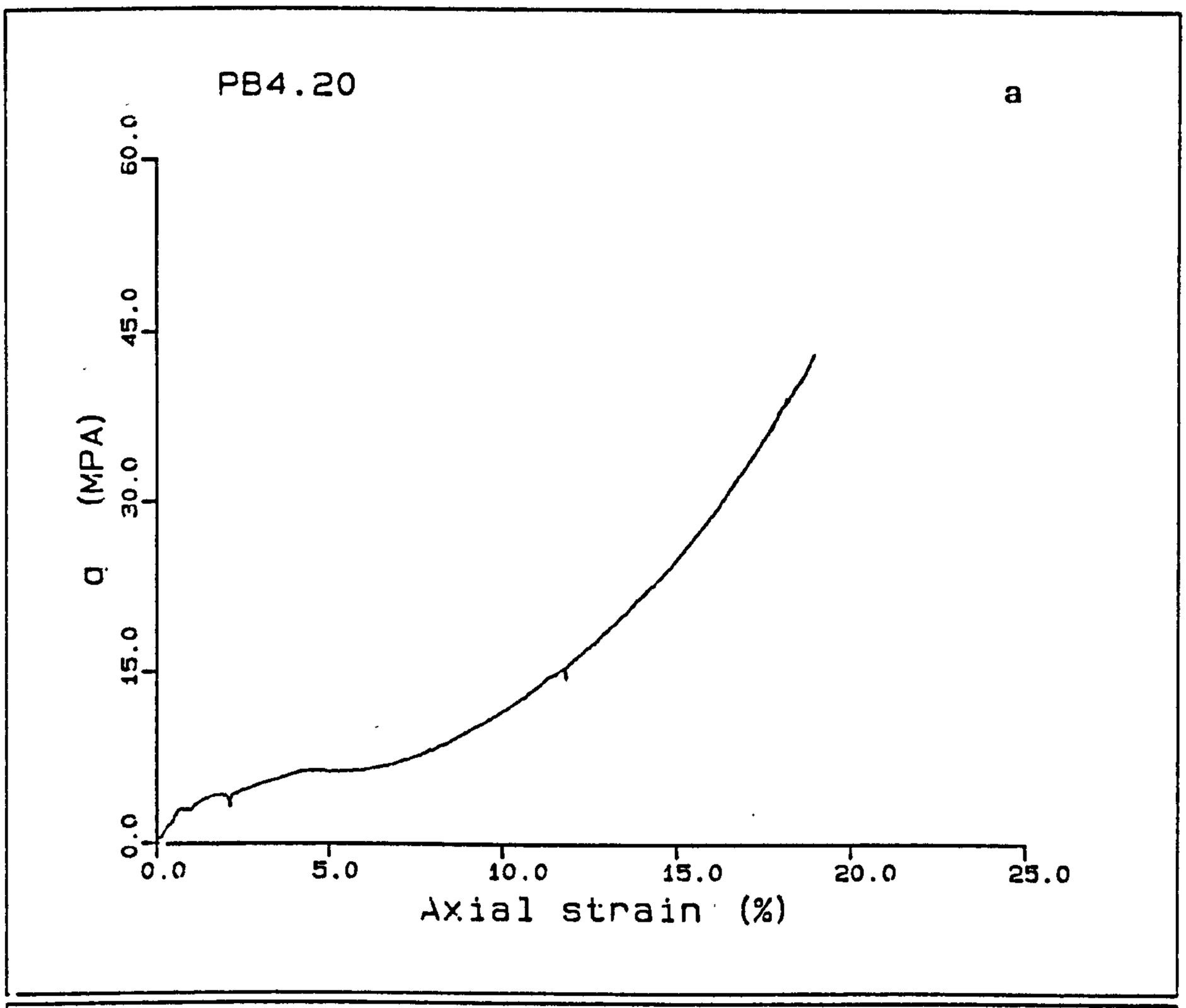

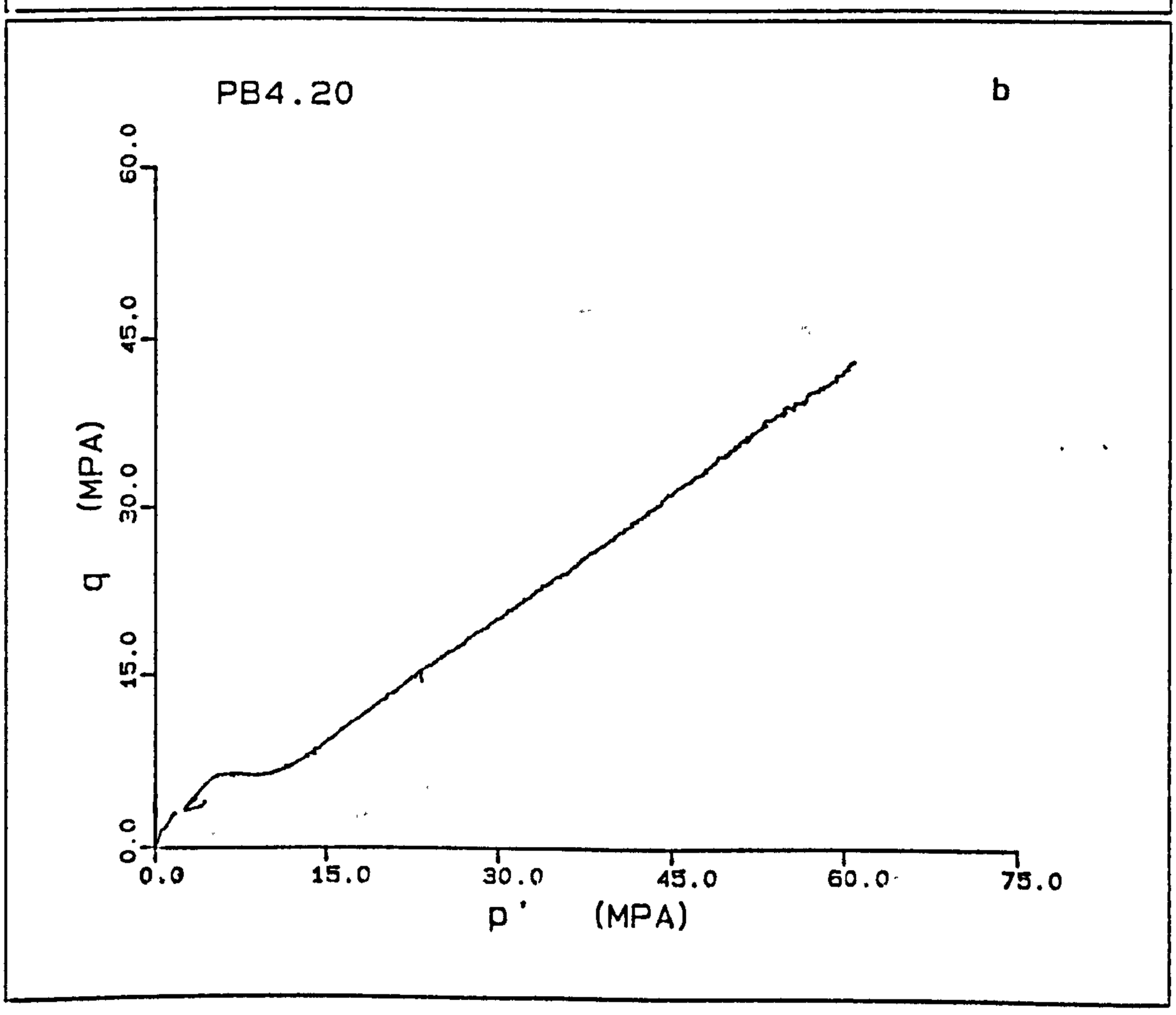

Figure A5.11(a-h) K_o test PB4.20.

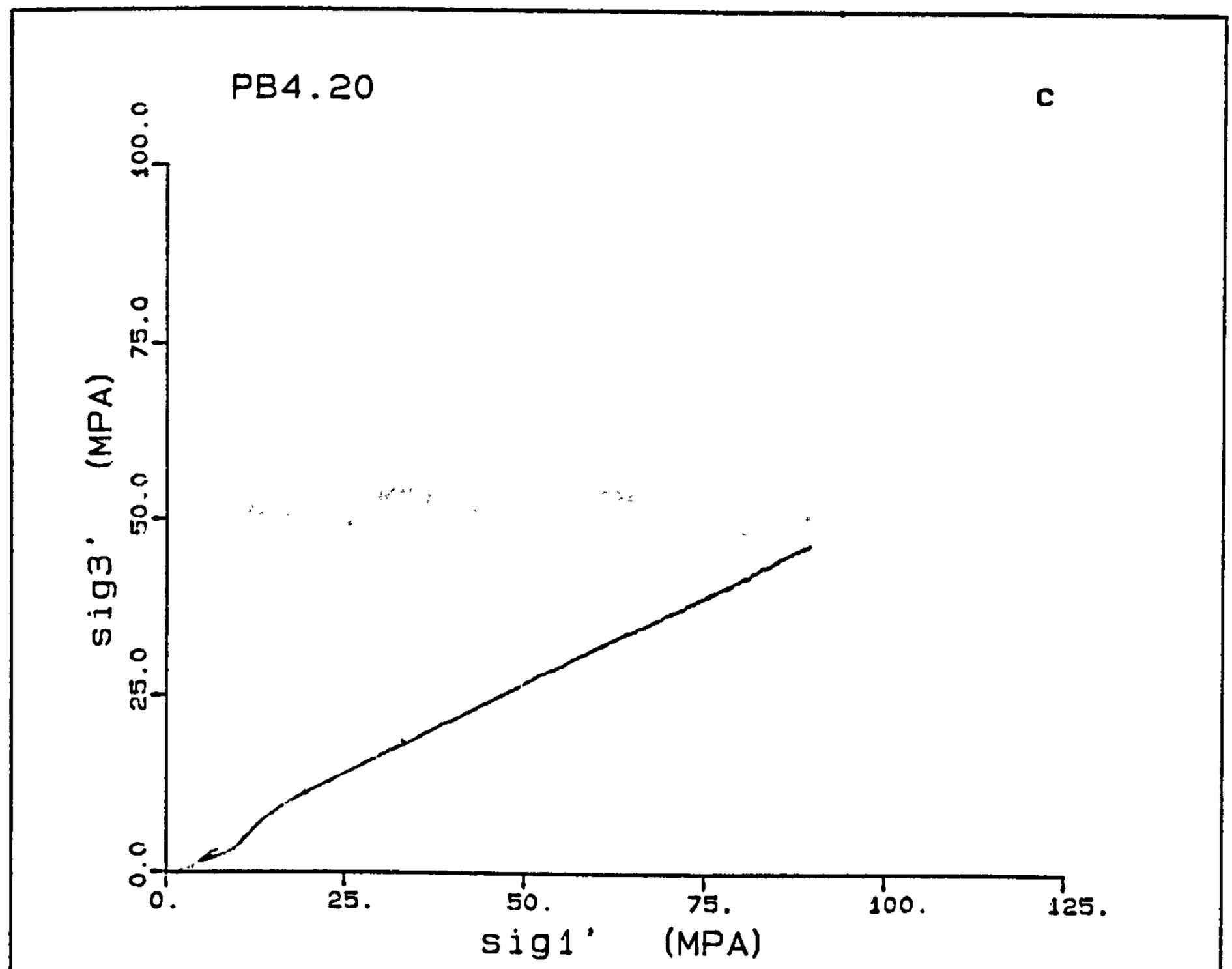
PB4.20
c
100.0
75.0
50.0
25.0
0.0
sig3' (MPA)
0.
25.
50.
75.
100.
125.
sig1' (MPA)

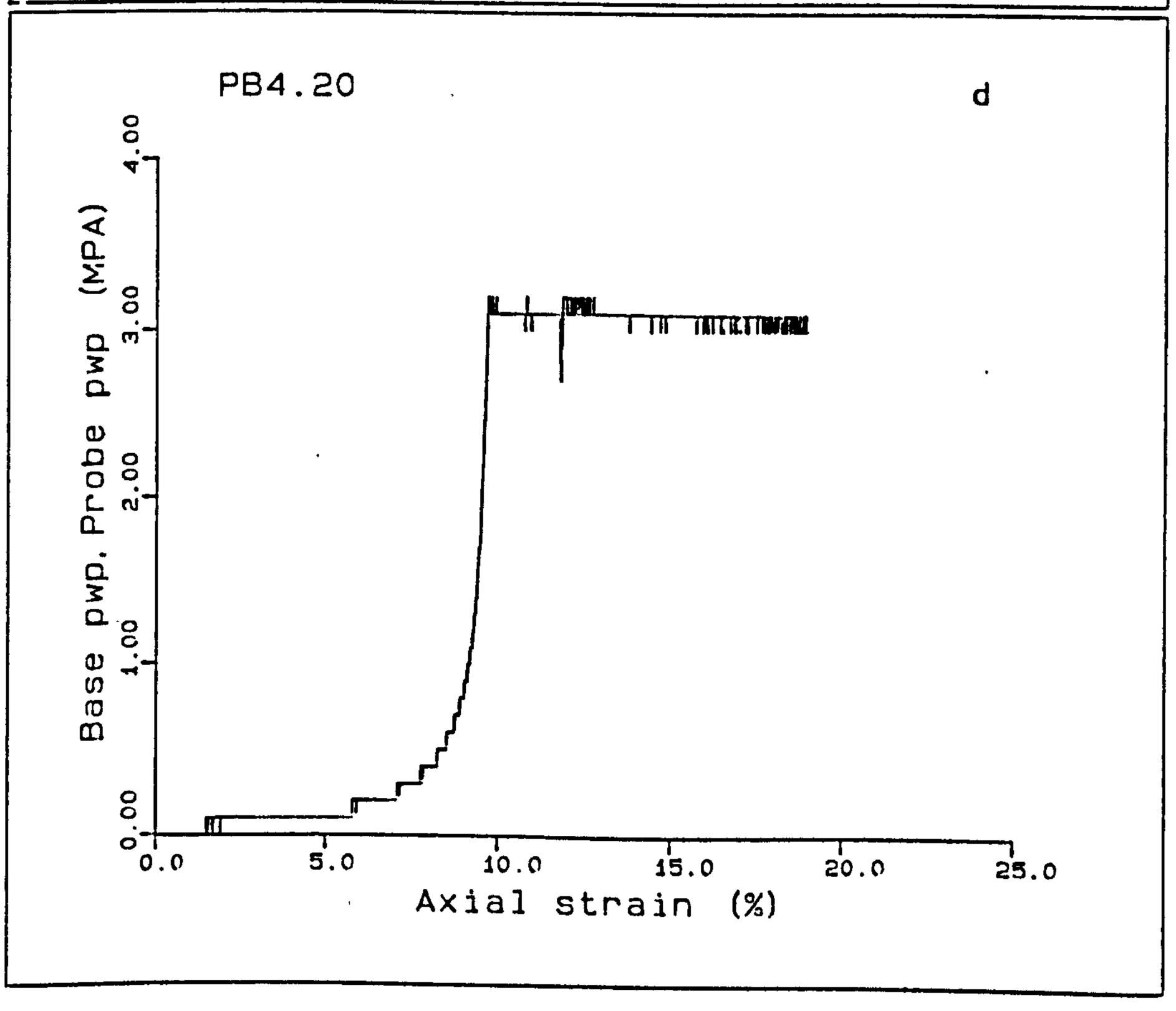
PB4.20
d
4.00
3.00
2.00
1.00
0.00
Base pwp, Probe pwp (MPA)
0.0
5.0
10.0
15.0
20.0
25.0
Axial strain (%)

PB4.20

e

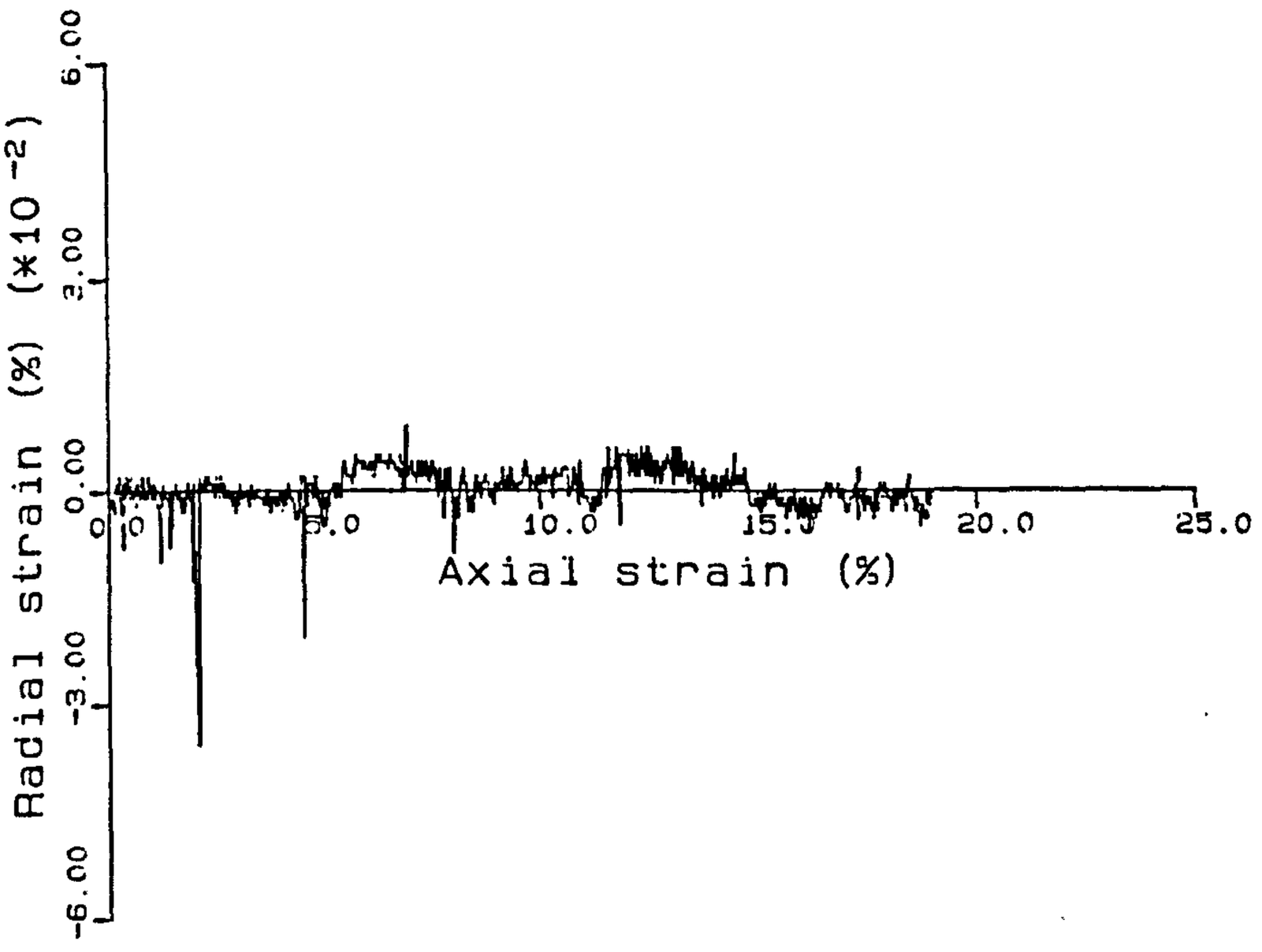

f

PB4.20

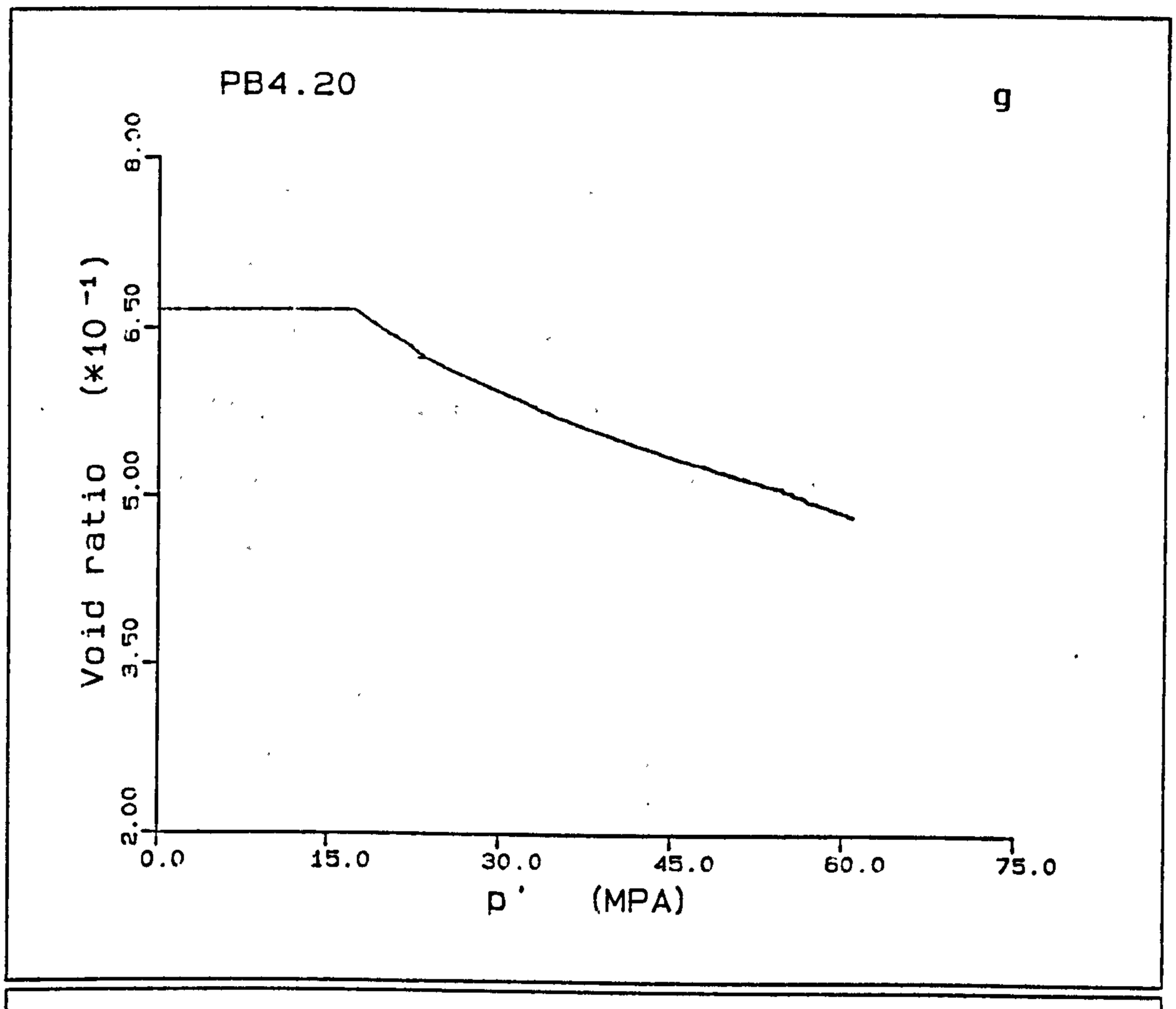
PB4.20
g
Void ratio (*10 -1)
8.00
6.50
5.00
3.50
2.00
0.0
15.0
30.0
45.0
60.0
75.0
p' (MPA)

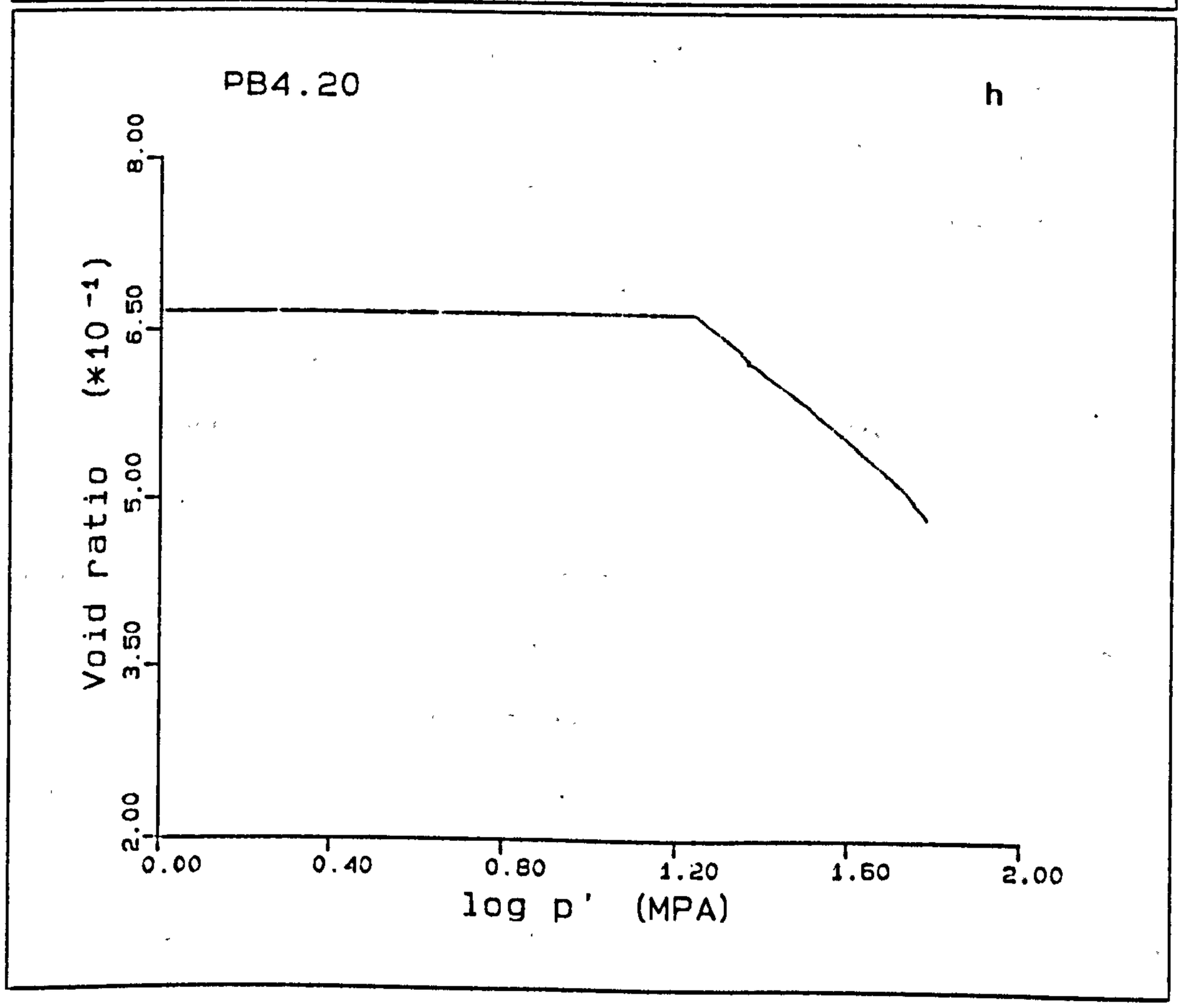
PB4.20
h
Void ratio (*10 -1)
8.00
6.50
5.00
3.50
2.00
0.00
0.40
0.80
1.20
1.60
2.00
log p' (MPA)

PB5.20

This sample was deformed at a rate of 0.08mm/min, Table A5.2, and is the fastest deformation rate employed in this series of tests. The initial elastic part of the deformation has a large step in it, despite this an initial modulus was obtained, 0.35GPa, the sample yielding at 3.6MPa. There was a slight decrease in the load in the post-peak deformation of 0.1MPa. The compaction behaviour is seen to be linear in deviatoric stress - mean effective stress space, with $\bar{K}_o$ values for the transitional and normal consolidation sections being 1.000 and 0.538 respectively. The plot of radial strain versus axial strain shows little general variation in radial strain, being predominantly less than $5*10^{-3}$%, however some peaks exist due to the manual adjustment of the cell pressure in the maintainance of K_o. The peaks in the radial strain occur at 0.8%, 4.7%, 4.9%, and 6.9% axial strain with values of $-52*10^{-3}$%, $17*10^{-3}$%, $-31*10^{-3}$% and $32*10^{-3}$%, the first accounting for the initial step in the deformation.

The faster rate of loading led to the build up of pore pressures at the undrained top of the sample, the excess pore pressures start increasing at an axial strain of approximately 11.2% and reach a maximum of 0.2MPa above the back pressure of 3.0MPa, at an axial strain of 22.1%.

Again as in PB3.20 the e-log p' plot, Fig. A5.12h, can be split up into three sections, an initial steep section, an intermediate more shallow slope, and a second steep slope at increasingly higher stresses, no abrupt change is seen as in PB4.20.

The peak compressibility (M_v) is equal to $5.8*10^{-3}MPa^{-1}$ at a vertical effective stress of 10MPa, with both the C_v and the permeability gradually decreasing from the initial values of 7.5mD to $174m^2/yr$ and 0.0042mD at 115.6MPa. The slopes of the log k(1+e)

versus log e plots show a slightly concave upwards trend, Fig. A5.121.

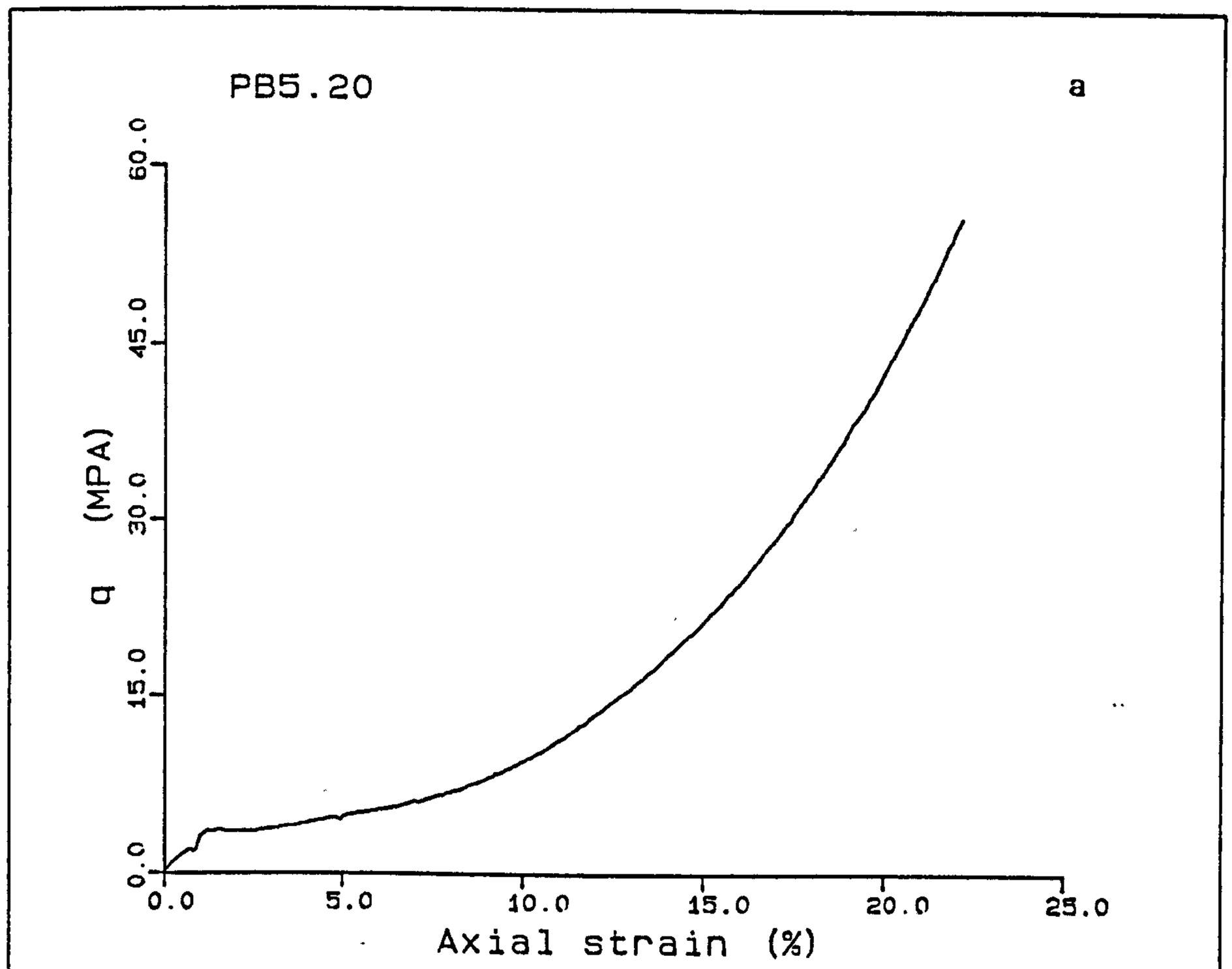

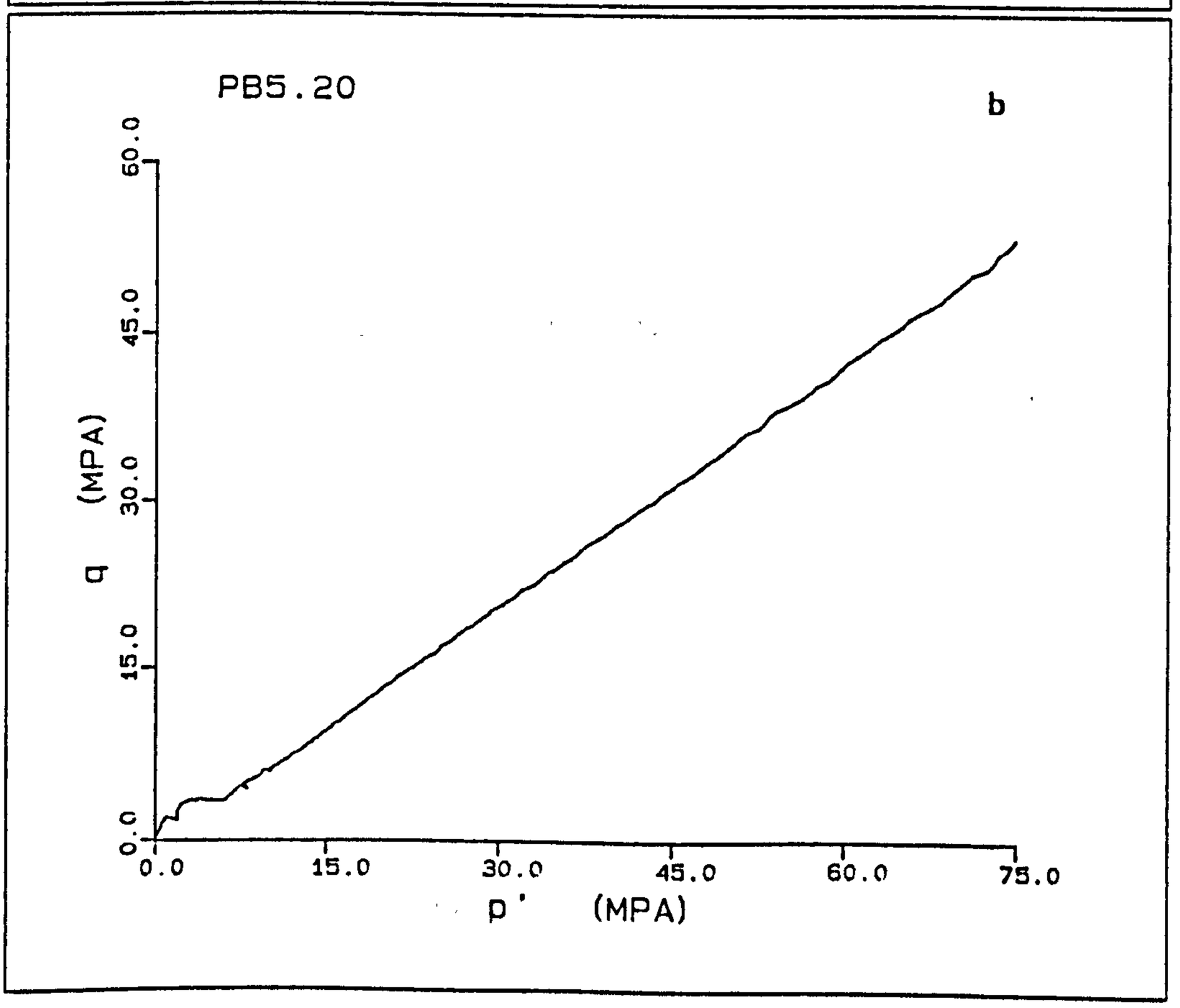

Figure A5.12(a-l) K_o test PB5.20.

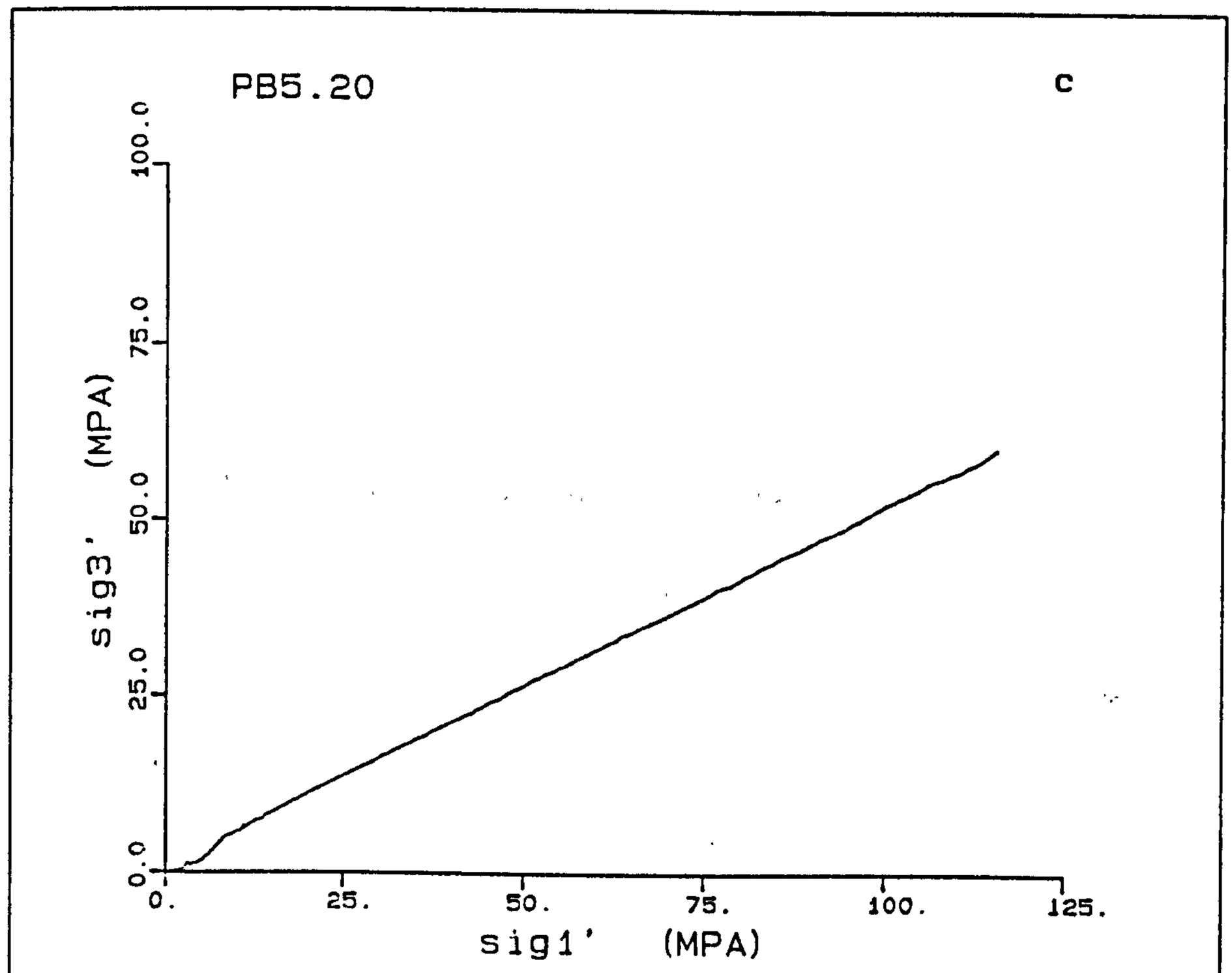
PB5.20
c
sig3' (MPA)
100.0
75.0
50.0
25.0
0.0
0.
25.
50.
75.
100.
125.
sig1' (MPA)

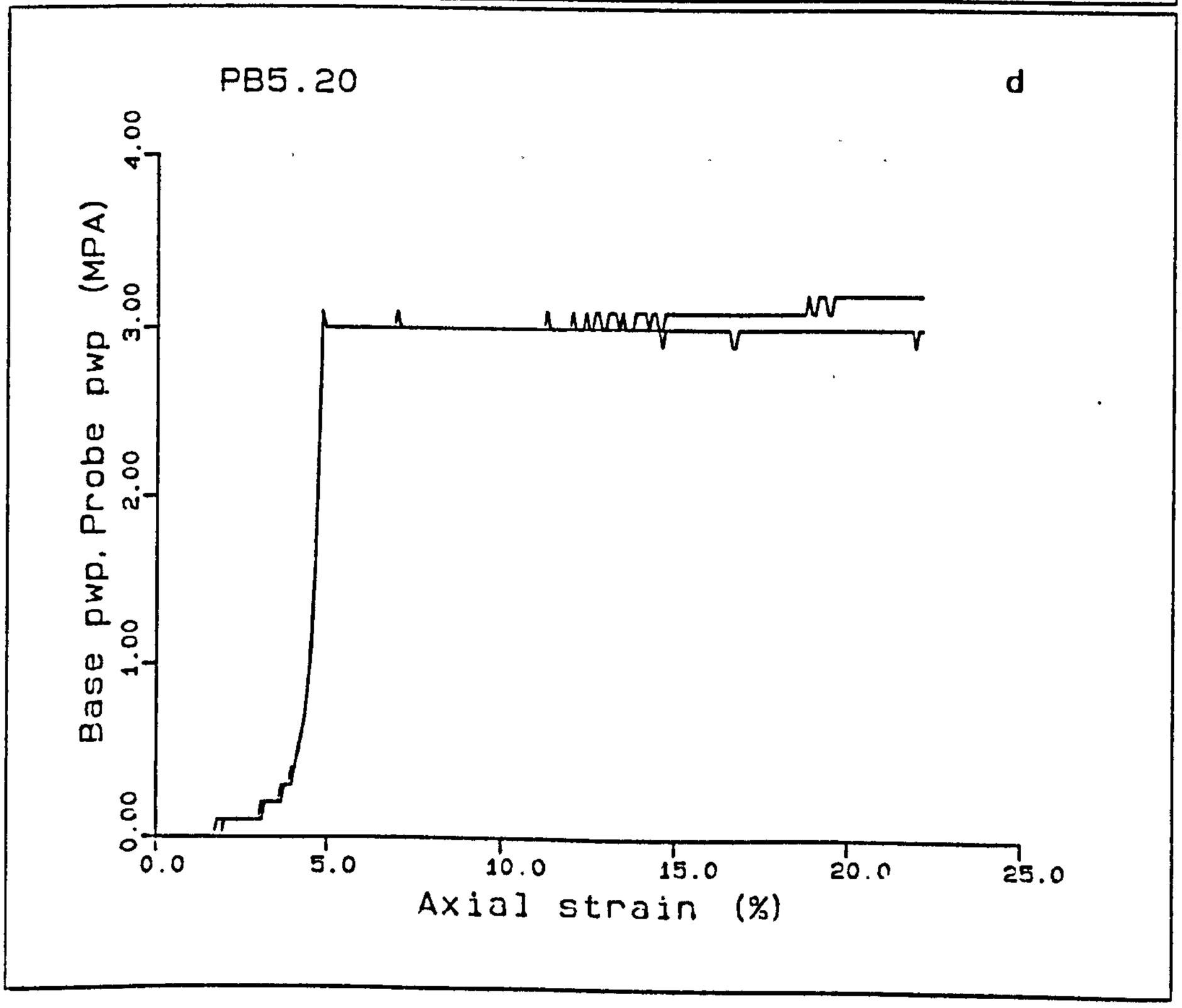
PB5.20
d
Base pwp, Probe pwp (MPA)
4.00
3.00
2.00
1.00
0.00
0.0
5.0
10.0
15.0
20.0
25.0
Axial strain (%)

PB5.20

e

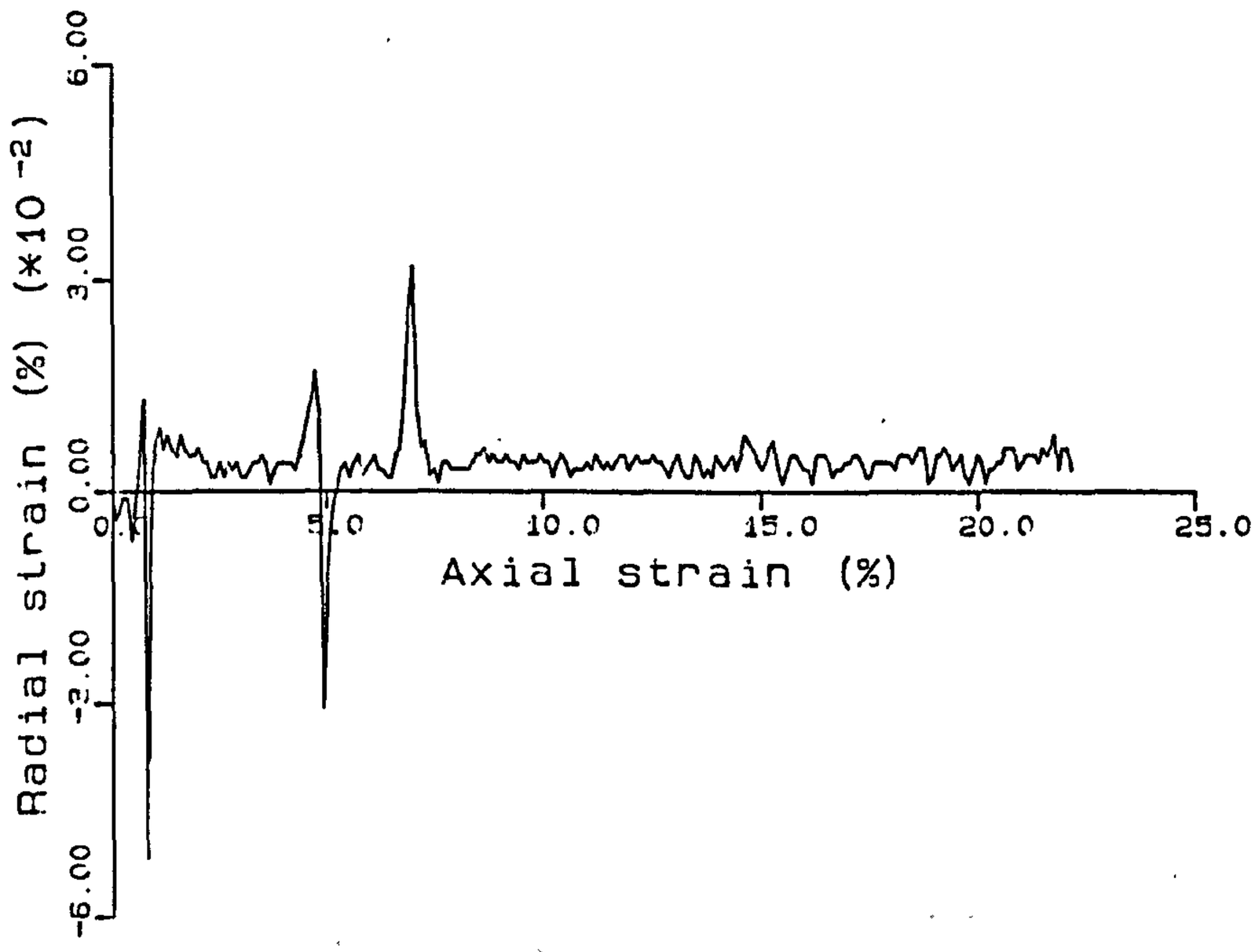

f

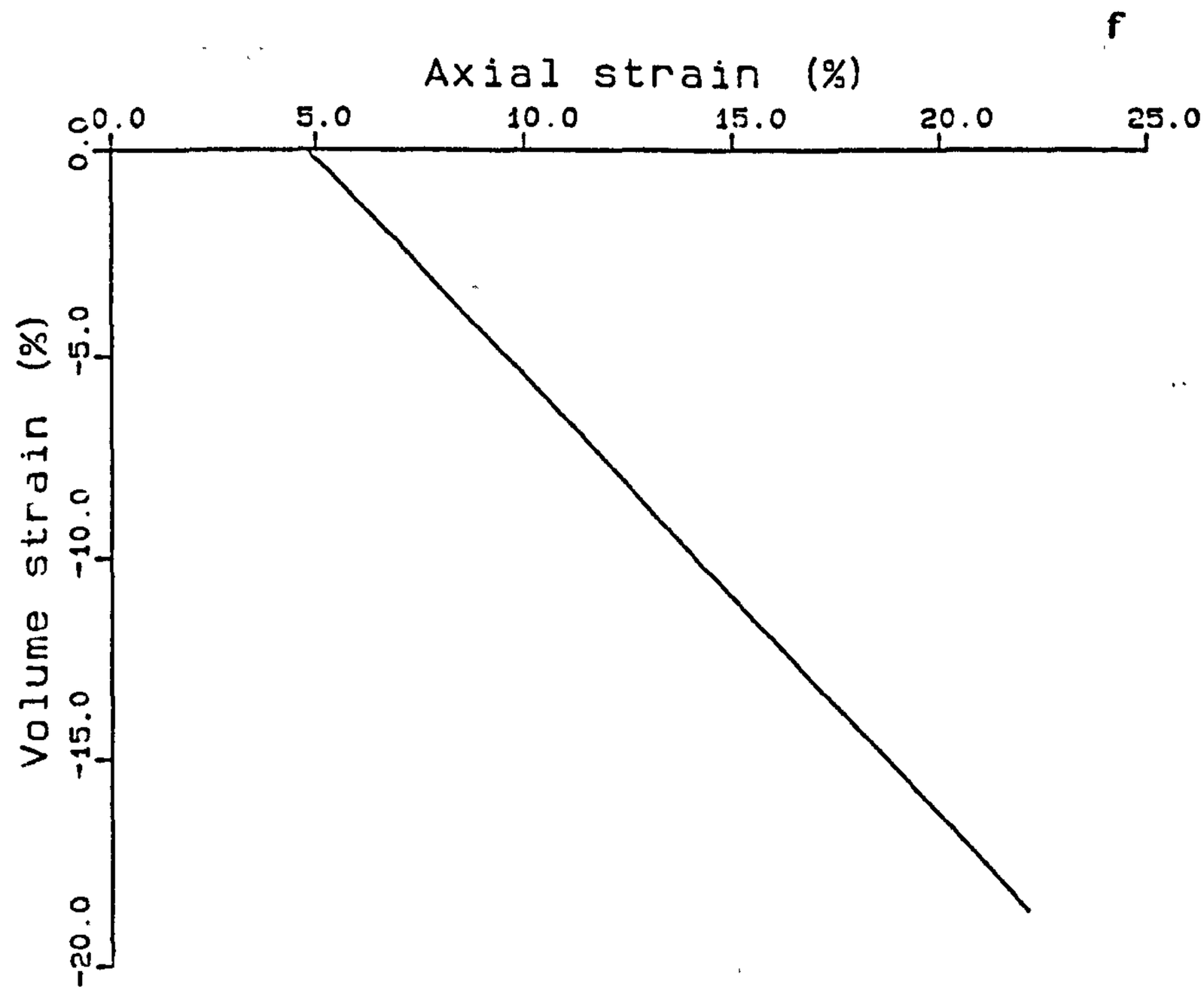

PB5.20

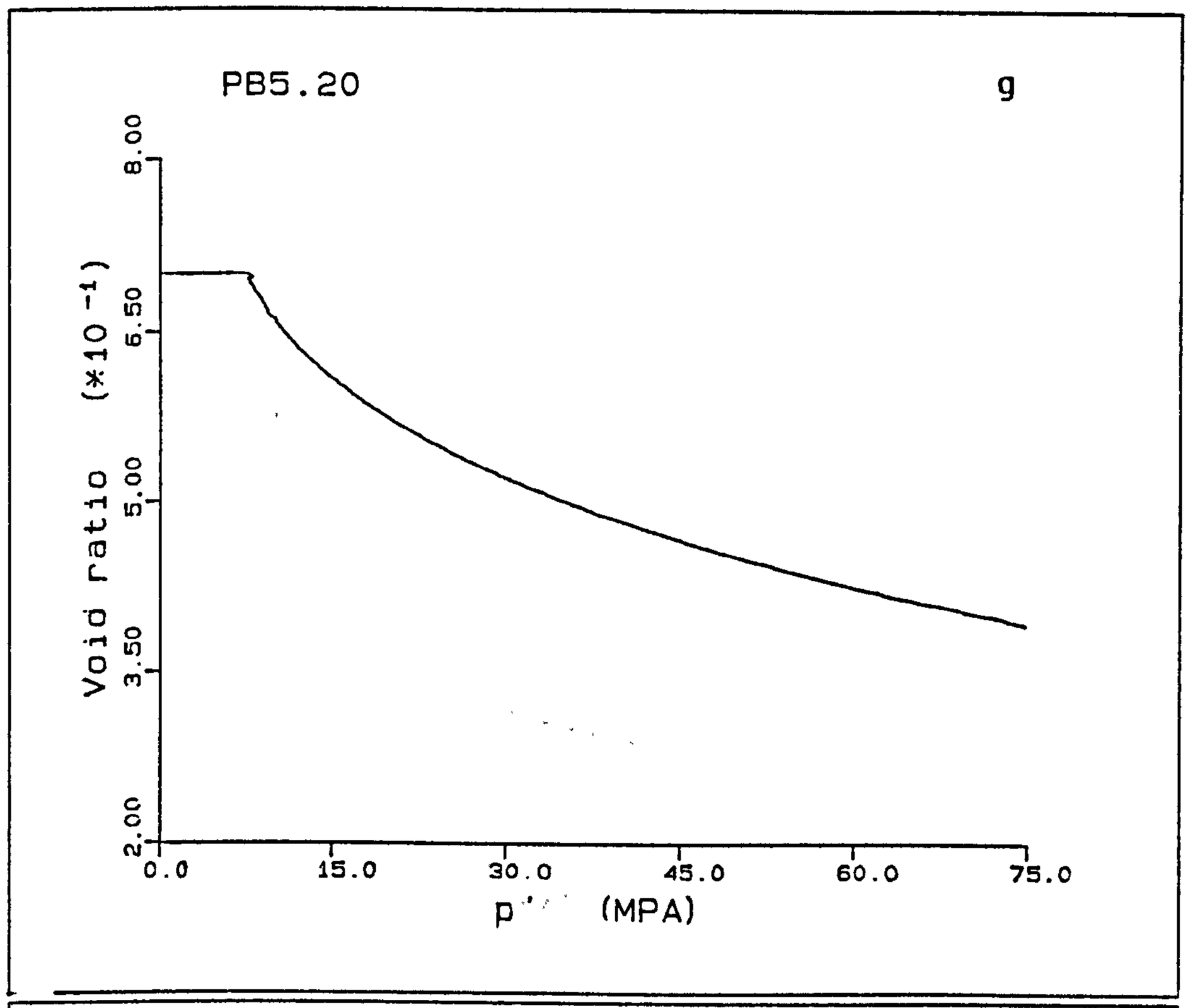
PB5.20
g
8.00
6.50
5.00
3.50
2.00
Void ratio (*10 -1)
0.0
15.0
30.0
45.0
60.0
75.0
p' (MPA)

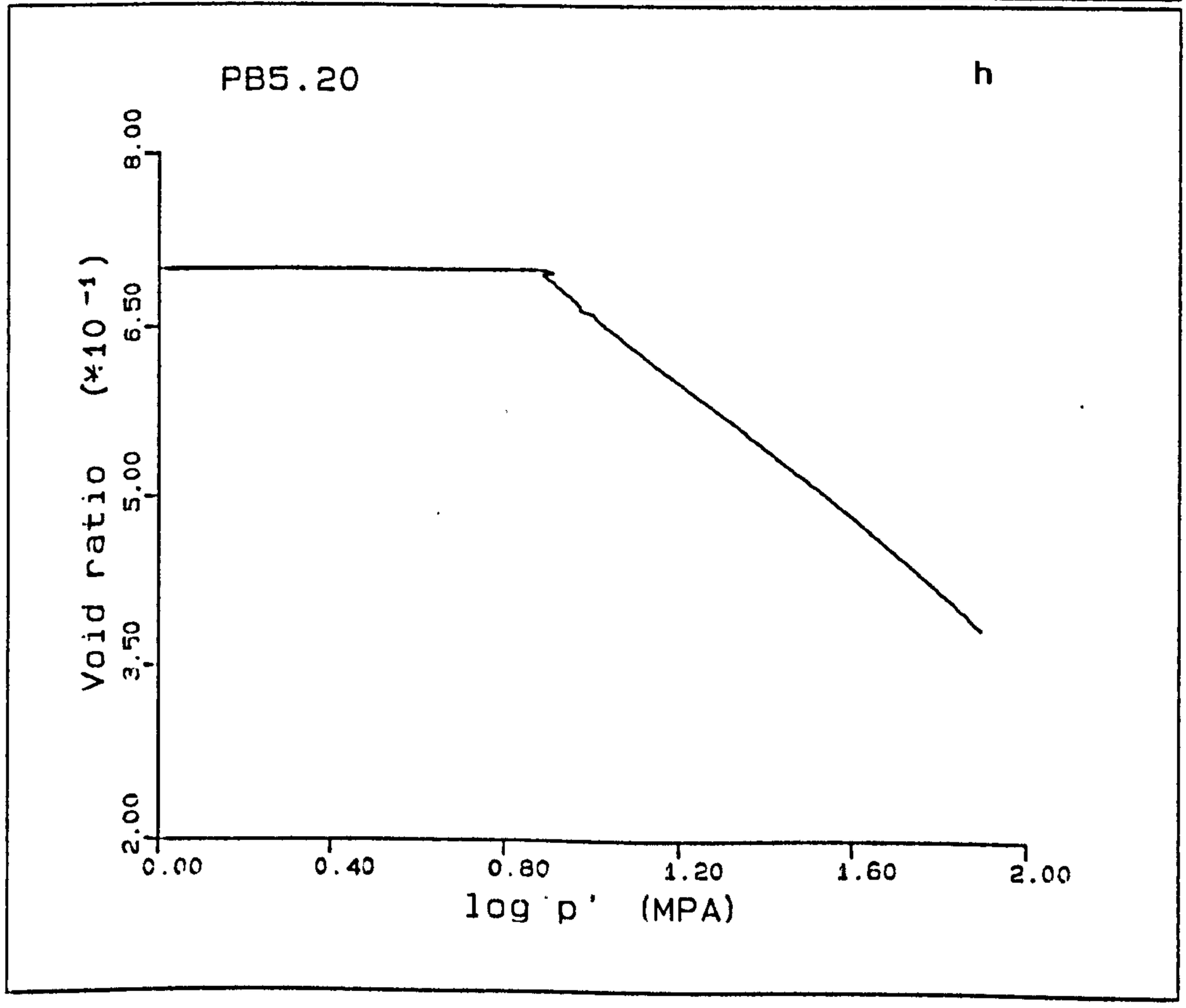
PB5.20
h
8.00
6.50
5.00
3.50
2.00
Void ratio (*10 -1)
0.00
0.40
0.80
1.20
1.60
2.00
log p' (MPA)

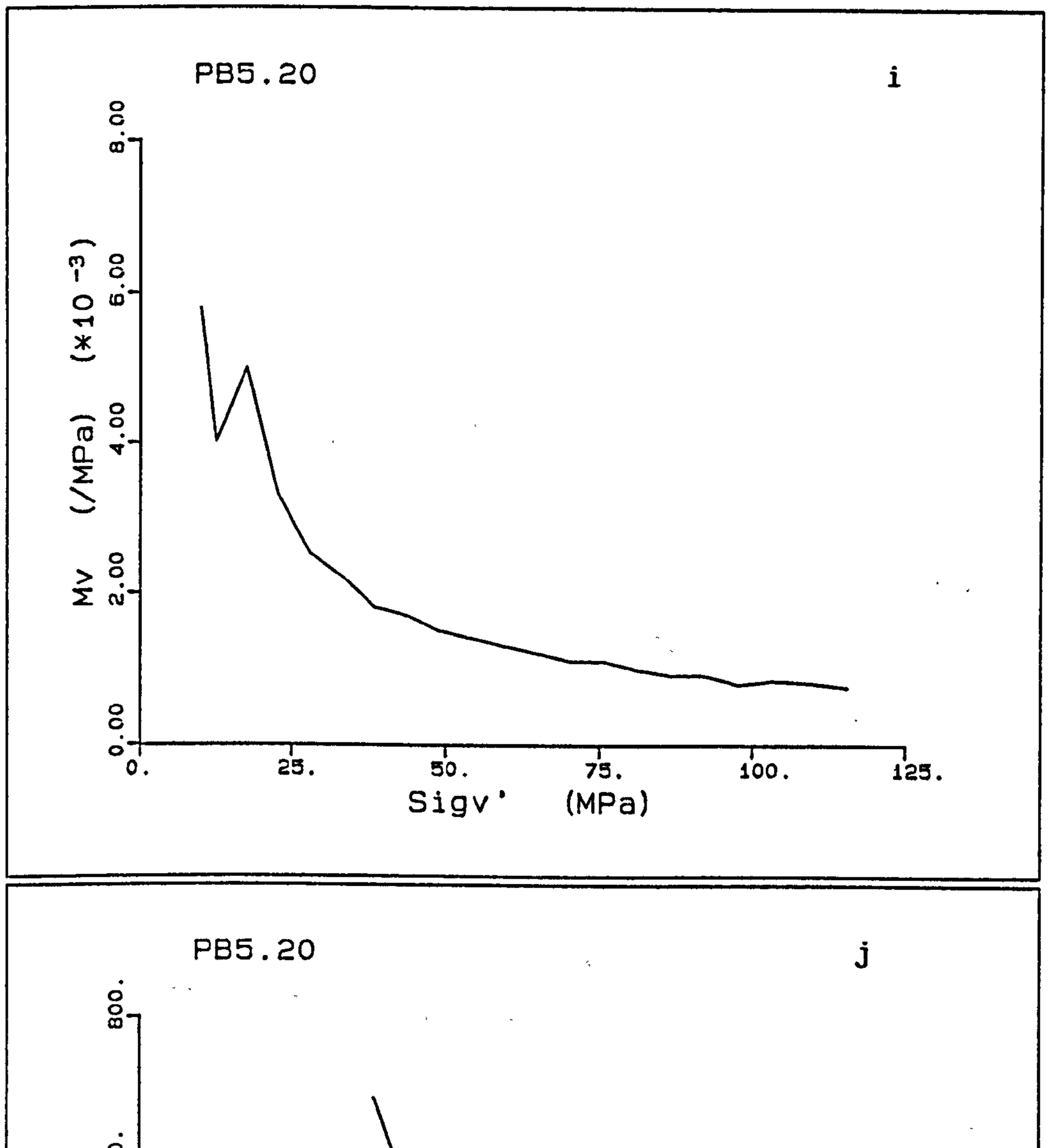
PB5.20
i
8.00
6.00
4.00
2.00
0.00
(*10 -3)
Mv (/MPa)
0.
25.
50.
75.
100.
125.
Sigv' (MPa)
PB5.20
j
800.
600.
400.
200.
0.
Cv (m2/yr)
0.
25.
50.
75.
100.
125.
Sigv' (MPa)

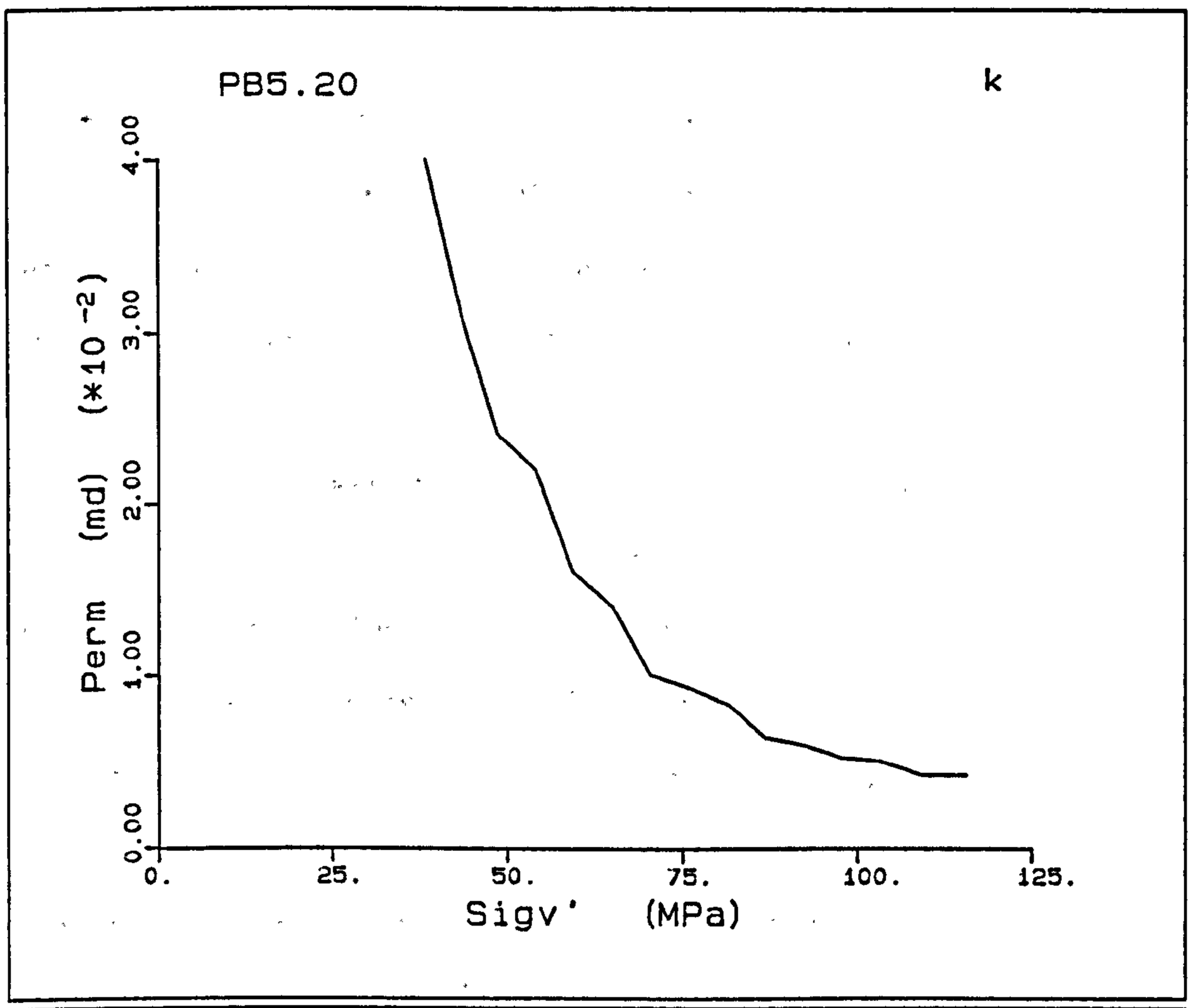
PB5.20
k
Perm (md) (*10 -2)
4.00
3.00
2.00
1.00
0.00
0.
25.
50.
75.
100.
125.
Sigv' (MPa)

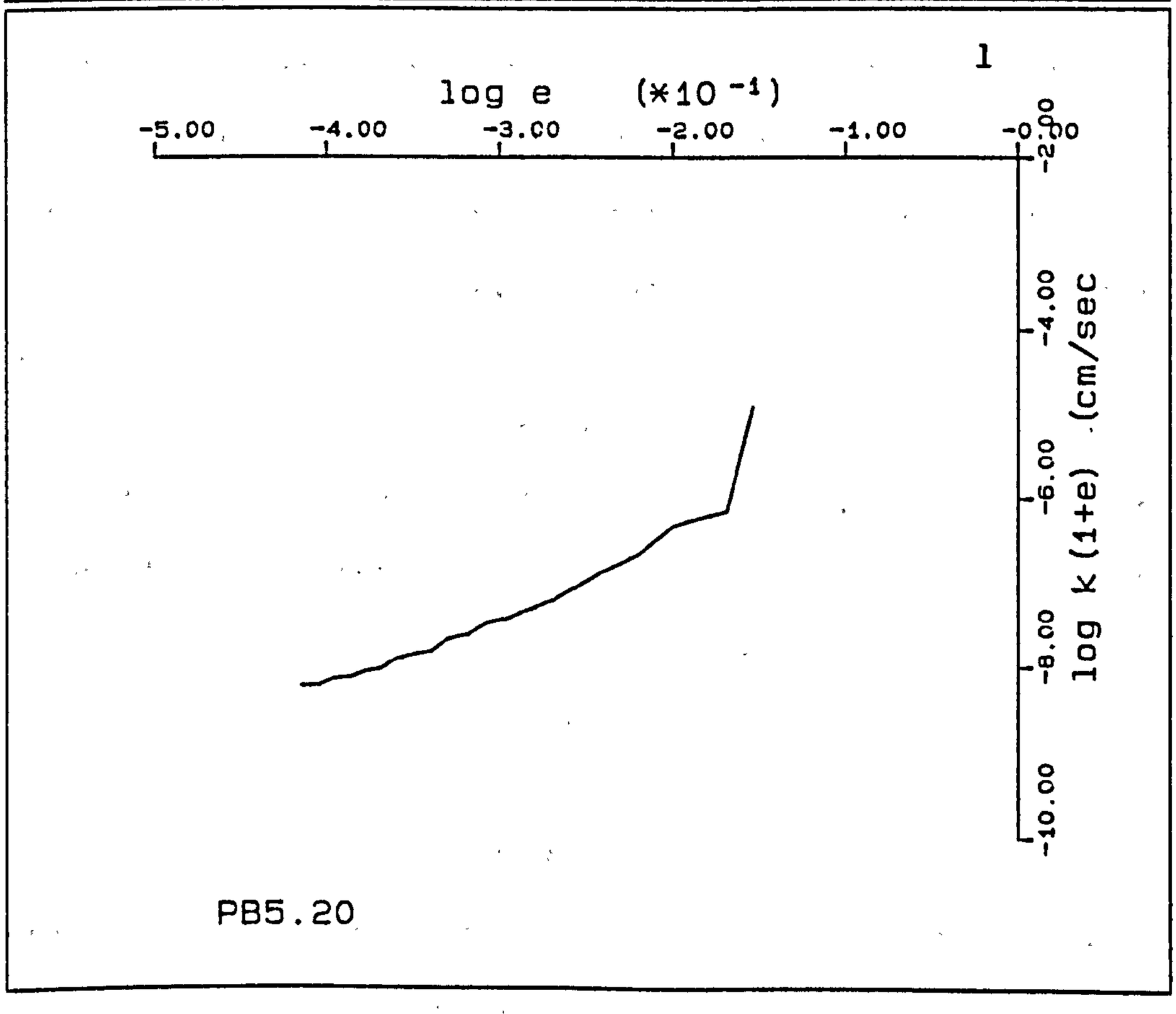
l
log e (*10 -1)
-5.00
-4.00
-3.00
-2.00
-1.00
-0.00
-2.00
-4.00
-6.00
-8.00
-10.00
log k (1+e) (cm/sec
PB5.20

PB6.20

This was the last of the 0 block samples, and was a repeat of PB5.20, performed at the same deformation rate, though in this test the servo mechanism controlling the zero lateral strain condition, was not adjusted manually with the resulting gradual increase in radial strain.

This experiment showed no linear elastic section in stress-strain space, Fig. A5.13a, this has been attributed to a gradual breakdown of the cementation during the compaction. The load increase levels off at a deviatoric stress of 5.2MPa, the post-yield transitional deformation being seen as a slight increase in q, after which the load increases more rapidly in q-p' space (Fig. A5.13b), corresponding to the normal consolidation deformation. The $\bar{K}_o$ values for these sections are $\bar{K}_{oe}$=0.367, $\bar{K}_{opc}$= 0.854, $\bar{K}_{onc}$=0.500. The normal consolidation is essentially linear in q-p' space with a deviation or a gradual increase in q above the linear trend at a mean effective stress of 39MPa, after which the K_o returns to the linear trend. This could be interpreted as a curve, but there is no evidence to support this at the moment.

The radial strain associated with the deformation gradually increasing from an average of $-7*10^{-3}$% to $7*10^{-3}$%, with some slight deviations off this general trend. The largest recorded deviations appearing at 1.4% and 4.5% axial strain with radial strains of $-31*10^{-3}$% and $16*10^{-3}$% respectively. The e-log p' plot, Fig. A5.13h, shows a trend of continually increasing slope, there is a step in the curve with a maximum offset at 14MPa mean effective stress. The pore pressure build up occured in this test, as in PB5.20, with the excess pressure occurring at an axial strain of 7% which gradually increases to reach 0.3MPa at an axial strain of 22.6%.

The peak M_v, Fig. A5.13i, of $5*10^{-3}MPa^{-1}$ gradually decreases to a value of $9*10^{-4}MPa^{-1}$ at 114MPa. The C_v and permeability gradually drops from $53066m^2/yr$ and 6.2mD to values of $196m^2/yr$ and 0.0056mD at a vertical effective stress of 114MPa. The trend of k(1+e) against e in log - log space shows the same slope as in PB5.20, in the normally consolidated range.

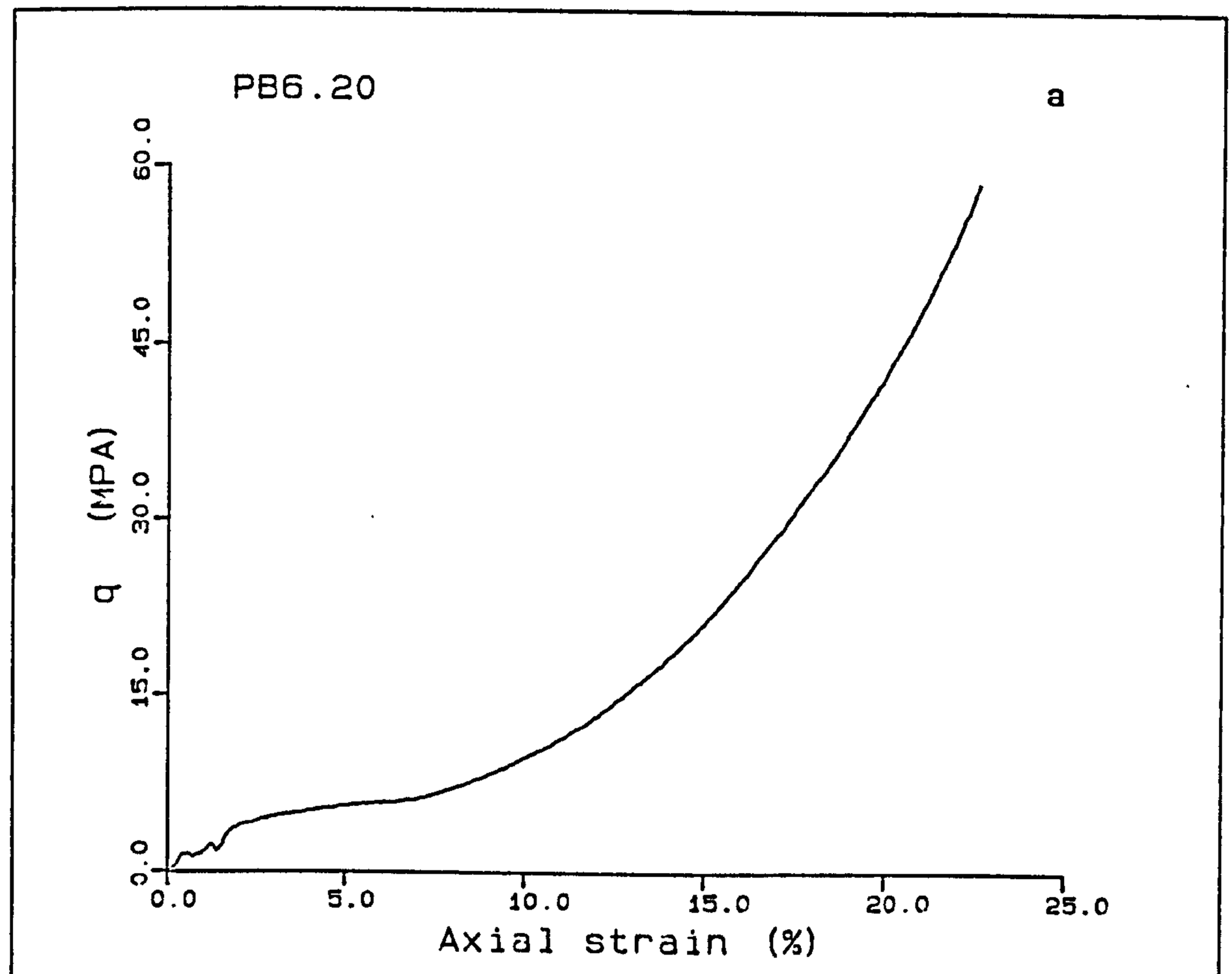

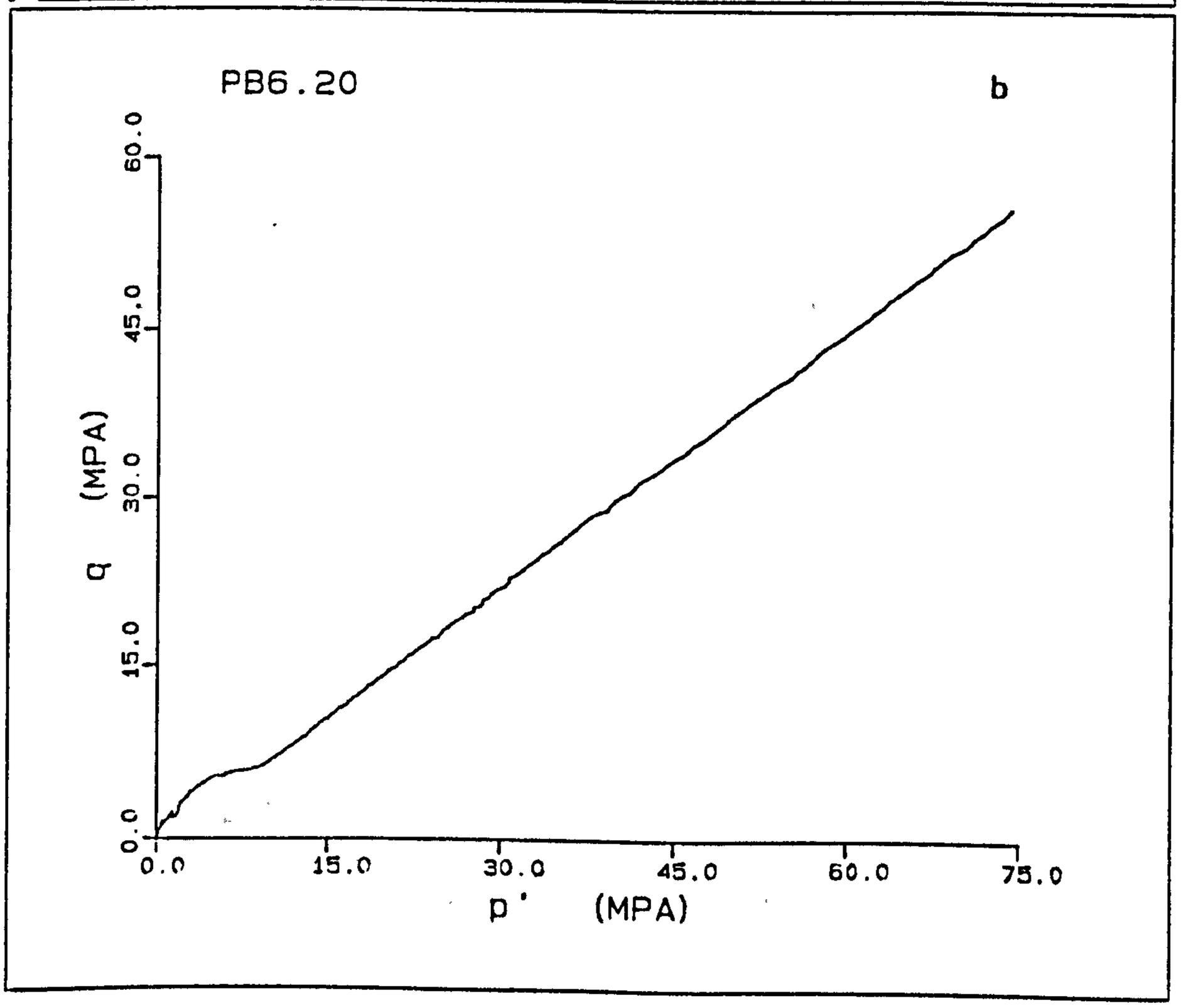

Figure A5.13(a-l) K_o test PB6.20.

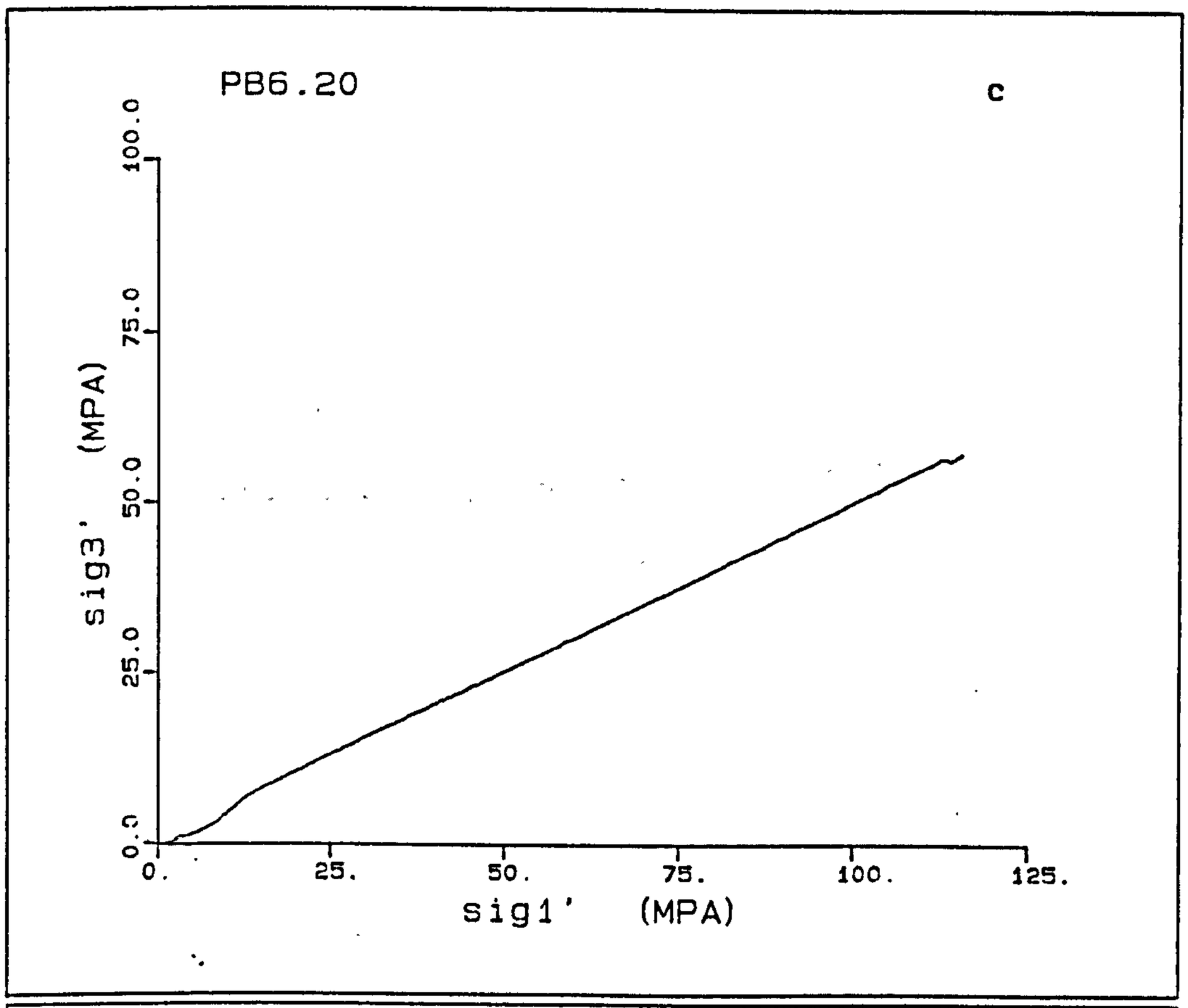
PB6.20
c
100.0
75.0
50.0
25.0
0.0
sig3' (MPA)
0.
25.
50.
75.
100.
125.
sig1' (MPA)

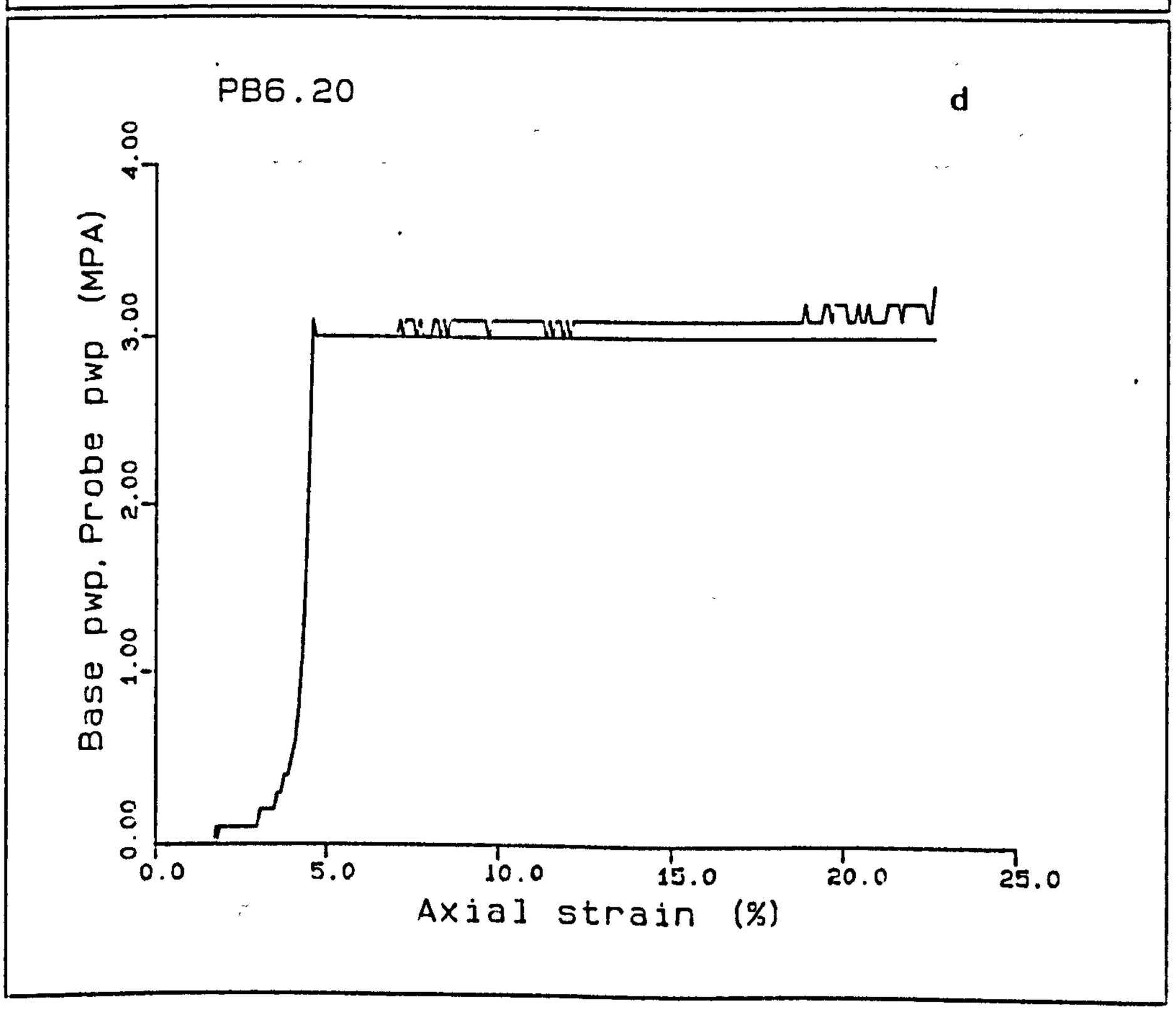
PB6.20
d
4.00
3.00
2.00
1.00
0.00
Base pwp, Probe pwp (MPA)
0.0
5.0
10.0
15.0
20.0
25.0
Axial strain (%)

PB6.20

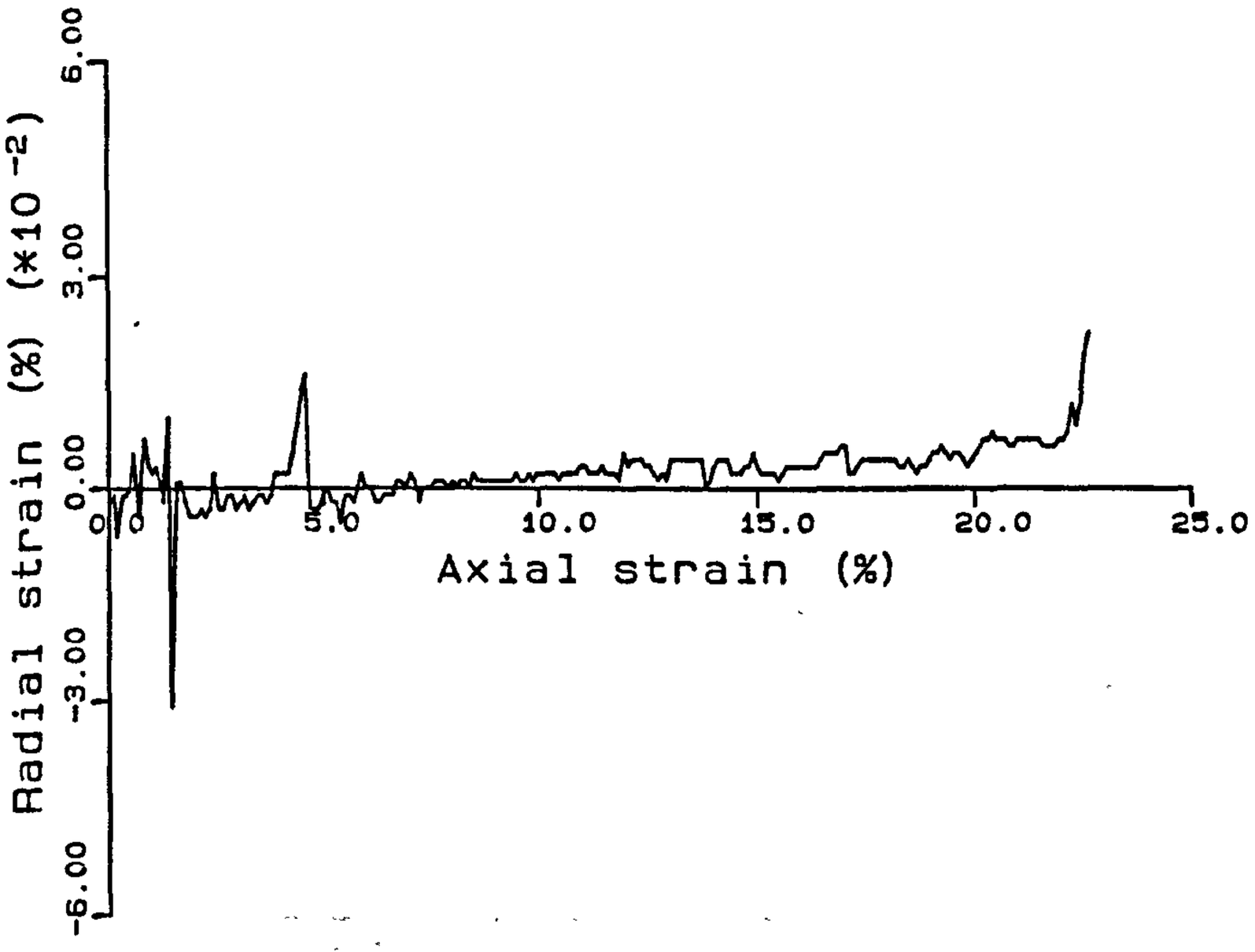
e
Radial strain (%) (*10 -2)
6.00
3.00
0.00
-3.00
-6.00
0.0
5.0
10.0
15.0
20.0
25.0
Axial strain (%)

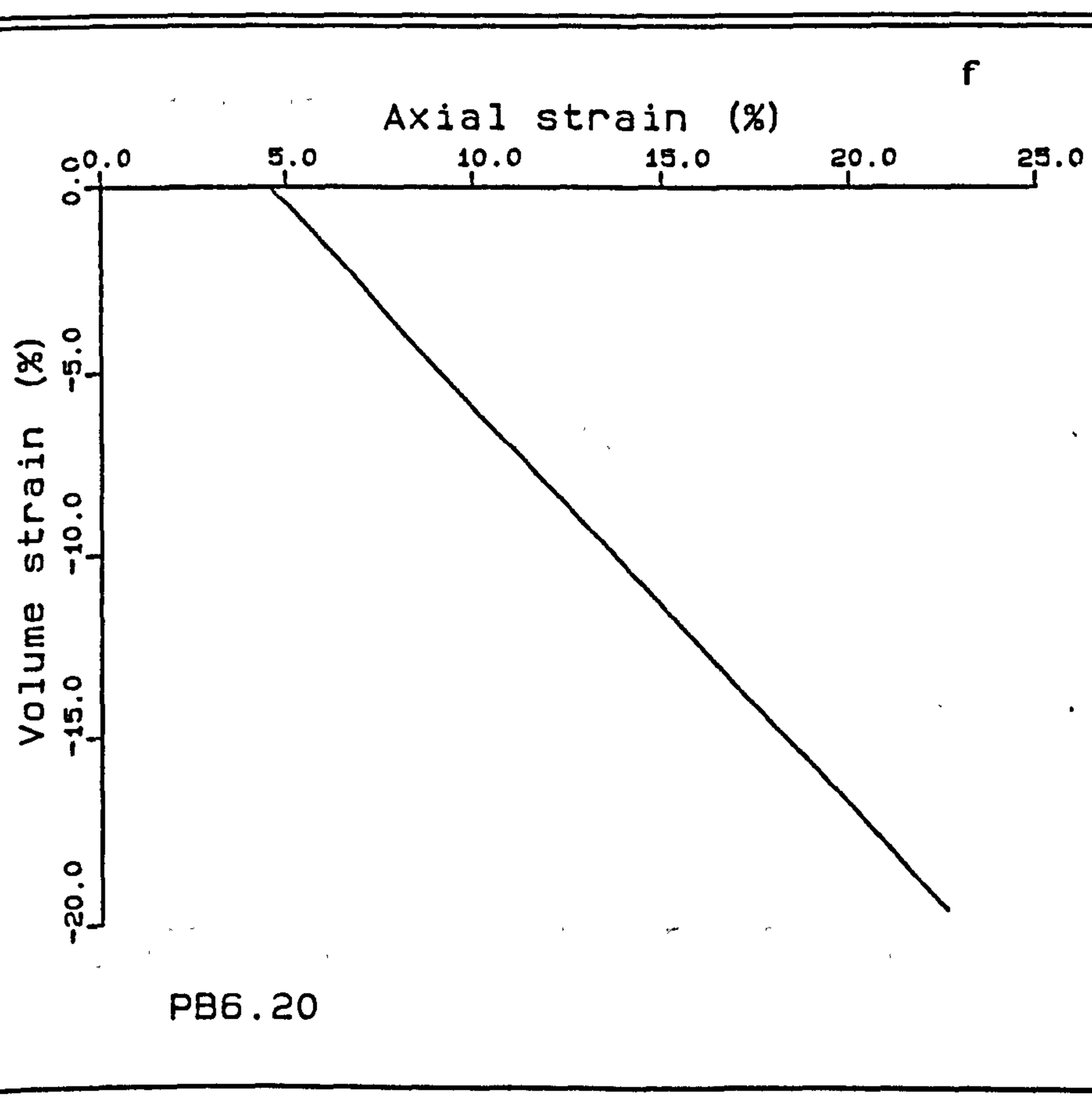
f
Axial strain (%)
0.0
5.0
10.0
15.0
20.0
25.0
Volume strain (%)
0.0
-5.0
-10.0
-15.0
-20.0

PB6.20

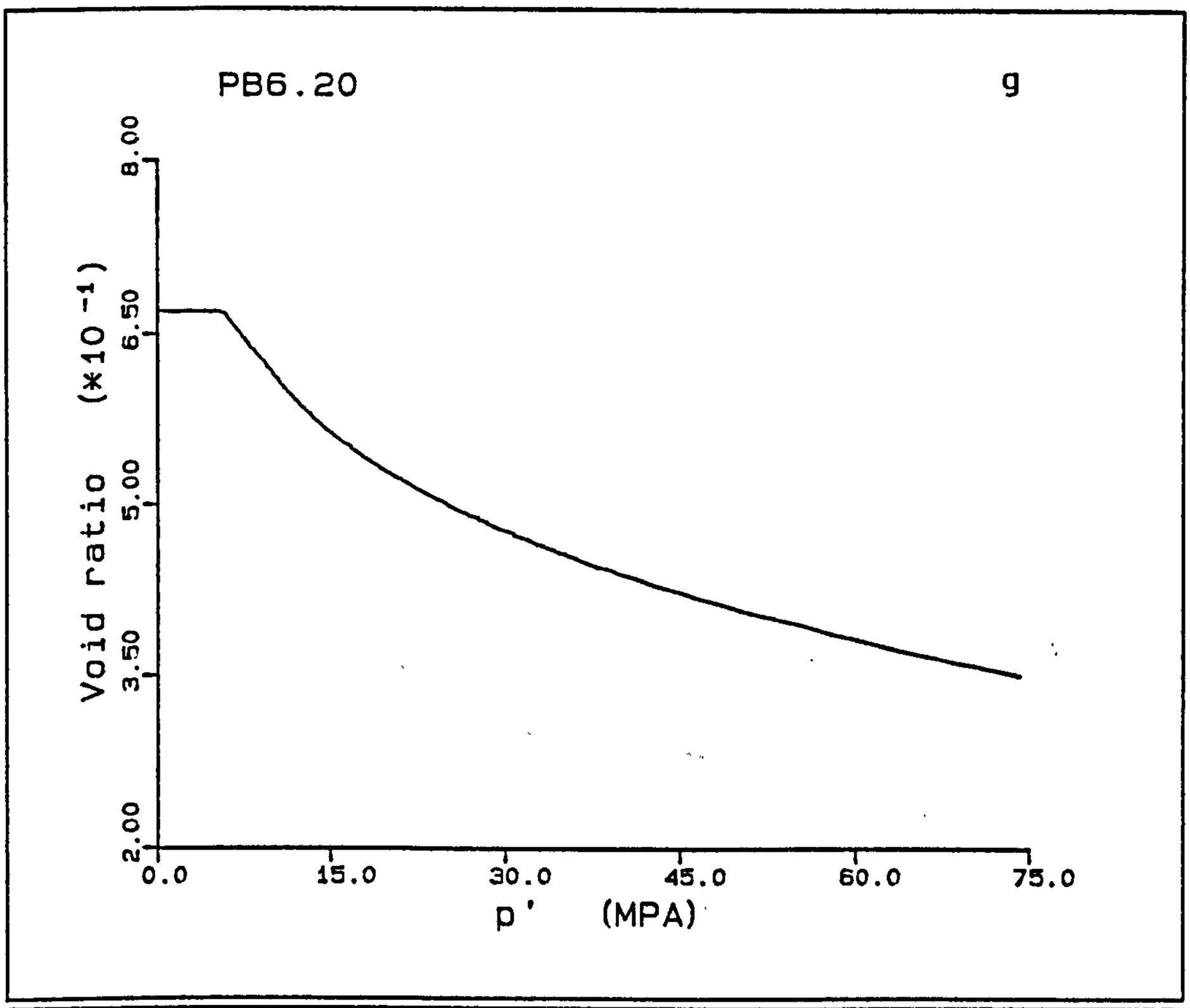
PB6.20
g
8.00
6.50
5.00
3.50
2.00
(*10 -1)
Void ratio
0.0
15.0
30.0
45.0
60.0
75.0
p' (MPA)

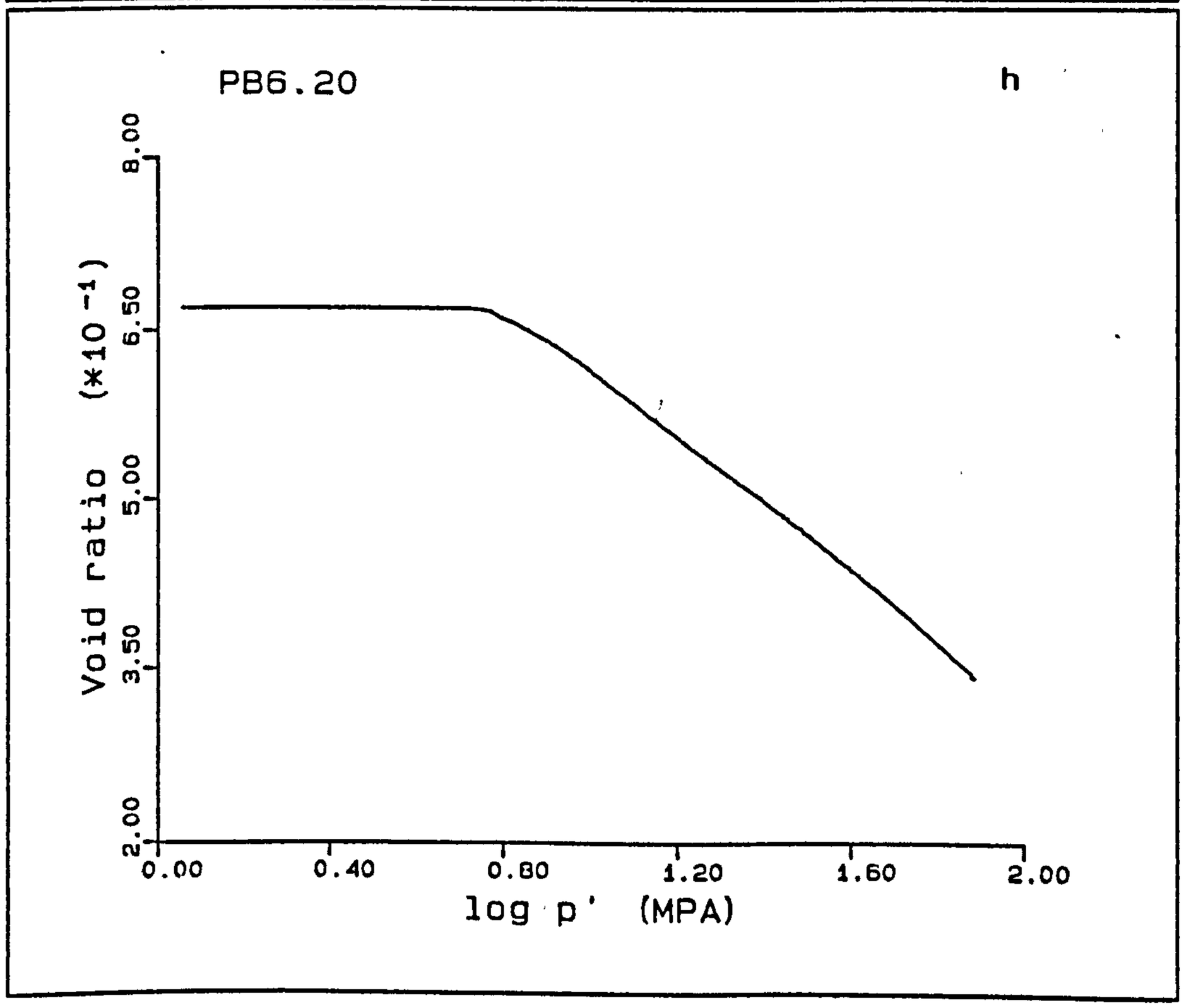
PB6.20
h
8.00
6.50
5.00
3.50
2.00
(*10 -1)
Void ratio
0.00
0.40
0.80
1.20
1.60
2.00
log p' (MPA)

PB6.20 i

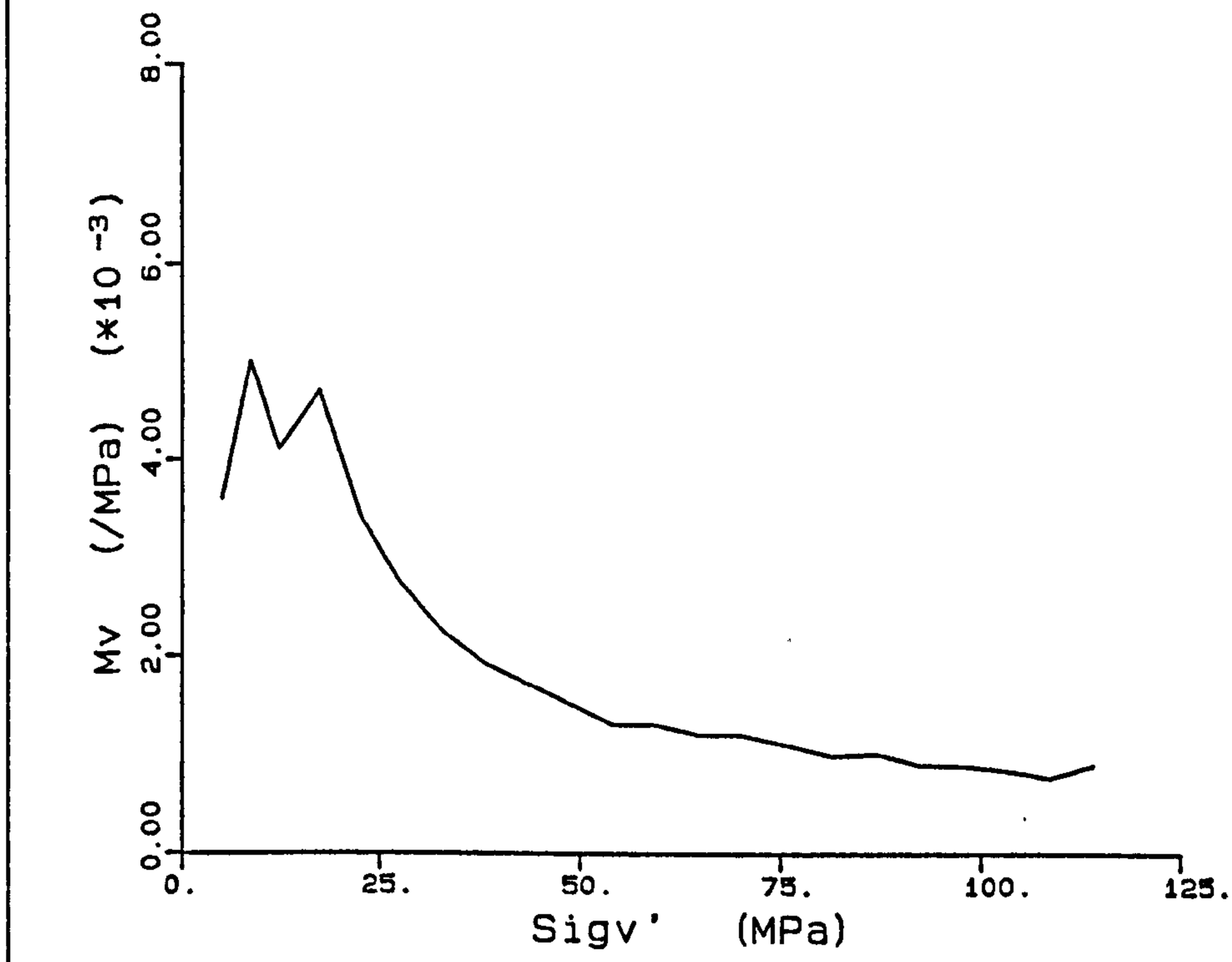

PB6.20 j

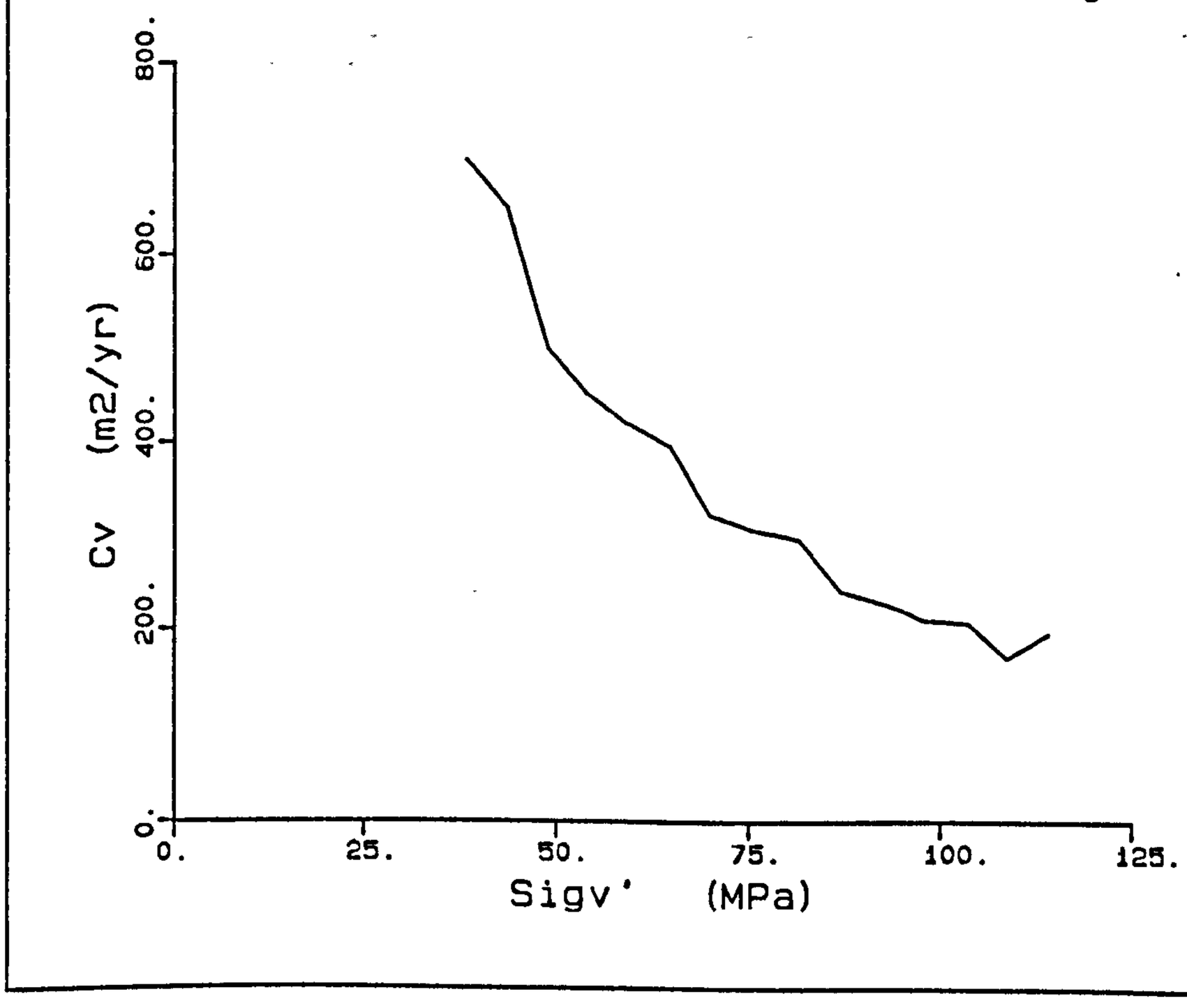

PB6.20

k

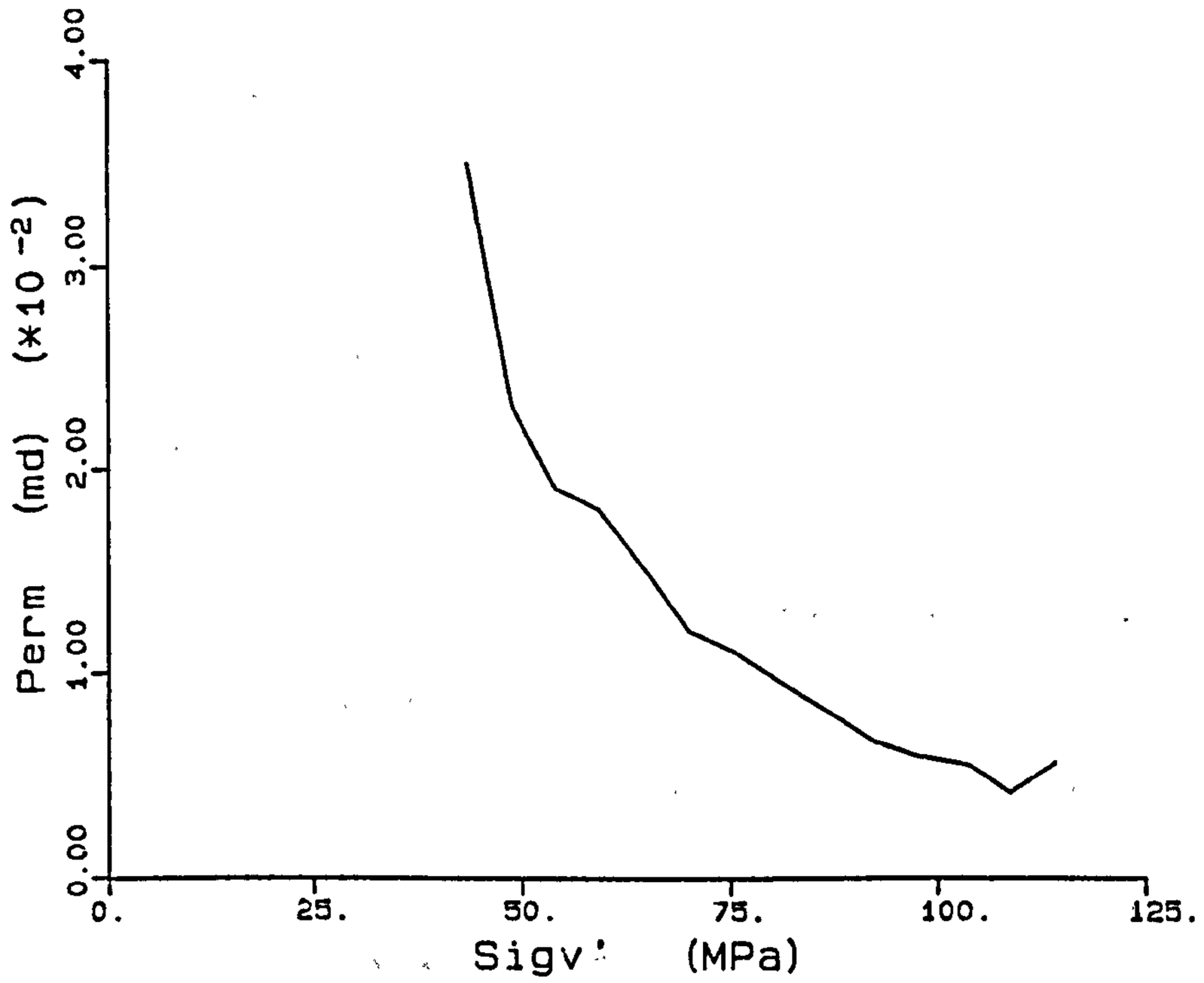

l

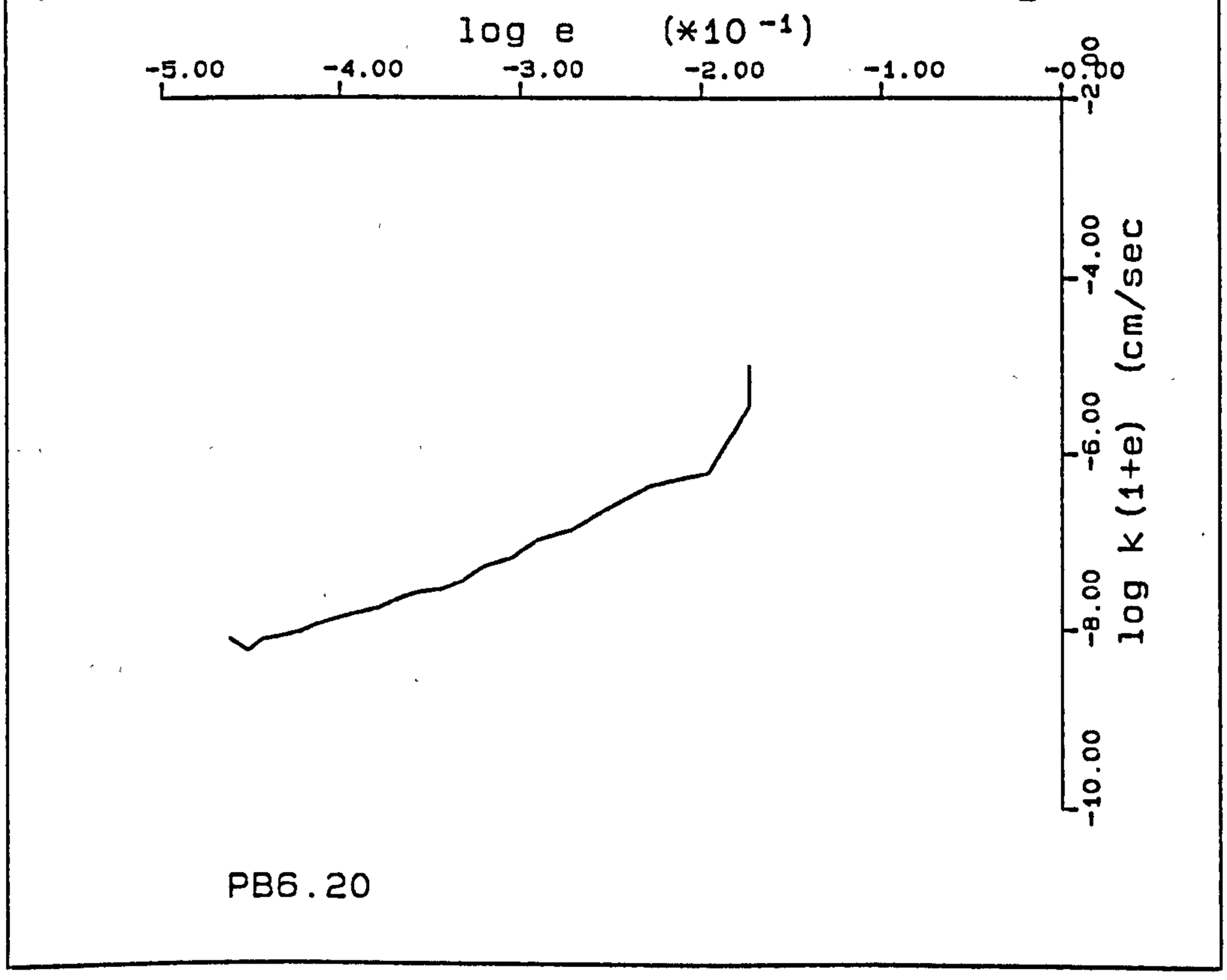

PB6.20

PB7.20

PB7.20 was the first sample from M block, and was deformed at a rate of 0.008mm/min. The initial stiff, elastic response, has a Young's modulus of 1.72GPa. As the yield point is approached, a step occurs, with the load decreasing and recovering to a yield stress of 5.0MPa. The constant deviatoric stress section is followed by a nearly linear work hardening section in q-p' space. At an axial strain of about 10% there is a slight deviation towards lower deviatoric stress than that predicted by the linear trend, and at 15.5% axial strain, a larger deviatoric stress occurs, thereafter the linear trend is re-established. These variations correspond to a decrease in the radial strain at 10% axial strain and a slight increase at around 15% axial strain. The deviation of radial strain throughout the experiment was less than $10*10^{-3}$%. Three peaks occured outside this general range at 0.6%, 12.5% and 15.6% axial strain with radial strains of $-21*10^{-3}$%, $-10*10^{-3}$%, and $-27*10^{-3}$%. The $\bar{K}_o$ values for the pore collapse and normal consolidation deformations are 1.294 and 0.516 respectively; the high value for the transition section is due to the decrease in the deviator stress of 0.5MPa.

The volume starts to record at an axial strain of 6.2% where the pore pressures reach 3.1MPa, no build up of excess pore pressures is seen in this experiment. The e-log p' plot (Fig. A5.14h) shows increasing slopes of the plot at increasingly higher stress, as seen in tests PB3.20 and PB5.20.

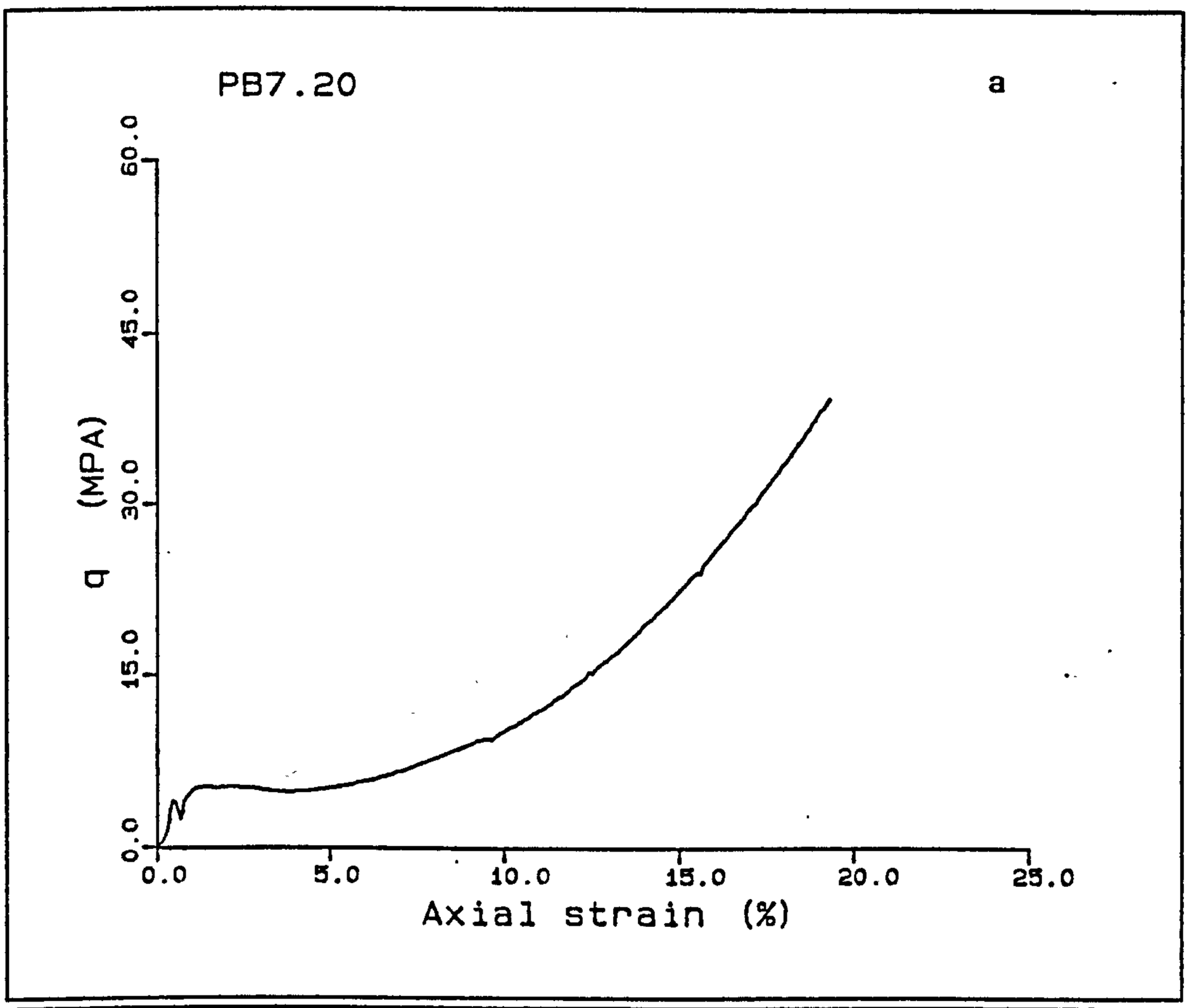

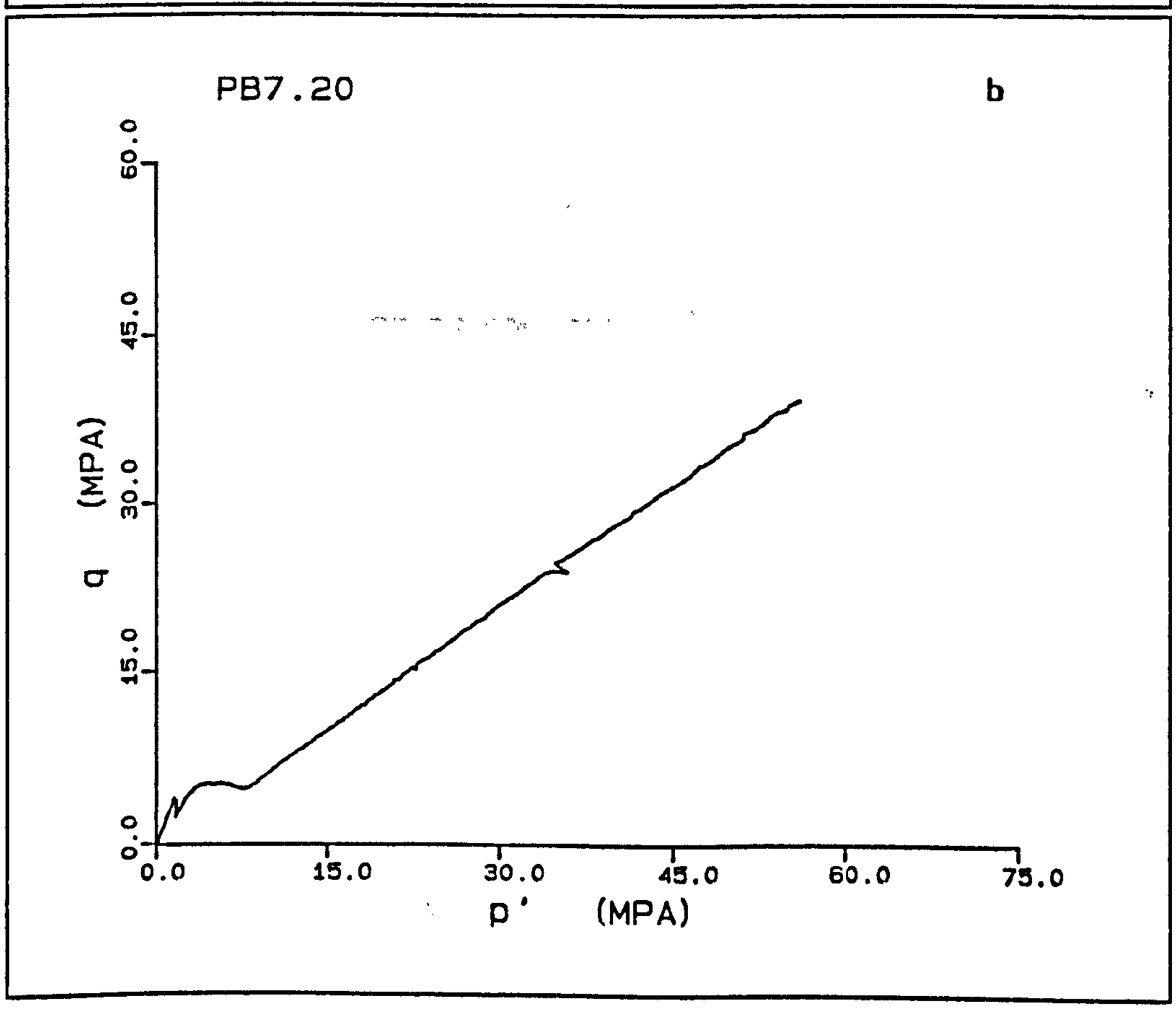

Figure A5.14(a-h) K_o test PB7.20.

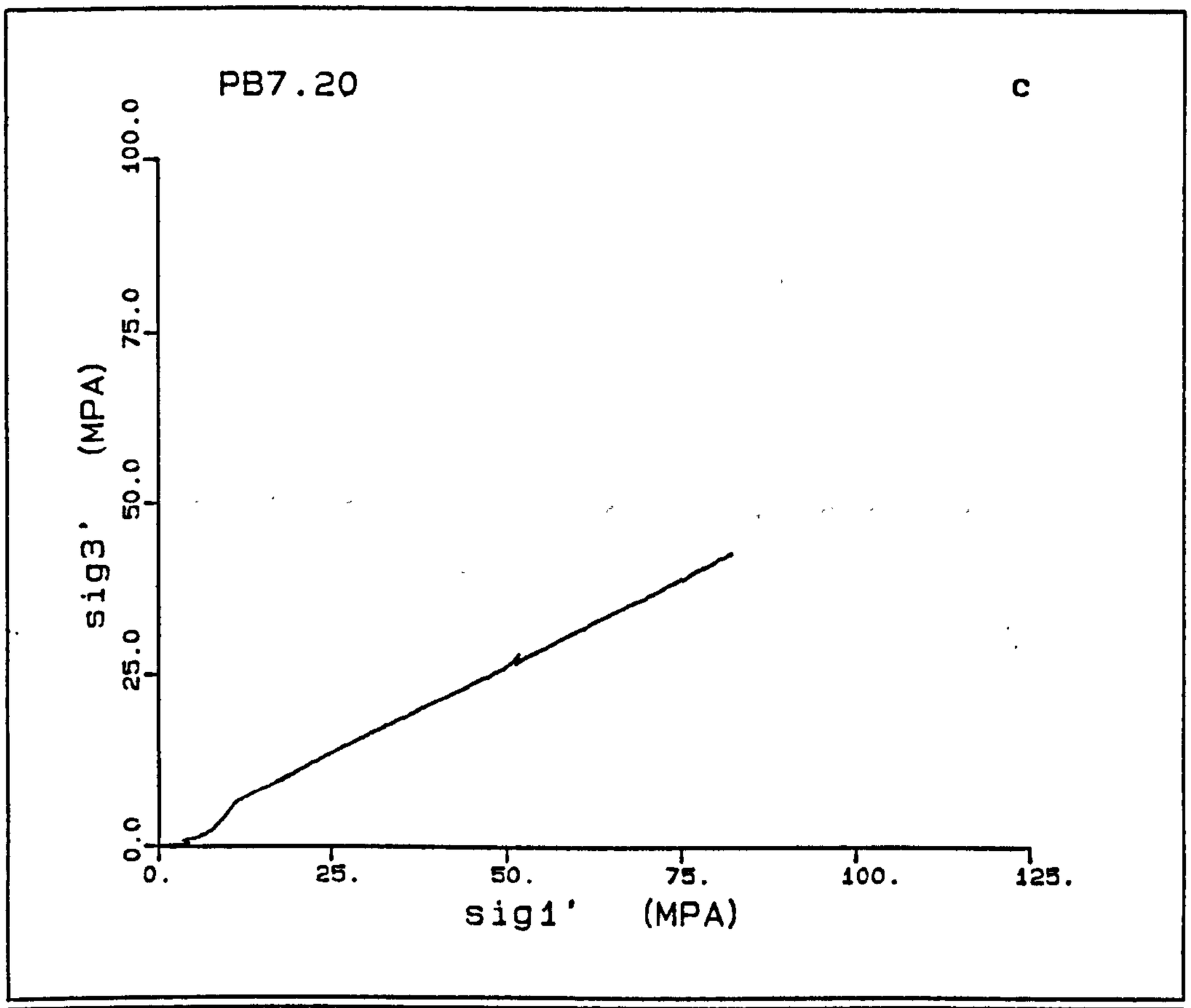
PB7.20
c
sig3' (MPA)
100.0
75.0
50.0
25.0
0.0
0.
25.
50.
75.
100.
125.
sig1' (MPA)

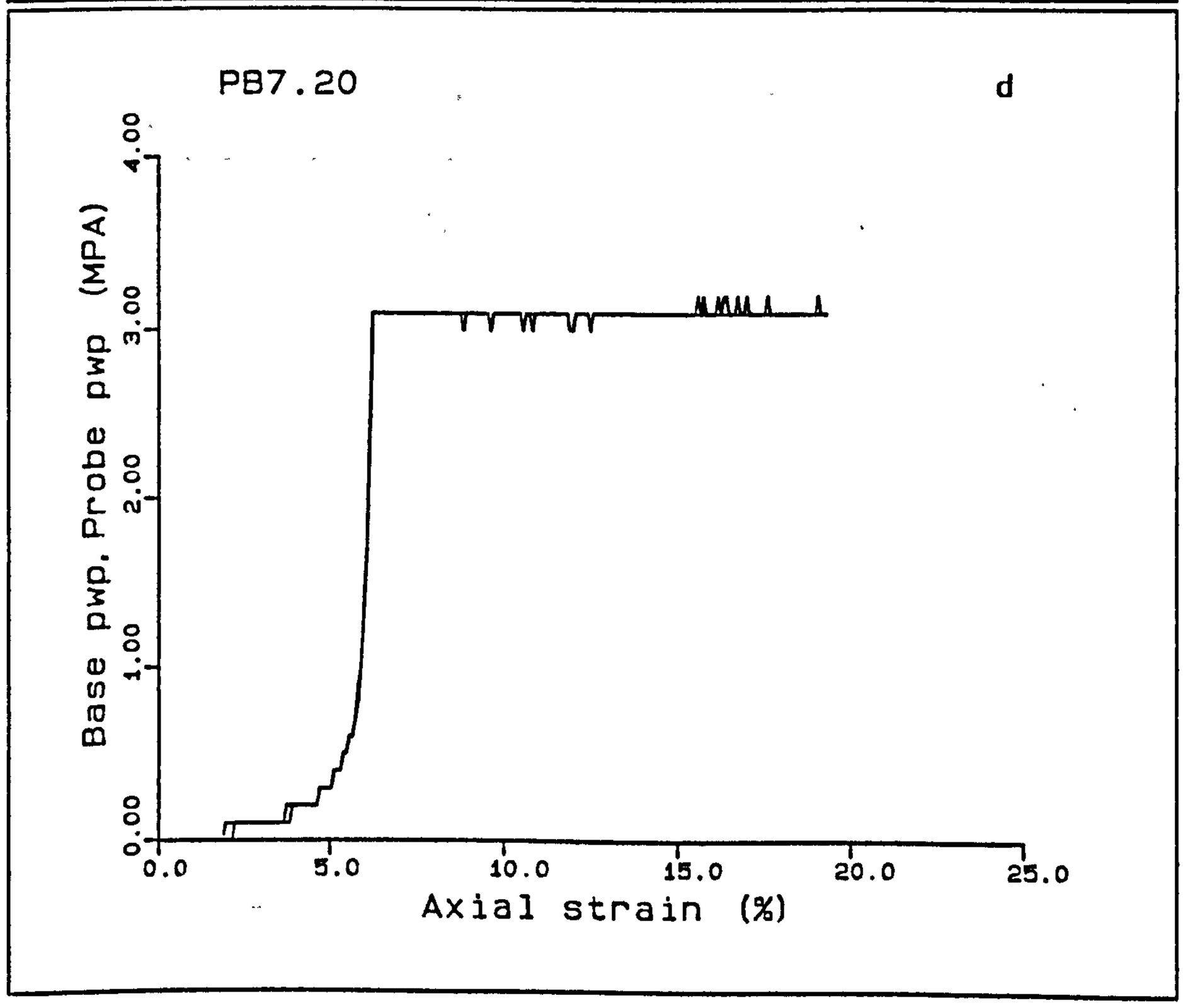
PB7.20
d
Base pwp. Probe pwp (MPA)
4.00
3.00
2.00
1.00
0.00
0.0
5.0
10.0
15.0
20.0
25.0
Axial strain (%)

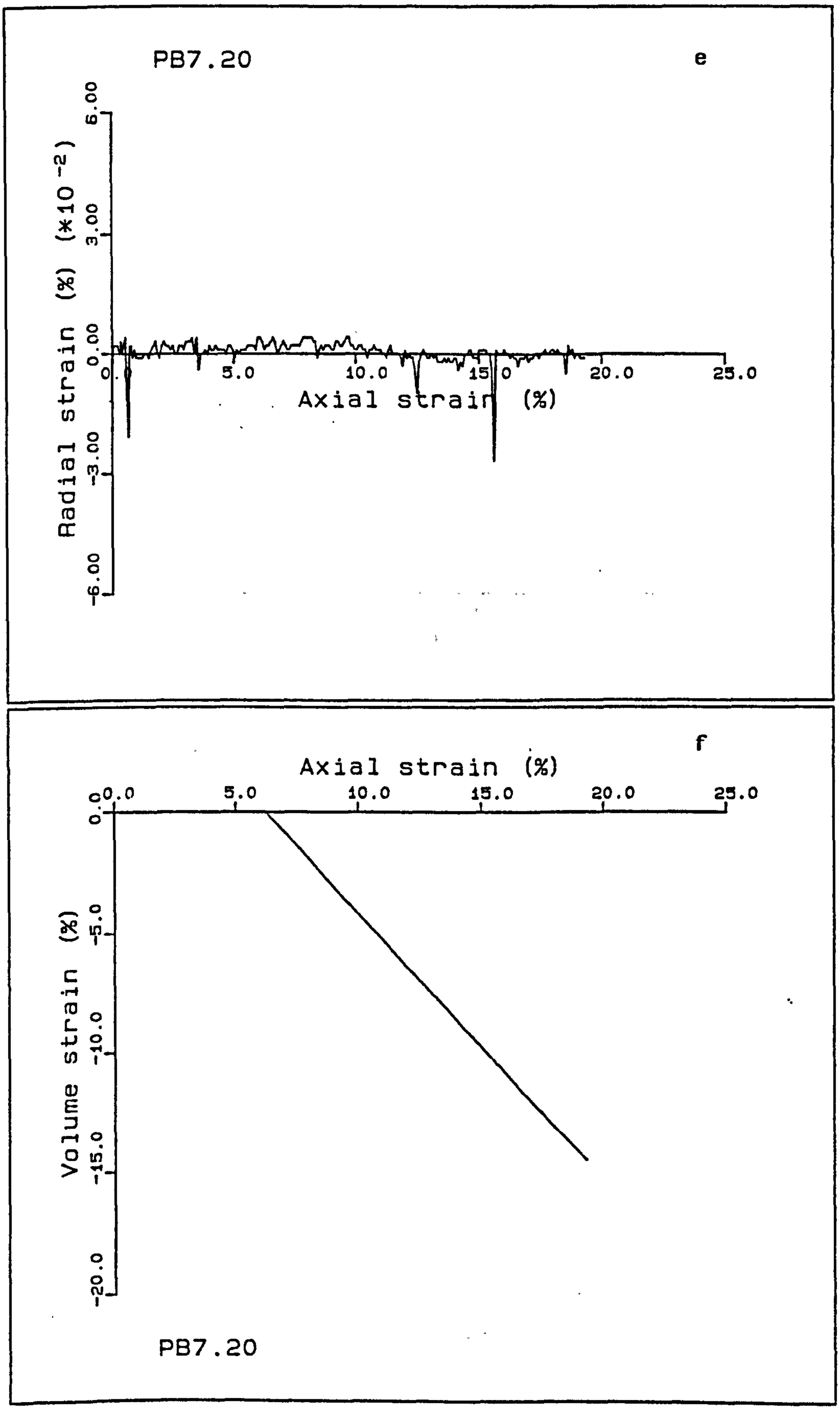
PB7.20
e
Radial strain (%) (*10 -2)
6.00
3.00
0.00
-3.00
-6.00
0.0
5.0
10.0
15.0
20.0
25.0
Axial strain (%)
f
Axial strain (%)
0.0
5.0
10.0
15.0
20.0
25.0
Volume strain (%)
0.0
-5.0
-10.0
-15.0
-20.0
PB7.20

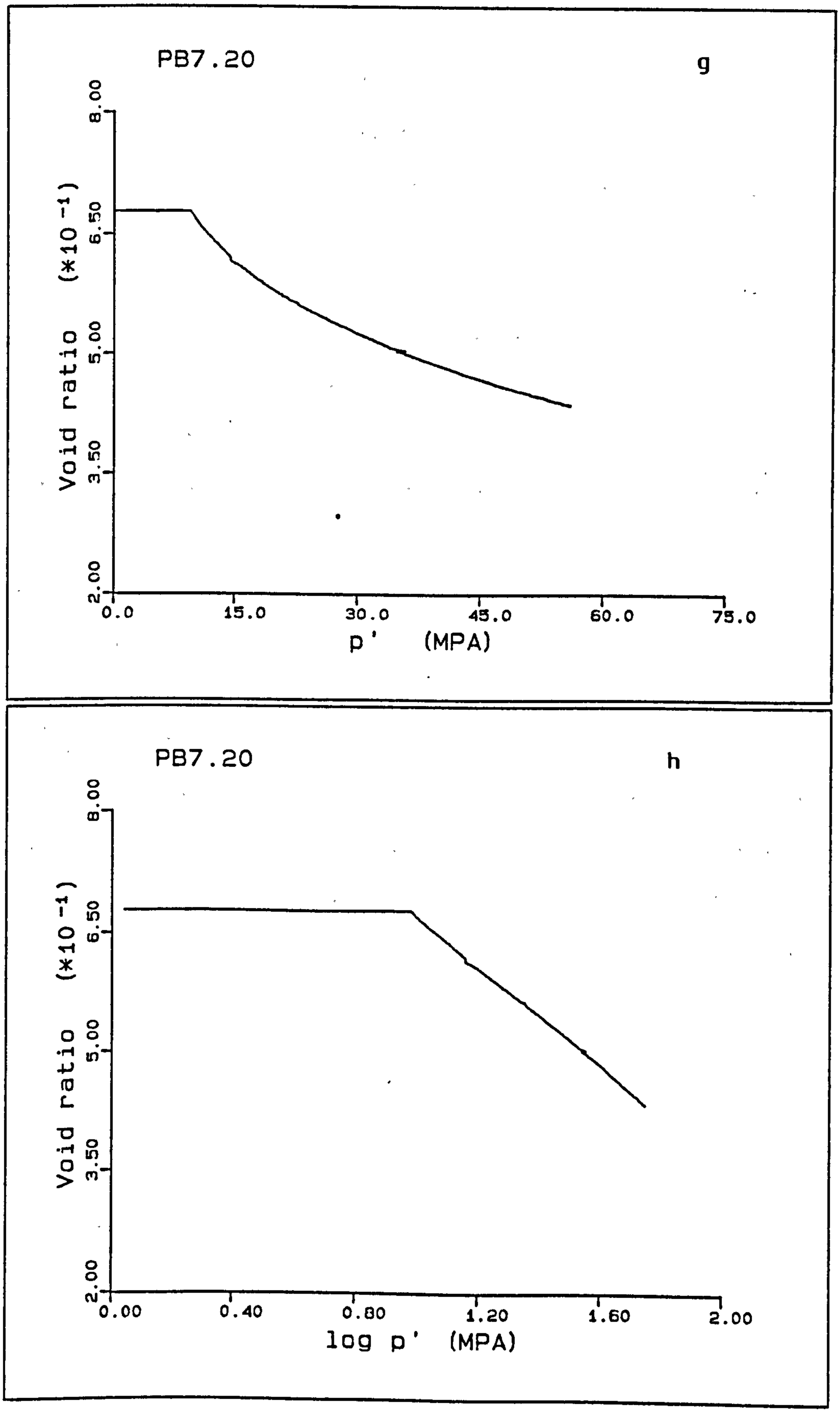
PB7.20
g
8.00
6.50
5.00
3.50
2.00
Void ratio (*10 -1)
0.0
15.0
30.0
45.0
60.0
75.0
p' (MPA)
PB7.20
h
8.00
6.50
5.00
3.50
2.00
Void ratio (*10 -1)
0.00
0.40
0.80
1.20
1.60
2.00
log p' (MPA)

PB8.20

This sample was used to repeat PB3.20 using a sample from M block. The Young's modulus for the cemented region of the deformation is 1.49GPa, the sample yielding at a deviatoric stress of 4.5MPa. Again near the yield, a step occurs due to a decrease in load which is subsequently recovered. The post-yield deformation is seen as a decrease in load sustainable by the sample in the transitional section, this being seen by a $\bar{K}_{opc}$ of 1.441. The work hardening or normally consolidated behaviour is seen to show a linear trend in Fig.A.15b, with a small deviation off the trend in the first part of the plastic stage. The $\bar{K}_o$ values of the elastic and work hardening deformations are 0.377 and 0.529 respectively. The radial strain variation were generally kept below $6*10^{-3}$%, with three peaks outside this range at axial strains of 0.5%, 3% and 21.3% with radial strains $-12*10^{-3}$%, $6*10^{-3}$% and $14*10^{-3}$% respectively.

The volume strains are recorded after 3.0% axial strain, where the pore pressures reach 3.1MPa, the loading of the back pressure regulator. The base pore pressure then decreases to 3.0MPa at an axial strain of 5%. The e-log p' diagram shows better than any of the previous tests the three deformational trends, in volume change with increasing pressure.

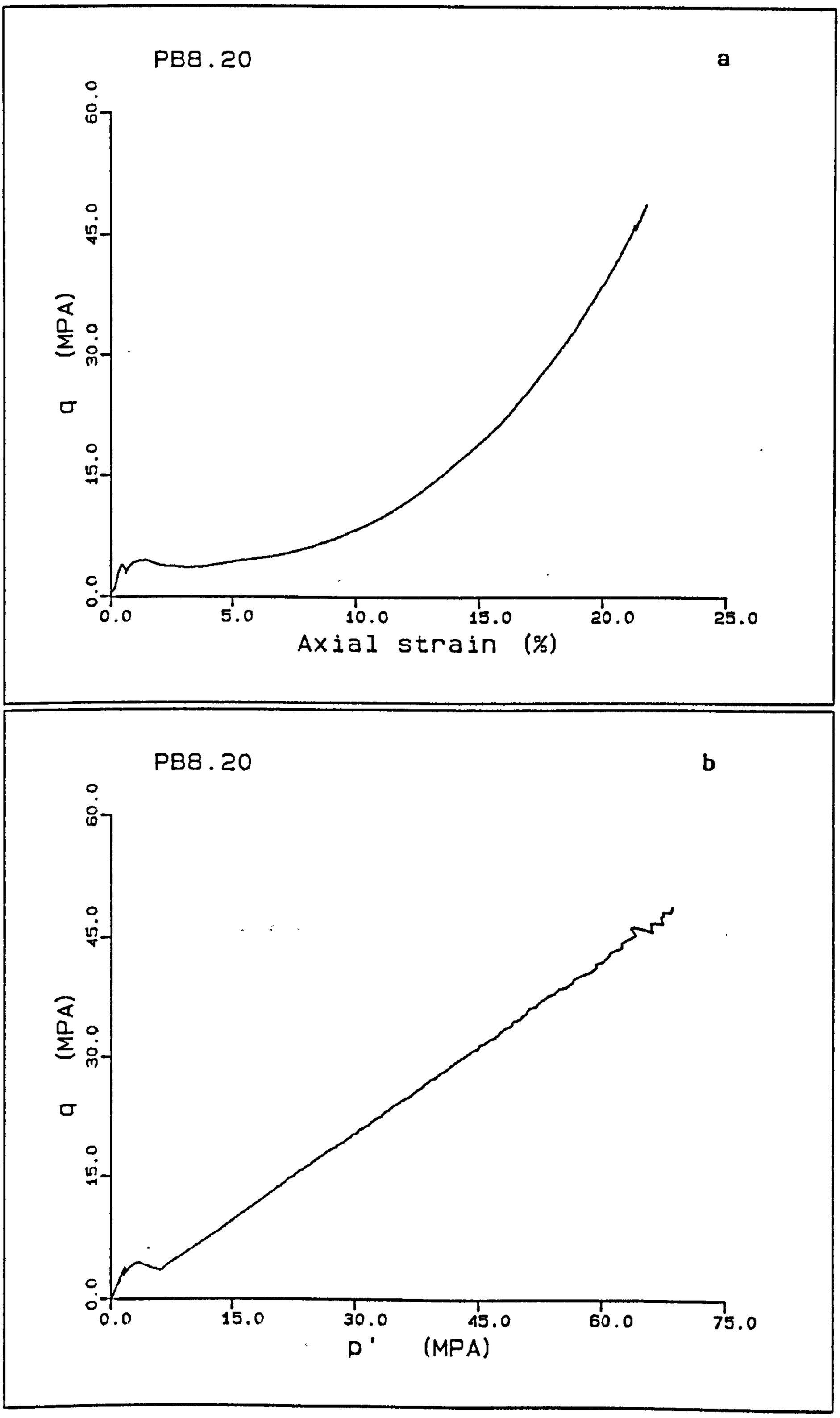

Figure A5.15(a-h) K_o test PB8.20.

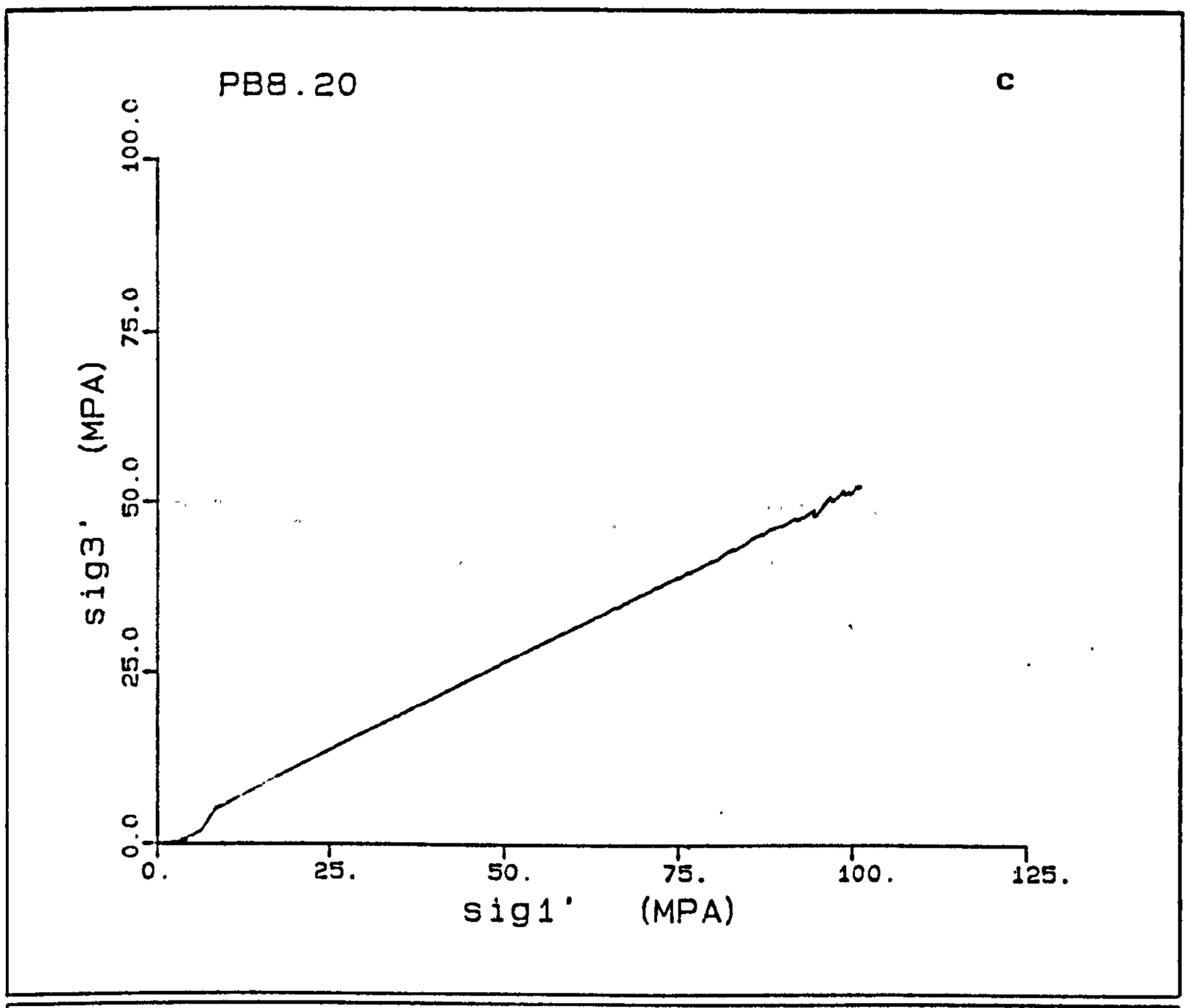
PB8.20
c
sig3' (MPA)
0.0
25.0
50.0
75.0
100.0
0.
25.
50.
75.
100.
125.
sig1' (MPA)

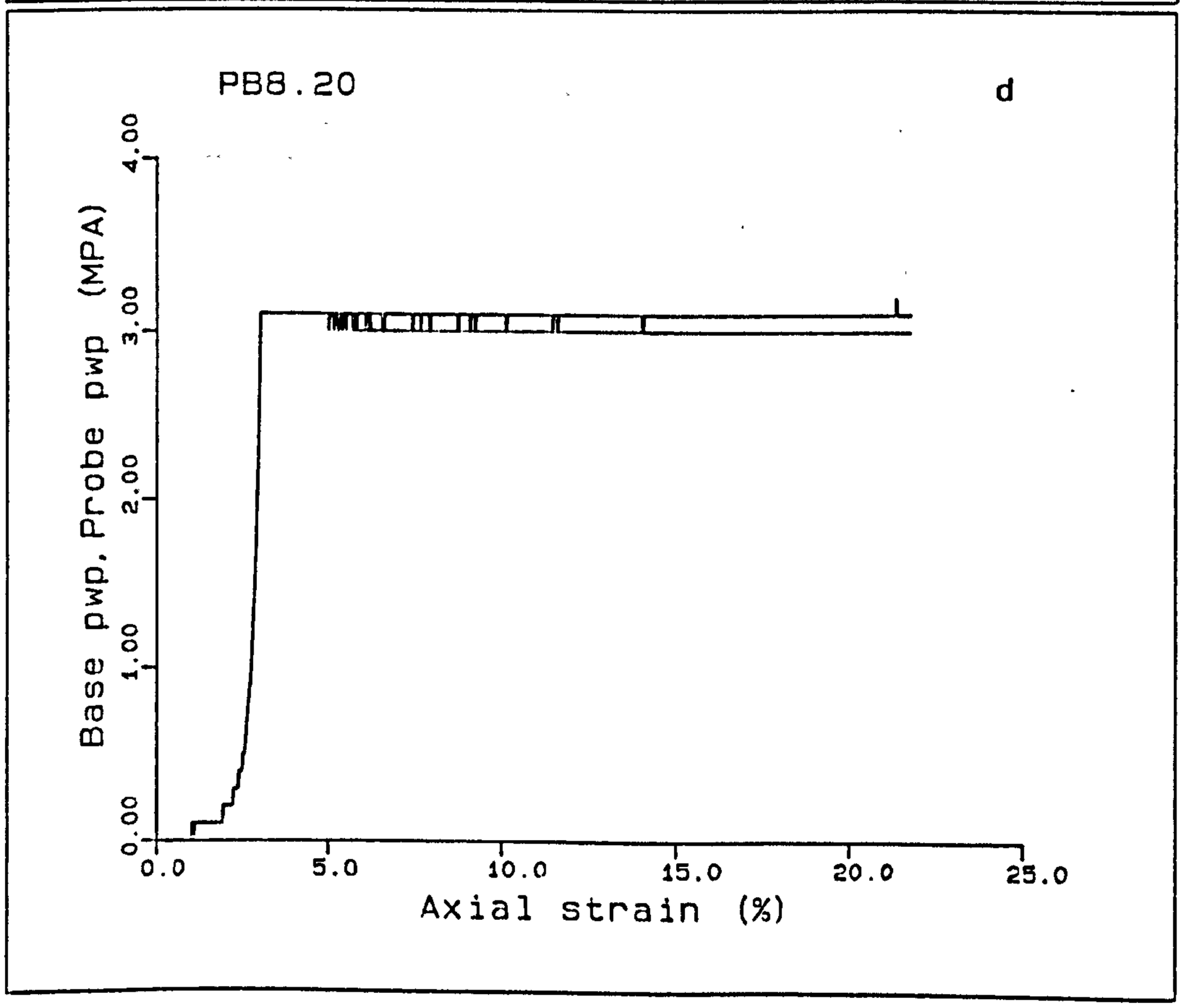
PB8.20
d
Base pwp, Probe pwp (MPA)
0.00
1.00
2.00
3.00
4.00
0.0
5.0
10.0
15.0
20.0
25.0
Axial strain (%)

PB8.20

e

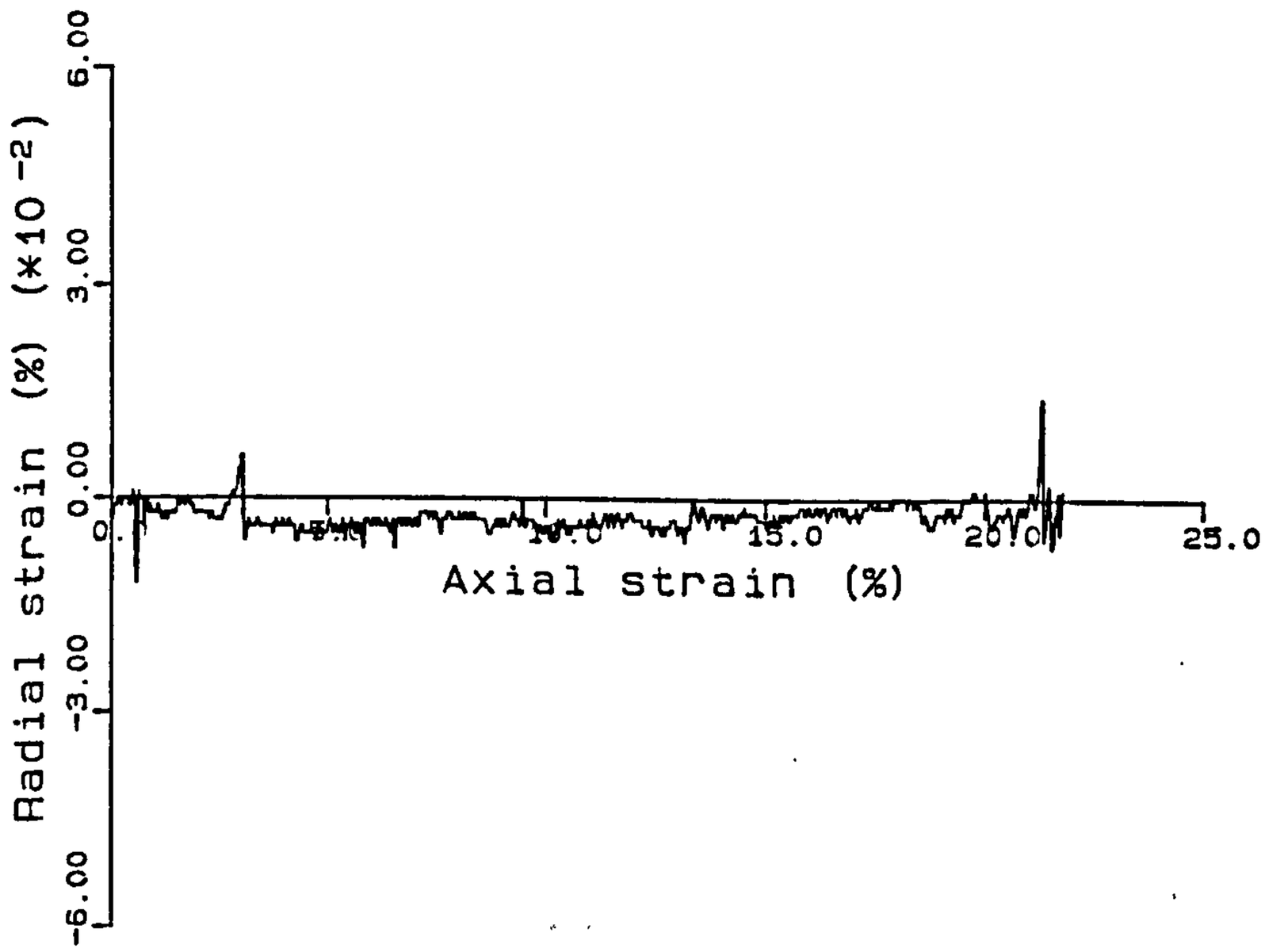

f

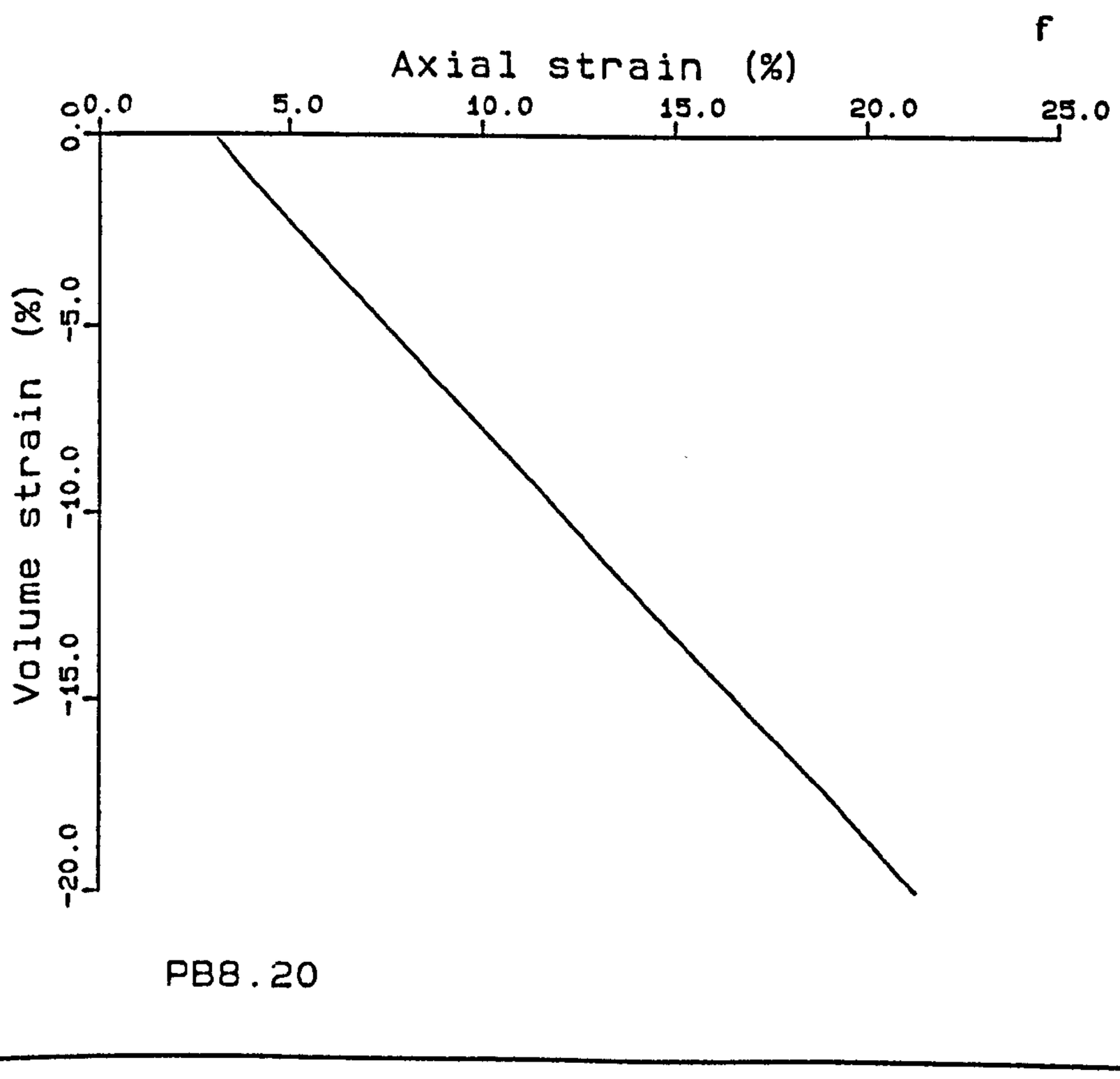

PB8.20

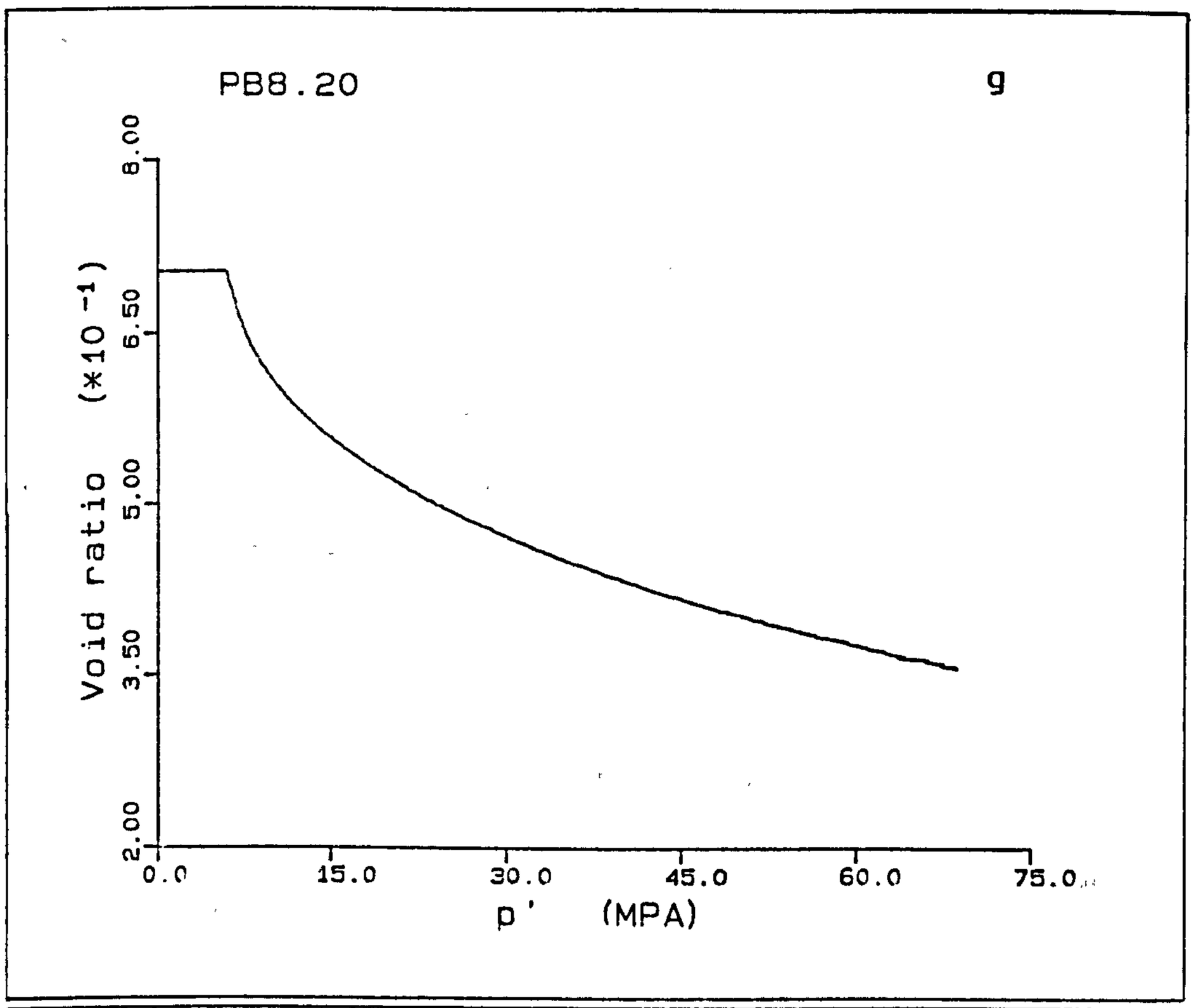
PB8.20
g
8.00
6.50
5.00
3.50
2.00
(*10 -1)
Void ratio
0.0
15.0
30.0
45.0
60.0
75.0
p' (MPA)

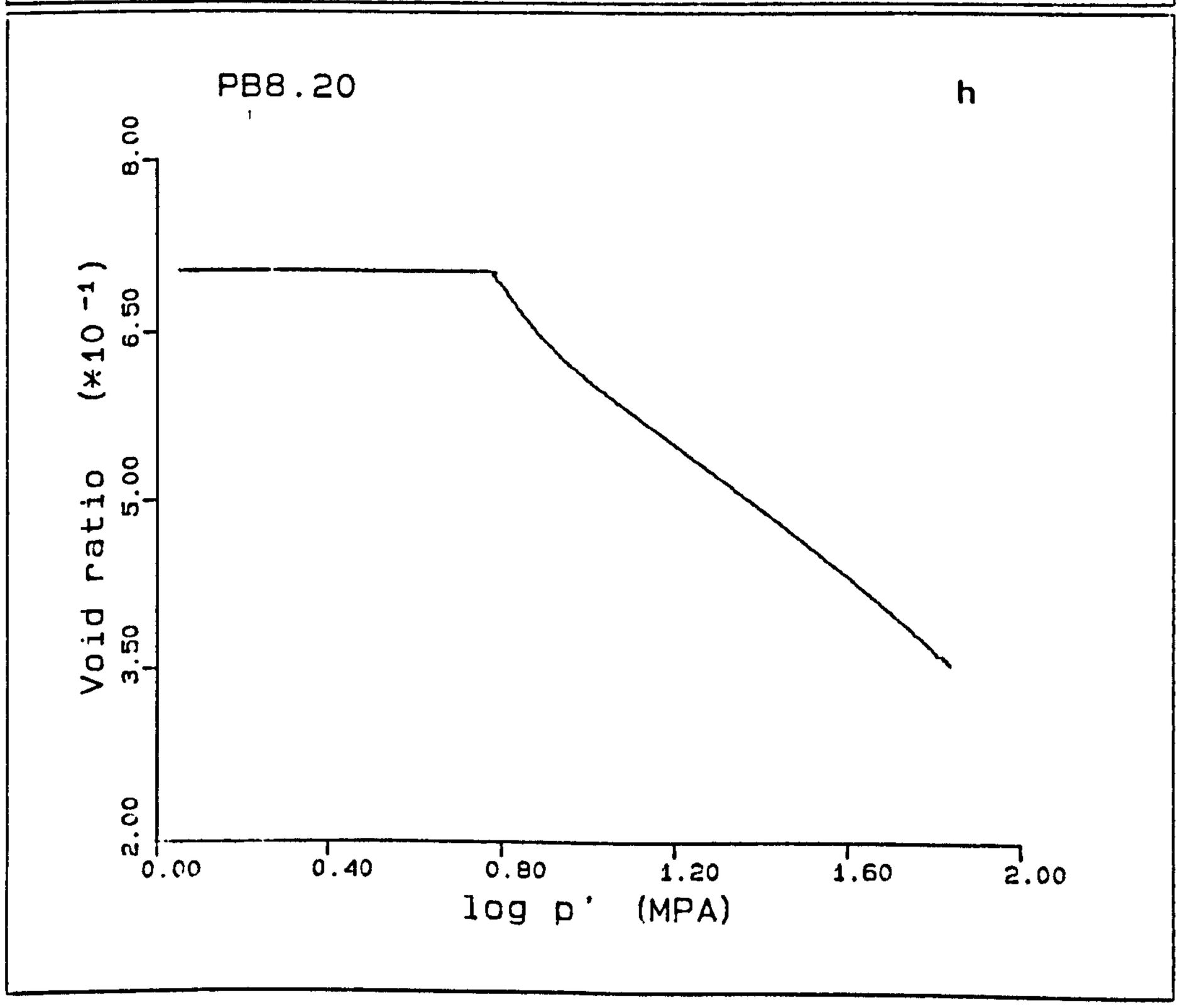
PB8.20
h
8.00
6.50
5.00
3.50
2.00
(*10 -1)
Void ratio
0.00
0.40
0.80
1.20
1.60
2.00
log p' (MPA)

A5.3) SAMPLE SHAPE

In this series of tests all of the chalk samples used were from Pegwell Bay, Kent (Chap. 3.5.2). The tests PB9.20, PB15.20, PB16.20 and PB17.20 were used to determine the effect of the height to diameter ratio on the compactional behaviour of chalks, Table A5.3. PB8.20 was also used in this study. PB8.20 and PB9.20 were tested at the same deformation rate but with different heights, while PB15.20, PB16.20 and PB17.20 were tested at the same strain rate but with differing height to diameter (H/D) ratios. Thus, by combining the two sets of tests, we can see the effects of varying strain rates on samples of similar height to diameter ratios.

The test conditions and details concerning the samples are presented in Table A5.3.

Table A5.3

Sample	Porosity %	Rate of loading mm/min	Average height mm	Average diameter mm	Saturated weight g	Dry weight g	Specific gravity g/cm3
PB9.20	41.3	0.03	24.81	37.66	54.42	43.58	2.69
PB15.20	42.5	0.01	73.83	37.62	161.38	126.82	2.69
PB16.20	42.5	0.0068	50.16	37.62	109.77	86.10	2.69
PB17.20	43.0	0.0033	24.38	37.56	53.24	41.38	2.69

PB9.20

This is a sample from M block of height 24.81mm with a height to diameter ratio of 0.658. It was deformed at a rate of 0.03mm/min, and is directly comparable to PB8.20. The initial deformation shows an irregular response to loading, and no initial modulus was obtained. The yield point occurs at 6.1MPa, the post-yield deformation being characterised by a decrease in load. The normal consolidation deformation shows a linear trend in q-p' space with no significant deviation off this trend. The $\bar{K}_o$ values for the deformation of this sample are $\bar{K}_{oe}$=0.324, $\bar{K}_{opc}$=1.470 (reflecting the decrease in the load carrying capacity of the chalk), and $\bar{K}_{onc}$=0.532. The variation in radial strain with the deformation is predominantly below $10*10^{-3}$%, with peaks outside this range occurring at 7.2% and 9.7% axial strain, the accompanying radial strains being $17*10^{-3}$% and $-10*10^{-3}$%. These are not seen as deviations in stress-strain or q-p' space.

The volume change measurements begin at an axial strain of 7.2% where a pore pressure of 3.2MPa is reached, this decreases to 3.1MPa by 7.5% axial strain, thereafter remaining constant. The plot of axial strain versus volume strain shows a decrease in slope at 17.7% axial strain despite no apparent change in the radial strain variation. The e - log p' plot shows the three stage volume deformation.

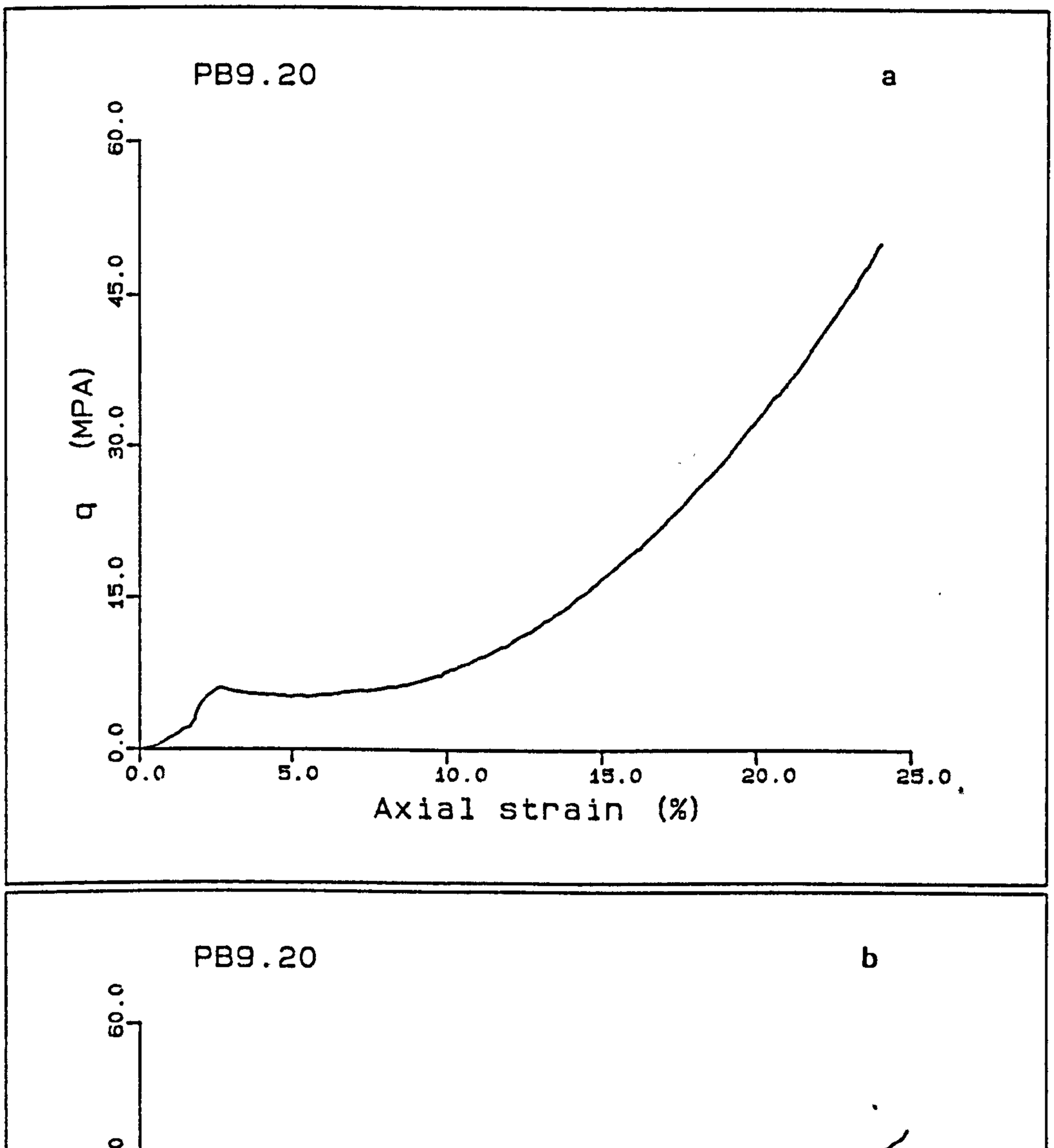

Figure A5.16(a-h) K_o test PB9.20.

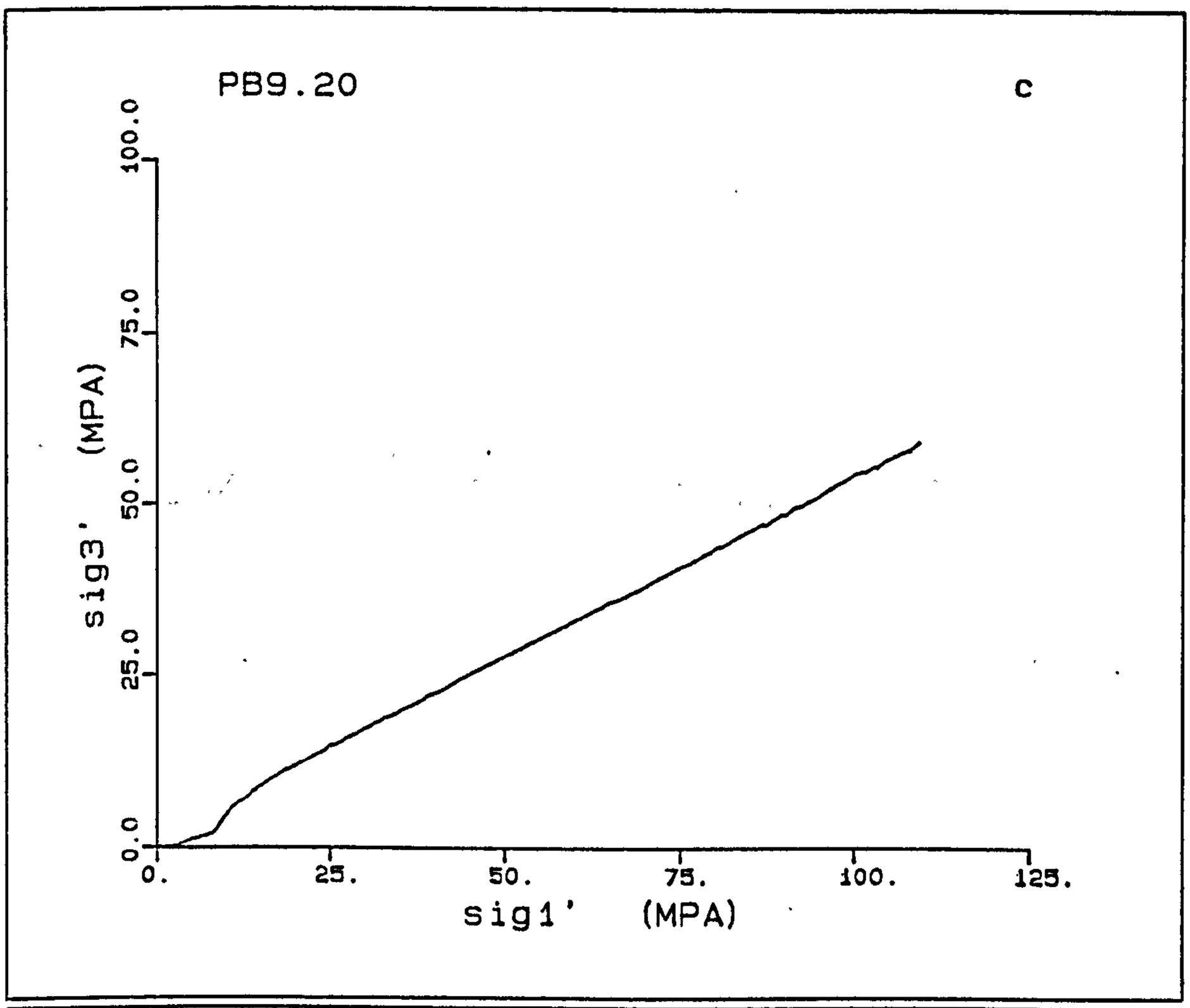
PB9.20
c
sig3' (MPA)
100.0
75.0
50.0
25.0
0.0
0.
25.
50.
75.
100.
125.
sig1' (MPA)

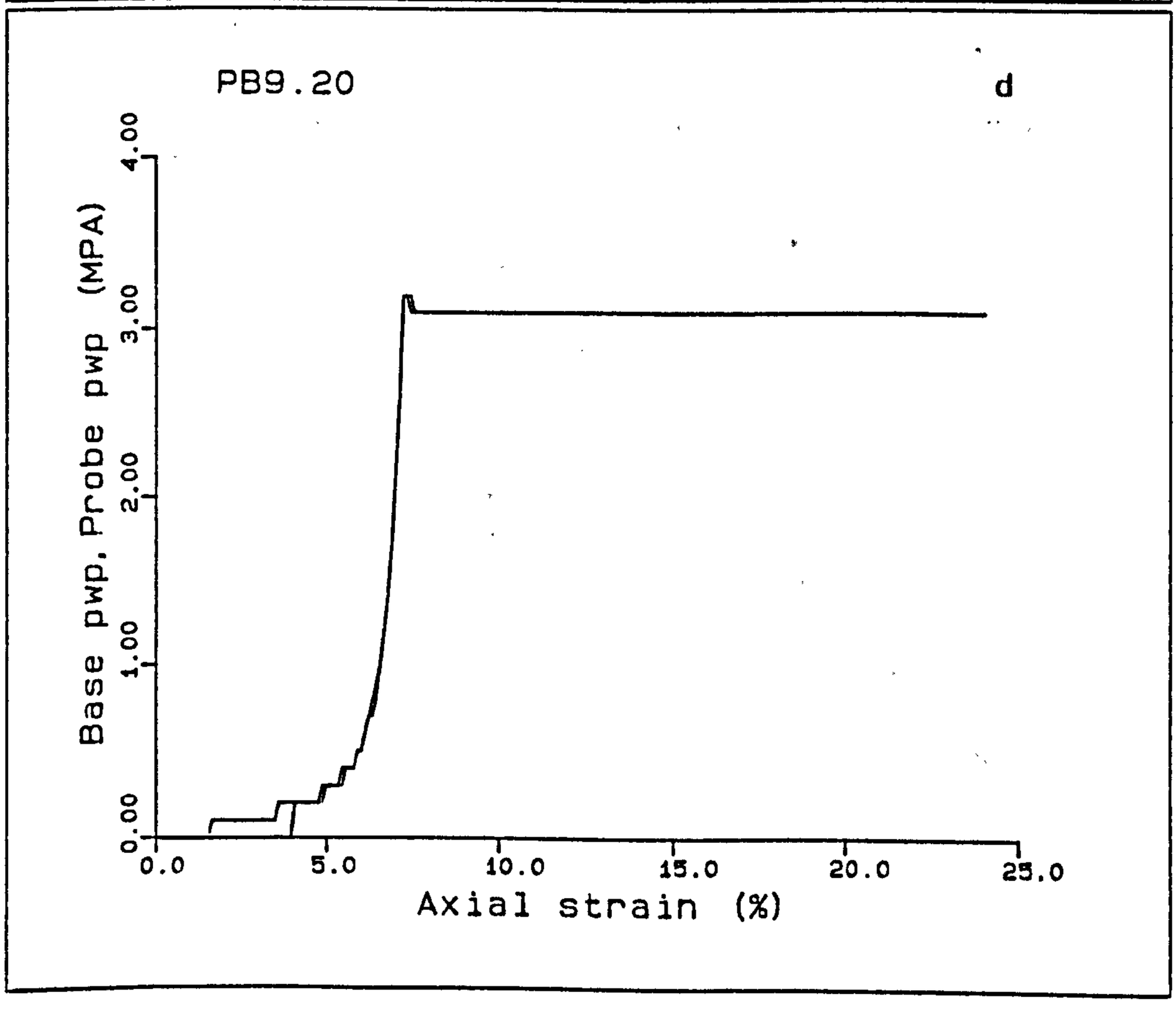
PB9.20
d
Base pwp, Probe pwp (MPA)
4.00
3.00
2.00
1.00
0.00
0.0
5.0
10.0
15.0
20.0
25.0
Axial strain (%)

PB9.20

e

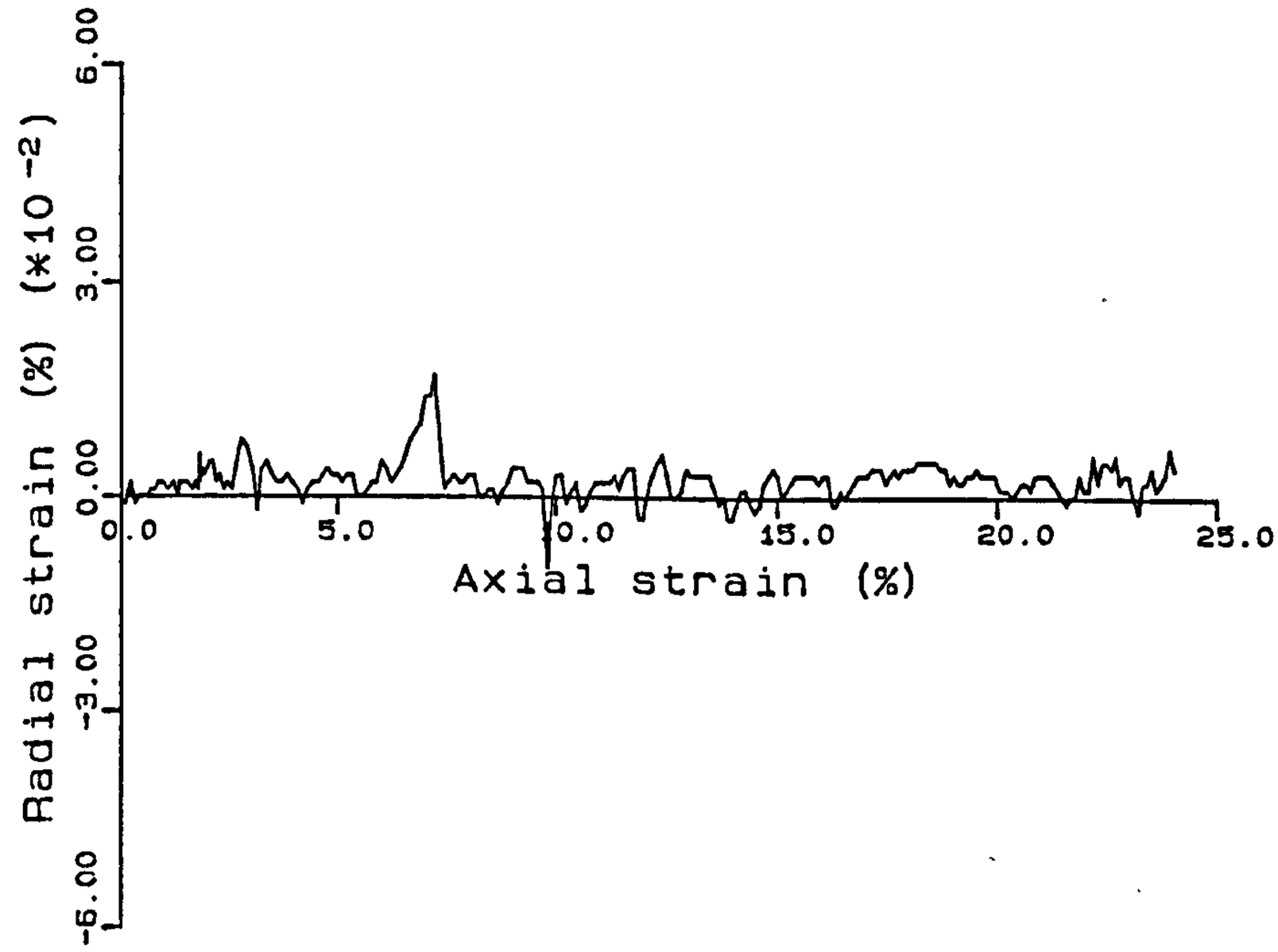

f

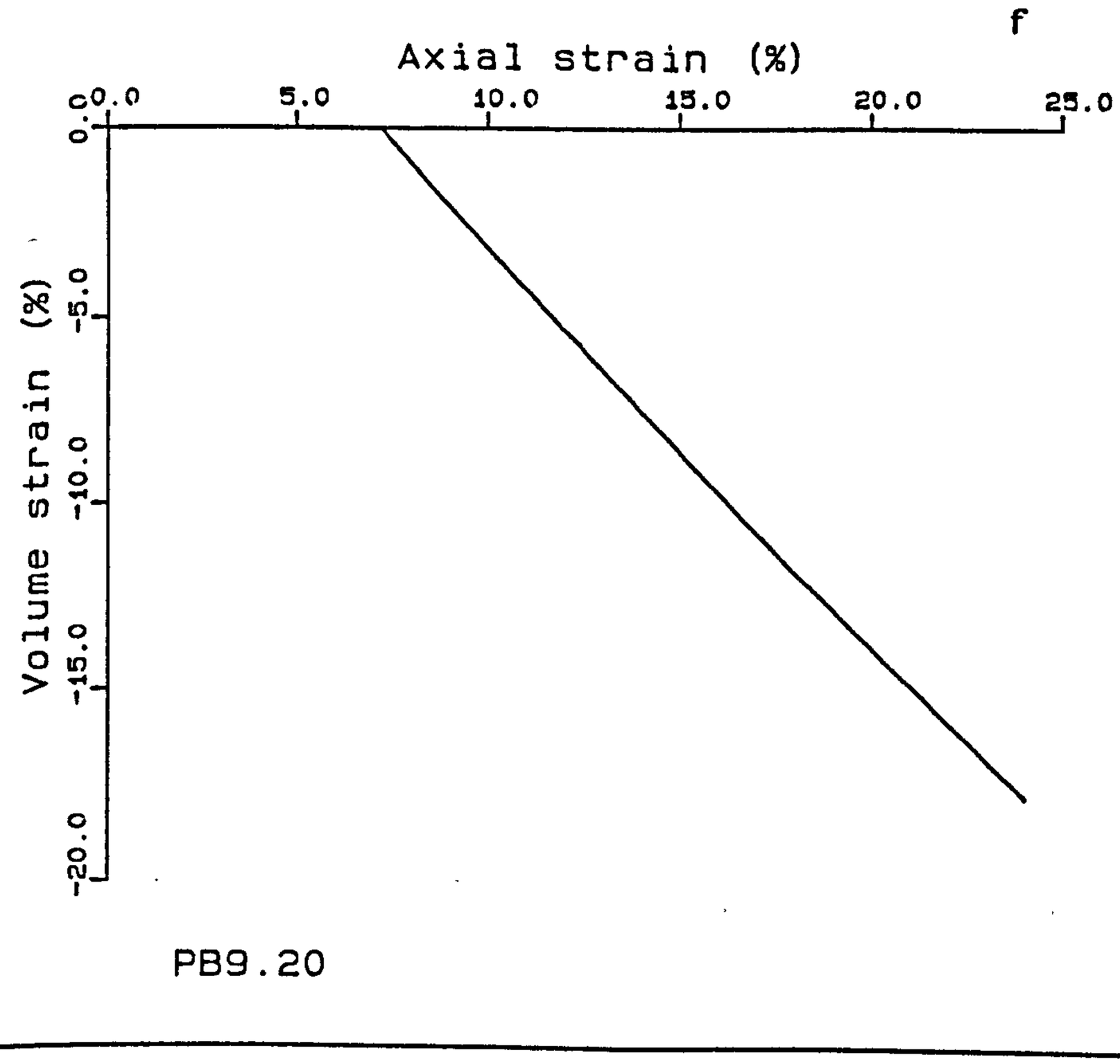

PB9.20

PB9.20

e

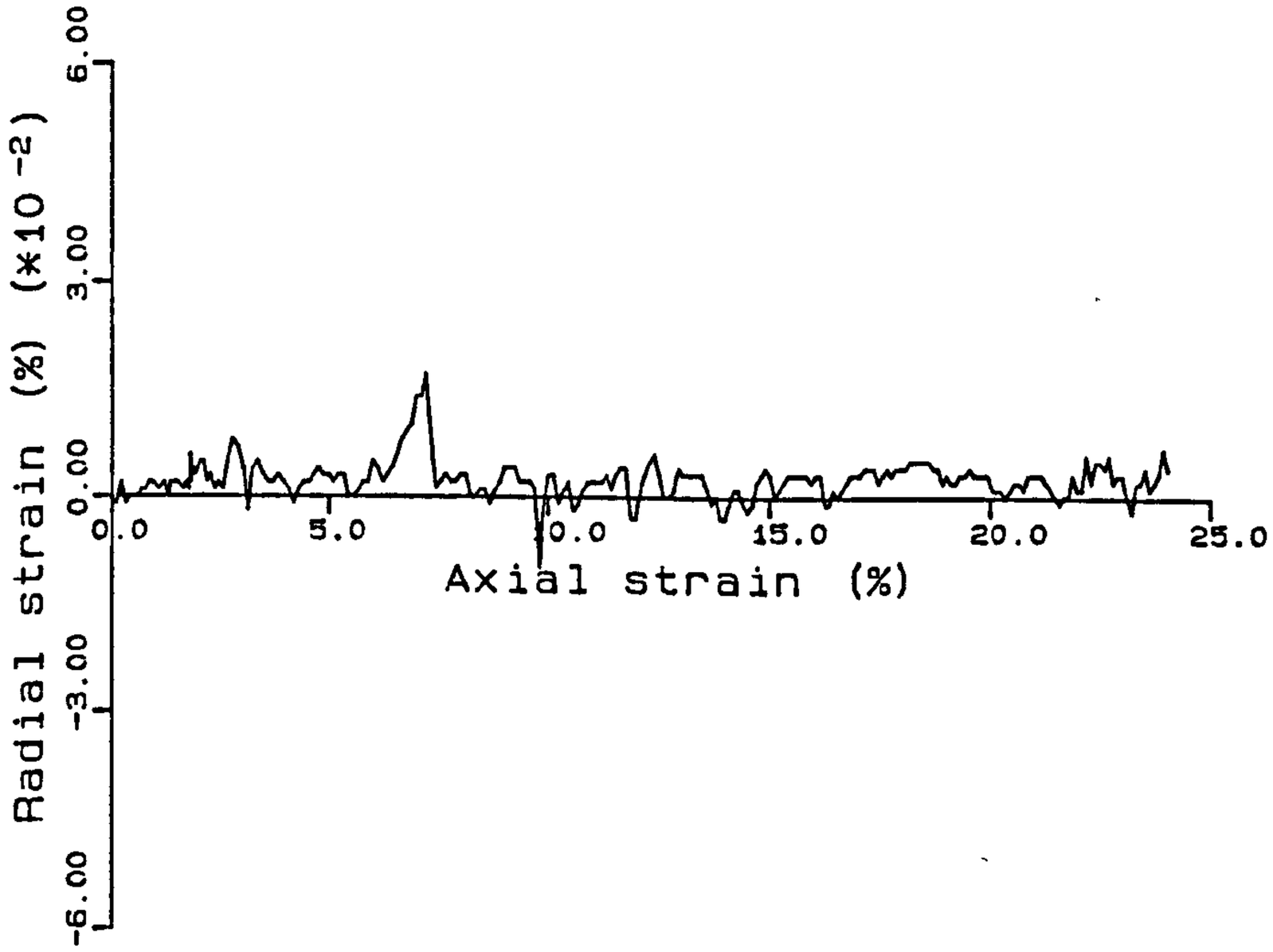

f

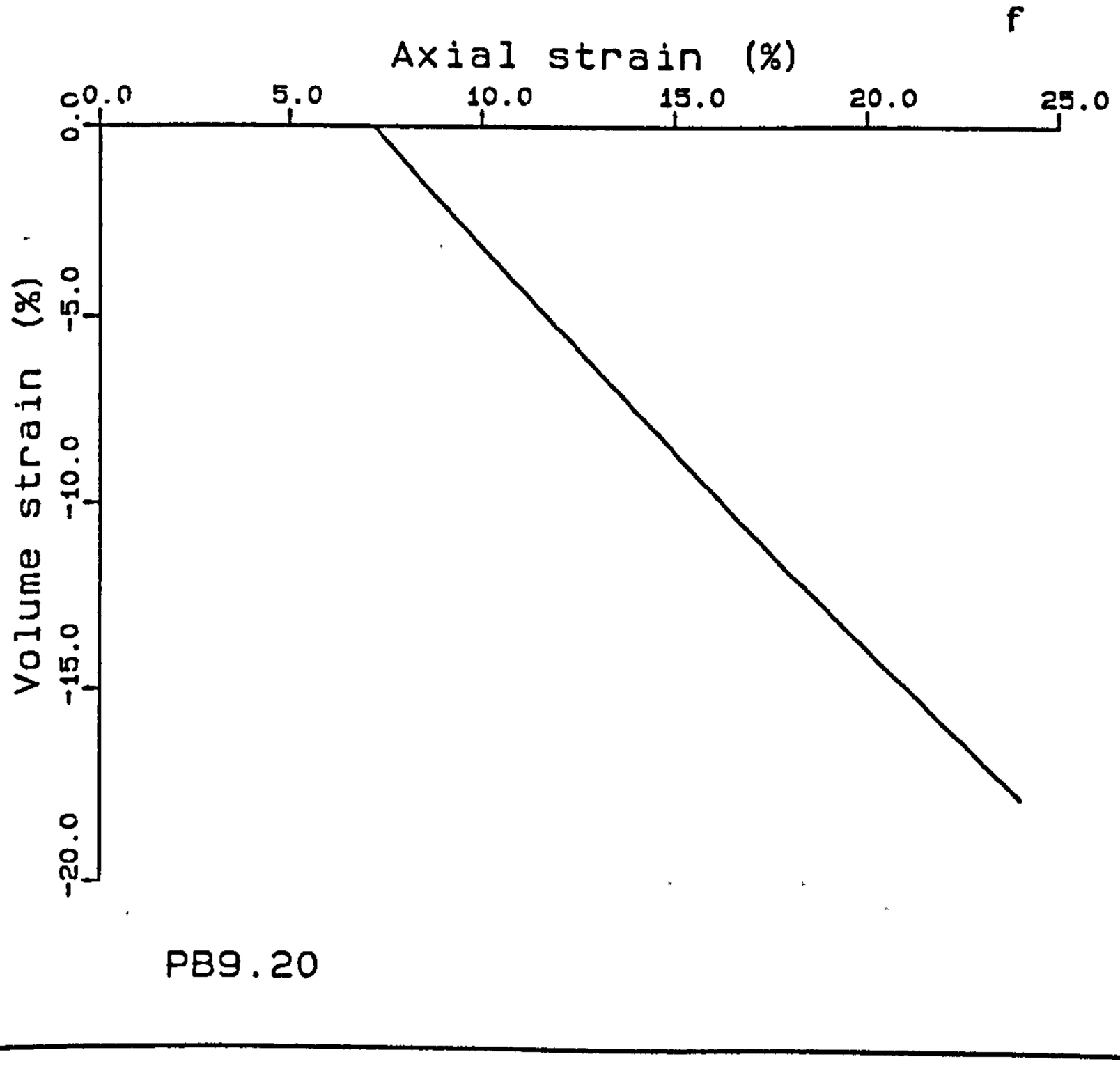

PB9.20

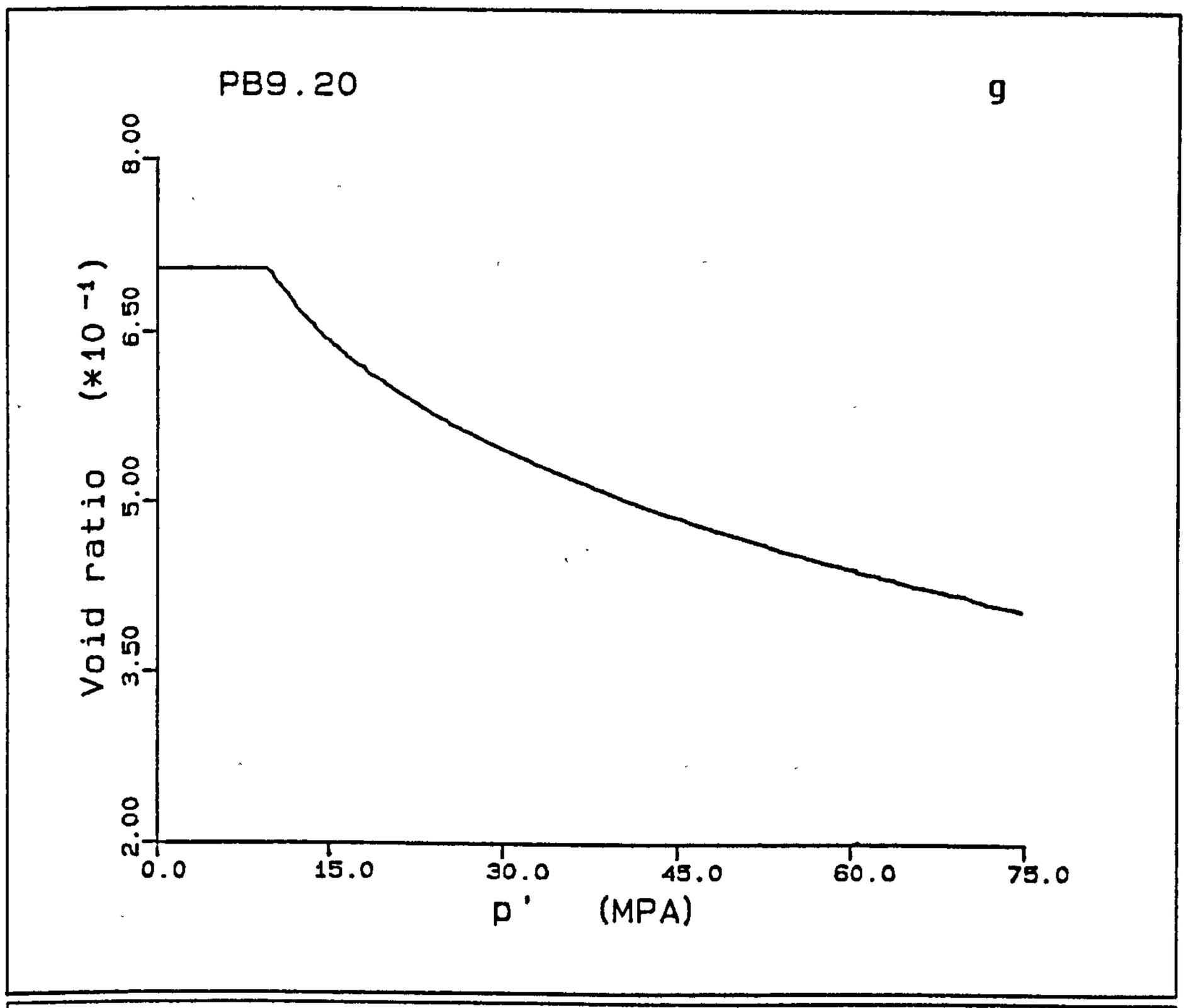
PB9.20
g
8.00
6.50
5.00
3.50
2.00
Void ratio (*10 -1)
0.0
15.0
30.0
45.0
60.0
75.0
p' (MPA)

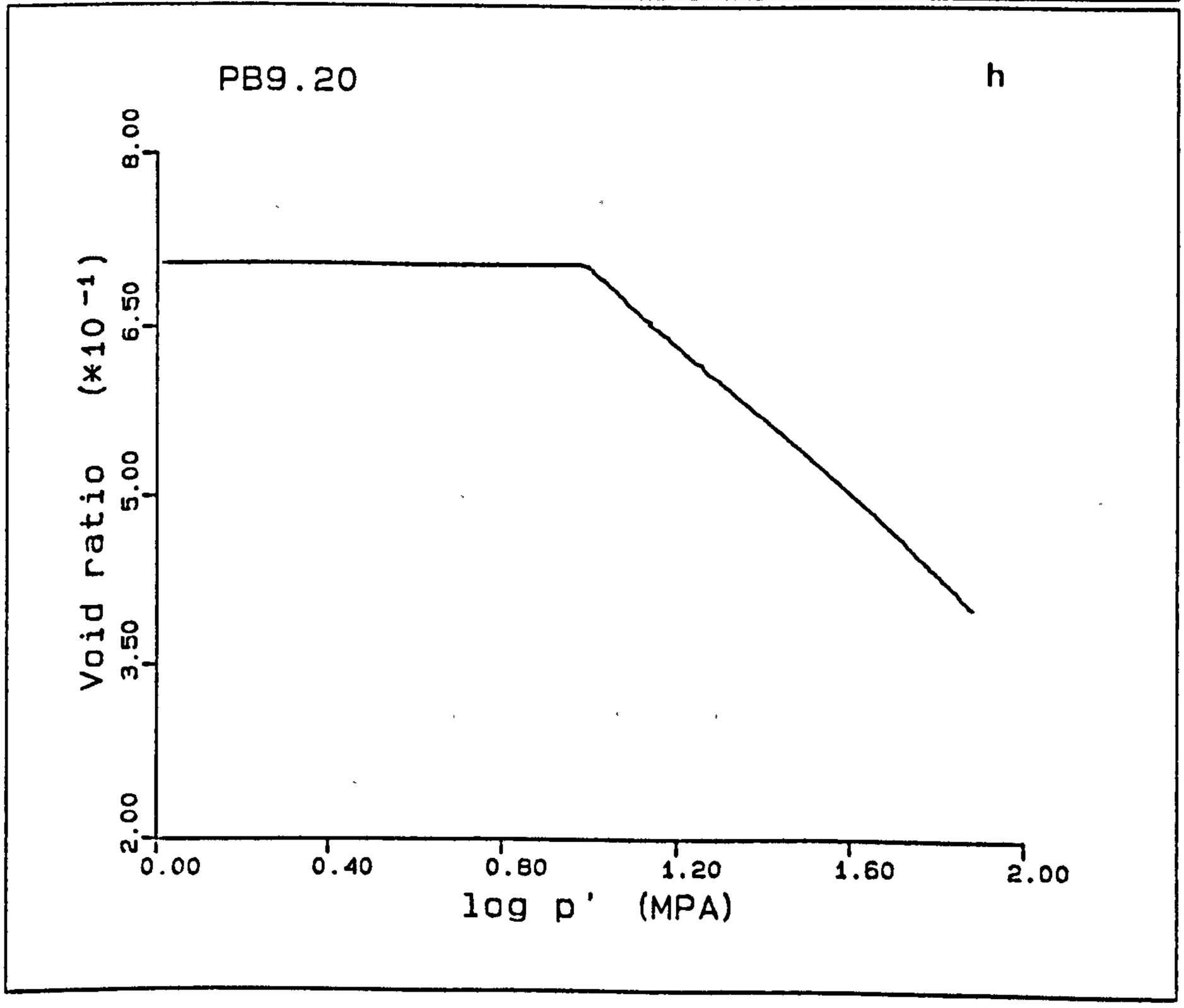
PB9.20
h
8.00
6.50
5.00
3.50
2.00
Void ratio (*10 -1)
0.00
0.40
0.80
1.20
1.60
2.00
log p' (MPA)

PB15.20

This sample is from P block, has a height of 76.83mm with a H/D ratio of 1.962, it was deformed at a rate of 0.01mm/min. The cell pressure at the start of the test was higher than in previous tests at 2.2MPa, this results in the transition stage of deformation being reduced or eliminated in q-p' space. The yield point occurs at 3.5MPa deviatoric stress, deformation continues straight into the linear plastic deformation section in q-p' space, Fig. A5.17b. The stress-strain curve has a large axial deformation at constant deviatoric stress, this is probably represented as a point in q-p' space, large volume strains occurring at more or less constant q and p'. The normal consolidation compaction is to a large extent linear, with two deviations seen at 15.7 and 17.6MPa mean effective stress.

The radial strains remains fairly constant up to an axial strain of 11.7%, after which the radial strain decreases to approximately $30*10^{-3}$% with two peaks at 12% and 12.6% axial strain, Fig. A5.17e. The $\bar{K}_o$ values for the compactional deformations are $\bar{K}_{oe}$= 0.311, $\bar{K}_{opc}$= 0, and $\bar{K}_{onc}$= 0.528.

The volume strain starts recording at axial strain of 1.8% with a pore pressure of 3.0MPa. The axial strain vs volume strain plot, Fig. A5.17f, plunges to higher slopes as a result of the negative radial strain. The e - log p' plot shows the three behavioural characteristics noted earlier, with an abrupt change in initial slope to intermediate shallow slope, probably as a result of the high p' at yield, with the subsequent intermediate behaviour at constant q and p'.

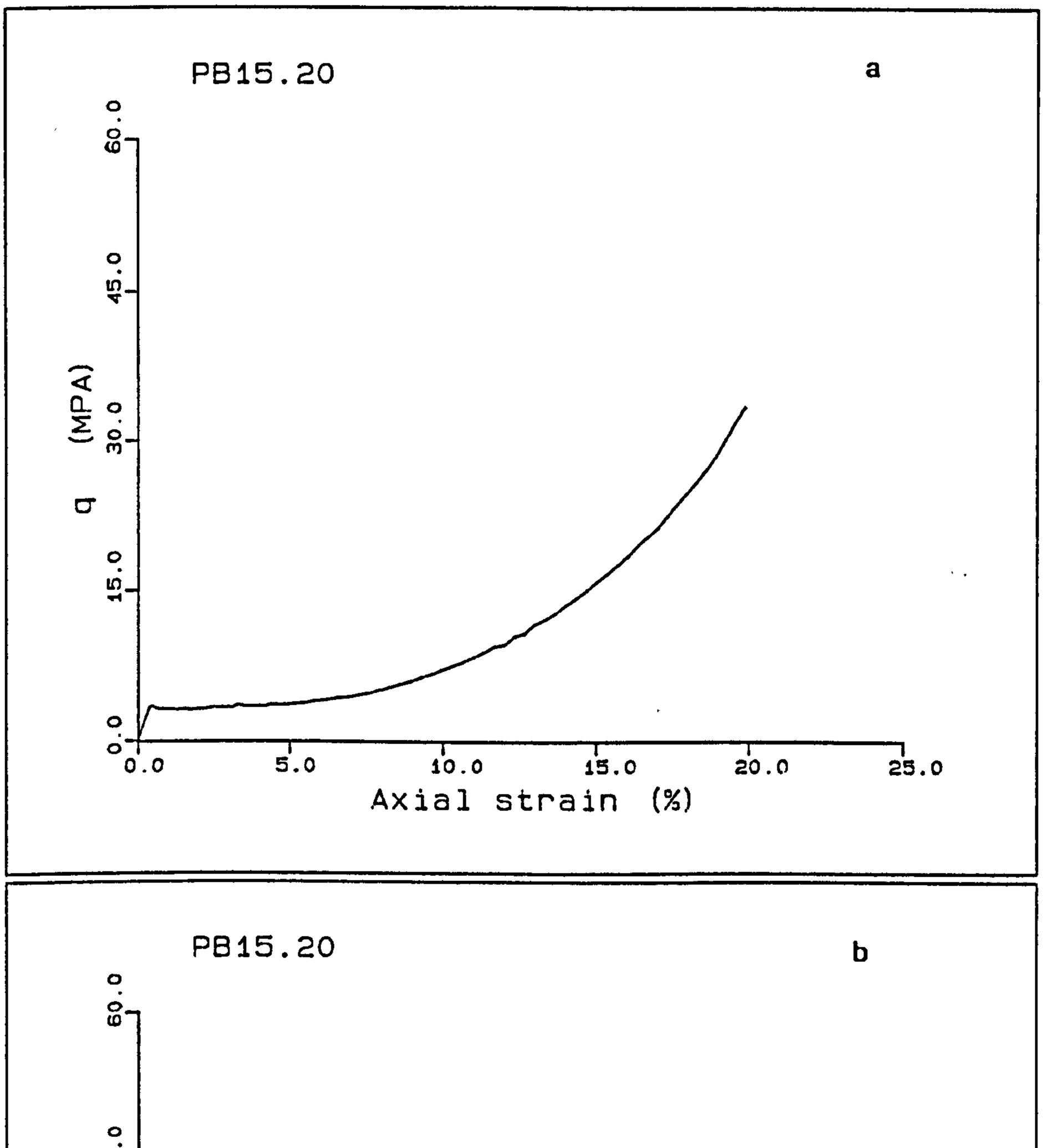

Figure A5.17(a-h) K_o test PB15.20

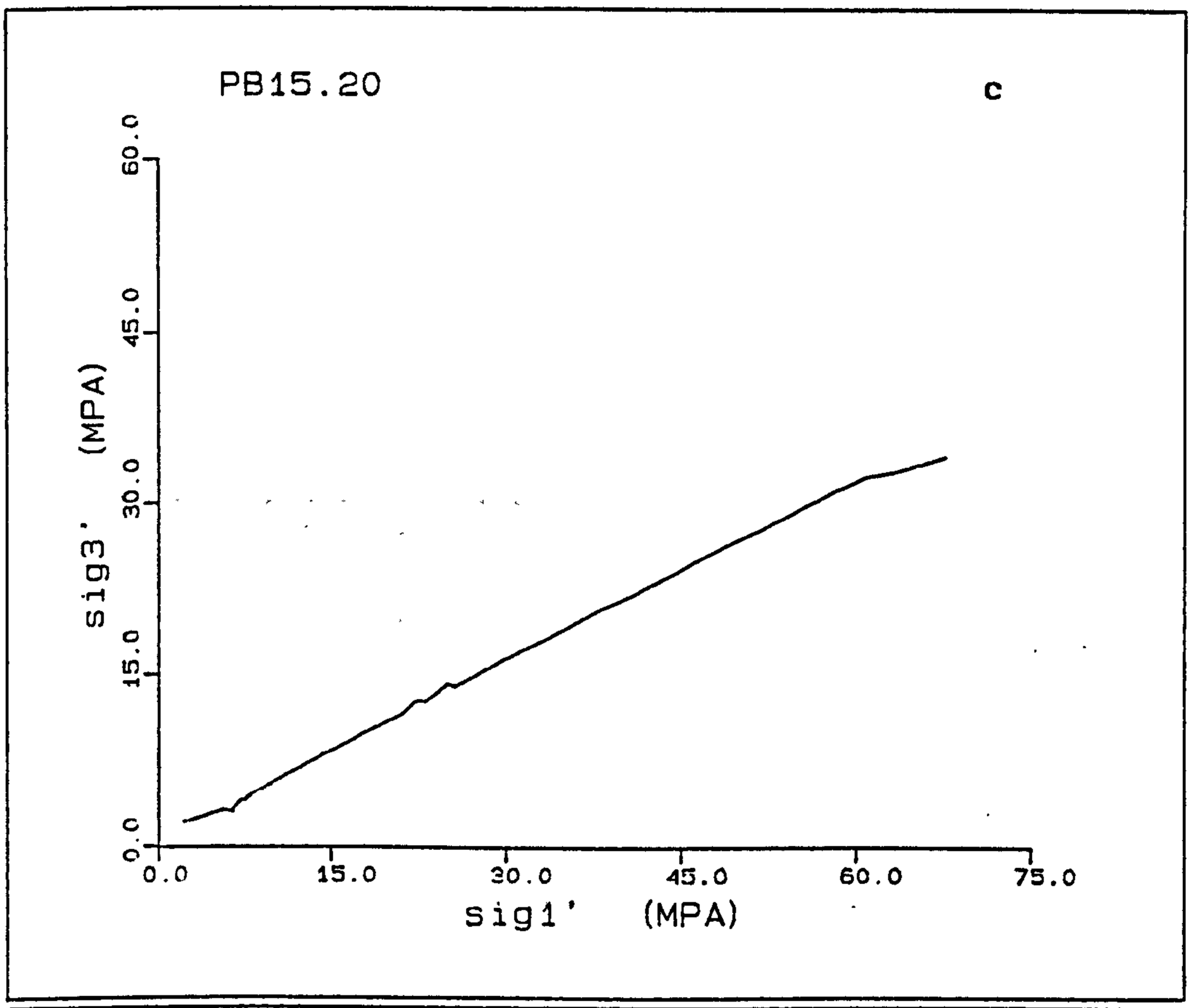
PB15.20
c
sig3' (MPA)
60.0
45.0
30.0
15.0
0.0
0.0
15.0
30.0
45.0
60.0
75.0
sig1' (MPA)

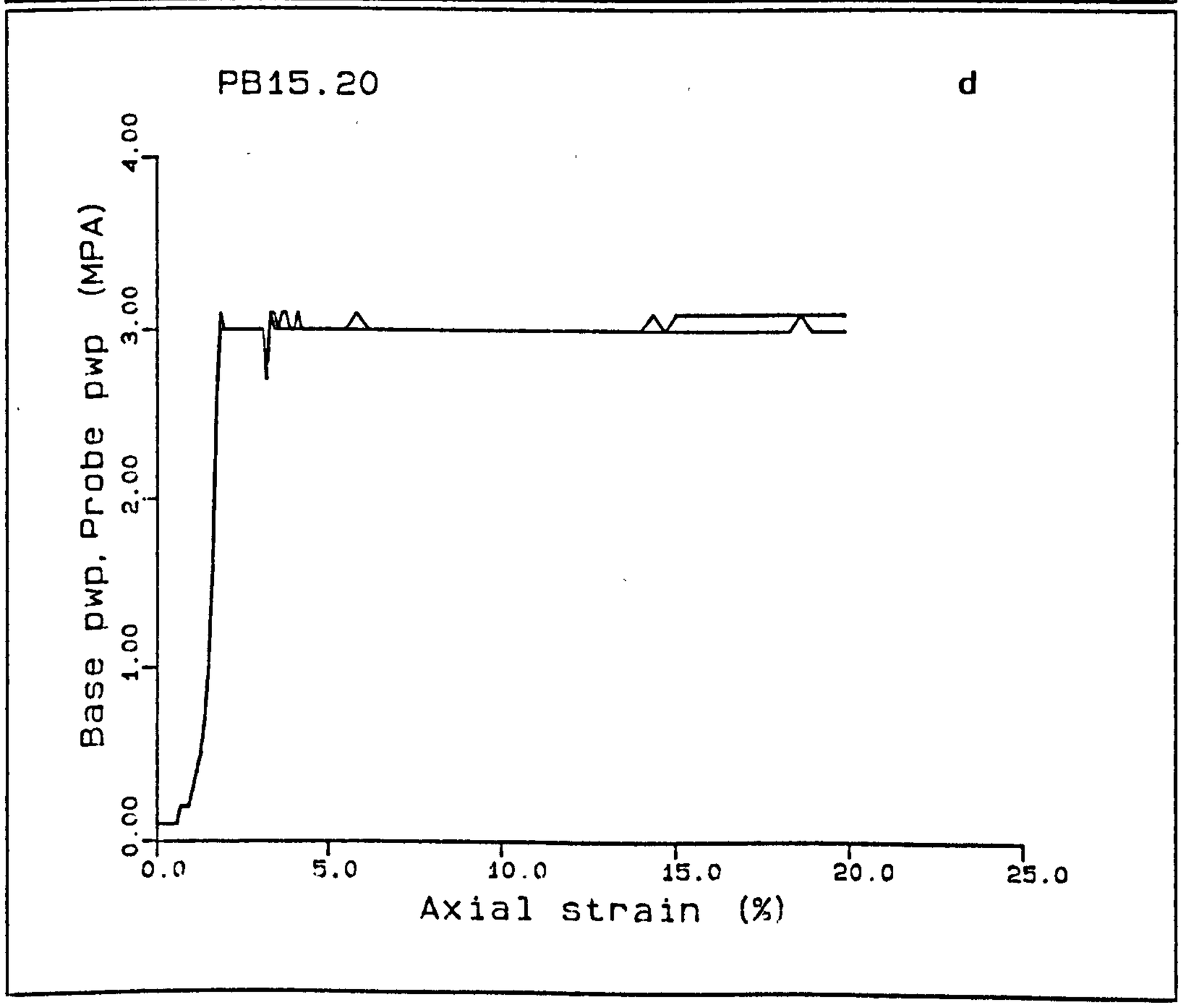
PB15.20
d
Base pwp, Probe pwp (MPA)
4.00
3.00
2.00
1.00
0.00
0.0
5.0
10.0
15.0
20.0
25.0
Axial strain (%)

PB15.20

e

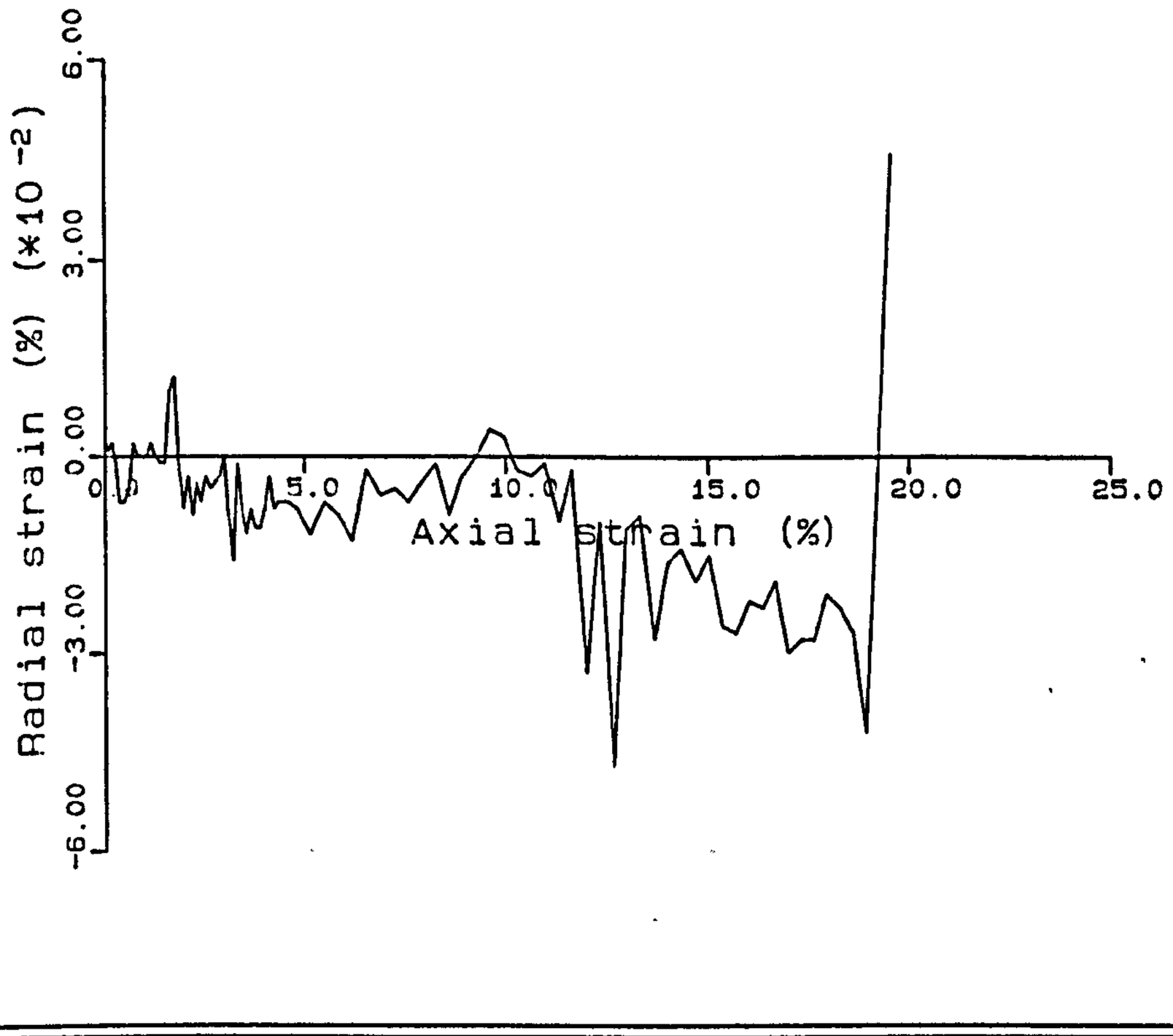

f

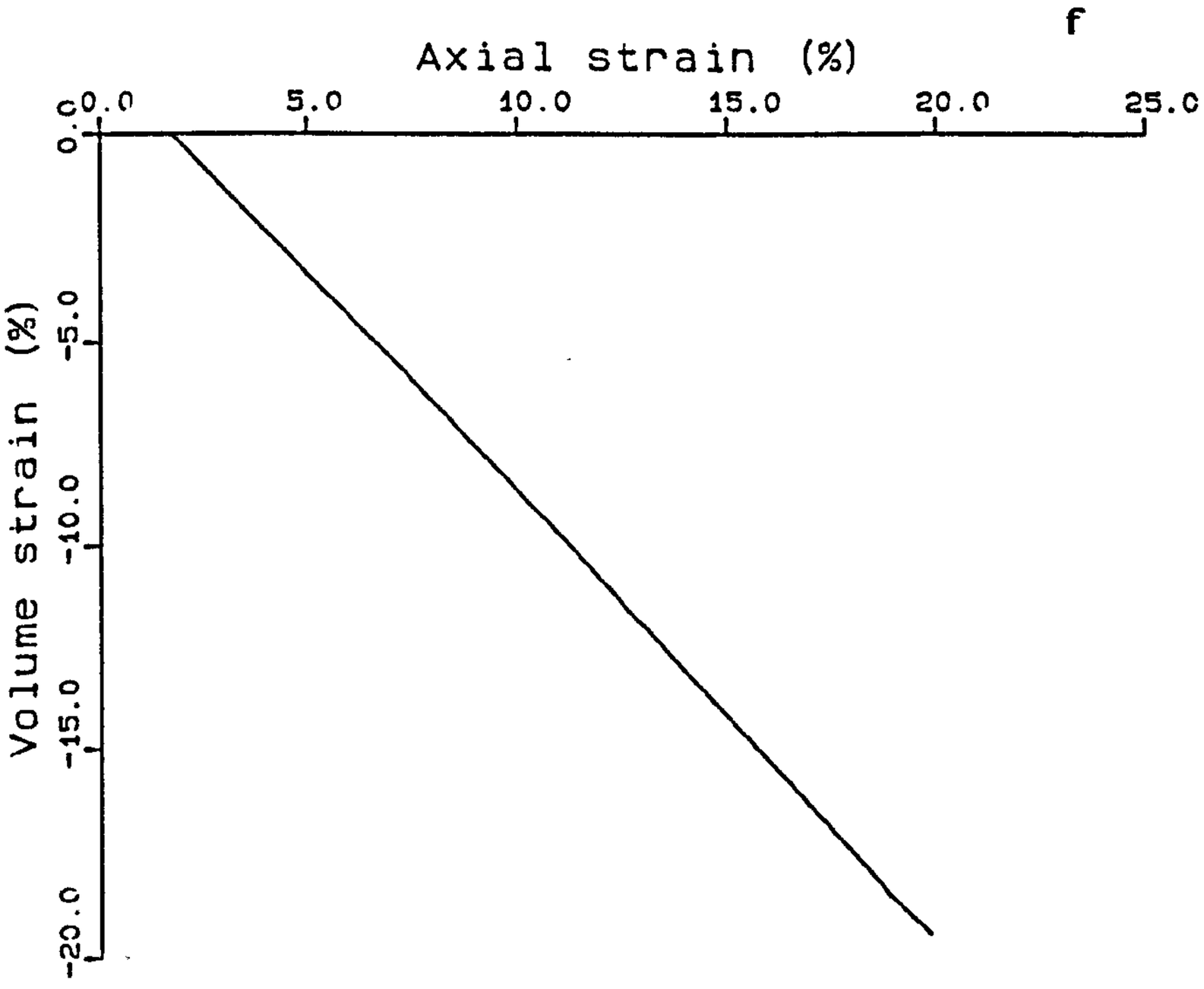

PB15.20

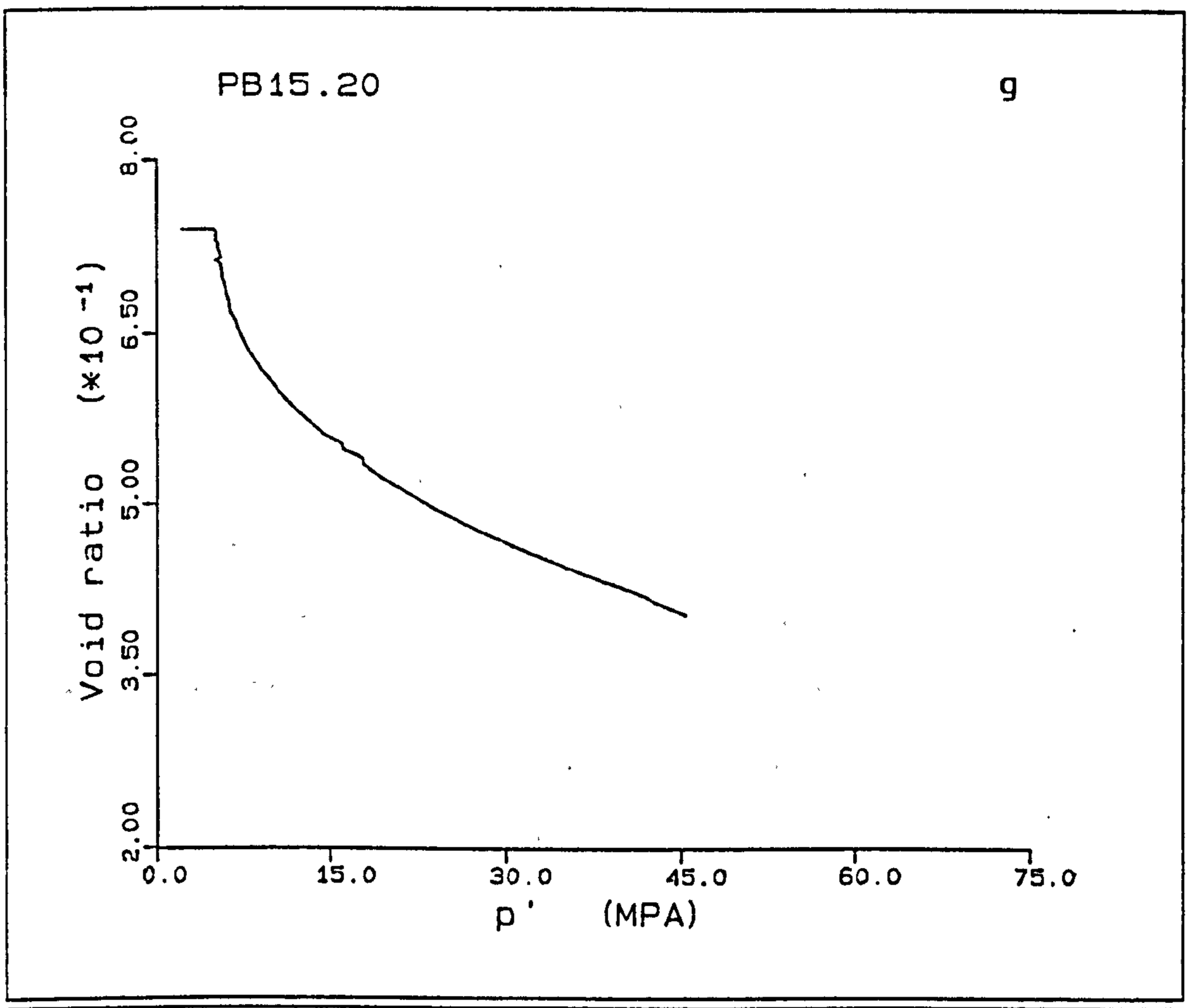
PB15.20
g
8.00
6.50
5.00
3.50
2.00
(*10 -1)
Void ratio
0.0
15.0
30.0
45.0
60.0
75.0
p' (MPA)

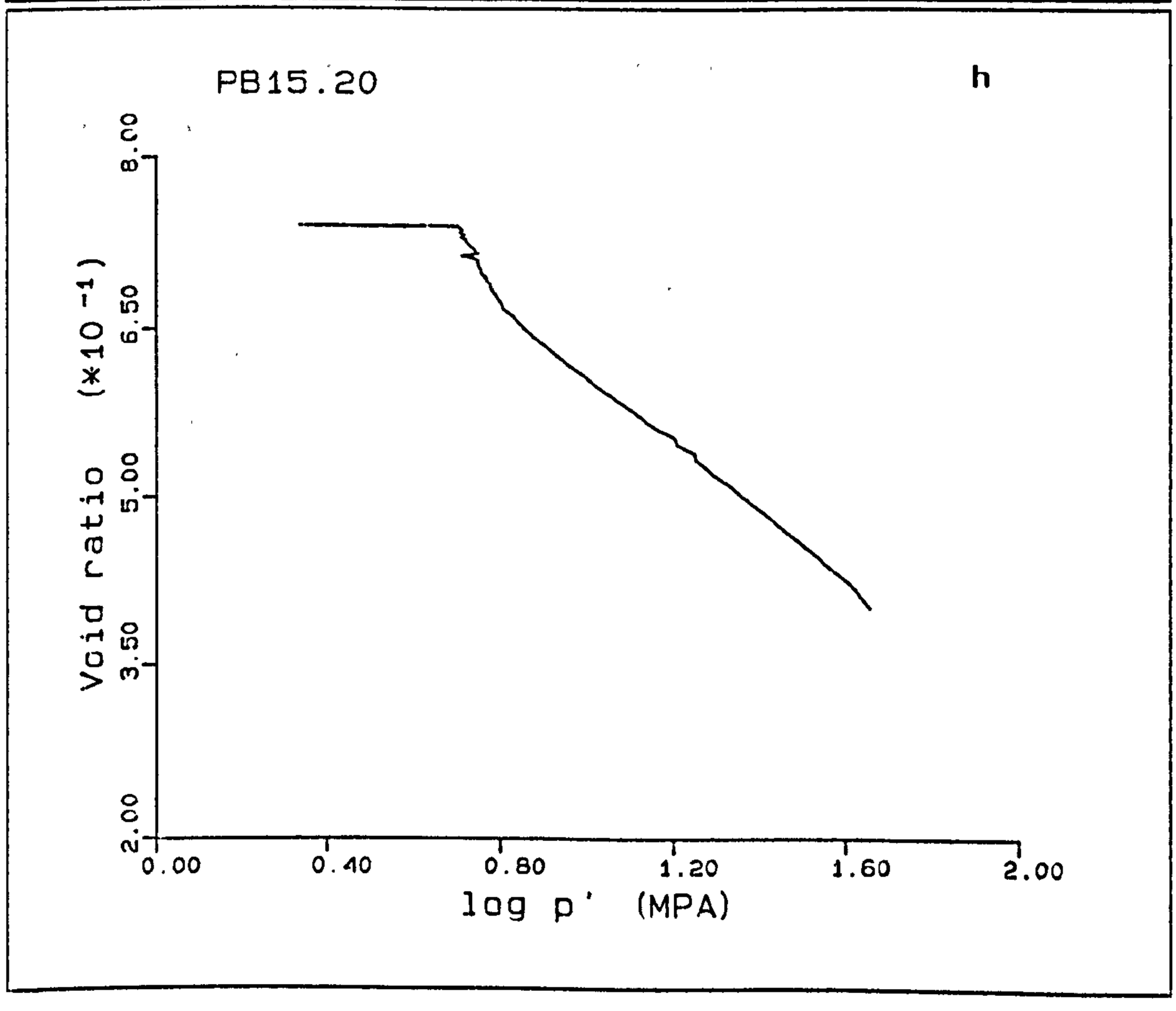
PB15.20
h
8.00
6.50
5.00
3.50
2.00
(*10 -1)
Void ratio
0.00
0.40
0.80
1.20
1.60
2.00
log p' (MPA)

PB16.20

The sample was taken from P block and is a 50.16mm high sample, the H/D ratio being 1.333, the chalk being deformed at a rate of 0.0068mm/min. The initial deformation shows an irregular load increase with strain, the initial modulus and the yield being indeterminate; though a maximum deviatoric stress of 3.9MPa occurs before a slight decrease in the pore collapse deformation. The work hardening deformation shows a linear increase of q with p, with only small deviations from this trend. The radial strains are kept to a variation below $20*10^{-3}$%, with one exception at 16% axial strain, where a radial strain of $-36*10^{-3}$% occurs. This is seen as a kick in the stress strain, q-p', and void ratio plots. The volume strain - axial strain plots show no apparent change due to this deviation.

The values of $\bar{K}_o$ obtained for the compaction are, $\bar{K}_{oe}$=0.472, $\bar{K}_{opc}$=1.023, $\bar{K}_{onc}$=0.523, for the elastic, pore collapse, and normal consolidation deformations respectively.

The e - log p' plot, Fig. A5.18h, shows the initial decrease in the void ratio with small change in p', the gradient of the plot decreases with increasing pressure. In this experiment the top pore pressure transducer was not used in the calculations as it proved to be faulty.

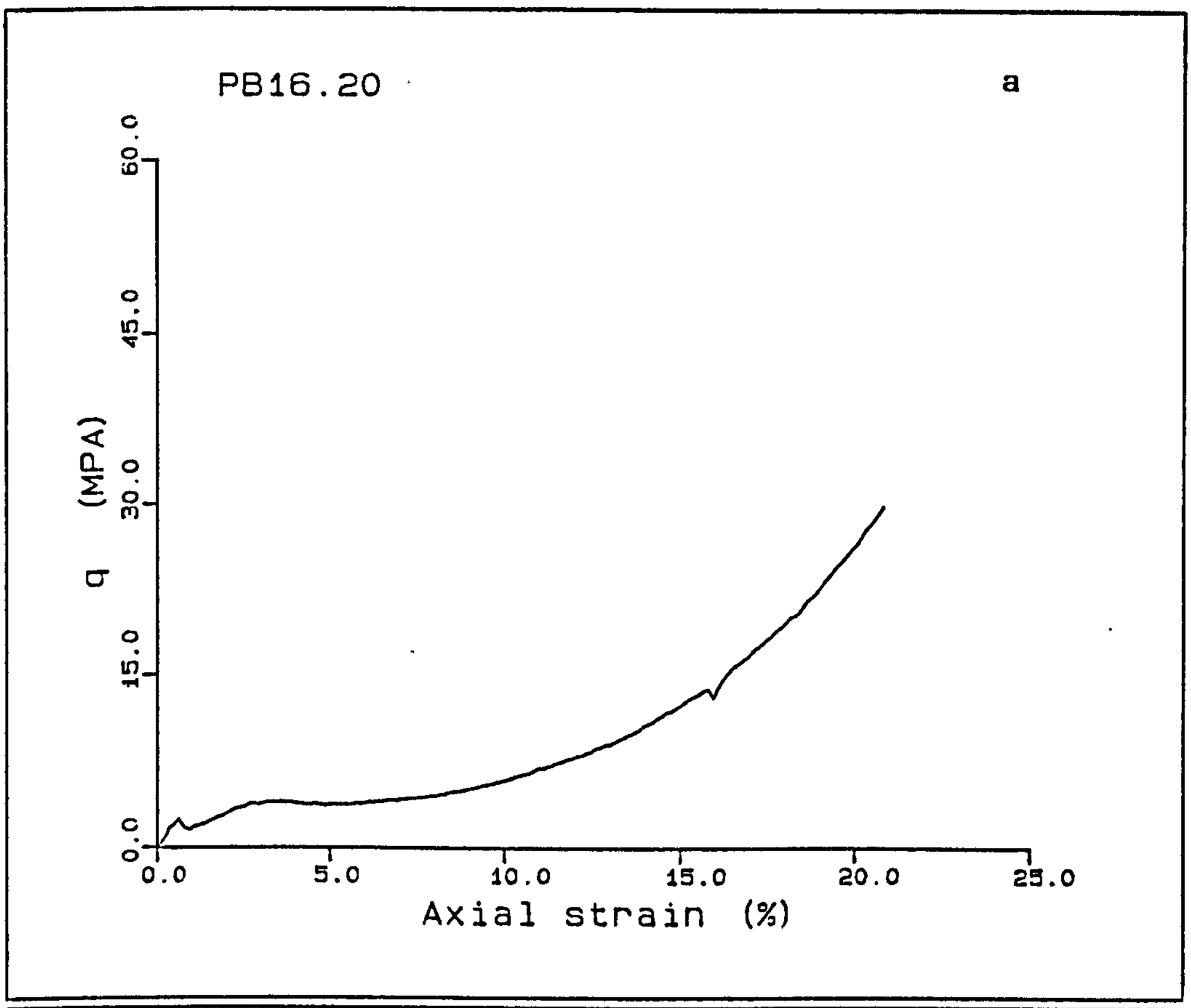

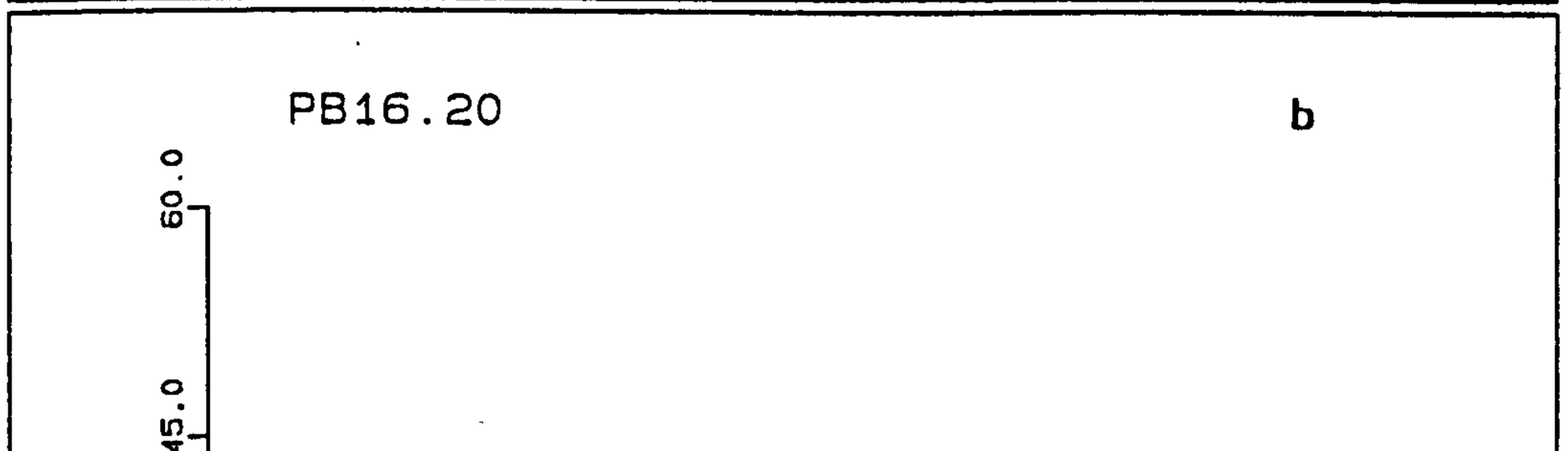

Figure A5.18(a-h) K_o test PB16.20.

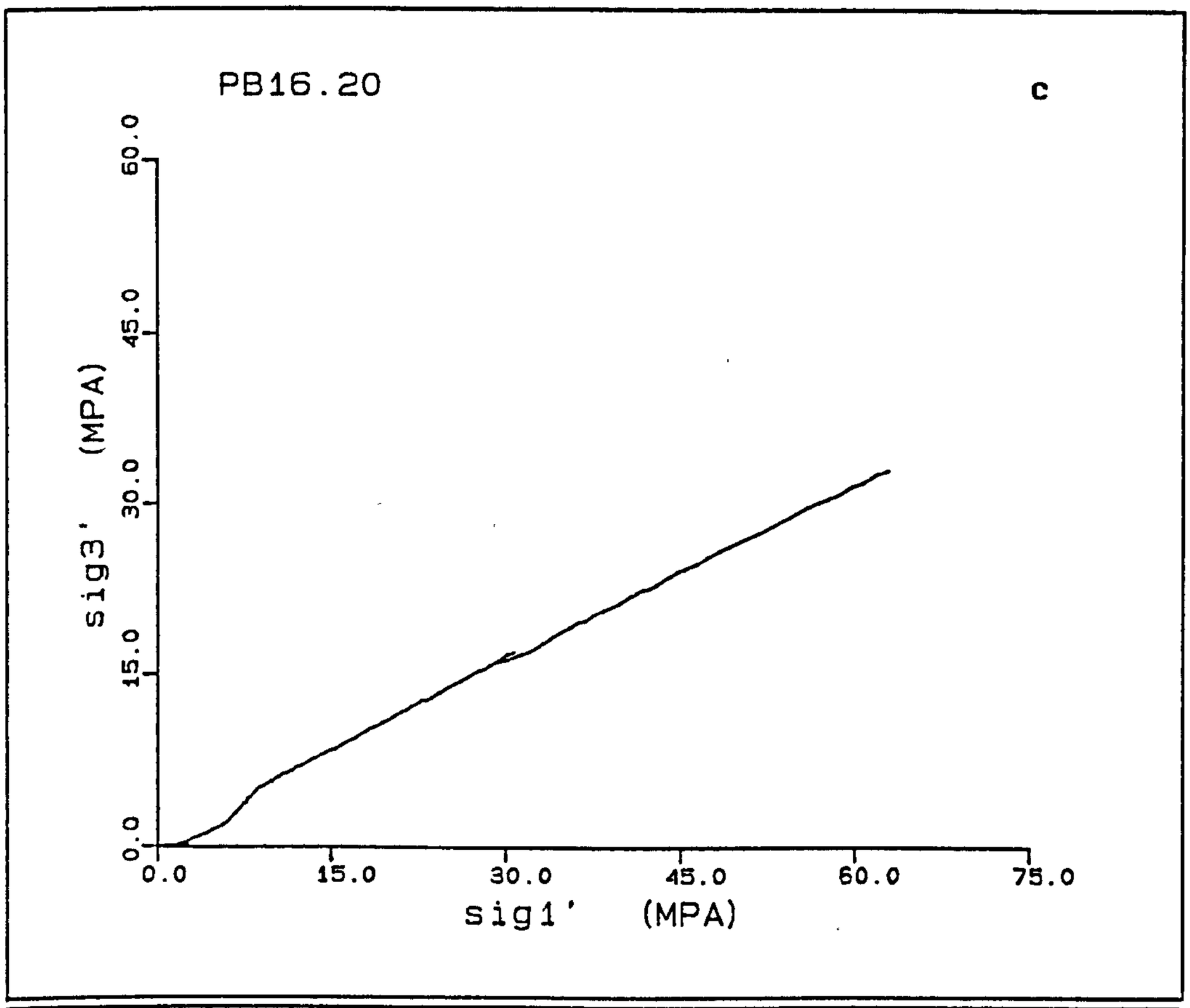
PB16.20
c
60.0
45.0
30.0
15.0
0.0
sig3' (MPA)
0.0
15.0
30.0
45.0
60.0
75.0
sig1' (MPA)

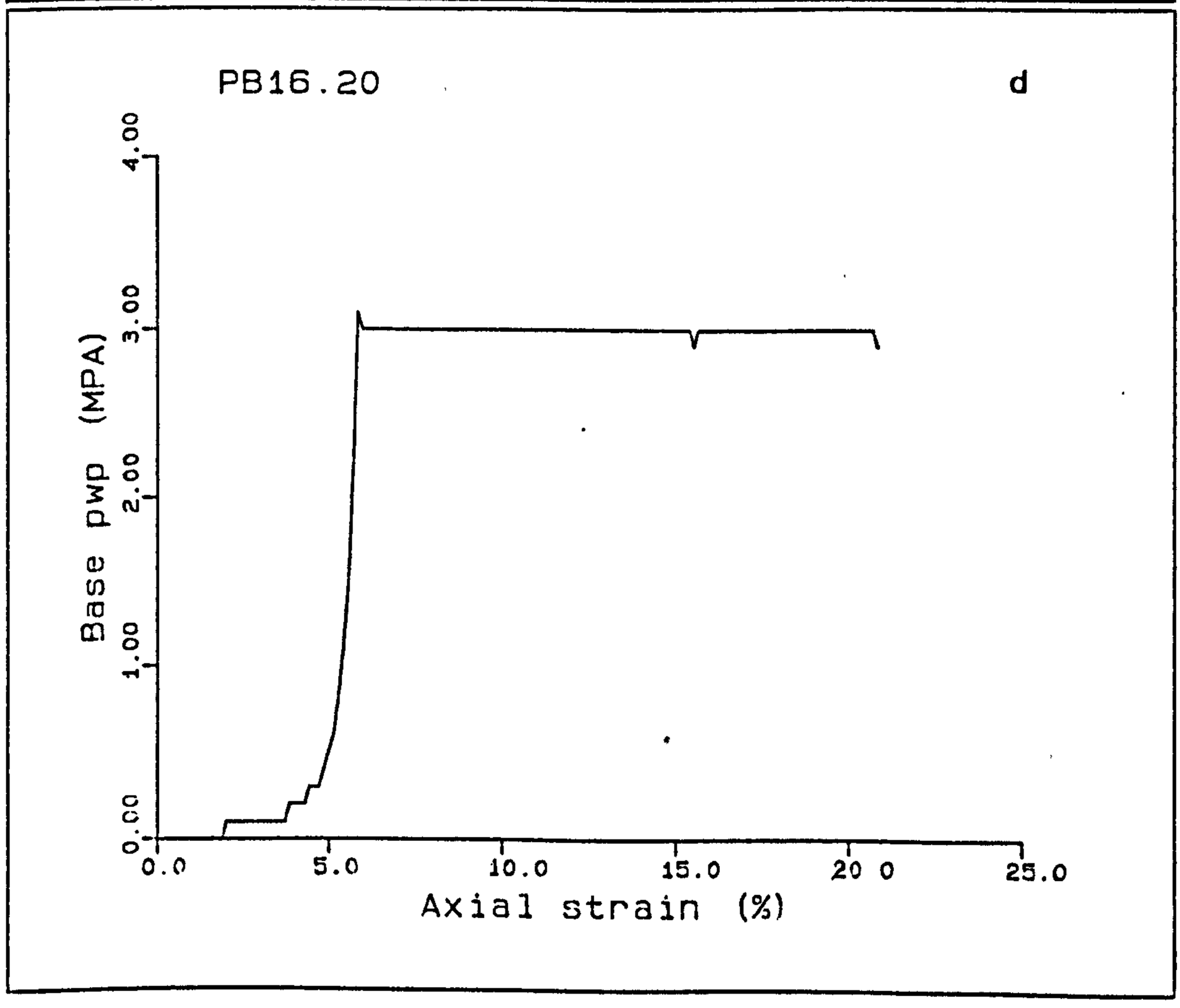
PB16.20
d
4.00
3.00
2.00
1.00
0.00
Base pwp (MPA)
0.0
5.0
10.0
15.0
20 0
25.0
Axial strain (%)

PB16.20

e

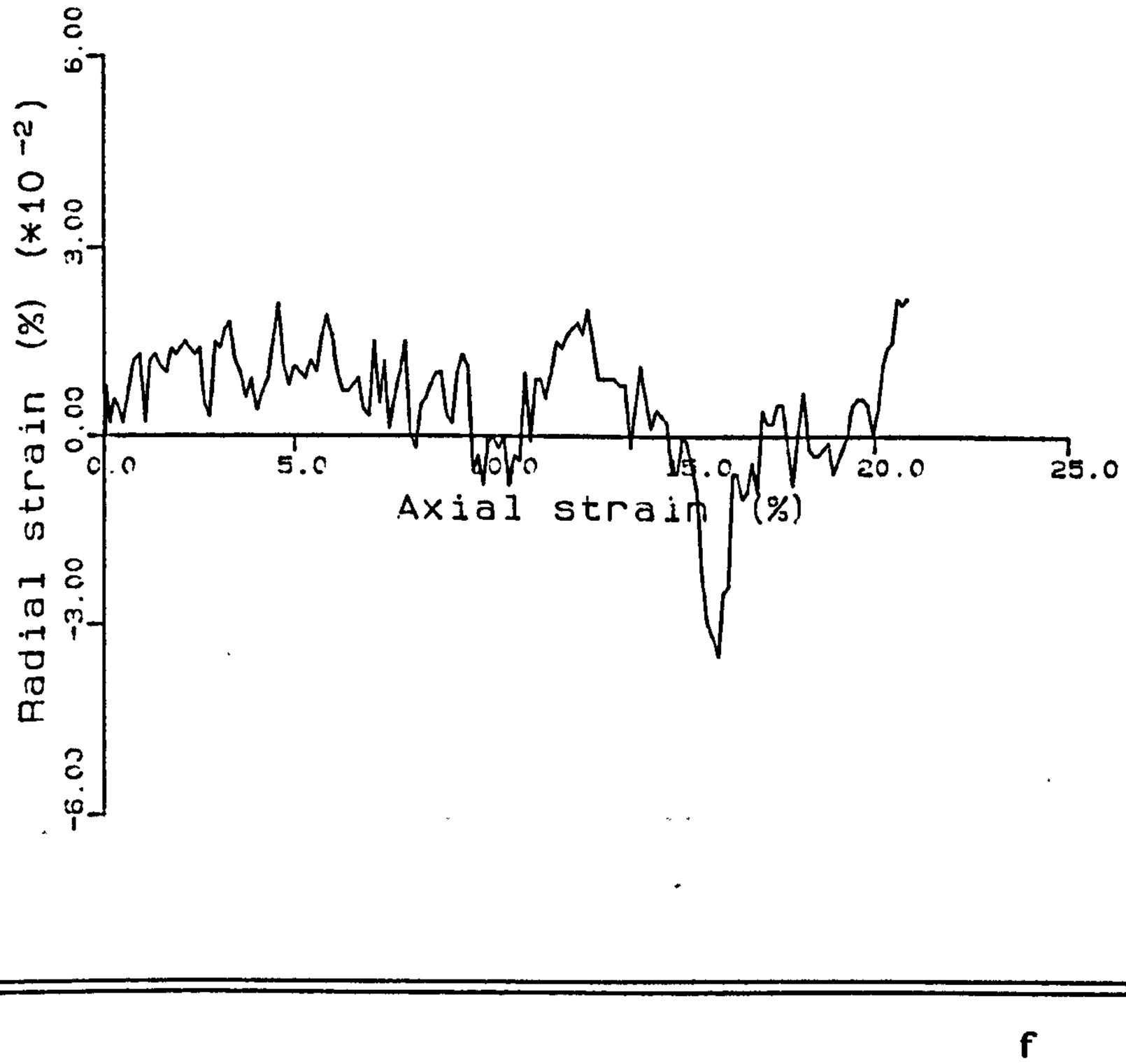

f

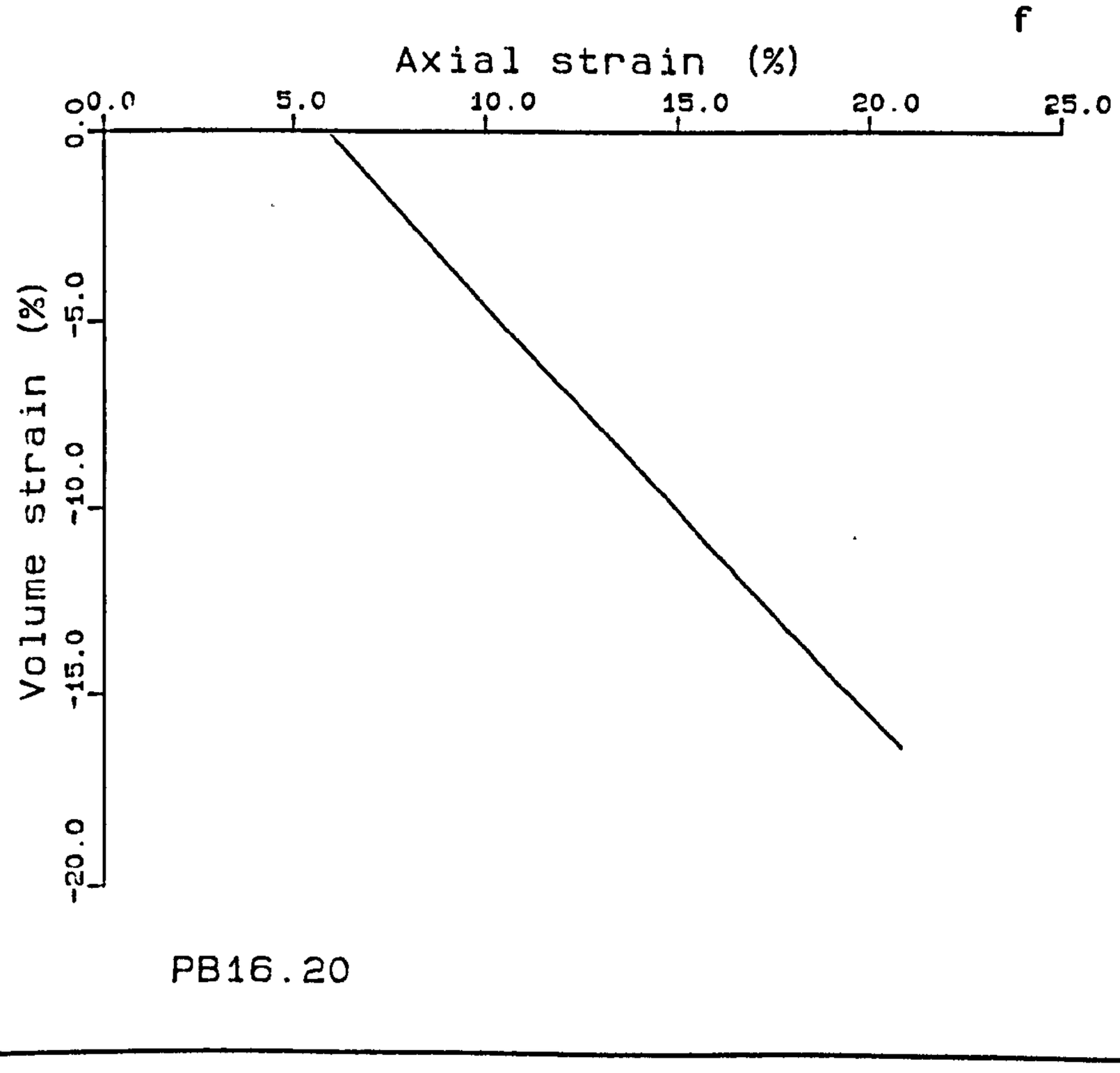

PB16.20

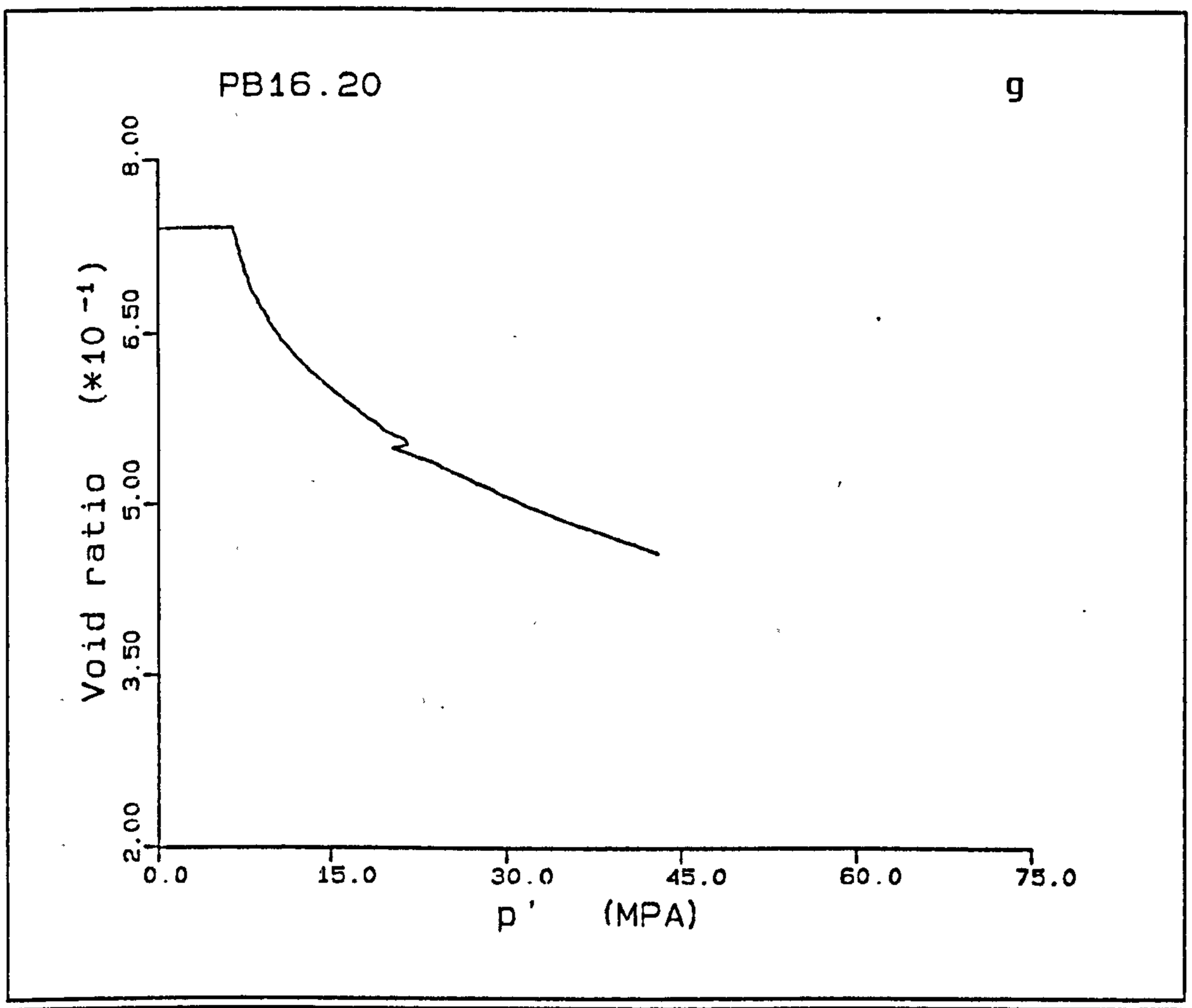
PB16.20
g
Void ratio (*10 -1)
8.00
6.50
5.00
3.50
2.00
0.0
15.0
30.0
45.0
60.0
75.0
p' (MPA)

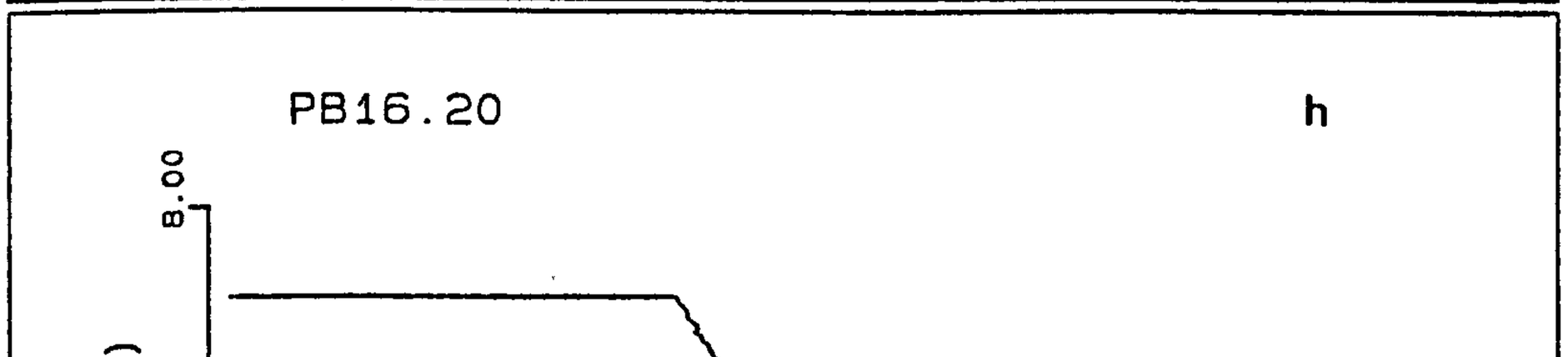
PB16.20
h
Void ratio (*10 -1)
8.00
6.50
5.00
3.50
2.00
0.00
0.40
0.80
1.20
1.60
2.00
log p' (MPA)

PB17.20

This is a sample from P block of height 24.38mm and H/D ratio of 0.649, it was deformed at a rate of 0.0033mm/min. The initial elastic deformation shows a small tangential Young's modulus of 0.39GPa, the yield point being 3.6MPa deviatoric stress. The post-peak deformation of the chalk is seen as a decrease in load of 0.7MPa; with continued deformation, a linear increase of q with p' occurs in the normal consolidation deformation. The main deviation seen in the plot Fig.A5.19b, is due to an increase in the pumping rate of the cell pressure controlling system. The load is seen to decrease, during which time the servo tries to maintain K_o and recover to the same load, this forms a loop in Fig. A5.19b and A5.19c. The $\bar{K}_o$ values for the deformation of the chalk are 0.250, 1.528 and 0.533 for the elastic, pore collapse and normal consolidation compactions respectively. The radial strain varies within a range of $10*10^{-3}$%, only twice going outside this range, Fig. A5.19e.

The volume starts recording at an axial strain of 7.5% when pore pressure equals 3.0MPa, after a slight overrun to 3.1MPa. The pore pressure at the top of the sample is not used as irregular readings were obtained; between these intervals, the top pore pressure could be seen to be equal to the back pressure. The e - log p' plot shows the three stage deformation, seen in previous tests.

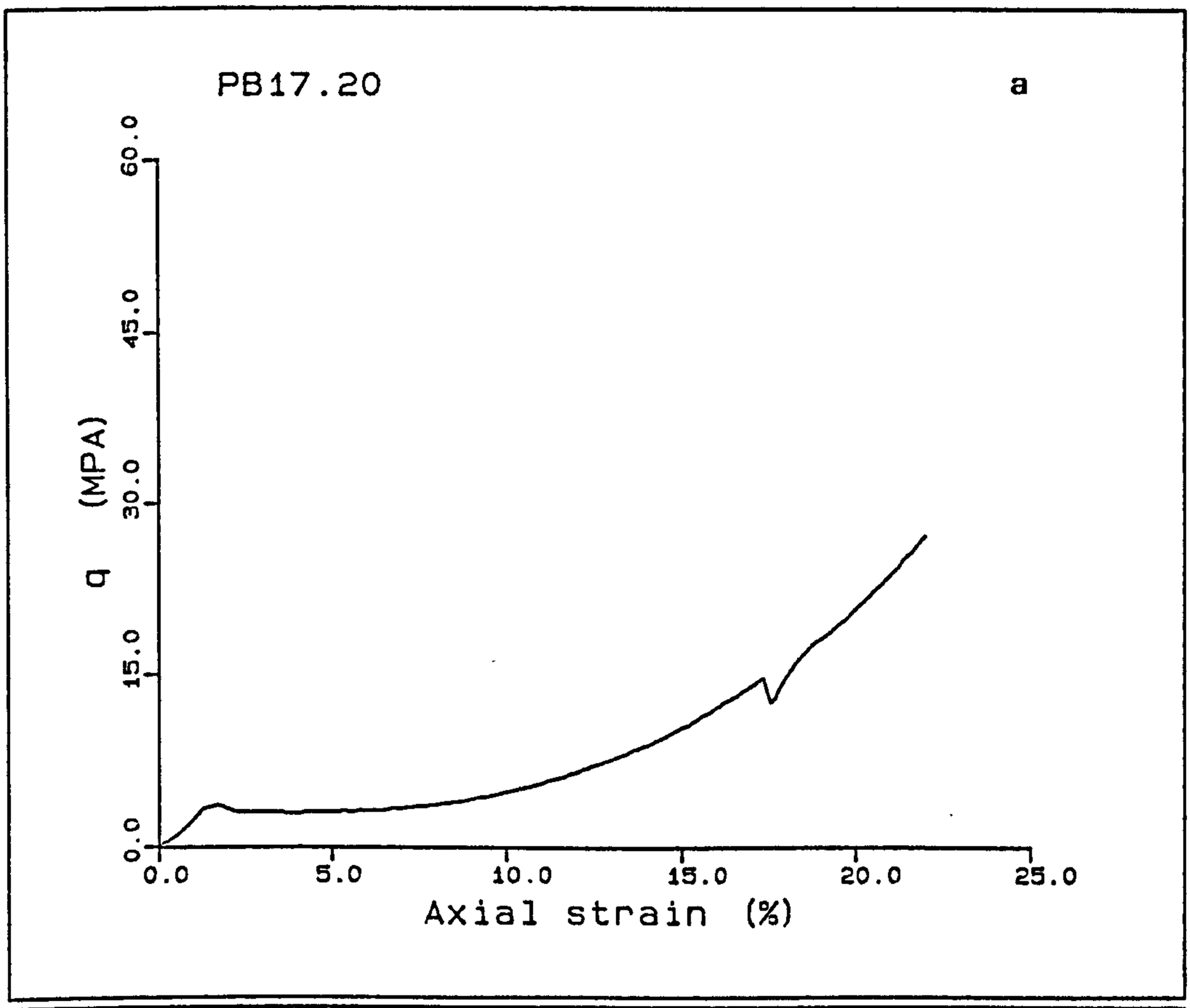

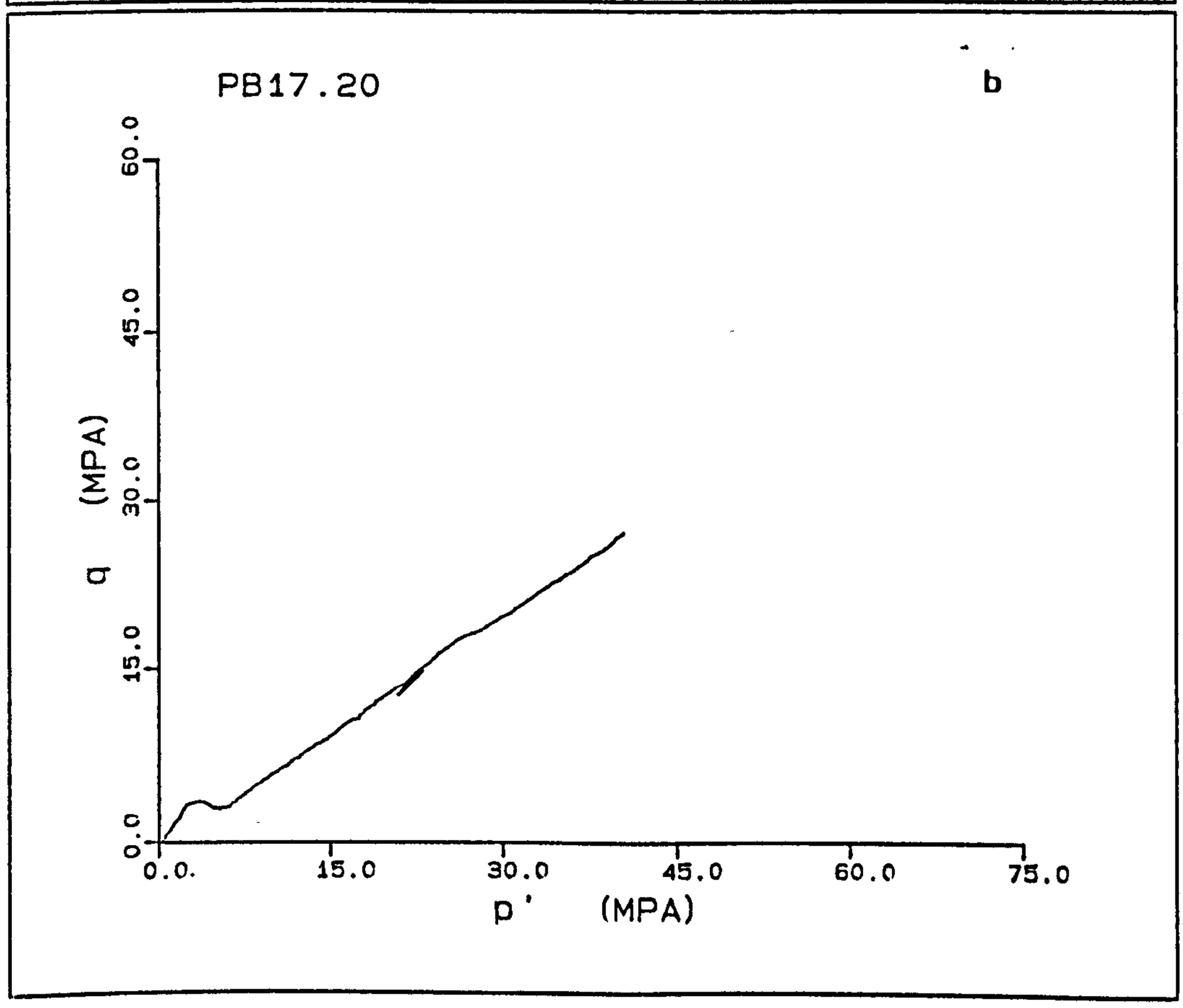

Figure A5.19(a-h) K_o test PB17.20.

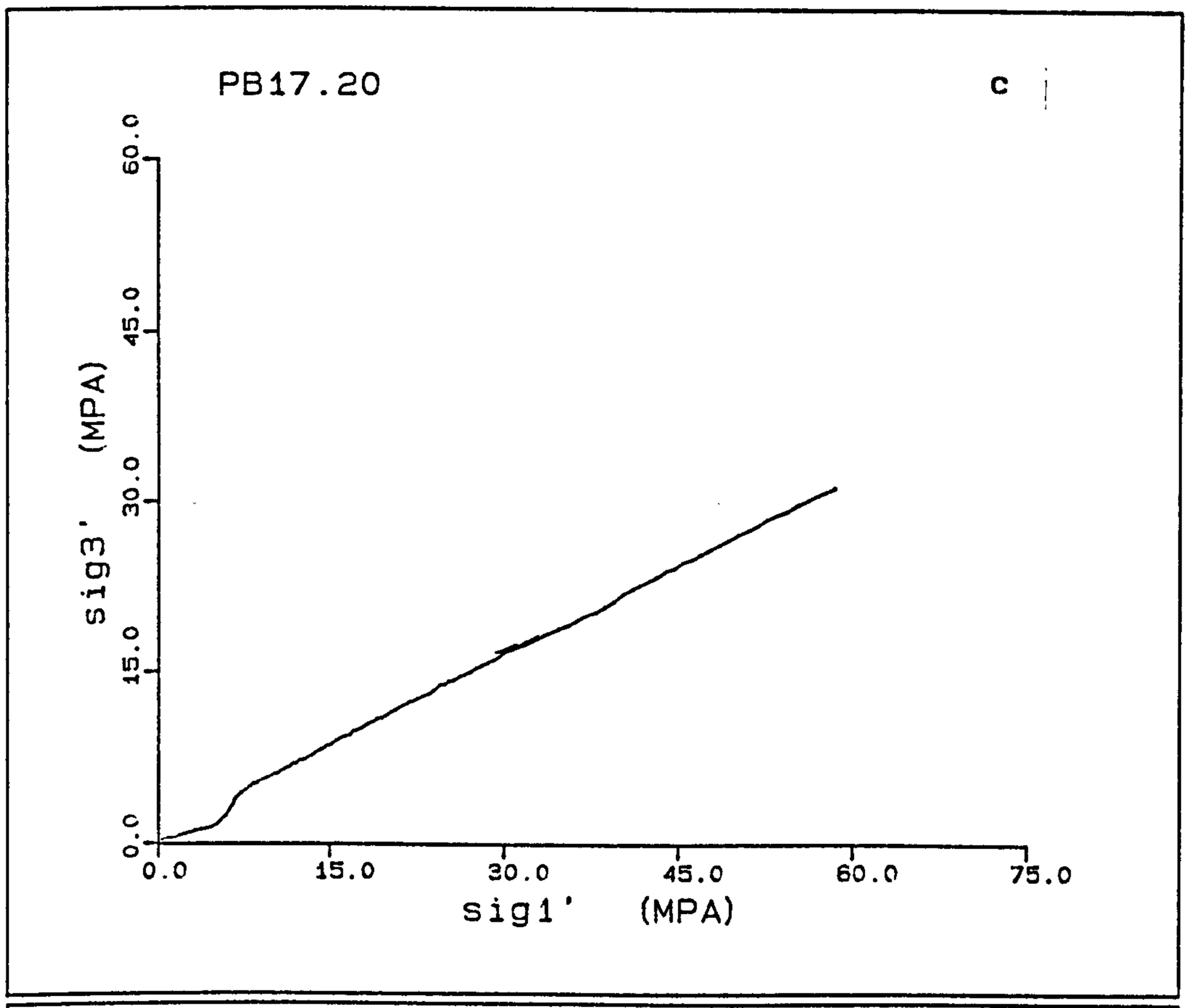
PB17.20
c
sig3' (MPA)
60.0
45.0
30.0
15.0
0.0
0.0
15.0
30.0
45.0
60.0
75.0
sig1' (MPA)

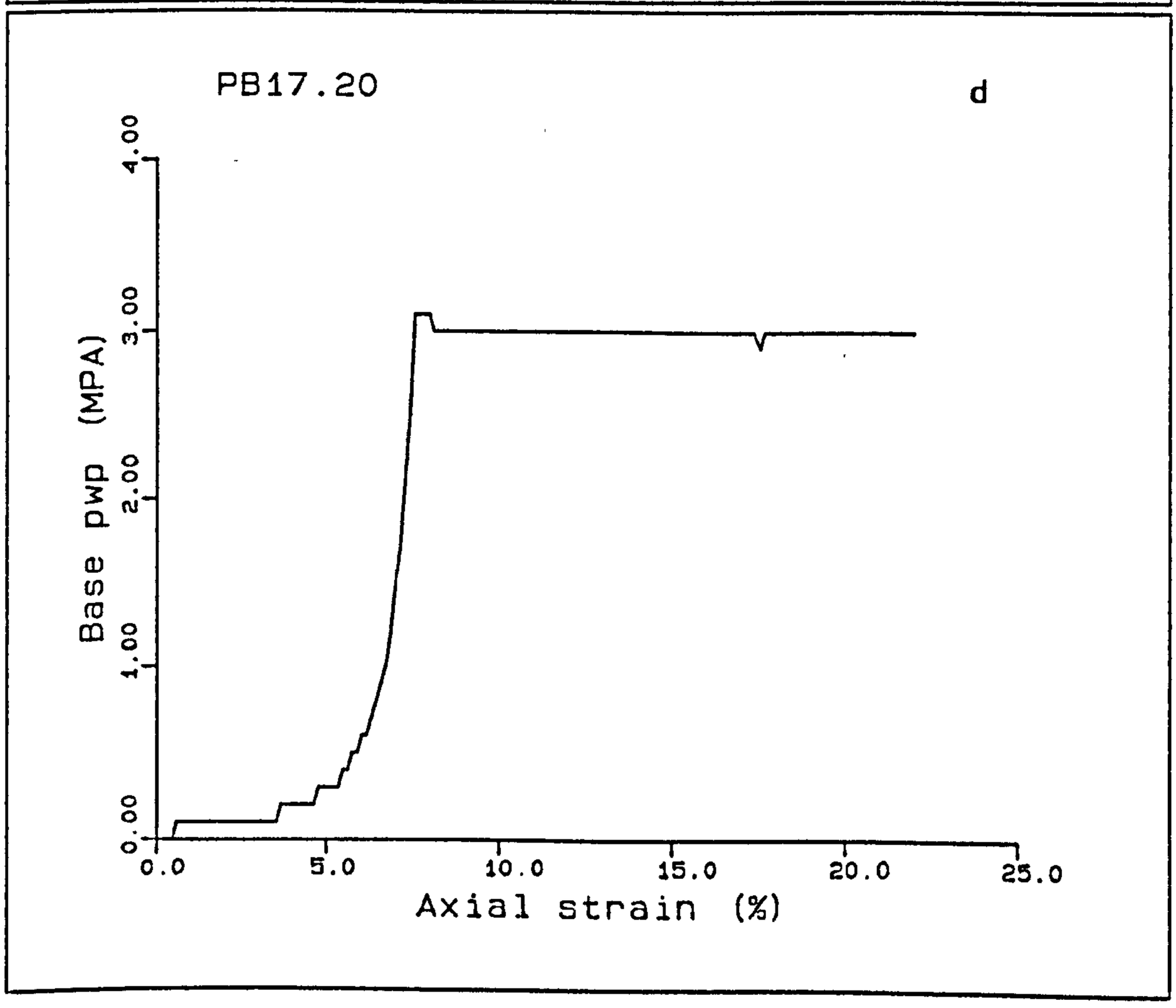
PB17.20
d
Base pwp (MPA)
4.00
3.00
2.00
1.00
0.00
0.0
5.0
10.0
15.0
20.0
25.0
Axial strain (%)

PB17.20

e

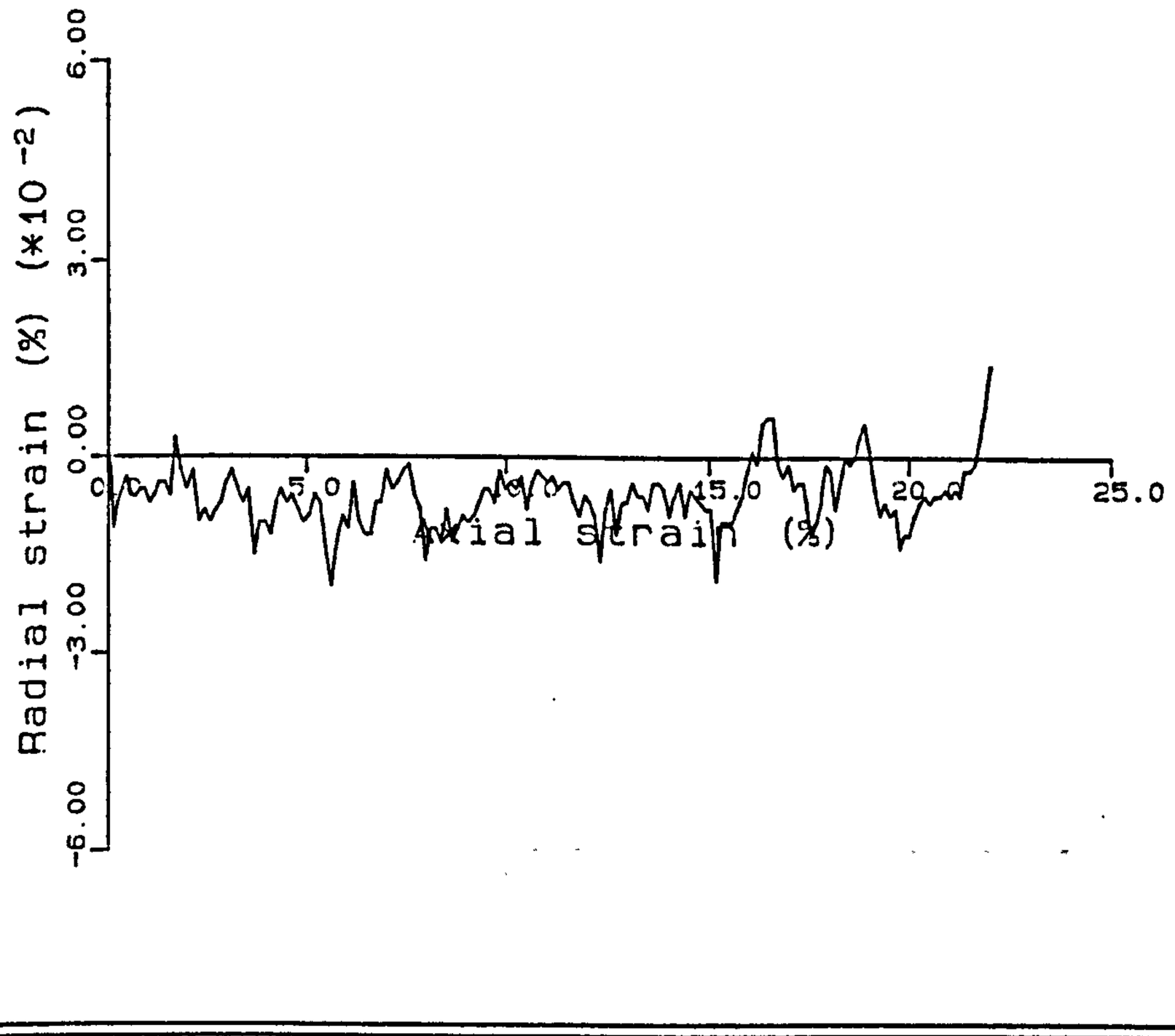

f

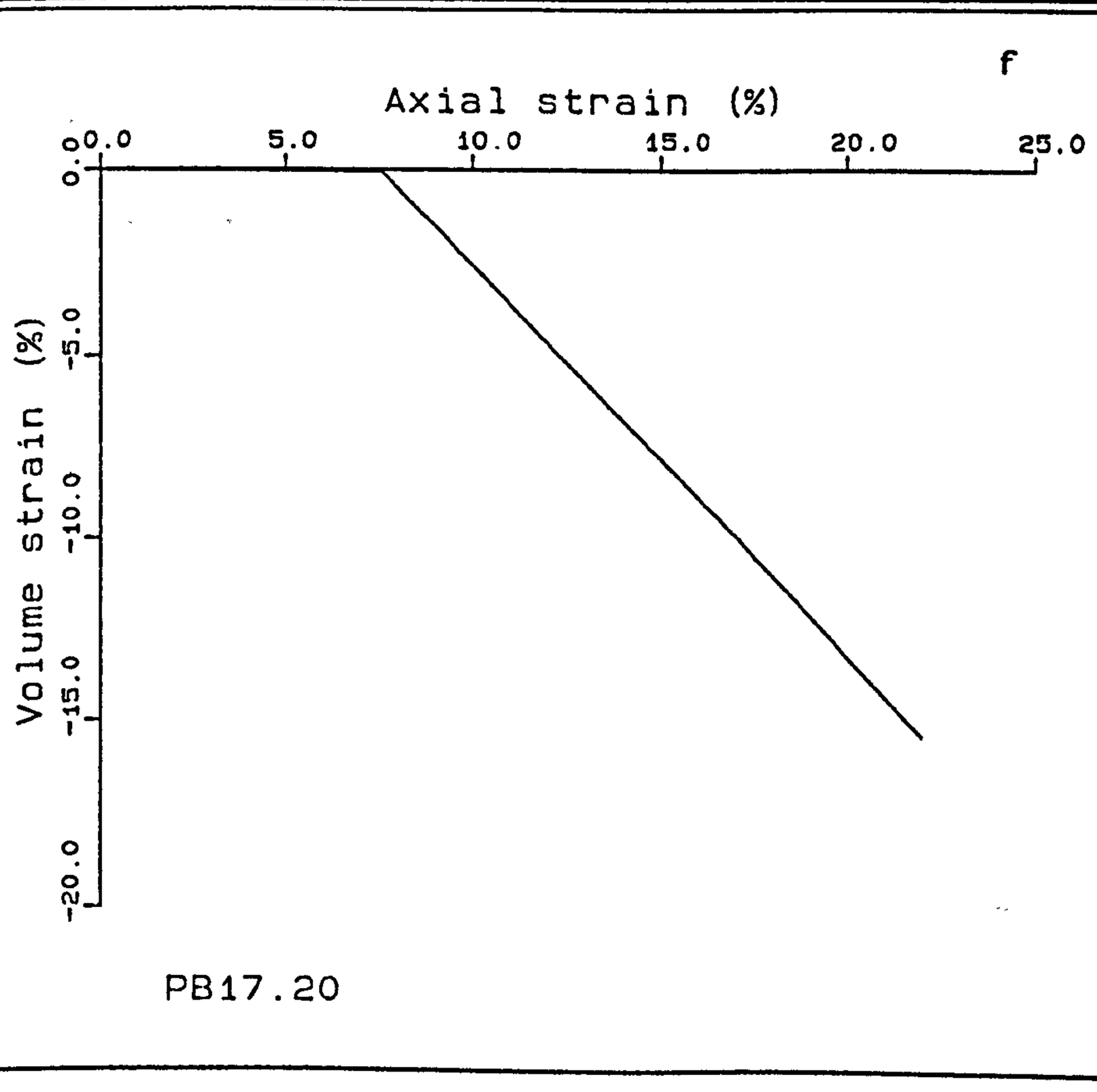

PB17.20

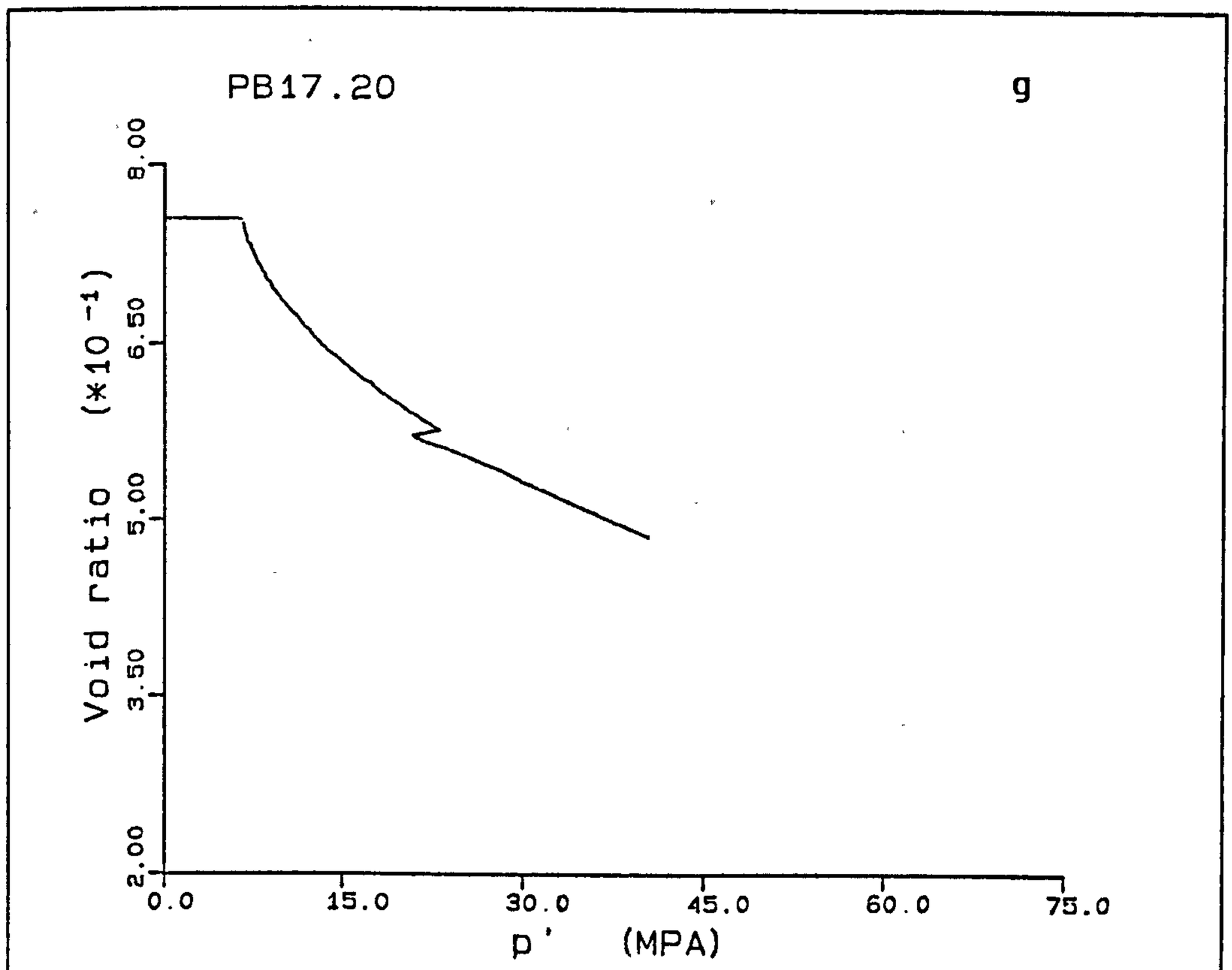
PB17.20
g
Void ratio (*10 -1)
8.00
6.50
5.00
3.50
2.00
0.0
15.0
30.0
45.0
60.0
75.0
p' (MPA)

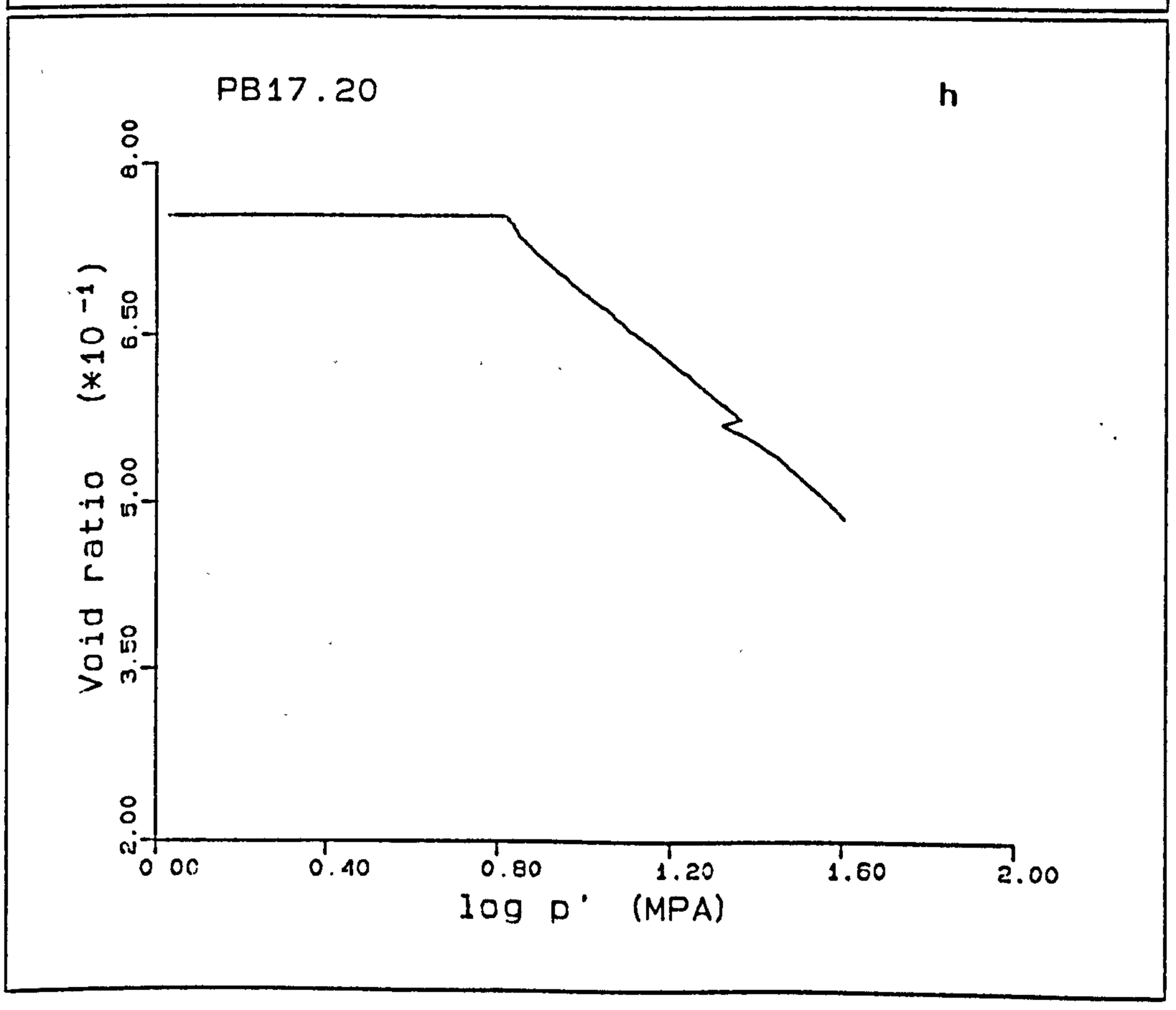
PB17.20
h
Void ratio (*10 -1)
8.00
6.50
5.00
3.50
2.00
0.00
0.40
0.80
1.20
1.60
2.00
log p' (MPA)

A5.4) BUTSER HILL CHALKS

The Pegwell Bay chalk samples used in this study had low yield points, approximately 5MPa deviatoric stress, and a low pecentage of impurities, defined as the insoluble residue (Chap. 3.5.2). In comparison, chalks from Butser Hill were tested, which have a lower porosity, Table A5.4, higher yield point and approximately 13% content of insoluble residue, or a calcimetry of 87%. The chalks are riddled with three stages of burrowing, so slight differences between samples were expected. Various tests were performed on these samples, K_o tests, drained and undrained shear tests and one hydrostatic test. The samples will be dealt with in these sub-sections. All of the samples used were obtained from one block, and sampled in the same direction, in case any directional anisotropy was present. This was done to keep any variation between samples to a minimum.

In these tests the second radial strain belt was used which enabled shearing to occur after K_o consolidation. New volume gauges were also used which enabled a back pressure to be applied before loading which enabled complete saturation of the samples.

The effect of temperature on the compaction of these chalks has been investigated. The samples were heated prior to loading, in undrained and drained conditions, these heating results are included with the appropriate experiment. The exception to this is test BH15.100 which had a membrane failure, the heating sequence of this test is included with BH16.100.

The summary of the K_o tests is presented in Table A5.4.

Table A5.4

Sample	Porosity %	Rate of loading mm/min	Average height mm	Average diameter mm	Saturated weight g	Dry weight g	Specific gravity g/cm3	Temperature ^{o}C
BH3.20	36.7	0.03	76.28	37.49	173.00	144.23	2.71	20
BH4.20	37.2	0.02	76.20	37.51	174.32	143.30	2.71	20
BH5.20	36.8	0.02	76.26	37.52	174.81	144.31	2.71	20
BH7.20	36.2	0.02	76.22	37.57	177.00	146.08	2.71	20
BH14.60	36.9	0.04	76.28	37.54	175.98	144.16	2.71	60
BH16.100	37.3	0.04	76.22	37.51	175.34	143.12	2.71	100
BH17.60	36.9	0.04	76.37	37.58	176.16	144.63	2.71	60
BH18.20	36.2	0.04	76.24	37.65	177.30	146.59	2.71	20

BH3.20

This test was performed on 36.7% porosity chalk, and is a K_o test followed by an undrained shear, only the K_o part of the tests will be discussed here. The sample was deformed at a rate of 0.03mm/min, as with the previous chalk tests. The stress-strain curve (Fig. A5.20a) shows that there is a well defined elastic section of the deformation, which has a tangential Young's modulus of 1.30GPa, and a yield point of 11.71MPa. This is seen as a peak deviatoric stress, the load increases after this to 11.8MPa thereafter decreasing to 11.3MPa. This is followed by the linear increase in q with p' in the normal consolidation compaction. A small loop occurs as the load dropped, probably due to the manual adjustment of the cell pressure. The radial strain for the deformation initially increased to $20*10^{-3}$% where it was maintained with a variation of $10*10^{-3}$%, one deviation occurs outside this range at an axial strain of 5.3% and a radial strain of $1*10^{-3}$%, this forming the loop in Fig. A5.20b mentioned above. At an axial strain of 13.1% the test was stopped and an undrained shear performed, USB3.20 (after the pore pressure which had built up in the experiment had dissipated). The new volume gauge supplied a back pressure at 2.0MPa $\pm$0.1MPa, the large variation being due to the fact that the air regulator was fully open, and hence has no effect on the air flow, consequently the volume gauge was open to the laboratory air supply. The pore pressure at the top of the sample can be seen to increase from the start of the experiment from the initial back pressure value to 2.9MPa at 11.3% axial strain, after which the sample was drained from both ends. The values of $\bar{K}_o$ for the deformations are $\bar{K}_{opc}$=1.018, and $\bar{K}_{onc}$=0.572; $\bar{K}_{oe}$ was indeterminate as no constant value was seen for the deformation.

The whole volume strain can now be seen, the void ratio plots are essentially the same as the Pegwell Bay samples, the e-log p' plot showing a normal trend of two linear portions about a yield point. The volume gauge used in this experiment was the high pressure volume gauge.

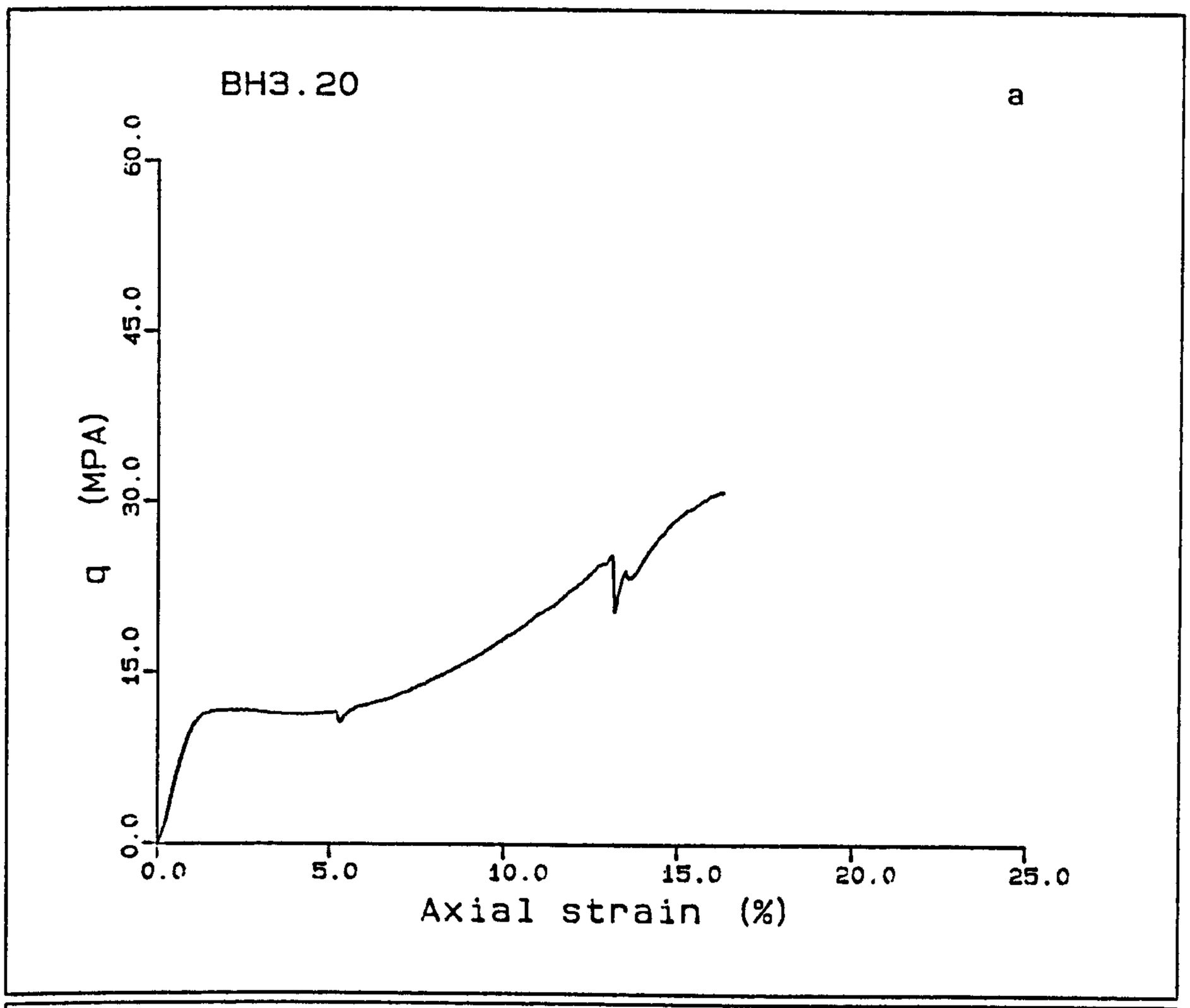

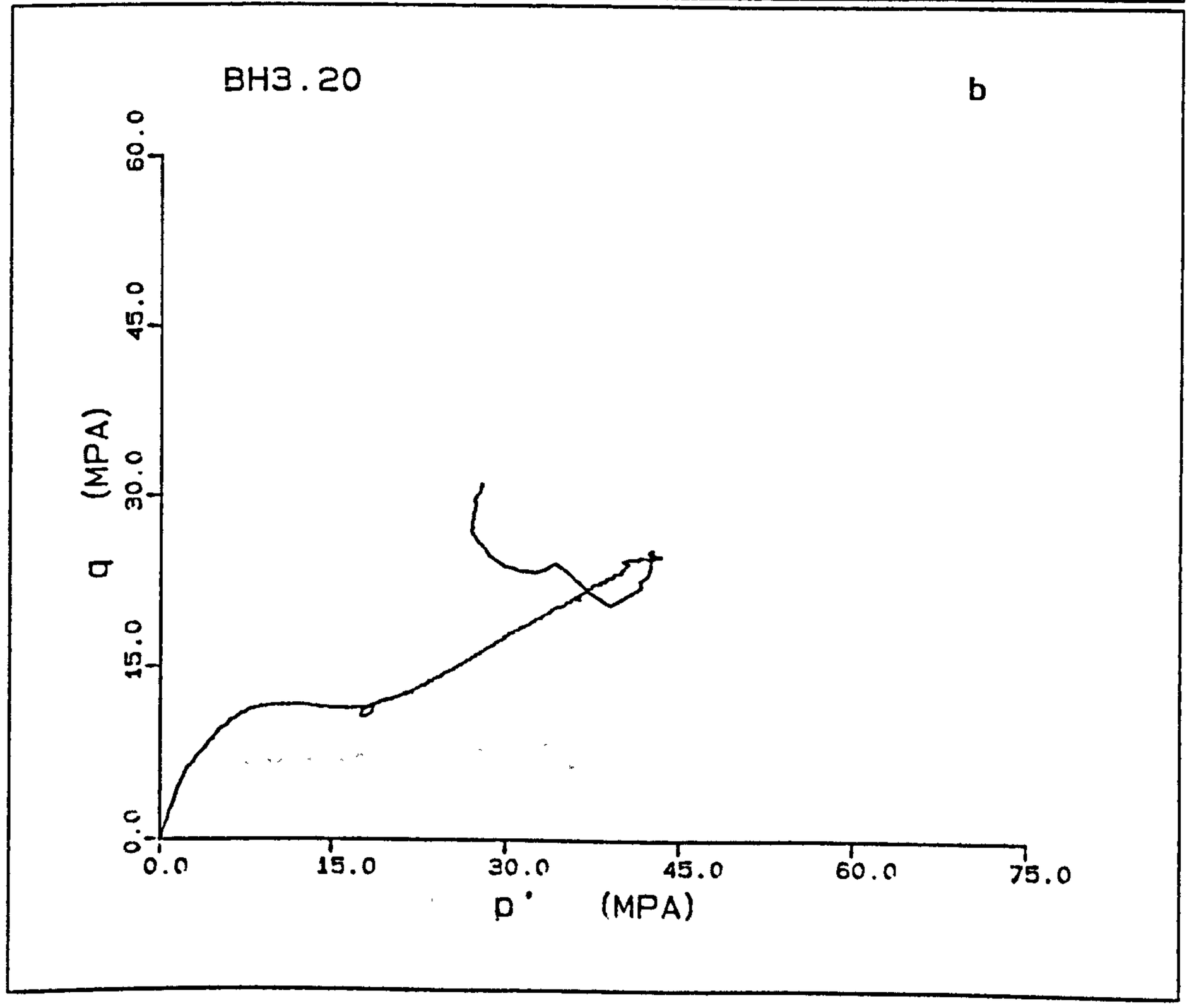

Figure A5.20(a-h) K_o test BH3.20.

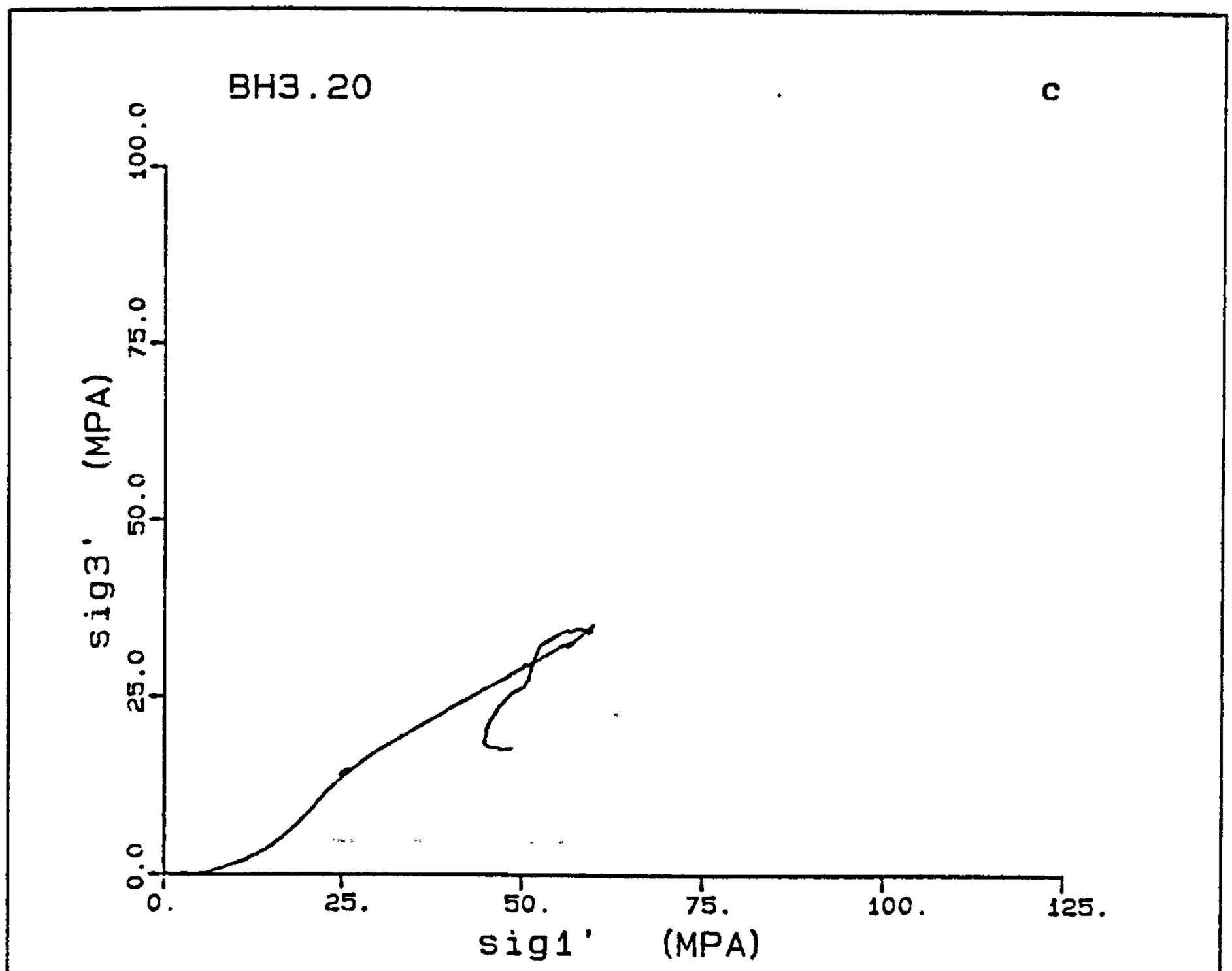
BH3.20
c
100.0
75.0
50.0
25.0
0.0
sig3' (MPA)
0.
25.
50.
75.
100.
125.
sig1' (MPA)

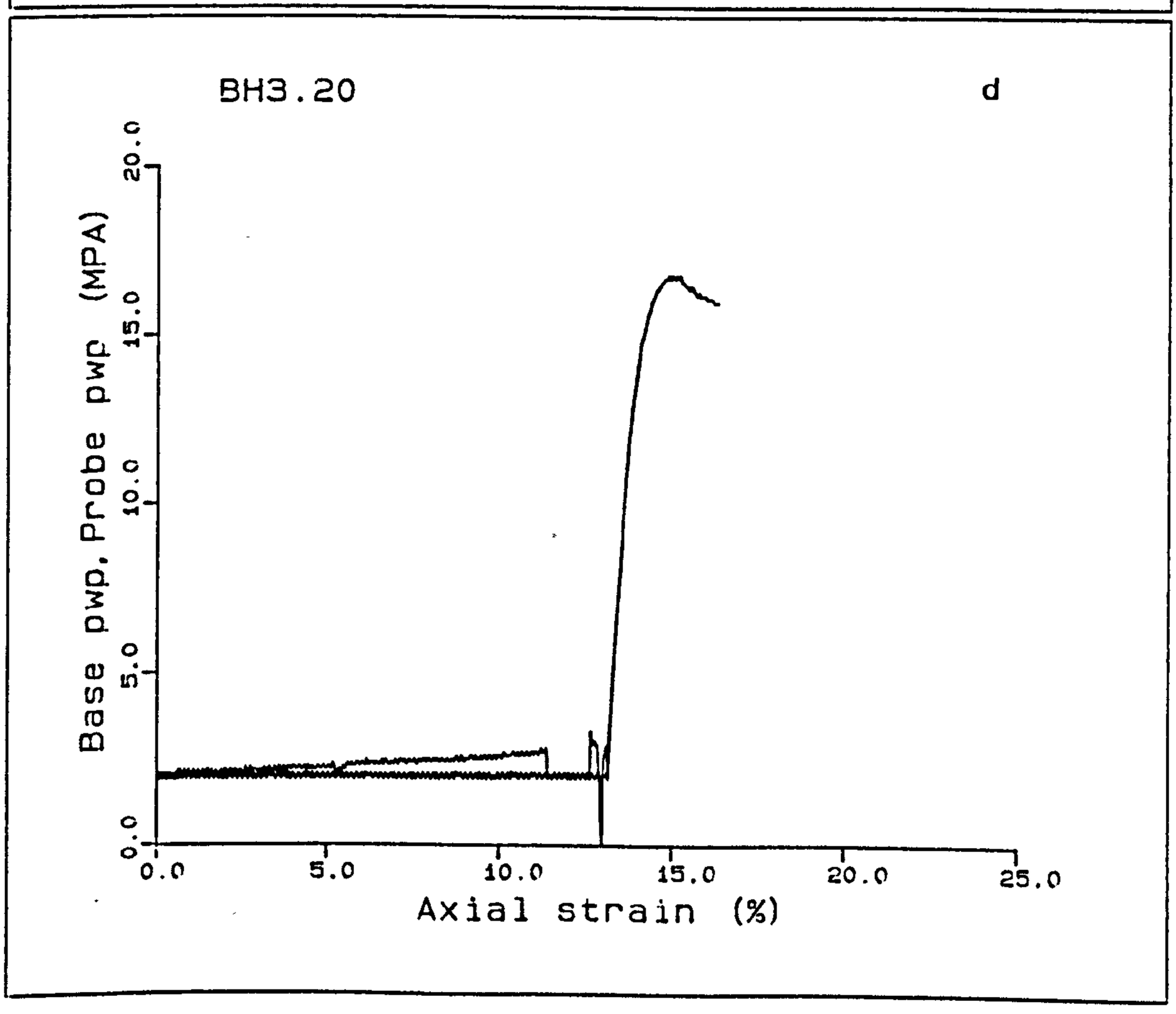
BH3.20
d
20.0
15.0
10.0
5.0
0.0
Base pwp, Probe pwp (MPA)
0.0
5.0
10.0
15.0
20.0
25.0
Axial strain (%)

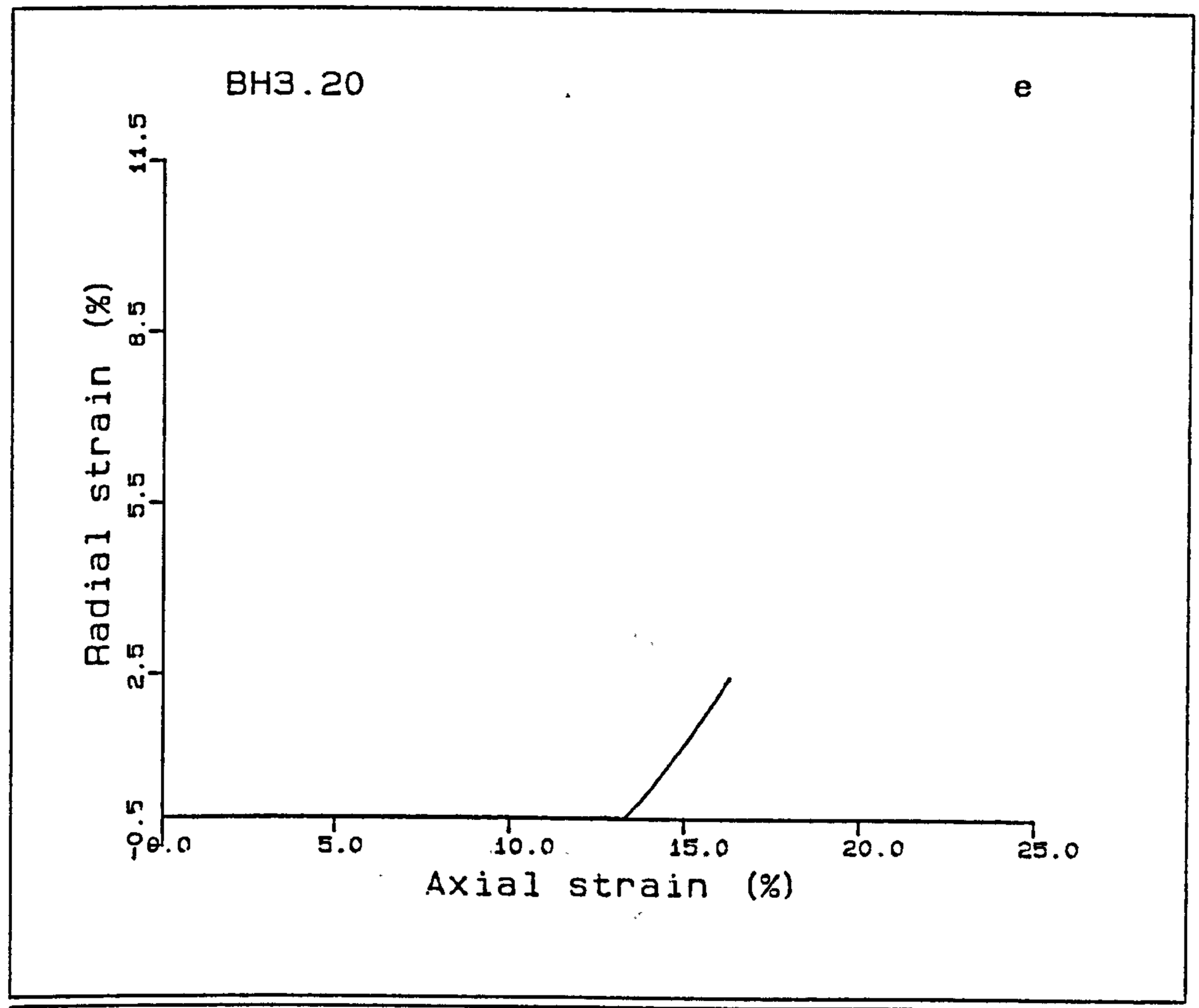
BH3.20
e
Radial strain (%)
11.5
8.5
5.5
2.5
-0.5
0.0
5.0
10.0
15.0
20.0
25.0
Axial strain (%)

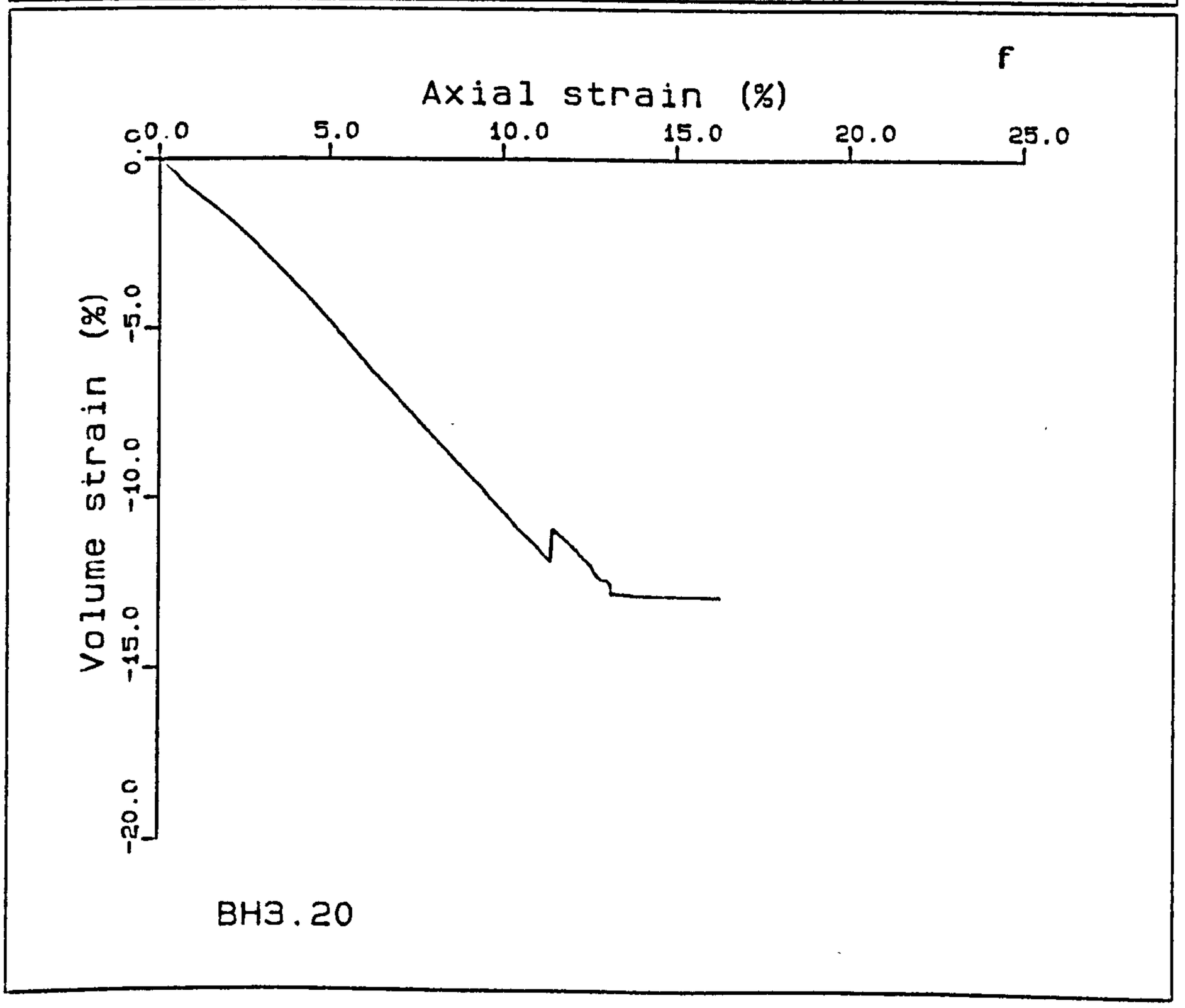
f
Axial strain (%)
0.0
5.0
10.0
15.0
20.0
25.0
0.0
-5.0
-10.0
-15.0
-20.0
Volume strain (%)
BH3.20

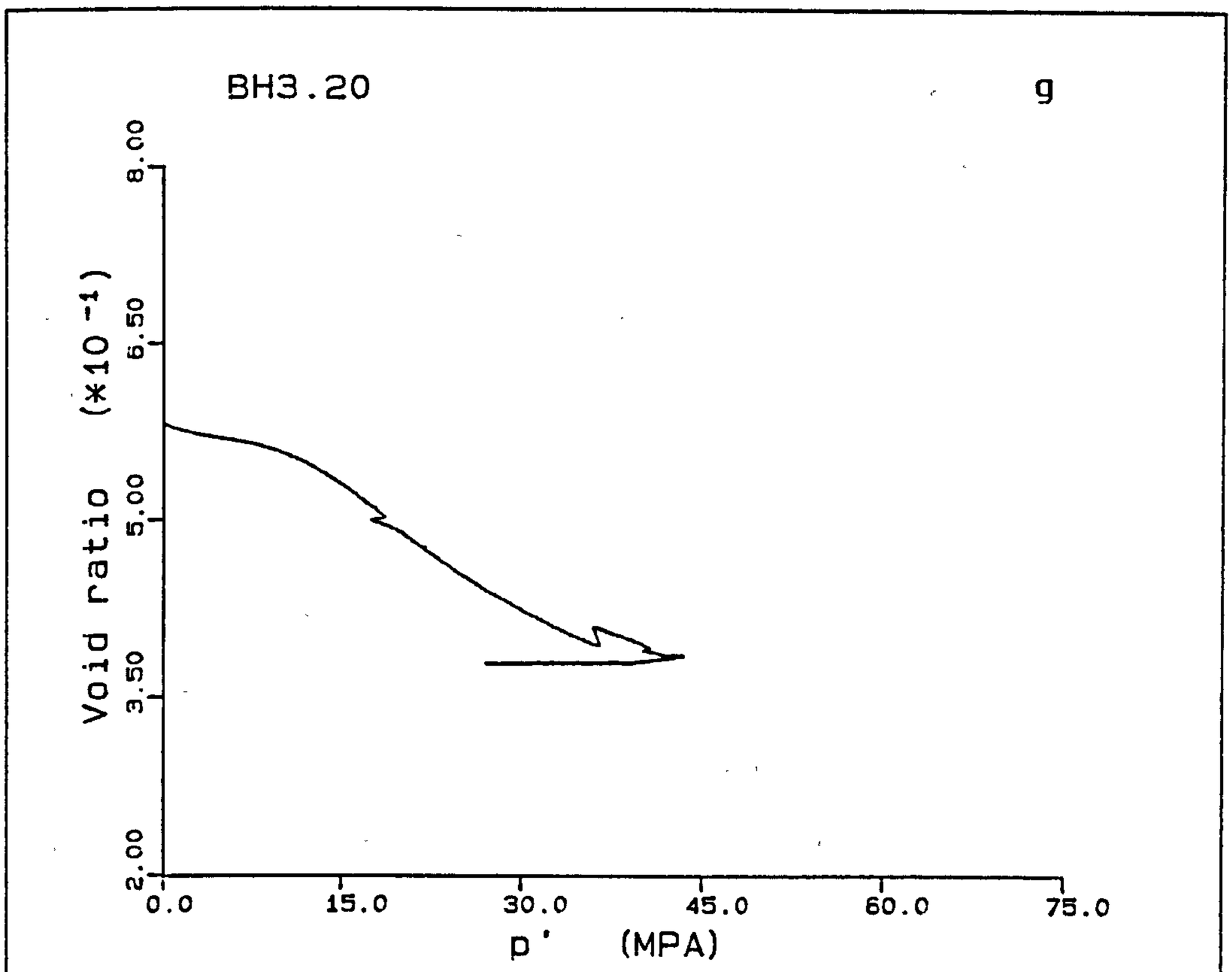
BH3.20
g
Void ratio (*10 -1)
8.00
6.50
5.00
3.50
2.00
0.0
15.0
30.0
45.0
60.0
75.0
p' (MPA)

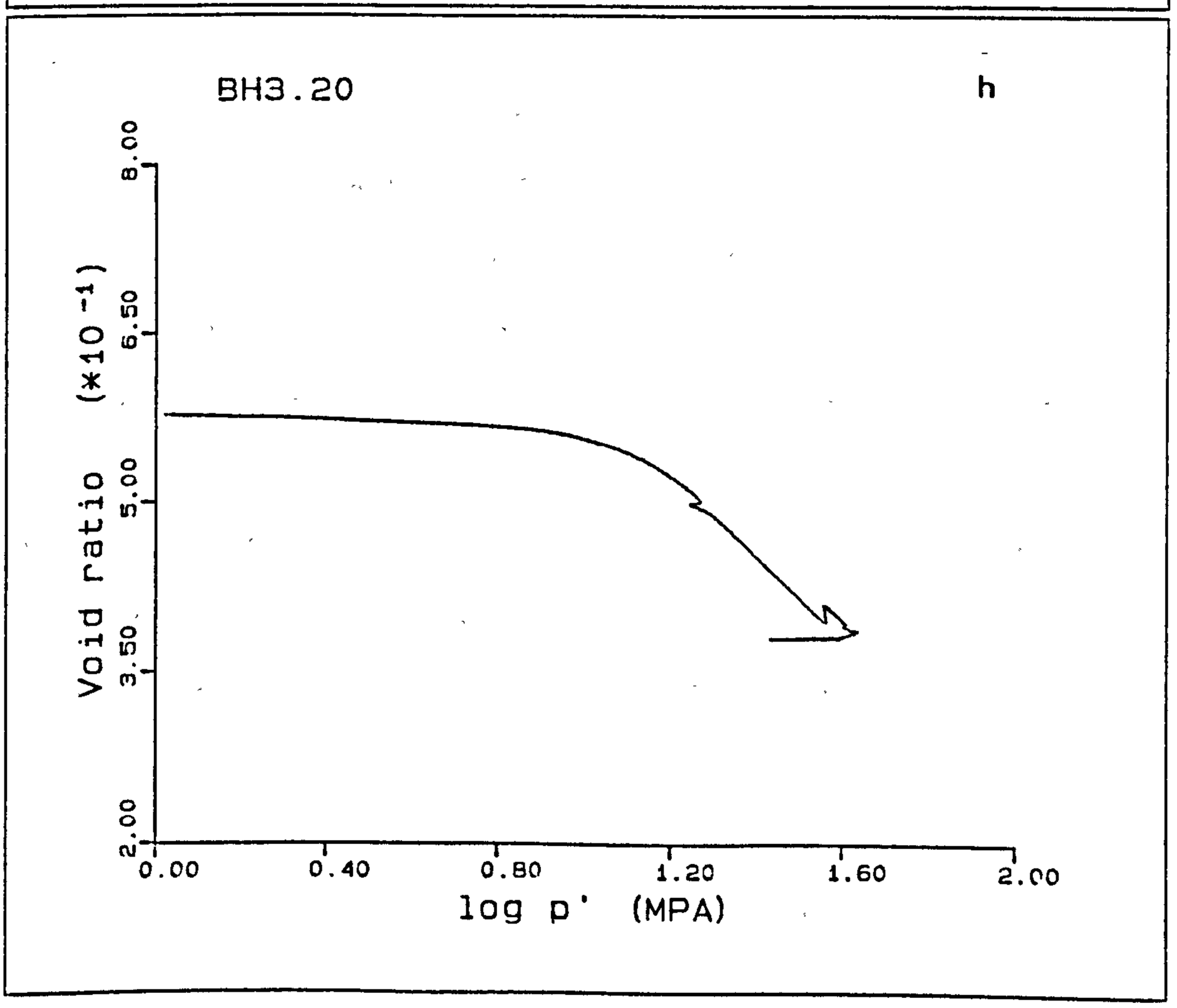
BH3.20
h
Void ratio (*10 -1)
8.00
6.50
5.00
3.50
2.00
0.00
0.40
0.80
1.20
1.60
2.00
log p' (MPA)

BH4.20

This is a 37.2% porosity sample which was deformed at a rate of 0.02mm/min. The sample shows an initial elastic deformation with a tangential modulus of 1.50GPa, the yield being well defined, by a peak at 11.72MPa. The pre-yield response has an initial K_{oe} of 0, i.e. a drained shear test, up to a maximum effective stress of 6MPa, the rest of the elastic section deforming with a K_{oe} of 0.405, the section being curved in Fig. A5.21b. The post-yield deformation of the chalk is accompanied by a large decrease in the load carrying capacity of the sample, the deviatoric stress decreasing to 10.3MPa, a drop of 1.4MPa, the cell pressure increasing steadily throughout this section. Subsequently the load increases steadily with some slight variation due to problems with the cell pressure control system. The $\bar{K}_o$ values obtained for these deformations are $\bar{K}_{opc}$=1.470 and $\bar{K}_{onc}$=0.558. The radial strain for this experiment initially varied a great deal in the $\bar{K}_o$=0 section with radial strains upto 0.5%, but after reaching the $\bar{K}_o$=0.405 section at a maximum effective stress of 6MPa, the strains remained at 0.158%, with an average variation of $\pm 7*10^{-3}$%. The radial strain, dropped to 0.120% over the erratic section at the start of the normally consolidated deformation, the radial strain was then recovered and limited to its 0.158% value, up to an axial strain of 13%. This was followed by an undrained shear test USB4.20. The back pressure in this experiment was 1.9MPa, the pore pressure at the top of the sample increasing from the mean value (fluctuations being due to cell pressure variations which caused the initial problems in the radial strain) to 2.3MPa at 13% axial strain. The volume change plot shows linear slopes before and after yield, with a slight initial variation at the start of the normal consolidation deformation.

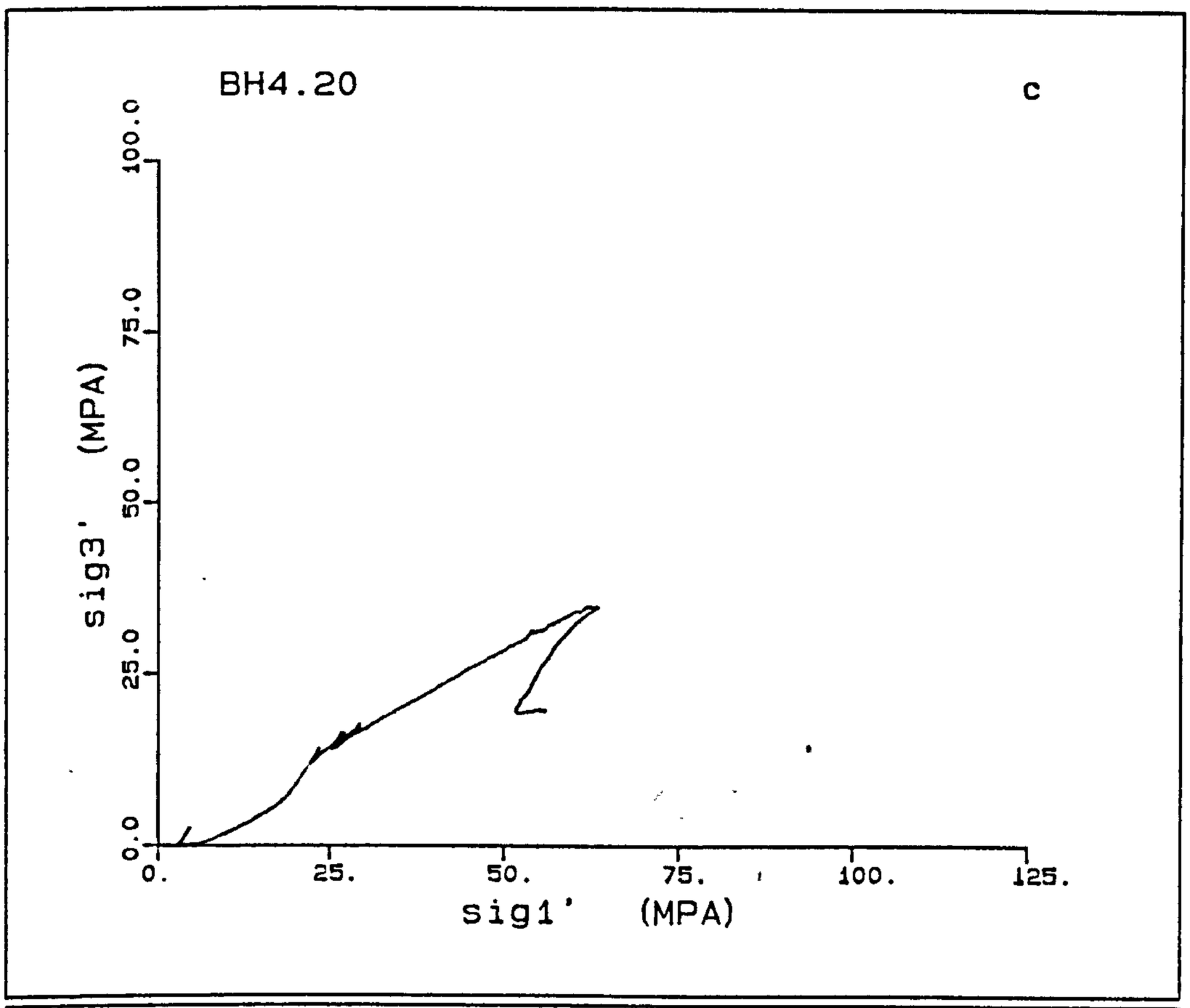
BH4.20
c
sig3' (MPA)
100.0
75.0
50.0
25.0
0.0
0.
25.
50.
75.
100.
125.
sig1' (MPA)

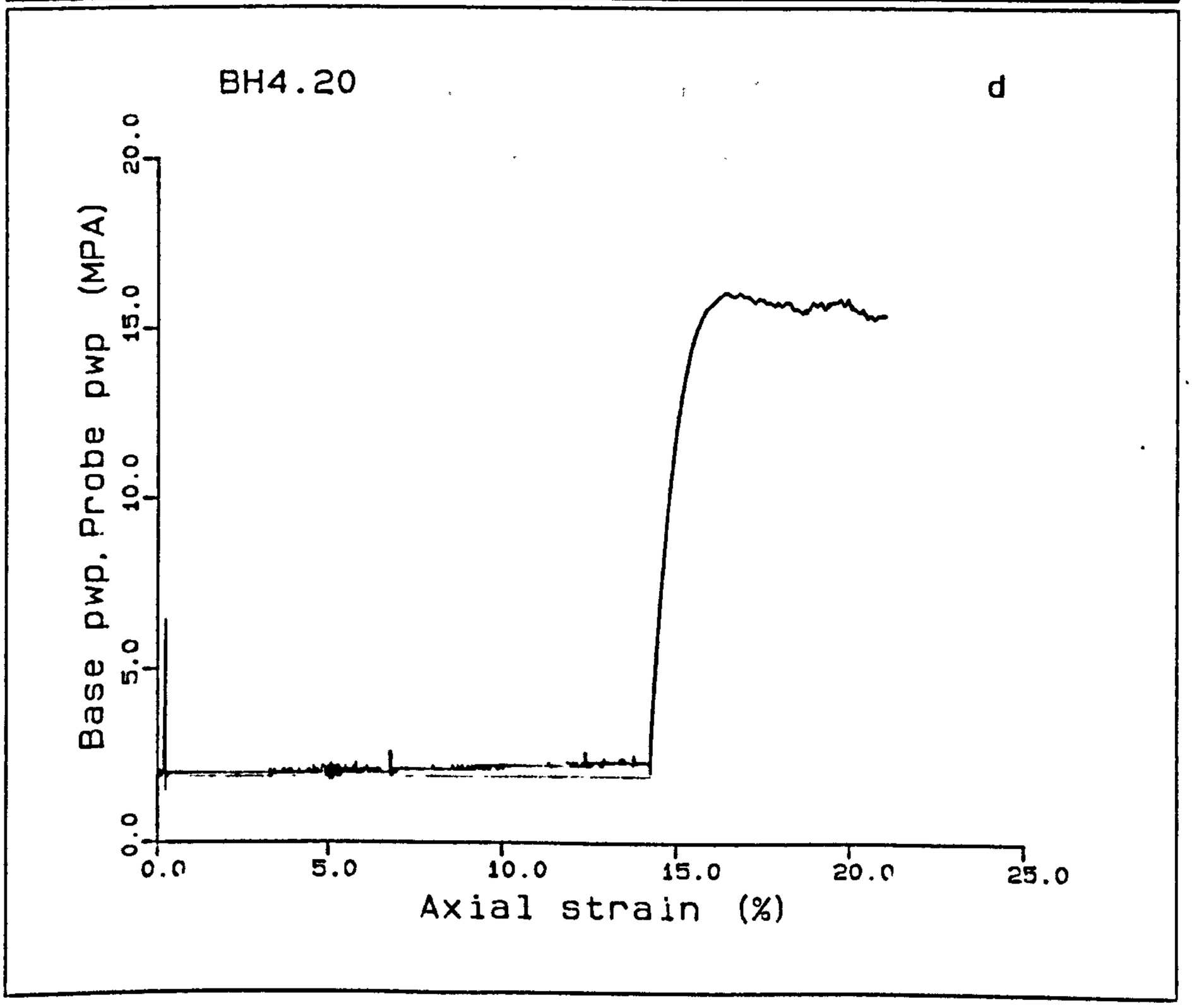
BH4.20
d
Base pwp, Probe pwp (MPA)
20.0
15.0
10.0
5.0
0.0
0.0
5.0
10.0
15.0
20.0
25.0
Axial strain (%)

BH4.20

e

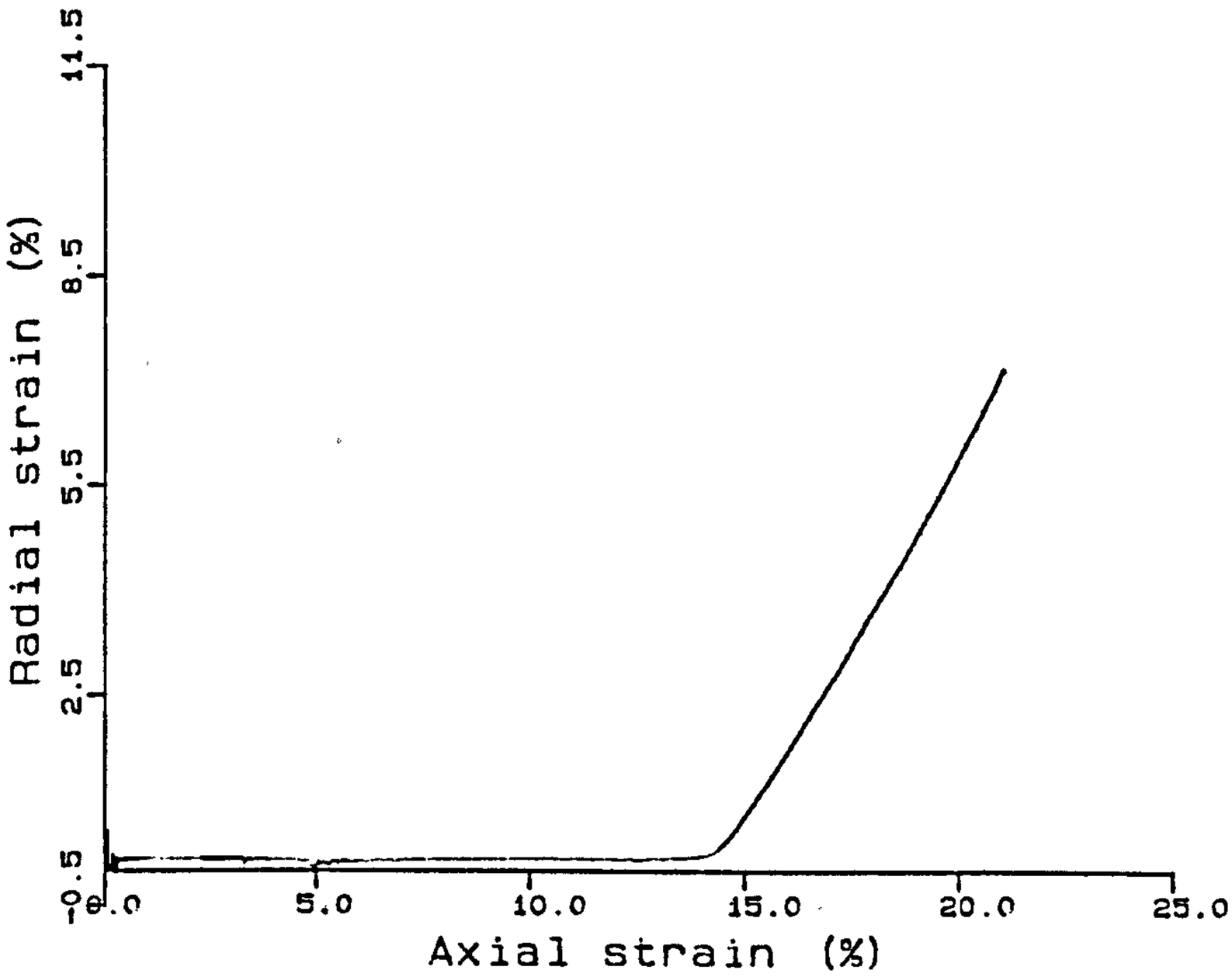

f

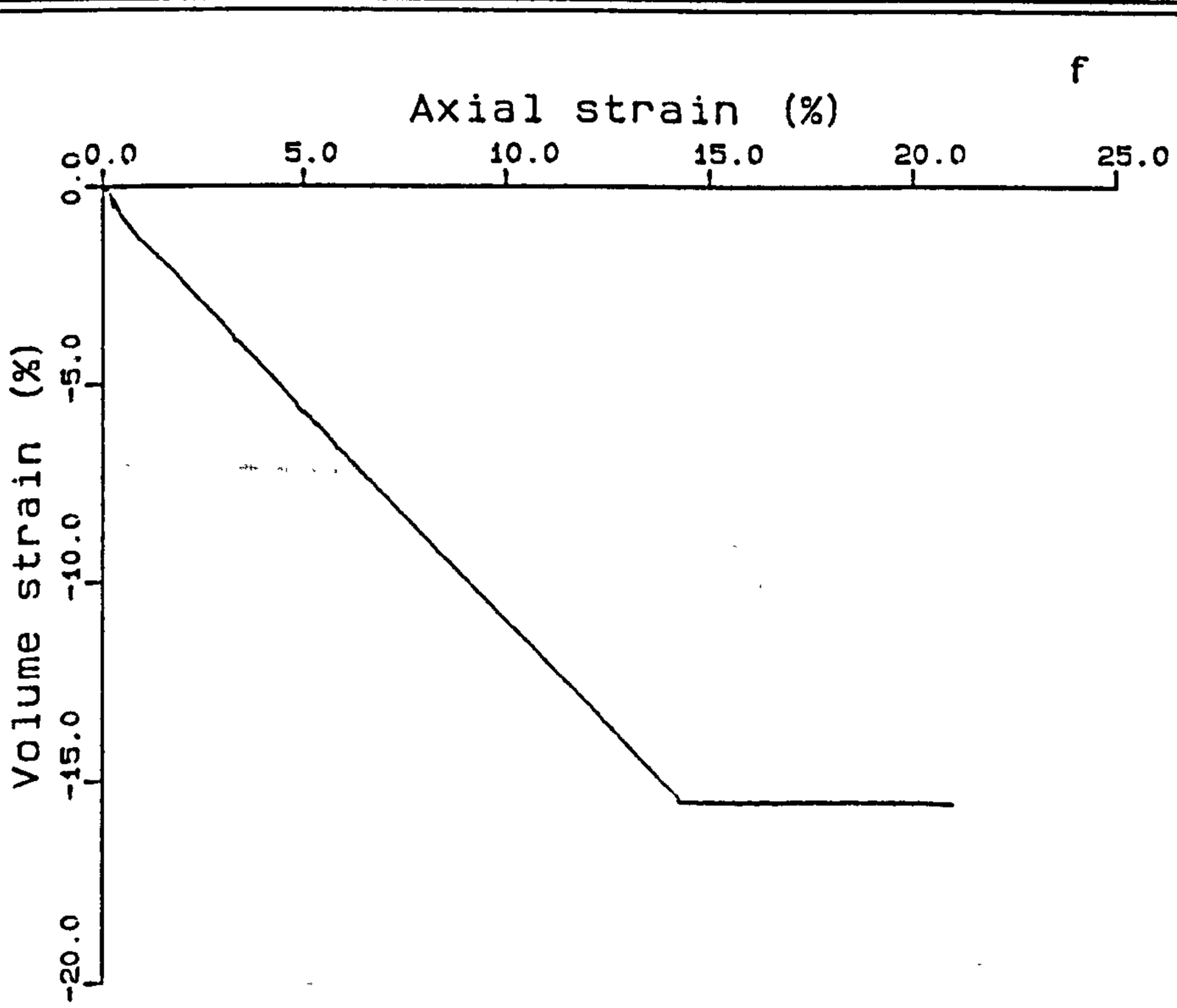

BH4.20

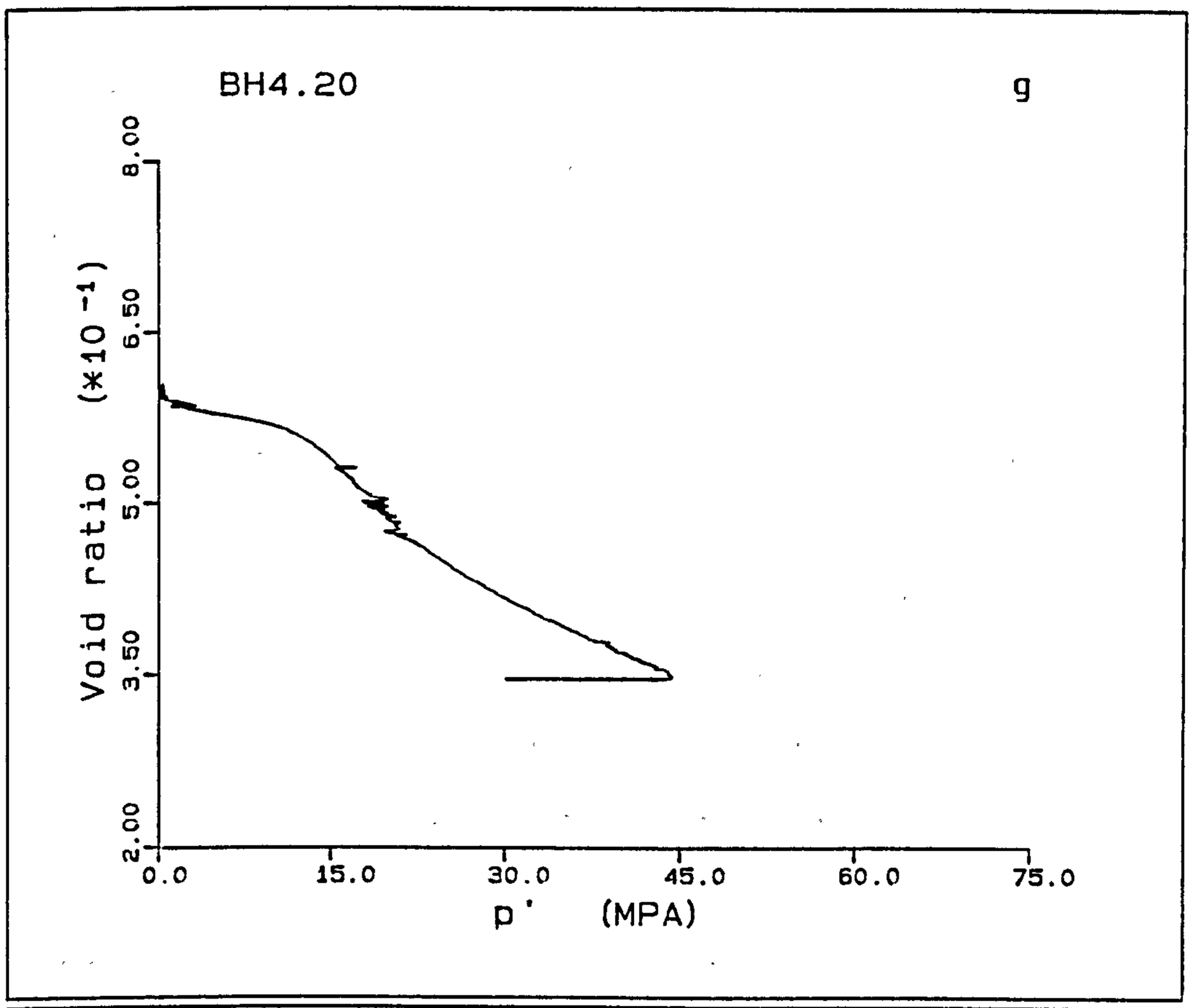
BH4.20
g
Void ratio (*10 -1)
8.00
6.50
5.00
3.50
2.00
0.0
15.0
30.0
45.0
60.0
75.0
p' (MPA)

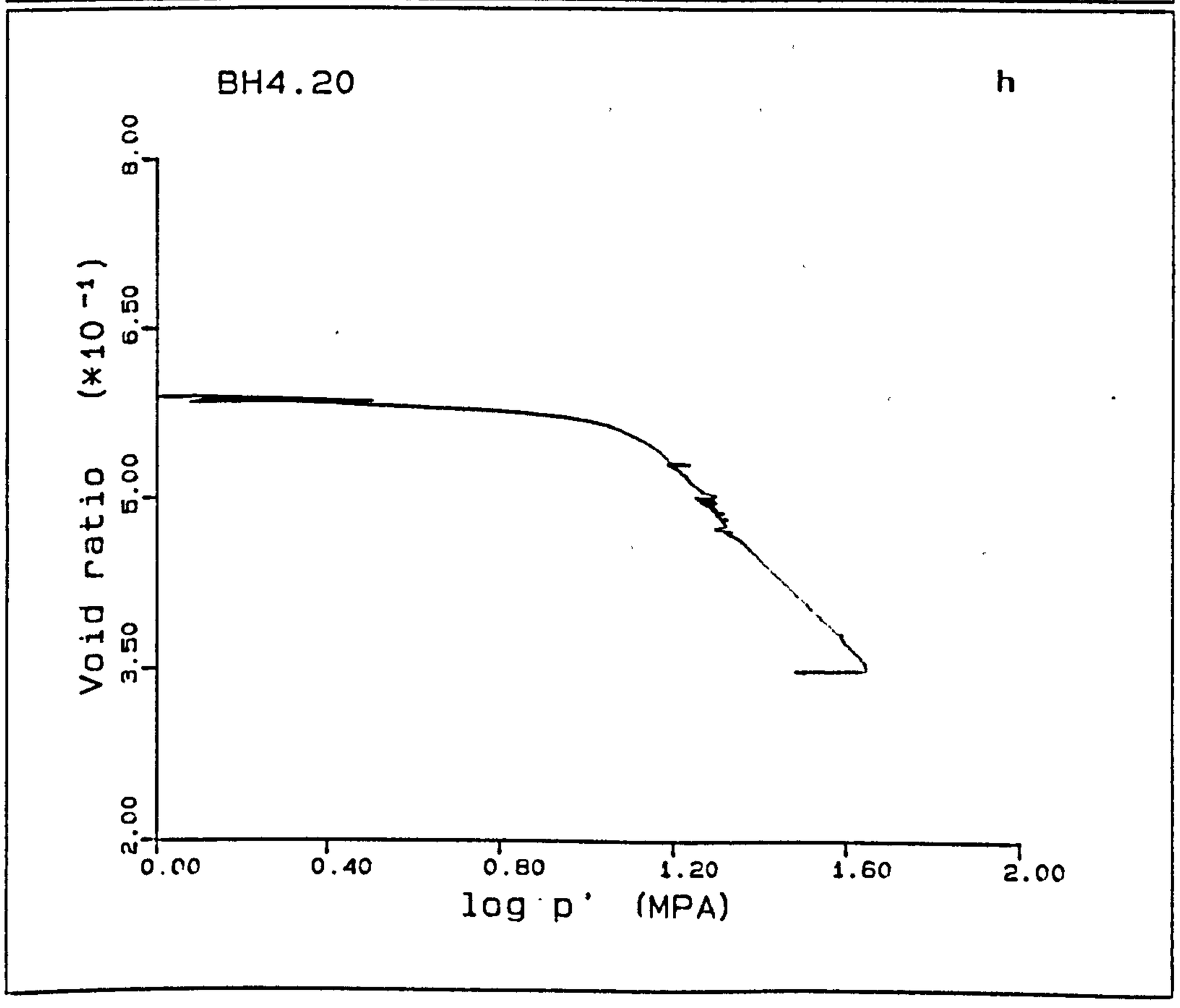
BH4.20
h
Void ratio (*10 -1)
8.00
6.50
5.00
3.50
2.00
0.00
0.40
0.80
1.20
1.60
2.00
log p' (MPA)

BH5.20

This sample of 36.8% porosity Butser Hill chalk was deformed at a constant deformation rate of 0.02mm/min, the sample following a K_o deformation up to an axial strain of 9.2%, it then being deformed under undrained shear conditions as USB5.20. The sample deforms initially with a tangential modulus of 0.72GPa, the chalk yielding at a deviatoric stress of 10.24MPa. The post-yield deformation does not show a reduction in load but a small increase. As in the last experiment, the start of normal consolidation was associated with problems with the cell pressure controlling system. The drop in load at 5.9% axial strain was the samples reaction to an increase in the rate at which the cell pressure controlling system pump operates. The $\bar{K}_o$ values for the elastic, pore collapse (plastic) and normal consolidation (work hardening) deformations are 0.215, 0.978, and 0.613 respectively. The radial strain initially increases by 0.340% up to 0.02% axial strain, after which it remains constant within a range of 15*10-3% above the 0.340% value. The radial strain went outside this value during the initial part of the normal consolidation curve, occasionally dropping momentarily to 0.290% radial strain. The pore pressure starts at a back pressure of 1.9MPa, the top pore pressure building up to 2.1MPa at 9.2% axial strain. The volume changes seen are similar to those of BH3.20 and BH4.20.

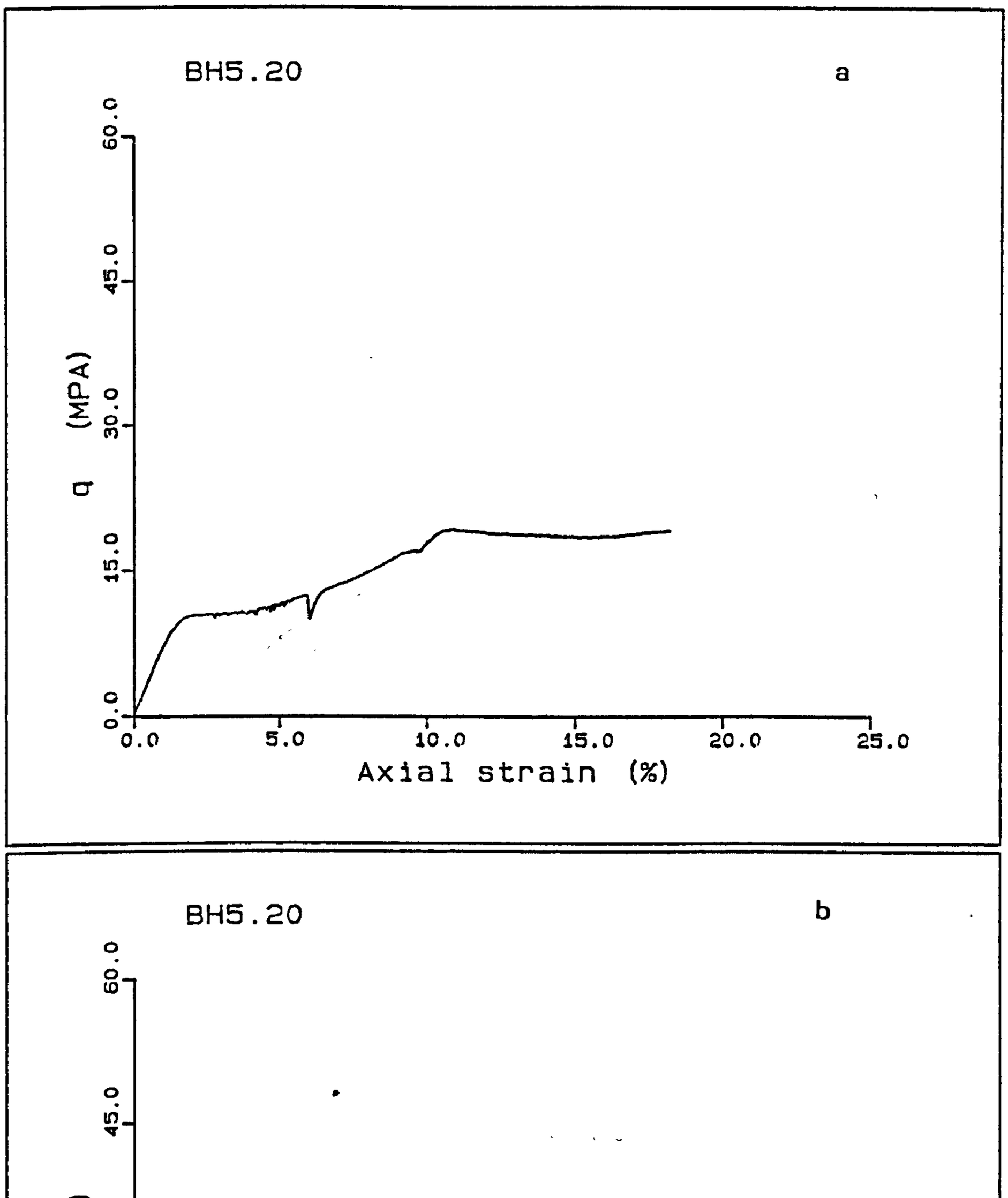

Figure A5.22(a-h) K_o test BH5.20.

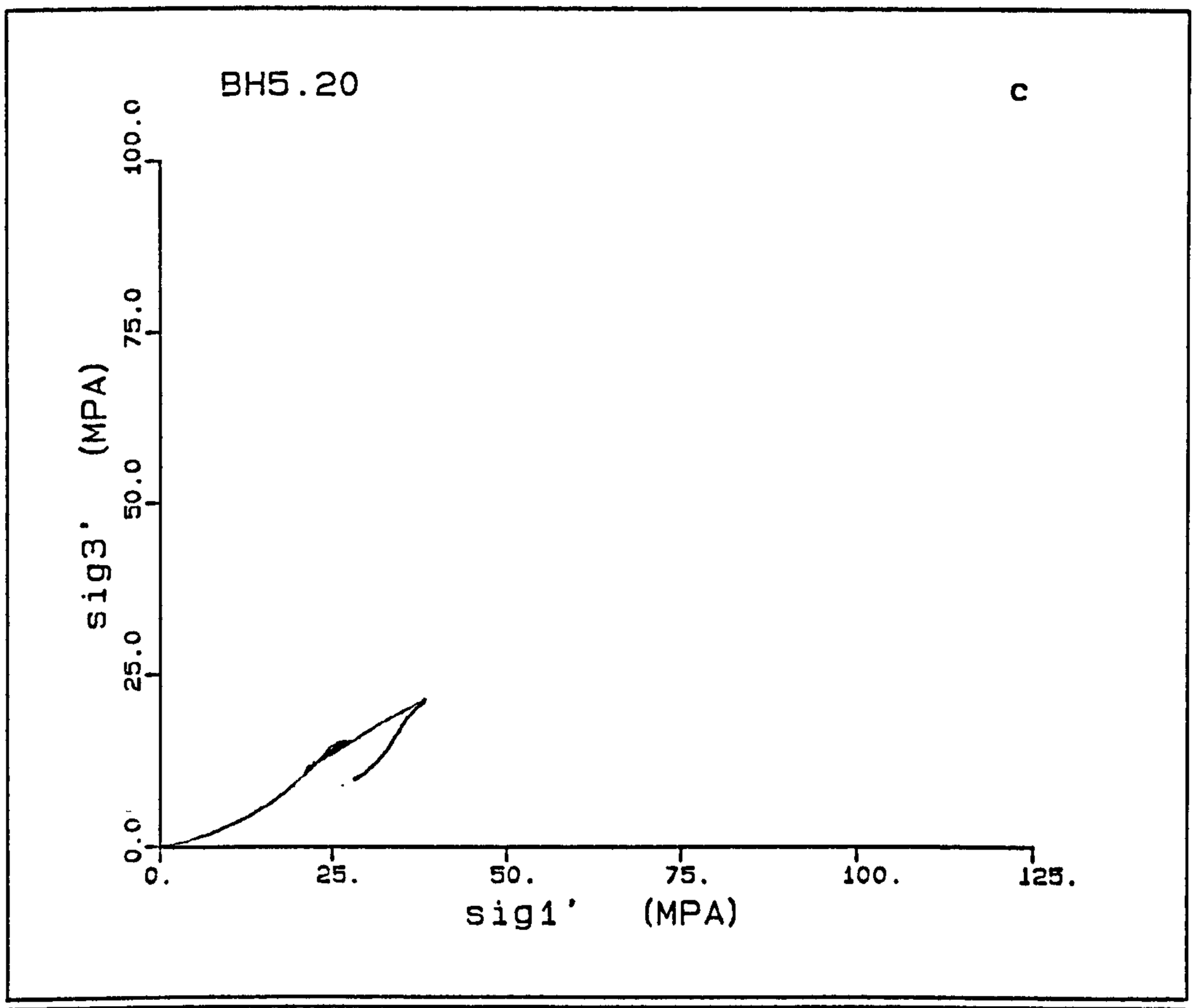
BH5.20
c
sig3' (MPA)
100.0
75.0
50.0
25.0
0.0
0.
25.
50.
75.
100.
125.
sig1' (MPA)

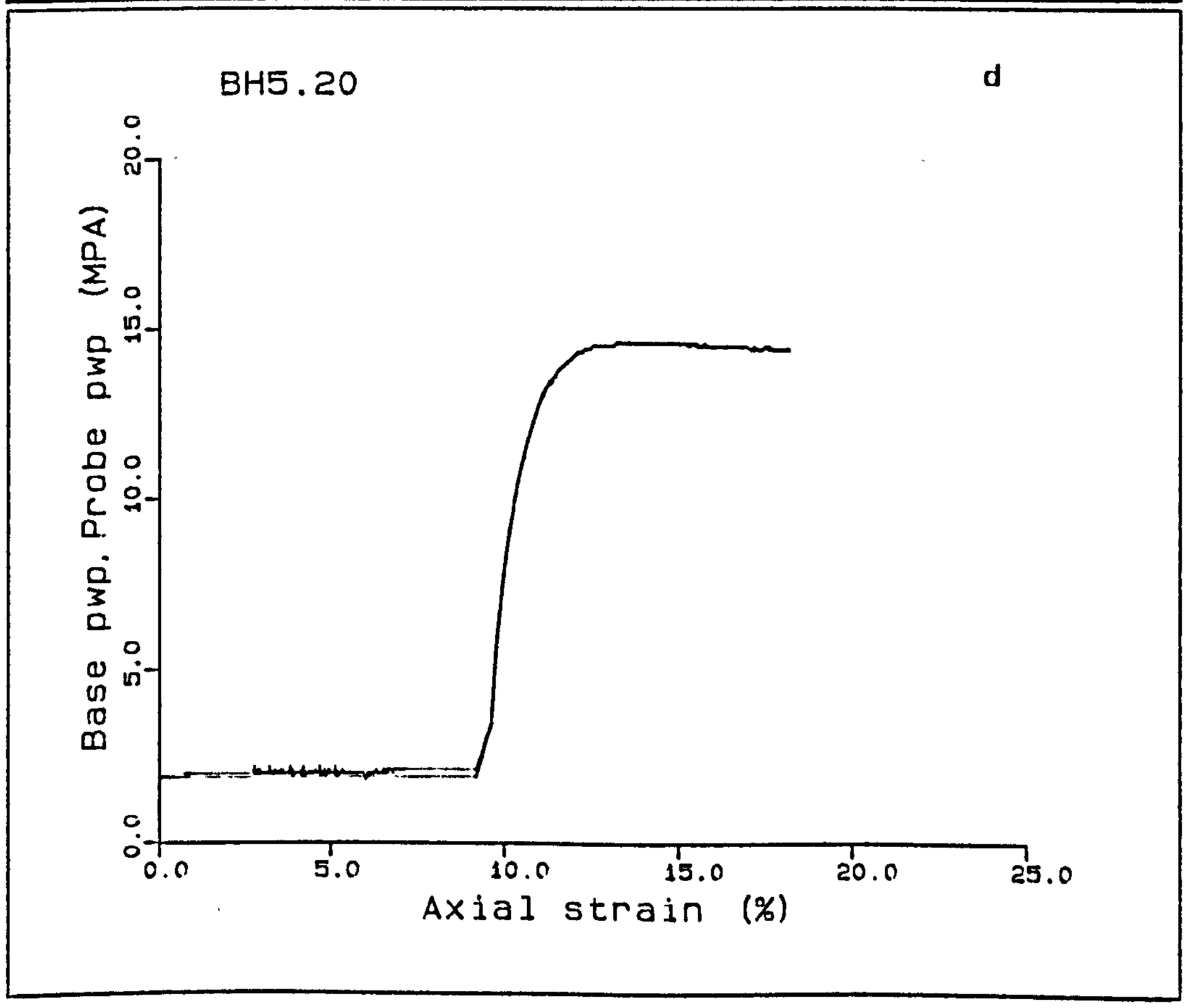
BH5.20
d
Base pwp, Probe pwp (MPA)
20.0
15.0
10.0
5.0
0.0
0.0
5.0
10.0
15.0
20.0
25.0
Axial strain (%)

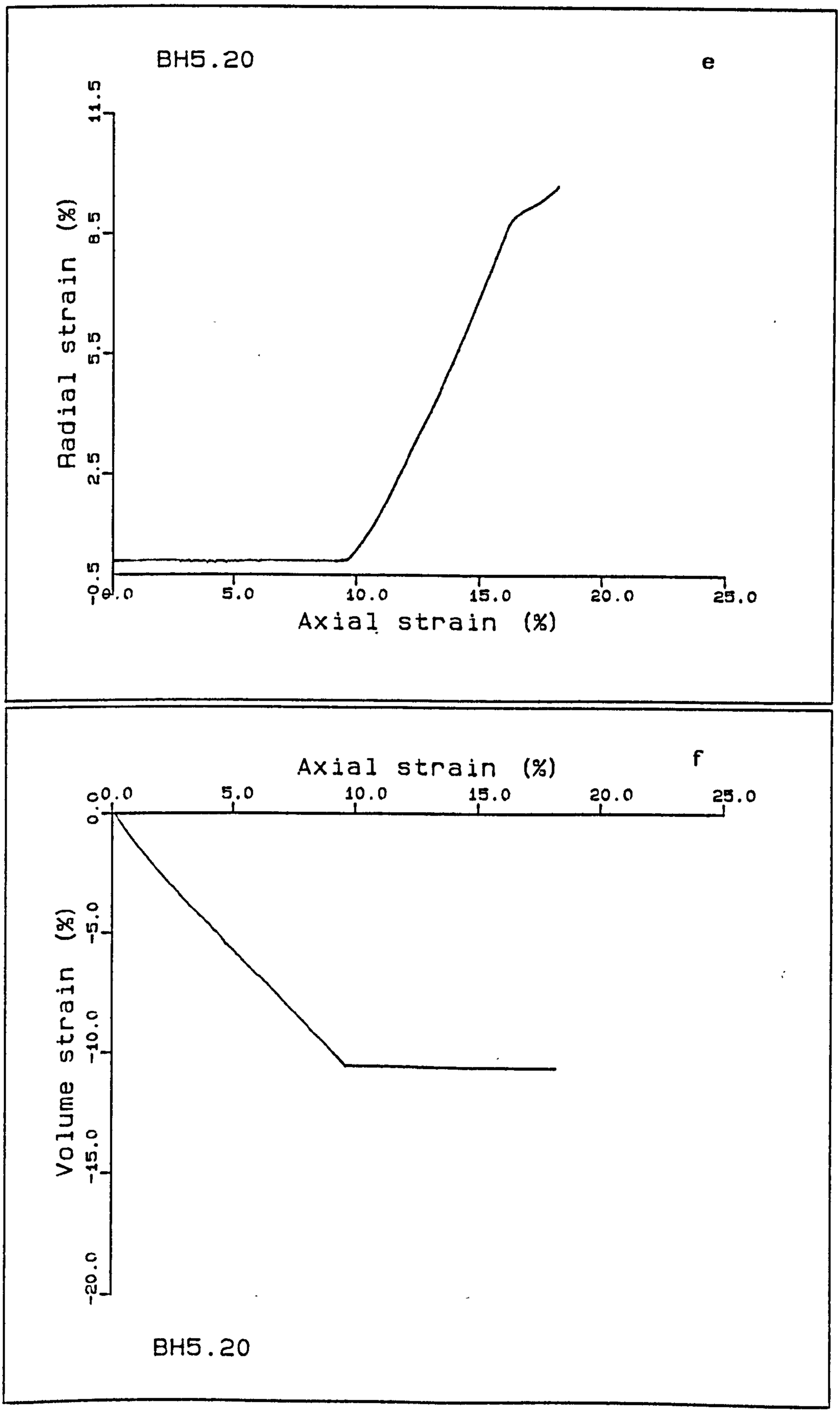
BH5.20
e
Radial strain (%)
11.5
8.5
5.5
2.5
-0.5
0.0
5.0
10.0
15.0
20.0
25.0
Axial strain (%)
f
Axial strain (%)
0.0
5.0
10.0
15.0
20.0
25.0
Volume strain (%)
0.0
-5.0
-10.0
-15.0
-20.0
BH5.20

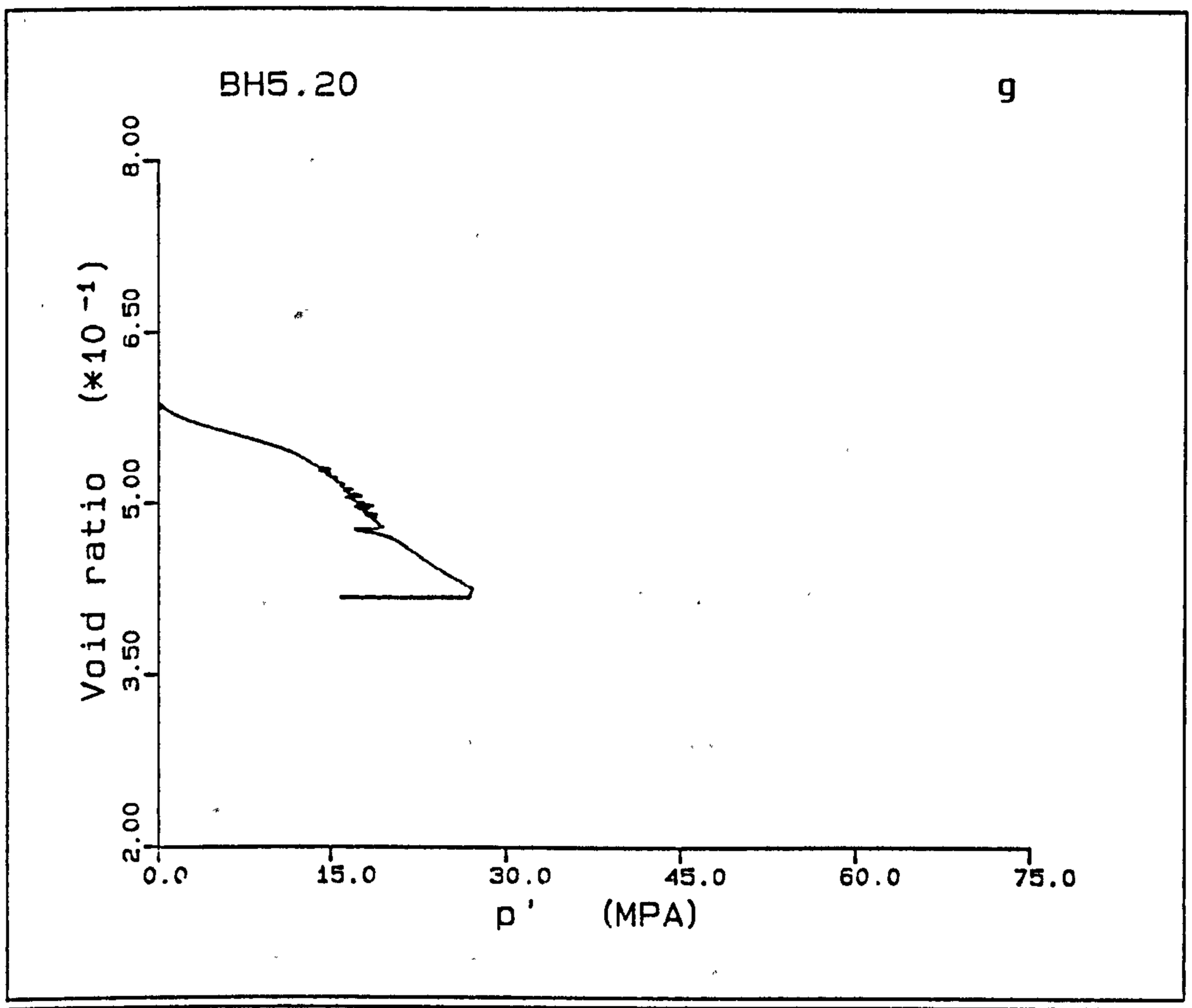
BH5.20
g
Void ratio (*10 -1)
8.00
6.50
5.00
3.50
2.00
0.0
15.0
30.0
45.0
60.0
75.0
p' (MPA)

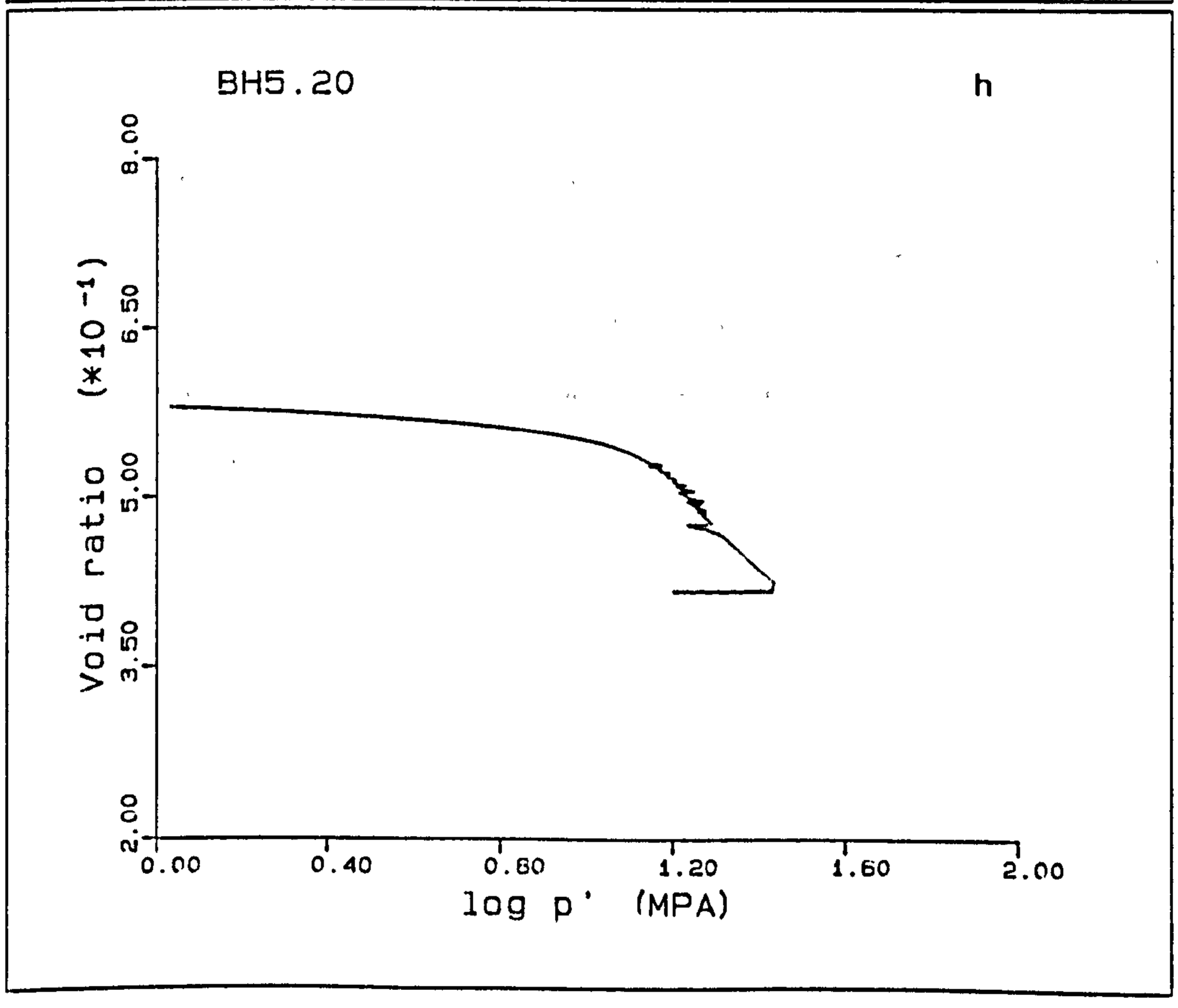
BH5.20
h
Void ratio (*10 -1)
8.00
6.50
5.00
3.50
2.00
0.00
0.40
0.80
1.20
1.60
2.00
log p' (MPA)

BH7.20

BH7.20 is a 36.2% chalk which was deformed at 0.02mm/min, the sample deforming under K_o conditions, again showed a two staged elastic response to stress, the first part of which has a $\bar{K}_o$=0, i.e. drained shear, up to an approximate mean effective stress of 6MPa. At higher values of p', the minimum effective stress increases with the maximum effective stress, a curved section of the K_o stress path being seen in Fig. A5.23c. The elastic modulus for the elastic deformation is 1.48GPa, the yield of the structure occurring at 12.21MPa deviatoric stress. The post-yield response of the sample to strain is a decrease of the deviatoric stress to 11.7MPa, after which the stress increases in the normally consolidated part of the deformation. The $\bar{K}_o$ values for these sections are 1.052 and 0.568. The radial strains for this experiment, Fig. A5.23e, vary by $+15*10^{-3}$% about the zero strain.

Only the base pore pressure is presented in Fig A5.23, because the output from the top pore pressure transducer was erratic again. Between these erratic readings, a gradual increase in the pore pressure at the undrained end of the sample to 2.0MPa at 10.8% axial strain was observed. The volume change shows two linear trends pre- and post-yield.

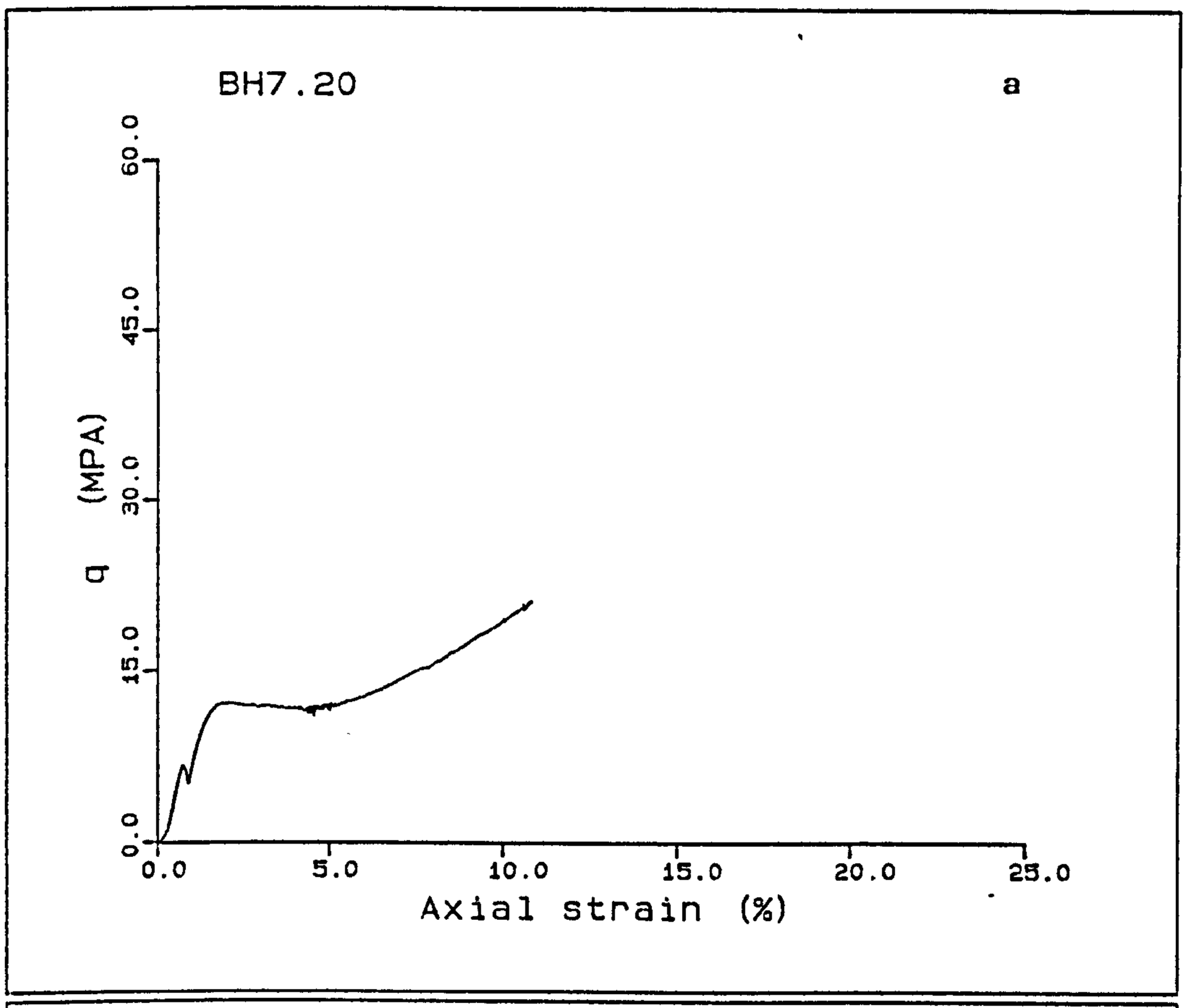

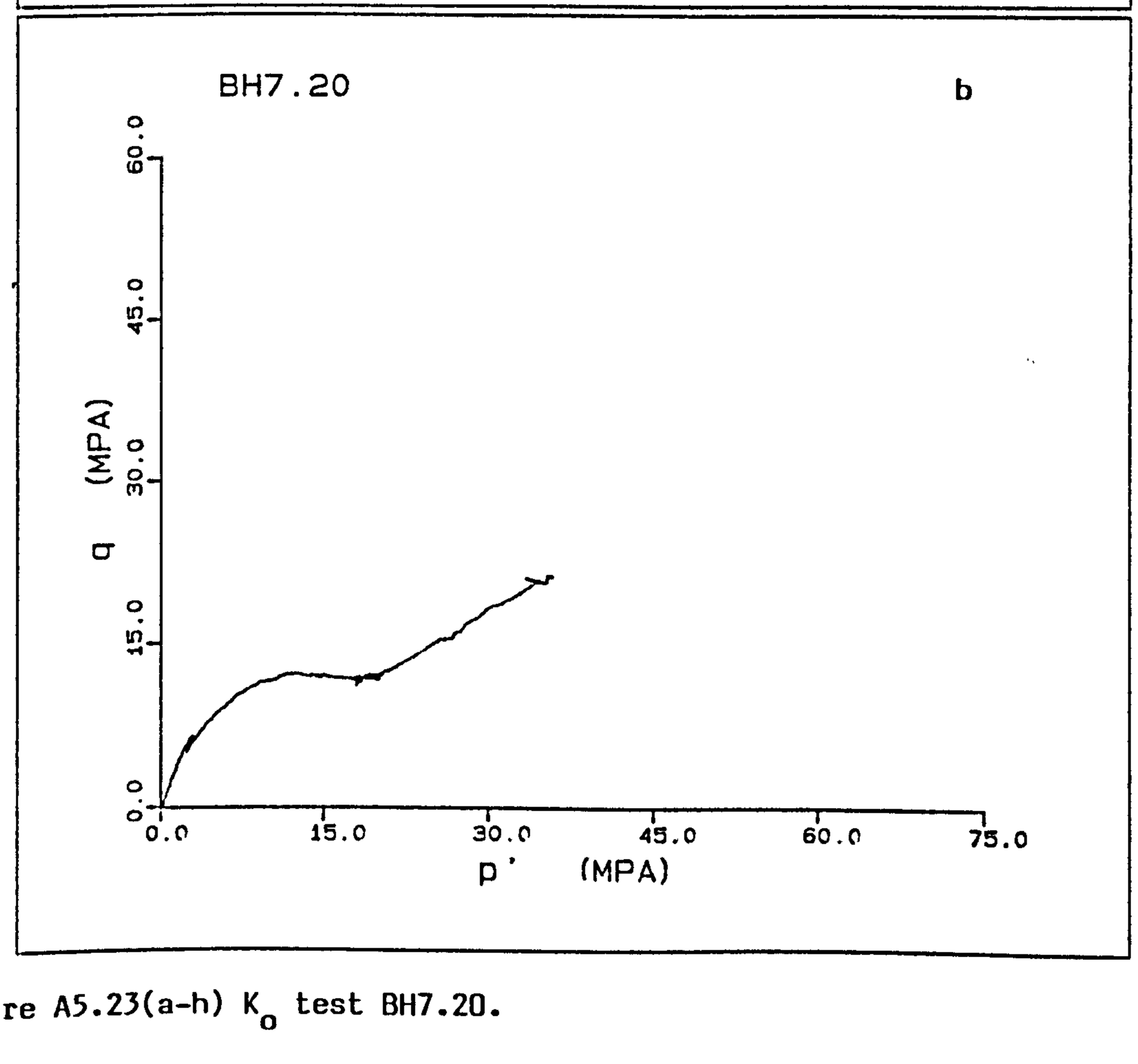

Figure A5.23(a-h) K_o test BH7.20.

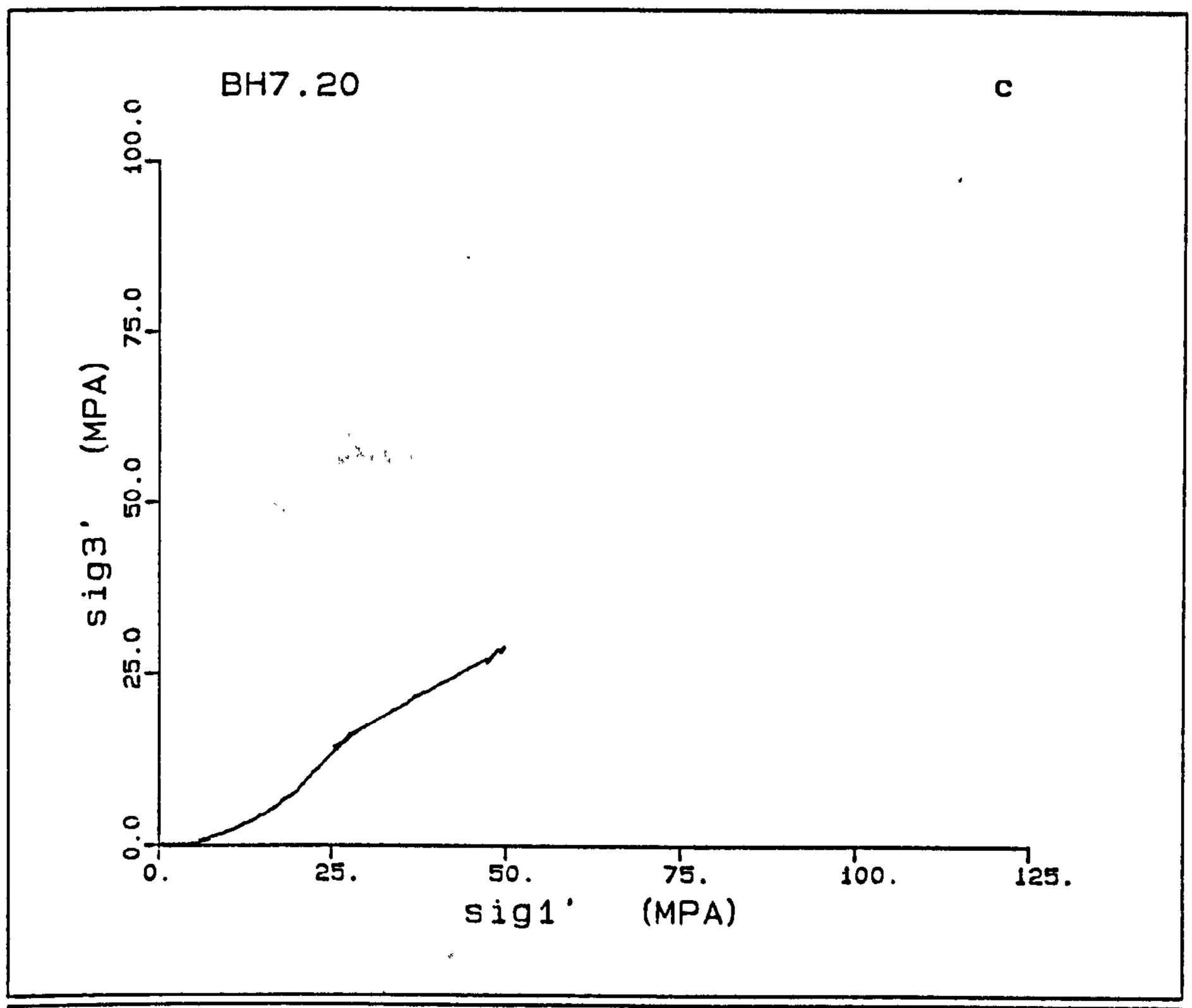
BH7.20
c
100.0
75.0
50.0
25.0
0.0
sig3' (MPA)
0.
25.
50.
75.
100.
125.
sig1' (MPA)

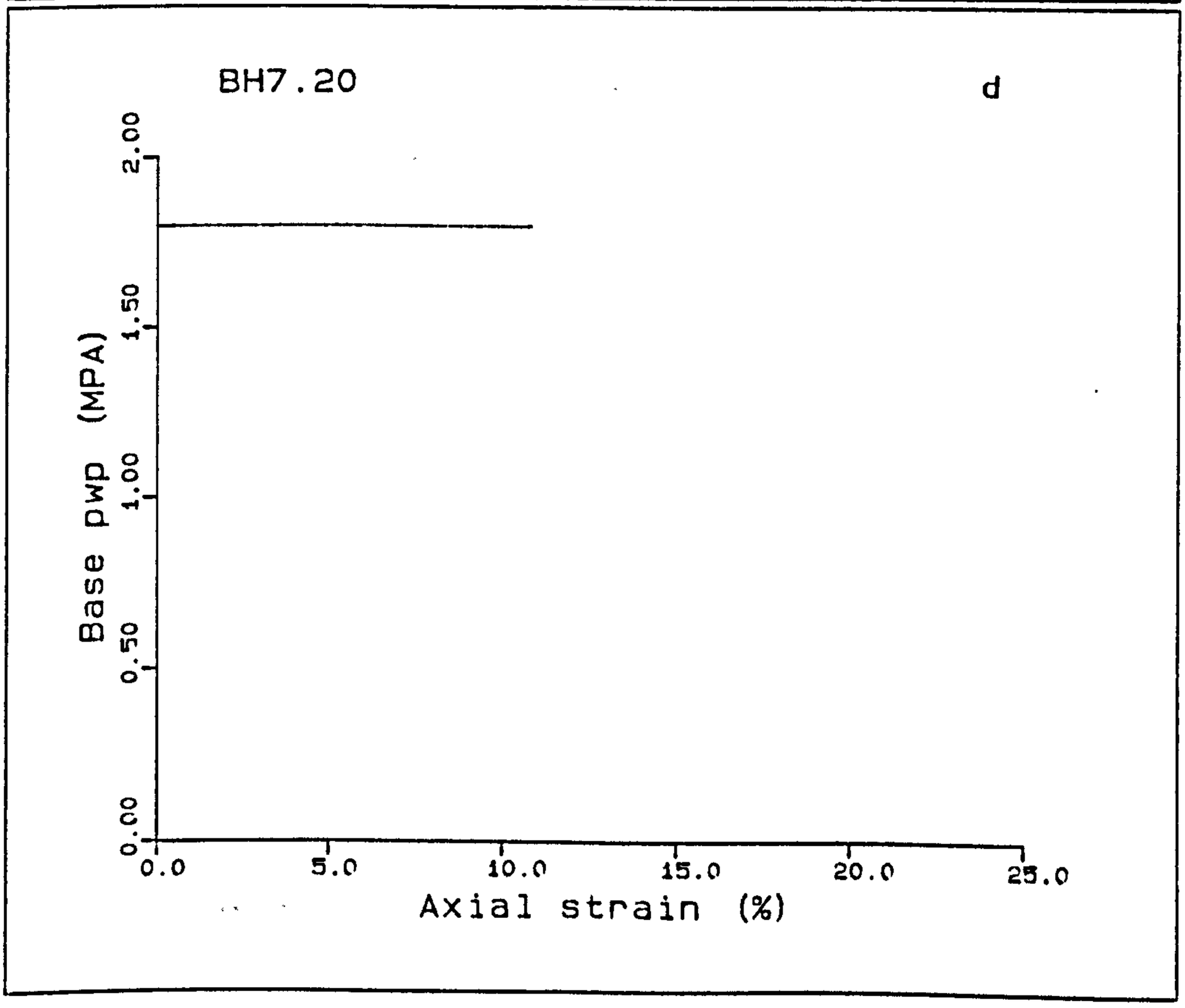
BH7.20
d
2.00
1.50
1.00
0.50
0.00
Base pwp (MPA)
0.0
5.0
10.0
15.0
20.0
25.0
Axial strain (%)

BH7.20

e

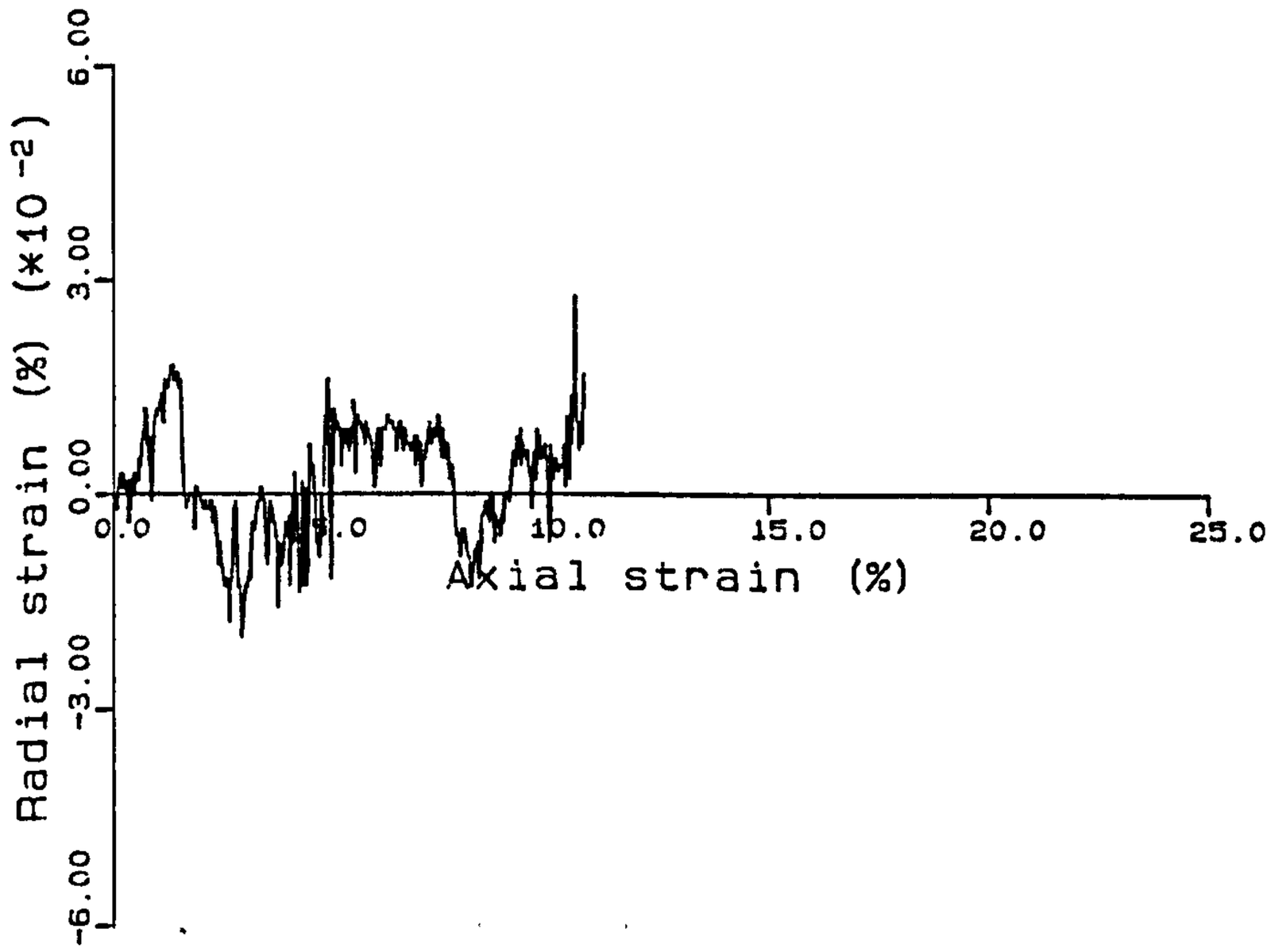

f

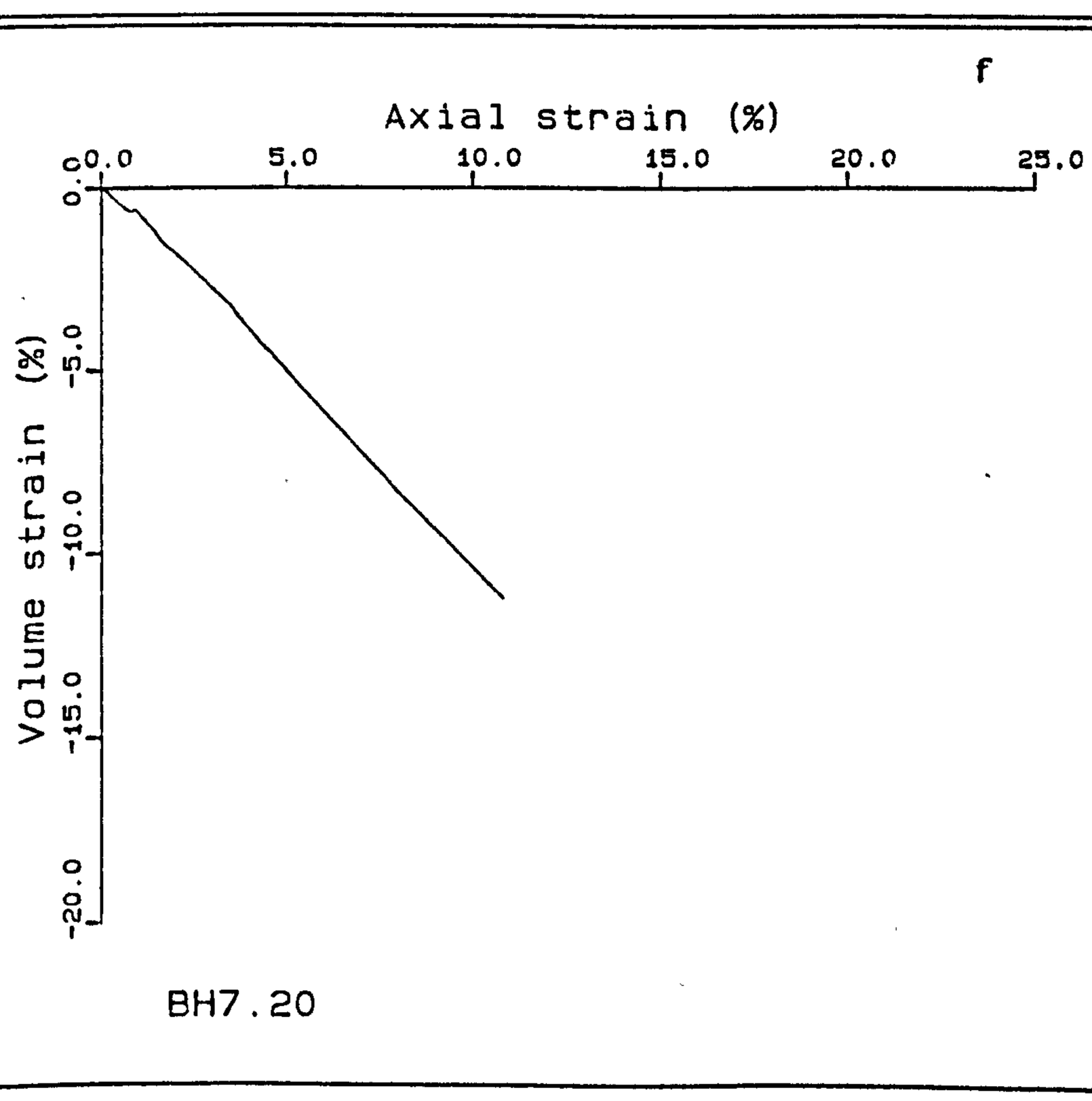

BH7.20

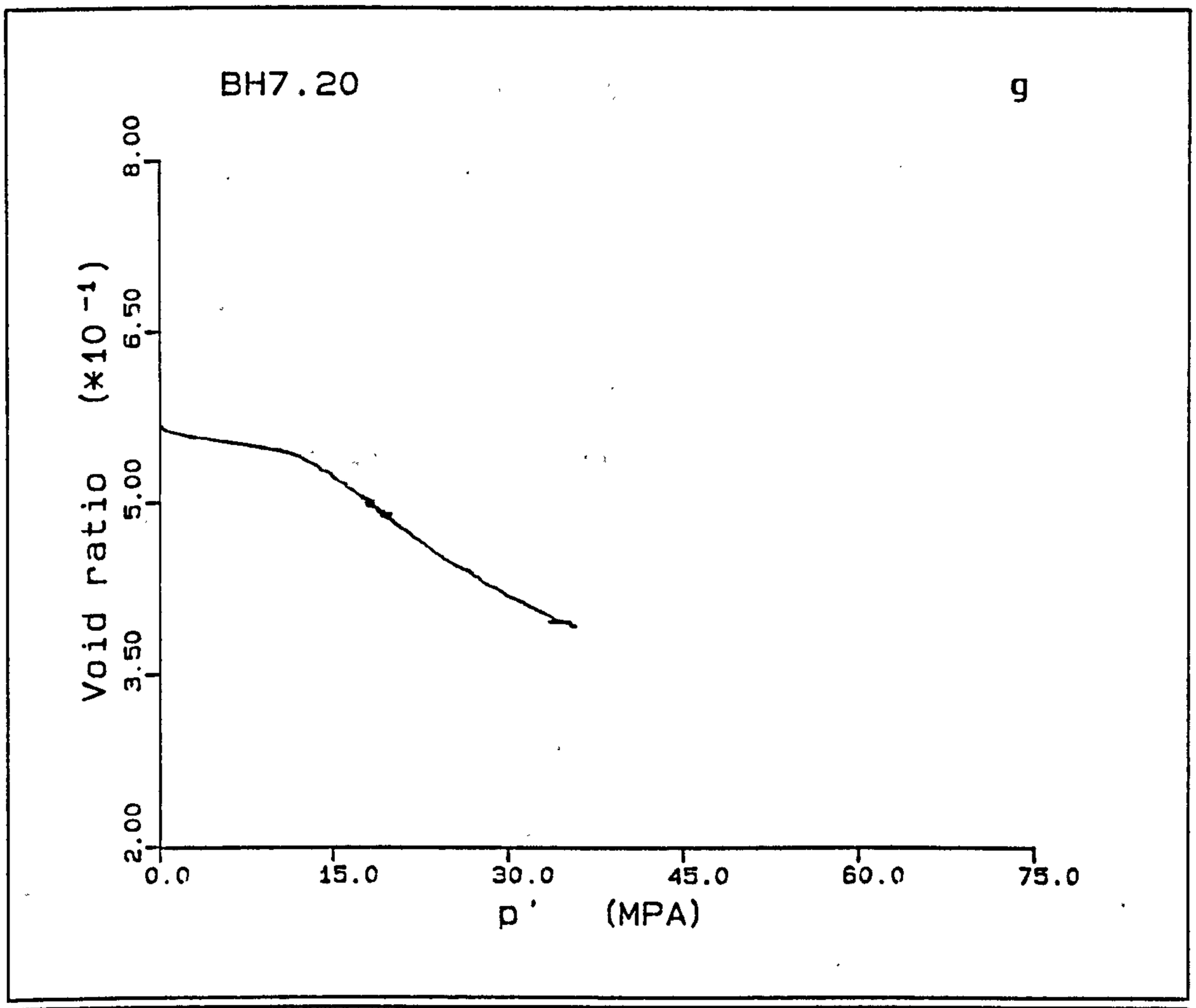
BH7.20
g
8.00
6.50
5.00
3.50
2.00
(*10 -1)
Void ratio
0.0
15.0
30.0
45.0
60.0
75.0
p' (MPA)

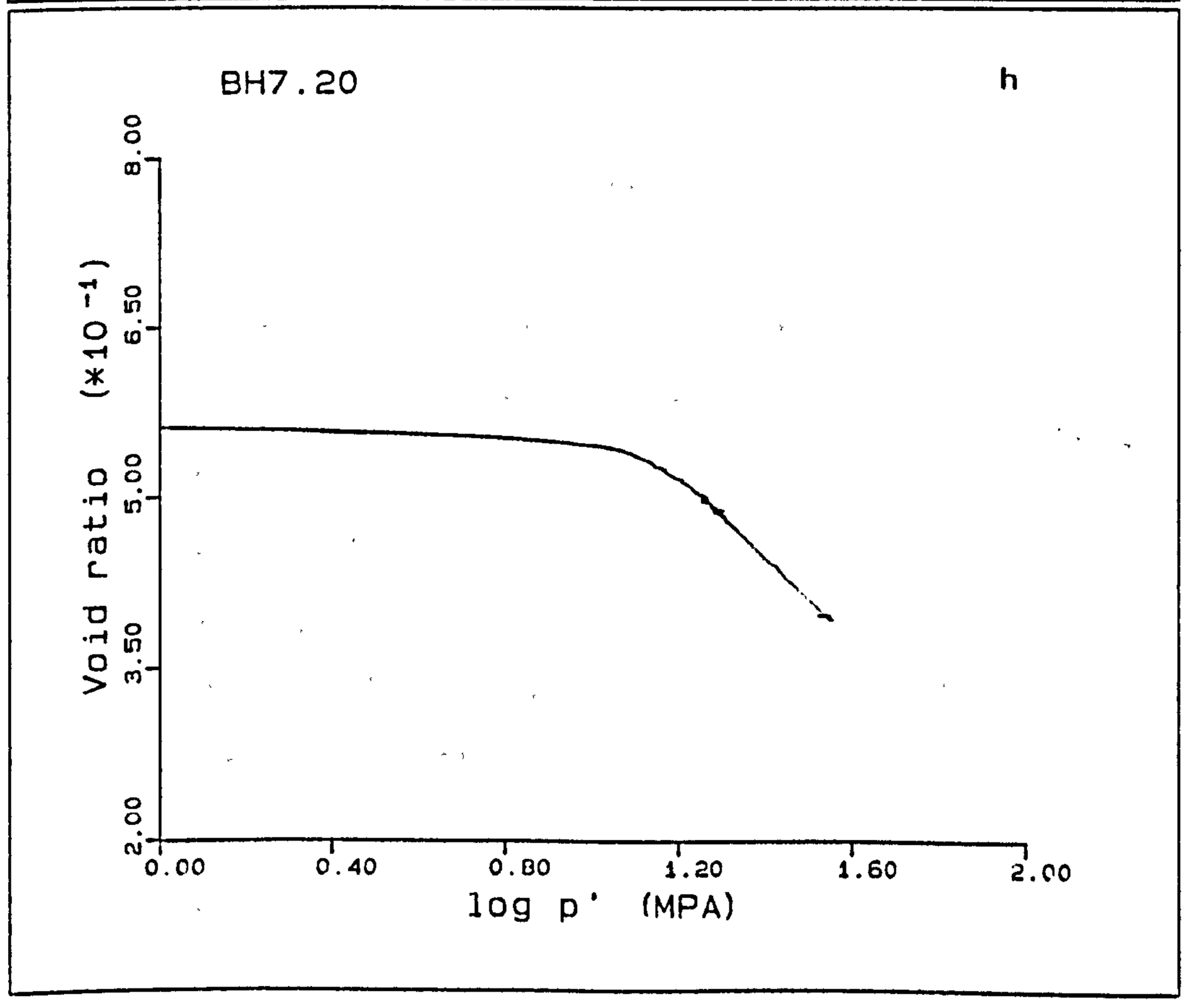
BH7.20
h
8.00
6.50
5.00
3.50
2.00
(*10 -1)
Void ratio
0.00
0.40
0.80
1.20
1.60
2.00
log p' (MPA)

BH18.20

The K_o test performed on the chalk was followed by an undrained shear test, USB18.20. The 36.2% porosity sample was deformed at 0.04mm/min, this was so that it was directly comparable with the elevated temperature tests BH14.60, BH15.100, BH16.100, and BH17.60. The elastic response to stress shows an initial linear reaction which reduces in modulus towards the peak, the linear trend having a modulus of 1.84GPa, the yield occurring at a deviatoric stress of 12.58MPa. The post-yield deformation is seen as a decrease in the load carrying capacity of the chalk, the load decreasing to 12.2MPa. After the pore collapse deformation the load increases linearly with mean effective stress. The $\bar{K}_o$ values for the stages of the deformation are $\bar{K}_{oe}$=0.047, a stress path close to a drained shear test, $\bar{K}_{opc}$=1.023 and $\bar{K}_{onc}$=0.574. The radial strains range in value from $20*10^{-3}$% to $8*10^{-3}$% on average, with a decrease to $-13*10^{-3}$% at 13.16% axial strain, where the cell pressure pumping rate needed increasing. There is also a decrease to $-6*10^{-3}$% at 0.18% axial strain.

The pore pressure increases at the top of the sample from a back pressure of 1.8MPa at zero axial strain to 3.2MPa at 14.1% axial strain, after which the sample was deformed in an undrained shear test. Fig. A5.24h shows an initial post-peak steep slope which becomes linear at higher stresses.

BH18.20 has an initial M_v of $6.5*10^{-4}MPa^{-1}$ increasing to a maximum compressibility of $3.2*10^{-3}MPa^{-1}$ at a vertical effective stress of 31.6MPa, the yield point occurring at a stress of 29.4MPa. After this, the value decreases to $1.3*10^{-3}MPa^{-1}$ at 77.5MPa. The C_v and permeability have values of $10086m^2/yr$ and 0.21mD at 6.1MPa effective stress, gradually decreasing to $21.2m^2/yr$ and 0.00087mD at 77.5MPa.

The reduction in log k(1+e), Fig. A5.241 is seen to be linear with log e.

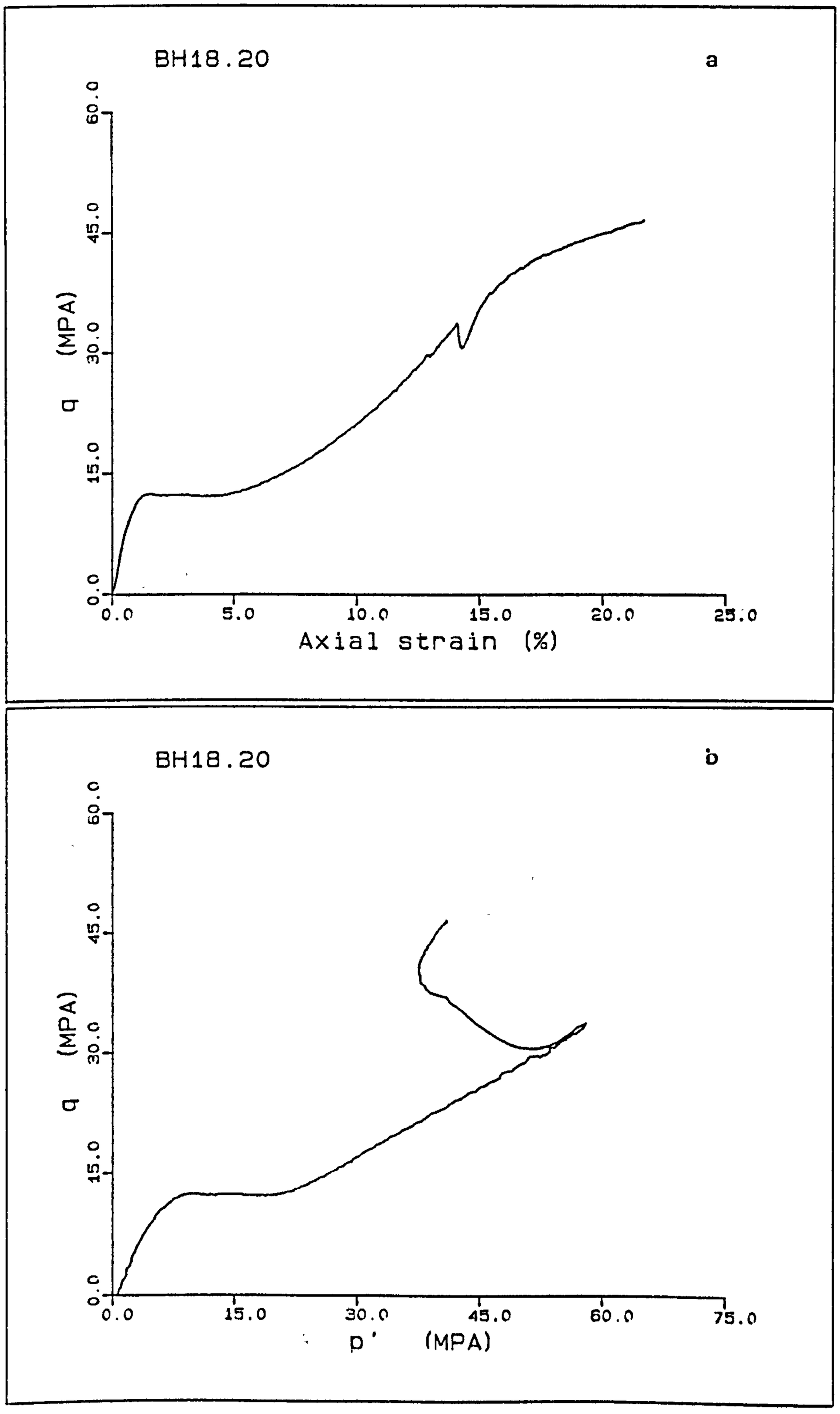

Figure A5.24(a-l) K_o test BH18.20.

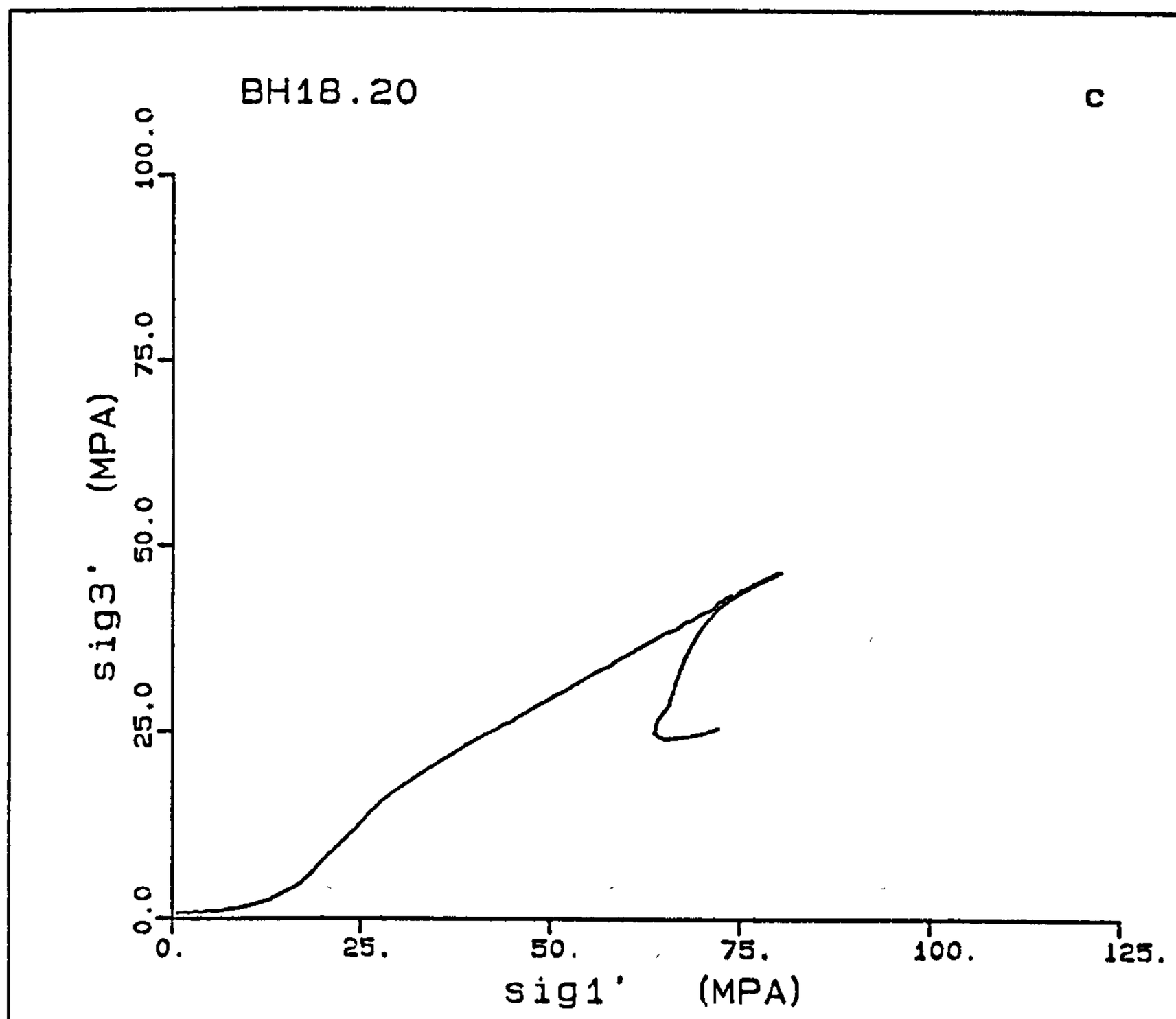
BH18.20
c
sig3' (MPA)
100.0
75.0
50.0
25.0
0.0
0.
25.
50.
75.
100.
125.
sig1' (MPA)

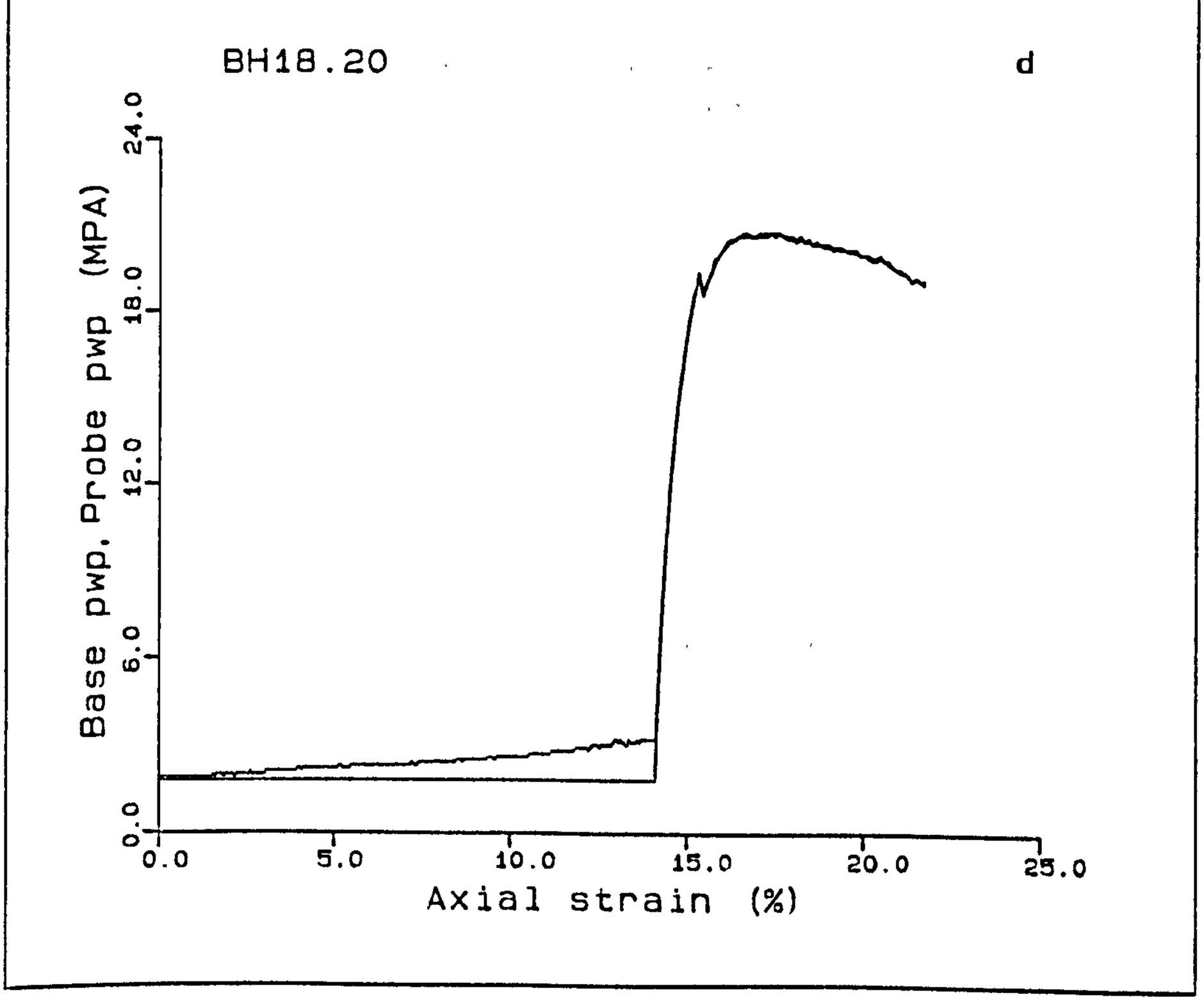
BH18.20
d
Base pwp, Probe pwp (MPA)
24.0
18.0
12.0
6.0
0.0
0.0
5.0
10.0
15.0
20.0
25.0
Axial strain (%)

BH18.20

e

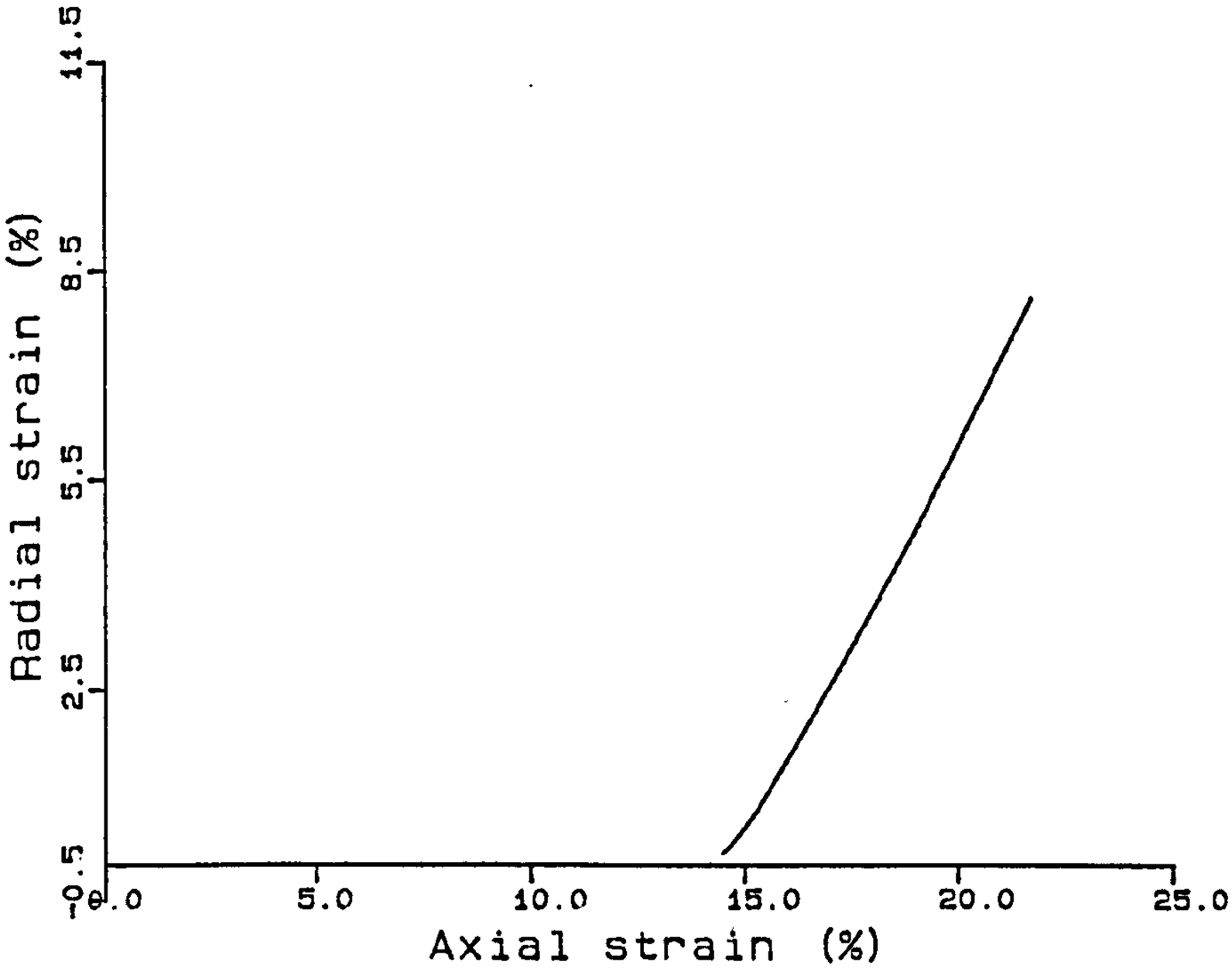

f

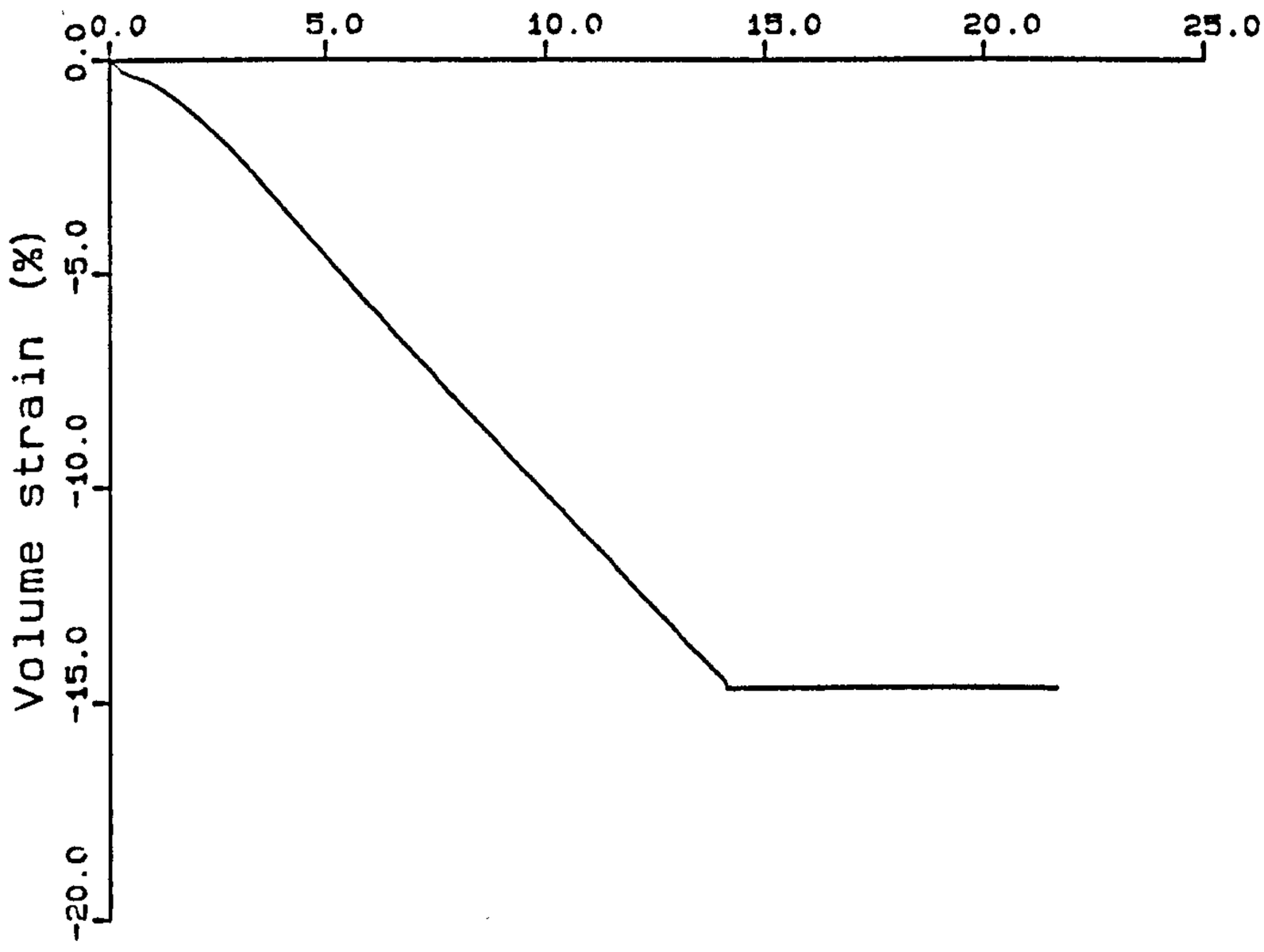

BH18.20

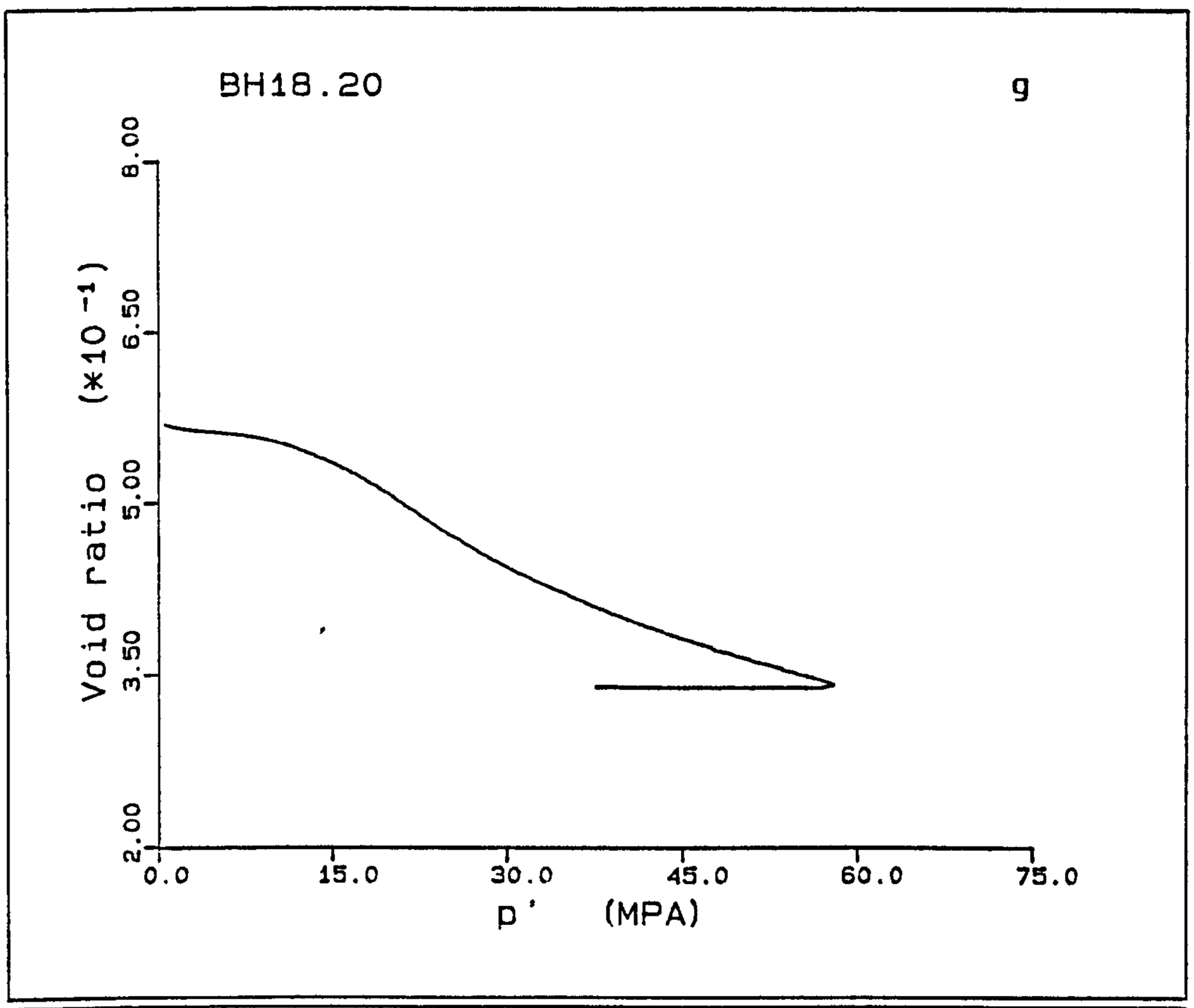
BH18.20
g
8.00
6.50
5.00
3.50
2.00
(*10 -1)
Void ratio
0.0
15.0
30.0
45.0
60.0
75.0
p' (MPA)

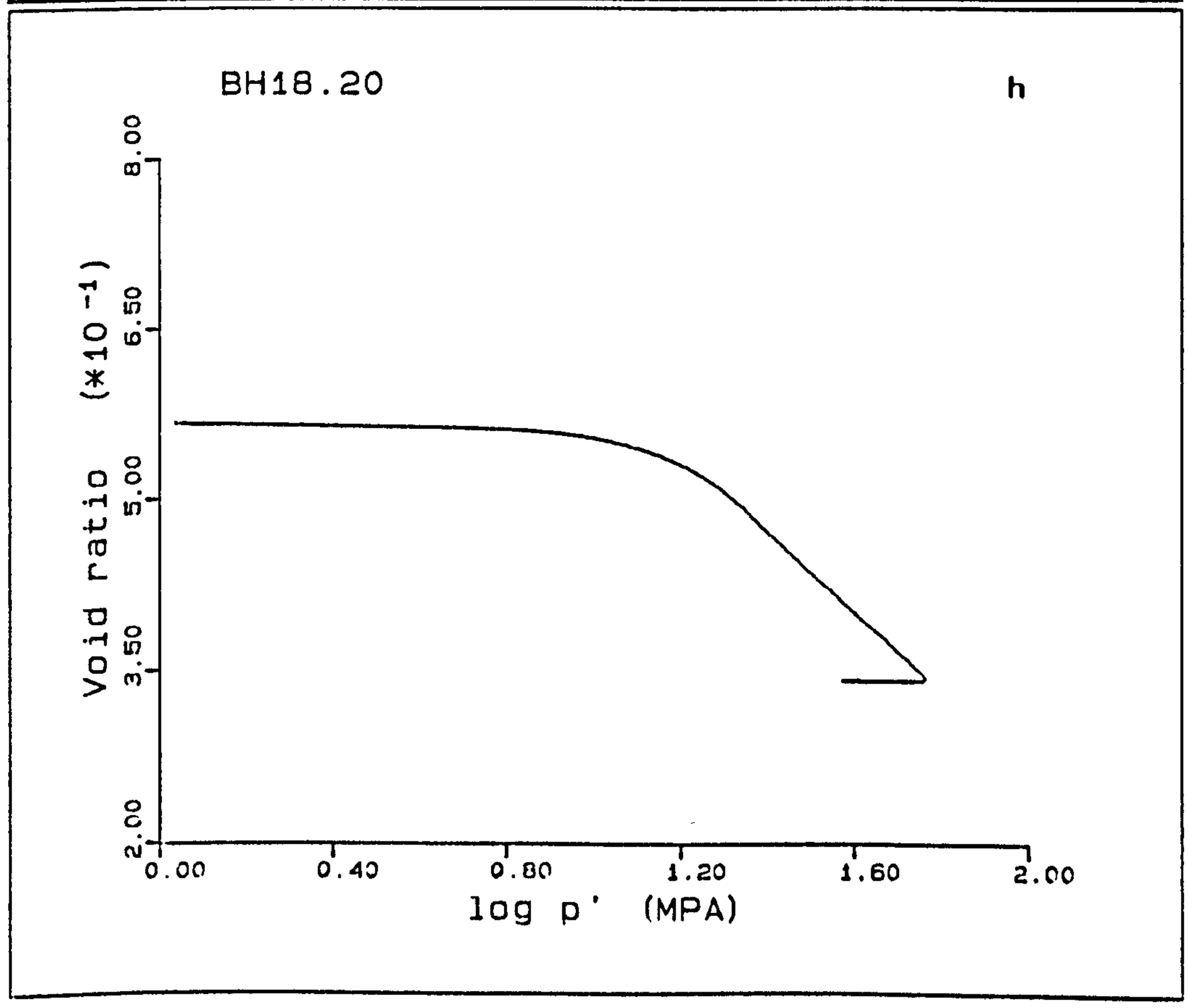
BH18.20
h
8.00
6.50
5.00
3.50
2.00
(*10 -1)
Void ratio
0.00
0.40
0.80
1.20
1.60
2.00
log p' (MPA)

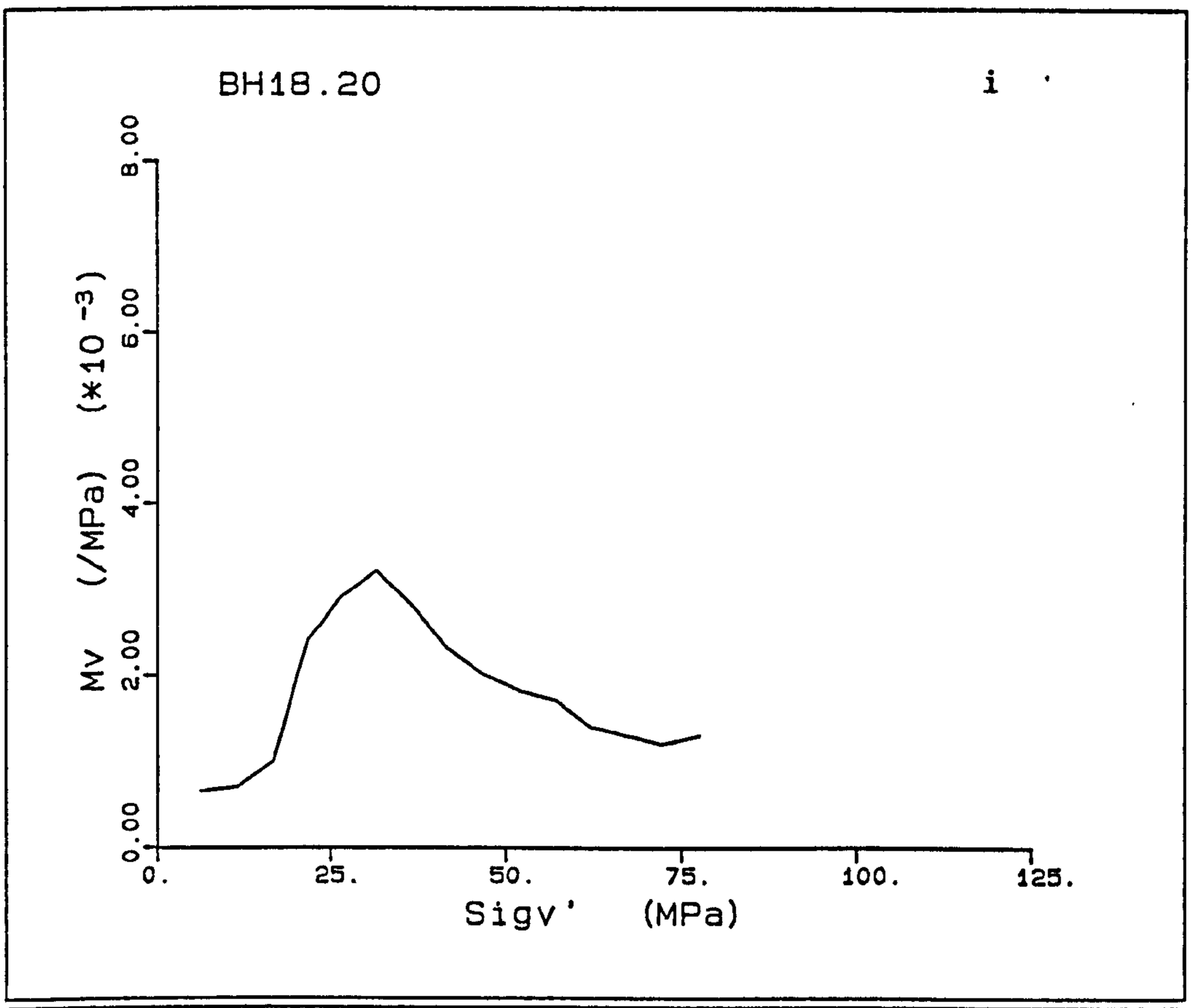
BH18.20
i
Mv (/MPa) (*10 -3)
8.00
6.00
4.00
2.00
0.00
0.
25.
50.
75.
100.
125.
Sigv' (MPa)

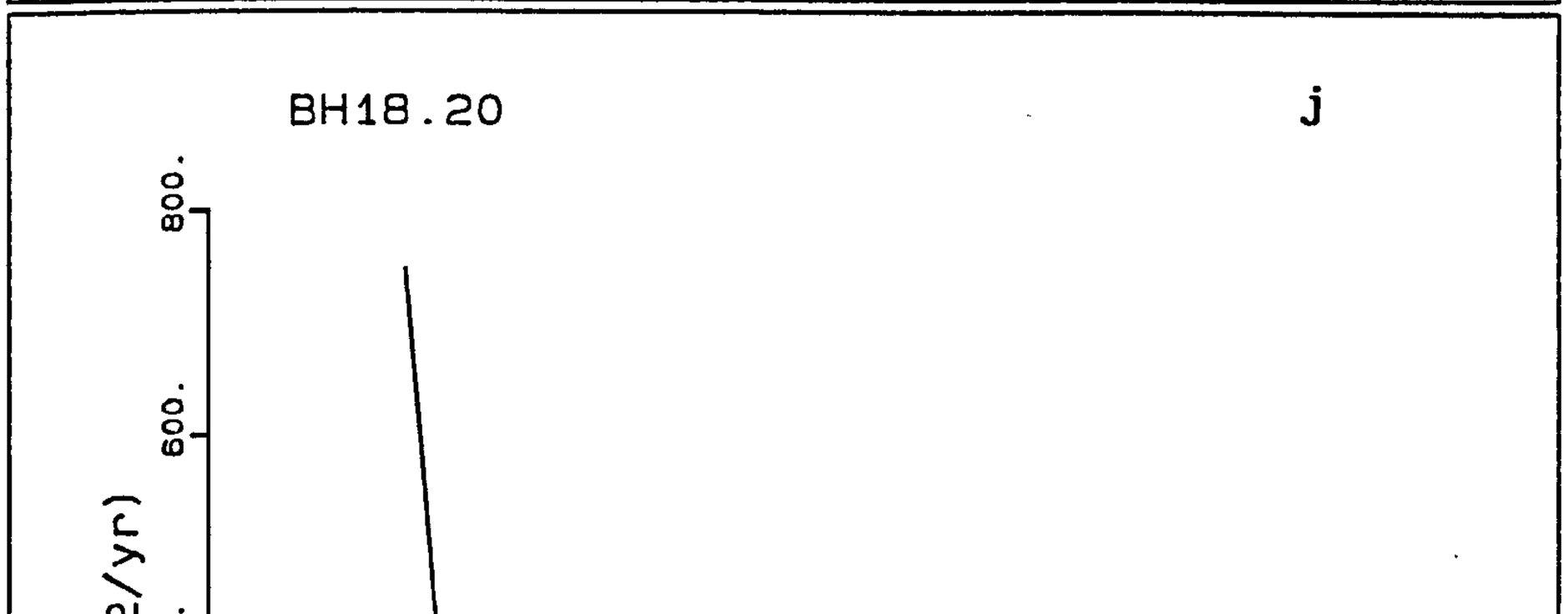
BH18.20
j
Cv (m2/yr)
800.
600.
400.
200.
0.
0.
25.
50.
75.
100.
125.
Sigv' (MPa)

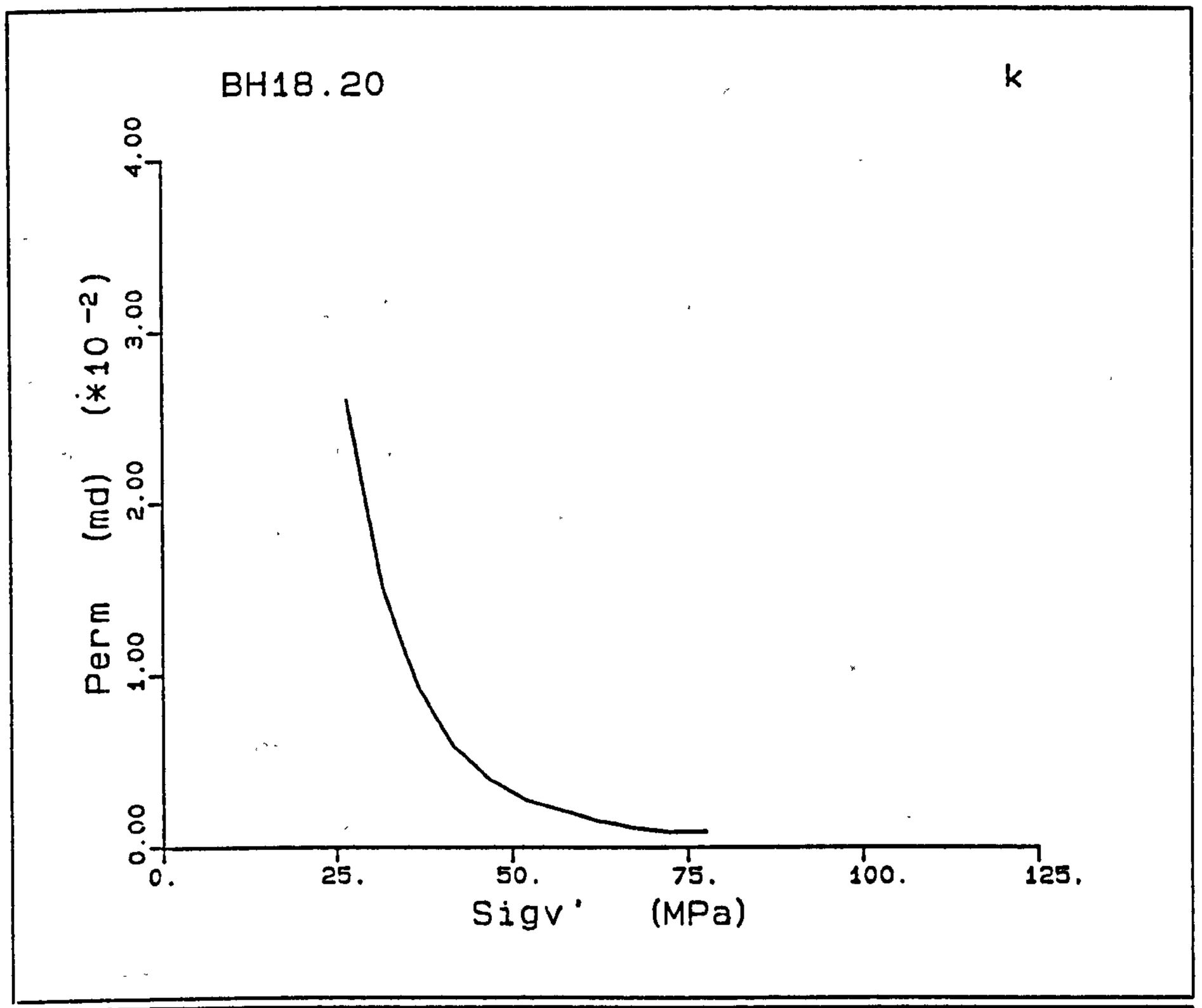
BH18.20
k
Perm (md) (*10 -2)
4.00
3.00
2.00
1.00
0.00
0.
25.
50.
75.
100.
125.
Sigv' (MPa)

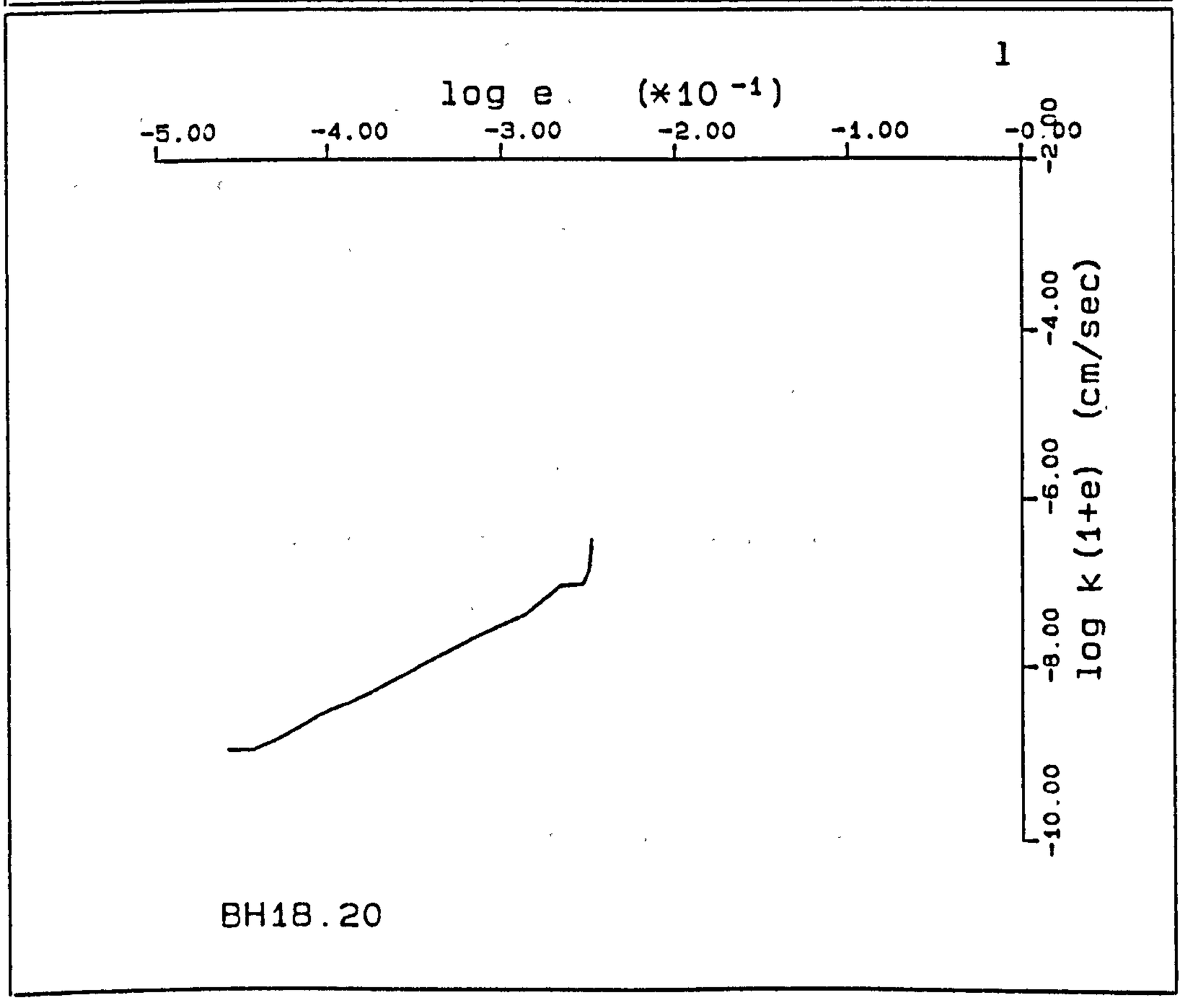
1
log e (*10 -1)
-5.00
-4.00
-3.00
-2.00
-1.00
-0.00
-2.00
-4.00
-6.00
-8.00
-10.00
log k (1+e) (cm/sec)
BH18.20

BH14.60

This sample is of 36.9% porosity, and was deformed at a rate of 0.04mm/min. After an initial heating of the sample to $60^{o}C$, the sample deformed with an elastic tangential modulus of 1.26GPa, the yield occurring at 10.55MPa. A drop is seen in the deviatoric stress as the yield is approached, probably due to a manual increase in the cell pressure pumping rate. The post-yield deformation is accompanied by a decrease in the load to 10.3MPa, and a gradual increase in load with the compaction of the chalk. At 9% axial strain the cell pressure could not maintain K_o so the cell pressure pumping rate was increased; as a result of this, the load on the sample dropped. The K_o was not recovered until an axial strain of 10.7% was reached. The $\bar{K}_o$ for the pore collapse and normally consolidated deformations are 0.969 and 0.567 respectively, the initial elastic $\bar{K}_{oe}$ being close to a drained shear, Fig. A5.25c. The radial strain was generally maintained within a range of $20*10^{-3}$% with the exception of the deviation mentioned above, and another at an axial strain of 6% where the radial strain reached $-55*10^{-3}$%, which is $10*10^{-3}$% outside the average range. The pore pressure gradually increases at the top of the sample from the back pressure value of 1.7MPa to 2.2MPa at 15.3% axial strain. The large deviation off K_o can be seen by two decreases separated by an increase in the top pore pressure reading. The volume strain plots show the deviation off K_o, with the e - log p' plot showing a slight curvature at higher axial strains.

The coefficient of volume compressibility increases from $1*10^{-3}MPa^{-1}$ to $3.9*10^{-3}MPa^{-1}$ at an effective stress of 31.2MPa, the yield occurring at a maximum effective stress of 15.6MPa, the M_v initially starting to increase at approximately 15MPa. The peak C_v of $13160m^2/yr$ occurs at 10.6MPa while the peak permeability of 0.18mD is

seen at a vertical effective stress of 20.9MPa. Fig. A5.251 shows that the function of permeability decreases with the same slope as BH18.20.

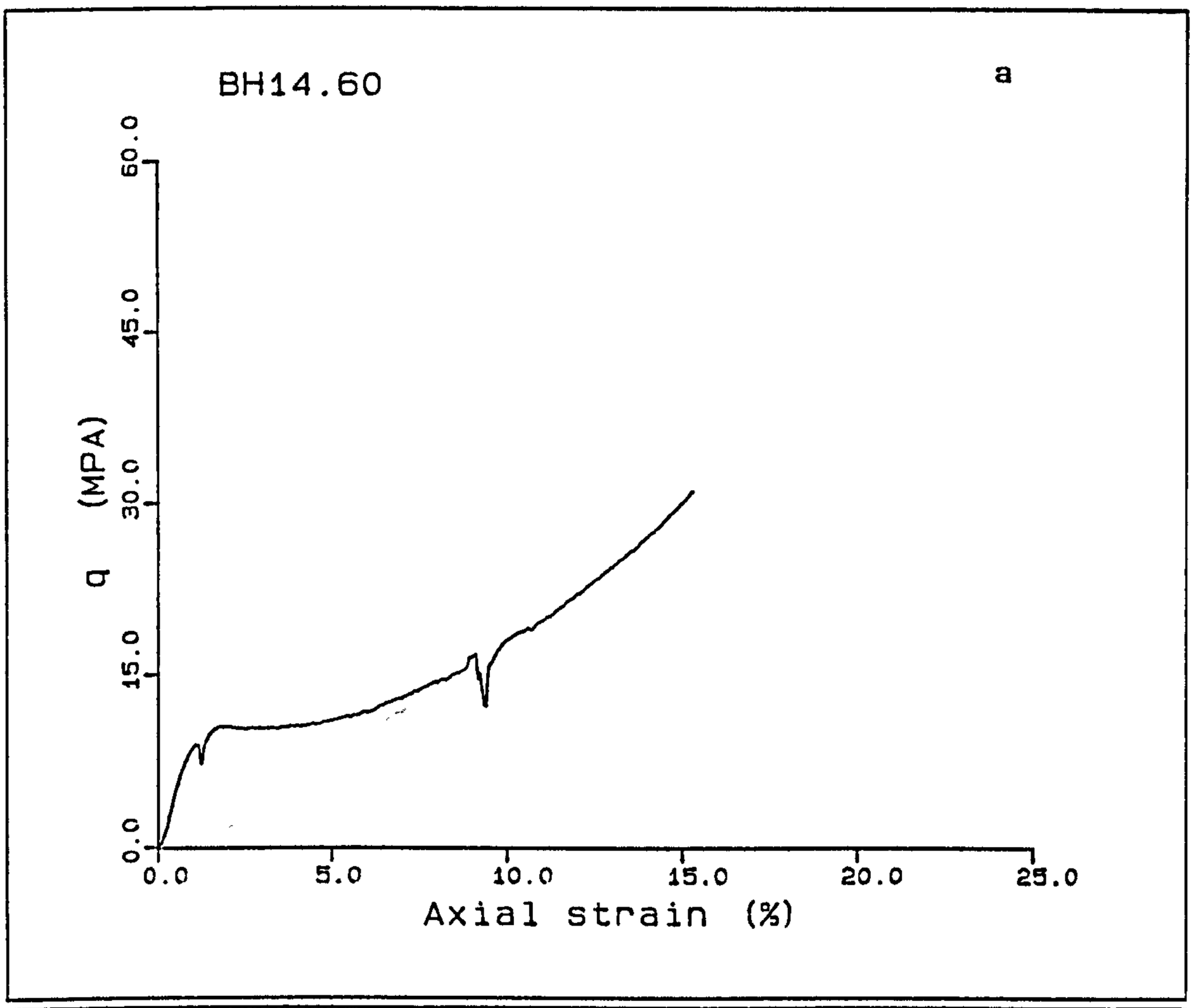

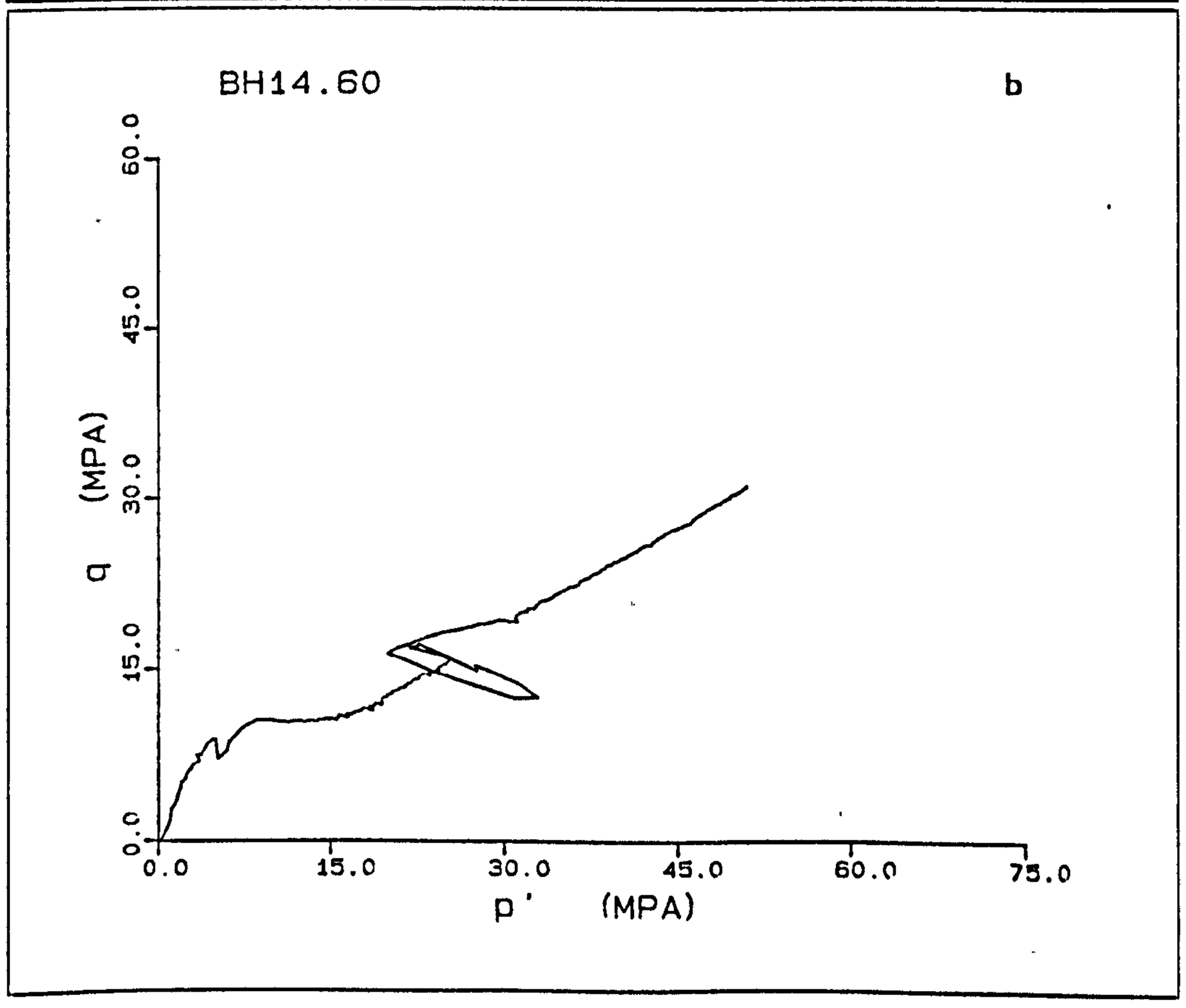

Figure A5.25(a-m) K_o test BH14.60.

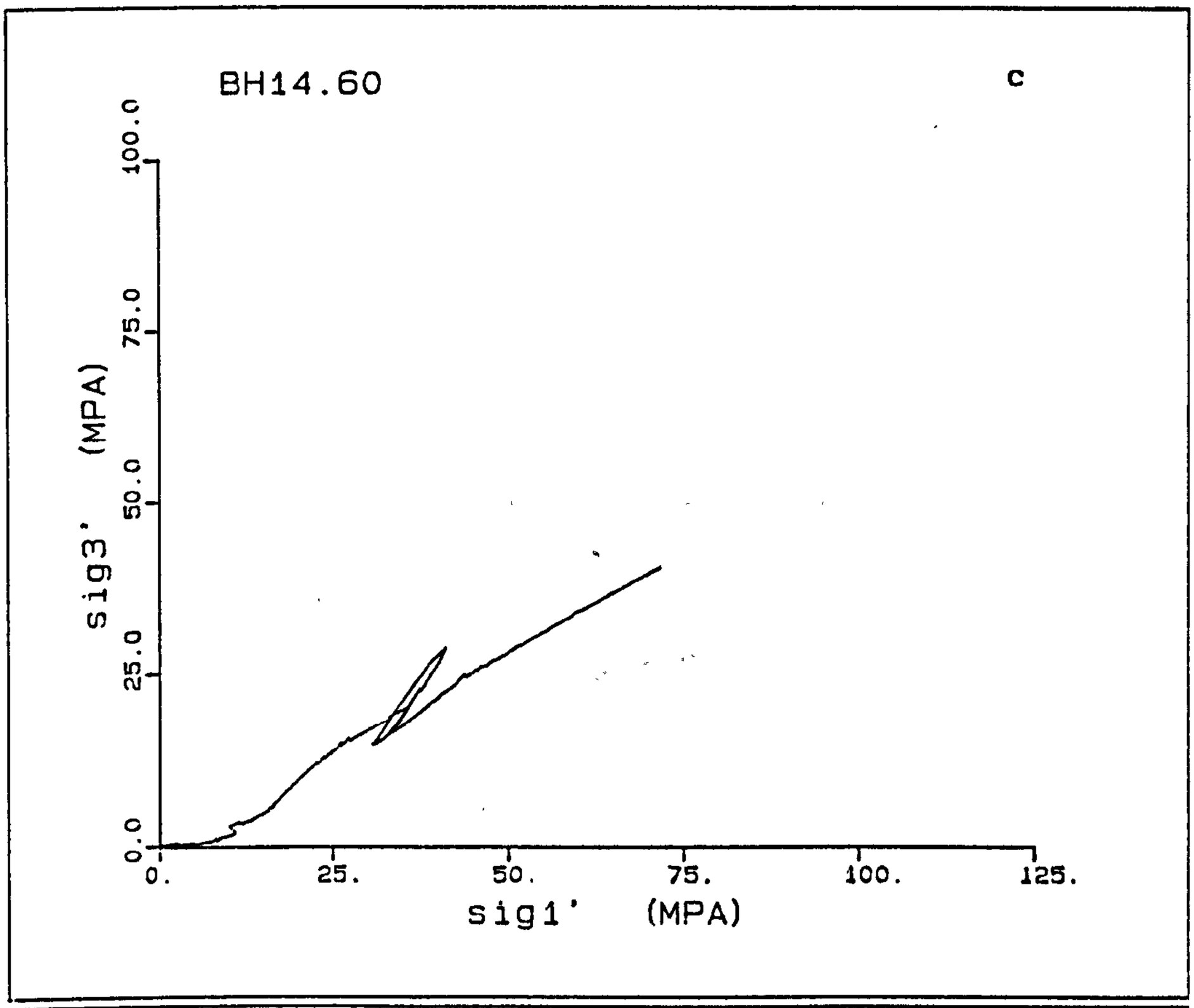
BH14.60
c
100.0
75.0
50.0
25.0
0.0
sig3' (MPA)
0.
25.
50.
75.
100.
125.
sig1' (MPA)

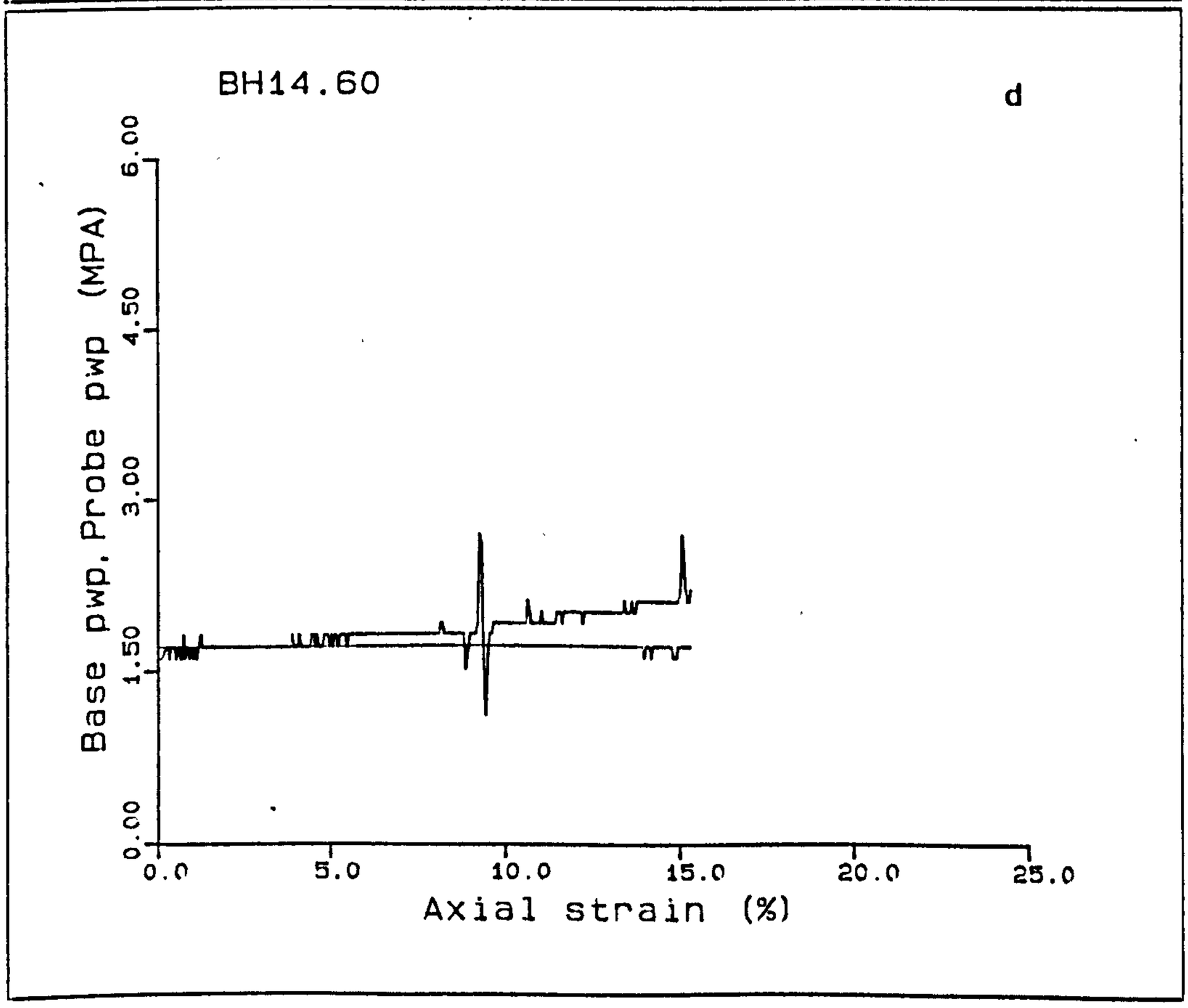
BH14.60
d
6.00
4.50
3.00
1.50
0.00
Base pwp, Probe pwp (MPA)
0.0
5.0
10.0
15.0
20.0
25.0
Axial strain (%)

BH14.60

e

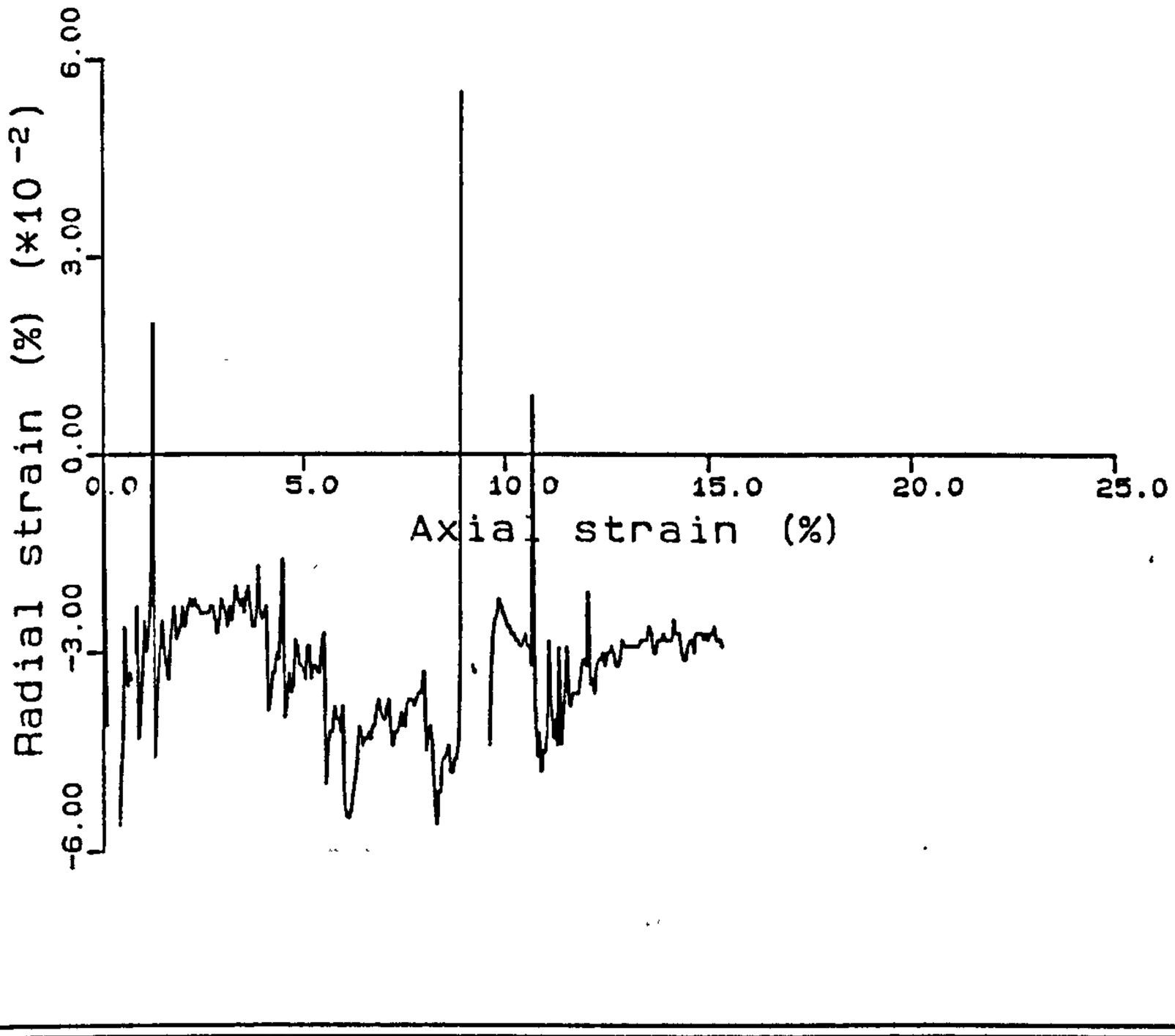

f

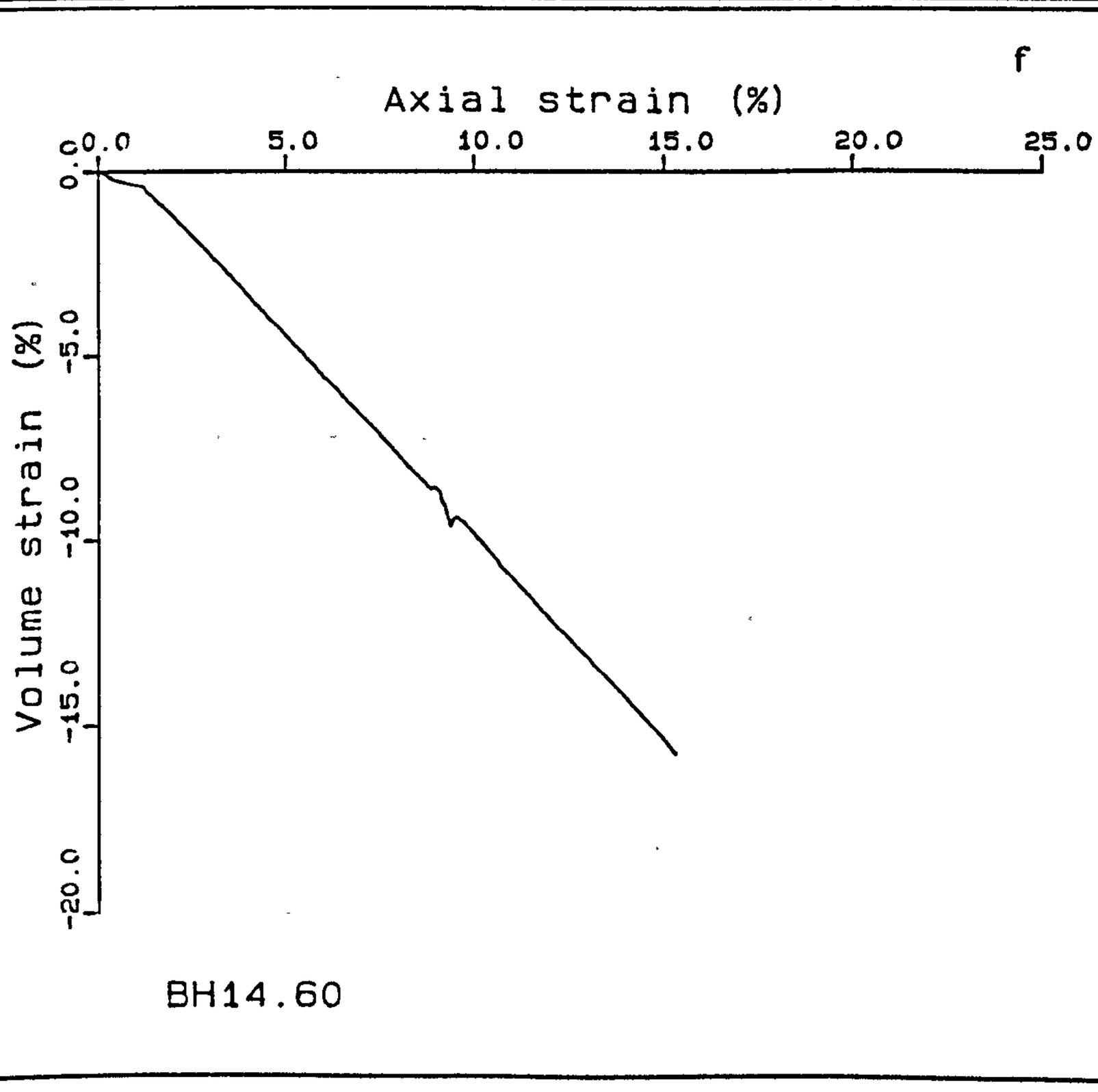

BH14.60

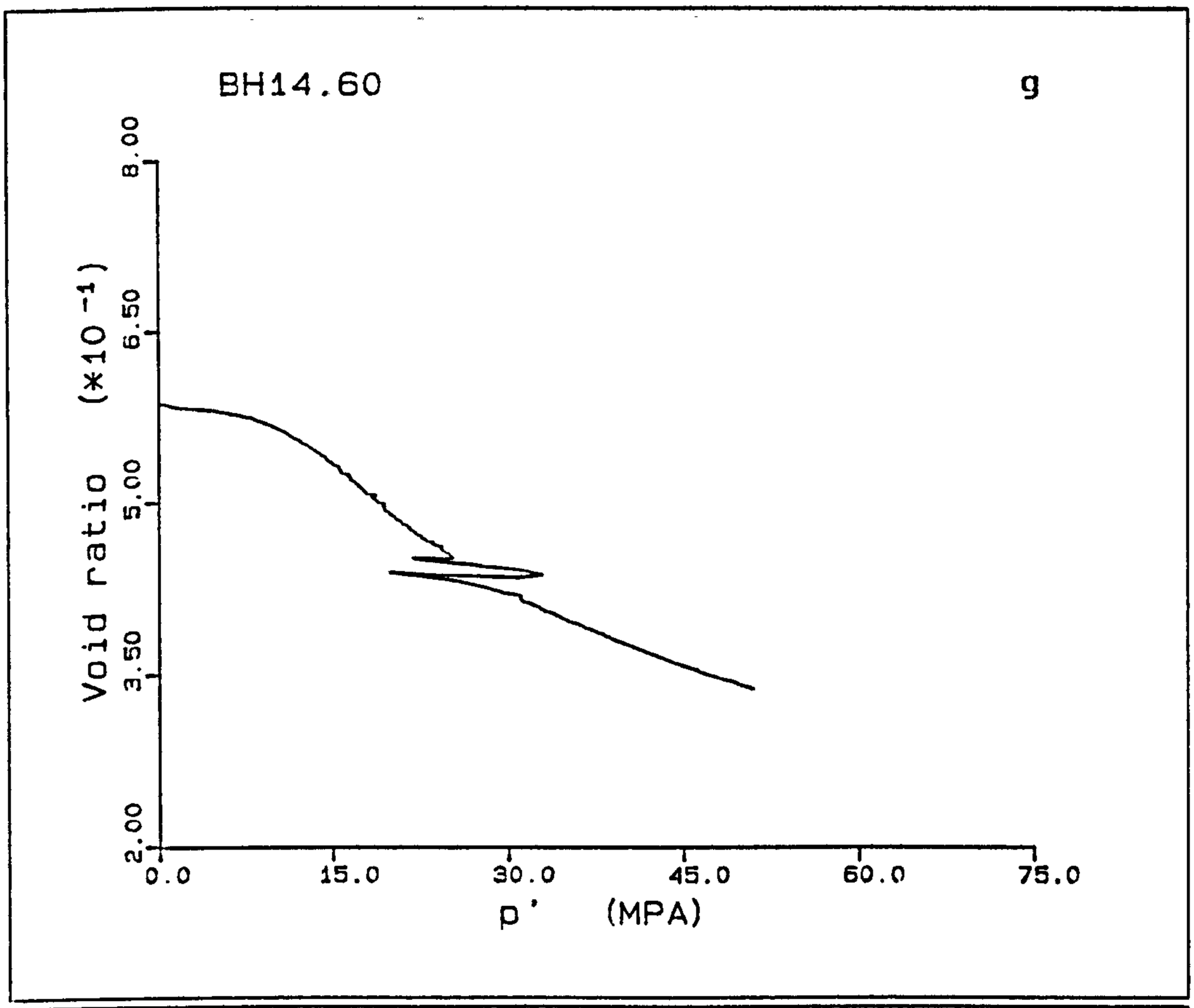
BH14.60
g
Void ratio (*10 -1)
8.00
6.50
5.00
3.50
2.00
0.0
15.0
30.0
45.0
60.0
75.0
p' (MPA)

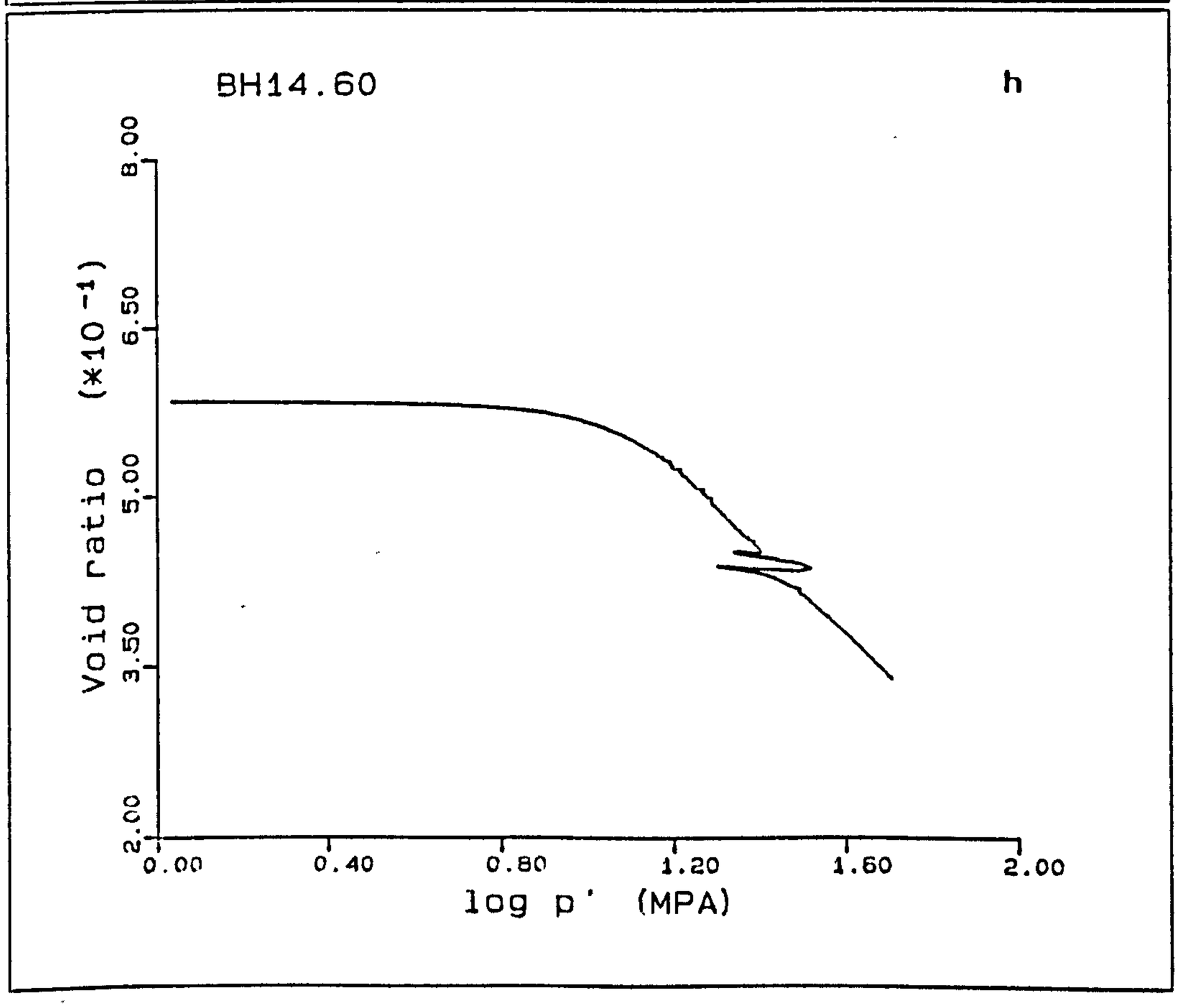
BH14.60
h
Void ratio (*10 -1)
8.00
6.50
5.00
3.50
2.00
0.00
0.40
0.80
1.20
1.60
2.00
log p' (MPA)

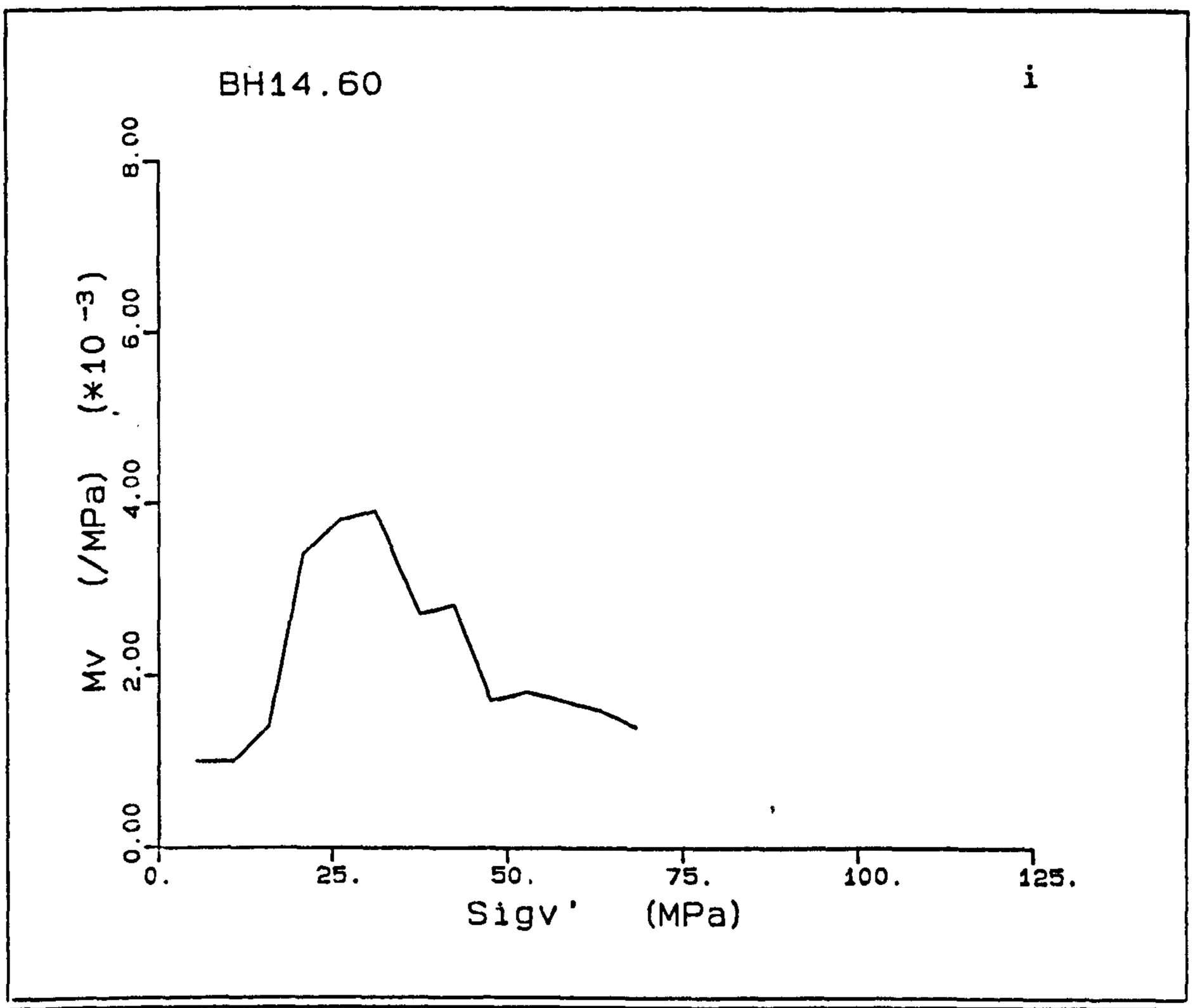
BH14.60
i
Mv (/MPa) (*10 -3)
8.00
6.00
4.00
2.00
0.00
0.
25.
50.
75.
100.
125.
Sigv' (MPa)

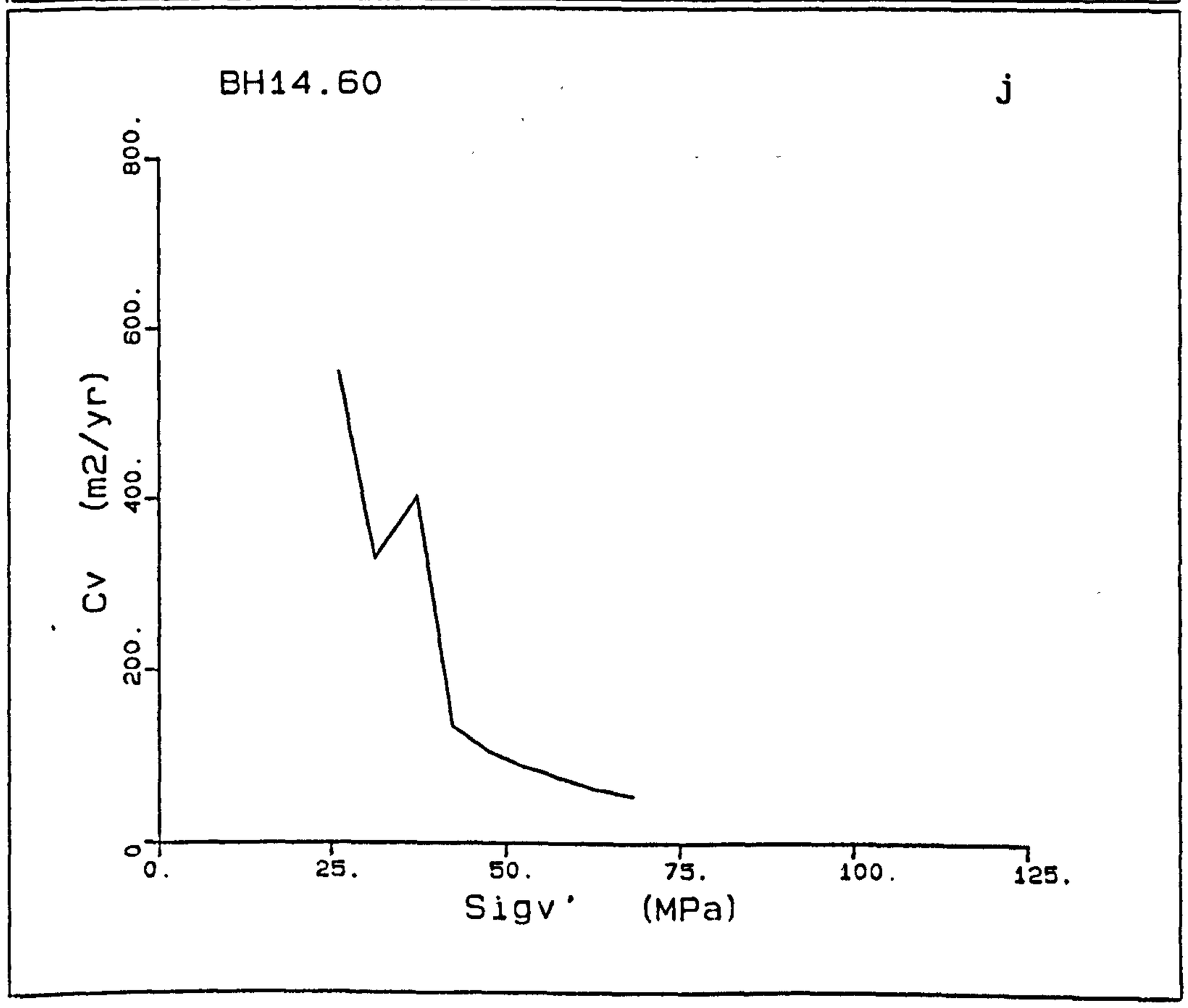
BH14.60
j
Cv (m2/yr)
800.
600.
400.
200.
0
0.
25.
50.
75.
100.
125.
Sigv' (MPa)

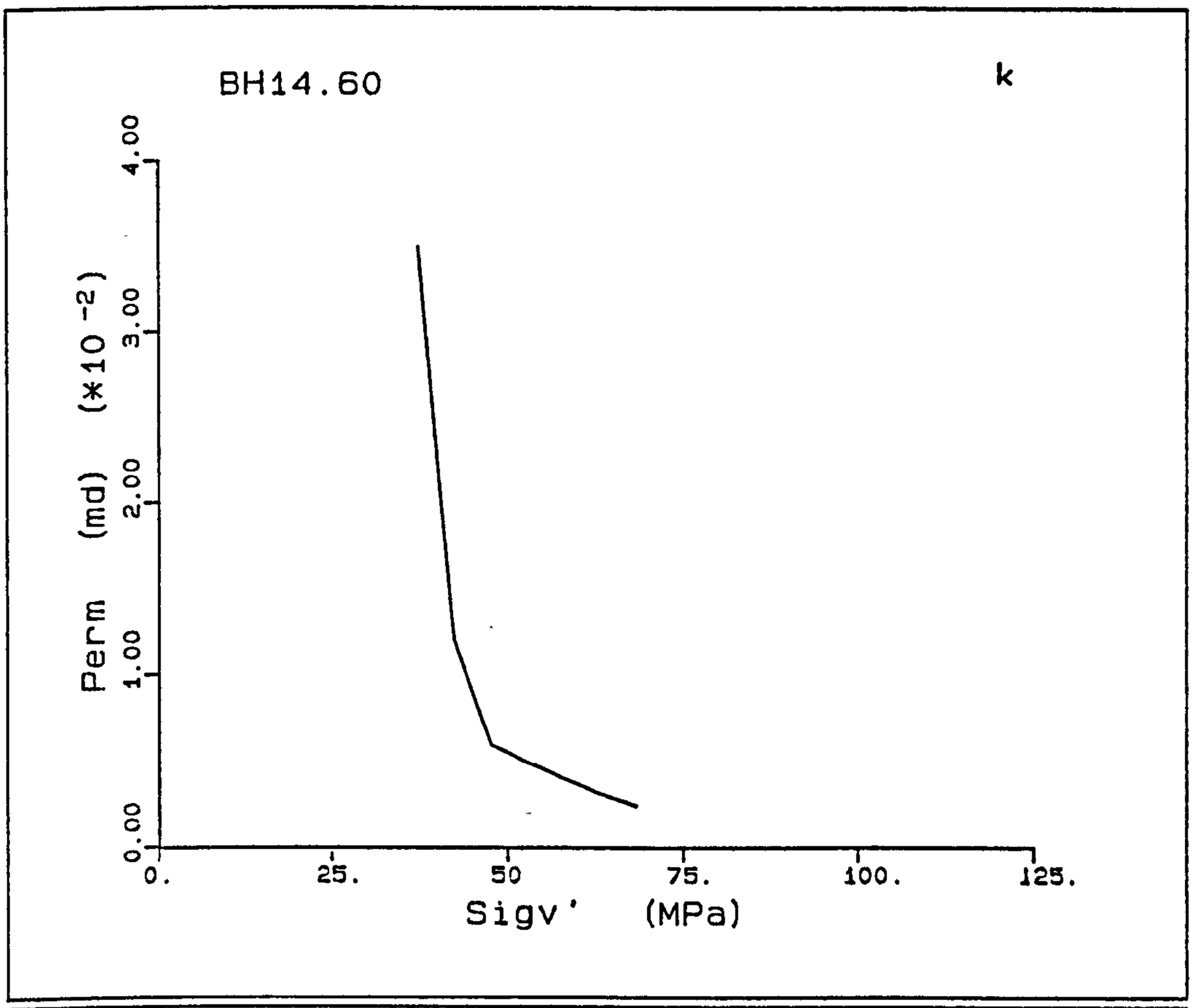
BH14.60
k
Perm (md)
(*10 -2)
4.00
3.00
2.00
1.00
0.00
0.
25.
50
75.
100.
125.
Sigv' (MPa)

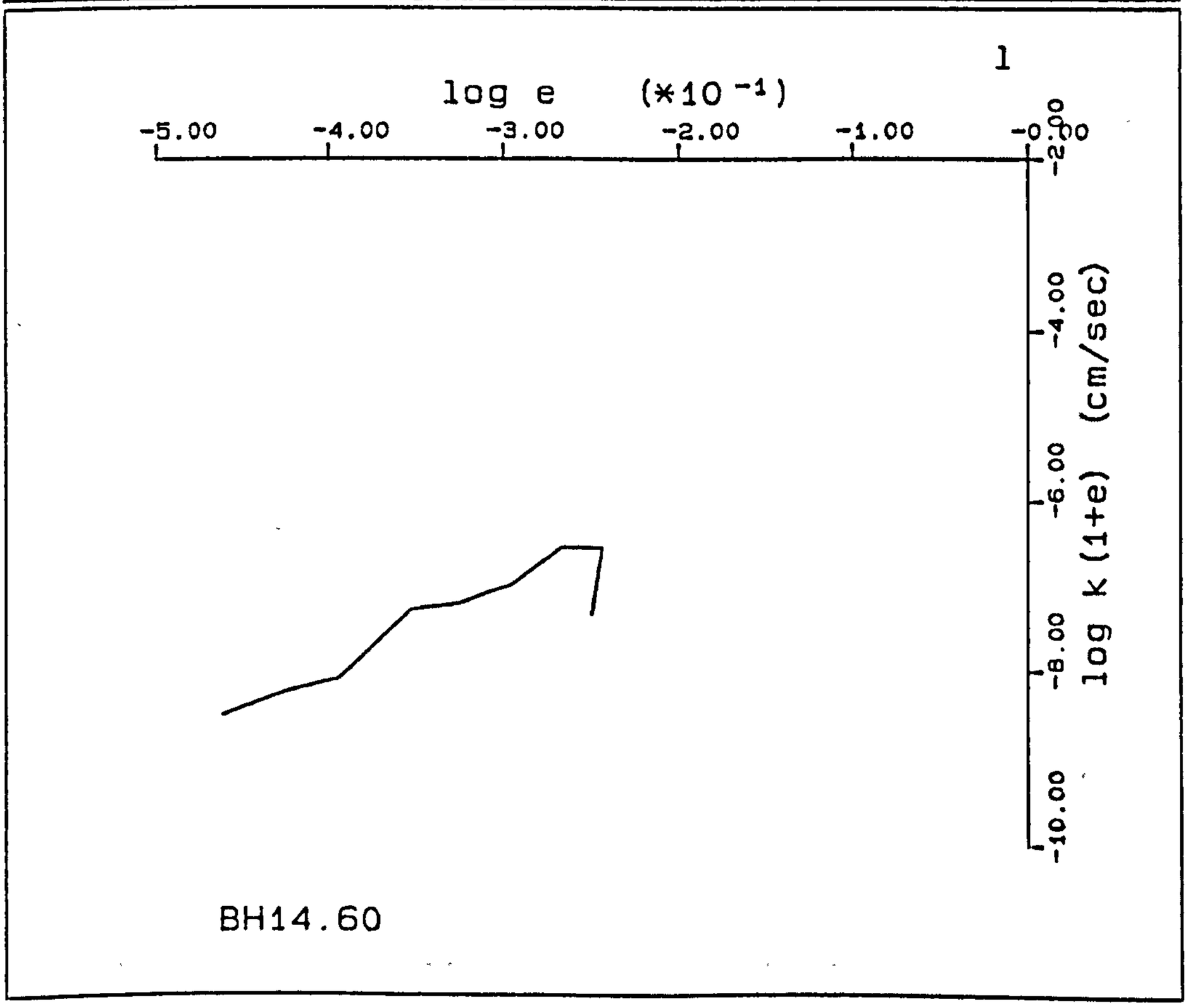
l
log e (*10 -1)
-5.00
-4.00
-3.00
-2.00
-1.00
-0.00
-2.00
-4.00
-6.00
-8.00
-10.00
log k (1+e) (cm/sec)
BH14.60

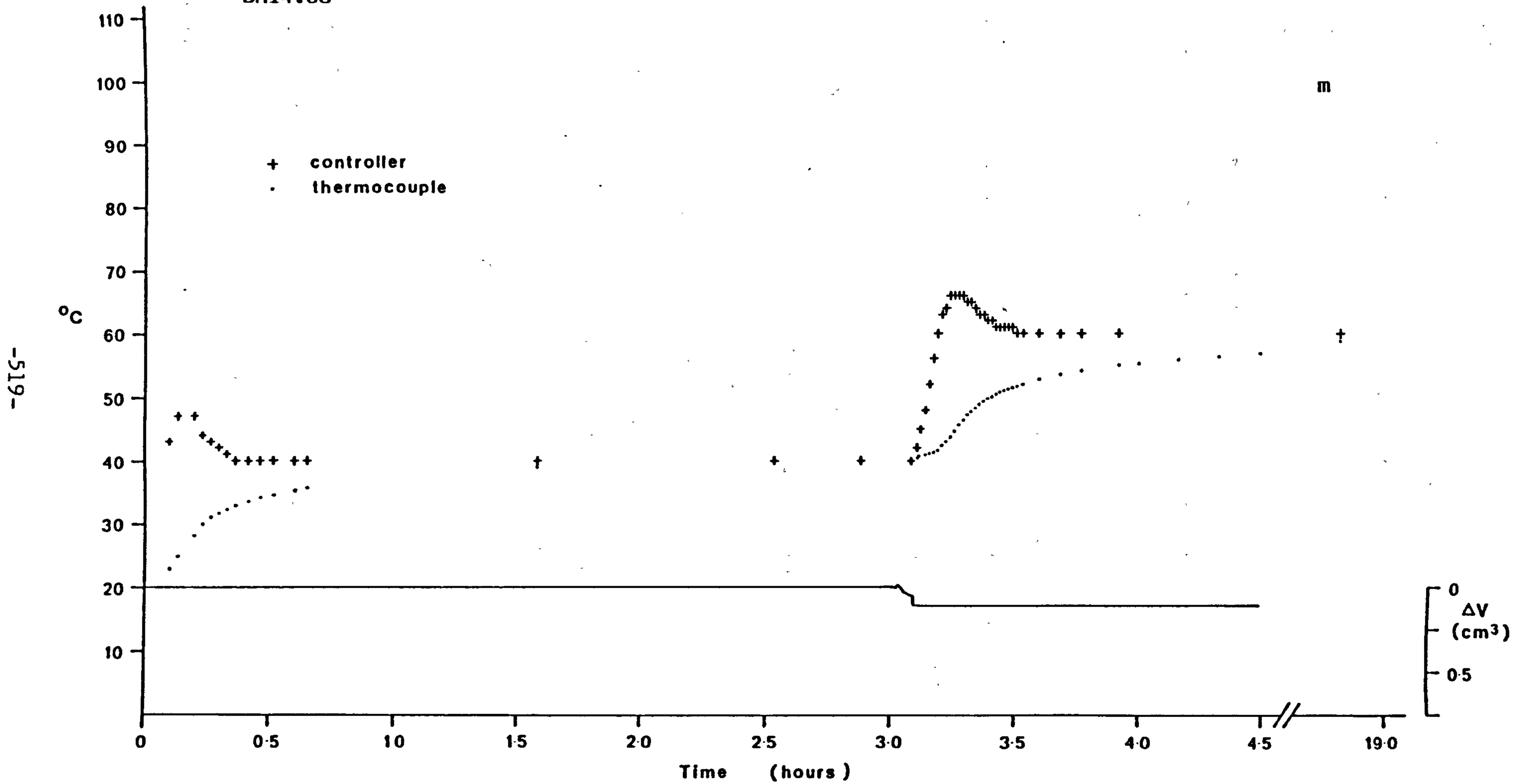
BH14.60
+ controller
· thermocouple
m
°C
110
100
90
80
70
60
50
40
30
20
10
0
0·5
1·0
1·5
2·0
2·5
3·0
3·5
4·0
4·5
19·0
Time (hours)
0
ΔV
(cm³)
0·5

BH16.100

This test was again deformed at a rate of 0.04mm/min, and the sample is a 37.3% chalk. The test was started initially at a higher cell pressure so that the undrained pore pressure response to temperature could be observed. The initial tangential modulus is 1.36GPa, the yield occurring at 11.78MPa, after which the load increases at an increasing rate. A deformation with a reasonably constant deviatoric stress is still seen in the q-p' plot, though the change from this section to the normal consolidation deformation, of linear increase in q with p' is gradual. No deviation from this linear trend is seen, and the $\bar{K}_o$ values for the pore collapse and normal consolidation compactions are 0.915 and 0.547, respectively. The elastic $\bar{K}_{oe}$ gradually increases from zero. The radial strain in the experiment can be seen to be held within a range of $20*10^{-3}$%, about a mean value of $5*10^{-3}$%. The pore water pressure at the top of the sample gradually increases with axial strain from the back pressure value of 1.8MPa at zero strain to 2.2MPa at 14.2% axial strain. The axial strain - volume strain plot is affected by the negative radial strain undergone by the sample, the plot becoming steeper at this point. Fig. A5.26h seems curved again but the affect is not as pronounced as in the Pegwell Bay samples.

The initial compressibility of the sample is $7.4*10^{-4}MPa^{-1}$, this increases to $1.6*10^{-3}MPa^{-1}$ at 67.3MPa. The peak C_v occurs at 16.3MPa, with a maximum permeability of 1.4mD, the yield point occurs at a vertical effective stress of 16.7MPa. These values decrease to $93.4m^{2}/yr$ and 0.048mD at a vertical effective stress of 67.3MPa. The decrease of k(1+e) with e in log - log space is of identical slope to BH18.20.

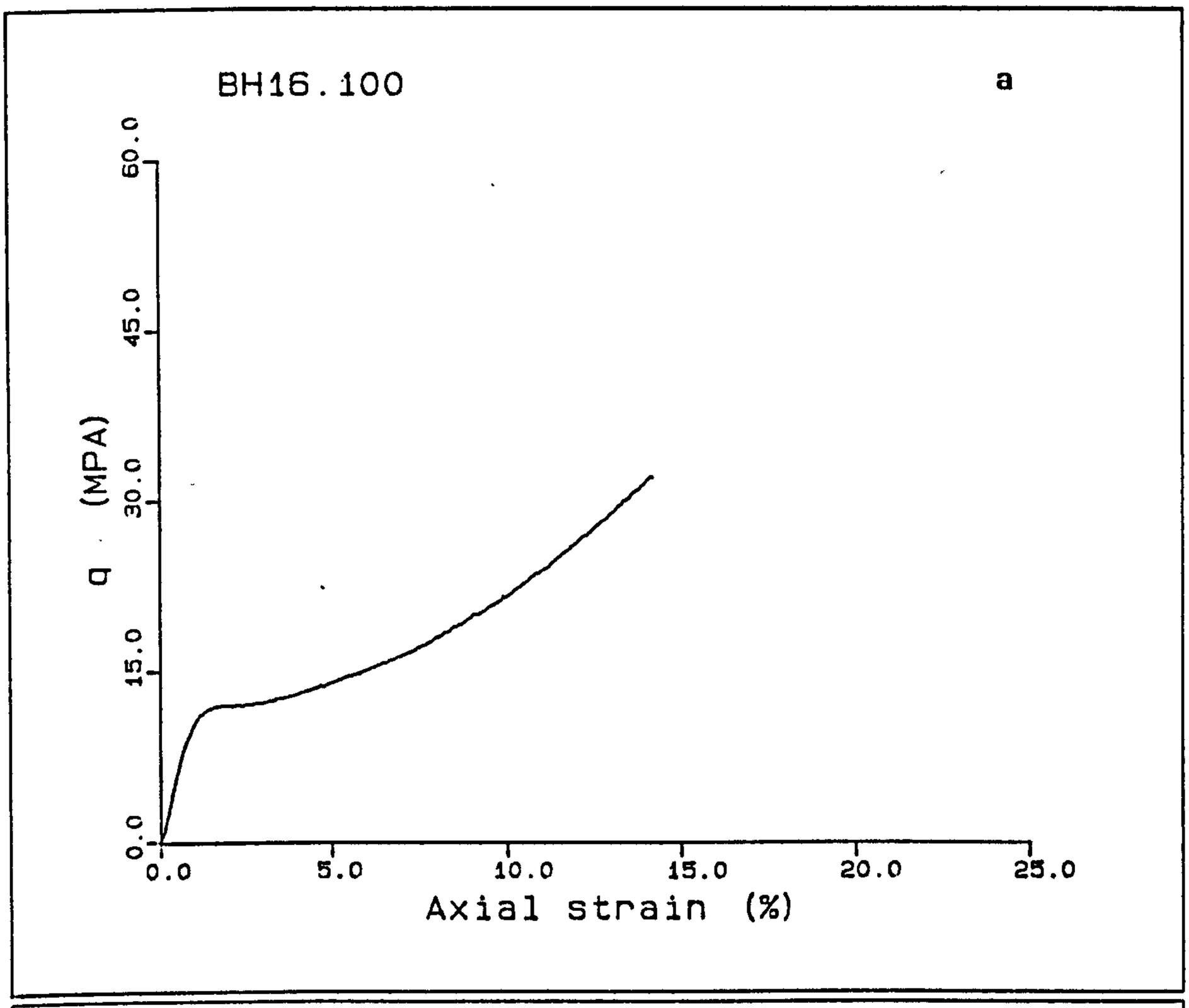

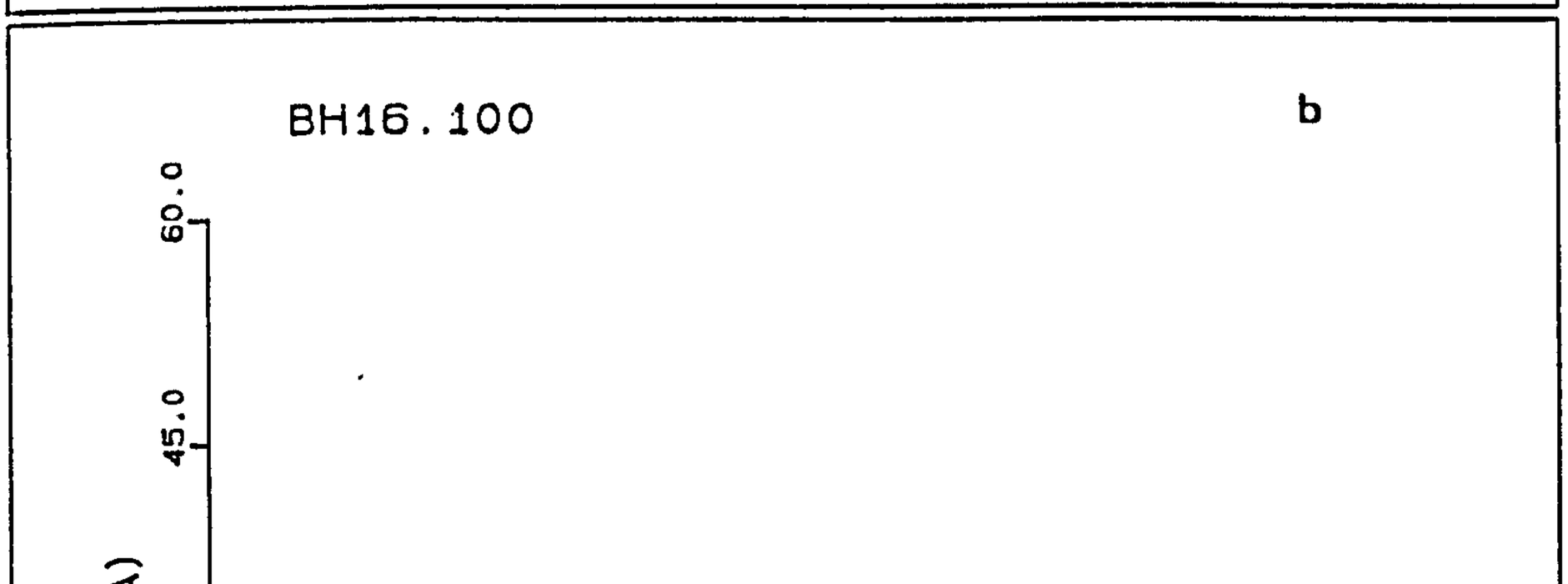

Figure A5.26(a-n) K_o test BH16.100.

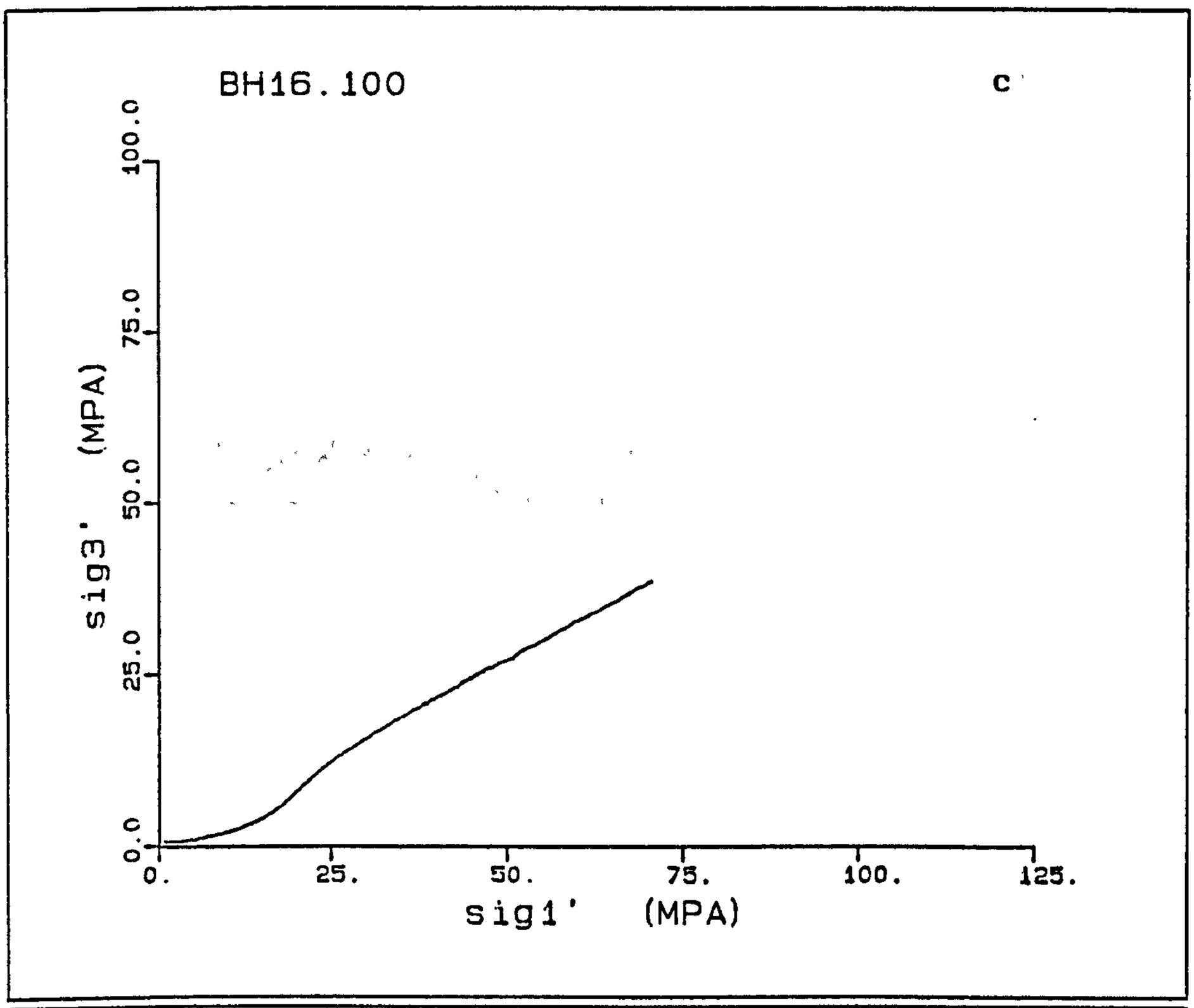
BH16.100
c
100.0
75.0
50.0
25.0
0.0
sig3' (MPA)
0.
25.
50.
75.
100.
125.
sig1' (MPA)

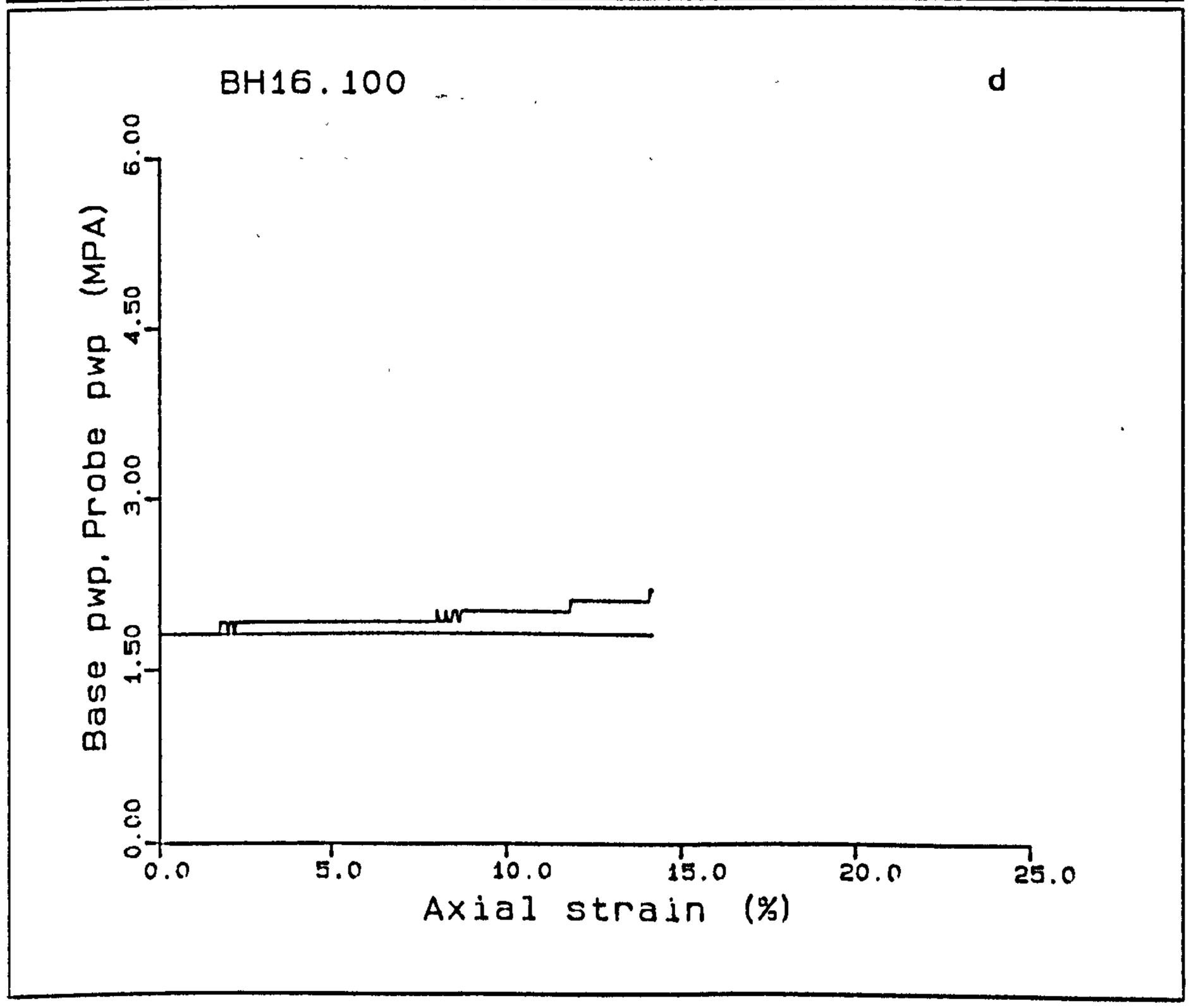
BH16.100
d
6.00
4.50
3.00
1.50
0.00
pwp, Probe pwp (MPA)
Base
0.0
5.0
10.0
15.0
20.0
25.0
Axial strain (%)

BH16.100

e

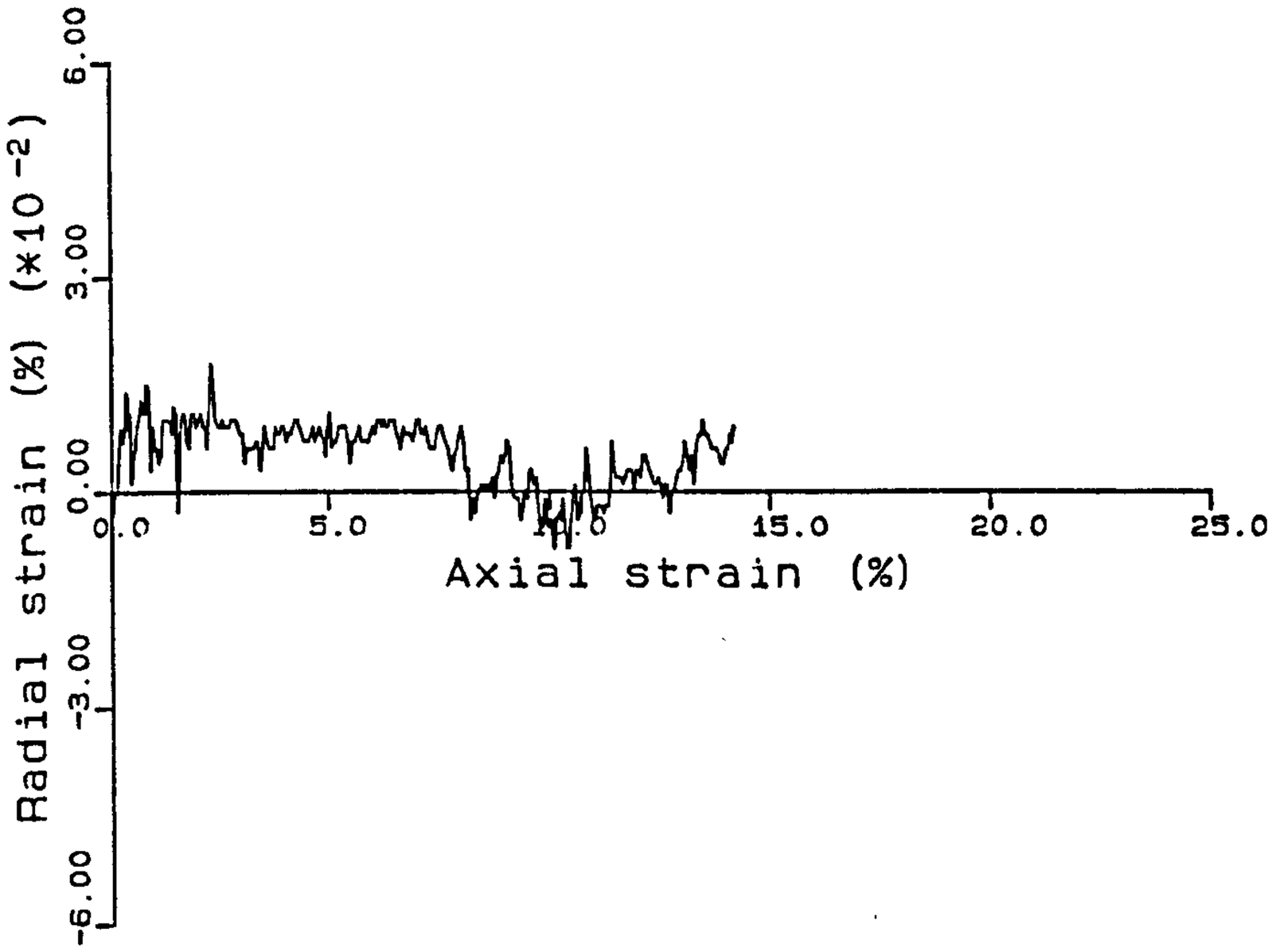

f

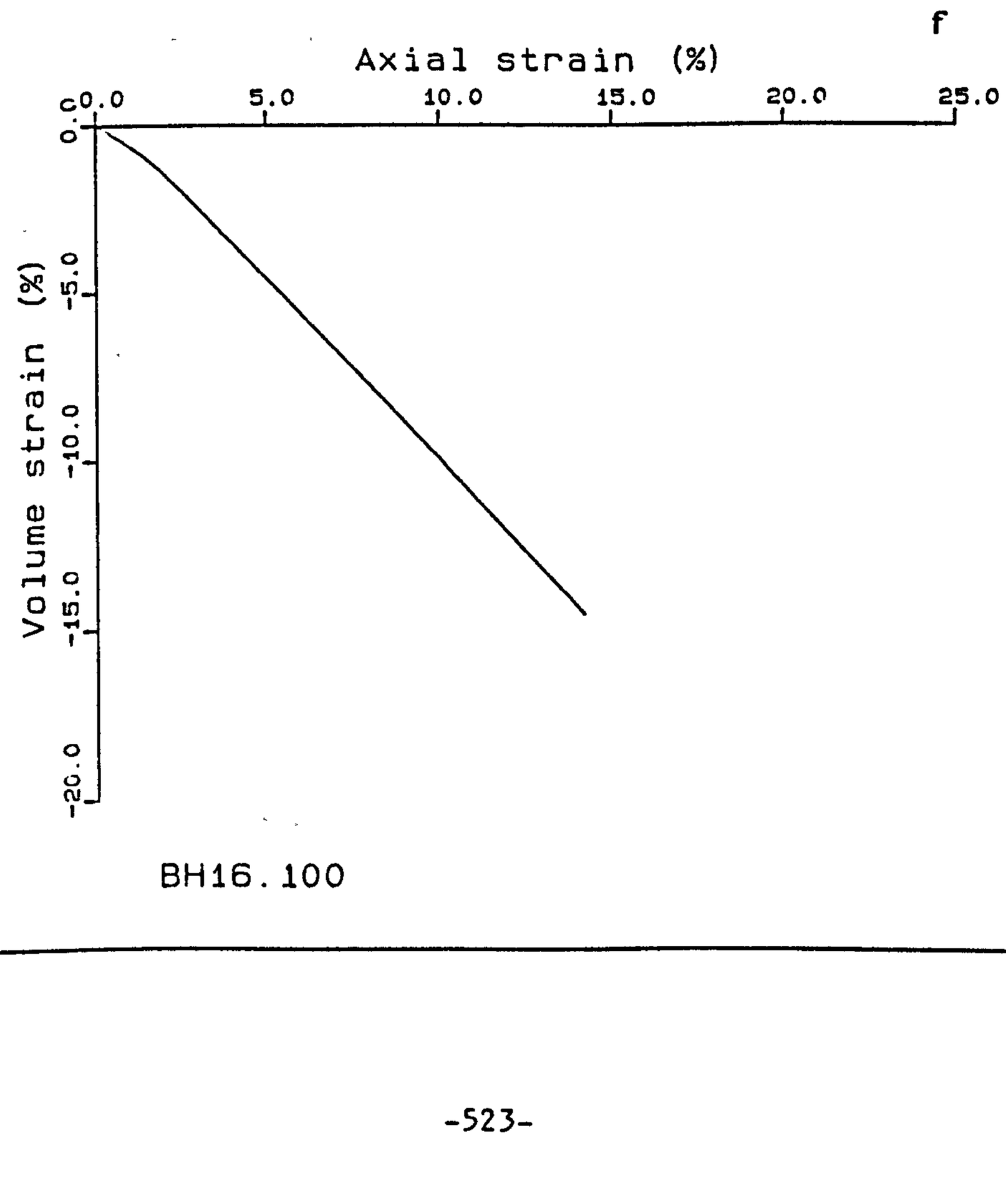

BH16.100

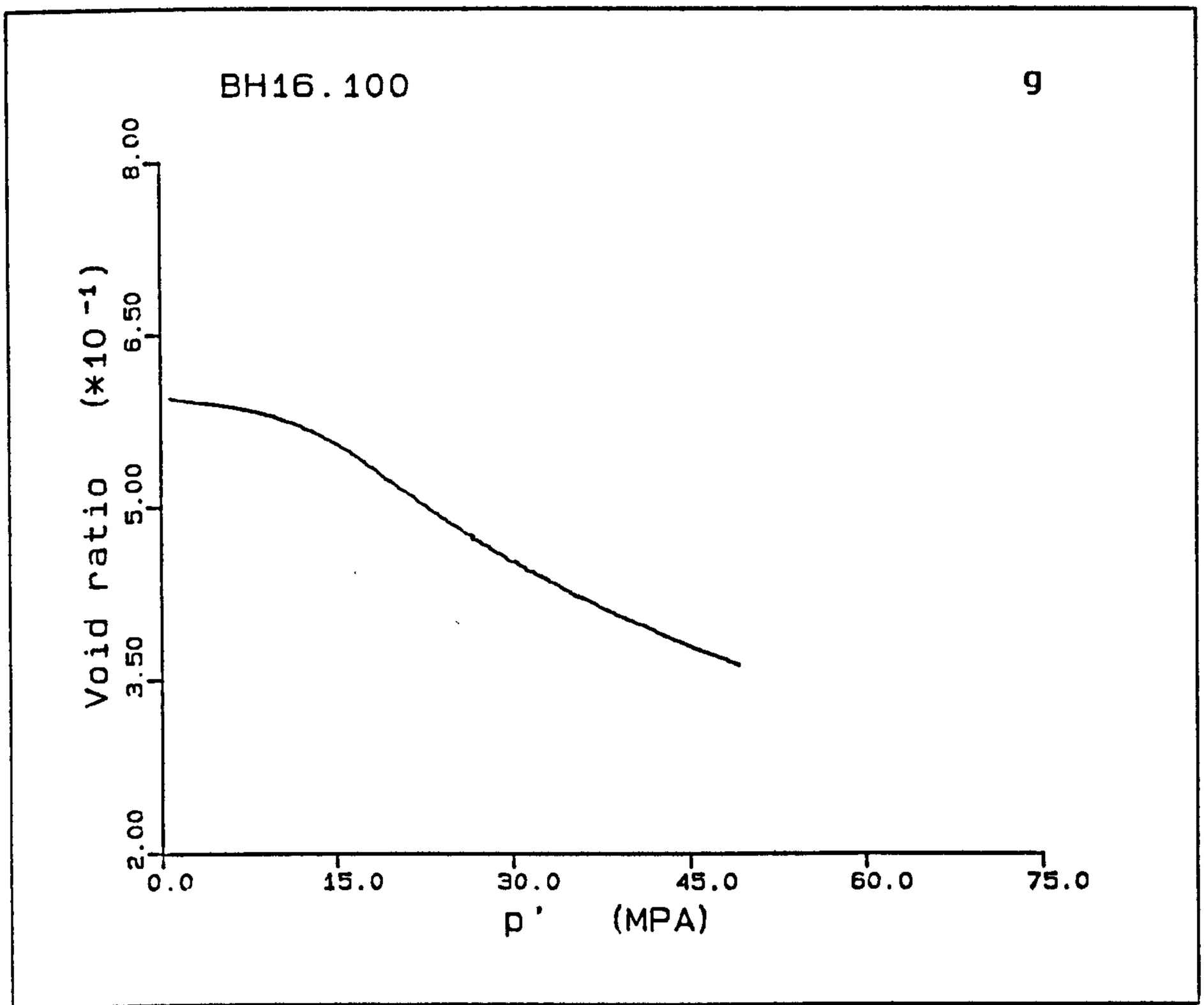
BH16.100
g
8.00
6.50
5.00
3.50
2.00
Void ratio (*10 -1)
0.0
15.0
30.0
45.0
60.0
75.0
p' (MPA)

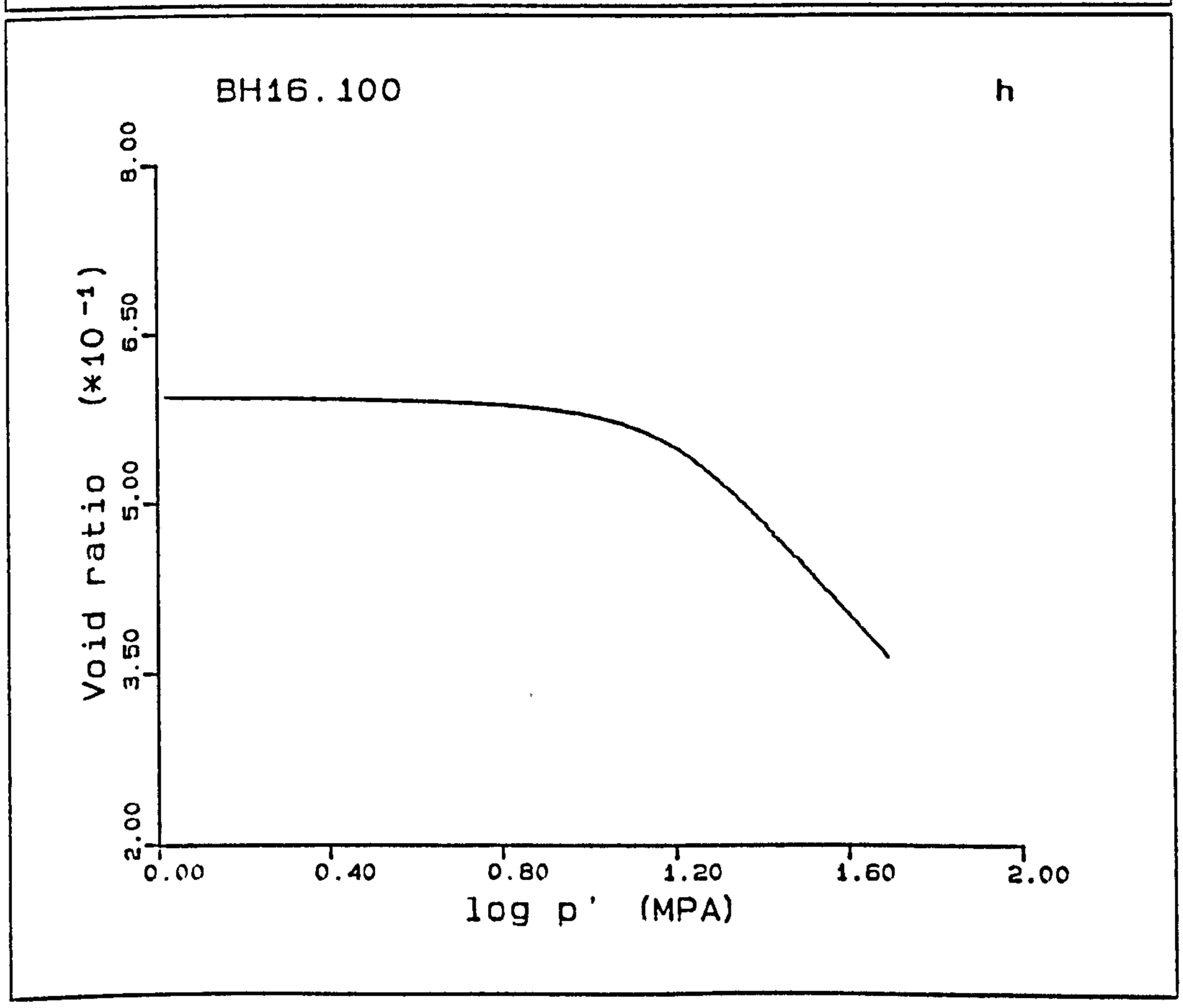
BH16.100
h
8.00
6.50
5.00
3.50
2.00
Void ratio (*10 -1)
0.00
0.40
0.80
1.20
1.60
2.00
log p' (MPA)

BH16.100

i

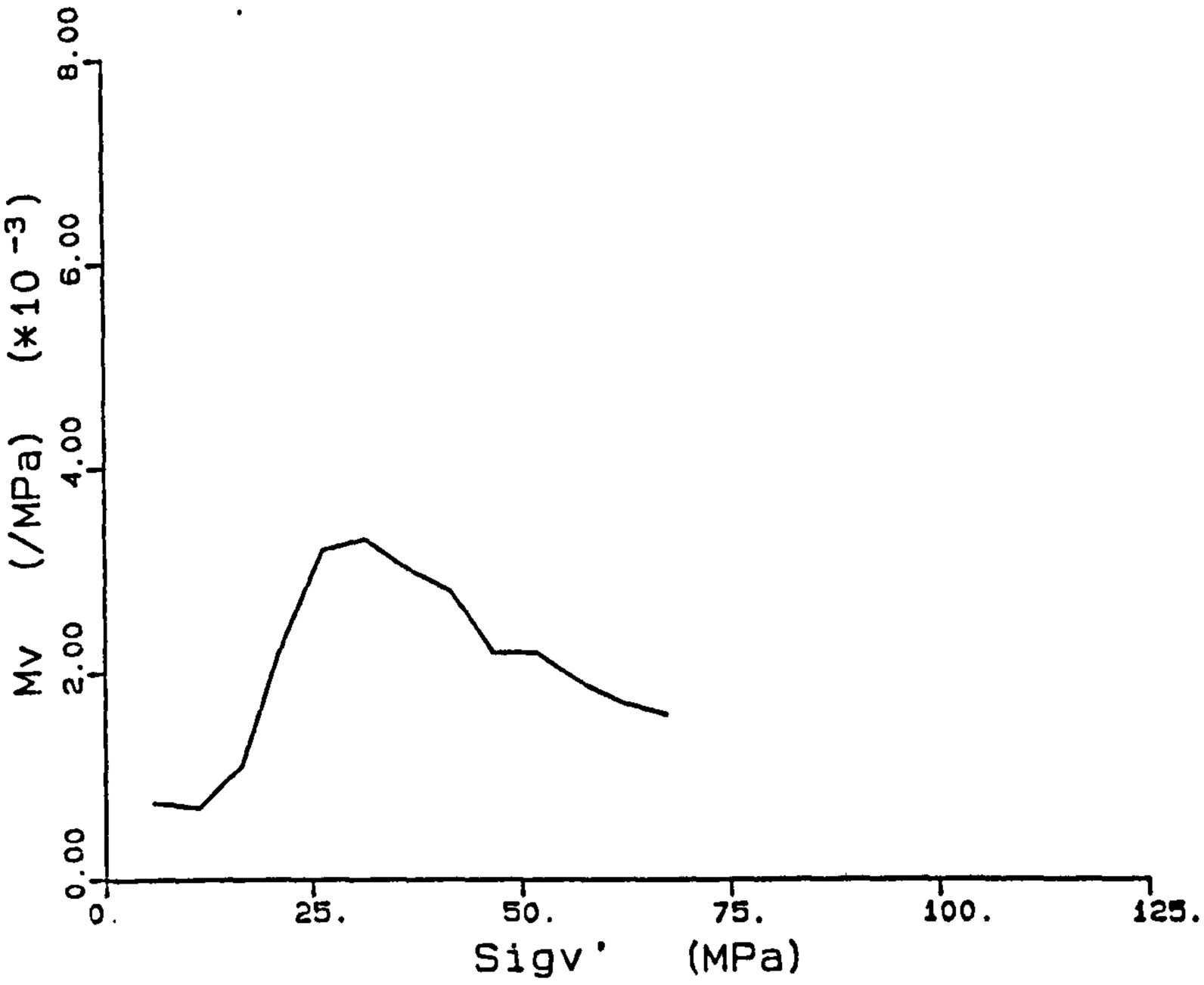

BH16.100

j

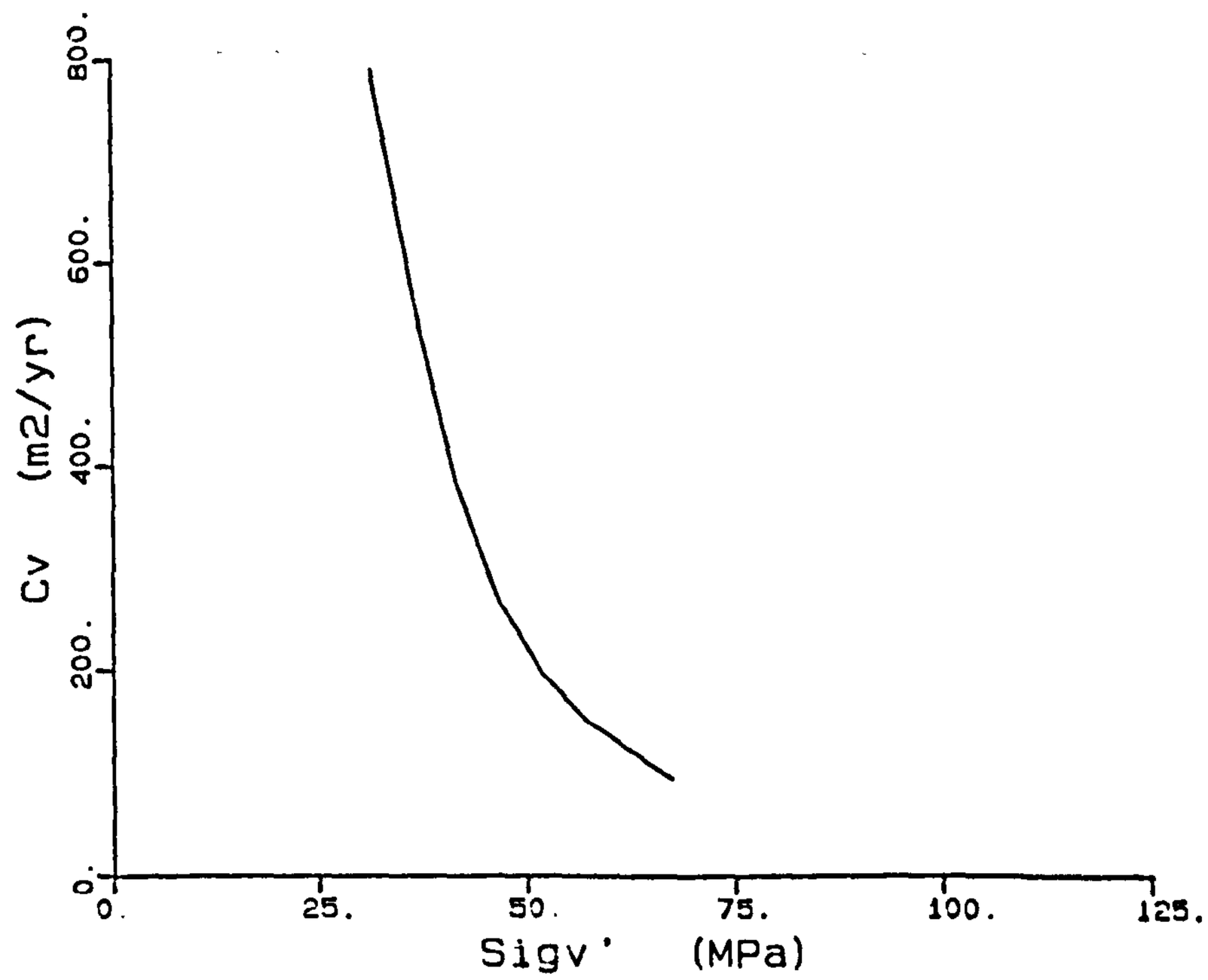

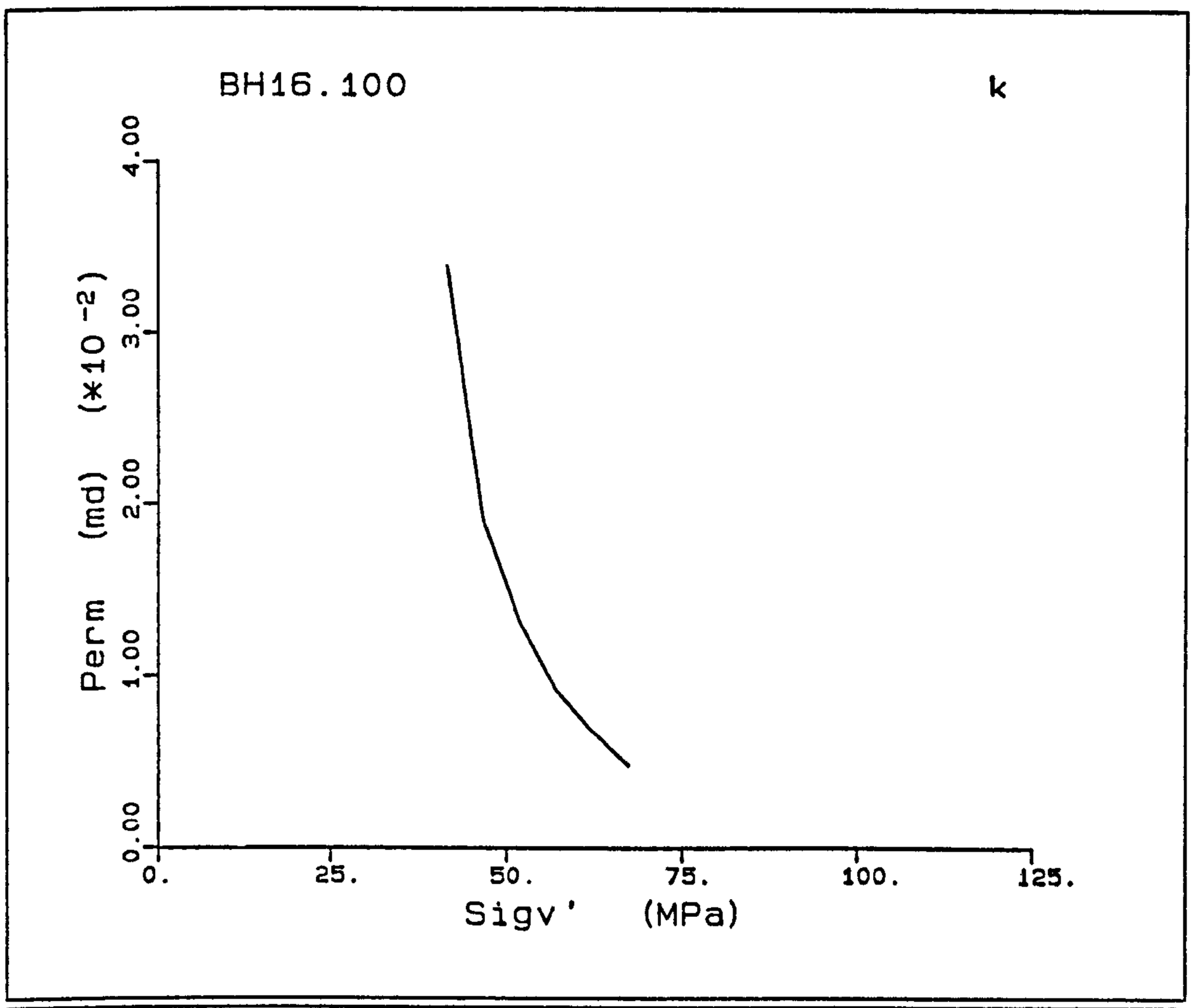
BH16.100
k
Perm (md) (*10 -2)
4.00
3.00
2.00
1.00
0.00
0.
25.
50.
75.
100.
125.
Sigv' (MPa)

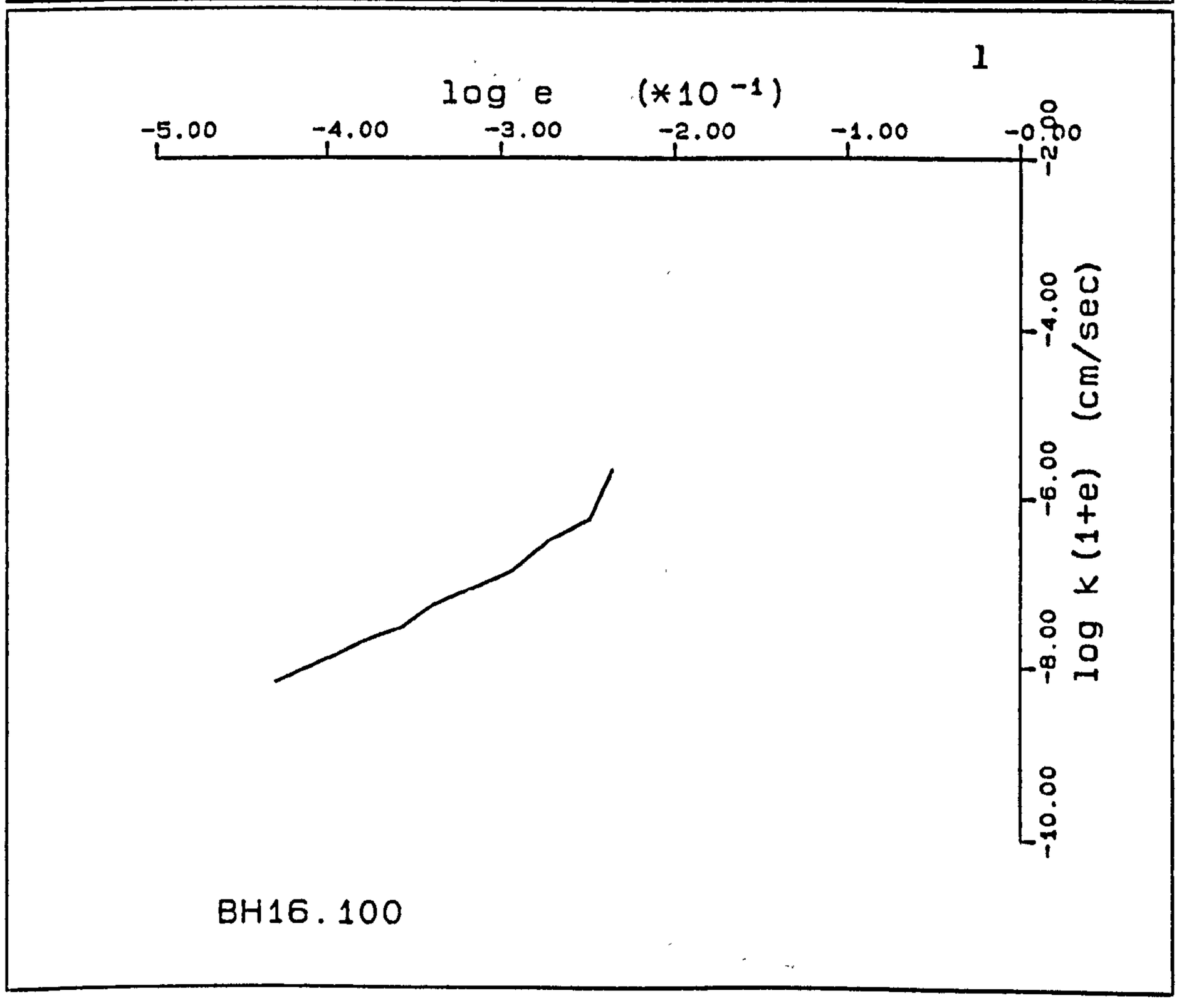
1
log e (*10 -1)
-5.00
-4.00
-3.00
-2.00
-1.00
-0.00
-2.00
-4.00
-6.00
-8.00
-10.00
log k (1+e) (cm/sec)
BH16.100

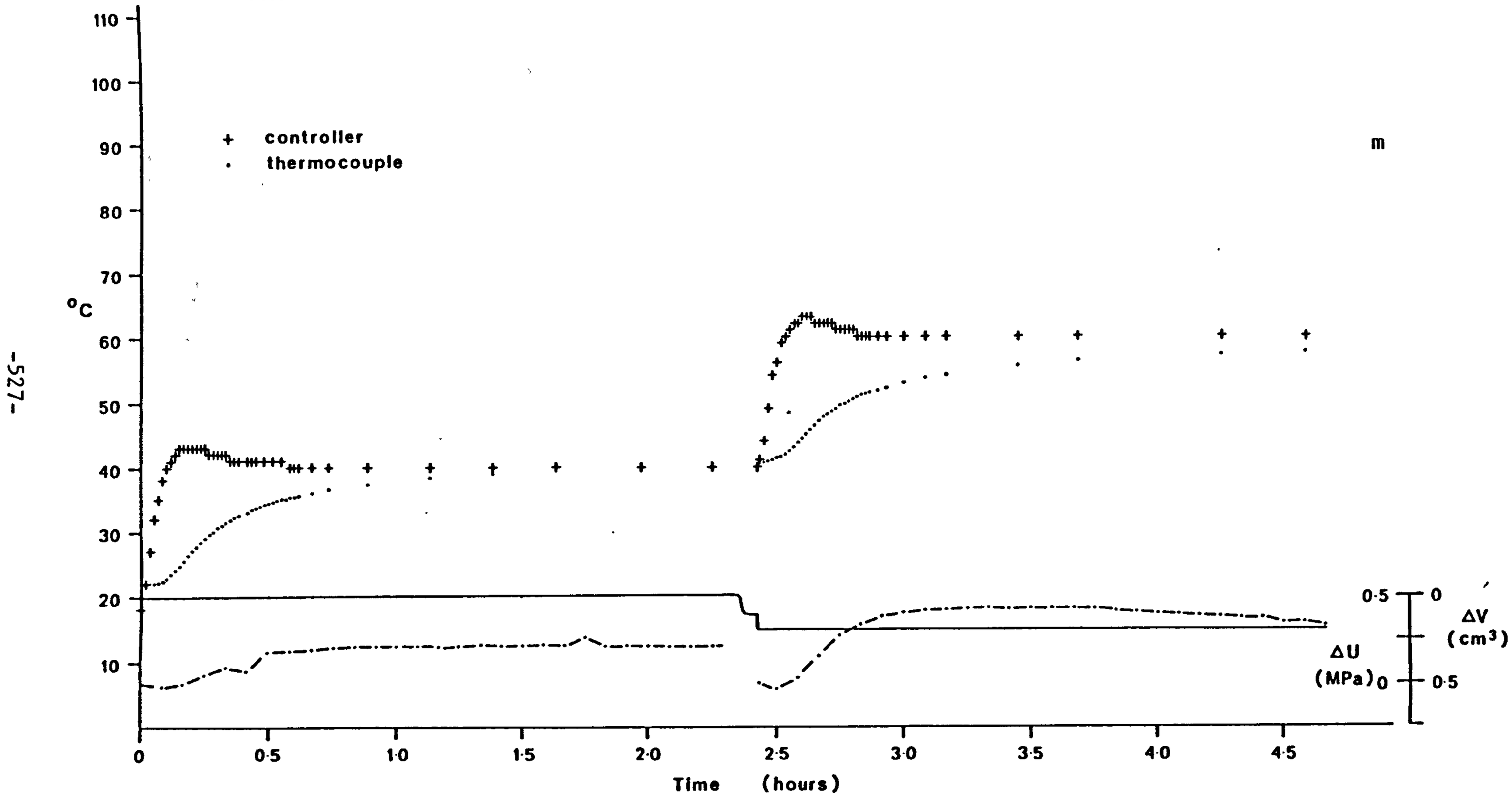
BH16.100
+ controller
· thermocouple
m
°C
110
100
90
80
70
60
50
40
30
20
10
0
0·5
1·0
1·5
2·0
2·5
3·0
3·5
4·0
4·5
Time (hours)
ΔU (MPa)
0·5
0
0·5
ΔV (cm³)

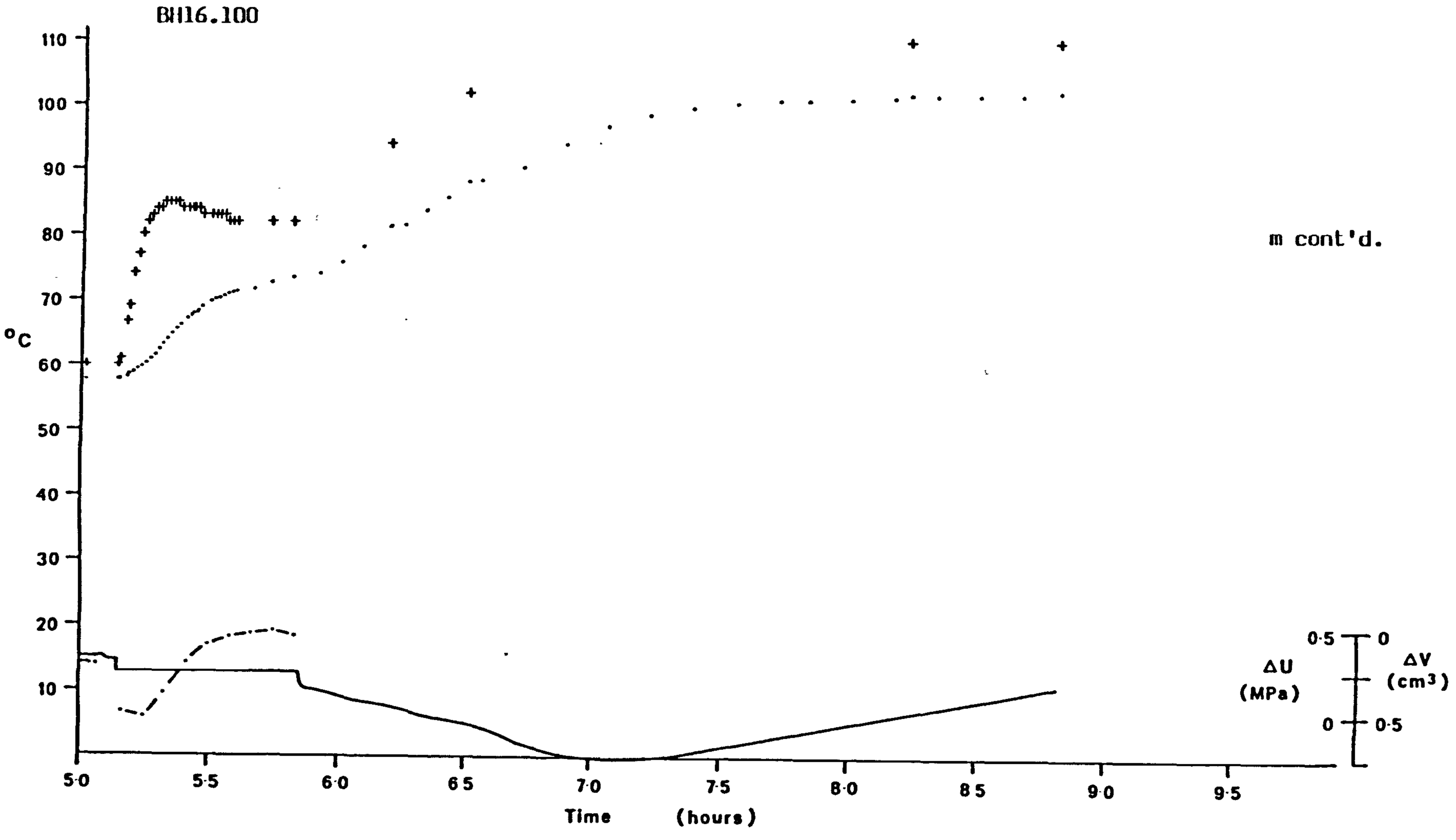
BH16.100
110
100
90
80
70
60
50
40
30
20
10
°C
5·0
5·5
6·0
6 5
7·0
7·5
8·0
8 5
9·0
9·5
Time (hours)
0·5
0
ΔU (MPa)
ΔV (cm³)
0
0·5

m cont'd.

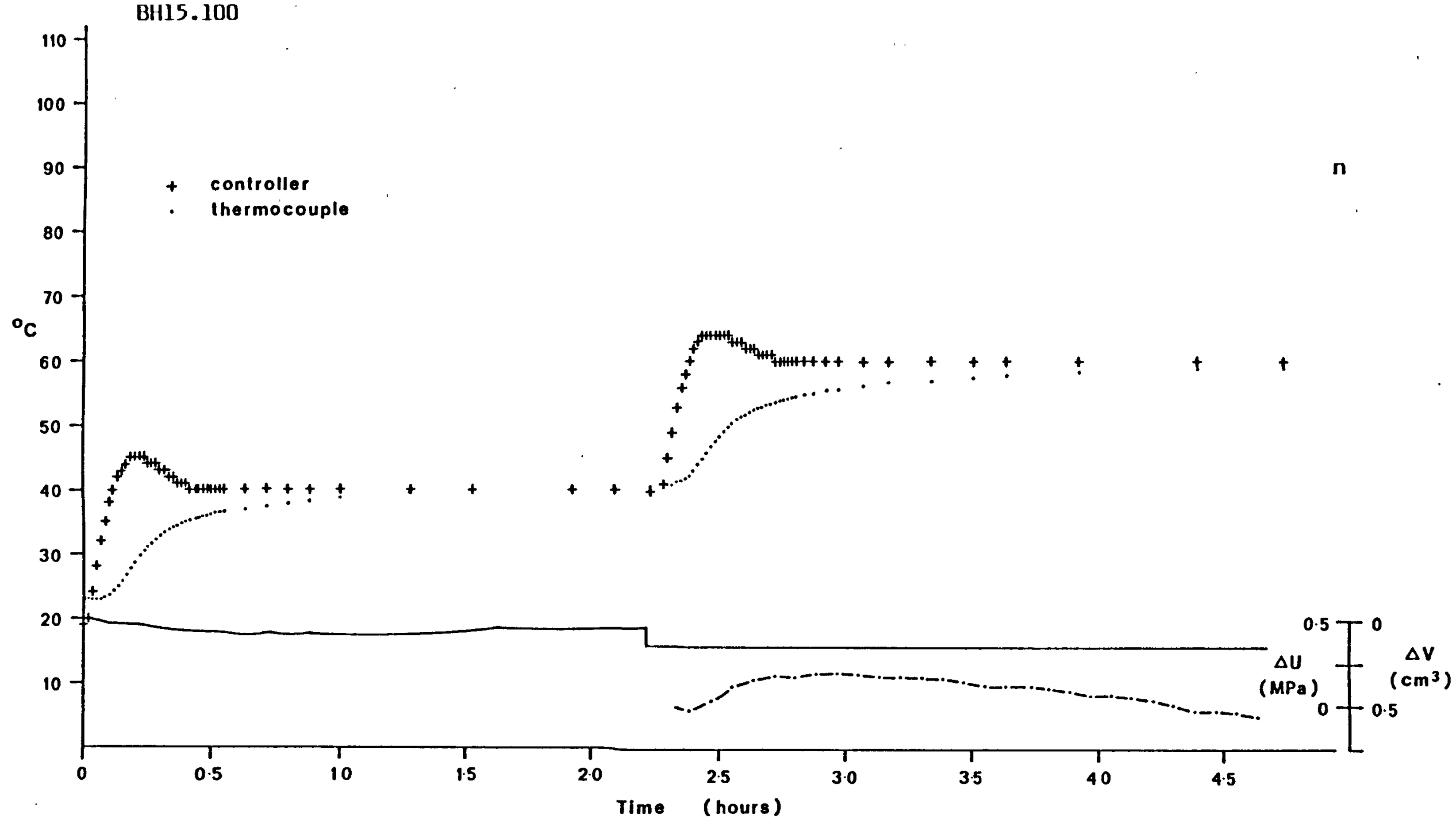
BH15.100
+ controller
· thermocouple
°C
110
100
90
80
70
60
50
40
30
20
10
0
0·5
1·0
1·5
2·0
2·5
3·0
3·5
4·0
4·5
Time (hours)
ΔU (MPa)
ΔV (cm³)
0·5
0
0
0·5

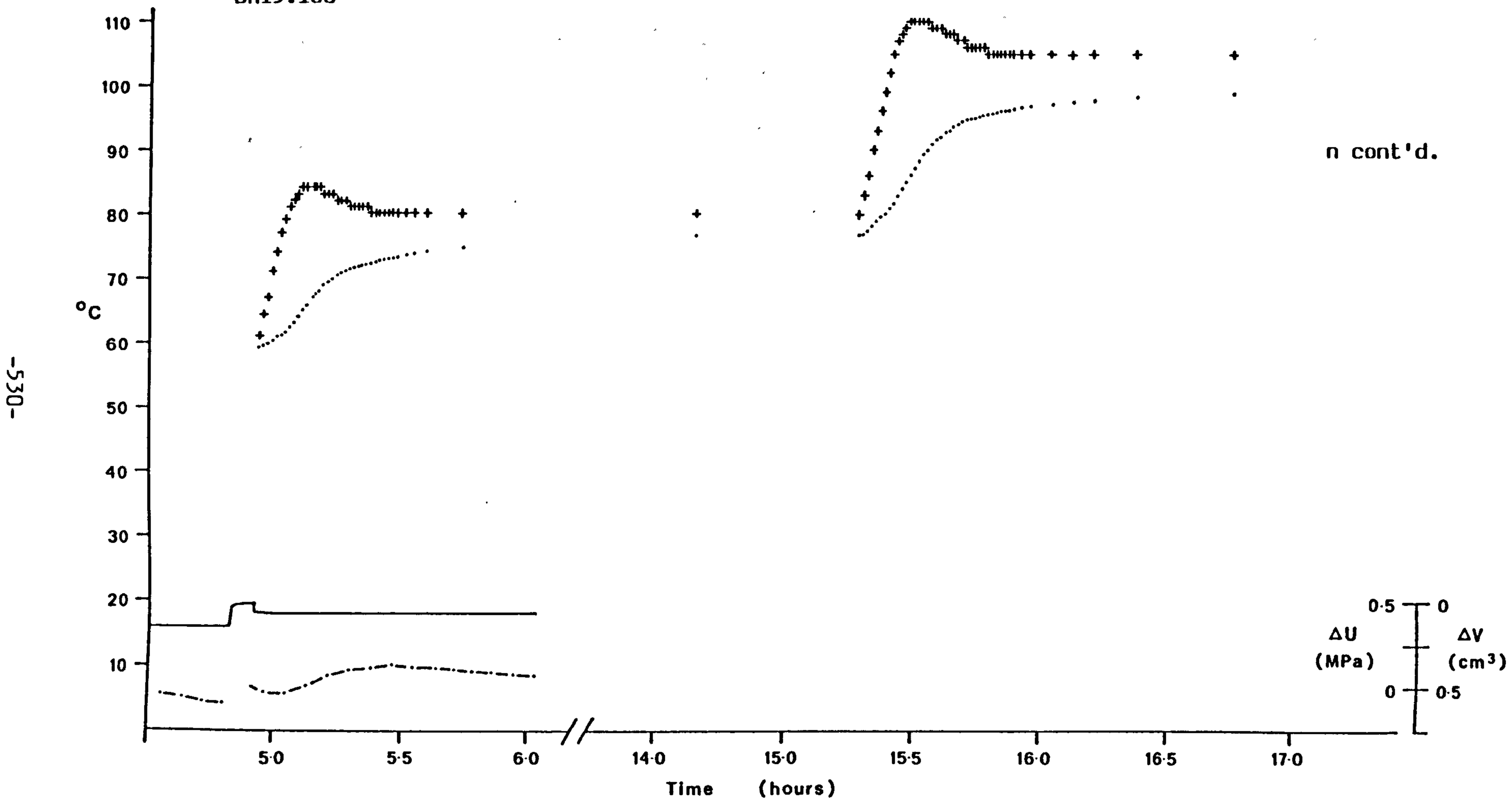
BH15.100
110
100
90
80
70
60
50
40
30
20
10
°C
n cont'd.
0·5
0
ΔU
(MPa)
ΔV
(cm³)
0
0·5
5·0
5·5
6·0
14·0
15·0
15·5
16·0
16·5
17·0
Time (hours)

BH17.60

This sample was a repeat of BH14.60 which underwent a large deviation off K_o. This sample had an initial porosity of 36.9% and was deformed under K_o conditions at a rate 0.04mm/min. The stress increase in the sample reacted linearly to initial strain with a Young's modulus of 1.17GPa, the yield of the chalk structure is taken at 11.0MPa, where a step occurs after a decrease and recovery in the deviatoric stress. The decrease in load is interpreted as a collapse of a burrow or cavity, as there is a sudden decrease in the radial strain and an increase in volume strain and pore pressure. After yield, the pore collapse deformation shows a slight increase in deviatoric stress followed by a decrease from 11.0 to 10.6MPa, the q then increasing linearly with p', Fig. A5.27b. The values of $\bar{K}_o$ obtained for the deformations are 0.140, 0.944 and 0.560 for the elastic, pore collapse and normal consolidation regions respectively. The radial strains increase initially, to drop when the pre-yield collapse occurs to $-14*10^{-3}$% radial strain. For the rest of the test, the strains are kept to $\pm 5*10^{-3}$% about $24*10^{-3}$% and only goes over this range at axial strains of 8.4 and 10.9%, when radial strains of $15*10^{-3}$% are recorded on both occasions.

The top pore pressure starts at a back pressure of 1.8MPa and increases to 5.8MPa during the collapse of the burrow, after this it reduces to 2.5MPa. With increasing compaction the top pore pressure gradually increases to 3.8MPa at an axial strain of 13.4%. The volume change plots are shifted to lower values due to the collapse, Figs. A5.27f-h, otherwise they show the same trends as in other Butser Hill chalks, the e - log p' plot showing two linear trends about the yield point.

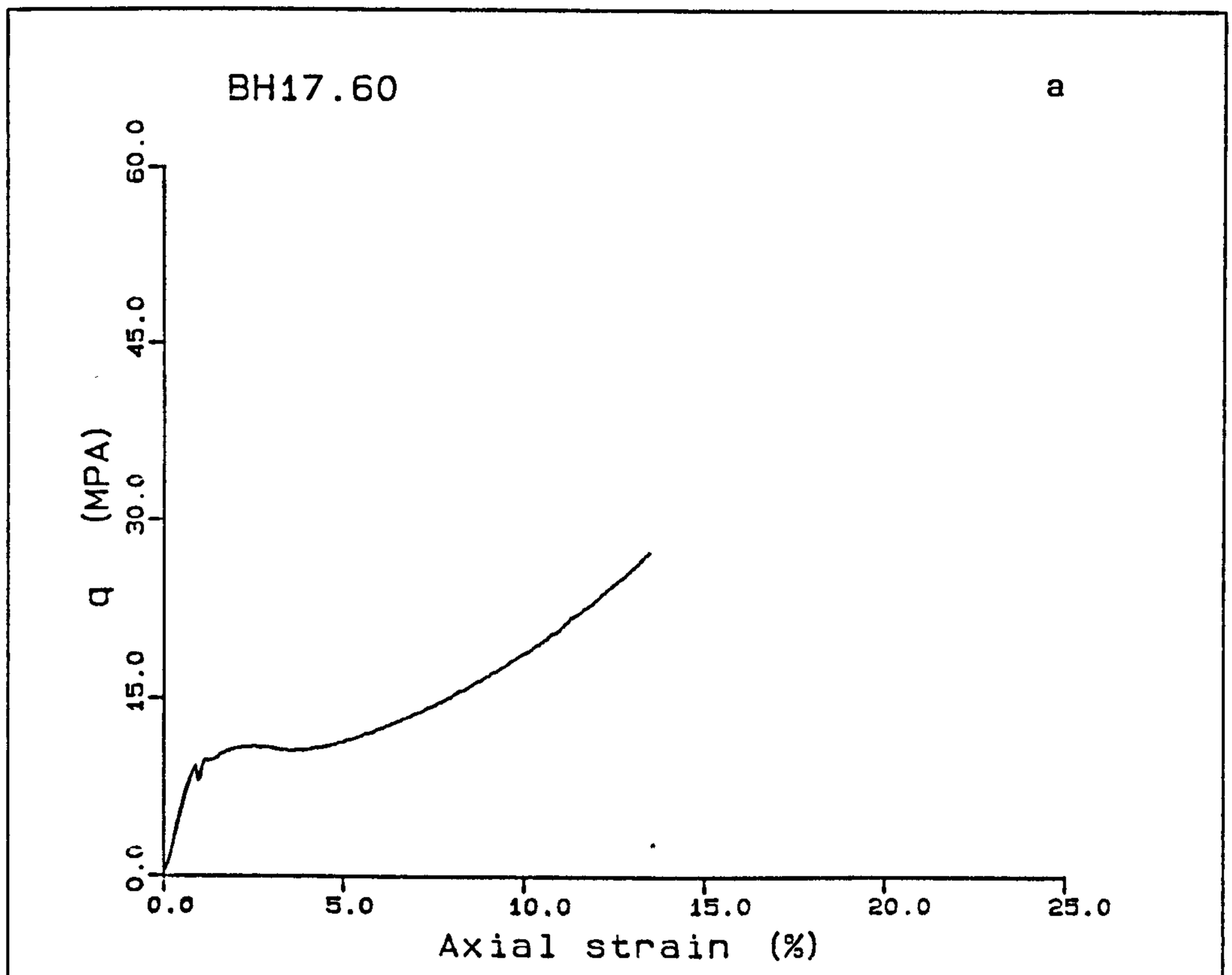

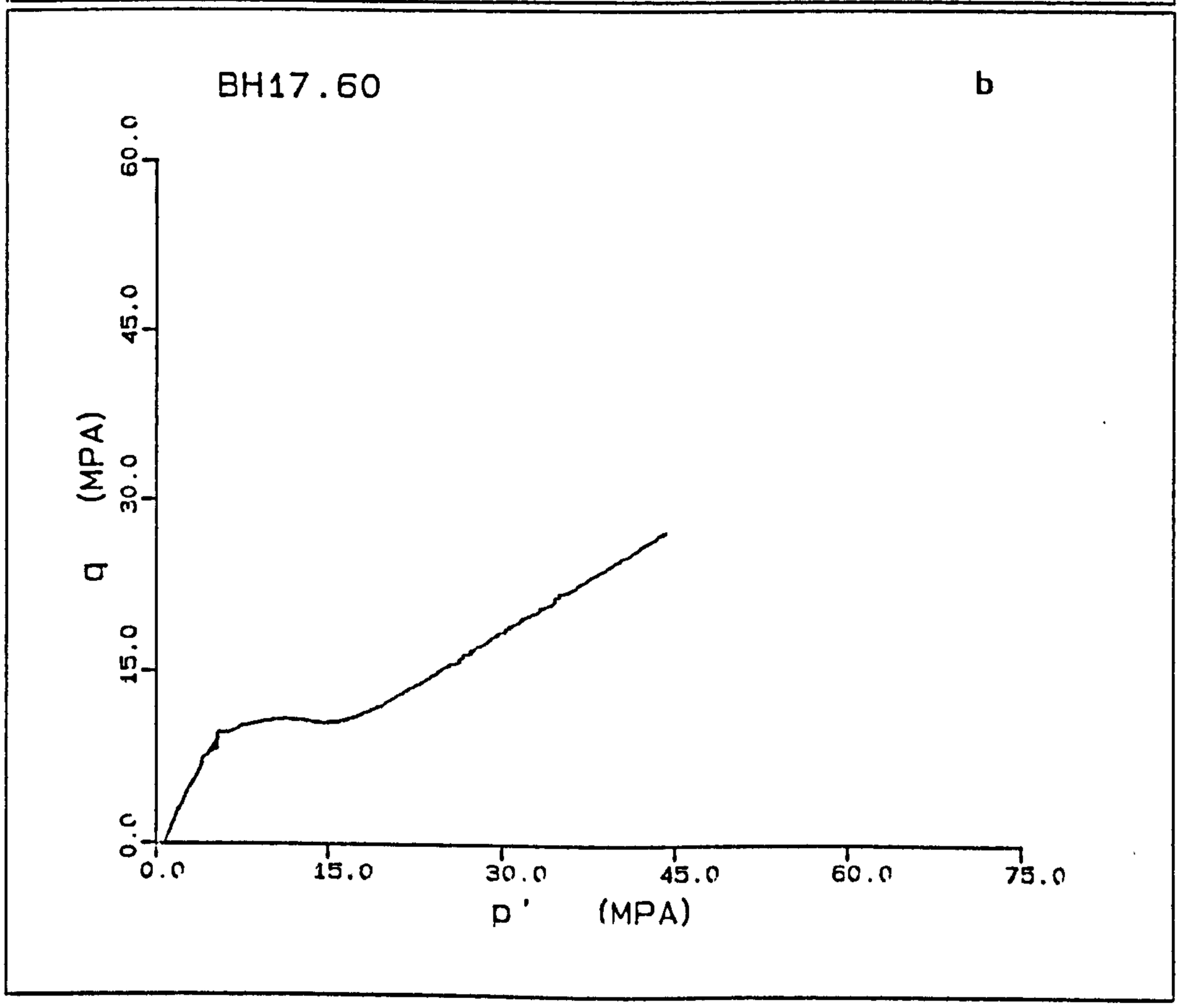

Figure A5.27(a-i) K_o test BH17.60.

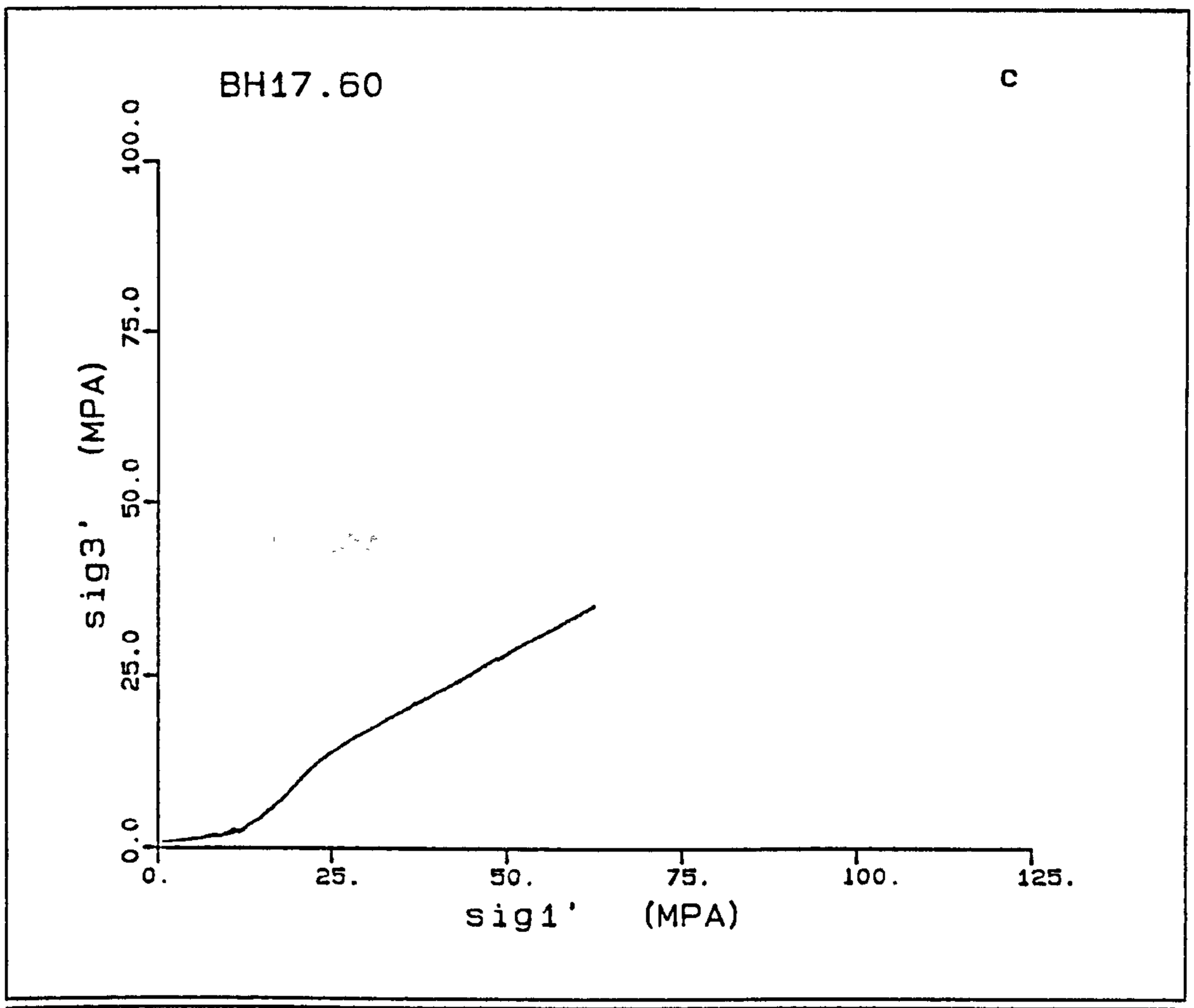
BH17.60
c
100.0
75.0
50.0
25.0
0.0
sig3' (MPA)
0.
25.
50.
75.
100.
125.
sig1' (MPA)

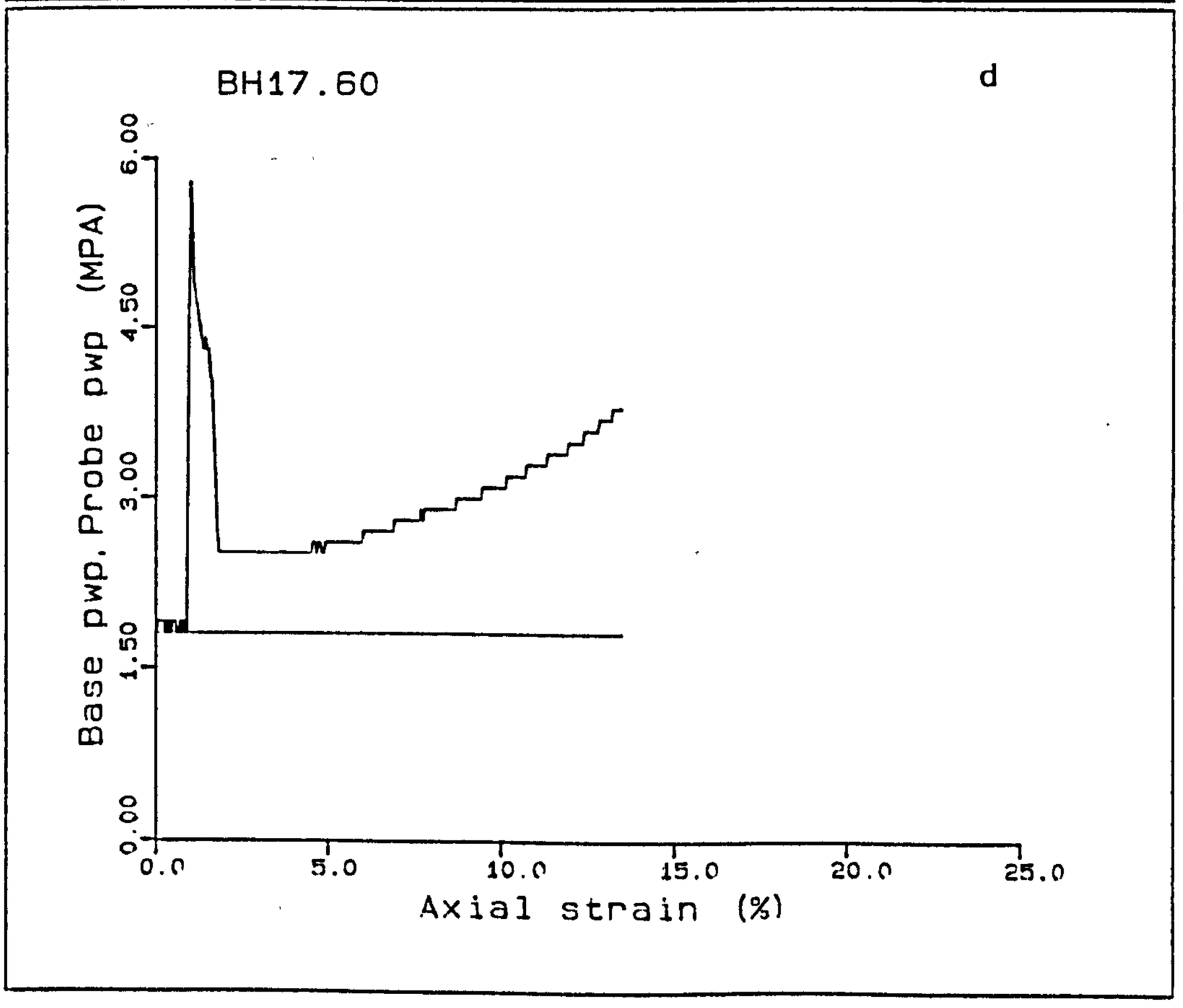
BH17.60
d
6.00
4.50
3.00
1.50
0.00
Base pwp, Probe pwp (MPA)
0.0
5.0
10.0
15.0
20.0
25.0
Axial strain (%)

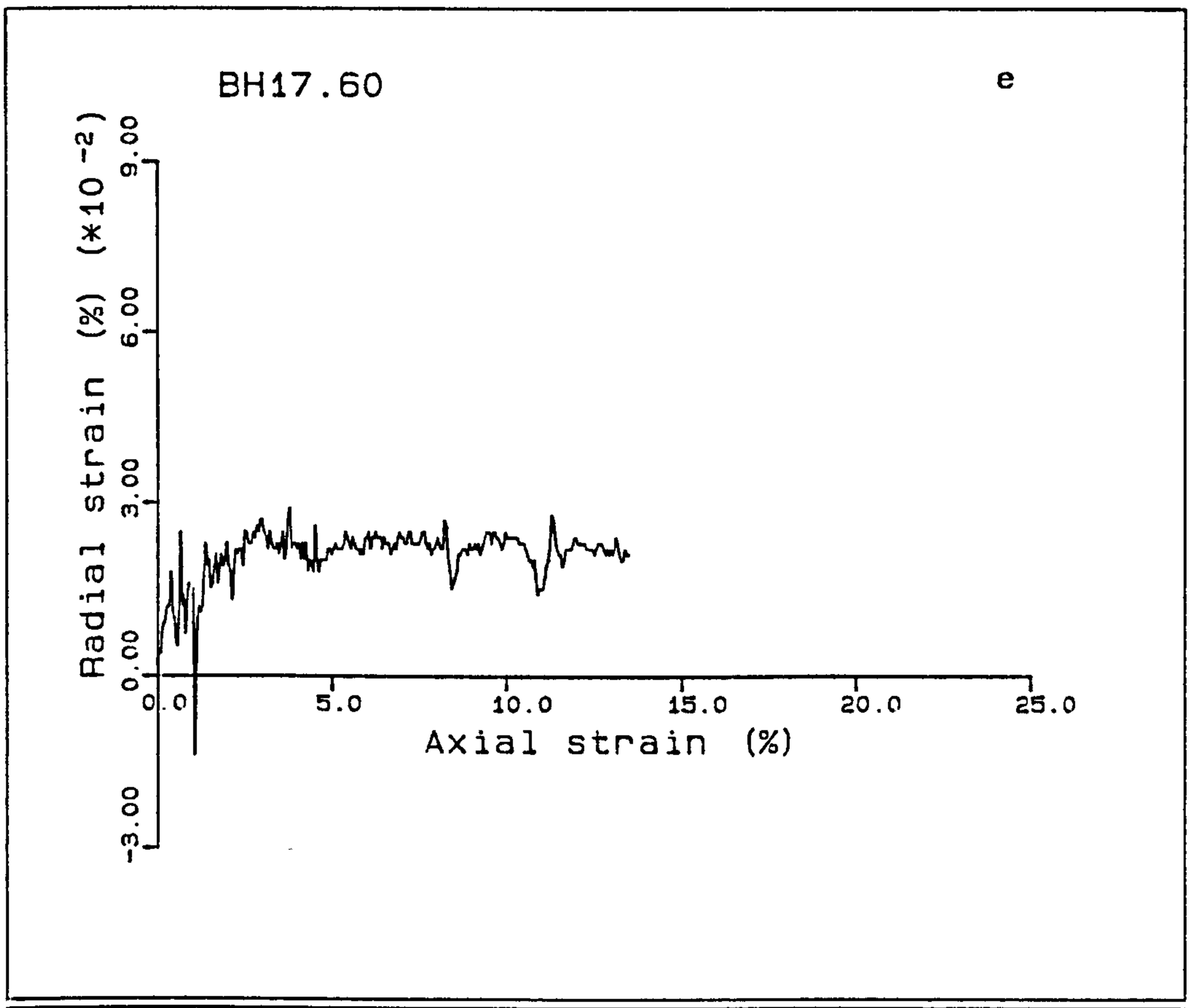
BH17.60
e
Radial strain (%) (*10 -2)
9.00
6.00
3.00
0.00
-3.00
0.0
5.0
10.0
15.0
20.0
25.0
Axial strain (%)

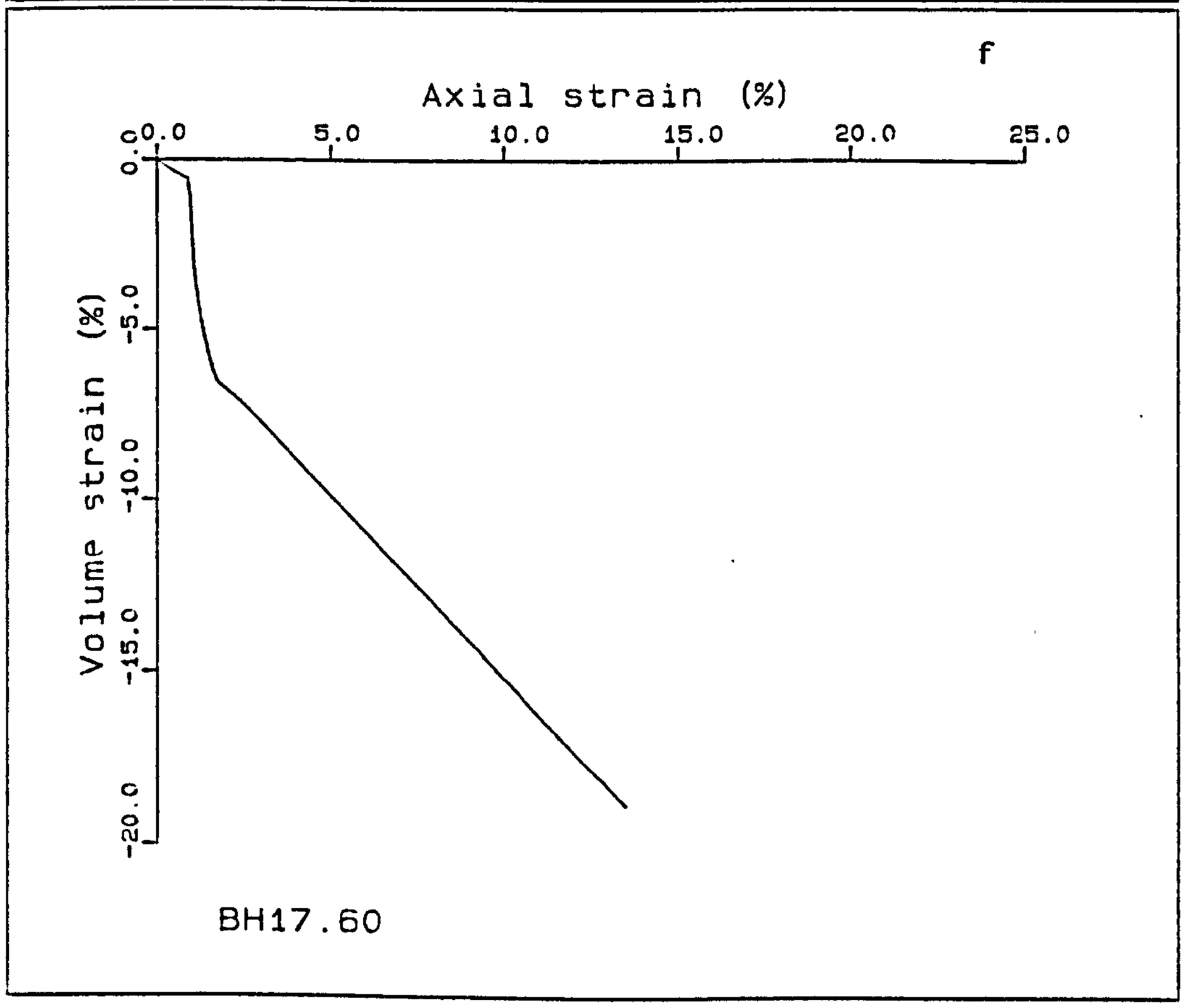
f
Axial strain (%)
0.0
5.0
10.0
15.0
20.0
25.0
0.0
-5.0
-10.0
-15.0
-20.0
Volume strain (%)
BH17.60

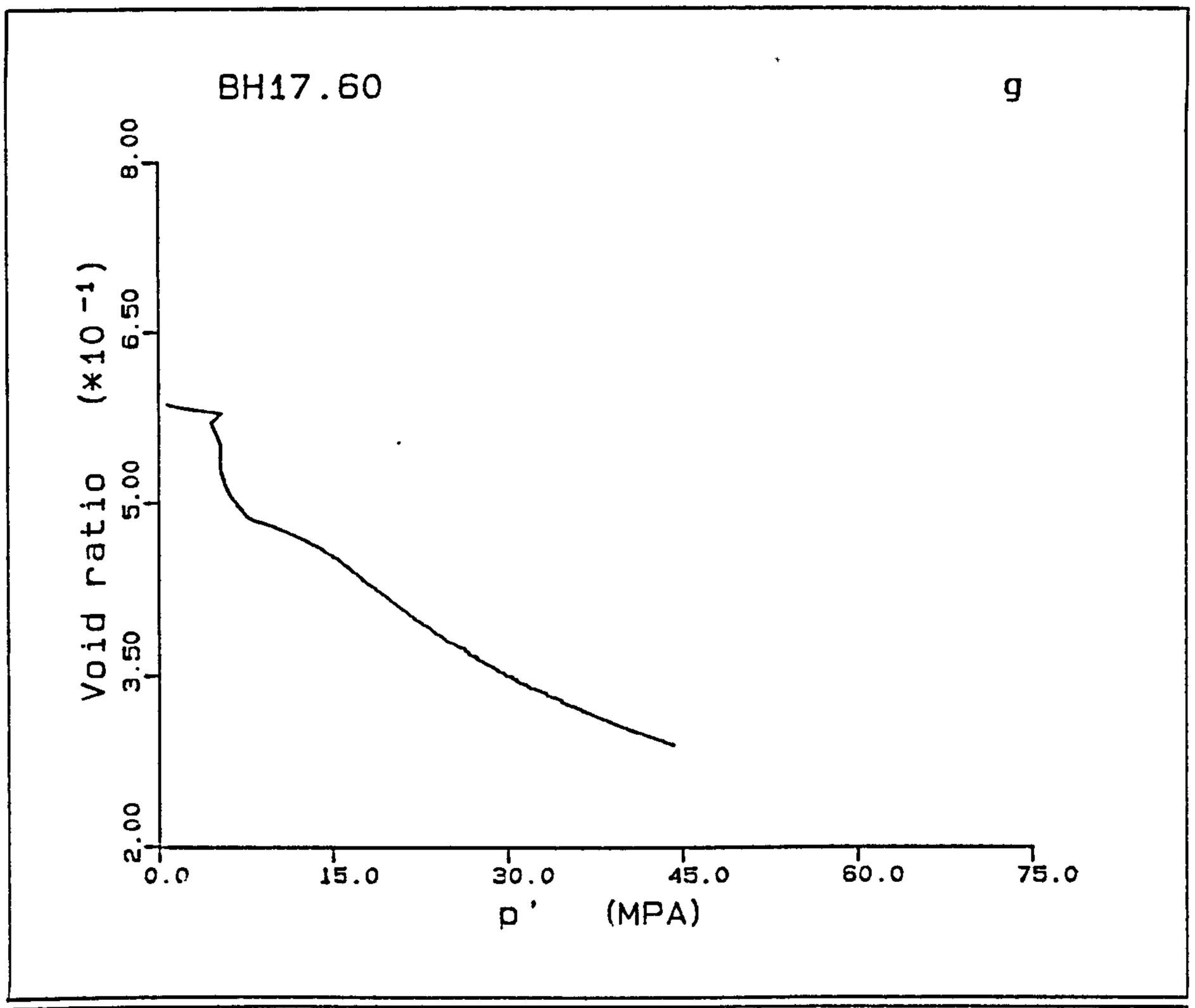
BH17.60
g
Void ratio (*10 -1)
8.00
6.50
5.00
3.50
2.00
0.0
15.0
30.0
45.0
60.0
75.0
p' (MPA)

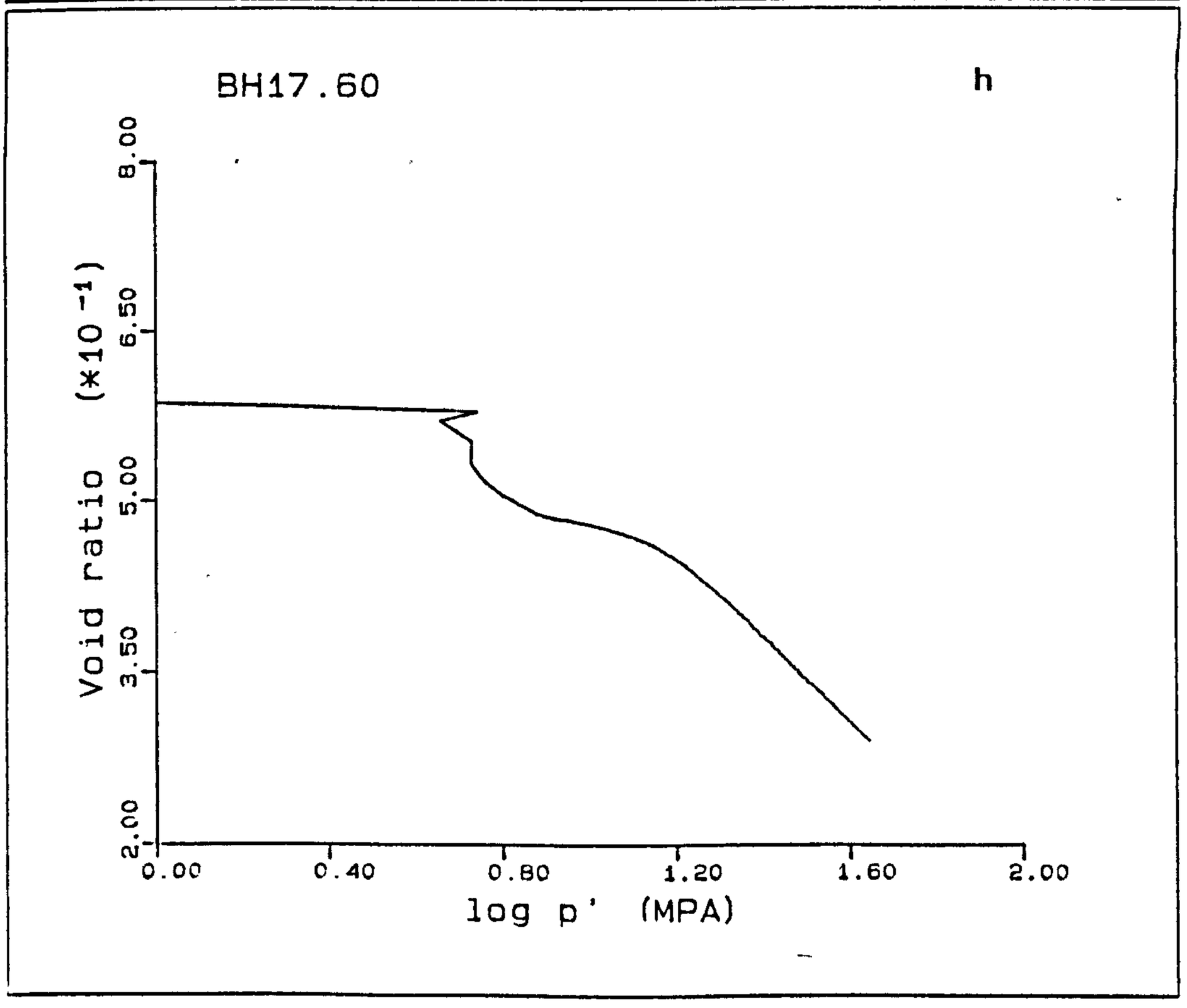
BH17.60
h
Void ratio (*10 -1)
8.00
6.50
5.00
3.50
2.00
0.00
0.40
0.80
1.20
1.60
2.00
log p' (MPA)

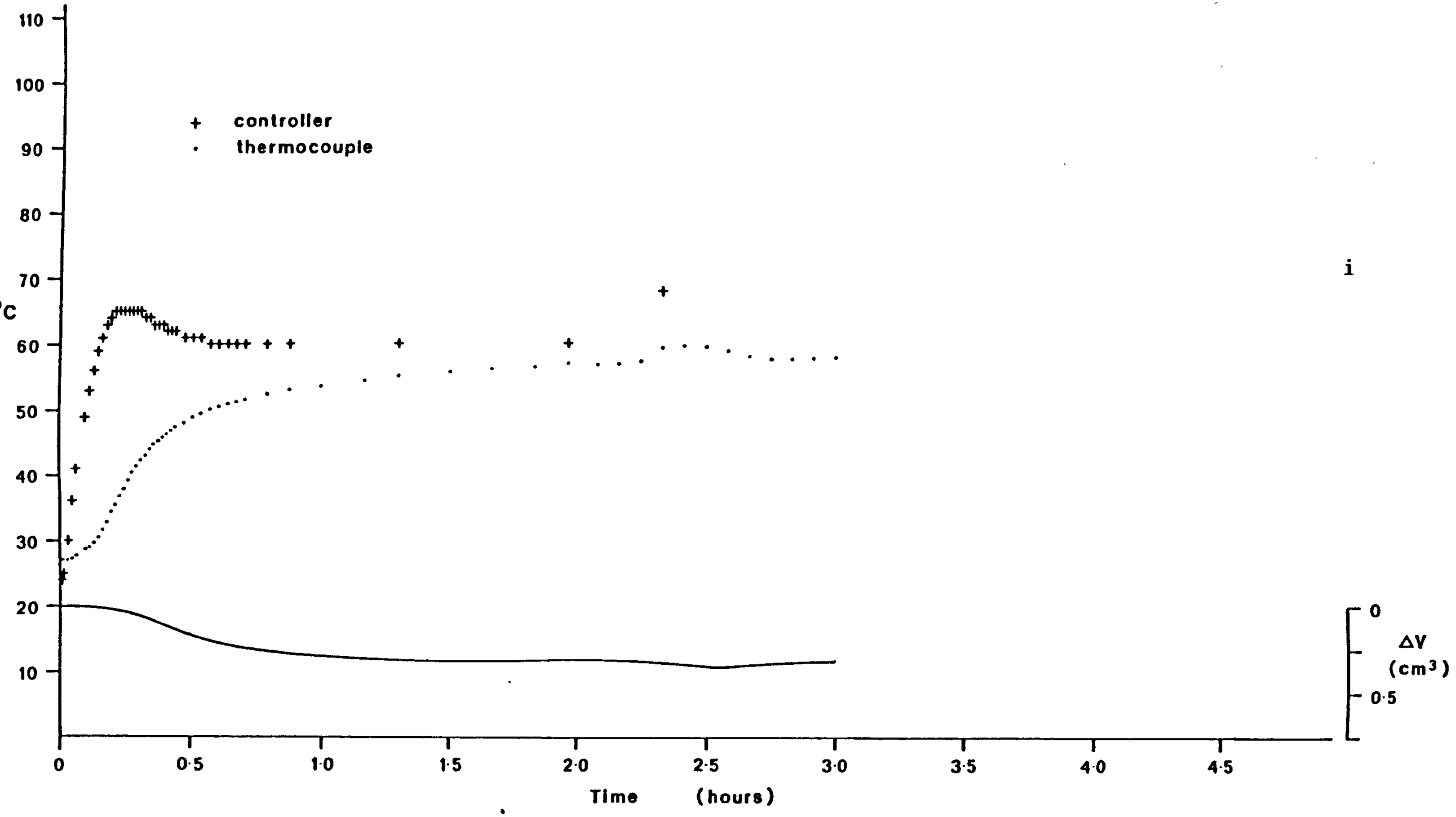
BH17.60
110
100
90
80
70
60
50
40
30
20
10
°C
+ controller
· thermocouple
0
0·5
1·0
1·5
2·0
2·5
3·0
3·5
4·0
4·5
Time (hours)
0
ΔV
(cm³)
0·5

A5.5) HYDROSTATIC TEST

BH6.20

This sample is a 36.9% porosity sample and tested by gradually increasing the cell pressure, from which we can obtain the isotropic (hydrostatic) yield point of the Butser Hill chalk, Fig. A5.28. This is a stress controlled test as opposed to the previous tests performed, which are strain controlled. The plots of void ratio against mean effective stress (also maximum effective stress), and void ratio versus log mean effective stress show a yield point of 20.87MPa mean effective stress. This was obtained from the intersection of slopes from the normal - normal plot.

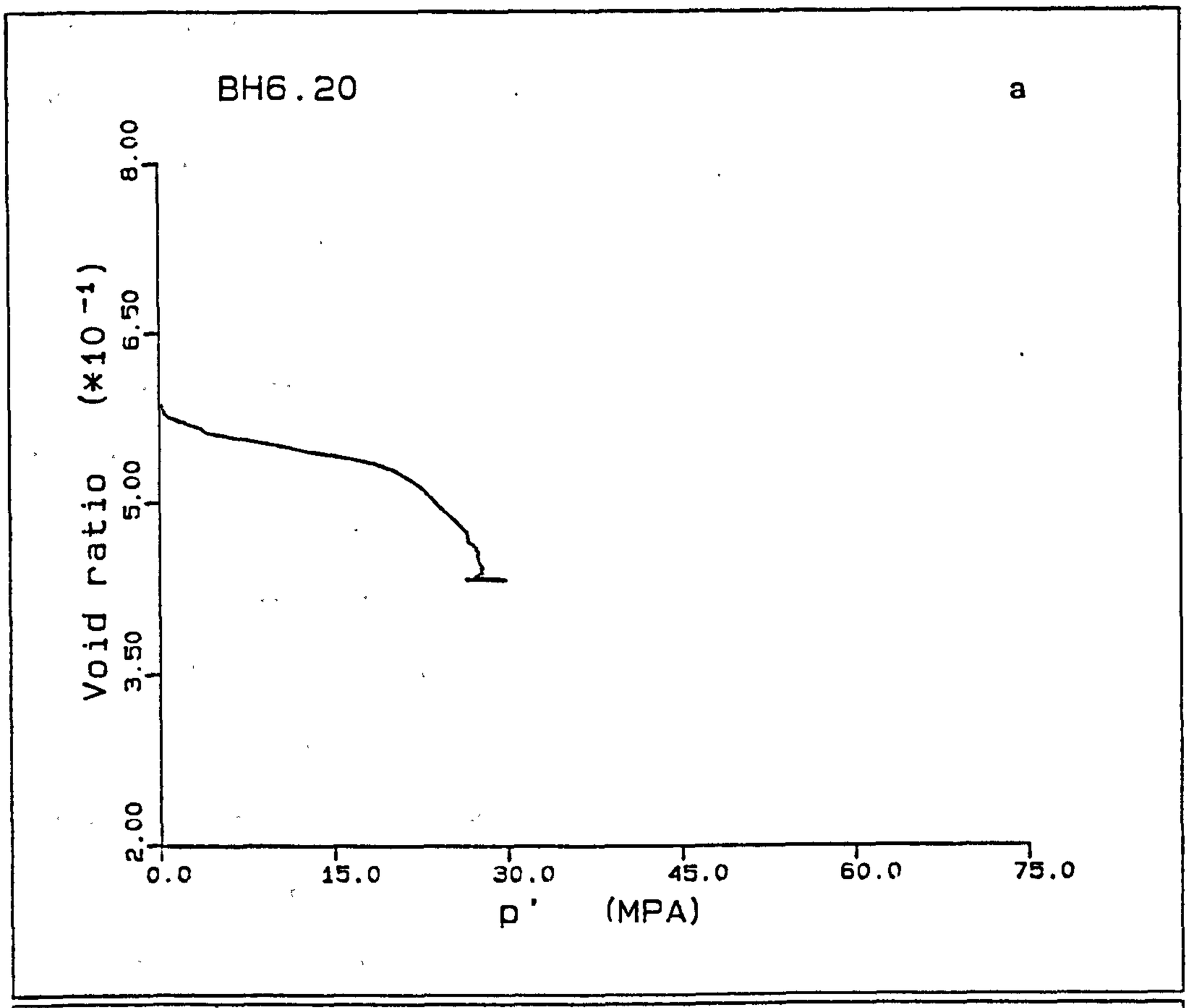

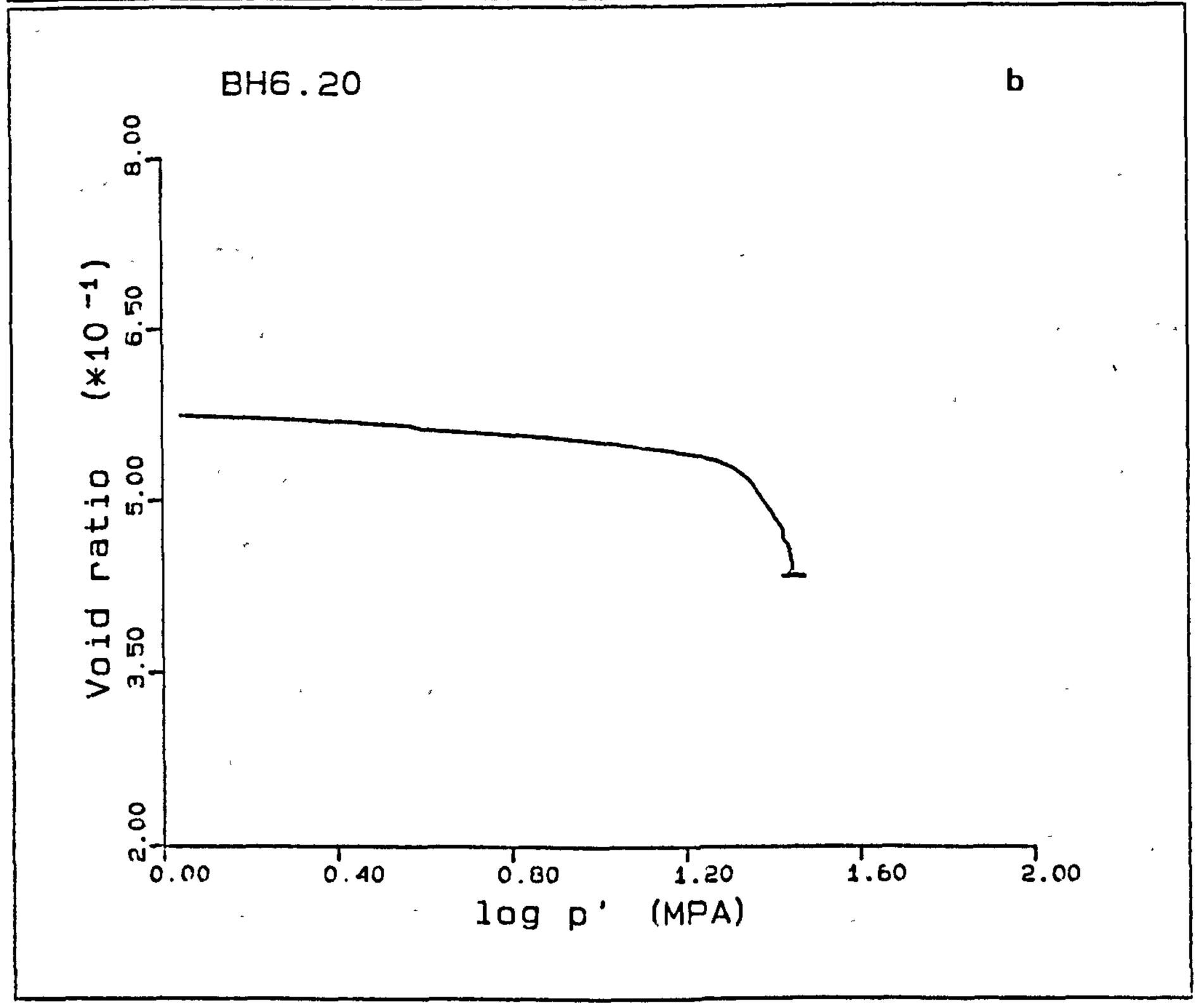

Figure A5.28(a-b) Hydrostatic test BH6.20.

A5.6) DRAINED SHEAR TESTS

These tests were performed at constant cell pressure the sample being loaded at a constant rate of deformation. These were performed to obtain the approximate shape of the yield envelope. The experiments will be described 'en masse', and are tabulated in Table A5.5. Five tests were performed BH8.20, BH10.20, BH11.20, BH12.20 and BH20.20, Figs. A5.29-33, and the yield envelope determined. In BH8.20, BH12.20, BH20.20, the deformation was continued to obtain the failure point also. This was only achieved in BH12.20. In these tests the cross sectional area of the sample was determined using the volume strain, as the sample at large radial strains came into contact with the radial strain belt, at which point the pads would tend to be pulled around the sample and off the diameter.

The confining pressure for BH8.20, BH10.20, BH11.20, BH12.20 and BH20.20, were 18.2MPa, 5.7MPa, 10.7MPa, 15.0MPa and 15.6MPa, the loading rate being 0.01mm/min for all of the shear tests. The yield points for the elastic breakdown are 6.72MPa, 11.47MPa, 11.37MPa, 7.14MPa, and 6.72MPa respectively, the maximum value of these tests reach approximately the same value as obtained from the K_o tests. The Young's moduli for these tests are 2.86GPa, 2.10GPa, 2.05GPa, 2.16GPa, and 1.48GPa, with the exception of of BH20.20 all of these are higher than the Young's moduli obtained from the K_o tests, which average 1.4GPa.

BH11.20 was performed when the membrane was leaking a large pore pressure gradient occurring across the sample, but is included here as the yield point is well defined. An average pore pressure was taken to determine the mean effective stress. BH10.20 shows a brittle failure with a well defined peak, it is the only sample tested that shows the brittle failure and occurs due to the low cell pressure

during shearing. The elastic behaviour can be seen as two trends with the tangential modulus decreasing with increasing strain. BH12.20 shows a drop in the load in the post-yield deformation from 14.4MPa to 12.0MPa, this is accompanied by a small decrease in the radial strain from 0.505% to 0.497%, whereas there would normally be an increase in the radial strain of between $20*10^{-3}$%, no change is seen in the cell pressure or the pore pressure.

The failure obtained in BH12.20 occurs around 34.4MPa at an axial strain of 31.1%, at maximum stress no constant volume shearing is seen.

Table A5.5

Sample	Porosity %	Rate of loading mm/min	Average height mm	Average diameter mm	Saturated weight g	Dry weight g	Specific gravity g/cm3
BH8.20	36.3	0.01	76.34	37.51	176.87	145.58	2.71
BH10.20	37.3	0.01	76.28	37.62	173.40	143.89	2.71
BH11.20	37.5	0.01	76.32	37.65	175.67	143.74	2.71
BH12.20	37.0	0.01	76.36	37.52	175.68	144.08	2.71
BH20.20	36.9	0.01	76.22	37.54	175.58	144.12	2.71
BH6.20	36.9	---	76.28	37.56	174.99	144.31	2.71

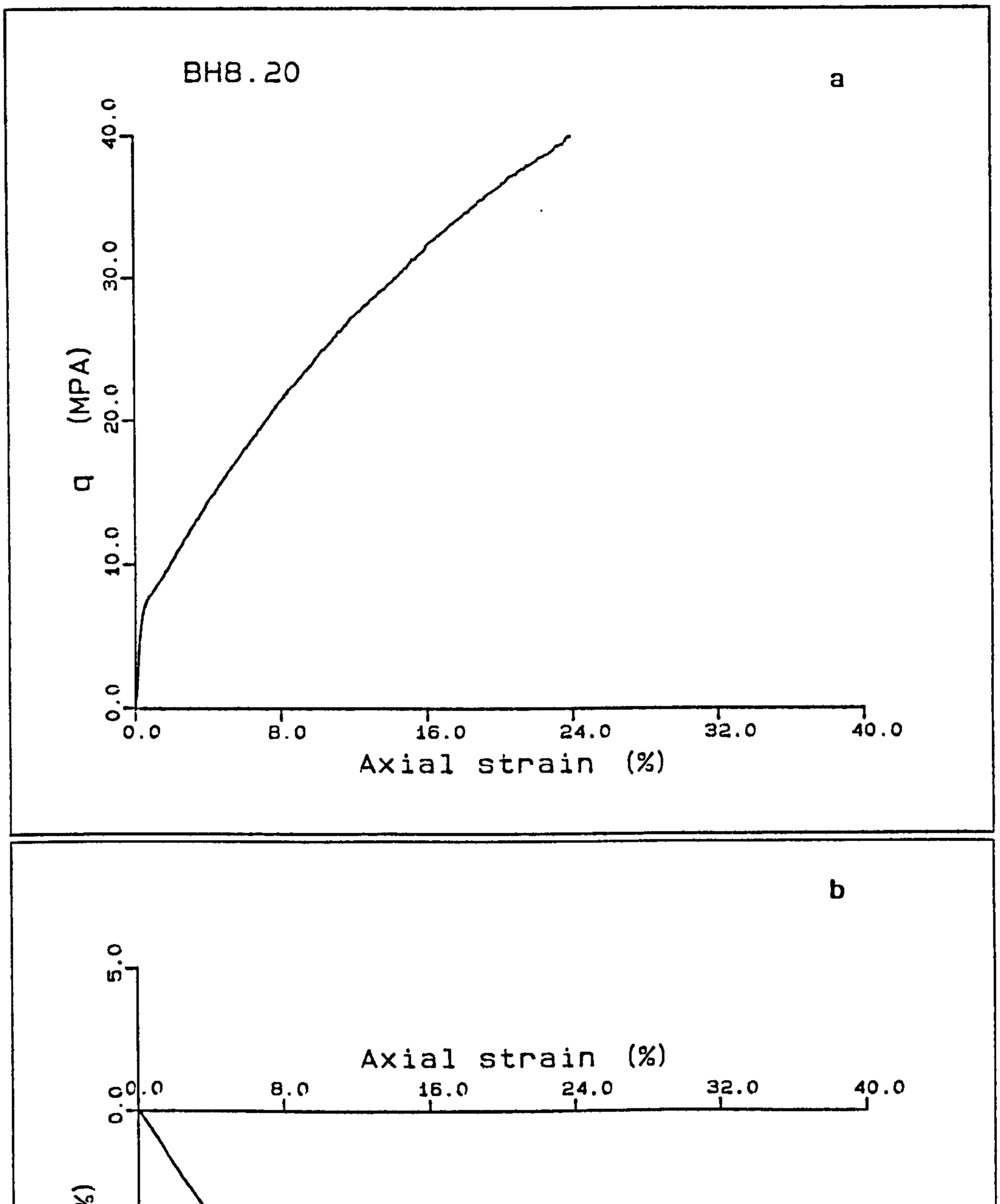

Figure A5.29(a-b) Drained loading test BH8.20.

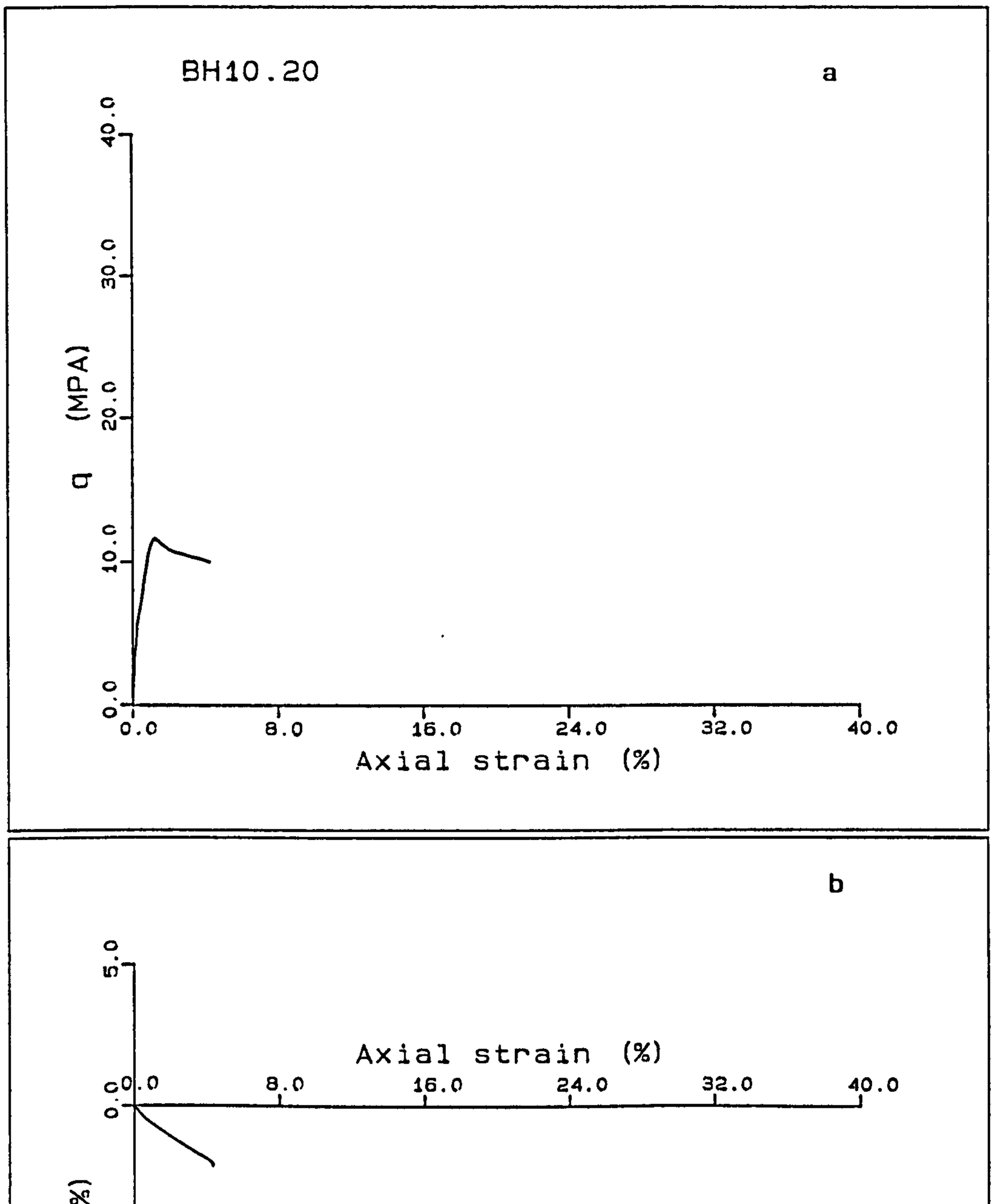

Figure A5.30(a-b) Drained loading test BH10.20.

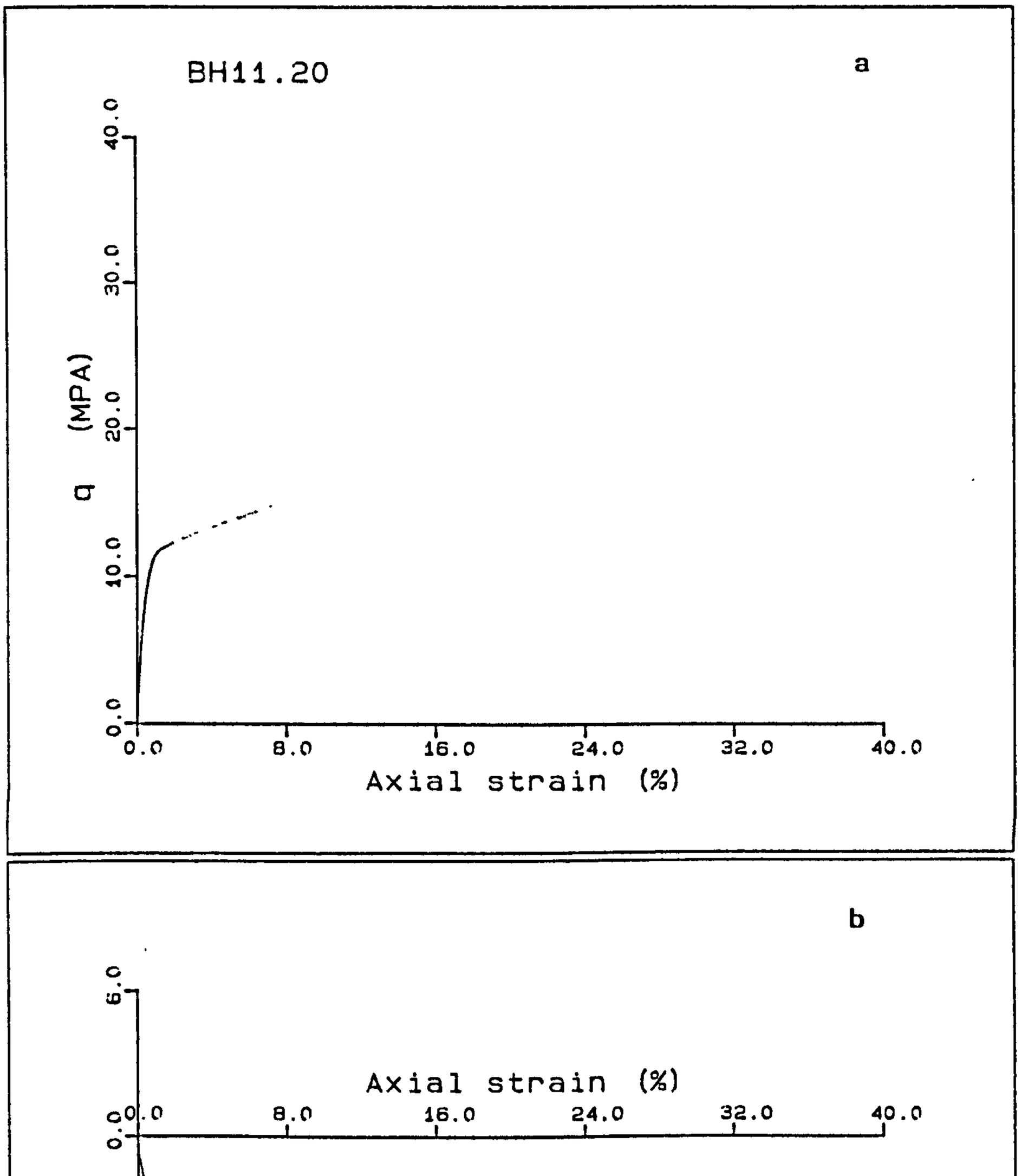

Figure A5.31(a-b) Drained loading test BH11.20.

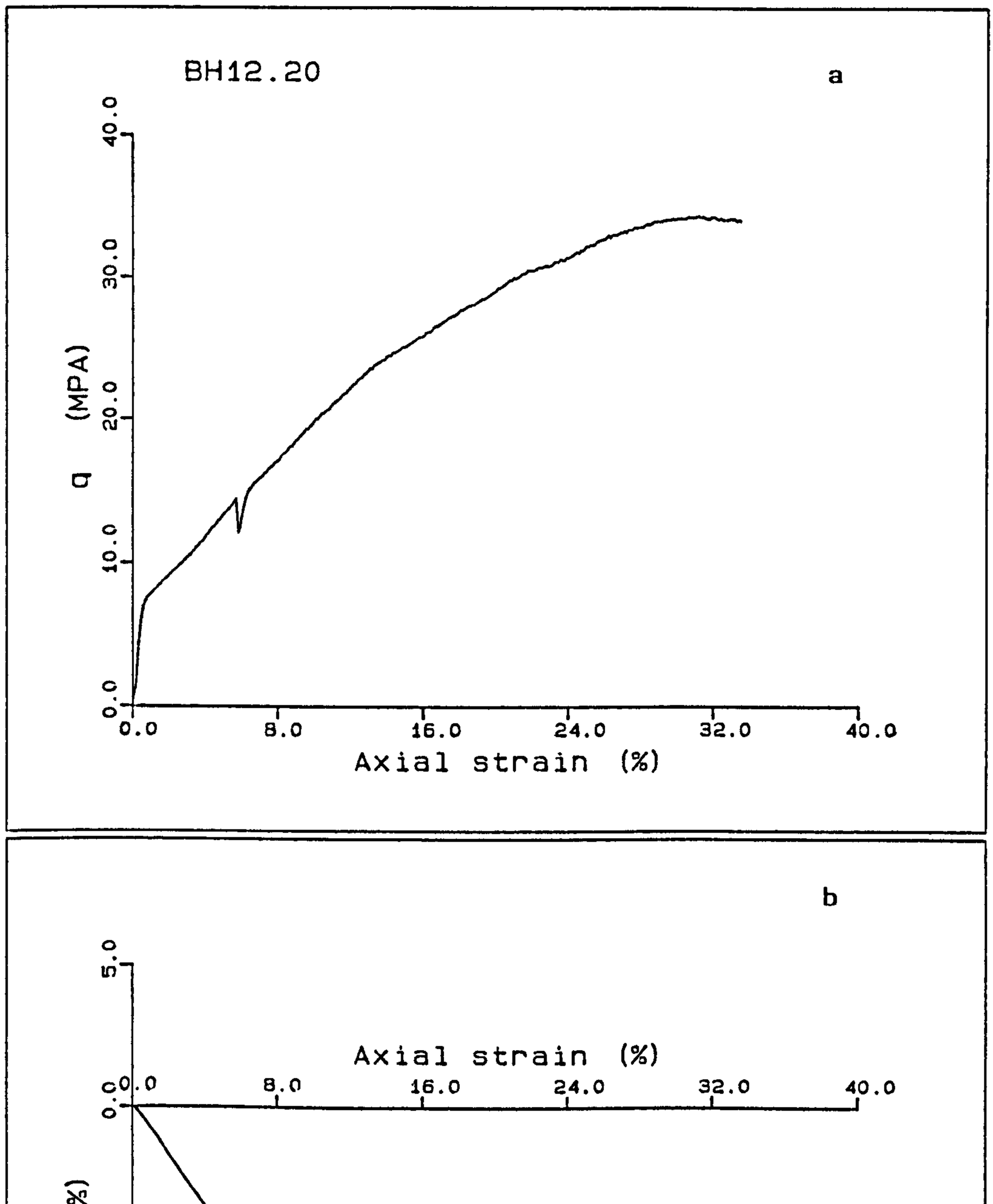

Figure A5.32(a-b) Drained loading test BH12.20.

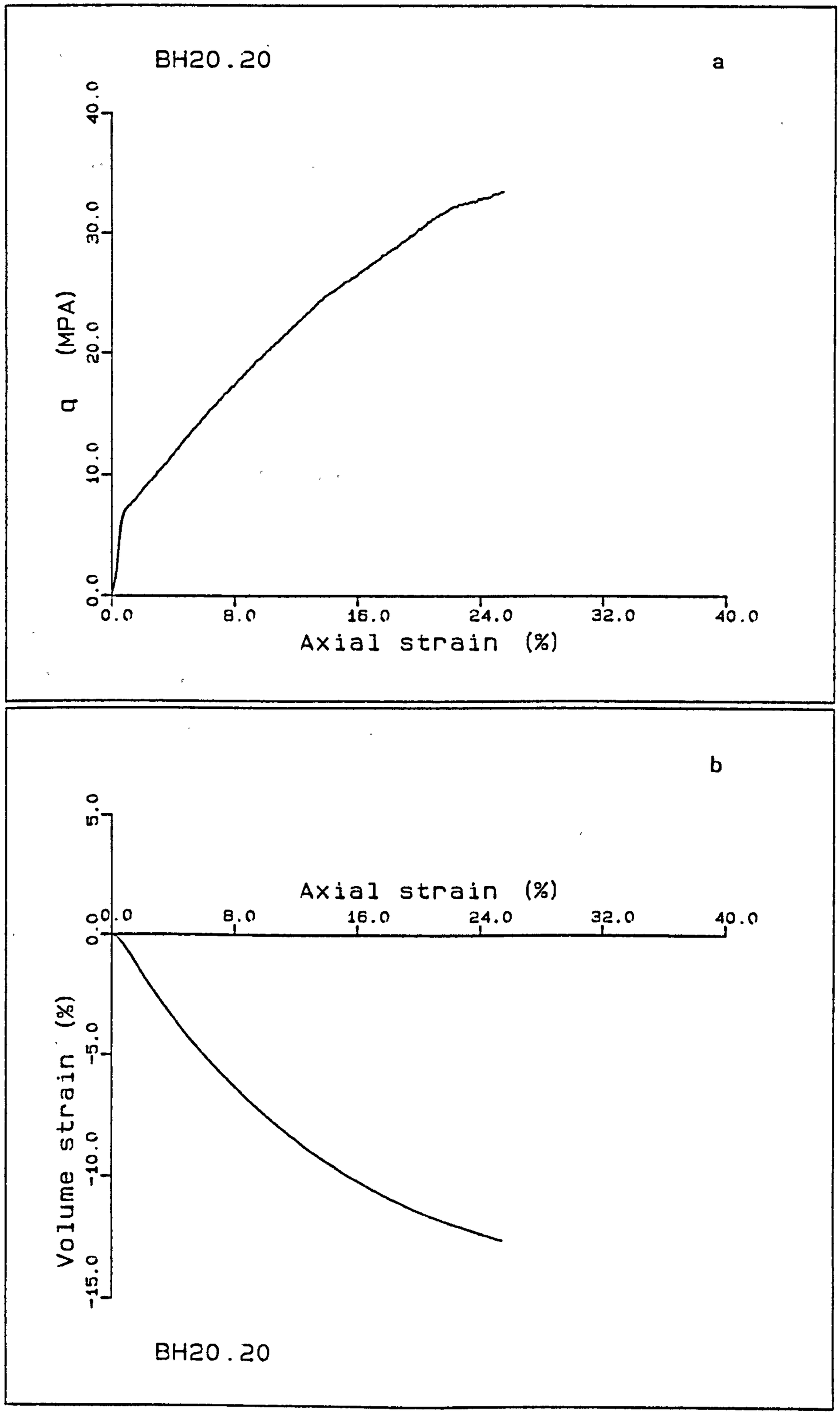

Figure A5.33(a-b) Drained loading test BH20.20.

A5.7) UNDRAINED SHEAR TESTS

Undrained shear tests were performed at constant cell pressure. Four samples were consolidated along the K_o stress path to different cell pressures, then deformed in undrained shear. USB3.20, USB4.20, USB5.20 and USB18.20 were sheared post-yield, while one test BH19.20 was isotropically consolidated to 12.6MPa, and sheared "inside the yield envelope". The peak deviatoric stress for this test is well defined at 10.41MPa, the Young's modulus gradually decreasing with increasing strain. The consolidation pressures of the anisotropically consolidated samples decreased with time due to problems with the confining pressure controlling system:

USB3.20 34.4 decreasing to 17.7MPa

USB4.20 34.7 decreasing to 19.7MPa

USB5.20 21.5 decreasing to 9.9MPa

USB18.20 46.7 decreasing to 24.0MPa increasing to 25.5MPa.

The shear data are presented in Figs. A5.35-39, and combined in Fig. A5.34. They show a decrease in load due to a slowing of the deformation rate from the K_o deformation rate to the shearing deformation. The shearing was performed at 0.01mm/min to be compatible with the drained shear tests, (an exception to this was USB3.20), this slow deformation rate also allows the dissipation of any pore pressures gradients present at the end of consolidation.

USB3.20 shows a drop in load, it also shows a small peak at 8MPa deviatoric stress due to a slowing down of the deformation rate from 0.0075mm/min to 0.003mm/min, this is seen as a kick in the q-p' diagram. Peak load is not reached in this test though the excess pore pressure increases with strain to a value 1MPa lower than the cell pressure. The stress ratio changed through the undrained shear, the modulus being seen to decrease with increasing axial strain.

USB4.20 shows no maximum load, but shows a peak pore pressure occurring 3MPa below the cell pressure, where the stress ratio levels off. USB5.20 shows a peak in the deviatoric stress, which at larger strains decreases and starts to increase again. USB18.20 shows a steady increase in the deviatoric stress after a change in the modulus of the stress-strain slope, the excess pore water pressure reaching a peak and the stress ratio changing modulus. The pore pressures at peak are 3MPa smaller than the cell pressure.

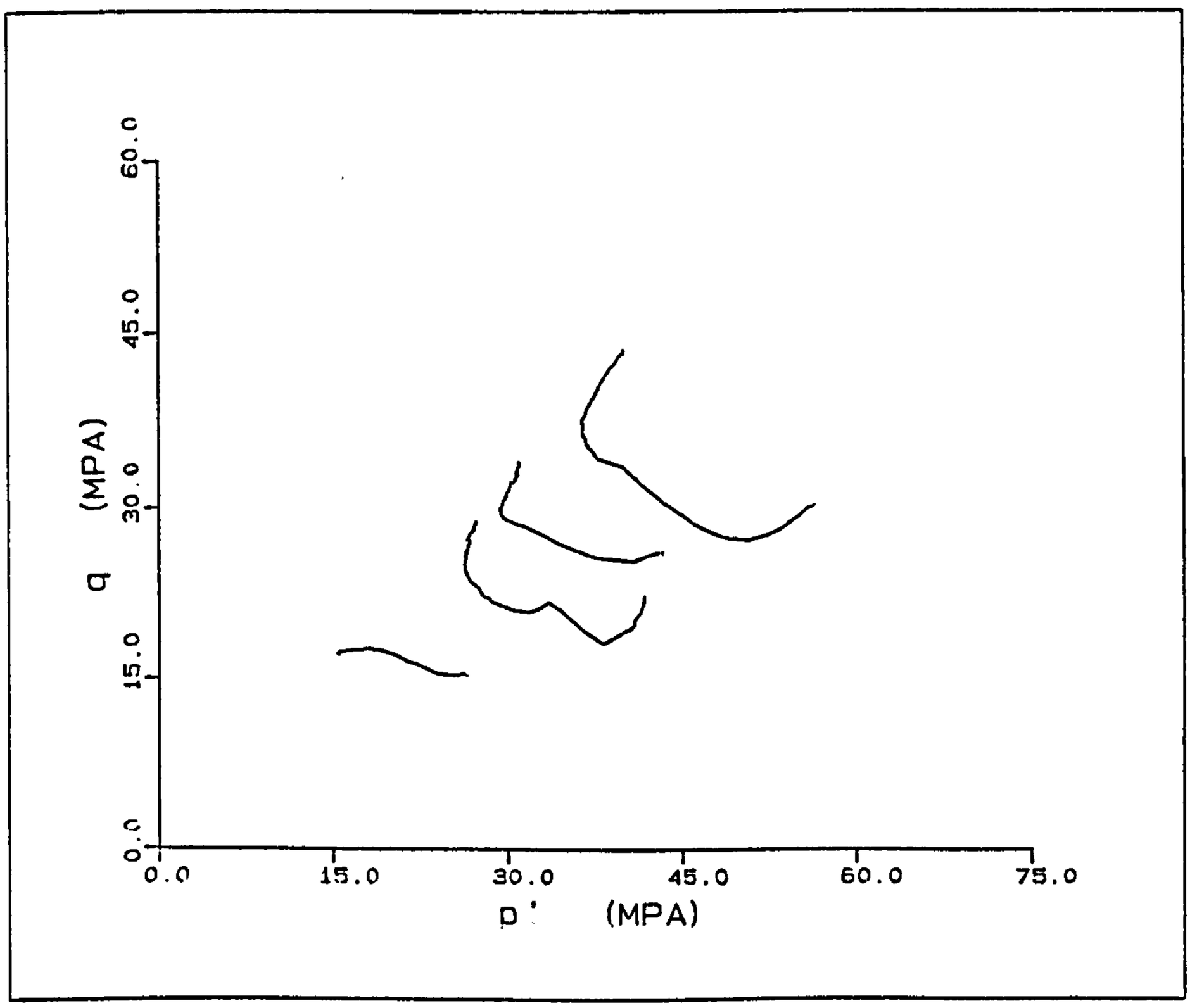

Figure A5.34 Combined stress paths from four anisotropically consolidated undrained loading tests.

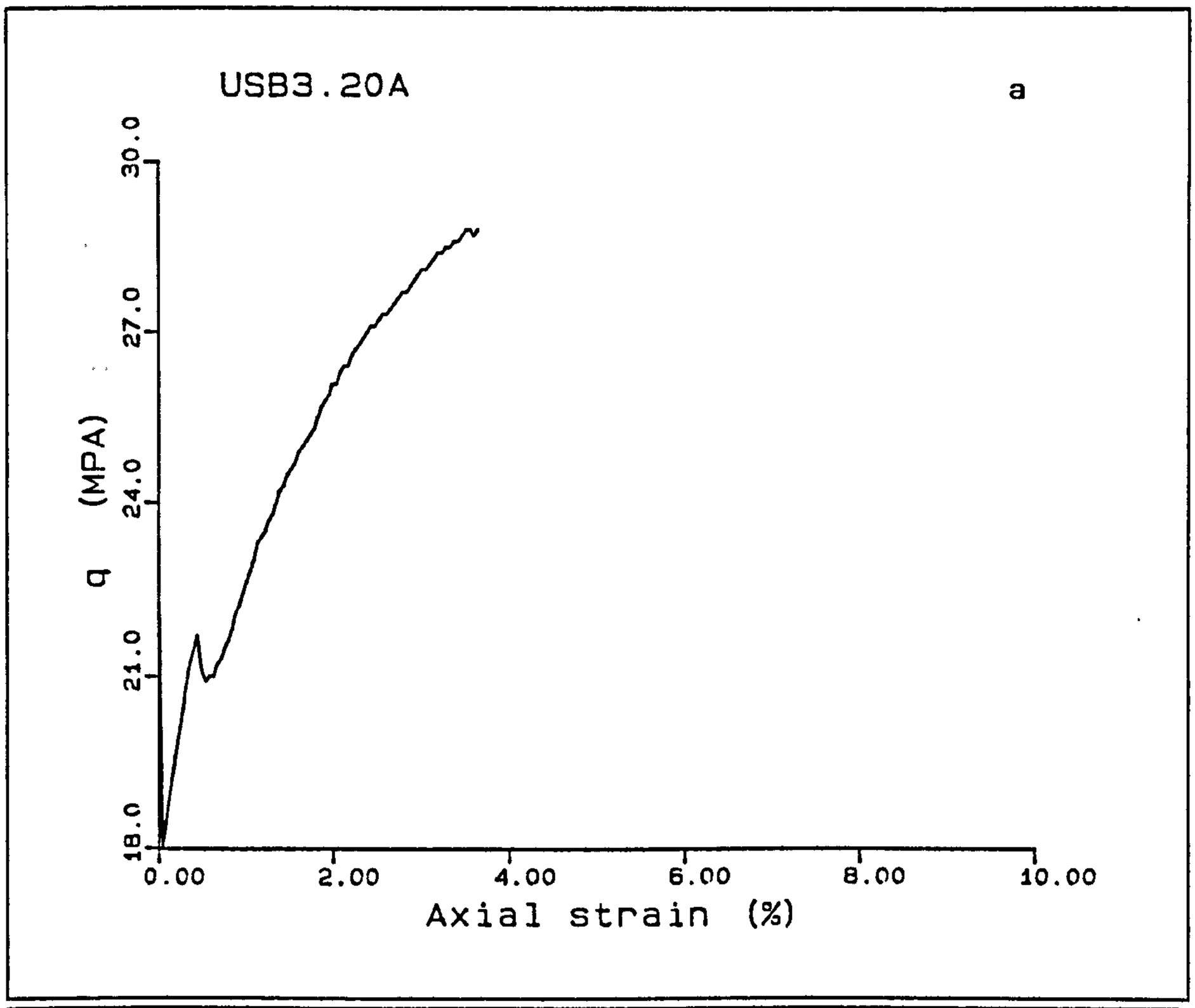

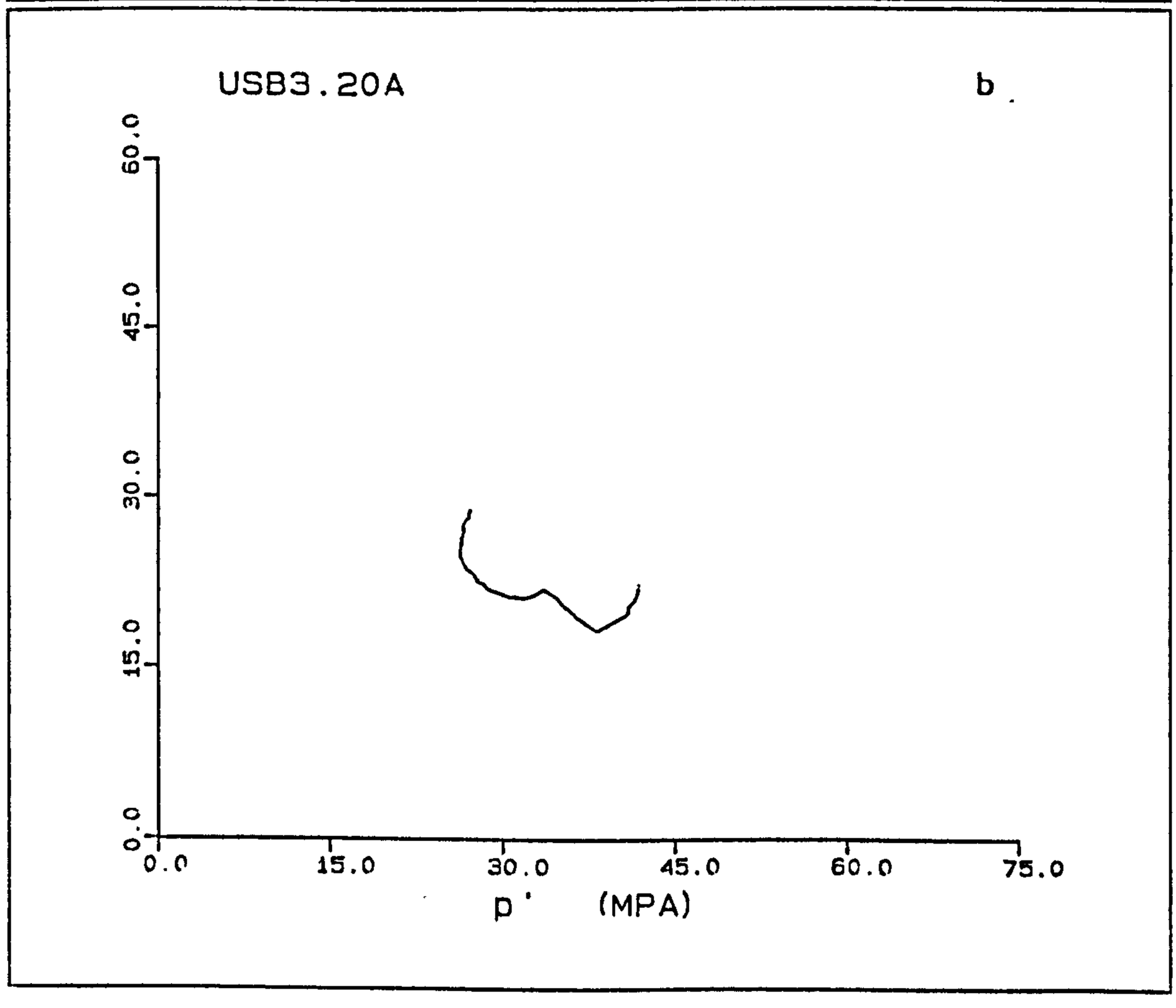

Figure A5.35(a-d) Undrained loading test USB3.20.

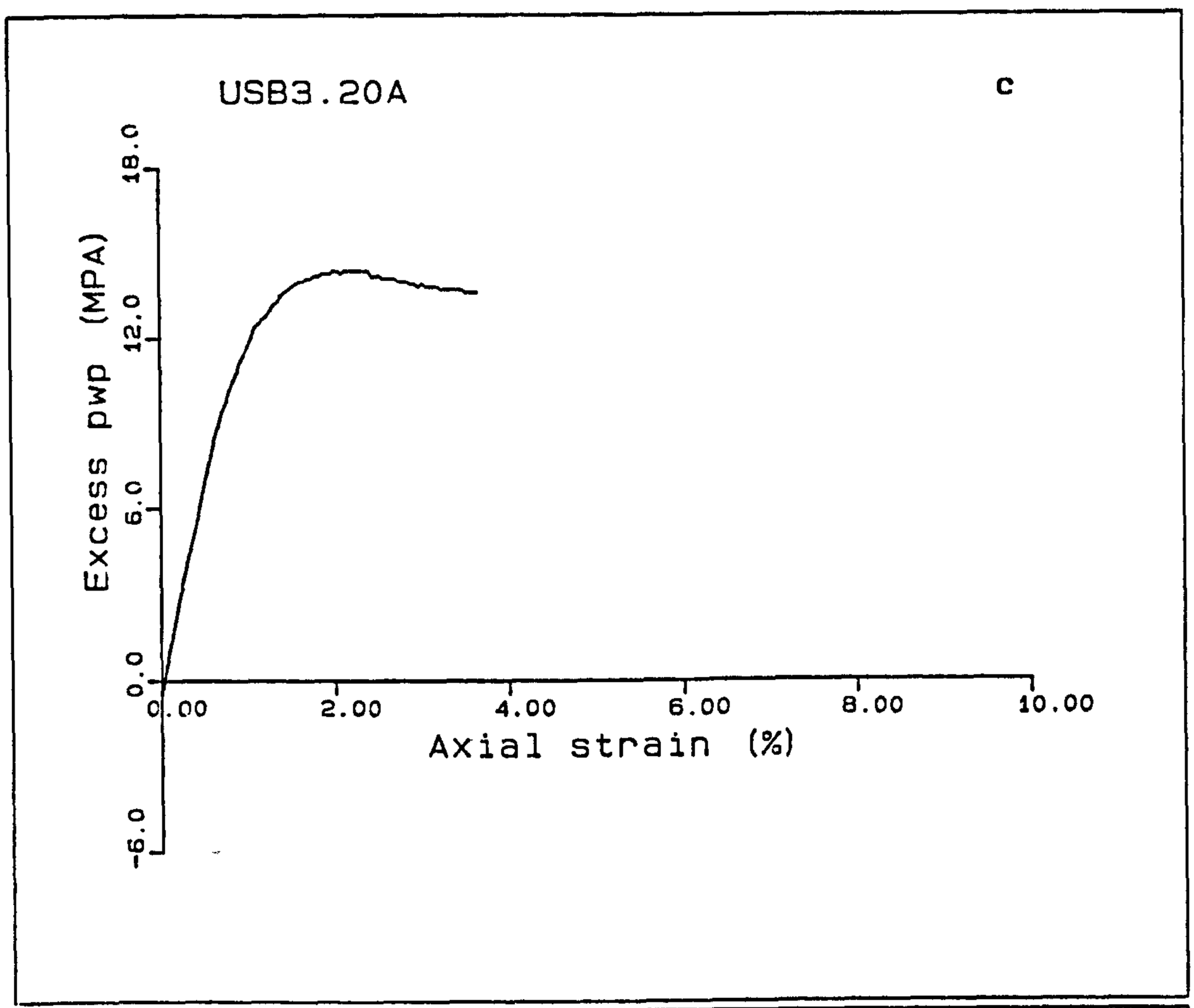
USB3.20A
c
Excess pwp (MPA)
18.0
12.0
6.0
0.0
-6.0
0.00
2.00
4.00
6.00
8.00
10.00
Axial strain (%)

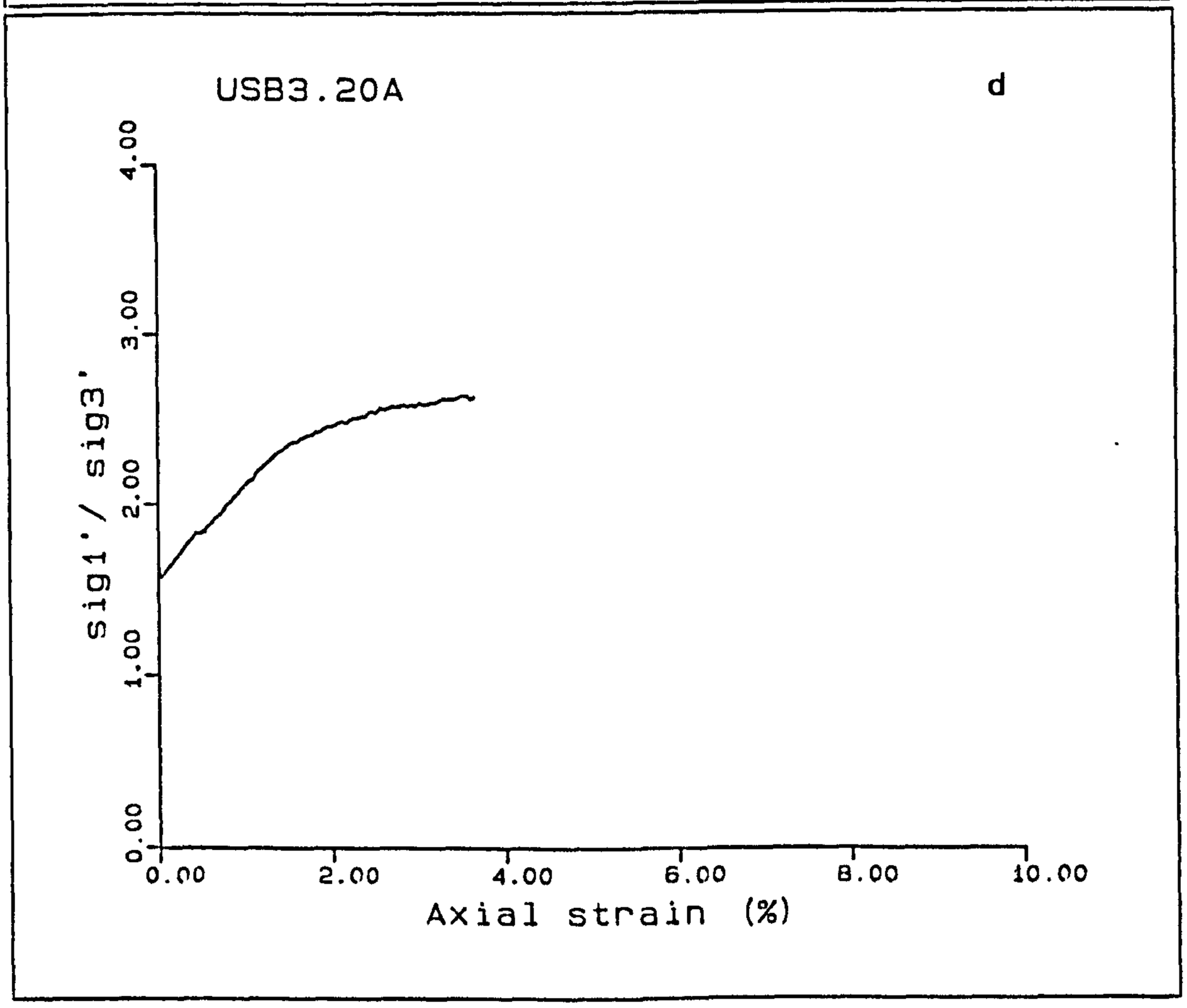
USB3.20A
d
Sig1' / sig3'
4.00
3.00
2.00
1.00
0.00
0.00
2.00
4.00
6.00
8.00
10.00
Axial strain (%)

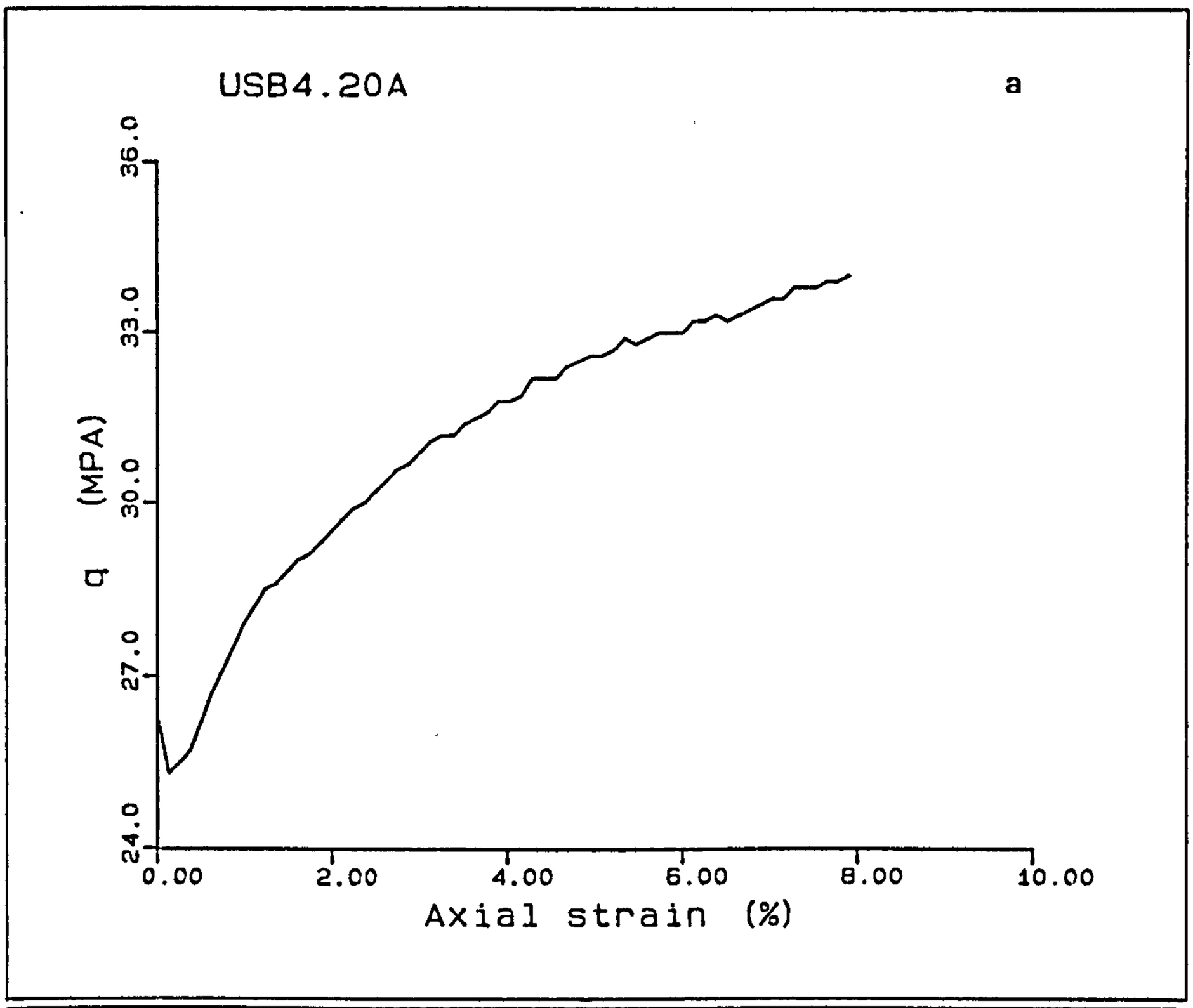

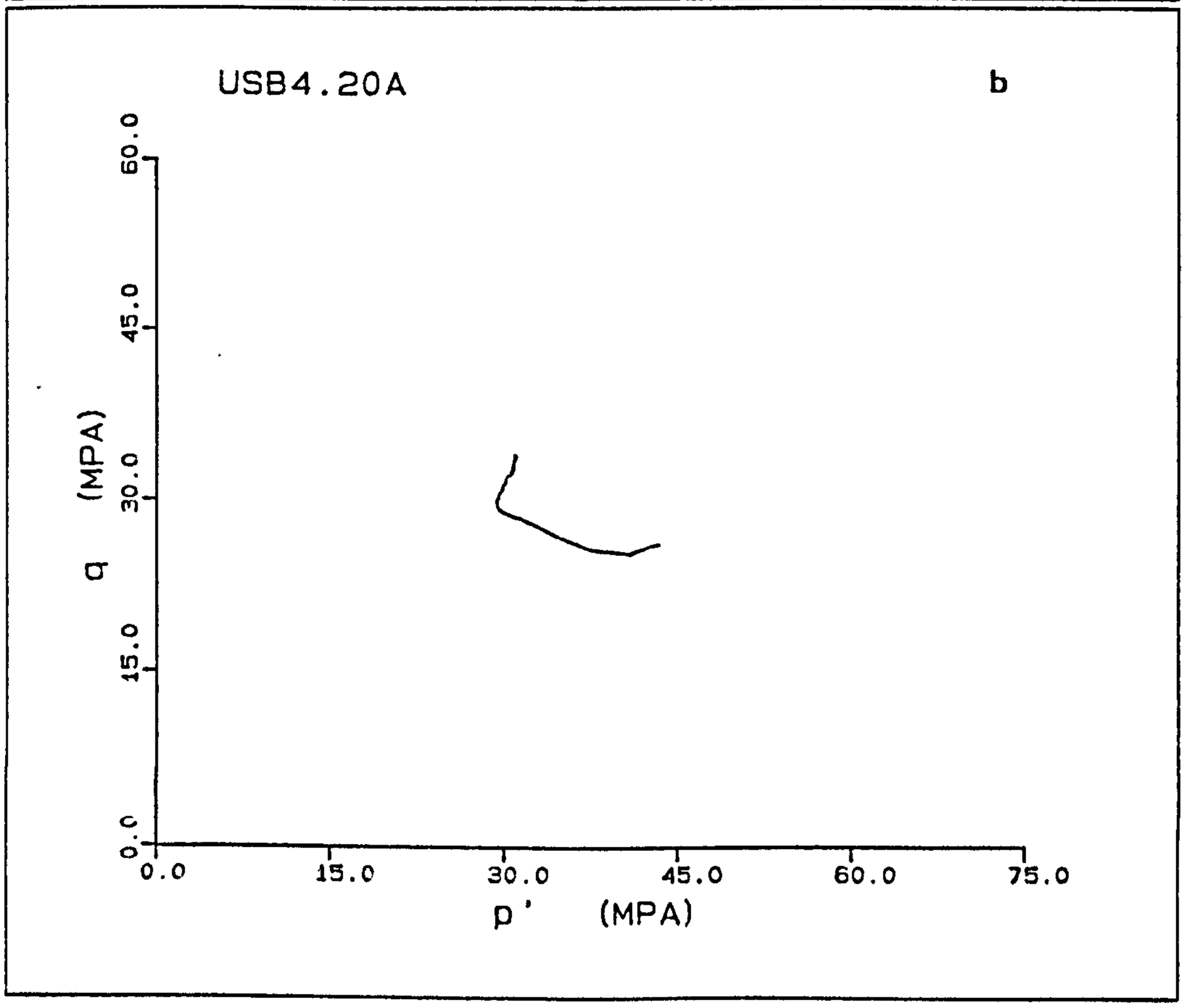

Figure A5.36(a-d) Undrained loading test USB4.20.

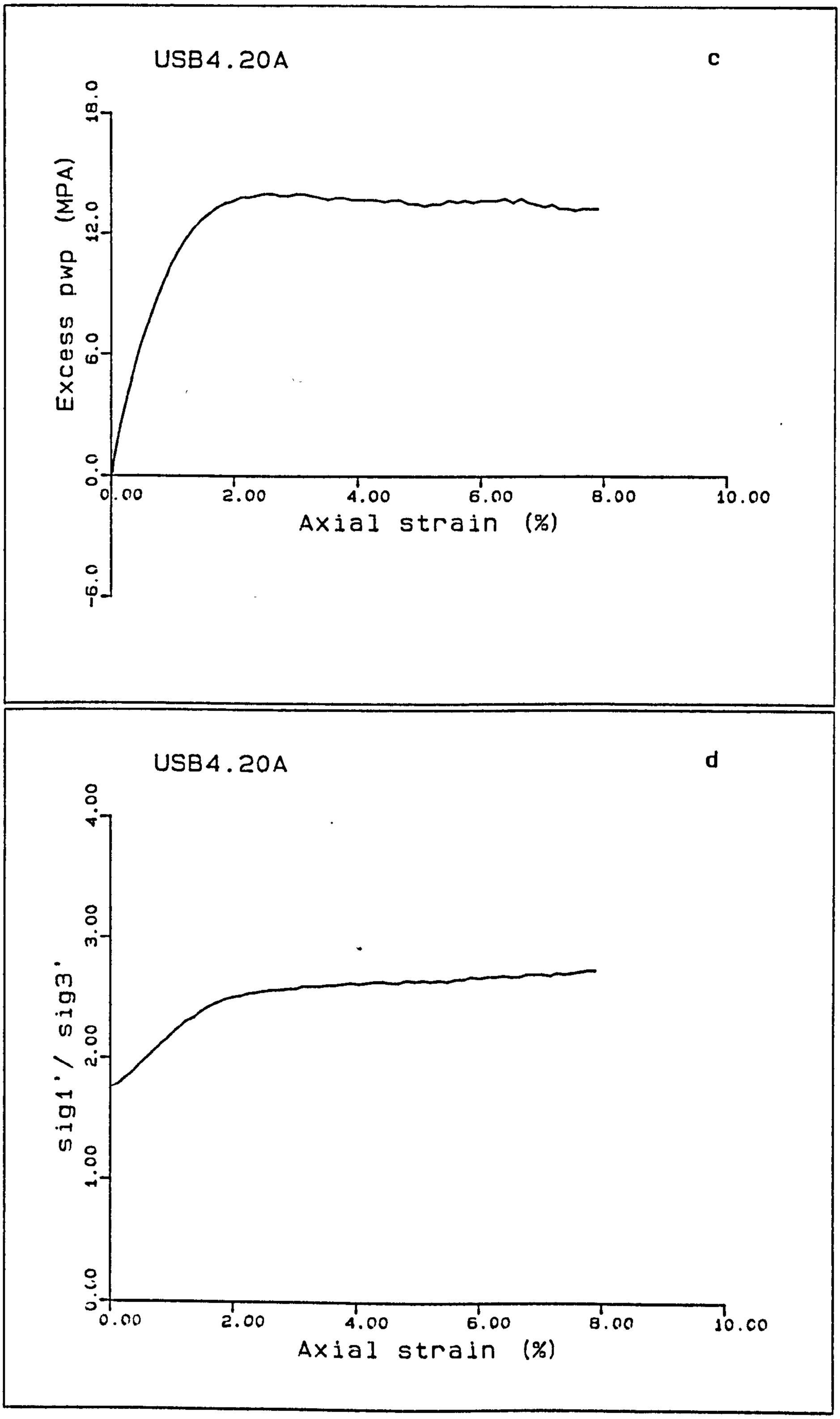
USB4.20A
c
Excess pwp (MPA)
18.0
12.0
6.0
0.0
-6.0
0.00
2.00
4.00
6.00
8.00
10.00
Axial strain (%)
USB4.20A
d
sig1' / sig3'
4.00
3.00
2.00
1.00
0.00
0.00
2.00
4.00
6.00
8.00
10.00
Axial strain (%)

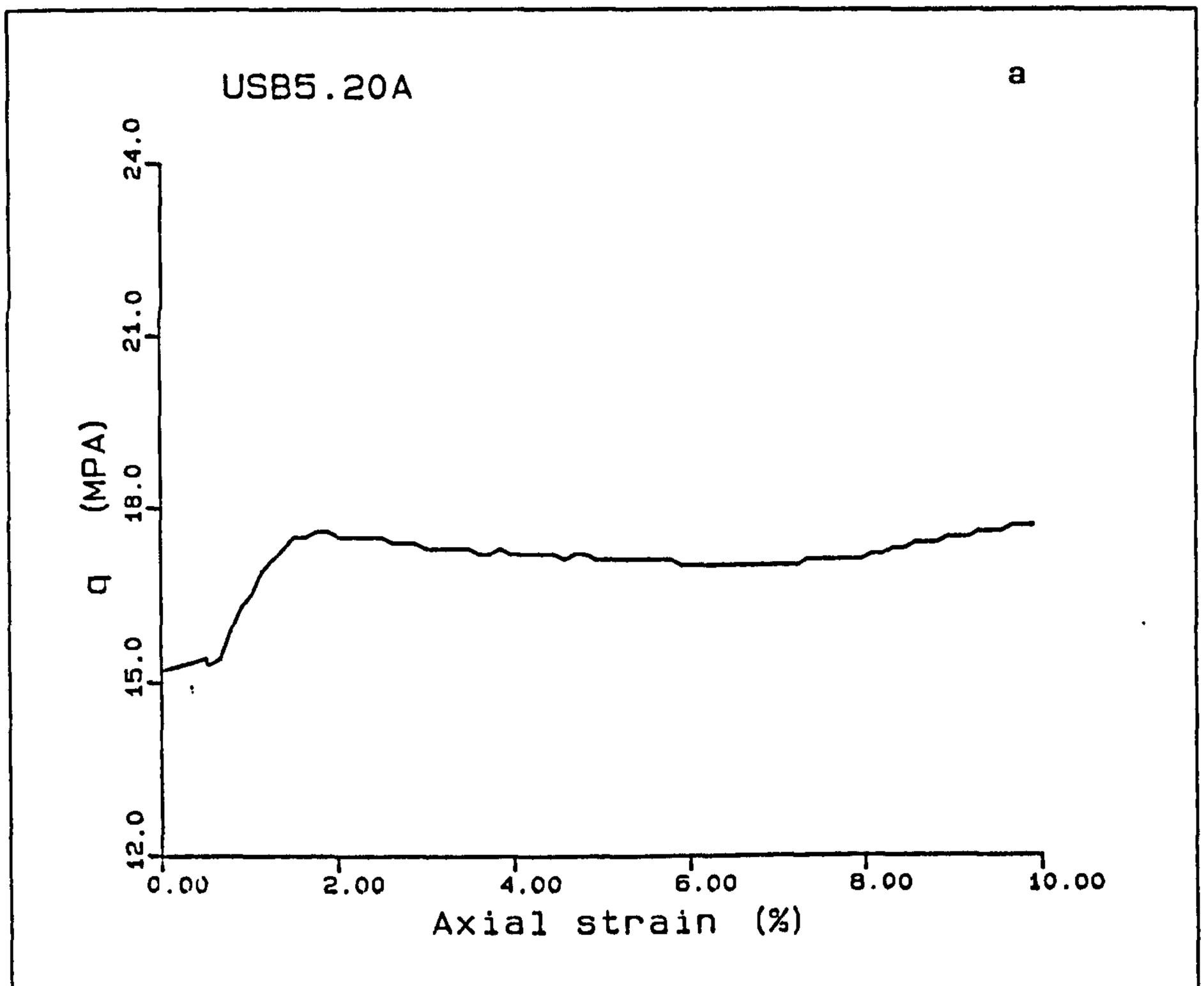

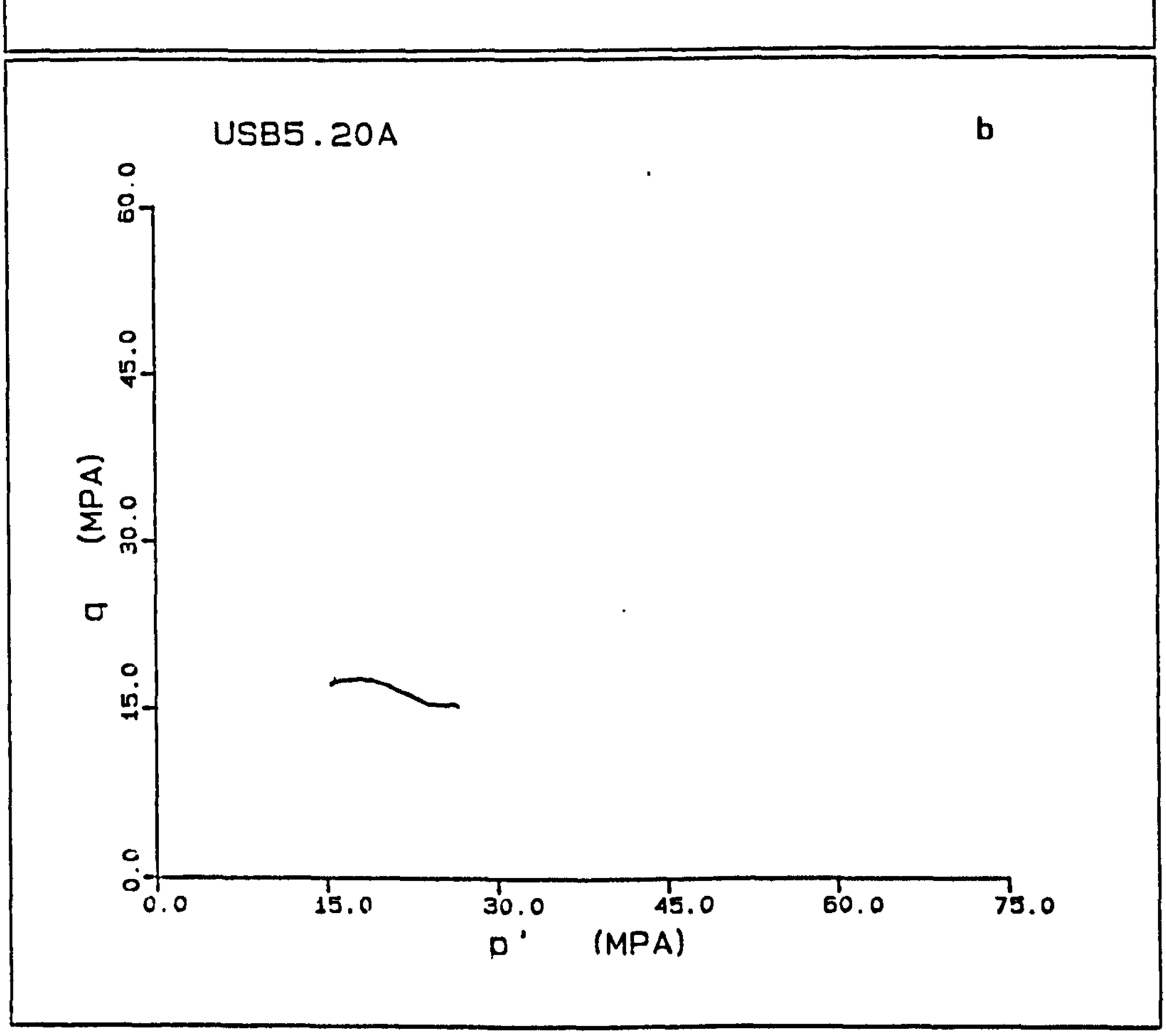

Figure A5.37(a-d) Undrained loading test USB5.20.

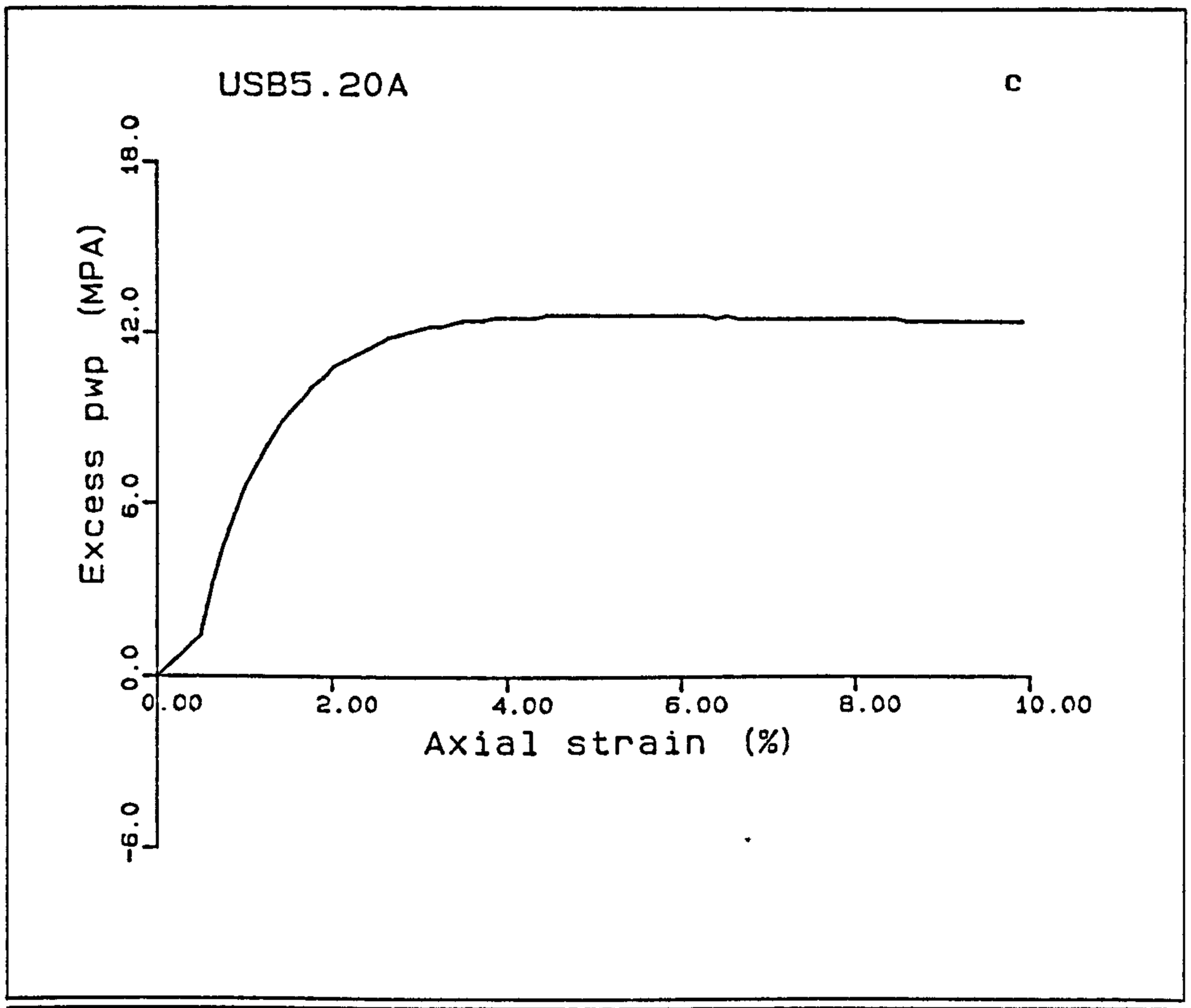
USB5.20A
c
Excess pwp (MPA)
18.0
12.0
6.0
0.0
-6.0
0.00
2.00
4.00
6.00
8.00
10.00
Axial strain (%)

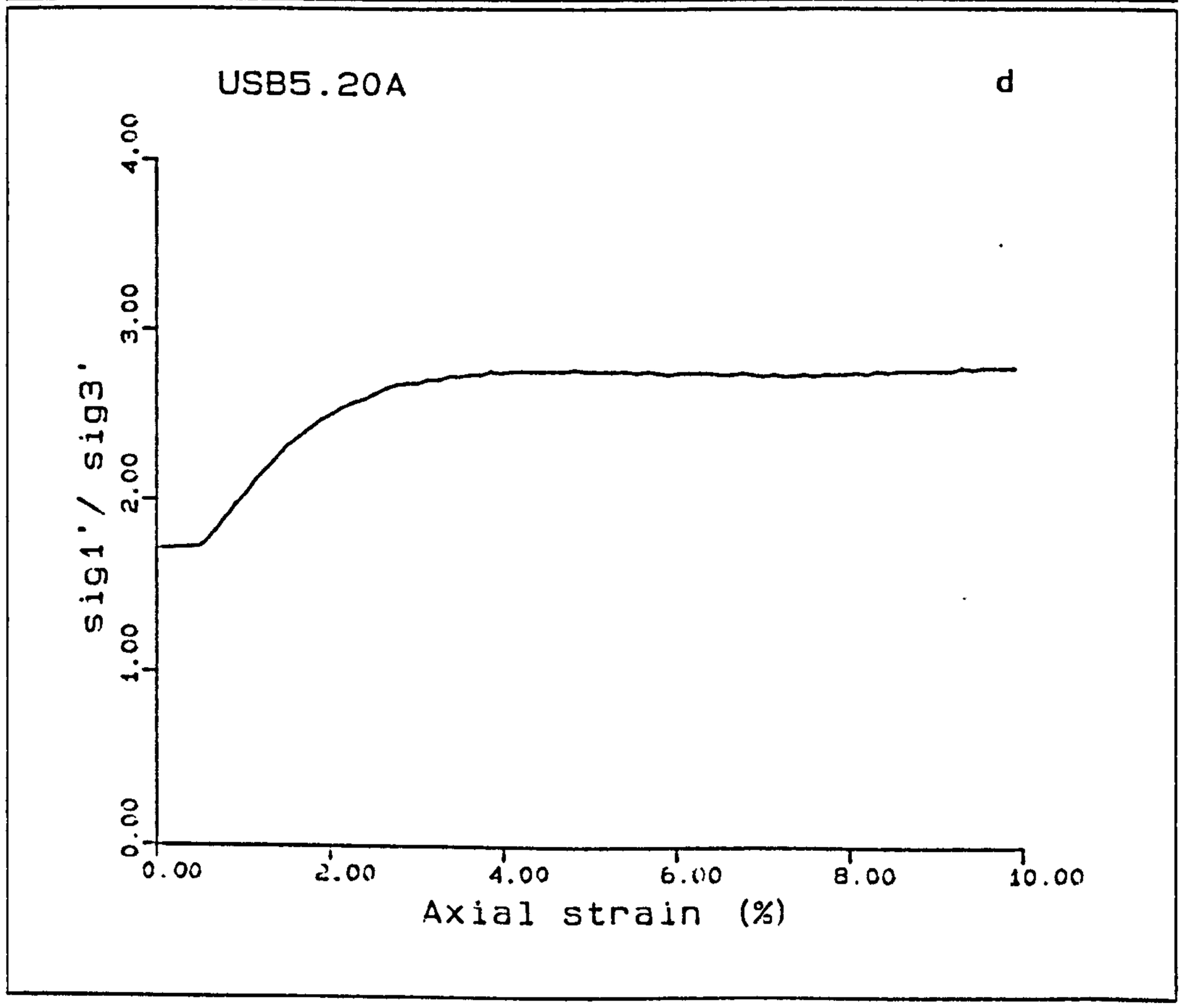
USB5.20A
d
sig1' / sig3'
4.00
3.00
2.00
1.00
0.00
0.00
2.00
4.00
6.00
8.00
10.00
Axial strain (%)

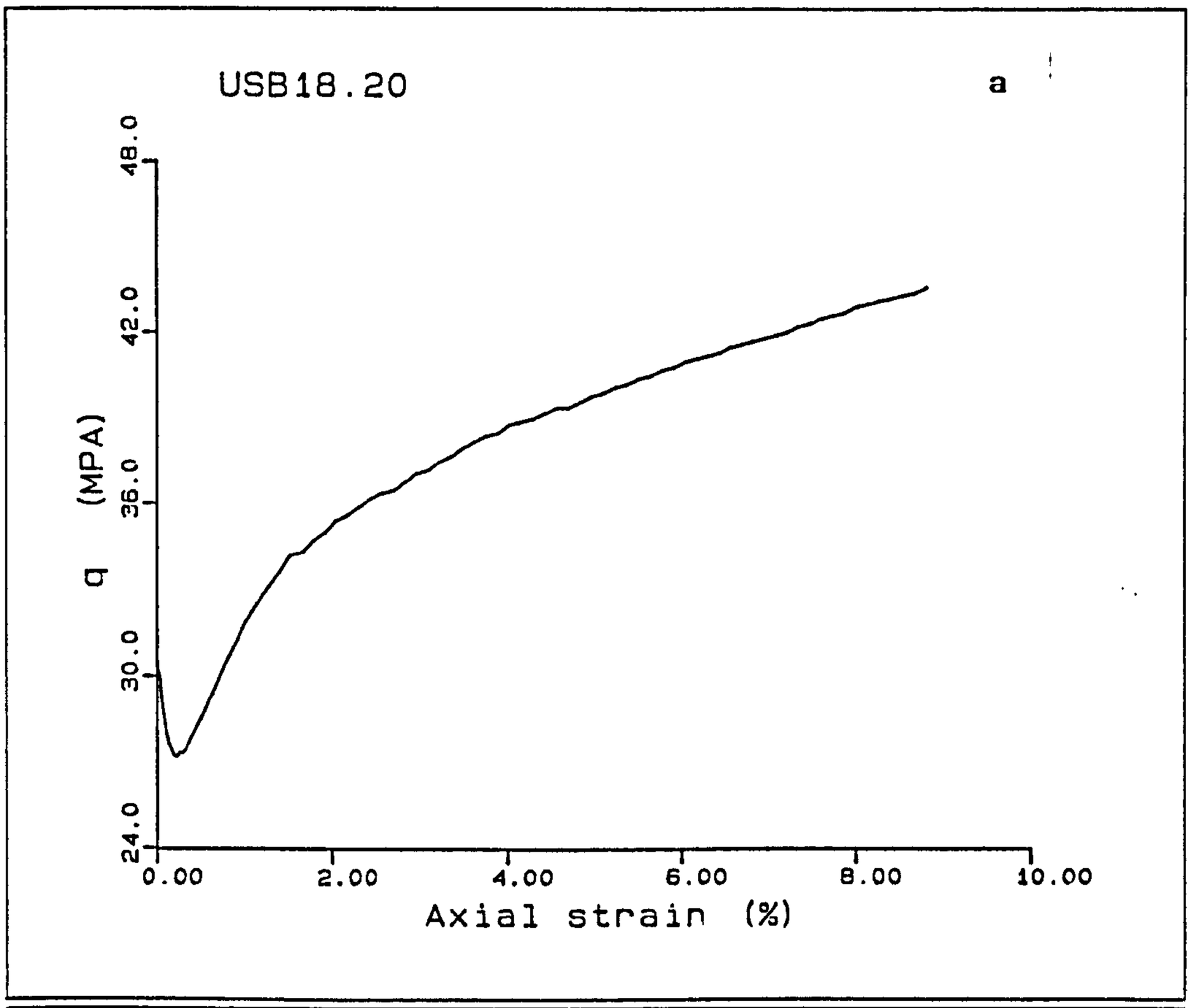

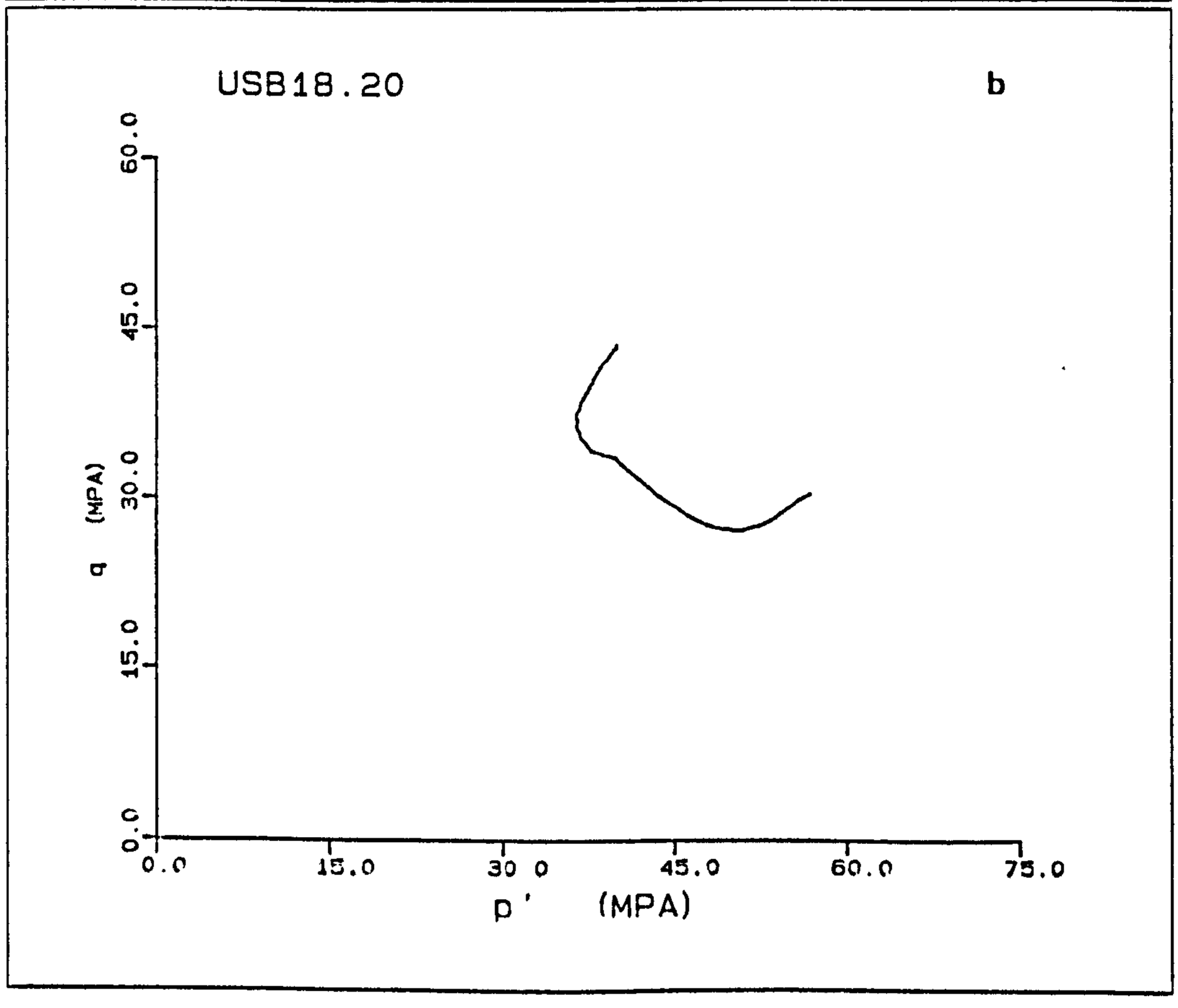

Figure A5.38(a-d) Undrained loading test USB18.20.

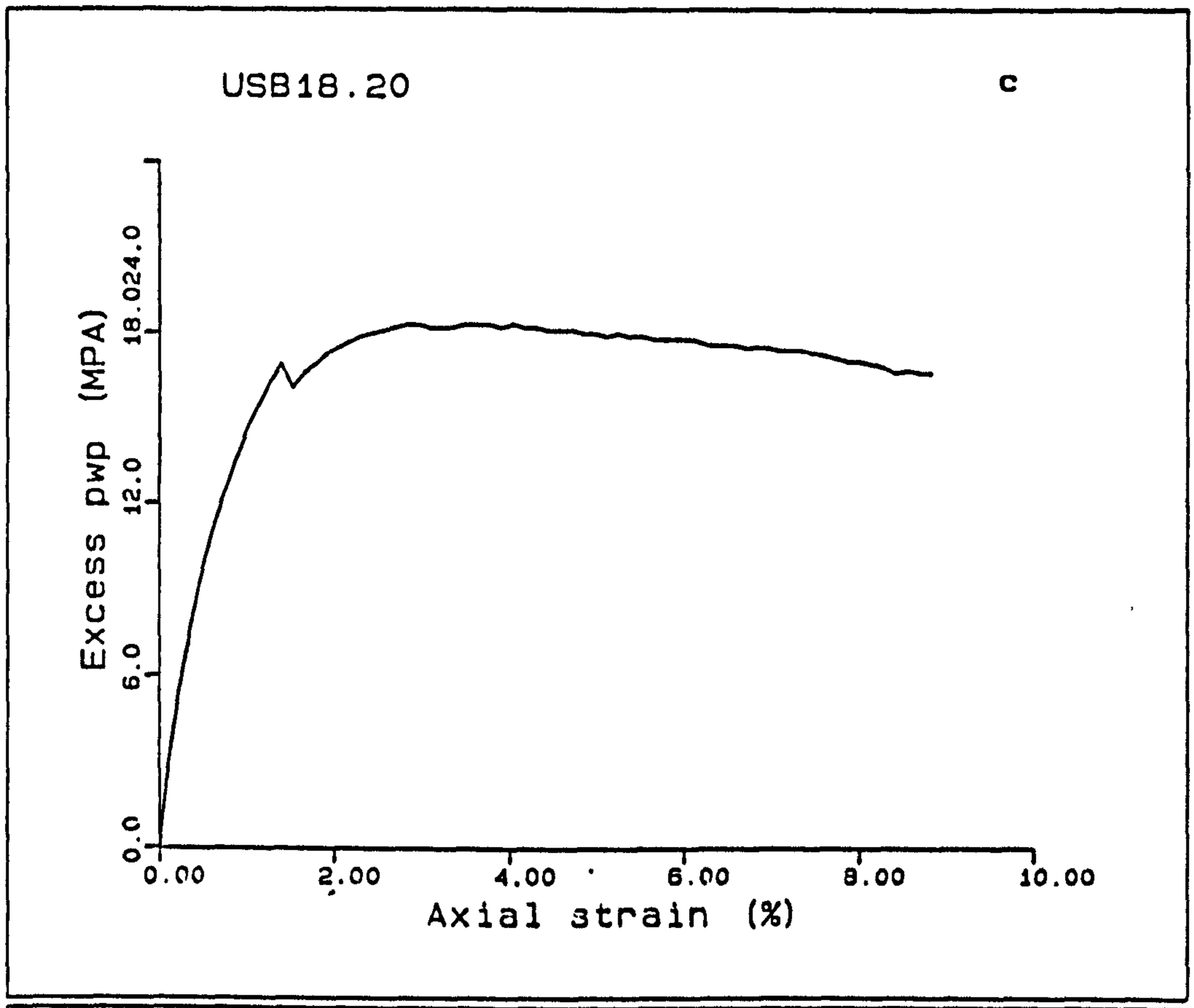
USB18.20
c
Excess pwp (MPA)
0.0
6.0
12.0
18.0
0.00
2.00
4.00
6.00
8.00
10.00
Axial strain (%)

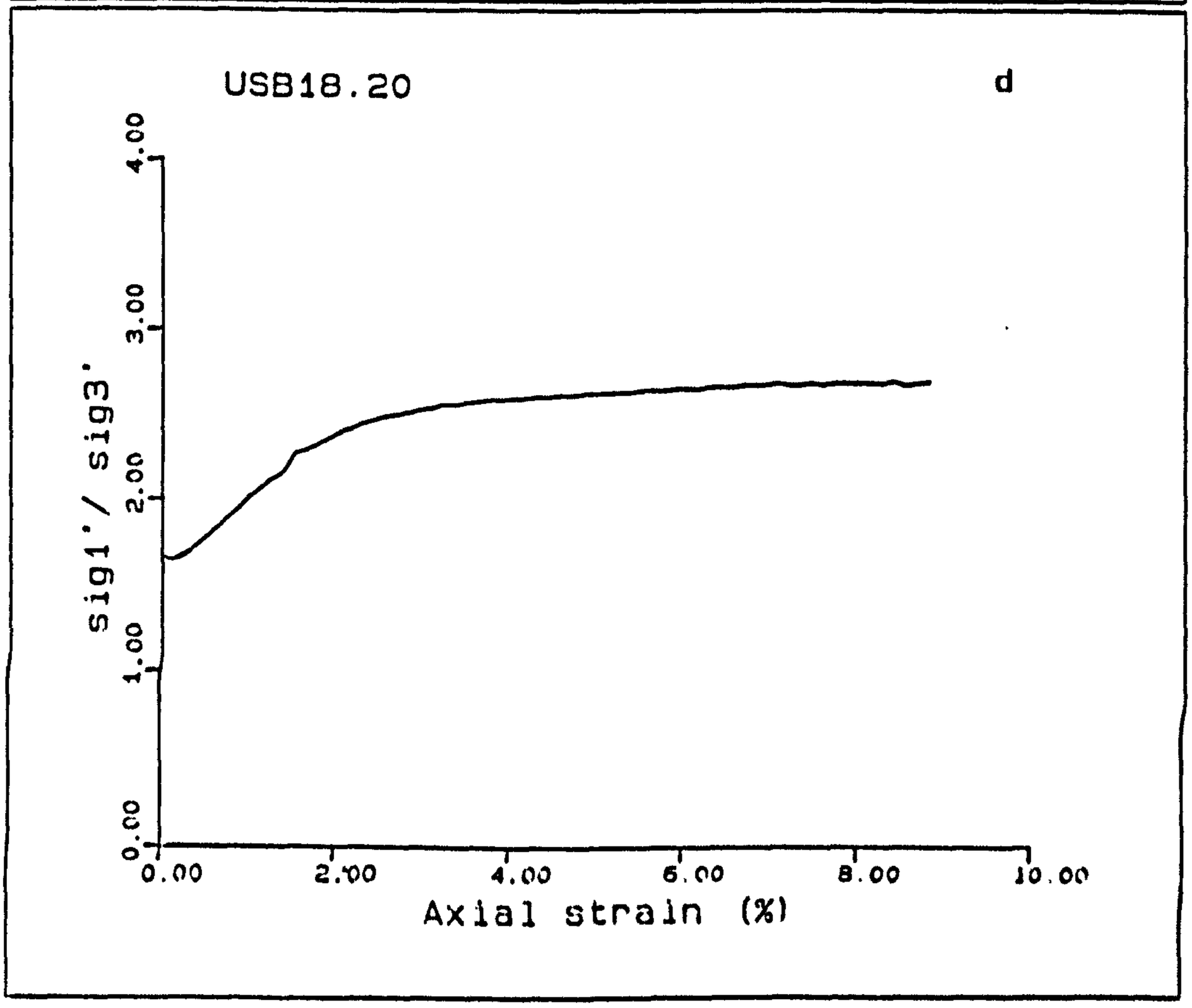
USB18.20
d
Sig1' / sig3'
0.00
1.00
2.00
3.00
4.00
0.00
2.00
4.00
6.00
8.00
10.00
Axial strain (%)

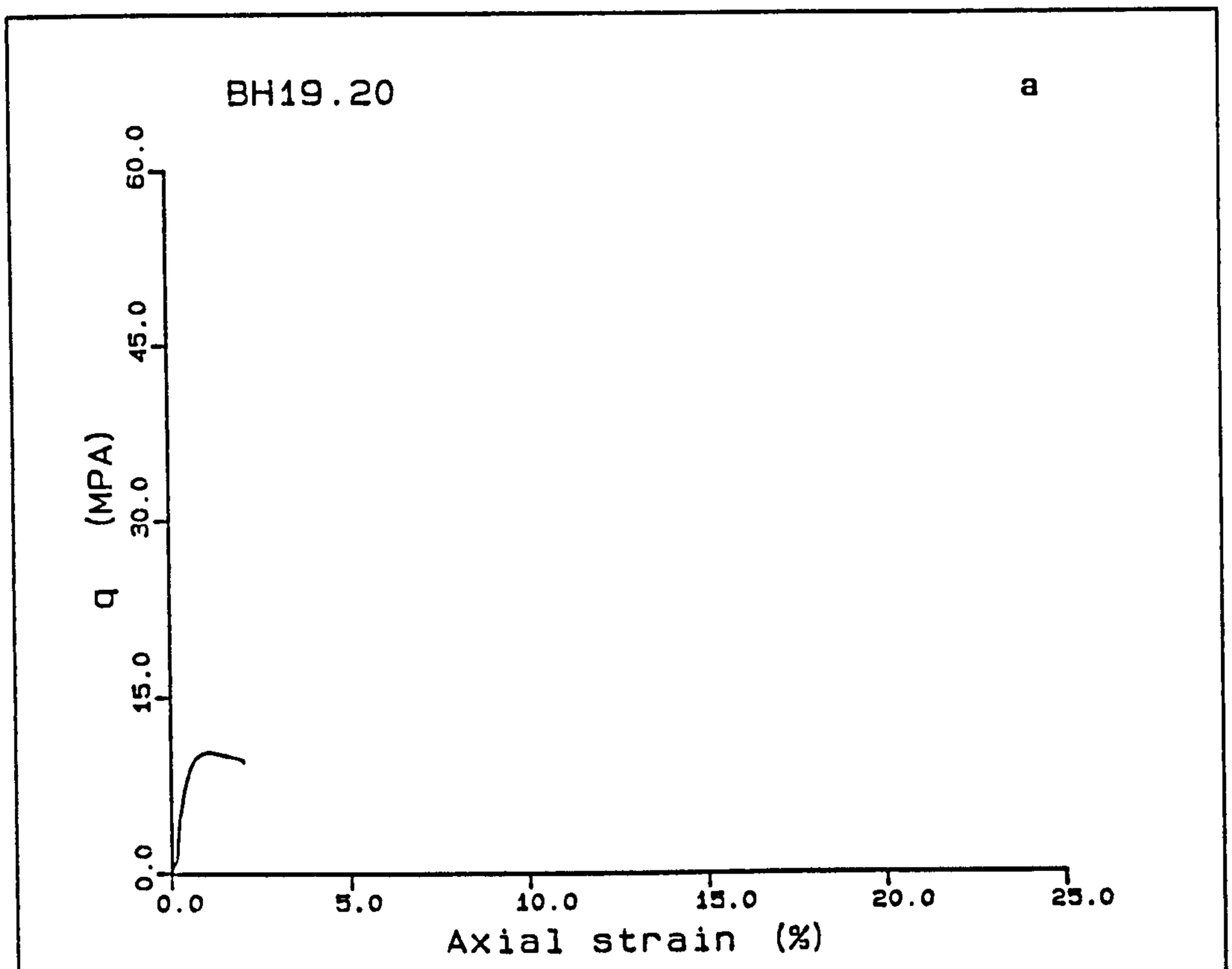

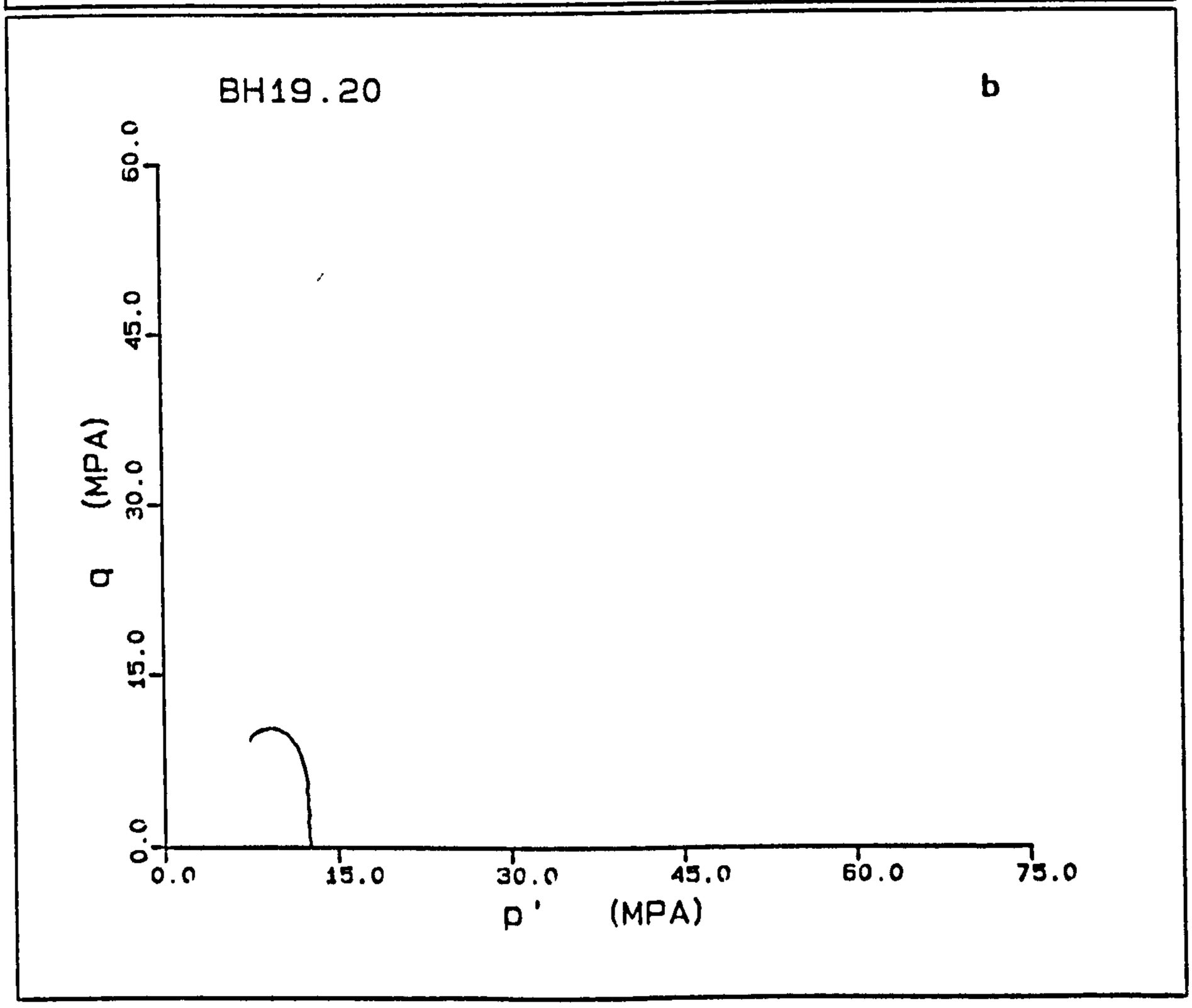

Figure A5.39(a-b) Undrained loading test BH19.20.

APPENDIX 6

EQUIPMENT SPECIFICATIONS

A6.1) SPECIFICATIONS FOR THE COMPONENTS OF THE TRIAXIAL CELL HEATING SYSTEM

CONTROLLING UNIT:

controller:

Eurotherm three term PID temperature controller type 805

supply voltage	110v 50/60 Hz
output	logic, non isolated, time proportioning between 2 and 20 seconds, 12MA 15v dc.
scale range	-50°C to +500°C
input	chromel - alumel, K type thermocouple range -50°C to +500°C

thyrister:

Eurotherm Eurocube 425

operating input voltage	110v
RMS voltage rating	13
output current and voltage	15A, 240v
input	logic, 5-10v dc, 10-25v dc, 4-20MA SSC.
firing mode	on - off thyrister, solid state contactor.

HEATING ELEMENT:

Surface heating BICC Pyrotenax stainless steel sheathed ceramically

insulated heating element:

heating cable reference	HSQIM4000
length	2M long with 2M lead in cable on each end.
diameter	3.2 mm outside diameter
supply voltage	110v a.c. single phase
electrical input	750 watts
nominal resistance	16 ohms
design temperature	250^{o}C

A6.2) SPECIFICATIONS OF COMPONENTS OF THE DRAINAGE SYSTEM

BACK PRESSURE REGULATOR:

Tescom 26-1700 series back pressure regulator.

seal	valve and seat (KEL-F-81)
maximum back pressure	70MPa (10,000 psig)
flow capacity	C_v = 0.6

VOLUME GAUGE:

I.C. volume change transducer

capacity	50cm^3 or 100cm^3
diameter	7.62cm (3") or 10.16cm (4")
height	15.24cm (6") or 15.24cm (6")
maximum back pressure	1.4 MPa (200 psi)
sensitivity	0.01cm^3 or 0.02cm^3
displacement transducer type	LS24 TCI
resistance	350 ohms nominal
range	full scale 26.9mm
output	5.3mv/v

TRANSDUCERS:

Manufacturer: Shape Instruments, The Western Centre, Western Road, Bracknell, Berkshire. RG12 1RW.

pressure transducer type	SP1082
range	0 to 70 MPa (0 to 10,000 psi)
fitting	1/4" BSP (male)

AIR REGULATOR:

Manostat; model number E162

Suppliers and Manufacturers: John Watson and Smith Ltd., Craven Road, Leeds. LS6 2EU.

Pressure range	0.014 to 0.83 MPa (2 to 120 psi)
port size	1/4" BSP

A6.3) STRAIN GAUGES USED ON THE RADIAL STRAIN BELT

Manufacturer: Micro-Measurements Division, Measurements Group Inc., Raleigh, North Carolina.

Supplied by: Welwyn Strain Measurements

Strain Gauges;

WK-06-250BG-350

WK=-269^{o}C to 290^{o}C Normal operation

-269^{o}C to 400^{o}C special or short term conditions

W = fully encapsulated gauge,glass fibre reinforced epoxy phenolic resin. High endurance lead wires.

K = Modified Karma alloy used for high performance self-temperature

-compensated gauge

06 = Self-Temperature-Compensation, the approximate thermal expension in PPM/^{O}F of the structural material on which the gauge is to be used.

250 = Active gauge length in millimetres

BG = Grid and tab geometry

250BG:

Gauge length = 6.35mm

Overall length = 9.53mm

Grid width = 3.18mm

Overall width = 3.18mm

350 = Resistance in ohms